NUCLEAR PHYSICS

JOURNAL DEVOTED TO THE EXPERIMENTAL AND THEORETICAL STUDY OF THE FUNDAMENTAL CONSTITUENTS OF MATTER AND THEIR INTERACTIONS

EDITOR: L. ROSENFELD - COPENHAGEN
ASSOCIATE EDITOR: O. NATHAN - COPENHAGEN

VOLUME XVIII

NORTH-HOLLAND PUBLISHING COMPANY - AMSTERDAM

EDTIORIAL BOARD

AUSTRALIA & NEW ZEALAND:	H. Messel (Sydney), M. L. Oliphant (Canberra)
AUSTRIA:	B. Karlik, (Vienna), H. Thirring (Vienna)
BELGIUM:	M. de Hemptinne (Louvain), J. Verhaeghe (Ghent)
CANADA:	G. Volkoff (Vancouver)
DENMARK:	C. Møller (Copenhagen), S. Rozental (Copenhagen), G. E. Brown (Copenhagen)
FINLAND:	L. Simons (Helsinki)
FRANCE:	A. Berthelot (Saclay), S. Gorodetzky (Strasbourg)
GERMANY (DEM. REP.):	G. Hertz (Leipzig)
GERMANY (FED. REP.):	W. Gentner (Freiburg i. B.), J. H. D. Jensen (Heidelberg)
GREAT BRITAIN:	S. Devons (Manchester), T. H. R. Skyrme (Harwell)
HUNGARY:	L. Janossy (Budapest)
INDIA:	H. Bhabha (Bombay), R. Ramanna (Trombay)
IRISH REPUBLIC:	J. McConnell (Maynooth)
ISRAEL:	G. Racah (Jerusalem)
ITALY:	E. Amaldi (Rome)
JAPAN:	S. Kikuchi (Tokyo), S. Tomonaga (Tokyo)
MEXICO:	M. Moshinsky (Mexico)
NETHERLANDS:	H. Brinkman (Groningen), S. R. de Groot (Leiden)
NORWAY:	E. Hylleraas (Oslo), A. Lundby (Oslo), H. Wergeland (Trondheim)
POLAND:	L. Infeld (Warsaw)
PORTUGAL:	J. M. Araújo (Porto), J. R. de Almeida Santos (Coimbra)
SOUTH AMERICA:	G. Beck (Saõ Paulo), J. Leite Lopes (Rio de Janeiro)
SPAIN:	J. M. Otero (Madrid), C. Sanchez del Rio (Madrid)
SWEDEN:	O. Klein (Stockholm), K. Siegbahn (Uppsala), I. Waller (Uppsala)
SWITZERLAND:	P. Huber (Basel), P. Scherrer (Zürich)
U.A.R. & ARAB COUNTRIES:	F. El Bedewi (Alexandria), M. G. Nooh (Cairo)
U.S.A.	H. H. Barschall (Madison, Wisconsin), V. Weisskopf (Cambridge, Mass.)
U.S.S.R.:	M. A. Markov (Moscow), I. S. Shapiro (Moscow), D V. Skobeltzyn (Moscow)
YUGOSLAVIA:	I. Supek (Zagreb)

NUCLEAR PHYSICS

JOURNAL DEVOTED TO THE EXPERIMENTAL AND THEORETICAL STUDY OF THE FUNDAMENTAL CONSTITUENTS OF MATTER AND THEIR INTERACTIONS

EDITOR: L. ROSENFELD · COPENHAGEN

VOLUME XVIII

AUGUST 1960—SEPTEMBER 1960

NORTH-HOLLAND PUBLISHING COMPANY-AMSTERDAM

PRINTED IN THE NETHERLANDS

2.F

Nuclear Physics **18** (1960) 1—13; © *North-Holland Publishing Co., Amsterdam*

Not to be reproduced by photoprint or microfilm without written permission from the publisher

DIRECT INTERACTION IN THE p—2p REACTION

A. M. GREEN and G. E. BROWN,

Department of Mathematical Physics, University of Birmingham

Received 7 April 1960

Abstract: An analysis of p—2p reactions is carried out and it is pointed out that with good energy resolution in detection of the particles, it would be possible to obtain important information about the energies of shell-model levels. Treatment of the direct-interaction part of the process as a surface reaction is justified. Calculations in the direct-interaction formalism show strong correlations in angle of the two emitted protons.

1. Introduction

Recent experimental studies have shown the p—2p reaction to be a very interesting and useful one. In particular, it can be used as a tool to investigate shell-model levels down in the nucleus [1]) and is, at present, almost our sole source of knowledge about these levels, since other methods usually give information only about the separation energies of the last particles.

In addition, Eisberg [2]) has proposed using this reaction to find out what proportion of the events take place in the nuclear surface. Such events would be expected to exhibit a strong correlation in angle, whereas the statistical events would not. Experiments of Eisberg and Griffiths [3]) have been interpreted as indicating a strong correlation in angle for a large proportion of the proton pairs, and that the events take place in the surface.

A theoretical analysis of these experiments [4]) assumes the momenta of the struck proton to have a distribution up to a maximum momentum k_F; the corresponding Fermi energy E_F is found to be 1—2 MeV which seems unreasonably small. There is no doubt that the direct interaction part of this process takes place in the nuclear surface, because protons from any events occurring within the nucleus will almost certainly be absorbed into compound states before getting out [5]). However, replacement of the nuclear surface by a Fermi sea drops the most important feature of direct interaction theories, namely, the centre of rotation; without it, angular momenta cannot be defined. Angular momentum considerations are of primary importance in determining the position of the peak in the differential cross section in direct interactions. Furthermore, the momenta k_F obtained by McCarthy *et al.* cannot signify the actual momenta of the nucleons in the surface since with such small momenta, one is precluded by the uncertainty principle from localizing the par-

ticles within a region less than several times the extent of the nuclear surface. We shall return later to a discussion of the results of McCarthy *et al.* and show why they obtain such a small k_F.

Our main interest in giving a theoretical description of the p—2p process is to see if it can be used at energies lower than the 185 MeV employed by Tyrén *et al.* to study shell model levels. If, for example, such studies can be carried out for incident energies of $\approx$ 50 MeV, the problem of determining the energies of the final protons becomes much easier, and there is more hope of extending the method to heavy nuclei where the shell model levels are closer together.

In giving such a description, we wish also to obtain a rough estimate of cross sections and, in this way, predict in which cases one would expect a large amount of direct interaction in the process.

In section 2 we discuss the physical picture behind the process, why one expects it to proceed by direct interaction, and the justification of the use of procedures invented for stripping reactions. In sect. 3 we develop the necessary formalism, and in sect. 4 compare our results with existing experimental data. In sect. 5 we discuss the results and indicate interesting experiments.

2. The Physical Picture

The p—2p reaction would appear to be a very useful tool for investigating the shell-model levels down in the nucleus. Consider the diagram in fig. 1.

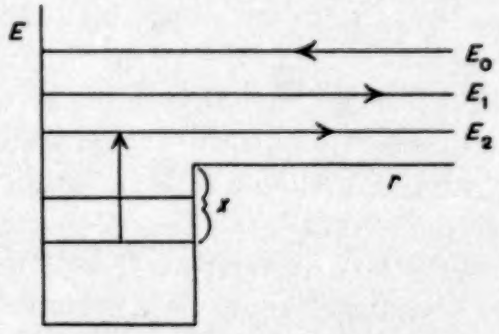

Fig. 1. Schematic picture of the p—2p reaction.

Here E_0 is the energy of the incoming proton and E_1 and E_2 are the energies of the two outgoing protons. The quantity $x = E_0 - E_1 - E_2$ represents the energy needed to eject the second proton from the nucleus. We neglect here the recoil energy of the residual nucleus; if it is not negligible, correction for it can easily be made.

If the nucleus consisted of non-interacting particles in stationary levels in a potential well, the p—2p process would occur only for certain definite values B_1 of x corresponding to the binding energies of the particle in the well. Although this is clearly not the situation, some effects of the underlying single-particle

structure remain in the process [6]). Restricting our considerations to those protons ejected in the direct-interaction process, we would expect giant resonances centred about B_1 to occur, of width $2W$, where W is the absorption for holes at the relevant excitation energy of the residual nucleus. In other words, the hole excitation formed in knocking the particle out of the shell-model state has a finite lifetime, decaying into compound states in a time $\approx \hbar/W$. These hole excitations are completely analogous to the single-particle excitations which are observed in low-energy neutron scattering, where they are called giant resonances. The absorption W for holes can be computed as a function of excitation energy [7]) in the same way as that for particles is calculated [8–10]). The calculations referred to have all been carried out for the case of the infinite nucleus, and it is clear here that, aside from the curvature of the Fermi surface, there is complete symmetry between particles and holes. It is well known that the value of W corresponding to neutron giant resonances at zero bombarding energy is $\approx$ 1—1.5 MeV, and this corresponds to an excitation energy of $\approx$ 8 MeV in a typical nucleus, if we take this to be the separation energy of the last particle. If, therefore, a value of x equal to 16 MeV is needed to eject a proton in the p—2p process, leaving the nucleus at an excitation energy of $\approx$ 8 MeV, the half-width of the hole giant resonance will be $\approx$ 1—1.5 MeV. Thus, for suitable angles, one would expect the cross section to behave as shown in fig. 2, with a

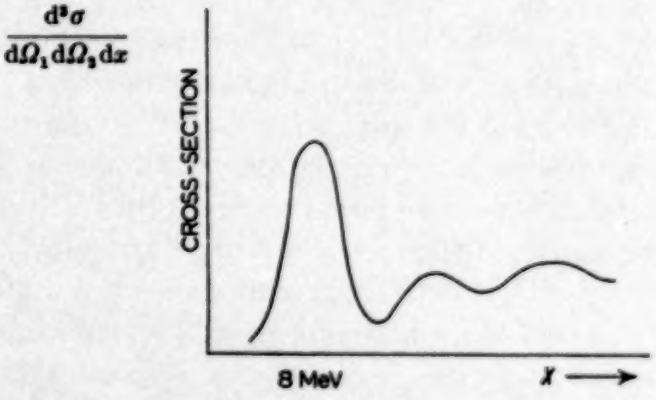

Fig. 2. Typical energy spectrum.

sharp peak corresponding to the ejection of protons filling the last shell-model level, occurring at $x = 8$ MeV, and then further peaks, corresponding to the lower shell-model levels, which become broader with increasing x. Such peaks were, incidentally, not observed in the Minnesota experiments; however, their energy resolution of 15 % would appear to be insufficient when folded in with the width $2W$ of the excitation.

One circumstance makes the observation of hole excitations more favourable

than that of particle excitations: namely, the former have no escape width, whereas at positive bombarding energies the latter have an escape width Γ, so that the total width of the excitation is $2W+\Gamma$, and this escape width increases rapidly with increasing energy, so that the particle excitations broaden out very quickly. We shall also see that the differential cross sections in the p—2p process will peak at different angles for different shell-model levels, and thus will help to distinguish the angular momentum of the hole excitation.

In the future we shall carry out the calculations as if the protons were in stationary states in a shell-model well; we must remember that the effect of interactions is simply to give each of these levels a width $2W$ as far as the direct-interaction part of the reaction is concerned.

Since we are mainly interested in using the p—2p process as a tool to observe the hole excitations, our description of the reaction mechanism will be carried out with the purpose of finding optimum angles of observation and to make sure that a measurable number of protons might be expected. Relatively crude calculations should suffice for this.

We consider the entire direct-interaction process to occur in the surface of the nucleus. That this is a reasonable assumption follows from the work of Elton and Gomes [5]) who find, in considering the p—p′ reaction, that only $\approx 10\,\%$ of the protons making collisions inside the nucleus are able to get out. This results partly from their short mean free path inside the nucleus, and also because their absorption is accentuated by an effect, analogous to total internal reflection of light, at the edge of the nucleus. Most of the protons p′ strike the edge of the nucleus at an acute angle, and are reflected several times, since only the wave number perpendicular to the surface is relevant to their transmission probability. These effects are much stronger in the p—2p process, where the initial energy is distributed between two protons, which, even if they strike the edge of the nucleus head on, have little chance of being transmitted. Therefore, one would expect the p—2p process to be much more completely confined to the surface than the p—p′ one, and to be more similar, in this respect, to deuteron stripping reactions. We shall, therefore, employ the cut-off Born approximation as used by Butler [11]). It is, of course, clear that this cut-off procedure is a crude way of taking the distortion of the incident and emergent waves into account, but it works exceedingly well in describing the angular distributions in stripping reactions. It should, however, be remembered that it does not reproduce the absolute values of the cross sections very well.

3. Development

The reaction is described by Butler's direct nuclear reaction formalism, in which differential cross sections are obtained from perturbation theory i.e. by means of the matrix element of the nucleon-nucleon potential between the

initial and final states of the system. This matrix element is of the form

$$M = \int \mathrm{d}\tau \Psi_f^*(\tau) V \Psi_i(\tau), \tag{3.1}$$

where τ denotes all the spatial and spin coordinates needed to specify the system; Ψ_i is the initial state of the system, and so in the case of the (p, 2p) reaction is the product of the wave function of the struck nucleus and that of the incident proton, which is taken to be a plane wave of wave number k_0; Ψ_f is the final state of the system, and in this case, is the product of the wave-function of the residual nucleus and those of the emergent protons, which are also taken to be plane waves of wave numbers k_1 and k_2; V is the interaction between the incident and struck proton. The integration is carried out only over the space outside a sphere of radius R, in line with the use of the cut-off Born approximation.

If the zero-range approximation is made for V, the matrix element M reduces to the form

$$M = V' \int_{r>R} \mathrm{d}^3 r \frac{\mathrm{e}^{-i\mathbf{k}_1\cdot\mathbf{r}}}{\Omega^{\frac{1}{2}}} \frac{\mathrm{e}^{-i\mathbf{k}_2\cdot\mathbf{r}}}{\Omega^{\frac{1}{2}}} \mathrm{e}^{i\mathbf{k}_0\cdot\mathbf{r}} A_l Y_l^m(\theta, \phi) h_l^{(1)}(ikr), \tag{3.2}$$

where $A_l Y_l^m(\theta, \phi) h_l^{(1)}(ikr)$ is the wavefunction of the struck proton ($h_l^{(1)}$ is a spherical Hankel function), V' is given by $V' = \int \mathrm{d}^3 r V(r)$, and Ω is the volume in which the wavefunction of the emergent protons is normalised. The radial limit on $\mathbf{r}$ was justified in sect. 2.

Using the procedure in Butler's article, the value of this integral is found to be

$$M = \frac{V'}{\Omega} A'_l [4\pi(2l+1)]^{\frac{1}{2}} \frac{R^2}{\rho^2 + k^2} W r[j_l(\rho r), h_l^{(1)}(ikr)]_{r=R}, \tag{3.3}$$

where $\boldsymbol{\varrho} = \mathbf{k}_1 + \mathbf{k}_2 - \mathbf{k}_0$ is the momentum furnished by the nucleus for given $\mathbf{k}_1, \mathbf{k}_2$.

Therefore the differential cross section is

$$\frac{\mathrm{d}\sigma}{\mathrm{d}\Omega_1 \mathrm{d}\Omega_2 \mathrm{d}E_1} = \frac{2\pi}{\hbar} \frac{M_0}{\hbar k_0} \frac{2M_0^3}{(2\pi\hbar)^6} \sqrt{E_1(E - E_1)} (\Omega M)^2, \tag{3.4}$$

where

$$E_1 + E_2 = E_0 - B = E \tag{3.5}$$

(B is the binding energy of the proton that was formerly bound) and M_0 is the mass of a proton.

The above is for spinless particles; but if V is considered to be independent of spin, the only change, when spin is introduced, is that the factor $2l+1$ in M is replaced by $2(l+1)$, when the bound proton was formerly in a $j = l + \frac{1}{2}$ state, and by $2l$ when in a $j = l - \frac{1}{2}$ state.

Instead of using the zero-range approximation for V, the t-matrix [12]) can

be used to give

$$\frac{\mathrm{d}\sigma}{\mathrm{d}\Omega_1 \mathrm{d}\Omega_2 \mathrm{d}E_1} = C\left(\frac{\mathrm{d}\sigma}{\mathrm{d}\Omega_1}\right)_{\mathrm{lab}} \frac{1}{\sqrt{E_1}} \sqrt{E_1(E-E_1)}(\Omega M)^2, \tag{3.6}$$

where C is a constant, $(\mathrm{d}\sigma/\mathrm{d}\Omega_1)_{\mathrm{lab}}$ is the differential cross-section for free p—p scattering in the laboratory system, where a proton of energy E_0 collides with another proton nearly at rest (i.e. $\rho \ll k_0$) and the two emerge with energies E_1 and E_2.

From experiment [13]) the equivalent differential cross section in the centre-of-mass system is isotropic with the value 11 mb/sr² at 40 MeV. In the p—2p experiments we shall need the differential cross section off the energy shell; we assume it to be isotropic in the c.m.s. of the two colliding nucleons, and to have the same value as found in proton-proton collisions at energy E_0. The value obtained for the absolute cross section depends strongly on the latter assumption, since the proton-proton cross section is strongly energy dependent in the region of E_0 we consider. The cross section in the laboratory system is obtained from that in the c.m.s. by the following relation:

$$\left(\frac{\mathrm{d}\sigma}{\mathrm{d}\Omega_1}\right)_{\mathrm{lab}} = \frac{|1-\gamma\cos\theta_1|}{[1+\gamma^2-2\gamma\cos\theta_1]^{\frac{3}{2}}}\left(\frac{\mathrm{d}\sigma}{\mathrm{d}\Omega}\right)_{\mathrm{c.m.}} = F(E_1,\theta_1)\left(\frac{\mathrm{d}\sigma}{\mathrm{d}\Omega}\right)_{\mathrm{c.m.}}, \tag{3.7}$$

where γ is the ratio of the velocity of the centre-of-mass in the laboratory system (which is constant in this case and equals $\frac{1}{2}|\mathbf{k}_0|$) to the velocity of the observed particle in the laboratory system, i.e. $|\mathbf{k}_1|$; θ_1 is the angle, in the laboratory, through which the particle is scattered; θ is the angle in the centre-of-mass system, the two being connected by

$$\tan\theta = \frac{\sin\theta_1}{\cos\theta_1-\gamma}. \tag{3.8}$$

4. Comparison with Experimental Data

The only experimental data existing at these energies are those of Griffiths and Eisberg, which are for 40 MeV protons incident on Ni^{58} and Cu. One coincidence counter was fixed at 25° to the incident direction and the other at a variable angle θ_1, as shown in fig. 3. In the data that we use, all coincidences with E_1 and E_2 greater than 10 MeV were registered. We shall calculate quantities for this case, and also for a theoretically simpler case, in which we hope experiments will be carried out in the future. The cross section is considered to be the sum of the contributions from the top four proton shell model levels, namely the $1F_{\frac{7}{2}}$, $1D_{\frac{3}{2}}$, $2S_{\frac{1}{2}}$ and $1D_{\frac{5}{2}}$. By interpolation from the article by Ross, Mark and Lawson [14]), who have calculated energy levels in a velocity-dependent potential, we find that the

binding energies of particles in the above levels are respectively 8 MeV, 11.6 MeV, 13 MeV and 17 MeV. To reproduce these with a square well, we need depths of 39 MeV, 40.8 MeV, 41.5 MeV and 43.5 MeV respectively, for a radius of 5×10^{-13} cm. The value of the cut-off radius is rather empirical, and is usually

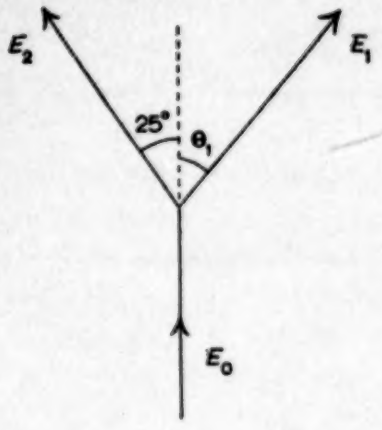

Fig. 3. Experimental set-up used in calculation.

chosen to be 1 or 2×10^{-13} cm larger than the potential-well radius. In this case, it is taken to be 7×10^{-13} cm.

We now carry out calculations in both Born approximation and impulse approximation.

4.1. BORN APPROXIMATION

The differential cross section is first calculated using M from equation (3.2) i.e. using Born approximation together with the zero-range approximation for the potential. We take $V(r) = V_0 \exp(-r/b)/(r/b)$, where $V_0 = 50$ MeV and $b = 1.2\times10^{-13}$ cm to calculate V'.

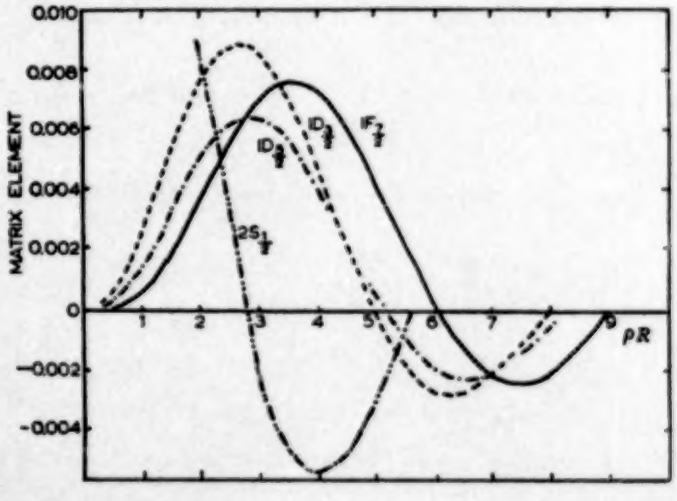

Fig. 4. Matrix elements for the top four filled shell-model levels in Ni^{58}.

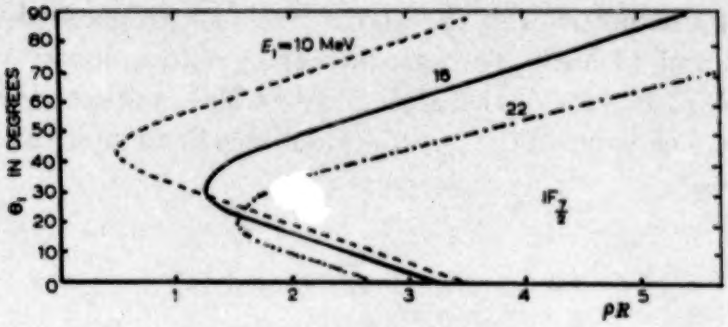

Fig. 5. θ_1 as a function of ρR for the $1F_{\frac{7}{2}}$ level.

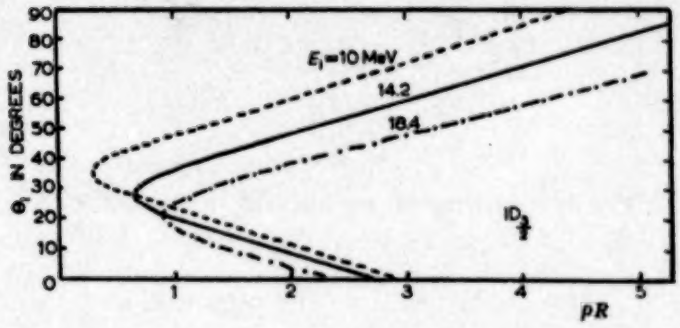

Fig. 6. θ_1 as a function of ρR for the $1D_{\frac{3}{2}}$ level.

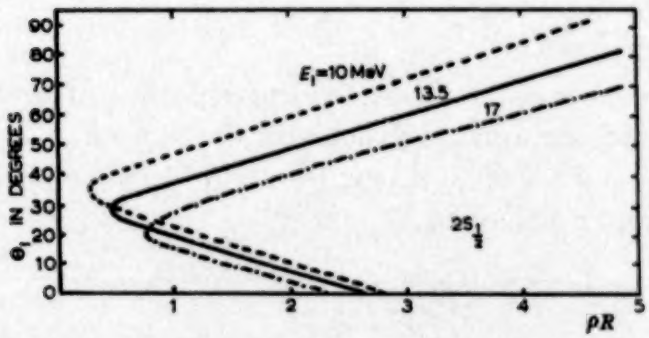

Fig. 7. θ_1 as a function of ρR for the $2S_{\frac{1}{2}}$ level.

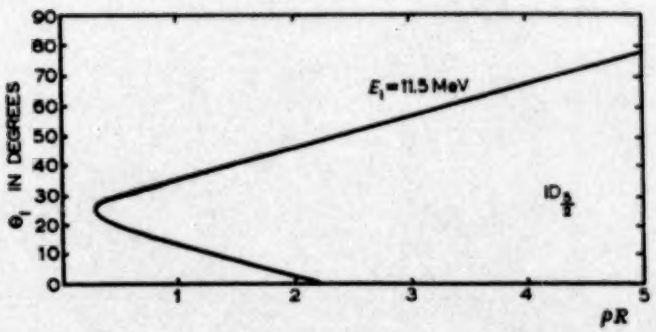

Fig. 8. θ_1 as a function of ρR for the $1D_{\frac{3}{2}}$ level.

The differential cross section given by equation (3.4) (modified for spin) is dependent on the angle θ_1, through the quantity ρ as shown in figs. 4—8. In most (p, 2p) experiments at this energy, owing to the scarcity of events, the differential cross section in integrated over energies. This is the procedure used in subsection 4.2, where the contributions to the cross section from the four energy levels are integrated over energy ranges, which ensure E_1 and E_2 both greater than 10 MeV. e.g. the $1F_{\frac{7}{2}}$ contribution is integrated from $E_1 = 10$ MeV to 22 MeV.

However, we first illustrate the results by a theoretically simpler case, where only particles in the $1F_{\frac{7}{2}}$ level are involved i.e. when only coincidences with $E_1 = E_2 = 16$ MeV are recorded, giving fig. 9. This illustrates the strong correlation one would expect to find in experiments with good energy resolution.

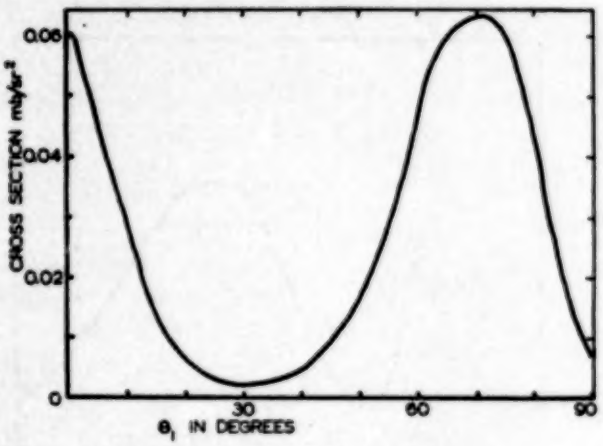

Fig. 9. Angular correlation in the idealized case of $E_1 = E_2 = 16$ MeV.

4.2. IMPULSE APPROXIMATION

We now go over to the impulse approximation by replacing the potential V by the t-matrix. This modification is important, because the t-matrix depends markedly on angle in the laboratory system, even though the proton-proton differential cross section is isotropic in the centre-of-mass system.

Using equations (3.6) and (3.7), the replacement of V is carried out by multiplying each differential cross section $d\sigma/d\Omega_1 d\Omega_2 dE_1$ of the method described in subsection 4.1 by the appropriate factor

$$C\left(\frac{d\sigma}{d\Omega}\right)_{c.m.} \frac{F(E_1, \theta_1)}{\sqrt{E_1}} \Big/ \frac{2\pi}{\hbar} \frac{M_0}{\hbar k_0} \frac{2M_0^3}{(2\pi\hbar)^6},$$

i.e. by $C' F(E_1, \theta_1)/\sqrt{E_1}$ where C' is a constant, and then integrating over energies as before. The quantity $F(E_1, \theta_1)$ is plotted in fig. 10. Angles $\theta_1 < 20°$ are not considered since F becomes very large in this region. In addition there are no experimental data for such angles. We still limit the integration over

energies so that E_1 and $E_2 \geqq 10$ MeV. since further modification is necessary to include protons of lower energy.

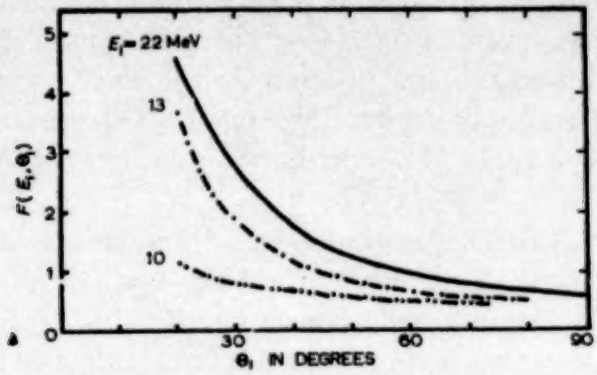

Fig. 10. $F(E_1, \theta_1)$ as a function of θ_1 for various values of E_1.

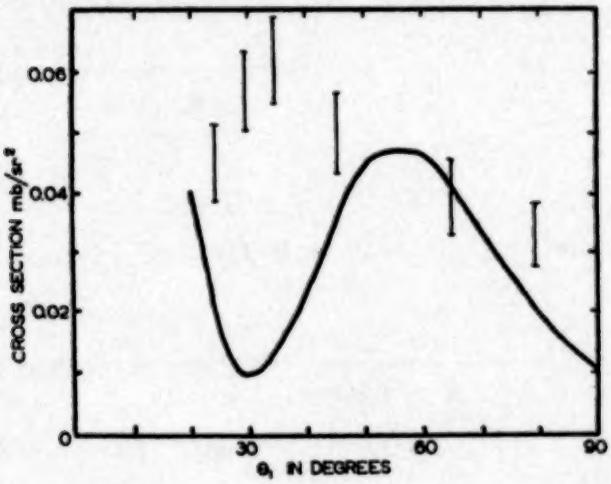

Fig. 11. Angular correlation, when protons from the top two shell model levels contribute.

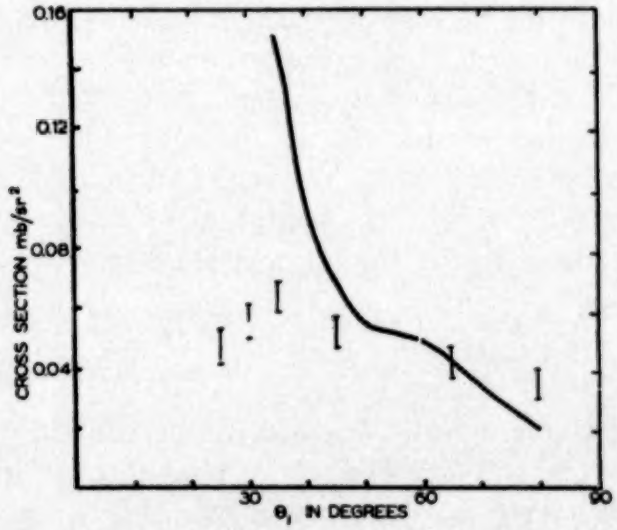

Fig. 12. Angular correlation, when protons from the four shell model levels contribute.

If we assume that only the top two proton levels, namely $1F_{\frac{7}{2}}$ and $1D_{\frac{3}{2}}$, contribute to the total differential cross section, we get fig. 11. The $1D_{\frac{3}{2}}$ level contributes only little, so that the main contribution comes from the $1F_{\frac{7}{2}}$ level. When all four levels contribute we get fig. 12. The relative Minnesota data are also plotted.

5. Conclusions and Discussion

It should be noted, first of all, that the agreement between theoretical calculations and the Minnesota experimental data, as shown in figs. 11 and 12, is not very good. A number of reasons might be adduced for this.

The rise in our curve at small angles in fig. 12, which is not observed in the experimental results, is due to the overwhelming contribution here from the $2S_{\frac{1}{2}}$ protons. However, the cut-off theory may give the ratio of $2S_{\frac{1}{2}}$ to $1F_{\frac{7}{2}}$ contributions badly; in the case of deuteron stripping a more realistic treatment of the distortion by Tobocman and Kalos [15]) gave a somewhat different ratio of S to P and S to D contribution than the cut off calculation, although the P to D ratio is given well by the cut off calculations.

Even if our calculation gives absolute values only roughly, a number of interesting qualitative features are shown.

Firstly, in the region of minimum momentum transfer ρ to the nucleus the F and D contributions are minimal (see figs. 5 and 6 and fig. 9). This is because the $j_l(\rho R)$ in eq. (3.3) goes to zero as $\rho \to 0$ for non-zero l; this illustrates the importance of angular momentum arguments of the type emphasized by Butler, Austern and Pearson [16]). Since the nucleus loses angular momentum l in the process, $l = |\boldsymbol{\varrho} \wedge \mathbf{R}|$, where $\mathbf{R}$ is the radius vector of the region in which the process takes place, in so far as this region can be localized. For $\rho = 0$ and non-zero l, this approximate equality cannot be satisfied.

In the neighbourhood of $\rho = 0$, the contribution from $l = 0$ is, however, large; the maximum of $j_0(\rho R)$, which is $j_0 = 1$, occurs for $\rho = 0$, and this is, in fact, larger than the maxima of Bessel functions of non-zero order (e.g., the maximum value of $j_3(\rho R)$ is 0.24 and occurs for $\rho R = 4.5$; in general, $j_l(\rho R)$ is maximum for ρR slightly greater than l). Hence, in the region of zero momentum transfer to the nucleus, contributions from S states predominate.

The latter qualitative point probably holds at higher energies, in the 100—200 MeV region, where the strong absorption forces the contributions to come mainly from the surface region. It is tempting to interpret the large peak in the Uppsala data for Ca as coming from the $2S_{\frac{1}{2}}$ protons, bound by about 14 MeV (their counters were set so that they selected small values of ρ). This binding energy would fit in well with our estimate of 13 MeV for the binding energy of the $2S_{\frac{1}{2}}$ proton in Ni. Presumably contributions from the D particles, which should lie on each side of the $2S_{\frac{1}{2}}$ peak, are obscured by the large

magnitude of the latter. Although the probability of $2S_{\frac{1}{2}}$ particles being in the surface of the nucleus is relatively small compared with that of particles of high angular momentum, they are strongly favoured in processes requiring very small momentum transfers ρ by the above angular-momentum rule.

The observation of any angular correlation in the Minnesota experiments depended on the bias of the counters being such that only particles with E_1 and E_2 greater than 10 MeV were detected, so as to cut out most of the statistical protons. We can see this by making a rough estimate of the contribution from the latter. In Ni the binding energy of neutrons exceeds that of protons by about the Coulomb barrier for the latter. Consequently, let us take the cross section for statistical p—2p processes to be about $\frac{1}{2}$ of geometrical, or ≈ 400 mb. If this is assumed to be isotropic, then

$$\frac{d\sigma_{pp}^{stat}}{d\Omega_1 d\Omega_2} \approx \frac{400}{(4\pi)^2} \text{mb/sr}^2$$

or about 3 mb/sr^2. This is much larger than the cross sections for direct interaction computed here. However, the statistical distribution will peak for E_1+E_2 of the order of twice the Coulomb barrier, so that for $E_1+E_2 \geqq 20$ MeV the contribution from statistical protons will be down by a factor of about 100 from the value if would have if protons of all energies were accepted. It does not appear, therefore, that direct emission makes a large contribution to the overall process. But it accounts for essentially all of the high-energy end of the spectrum.

We do not believe the description by McCarthy *et al.* [4]) which involves a replacement of the nuclear surface by a Fermi gas, to be a useful one, since in going over to the infinite nucleus, it drops the centre of rotation. It was just the angular momentum considerations that we found to be most important. Within our formalism we can, however, understand why they obtain such a low value for their Fermi energy E_F. In our theory, in which the main features of the angular distribution are determined by the Bessel function $j_l(\rho R)$, the maximum cross section not only occurs for $\rho R \approx l$, but the width of the maximum is given by $\delta\rho R \approx 1$, i.e., by a change in the argument of the Bessel function of about one unit. If one were to fit the experimental data by assuming the second proton to be picked up out of a Fermi sea, it is clear that the Fermi momentum k_F would have to be chosen so that $k_F \approx \delta\rho \approx 1/R$, since the vectorial addition of this momentum to the final momenta must then produce the width of the peak in the angular correlation. One would, therefore, obtain a Fermi energy $E_F \approx \hbar^2/2MR^2$, where M is the mass of the proton, and this is approximately equal to 1 MeV. However, we see from the above discussion that k_F does not really have the significance of the Fermi momentum of particles in the surface.

Finally, we hope that the treatment here given will encourage further

experimental work with improved energy resolution. This should be possible now that cyclotrons in this energy range are becoming available. We believe that very interesting information can be obtained from these with respect to the shell-model levels, as illustrated in fig. 2. This will allow one to determine empirically the energy dependence of the shell-model potential for energies below the separation energy, where almost no experimental information is available.

One of us (A. M. G.) is grateful to the Department of Scientific and Industrial Research for the award of a maintenance grant.

References

1) H. Tyrén, P. Hillman and Th. A. J. Maris, Nuclear Physics **7** (1958) 10
2) R. M. Eisberg, UCRL-2240 (1953)
3) R. J. Griffiths and R. N. Eisberg, Nuclear Physics **12** (1959) 225
4) I. E. McCarthy, E. V. Jezak and A. J. Kromminga, Nuclear Physics **12** (1959) 274
5) L. R. B. Elton and L. C. Gomes, Phys. Rev. **105** (1957) 1027
6) G. E. Brown, Rev. Mod. Phys. **31** (1959) 893
7) E. P. Pendlebury, private communication
8) M. Cini and S. Fubini, Nuovo Cim. **2** (1955) 75
9) K. A. Brueckner, R. J. Eden and N. C. Francis, Phys. Rev. **100** (1955) 891
10) A. M. Lane and C. F. Wandel, Phys. Rev. **98** (1955) 1524
11) S. T. Butler, Phys. Rev. **106** (1957) 272
12) N. Austern, S. T. Butler and H. McManus, Phys. Rev. **92** (1953) 350
13) L. H. Johnson and D. A. Swenson, Phys. Rev. **111** (1958) 221
14) A. A. Ross, R. D. Lawson and H. Mark, Phys. Rev. **104** (1956) 408
15) W. Tobocman and M. H. Kalos, Phys. Rev. **97** (1955) 132
16) S. T. Butler, N. Austern and C. Pearson, Phys. Rev. **112** (1958) 1227

7.C

Nuclear Physics **18** (1960) 14—22; © *North-Holland Publishing Co., Amsterdam*

Not to be reproduced by photoprint or microfilm without written permission from the publisher

PION-NUCLEON ATTRACTION AT SHORT DISTANCES

S. DONIACH and E. YAMADA †

Department of Theoretical Physics, University of Liverpool

Received 10 March 1960

Abstract: It is suggested that a theory which treats the π-meson as a strongly bound nucleon-antinucleon state could provide an explanation for the observed isobaric-spin dependence of the meson-nucleon s-wave scattering length. The consistency of this proposal is tested using a simple model.

1. Discussion of a Model and Conclusions

The observed attraction in the s-wave, $T = \frac{1}{2}$, pion-nucleon scattering phase shift has so far proved rather hard to reconcile with the usual one or two pion approximations of the Yukawa type meson theory (Edwards and Matthews [1])). In this paper we propose a qualitative explanation of this effect on the basis of a strong coupling model for the nucleon-antinucleon system.

It is supposed that a nucleon and antinucleon interact so strongly at short distances that they form a bound state — the pion. Such an idea was first proposed by Fermi and Yang [2]) and has since been taken up by a number of other people. (See, e.g. the paper by Maki [3]) and references given there). But at this stage the idea does not necessarily go beyond the usual Yukawa theory; the nucleon-antinucleon scattering matrix must certainly contain a pole corresponding to the pion state, independently of any model for their interaction. Our proposal is, however, that the basic nucleon-antinucleon interaction should not be treated as having purely pseudoscalar properties, but must involve various types of exchange of isobaric spin, ordinary spin and parity. This observation has two main consequences: (i) the nucleon-antinucleon system may have bound states other than the isobaric triplet ($T = 1$) pseudoscalar pion state (though they need not necessarily be stable ones); (ii) in addition to the usual Yukawa mechanism for pion-nucleon interaction, which in the present model proceeds via annihilation and creation of nucleon-antinucleon pairs, the basic interaction now provides a further mechanism for pion nucleon interaction which proceeds via the direct interaction of a constituent nucleon or antinucleon in the pion with the external nucleon (fig. 1). It is this direct process which, we propose, may lead to a short range pion-nucleon attraction of the observed type ††.

† On leave of absence from Nagoya University, Nagoya, Japan.

†† We find that S. Ataka [4]) has independently put forward a similar proposal.

This hypothesis appears plausible on order of magnitude grounds on account of the considerable strength required of an interaction which can bind the pion: for this purpose it must have total energy (well depth) of order at least $2M$, where M is the nucleon mass; and if we suppose its range to be about $1/M$ (in units of length), the Born approximation s-wave scattering length for the direct pion-nucleon scattering process will be of order $2\mu 2M(1/M)^3 \approx 0.1\mu^{-1}$, where μ is the pion rest-mass, which is comparable with the observed scattering lengths. However, for matrix elements of the type of fig. 1b) to exist for s-waves, the basic interaction must contain scalar or vector components since no spin or parity is to be exchanged at this vertex. Furthermore the observed scattering is strongly dependent on the relative isobaric spin states of meson and nucleon.

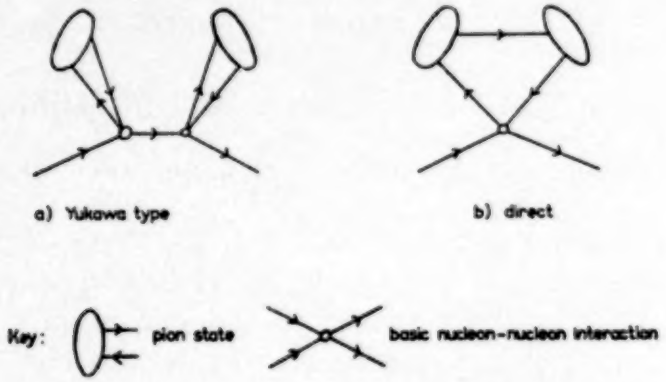

Fig. 1. Pion-nucleon interaction mechanisms.

Can an interaction which leads to strongest binding for a pseudoscalar, $T = 1$, pion satisfy these conditions?

To answer this question some sort of a model is required for the basic interaction. In sect. 2 we consider the general form of an interaction of contact (δ-function) type between identical fermions. On account of the exclusion principle this interaction must contain mixtures of scalar, vector, etc., components, and is now determined by 5 real parameters as opposed to 10 for a non-antisymmetrized interaction. With this degree of freedom still remaining it should not be difficult to satisfy the above conditions, and we proceed to estimate in more detail what range of parameters is likely to lead to the observed type of pion-nucleon attraction, using a Born approximation argument. In sect. 3 we consider the bound-state problem in a two-body covariant approximation which is subject to the usual strong-coupling difficulties. For this equation the pseudoscalar state appears the most easily bound, but the condition that the lowest state should have $T = 1$ imposes a stronger restriction on the form of the basic interaction. It turns out that the latter restriction does not contradict the condition that the direct interaction mechanism can lead to the observed type of pion-nucleon attraction, so that we have shown our main hypothesis to be consistent, within the limitations of our approach.

2. Properties of the Direct Interaction

We start this section by considering the general form of a contact interaction between identical fermions. Consider matrix elements of the form

$$\mathscr{H}_{\text{int}} = f\mathcal{O}_{\alpha\beta\gamma\delta}\bar{\psi}_\alpha(\mathbf{x})\psi_\beta(\mathbf{x})\bar{\psi}_\gamma(\mathbf{x})\psi_\delta(\mathbf{x}), \tag{2.1}$$

where f is a coupling constant and the ψ_α are nucleon wave functions, spinor suffix α, with spinor summation implied. $\mathcal{O}_{\alpha\beta\gamma\delta}$ is a two-particle spinor and isobaric spin operator which can generally be written in the form

$$\mathcal{O} = \tfrac{1}{4}(3+\boldsymbol{\tau}_1\cdot\boldsymbol{\tau}_2)\mathscr{A}+\tfrac{1}{4}(1-\boldsymbol{\tau}_1\cdot\boldsymbol{\tau}_2)\mathscr{S} \tag{2.2}$$

where $\mathscr{A}$ and $\mathscr{S}$ are linear combinations of the Lorentz-invariant γ-matrix products

$$\begin{aligned} &S = I^1I^2, \qquad V = \gamma_\mu{}^1\gamma_\mu{}^2, \\ &T = (\tfrac{1}{2}i[\gamma_\mu,\gamma_\nu])^1(\tfrac{1}{2}i[\gamma_\mu,\gamma_\nu])^2, \qquad A = (i\gamma_5\gamma_\mu)^1(i\gamma_5\gamma_\mu)^2, \qquad P = \gamma_5{}^1\gamma_5{}^2 \end{aligned} \tag{2.3}$$

By the exclusion principle the expression (2.1) must be antisymmetric under interchange of the wave functions ψ or $\bar{\psi}$. Therefore, since $\frac{1}{4}(3+\boldsymbol{\tau}_1\cdot\boldsymbol{\tau}_2)$, $\frac{1}{4}(1-\boldsymbol{\tau}_1\cdot\boldsymbol{\tau}_2)$ are isobaric triplet and singlet projection operators, $\mathscr{A}$ and $\mathscr{S}$ should be purely antisymmetric and symmetric, respectively, against particle interchange. From the Fierz identities one finds five independent linear combinations of the γ products, three antisymmetric, two symmetric, satisfying the above requirements:

$$\begin{aligned} &\mathscr{A}_1 = \tfrac{1}{4}(S+P-T), \qquad \mathscr{A}_2 = \tfrac{1}{4}(V-A), \qquad \mathscr{A}_3 = \tfrac{1}{2}(A-T+2P), \\ &\mathscr{S}_1 = \tfrac{1}{4}(S+P+\tfrac{1}{3}T), \qquad \mathscr{S}_2 = \tfrac{1}{4}(V+A-\tfrac{2}{3}T-4P). \end{aligned} \tag{2.4}$$

Hence a general contact interaction between identical fermions must be of the form given by eqs. (2.1), (2.2), where

$$\mathscr{A} = a_1\mathscr{A}_1+a_2\mathscr{A}_2+a_3\mathscr{A}_3; \quad \mathscr{S} = s_1\mathscr{S}_1+s_2\mathscr{S}_2 \tag{2.5}$$

and a and s are arbitrary real coefficients.

Using this contact model for the basic nucleon-antinucleon interaction we now consider in somewhat more detail the dependence on isobaric spin, etc., of the direct pion-nucleon interaction mechanism proposed in sect. 1. We confine ourselves to a consideration of the sign of the isobaric spin dependent part of the Born approximation direct scattering matrix element (fig. 1b), since it so happens that this can be evaluated without any detailed knowledge of the pion wave function. It is hoped that this calculation will indicate what sort of basic interaction is needed to give the observed type of isobaric spin dependence for the pion-nucleon attraction, since, apart from radiative corrections, which we assume not too important in the low energy limit, this sign would still be

preserved in an exact treatment of the static source s-wave scattering problem, as in the Wentzel pair theory. Of course the usual Yukawa process (fig. 1a) also contributes to the s-wave phase shift. The magnitude of this contribution is rather dependent on the pion-nucleon coupling type, pseudoscalar or pseudovector, which, in the present model is deduced from the details of the pion wave function and the form of the basic interaction. In the pseudovector limit, the s-wave contribution is extremely small, while in the pseudoscalar case the predicted scattering is purely repulsive [1]), so that we do not consider this contribution in further detail.

In the Born approximation the S-matrix element for the direct pion nucleon scattering process reads, in the forward scattering limit,

$$S_{\mathrm{B}} = 2if\mathcal{O}_{\alpha\beta\gamma\delta}\int \mathrm{d}^4x\langle\pi(k)|\bar{\psi}_\alpha(x)\psi_\beta(x)|\pi(k)\rangle\langle q|\bar{\psi}_\gamma(x)\psi_\delta(x)|q\rangle, \tag{2.6}$$

where $|\pi(k)\rangle$ represents a bound pion state, four-momentum k, and $|q\rangle$ a free nucleon state, momentum q. The interaction is as defined above. Since the nucleon number is conserved at the direct interaction vertex, the transfer of spin, isobaric spin and parity from meson to nucleon must have a boson symmetry character. Therefore, by a generalized Furry's theorm (Pais and Jost [5])) the only components of $\mathcal{O}_{\alpha\beta\gamma\delta}$ to contribute to this process are

$$S,\ P,\ A,\ \boldsymbol{\tau}^1\cdot\boldsymbol{\tau}^2V,\ \boldsymbol{\tau}^1\cdot\boldsymbol{\tau}^2T. \tag{2.7}$$

For s-waves, only the forward scattering limit is of interest, so that only the scalar and vector terms in eq. (2.7) will contribute to this process, and of these the scalar part is independent of the isobaric spin, leaving the vector part to carry the isobaric spin dependence:

$$S_{\mathrm{B(v)}} = 2if\tfrac{1}{4}(a_2-s_2)\int \mathrm{d}^4x\langle\pi(k)|\bar{\psi}(x)\boldsymbol{\tau}\gamma_\mu|\pi(k)\rangle\cdot\langle q(\bar{\psi})(x)\boldsymbol{\tau}\gamma_\mu\psi(x)|q\rangle. \tag{2.8}$$

The form of the isobaric spin dependence of (2.8) follows from invariance in isobaric spin space: since $|\pi(k)\rangle$ is a $T=1$ state, $\langle\pi|\boldsymbol{\tau}|\pi\rangle$ must be proportional to matrix elements of the isobaric spin 1 vector operator $\boldsymbol{\omega}$. This can conveniently be represented by introducing an effective pion field $\boldsymbol{\phi}_\alpha(\mathbf{x})$, in terms of which (2.8) is represented as a first order S-matrix element of the effective symmetrized interaction

$$\mathcal{H}_{\mathrm{eff}} = F\boldsymbol{\omega}_{\alpha\beta}\left[\boldsymbol{\phi}_\alpha(\mathbf{x}),\ \left(\frac{1}{i}\,\partial_\mu\boldsymbol{\phi}_\beta(\mathbf{x})\right)\right]\bar{\psi}(\mathbf{x})\boldsymbol{\tau}\gamma_\mu\psi(\mathbf{x}). \tag{2.9}$$

It remains to determine the relation between the effective coupling constant F and the constants in eq. (2.8). Fortunately the magnitude of the matrix element (2.8) can be directly determined from current conservation since for normalized pion states

$$\langle\pi|i\int \mathrm{d}\sigma_\mu(\bar{\psi}\tfrac{1}{2}\tau_3\gamma_\mu\psi)|\pi\rangle = 1. \tag{2.10}$$

Thus, the required relation is

$$\tfrac{1}{2}F = 2\mu^{-1}f_{\frac{1}{2}}(a_2-s_2). \tag{2.11}$$

In the static limit (2.9) gives rise to Born approximation scattering lengths proportional to

$$F\mu^2 \times \begin{cases} +1 & \text{for} \quad T=\frac{3}{2} \\ -2 & \text{for} \quad T=\frac{1}{2} \end{cases} \tag{2.12}$$

in the two-pion nucleon isobaric spin states, Thus, in order to have more attraction in the $T=\frac{1}{2}$ than $T=\frac{3}{2}$ states we require

$$a_2-s_2 > 0. \tag{2.13}$$

Hence, the right sort of isobaric spin dependence can result, provided that the basic interaction has a non-zero vector component whose sign is determined through (2.13).

Before going on to consider the bound state problem, it is of interest to test the effect of the condition (2.13) on the sign of the Born approximation matrix element for nucleon-nucleon scattering. It seems reasonable that this matrix element should be either repulsive or zero, since, on account of its strength, any attractive effects of the interaction would tend to de-saturate the inter-nucleon force. In the static nucleon-nucleon limit one has

$$(S, \ V, \ T, \ A, \ P) \to (I^1I^2, \ I^1I^2, \ \boldsymbol{\sigma}^1\cdot\boldsymbol{\sigma}^2, \ \boldsymbol{\sigma}^1\cdot\boldsymbol{\sigma}^2, \ 0). \tag{2.14}$$

and since the interaction (2.1), (2.2) is antisymmetrised through (2.4) only the $J=0$, $T=1$ and $J=1$, $T=0$ two-nucleon states will yield non zero matrix elements of $\mathscr{H}_{\text{int}}$ in this limit:

$$\langle \mathscr{H}_{\text{int}} \rangle_{\text{NN}} = \begin{cases} a_1+a_2 & \text{for} \quad J=0, \ T=1, \\ s_1+s_2 & \text{for} \quad J=1, \ T=0. \end{cases} \tag{2.15}$$

For (2.15) to be repulsive or zero, one has then the conditions

$$a_1+a_2 \geqq 0; \quad s_1+s_2 \geqq 0,$$

which do not conflict with (2.13).

3. Nucleon-Antinucleon Bound States

In this section we try to answer the question whether an interaction which binds most strongly the pseudoscalar, $T=1$, nucleon-antinucleon state can also have the type of spin and isobaric spin dependence, defined through condition (2.13), which could lead to the observed type of s-wave pion-nucleon attraction. For this purpose we consider the bound state solutions of a covariant

two-body wave equation of the Bethe-Salpeter-Nambu type

$$(\gamma_\mu^1 \partial_\mu^1 + M)(\gamma_\mu^{T\,2} \partial_\mu^2 - M)\Psi(x_1, x_2) = -i \int \mathrm{d}x_3 \mathrm{d}x_4 \mathscr{K}(x_1 x_2 x_3 x_4)\Psi(x_3, x_4) \quad (3.1)$$

where the x carry both four-vector and spinor suffixes and γ^T acts to the right on antinucleon spinors (the suffix T denotes the transpose). This approach becomes rather doubtful under strong-coupling conditions, when the binding energies become of order of the two-particle rest mass, since, as will be seen below, some of the solutions have anomalous properties of the Klein-paradox type. Since it would require a many-pair treatment to overcome these difficulties we can only regard the present work as giving some sort of qualitative indication as to the binding properties of the basic interaction, and do not attempt any quantitative calculation of the bound state properties. To relate the kernel $\mathscr{K}$ of (3.1) to the basic interaction introduced in sect. 2, eq. (3.1) can be derived in a two-body approximation as an equation of motion for the Feynman amplitude

$$\Psi(x_1, x_2) = \langle 0|N(\psi(x_1)\bar{\psi}(x_2))|\pi\rangle. \quad (3.2)$$

For this purpose the wave equation for the ψ is deduced using $(-\mathscr{H}_{\mathrm{int}})$ of (2.1) as a Lagrangian density, and the free field commutation relations are used (Maki [3])). However, the resulting two-body equation diverges on account of the contact character of $\mathscr{H}_{\mathrm{int}}$, and to avoid this we introduce a form factor which, in order to be able to solve explicitly for the bound states, we assume to be of separable form †.

Introducing centre of mass and relative momenta through

$$P = (p_1 + p_2), \quad q = \tfrac{1}{2}(p_1 - p_2), \quad (3.3)$$

the two-body equation (3.1) now takes the form, in momentum representation,

$$[\gamma_\mu^1(\tfrac{1}{2}P_\mu + q_\mu) - iM][\gamma_\mu^{T\,2}(\tfrac{1}{2}P_\mu - q_\mu) + iM]\Psi(P, q) = -2i \int \mathrm{d}q' H(q) H(q') \mathscr{O} \Psi(P, q'), \quad (3.4)$$

where $H(q)$ is a cut-off function, and since $\mathscr{O}$ is fully antisymmetrized through (2.2), (2.5), the spinor product can equally be represented as

$$\mathscr{O}\Psi \equiv \mathscr{O}_{\alpha\beta\gamma\delta}\Psi_{\delta\gamma} = -\mathscr{O}_{\alpha\beta\gamma\delta}\Psi_{\beta\gamma}. \quad (3.5)$$

We now define an external spinor wave function

$$\Lambda_{\alpha\beta}(P) = \int \mathrm{d}q\, H(q)\Psi_{\alpha\beta}(P, q) \quad (3.6)$$

† Some care must be employed in the use of a separable form factor in order to preserve crossing symmetry. In the bound state case, the antisymmetry requirement, $\langle 0|N(\psi\bar{\psi})|\pi\rangle = -\langle 0|N(\bar{\psi}\psi)|\pi\rangle$ is still satisfied in the separable equation (3.4).

which satisfies a matrix eigenvalue equation

$$\Lambda = fX\mathcal{O}\Lambda, \tag{3.7}$$

where X is a spinor operator defined by

$$X = i\int \mathrm{d}q \frac{H^2(q)}{(\gamma_\mu^1(\frac{1}{2}P_\mu+q_\mu)-iM)\,(\gamma_\mu^{T\,2}(\frac{1}{2}P_\mu-q_\mu)+iM)} \tag{3.8}$$

and the q_4 integration is taken around a Feynman contour. Then if $H(q)$ depends only on q^2, X must generally have the covariant form

$$X = -\tfrac{1}{4}(P_\mu\gamma_\mu^1)(P_\nu\gamma_\nu^{T\,2})T(P^2)-\tfrac{1}{4}(\gamma_\mu^1\gamma_\mu^{T\,2})I(P^2) + [\tfrac{1}{4}(P_\mu\gamma_\mu^1)(P_\nu\gamma_\nu^{T\,2})-iMP_\mu(\gamma_\mu^1-\gamma_\mu^{T\,2})+M^2]S(P^2), \tag{3.9}$$

where T, I, S are real functions of P_2 defined through

$$\left.\begin{matrix} S \\ I\delta_{\mu\nu}+\ T\ P_\mu P_\nu/P^2 \end{matrix}\right\} = i\int \mathrm{d}q \frac{H^2(q)\times\begin{cases}1\\ q_\mu q_\nu\end{cases}}{((\frac{1}{2}P+q)^2+M^2)\,((\frac{1}{2}P-q)^2+M^2)}. \tag{3.10}$$

For a particular eigenvalue, (3.7) has the character of a Kemmer equation with non degenerate mass operator since $\frac{1}{2}(\gamma_\mu^1-\gamma_\mu^{T\,2})$ has the properties of the Kemmer-Duffin β_μ as most easily can be seen by a charge conjugation of the equation with respect to the antiparticle 2, when $\frac{1}{2}(\gamma_\mu^1-\gamma_\mu^{T\,2})$ becomes of the well-known form $\frac{1}{2}(\gamma_\mu^1+\gamma_\mu^2)$. However, we find it more convenient to use a direct product representation for the two-particle spinors, based on the set of 16 γ-matrices. This has the advantage of being manifestly Lorentz covariant in the nucleon-antinucleon case: $\langle 0|N(\psi_\alpha\bar{\psi}_\beta)|\pi\rangle$ transforms in the same way as a one-particle spinor operator. With this definition the multiplication rule becomes

$$(\gamma_\mu^1\Lambda)_{\alpha\beta} = (\gamma_\mu)_{\alpha\delta}\Lambda_{\delta\beta}; \qquad (\gamma_\mu^{T\,2}\Lambda)_{\alpha\beta} = \Lambda_{\alpha\delta}(\gamma_\mu)_{\delta\beta} \tag{3.11}$$

and in the rest frame, $P_\mu = (\mathbf{0}, i\mu)$, where μ is the bound state rest mass, (3.7) splits into a set of 2×2 submatrices whose eigenfunctions are linear combinations of the pairs †

$$(1, \gamma_4), \quad (\gamma_i, \gamma_{i4}), \quad (\gamma_{5i}, \gamma_{5i4}), \quad (\gamma_5, \gamma_{54}). \tag{3.12}$$

which transform respectively as scalar, vector, pseudovector and pseudoscalar states.

The interaction operator, $\mathcal{O}_{\alpha\beta\gamma\delta}$, is diagonal in this representation and in

† In a general frame, with centre of mass momentum-vector P_μ, the eigenfunctions (3.12) undergo a transformation of the type

$$(\gamma_5, \gamma_5\gamma_4) \to (\gamma_5, i\gamma_5\gamma_\mu P_\mu/\sqrt{-P^2}).$$

The five coefficients thereby introduced form (in this example) an eigenvector for the five-dimensional submatrix decomposition of the Kemmer equation.

order to get some idea of the eigensolutions of (3.7) it is convenient to consider cases where $\mathcal{O}$ projects onto only one part of a pair in (3.12). Eq. (3.7) then reduces to a linear equation for this particular state, and the eigenvalue μ satisfies the relation

$$\langle X(-\mu^2)\rangle_A^{-1} = f, \tag{3.13}$$

where $\langle X\rangle_A$ is the diagonal element of X of eq. (3.9) with respect to the state in question. $\langle X\rangle^{-1}$ thus plays the role of an internal kinetic energy for the bound state. The dependence of $\langle X\rangle$ on μ is sketched in fig. 2 for a particular analytic form of the cut-off function

$$H(q) = \frac{\lambda^2}{\lambda^2+q^2}. \tag{3.14}$$

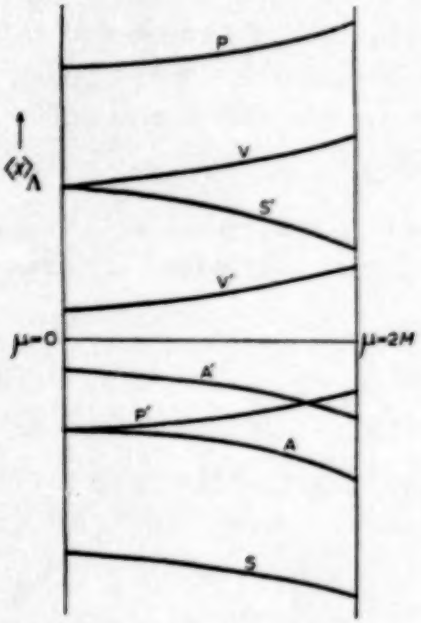

Fig. 2. Sketch of the dependence of diagonal matrix elements $\langle X\rangle_A = \frac{1}{4}\,\mathrm{Tr}\,(\gamma^A X \gamma^A)$ on the rest mass μ. Here,

$$\gamma^A = \begin{cases}1 & (S)\\ \gamma_4 & (S')\end{cases}; \quad \begin{cases}\gamma_i & (V)\\ \gamma_{4i} & (V')\end{cases}; \quad \begin{cases}\gamma_{5i} & (A)\\ \gamma_{5i4} & (A')\end{cases}; \quad \begin{cases}\gamma_5 & (P)\\ \gamma_{54} & (P')\end{cases}.$$

In this simple case X can be evaluated analytically by the Feynman parametrization technique. It may now be seen that many of the solutions have an anomalous character: the internal kinetic energy may increase with decreasing binding energy (increasing rest mass) of the pair, or even become negative. This is the behaviour we attribute to the Klein paradox. But since the state most easily bound, namely that with pseudoscalar wave function component γ_5, has a normal behaviour, it seems reasonable to draw qualitative conclusions from its properties. We thus conclude that it is fairly easy to choose an interaction operator $\mathcal{O}$, which, provided it has non-zero projection onto the γ_5

wave function, will lead to a pseudoscalar state as the most easily bound state, in agreement with the conclusions of Fermi and Yang. However, we must now discuss the much stronger condition that the lowest bound state should have $T = 1$, since no isobaric spin zero pion has been observed with comparable mass.

In the direct product representation the isobaric spin eigenfunctions are represented by the three τ_i for triplet states and by the unit matrix for the singlet state, so that the operator $\boldsymbol{\tau}^1 \cdot \boldsymbol{\tau}^2$ has eigenvalues $+3$, -1, for isobaric spin 0, 1, nucleon-antinucleon states.

Thus the effective nucleon-antinucleon interaction operator becomes

$$\mathcal{O} = \begin{cases} \frac{1}{2}(\mathscr{A}+\mathscr{S}) & \text{for } T = 1, \\ \frac{1}{2}(3\mathscr{A}-\mathscr{S}) & \text{for } T = 0, \end{cases} \tag{3.15}$$

where $\mathscr{A}$, $\mathscr{S}$ are defined in (2.5). A possible reason for reduced binding in the $T = 0$ state could therefore arise out of the change in sign of the symmetric part of the interaction. On evaluation one finds

$$\langle \mathscr{A} \rangle_{\mathrm{P}} = \tfrac{1}{4}\mathrm{Tr}(\gamma_5 \mathscr{A} \gamma_5) = -a_2 - 4a_3; \qquad \langle \mathscr{S} \rangle_{\mathrm{P}} = s_1 - 4s_2. \tag{3.16}$$

Since the mixing in of the γ_{54} component in (3.9) is proportional to (μ/M) we neglect this for the $T = 1$ state and find as a condition for binding to be possible

$$\langle \mathscr{A} \rangle_{\mathrm{P}} + \langle \mathscr{S} \rangle_{\mathrm{P}} > 0. \tag{3.17}$$

A similar approximation for the $T = 0$ solution suggests a condition

$$3\langle \mathscr{A} \rangle_{\mathrm{P}} - \langle \mathscr{S} \rangle_{\mathrm{P}} < \langle \mathscr{A} \rangle_{\mathrm{P}} + \langle \mathscr{S} \rangle_{\mathrm{P}} \tag{3.18}$$

for the $T = 0$ coupling to be weaker than that in the $T = 1$ state. Combining these results in one condition, using (3.16), we have

$$s_1 - 4s_2 > |a_2 + 4a_3| \geqq 0. \tag{3.19}$$

Thus it is possible, by suitable choice of parameters, e.g. $s_2 < 0$ together with $|a_2| < |s_2|$ etc., to satisfy both condition (3.19) for $T = 1$ lowest state, and (2.13) for $T = \frac{1}{2}$ pion-nucleon attraction. We therefore conclude that, within the limitations of the model, these two conditions are not in direct contradiction with each other.

E. Yamada wishes to thank Professor Fröhlich for his hospitality at the Department of Theoretical Physics.

References

1) S. F. Edwards and P. T. Matthews, Phil. Mag. **42** (1957) 1
2) E. Fermi and C. N. Yang, Phys. Rev. **76** (1949) 1739
3) Z. Maki, Prog. Theor. Phys. **16** (1956) 667
4) Y. Ataka, Prog. Theor. Phys. **22** (1959) 321
5) A. Pais and R. Jost, Phys. Rev. **82** (1952) 840

1.D.3

Nuclear Physics **18** (1960) 23—39; © *North-Holland Publishing Co., Amsterdam*

Not to be reproduced by photoprint or microfilm without written permission from the publisher

LOW LYING LEVELS OF Li^7 AND Be^8 IN THE CLUSTER MODEL

L. D. PEARLSTEIN, Y. C. TANG and K. WILDERMUTH

Florida State University, Tallahassee, Florida †

Received 2 March 1960

Abstract: A study of the first few levels of Li^7 and Be^8 has been conducted. To calculate the appropriate energies, a variational procedure was adopted in which some of the long-range nuclear correlations were incorporated in the wave function wherein they appear as favoured cluster configurations, i.e. alpha, triton groups. Agreement with experiment was obtained for the three rotational levels of Be^8 and the two rotational levels of Li^7. For the first change of parity level in the latter nucleus, however, arguments are presented indicating that the inclusion of a deuteron substructure would reproduce the properties of this level.

1. Introduction

The Cluster Model [1]) of the atomic nuclei has been fairly successful in explaining qualitatively many features of nuclear phenomena in the low-energy region. For the description of the nuclear bound and virtual states, it has been shown [1, 2]) that this model leads quite naturally to the prediction of correct level classifications, and for scattering and reaction phenomena, the survey of reduced level width [3]) has also supported this method. Briefly, this model is characterized by the fact that it takes into consideration some of the relatively long range correlations in nuclei in a consistent manner. Thus, besides the energetically favoured closed shell structures, there must also exist in nuclei other energetically favoured substructures, such as alpha-clusters and triton-clusters. In describing the behaviour of nuclei in the low-energy region, it is therefore essential to include these long range correlations in the wave functions which describe the system. (In many respects, this method resembles the method of resonating group structures devised by Wheeler [4]).)

In this investigation, we calculate quantitatively the energies of the ground states and the first few excited states of Li^7 and Be^8. For the binding energy of the ground state of Be^8, the calculation is not completely new since it has already been carried out in an analogous fashion by Edwards [5]) and Biel [6]). These authors, however, came to contradictory conclusions, thus indicating a need for further work ††. For all the levels of nuclei considered, quantitative

† This work is partially supported by the Air Force Office of Scientific Research, Contract AF 49(638)-427, and the National Science Foundation.

†† *Editor's Note.* For a careful and detailed discussion of the interaction between α-particles, see A. Herzenberg, Nucl. Phys. **3** (1957) 1; A. Herzenberg and A. S. Roberts, Nucl. Phys. **3** (1957) 314.

estimates may also be inferred from the intermediate coupling picture of the shell model [7]). We believe, however, that our method is not as limited as the latter model in two respects. First, the level structure is better understood from the point of view of the cluster model, and second, we need no adjustable parameters once a realistic force, which explains low-energy two-nucleon behaviour, is included.

In section 2, we describe the method of calculation to be followed in this investigation. The case of Be^8 is considered in section 3 and Li^7 in section 4. Finally in section 5, we conclude with a review of the results and discuss the various approximations which have been made.

2. Method of Calculation

The total energies of the various states of the system are obtained by the usual variational calculations. We minimize the expression

$$E = \frac{\int \psi^* H \psi \mathrm{d}\tau}{\int \psi^* \psi \mathrm{d}\tau} \tag{1}$$

with respect to the parameters in the variational wave function ψ. In eq. (1), H is the Hamiltonian operator and has the form

$$H = -\frac{\hbar^2}{2M} \sum_{\text{all particles}} \nabla_i^2 + \sum_{\text{all pairs}} V_{ij}, \tag{2}$$

where V_{ij} is the nuclear two-body potential. In accordance with the basic requirements of the cluster model [1]), ψ is chosen to be the anti-symmetrized product of two factors, one of which representing the internal structures of the clusters and the other describing the relative motion among the clusters.

To facilitate computations, we make the further assumption that the mutual interaction of the clusters (interaction energy) does not depend in first approximation upon the hard-core part of the nuclear two-body force †. Thus we calculate this part of the energy by using a simple Serber force with no saturating properties (without hard core) which, however, is consistent with all low energy two-nucleon phenomena. This potential is of the form [8])

$$V_{ij} = -V_0 \mathrm{e}^{-\kappa r_{ij}^2} \{W[1 - \tfrac{1}{4}(1+\boldsymbol{\sigma}_i \cdot \boldsymbol{\sigma}_j)(1+\boldsymbol{\tau}_i \cdot \boldsymbol{\tau}_j)] + b[\tfrac{1}{2}(1+\boldsymbol{\sigma}_i \cdot \boldsymbol{\sigma}_j) - \tfrac{1}{2}(1+\boldsymbol{\tau}_i \cdot \boldsymbol{\tau}_j)]\}, \tag{3}$$

with $V_0 = 68.6$ MeV, $\kappa = 4.16 \times 10^{25}$ cm^{-2}, $W = 0.41$ and $b = 0.09$. As to the internal energies of the clusters, the hard-core part of the two-body potential certainly plays a dominant role; consequently it is entirely incorrect to calculate them with a potential of the form (3). Fortunately, Mang and Wild [9]) have

† This assumption is expected to be valid as long as the separation of the clusters is considerably greater than the hard-core radius; a condition which is very likely fulfilled for light nuclei. At present the only justification is the relative success of our calculation.

recently calculated with rather realistic nuclear forces the binding energies of the alpha-cluster and triton-cluster as a function of their respective width parameters. They obtained values for the binding energies of free alpha particle and triton in good agreement with the experimentally measured values. Therefore, it seems reasonable to adopt their values in our calculation.

To summarize, we calculate the interaction energies by a Serber force of the form (3) and adopt Mang and Wild's values for the internal energies of the clusters, and then proceed to minimize the total energy of the system with respect to the parameters in the trial wave functions. The Coulomb energy is not included in the variational procedure, since it is expected to be a slowly varying function of the appropriate parameters and, moreover, it is only a small correction. We merely estimate it in a rough manner and incorporate it in our final results.

3. Ground States and Excited States of Be^8

It has been shown in ref. [1]) that the wave functions of the ground state and the first two excited states of Be^8 are described approximately by

$$\psi = \mathrm{A}\{\psi_0(\alpha_1)\psi_0(\alpha_2)\chi(\mathbf{R}_{\alpha_1}-\mathbf{R}_{\alpha_2})\}, \tag{4}$$

where $\psi_0(\alpha_1)$ and $\psi_0(\alpha_2)$ are wave functions of the alpha-clusters in the ground state, and $\chi(\mathbf{R}_{\alpha_1}-\mathbf{R}_{\alpha_2})$ describes the relative motion of these clusters. The operator A denotes the complete antisymmetrization of the wave function (4) with respect to the exchange of any pair of nucleons.

For the internal wave functions of the two alpha-clusters, we write, for their space part

$$\psi_0(\alpha_1)\psi_0(\alpha_2) = \mathrm{e}^{-\frac{1}{2}\alpha\sum_{i=1}^{4}\bar{\mathbf{r}}_i^2-\frac{1}{2}\alpha\sum_{i=5}^{8}\bar{\mathbf{r}}_i^2}, \tag{5}$$

with

$$\begin{aligned} \bar{\mathbf{r}}_2 &= \mathbf{r}_2-\mathbf{R}_1, \quad \bar{\mathbf{r}}_6 = \mathbf{r}_2-\mathbf{R}_2, \\ \bar{\mathbf{r}}_3 &= \mathbf{r}_3-\mathbf{R}_1, \quad \bar{\mathbf{r}}_7 = \mathbf{r}_2-\mathbf{R}_2, \\ \bar{\mathbf{r}}_4 &= \mathbf{r}_4-\mathbf{R}_1, \quad \bar{\mathbf{r}}_8 = \mathbf{r}_8-\mathbf{R}_2, \end{aligned} \tag{6}$$

and

$$\mathbf{R}_1 = \tfrac{1}{4}(\mathbf{r}_1+\mathbf{r}_2+\mathbf{r}_3+\mathbf{r}_4), \quad \mathbf{R}_2 = \tfrac{1}{4}(\mathbf{r}_5+\mathbf{r}_6+\mathbf{r}_7+\mathbf{r}_8).$$

For that part of the wave function which describes the relative motion, we use

$$\chi(\mathbf{R}_{\alpha_1}-\mathbf{R}_{\alpha_2}) = R^n\mathrm{e}^{-\beta R^2}Y_{lm}(\Omega), \tag{7}$$

where $R = |\mathbf{R}_{\alpha_1}-\mathbf{R}_{\alpha_2}|$ and Ω denotes the orientation of the vector $(\mathbf{R}_{\alpha_1}-\mathbf{R}_{\alpha_2})$.

As was pointed out in ref. [1]) it is convenient for computational purposes to write eq. (4) in a parameter representation:

$$\psi = \mathrm{A}\left\{\int g(\mathbf{r}'_1 \ldots \mathbf{r}_8')\delta(\mathbf{r}_1-\mathbf{r}'_1)\ldots\delta(\mathbf{r}_8-\mathbf{r}_8')\mathrm{d}\mathbf{r}'_1\ldots\mathrm{d}\mathbf{r}_8'\right\}, \tag{8}$$

with $\mathbf{r}_1, \ldots, \mathbf{r}_8$ representing the space, spin and isobaric spin coordinates of the eight nucleons. Here, $\delta(\mathbf{r}_1-\mathbf{r}'_1), \ldots, \delta(\mathbf{r}_8-\mathbf{r}'_8)$ are eigenfunctions which state that nucleon 1 has position $\mathbf{r}'_1$, spin $+\frac{1}{2}$ and isobaric spin $+\frac{1}{2}$, nucleon 2 has position $\mathbf{r}'_2$, spin $+\frac{1}{2}$ and isobaric spin $-\frac{1}{2}$, and so on. As for $g(\mathbf{r}'_1 \ldots \mathbf{r}'_8)$, we may easily see from eqs. (4), (5) and (7) that it must be of the form

$$g(\mathbf{r}'_1, \ldots \mathbf{r}'_8) = e^{-\frac{1}{2}\alpha \sum_1^4 \bar{r}_i'^2 - \frac{1}{2}\alpha \sum_5^8 \bar{r}_i'^2} R'^n e^{-\beta R'^2} Y_{lm}(\Omega'). \tag{9}$$

In our calculations, n is equal to 4 and α, β are the variational parameters. We should like to point out here that if $\alpha = \beta$, the function ψ reduces to the usual shell model wave function in an oscillator potential with width parameter α †. In this particular case, it is then necessary, in order to satisfy the Pauli exclusion principle, that $n = 4$. In our calculation, since the wave function ψ is merely a trial function, we really have no a priori reason to assume that n must be equal to 4. In fact, we have used $n = 0$ and 2 and obtained results for the energies of the first two states of Be^8 which are essentially identical to those for $n = 4$ ††. However, due to the fact that the wavefunction goes to zero as α approaches β for $n < 4$, computational difficulties arose. Thus we contend that $n = 4$ is indeed a more desirable choice for our variational procedure. As to the choice of l, it is of course natural to choose, for the three lowest energy states of Be^8 the values 0, 2 and 4. It is important to mention at this point that for $\alpha \neq \beta$, we have effectively included highly excited shell model states.

To proceed, the expectation value of any operator $Q(1, \ldots, 8)$ which depends on the coordinates of the 8 nucleons is written as

$$\begin{aligned} N^2\langle Q\rangle = 2(8!)\int\Big[\int & g(\mathbf{r}''_1 \ldots \mathbf{r}''_8)\{\delta(\mathbf{r}_1-\mathbf{r}''_1) \ldots \delta(\mathbf{r}_8-\mathbf{r}''_8) \\ & -4\delta(\mathbf{r}_1-\mathbf{r}''_1) \ldots \delta(\mathbf{r}_8-\mathbf{r}''_4)\delta(\mathbf{r}_5-\mathbf{r}''_5) \ldots \delta(\mathbf{r}_4-\mathbf{r}''_8) \\ & +3\delta(\mathbf{r}_1-\mathbf{r}''_1) \ldots \delta(\mathbf{r}_7-\mathbf{r}''_3)8(\mathbf{r}_8-\mathbf{r}''_4) \ldots \delta(\mathbf{r}_3-\mathbf{r}''_7)\delta(\mathbf{r}_4-\mathbf{r}''_8)\} \\ & d\mathbf{r}''_1 \ldots d\mathbf{r}''_8 Q(1, \ldots, 8)\int\{g(\mathbf{r}'_1 \ldots \mathbf{r}_8') \\ & \delta(\mathbf{r}_1-\mathbf{r}'_1) \ldots \delta(\mathbf{r}_8-\mathbf{r}'_8)d\mathbf{r}'_1 \ldots d\mathbf{r}'_8\}\Big] d\mathbf{r}_1 \ldots d\mathbf{r}_8, \end{aligned} \tag{10}$$

where N^2 is the normalization factor, and from which the spin and isobaric spin dependence has been removed.

3.1. THE NORMALIZATION; KINETIC AND POTENTIAL INTEGRALS

The normalization factor can be obtained by introducing eq. (9) into eq. (10) and setting Q equal to unity. Integrating over all coordinates of the nucleons

† The width parameter of an oscillator potential is defined as $M\omega/\hbar$, where ω is equal to the frequency of the oscillator potential.

†† This equivalence is attributed to the complete anti-symmetrization of our wave function.

and over all parameter coordinates $\mathbf{r}'_1 \ldots \mathbf{r}'_8$, $\mathbf{r}''_1 \ldots \mathbf{r}''_8$ except the relative parameter coordinates $\mathbf{R}'$ and $\mathbf{R}''$, we finally obtain

$$N^2 = 2(8!)[A_0 - 4A_1 + 3A_2], \tag{11}$$

with the direct term

$$A_0 = 2^6 \frac{\pi^9}{\alpha^9} I(2\beta) \tag{12}$$

and the exchange terms

$$A_1 = 2^{12} \left(\frac{\pi^5}{6\alpha^5}\right)^{\frac{3}{2}} J(\tfrac{5}{3}\alpha+\beta, \tfrac{8}{3}\alpha, \tfrac{5}{3}\alpha+\beta), \tag{13}$$

$$A_2 = 2^9 \left(\frac{\pi^5}{2\alpha^5}\right)^{\frac{3}{2}} J(\alpha+\beta, 0, \alpha+\beta), \tag{14}$$

where

$$I(p) = \int R'^{2n+2} e^{-pR'^2} |Y_{lm}(\Omega')|^2 dR' d\Omega' \tag{15}$$

and

$$J(p, q, s) = \int R''^{n+2} R'^{n+2} e^{-pR''^2 + q\mathbf{R}'' \cdot \mathbf{R}' - sR'^2} Y^*_{lm}(\Omega'') Y_{lm}(\Omega') dR'' dR' d\Omega'' d\Omega'. \tag{16}$$

Similarly, for the expectation value of the kinetic energy, we use the operator

$$T = -\sum_{i=1}^{8} \frac{\hbar^2}{2M} \nabla_i^2 \tag{17}$$

in eq. (10). The result is

$$\langle T \rangle = \frac{\hbar^2}{2M}(2\beta n + 3\beta + 18\alpha) - 2(8!)\frac{\hbar^2}{2M}\frac{1}{N^2}(C_0 - 4C_1 + 3C_2) - 2(8!)\frac{\hbar^2}{2M}\frac{n(n+1) - l(l+1)}{2N^2}(B_0 - 4B_1 + 3B_2), \tag{18}$$

with

$$B_0 = 2^6 \frac{\pi^9}{\alpha^9} K(2\beta), \tag{19}$$

$$B_1 = 2^{12} \left(\frac{\pi^5}{6\alpha^5}\right)^{\frac{3}{2}} L(\tfrac{5}{3}\alpha+\beta, \tfrac{8}{3}\alpha, \tfrac{5}{3}\alpha+\beta), \tag{20}$$

$$B_2 = 2^9 \left(\frac{\pi^5}{2\alpha^5}\right)^{\frac{3}{2}} L(\alpha+\beta, 0, \alpha+\beta), \tag{21}$$

where

$$K(p) = \int R'^{2n} e^{-pR'^2} |Y_{lm}(\Omega')|^2 dR' d\Omega', \tag{22}$$

$$L(p, q, s) = \int R''^{n} R'^{n+2} e^{-pR''^2 + q\mathbf{R}'' \cdot \mathbf{R}' - sR'^2} Y^*_{lm}(\Omega'') Y_{lm}(\Omega') dR'' dR' d\Omega'' d\Omega'. \tag{23}$$

After some tedious integrations we find

$$C_0 = \frac{2\beta n+3\beta+18\alpha}{2} A_0, \tag{24}$$

$$C_1 = \left[\frac{2n+21}{2}\alpha + \Lambda(\tfrac{5}{3}\alpha+\beta, \tfrac{8}{3}\alpha)\right] A_1, \tag{25}$$

$$C_2 = \left[\tfrac{15}{2}\alpha + (n+3)\frac{\alpha^2+\beta^2}{\alpha+\beta}\right] A_2, \tag{26}$$

where

$$\Lambda(p, q) = (2n+3)\frac{\beta(\beta-\alpha)}{p}\left(1-\frac{q^2}{4p^2}\right)^{-1} \times \frac{{}_2F_1\left(-\tfrac{1}{2}(n-l+2); -\tfrac{1}{2}(n-l); -\tfrac{1}{2}(2n+3); 1-\dfrac{q^2}{4p^2}\right)}{{}_2F_1\left(-\tfrac{1}{2}(n-l); -\tfrac{1}{2}(n-l); -\tfrac{1}{2}(2n+1); 1-\dfrac{q^2}{4p^2}\right)}, \tag{27}$$

${}_2F_1$ being a hypergeometric function [10]). To arrive at eq. (27), we have used the fact that in our case, $n-l$ is an even integer greater than or equal to zero.

For the expectation value of the potential energy operator, we note that for a Serber potential of the form (3), the contributions from the Heisenberg and Bartlett forces cancel with each other and hence, need not be considered. Therefore, the final expression for $\langle V\rangle$ is

$$\langle V\rangle = 2(8!)(-WV_0)\left(\frac{\alpha}{2\pi}\right)^{\frac{3}{2}}\frac{1}{N^2} \times \{24P_1+12P_2-48P_3-12P_4+12P_5-96P_6+24P_7-12P_8+96P_9\}, \tag{28}$$

a result previously determined by Biel [6]). In eq. (28), the quantities P_i are independent integrals which are defined by

$$P_1 = 2^6\frac{\pi^9}{\alpha^9}\left(\frac{\pi}{\kappa+\frac{1}{2}\alpha}\right)^{\frac{3}{2}} I(2\beta), \tag{29}$$

$$P_2 = 2^9\left(\frac{\pi^6}{3\alpha^6}\right)^{\frac{3}{2}}\left(\frac{\pi}{\kappa+\frac{2}{3}\alpha}\right)^{\frac{3}{2}} I\left(\frac{2\alpha\kappa}{2\alpha+3\kappa}+2\beta\right), \tag{30}$$

$$P_3 = 2^{12}\left(\frac{\pi^5}{6\alpha^5}\right)^{\frac{3}{2}}\left(\frac{\pi}{\kappa+\frac{1}{2}\alpha}\right)^{\frac{3}{2}} J(\tfrac{5}{3}\alpha+\beta, \tfrac{8}{3}\alpha, \tfrac{5}{3}\alpha+\beta), \tag{31}$$

$$P_4 = 2^9\left(\frac{\pi^5}{\alpha^5}\right)^{\frac{3}{2}}\left(\frac{\pi}{\kappa+\frac{3}{4}\alpha}\right)^{\frac{3}{2}} J\left(\frac{5\alpha+8\kappa}{3\alpha+4\kappa}\alpha+\beta, \frac{8\alpha+8\kappa}{3\alpha+4\kappa}\alpha, \frac{5\alpha+8\kappa}{3\alpha+4\kappa}\alpha+\beta\right), \tag{32}$$

$$P_5 = 2^{12}\left(\frac{\pi^6}{3\alpha^6}\right)^{\frac{3}{2}} J(\tfrac{5}{3}\alpha+\beta+4\kappa, \tfrac{8}{3}\alpha+8\kappa, \tfrac{5}{3}\alpha+\beta+4\kappa), \tag{33}$$

$$P_6 = 2^9\left(\frac{\pi^5}{\alpha^5}\right)^{\frac{1}{2}}\left(\frac{\pi}{\kappa+\frac{3}{4}\alpha}\right)^{\frac{1}{2}} J\left(\frac{5\alpha+8\kappa}{3\alpha+4\kappa}\alpha+\beta, \frac{8\alpha+16\kappa}{3\alpha+4\kappa}\alpha, \frac{5\alpha+12\kappa}{3\alpha+4\kappa}\alpha+\beta\right), \quad (34)$$

$$P_7 = 2^9\left(\frac{\pi^5}{2\alpha^5}\right)^{\frac{1}{2}}\left(\frac{\pi}{\kappa+\frac{1}{2}\alpha}\right)^{\frac{1}{2}} J(\alpha+\beta, 0, \alpha+\beta), \quad (35)$$

$$P_8 = 2^9\left(\frac{\pi^5}{\alpha^5}\right)^{\frac{1}{2}}\left(\frac{\pi}{\kappa+\alpha}\right)^{\frac{1}{2}} J\left(\frac{\alpha+2\kappa}{\alpha+\kappa}\alpha+\beta, \frac{2\kappa}{\alpha+\kappa}\alpha, \frac{\alpha+2\kappa}{\alpha+\kappa}\alpha+\beta\right), \quad (36)$$

$$P_9 = 2^{12}\left(\frac{\pi^5}{6\alpha^5}\right)^{\frac{1}{2}}\left(\frac{\pi}{\kappa+\frac{2}{3}\alpha}\right)^{\frac{1}{2}} J\left(\frac{2\alpha+5\kappa}{2\alpha+3\kappa}\alpha+\beta, 0, \alpha+\beta\right). \quad (37)$$

All the integrals listed are rather elementary and can be readily calculated to give the following results:

$$I(p) = \frac{\sqrt{\pi}}{2^{n+2}}(2n+1)!!p^{-\frac{1}{2}(2n+3)}, \quad (38)$$

$$J(p, q, s) = \frac{\pi^2[(n+l+1)!!]^2}{2^{n+l+2}(2l+1)!!}\frac{q^l}{(ps)^{\frac{1}{2}(n+l+3)}} \times \left(1-\frac{q^2}{4ps}\right)^{-\frac{1}{2}(2n+3)} {}_2F_1\left(\tfrac{1}{2}(-n+l), \tfrac{1}{2}(-n+l); l+\tfrac{3}{2}; \frac{q^2}{4ps}\right), \quad (39)$$

$$J(p, 0, s) = \frac{\pi^2}{2^{n+2}}[(n+1)!!]^2\delta_{l0}(ps)^{-\frac{1}{2}(n+3)}, \quad (40)$$

with similar expressions for $K(p)$, $L(p, q, s)$ and $L(p, 0, s)$. In integrating eq. (16), use is made of the expansion [10])

$$e^{-qR''\cdot R'} = 4\pi\sum_{l,m}(-1)^l\sqrt{\frac{\pi}{2qR''R'}}I_{l+\frac{1}{2}}(qR''R')Y^*_{lm}(\Omega'')Y_{lm}(\Omega'), \quad (41)$$

where $I_{l+\frac{1}{2}}(qR''R')$ are Bessel functions of half integral order of the imaginary argument $iqR''R'$.

3.2. NUMERICAL CALCULATIONS

As mentioned in section 2, we adopt the results of Mang and Wild [9]) for the internal energies of the alpha-clusters. Their results are, however, given in graphical form, which is not very convenient for machine calculations. Thus, we fir their curve with an analytical equation of the form

$$E_\alpha = -28.8+22.6\left(\frac{\alpha-\alpha_0}{\alpha_0}\right)^2 \text{MeV}, \quad (42)$$

with $\alpha_0 = 3.569\times10^{25}$ cm^{-2}. As was noted by Mang and Wild, the rms radius they calculated for a free apha-particle was 1.75×10^{-13} cm rather than

1.61×10^{-13} cm found experimentally [11]). To ensure that our results will not be unduly affected by this larger radius of the free alpha-particle, we have shifted their curve without altering its shape to correspond to the correct alpha-particle radius. Thus, instead of eq. (42), we use

$$E_\alpha = -28.8+22.6\left(\frac{\alpha-\alpha'}{\alpha_0}\right)^2 \text{MeV}, \tag{43}$$

with $\alpha' = 4.34\times10^{25}\,\text{cm}^{-2}$.

Calculations with both eqs. (42) and (43) have been carried out. In both cases, the results for the binding energies of the first three states of Be^8 are generally the same. The difference is only about 1 MeV for the second excited state and even less for the ground state and the first excited state; the level distances are essentially unaffected. Thus, in this paper, we shall only present the results calculated with eq. (43).

For the sake of simplicity, we have redefined our variational parameters as follows:

$$y = \kappa/\alpha, \quad x = \beta/\alpha. \tag{44}$$

The quantity we ultimately determine is E_0, the negative of the separation energy into two free alpha-particles in the absence of the Coulomb interaction, i.e.

$$E_0 = E-2E_\alpha(\text{free}). \tag{45}$$

The final computations have been done on an IBM-650 electronic computer. The results obtained are shown in fig. 1†, in which we plot E_0 as a function of x, with y chosen to give the minimum value of E_0. If we now add the Coulomb energy estimated to be about 1.8 MeV [12]) to E_0 (minimum), a comparison can

TABLE 1

Comparison between the calculated and experimental separation energies for the first three states in Be^8

	Separation energy in MeV	
	Calculated	Experimental
Ground state	+0.5	−0.1
First excited state	−2.8	−3.0
Second excited state	−11.1	−11.8

be made with the experimental separation energy in the various states. This comparison is listed in table 1, in which the experimental values are taken from the recent tabulation of Ajzenberg and Lauritzen [13]).

† The occurrence of a relative minimum in the resonant state in some sense corresponds to the "tunnel effect" since the appropriate clusters must pass through an energetically unfavoured configuration to separate.

The values of the variational parameters x and y which yield E_0 (minimum) are as follows:

$$\begin{aligned} &\text{ground state:} && y = 0.96, \quad x = 0.728, \\ &\text{1st excited state:} && y = 0.96, \quad x = 0.693, \\ &\text{2nd excited state:} && y = 0.99, \quad x = 0.653. \end{aligned} \tag{46}$$

It is seen that for all three states, x is quite different from unity. Thus our wave functions are substantially different from those in an oscillator shell model.

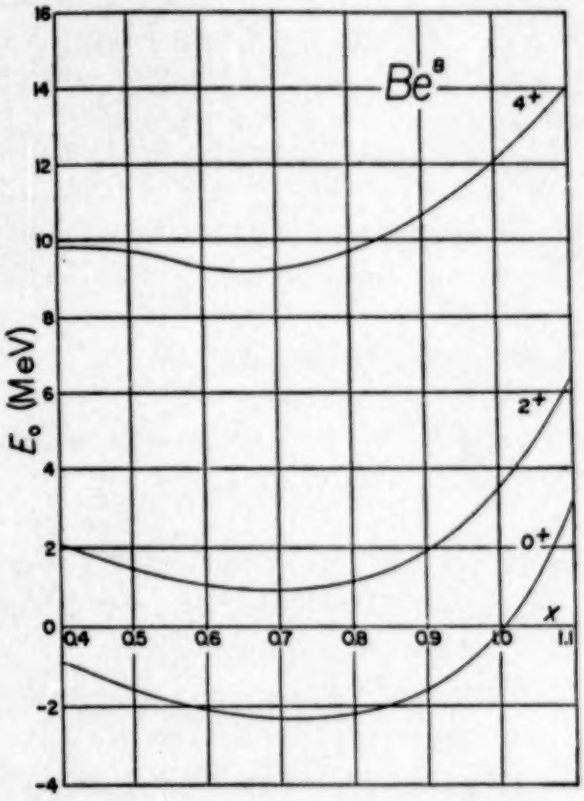

Fig. 1. E_0 as a function of x for the first three levels of Be^8.

We also note that x decreases with the excitation energy, which indicates that for higher excitations, the Be^8 nucleus approaches a dumbbell shape. A similar tendency in the behaviour of y would be expected, since y is directly related to the sizes of the clusters; however, eq. (46) shows a slight contrary behaviour. A detailed examination of the interaction energy as a function of y leads us to believe that this discrepancy can be attributed to our approximate method of calculating this energy wherein we have neglected the hard core. Presumably, the inclusion of this hard core effect would reduce the separation energy in the ground state while leaving the respective separation energies of excited states relatively unaltered. Unfortunately, we must also infer that our procedure would probably give poor results for $A > 12$.

4. Ground States and Excited States of Li^7

For the discussion of the low lying energy levels of Li^7 we shall use an alpha-cluster plus a triton-cluster representation and further make the assumption that both those clusters are not broken up. That is, for the trial wave function, we shall use the form †

$$\psi = A\left\{\int g(\mathbf{r}'_1 \ldots \mathbf{r}'_7)\delta(\mathbf{r}_1-\mathbf{r}'_1)\ldots\delta(\mathbf{r}_7-\mathbf{r}'_7)d\mathbf{r}'_1\ldots d\mathbf{r}'_7\right\}, \tag{47}$$

with

$$g(\mathbf{r}'_1 \ldots \mathbf{r}'_7) = e^{-\frac{1}{2}\alpha\sum_{i=1}^{4}\bar{r}_i'^2-\frac{1}{2}\alpha\sum_{i=5}^{7}\bar{r}_i'^2} R'^n e^{-\frac{3}{7}\beta R'^2} Y_{lm}(\Omega'). \tag{48}$$

It should be pointed out here that only two parameters α and β are present in the trial wave function (47). A priori, we certainly should expect that the alpha cluster and triton cluster have width parameters distinct from each other. Thus, our trial wave function is not expected to yield the optimum values for the binding energies of Li^7; more appropriately, we should certainly use a three-parameter variational wave function. This has not been done, mainly because the computations involved become too complicated. By a crude estimate, we expect that if a more reasonable trial function is used, our calculated values for the total energies of the various states considered will be lowered by around 1.3 MeV.

Again for $\alpha = \beta$ (or $x = 1$), the wave function (47) goes over to the shell model wave function in an oscillator potential of width parameter α. Any deviation of x from unity thus gives a measure of the difference between our wave function and the shell model one.

As in the case of Be^8, Coulomb energy has not been included in the variational procedure; it has again only been incorporated as a perturbation. The spin-orbit force is also left out in the variation. Both these simplifications would certainly inject errors into our calculations; however, we anticipate that the resulting errors will be rather small.

As to the choices of n and l, similar arguments as in section 3 lead to the following selections:

ground state: $n = 3,\ l = 1$

1st excited state: $n = 3,\ l = 3$

2nd excited state: $n = 4,\ l = 0.$

In analogy to eq. (10) we may write down the similar relation for Li^7:

† Similar notations will be used for corresponding quantities in sections 3 and 4. Different notations will be employed only if confusion may possibly arise.

$$
\begin{aligned}
N^2\langle Q\rangle = 7!\int\Big[\int g(\mathbf{r}_1''\ldots\mathbf{r}_7'')\{&\delta(\mathbf{r}_1-\mathbf{r}_1'')\ldots\delta(\mathbf{r}_7\ldots\mathbf{r}_7'')\\
&-3\delta(\mathbf{r}_1-\mathbf{r}_5'')\ldots\delta(\mathbf{r}_5-\mathbf{r}_1'')\ldots\delta(\mathbf{r}_7-\mathbf{r}_7'')\\
&+3\delta(\mathbf{r}_1-\mathbf{r}_5'')\delta(\mathbf{r}_2-\mathbf{r}_6'')\ldots\delta(\mathbf{r}_5-\mathbf{r}_1'')\delta(\mathbf{r}_6-\mathbf{r}_2'')\delta(\mathbf{r}_7-\mathbf{r}_7'')\\
&-\delta(\mathbf{r}_1-\mathbf{r}_5'')\delta(\mathbf{r}_2-\mathbf{r}_6'')\delta(\mathbf{r}_3-\mathbf{r}_7'')\delta(\mathbf{r}_4-\mathbf{r}_4'')\\
&\delta(\mathbf{r}_5-\mathbf{r}_1'')\delta(\mathbf{r}_6-\mathbf{r}_2'')\delta(\mathbf{r}_7-\mathbf{r}_3'')\}d\mathbf{r}_1''\ldots d\mathbf{r}_7''\\
&\times Q(1,\ldots,7)\int\{g(\mathbf{r}'_1\ldots\mathbf{r}'_7)\delta(\mathbf{r}_1-\mathbf{r}'_1)\ldots\delta(\mathbf{r}_7-\mathbf{r}'_7)\\
&d\mathbf{r}'_1\ldots d\mathbf{r}'_7\}\Big]d\mathbf{r}_1\ldots d\mathbf{r}_7.
\end{aligned}
\tag{49}
$$

4.1. THE NORMALIZATION; KINETIC AND POTENTIAL INTEGRALS

It may again be easily shown that

$$N^2 = 7![A_0-3A_1+3A_2-A_3], \tag{50}$$

where the subscripts 0, 1, 2, 3 denote no exchange, single exchange, double exchange and triple exchange, respectively, and

$$A_0 = 12^3\left(\frac{\pi^5}{12\alpha^5}\right)^{\frac{3}{2}} I(\tfrac{12}{7}\beta), \tag{51}$$

$$A_1 = 12^3(\tfrac{12}{7})^3(\tfrac{1}{17})^{\frac{3}{2}}\left(\frac{\pi}{\alpha}\right)^6 M(\tfrac{169}{119}\alpha+\beta, \tfrac{240}{119}\alpha, \tfrac{169}{119}\alpha+\beta), \tag{52}$$

$$A_2 = 12^3(\tfrac{12}{7})^3(\tfrac{1}{20})^{\frac{3}{2}}\left(\frac{\pi}{\alpha}\right)^6 M(\tfrac{37}{35}\alpha+\beta, -\tfrac{24}{35}\alpha, \tfrac{37}{35}\alpha+\beta), \tag{53}$$

$$A_3 = 12^3(\tfrac{12}{7})^3(\tfrac{1}{9})^{\frac{3}{2}}\left(\frac{\pi}{\alpha}\right)^6 M(\tfrac{25}{7}\alpha+\beta, -\tfrac{48}{7}\alpha, \tfrac{25}{7}\alpha+\beta), \tag{54}$$

with

$$M(p, q, s) = J(\tfrac{6}{7}p, \tfrac{6}{7}q, \tfrac{6}{7}s). \tag{55}$$

Similarly, for the expectation value of the kinetic energy operator, we have

$$
\begin{aligned}
\cdot\langle T\rangle = &\frac{\hbar^2}{2M}(2\beta n+3\beta+15\alpha)-7!\frac{\hbar^2}{2M}\frac{1}{N^2}(C_0-3C_1+3C_2-C_3)\\
&-7!\frac{\hbar^2}{2M}\frac{n(n+1)-l(l+1)}{\frac{12}{7}N^2}(B_0-3B_1+3B_2-B_3),
\end{aligned}
\tag{56}
$$

where B_0, B_1, B_2, B_3 have the same form as A_0, A_1, A_2, A_3 in eqs. (51)—(54) except that an additional factor R'^{-2} appears in the definition of $I(p)$ and $M(p, q, s)$. Further, in eq. (56),

$$C_0 = A_0(\tfrac{15}{2}\alpha+\tfrac{1}{2}(2n+3)\beta), \tag{57}$$

$$C_1 = A_1[(n+9)\alpha+\Lambda(\tfrac{169}{119}\alpha+\beta, \tfrac{240}{119}\alpha)], \tag{58}$$

$$C_2 = A_2[(n+9)\alpha+\Lambda(\tfrac{37}{35}\alpha+\beta, \tfrac{24}{35}\alpha)], \tag{59}$$

$$C_3 = A_3[(n+9)\alpha+\Lambda(\tfrac{25}{7}\alpha+\beta, \tfrac{48}{7}\alpha)], \tag{60}$$

where Λ is defined by eq. (27).

The total potential energy (without Coulomb interaction) may be easily subsumed in the form

$$\langle V\rangle = 7!(-WV_0)\frac{1}{N^2}\{18P_1+9P_2-24P_3-6P_4+9P_5-60P_6+72P_7 \\ +18P_8-3P_9-6P_{10}-12P_{11}-3P_{12}-12P_{13}\}, \tag{61}$$

wherein the quantities P_i are independent integrals given by

$$P_1 = 12^3\left(\frac{\pi}{\alpha}\right)^6\left(\frac{\pi}{12\alpha+24\kappa}\right)^{\frac{3}{2}} I(\tfrac{12}{7}\beta), \tag{62}$$

$$P_2 = 12^3\left(\frac{\pi}{\alpha}\right)^6\left(\frac{\pi}{12\alpha+17\kappa}\right)^{\frac{3}{2}} I\left(\frac{12\alpha\kappa}{12\alpha+17\kappa}+\tfrac{12}{7}\beta\right), \tag{63}$$

$$P_3 = \Gamma\left(\frac{\pi}{17\alpha+34\kappa}\right)^{\frac{3}{2}} M(\tfrac{169}{119}\alpha+\beta, \tfrac{240}{119}\alpha, \tfrac{169}{119}\alpha+\beta), \tag{64}$$

$$P_4 = \Gamma\left(\frac{\pi}{17\alpha+20\kappa}\right)^{\frac{3}{2}} M\left(\frac{169\alpha+268\kappa}{119\alpha+140\kappa}\alpha+\beta, \frac{240\alpha+144\kappa}{119\alpha+140\kappa}\alpha, \frac{169\alpha+268\kappa}{119\alpha+140\kappa}\alpha+\beta\right), \tag{65}$$

$$P_5 = \Gamma\left(\frac{\pi}{17\alpha}\right)^{\frac{3}{2}} M(\tfrac{169}{119}\alpha+\beta+\tfrac{24}{7}\kappa, \tfrac{240}{119}\alpha+\tfrac{48}{7}\kappa, \tfrac{169}{119}\alpha+\beta+\tfrac{24}{7}\kappa), \tag{66}$$

$$P_6 = \Gamma\left(\frac{\pi}{17\alpha+22\kappa}\right)^{\frac{3}{2}} M\left(\frac{169\alpha+254\kappa}{119\alpha+154\kappa}\alpha+\beta, \frac{240\alpha+480\kappa}{119\alpha+154\kappa}\alpha, \frac{169\alpha+422\kappa}{119\alpha+154\kappa}\alpha+\beta\right), \tag{67}$$

$$P_7 = \Gamma\left(\frac{\pi}{20\alpha+28\kappa}\right)^{\frac{3}{2}} M\left(\frac{37\alpha+95\kappa}{35\alpha+49\kappa}\alpha+\beta, -\frac{24\alpha+48\kappa}{35\alpha+49\kappa}\alpha, \frac{37\alpha+53\kappa}{35\alpha+49\kappa}\alpha+\beta\right), \tag{68}$$

$$P_8 = \Gamma\left(\frac{\pi}{20\alpha+40\kappa}\right)^{\frac{3}{2}} M(\tfrac{37}{35}\alpha+\beta, -\tfrac{24}{35}\alpha, \tfrac{37}{35}\alpha+\beta), \tag{69}$$

$$P_9 = \Gamma\left(\frac{\pi}{20\alpha+12\kappa}\right)^{\frac{3}{2}} M\left(\frac{37\alpha+81\kappa}{35\alpha+21\kappa}\alpha+\beta, -\frac{24\alpha+132\kappa}{35\alpha+21\kappa}\alpha, \frac{37\alpha+81\kappa}{35\alpha+21\kappa}\alpha+\beta\right), \tag{70}$$

$$P_{10} = \Gamma\left(\frac{\pi}{20\alpha+20\kappa}\right)^{\frac{3}{2}} M\left(\frac{37\alpha+67\kappa}{35\alpha+35\kappa}\alpha+\beta, -\frac{24\alpha-36\kappa}{35\alpha+35\kappa}\alpha, \frac{37\alpha+67\kappa}{35\alpha+35\kappa}\alpha+\beta\right), \tag{71}$$

$$P_{11}=\Gamma\left(\frac{\pi}{9\alpha+18\kappa}\right)^{\frac{3}{2}} M\left(\tfrac{25}{7}\alpha+\beta,\ -\tfrac{48}{7}\alpha,\ \tfrac{25}{7}\alpha+\beta\right), \tag{72}$$

$$P_{12}=\Gamma\left(\frac{\pi}{9\alpha+12\kappa}\right)^{\frac{3}{2}} M\left(\frac{75\alpha+108\kappa}{21\alpha+28\kappa}\alpha+\beta,\ -\frac{144\alpha+176\kappa}{21\alpha+28\kappa}\alpha,\ \frac{75\alpha+108\kappa}{21\alpha+28\kappa}\alpha+\beta\right), \tag{73}$$

$$P_{13}=\Gamma\left(\frac{\pi}{9\alpha+6\kappa}\right)^{\frac{3}{2}} M\left(\frac{75\alpha+122\kappa}{21\alpha+14\kappa}\alpha+\beta,\ -\frac{144\alpha+288\kappa}{21\alpha+14\kappa}\alpha,\ \frac{75\alpha+178\kappa}{21\alpha+14\kappa}\alpha+\beta\right), \tag{74}$$

with

$$\Gamma = 12^3\left(\tfrac{12}{7}\right)^3\left(\frac{\pi}{\alpha}\right)^{9/2}. \tag{75}$$

In eq. (61), P_1, P_2 relate to the no-exchange potential integrals, P_3 to P_6 to the single-exchange integrals, P_7 to P_{10} to the double-exchange integrals, and P_{11} to P_{13} to the triple-exchange integrals. All those integrals may be readily integrated by the general formulae (38) and (39).

4.1 NUMERICAL CALCULATIONS

The curve of Mang and Wild for the internal energy of a triton cluster versus its width parameter is fitted by an analytical equation of the form

$$E_T = -7.1+8.6\left(1-\frac{1.41}{y}\right)^2 \text{MeV}, \tag{76}$$

where y is defined by eq. (44). In deriving this equation, we have again shifted their curve without altering its shape, a procedure necessary to give the rms radius of a free triton the value 1.84×10^{-13} cm [14]).

At present, we shall set aside a discussion of the positive parity state and limit ourselves to the first two negative parity levels of Li^7 †. The results obtained for E_0, now defined by

$$E_0 = E-E_\alpha(\text{free})-E_T(\text{free}) \tag{77}$$

as a function of x, are plotted in fig. 2, where y is chosen to give the minimum value of E_0. Further, by adding a Coulomb energy estimated to be about 0.85 MeV, we obtain values for the separation energies which are tabulated and compared to the experimentally observed values [13]) in table 2.

We note that the agreement between the calculated and the experimental values are only fair. However, the calculated level spacing of 5.6 MeV compares very favourably with the experimental value of 5.7 MeV. As has already been mentioned, better agreement could probably be attained if we had used a

† Spin-orbit interaction has not been considered in our work; hence, the observed $\frac{3}{2}^-$, $\frac{1}{2}^-$, $\frac{7}{2}^-$, and $\frac{5}{2}^-$ states degenerate into two states, and consequently we use the respective appropriate experimental "centre of mass" energy for comparison between theory and experiment. To compute the "centre of mass" energy, we have assumed that the $\frac{5}{2}^-$ state exists at 6.5 MeV [18]).

three-parameter variational wave function. In fact, if we add 1.3 MeV as mentioned in the second paragraph of this section to the second column of table 2, the agreement is much improved. However, as has also been pointed out,

TABLE 2

Comparison between the calculated and experimental separation energies for the first two states in Li^7

	Separation energy in MeV	
	Calculated	Experimental
Ground state	+0.2	+2.3
First excited state	−5.4	−3.4

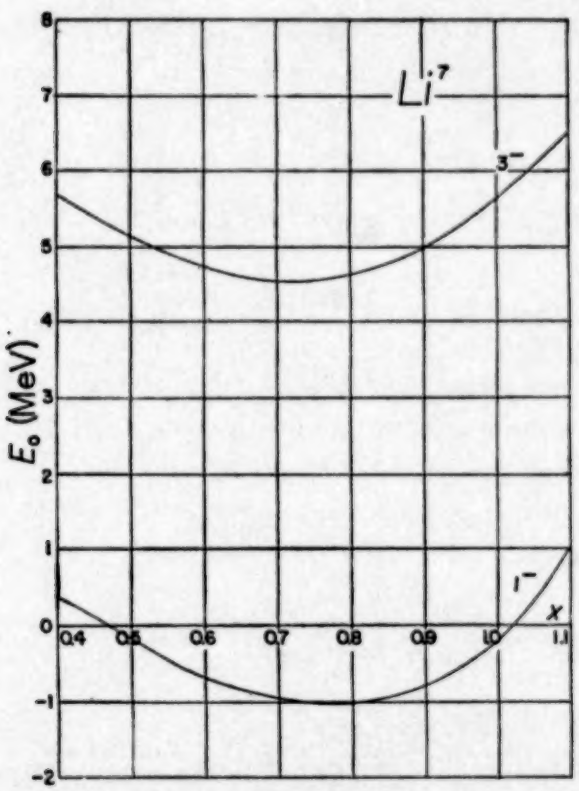

Fig. 2. E_0 as a function of x for the first two levels of Li^7

the calculation with a three-parameter trial function is immensely tedious; hence, at the present moment, we do not intend to proceed in this direction for this particular nucleus.

The values of x and y which yield E_0 (minimum) are:

$$\begin{aligned} &\text{ground state:} \quad y = 1.04, \quad x = 0.775, \\ &\text{1st excited state:} \quad y = 1.08, \quad x = 0.720. \end{aligned} \tag{78}$$

We now return to a consideration of the broad positive parity state at 6.5 MeV excitation energy [13]). The wave function we have previously used, with $n = 4$, $l = 0$, would predict that this level has an assignment of $\frac{1}{2}^+$. However, an examination of the present experimental status indicates that the most probable classification is either $\frac{1}{2}^+$ or $\frac{3}{2}^+$ with an equal possibility for the presence of both states [13, 15]). Since it is most likely that a $\frac{3}{2}^+$ state is present † we must necessarily conclude that the aforementioned wave function is incorrect. Consequently, it is necessary to search for another structure for a trial wave function, one in which the triton is fractured. The lowest lying state

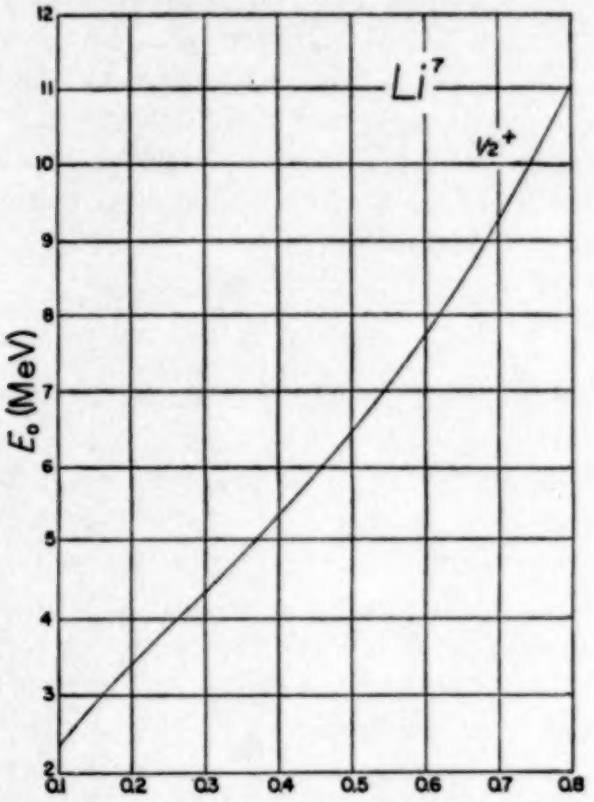

Fig. 3. E_0 as a function of x for the positive parity level of Li^7

with such a configuration would be one in which the deuteron cluster is in a relative 2s-state with respect to the alpha-cluster and the remaining nucleon in a 2s-state relative to their centre of mass. This structure would give rise [15]) to two closely lying positive parity states of level assignment $\frac{1}{2}^+$ and $\frac{3}{2}^+$. Our contention that the triton-cluster is excited is further supported by the fact that the excitation energy of this level is adequate to break up a free triton.

Now, recalling that the above wave function produces a $\frac{1}{2}^+$ state it becomes necessary to determine the relative importance of the original wave function which describes the motion of two unexcited clusters; therefore, we have per-

† The situation [13]) in Li^7 indicates that possibly both are present, while the status [16]) of Be^7 demands the presence of a $\frac{1}{2}^+$ state.

formed the appropriate calculation. The results are shown in fig. 3 where again we plot E_0 versus x. An examination of this curve reveals the absence of a relative minimum. Consequently, we must conclude that the excited triton plays the dominant role.

Assuming that this latter mechanism is indeed responsible for the behaviour of this positive parity state, we would then predict that another positive parity state, corresponding to the virtual singlet spin state of the deuteron, would exist at an excitation of about 9 MeV. Consequently we contend that the 9.6 MeV level [13]) in Li^7 might be this $\frac{1}{2}^+$ state.

We may add that the experimental evidence indicating the absence of any negative parity levels below 6 MeV in Li^6 presents another argument in favour of our contention †. This absence can be explained by the fact that the two nucleons do not interact strongly in a relative p-state.

There now remains the need for a quantitative examination of these effects, which is planned for the immediate future. Moreover, there is an urgent need for further experimental clarification.

5. Concluding Remarks

The results of our calculation indicate that reasonably good agreement with experiment for the first few levels of the nuclei considered can be obtained if the features of long range nuclear correlations (cluster structures) are included in the wave functions. Not only have we been able to predict the ground state energies of the nuclei Be^8 and Li^7, but also we can calculate the level spacings.

In our calculation, we have made the assumption that the hard-core part of the nuclear force has no effect on the interaction energy between the clusters, and hence is included only in the computation of the internal energies of the clusters. This assumption is justified a posteriori by the results of our calculation. We must point out, however, that if one wishes to go over to heavier nuclei ($A > 12$), the hard-core force must be taken into account in a more consistent manner.

For the calculation of the energies of the virtual levels, the variational procedure yields relative minima (see figs. 1 and 2), which indicates that these levels can disintegrate into a configuration of free clusters only by going through energetically unfavoured regions. Therefore, the life time of these states must be closely connected with the depth of the relative minima. For instance, we notice that in Be^8, the depth of the minima decreases with increasing excitation energy of the levels, in agreement with the experimental fact that the level width increases with the excitation energy.

We have concluded that the first positive parity level in Li^7 must be repre-

† There is some weak evidence on the existence of a negative parity level in Li^8 at about 7 MeV excitation [17]).

sented by a wave function in which the triton has a large probability of being fractured. This conclusion was reached by a careful examination of the experimental data in Li^7 and Li^6 as previously reported. We are now in the process of determining quantitatively the properties of such a configuration. Also we have begun a detailed investigation of the 16.7 MeV level in He^5 which presumably must also be described by an analogous wave function.

To reduce the complexity of our calculations, we have made some further simplifying assumptions:

(1) For Li^7, our trial wave function is not the optimum one. Preferably, a three-parameter function should be used, i.e., the triton an alpha width parameters should be independently varied. As has been previously mentioned, this simplification gives rise to an error of approximately 1.3 MeV.

(2) The Coulomb and the spin-orbit energies are incorporated in a rough additive manner.

Finally, it is necessary to remark that we have redone a part of these calculations with a Serber force of Yukawa structure which has the same average properties in the low-energy region as the Gaussian potential of eq. (3). The results thereby obtained were essentially identical to those arrived at with the original potential. Since calculations with the latter are nearly prohibitive we anticipate using a Gaussian potential in any future investigations of the properties of light nuclei.

References

1) K. Wildermuth and Th. Kanellopoulos, Nuclear Physics **1** (1953) 150; **9** (1958/59) 449; CERN Report 59-23
2) R. K. Sheline and K. Wildermuth (to be published)
3) B. Roth and K. Wildermuth (to be published)
4) J. A. Wheeler, Phys. Rev. **52** (1937) 1083, 1107
5) S. F. Edwards, Proc. Cambridge Phil. Soc. **48** (1952) 652
6) S. F. Biel, Proc. Phys. Soc. A **70** (1957) 866
7) J. P. Elliott and A. M. Lane, The Nuclear Shell Model, Encyclopedia of Physics **39** (1957) 241
8) Lederer, Diplomarbeit (München, 1957)
9) H. J. Mang and W. Wild, Z. Physik **154** (1959) 182
10) Magnus and Oberhettinger, Functions of Mathematical Physics, (Chelsea Publishing Company New York, 1954)
11) R. Hofstadter, Rev. Mod. Phys. **28** (1956) 214
12) A. Herzenberg, Nuovo Cimento **1** (1955) 986
13) F. Ajzenberg and T. Lauritzen, Nuclear Physics **11** (1959) 1
14) B. C. Carlson and I. Talmi, Phys. Rev. **96** (1954) 436
15) A. M. Lane, AERE Report T/R 1289, 1954 (unpublished)
16) J. B. Marion, G. Weber and F. S. Mozer, Phys. Rev. **104** (1956) 1402
17) A. Galonsky and M. T. McEllistrem, Phys. Rev. **98** (1955) 590
18) C. A. Levinson and M. K. Banerjee, Ann. Phys. **2** (1957) 471

1.D.2:
1.E.3

Nuclear Physics **18** (1960) 40—45; © *North-Holland Publishing Co., Amsterdam*

Not to be reproduced by photoprint or microfilm without written permission from the publisher

GYROMAGNETIC FACTORS OF DEFORMED ODD-MASS NUCLEI WITH $153 \leqq A \leqq 187$

E. M. BERNSTEIN † and J. DE BOER

Institute for Theoretical Physics, University of Copenhagen

Received 20 April 1960

Abstract: Recently available experimental data are combined to obtain accurate values of the reduced magnetic dipole transition probabilities between rotational states of deformed odd-mass nuclei. These results are interpreted on the basis of the rotational model to yield the gyromagnetic factors g_R and g_K. It appears that the values of g_R vary rather smoothly with the atomic number and have a minimum at $A \approx 170$, and that g_R is smaller for odd neutron nuclei than for odd proton nuclei.

According to the collective model of Bohr and Mottelson [1, 2]) the transitions between the levels of a rotational band can be expressed in terms of parameters which are related to the intrinsic nuclear configuration. These parameters are the following: the ground state spin I_0 and the parity, the effective moment of inertia $\Im_0$, the intrinsic quadrupole-moment Q_0 and the gyromagnetic factors g_R and g_K. In addition to the ground-state spin very accurate values of $\Im_0$ and Q_0 have been determined from Coulomb-excitation experiments and have been compared with theoretical predictions. In this paper, we have combined the data of several recent experiments to obtain the most accurate values of the gyromagnetic factors g_R and g_K for highly deformed odd-mass nuclei ††.

The determination of the g-factors for odd-mass nuclei requires experimental values for both the ground-state magnetic moment μ_0 and the magnetic dipole transition probability $B(\mathrm{M1})$ between any two rotational states. The g-factors are related to these quantities by the following equations †††:

$$g_R = \frac{\mu_0}{I_0} - \frac{M_0}{I_0+1}, \tag{1}$$

$$g_K = \frac{\mu_0}{I_0} + \frac{M_0}{I_0(I_0+1)}, \tag{2}$$

$$M_0 = \pm \left\{ \frac{4.19\, B(\mathrm{M1}; I_1 \to I_f)}{\langle I_1 1 I_0 0 | I_1 1 I_f 0 \rangle^2} \right\}^{\frac{1}{2}}. \tag{3}$$

† U.S. National Science Foundation Fellow (1959/60).

†† Earlier, less accurate determinations of g_R for these nuclei yielded $(g_R)_{av} \approx 0.3$ (see refs. [2–6])).

††† These equations hold for $I_0 = K \neq \frac{1}{2}$. For $K = \frac{1}{2}$, eqs. (1), (2) and (3) are replaced by similar relations containing an additional parameter b_0 (see ref. [2]), p. 532); g_R, g_K and b_0 can be determined, if $B(\mathrm{M1})$-values are known for two transitions in the rotational band.

Here, $B(\mathrm{M1})$ is expressed in units of $(e\hbar/2Mc)^2$ and $\langle I_1 1 I_0 0 | I_1 1 I_f I_0 \rangle$ is a vector addition coefficient. The sign of M_0 is the same as the sign of δ, where δ^2 is the E2/M1 gamma ray intensity ratio in the transition between the rotational states with spin I_1 and I_f. The sign of δ is the same as defined in ref. [2]).

From the available data it is possible to obtain $B(\mathrm{M1})$ either for the transition from the first rotational state to the ground state ($I_0+1 \rightarrow I_0$), or for the cascade transition from the second rotational state to the first rotational state ($I_0+2 \rightarrow I_0+1$). In most cases, however, the values determined for the cascade transition are more accurate. The quantity $B(\mathrm{M1})$ cannot be measured directly; it depends on several experimental quantities through the relations

$$B(\mathrm{M1}) = 0.70 \frac{(\Delta E)^2}{\delta^2} B_{\mathrm{d}}(\mathrm{E2}), \tag{4}$$

$$B_{\mathrm{d}}(\mathrm{E2}; I_0+1 \rightarrow I_0) = \frac{2I_0+1}{2I_0+3} B_{\mathrm{ex}}(\mathrm{E2}; I_0 \rightarrow I_0+1), \tag{5}$$

$$B_{\mathrm{d}}(\mathrm{E2}; I_0+2 \rightarrow I_0+1) = \frac{\delta^2}{1+\delta^2} \frac{1}{\lambda} \left\{ \frac{\Delta E_{I_0+2 \rightarrow I_0}}{\Delta E_{I_0+2 \rightarrow I_0+1}} \right\}^5 \frac{2I_0+1}{2I_0+5} B_{\mathrm{ex}}(\mathrm{E2}; I_0 \rightarrow I_0+2). \tag{6}$$

Here, ΔE denotes the transition energy in MeV, $B_{\mathrm{d}}(\mathrm{E2})$ and $B_{\mathrm{ex}}(\mathrm{E2})$ are the reduced electric quadrupole transition probabilities for decay and excitation expressed in units of $10^{-48} e^2\ \mathrm{cm}^4$, and λ is the crossover to cascade gamma ray branching ratio of the second rotational state. Although the entire conception of expressing the magnetic properties of deformed nuclei in terms of two g-factors (eqs. (1), (2) and (3)) is based on the validity of the rotational model, it should be noted that the $B(\mathrm{M1})$ values are obtained in a manner which is independent of the model.

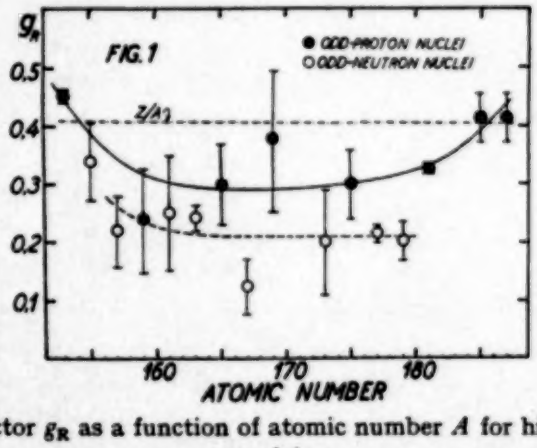

Fig. 1. Gyromagnetic factor g_R as a function of atomic number A for highly deformed odd-mass nuclei.

The experimental data which were used for the calculations are listed in table 1 along with the values of g_R and g_K. In fig. 1, g_R is plotted as a function of the atomic number. Although the errors of most points are too large to present a

TABLE I

g-factors for highly

Isotope	I_0	μ_0 (nucl. magn.)	ΔE (keV)	Trans. $I_1 \to I_f$	$B_{ex}(E2; I_f \to I_1)$ (10^{-48} cm^4 e^2)
$_{63}Eu^{153}$	$\frac{5}{2}$	$+1.507 \pm 0.002$ [29])	109 ± 2 [5, 13, 18, 19]) 192 ± 2 [5, 13, 18, 19])	$\frac{5}{2} \to \frac{7}{2}$ $\frac{5}{2} \to \frac{5}{2}$	0.70 ± 0.04 [13])
$_{64}Gd^{155}$	$\frac{3}{2}$	-0.28 ± 0.03 [10, 8])	86.45 [20, 21]) 146.55 [20, 21])	$\frac{7}{2} \to \frac{5}{2}$ $\frac{7}{2} \to \frac{3}{2}$	1.12 ± 0.15 [22])
$_{64}Gd^{157}$	$\frac{3}{2}$	-0.37 ± 0.04 [10])	76.5 ± 1 [5, 13, 20, 22]) 131 ± 1 [5, 13, 20, 22])	$\frac{7}{2} \to \frac{5}{2}$ $\frac{7}{2} \to \frac{3}{2}$	1.21 ± 0.10 [22])
$_{65}Tb^{159}$	$\frac{3}{2}$	$+1.52 \pm 0.08$ [9])	79.51 [20]) 137.50 [20])	$\frac{7}{2} \to \frac{5}{2}$ $\frac{7}{2} \to \frac{3}{2}$	1.45 ± 0.06 [13])
$_{66}Dy^{161}$	$\frac{5}{2}$	-0.375 ± 0.04 [9, 11])	43.83 [20])	$\frac{7}{2} \to \frac{5}{2}$	2.54 ± 0.25 [23])
$_{66}Dy^{163}$	$\frac{5}{2}$	$+0.52 \pm 0.05$ [9, 11])	94.6 ± 1 [5, 19, 20, 23]) 170 ± 1 [5, 19, 20, 23])	$\frac{9}{2} \to \frac{7}{2}$ $\frac{9}{2} \to \frac{5}{2}$	0.67 ± 0.13 [23])
$_{67}Ho^{165}$	$\frac{7}{2}$	$+3.29 \pm 0.17$ [12])	109.93 [20]) 204.63 [20])	$\frac{11}{2} \to \frac{9}{2}$ $\frac{11}{2} \to \frac{7}{2}$	0.63 ± 0.04 [13])
$_{68}Er^{167}$	$\frac{7}{2}$	-0.5 ± 0.1 [13])	100.0 ± 1 [5, 16, 20]) 178.5 ± 1 [5, 13, 20])	$\frac{11}{2} \to \frac{9}{2}$ $\frac{11}{2} \to \frac{7}{2}$	0.60 ± 0.04 [13])
$_{69}Tm^{169}$	$\frac{1}{2}$ [a])	-0.21 ± 0.02 [32])	109.78 [33]) 118.20 [33]) 20.75 [33]) 130.53 [33])	$\frac{5}{2} \to \frac{3}{2}$ $\frac{5}{2} \to \frac{1}{2}$ $\frac{7}{2} \to \frac{5}{2}$ $\frac{7}{2} \to \frac{3}{2}$	3.37 ± 0.07 [13])
$_{70}Yb^{173}$	$\frac{5}{2}$	-0.665 ± 0.01 [11, 14])	101.0 ± 0.5 [5, 13, 23]) 179.7 ± 0.5 [5, 13, 23])	$\frac{9}{2} \to \frac{7}{2}$ $\frac{9}{2} \to \frac{5}{2}$	0.89 ± 0.18 [23])
$_{71}Lu^{175}$	$\frac{7}{2}$	$+2.0 \pm 0.2$ [15])	137 ± 2 [4, 19, 20, 24]) 251 ± 2 [4, 19, 20, 24])	$\frac{11}{2} \to \frac{9}{2}$ $\frac{11}{2} \to \frac{7}{2}$	0.57 ± 0.08 [24])
$_{72}Hf^{177}$	$\frac{7}{2}$	$+0.61 \pm 0.03$ [16])	137.09 [25]) 250.00 [25])	$\frac{11}{2} \to \frac{9}{2}$ $\frac{11}{2} \to \frac{7}{2}$	0.49 ± 0.04 [26])
$_{73}Hf^{179}$	$\frac{9}{2}$	-0.47 ± 0.03 [16])	143 ± 3 [5, 13, 20, 26]) 269 ± 3 [5, 13, 20, 26])	$\frac{13}{2} \to \frac{11}{2}$ $\frac{13}{2} \to \frac{9}{2}$	0.40 ± 0.06 [26])
$_{73}Ta^{181}$	$\frac{7}{2}$	$+2.340$ [17])	136.1 [20])	$\frac{9}{2} \to \frac{7}{2}$	1.94 ± 0.06 [6, 19, 26])
$_{75}Re^{185}$	$\frac{5}{2}$	$+3.144$ [13])	159 ± 3 [5, 13]) 284 ± 3 [5, 13])	$\frac{9}{2} \to \frac{7}{2}$ $\frac{9}{2} \to \frac{5}{2}$	0.69 ± 0.06 [5, 6])
$_{75}Re^{187}$	$\frac{5}{2}$	$+3.176$ [13])	166 ± 3 [5, 13]) 300 ± 3 [5, 13])	$\frac{9}{2} \to \frac{7}{2}$ $\frac{9}{2} \to \frac{5}{2}$	0.64 ± 0.06 [5, 6])

The g-factors are obtained from the ground-state magnetic moment (column 3), the relative sign of the E2 to M1 transition matrix elements (col. 9) and the reduced magnetic dipole transition probability (col. 10) (see eqs. (1), (2), (3)). B(M1) is determined from the transition energies (col. 4), the reduced E2 transition probability for excitation (col. 6), the cascade to crossover gamma-ray branching ratio (col. 7) and the E2 to M1 gamma-ray mixing ratio (col. 8) (see eqs. (4), (5), (6)). Where more than one reference is given, the quoted value is a weighted average.

[a]) See footnote ††† on page 40.

deformed odd-mass nuclei

Branching ratio crossover/casc.	δ^2	sign δ	$B(M1; I_1 \to I_f)$ $\left(\frac{e\hbar}{2Mc}\right)^2$	g_R	g_K
0.19 ±0.01 [3, 5, 19, 27])	0.47 ±0.05 [5, 19])	+	0.021 ±0.003	0.452±0.012	+0.664±0.009
0.25 ±0.05 [3, 5])	0.038±0.011 [5, 30])	−	0.152 ±0.041	0.34 ±0.07	−0.54 ±0.05
0.29 ±0.07 [3, 5])	0.040±0.016 [5, 30])	−	0.120 ±0.029	0.22 ±0.06	−0.56 ±0.05
0.145±0.025 [3, 4])	0.02 ±0.01 [4])	+	0.330 ±0.058	0.24 ±0.09	+1.53 ±0.08
	0.025±0.012 [c]) [19])	−	0.101 ±0.050	0.25 ±0.10	−0.311±0.042
5.6 ±0.5 [5, 19, 28])	6.7 ±2.0 [5, 19])	−	0.0011±0.0003	0.243±0.021	+0.194±0.020
0.14 ±0.02 [3, 4, 19, 27])	0.031±0.009 [5, 19])	+	0.542 ±0.082	0.30 ±0.07	+1.120±0.015
0.48 ±0.13 [5])	0.106±0.038 [5])	−	0.094 ±0.026	0.124±0.047	−0.219±0.030
0.106±0.010 [19, 33])	0.020±0.005 [4])	−	0.125 ±0.013	0.38 ±0.12	−1.79 ±0.21
47.5 ±8 [33])	(9.8 ±1)×10^{-4} [33])		0.108 ±0.029 [b])		
0.32 ±0.10 [5])	0.047±0.014 [5])	−	0.20 ±0.07	0.20 ±0.09	−0.453±0.035
0.87±0.09 [3, 4, 19, 27])	0.22±0.02 [5, 19])	+	0.096±0.017	0.30 ±0.06	+0.65 ±0.06
3.6 ±0.6 [3, 5, 27])	10 ±5 [5])	−	0.0022±0.0011	0.215±0.014	+0.162±0.010
0.50 ±0.05 [3, 5, 27])	0.15 ±0.06 [5])	−	0.165 ±0.031	0.203±0.034	−0.172±0.015
	0.198±0.008 [6, 19, 31])	+	0.100 ±0.005	0.327±0.009	+0.767±0.003
0.195±0.02 [5, 6, 27])	0.033±0.004 [5, 6])	+	0.653 ±0.065	0.413±0.042	+1.597±0.017
0.20 ±0.02 [5, 6, 27])	0.030±0.004 [5, 6])	+	0.684 ±0.68	0.413±0.043	+1.617±0.017

[b]) In addition to the experimental data quoted in the table, the half-lifes of the 118.20 keV and 138.95 keV states [(6.2±1.0)×10^{-11} s and (2.9±0.7)×10^{-10} s; ref. [34])] were used to determine the $B(M1)$ value.

[c]) This value of δ^2 is obtained by combining the results of ref. [19]) with the theoretical E2 intensity rules predicted by the rotational model.

detailed picture, some systematic trends in the values of g_R seem to be present:

1) in general, the values are appreciably less than Z/A;

2) the values lie on a reasonably smooth concave curve which has a minimum at $A \approx 170$;

3) the values for odd-proton nuclei are larger than those for odd-neutron nuclei.

These features are in good agreement with recent theoretical calculations [7]) of g_R.

The values of g_K depend mainly on the magnetic moments and are relatively insensitive to the magnetic dipole transition probabilities. Therefore, the present determinations do not differ appreciably from earlier tabulations [2–6, 35]).

The authors wish to express their appreciation to Professor Niels Bohr and the staff of the Institute for Theoretical Physics in Copenhagen for their kind hospitality. It is a pleasure to thank Drs. B. R. Mottelson and S. G. Nilsson for several stimulating and helpful discussions. We would also like to acknowledge two postdoctoral fellowships offered by the U.S. National Science Foundation (E. M. B.) and the Ford Foundation (J. de B.).

References

1) Aa. Bohr and B. R. Mottelson, Mat. Fys. Medd. Dan. Vid. Selsk. **27** No. 16 (1953)
2) K. Alder, Aa. Bohr, T. Huus, B. Mottelson and Aa. Winther, Revs. Mod. Phys. **28** (1956) 437
3) N. P. Heydenburg and G. M. Temmer, Phys. Rev. **104** (1956) 981
4) M. Martin, P. Marmier and J. de Boer, Helv. Phys. Acta **31** (1958) 435
5) J. de Boer, M. Martin and P. Marmier, Helv. Phys. Acta **32** (1959) 377
6) F. K. McGowan and P. H. Stelson, Phys. Rev. **109** (1958) 901
7) B. R. Mottelson and S. G. Nilsson, private communication
8) W. Low and D. Shaltiel, Phys. Rev. **115** (1959) 424
9) J. G. Park, Proc. Roy. Soc. A **245** (1958) 118
10) D. R. Speck, Phys. Rev. **101** (1956) 1725
11) A. H. Cooke and J. G. Park, Proc. Phys. Soc. A **69** (1956) 282
12) J. M. Baker and B. Bleaney, Proc. Roy. Soc. A **245** (1958) 156
13) D. Strominger, J. M. Hollander and G. T. Seaborg, Revs. Mod. Phys. **30** (1958) 585
14) K. Krebs and H. Nelkowski, Z. Physik **141** (1955) 254
15) A. Steudel, Naturwissensch. **44** (1957) 371
16) D. R. Speck, Bull. Am. Phys. Soc. **1** (1956) 282
17) L. H. Bennet and J. I. Budnik, Bull. Am. Phys. Soc. **4** (1959) 417
18) M. C. Olesen and B. Elbek, Nuclear Physics **15** (1960) 134
19) E. M. Bernstein and R. Graetzer, Phys. Rev. (submitted)
20) E. L. Chupp, J. W. M. DuMond, F. J. Gordon, R. C. Jopson and Hans Mark, Phys. Rev. **112** (1958) 518
21) F. Boehm and E. N. Hatch, Bull. Am. Phys. Soc. **2** (1957) 231
22) V. Ramšak, M. C. Olesen and B. Elbek, Nuclear Physics **6** (1958) 451
23) B. Elbek, K. O. Nielsen and M. C. Olesen, Phys. Rev. **108** (1957) 406
24) B. Elbek, M. C. Olesen and O. Skilbred, Nuclear Physics **10** (1959) 294
25) P. Marmier and F. Boehm, Phys. Rev. **97** (1955) 103
26) M. C. Olesen, O. Hansen, B. Elbek and O. Skilbreid, to be published
27) G. Goldring and G. T. Paulissen, Phys. Rev. **103** (1956) 1314

28) N. P. Heydenburg and G. F. Pieper, Phys. Rev. **107** (1957) 1297
29) G. K. Woodgate, P. G. H. Sandars and F. Pichanik, Proc. Roy. Soc. (submitted)
30) J. H. Bjerregaard and U. Meyer-Berkhout, Z. Naturf. **11a**, (1956) 273
31) P. Debrunner, E. Heer, W. Kuendig and R. Ruetschi, Helv. Phys. Acta **29** (1956) 463
32) K. H. Lindenberger, Z. Physik **141** (1955) 476
33) E. N. Hatch, F. Boehm, P. Marmier and J. W. M. DuMond, Phys. Rev. **104** (1956) 745
34) A. E. Blaugrund, Phys. Rev. Lett. **3** (1959) 226
35) B. R. Mottelson and S. G. Nilsson, Mat. Fys. Skr. Dan. Vid. Selsk. **1**, No. 8 (1959)

2.F

Nuclear Physics **18** (1960) 46—64; © *North-Holland Publishing Co., Amsterdam*

Not to be reproduced by photoprint or microfilm without written permission from the publisher

QUASI-ELASTIC SCATTERING OF 153 MeV PROTONS BY p-STATE PROTONS IN C^{12}

I. Experimental

T. J. GOODING and H. G. PUGH

AERE, Harwell, Didcot, Berks

Received 31 March 1960

Abstract: For the reaction $C^{12}(p, 2p)B^{11}$ at 153 MeV, the energies of the two protons emitted in each event are measured with plastic scintillators, and added. The summed-energy spectrum shows a well-defined peak corresponding to an energy loss of 16 MeV in the reaction, and events in this peak are interpreted as those in which a proton is knocked out of the p-shell in carbon. For coplanar p-state events, angular correlations and energy spectra are measured with one counter fixed at 15°, 20°, 30°, 40°, 60° and 80° relative to the incident beam and the angle of the other varied between 15° and 80° on the other side of the beam. The angular correlations are sharply peaked, while for the peak the separation angle between the two outgoing protons depends markedly on the angle at which one proton is detected, varying from 35° when the fixed counter is set at 15° to 110° when it is at 80°. The results are consistent with the mechanism of quasi-elastic p—p scattering when the momentum distribution of the struck protons is taken into account.

A rough value is obtained for the total cross-section for p-state events. It is about one-sixth of the expected value in the absence of absorption, thus showing the importance of this process. By comparison of the experimental results with distorted-wave calculations it should be possible to determine the momentum distribution of the p-state protons and the magnitude of the distortion effects themselves.

1. Introduction

Many experimental studies of (p, 2p) reactions have been made. The interaction is believed to proceed at high energies through the mechanism of quasi-elastic scattering in which the incident proton strikes a single proton in the target nucleus and both scattered and recoil protons are emitted. The name 'quasi-elastic scattering' arises because the interaction between the two protons is similar to elastic proton-proton scattering while the reaction as a whole is inelastic since a proton is ejected from the target nucleus.

Chamberlain and Segrè [1]) originally studied the reaction as a test of this mechanism. They bombarded lithium with 340 MeV protons and looked for two protons emitted in coincidence. With one counter fixed the maximum coincidence rate appeared when the other counter was at an angle approximately equal to that expected from p—p scattering inside the nucleus. Their results were qualitatively in agreement with those expected if the nucleus were a Fermi gas of particles in a square well.

Later Cladis *et al.* [2]) and Wilcox and Moyer [3]) at 340 MeV, and Azhgirey

et al. [4]) at 660 MeV studied the reaction to obtain momentum distributions for the struck particles. Cladis and Azhgirey studied the spectrum of protons emitted at a particular angle while Wilcox and Moyer further specified each event by requiring a coincident proton in a second counter. All these experiments were analyzed semi-classically and the distortion caused by the nuclear potential was neglected. At high energies this procedure is reasonable, but at low energies distortion is expected to be severe.

Griffiths and Eisberg [5]) found that for 40 MeV protons incident on medium-weight nuclei the primary interaction is still a quasi-elastic process but that the distortion effects are so severe that the reaction is limited to the surface of the nucleus. At 153 MeV for a light nucleus most of the nuclear volume can contribute to the reaction, while distortion effects are not negligible. We should therefore at this energy be able, by comparison of the experimental results with both detailed distorted-wave calculations and with calculations which do not include distortion, to study not only the momentum distribution but the distortion effects themselves.

The experiments of Cladis and Azhgirey gave a momentum distribution for all nucleons inside the nucleus, while Wilcox and Moyer obtained the momentum distribution for protons. If one could specify the shell-model state of the struck proton the momentum distribution obtained would be the Fourier transform of the wave function for that state. Tyrén, Maris and Hillman [6]) have shown that it is possible to determine the initial state by measuring the energies of both outgoing protons and considering the energy balance for the reaction. In our experiment we consider the p-state in C^{12}.

We have studied the reaction C^{12}(p, 2p)B^{11} at 153 MeV and have measured for each coplanar event the energies of both protons emitted. We have selected from these events those for which the energy balance shows that the struck proton was in the p-state. For these p-state events we have measured energy spectra as a function of the angles of both protons and have obtained differential cross-sections and angular correlations between the protons. We thus have for coplanar p-state events a complete set of data on the reaction for comparison with the distorted partial waves analysis of Nuttall and Riley [7]) and with simplified calculations which will be dealt with in the following paper [8]).

2. Principles of the Method

We require to study (p, 2p) interactions in which a proton is removed from a specified state in C^{12}. Each state can be characterized by its binding-energy E_B, which is the energy required to remove a proton from that state, and this can be determined from the energy balance equation

$$E_0 = E_1 + E_2 + E_R + E_B, \tag{1}$$

where E_0 is the energy of the incident proton, E_1 and E_2 are the energies of the outgoing protons and E_R is the kinetic energy of the recoil nucleus. Since E_R is of the order of 1 MeV which is small compared with the observed differences in E_B for different proton states in C^{12} it may be neglected in the equation, and if we measure E_1 and E_2 the binding-energy E_B is determined and the state is specified. We can then proceed to study the reaction in detail for scattering from this state.

We measure E_1 and E_2 using total-energy counters (to be called the E-counters) which can detect all protons of energy greater than 13 MeV. The experiments of Tyrén, Hillman and Maris were severely limited because they used range telescopes and detected only events in which the two proton energies were equal to some predetermined value. By using E-counters we gain in counting-rate and it is possible to study more details of the reaction.

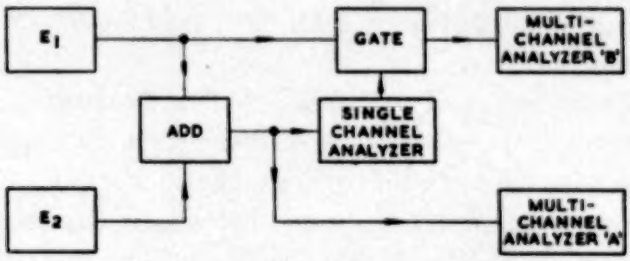

Fig. 1. Schematic diagram of the experiment.

A schematic diagram of the experiment is shown in fig. 1. The responses of the two E-counters are arranged to be linear and exactly equal, so that the pulses from them can be added electronically to give an unambiguous result for (E_1+E_2) which is displayed on the multichannel analyzer A. A typical spectrum for carbon is shown in fig. 4 together with the peak for scattering from hydrogen to show the energy resolution of the experiment. For hydrogen the summed peak is at the energy of the incident beam because the struck proton is unbound and no energy is lost in the reaction. There are two peaks in the carbon spectrum, 16 MeV and 34 MeV below the incident energy of 153 MeV, corresponding to events in which protons are knocked out of the p-state and s-state respectively. The arrow indicates the point below which we might detect competing reactions in which a deuteron or third particle may be emitted. The p-state peak is unambiguously due to (p, 2p) events and we do not need special counters to discriminate against deuterons. For a fuller discussion of the binding energy spectrum see section 4.

In order to study E_1 and E_2 separately for p-state events, we feed the summed pulse into a single-channel analyzer which when E_1+E_2 is equal to 137 MeV opens a gate for E_1 to be displayed on the mutli-channel analyzer B. Since E_1+E_2 is specified we have then measured for each p-state event the energies

of both protons emitted at definite angles relative to the incident beam. With both energies and angles measured the kinematics of each event is completely specified, including the recoil momentum of the residual nucleus.

In our experiment we fix the angle of one counter and measure the energy spectra of protons in that counter for a wide range of angles of the other counter. These spectra give the angular correlations for all p-state events and for p-state events in which the energy is shared between the two protons in specified ways. We also study the effect on these angular correlations of the angle of the fixed counter.

3. Apparatus and Procedure

An unpolarized beam of about 2×10^7 protons per second was extracted from the Harwell 2.8 m synchrocyclotron and focused by magnetic quadrupoles to a 1.3 cm diameter spot at the centre of a vacuum scattering chamber (see fig. 2).

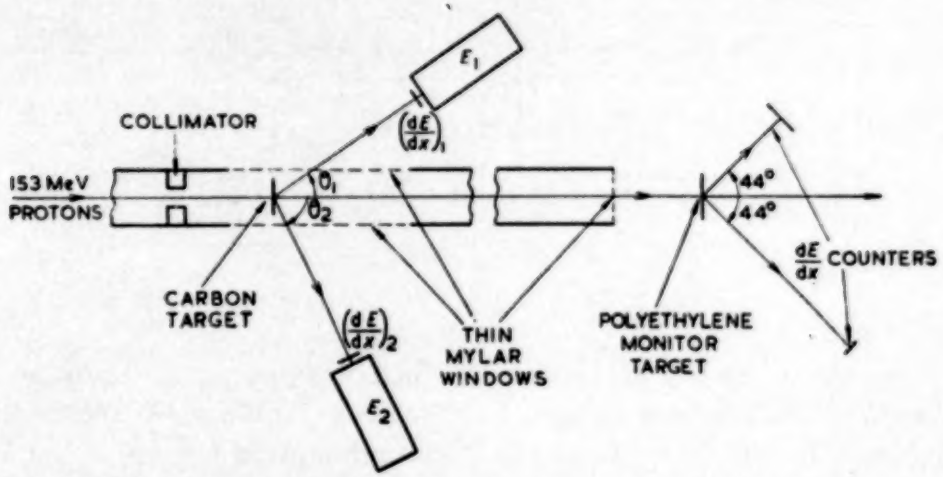

Fig. 2. Schematic diagram of the vacuum chamber and arrangement of counters. This diagram is not drawn to scale.

A circular collimator of 2 cm diameter was used to remove any protons outside the main beam. The mean energy of the beam was 153 MeV and the energy spread was 7 MeV full-width at half-height. The target consisted of a 0.143 g/cm² sheet of graphite which, in order to minimise the energy lost by the outgoing protons, could be rotated to any angle relative to the incident beam. The vacuum chamber was 5 cm square in cross-section with 0.005 cm Mylar side windows and extended about four feet behind the target to eliminate scattering from the air. The beam after emerging from the vacuum chamber was monitored by scattering from a 0.083 g/cm² polyethylene target with dE/dx-counters placed at 44° on either side of the beam. Because of the extent of the beam spot at the monitor target, the solid angle subtended by one counter was made considerably larger than that subtended by the other.

The protons leaving the carbon target were defined in angle and direction by circular dE/dx-counters subtending solid angles of about 0.01 steradians at the target. These counters were mounted on arms which could be rotated about the target from 15° to 165° on either side of the beam. The arms were aligned visually and with X-ray films, to an accuracy of about one degree. The dE/dx-counters were made from plastic scintillator NE 102, 0.125 cm thick, coupled to RCA 7264 photomultipliers.

A block diagram of the electronics is shown in fig. 3. Because of their reliability and ease of construction we have used transistorized circuits everywhere

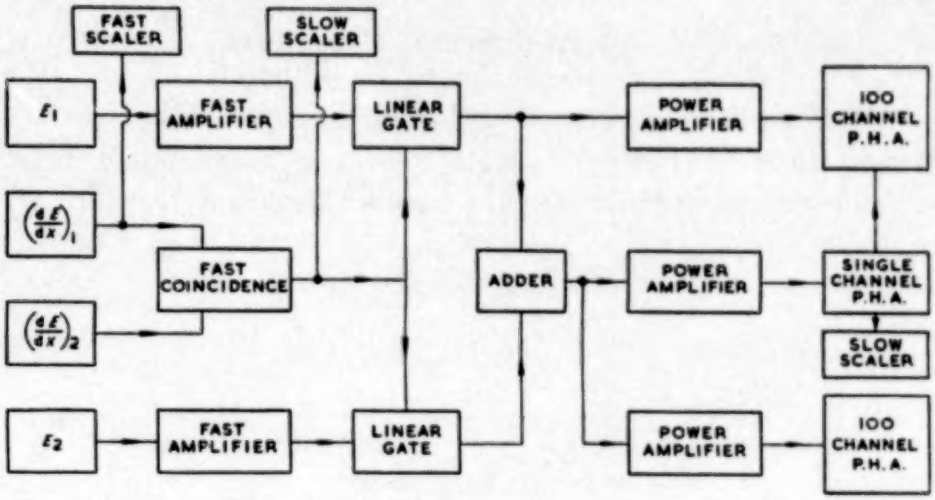

Fig. 3. Block diagram of the electronics.

except for the pulse-height analyzers which were standard equipment. The transistorized circuits were designed by Candy, Chaplin, Cole and Owens and are discussed in refs. [9–12]). The two dE/dx-pulses were fed into a coincidence circuit [9]) whose resolving curve was 7 nsec wide at half-height with a flat top of 6 nsec. The resolving time could not be made very short because of the finite times taken by protons of different energies to reach the detectors, 30 cm from the target. Two protons of 20 MeV and 120 MeV would differ in their times of flight by about 2.7 nsec, so that the coincidence resolving time (2τ) must be at least 5.4 nsec.

The energies of the two protons were found by measuring the light outputs when they were stopped in NE 102 plastic scintillators. We have shown [13]) that by introducing a thin absorber in front of a plastic scintillator the light output from the scintillator can be made a linear function of the proton energy incident on the absorber. The absorber in each case was the dE/dx-counter which together with thin windows and the air path would just stop 13 MeV protons. The E-counters were cylinders of NE 102, 7.5 cm in diameter and 18 cm long, coupled through a short light guide to EMI 9531B photomultipliers. The pulses taken from the anodes of the photomultipliers at a maximum level of 2 mA

into 100 Ω were 50 nsec long at the base and were passed through linear gates [10]) opened for 60 nsec by the output of the dE/dx-coincidence circuit.

The peak counting rates in the dE/dx-counters were determined at each setting of the counters with a 20 MHz transistorized scaler [11]). By reducing the beam the counting rates were kept below 500 per sec; with a duty cycle of 0.8 % this corresponds to a peak counting rate of about 6×10^4 per sec. At each coincidence input the dead time was about 10^{-7} sec and the percentage loss of coincidences was less than 2 %. The dead times at the outputs of the coincidence circuit and linear gates were 10 μsec and 50 μsec respectively, and for our observed coincidence rate of about one per sec the loss was negligible. The random coincidence-rates were determined by delaying the output pulses from one pair of dE/dx- and E-counters by an integral number of r.f. cycles of the machine. The random coincidence rate was never greater than 20 % of the total and the beam intensity was constant within 5 % so that the subtraction of random events was reliable within 2 % of the real counting rate.

Since the coincidence rate was very low there was no necessity for fast circuitry after the linear gates, so the fast pulses from the gates were stretched to about 2 μsec by the gate amplifiers. The maximum pulse height from these amplifiers was kept below 5 V so that the transistorized circuits could be given an output impedance of 100 Ω without requiring excessive power dissipation in the transistors. Where it was necessary to use standard electronic equipment such as the pulse-height analyzers the pulses were amplified to 50 V maximum by transistorized power amplifiers [10]). The gates were linear within $\frac{1}{2}$ % of the maximum signal and the pedestal was less than $\frac{1}{2}$ % of this maximum signal. The amplifiers used in various parts of the system were found to be linear within 0.2 % of the maximum signal. All the amplifiers employed negative feedback over rings of two or three to give stability and no trouble was experienced in this respect.

For obtaining the summed spectrum the important criterion is that pulses reaching the adder for a fixed proton energy in either E-counter shall give the same output from the adder. The electronics was first set up using a pulse generator so that equal pulses fed into the two gates separately gave equal outputs from the gate amplifiers and from the adder. The gains of the power amplifiers were set equal and the relative calibration of the single-channel and multi-channel pulse-height analyzers was determined.

The final adjustments were made by scattering the beam from the hydrogen in a polyethylene target. The two counters were set at 30° and 58° to the incident beam, so that protons of 112 and 41 MeV were detected in coincidence, and the summed spectrum was recorded. The angles of the counters were interchanged and any unbalance of the system showed up as a shift in the summed peak. This check was applied frequently throughout the experiment and adjustments were made when necessary by altering the voltage on one photomultiplier.

The window of the single-channel pulse-height analyzer was set to select summed pulses corresponding to p-state events. The output from the analyzer could be used to gate either multichannel analyzer, and by self-gating the summed spectrum the setting of the window (shown in fig. 4) was checked. The summed spectrum was normally displayed ungated while the spectrum from one of the counters was displayed on the gated analyzer which was calibrated by scattering at various angles from hydrogen.

Measurements were made at a variety of angles for the two counters. With one counter fixed the angle of the other counter was varied between 15° and 80° relative to the proton beam. This was repeated for several angles of the fixed counter. Combinations such as (30°, 40°) and (40°, 30°) must give the same information and where such measurements were duplicated the results always agreed within the statistical error. In order to estimate the total cross-section for the reaction some measurements were made with one counter raised out of the plane defined by the incident beam and the other proton.

4. The Binding Energy Spectrum

The energy balance for the (p, 2p) reaction is given by eq. (1). The binding energy E_B may be split into two parts

$$E_B = Q + E^*, \tag{2}$$

where Q is the energy required for the reaction if the residual nucleus is left in its ground state, while E^* is the excitation energy of the residual nucleus.

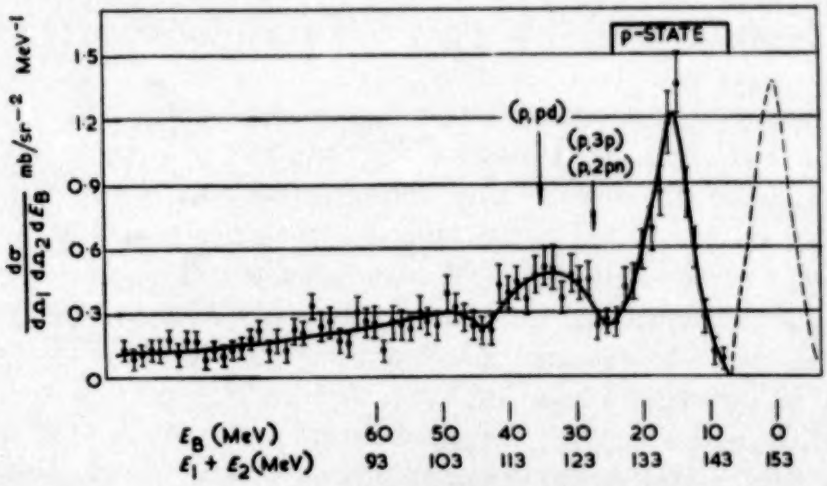

Fig. 4. A typical spectrum of $(E_1 + E_2)$ for carbon, measured at (40°, 30°). The counting statistics for the points are displayed while the absolute error on the cross-section is ±20 %. The arrows indicate the points below which reactions other than (p, 2p) reactions may be detected, and the bracket shows selected p-state events. The spectrum for free p−p scattering is shown dotted for comparison.

The summed spectrum for carbon given in fig. 4 is typical of the spectra obtained at all pairs of angles for the two counters, with two main peaks at $E_B = 16$ MeV and 34 MeV. The binding-energy calibration is accurate to ± 3 MeV, neglecting the recoil energy E_R which is of the order of 1 MeV. Since the Q-value for the reaction $C^{12}(p, 2p)B^{11}$ is 15.96 MeV, events in the first peak must leave the B^{11} nucleus in its ground state or in states near the ground state while for the second peak the nucleus is left in excited states near 18 MeV. The energy resolution of the experiment, shown in the peak obtained for scattering from hydrogen is about 7 MeV, which is the spread of the incident beam. It would thus be impossible to identify the individual states in B^{11} which are produced.

On the single-particle shell model, if a p-state proton is removed from C^{12} the ground state of B^{11} remains, while the removal of an s-state proton results in a broad state at high excitation. Accordingly we interpret events in the two peaks as those in which the incident proton knocks out p-state and s-state protons respectively. Because of correlations between the struck proton and individual particles in the nucleus, the single-particle shell-model is not an exact description and the residual B^{11} may be left in one of a group of levels near the theoretical single-hole states. One would expect, particularly in the p-state peak where individual states must be sharp, to see fine structure. However, for measuring the angular correlations it is not necessary to consider the fine structure of the p-state so our broad resolution is not a disadvantage.

We have to consider the likelihood of detecting events other than (p, 2p) interactions, because our counters do not distinguish between protons and other charged particles and because an undetected third particle may have been emitted. The Q-values for the most likely competing reactions are

$$\begin{aligned} C^{12}(p, 2p)B^{11} &\quad - \quad 15.96 \text{ MeV}, \\ C^{12}(p, pd)B^{10} &\quad - \quad 25.19 \text{ MeV}, \\ C^{12}(p, 3p)Be^{10} &\quad - \quad 27.19 \text{ MeV}, \\ C^{12}(p, 2pn)B^{10} &\quad - \quad 27.42 \text{ MeV}. \end{aligned}$$

Deuterons give the same response from the counters as protons of about 10 MeV less energy [13]), so that (p, pd) events cannot appear in the summed spectrum at binding energies less than about 35 MeV. The (p, pd) reaction should give peaks in the summed spectrum and this may be the explanation of a broad peak which always appears at $E_B \approx 50$ MeV. Scattering from the s-state leaves B^{11} in unbound states which decay by evaporation of slow neutrons, protons or other particles so that s-state events are usually of the form (p, 2px) where x is a slow particle. There may, however, be some events in which three fast nucleons are emitted and since only two particles are detected these events will give a broad background in the spectrum at high binding energies. These events can

occur when one of the outgoing protons is scattered inside the nucleus, and their theoretical description is difficult.

Events with binding-energy less than 27 MeV are unambigously (p, 2p) interactions and we have chosen to study these in detail. By studying the p-state peak alone we simplify the theoretical analysis of the results.

5. Cross-sections

The absolute values of the differential cross-sections were determined to an accuracy of $\pm 20\,\%$ by comparison with the monitor counting-rate and the known p—p cross-section.

A correction has to be applied for nuclear absorption in the E-counters since inelastic collisions with carbon nuclei in the scintillator will lead to loss of light and produce a tail on the pulse-height distribution. The percentage of inelastic collisions in a plastic scintillator for 10, 40 and 68 MeV protons has been measured [14]) and we have calculated it up to 150 MeV from the known total reaction cross section in carbon [15–17]). We have neglected the small effect due to the hydrogen in the scintillator. Fig. 5 shows the percentage of events

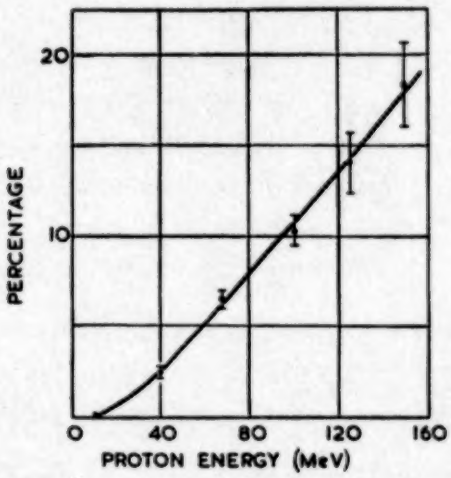

Fig. 5. The percentage of protons of a given energy which gives less than the full light output when stopped in a plastic scintillator.

degraded from the peak for incident protons of different energies. In our experiment we detect two protons whose total energy is approximately 137 MeV by gating on the summed peak and an inelastic scattering in either counter will cause the loss of an event. The percentage loss of coincident events for various combinations of energies is given in table 1. The percentage loss of p-state events is thus independent of the way the total energy is shared, and an overall increase in the cross-sections may be made to allow for it. Because this factor is constant the single energy spectra are not distorted in any way.

TABLE 1

The correction to be applied to the cross-sections to allow for nuclear absorption in the E-counters

E_1(MeV)	% loss	E_2(MeV)	% loss	% loss of events
20	0.6±0.1	117	13.0±1.5	13.5±1.5
40	2.5±0.2	97	10.3±0.8	12.6±0.8
68.5	6.5±0.5	68.5	6.5±0.5	12.6±1.0

We have to consider the effect of our finite angular resolution on the cross-sections. The coordinate system for the experiment is shown in fig. 6, the differential cross-section

$$\frac{d\sigma}{d\Omega_1 d\Omega_2}(\theta_1, \theta_2)$$

being measured for $\phi_2 = 0$ in which case the two counters are coplanar with the incident beam. If the angular correlations as θ_2 and ϕ_2 are varied are much

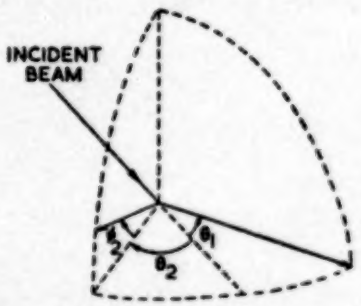

Fig. 6. The coordinate system used to integrate the differential cross-sections.

broader than the angular resolution of the experiment, no corrections will have to be applied. The angular resolution was tested for free p—p scattering in a polyethylene target. With $\theta_1 = 44°$ and $\phi_2 = 0$ the counting rate was plotted as a function of θ_2, giving a resolution curve with full-width at half-height of 7°, whereas the coplanar angular correlations for p-state events in carbon are all 40°—50° wide (fig. 7). With θ_1 and θ_2 fixed at 44° the resolution curve as ϕ_2 is varied has a full-width at half-height of 10°, slightly greater than in the plane because of the finite extent of the beam. To test the adequacy of this angular resolution some measurements were made for non-coplanar p-state events. With θ_1 and θ_2 fixed at 40° the counting rate of p-state events dropped to half when ϕ_2 was changed to ±25°, and the same result was obtained when θ_1 and θ_2 were both 20°. Thus the angular correlations for both coplanar and non-coplanar events are much broader than the angular resolution, and the correlations and differential cross-sections should not be distorted.

In order to integrate the differential cross-section it is necessary to make some assumption about the angular correlations for non-coplanar events at values of θ_1 and θ_2 for which they have not been measured. The above results at (20°, 20°) and (40°, 40°) suggest that they do not vary very much. We assume that the angular correlations as ϕ_2 is varied are independent of θ_1 and θ_2 and, for simplicity, that the cross-section is constant for $|\phi_2| < 25°$ and zero for $|\phi_2| > 25°$. When the angle of the first proton is fixed we integrate over the solid angle $d\Omega_2$ for the second proton using the coordinate system of fig. 6, where the element of solid angle $d\Omega_2$ is $\cos\phi_2\, d\theta_2 d\phi_2$. For integrations over $d\Omega_1$, we use the normal system of spherical polar coordinates (θ'_1, ϕ'_1) in which the direction of the beam is taken as polar axis. θ'_1 is, of course, equal to θ_1.

The differential cross-section for emission of protons from p-state events into a counter at θ_1 is then

$$\frac{d\sigma}{d\Omega_1}(\theta_1) = \int_{-25°}^{+25°} \cos\phi_2 d\phi_2 \int_0^{\pi} \frac{d\sigma}{d\Omega_1 d\Omega_2}(\theta_1 = \text{const.},\ \theta_2) d\theta_2.$$

We can also obtain the cross-section for p-state events with a given separation angle between the outgoing protons. Since ϕ_2 is not very large, the separation angle is very nearly $\theta_1+\theta_2$.

$$\frac{d\sigma}{d(\theta_1+\theta_2)} = \int_{-25°}^{+25°} \cos\phi_2 d\phi_2 \int_0^{\pi} d\phi'_1 \int_0^{\pi} \frac{d\sigma}{d\Omega_1 d\Omega_2}(\theta_1+\theta_2 = \text{const.},\ \theta'_1) \sin\theta'_1 d\theta'_1,$$

where the integral over ϕ'_1 extends from 0 to π to allow for the fact that two protons are emitted in each event. This expression may be further integrated over $(\theta_1+\theta_2)$ to give the total cross-section for p-state events. The results of these integrations are given in the next section.

6. Results

In our results each measurement, except where otherwise stated, is displayed with the error due to counting statistics while the absolute scale for the differential cross-sections is uncertain within ±20 %. The lines through the points are intended to guide the eye; they have no theoretical significance.

Fig. 7 shows the angular correlations for coplanar p-state events, displayed for six values of θ_1 and plotted as a function of the separation angle $(\theta_1+\theta_2)$ between the two outgoing protons. The differential cross-section $d\sigma/d\Omega_1 d\Omega_2$ represents the total number of p-state coincidences at a given pair of angles (θ_1, θ_2) and is tabulated in table 2. The angular correlations are peaked, with a width at half-height of 40°—50°. Since they have a similar width out of the plane of scattering (see section 5) this means that the second proton tends to be emitted into less than 5 % of the total solid angle (4π) available, and strongly

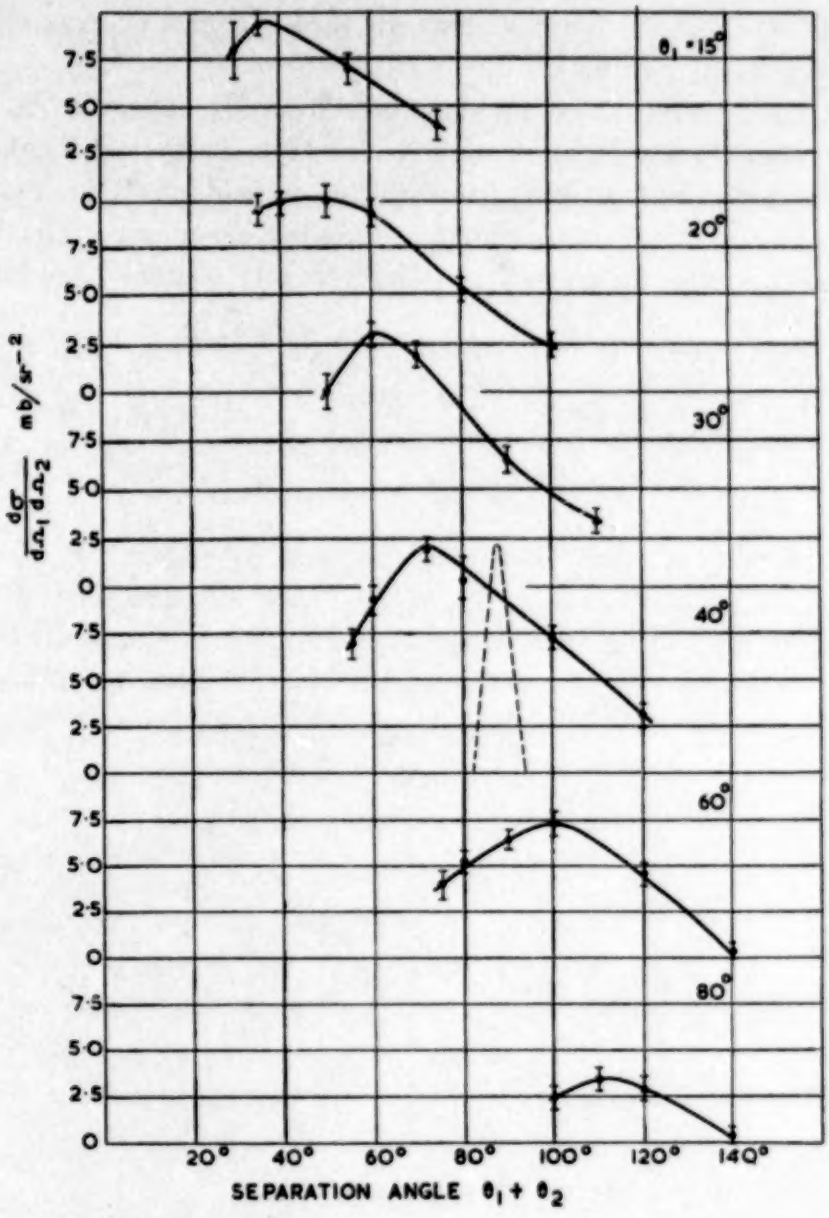

Fig. 7. The differential cross-section for coplanar p-state events for 6 values of θ_1. The angular resolution for free p−p scattering is shown dotted. The relative errors are equal to the statistical errors displayed, while the absolute error on the cross-section is ±20 %. These results are tabulated in table 2.

TABLE 2

The differential cross-section $d\sigma/d\Omega$, $d\Omega_2$ in mb · sr^{-2} for coplanar p-state events at angles θ_1 and θ_2 relative to the proton beam. The absolute scale for these cross-sections is uncertain to ±20 %.

θ_1 \ θ_2	15°	20°	30°	40°	60°	80°
15°	8.0±1.5	9.3±0.7		7.1±0.7	3.9±0.7	
20°	9.3±0.7	9.9±0.5	10.1±0.7	9.3±0.7	5.2±0.5	2.5±0.5
30°		10.1±0.7	13.1±0.5	11.8±0.5	6.5±0.5	3.6±0.5
40°	7.1±0.7	9.3±0.7	11.8±0.5	10.4±1.0	7.3±0.5	3.0±0.5
60°	3.9±0.7	5.2±0.5	6.5±0.5	7.3±0.5	4.4±0.5	0.3±0.3
80°		2.5±0.5	3.6±0.5	3. 0±0.5	0.3±0.3	

supports the idea that the reaction proceeds through quasi-elastic p—p scattering inside the carbon nucleus.

The striking feature of the angular correlations is, however, the marked dependence on θ_1 of the separation angle for the peak. This effect is not expected from the kinematics of scattering from stationary protons. If the momenta of the incident and outgoing protons are $\mathbf{p}_0$, $\mathbf{p}_1$ and $\mathbf{p}_2$ the momentum and energy conservation equations for scattering from stationary protons bound by E_B are

$$\mathbf{p}_0 = \mathbf{p}_1+\mathbf{p}_2, \quad p_0^2 = p_1^2+p_2^2+2mE_B.$$

Hence

$$\cos(\theta_1+\theta_2) = \frac{mE_B}{p_1p_2}.$$

If $E_B = 0$ this reduces to free p—p scattering and $(\theta_1+\theta_2) = 90°$, while for $E_B = 16$ MeV the separation angle is slightly less than 90°. The separation angles for the peaks of fig. 7 are plotted in fig. 8 as a function of θ_1 and the non-relativistic separation angles for free and bound p—p scattering are shown for comparison.

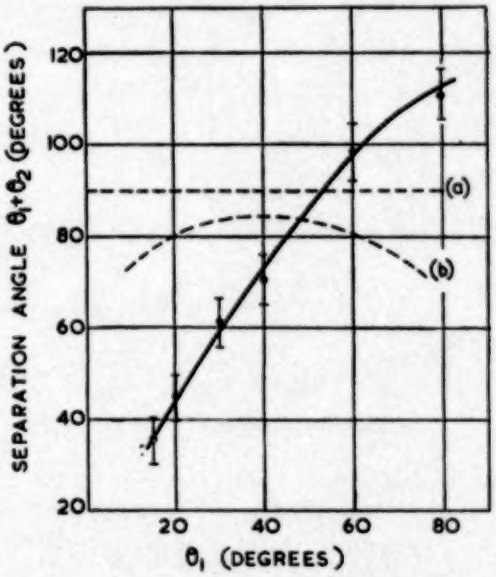

Fig. 8. The separation angle $(\theta_1+\theta_2)$ for the maximum cross-section when one counter is set at θ_1, plotted as a function of θ_1. The non-relativistic separation angles for scattering from stationary protons are shown for two cases: (a) free protons, (b) protons bound by 16 MeV.

The differential cross-section for the special case $\theta_1 = \theta_2$ and the maximum cross-section for particular values of θ_1 are plotted in figs. 9(a) and (9b). It will be seen that the maximum counting-rate occurs when both counters are at 30°. The differential cross-section as a function of both θ_1 and θ_2 is shown in fig. 10 as a contour diagram. This shows that for any value of θ_1 or θ_2 the maximum

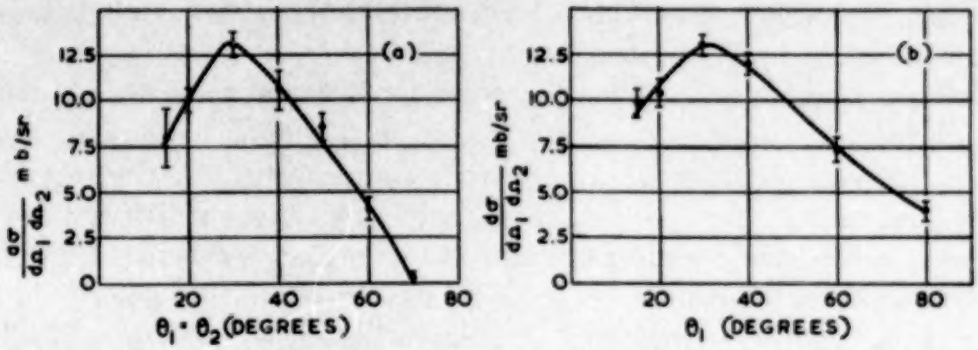

Fig. 9. (a) The differential cross-section for coplanar p-state events for the special case $\theta_1 = \theta_2$.
(b) The maximum cross-section observed for different values of θ_1. The value of $(\theta_1+\theta_2)$ at which this maximum occurs is plotted in fig. 8.

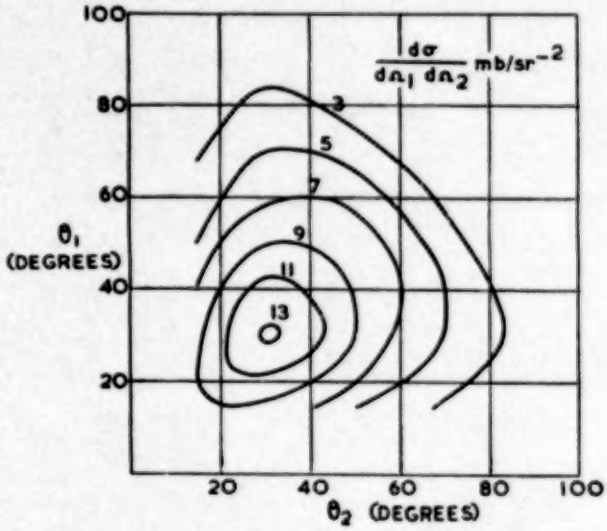

Fig. 10. The differential cross-section for p-state events as a function of θ_1 and θ_2 displayed as a contour diagram.

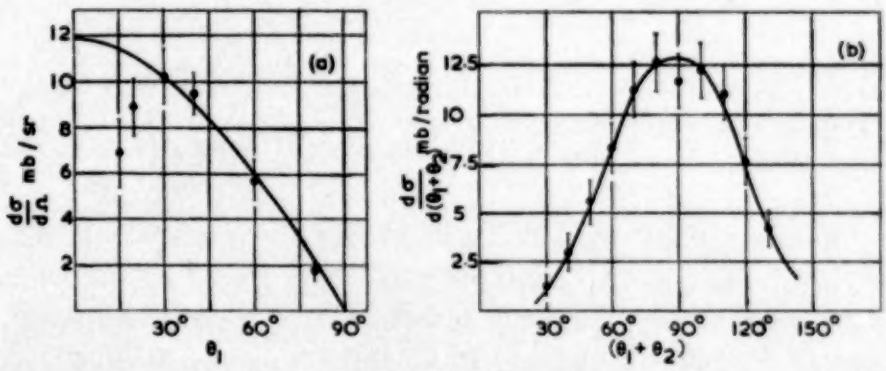

Fig. 11. (a) The cross-section for emission into a counter at θ_1 of one of the protons from a p-state event. The laboratory cross-section for free p−p scattering, normalized to the point at 30°, is shown for comparison.
(b) The cross-section for p-state events with the separation angle $(\theta_1+\theta_2)$. The approximations made in obtaining these cross-sections are described in the text.

counting-rate occurs when the other counter is near 30°, with the overall maximum when both counters are at 30°.

The differential cross-section for emission into a counter placed at θ_1 of one of the protons from a p-state event is shown in fig. 11 (a) together with the differential cross-section in laboratory space for free p—p scattering, normalized to the point at 30°. Except at small angles the two angular distributions have much the same form, and in particular there are very few events beyond 90°. The cross-section for p-state events with a given separation angle $(\theta_1+\theta_2)$ is shown in fig. 11(b). The most probable separation angle is seen to be about 90°,

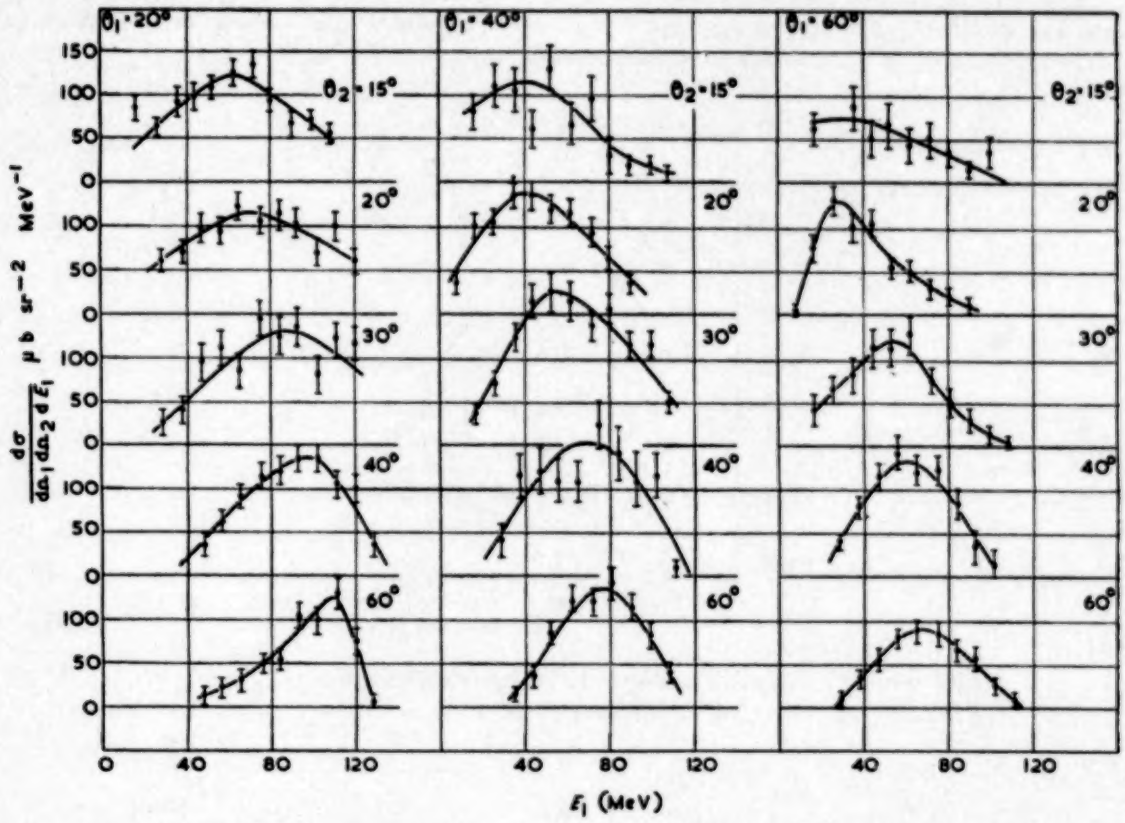

Fig. 12. The energy spectra of protons detected at θ_1 for p-state events in which the second proton is detected at various values of θ_2. The relative errors are equal to those displayed, while the absolute error on the cross-section is ±20 %. These results are tabulated in table 3.

which is the separation angle obtained in free p—p scattering. The results shown in figs. 11(a) and 11(b) are obtained from the angular correlations of fig. 7 by the integrations described in section 5. The errors displayed include counting statistics and uncertainty in extrapolating the angular correlations but not the absolute error of ±20 % in the monitor. These results will be distorted if detailed measurements show the assumption made about the non-coplanar angular correlations to be untrue.

Integration of fig. 11(b) over $(\theta_1+\theta_2)$ gives the total cross-section for p-state

events as 16 ± 4 mb. The uncertainty quoted includes all known errors but the figure may be altered significantly if the non-coplanar angular correlations do in fact vary very much. This total cross-section is about two thirds of the cross-section for free p—p scattering. Since there are expected to be four p-state protons in C^{12} the effect of nuclear absorption is to reduce the cross-section by a factor of ≈ 6.

TABLE 3

The differential cross-section $d\sigma/d\Omega_1 d\Omega_2 dE_1$ in $\mu b \cdot sr^{-2} \cdot MeV^{-1}$ for coplanar p-state events at angles θ_1 and θ_2 relative to the proton beam. The absolute scale for these cross-sections is uncertain to ± 20 %

E_1, E_2 (MeV)	$\theta_1 = 20°$ $\theta_2 = 15°$	20 20	30 20	40 20	60 20	40 15
17, 120	86±11	60±12	112±21	100±13	74±12	80±20
26, 111	61±10	100±16	119±21	105±13	130±16	110±25
35, 102	92±16	70±14	81±21	135±15	100±14	105±25
44, 93	98±14	102±16	134±21	135±15	104±15	60±20
53, 84	108±13	112±16	126±21	120±14	54±10	130±27
62, 75	123±16	106±16	146±21	115±14	50±10	65±20
72, 65	133±16	122±16	86±19	93±13	32± 8	90±25
81, 56	93±14	94±15	111±21	62±10	22± 7	30±20
90, 47	66±13	98±15	96±20	33± 7	12± 5	20±10
99, 38	71±11	72±13	39±16			20±10
108, 29	53±12	60±12	27±14			10± 5
E_1, E_2 (MeV)	$\theta_1 = 40$ $\theta_2 = 32$	40° 60°	40 40	60 15	60 30	60 60
17, 120	36± 9			59±22	39±13	5± 3
26, 111	71±12	4± 3	7± 7		65±16	12± 5
35, 102	126±16	17± 6	113±27	84±26	81±18	24± 6
44, 93	163±18	35± 8	107±27	50±21	113±20	53±10
53, 84	173±18	84±12	140±34	67±24	112±20	65±10
62, 75	163±18	122±14	173±34	42±19	127±21	85±11
72, 65	136±16	122±14	107±27	50±21	75±16	87±12
81, 56	155±17	142±17	107±27	34±17	49±14	80±11
90, 47	115±15	116±15	120±27	17±12	29±10	55±10
99, 38	113±15	82±12	113±29	34±17	13± 8	34± 7
108, 29	48±10	39± 9	40±20		4± 4	10± 4

Fig. 12 and table 3 show the energy spectra of the protons detected in the counter at θ_1 for various values of θ_2. Consider the five spectra with $\theta_1 = 20°$: when θ_2 is also 20° the spectrum is symmetrical about 68.5 MeV, as it must be since the two counters are identical. When θ_2 is increased the peak moves to higher energies, indicating that when the counters are at unequal angles the higher-energy protons tend to appear at the forward angle. This feature is again in agreement with the idea of quasi-elastic scattering, and it is reproduced through all the spectra. From these energy spectra we can derive angular correlations for p-state events in which the total energy is shared between the two

protons in specified ways. These may be simpler to interpret theoretically than the correlations for all events. Fig. 13 shows these angular correlations for three values of θ_1, and five values of E_1. The corresponding energy E_2 is of course 137 MeV$-E_1$. The most prominent feature of these angular correlations is the way in which the peaks move from small angles to large angles as E_1 is increased. This is the same effect as mentioned before: the higher energy protons tend to be emitted at the smaller angle.

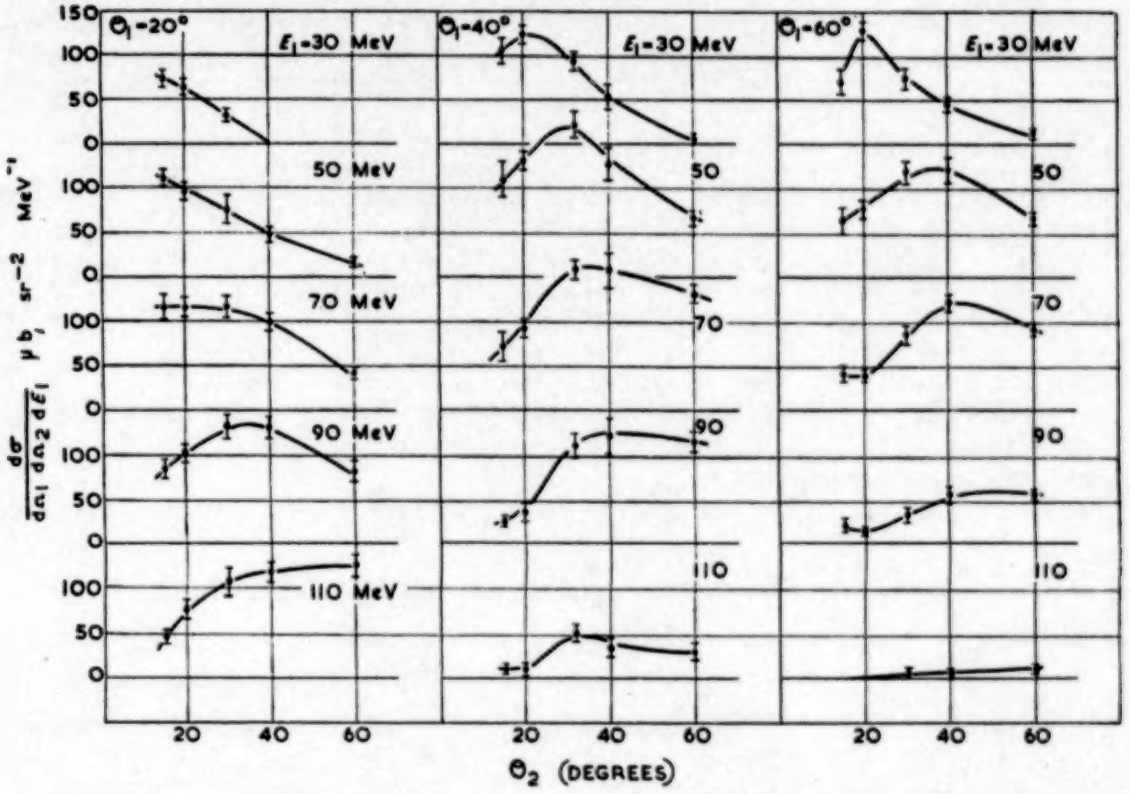

Fig. 13. Angular correlations for coplanar p-state events in which the proton emitted at θ_1 has the fixed energy E_1. The energy E_2 is 137 MeV$-$E$_1$. These correlations are derived from the data displayed in fig. 12.

7. Discussion

The results suggest strongly that the reaction proceeds by the mechanism of quasi-elastic scattering: the angular correlations are sharply peaked and the events are almost coplanar; very few protons are emitted at angles greater that 90° relative to the incident beam and the angular distribution is roughly the same as for free p$-$p scattering; the most probable separation angle between the outgoing protons is near 90°, and the higher energy proton tends to be emitted in the forward direction. The only apparent contradiction is the striking dependence of the separation angle $(\theta_1+\theta_2)$ on θ_1. This cannot be explained on the basis of scattering from stationary protons. However, one

can see qualitatively how it may be caused by the momentum distribution of the struck protons. Assuming the impulse approximation and neglecting the distorting effects of the nuclear potential one can consider the interaction as p—p scattering with a non-stationary target proton. In scattering from stationary free protons the separation angle between the outgoing protons is always 90°. If the struck proton is moving forward the modified centre-of-mass transformation reduces the angles of both protons. Thus if we set a counter at an angle relative to the proton beam of less than about 45° we are more likely to detect collisions with forward-going protons than with stationary or backward moving ones. The observed separation angle is therefore less when one of the protons is detected at a small angle. Similarly when the counter is set at a backward angle we are more likely to detect collisions with backward moving protons and the separation angle will be greater than 90°.

The importance of absorption in the reaction is illustrated by the fact that the total cross-section is roughly a factor of 6 less than the value expected in its absence. Nuclear absorption will have different effects for protons removed from different parts of the nucleus and thus the spatial distribution of p-state protons inside the nucleus has to be considered. Because of the centrifugal force p-state protons will be on the average nearer the surface than s-state protons, and the absorption will be different for scattering from protons in these states [18]). Refraction and reflection are likely to modify the angular correlations to some extent. Because we have such comprehensive experimental data available, comparison with a good quantum-mechanical calculation should give a great deal of information on the effects of refraction, reflection and absorption and on the momentum distribution of the p-state protons in C^{12}.

Nuttall and Riley [7]) are performing such a calculation. They consider the interaction as taking place in a complex energy-dependent Saxon-Woods potential and calculate exactly the distortion of the incoming and outgoing proton waves by that potential, for partial waves up to $l = 8$. Their preliminary results are in good agreement with our experimental measurements, but we must await their final calculations before making a detailed comparison. Meanwhile, in collaboration with Mr. K. F. Riley, we have investigated the effects of the momentum distribution and the necessity for including a detailed treatment of distortion. We have repeated Riley's 80 MeV WKB-calculation[19]) for 153 MeV incident protons. This reproduces the dependence of the angular correlations on θ_1 successfully. The effect is not changed when we replace the energy-dependent potential by a static potential nor when we alter the radius of the well while leaving the momentum distribution unchanged. A Born-approximation calculation gives the same general trend, provided we include a reasonable momentum distribution.

The Born approximation gives marked structure in the differential cross-sections which is considerably smoothed out in the WKB-calculations. This

structure is not observed in the experiment and it is not predicted by the partial waves analysis. We therefore conclude that the dependence of separation angle on θ_1 is due to the momentum distribution of the struck protons but that it is necessary to use the partial waves analysis to make detailed deductions from the experimental results.

The results of the W K B and Born approximation calculations are published in the following paper [8]).

We wish to thank Mr. R. G. C. Artus for help in constructing the apparatus and in making measurements, Mr. K. F. Riley for both experimental and theoretical assistance, Dr. G. B. B. Chaplin, Dr. C. J. N. Candy, Mr. A. J. Cole and Mr. A. R. Owens for designing the transistorized circuits, Dr. J. P. Schiffer, Mr. B. Rose and Dr. T. H. R. Skyrme for helpful discussions, and the cyclotron crew for providing a proton beam.

References

1) O. Chamberlain and E. Segré, Phys. Rev. **87** (1952) 81
2) J. B. Cladis, W. N. Hess and B. J. Moyer, Phys. Rev. **87** (1952) 425
3) J. M. Wilcox and B. J. Moyer, Phys. Rev. **99** (1955) 875
4) L. S. Azghirey *et al.*, Nuclear Physics **13** (1959) 258
5) R. J. Griffiths and R. M. Eisberg, Nuclear Physics **12** (1959) 225
6) H. Tyrén, P. Hillman and A. J. Maris, Nuclear Physics **6** (1958) 10
7) J. Nuttall and K. F. Riley, to be published
8) K. F. Riley, H. G. Pugh and T. J. Gooding, Nuclear Physics **18** (1960) 65
9) G. B. B. Chaplin and C. J. N. Candy, Nuclear Instruments **5** (1959) 242
10) G. B. B. Chaplin and A. J. Cole, Nuclear Instruments (to be published)
11) A. R. Owens, A. J. Cole and P. E. Dolley, Nuclear Instruments (to be published)
12) G. B. B. Chaplin, C. J. N. Candy and A. J. Cole, Proc. I.E.E. **106** B, no. 2892 (1959)
13) T. J. Gooding and H. G. Pugh, Nuclear Instruments (to be published)
14) D. H. Service, Minnesota Progress Report, November 1958
15) J. M. Cassels and J. D. Lawson, Proc. Phys. Soc. A **67** (1954) 125
16) T. J. Gooding, Nuclear Physics **12** (1959) 241
17) R. M. Eisberg, Proceedings of the Florida Optical Conference 1959
18) Th. A. J. Maris, Nuclear Physics **9** (1958—59) 577
19) K. F. Riley, Nuclear Physics **13** (1959) 3

2.F

Nuclear Physics **18** (1960) 65—74; © *North-Holland Publishing Co., Amsterdam*

Not to be reproduced by photoprint or microfilm without written permission from the publisher

QUASI-ELASTIC SCATTERING OF 153 MeV PROTONS BY p-STATE PROTONS IN C^{12}
II. Theoretical

K. F. RILEY †, H. G. PUGH and T. J. GOODING
AERE, Harwell, Berks.

Received 31 March 1960

Abstract: The cross-section for the reaction $C^{12}(p, 2p)B^{11}$ is calculated for events in which the residual nucleus is in its ground state. The direct interaction model is used, the reaction being considered in the impulse approximation as quasi-elastic scattering. Both WKB- and Born-approximation calculations predict the general features of the reaction fairly well, confirming the validity of the above picture. The most important features to be taken into account in a more detailed calculation are investigated.

1. Introduction: Direct Interactions and the Impulse Approximation

About twelve years ago it was pointed out by Serber [1]) that when a nucleon with energy of about 100 MeV or more is incident upon a nucleus, the mean free path of the nucleon inside the nucleus is comparable with the dimensions of the nucleus. This immediately leads to the possibility that an incident nucleon (which we will consider as a proton) can pass through the nucleus unaffected, or suffering at most only a small number of scatterings. Such an approach has led to attempts to describe the scattering of the proton as the sum of the contributions from individual nucleons in the nucleus, the scatterings taking place one at a time. This model is known as the 'direct interaction model'.

In the direct interaction model it is assumed that the two-body nuclear forces which cause the scattering of the proton are the same as those for free protons and that the scattering potential can be written as

$$V = \sum_i V_i, \tag{1}$$

where V_i is the potential due to one of the nucleons in the nucleus and the sum i runs over all the nucleons. Even with the assumption of two-body forces the scattering in the presence of other particles in the nucleus is too difficult to calculate and it is usual to make a further assumption, the 'impulse approximation'.

Chew and Goldberger [2]) first introduced the impulse approximation and applied it to the problem of deuteron pick-up. The approximation consists

† On attachment from Clare College, Cambridge.

essentially of replacing the scattering amplitude for the nucleon-nucleon interaction in the presence of the other nucleons in the nucleus, by the corresponding amplitude for free nucleon-nucleon scattering. The latter amplitudes can be obtained from experimentally measured cross-sections. Such a procedure is equivalent to neglecting the difference in states of the target particles in the two cases and will be the more valid the smaller the binding energy of the bound particle is compared with the other energies involved. The leading corrections to the 'impulse approximation cross-section' have been shown by Nuttall [3]) to be of the third order in the many-body scattering operator t, so that the error introduced is not so serious as the errors introduced by other approximations, such as the neglect of multiple scattering, which introduces corrections of second order in t. The effect of multiple scattering may be approximately taken into account by the use of a complex nuclear potential through which the nucleons have to pass. The real part of the nuclear potential allows for the effect of elastic multiple scattering, while the imaginary part excludes events in which inelastic multiple scattering occurs. This method is known as the distorted wave method.

If the essential correctness of the direct interaction model can be established, we shall be furnished with a powerful method of investigating the structure of the nucleus. Such quantities as density and momentum distributions could be studied and possible correlations between nucleons within nuclei investigated.

Experimentally there is much evidence to support the direct interaction model, even at comparatively low bombarding energies. The best evidence comes from experiments in which a second particle is ejected from the nucleus with considerable energy as a result of the passage of the incident proton through the nucleus. We picture these 'quasi-elastic' events as being caused by the scattering of the initial proton by a particle in the nucleus, after which both the incident proton and the recoiling particle emerge from the nucleus. In all such experiments above 20 MeV two typical features support the idea of direct interactions. The first is that in proton induced reactions the emission of a proton as one of the final particles is much more likely than that of a neutron. If a compound nucleus were formed we would expect roughly equal numbers of protons and neutrons. The second feature is that the particles tend to be ejected in a forward direction relative to the incident beam.

Previous experiments of this type have not specified the interaction in sufficient detail for a precise analysis to be made. The state of the residual nucleus has to be determined in order to define the energy conservation equation for the reaction. This was done in the experiment of Tyrén, Hillman and Maris [4]), but they did not study the angular correlation between the two outgoing protons. Gooding and Pugh [5]) have made an extensive experimental investigation of the (p, 2p) reaction on C^{12}. For coplanar events they have, by measuring the energies of both outgoing protons, selected events which leave the residual B^{11}

nucleus in or near its ground state. For these events they have measured proton energy spectra and angular correlations between the outgoing protons over a wide range of angles. Thus it is possible to test rather rigorously any theory of the reaction. The model likely to give the best results is the direct interaction model considered in the impulse approximation, together with an optical model approximation to multiple scattering. Nuttall and Riley [6]) are performing a partial-wave analysis of this type. In this paper we investigate by means of simpler calculations the broad agreement between theory and experiment and investigate what are the most important factors to be taken into consideration in a detailed analysis.

2. The Reaction $C^{12}(p, 2p)B^{11}$

In this reaction a proton is incident upon a C^{12} nucleus and the final state consists of two free protons and some state of B^{11}. We consider the reaction as proceeding via a direct interaction between the incident proton and a proton initially bound in the carbon nucleus. On the basis of the shell model, when the ejected proton comes from the outermost shell of the target nucleus, the state of the final nucleus will be its ground state. This is likely to be a good approximation if the nearest excited state is several MeV away.

In our calculations we consider only reactions proceeding to the ground state of the B^{11} nucleus. The experimental results give cross-sections for events in which the residual nucleus is left near its ground state, but the energy resolution is such that it is not possible to distinguish individual states. However one may hope that the poor energy resolution may, as in the work of Schiffer [7]), help by averaging the cross-sections to individual states in such a way that the average cross-section is well described by the shell model.

Nuttall [3]) has shown how to use the formal theory of rearrangement collisions to obtain the reaction matrix for the (p, 2p) process in the form

$$T\delta(\mathbf{K}_1-\mathbf{K}_f) = A^{\frac{1}{2}}(\chi_f|t_{pp}|\chi_1). \tag{2}$$

Here $(\chi_f|$ is a wave function describing the two final protons moving in an optical potential, together with an antisymmetrized wave function corresponding to the final state of the residual nucleus. $|\chi_1)$ consists of the product of an antisymmetrized ground state wave function for carbon and a wave function describing the motion of the incident particle in an optical potential. The δ-function describes the necessary momentum conservation for the whole system, A is the number of nucleons in the target nucleus (in our case $A = 12$) and t_{pp} is the antisymmetrized two-body scattering operator derived from the proton-proton potential.

The optical potential to be used in describing events which involve inelastic collisions is not well determined. In the fitting of experimental data on the

inelastic scattering of protons from carbon, Levinson and Banerjee [8]) found that the real part of the optical potential had to be reduced by a factor of about $\frac{2}{3}$ compared with the value determined from elastic scattering measurements. It is obvious that some reduction is necessary since we have to remove from the optical potential the contribution of the struck proton, its complete interaction with the incident proton being contained in t_{pp}. Thus it might seem that the appropriate potential to use is either that determined by elastic scattering from B^{11}, or $\frac{11}{12}$ times the optical potential measured for C^{12}, since there are effectively eleven nucleons moving in a volume corresponding to twelve. However, Fowler[9]) has pointed out the possibility of a larger reduction in the depth of the real part of the potential in inelastic processes due to correlation structure in the nucleus, and Rodberg [10]) has suggested a similar reduction on the grounds that the short range and the symmetry and spin dependence of nuclear forces make the contribution of the proton whose effect we must remove more important than those of the other nucleons. In view of the other uncertainties involved, we make the simplest choice, of $\frac{11}{12}$ of the optical potential for carbon as determined by elastic scattering.

We have solved eq. (2) for T using various approximations and the results of these calculations are presented in the following sections. A distorted wave calculation to evaluate T is being performed [6]) and will be published in due course, together with more detailed theoretical considerations.

3. Methods of Calculation

Using the impulse approximation approach and making the zero-range approximation for the two-body scattering, we can reduce the transition amplitude T to the product of a two-body scattering amplitude and a function depending both upon the initial and final states of the nucleus and upon the wave-functions describing the nucleons moving in the nuclear potential. The use of the zero-range approximation is not a serious restriction since we determine the two-body scattering amplitude from experimentally measured p—p cross-sections.

We have, however, the difficulty of deciding what free p—p transition amplitude to use, since in the interaction of the incident nucleon with the bound particle it is not possible to conserve both momentum and energy. There is no evidence to help us to decide, and we make the assumption that the scattering is determined by the initial relative momentum of the incident and struck particle and by their centre-of-mass scattering angle. With this assumption we can use the method of transformation of transition amplitudes developed by Møller [11]) and described in ref. [12]).

We neglect Coulomb effects, and in order to simplify the calculations we have restricted ourselves to events in which the two final protons and the initial one are coplanar.

On the basis of these assumptions we have calculated the cross-section for the reaction both in Born-approximation and using a WKB-method. The transition amplitude in Born-approximation can be written down immediately:

$$T = (2\pi)^{-\frac{1}{2}} \int e^{-i\mathbf{k}_1 \cdot \mathbf{r}_1} e^{-i\mathbf{k}_2 \cdot \mathbf{r}_2} (\mathbf{r}_1, \mathbf{r}_2 | t | \mathbf{r}'_1, \mathbf{r}'_2) \phi(\mathbf{r}'_2) e^{i\mathbf{k}_0 \cdot \mathbf{r}_1'} d\mathbf{r}_1 d\mathbf{r}_2 d\mathbf{r}'_1 d\mathbf{r}'_2, \quad (3)$$

where $\mathbf{k}_1$ and $\mathbf{k}_2$ are the momenta of the two final protons and $\mathbf{k}_0$ that of the incident one, whilst $\phi(\mathbf{r})$ is the overlap function between the initial and final states of the nucleus

$$\phi(1) = \int \psi_f^*(2, \ldots, A) \psi_i(1, \ldots, A) d2 \ldots dA. \quad (4)$$

Because of the necessary momentum conservation and the zero-range approximation, the expression for $|T|^2$ reduces to a single term

$$|T|^2 = \left|(\mathbf{k}_1 - \mathbf{k}_2 | t | \mathbf{k}_0 - (\mathbf{k}_1 + \mathbf{k}_2 - \mathbf{k}_0))\right|^2 |N(\mathbf{k}_1 + \mathbf{k}_2 - \mathbf{k}_0)|^2, \quad (5)$$

where

$$N(\mathbf{k}) = (2\pi)^{-\frac{1}{2}} \int \phi(\mathbf{r}) e^{-i\mathbf{k} \cdot \mathbf{r}} d\mathbf{r}. \quad (6)$$

Thus since the Born-approximation cross-section is proportional to the product of the momentum distribution of the target nucleons, evaluated at the point $\mathbf{k}_1 + \mathbf{k}_2 - \mathbf{k}_0$, and the square of the modulus of the corresponding t-matrix-element, it is essentially the classical cross-section.

In the WKB-method of evaluating T, we consider the interaction as taking place in the nuclear potential well which represents the effect of the nucleons not directly taking part in the two-body interaction. For calculational convenience we replace the nuclear potential by an equivalent spin-independent square well in so far as strength and size are concerned. On this model the nucleons move in straight-line trajectories, suffering changes of wave number upon entering and leaving the potential well and absorption whilst traversing it. Refraction is assumed to be negligible and, using this assumption, reflection is treated approximately. This calculation has been described in ref. [12]) together with the results for 80 MeV incident protons †.

4. Numerical Values and Results

For all calculations, an $l = 1$ simple harmonic-oscillator wave-function was used for the overlap function ϕ, giving

$$\phi(\mathbf{r}) = \left(\frac{8\nu^{\frac{5}{2}}}{3\pi^{\frac{1}{2}}}\right)^{\frac{1}{2}} r e^{-\frac{1}{2}\nu r^2} Y_1^{\mu} \quad (\mu = -1, 0, 1),$$

with a variety of values of ν. In all cases summation over final spin states was carried out. The energy dependence of the potential was found by interpolation,

† The isobaric spin argument given in ref. [12]) is incorrect and no factor $\frac{1}{2}$ appears in the cross-section.

from the values given by Glassgold and Kellogg [13]) for the elastic scattering of protons by carbon. The free p—p scattering cross-section was taken from the data compiled by Hess [14]), and a value of 16 MeV was taken for the binding energy of a p-shell proton in carbon.

Using a value of 2.8×10^{-13} cm for the radius R of the optical potential, and a value of $\nu = 0.3741$ chosen to fit Hofstadter's data [15]) for electron scattering from carbon, the cross-section was calculated in the WKB-approximation for an incident energy of 153 MeV and a variety of angles. Three values of θ_1 (see fig. 1) were used, 20°, 40° and 60°.

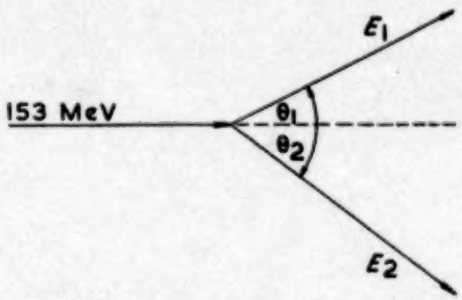

Fig. 1. The co-ordinate system.

The experimental angular correlations integrated over all energies for the two emitted protons are compared in fig. 2 with the WKB- and Born-approximation calculations for $\nu = 0.3741$. The WKB-results have all been multiplied by the factor 2.1 to fit the absolute values of the cross-section, while the Born-approximation results (shown by broken lines) are all multiplied by 0.38. It will be seen that the WKB-results fit the experimental data rather better than the Born-approximation. The Born-approximation as we would expect predicts far too high an absolute value for the cross-sections. The discrepancy in absolute magnitude between the WKB-results and the experiment may be due to several causes: the use of simple harmonic oscillator wave functions may give too few nucleons in the surface, outside the range of the absorptive potential; the radius chosen for the optical well will also affect the absolute magnitude of the cross-section since the simple harmonic-oscillator wave-function was not chosen to fit the radius of the potential well used; also the depth of the potential well may be less than the one we used. We have made no attempt to improve the agreement with experiment, apart from altering the radius of the complex potential, since we are principally concerned with discovering the major factors of importance in the description of the experiment. Altering the radius of the potential well from $R = 2.8\times10^{-13}$ cm to $R = 2.4\times10^{-13}$ cm increases the absolute magnitude of the cross-sections as expected without altering very much the shape of the angular correlations.

The most striking feature of the reaction is the fact that the maxima in the cross-sections do not occur at positions such that $(\theta_1+\theta_2)$ is constant for diffe-

rent values of θ_1. For free p—p scattering we would expect $\theta_1+\theta_2 = 90°$, or making allowance for the binding energy $\theta_1+\theta_2 \approx 80°$. The marked dependence on θ_1 of the separation angle $(\theta_1+\theta_2)$ for the maxima has been successfully described by both the preliminary results of the partial waves analysis [6]) and by the WKB-analysis, and we shall now consider the various factors which determine the position of the maximum. Since both the partial waves analysis

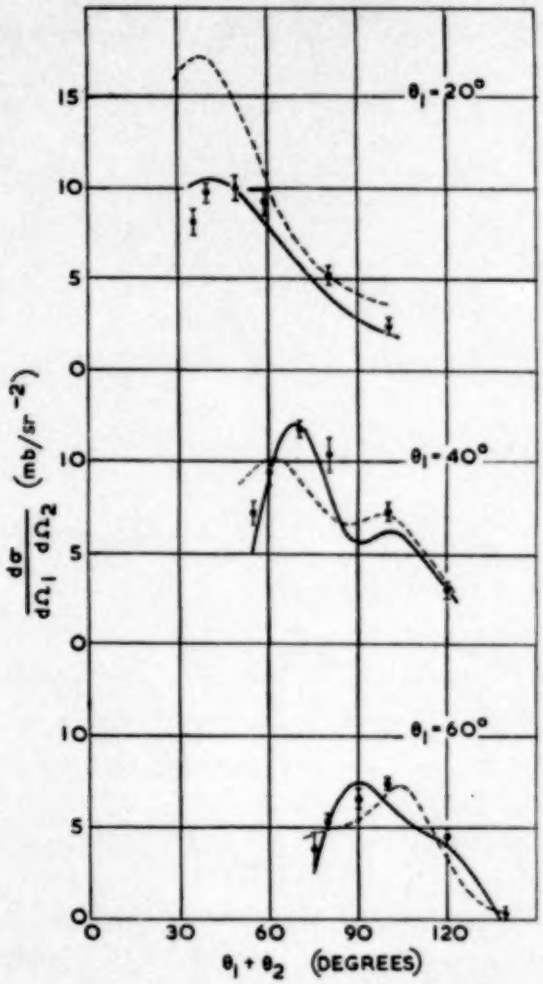

Fig. 2. Comparison of the experimental and theoretical angular correlations for coplanar p-state events. The WKB-results are indicated by the solid line and those of the Born-approximation by the broken one. For either method of calculation the normalization of all three correlations is the same (see text).

and the WKB-analysis successfully predict the correlation, and the former contains refraction effects while the latter takes no account of the deviations of the particles from straight lines, we may conclude that refraction is unimportant in determining the positions of the maxima. In the Born-approximation we completely remove the distorting effects of the nucleus on the plane waves representing the protons, and obtain for $|T|^2$ the product of the squared modulus of a two-body scattering amplitude and a nuclear momentum distribution.

It is easily shown that the only effect of the energy and angular dependence of the t-matrix is to reduce the cross-section for larger angle emission relative to that for smaller angles; at 153 MeV the effect of this will be very slight. Thus results obtained using the Born-approximation will be simply due to the momentum distribution of the struck protons. The parameters of the overlap function were chosen for the Born-approximation, to give a wave function whose Fourier transform corresponded to a most probable energy W for the target nucleon of 5 MeV, 10 MeV or 20 MeV (compared with about 12 MeV for

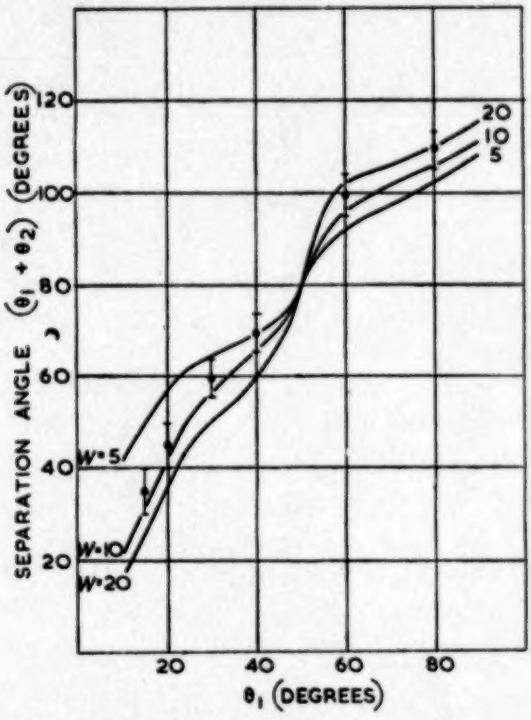

Fig. 3. The separation angle $(\theta_1+\theta_2)$ for maximum cross-section plotted as a function of θ_1, as calculated in Born-approximation for three values of W, the most probable energy of the struck nucleon.

the Hofstadter data). The calculated separation angles $(\theta_1+\theta_2)$ for the maximun cross-section with various values of θ_1 are plotted in fig. 3, together with the experimental results. It can be seen that the Born-approximation predicts the positions of the maxima very well, while in the physically reasonable range of W (10—20 MeV) the result is insensitive to the value of W chosen. As a test of the method, the Born-approximation calculation was repeated for $W \approx 2$ MeV and zero binding energy. The results approximated closely to those expected in free p—p scattering.

The energy spectra of protons detected at θ_1 when the other counter is placed at various values of θ_2 are expected to give the most sensitive test of the theory. The energy spectra observed at $\theta_1 = 20°$, $40°$ and $60°$ for various values of θ_2 are plotted in fig. 4 together with the WKB- and Born-approximation calculations for $\nu = 0.3741$ with their absolute magnitudes appropriately normalized.

The comparison between the two calculations at certain angles is interesting. For example, at $\theta_1 = \theta_2 = 40°$ the Born-approximation predicts a deep minimum at about 70 MeV, because this corresponds to collisions with almost stationary protons. In the WKB-calculation with the same overlap function this deep minimum is largely filled in, in much better agreement with experiment. This improvement is due to the inclusion of absorption, whose effect may be understood semi-classically in terms of the correlation between momentum and position for the struck protons. Absorption will reduce the cross-section for

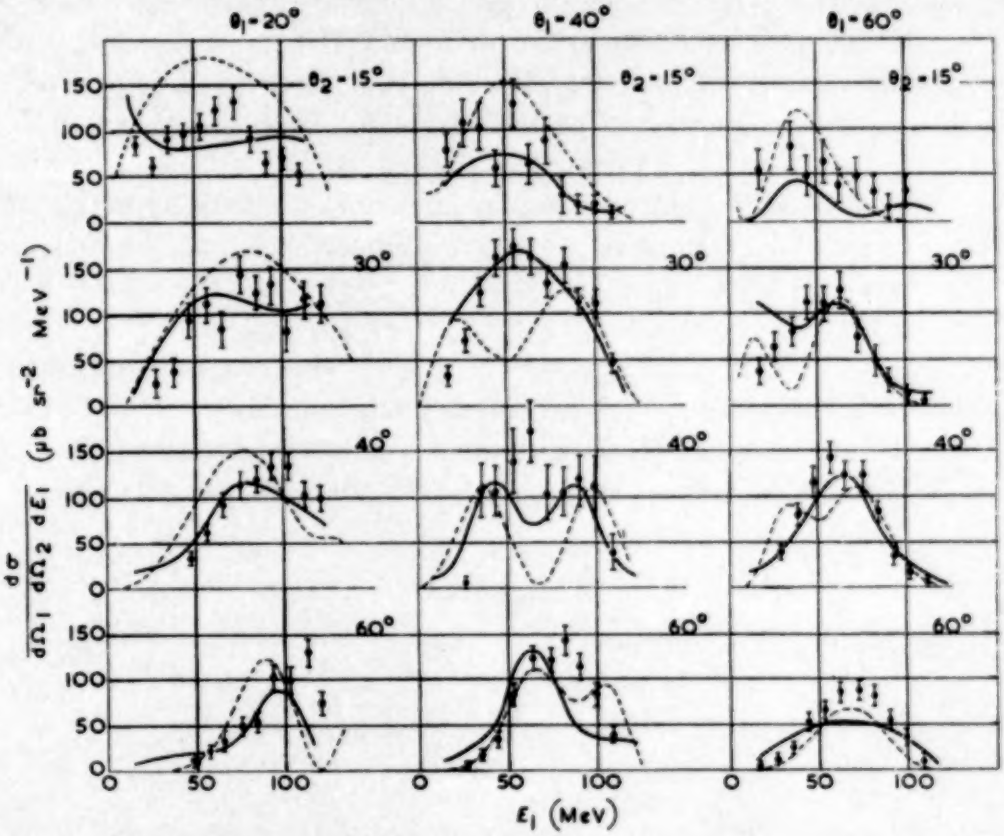

Fig. 4. The energy spectra of protons emitted at θ_1 for p-state events in which the second proton is emitted at various values of θ_2. The WKB-results are indicated by the solid line and those of the Born-approximation by the broken one. For either method of calculation the normalization of all spectra is the same (see text).

scattering near the centre of the nucleus relative to that for scattering from protons in the nuclear surface. Because $\langle \mathbf{k} \times \mathbf{r} \rangle = \mathbf{l}$ the slowly-moving protons are on the average at large radii and their effect will thus be more important in the WKB-calculation than in the Born-approximation which makes no distinction between different regions of the nucleus. This effect is further demonstrated in the angular correlations (fig. 2). The relative cross-sections for scattering at small separation angles is much too large in the Born-approximation, whereas the WKB-fit is much better. This is because these events can only be produced

by scattering from energetic protons, which must be near the centre of the nucleus.

5. Conclusions

Both the Born- and WKB-approximations predict the general features of the reaction fairly well provided that a reasonable momentum distribution for the struck protons is used. This is strong evidence for the validity of the impulse approximation and the description of the reaction by means of a direct interaction picture. The WKB-calculations give appreciably better agreement with experiment, showing that it is important to include the absorption effects which preferentially select slowly moving nucleons at large radii. This is especially noticeable in the energy spectra, which will give a most rigorous test to any theory of the reaction. We do not feel that it would be fruitful to make a comprehensive search for the best parameters to fit the data by means of the WKB-approximation, since it does not take proper account of the refraction and reflection effects on the particles travelling through the nucleus.

The authors wish to acknowledge the help of the Cambridge University Mathematical Laboratory in making time available on EDSAC 2 and to thank Drs. J. P. Schiffer and T. H. R. Skyrme for helpful discussions. One of us (K. F. R.)wishes to acknowledge a D.S.I.R. research studentship.

References

1) P. R. Serber, Phys. Rev. **72** (1947) 1114
2) G. F. Chew and M. L. Goldberger, Phys. Rev. **77** (1950) 470; **87** (1952) 778
3) J. Nuttall, Smith's Prize Essay, Cambridge University (1959)
4) H. Tyrén, P. Hillman and Th. A. J. Maris, Nuclear Physics **7** (1958) 1
5) T. J. Gooding and H. G. Pugh, Nuclear Physics **18** (1960) 46
6) J. Nuttall and K. F. Riley, to be published
7) J. P. Schiffer, L. L. Lee, Jr., and B. Zeidman, Phys. Rev. **115** (1959) 427
8) C. A. Levinson and M. K. Banerjee, Ann. of Phys. **2** (1957) 471
9) T. K. Fowler, Phys. Rev. Letters **1** (1958) 371
10) L. S. Rodberg, Annals of Physics (to be published)
11) C. Møller, Mat. Fys. Medd. Dan. Vid. Selsk. **22** ,No. 19 (1946); **23**, No. 1 (1948)
12) K. F. Riley, Nuclear Physics **13** (1959) 3
13) A. E. Glassgold and P. J. Kellogg, Phys. Rev. **109** (1958) 1291
14) W. N. Hess, Revs. Mod. Phys. **30** (1958) 368
15) R. Hofstadter, Revs. Mod. Phys. **28** (1956) 214

7.A

Nuclear Physics **18** (1960) 75—80; © *North-Holland Publishing Co., Amsterdam*

Not to be reproduced by photoprint or microfilm without written permission from the publisher

RESONANCE BEHAVIOUR OF SCATTERING AMPLITUDES IN DISPERSION RELATIONS

JOHN W. MOFFAT

RIAS, Baltimore 12, *Maryland, U.S.A.*

Received 29 April 1960

Abstract: A Breit-Wigner resonance behaviour of the total cross section for a model of pion-nucleon scattering is deduced from a relativistic dispersion relation and a physical energy spectrum. In virtue of the analyticity of the scattering amplitude in the cut plane of the energy an expression is derived for the scattering amplitude which has the form of the solution to the Hilbert problem in the theory of singular integral equations. The scattering amplitude is therefore determined by the behaviour of a phase angle ϑ. Points of discontinuity in ϑ correspond to the location of resonances and lead to a Breit-Wigner formula for the total cross section.

1. Introduction

The complete dispersion relations have been truncated on the basis of the dominance of the $(\frac{3}{2}, \frac{3}{2})$ resonance, and in this way very high energy phenomena have been excluded from consideration [1]). This yields an approximate set of relations which comprise a relativistic generalization of the static model. The shape of the resonance curve in the $(\frac{3}{2}, \frac{3}{2})$ state is determined by this set of relations once the location of the resonance is given. In this approach, one is faced with the problem of solving singular integral equations. Omnès [2]) has studied the properties of the simplest equations of the type

$$G(x) = F(x) + \frac{1}{\pi}\int_1^\infty \frac{e^{-i\delta}\sin\delta G(x')}{x'-x-i\varepsilon}\,dx'. \tag{1}$$

The general solution to (1) is derived by considering the standard Hilbert problem of the known difference of a function above and below a cut [3]). The solution is of the form

$$G'(x) = G(x) + \frac{L(x)}{(x-1)^n}\exp\left(\frac{P}{\pi}\int_1^\infty \frac{\vartheta(\zeta)d\zeta}{\zeta-x}\right)\exp i\vartheta, \tag{2}$$

where $\vartheta(1) = k\pi$ and ϑ tends to zero at infinity. $L(x)$ is an arbitary polynomial in x. The detailed behaviour of ϑ determines the explicit form of $L(x)$ and the value of n.

Some attention has been devoted recently to the problem of unstable elementary particles in field theory [4]). Schwinger [5]) has described a theory of unstable particles based on a study of the analytic properties of the one-particle Green's function for a spinless boson field. He shows that a description of unstable particles is already contained within the framework of the theory of Green's functions by emphasizing the basic analytic properties of these functions in the complex plane of the momentum. In the following, we shall show that by extending Schwinger's analysis to dispersion relations the form (2) results for the two-particle scattering amplitude simply from the analyticity of the scattering amplitude in the cut plane of the energy. Points of discontinuity in $\vartheta(E)$ as a function of the energy E correspond to the location of resonances and lead to a Breit-Wigner formula for the total cross section.

2. Analytic Properties of Scattering Amplitude

We shall consider two-particle scattering $p+k \to p'+k'$, where k and k' are the initial and final momenta of a neutral particle of mass μ and p and p' are the initial and final momenta of a particle of mass M. We neglect spin values of these particles and consider for definiteness a model of pion-nucleon scattering in which a real scalar field ("meson" of mass μ) is coupled to a complex scalar field ("nucleon" of mass M).

The vectors p, p' and k, k' satisfy the energy and mass shell relations †

$$p+k = p'+k', \qquad p^2 = p'^2 = M^2, \qquad k^2 = k'^2 = \mu^2. \tag{3}$$

The total invariant energy of the system is

$$W^2 = (p+k)^2 \tag{4}$$

and in the centre of mass system

$$W^2 = (\sqrt{K^2+M^2}+\sqrt{K^2+\mu^2})^2, \qquad \cos\theta = 1-\frac{\Delta^2}{2K^2}, \tag{5}$$

where Δ^2 is the invariant momentum transfer $(p-p')^2$, and K is the centre of mass momentum.

We shall assume that the scattering amplitude $T(W^2)$ for fixed Δ^2 is analytic in the cut plane with a branch point at Re $W^2 = E^2 = (M+\mu)^2$ and a branch line in the physical region extending to infinity. Then $T(W^2)$ satisfies a dispersion relation

$$T(W^2) = \frac{1}{\pi}\int_{-\infty}^{\infty} \frac{\mathrm{d}W'^2 A(W'^2)}{W'^2-W^2}, \tag{6}$$

where $A(W^2) = \mathrm{Im}\, T(W^2)$ and we have assumed that $T(W^2)$ is sufficiently

† In this paper natural units $\hbar = c = 1$ are used throughout.

bounded at infinity. When $T(W^2)$ is not sufficiently bounded, we can divide T by a polynomial in W^2.

Let us now proceed to study some of the consequences of the analyticity properties of $T(W^2)$ by using Schwinger's method of reasoning [5]). The singularities on the real axis of the energy variable consist of isolated poles and a continuous spectrum of singularities with branch points at $E^2 = (M+n\mu)^2$ for $n = 1, 2, \ldots$ The inverse scattering amplitude $T^{-1}(W^2)$ is discontinuous across the same branch cut as $T(W^2)$. The function $T^{-1}(W^2)$ has branch points at $(M+n\mu)^2$ for $n = 1, 2, \ldots$. Therefore, $T(W^2)$ and $T^{-1}(W^2)$ possess the same poles and zeros and the same cut along the real axis. For large W^2 the scattering amplitude $T(W^2)$ behaves like

$$T(W^2) \sim -\frac{N}{W^2} \quad \text{for} \quad W^2 \to \infty, \tag{7}$$

where N is a constant. Then for large W^2 the inverse scattering amplitude $T^{-1}(W^2)$ behaves like $-W^2/N$.

The function

$$Q(W^2) = T^{-1}(W^2) + \frac{W^2}{N} \tag{8}$$

satisfies $(1/W^2)Q(W^2) \to 0$ for $W^2 \to \infty$, and is regular everywhere in the cut plane with the cut along the real axis corresponding to the branch line of $T(W^2)$. We shall neglect any complex zeros that occur in $T(W^2)$. The function $(1/W^2)Q(W^2)$ has a pole at the origin and can be represented by

$$W^{-2}Q(W^2) = \frac{a}{W^2} - \frac{1}{\pi}\int_{-\infty}^{\infty} \frac{\mathrm{d}W'^2 H(W'^2)}{W'^2 - W^2}. \tag{9}$$

In virtue of (8) ,we get

$$T^{-1}(W^2) = a - W^2\left(\frac{1}{N} + \frac{1}{\pi}\int_{-\infty}^{\infty} \frac{\mathrm{d}W'^2 H(W'^2)}{W'^2 - W^2}\right). \tag{10}$$

When $T^{-1}(W^2)$ possesses neither poles nor zeros it can be represented in the physical region by

$$T^{-1}(W^2) = \frac{1}{N}[(M+\mu)^2 - W^2]R(W^2), \tag{11}$$

where $\log R(W^2) \to 0$ when $W^2 \to \infty$ in virtue of (8) and $\log R(W^2)$has a branch point at $(M+\mu)^2$ and a branch line extending to infinity. The function $\log R(W^2)$ can be represented analytically by

$$\log R(W^2) = \frac{1}{\pi}\int_{(M+\mu)^2}^{\infty} \frac{\mathrm{d}W'^2 \vartheta(W'^2)}{W'^2 - W^2}, \tag{12}$$

where at the singular point $W^2 = (M+\mu)^2$ the phase angle $\vartheta(W^2) = \pi$ in order

to generate the pole in $R(W^2)$ at $(M+\mu)^2$ and the continuous function $\vartheta(W^2)\to 0$ for $W^2\to\infty$. In order to simplify the following discussion, we have omitted the contribution of the unphysical region in (12). The scattering amplitude $T(W^2)$ then has the form

$$T(W^2)=\frac{N}{[(M+\mu)^2-W^2]}\exp\left(-\frac{1}{\pi}\int_{(M+\mu)^2}^{\infty}\frac{dW'^2\vartheta(W'^2)}{W'^2-W^2}\right). \tag{13}$$

We deduce the relation between the phase angle $\vartheta(W^2)$ and $H(W^2)$:

$$E^2H(E^2)\cot\vartheta(E^2)=-a+E^2\left(\frac{1}{N}+\frac{P}{\pi}\int_{(M+\mu)^2}^{\infty}\frac{dW'^2H(W'^2)}{W'^2-E^2}\right). \tag{14}$$

Moreover,

$$A(E^2)\cot\vartheta(E^2)=-\frac{P}{\pi}\int_{(M+\mu)^2}^{\infty}\frac{dW'^2A(W'^2)}{W'^2-E^2}. \tag{15}$$

In the derivation of (14) and (15), we have used the identity

$$\lim_{\epsilon\to 0}\frac{\epsilon}{(E^2-E_0^2)^2+\epsilon^2}=\pi\delta(E^2-E_0^2). \tag{16}$$

We can also deduce that in the physical region

$$A(E^2)=\frac{N}{[E^2-(M+\mu)^2]}\exp\left(-\frac{P}{\pi}\int_{(M+\mu)^2}^{\infty}\frac{dW'^2\vartheta(W'^2)}{W'^2-E^2}\right)\sin\vartheta(E^2) \tag{17}$$

and

$$E^2H(E^2)A(E^2)=\frac{1}{(\cot^2\vartheta+1)}. \tag{18}$$

Poles and zeros of the scattering amplitude $T(W^2)$ are generated in regions where rapid variations of the phase angle $\vartheta(E^2)$ become points of discontinuity[5]). As an illustration of this, we can choose ϑ such that $0\leqq\vartheta\leqq\pi$, then both $A(E^2)$ and $H(E^2)$ are small for ϑ near 0 or π, while for values of $\vartheta(E^2)$ which differ from 0 or π either $A(E^2)$ or $H(E^2)$ are correspondingly large. Let us designate by E_1 the centre located at $\frac{1}{2}\pi$ of a region of rapid variation of $\vartheta(E^2)$. Then a pole in $T(E^2)$ corresponds to a rapid increase in $A(E^2)$ and a rapid decrease in $H(E^2)$. When $E\approx E_1$, we can write

$$E_1^2H(E_1^2)A_1(E^2)=\frac{1}{(\cot^2\vartheta_1+1)} \tag{19}$$

and

$$H(E_1^2)E_1^2\cot\vartheta_1(E^2)=C_1^{-1}(E^2-E_1^2), \tag{20}$$

where C_1 is a positive constant with the dimensions of energy (in our units (length)$^{-1}$). In view of (19) and (20), we get

$$A_1(E^2)=\frac{C_1^2E_1^2H(E_1^2)}{(E^2-E_1^2)^2+(C_1E_1^2H(E_1^2))^2}. \tag{21}$$

The expression (21) holds in regions where $E \approx E_1$ and E_1 is a centre of rapid oscillation of $\vartheta(E^2)$.

3. Resonance Scattering

We are primarily concerned with the physical situation corresponding to the familiar energy spectrum associated with pion-nucleon scattering. There is a bound state corresponding to the one-nucleon pole at $E_0^2 = M^2$. In the interval $0 < E^2 < (M+\mu)^2$ the absorptive part $A(E^2)$ differs from zero only at the pole $E_0^2 = M^2$. The contribution due to the one-nucleon state is obtained from (21) in the limit as $H(E_0^2)$ tends to zero. We get

$$A_0(E^2) = \pi G^2 \delta(E^2 - M^2), \tag{22}$$

where $G^2 = C_0$ is the coupling constant. The bound state then yields the familiar contribution to the dispersion relation

$$\frac{G^2}{M^2 - E^2}. \tag{23}$$

For values of the energy E close to the resonance level E_1, the physical continuum above the threshold $(M+\mu)^2$ is characterized by the approximate expression

$$A_1(E^2) = \frac{1}{4\lambda_1 E_1} \frac{\Gamma_1^2}{(E-E_1)^2 + (\frac{1}{2}\Gamma_1)^2}, \tag{24}$$

where $\Gamma_1 = C_1 E_1 H(E_1^2)$ and $\lambda_1 = E_1 H(E_1^2)$ is a dimensionless quantity. In the case of forward scattering, we can introduce the total cross section corresponding to the resonance level E_1 by

$$\sigma_T = \frac{4\pi}{q}\left(\frac{2\lambda_1 E_1}{q}\right) A_1(E^2), \tag{25}$$

where q is the "pion" momentum in the centre of mass system. In virtue of (25), we get the single-level resonance formula

$$\sigma_T = \frac{2\pi}{q^2} \frac{\Gamma_1^2}{(E-E_1)^2 + (\frac{1}{2}\Gamma_1)^2} \tag{26}$$

for energy values E (in the continuum) close to the resonance of the "nucleon" isobar system. By giving the location of the resonance the shape of the curve can be determined [6]).

In the above considerations, we have only treated the case of strong coupling. The extension of Schwinger's theory to a complete description of unstable particles in dispersion relations including weak coupling will be deferred to another publication.

I thank Dr. T. Fulton and Dr. P. Schwed for discussion.

References

1) G. F. Chew, M. L. Goldberger, F. E. Low and Y. Nambu, Phys. Rev. **106** (1957) 1337
2) R. Omnès, Nuovo Cimento **8** (1958) 316
3) N. I. Muskhelishvili, Trud. Tbil. Mat. Inst. **10** (1941) 1
4) M. Lévy, Nuovo Cimento **13** (1959) 115;
P. T. Matthews and A. Salam, Phys. Rev. **112** (1958) 283;
R. E. Peierls, Proc. Glasgow Conference on Nuclear and Meson Physics, (Pergamon Press, London, 1954) 296;
J. Gunson and J. G. Taylor, Preprint (1960)
5) J. Schwinger, Ann. of Phys. **9** (1960) 169
6) M. Gell-Mann and K. M. Watson, Annual Review of Nuclear Science (1954) 219

7.A

Nuclear Physics **18** (1960) 81—84; © *North-Holland Publishing Co., Amsterdam*

Not to be reproduced by photoprint or microfilm without written permission from the publisher

A NOTE ON SCATTERING AND PRODUCTION AMPLITUDES

A. P. BALACHANDRAN † and N. R. RANGANATHAN ††

Department of Physics, University of Madras, India

Received 25 April 1960

Abstract: A relation between scattering and production amplitudes for processes involving an arbitrary number of final channels has been arrived at following a method due to Sucher and Day. Possible applications of this equation to $\pi-\pi$, $K-\bar{K}$ and $\pi+\pi \to K+\bar{K}$ scatterings are pointed out. Also a simple and exact expression for the $\gamma-\gamma$ scattering amplitude in terms of the amplitude for the process $\gamma+\gamma \to e^-+e^+$ has been obtained.

1. Introduction

In a recent paper, Sucher and Day [1]) derived an interesting integral equation for the production amplitude for a process $A+B \to C+D$ in terms of the "pure" production amplitude and the scattering amplitudes for the initial and final states. In this note we have derived in a similar way an integral equation for the production amplitude into a particular final channel when more than one final channel is available. From such equations we can hope to deduce some information on unknown scattering amplitudes, perhaps after making some suitable approximations. We point out for instance how in principle it is possible to study the amplitudes for the processes $\pi+\pi \to \pi+\pi$, $K+\bar{K} \to K+\bar{K}$ and $\pi+\pi \to K+\bar{K}$ if one knows nucleon-anti-nucleon interactions. Though this idea is known, the equation we employ for this purpose is not the usual one. Finally we have also obtained a rather simple result for the $\gamma-\gamma$ scattering amplitude in terms of the amplitude for the process $\gamma+\gamma \to e^-+e^+$.

2. The Integral Equation for $M_{f(j)i}$

We consider a process in which a given initial state $|i\rangle$ can go over into any one of the final states $|f_{(j)}\rangle$ ($j = 1, 2, \ldots n$). Following the notation in ref. [1]), we can then write

$$M_{f(j)i} = \langle f_{(j)}|T|i\rangle, \tag{1}$$

where

$$T = H_1 + H_1 G T \tag{2}$$

† Research Fellow of the University of Madras.

†† Atomic Energy Commission Senior Research Fellow.

with

$$G = (E - H_0 + i\varepsilon)^{-1}.$$

The "pure" production amplitude $P_{f_{(j)}i}$ is given by

$$P_{f_{(j)}i} = \langle f_{(j)}|T_p|i\rangle, \tag{3}$$

where

$$T_p = H_1 + H_1 G_p T_p$$

with

$$G_p = G(1 - \Lambda_{fi}). \tag{4}$$

Here, Λ_{fi} is a projection operator which has eigenvalue unity for any one of the initial or final states and has zero eigenvalue for all the other states.

We also define s_i as

$$s_i = \langle i|T_s|i\rangle, \tag{5}$$

where

$$T_s = H_1 + H_1 G_s T_s$$

with

$$G_s = G\left(1 - \sum_{j=1}^{n} \Lambda_{f_{(j)}}\right)$$

and

$$\Lambda_{f_{(j)}}|f_{(j)}\rangle = |f_{(j)}\rangle, \quad \Lambda_{f_{(j)}}|\rangle = 0. \tag{6}$$

In the last formula, $|\rangle$ denotes any state other than $|f_{(j)}\rangle$.

Using these amplitudes, we arrive at the following integral equation for $M_{f_{(j)}i}$:

$$M_{f_{(j)}i} = P_{f_{(j)}i} + P_{f_{(j)}i} \cdot M_{ii} + \sum_{k=1}^{n} [M_{f_{(j)}f_{(k)}} \cdot P_{f_{(k)}i} + M_{f_{(j)}f_{(k)}} \cdot P_{f_{(k)}i} \cdot M_{ii} - M_{f_{(j)}i} \cdot P_{if_{(k)}} \cdot M_{f_{(k)}i}], \tag{7}$$

where the "dot" product is defined as in ref. [1]), i.e. for instance,

$$M_{f_{(j)}f_{(k)}} \cdot P_{f_{(k)}i} = \sum_{m=q_k} \frac{M_{f_{(j)}f_{(k)}}(q_j, q_k) P_{f_{(k)}i}(q_k, q_i)}{E - E_m + i\varepsilon}, \tag{8}$$

where the sum is over the complete set of the k-th final state.

3. Pion and K-Meson Interactions

Consider the process

$$N + \bar{N} \to \pi + \pi, \tag{9}$$

with $|N\bar{N}\rangle \equiv |i\rangle$ and $|\pi\pi\rangle \equiv |f\rangle$. We then have

$$M_{fi} = P_{fi} + P_{fi} \cdot M_{ii} + M_{ff} \cdot P_{fi} + M_{ff} \cdot P_{fi} \cdot M_{ii} - M_{fi} \cdot P_{if} \cdot M_{fi}. \tag{10}$$

Making use of the experimental data available on the process $N+\bar{N} \to \pi+\pi$, we can evaluate M_{fi}, while M_{ii} can be arrived at using the results of Federbush *et al.* [2]). Since P_{fi} is independent of the $\pi-\pi$ interaction, it can be reasonably approximated by the renormalized Born term by setting up a Chew-Low type of integral equation for the process. In this calculation, in the absence of any knowledge on the $K-\pi$ interaction, we have also to assume that intermediate states involving K-meson pairs do not appreciably contribute to the P_{fi} in (10). The $\pi-\pi$ scattering amplitude can now be deduced by solving the integral equation (10) for M_{ff}. We are at present engaged in carrying out this programme. By a similar procedure one can also deduce the $K-\bar{K}$ scattering amplitude under neglect of the contribution of intermediate states involving pions to the corresponding P_{fi}. Now if we consider the processes

$$N+\bar{N} \to N+\bar{N}, \quad N+\bar{N} \to \pi+\pi, \quad N+\bar{N} \to K+\bar{K} \tag{11}$$

with $|N\bar{N}\rangle \equiv |i\rangle$, $|\pi\pi\rangle \equiv |f_{(1)}\rangle$ and $|K\bar{K}\rangle \equiv |f_{(2)}\rangle$, we have the equation

$$M_{f_{(1)}i} = P_{f_{(1)}i}+P_{f_{(1)}i} \cdot M_{ii}+\sum_{k=1}^{2} [M_{f_{(1)}f_{(k)}} \cdot P_{f_{(k)}i} + M_{f_{(1)}f_{(k)}} \cdot P_{f_{(k)}i} \cdot M_{ii}-M_{f_{(1)}i} \cdot P_{if_{(k)}} \cdot M_{f_{(k)}i}]. \tag{12}$$

Utilizing the information already deduced on the $\pi-\pi$ and $K-\bar{K}$ scattering amplitudes, one can hope to deduce the amplitude for the process $\pi+\pi \to K+\bar{K}$ from (12).

4. The $\gamma-\gamma$ Scattering Amplitude

The processes we consider here are

$$\gamma+\gamma \to \gamma+\gamma \quad \text{and} \quad \gamma+\gamma \to e^-+e^+ \tag{13}$$

with

$$|\gamma\gamma\rangle \equiv |i\rangle \quad \text{and} \quad |e^-e^+\rangle \equiv |f\rangle.$$

The $\gamma-\gamma$ scattering amplitude is then given by

$$M_{ii} = s_1+P_{if} \cdot M_{fi}+s_1 \cdot P_{if} \cdot M_{fi}. \tag{14}$$

Remembering that s_1 denotes the $\gamma-\gamma$ scattering that does not involve (e^-, e^+) pairs in the intermediate states, we have $s_1 = 0$ since even the lowest order diagram for $\gamma-\gamma$ scattering (i.e. the square diagram) involves electron pairs in the intermediate state †. Thus

$$M_{ii} = P_{if} \cdot M_{fi}. \tag{15}$$

† If we write a similar equation for $\pi+\pi \to N+N$ and solve for s_1, a large value of s_1, especially in the lower energy region, will indicate a $\pi-\pi$ direct interaction.

We have thus expressed the exact $\gamma-\gamma$ scattering amplitude in terms of the pure production amplitude for a pair annihilating into two photons and the exact amplitude for two photons creating a pair. It is interesting to note that $P_{1f} = M_{1f}$ to order e^2, so that M_{11} to order e^4 is given by the familiar result

$$M_{11} = M_{1f} \cdot M_{f1}. \tag{16}$$

5. Conclusion

We can also adopt the procedure of the paper for final states involving three particles as in the process $A+B \to C+D+E$. As a simple example we can take $|i\rangle \equiv |NN\rangle$ and $|f\rangle \equiv |NN\pi\rangle$ and we can then express M_{fi} in terms of the 'pure' production and scattering amplitudes. The main difficulty is the interpretation of M_{ff}, i.e. the process of three particles scattering into three particles. However, in our example, it is possible to express M_{ff} in terms of the $N-N$ and $\pi-N$ scattering amplitudes.

We note also that by this method we can estimate the final state inelastic interaction in processes like $\pi^- + p \to \Sigma^0 + K^0$, $\pi^- + p \to \Lambda^0 + K^0$ with $|i\rangle \equiv |\pi^- p\rangle$, $|f_{(1)}\rangle \equiv |\Sigma^0 K^0\rangle$ and $|f_{(2)}\rangle = |\Lambda^0 K^0\rangle$, where the amplitude $M_{f_{(2)} f_{(1)}}$ describes the final state inelastic interaction.

Perhaps it may also be interesting to apply to relations like equation (10) considerations about location of poles conjectured [3]) from a study of the analytic behaviour of the scattering amplitudes.

We wish to express our gratitude to Professor Alladi Ramakrishan for instructive discussions and thank Dr. S. K. Srinivasan and Mr. K. Venkatesan for helpful suggestions.

References

1) J. Sucher and T. B. Day, Nuovo Cim. **13** (1959) 1111
2) P. Federbush, M. L. Goldberger and S. B. Treiman, Phys. Rev. **112** (1958) 642
3) G. F. Chew, Phys. Rev. **112** (1958) 1380

7.C

Nuclear Physics **18** (1960) 85—90; © *North-Holland Publishing Co., Amsterdam*

Not to be reproduced by photoprint or microfilm without written permission from the publisher

RECOIL IN PION-NUCLEON SCATTERING

V. GUPTA

Tata Institute of Fundamental Research, Bombay

Received 16 March 1960

Abstract: The object of this paper is to show the dependence of the pion-nucleon scattering cross-section on nucleon recoil. To this end the method of canonical transformations has been used to obtain the scattering operator explicitly. Numerical results are given for $\pi^+ + p \rightarrow \pi^+ + p$ and the cross-section is found to decrease with increase of recoil. No attempt has been made to fit results with experiment as the calculation is in the lowest order perturbation theory.

1. Introduction

The calculation of recoil effects in pion nucleon processes has always been a problem. In ordinary perturbation theory the inclusion of nucleon recoil makes the summation over intermediate states virtally impossible. In the Chew-Low method recoil is neglected and the static model of the nucleon used. For low energy scattering this is a good approximation. Nevertheless, a method for calculating such effects is desirable and to this end we have used the method of canonical transformation (abbreviated as C.T. hereafter). The method of C.T. has been applied to various meson-nucleon problems †. To collision problems it has been applied by Heitler and Ma [4]) and Corinaldesi and Field [5]). These authors do not determine the C. T. as an operator (as is done in this paper), but determine its matrix elements in terms of those of the interaction.

In the next section we give the method of C.T. in general and then go on to apply it to scattering in section 3.

2. The Method of Canonical Transformation

Let H_0 be the free field Hamiltonian of our system and fH_1 the interaction term, where f is the coupling constant. We shall specialize to the pion-nucleon system straightaway for the sake of convenience. The technique outlined will be the same for other systems.

The equation we have to solve is

$$i\frac{\partial \Psi}{\partial t} = (H_0 + fH_1)\Psi(t), \quad (\hbar = c = 1). \tag{1}$$

† For application to nuclear forces see ref. [1]), to magnetic moments see ref. [2]) and to beta-decay see ref. [3]).

We go into the interaction representation by the C. T.

$$\Psi(t) = \mathrm{e}^{-iH_0 t}\Psi'(ft), \tag{2a}$$

obtaining

$$i\frac{\partial\Psi'}{\partial t} = fH_1\Psi'(t), \tag{2b}$$

where

$$H_1 = \mathrm{e}^{iH_0 t}H_1\mathrm{e}^{-iH_0 t}.$$

To eliminate H_1 we make the C.T.

$$\Psi'(t) = \mathrm{e}^{-ifS_1(t)}\Psi_1(t), \quad S_1(t) = \int^t H_1(t)\mathrm{d}t, \tag{3}$$

giving us

$$i\frac{\partial\Psi_1}{\partial t} = \{\tfrac{1}{2}f^2[iS_1, H_1] + \tfrac{1}{3}f^3[iS_1, [iS_1, H_1]] + \ldots\}\,\Psi_1(t). \tag{4}$$

Thus the required transformation is simply the indefinite time integral of the term we wish to eliminate. Having obtained the C.T. in the interaction representation it is now easy to obtain it in the Schrödinger representation.

An operator equation may be obtained for S_1, without going into the interaction representation, which is equivalent to eq. (3). Putting $\Psi(t) = \mathrm{e}^{-ifS_1}\Psi_1(t)$ in eq. (1) and requiring that terms of order f vanish we obtain

$$i\frac{\partial\Psi_1}{\partial t} = \{H_0 + \tfrac{1}{2}f^2[iS_1, H_1] + \tfrac{1}{3}f^3[iS_1, [iS_1, H_1]] + \ldots\}\,\Psi_1(t)$$

and

$$[iS_1, H_0] = -H_1. \tag{5}$$

Here S_1 and H_1 are of course time-independent.

The interpretation of the terms in eq. (4) is quite simple. If H_1 is linear in a_k^* and a_k (creation and annihilation operators of the pions), so is S_1 and the f^2 terms will involve the following combinations:

(i) $[a_k, a_{k'}^*]$ (this will yield nuclear force and self energy of nucleon to second order);

(ii) $a_k a_{k'}^*$ or $a_k^* a_{k'}$ (these will give scattering of a pion by a nucleon);

(iii) $a_k a_{k'}$ or $a_k^* a_{k'}^*$ (these will contribute to higher order terms, e.g. fourth order nuclear force).

Thus to obtain the total contribution to fourth order processes we should eliminate the f^2 terms from eq. (4). This will not give any more f^3 terms. Thus the operators for the fourth or higher order processes (like scattering, nuclear force, pion production) can be obtained by applying suitable transformations to eliminate the terms which would contribute.

The f^3 terms can be interpreted in a similar manner. For example the terms leading to one-pion production in a pion-nucleon collision will clearly involve $a_k^* a_{k'}^* a_{k''}$, that is two creation operators and one annihilation operator. Picking out such terms gives us the one-pion production operator. It should be remarked that the above technique does not require the nucleon to be static. Further, the operator so obtained automatically contains the contribution of all the Feynman graphs of that order. One has just to take its matrix elements between the required initial and final states. In the next section we give both the static and the recoil scattering operators.

3. Scattering Operator

Our system contains only one nucleon and we treat it non-relativistically. We use the symmetric pseudoscalar meson theory with pseudovector coupling. In momentum space

$$H_0 = H_N + H_\pi, \quad \text{with} \quad H_N = \frac{1}{2M} p^2, \quad H_\pi = \tfrac{1}{2} \sum_k \omega_k (a_k a_k^* + a_k^* a_k), \tag{6}$$

where $\omega_k = (k^2+\mu^2)^{\frac{1}{2}}$ the energy of a pion of momentum $\mathbf{k}$. We further use k to denote both the momentum and isobaric spin index λ. The interaction (the non-relativistic limit of the ps (pv) interaction $(f/\mu)\overline{\Psi}\gamma_5\gamma_\nu\tau_\alpha\Psi(\partial\phi_\alpha/\partial x_\nu)$) is

$$\begin{aligned} H_1 &= H_{N\pi} + H_R, \\ H_{N\pi} &= \sum_k (a_k V_k + a_k^* V_k^*), \\ H_R &= \frac{1}{2M} \sum_k \omega_k (a_k^* V_k^* - a_k V_k) + \frac{1}{M} \sum_k (a_k^* \mathbf{Q}_k^* + a_k \mathbf{Q}_k) \cdot \mathbf{p}\omega_k, \end{aligned} \tag{7}$$

where

$$V_k = \frac{\sqrt{4\pi}}{\mu} \frac{e^{i\mathbf{k}\cdot\mathbf{r}}}{\sqrt{2\omega_k}} (i\mathbf{k}\cdot\boldsymbol{\sigma})\tau_\lambda, \quad \mathbf{Q}_k = -i \frac{\sqrt{4\pi}}{\mu} \frac{e^{i\mathbf{k}\cdot\mathbf{r}}}{\sqrt{2\omega_k}} \tau_\lambda \boldsymbol{\sigma} \tag{8}$$

and $\mathbf{p}$ represents the nucleon momentum.

We are interested in scattering to the lowest order (i.e. f^2) and this can be obtained by making only one C.T., namely S_1. Further, we shall calculate terms linear in $\mathbf{p}$ only.

To this order, we obtain

$$S_1 = S_1^A + S_1^R + S_1^P,$$

where

$$S_1^{\mathrm{A}} = i\sum_k (a_k V_k - a_k^* V_k^*)\omega_k^{-1},$$

$$S_1^{\mathrm{R}} = -\frac{i}{2M}\sum_k (a_k V_k + a_k^* V_k^*) + \frac{i}{M}\sum_k (a_k \mathbf{Q}_k - a_k^* \mathbf{Q}_k^*)\cdot \mathbf{p}, \tag{9}$$

$$S_1^{\mathrm{P}} = \frac{i}{2M}\sum_k \omega_k^{-2}[a_k V_k(k^2+2\mathbf{k}\cdot\mathbf{p}) + a_k^* V_k^*(k^2-2\mathbf{k}\cdot\mathbf{p})].$$

Here S_1^{A}, S_1^{R} are required to eliminate the static and momentum-dependent interaction terms $H_{\mathrm{N}\pi}$ and H_{R} respectively; while S_1^{P} is necessary because of the nucleon kinetic energy H_{N}.

The transformation S_1 has been given in the Schrödinger representation. The f^2 term in eq. (5) contains

(i) the pure static term $\frac{1}{2}f^2[iS_1^{\mathrm{A}}, H_{\mathrm{N}\pi}]$,

(ii) the recoil terms $\frac{1}{2}f^2[iS_1^{\mathrm{A}}, H_{\mathrm{R}}]$ and $\frac{1}{2}f^2[iS_1^{\mathrm{R}}+iS_1^{\mathrm{P}}, H_{\mathrm{N}\pi}]$. We pick out the scattering operator (cf. section 2)

$$U_1 = U_1^{\mathrm{A}} + U_1^{\mathrm{R}}, \tag{10}$$

where the static part is

$$U_1^{\mathrm{A}} = -\tfrac{1}{2}\sum_{k,k'}\{[V_k, V_{k'}^*]a_{k'}^* a_k - [V_k^*, V_{k'}]a_{k'} a_k^*\}\omega_k^{-1}$$

and the recoil part is

$$U_1^{\mathrm{R}} = \frac{1}{4M}\sum_{k,k'}\{[V_k, V_{k'}^*]a_{k'}^* a_k + [V_k^*, V_{k'}]a_{k'} a_k^*\}\left(\frac{\mu^2}{\omega_k^2} - \frac{\omega_{k'}}{\omega_k}\right)$$
$$-\frac{1}{2M}\sum_{k,k'}\left[\left\{[V_k, \mathbf{Q}_{k'}^*\cdot\mathbf{p}]\frac{\omega_{k'}}{\omega_k} + \left[\left(\mathbf{Q}_k + \frac{V_k}{\omega_k^2}\mathbf{k}\right)\cdot\mathbf{p}, V_{k'}^*\right]\right\}a_{k'}^* a_k\right.$$
$$\left.-\left\{[V_k^*, \mathbf{Q}_{k'}\cdot\mathbf{p}]\frac{\omega_{k'}}{\omega_k} + \left[\left(\mathbf{Q}_k^* + \frac{V_k^*}{\omega_k^2}\mathbf{k}\right)\cdot\mathbf{p}, V_{k'}\right]\right\}a_{k'} a_k^*\right].$$

We now use the relation

$$[\mathbf{A}\cdot\mathbf{p}, A'e^{\pm i\mathbf{k}\cdot\mathbf{r}}] = [\mathbf{A}, A'e^{\pm i\mathbf{k}\cdot\mathbf{r}}]\cdot\mathbf{p} \pm \mathbf{A}\cdot\mathbf{k}A'e^{\pm i\mathbf{k}\cdot\mathbf{r}}$$

to transfer $\mathbf{p}$ to the right in U_1 and obtain it in the form

$$U_1 = U + \mathbf{U}_2\cdot\mathbf{p}.$$

In the laboratory system the nucleon will be at rest initially and will acquire a momentum due to collision with the incident pion. The effect of transferring the operator $\mathbf{p}$ to the right in U_1 is that the final momentum has been expressed

in terms of the initial momentum $\mathbf{p}$ and the pion momenta. We shall use the laboratory frame and drop the $\mathbf{U}_2 \cdot \mathbf{p}$ term. Let the initial pion be denoted by $\pi_{k_1\lambda_1}$ and the scattered pion by $\pi_{k_2\lambda_2}$, where we have made the isobaric spin index λ explicit. Then

$$\langle \pi_{k_2\lambda_2}|U|\pi_{k_1\lambda_1}\rangle = \mathscr{M} = \mathscr{M}^{\mathrm{A}} + \mathscr{M}^{\mathrm{R}},$$

where

$$\mathscr{M}^{\mathrm{A}} = -\tfrac{1}{2}[V_1, V_2^*]\,\frac{(\omega_1+\omega_2)}{\omega_1\omega_2}, \tag{11}$$

$$\mathscr{M}^{\mathrm{R}} = -\frac{1}{2M}\,\mathscr{M}^{\mathrm{A}}(\omega_1-\omega_2)\left(1-\frac{\mu^2}{\omega_1\omega_2}\right)$$
$$+\frac{1}{2M}\left\{\mathbf{Q}_2^*\cdot\mathbf{k}_1 V_1\,\frac{\omega_2}{\omega_1} - \mathbf{Q}_1\cdot\mathbf{k}_2 V_2^*\,\frac{\omega_1}{\omega_2}\right\}$$
$$+\frac{1}{2M}\left\{\left(\mathbf{Q}_1+\frac{V_1}{\omega_1^2}\mathbf{k}_1\right)\cdot\mathbf{k}_2 V_2^* + \left(\mathbf{Q}_2^*+\frac{V_2^*}{\omega_2^2}\mathbf{k}_2\right)\cdot\mathbf{k}_1 V_1\right\}.$$

We have used the notation $\omega_i \equiv \omega_{k_i}$ and $V_{k_i\lambda_i} \equiv V_i$. Here $\mathscr{M}^{\mathrm{A}}$ gives us the static part and this is the same as in ordinary perturbation theory when use is made of the energy conservation $\omega_1 = \omega_2$. Since the nucleon in our case will have kinetic energy, say E, after collision, the energy conservation equation we require is

$$\omega_1 = E+\omega_2. \tag{12}$$

Further, $\mathscr{M}$ is now an operator solely dependent on nucleon variables. We apply this to the reaction

$$\pi^+ + \mathrm{p} \to \pi^+ + \mathrm{p}, \tag{13}$$

a pure $T = \frac{3}{2}$ scattering, to estimate the recoil effects. Taking the isobaric spin matrix element and performing the average over initial and sum over final spin states, we obtain the total cross-section (to order μ/M)

$$\sigma(x, a) = 4\pi f^4\mu^{-2}(x^2-1)^{\frac{1}{2}}(a^2x^2-1)^{\frac{3}{2}}\,\frac{(1+a)}{ax}\left\{1-\frac{\mu}{M}(1-a)\left(1-\frac{1}{ax^2}\right)\right\}. \tag{14}$$

Here $a = (\omega_1-E)/\omega_1$ and $X = \omega_1/\mu$ are dimensionless quantities. When $E = 0$, that is the recoil parameter $a = 1$, σ reduces to σ_s, the usual static cross-section.

4. Results and Discussions

The numerical values of σ are given in table 1.

The first column gives the incident laboratory kinetic energy K(MeV), and

the second the corresponding value of X. The other columns give various values of σ in mb.

TABLE 1

The values of the cross-section for the scattering process $\pi^+ + p \to \pi^+ + p$

K (MeV)	X	$\sigma(\infty, a)$		
		$a=1$	$a=0.95$	$a=0.9$
69.5	1.5	3.2	2.5	1.8
139	2	14.0	11.6	9.4
208.5	2.5	34.4	29.0	24.3

Cross-sections are given in mb for various values of the recoil parameter a (cf. eqs. (14) sqq.); K is the incident pion laboratory kinetic energy.

It will be noticed that the cross-section decreases with the increase of recoil energy, that is, decrease of the recoil parameter a. The term with μ/M contributes less than 1 % to the cross-section for the energies considered. The percentage reduction in σ for fixed a is smaller for larger X. In reality the assumption of fixed a for various X is not justified. One would expect a to decrease (i.e. E will increase) with increase of the incident energy X. The suitable value of a has to be determined from a detailed solution of the energy-momentum conservation equations.

The main point which emerges from the calculation is that the μ/M terms are negligible and that recoil may be adequately taken into account by using the energy conservation $\omega_1 = E + \omega_2$ rather than $\omega_1 = \omega_2$ in the expression for the static cross-section. This is the procedure adopted in the Chew-Low formalism for scattering [6]) and pion-production [7]). Similar recoil effects would be expected for the other pion-nucleon scattering cross-sections. A calculation on the above lines is in progress for one-pion production in pion-nucleon collisions.

I wish to thank Dr. S. N. Biswas and Mr. B. M. Udgaonkar for helpful discussion and comments.

References

1) K. Nishijima, Prog. Theor. Phys. **6** (1951) 851, 911;
S. Sato, K. Itabashi and I. Sato, Prog. Theor. Phys. **14** (1955) 303
2) F. Villars, Helv. Phys. Acta **20** (1947) 476
3) R. J. Blin-Stoyle, V. Gupta and H. Primakoff, Nuclear Physics **11** (1959) 444
4) W. Heitler and S. T. Ma, Phil. Mag. **40** (1949) 651
5) E. Corinaldesi and G. Field, Phil. Mag. **40** (1949) 1159
6) G. F. Chew and F. E. Low, Phys. Rev. **101** (1956) 1570
7) J. Franklin, Phys. Rev. **105** (1957) 1101

1.D.2:
4.A

Nuclear Physics **18** (1960) 91—109; © *North-Holland Publishing Co., Amsterdam*
Not to be reproduced by photoprint or microfilm without written permission from the publisher

THE ELECTRIC QUADRUPOLE INTERACTION IN BETA DECAY

J. M. PEARSON † and M. A. PRESTON

Dept. of Physics, Hamilton College, McMaster University, Hamilton, Ontario

Received 15 March 1960

Abstract: In the β-decay of strongly deformed nuclei the electrostatic field in which the decay electron moves by no means possesses the spherical symmetry that it has been customary to assume in β-decay theory. The angular momentum of the electron will not be conserved and different, closely lying, rotational states of the daughter nucleus will be coupled together. In this work we consider the possibility that it is this electric quadrupole coupling, rather than a failure of pure rotational structure, that is responsible for the observed anomalies in the branching ratios of the first forbidden decays of Lu^{176}, Ta^{180} and Np^{238}. The general theory of the β-decay of strongly deformed nuclei is set up, taking into account the electric quadrupole coupling, and specialized to the case of first forbidden decays of even nuclei. The electron functions are obtained by an essentially exact method, the Dirac equation appropriate to a non-central interaction being solved numerically on a computer. It is found that the coupling effect on the branching ratio can be no larger than 4 % or so, which is far too small to account for the observed values.

1. Introduction

The calculation of transition rates (both beta and electro-magnetic) in nuclei is greatly confused by uncertainties in the nuclear wave functions. However, Alaga *et al.* [1]) have pointed out that a considerable simplification is possible for strongly deformed nuclei, where there is a well-defined separation of rotational and intrinsic nuclear structure. For then the *relative* transition rate, i.e. the branching ratio, of transitions of the same multipolarity L from an initial state I_i to two different daughter states, I_f^1 and I_f^2, belonging to the same rotational band, depends only on the rotational wave functions, being

$$\frac{w_0(I_f^1)}{w_0(I_f^2)} = \sqrt{\frac{2I_f^1+1}{2I_f^2+1}} \frac{\sum_{M_f} |\langle D^{I_f^1}_{M_f K_f} | D^L_{M_f - M_i,\, K_f - K_i} | D^{I_i}_{M_i K_i} \rangle|^2}{\sum_{M_f} |\langle D^{I_f^2}_{M_f K_f} | D^L_{M_f - M_i,\, K_f - K_i} | D^{I_i}_{M_i K_i} \rangle|^2}, \tag{1}$$

in the notation of Bohr and Mottelson [2]). Thus, although the absolute transition rate will still depend on the intrinsic nuclear structure the branching ratio will be independent of this and be essentially a geometric quantity.

† Now at Western Reserve University, Cleveland, Ohio. The work described herein is based on a Ph. D. thesis submitted by this author to McMaster University.

The most common such branched β-decays are from a 1^- parent state of an odd nucleus to the 0^+ and 2^+ states of the lowest rotational band of the even daughter, for which the branching ratio (1) becomes

$$\frac{w_0(I_f=0)}{w_0(I_f=2)}=2. \tag{2}$$

Well established departures from this value occur in three decays: those of Lu^{176}, Ta^{180} and Np^{236} (see, e.g. ref. [3])). For the first two the branching ratios are of the order of unity but such departures could conceivably be accounted for by the ignored B_{ij} matrix element, for which $L = 2$ (see, e.g., Konopinski and Uhlenbeck [4])). However, this cannot explain the anomalous branching of Np^{236}, in which it is the 0^+ transition that is enhanced, the branching ratio being ≈ 4. The only other possible state assignment to Np^{236}, consistent with the observed *ft* values of both branches being first forbidden, is 2^-. The ground state transition would then be pure $L = 2$, while the 2^+ transition would be a mixture of $L = 1$ and $L = 2$. Since the latter cannot interfere it follows that the expression (1) becomes $w_0(I_f = 0)/w_0(I_f = 2) < 0.7$, which makes the anomaly even worse. These failures in the intensity relation (1) could be interpreted as indicating a serious breakdown in pure rotational structure but in this work we wish to investigate a possible alternative explanation.

These strongly deformed nuclei possess large intrinsic quadrupole moments Q_0 so that there is a considerable departure from spherical symmetry in the electrostatic field in which the decay electron moves. Consequently, in the decay of these nuclei neither the angular momentum of the electron j_e, nor that of the daughter nucleus I_f, will be conserved. In particular, for the decays we have considered, the closely lying 0^+ and 2^+ states, having the same parity, may be expected to be coupled together quite strongly by the quadrupole interaction with the decay electron. Only asymptotically, when the decay electron is beyond the range of the quadrupole interaction, will the daughter nucleus be in a definite state. Consequently, if the daughter nucleus is observed to be in the 0^+ state it will actually have had the 2^+ state coupled in with it when the decay was taking place, and conversely for an observed 2^+ state. Therefore we no longer have eqs. (1) and (2) for the branching ratio but rather

$$\frac{w(I_f=0)}{w(I_f=2)}=\frac{a_1w_0(I_f=0)+a_2w_0(I_f=2)}{b_1w_0(I_f=2)+b_2w_0(I_f=0)}, \tag{3}$$

where in the limit of $Q_0 = 0$ we shall have $a_1 = b_1 = 1$, $a_2 = b_2 = 0$.

In section 2 we obtain an expression for the transition probability to states of the coupled daughter nucleus-electron system, in which the separate angular momenta are only asymptotically conserved. In the next section a set of exact equations is derived for a Dirac electron coupled by the quadrupole interaction

to the daughter nucleus. The angular part is separated, leaving a set of coupled first order equations for the electron radial functions. Section 4 is concerned with the method of solution of these equations and the actual numerical work is described in section 5. We limited ourselves to the case of Np^{236}, which was assumed to decay from a 1^- state. The intrinsic quadrupole moment of the daughter nucleus Pu^{236} has not been measured but we took its magnitude to be 15 b, the highest measured value in this region being that of U^{233}, which is 14 b (see, e.g. ref. [5])) †. Since the sign of Q_0 in this mass number region has been reported both as positive [7]) and negative [8]) we decided to consider both signs. A limitation is placed on the accuracy with which the branching ratio can be calculated by the fact that it is no longer independent of the intrinsic nuclear structure when a quadrupole coupling is present. However the fact that the *ft* values of the decays are normal and show no evidence of excessive cancellation of the nuclear matrix elements permits us to draw some conclusion concerning whether or not the quadrupole coupling has a significant effect on the branching ratio.

Since this work was completed we have found that other workers [9, 10]) have also been investigating the role of the quadrupole interaction in β-decay.

2. The Transition Probability to States of Coupled Angular Momenta

In the initial system the energies of the parent nucleus and of the absorbed neutrino, and their respective angular momenta I_1 and j_ν, are all conserved. The initial state, therefore, is expressed in the usual representation, i.e. one in which all these constants of motion, as well as the z-components of the two angular momenta M_1 and μ_ν are diagonal. The basic states can then be written as $\Psi^{M_1}_{I_1}\psi^{\mu_\nu}_{\kappa_\nu}(-q)$, where $\Psi^{\mu_\nu}_{\kappa_\nu}(-q)$ is the Dirac wave function of the appropriate absorbed neutrino of energy $-q$ and where the nuclear wave function becomes in the limit of pure rotational structure

$$\Psi^{M_1}_{I_1} = \sqrt{\frac{2I_1+1}{16\pi^2}}\,[X^{\tau_1}_{K_1}(\mathbf{r}')D^{I_1}_{M_1K_1}(\Theta)+(-)^{I_1-J}X^{\tau_1}_{-K_1}(\mathbf{r}')D^{I_1}_{M_1-K_1}(\Theta)] \qquad (4)$$

(see, e.g., Moszkowski [11])).

In the absence of a quadrupole coupling let us describe the final system in a representation in which the total angular momentum $\mathbf{J} = \mathbf{j}_e+\mathbf{I}_f$ and its z-component M are diagonal, rather than the z-components M_f and μ_e of I_f and j_e respectively. With the total energy W being a constant of the motion, the conservation of the electron energy W_e automatically follows from $W = W_e+E_{I_f}$, since E_{I_f}, the energy of the nuclear state I_f, is also conserved.

† However, recent data [6]) on the even nuclei in this mass number region suggest $|Q_0| \approx 10.7$ b for Pu^{236}.

For the basic states we write

$$\Xi(JMW, \kappa_e I_t) = \sum_{\mu_e} C \begin{pmatrix} J & j_e & I_t \\ M & \mu_e & M_t \end{pmatrix} \Psi_{I_t}^{M_t} \psi_{\kappa_e}^{\mu_e}(W_e), \tag{5}$$

in which the C factors are the Clebsch-Gordan coefficients, denoted by Condon and Shortley [12]) as $(j_e I_t \mu_e M_t | j_e I_t JM)$. Because we are considering just the lowest intrinsic state of an even nucleus the nuclear wave function here simplifies to

$$\Psi_{I_t}^{M_t} = \sqrt{\frac{2I_t+1}{8\pi^2}}\, X_0^{\tau_t}(\mathbf{r}') D_{M_t 0}^{I_t}(\Theta) \tag{6}$$

in the limit of pure rotational structure (see, e.g. ref. [11])). The electron function is just the usual central field Dirac spinor

$$\psi_{\kappa_e}^{\mu_e}(W_e) = \begin{bmatrix} -if_{\kappa_e}(W_e) X_{-\kappa_e}^{\mu_e} \\ g_{\kappa_e}(W_e) X_{\kappa_e}^{\mu_e} \end{bmatrix} \tag{7}$$

(see, e.g., ref. [13]). Here the $X_{\pm\kappa_e}^{\mu_e}$ are the two-component Pauli spinors

$$X_\kappa^\mu = \sum_{\tau=\pm\frac{1}{2}} C \begin{pmatrix} j & l_\kappa & \frac{1}{2} \\ \mu & \mu-\tau & \tau \end{pmatrix} Y_{l_\kappa}^{\mu-\tau}(\theta,\phi) \begin{bmatrix} \frac{1}{2}+\tau \\ \frac{1}{2}-\tau \end{bmatrix}. \tag{8}$$

The f and g are real radial functions satisfying the pair of first order coupled equations

$$\begin{aligned} (W_e - V_c + 1) f - \frac{dg}{dr} - (\kappa_e + 1)\frac{g}{r} &= 0, \\ (W_e - V_c - 1) g + \frac{df}{dr} - (\kappa_e - 1)\frac{f}{r} &= 0, \end{aligned} \tag{9}$$

V_c being the central potential. If the electron wave functions are normalized according to

$$\langle \psi_{\kappa'_e}^{\mu'_e}(W'_e) | \psi_{\kappa_e}^{\mu_e}(W_e) \rangle = \delta_{\kappa'_e \kappa_e} \delta_{\mu'_e \mu_e} \delta(W'_e - W_e), \tag{10}$$

the radial functions behave asymptotically as

$$\begin{aligned} f_{\kappa_e}(W_e) &\sim -\frac{1}{r}\sqrt{\frac{W_e-1}{\pi\rho}} \sin(\rho r + \delta + \varepsilon), \\ g_{\kappa_e}(W_e) &\sim \frac{1}{r}\sqrt{\frac{W_e+1}{\pi\rho}} \cos(\rho r + \delta + \varepsilon), \end{aligned} \tag{11}$$

where ρ is the asymptotic momentum $(W_e^2-1)^{\frac{1}{2}}$; δ is given by Rose [14]) and ε is some constant phase angle, zero only for a point nuclear charge.

The presence of a quadrupole interaction introduces an extra term H_Q into the total Hamiltonian H of the final system. As J and M are still constants of the motion we shall continue to use a representation in which they are diagonal. However, rather than finding what the other operators are that have replaced κ_e and I_f as constants of motion let us choose the new basic states belonging to given J, M and W according to the method of Lippmann and Schwinger [15]) as

$$Y(JMW,l) = \Xi(JMW,l) + \frac{\Xi(JMW,l)}{W-H+i\eta}, \tag{12}$$

where l labels the states such that $\Xi(JMW, l)$ is an abbreviation for $\Xi(JMW, \kappa_e^l I_f^l)$

It is clear that the states $Y(JMW, l)$ so defined will satisfy the same boundary conditions at the origin as do the $\Xi(JMW, l)$, i.e. they will be regular there, and asymptotically they will assume the form of central field eigenstates belonging to κ_e^l, I_f^l. Furthermore, these states are known to constitute a complete set (they are the so-called outgoing wave solutions) and since each state is characterized by different values of κ_e^l and I_f^l it follows that imposing on an eigenstate belonging to J, M and W the condition that it has certain values κ_e^l and I_f^l as "asymptotic eigenvalues" will uniquely define that state.

Although eq. (12) is the basis of a perturbation treatment it is used here simply to establish the required formal properties of the Y states: the intention is to calculate these states exactly, since it was felt that perturbation theory may be unreliable, besides being little simpler than an exact treatment. With $\Xi(JMW, l)$ being orthogonal,

$$\langle \Xi(J'M'W', l') | \Xi(JMW, l) \rangle = \delta_{JJ'}\delta_{MM'}\delta_{ll'}\delta(W'-W), \tag{13}$$

it follows that

$$\begin{aligned} \langle \Xi(J'M'W', l') | Y(JMW, l) \rangle &= \langle Y(J'M'W', l') | Y(JMW, l) \rangle \\ &= \delta_{JJ'}\delta_{MM'}\delta_{ll'}\delta(W'-W). \end{aligned} \tag{14}$$

This result, which occurs implicitly quite often in the literature is most easily proved by a straight-forward generalization of section 2 of the paper of Gell-Mann and Goldberger [16]). It does not depend on any perturbation treatment of H_Q, but requires only that this falls of sufficiently rapidly at large distances so that $\langle \Xi(JMW, l) | H_Q | \Xi(JMW, l) \rangle < \infty$, which is, of course, the case. However, the result holds only for true continuum states and will fail if the states are confined within a finite enclosure. Although eq. (14) shows that the states $Y(JMW, l)$ form an orthogonal set, it does not necessarily follow, of course, that they are eigenstates of the new constants of motion that have replaced κ_e and I_f; we do not need to know what these constants of motion are, nor do we attempt to determine them.

The β-decay transition rate can now be calculated in the usual way by using standard time-dependent perturbation theory with the $Y(JMW, l)$ states as the basic set of orthonormal states of the final system. Two viewpoints are possible as to what state is appropriate to observed quantum numbers $\kappa_e{}^{\nu'}, I_f{}^{\nu'}$:

1) These are "asymptotic quantum numbers", whence the rate of transitions directly to the state $Y(JMW, l')$ is required.

2) The state must be a true eigenstate belonging to $\kappa_e{}^{\nu'}$ and $I_f{}^{\nu'}$, i.e. it must be the central field state $\Xi(JMW, l')$. Hence the $Y(JMW, l)$ states which have to be retained as the basic set, since they rather than the $\Xi(JMW, l)$ states are eigenstates of H, must be projected onto the latter.

Now eq. (14) shows that the two viewpoints will lead to the same result, whence the dilemma is resolved. With H_β being the β-decay interaction Hamiltonian we shall have for the total transition rate to the observed nuclear state $I_f{}^{\nu'}$

$$w(I_f{}^{\nu'}) = 2\pi \int_1^{W_0{}^{\nu}} \mathrm{d}W_e{}^{\nu'} \sum_{\substack{J, M, l \\ \kappa_\nu, \mu_\nu}} \delta_{I_f{}^{l} I_f{}^{\nu}} |\langle Y(JMW, l)|H_\beta|\Psi_{I_1}^{M_1}\psi_{\kappa_\nu}^{\mu_\nu}(-q)\rangle|^2. \quad (15)$$

The summation with respect to l runs over all possible values of the asymptotic quantum numbers $\kappa_e{}^{l}, I_f{}^{l}$. The spectrum end-point $W_0{}^{\nu'}$ is appropriate to the nuclear state $I_f{}^{\nu'}$ and $W_e{}^{\nu'} = W - E_{I_f{}^{\nu}}$ is the asymptotic electron energy. The energy of the equivalent *emitted* neutrino is then given by $W_0{}^{\nu'} = W_e{}^{\nu'} + q$. The state density factor is just unity if δ-function normalization is adopted for the neutrino states as well as for the electron states.

We expand the final system states $Y(JMW, l)$ in terms of the discrete basic set consisting of eigenstates of nuclear and electron angular momenta,

$$Y(JMW, l) = \sum_{I_f \kappa_e \mu_e} C \begin{pmatrix} J & j_e & I_f \\ M & \mu_e & M_f \end{pmatrix} \Psi_{I_f}^{M_f} \begin{bmatrix} -iF_{\kappa_e I_f}(JW, l) X_{-\kappa_e}^{\mu_e} \\ G_{\kappa_e I_f}(JW, l) X_{\kappa_e}^{\mu_e} \end{bmatrix}. \quad (16)$$

This represents a mixture of the coupled nuclear states, each of which is associated with all possible angular momentum states of the electron. The angular part of the electron wave functions must be as in the central field case, but W_e is no longer a constant of the motion and so the radial dependence will be different. In writing the radial functions it is tacitly assumed that they are independent of both M and μ_e: this is shown in section 3 but is assumed here for brevity of notation. However, the functions will in general depend on both J and I_f, the nuclear state with which they are associated. The dependence on the asymptotic quantum numbers takes the form of the following asymptotic behaviour:

$$\begin{aligned} F_{\kappa_e I_f}(JW, l) &\sim -\delta_{\kappa_e \kappa_e{}^{l}} \delta_{I_f I_f{}^{l}} \frac{1}{r} \sqrt{\frac{W_e{}^{l} - 1}{\pi \rho^{l}}} \sin(\rho^{l} r + \delta^{l} + \varepsilon), \\ G_{\kappa_e I_f}(JW, l) &\sim \quad \delta_{\kappa_e \kappa_e{}^{l}} \delta_{I_f I_f{}^{l}} \frac{1}{r} \sqrt{\frac{W_e{}^{l} + 1}{\pi \rho^{l}}} \cos(\rho^{l} r + \delta^{l} + \varepsilon). \end{aligned} \quad (17)$$

The asymptotic momentum ρ^i corresponds to $W_e{}^i$ and δ^i is the value of δ, appearing in eq. (11), appropriate to $W_e{}^i$ and $\kappa_e{}^i$. The constant phase angle ε will generally be different from that in the central field case. In the limit of vanishing quadrupole moment we have, of course,

$$\begin{aligned} F_{\kappa_e I_t}(JW, l) &= \delta_{\kappa_e \kappa_e{}^i}\delta_{I_t I_t{}^i} f_{\kappa_e{}^i}(W_e{}^i), \\ G_{\kappa_e I_t}(JW, l) &= \delta_{\kappa_e \kappa_e{}^i}\delta_{I_t I_t{}^i} g_{\kappa_e{}^i}(W_e{}^i), \end{aligned} \tag{18}$$

where the functions f and g are the usual central field radial functions, satisfying eqs. (9) and (10). Thus the essential difference from the central field case is that states which asymptotically have the form of central fields states will, in the region close to the nucleus, be coupled in with other states belonging to different values of κ_e and I_t, and which vanish asymptotically.

A multipole expansion of the matrix element of H_β, appearing in eq. (15), into products of quantities dependent on the lepton states and nuclear matrix elements of various spherical tensor operators can now be effected, exactly as in the standard theory. It will be seen from the numerical results in section 5 that the degree of forbiddenness approximation adopted in the standard theory is valid here. That is, although electron states that in the central field limit would give a dominant contribution to the transition probability are here coupled in with electron states corresponding to higher degrees of forbiddenness, the coupling is not strong enough to make the contribution of these latter states any more significant. Thus the present theory considers only the same combinations of electron and neutrino angular momenta and the same spherical tensor operators in nuclear space as does the standard theory, but they are, of course, involved in a much more complicated way because of the coupling. To each asymptotic pair of eigenvalues $\kappa_e{}^i$ and $I_t{}^i$, there will correspond several sets of terms each characterized by different values of κ_e and I_t.

Because of the great complexity of the problem we do not attempt to derive general expressions for an arbitrary degree of forbiddenness but instead consider just the case of present interest: that of a non-unique first forbidden transition. We assume the currently accepted VA form of the interaction and make the fairly common approximation of ignoring the contribution of the second rank tensor that corresponds to the B_{ij} matrix element, so that there will appear just the following operators, all of which are to be regarded as containing the appropriate coupling constants: $Y_1{}^m(\mathbf{r})$, $T_{11}^m(\mathbf{r}, \boldsymbol{\sigma})$, and $T_{10}^m(\mathbf{r}, \boldsymbol{\alpha})$ (see, e.g., Rose and Osborn [17])).

Using the nuclear wave functions (4) and (6), which describe pure rotational structure, we can write for the nuclear matrix elements of an arbitrary spherical tensor $T_L{}^m(\omega)$ of rank L:

$$\langle \Psi_{I_t}^{M_t} | T_L{}^m(\omega) \Psi_{I_1}^{M_1} \rangle = \sqrt{\frac{1}{2I_t+1}}\, C\begin{pmatrix} I_t & I_1 & L \\ M_t & M_1 & m \end{pmatrix} C\begin{pmatrix} I_t & I_1 & L \\ 0 & K_1 & -K_1 \end{pmatrix} M_L(\omega') \tag{19}$$

Here we have the characteristic separation into a purely geometric factor and the intrinsic nuclear matrix element

$$M_L(\omega') = \sqrt{\frac{2I_1+1}{2}} \{\langle X_0^{\tau_1}(\mathbf{r}')|T_L^{-K_1}(\omega')|X_{K_1}^{\tau_1}(\mathbf{r}')\rangle + (-)^{I_f+I-L}\langle X_0^{\tau_1}(\mathbf{r}')|T_L^{K_1}(\omega')|X_{-K_1}^{\tau_1}(\mathbf{r}')\rangle, \tag{20}$$

where the prime on ω' signifies that $T_L^M(\omega')$ is to be expressed in the nuclear fixed co-ordinate system.

In the first forbidden approximation the only values of j_ν which give a contribution are $\frac{1}{2}$ and $\frac{3}{2}$. Then with $I_1 = 1$ it follows from $\mathbf{J} = \mathbf{I}_1+\mathbf{j}_\nu$ that the significant values of J are $\frac{1}{2}$, $\frac{3}{2}$ and $\frac{5}{2}$, and we can write eq. (15) in the form

$$w(I_f^{\tau}) = 2\pi \int_1^{W_0^{\nu}} \mathrm{d}W_e^{\tau} \sum_{J,l} \delta_{I_f^{\tau} I_f^{\nu}} Q_{J,l}, \tag{21}$$

where the quantities $Q_{J,l}$ are given in the appendix. There the abbreviated notation $F_{\kappa_e I_f}$ for $F_{\kappa_e I_f}(JW, l)$, etc., is adopted. No confusion can occur if it is made explicit which $Q_{J,l}$ is being referred to. The expressions for $Q_{J,l}$ are written in such a way that within the square brackets the normal central field terms are separated from the coupling terms. The usual approximation of evaluating the lepton functions at the average nuclear radius R has been made.

It has been checked that eq. (21) reduces to the correct central field limit; in particular it gives the rquired value 2 for the branching ratio in this limit. It will be noticed that in the presence of a quadrupole interaction the branching ratio is no longer independent of the intrinsic nuclear structure.

3. The Coupled Equations of the Electron Wave Functions

The expansion (16) of the basic states $Y(JMW, l)$ of the final system consisting of the daughter nucleus and the decay electron, based on the fact that they are eigenstates of J and M, leaves undetermined only the radial functions $F_{\kappa_e I_f}(JW, l)$ and $G_{\kappa_e I_f}(JW, l)$. The further fact that the states are also eigenstates of the final system Hamiltonian H now leads to a system of equations in the radial functions. It will, of course, be impossible to obtain a system of equations that define the functions completely, since the states are not chosen to be eigenstates of the remaining constants of motion. The complete definition will depend, rather, on the imposition of the boundary condition (17).

We have

$$H|Y(JMW, l)\rangle \equiv (H_{\mathrm{nuc}}+H_e+H_Q)|Y(JMW, l)\rangle = W|Y(JMW, l)\rangle, \tag{22}$$

where H_{nuc} is the nuclear Hamiltonian and H_e is the familiar Dirac Hamiltonian for an electron in a central field,

$$H_e = -\boldsymbol{\alpha}\cdot\boldsymbol{\varrho}-\beta+V_e \tag{23}$$

in the usual notation. The Hamiltonian H_Q of the interaction of the electron with the nuclear quadrupole moment is

$$H_Q = -\tfrac{1}{2}e^2Q_0f(r)P_2\,(\cos\theta'), \tag{24}$$

where θ' is the polar angle of the electron position vector with respect to the symmetry axis of the nucleus and $f(r)$ is a radial function which outside the nucleus is r^{-3} but inside the nucleus depends on the charge distribution.

Eq. (22) can be simplified by removing from it the dependence on the intrinsic nuclear structure, this being the same for both of the coupled states of the daughter nucleus. Let us write, with an obvious meaning,

$$H_{\text{nuc}} = H_{\text{rot}} + H_{\text{int}}$$

and

$$W^* = W - E_0, \tag{25}$$

where E_0 is the energy of the ground state ($I_f = 0$) of the daughter nucleus, i.e., it is the energy associated with the intrinsic nuclear structure. Then (23) becomes

$$(H_{\text{rot}} + H_e + H_Q)|\Phi(JMW,l)\rangle = W^*|\Phi(JMW,l)\rangle, \tag{26}$$

where, from eqs. (6) and (16)

$$\Phi(JMW,l) = \sum_{I_f\kappa_e\mu_e} \sqrt{\frac{2I_f+1}{8\pi^2}}\, C\begin{pmatrix} Jj_eI_f \\ M\mu_eM_f\end{pmatrix}\begin{bmatrix} -iF_{\kappa_eI_f}(JW,l)X^{\mu_e}_{-\kappa_e} \\ G_{\kappa_eI_f}\quad (JW,l)X^{\mu_e}_{\kappa_e}\end{bmatrix} D^{I_f}_{M_f0}(\Theta). \tag{27}$$

The angular dependence is removed from eq. (26) by introducing the quantities

$$\pm\,\Omega^{I'_f\kappa'_e}_{JM} = \sum_{\mu'_e} \sqrt{\frac{2I_f+1}{8\pi^2}}\, C\begin{pmatrix} J\ j'_e\ I'_f \\ M\mu'_eM'_f\end{pmatrix}\begin{bmatrix} X^{\mu'_e}_{-\kappa'_e} \\ X^{\mu'_e}_{\kappa'_e}\end{bmatrix} D^{I'_f}_{M'_f0}(\Theta) \tag{28}$$

and then forming the scalar products of both sides of (26) with $\langle\pm\Omega^{I'_f\kappa'_e}_{JM}|$.

This gives

$$\langle\pm\Omega^{I'_f\kappa'_e}_{JM}|H_{\text{rot}} + H_e + H_Q|\Phi(JMW,l)\rangle = W^*\{-iF_{\kappa'_eI'_f}(JW,l) + G_{\kappa'_eI'_f}(JW,l)\}, \tag{29}$$

which reduces to a system of first order coupled equations in the radial functions on working out the left-hand side, term by term. The calculation is straightforward, being based essentially on the standard results of the quantum theory of angular momentum (see, e.g., Rose [18]) †), but is somewhat lengthy

† Note that Rose's D functions are the complex conjugates of the ones we have used, which are the usual ones adopted in the collective model literature (see, e.g., ref. [11])).

and so will not be presented here. In writing down the coupled equations it will be convenient to use for the radial functions the notation introduced at the end of the preceding section: no ambiguity can arise since different values of J and W are not coupled together and the equations obviously do not contain any reference to the asymptotic quantum numbers $\kappa_e{}^1$ and $I_f{}^1$ The coupled equations take the form

$$(W^*-V_c+1)F_{\kappa_e 0}-\frac{dG_{\kappa_e 0}}{dr}-(\kappa_e+1)\frac{G_{\kappa_e 0}}{r}+e^2Q_0f(r)\sum_{\kappa'_e}a^{\kappa_e}_{\kappa'_e}F_{\kappa'_e 2}=0,$$

$$(W^*-V_c-1)G_{\kappa_e 0}+\frac{dF_{\kappa_e 0}}{dr}-(\kappa_e-1)\frac{F_{\kappa_e 0}}{r}+e^2Q_0f(r)\sum_{\kappa'_e}a^{\kappa_e}_{\kappa'_e}G_{\kappa'_e 2}=0,$$

$$\begin{aligned}(W^*-E_2{}^*-V_c+1)F_{\kappa_e 2}-\frac{dG_{\kappa_e 2}}{dr}-(\kappa_e+1)\frac{G_{\kappa_e 2}}{r}\\+e^2Q_0f(r)\sum_{\kappa'_e}\{b^{\kappa_e}_{\kappa'_e}F_{\kappa'_e 0}+c^{\kappa_e}_{\kappa'_e}F_{\kappa'_e 2}\}=0,\end{aligned}\tag{30}$$

$$\begin{aligned}(W^*-E_2{}^*-V_c-1)G_{\kappa_e 2}+\frac{dF_{\kappa_e 2}}{dr}-(\kappa_e-1)\frac{F_{\kappa_e 2}}{r}\\+e^2Q_0f(r)\sum_{\kappa'_e}\{b^{\kappa_e}_{\kappa'_e}G_{\kappa'_e 0}+c^{\kappa_e}_{\kappa'_e}G_{\kappa'_e 2}\}=0,\end{aligned}$$

where

$$a^{\kappa_e}_{\kappa'_e}=(-)^{j_e+l\kappa_e+\frac{1}{2}}\{\tfrac{1}{20}(2j'_e+1)(2l_{-\kappa'_e}+1)\}^{\frac{1}{2}}C\begin{pmatrix}l_{-\kappa_e} & l_{-\kappa'_e} & 2\\ 0 & 0 & 0\end{pmatrix}W(l_{-\kappa_e}j_el_{-\kappa'_e}j'_e,\tfrac{1}{2}2),$$

$$b^{\kappa_e}_{\kappa'_e}=(-)^{l-\kappa_e+J-\frac{1}{2}}\delta_{Jj'_e}\{\tfrac{1}{20}(2j_e+1)(2l_{-\kappa'_e}+1)\}^{\frac{1}{2}}C\begin{pmatrix}l_{-\kappa_e} & l_{-\kappa'_e} & 2\\ 0 & 0 & 0\end{pmatrix}W(l_{-\kappa_e}j_el_{-\kappa'_e}j'_e,\tfrac{1}{2}2),$$

$$\begin{aligned}c^{\kappa_e}_{\kappa'_e}=(-)^{l-\kappa_e+j_e+\frac{1}{2}}\{\tfrac{5}{14}(2j_e+1)(2j'_e+1)(2l_{-\kappa'_e}+1)\}^{\frac{1}{2}}\\\times C\begin{pmatrix}l_{-\kappa'_e} & l_{-\kappa'_e} & 2\\ 0 & 0 & 0\end{pmatrix}W(l_{-\kappa_e}j_el_{-\kappa'_e}j'_e,\tfrac{1}{2}2)W(j'_e2J2,j_e2).\end{aligned}$$

The coefficients $W(abcd, ef)$ are the usual Racah coefficients, and $E_2{}^*$ is the excitation energy of the state $I_f = 2$, i.e., $E_2{}^* = E_2 - E_0$.

It will be seen that the radial functions are independent of the magnetic quantum numbers. Also the equations reduce to the central field form (9) in the limit of Q_0 being zero. The summation with respect to κ'_e occurring in the equations goes over all values that are coupled in with κ_e by the quadrupole interaction, i.e. that satisfy

$$|j'_e-j_e|\leqq 2\leqq j'_e+j_e \tag{31}$$

and

$$l_{\kappa_e}+l_{\kappa'_e}\ (\text{or } l_{-\kappa_e}+l_{-\kappa'_e})=\text{even integer}. \tag{32}$$

With I_t and I'_t satisfying a relation similar to eq. (31) it readily follows that the two triangular relations implied by

$$\mathbf{j}_e + \mathbf{I}_t = \mathbf{j}'_e + \mathbf{I}'_t = \mathbf{J}$$

can be simultaneously satisfied.

For each pair of coupled (κ_e, I_t) values belonging to a given J there will correspond a pair of equations and because of eq. (32) the complete system of coupled equations will separate into two sets. We shall not write down explicitly the coupled equations that eq. (30) gives for the J values of interest but will merely state the different (κ_e, J_t) values that are coupled together.

a) $J = \frac{1}{2}$: two sets, each of six equations.
Set I: (1,0), (−2,2), (3,2).
Set II: (−1,0), (2,2), (−3.2),

b) $J = \frac{3}{2}$: two sets, each of ten equations.
Set I: (2,0), (−1,2), (2,2), (−3,2), (4,2).
Set II: (−2,0), (1,2), (−2,2), (3,2), (−4,2).

c) $J = \frac{5}{2}$: two sets, each of twelve equations.
Set I: (3,0), (1,2), (−2,2), (3,2), (−4,2), (5,2).
Set II: (−3,0), (−1,2), (2,2), (−3,2), (4,2), (−5,2).

4. The Boundary Conditions on the Electron Functions

A particular system of the equations (30) will uncouple asymptotically into n pairs of central field equations of the form (9), each one of which is characterized by one of the n different pairs of (κ_e, I_t) values that are coupled together. Therefore each of these (κ_e, I_t) values, but only these, can be asymptotic quantum numbers.

In section 2 it has been stated that the $Y(JMW, l)$ states are orthogonal and are uniquely defined by the asymptotic quantum numbers. It follows that the particular system must be n-fold degenerate. On the other hand, such a system contains $2n$ equations in $2n$ functions so that there must be $2n$ linearly independent solutions. It is, however, easy to show that of the complete set of solutions of eq. (30) half must be regular at the origin and half irregular, provided only that the potential functions occurring in eqs. (30) do not contain any essential singularities, i.e., provided that there are regular solutions at all. In solving the coupled equations (30), then, we are confronted with a minor problem in the form of two-point boundary conditions: the solutions have to be regular at the origin and asymptotically satisfy eq. (17). Only in the central field case will the boundary condition at the origin determine the asymptotic form.

For the required solutions $F_{\kappa_0 l_l'}(JW, l)$, $G_{\kappa_0 l_l'}(JW, l)$ let us adopt the contracted notation F_i^l, G_i^l, respectively. Let us also write a particular solution to all $2n$ functions, e.g., the set $F_1^l, G_1^l, \ldots, F_i^l, G_i^l, \ldots F_n^l, G_n^l$ as a column vector ϕ^l, called a solution vector. Then any solution vector whatsoever can be written as

$$\sum_l A_l \phi^l, \tag{33}$$

since the completeness of the set of the ϕ^l must follow from that of the $Y(JMW, l)$. The $2n \times n$ matrix whose columns are $\phi^1, \ldots \phi^l, \ldots \phi^n$ we write as $\{\phi\}$.

Outside of the nucleus the quadrupole coupling term in eq. (30) falls off as r^{-3}, while all other terms fall off as r^{-1} at the most. Hence the solutions F_i^l, G_i^l will tend to the form of central field solutions long before these latter assume their asymptotic form (11). The boundary condition (17) can therefore be replaced by

$$\left.\begin{matrix} F_i^l \\ G_i^l \end{matrix}\right\} \to \delta_{il} \begin{cases} f_i \\ g_i \end{cases}, \tag{34}$$

where f_i, g_i are abbreviations for the $f_{\kappa_0 i}, g_{\kappa_0 i}$ of eq. (11). The $\to$ sign is used here in contrast to the $\sim$ sign to indicate the greater rate at which the right hand side of the expression is approached. From eq. (34) we have for the matrix of regular solutions

$$\{\phi\} \to \begin{pmatrix} f_1 & \cdots & 0 & \cdots & 0 \\ g_1 & & 0 & & 0 \\ 0 & & \cdot & & \cdot \\ 0 & & \cdot & & \cdot \\ \cdot & & 0 & & \cdot \\ \cdot & & 0 & & \cdot \\ \cdot & & f_i & & \cdot \\ \cdot & & g_i & & \cdot \\ \cdot & & 0 & & \cdot \\ \cdot & & 0 & & \cdot \\ \cdot & & \cdot & & 0 \\ \cdot & & \cdot & & 0 \\ 0 & & 0 & & f_n \\ 0 & \cdots & 0 & \cdots & g_n \end{pmatrix} \tag{35}$$

Suppose now that we compute *any* complete set of regular solutions to eq. (30). This can be done quite easily since it is sufficient to integrate the equations outwards from the origin with starting values chosen to guarantee the linear independence of the solutions; no attention to the asymptotic boundary conditions is necessary. Let us write these solutions as $\mathscr{F}_i^l$, $\mathscr{G}_i^l$ where l again varies from 1 to n, and the matrix of the solutions as $\{\xi\}$. Then it follows from eqs. (33)

and (35) that in the region of vanishing quadrupole interaction $\{\xi\}$ *must* have the following form

$$\{\xi\} \rightarrow \begin{pmatrix} C_{11}\dfrac{f_1}{g_1} & \cdots & C_{1i}\dfrac{f_1}{g_1} & \cdots & C_{1n}\dfrac{f_1}{g_1} \\ \vdots & & \vdots & & \vdots \\ C_{i1}\dfrac{f_i}{g_i} & \cdots & C_{ii}\dfrac{f_i}{g_i} & \cdots & C_{in}\dfrac{f_i}{g_i} \\ \vdots & & \vdots & & \vdots \\ C_{n1}\dfrac{f_n}{g_n} & \cdots & C_{ni}\dfrac{f_n}{g_n} & \cdots & C_{nn}\dfrac{f_n}{g_n} \end{pmatrix}. \qquad (36)$$

The essential content of this statement is that in the central field region the ratio $\mathscr{F}_i^l/\mathscr{G}_i^l$ should be the same for all solutions l. If the computed functions do not satisfy this at some particular value of r, this must be due simply to the fact that the quadrupole interaction is still not negligible (to within the limits of computational accuracy) and that what has been chosen to be called the central field region has not yet been reached. This result would not be possible were there no set of solutions that behaved according to eq. (35) in the central field region. The C_{il} coefficients are determined by continuing the integration out into the central field region and requiring that the amplitudes of the f_i and g_i functions be such that (11) is satisfied.

The required solutions F_i^l and G_i^l are then connected with the computed functions $\mathscr{F}_i^l$ and $\mathscr{G}_i^l$ by

$$F_i^l = \sum_m \{C^{-1}\}_{ml}\,\mathscr{F}_i^m, \text{ etc.}, \qquad (31)$$

where the matrix $\{C^{-1}\}$ is $\{C_{ij}\}^{-1}$. This linear transformation, the coefficients of which are determined in the central field region, is valid everywhere.

5. The Computation and Numerical Results

The numerical solution of the coupled equations (30) was performed on the Bendix G15D computer at McMaster University by the variant of the fourth order Runge-Kutta method due to Gill [19]). Because of the length of computation only one energy value, $W^* = 1.3mc^2$, was taken, trial computations having shown that there was no critical dependence on energy. A uniform charge distribution within the nucleus was assumed. Then the potential functions

appearing in eq. (30) became

$$V_c = \begin{cases} -\dfrac{aZ}{r} & \text{for } r > R, \\ \dfrac{aZ}{2R^3}(r^2 - 3R^2) & \text{for } r < R, \end{cases} \tag{38}$$

$$f(r) = \begin{cases} \dfrac{1}{r^3} & \text{for } r > R. \\ \dfrac{r^2}{R^5} & \text{for } r < R, \end{cases} \tag{39}$$

Had a point nucleus been assumed, the quadrupole interaction would have introduced an essential singularity and regular solutions would not have existed. The value R was taken to be $1.2A^{\frac{1}{3}} \times 10^{-13}$ cm.

The general method of solution has been outlined in the previous section: it is sufficient to compute *any* complete set of regular solutions, $\mathcal{F}_i^l$, $\mathcal{G}_i^l$. We obtained such a set by noting that at the origin the quadrupole coupling vanishes, so that wave equations uncouple into central field equations, as at large distances from the nucleus. Then there will exist a complete set of solutions such that each solution assumes a different (κ_e, I_t) pair of values as constants of the motion at the origin. Thus this set will behave at the origin in exactly the same way as the *required* set does asymptotically. Our method of computing a set of solutions, then, was to put all but one of the pairs $\mathcal{F}_i^l$, $\mathcal{G}_i^l$ equal to zero at the origin, the remaining pair taking just its central field value. With these starting values the solutions to eq. (30) were then computed by an outwards integration. Different solutions were obtained by taking different pairs of functions $\mathcal{F}_i$, $\mathcal{G}_i$ to be non-vanishing at the origin. In the event of there being no quadrupole interaction this would be the only pair of functions that did not vanish *everywhere*.

The actual method of starting the integration requires further consideration. Although the solutions are chosen to be regular at the origin this is still a singular point and hence cannot be included within the domain of computation. Since the potentials (38) and (39) vary slowly near the origin the integration was begun at $r = \frac{1}{5}R$ with functions appropriate to a constant central potential $V_c(r = 0)$. These are just the spherical Bessel functions for energy $W_e^l - V_c(r = 0)$.

The integration was continued out to $r = 5R$ at which point the quadrupole interaction has fallen to 1 % of the central interaction, in our case, so it may be expected that at this distance the electron functions are very close to their central field form (36). This was found to be the case: the ratios $\mathcal{F}_i^l/\mathcal{G}_i^l$ at this point were the same for all solutions l to within 1 %. The determination of the

absolute values of the C_{il} requires that the integration be carried out to the asymptotic region in order to fix the normalization constants of the f_i, g_i. However, it will be seen that this was unnecessary.

Let us assume arbitrary values for the f_i, g_i at $r = 5R$, consistent, of course, with their having the correct ratio. Then from (36) we can calculate coefficients

$$C'_{il} = A_i C_{il}, \tag{40}$$

where A_i is the unknown normalization constant for f_i, g_i. It then readily follows that eq. (37) becomes

$$F_i^l = \frac{1}{A_i} \sum_m \{C'^{-1}\}_{ml} \mathscr{F}_i^m, \quad \text{etc.} \tag{41}$$

Now, whether or not particular F_i^l, G_i^l lead to significant departures from the central field case depends essentially upon the ratios of these functions to the corresponding central field functions at the nuclear radius, i.e. upon the coupling parameters

$$\left(\frac{F_i^l}{f_i}\right)_R, \quad \left(\frac{G_i^l}{g_i}\right)_R.$$

The computation was therefore repeated with the same starting values, but with $Q_0 = 0$. The new, non-vanishing solutions were found to be identical to $\mathscr{F}_i^l$, $\mathscr{G}_i^l$, respectively, to within less than 0.1 %. Hence we may set

$$f_i = \frac{1}{A_i} \mathscr{F}_i^l, \text{ etc.} \tag{42}$$

whence the coupling parameters do not depend on the normalization constants.

We now summarize the results. Firstly, the required functions F_i^l, G_i^l depend hardly at all on the sign of Q_0 but only on its magnitude. Secondly, the functions F_i^l, G_i^l, which may be regarded as the principal functions since these are the only functions that do not vanish beyond the region of significant quadrupole interaction, are identical everywhere to the central field functions f_i, g_i to within less than $\frac{1}{2}$ %, for all three values of J : $\frac{1}{2}$, $\frac{3}{2}$, and $\frac{5}{2}$. Hence there is no significant modification of the central field states and the only consequence the quadrupole interaction can have is essentially a coupling in of the different angular momentum states close to the nucleus. For $i \neq l$ all but two of the coupling parameters are less than $\frac{1}{2}$ % and are therefore ignored. For $J = \frac{3}{2}$ and asymptotic quantum numbers $\kappa_e^l = -1$, $I_l^l = 2$ we have

$$\left(\frac{F_{2,0}^{-1,2}}{f_{1,2}}\right)_R = -\frac{1}{30},$$

and for $J = \frac{3}{2}$ and asymptotic quantum numbers $\kappa_e{}^I = 1$, $I_f{}^I = 2$

$$\left(\frac{G^{1,2}_{2,0}}{g_{1,2}}\right)_R = -\frac{1}{30}$$

also. Both of these correspond to a mixing of the two nuclear states and furthermore the coupled κ_e values both correspond to first forbidden transitions: hence the approximation in the multipole expansion of eq. (15) is justified. Now because all the electron functions can be expressed in terms of central field functions and because of the numerical equality of the two coupling parameters for $i \neq l$, it turns out that all the electron terms appearing in the $Q_{J,l}$ of (21) can be expressed in terms of tabulated functions [20]). Thus the absolute values of our electron functions do not have to be computed and it is unnecessary to continue the integration beyond the region of negligible quadrupole interaction.

The effect of the coupling on the branching ratio can now be given in terms of the nuclear matrix elements that appear in the expressions given in the appendix for the $Q_{J,l}$; clearly only the $I_f = 2$ transition is affected. The term in $\mathrm{Im}\, M_{11}(\mathbf{r}, \sigma) M^*_{10}(\mathbf{r}, \alpha)$ is reduced by about 1 % but all the other terms are increased by between 1 and 4 %. A precise statement about the branching ratio would, of course, require a knowledge of the matrix elements but it is at least clear that unless there is a massive cancellation of the matrix elements then it will be impossible to account for the observed anomalies in this way. And because the ft values of the decays are quite normal, unlike the famous case of RaE, it is difficult to believe that such cancellations exist. In fact, the most probable effect of the quadrupole coupling would be to enhance the $I_f = 2$ transition, whereas it is actually the $I_f = 0$ transition that is observed to be excessive.

6. Conclusion

The acutal computation was performed for only one value of the energy but it is clear that no significant change to our general result would follow from repeating it at different energies and integrating over the spectrum. A similar remark applies to a possible dependence on the nuclear radius R and the charge distribution within the nucleus. Furthermore the value of Q_0 that we have taken, 15 b, is probably excessive, so that we have really obtained an upper limit on the quadrupole coupling effect. It is fairly clear, therefore, that the anomalous branching must be due to a failure in pure rotational structure, after all.

We wish to thank Mr. Edward Beaver of the McMaster University staff for his proficient management of the Bendix computer. One of the authors (J. M. P.) is grateful for partial financial support by the United States Air Force Office of Scientific Research, during the period in which this paper was prepared.

Appendix

Expressions of the $Q_{J,I}$ of eq. (21):

$$Q_{\frac{1}{2},1}=\frac{1}{27\pi}\left[\tfrac{1}{6}q^4(F_{1,0}^2+G_{-1,0}^2)+\tfrac{1}{3}\frac{q^3}{R}(F_{1,0}G_{1,0}-F_{-1,0}G_{-1,0})\right.$$
$$+\tfrac{1}{2}\frac{q^2}{R^2}\{G_{1,0}^2+F_{-1,0}^2+\tfrac{1}{2}(F_{2,2}^2+G_{-2,2}^2)\}-\frac{1}{3\sqrt{2}}\frac{q^3}{R}(F_{1,0}G_{2,2}+G_{-1,0}F_{2,2})$$
$$\left.+\frac{1}{\sqrt{2}}\frac{q^2}{R^2}(F_{2,2}F_{-1,0}-G_{1,0}G_{-2,2})\right]|M_1(\mathbf{r})|^2$$
$$+\tfrac{2}{27}q^2(F_{1,0}^2+G_{-1,0}^2)|M_{10}(\mathbf{r},\boldsymbol{\alpha})|^2+\tfrac{1}{81}\left[\tfrac{2}{3}q^4(F_{1,0}^2+G_{-1,0}^2)\right.$$
$$-\tfrac{8}{3}\frac{q^3}{R}(F_{1,0}G_{1,0}-F_{-1,0}G_{-1,0})+\tfrac{1}{2}\frac{q^2}{R^2}\{F_{2,2}^2+G_{-2,2}^2+8(G_{1,0}^2+F_{-1,0}^2)\}$$
$$\left.-\frac{4}{3\sqrt{2}}\frac{q^3}{R}(F_{1,0}G_{-2,2}+G_{-1,0}F_{2,2})+\frac{4}{\sqrt{2}}\frac{q^2}{R^2}(G_{1,0}G_{-2,2}-F_{-1,0}F_{2,2})\right]|M_{11}(\mathbf{r},\boldsymbol{\sigma})|^2$$
$$+\frac{1}{27\sqrt{6\pi}}\left[\frac{q^2}{R^2}\{F_{2,2}^2+G_{-2,2}^2-4(G_{1,0}^2+F_{-1,0}^2)\}-\sqrt{2}\frac{q^3}{R}(F_{1,0}G_{-2,2}+G_{-1,0}F_{2,2})\right.$$
$$\left.+\sqrt{2}\frac{q^2}{R^2}(G_{1,0}G_{-2,2}-F_{-1,0}F_{2,2})\right]\mathrm{Re}\,M_1(\mathbf{r})M_{11}^*(\mathbf{r},\boldsymbol{\sigma})$$
$$+\frac{1}{27\sqrt{\pi}}\left[\tfrac{2}{3}q^3(F_{1,0}^2+G_{-1,0}^2)+2\frac{q^2}{R^2}(F_{1,0}G_{1,0}-F_{-1,0}G_{-1,0})\right.$$
$$\left.-\sqrt{2}\frac{q^2}{R}(F_{1,0}G_{-2,2}+G_{-1,0}F_{2,2})\right]\mathrm{Im}\,M_1(\mathbf{r})M_{10}^*(\mathbf{r},\boldsymbol{\alpha})$$
$$+\tfrac{1}{27}\sqrt{\tfrac{2}{3}}\left[\tfrac{4}{3}q^3(F_{1,0}^2+G_{-1,0}^2)-4\frac{q^2}{R}(F_{1,0}G_{1,0}-F_{-1,0}G_{-1,0})\right.$$
$$\left.-\sqrt{2}\frac{q^2}{R}(F_{10}G_{-2,2}+G_{-1,0}F_{2,2})\right]\mathrm{Im}\,M_{11}(\mathbf{r},\boldsymbol{\sigma})M_{10}^*(\mathbf{r},\boldsymbol{\alpha}).$$

$$Q_{\frac{3}{2},1}=\frac{1}{27\pi}\left[\tfrac{1}{30}q^4(F_{1,2}^2+G_{-1,2}^2)+\tfrac{1}{6}\frac{q^3}{R}(F_{1,2}G_{1,2}-F_{-1,2}G_{-1,2})\right.$$
$$+\frac{q^2}{R^2}\{F_{2,0}^2+G_{-2,0}^2+\tfrac{1}{4}(F_{2,2}^2+G_{-2,2}^2+F_{-1,2}^2+G_{1,2}^2)\}$$
$$+\tfrac{1}{3}\frac{q^3}{R}\{(F_{1,2}G_{-2,0}+G_{-1,2}F_{2,0}+\tfrac{1}{2}(F_{1,2}G_{-2,2}+G_{-1,2}F_{2,2})\}$$

$$+\frac{q^2}{R^2}\{F_{2,0}F_{2,2}+G_{-2,0}G_{-2,2}+G_{1,2}G_{-2,0}-F_{-1,2}F_{2,0}$$

$$+\tfrac{1}{2}(G_{1,2}G_{-2,2}-F_{-1,2}F_{2,2})\}\Big]|M_1(\mathbf{r})|^2+\tfrac{1}{27}q^2(F_{1,2}^2+G_{-1,2}^2)|M_{10}(\mathbf{r},\alpha)|^2$$

$$+\tfrac{1}{81}\Big[\tfrac{7}{30}q^4(F_{1,2}^2+G_{-1,2}^2)-\tfrac{4}{3}\frac{q^3}{R}(F_{1,2}G_{1,2}-F_{-1,2}G_{-1,2})$$

$$+2\frac{q^2}{R^2}\{F_{2,0}^2+G_{-2,0}^2+F_{-1,2}^2+G_{1,2}^2+\tfrac{1}{4}(F_{2,2}^2+G_{-2,2}^2)\}$$

$$+\tfrac{4}{3}\frac{q^3}{R}\{F_{1,2}G_{-2,0}+G_{-1,2}F_{2,0}+\tfrac{1}{2}(F_{1,2}G_{-2,2}+G_{-1,2}F_{2,2})\}$$

$$+2\frac{q^2}{R^2}\{F_{2,0}F_{2,2}+G_{-2,0}G_{-2,2}+G_{1,2}G_{-2,2}-F_{-1,2}F_{2,2}$$

$$+2(G_{1,2}G_{-2,0}-F_{-1,2}F_{2,0})\}\Big]|M_{11}(\mathbf{r},\sigma)|^2$$

$$+\frac{1}{27\sqrt{6\pi}}\Big[\tfrac{1}{5}q^4(F_{1,2}^2+G_{-1,2}^2)+\frac{q^2}{R^2}\{F_{2,2}^2+G_{-2,2}^2-2(F_{-1,2}^2+G_{1,2}^2)+4(F_{2,0}^2+G_{-2,0}^2)\}$$

$$+\frac{q^3}{R}\{F_{2,2}G_{-1,2}+G_{-2,2}F_{1,2}+2(F_{1,2}G_{-2,0}+G_{-1,2}F_{2,0})\}$$

$$+\frac{q^2}{R^2}\{F_{2,2}F_{-1,2}-G_{-2,2}G_{1,2}\}$$

$$+2(F_{2,0}F_{-1,2}-G_{-2,0}G_{1,2})+4(F_{2,0}F_{2,2}+G_{-2,0}G_{-2,2})\}\Big]\,\mathrm{Re}\,M_1(\mathbf{r})M_{11}^*(\mathbf{r},\sigma)$$

$$+\frac{1}{27\sqrt{\pi}}\Big[\tfrac{1}{3}q^3(F_{1,2}^2+G_{-1,2}^2)+\frac{q^2}{R}(F_{1,2}G_{1,2}-G_{-1,2}F_{-1,2})$$

$$+\frac{q^2}{R}\{F_{1,2}G_{-2,2}+G_{-1,2}F_{2,2}+2(F_{2,0}G_{-1,2}+G_{-2,0}F_{1,2})\}\Big]\,\mathrm{Im}\,M_1(\mathbf{r})M_{10}^*(\mathbf{r},\alpha)$$

$$+\tfrac{1}{27}\sqrt{\tfrac{2}{3}}\Big[\tfrac{2}{3}q^3(F_{1,2}^2+G_{-1,2}^2)+2\frac{q^2}{R}(F_{-1,2}G_{-1,2}-F_{1,2}G_{1,2})$$

$$+\frac{q^2}{R}\{F_{1,2}G_{-2,2}+G_{-1,2}F_{2,2}+2(F_{1,2}G_{-2,0}+G_{-1,2}F_{2,0})\}\Big]\,\mathrm{Im}\,M_{11}(\mathbf{r},\sigma)M_{10}^*(\mathbf{r},\alpha).$$

$$Q_{\frac{1}{2},\frac{1}{2}}=\frac{1}{540\pi}q^4(F_{1,2}^2+G_{-1,2}^2)|M_1(\mathbf{r})|^2+\tfrac{1}{810}q^4(F_{1,2}^2+G_{-1,2}^2)|M_{11}(\mathbf{r},\sigma)|^2$$

$$-\sqrt{\frac{1}{6\pi}}\tfrac{1}{135}q^4(F_{1,2}^2+G_{-1,2}^2)\,\mathrm{Re}\,M_1(\mathbf{r})M_{11}^*(\mathbf{r},\sigma).$$

References

1) G. Alaga, K. Alder, A. Bohr and B. R. Mottelson, Mat. Fys. Medd. Dan. Vid. Selsk. **29** No. 9 (1955)
2) A. Bohr and B. R. Mottelson, Mat. Fys. Medd. Dan. Vid. Selsk. **27**, No. 16 (1953)
3) D. Strominger, J. M. Hollander and G. T. Seaborg, Rev. Mod. Phys. **30** (1958) 585
4) E. J. Konopinski and G. E. Uhlenbeck, Phys. Rev. **60** (1941) 308
5) K. Alder, A. Bohr, T. Huus, B. R. Mottelson and A. Winther, Rev. Mod. Phys. **28** (1956) 432
6) R. E. Bell, private communication
7) T. E. Manning, M. Fred. and F. S. Tomkins, Phys. Rev. **102** (1956) 1108
8) K. L. van der Sluis, ORNL 2236 (1956)
8) M. Fred, F. S. Tomkins and W. F. Meggers, Phys. Rev. **98** (1955) 1514;
M. H. L. Pryce, Phys. Rev. Lett. **3** (1959) 375
9) R. Weiner and Ch. Iusim, private communication and JETP (to be published)
10) M. Micu, private communication
11) S. A. Moszkowski, Handbuch der Physik, Bd. XXXIX (Springer-Verlag, Berlin, 1957)
12) E. U. Condon and G. H. Shortley, Theory of Atomic Spectra (Cambridge University Press, 1935)
13) H. A. Bethe and E. E. Salpeter, Handbuch der Physik, Bd. XXXV (Springer-Verlag, Berlin, 1957)
14) M. E. Rose, Phys. Rev. **51** (1937) 484
15) B. A. Lippmann and J. Schwinger, Phys. Rev. **79** (1950) 469
16) M. Gell-Mann and M. L. Goldberger, Phys. Rev. **91** (1953) 398
17) M. E. Rose and R. K. Osborn, Phys. Rev. **93** (1954) 1315
18) M. E. Rose, Elementary Theory of Angular Momentum (John Wiley and Sons, New York, 1957)
19) S. Gill, Proc. Camb. Phil. Soc. **47** (1951) 96
20) M. E. Rose, C. L. Perry and N. M. Dismuke, Oak Ridge National Laboratory Report no. 1459

2.F

Nuclear Physics **18** (1960) 110—121; © *North-Holland Publishing Co., Amsterdam*

Not to be reproduced by photoprint or microfilm without written permission from the publisher

SYMMETRY PROPERTIES OF THE DISTORTED WAVE THEORY OF DIRECT NUCLEAR REACTIONS

G. R. SATCHLER

Oak Ridge National Laboratory, Oak Ridge, Tennessee

Received 19 April 1960

Abstract: It is shown that under certain simple conditions often nearly realized experimentally the transition amplitudes in the distorted wave Born approximation theory of direct nuclear reactions have a simple symmetry under interchange of the distorted waves for initial and final states. For observations on the reaction the symmetry is equivalent to rotating coordinate axes by π about the recoil direction. This property is used to show in detail how the initial and final distortions have opposing effects for some phenomena (such as polarization of emitted particles or change of symmetry axis for the distribution of subsequent γ-rays) but are cooperative for others (such as the differential cross-section). Some conclusions are drawn about distortion effects in various types of reaction.

1. Introduction

Experiments on direct nuclear reactions at medium energies, such as deuteron stripping, are often interpreted in terms of Born-approximation theories which use plane waves to describe the incident and emitted particles. However, much work has been done in recent years to improve on these simple theories by the use of distorted waves [1]). These distorted waves take into account the elastic scattering of the incident particles before the reaction, and of the emergent particles afterwards. In practice they are usually taken as the waves distorted by elastic scattering from an optical potential, adjusted so as to give a reasonable description of the observed elastic scattering of that pair of particles at the same energy. These more sophisticated theories modify somewhat the predictions of the plane wave Born approximation; for example they allow the outgoing particles to be polarized, an effect absent from the plane wave theory.

The initial and final state distortions have opposing effects in some ways. For example, it was argued on semi-classical grounds [1]) that in a deuteron stripping reaction the two distortions tended to produce polarizations of opposite sign for the emitted nucleon, and this has been demonstrated analytically under certain conditions by considering the detailed structure of the matrix elements involved [2]). The purpose of the present paper is to show how these and similar properties follow in a very simple geometric way, under certain conditions which are often close to those realized in actual experiments. To do this we use the relation (3) between the distorted waves with outgoing scattered

waves and those with incoming scattered waves to demonstrate a symmetry property of the distorted wave matrix elements.

Since explicit calculation with the distorted wave theories requires much numerical work, any information of this or a similar nature [3]) which can be obtained from the general properties of the theory, is of considerable value both in testing the validity of the theories and in understanding the results of calculation with them.

2. The Distorted Wave Theory

The elastically distorted waves used to describe the relative motion of the incident particle and target nucleus, or emergent particle and residual nucleus, are solutions of the Schrödinger equation

$$[\nabla^2+k^2-(2m/\hbar^2)U(r)]\phi(\mathbf{k},\mathbf{r}) = 0. \tag{1}$$

(Except for some comments in section 5, we are assuming the distorting potentials U are spin-independent. While spin-orbit coupling is undoubtedly present if the particles have spin, it is not expected to play an important role). The relative momentum of the pair is $\hbar\mathbf{k}$, and m is their reduced mass. We use two types of solution of eq. (1), denoted by a superscript $(+)$ or $(-)$ according to their asymptotic form being a plane wave plus outgoing or incoming spherical waves,

$$\begin{aligned}\phi^{(+)}(\mathbf{k},\mathbf{r}) &\to \exp(i\mathbf{k}\cdot\mathbf{r})+\frac{1}{r}f(\theta)\exp(ikr),\\ \phi^{(-)}(\mathbf{k},\mathbf{r}) &\to \exp(i\mathbf{k}\cdot\mathbf{r})+\frac{1}{r}f(\pi-\theta)^*\exp(-ikr),\end{aligned} \tag{2}$$

where θ is the angle between $\mathbf{k}$ and $\mathbf{r}$. There is a relation between these two solutions, already reflected in eq. (2),

$$\phi^{(-)}(\mathbf{k},\mathbf{r}) = \phi^{(+)}(-\mathbf{k},\mathbf{r})^*. \tag{3}$$

If the potential U in eq. (1) is complex (the imaginary part simulating absorption), the relation (3) still holds if we interpret $\phi^{(+)}$ as a solution with U and $\phi^{(-)}$ as a solution with its complex conjugate U^*.

The distorted wave Born approximation for the transition amplitude for a reaction A(a, b)B is proportional to the matrix element [1])

$$T(\mathbf{k}_1\to\mathbf{k}_2) = \langle\phi_2^{(-)}(\mathbf{k}_2,\mathbf{r}_b)|V_{AB}|\phi_1^{(+)}(\mathbf{k}_1,\mathbf{r}_a)\rangle. \tag{4}$$

The distorted waves ϕ_1 and ϕ_2 are both solutions of an equation like (1), but in general with different potentials U_1 and U_2. If the potential U_2 describing the scattering of b on B is complex [4]), $\phi_2^{(-)}$ is the solution found using U_2^* in

eq. (1), although one need never compute it that way because of the relation (3). The simple plane wave Born approximation follows immediately by neglecting in the matrix element (4) all but the first term of the distorted waves (2). V_{AB} is the matrix element of the interaction responsible for the reaction, taken between the initial and final *internal* states of the four particles [1]). It is a function of the relative coordinates $\mathbf{r}_a$ and $\mathbf{r}_b$, but its detailed structure need not concern us here.

3. The Symmetry Property

Now consider the same transition, but interchange the distorted waves describing the relative motion of the pairs a, A and b, B. Denoting this by a tilde, we have

$$\tilde{T}(\mathbf{k}_1 \to \mathbf{k}_2) = \langle \phi_1^{(-)}(\mathbf{k}_2, \mathbf{r}_b) | V_{AB} | \phi_2^{(+)}(\mathbf{k}_1, \mathbf{r}_a) \rangle. \tag{5}$$

It is apparent from eq. (1) that this is not the same as interchanging the potentials U_1 and U_2, because in general the reduced masses m_a and m_b of the pairs a, A and b, B will be different. Instead we must interchange $m_a U_1$ and $m_b U_2$. This applies equally to any Coulomb interaction which is included in the potentials; to the extent that this is important the interchange of distorted waves is unphysical when $m_a Z_a Z_A \neq m_b Z_b Z_B$ because it involves changing the electric charges on the particles. However, the importance of Coulomb effects falls off with increasing energy and they may be neglected in many cases of interest where the influence of the stronger nuclear potential is still important. Of course, this difficulty does not arise for inelastic scattering.

When $k_1 = k_2$, $\mathbf{r}_a = \mathbf{r}_b$ and V_{AB} is local in $\mathbf{r}_a$ and $\mathbf{r}_b$, the property (3) immediately gives us a relation between T and $\tilde{T}$

$$T(\mathbf{k}_1 \to \mathbf{k}_2) = \tilde{T}(-\mathbf{k}_2 \to -\mathbf{k}_1). \tag{6}$$

Of course, this applies when both amplitudes are referred to the *same* set of quantization axes (there are angular momentum quantum numbers, namely the nuclear spins and their z-components, associated with V_{AB}). Suppose we choose these with z-axis along $\mathbf{n} = \mathbf{k}_1 \times \mathbf{k}_2$ and x-axis along $\mathbf{Q} = \mathbf{k}_1 - \mathbf{k}_2$.

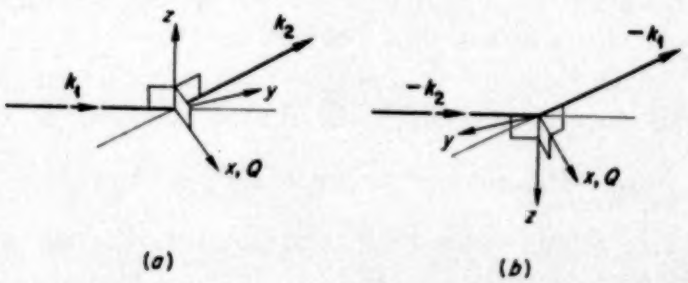

Fig. 1. (*a*) Coordinate axes used in the text. (*b*) Equivalent transition when the distorted waves are interchanged.

Because $\mathbf{k}_1$ and $\mathbf{k}_2$ are equal in magnitude, $\mathbf{Q}$ makes equal angles with them. These axes are illustrated in fig. 1. Then eq. (6) states that the T for fig. 1(*a*) is equal to the $\tilde{T}$ for fig. 1(*b*). Thus we see that interchanging the distorted waves was equivalent to rotating our coordinate axes by π around $\mathbf{Q}$, and if is this property we shall use in the next section. If the distorted waves are the same for initial and final states, $\phi_1 = \phi_2$ (which will happen when $m_a U_1 = m_b U_2$), then $T = \tilde{T}$ and eq. (6) implies T is invariant under this rotation.

We must now discuss the physical conditions under which the symmetry property (6) holds. They are the following:

(i) The magnitude of the initial and final momenta are the same, $k_1 = k_2$ (but see also the Appendix). This requires the energy release Q of the process to be given by

$$Q = E_a \left(\frac{m_a}{m_b} - 1 \right), \tag{7}$$

where E_a is the incident energy in the centre of mass system. This is often well satisfied by (d, p), (d, n), (d, t) and (d, He^3) reactions with medium energy deuterons (and of course the inverse reactions). For inelastic scattering (a, a') this condition implies $Q/E_a = 0$, or the adiabatic condition. While never exactly satisfied, for particles of moderate energy E_a and excitation of low-lying states Q/E_a is quite small. Again, $Q = 0$ is implied for (n, p) reactions, and this may be realized. Rearrangement collisions involving α-particles seldom come close to satisfying condition (7) because of the tight binding of the α-particle. But the point of view here is that while the condition $k_1 = k_2$ is required to establish the mathematical equality (6), the underlying physical symmetry has a much wider, if approximate, validity.

(ii) We may put $\mathbf{r}_a = \mathbf{r}_b$ in the integrand of (4). This will always be true for inelastic scattering without exchange for then a and b refer to the same particle. For rearrangement collisions it will require a zero-range interaction V, which is often a good approximation [1]). (See the Appendix for the modification necessary when recoil is taken into account). Again we expect the underlying physical symmetry to persist for finite, but short, range interactions. A condition alternative to $\mathbf{r}_a = \mathbf{r}_b$ is for V_{AB} to be symmetric in $\mathbf{r}_a$ and $\mathbf{r}_b$, but this is seldom, if ever, satisfied.

(iii) Finally we require V_{AB} to be local in the coordinates $\mathbf{r}_a$ and $\mathbf{r}_b$. This is certainly a good approximation if V is the actual two-body potential, and even if it is a pseudo-potential of the Watson-Brueckner type the non-locality is of short range and probably negligible for our purpose.

Higher order processes will violate the last two requirements. The *exact* amplitude for the reaction can be written in the form (4), except that V is replaced by some transition operator. The direct reaction amplitude (4) results from the first term of an expansion of this operator in powers of V (whether V is

an actual or a pseudo-potential). Higher powers correspond to multiple collisions, and will be non-local integral operators of longer range.

4. Applications

Application of the symmetry (6) is based upon the equivalence between interchanging the distorted waves and rotating the coordinate axes by π about the recoil direction $\mathbf{Q} = \mathbf{k}_1 - \mathbf{k}_2$. This rotation must also relate the observables of the reaction predicted by the two matrix elements T and $\tilde{T}$. A simple case would be to use a plane wave for ϕ_1 but a distorted wave for ϕ_2; then we could compare the effects of distorting only the emitted waves with the effects of distorting only the incident waves. For example if the first situation had predicted the emitted particles would be polarized along the positive z-axis of fig. 1(*a*), then the second would lead to the same result but referred to the rotated axes of fig. 1(*b*); that is, a polarization of *opposite* sign (as had been predicted on semi-classical grounds for deuteron stripping [1])). The change of sign is a consequence of the vector nature of the polarization. When the two distorted waves are identical, $\phi_1 = \phi_2$, the reaction is invariant under this rotation, or $T = \tilde{T}$, and the polarization must vanish: i.e., the effects of the initial and final distortions have exactly cancelled. This will occur in deuteron stripping when the distorting deuteron potential has the same size but is only half as strong as that for the emitted nucleons, because the deuteron mass is twice that of a nucleon. Since we expect the two potentials to have roughly the same strength this would support the statement sometimes made that distortion of the deuteron waves is the dominant effect in deuteron stripping.

This cancellation does not occur for all observables, as we shall see below. For example if the emitted particles were deuterons with spin 1, they could possess a tensor polarization in addition to the vector type, and this would not vanish when $\phi_1 = \phi_2$. A further example is the differential cross-section. This is a scalar, and unaffected by the rotation of coordinate axes; in other words the initial and final distorted waves have exactly the same effect. When both are present they reinforce rather than tending to cancel.

All measurable quantities depend quadratically on the matrix elements T, and it is convenient to define density matrixes and from them [5]), statistical tensors ρ_{kq}. The precise definition of the ρ_{kq} will depend somewhat on the reaction and the observable being discussed [3, 6, 7]), but suffice it to say they are spherical tensors, behaving under coordinate rotations like the spherical harmonics Y_k^{q*}. Let us denote the tensors derived from $\tilde{T}$ by $\tilde{\rho}_{kq}$. Then the rotation which relates T and $\tilde{T}$ must also relate ρ_{kq} and $\tilde{\rho}_{kq}$. Referred to the axes shown in fig. 1(*a*), we have

$$\tilde{\rho}_{kq} = (-)^k \rho_{k\,-q}. \tag{8}$$

(Only tensors of the same rank k may be related by a rotation, although different z-components q may be involved.) The differential cross-section is proportional to the sclar $\rho_{00} = \tilde{\rho}_{00}$, thus is the same for T and $\tilde{T}$ as already noted. The vector polarization of the emitted particles is a tensor of rank 1, and directed perpendicular to the reaction plane; hence it can be written as ρ_{10}. Since $\tilde{\rho}_{10} = -\rho_{10}$, the change of sign upon interchanging the distorted waves is made evident. The higher rank polarization which is also possible for spin−1 deuterons corresponds to $k = 2$ so does not change sign, although the $\pm q$ components become interchanged. Of course, the corresponding changes are seen in the asymmetry produced by using polarized incident particles a.

When the two distorted waves are the same, eq. (8) reduces to a symmetry property of the ρ_{kq},

$$\rho_{kq} = (-)^k \rho_{k\,-q}, \quad \text{if} \quad \phi_1 = \phi_2. \tag{9}$$

In particular, tensors ρ_{k0} of odd rank k vanish.

The angular distribution of any radiation emitted by the residual nucleus B is determined by the statistical tensors ρ_{kq} which describe the orientation of its spin [5]). For example, the probability of radiation in the direction (θ, ϕ) in coincidence with particles b emitted along $\mathbf{k}_2$ can be written [3, 6, 7])

$$W(\theta\phi; \mathbf{k}_1\mathbf{k}_2) = \sum_{kq} a_k \rho_{kq}(J_B) Y_k^q(\theta, \phi). \tag{10}$$

The real coefficients a_k depend only on the residual nuclear transition, and are independent of q, while the dependence on the direction of $\mathbf{k}_2$ is contained in the ρ_{kq}. If parity is conserved in the reaction (a, b) the $\rho_{kq}(J_B)$ vanish if q is odd (in the axes of fig. 1), while if parity is conserved in the radiative transition and only the direction of the radiation is observed, only even k enter the series (10). Thus we have quite generally in these axes

$$W(\theta, \phi) = W(\theta, \pi+\phi) = W(\pi-\theta, \phi). \tag{11}$$

Further, since W is real, the $\rho_{kq}(J_B)$ must have the symmetry $\rho_{kq} = (-)^q \rho_{k\,-q}{}^*$, so that relation (8) becomes

$$\tilde{\rho}_{kq}(J_B) = (-)^{k-q} \rho_{kq}(J_B)^*. \tag{12}$$

To see the connection between the angular correlation W, predicted by the Born approximation, and the $\tilde{W}$ obtained when the distorted waves are then interchanged, let us write for $q \neq 0$

$$\rho_{kq} = |\rho_{kq}| \exp(-iq\alpha_{kq}). \tag{13}$$

Then W becomes

$$W(\theta\phi) = \sum_k (2k+1)^{\frac{1}{2}} a_k \{\rho_{k0} P_k(\theta) + 2 \sum_{q>0} (-)^q \bar{P}_k^q(\theta) |\rho_{kq}| \cos q(\phi - \alpha_{kq})\}, \tag{14}$$

where $\bar{P}_k^q = [(k-q)!/(k+q)!] P_k^q$. In the simple plane wave theory the phases

α_{kq} are all equal to the azimuth angle of the recoil direction **Q**, which is zero with our choice of axes (fig. 1(a)) (or that angle plus π/q if ρ_{kq} is negative). Then the distribution (14) has **Q** as axis of axial symmetry. In general the distorted wave theories will lead to different α_{kq}, hence destroying this symmetry, although when selection rules limit k to 0 or 2 only (so only α_{22} enters eq. (14)) the distorted wave effect can be represented as a rotation of the symmetry axis away from **Q** by the angle α_{22} (or $\alpha_{22}-\frac{1}{2}\pi$ if ρ_{22} is negative). In addition the magnitudes $|\rho_{kq}|$ are altered from the plane wave predictions so the degree of anisotropy is also changed. Upon interchanging the distorted waves we have immediately from eq. (12) when k and q are even that the phase angles change sign, $\tilde{\alpha}_{kq} = -\alpha_{kq}$, while the magnitudes are unaltered $|\tilde{\rho}_{kq}| = |\rho_{kq}|$. This of course corresponds to rotating the radiation pattern by π around **Q**, so $\tilde{W}(\theta, \phi) = W(\theta, -\phi)$. When the distorted waves are the same in initial and final states so $\tilde{W} = W$, we must have $\alpha_{kq} = 0$ (or π/q). Then the recoil **Q** is regained as an axis of symmetry although the $|\rho_{kq}|$ and hence the degree of anisotropy may still differ considerably from the plane wave prediction; also, while there is now left-right and back-forward symmetry relative to **Q**, there may be still a lack of axial symmetry around **Q**. So with inelastic scattering when the adiabatic approximation is good we should have $\alpha_{kq} \approx 0$ (or π/q), while with a rearrangement like deuteron stripping where the two distorted waves are not expected to be similar we may find large changes in α_{kq}. The numerical calculations to date [6, 8]) seem to support these conclusions. Again we see the initial and final distorted waves tending to cancel in their effect on the shifts α_{kq}, but reinforcing in changing the magnitudes $|\rho_{kq}|$.

When we do not observe the emitted particles b, we must average the correlation (10) over the directions $\mathbf{k}_2$. If θ is the angle between the radiation and a z-axis chosen parallel to the incident particles a, the non-coincident distribution is

$$I(\theta) = \sum_k (2k+1)^{\frac{1}{2}} a_k \langle \rho'_{k0} \rangle P_k(\theta),$$

where $\langle \rho'_{k0} \rangle$ is the $\rho'_{k0}(J_B)$ referred to these new axes and averaged over the angular distribution of b. Again k takes only even values. To see the effect of interchanging distorted waves we express ρ'_{k0} in terms of the $\rho_{kq}(J_B)$ used above which are referred to the axes of fig. 1(*a*),

$$\rho'_{k0} = \sum_q \rho_{kq} D^k_{q0}(\theta_R \tfrac{1}{2}\pi 0)^*,$$

where D^k_{q0} is a rotation matrix element [5]) and θ_R is the angle between **Q** and $\mathbf{k}_1$. Then using eq. (8)

$$\tilde{\rho}'_{k0} = \sum_q \rho_{kq} D^k_{-q0}(\theta_R \tfrac{1}{2}\pi 0)^*,$$

so there is no simple relation between $\tilde{I}(\theta)$ and $I(\theta)$ except when the two distort-

ed waves are the same and $\bar{I} = I$. This is not surprising since the relations (6), (8) and (9) correspond to a rotation about $\mathbf{Q}$, whose direction is being averaged when computing I and $\bar{I}$.

Finally we consider the circular polarization C of any γ-rays emitted by the residual nucleus in a direction (θ, ϕ) and detected in coincidence with particles b along $\mathbf{k}_2$. This is an example of a measurement depending upon the *odd* moments of the polarization of the residual nucleus; another example which has been studied experimentally is the up-down asymmetry in the emission of any β-rays following the reaction [9]). C is defined as the excess intensity of right-hand over left-hand photons divided by the total intensity, and can be written in terms of the same parameters as the directional correlation (10) except that we must now include odd values of k [7]),

$$C(\theta\phi; \mathbf{k}_1\mathbf{k}_2) = \frac{\sum\limits_{k\ \mathrm{odd},\, q} a_k \rho_{kq}(J_\mathrm{B}) Y_k^q(\theta\phi)}{\sum\limits_{k\ \mathrm{even},\, q} a_k \rho_{kq}(J_\mathrm{B}) Y_k^q(\theta\phi)} . \tag{15}$$

Using the axes of fig. 1(*a*) (so q has to be even) and the relation (8) leads to the polarization predicted when the distorted waves are interchanged

$$\bar{C}(\theta, \phi) = -C(\theta, -\phi), \tag{16}$$

which again corresponds to a rotation of π about $\mathbf{Q}$. In the simplest case when selection rules only allow $k = 0$ or 1 (for example emission from a nuclear level with spin $\frac{1}{2}$), C does not depend on ϕ and $\bar{C} = -C$. When the two distorted waves are the same we have $\bar{C} = C$. Then eq. (16) does not lead to complete extinction of the polarization in general, but gives $C = 0$ in the x–y, y–z, and x–z planes of fig. 1(*a*). In particular, C vanishes along $\mathbf{k}_1 \times \mathbf{k}_2$ (unless the total intensity itself vanishes in this direction, in which case the limiting value as θ tends to zero depends on ϕ). Again we expect this to be the situation, approximately, in inelastic scattering, but not in rearrangement collisions where $m_\mathrm{a} U_\mathrm{a} = m_\mathrm{b} U_\mathrm{b}$ is unlikely to be satisfied.

Similar remarks apply to the distribution of β-rays in coincidence with particles b. This can be written in the form (10), where the parity non-conserving terms now allow odd k values to appear. If ε is the up-down asymmetry, or relative excess of β-rays along $\mathbf{k}_1 \times \mathbf{k}_2$ over those along $-(\mathbf{k}_1 \times \mathbf{k}_2)$, then $\bar{\varepsilon} = -\varepsilon$, and both vanish if the two distorted waves are the same.

5. Spin-Orbit Coupling

So far we have neglected the effects on the elastic scattering waves of any spin-orbit coupling which may be present if the particles a or b have spin. This is not unreasonable at medium energies since optical model analyses indicate a spin-orbit coupling of only a few MeV in an overall potential of depth

50 MeV or greater, although this may not be a fair estimate of its effects under all conditions as we shall see. For our discussion of the effects of interchanging initial and final distorted waves it only makes sense to include spin-orbit coupling when particles a and b have the same spin. The distorted waves (2) have to be replaced by matrices in spin space $\phi_{\mu\sigma}(\mathbf{k}, \mathbf{r})$, where μ, σ are values of the z-component of spin of the particle a or b (we are still neglecting any coupling to the *nuclear* spin). The relation (3) between incoming and outgoing wave solutions becomes

$$\phi^{(-)}_{\mu\sigma}(\mathbf{k}, \mathbf{r}) = (-)^{\mu-\sigma}\phi^{(+)}_{-\mu,-\sigma}(-\mathbf{k}, \mathbf{r})^*, \tag{17}$$

in a representation in which angular momentum functions behave under time reversal [5]) like $K\psi_{jm} = (-)^{j-m}\psi_{j\,-m}$. Similarly the transition amplitude (4) must now be written explicitly as a spin matrix

$$T(\sigma_1\mathbf{k}_1 \to \sigma_2\mathbf{k}_2) = \sum_{\mu_1\mu_2} \langle \phi^{(-)}_{2,\mu_2\sigma_2}(\mathbf{k}_2, \mathbf{r}_b) | V^{\mu_1\mu_2}_{AB} | \phi^{(+)}_{1,\mu_1\sigma_1}(\mathbf{k}_1, \mathbf{r}_a) \rangle,$$

where the sum over μ_1 and μ_2 allows the possibility of spin-flip during the elastic scatterings. Interchanging the distorted waves ϕ_1 and ϕ_2 does not lead to any simple result except when $V^{-\mu_2-\mu_1}_{AB} = \pm V^{\mu_1\mu_2}_{AB}$. This will occur if V is spin-independent. It is also true if the selection rules implicit in V_{AB} demand that the transition occur with the transfer to the nucleus of a definite amount of angular momentum S from the spins of a and b. That is, if the difference in orbital momentum of a and b contributes † L so that the total angular momentum transfer is $\mathbf{J}_B - \mathbf{J}_A = \mathbf{L} + \mathbf{S}$, and if only one value of S contributes, then $V^{-\mu_2-\mu_1}_{AB} = (-)^S V^{\mu_1\mu_2}_{AB}$. For example, if V is spin independent we have $S = 0$. Under these conditions and with eq. (17) we have the analogue of eq. (6) when $k_1 = k_2$ and $\mathbf{r}_a = \mathbf{r}_b$,

$$T(\sigma_1\mathbf{k}_1 \to \sigma_2\mathbf{k}_2) = (-)^{S+\sigma_1-\sigma_2}\bar{T}(-\sigma_2, -\mathbf{k}_2 \to -\sigma_1, -\mathbf{k}_1).$$

Then it is easy to show that the statistical tensors $\rho_{kq}(J_B)$ describing the orientation of the residual nucleus B still obey the relation (8) provided the polarization of the outgoing particles b is not observed and the incident particles a are unpolarized. Hence the discussion in the last section concerning the differential cross section and any radiation emitted by B still holds if there is a unique spin transfer S. The polarization of particles b, or the effect of using polarized particles a, however, still do not show any simple behaviour upon interchanging distorted waves. Even if the spins of a and b are not directly coupled to the nucleus by the interaction V_{AB}, they are indirectly through the coupling to their orbital motion which is the source of the angular momentum transfer to the nucleus. Thus it matters for the spin polarization whether the spin-orbit coupling

† This L has the significance that in the simplest plane wave theory [1]) the differential cross-section is proportional to $j_L(QR)^2$.

is experienced before or after this transfer. Even when the two distorted waves are similar the spin-orbit coupling allows a non-zero polarization, and will thus be the dominant effect in producing polarization in inelastic scattering when the adiabatic approximation is good and the "central" distortion effects have cancelled.

6. Discussion

We have seen how the effects of initial and final distorted waves tend to cancel for some quantities such as the polarization of emitted particles and the change of symmetry axis for an angular correlation, but reinforce for others, such as the differential cross-section and change in degree of anisotropy of a correlation. These results were deduced under the conditions that the initial and final momenta had similar magnitudes and that the interaction was local and (except for non-exchange inelastic scattering) of short range. Again we emphasize our belief that these conclusions have a much wider range of (approximate) validity, and reflect the physical conditions which are appealed to in semiclassical arguments.

These results may be supplemented by others found in numerical calculations [1]) concerning the relative effects of a repulsive Coulomb field and an attractive nuclear potential in a given distorted wave. While both cut down the total cross-section, they seem to have opposing effects on the shape of the differential cross-section. This is presumably because while they both produce reflection, they will refract in opposite directions. On the other hand the relative effects of distorting the motion of the incident and the emitted particles with which we are concerned here shows itself through a preference for the reaction to take place on one *side* of the nucleus (relative to the $x-z$ plane of fig. 1 which contains the recoil **Q**). There is an unsymmetrical illumination of the nucleus by the incident and outgoing beams except when the two distorted waves are identical. Clearly this will show in the angular distribution of any further radiation no longer having **Q** as symmetry axis. It also allows the emitted particles to be polarized [1]). Interchanging the distorted waves shifts the asymmetry of illumination from one side to the other, thus changing the sense of these effects while quantities like the differential cross-section remain unaltered.

Appendix

The conditions for eq. (6) to hold are actually that $\mathbf{r}_a$ be proportional to $\mathbf{r}_b$ in the integrand of the matrix element (5): $\mathbf{r}_b = \alpha \mathbf{r}_a$, where α is a constant, with the compensating requirement that $k_1 = \alpha k_2$. This is appropriate to stripping or knock-on reactions when the nuclear recoil is taken into account; a zero-range interaction then leads to $\mathbf{r}_b = (M_A/M_B)\mathbf{r}_a$, where M_A and M_B are the

masses of the target and residual nuclei [1]). We then require $k_1 = k'_2 = (M_A/M_B)k_2$, so that the energy release (7) now becomes

$$Q = E_0 \frac{M_A}{M_A+M_a}\left\{\frac{M_B M_a(M_B+M_b)}{M_A M_b(M_A+M_a)} - 1\right\},$$

where M_a, M_b are now the actual (not reduced) masses of a and b, and E_0 is the incident energy in the *lab*. The condition on the potentials in eq. (1) for the two distorted waves to be the same, previously written as $m_a U_a = m_b U_b$, now becomes

$$\frac{M_A M_a}{M_A+M_a} U_a(r) = \left(\frac{M_A}{M_B}\right)^2 \frac{M_B M_b}{M_B+M_b} U_b\left(\frac{M_A}{M_B} r\right)$$

for all r. So if the potentials are written as a strength times a form factor, say

$$U(r) = (V+iW) f\left(\frac{r-R}{a}\right),$$

they must have the same shape, $f_a = f_b$, but with strengths in the ratio

$$\frac{V_a}{V_b} = \frac{W_a}{W_b} = \frac{M_A M_b(M_a+M_A)}{M_B M_a(M_b+M_B)},$$

and dimensions in the ratio

$$\frac{R_a}{R_b} = \frac{a_a}{a_b} = \frac{M_B}{M_A}.$$

When the particles are charged, the potentials U contain in addition a Coulomb term. The condition for equal distorted waves here becomes

$$\frac{Z_a Z_A}{Z_b Z_B} = \frac{M_b(M_a+M_A)}{M_a(M_b+M_B)},$$

where $Z_i e$ is the charge on particle i. In terms of the Coulomb parameters $\eta_a = Z_a Z_A e^2/\hbar v_a$ (v_a being the relative velocity of a and A) this is just $\eta_a = \eta_b$.

With these conditions, quantities like the polarization of particles b and the shift of the correlation symmetry axis from Q should vanish in the distorted wave Born approximation.

References

1) N. Austern, Fast Neutron Physics, edited by J. B. Marion and J. L. Fowler (Interscience, New York, 1960) Ch. VD, and other references cited there

2) M. Y. Refai, unpublished (private communication from H. C. Newns, 1958); S. Okai, Progress of Theoretical Physics **22** (1959) 89

3) R. Huby, M. Y. Refai and G. R. Satchler, Nuclear Physics **9** (1958) 94
4) L. C. Biedenharn, Nuclear Physics **10** (1959) 620
5) S. Devons and L. J. B. Goldfarb, Handbuch der Physik, Ed. S. Flügge (Springer, Berlin, 1957) **42**, 362;
L. C. Biedenharn and M. E. Rose, Revs. Mod. Phys. **25** (1953) 729
6) W. Tobocman and G. R. Satchler, Phys. Rev. (to be published)
7) G. R. Satchler, Nuclear Physics **16** (1960) 674
8) C. A. Levinson and M. K. Banerjee, Annals of Physics **3** (1958) 67
9) L. F. Chase and G. Igo, Phys. Rev. **116** (1959) 170

1.E.1:
4.A

Nuclear Physics 18 (1960) 122—130; © *North-Holland Publishing Co., Amsterdam*
Not to be reproduced by photoprint or microfilm without written permission from the publisher

INVESTIGATION OF POLARIZATION OF INTERNAL CONVERSION ELECTRONS EMITTED AFTER β^--DECAY IN HEAVY ELEMENTS

M. E. VISHNEVSKY, V. A. LYUBIMOV, E. F. TRETYAKOV and G. I. GRISHUK
Institute of Theoretical and Experimental Physics of the USSR Academy of Sciences, Moscow

Received 20 December 1959

Abstract: The polarization of internal conversion electrons produced in some transitions occurring after β^--decay of Tm^{170}, Re^{186}, Hg^{203} and Pa^{233} has been measured. The conversion electrons were found to be polarized in the direction of emission of the β-particles from Tm^{170} and Re^{186} and opposite to the direction of emission of β-particles from Hg^{203} and Pa^{233}. The most probable values of the ground state spins of β-decaying nuclei are determined for Hg^{203} and Pa^{233}. Agreement between the experimental and theoretical results has been obtained for Tm^{170} and Re^{186} for which all transition constants are known.

1. Introduction

Non-conservation of parity in weak interactions is now a reliably established fact. In some cases the regularities of weak interactions can be employed to study the characteristics of nuclear transitions. Thus, the old methods of nuclear spectroscopy can be supplemented by new "non-classical" methods (experiments with polarized particles involved in weak interactions).

A method of this type which should be especially convenient for investigation of heavy nuclei is the measurement of polarization of internal conversion electrons emitted after β-decay. The polarization of conversion electrons emitted after β-decay was predicted by A. I. Alikhanov and V. A. Lyubimov [1]) and subsequently detected by two of us (V. L. and M. V.) [2]). The theory of this phenomenon has been developed by V. B. Berestetsky and A. P. Rudik [3]) and B. V. Geshkenbein [4]).

2. Experimental Arrangement

Internal conversion electrons are polarized in the direction of polarization of the nuclei produced in the preceding β-decay. If conversion electrons are selected at an angle of 90° with respect to the direction of the β-particle momentum the polarization will be transverse and its measurement is thus facilitated. Transverse polarization of the conversion electrons was determined from the azimuthal asymmetry of Mott scattering on gold nuclei. The scheme of the apparatus is depicted in fig. 1.

The β-electrons from a thin source (B) were recorded by counters 1 and 2. Conversion electrons emitted after β-decay were selected by a toroidal spectrometer and after scattering in the gold scatterer through a mean angle of 135°

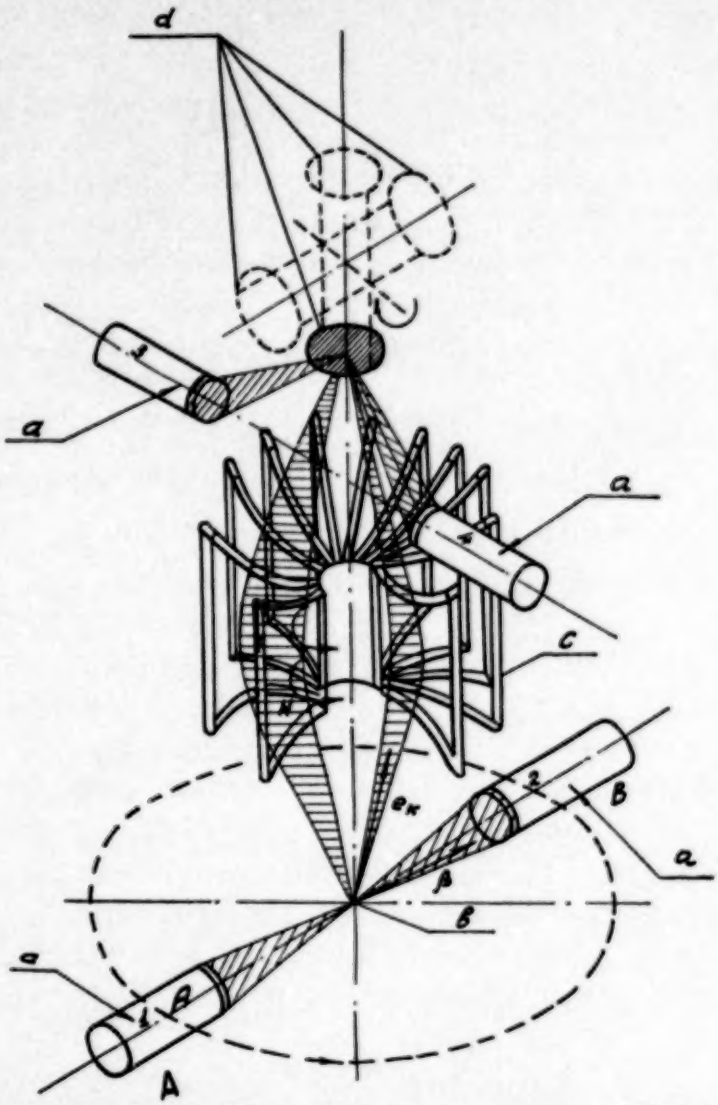

Fig. 1. Experimental arrangement; a = scintillation counters, b = source, c = toroidal coil, d = scatterers.

they were detected by counters 3 and 4 connected respectively with counters 1 and 2 in double coincidence. Counters 3 and 4 were oriented in a plane perpendicular to the axis of counters 1 and 2.

Since the conversion electrons were monochromatic and their transverse polarization weakly depended on the angle between the directions of the β- and conversion electrons in the region of $\approx 90°$, a large-angle high-efficiency magnetic spectrometer [5]) possessing a high resolution with respect to electron energy could be employed to separate the conversion electrons from the β-particles.

Counters 1 and 2 select from the source oppositely directed β-particles. Thus, depending on which of the two β-counters 1 or 2 the pulses in conversion electron counters 3 and 4 coincide, one measures the azimuthal scattering asymmetry of electrons possessing oppositely directed spins. This is equivalent to the usual substitution of a "left" counter for a "right" counter in scattering asymmetry measurements. Moreover, in the measurements a real rotation of counters 3 and 4 through 180° was performed (position of counters AA and AB; position AA is represented in fig 1). Under such conditions asymmetry due to the apparatus can be excluded without further measurements. This can be seen from the following. The conversion electron- β-electron coincidence rate minus the background can be written as follows:

$$(N_{13})_{AA} = q(\eta_1\eta_3)_{AA}\eta_{13}(1-S\langle\sigma\rangle), \qquad (N_{13})_{AB} = q(\eta_1\eta_3)_{AB}\eta_{13}(1+S\langle\sigma\rangle),$$
$$(N_{14})_{AA} = q(\eta_1\eta_4)_{AA}\eta_{14}(1+S\langle\sigma\rangle), \qquad (N_{14})_{AB} = q(\eta_1\eta_4)_{AB}\eta_{14}(1-S\langle\sigma\rangle),$$
$$(N_{23})_{AA} = q(\eta_2\eta_3)_{AA}\eta_{23}(1+S\langle\sigma\rangle), \qquad (N_{23})_{AB} = q(\eta_2\eta_3)_{AB}\eta_{23}(1-S\langle\sigma\rangle),$$
$$(N_{24})_{AA} = q(\eta_2\eta_4)_{AA}\eta_{24}(1-S\langle\sigma\rangle), \qquad (N_{24})_{AB} = q(\eta_2\eta_4)_{AB}\eta_{24}(1+S\langle\sigma\rangle).$$

Here, the q are proportionality coefficients, η_i are solid angles, efficiencies and other quantities determining the probability for detection of an electron by a counter. The η_i may differ in positions AA and AB. The quantities η_{ik} depend on the counter combination (for example, coincidence efficiency for channel ik). In a good approximation the η_{ik} do not depend on the positions of counters AA and AB. Further, S is the asymmetry of transversely polarized electrons after single scattering on gold, account being taken of the geometry of the apparatus. Finally, $\langle\sigma\rangle$ is the degree of transverse polarization of the electrons.

It can readily be seen that a combination depending only on the electron polarization can be set up from the 8 measured numbers $(N_{ik})_{AA,AB}$. Indeed, the asymmetry coefficient

$$R = \sqrt[4]{\left(\frac{N_{13}N_{24}}{N_{14}N_{23}}\right)_{AA}\left(\frac{N_{14}N_{23}}{N_{13}N_{24}}\right)_{AB}} = \frac{1-S\langle\sigma\rangle}{1+S\langle\sigma\rangle}$$

does not contain any instrumental asymmetry factor.

As a rule auxiliary measurements with a scatterer made of a light material are carried out to exclude any instrumental asymmetry. Azimuthal asymmetry due to electron polarization should practically be absent in this case. There is no necessity in carrying out such measurements in our case. Measurements with an aluminium scatterer were performed solely with the purpose of control and in all substances studied by us the role of instrumental asymmetry was practically nil. Thus,

$(R_{Al})_{Tm^{170}} = 1.00\pm0.02$, $(R_{Al})_{Pa^{233}} = 0.98\pm0.02$ $(E_\gamma = 312.6$ keV),
$(R_{Al})_{Pa^{233}} = 1.01\pm0.03$ $(E_\gamma = 74.8$ keV), $(R_{Al})_{Hg^{203}} = 0.97\pm0.03$.

The measurements were performed in the following order: with a gold scatterer, then with an aluminium scatterer and with an empty frame (for exclusion of scattering from the apparatus walls and scatterer frame). The random coincidence rate was measured separately in each case. All measurements as well as changing of the scatterers were performed automatically and the results were recorded by the corresponding counter set. Measurements in position AA and position AB were made during approximately equal periods of time. It can be seen from the determination of the asymmetry coefficients R and fig. 1 that if R is larger (smaller) than unity, the internal conversion electrons emitted after β^--decay will be correspondingly polarized opposite to (along) the direction of emission of the β^--particles.

3. Measurements

3.1. THULIUM Tm^{170}

The decay of Tm^{170} is accompanied by strong γ-ray conversion and the Tm^{170} transition constants are well known [6]). This case is therefore very convenient for experimental verification of the theory of conversion electron polarization. In about 24 % of cases β-decay leads to an excited Yb^{170} level with $E_\gamma = 84.23$ keV, de-excitation of this level involving the emission of an internal conversion electron of multipolarity E2:

$$1^- \xrightarrow[E_\beta = 864\ \text{keV}]{} 2^+ \xrightarrow[E_\gamma = 84.2\ \text{keV}]{} 0^+.$$

Polarization measurements were carried out on conversion electrons emitted from the L shell ($E_{eL} = 75$ keV). Scattering asymmetry measurements on a gold scatterer (thickness 0.07 mg/cm^2) yielded

$$R_{Au} = \sqrt[4]{\left(\frac{N_{13}N_{24}}{N_{14}N_{23}}\right)_{AA}\left(\frac{N_{14}N_{23}}{N_{13}N_{24}}\right)_{AB}} = 0.83 \pm 0.03,$$

which corresponds to

$$2S\langle\sigma\rangle = 2\,\frac{1-R}{1+R} = +0.19 \pm 0.03.$$

An asymmetry of this magnitude signifies that the conversion electrons are polarized along the direction of the emitted β^--electron.

A correction to account for the finite thickness of the scatterer should be introduced into the measured asymmetry value. Careful measurements of this correction for electrons of various energies and similar scattering positions have been made in ref. [7]). After taking into account the finite thickness of the scatterer one gets

$$(2S\langle\sigma\rangle)_0 = +0.22 \pm 0.03.$$

Hence, using the tabulated data from ref. [8]) and the corrections to these data presented in ref. [7]) one obtains, by taking into account the geometry of the apparatus, the following value for the conversion electron polarization:

$$\langle \sigma \rangle_{\text{exp}} = +(0.55 \pm 0.08) \frac{\mathbf{v}}{c}$$

(for an average value of $v/c = 0.78$ for the recorded part of the β-spectrum).

According to Geshkenbein's theory [4]) the polarization of conversion electrons from the L level in electric transitions is

$$\langle \sigma \rangle = \alpha \frac{l(l+1)+J_2(J_2+1)-J_3(J_3+1)}{2l(l+1)J_1(1+|\eta_{L_i}|^2)} \left\{ \left(\frac{\mathbf{v}\cdot\mathbf{n}}{c} \right) \mathbf{n} + \sqrt{l(l+1)}\ (\mathrm{Re}\ \eta_{L_i}) \left[\frac{\mathbf{v}}{c} - \left(\frac{\mathbf{v}\cdot\mathbf{n}}{c} \right) \mathbf{n} \right] \right\},$$

where α is a quantity which depends on the same combination of constants and matrix elements as the angular distributition of electrons emitted during β-decay of polarized nuclei. We have

$$\alpha = \frac{\lambda_{J_1 J_2} |C_A|^2 |M_{GT}|^2 + 2\delta_{J_1 J_2} \sqrt{\dfrac{J_2}{(J_2+1)}}\ \mathrm{Re}\ (C_V C_A^* M_F M_{GT}^*)}{|C_A|^2 |M_{GT}|^2 + |C_V|^2 |M_F|^2},$$

with

$$\lambda_{J_1 J_2} = \frac{J_2(J_2+1) - J_1(J_1+1) + 2}{2(J_2+1)}.$$

Here, M_F, M_{GT} are the nuclear matrix elements, l is the multipolarity of the γ-quantum, J_1 the nuclear spin before β-decay, J_2 the nuclear spin before conversion, J_3 the nuclear spin after conversion, $\mathbf{v}/c$ the electron velocity, $\mathbf{n}$ a unit vector defining the direction of emission of the conversion electron and η_{L_i} is a function of the radial integrals.

The main contribution to the polarization is made by electrons from the L_{II} and L_{III} shells. According to Geshkenbein's calculations $\eta_{L_{II}} = 0.51 \pm 0.25i$, and $\eta_{L_{III}} = 0.534$, whence one gets for the polarization

$$\langle \sigma \rangle_{\text{th}} = +0.488 \frac{\mathbf{v}}{c},$$

which is in good agreement with the experimental value.

3.2. PROTACTINIUM Pa^{233}

The decay scheme of protactinium and its transition characteristics have been presented in ref. [6]). We have been primarily interested in measuring the polarization of conversion electrons produced in de-excitation of the 312.6 keV

U^{233} excited state:

$$(\tfrac{1}{2}, \tfrac{3}{2}, \tfrac{5}{2}) \xrightarrow[E_\beta = 257\ \text{keV}]{} \tfrac{3}{2}^+ \xrightarrow[E_\gamma = 312.6\ \text{keV}]{} \tfrac{5}{2}^+.$$

Polarization of conversion electrons from the K shell produced as a result of M1 transitions with $E_\gamma = 312.6$ keV was measured. The experimental value of the scattering asymmetry is $R = 1.10 \pm 0.02$. The electrons are polarized opposite the direction of the β-particle momentum.

After introduction of corrections for the finite thickness of the scatterer (0.45 mg/cm^2) and also for the admixture of cascade transitions, the following experimental polarization value was obtained:

$$\langle \sigma \rangle_{\text{exp}} = -(0.48 \pm 0.14) \frac{v}{c}$$

(the mean value of v/c is 0.56).

For the assumed values of the Pa^{233} ground state spin $(\frac{1}{2}, \frac{3}{2}, \frac{5}{2})$ the computed polarization values are

$$\langle \sigma \rangle_{\frac{1}{2}} = -0.334 \frac{v}{c}, \qquad \langle \sigma \rangle_{\frac{3}{2}} = (-0.334 \div +0.200) \frac{v}{c}, \qquad \langle \sigma \rangle_{\frac{5}{2}} = 0.200 \frac{v}{c}.$$

If the spin of the Pa^{233} ground state is $\frac{3}{2}$, the transition occurs between the levels $\frac{3}{2} \to \frac{3}{2}$. In this case the calculated polarization value depends on a combi-

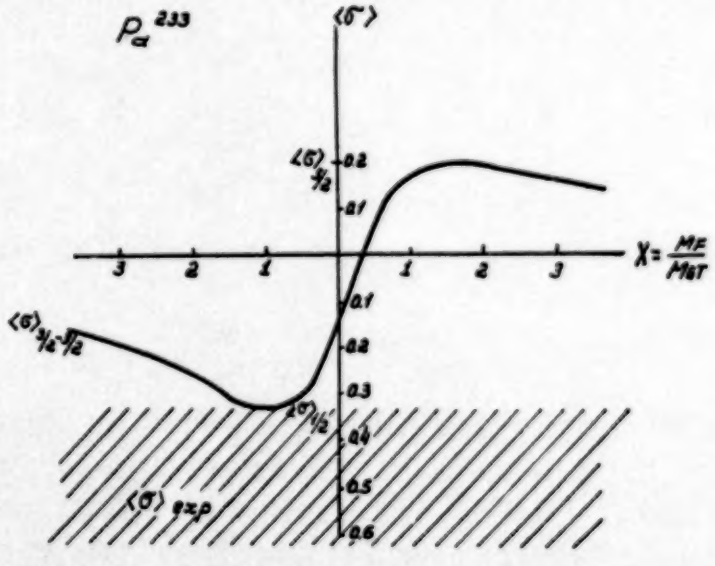

Fig. 2. Polarization $\langle\sigma\rangle$ calculated as a function of the ratio of the $Pa^{233} \to U^{233}$ β-transition matrix elements.

nation of the β-transition matrix elements. The computed polarization value as a function of the matrix element ratio $X = M_F/M_{GT}(C_A = -1.2C_V)$ and also the experimental value of $\langle\sigma\rangle$ are presented in fig. 2. Since experimental

errors as well as some inaccuracy in the intensities of transitions between levels of the daughter U^{233} nucleus are possible, our data may be considered consistent with the theoretical data, provided the Pa^{233} ground state spin is $\frac{1}{2}$ or $\frac{3}{2}$. In the latter case there is interference between the Fermi and Gamov-Teller interactions and the matrix elements have opposite signs.

As a check, measurements were carried out on the polarization of conversion electrons produced by 74.5 keV γ-quanta in the transition between two excited U^{233} levels:

$$(\tfrac{1}{2}, \tfrac{3}{2}, \tfrac{5}{2}) \xrightarrow[E_\beta = 145\ \text{keV}]{} \tfrac{3}{2}^+ \xrightarrow[E_\gamma = 74.5\ \text{keV}]{} \tfrac{5}{2}^+.$$

This transition is almost similar to the preceding one and merely differs in the β-particle and conversion electron energy. The asymmetry value obtained, corresponds to the same direction of the conversion electrons as in the case of the 312.6 keV transition.

3.3. MERCURY Hg^{203}.

A study of the polarization of conversion electrons accompanying β-decay of Hg^{203} is interesting in that it should permit one to determine the spin of the ground state of Hg^{203}, a quantity which at present is known with a low degree of accuracy $(\frac{1}{2}, \frac{3}{2}, \frac{5}{2})$ [6]. A characteristic feature of Hg^{203} decay is that the conversion electrons possess energies exceeding the end point energy of the β-spectrum. Owing to this circumstance the measurements were carried out [2] on a spectrometer with a lower resolution. The measurements revealed that the electrons were polarized opposite the direction of emission of the particles, the magnitude of the polarization being

$$\langle \sigma \rangle = (-0.32 \pm 0.09) \frac{\mathbf{v}}{c}$$

for an average value of $v/c = 0.55$. The calculated polarization values are

$$\langle \sigma \rangle_{\frac{1}{2}} = 0.495 \frac{\mathbf{v}}{c}, \qquad \langle \sigma \rangle_{\frac{3}{2}} = (+0.495 \div -0.297) \frac{\mathbf{v}}{c}, \qquad \langle \sigma \rangle_{\frac{5}{2}} = -0.297 .$$

The calculated and experimental polarization values are presented in fig. 3.

The results of the measurements are consistent with a value of $\pm\frac{5}{2}$ and $\pm\frac{3}{2}$ for the Hg^{203} ground state spin and are inconsistent with a value of $\pm\frac{1}{2}$ †.

In the case of a $\frac{3}{2} \rightarrow \frac{3}{2}$ transition, interference takes place between Fermi and Gamov-Teller interactions. The matrix element signs are the same.

† A different interpretation of the experimental results has been proposed in ref. [2]). The experimental results were compared with Geshkenbein's formula [4]) in which the polarization sign was found to be wrong. The error in the formula was detected by Geshkenbein after we had measured the polarization of conversion electrons from Tm^{170} for which all the transition characteristics were known. It was found that the result thus obtained was opposite in sign to the theoretical value computed by the old formula.

3.4. RHENIUM Re^{186}

The same experimental arrangement as employed in ref. [2]) was used to measure the sign of the polarization of conversion electrons emitted after β decay of Re^{186}. Decay of Re^{186} is similar to that of Tm^{170}. As in the case of

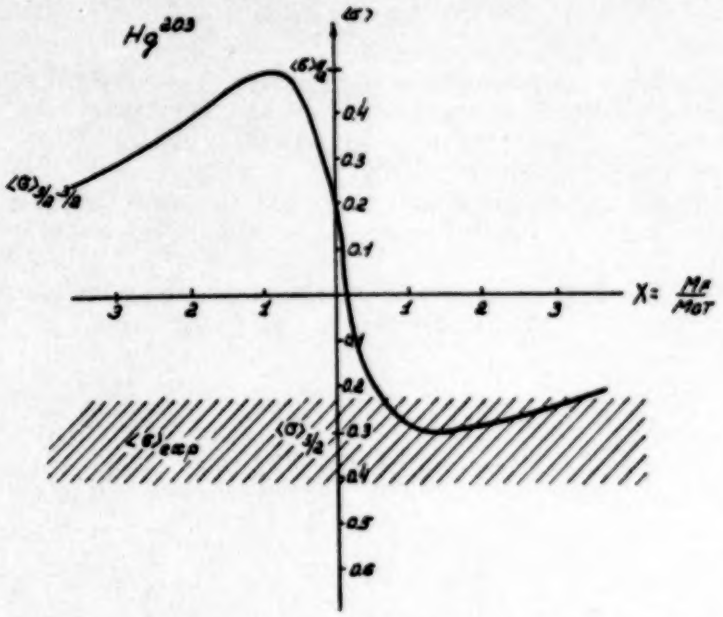

Fig. 3. Polarization $\langle\sigma\rangle$ calculated as a function of the $Hg^{203} \rightarrow Tl^{203}$ β-transition matrix elements.

Tm^{170} decay the conversion electrons accompanying β-decay of Re^{186} are polarized in the direction of the β-particle momentum.

4. Conclusion

Polarization of conversion electrons emitted after β-decay in various transition schemes has been measured. Conversion electrons from K and L shells involved in transitions of various multipolarities have been investigated. It has been detected experimentally that conversion electrons can be polarized along as well as opposite the direction of motion of the β-electron. In all cases in which the transition characteristics were known the magnitude and direction of polarization were found to agree with the theoretical predictions.

A study of conversion electron polarization, carried out with not all spins of the levels between which the transitions occurred were known, could be applied to determine the unknown characteristics (or those known with a low accuracy). Evidently this method should be especially useful for determination of the spin of the ground state of a decaying nucleus, providing that the spins of the daughter nuclear levels are known. Determination of this parameter on the basis of β-spectroscopy data (from the magnitude of and shape of the Kurie plot) is frequently ambiguous.

The authors are thankful to A. I. Alikhanov for his constant interest in this work and to B. V. Geshkenbein for creative cooperation and discussion of the results. The authors are also grateful to S. V. Markizov for help in the work.

References

1) A. I. Alikhanov, Report at International High Energy Physics Conference in Kiev, July 1959
2) V. A. Lyubimov and M. E. Vishnevsky, JETP **35** (1958) 1577
3) V. B. Berestetsky and A. P. Rudik, JETP **35** (1958) 159
4) B. V. Geshkenbein, JETP **35** (1958) 1235
5) E. F. Tretyakov, L. L. Goldin and G. I. Grishuk, Prib. Tekhn. Izmer. **6** (1957) 22
6) B. S. Dzhelepov and L. K. Peker, Decay Schemes of Radioactive Nuclei, Izdat. Acad. Nauk SSSR (1956)
7) A. I. Alikhanov, G. P. Eliseyev and V. A. Lyubimov, JETP **34** (1957) 1045
8) N. Sherman, Phys. Rev. **103** (1956) 1601

3.C

Nuclear Physics **18** (1960) 131—137; © *North-Holland Publishing Co., Amsterdam*

Not to be reproduced by photoprint or microfilm without written permission from the publisher

INVESTIGATION OF INTERNAL BREMSSTRAHLUNG CROSS-SECTION WITH SPECIFIED ELECTRON AND PHOTON ENERGIES

J. E. THUN, B. G. PETTERSSON and K. SIEGBAHN

Institute of Physics, Upsala, Sweden

Received 1 April 1960

Abstract: The internal bremsstrahlung from P^{32} is measured by a coincidence arrangement, where the electrons are detected in a lens spectrometer and the photons in a NaI(Tl) scintillation crystal.

By selecting a certain energy in the β-spectrometer it was possible to test the differential probability for the internal bremsstrahlung emission as given by the theory of Knipp and Uhlenbeck. The angle between the electron and photon is chosen to be 90°. The result shows good agreement for all electron energies chosen.

1. Introduction

The theory of the Internal Bremsstrahlung (IB) was first worked out by Knipp and Uhlenbeck [1]) and by Bloch [2]). The IB-probability was calculated with the second order perturbation method for the case of the Fermi polar vector interaction and an allowed beta-transition. Knipp and Uhlenbeck introduced, however, an alternative method. The probability of the IB-process was here regarded as the product of the probabilities of two independent steps:

1) The probability for the emission of a beta-particle with energy W_e as calculated from conventional beta-theory;

2) The probability for such an electron to radiate a quantum of energy k when leaving the nucleus.

The two methods gave the same results in the case treated by Knipp and Uhlenbeck. Later it was shown by Chang and Falkoff [3]) who carried out calculations with both methods for different types of interaction in once and twice forbidden transitions, that even if the results are not exactly the same in both cases, the close agreement between them justifies the use of the simpler method of Knipp and Uhlenbeck.

The influence of nuclear charge on the radiation was not taken into account by the above-mentioned authors. This Coulomb effect has later been treated by Nilsson [4]) and Lewis and Ford [5]).

The theory of Knipp-Uhlenbeck gives the expression for the probability of the emission of a photon with energy k

$$S(k) = \int_{1+k}^{W_0} \mathrm{d}W_e P(W_e)\Phi(W_e, k), \qquad (1)$$

where $P(W_e)\mathrm{d}W_e$ is the distribution of the beta-spectrum and $\Phi(W_e, k)$ the probability that an electron of energy W_e emits a photon of energy k. The function $\Phi(W_e, k)$ is given by

$$\Phi(W_e, k) = \frac{\alpha p}{\pi p_e k}\left\{\frac{W_e^2+W^2}{W_e \cdot p}\log(W+p)-2\right\}. \qquad (2)$$

Here, $\alpha = \frac{1}{137}$ is the Sommerfeld fine structure constant; W_e, W and p_e, p are the energies and momenta of the electron before and after the photon emission respectively, expressed in mc^2 units. For $P(W_e)\mathrm{d}W_e$ one can use the experimentally measured beta-distribution, which is a great advantage as it eliminates the difficulty of dealing with the lack of uniqueness in the beta-interaction.

The differential probability $\mathrm{d}\Phi$, that is the probability that a beta-particle of energy W_e will radiate a quantum of energy k per unit photon energy interval at an angle θ between $\mathbf{k}$ and $\mathbf{p}$, is given by

$$\mathrm{d}\Phi(W_e, k, \theta) = \frac{\alpha p}{4\pi^2 p_e k}\left\{\frac{W_e^2+W^2}{W_e(W-p\cos\theta)} - \frac{1}{(W-p\cos\theta)^2} - 1\right\}\mathrm{d}\Omega_k. \qquad (3)$$

The first experimental evidence of the IB was found some thirty years ago and during the following decades several investigations were carried out [6]. No extensive comparisons with theory could be made, however, until the arrival of the scintillation detector. Since then many experiments have been performed, intended to test the photon energy distribution and the photon angular distribution.

The energy distribution has been investigated by Madansky and Rasetti [7], Novey [8], Bogliano *et al.* [9] and by Boehm and Wu [10]. The beta-emitters used were P^{32}, S^{35}, Y^{91}, Pm^{147} and RaE. Photon energies below 250 keV were recorded and the agreement with theory was in all cases rather good. Later on the upper limit of the photon spectrum recorded was extended by Michalowicz [11] to 400 keV and by Goodrich and Payne [12] to 900 keV. These two investigations also give a fairly good agreement with theory.

In 1955, however, Lidén and Starfelt [13] got a result which shows agreement for energies below 600 keV, but at 800 keV they found an excess over the theoretical value of 45 % and at 1000 keV an excess of 70 %.

Finally Langevin-Joliot [14] arrived at experimental results which were two times as high as the theoretically expected values over the whole energy range investigated (up to 1100 keV).

Novey [8] investigated the angular correlation between electrons and photons in a coincidence experiment. Electrons with energies over 50 keV and photons of energies over 40 keV were accepted. The substances investigated were P^{32} and RaE. The results normalized at a certain angle show a very good agreement with the theoretically calculated angular distribution curve.

In 1959 Persson and Johansson [15]) reported an experiment on the absolute probabilities for the emission of IB per beta-decay. They chose three different angles (25°, 45°, 90°) between photon and electron directions and recorded coincidences between beta-particles with energy greater than 150 keV and photons of energies in the region of 200 to 1000 keV. The agreement was good.

Common to all experiments is that the probability $S(k)$ defined in eq. (1) has been measured. No previous attempts to test the dependence of the differential probability $d\Phi$ (eq. (3)) on the beta-energy W_e have been reported. In such a measurement one has a possibility to detect errors in the theory, which otherwise can be wiped out in the integration over all beta-energies.

The present investigation is a test of that part of the theory.

2. Experiment

2.1. SOURCE

P^{32} was available carrier-free with a specific activity of 5 c/g in a weak acid solution. The source was prepared by letting a drop of this dry on a thin zapon film. The diameter of the source was $\approx$ 3 mm and the thickness in the order of 100 $\mu g/cm^2$. The zapon film was mounted on a aluminium ring with 1.5 cm inside diameter. The ring in turn was mounted in a lucite holder with minimum mass in the horizontal plane and fitted into an aluminium cup, thick enough to prevent the electrons from reaching the gamma-detector.

2.2. EQUIPMENT

The experimental arrangement is shown in fig. 1. A magnetic lens spectrometer with momentum resolution adapted for electron-gamma angular corre-

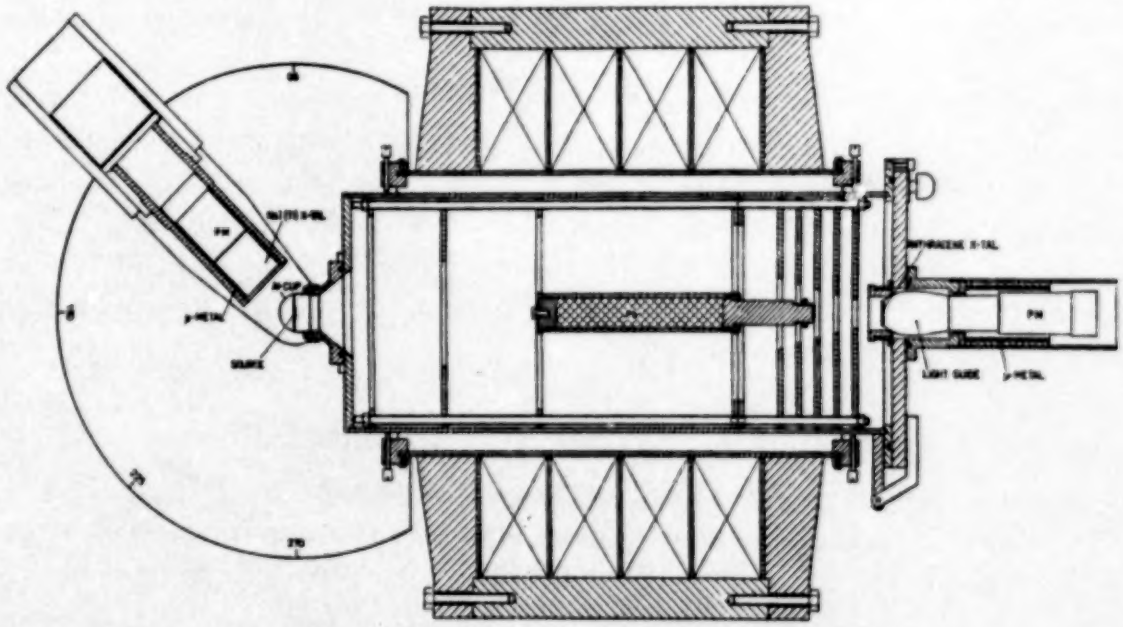

Fig. 1. Electron-gamma angular correlation spectrometer.

lation experiments was used for the measurements. This instrument has been described by Gerholm and Pettersson [16]). The momentum resolution was set at 8 % with a transmission of 2.5 %. The focussed electrons were detected by a 25×2 mm thick anthracene crystal coupled to an EMI 6342 photomultiplier, the photons by a NaI(Tl) 6.4×5.1 cm thick crystal coupled to a DuMond 6363 photomultiplier.

The pulses from each detector were fed to a linear amplifier, followed by a differential discriminator. The coincidence unit of a fast-slow type had a resolving time of 34 ns.

3. Measurements

To check that electrons scattered in source-holder and aluminium cup did not contribute to the coincidences through external bremsstrahlung (EB), the coincidence rates in the 180° resp. 90° positions were measured for photon energies above 100 keV and electrons of 600 keV energy. From these measurements it could be concluded that the contribution from EB was less than 1 % of the coincidence rate in the 90° position.

In the final experiment the gamma-channel was set to accept pulses between 200 and 300 keV. For the beta-spectrometer three different energies were chosen, 350, 680 and 1000 keV. The coincidences were recorded for periods of approximately one hour. For every reading the corresponding single counting rates were measured. Calibration of the discriminator setting of the gamma-channel was performed frequently by means of the 279 keV gamma-line in Hg^{203}.

The resolving time was calculated from the formula $N_{acc} = 2\tau_0 N_\gamma N_\beta$, by recording the number of coincidences when inserting a long delay time in the coincidence circuit.

As the ratio of true to accidental coincidences was unity, the number of accidental coincidences was measured with the same accuracy as the number of true and accidental coincidences together. The resolving time of the coincidence unit was constant within 1 % through the whole measuring period.

The delay curve of the coincidence circuit was also checked each day and the setting of the delay time was adjusted to be in the middle of the flat region of maximum efficiency.

4. Calculation of the Theoretically Expected Value

The most suitable figure to calculate is the probability for IB expressed as photons per beta disintegration. There are several advantages, e.g. no absolute knowledge of the source strength is needed. We write

$$C_k \mathrm{d}k = \int_{W_1}^{W_2} N_0 P(W+k) f(W) \mathrm{d}W \mathrm{d}\Phi(W+k, k, \theta) \omega_\beta \varepsilon_\beta \omega_\gamma \varepsilon_\gamma \mathrm{d}k,$$

and integrating we get

$$C = \int_{k_1}^{k_2} C_k \mathrm{d}k.$$

Here C is the coincidence rate, the coincidences being recorded between photons in the energy interval k_1 to k_2 and beta-particles of energy W. The photons are emitted from electrons with energy $W_e = W+k$. The quantity N_0 is the disintegration rate, $P(W+k)$ the experimentally measured beta-distribution, $\mathrm{d}\Phi$ the above-mentioned differential probability, $f(W)$ the window-curve for the beta-spectrometer, ω_β the transmission of the beta-spectrometer, ε_β the efficiency of the anthracene crystal, ω_γ the solid angle subtended by the NaI-crystal, $\varepsilon_\gamma(k)$ the efficiency of the gamma-channel to detect a photon of energy k.

The counting rate in the beta-spectrometer N_β is given by

$$N_\beta = \int_{W_1}^{W_2} N_0 P(W) f(W) \mathrm{d}W \omega_\beta \varepsilon_\beta.$$

The integrals can be considerably simplified as $P(W)$ varies approximately linearly in the energy interval $W_1 - W_2$ accepted in the spectrometer. Therefore,

$$\frac{C}{N_\beta} = \frac{\int_{k_1}^{k_2} P(\overline{W}+k)\,\mathrm{d}\Phi(\overline{W}+k, k, \theta)\omega_\gamma \varepsilon_\gamma \mathrm{d}k}{P(\overline{W})},$$

where $\overline{W}$ is the energy focussed in the spectrometer. The above integral can more conveniently be written as

$$\frac{C}{N_\beta} = \frac{\int_0^\infty P(\overline{W}+k)\mathrm{d}\Phi(\overline{W}+k, k, \theta)p_\gamma(k)\mathrm{d}k}{P(\overline{W})},$$

where $p_\gamma(k)$ is the probability that a photon of energy k is accepted in the discriminator window. A plot of the integrand in the numerator is shown in fig. 2.

The values of $P(\overline{W})$ and $P(\overline{W}+k)$ are taken from the experimentally measured beta-spectrum, and $\mathrm{d}\Phi$ is calculated from eq. (3). The factor $p_\gamma(k)$ for a certain k was calculated in the following way. The ratio peak/total and absolute efficiency $\omega_\gamma \varepsilon_\gamma$ for an ideal crystal at the distance used were taken from ref. [17]). The energy distributions of certain calibration lines were measured in the actual geometry. The sources used were Hg^{203} (279 keV), Cs^{137} (662 keV), Co^{60} (1.2 MeV). The contribution from photopeaks falling within the discriminator window was calculated from the formula

$$\frac{N_{\text{peak}}}{N_{\text{total}}} = f_{\text{peak}} \times \left(\frac{\text{peak}}{\text{total}}\,\omega_\gamma \varepsilon_\gamma\right)_{\text{theory}},$$

where f_{peak} is the fraction of the photopeak falling within the window. The part

of a Compton distribution falling within our window was calculated from

$$\frac{N_{\text{Compton}}}{N_{\text{total}}} = f_{\text{Compton}} \times \left(\frac{\text{peak}}{\text{total}}\,\omega_\gamma \varepsilon_\gamma\right)_{\text{theory}},$$

where f_{Compton} is the ratio between the number of counts from the accepted part of the Compton distribution and the number of counts in the photopeak.

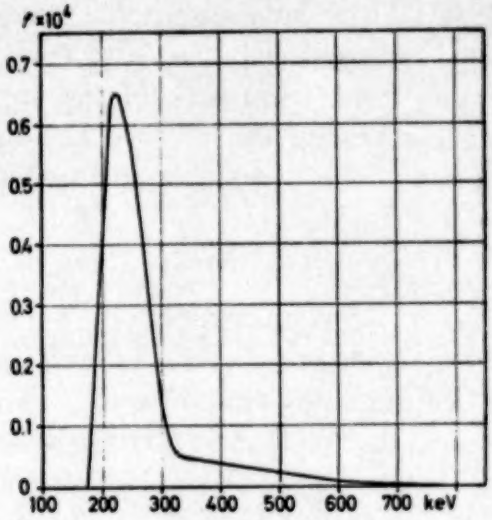

Fig. 2. The expression $f \equiv \mathrm{d}\Phi(\bar{W}+k,\ k,\ 90°)P(\bar{W}+k)p_\gamma(k)$ for $\bar{W} = 2.96$ ($E = 1000$ keV) as a function of photon energy k.

The integral is numerically evaluated for different angles θ to make a correction for the finite solid angles possible. With a 5.5 cm distance source-gamma detector, the value calculated in this way differs 10 % from the value for θ exactly equal to 90°.

5. Treatment of Data and Results

The real coincidence rate was calculated by subtracting the number of accidental coincidences from the measured rate. For each energy about 6000 true coincidences were recorded. As the gamma counting rate was measured, small drifts due to variations in the window width or position could be corrected for. The energy limits of the window was determined from the average of several careful calibrations of the gamma counter.

TABLE 1

Experimental and theoretical values of $\frac{C}{N_\beta} \times 10^3$

Energy (keV)	Experiment	Theory
350	2.24±0.08	2.01±0.06
680	1.97±0.07	1.94±0.06
1000	1.35±0.05	1.38±0.04

The experimental results compared with the values calculated from theory are given in table 1.

The errors in the experimental figures are the statistical ones and the errors in the theoretical values are due to uncertainties in the approximations made when the integrals are calculated.

6. Discussion

Earlier deviations from theory have been found mainly for high energy gammas. It is, however, difficult to measure the IB cross-section for these gammas because of low detection efficiency and low emission probability. High energy photons can only be emitted from beta-particles originally created with high energy. It was therefore considered worth-while to test the IB probability for high energy beta-particles at these must be connected with possible departures from theory. To avoid the large correction connected with high energy gammas and to obtain a reasonable coincidence rate, a gamma energy of 250 keV was selected.

The data presented in column 3 of table 1 have inherent corrections for Compton-distribution from high energy gammas scattering of such gammas into the crystal from outside and backscattering of gammas from multiplier and multiplier shielding. The total correction is less than 20 % with an uncertainty well below 10 % thereof. The data were not influenced by EB as pointed out earlier.

The agreement with theory is good, especially for high energy beta particles.

References

1) J. K. Knipp and G. E. Uhlenbeck, Physica **3** (1936) 425
2) F. Bloch, Phys. Rev. **50** (1936) 2272
3) C. S. W. Chang and D. L. Falkoff, Phys. Rev. **76** (1949) 365
4) S. B. Nilsson, Ark. f. Fysik **10** (1956) 467
5) R. R. Lewis and G. W. Ford, Phys. Rev. **107** (1957) 756
6) S. Bramson, J. de Phys. et Rad. **66** (1930) 721;
C. S. Wu, Phys. Rev. **59** (1941) 481;
K. Siegbahn, Ark. f. Mat., Fys., Astr. **34A** (1946) 6
7) L. Madansky and F. Rasetti, Phys. Rev. **83** (1951) 187
8) T. B. Novey, Phys. Rev. **89** (1953) 672
9) P. Bogliano *et al.*, Phys. Rev. **89** (1953) 679
10) F. Boehm and C. S. Wu, Phys. Rev. **93** (1954) 518
11) A. Michalowicz, J. de Phys. et Rad. **15** (1954) 156
12) M. Goodrich and W. B. Payne, Phys. Rev. **94** (1954) 405
13) K. Lidén and N. Starfelt, Phys. Rev. **97** (1955) 419
14) H. Langevin-Joliot, Ann. de Physique **2** (1957) 16
15) B. Persson and S. A. E. Johansson, Nuclear Physics **12** (1959) 432
16) T. R. Gerholm and B. G. Pettersson, Nuclear Instruments **4** (1959) 107
17) R. L. Heath, AEC Research and Development Report IDO -16408 (unpublished);
S. H. Vegors, L. L. Marsden and R. L. Heath, AEC Research and Development Report IDO-16370 (unpublished)

4.B

Nuclear Physics 18 (1960) 138—148; © *North-Holland Publishing Co., Amsterdam*

Not to be reproduced by photoprint or microfilm without written permission from the publisher

ON THE PSEUDOSCALAR INTERACTION IN $0^- \rightarrow 0^+$ BETA TRANSITIONS

DUBRAVKO TADIĆ

Institute "Rudjer Bošković", Zagreb

Received 19 April 1960

Abstract: The correction factors for the spectrum and longitudinal polarization of electrons in $0^- \rightarrow 0^+$ transitions for the axial vector and pseudoscalar interaction are calculated in the non-relativistic approximation up to the order $(v/c)^2$. Various possible non-relativistic approximations are discussed. Numerical analysis was undertaken for $Pr^{144} \rightarrow Nd^{144}$ transitions. Different results obtained in earlier analyses are explained. From measurements of longitudinal polarization of electrons it seems that $0^- \rightarrow 0^+$ transitions are difficult to explain by pure axial vector interaction.

1. Introduction

A very important question in the theory of β decay is the existence of some kind of pseudoscalar interaction. The measurements of the spectra and longitudinal polarization of electrons in $0^- \rightarrow 0^+$ transitions can give some information about the above problem.

Measurements of the spectra of $Pr^{144} \rightarrow Nd^{144}$ transition have been made by Graham *et al.* [1]) and by Porter *et al.* [2]). They have found that the results obtained by comparing theory and experiment are very insensitive to an admixture of pseudoscalar interaction in theoretical expressions. By analyzing longitudinal polarization in the decay of Ho^{166} W. Bühring [3]) concluded that the contribution of the pseudoscalar interaction was very small (but his theoretical expression for longitudinal polarization was not quite correct; see the Appendix). From the measurements of longitudinal polarization in the decay of Pr^{144} Cohen *et al.* [4]) found an upper limit for the contribution of the pseudoscalar interaction. Their limitation is not consistent with spectrum shape measurements [1, 2]), as will be shown later (see formula (43)).

Such different results were obtained owing to different approximations of the β decay theory used by various authors. It has been shown by Alaga *et al.* [6]), Rose *et al.* [7]) and Konopinski [8]) that if β decay is described by the relativistic Hamiltonian in the usual manner, the nuclear matrix elements are still functions of the electron energy. To take this into account it is necessary to make the non-relativistic approximation in the theory of β decay. The most suitable way of doing this is to use the Foldy-Wouthuysen transformation [6, 7, 9]).

The pseudoscalar interaction is, of course, very sensitive to the assumptions taken into account in deriving the non-relativistic approximation.

2. Some Results

In the non-relativistic approximation the terms up to the order of $(v/c)^2$ were taken into account. The most general correction factor for the spectrum in the case of $0^- \to 0^+$ transitions is

$$\begin{aligned} C_\beta = g_A^2 \Big\{ & |\langle \boldsymbol{\sigma} \cdot \mathbf{r} f_1 \rangle|^2 C_1 + 2\langle \boldsymbol{\sigma} \cdot \mathbf{r} f_1 \rangle \left\langle \frac{i\boldsymbol{\sigma} \cdot \mathbf{p}}{M} + f_2 \right\rangle^* C_2 + \langle \boldsymbol{\sigma} \cdot \mathbf{r} f_1 \rangle \langle \boldsymbol{\sigma} \cdot \mathbf{r} f_3 \rangle^* \frac{C_3}{M} \\ & + \left| \left\langle \frac{i\boldsymbol{\sigma} \cdot \mathbf{p}}{M} + f_2 \right\rangle \right|^2 C_4 + \left\langle \frac{i\boldsymbol{\sigma} \cdot \mathbf{p}}{M} + f_2 \right\rangle \langle \boldsymbol{\sigma} \cdot \mathbf{r} f_3 \rangle^* \frac{C_5}{M} \\ & + \langle \boldsymbol{\sigma} \cdot \mathbf{r} r^2 f_1 \rangle \langle \boldsymbol{\sigma} \cdot \mathbf{r} f_1 \rangle^* \bar{C}_1 + 2\langle \boldsymbol{\sigma} \cdot \mathbf{r} r^2 f_1 \rangle \left\langle \frac{i\boldsymbol{\sigma} \cdot \mathbf{p}}{M} + f_2 \right\rangle^* \bar{C}_2 \\ & + \left| \left\langle r^2 \left(\frac{i\boldsymbol{\sigma} \cdot \mathbf{p}}{M} + f_2 \right) \right\rangle \right|^2 \bar{C}_4 \Big\} + g_A g_P \Big\{ \langle \boldsymbol{\sigma} \cdot \mathbf{r} f_1 \rangle \langle \boldsymbol{\sigma} \cdot \mathbf{r} f_4 \rangle^* \frac{C_6}{M} \\ & + \left\langle \frac{i\boldsymbol{\sigma} \cdot \mathbf{p}}{M} + f_2 \right\rangle \langle \boldsymbol{\sigma} \cdot \mathbf{r} f_4 \rangle^* \frac{C_7}{M} + \langle \boldsymbol{\sigma} \cdot \mathbf{r} f_1 \rangle \langle \boldsymbol{\sigma} \cdot \mathbf{r} f_5 \rangle^* C_8 \\ & + \left\langle \frac{i\boldsymbol{\sigma} \cdot \mathbf{p}}{M} + f_2 \right\rangle \langle \boldsymbol{\sigma} \cdot \mathbf{r} f_5 \rangle^* C_9 \Big\} + g_P^2 |\langle \boldsymbol{\sigma} \cdot \mathbf{r} f_5 \rangle|^2 C_{10}. \end{aligned} \tag{1}$$

Here, g_A and g_P are the axial vector and pseudoscalar coupling constants, and the expressions between $\langle\ \rangle$ are nuclear matrix elements, the f_i being unknown functions of nuclear potentials and operators. We have further

$$C_1 = M_0 - \tfrac{2}{3} q N_0 + \tfrac{1}{9} q^2 L_0, \tag{2}$$

$$C_2 = N_0 - \tfrac{1}{3} q L_0, \tag{3}$$

$$C_3 = \tfrac{1}{9} q^2 (W - V + q) L_0 + (W - V - \tfrac{1}{3} q) M_0 - \tfrac{2}{3} q (W - V + \tfrac{1}{3} q) N_0 - \tfrac{1}{9} q^2 P_0 - Q_0, \tag{4}$$

$$C_4 = C_{10} = L_0, \tag{5}$$

$$C_5 = (W - V - \tfrac{1}{3} q) M_0 + R_0 - \tfrac{1}{3} q (W - V + q) L_0 + \tfrac{1}{3} q P_0, \tag{6}$$

$$C_6 = M_0 - U Q_0 - \tfrac{2}{3} q (2 Q_0 + N_0) + \tfrac{1}{9} q^2 (L_0 - U P_0 - 4 R_0), \tag{7}$$

$$C_7 = U R_0 + N_0 + \tfrac{1}{3} q (U P_0 - L_0 + 4 R_0), \tag{8}$$

$$C_8 = \tfrac{1}{3} q P_0 - R_0, \tag{9}$$

$$C_9 = P_0, \tag{10}$$

$$\bar{C}_1 = \tfrac{8}{45} q^3 N_0 - \tfrac{1}{45} q^4 L_0 - \tfrac{1}{3} q^2 M_0, \tag{11}$$

$$\bar{C}_2 = \tfrac{4}{45} q^3 L_0 + \tfrac{1}{3} q M_0 - \tfrac{4}{9} q^2 N_0, \tag{12}$$

$$\bar{C}_4 = \tfrac{2}{3}qN_0 - \tfrac{1}{3}q^2L_0, \tag{13}$$

$$U = W - V - q, \tag{14}$$

$$V = -\frac{\alpha Z}{r_0}. \tag{15}$$

All other notations have the usual meaning. The terms C_1, C_2, C_4, C_8, C_9, C_{10} were calculated by Konopinski *et al.* [10]) and by Smith [11]); C_6, C_7 were calculated by Rose *et al.* [7]), but in Rose's published results there are a number of misprints.

Longitudinal polarization was calculated according to the method of Alder *et al.* [12]). It is of the form [13])

$$\mathbf{P} = -\frac{\mathbf{p}_e}{W}\frac{P}{C_\beta}, \tag{16}$$

where $\mathbf{p}_e$ is the momentum of the electron. Here P/C_β plays the same role as the correction factor C_β for the spectra, because it measures the deviation from the allowed shape v/c. We have

$$\begin{aligned} P = g_A^2 \Big\{ & |\langle \boldsymbol{\sigma}\cdot\mathbf{r}f_1\rangle|^2 P_1 + 2\langle \boldsymbol{\sigma}\cdot\mathbf{r}f_1\rangle \Big\langle \frac{i\boldsymbol{\sigma}\cdot\mathbf{p}}{M} + f_2 \Big\rangle^* P_2 + \langle \boldsymbol{\sigma}\cdot\mathbf{r}f_1\rangle\langle \boldsymbol{\sigma}\cdot\mathbf{r}f_3\rangle^* \frac{P_3}{M} \\ & + \Big| \Big\langle \frac{i\boldsymbol{\sigma}\cdot\mathbf{p}}{M} + f_2 \Big\rangle \Big|^2 P_4 + \Big\langle \frac{i\boldsymbol{\sigma}\cdot\mathbf{p}}{M} + f_2 \Big\rangle \langle \boldsymbol{\sigma}\cdot\mathbf{r}f_3\rangle^* \frac{P_5}{M} \\ & + \langle \boldsymbol{\sigma}\cdot\mathbf{r}r^2 f_1\rangle\langle \boldsymbol{\sigma}\cdot\mathbf{r}f_1\rangle^* \bar{P}_1 + 2\langle \boldsymbol{\sigma}\cdot\mathbf{r}r^2 f_1\rangle \Big\langle \frac{i\boldsymbol{\sigma}\cdot\mathbf{p}}{M} + f_2 \Big\rangle^* \bar{P}_2 \\ & + \Big| \Big\langle r^2 \Big(\frac{i\boldsymbol{\sigma}\cdot\mathbf{p}}{M} + f_2 \Big) \Big\rangle \Big|^2 \bar{C}_4 \Big\} + g_A g_P \Big\{ \langle \boldsymbol{\sigma}\cdot\mathbf{r}f_1\rangle\langle \boldsymbol{\sigma}\cdot\mathbf{r}f_4\rangle^* \frac{P_6}{M} \\ & + \Big\langle \frac{i\boldsymbol{\sigma}\cdot\mathbf{p}}{M} + f_2 \Big\rangle \langle \boldsymbol{\sigma}\cdot\mathbf{r}f_4\rangle^* \frac{P_7}{M} + \langle \boldsymbol{\sigma}\cdot\mathbf{r}f_1\rangle\langle \boldsymbol{\sigma}\cdot\mathbf{r}f_5\rangle^* P_8 \Big\} + g_P^2 |\langle \boldsymbol{\sigma}\cdot\mathbf{r}f_5\rangle|^2 P_{10}, \end{aligned} \tag{17}$$

with

$$P_1 = (\tfrac{1}{9}q^2A_0 - \tfrac{2}{3}qC_0 - B_0)n, \tag{18}$$

$$P_2 = (C_0 - \tfrac{1}{3}qA_0)n, \tag{19}$$

$$P_3 = [\tfrac{1}{9}q^2(W - V + q)A_0 + (W - V - \tfrac{1}{3}q)B_0 - \tfrac{2}{3}q(W - V + \tfrac{1}{3}q)C_0 - \tfrac{2}{3}qD_0]n, \tag{20}$$

$$P_4 = A_0 n, \tag{21}$$

$$P_5 = -[\tfrac{1}{3}q(W - V + q)A_0 - (W - V - \tfrac{1}{3}q)C_0 - D_0]n, \tag{22}$$

$$P_6 = [\tfrac{1}{9}q^2A_0 - B_0 - \tfrac{2}{3}qC_0 - \tfrac{2}{3}q(W - V - \tfrac{1}{3}q)D_0]n, \tag{23}$$

$$P_7 = [(W - V + \tfrac{1}{3}q)D_0 - \tfrac{1}{3}qA_0 + C_0]n, \tag{24}$$

$$P_8 = D_0 n, \tag{25}$$

$$P_{10} = -A_0 n, \tag{26}$$

$$\bar{P}_1 = (\tfrac{8}{45}q^3 C_0 + \tfrac{1}{3}q^2 B_0 - \tfrac{1}{45}q^4 A_0)n, \tag{27}$$

$$\bar{P}_2 = (\tfrac{4}{45}q^3 A_0 - \tfrac{1}{3}q B_0 - \tfrac{4}{9}q^2 C_0)n, \tag{28}$$

$$\bar{P}_4 = (\tfrac{2}{3}q C_0 - \tfrac{1}{3}q^2 A_0)n, \tag{29}$$

in these formulae,

$$n = \cos(\Delta_1 - \Delta_{-1}). \tag{30}$$

The definitions of A_0, B_0, C_0, D_0 and Δ_k are given in the Appendix.

A great number of unknown parameters makes the analysis of experimental results very difficult. If some further assumptions are taken into account it is possible to limit the number of parameters. The results for some extreme cases are given below.

2.1. CASE I

Assuming that the nuclear potential is an even operator [9]) and that the Foldy-Wouthuysen approximation can be limited to terms of the order v/c, the approximation first proposed by Rose *et al.* [7]) is obtained. This approximation was used in the explanation of spectrum shape measurements [1, 2]). The correction factors are given by

$$C_\beta = |\langle \boldsymbol{\sigma} \cdot \mathbf{r} \rangle|^2 g_A{}^2 \left\{ C_1 + 2fC_2 + \frac{C_3}{M} + f^2 C_4 + f\frac{C_5}{M} + \Gamma\frac{C_6}{M} + \Gamma f\frac{C_7}{M} + s\bar{C}_1 + 2sf\bar{C}_2 + tf^2\bar{C}_4 \right\}, \tag{31}$$

$$P = |\langle \boldsymbol{\sigma} \cdot \mathbf{r} \rangle|^2 g_A{}^2 \left\{ P_1 + 2fP_2 + \frac{P_3}{M} + f^2 P_4 + f\frac{P_5}{M} + \Gamma\frac{P_6}{M} + \Gamma f\frac{P_7}{M} + s\bar{P}_1 + 2sf\bar{P}_2 + tf^2\bar{P}_4 \right\}, \tag{32}$$

where

$$f = \frac{\left\langle \frac{i\boldsymbol{\sigma} \cdot \mathbf{p}}{M} \right\rangle}{\langle \boldsymbol{\sigma} \cdot \mathbf{r} \rangle}, \quad \Gamma = \frac{g_P}{g_A}, \tag{33}$$

$$s = \frac{\langle \boldsymbol{\sigma} \cdot \mathbf{r} r^2 \rangle}{\langle \boldsymbol{\sigma} \cdot \mathbf{r} \rangle}, \quad t = \frac{\langle r^2 \boldsymbol{\sigma} \cdot \mathbf{p} \rangle}{\langle \boldsymbol{\sigma} \cdot \mathbf{p} \rangle}, \quad s \approx t \approx r_0{}^2. \tag{34}$$

Numerical analyses were undertaken for Pr^{144}. Measurements of longitudinal polarization [4, 14–16]) were performed at different energies, and all results are approximately $-v/c$ (allowed shape). The spectrum is also approximately of allowed shape. It was reasonable to search for such parameters f and Γ for which the deviation of the spectra and longitudinal polarization from the allowed shape would be less than 3.5 %. A_0, B_0, C_0, D_0 were obtained by

interpolating numerical tables for the spectra [17]). As finite size corrections and screening were not taken into account the results are not very accurate for $f > 0$. For these values of f a destructive interference of the relativistic and non-relativistic part of the axial vector contribution occurs which gives a too large ft value.

The region of f and Γ satisfying the spectrum shape and longitudinal polarization is presented in fig. 1. The experimental results are natural and easy to reproduce for $f < 0$. That is not consistent with theoretical estimations. Pursey [18]) and Feenberg *et al.* [19]) † deduced that f was always positive and of a magnitude of about $0 < f < 15$.

On the basis of the shell model Pearson [20]) deduced for the magnitude $2.5 < f < 9$.

For most combinations of parameters longitudinal polarization is here somewhat larger in absolute value than $|v/c|$. Of course, the contrary is not excluded.

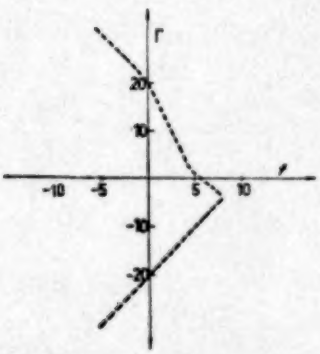

Fig. 1. The parameter Γ defined by eq. (33) is plotted as a function of the parameter f defined by (33). The region to the left from the curve is in agreement with the experiments. For $f < -5$, results are very insensitive to Γ.

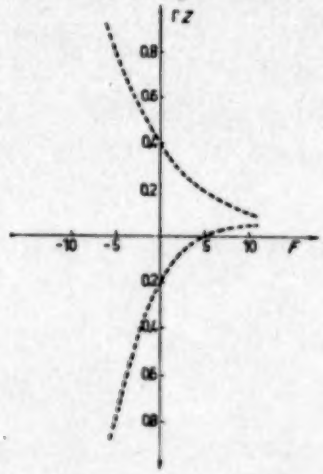

Fig. 2. The parameter ΓZ defined by eq. (38) or (45) is plotted as a function of the parameter F defined by eq. (37) or (44). The region to the left of the curve is in agreement with the experimental results.

2.2. CASE II

Assuming that the nuclear potential is of the form $U_e = \sum_{K=1}^{A} \beta_K V_K(r)$, the approximation proposed by Alaga *et al.* [6]) and Konopinski [8]) is obtained. It is really the shell model approximation. The total Hamiltonian for this approximation is given in the Appendix (eq. A (12)). The correction factors are given by

$$C_\beta = |\langle \boldsymbol{\sigma} \cdot \mathbf{r} \rangle|^2 g_A^2 \left\{ C_1 + 2FC_2 + \frac{C_3}{M} + F^2 C_4 + F\frac{C_5}{M} + 2\Gamma Z C_8 + 2F\Gamma Z C_9 \right.$$
$$\left. + (\Gamma Z)^2 C_{10} + S\bar{C}_1 + 2SF\bar{C}_2 + TF^2\bar{C}_4 \right\}, \tag{35}$$

† Rose *et al.* [7]) use a γ_5 matrix of opposite sign to that used by Feenberg *et al.* [19]), Konopinski *et al.* [10]) and the present work. If this is taken into account Rose's and Feenberg's results for the non-relativistic approximation are equivalent and have the same sign.

$$P = |\langle \boldsymbol{\sigma} \cdot \mathbf{r} \rangle|^2 g_A^2 \left\{ P_1 + 2FP_2 + \frac{P_3}{M} + F^2 P_4 + F\frac{P_5}{M} + 2\Gamma Z P_8 + (\Gamma Z)^2 P_{10} + S\bar{P}_1 + 2SF\bar{P}_2 + TF^2\bar{P}_4 \right\}, \tag{36}$$

where

$$F = \frac{\left\langle i\frac{\boldsymbol{\sigma}\cdot\mathbf{p}}{M}\left(1+\frac{V}{M}\right) - 2\boldsymbol{\sigma}\cdot\mathbf{r}G(r)\right\rangle}{\langle \sigma r \rangle}, \tag{37}$$

$$Z = \frac{\langle \boldsymbol{\sigma}\cdot\mathbf{r}G(r)\rangle}{\langle \boldsymbol{\sigma}\cdot\mathbf{r}\rangle}, \quad \Gamma = \frac{g_P}{g_A}, \tag{38}$$

$$S \approx T \approx r_0^2. \tag{39}$$

The terms with the derivatives of the pseudoscalar interaction are neglected here, which is a good approximation if the assumption $|g_P/g_A| < 1$ is taken into account

For the nuclear potentials the following expression holds:

$$\frac{1}{4M^2}\frac{1}{r}\frac{dV}{dr} = -G(r); \quad G(r) = |G(r)|. \tag{40}$$

Alaga *et al.* [6]) estimated for a square well potential that †

$$\frac{\frac{i}{4M^2}\left\langle \boldsymbol{\sigma}\cdot\mathbf{r}\frac{1}{r}\frac{dV}{dr}\right\rangle}{\langle \boldsymbol{\sigma}\cdot\mathbf{r}\rangle} \approx \frac{iE^2}{6M} = 0.95i. \tag{41}$$

In comparison with the spin orbit coupling term another estimation was proposed by Konopinski [8]) (see Appendix eq. A (12)), namely

$$\frac{i}{4M^2}\left\langle \boldsymbol{\sigma}\cdot\mathbf{r}\frac{1}{r}\frac{dV}{dr}\right\rangle \approx -iC\langle \boldsymbol{\sigma}\cdot\mathbf{r}\rangle, \tag{42}$$

where

$$C = \overline{G(r)} = 2 - 4mc^2.$$

The terms containing only V are rather small for a square well potential and may be neglected.

The region of F and ΓZ satisfying the spectrum and the polarization is given in fig. 2. A negative value for F could perhaps be understood if the estimation (42) is introduced into the matrix element (37). If F is positive the same remarks about the accuracy of the treatment and for the ft-value as in case I are valid.

Case II corresponds to the treatment of Bühring [3]), and for $F = 0$ to that of Cohen *et al.* [4]). The only difference is that some higher order corrections for the

† The sign of this expression is doubtful.

axial vector coupling are taken into account. For $F = 0$ one obtains

$$-0.2 < \Gamma Z < 0.4. \tag{43}$$

According to (41) $|g_P/g_A| < 0.4$ and according to (42) $|g_P/g_A| < 0.1$. For $f = 0$, Case I gave $|g_P/g_A| < 20$. Thus, Cases I and II give quite different limitations for the pseudoscalar coupling constant.

It is quite easy to obtain the longitudinal polarization which is in absolute value approximately $|v/c|$ or somewhat smaller and practically constant in energy. The shape of the correction factor for the polarization for some interesting examples is given in fig. 3.

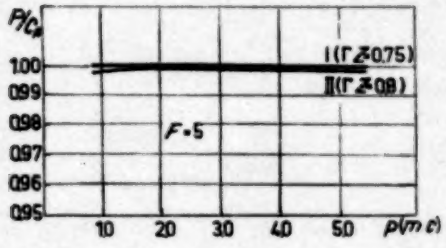

Fig. 3. The theoretical correction factor for longitudinal polarization P/C_β is plotted as a function of the electron momentum. The longitudinal polarization is given by $-(v/c)P/C_\beta$. The parameters F and ΓZ are defined by eqs. (37) and (38) or by eqs. (44) and (45). For $\Gamma Z > 0.8$, the results are not in agreement with spectrum shape measurements [1, 2]).

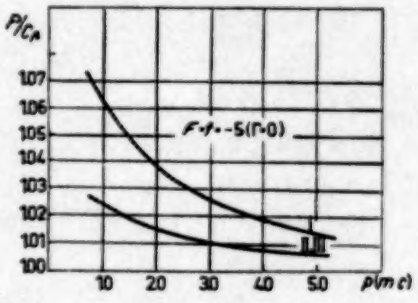

Fig. 4. The theoretical correction factor for longitudinal polarization P/C_β for pure axial vector coupling is plotted as a function of the electron momentum. The parameter f or F is defined by eqs. (33), (37) or (44). Curve I is obtained in plane wave approximation and without higher order corrections C_3, C_5, $\bar{C}_1$, $\bar{C}_2$, $\bar{C}_4$, P_3, P_5, $\bar{P}_1$, $\bar{P}_2$ and $\bar{P}_4$. Curve II is obtained with Coulomb wave functions for electrons but still without higher order corrections. Curve III, obtained with all corrections, is practically the same as curve II.

2.3. CASE III

If Herbst's [21]) suggestion for the non-relativistic approximation is accepted the correction factors are still of the form (35) and (36). The nuclear matrix elements are now defined by

$$F = \frac{\left\langle i\left(\frac{\boldsymbol{\sigma}\cdot\mathbf{p}}{M} - \boldsymbol{\sigma}\cdot\mathbf{V} - \theta\right)\right\rangle}{\langle \boldsymbol{\sigma}\cdot\mathbf{r}\rangle}, \tag{44}$$

$$Z = \frac{\frac{1}{M}\langle \boldsymbol{\sigma}\cdot\mathbf{r} f(r) + \phi\rangle}{\langle \boldsymbol{\sigma}\cdot\mathbf{r}\rangle}. \tag{45}$$

The notations are the same as in ref. [21]): $f(r)/M$ is the factor of the spin orbit coupling term, $\mathbf{V}$, ϕ and θ are nuclear potentials. The results given in fig. 2 still hold.

2.4. CASE IV

For $g_P = 0$, pure axial vector coupling is obtained from eqs. (31), (32) or (35), (36). This case was investigated in detail in ref. [13]). The possible region for f or F is easily deduced from fig. 1 or 2 for $\Gamma = 0$ or $\Gamma Z = 0$.

The most interesting result is that the polarization for all possible cases is somewhat larger in absolute value than $|v/c|$. In fig. 4 some curves for $f = -5$ are given.

Of course, it is not excluded to obtain an absolute polarization $< |v/c|$ if the variation of the lepton wave functions over the nucleus is taken into account with higher accuracy, as for example is done by Alaga and Jakšić [22, 23]). An argument against this possibility is that the polarization is quite insensitive to high order corrections, as is seen from fig. 4. This is a very important question because the experiments [4, 14–16]) favour a polarization $<|v/c|$.

3. Conclusion

It is quite impossible to reach any definite conclusion about the presence of the pseudoscalar interaction. It is remarkable that for pure axial vector interaction the theoretical polarization is always larger in absolute value than $|v/c|$. If experiments definitely gave a polarization smaller than $|v/c|$, it would mean that some new interaction had to be included, or that something is wrong in the treatment of the axial vector interaction.

It will be of great importance to measure the correction factor for longitudinal polarization (16) as a function of the electron energy.

I am very grateful to Dr. G. Alaga for suggesting the problem and for constant help and encouragement during this work. I should like to acknowledge some illuminating discussions with Dr. B. Jakšić, L. Šips and some other members of our theoretical group.

Appendix

The usual notation is used here (see ref. [7])). Combinations of the radial wave functions are as follows:

$$f_\nu g_{-\nu} = p^2 F \frac{p}{W} r_0^{2\nu-2} A_{\nu-1}, \tag{A1}$$

$$f_{-\nu} g_\nu = p^2 F \frac{p}{W} r_0^{2\nu} B_{\nu-1}, \tag{A2}$$

$$f_\nu f_{-\nu} - g_\nu g_{-\nu} = 2p^2 F \frac{p}{W} r_0^{2\nu-1} C_{\nu-1}, \tag{A3}$$

$$f_\nu f_{-\nu} + g_\nu g_{-\nu} = 2p^2 F \frac{p}{W} r_0^{2\nu-1} D_{\nu-1}, \tag{A4}$$

$$A_0 \to 1, \tag{A5}$$

$$B_0 \to -\tfrac{1}{6}p^2 - \tfrac{2}{3}W\xi - \xi^2, \tag{A6}$$

$$C_0 \to -\tfrac{1}{3}W - \xi, \tag{A7}$$

$$D_0 \to \tfrac{1}{3}, \tag{A8}$$

$$\xi = \frac{\alpha Z}{2r_0}, \tag{A9}$$

$$\cos(\Delta_\kappa - \Delta_{-\kappa}) = \frac{\kappa S_\kappa}{\left[\kappa^2 + \left(\frac{\alpha Z}{p}\right)^2\right]^{\frac{1}{2}}}, \quad S_\kappa = \frac{\kappa}{|\kappa|}, \tag{A10}$$

$$\sin(\Delta_\kappa - \Delta_{-\kappa}) = \frac{(-\alpha Z/p) S_\kappa}{\left[\kappa^2 + \left(\frac{\alpha Z}{p}\right)^2\right]^{\frac{1}{2}}}. \tag{A11}$$

All results are in agreement with those of Alder *et al.* [12]) and of Rakavy [4, 5]). The Lee-Whiting [24]) rules for the transformation from spectrum to polarization gave incomplete expressions for some of the terms without derivatives of the lepton wave functions, and for all terms with such derivatives.

To control the results the calculation for plane waves ($Z = 0$) was performed by several different methods. The approximate expressions A(5—8) lead to the same results.

The total nuclear Hamiltonian for the approximation of Case II is given by

$$H' = \frac{1}{2M}(\mathbf{p} - e\mathbf{A})^2\tau_P + \frac{g_V}{2M}(\mathbf{p}\cdot\mathbf{L}_V + \mathbf{L}_V\cdot\mathbf{p})\tau_+ - \frac{ie}{2M}\boldsymbol{\sigma}\cdot(\mathbf{p}\times\mathbf{A} + \mathbf{A}\times\mathbf{p})\tau_P$$

$$+ \frac{ig_V}{2M}\boldsymbol{\sigma}\cdot(\mathbf{p}\times\mathbf{L}_V + \mathbf{L}_V\times\mathbf{p})\tau_+ + g_A\boldsymbol{\sigma}\cdot\mathbf{L}_A\tau_+ + g_V L_V\tau_+$$

$$+ \frac{g_A}{2M}(\boldsymbol{\sigma}\cdot\mathbf{p}L_A + L_A\boldsymbol{\sigma}\cdot\mathbf{p})\tau_+ - \frac{g_P}{2M}(\boldsymbol{\sigma}\cdot\mathbf{p}L_P - L_P\boldsymbol{\sigma}\cdot\mathbf{p})\tau_+$$

$$+ \frac{1}{4M^2}\frac{1}{r}\frac{dV}{dr}\boldsymbol{\sigma}\cdot\mathbf{l} \tag{a}$$

$$- \frac{e}{4M^2}\Big\{4V\mathbf{A}\cdot\mathbf{p} - 2i\mathbf{A}\cdot\mathbf{r}\frac{1}{r}\frac{dV}{dr} + \frac{1}{r}\frac{dV}{dr}\boldsymbol{\sigma}\cdot(\mathbf{r}\times\mathbf{A})$$

$$+ 2V\boldsymbol{\sigma}\cdot(\boldsymbol{\nabla}\times\mathbf{A}) - 2iV\boldsymbol{\nabla}\cdot\mathbf{A}\Big\}\tau_P \tag{b}$$

$$+ \frac{g_V}{4M^2}\Big\{4V\mathbf{L}_V\cdot\mathbf{p} - 2i\mathbf{L}_V\cdot\mathbf{r}\frac{1}{r}\frac{dV}{dr} + \frac{1}{r}\frac{dV}{dr}\boldsymbol{\sigma}\cdot(\mathbf{r}\times\mathbf{L}_V)$$

$$+ 2V\boldsymbol{\sigma}\cdot(\boldsymbol{\nabla}\times\mathbf{L}_V) - 2iV\boldsymbol{\nabla}\cdot\mathbf{L}_V\Big\}\tau_+ \tag{c}$$

$$+\frac{g_A}{2M^2}\left\{2L_A V\boldsymbol{\sigma}\cdot\mathbf{p}-iL_A\boldsymbol{\sigma}\cdot\mathbf{r}\frac{1}{r}\frac{dV}{dr}-iV\boldsymbol{\sigma}\cdot\boldsymbol{\nabla}L_A\right\}\tau_+ \qquad \text{(d)}$$

$$+\frac{ig_P}{4M^2}\left\{L_P\boldsymbol{\sigma}\cdot\mathbf{r}\frac{1}{r}\frac{dV}{dr}+2V\boldsymbol{\sigma}\cdot\boldsymbol{\nabla}L_P\right\}\tau_+ \qquad \text{(e)}$$

$$+U_C+U_e+H_L+H_\gamma. \qquad \text{(A12)}$$

The summation over individual nucleons is understood. Here, $\mathbf{A}$ is the electromagnetic potential; $\mathbf{L}_V$, L_V, $\mathbf{L}_A$, L_A and L_P are the lepton covariants for the vector, axial vector and pseudoscalar interaction respectively; U_C is the Coulomb potential U_e the nuclear potential, H_L and H_γ the Hamiltonians for the lepton and electromagnetic fields respectively; βV is the relativistic shell model potential; $\tau_P=\frac{1}{2}(1+\tau_3)$, $\tau_+=\frac{1}{2}(\tau_1+i\tau_2)$; τ_1 are the usual isobaric spin operators.

The first seven terms correspond to the approximation of Case I. The term (a) is the spin orbit coupling term. The term (e) was first derived by Alaga *et al.* [6]) and partially by Konopinski [8]).

Jensen *et al.* [25]) gave semi-empirical arguments for the influence of the spin orbit coupling on γ transitions. The same argument holds perhaps for the vector coupling in β decay, if the Gell-Mann form of the theory [26–28]) is accepted. In the empirical form of the spin orbit coupling

$$-\xi(r)\boldsymbol{\sigma}\cdot(\mathbf{r}\times\mathbf{p}), \qquad \text{(A13)}$$

$\mathbf{p}$ can be replaced by

$$\mathbf{p}-e\mathbf{A}\tau_P+g_V\mathbf{L}_V\tau_+ \qquad \text{(A14)}$$

and some parts of the terms (A12b) and (A12c) are deduced.

It is interesting to note that Morita's treatment [29, 30]) in the theory of allowed decays would give in the plane wave approximation exactly the same results as Case I if the relations of Feenberg *et al.* [19]) and Yamada [31]) between the nuclear matrix elements are used. It seems that it is not too satisfactory to use these relations in the analysis of experimental results. (Feenberg's and Yamada's results are based on the same assumptions as the approximation in Case I.)

References

1) R. L. Graham, J. S. Geiger and T. A. Eastwood, Can. J. Phys. **36** (1958) 1084
2) F. T. Porter and P. P. Day, Phys. Rev. **114** (1959) 1286
3) W. Bühring, Z. f. Phys. **115** (1959) 566
4) S. G. Cohen and R. Wiener, Nuclear Physics **15** (1960) 79
5) G. Rakavy, Nuclear Physics **14** (1960) 661
6) G. Alaga, O. Kofoed-Hansen and A. Winther, Mat. Fys. Medd. Dan. Vid. Selsk. **28**, No. 3 (1953)
7) M. E. Rose and R. K. Osborn, Phys. Rev. **93** (1954) 1315
8) E. J. Konopinski, Phys. Rev. **94** (1954) 492

9) L. L. Foldy and S. A. Wouthuysen, Phys. Rev. **78** (1950) 29
10) E. J. Konopinski and G. E. Uhlenbeck, Phys. Rev. **60** (1941) 308
11) A. M. Smith, Phys. Rev. **82** (1951) 955
12) K. Alder, B. Stech and A. Winther, Phys. Rev. **107** (1957) 728
13) D. Tadić, Glasnik mat. fiz. i astr. **13** (1958) 267
14) M. A. Grace, Proc. Roy. Soc. **246** (1958) 454
15) I. S. Geiger, G. I. Ewan, R. L. Graham and D. R. Mac Kenzie, Phys. Rev. **112** (1958) 1684
16) W. A. W. Mehlhop, E. D. Lambe and T. A. Pond, Bull. Am. Phys. Soc. **5** (1960) 9
17) M. E. Rose, C. L. Perry and N. M. Dismuke, ORNL-1459
18) D. L. Pursey, Phil. Mag. **42** (1951) 1193
19) T. Ahrens and E. Feenberg, Phys. Rev. **86** (1952) 64
20) M. J. Pearson, Can. J. Phys. **38** (1960) 148 and private communication
21) R. F. Herbst, Phys. Rev. **96** (1954) 372
22) G. Alaga and B. Jakšić, Phys. Rev. **103** (1956) 1441
23) G. Alaga and B. Jakšić, Glasnik mat. fiz. i astr. **13** (1957) 31
24) G. E. Lee-Whiting, Can. J. Phys. **36** (1958) 1199
25) J. Jensen and M. Goeppert-Mayer, Phys. Rev. **85** (1952) 1040
26) R. P. Feynman and M. Gell-Mann, Phys. Rev. **109** (1958) 193
27) M. Gell-Mann, Phys. Rev. **111** (1958) 362
28) M. Gell-Mann, Rev. Mod. Phys. **31** (1959) 834
29) M. Morita, Phys. Rev. **113** (1959) 158
30) M. Morita, Nuclear Physics **14** (1959) 106
31) M. Yamada, Progr. Theoret. Phys. **9** (1953) 268

8.B

Nuclear Physics **18** (1960) 149—152; © *North-Holland Publishing Co., Amsterdam*

Not to be reproduced by photoprint or microfilm without written permission from the publisher

STRONG INTERACTIONS AND ISOBARIC GAUGE INVARIANCE

V. GUPTA

Tata Institute of Fundamental Research, Bombay

Received 21 April 1960

Abstract: Isobaric gauge invariance of the free fermion Lagrangian is demanded and it is shown that it is possible to introduce the pion field and its pseudoscalar and pseudovector couplings under a restricted gauge transformation. It is also possible to introduce the vector coupling in a similar way. The removal of the restrictions on the gauge would require the introduction of additional interaction terms.

1. Introduction

It is known [1]) that the electromagnetic field and its interaction with a charged fermion may be introduced by requiring the free fermion Lagrangian to be invariant under the gauge transformation $\psi \rightarrow \exp(ie\alpha(x_\mu))\psi$. Salam and Gell-Mann [2]) have shown the possibility of generating a weak interaction current by requiring the invariance of the strong interaction Lagrangian (including only pseudoscalar pion coupling) under suitable isobaric gauge transformations. Our aim is to investigate whether the strong interaction Lagrangian (pion couplings only) may be generated by requiring the free fermion Lagrangian to be invariant under isobaric gauge transformations. Following Yang and Mills [1]) we define the isobaric gauge as an arbitrary way of choosing the orientation of the isobaric spin axes at all space-time points. Yang and Mills further demand that physical processes be independent of this arbitrariness.

A general infinitesimal isobaric gauge transformation will be of the form †

$$\psi \rightarrow \psi + igI'T\psi,$$

where g is a real number and I' and T are hermitian operators: I' is a combination of the Dirac matrices and T contains the dependence on isobaric space. To give isobaric spin conservation, T should be of the form [1]) $\tau \cdot \alpha(x_\mu)$ where τ are the Pauli spin matrices in isobaric space and $\alpha(x_\mu)$ a hermitian isobaric vector which specifies the isobaric gauge. Having chosen T as above, the possible choices for I', which preserve invariance under proper Lorentz transformations, are either γ_5 or 1.

† One could, however, have a more general transformation, for example, $\psi \rightarrow \psi + ig\gamma_\mu(\partial_\mu\alpha)\cdot\tau\psi$. We shall not consider such transformations.

The next section gives the generation of the pseudoscalar (ps) and pseudovector (pv) interaction terms. In section 3 we consider the generation of the scalar and vector couplings.

2. The ps and pv Pion Couplings

For simplicity we limit ourselves to the nucleon isobaric doublet. The free nucleon Lagrangian density is ($\hbar = c = 1$)

$$\begin{aligned} L_0 &= L_0^{(1)} + L_0^{(2)}, \\ L_0^{(1)} &= -\tfrac{1}{2}(\bar{\psi}\gamma_\mu \partial_\mu \psi - \partial_\mu \bar{\psi}\gamma_\mu \psi), \quad L_0^{(2)} = -m\bar{\psi}\psi, \end{aligned} \tag{1}$$

where ψ is a two-component spinor in isobaric space and we use the convention $\gamma_\mu^\dagger = \gamma_\mu$ ($\mu = 1, 2, 3, 4$), $\gamma_5^\dagger = \gamma_5$ and $\partial_\mu \equiv \partial/\partial x_\mu$; $x_\mu = (x_1, x_2, x_3, it)$.

Consider the infinitesimal gauge transformation †

$$\psi \to (1 + ig\gamma_5 \boldsymbol{\tau} \cdot \boldsymbol{\alpha})\psi \tag{2}$$

where g is a real number corresponding to the coupling strength (like the electric charge in the electromagnetic case). Requiring (1) to be invriant under (2), one finds that it is necessary to introduce a spin zero isobaric vector field $\boldsymbol{\phi}(x_\mu)$ which transforms as

$$\boldsymbol{\phi} \to \boldsymbol{\phi} + \boldsymbol{\alpha}. \tag{3}$$

Further one has to introduce the coupling terms

$$L_1 = ig\bar{\psi}\gamma_\mu \gamma_5 \boldsymbol{\tau} \cdot \partial_\mu \boldsymbol{\phi} \psi, \quad L_2 = 2mig\bar{\psi}\gamma_5 \boldsymbol{\tau} \cdot \boldsymbol{\phi}\psi. \tag{4}$$

Then $L_0 + L_1 + L_2$ is invariant under (2) and (3) under the restrictions, in isobaric space,

$$\boldsymbol{\alpha} \cdot \boldsymbol{\phi} = 0, \tag{5a}$$

$$\boldsymbol{\alpha}_\Lambda \partial_\mu \boldsymbol{\phi} = 0. \tag{5b}$$

Eqs. (5a) and (5b) are required to ensure the invariance of $L_0^{(2)} + L_2$ and $L_0^{(1)} + L_1$ respectively.

The parity of the $\boldsymbol{\phi}$ field is undetermined. If we assume it to be pseudoscalar and identify it with the pion field, then L_1 and L_2 are the usual pv and ps coupling terms. An interesting feature is the relation obtained between the two coupling constants g_{ps} and g_{pv}, namely

$$g_{ps} = 2mg_{pv}. \tag{6}$$

This is just the relation obtained when the equivalence of the ps and pv couplings is shown [3]), to first order, by the Dyson-Foldy transformation.

† R. P. Feynmann, M. Gell-Mann and M. Lévy have recently considered similar transformations (A. Salam, private communication).

Above, the relation (6) emerges automatically. Since we have introduced the boson field $\boldsymbol{\phi}$ we must add its free Lagrangian density $L_\pi = -\frac{1}{2}(-\dot{\boldsymbol{\phi}}^2+|\nabla\boldsymbol{\phi}|^2+ +\mu^2\boldsymbol{\phi}^2)$ and require the total Lagrangian density $L = L_0+L_\pi+L_1+L_2$ to be invariant. Now $\boldsymbol{\phi}^2$ is invariant owing to (5a). The term arising from the rest of L_π is essentially $\nabla\boldsymbol{\phi}\cdot\nabla\boldsymbol{\alpha}-\dot{\boldsymbol{\phi}}\cdot\dot{\boldsymbol{\alpha}}$. This can be shown to be zero by applying $\Box \equiv \nabla^2-\partial^2/\partial t^2$ to (5a) and imposing the restriction, in space-time,

$$\Box\boldsymbol{\alpha} = c\boldsymbol{\alpha}, \tag{7}$$

where c is an arbitrary constant † or zero.

We can also introduce in the total Lagrangian density a pion-pion interaction term $\boldsymbol{\phi}^4$, which is invariant owing to (5a).

Though we had limited the above analysis to the nucleon doublet it is valid for any fermion isobaric doublet. Thus under the 'doublet approximation' [4]) for the baryons their pion couplings can be derived in the above manner.

3. Scalar and Vector Pion Couplings

It seems natural that the use of 1 instead of γ_5 in the above transformation (2) will lead to the scalar and vector couplings. Proceeding as above we require invariance of L_0 under

$$\psi \to \psi+ig'\boldsymbol{\tau}\cdot\boldsymbol{\alpha}\psi \tag{8}$$

and introduce the field $\boldsymbol{\phi} \to \boldsymbol{\phi}+\boldsymbol{\alpha}$. Since $L_0^{(2)}$ is invariant under (8), it is possible to introduce the vector coupling

$$L_3 = -ig'\bar{\psi}\gamma_\mu\boldsymbol{\tau}\cdot\partial_\mu\boldsymbol{\phi}\psi.$$

Invariance of L_0+L_3 is obtained under the restriction (5b) above. For the invariance of L_π one has to make the additional restrictions (5a) and (7).

To obtain parity conservation one has to assume that the boson field $\boldsymbol{\phi}$ thus introduced has even parity.

It may be remarked that under the gauge restriction $\partial_\mu\boldsymbol{\alpha} = 0$, i.e. $\boldsymbol{\alpha}$ a constant in space-time, $L_0^{(1)}$ becomes invariant under both (2) and (8). Then, in the case of the transformation (2) it is only possible to introduce the pseudoscalar coupling under the restriction (5a); L_π is then also invariant. Under (8), since L_0 is invariant, according to our point of view the introduction of a $\boldsymbol{\phi}$ field and its interaction with ψ would be artificial.

4. Conclusion

We have seen that the insistence on the isobaric gauge invariance of the free Lagrangian of a fermion isobaric doublet leads to the introduction of a spin

† Invariance of $(\Box^2-\mu^2)\boldsymbol{\phi} = 0$ under (3) gives $c = \mu^2$.

zero isobaric vector field. The parity of this boson field is undetermined. Further it is only possible to introduce the ps, pv and vector pion couplings. The gauge is restricted by the conditions (5) in isobaric space and (7) in space-time.

Under the restriction that the rotation α at each space time point be the same and satisfy (5a) it is only possible to introduce the ps coupling.

The removal of the restrictions would necessitate the introduction of further (possibly non-linear) interaction terms. Our attempts to generate K-meson interactions by similar methods have been, so far, unsuccessful.

I am grateful to Dr. B. Banerjee, Dr. S. N. Biswas and Mr. B. M. Udgaonkar for comments.

References

1) C. N. Yang and R. L. Mills, Phys. Rev. **96** (1954) 191
2) A. Salam, Lecture at the 47th Indian Science Congress, Bombay, 1960
3) H. A. Bethe, F. de Hoffmann and S. S. Schweber, Mesons and Fields (1955) Vol. II, p. 411
4) M. Gell-Mann, Phys. Rev. **106** (1957) 1296

8.C

Nuclear Physics **18** (1960) 153—160; © *North-Holland Publishing Co., Amsterdam*

Not to be reproduced by photoprint or microfilm without written permission from the publisher

A POSSIBLE MODEL FOR THE FOUR-FERMION COUPLING

E. VAN DER SPUY

Universitetets Institut for Teoretisk Fysik, Copenhagen †

Received 17 February 1960

Abstract: Starting from a possible modification of the photon-propagator in electrodynamics, below a fundamental length, a generalization of the cohesive vector meson field thus introduced gives a possible model for the four-fermion coupling effective in, for example, β decay. The model is based on a charged intermediate vector meson field of the same coupling constant as for electrodynamics. The fundamental implications of a cohesive field demand a partition of Hilbert space as proposed by Heisenberg. Some implications of the model relative to the universality of the coupling and the mass of the cohesive meson are briefly indicated.

1. Introduction

The purpose of the present discussion is to indicate a possible basis for the weak four-fermion coupling involved in β decay, and the like. The suggestion arose in the course of research on a consistent modification of field propagators below a fundamental length, or at very high momenta. In view of the fundamental problems associated with the model to be suggested, and which the present author aims to discuss in more detail in due course, it seems appropriate nevertheless to sketch some of the associated detail and hence to start with the problem of the self-energy in electrodynamics. Of course, one may be inclined to hold the view that the calculation of the complete self-energy is meaningless in sofar as it may not be an experimentally separable quantity. Such a view would however be tenable only in a closed and limited system in which only one mass occurs. For any theory covering a whole complex of known particles this view is at least undesirable insofar as some small mass differences are only too naturally described in terms of electromagnetic self-energy differences, for example.

If one hence assumes self-energy to be calculable, it is useful to consider the electromagnetic self-energy of the electron. It is well-known that in the usual field theory the first order perturbation calculation diverges logarithmically. One may, of course, suggest that perturbation theory is just inappropriate. As the fine structure constant $\alpha = e^2/4\pi\hbar c$ is so small, this is only useful if one countenances the complete electromagnetic self-energy not to be a regular function of α round the point $\alpha = 0$. As this is such a pessimistic basis to start from, it will be assumed not to be the case. Then one feels, if one starts with the

† On leave of absence from Physics Department, University, Stellenbosch.

skeleton self-energy diagram in electrodynamics and uses fully dressed propagators that, since in normal field theory [1]) these propagators are at least as divergent as the free field propagators, the full self-energy would (only with completely fortuitous exceptions) very likely be divergent. Any calculation of self-energy is thus driven to invoke modifications or cut-offs of the propagators at high momenta. These are essentially of two kinds: those that do not preserve the usual feature of microcausality, (such as most assumptions of a non-local interaction), or those that employ a cut-off preserving microcausality. Although the finiteness of all practical wave packets may make deviations from microcausality impossible to pin down unequivocally in practice, if confined to small enough domains, it shall be assumed as a basis of discussion that microcausality should be preserved.

One has then to employ a causal cut-off. Physically this means adding negative contributions to the propagators at high momenta, with the cut-off mass(es) defined as by Feynman, in a causal way. This, however, necessarily implies [1, 2]) in the more usual conception of Hilbert space that there are contributions from negative norm states at high momenta. This would violate conservation of probability, unless one imagines with Heisenberg [2]) the partition of the total Hilbert space in the case of indefinite metric, into Hilbert space I which contains all physical states, with positive norm, and for which the probability is rigidly conserved and the S matrix unitary, and Hilbert space II, containing the so-called ghost states which do not play a direct physical role and are hence never observed as such. The S matrix is considered to show no coupling of the states of Hilbert space II with those of Hilbert space I insofar as the theory is translation invariant [2]). Hilbert space II can, however, locally play a role in, for example, the modification of a propagator and as such would indirectly affect the magnitude of observables. The ghost states have their effect in localized regions in the description of virtual or intermediate states.

2. Modified Photon Propagator

To make this more specific, consider the calculation of the first order electron self-energy contribution. Since α is small, this contribution is likely to be the most important, in terms of the above premises. Since integration is over virtual photon momenta, one has to consider a causal cut-off of the photon propagator in view of the above discussion. There are many ways of doing this and the present author is now considering ways of narrowing down the possibilities in a self-consistent and useful manner.

It seems useful to consider modifying the photon propagator from $1/k^2$ to

$$D(k^2) = \frac{1}{k^2+\rho^2 k^4}$$

which appears to endow virtual photons with a mass proportional to k^4. Since

$$D(k^2) = \frac{1}{k^2+\rho^2 k^4} = \frac{1}{k^2} - \frac{\rho^2}{1+\rho^2 k^2} = \frac{1}{k^2} - \frac{1}{\mu^2+k^2} \tag{1}$$

with $\mu = 1/\rho$, this modification is just equivalent to the Feynman cut-off with regulator of mass μ. The latter is made a causal cut-off by using μ with a small negative imaginary part, as done by Feynman. The μ-field is then a neutral vector meson field, which may be viewed as a cohesive field in the well-known way. Owing to the minus sign in the last mentioned expression for $D(k^2)$, the μ-field must belong to Hilbert space II and as such a particle of mass μ will not be observed on this view, even if μ is finite.

Now, it is well-known that the electron self-energy, with $D(k^2)$ for the propagator and the electron propagator and vertex parts unmodified, is finite and to the first order chiefly proportional to $\log \mu/m_e$. If μ is finite, one can calculate the electron self-energy, and in this sense $D(k^2)$ is a possible modified propagator. One realizes that the modification, even if essentially the appropriate one, probably merely expresses in an equivalent way and in terms of perhaps inappropriate but more familiar concepts, that modification in quantum electrodynamics which is anticipated to occur below the fundamental length (here proportional to ρ). As such the modification may for instance be the expression of a complete solution of a closed system of quantum electrodynamics which has not yet been found, or it may be the equivalent expression for describing the essentially open system of electrons, photons, etc., in terms of electron and photon fields alone.

In neither case is μ likely to be very much larger than the light meson masses. In this case the electromagnetic self-energy of the electron is only a few percent of its rest mass. The rest of the mass would then have to be explained in some other way. With the above propagator, the full mass can only come from electromagnetic self-energy when unphysically large photon momenta (and μ) are involved in the integration (momenta $\approx e^{137} m_e c$). A cut-off of the photon propagator and a related cut-off of the electron propagator and the vertex part at a wavelength roughly of the order of $\alpha\hbar/m_e c \approx e^2/m_e c^2$ or of the order of the Compton wavelengths of the light mesons, seems to be suggested by a possible consistent model. This statement is however tentative and is the subject of further research.

In the spirit of the above discussion a vector meson of mass μ is not observable, but the modification of the propagator is. If μ is of the order of the light meson masses, electron-electron scattering at centre of mass energies of 100 MeV (bombarding stationary electrons with accelerated electrons in the GeV range) will be much affected. Such modifications in the photon propagator will hence be amenable to experiment in the near future. Due to the complexity of what one is investigating, it seems rather important to take a case which has a chance

of being as pure as possible, for example the electron-electron scattering, rather than aiming at an experiment which may be easier but may relate to a really different phenomenon (such as electron-muon, muon-muon scattering, etc.) which is very likely to be more complicated.

3. Charged Cohesive Meson Field

After this investigation of the nature of one possible modification of the photon propagator, we take eq. (1) as a basis of discussion (as a law of nature, say) and we consider now some of the further consequences. The modification may mean that the wave-equation for the total vector potential A_μ^{t} should now read

$$(\Box+\rho^2\Box^2)A_\mu^{\mathrm{t}}(x) = e(\overline{\Psi}\gamma_\mu\Psi)$$

in the presence of the electron spinor field $\Psi(x)$ only. It is clear that the retarded Green's function for the operator $\Box+\rho^2\Box^2$ is $D_R^0-D_R^\mu$ with the usual definition of D_R^0, D_R^μ. Hence the latter equation solves as

$$A_\mu^{\mathrm{t}}(x) = A_{\mu\,\mathrm{in}}^{\mathrm{t}}+e\int(D_R^0-D_R^\mu)(\overline{\Psi}\gamma_\mu\Psi)\mathrm{d}^4x_1.$$

This solution is, however, equivalent to the sum of the solutions of two separate equations

$$\Box A_\mu = e(\overline{\Psi}\gamma_\mu\Psi), \qquad (\Box+\mu^2)\Phi_\mu = -e(\overline{\Psi}\gamma_\mu\Psi), \tag{2}$$

such that $A_\mu^{\mathrm{t}} = A_\mu+\Phi_\mu$. The operator Φ_μ represents the neutral cohesive vector meson field which leads to a finite self-energy, and in the spirit of the present discussion always occurs with the electromagnetic field and in the presence of matter, as a properly virtual field. The separation (2) is thus a formal device for the generalization to a more general cohesive field, now to be effected.

Consider thus that matter generates in addition a charged cohesive vector meson field Φ_μ^{c}, with the same coupling constant e and mass μ. Hence generalize in a natural way

$$(\Box+\mu^2)\Phi_\mu^{\mathrm{c}} = -e\sum_{a,\,b}(\overline{\Psi}_a\gamma_\mu\alpha\Psi_b), \tag{3}$$

where the mixed spinor matter current is taken to be empirically determined. For simplicity, one should hence expect the mixed current

$$J_\mu = \sum_{a,\,b}(\overline{\Psi}_a\gamma_\mu\alpha\Psi_b) = (\bar{\nu}\gamma_\mu\alpha\mu^+)+(\bar{\nu}\gamma_\mu\alpha e^+)+(\bar{n}\gamma_\mu\alpha p)+\ldots,$$

stating only the elements corresponding to the well-known vertices of the Puppi-triangle explicitly. No attempt will be made to specify the remaining current elements, except to say that it may have to be a complete current to give the type of current conservation discussed below, and elsewhere[3]). The

operator Φ_μ^c clearly represents a charged field and if the operator α corresponds to a V—A four-fermion interaction, Φ_μ^c will be of mixed parity. In view of the nature of the cohesive field, and of the fact that eq. (3) can, sofar at least, be easily split in two equations, each for a part of definite parity, this presents no problem.

Since Φ_μ^c is a completely virtual cohesive field, it will be assumed that the correct solution of eq. (3) is

$$\Phi_\mu^c = -e\int D_R^\mu \sum_{a,b} (\overline{\Psi}_a \gamma_\mu \alpha \Psi_b) \mathrm{d}^4 x_1. \tag{4}$$

If one now calculates the energy in the cohesive field Φ_μ^c by the usual vector meson theory, one obtains a possible model for the four-fermion coupling. To get a rough indication of the order of μ and e which would give the correct magnitude of this coupling, consider those sets of four-fermions for which the static approximation to the field energy is close enough. Thus the corresponding part of the interaction energy density residing in the cohesive field is

$$\tfrac{1}{2}\mu^2 \Phi_\mu^{c*} \Phi_\mu^c = \tfrac{1}{2}\mu^2 e^2 \sum_{a,b,c,d} \left\{\int D_R^\mu (\overline{\Psi}_a \gamma_\mu \alpha \Psi_b) \mathrm{d}^4 x_1\right\} \left\{\int D_R^\mu (\overline{\Psi}_c \gamma_\mu \alpha \Psi_d) \mathrm{d}^4 x_2\right\}.$$

A typical four-fermion coupling energy in the static approximation is

$$\mathscr{E}_{\mathrm{NL}} = \tfrac{1}{2}\mu^2 e^2 \left\{\int D_R^\mu (\overline{\Psi}_a \gamma_\mu \alpha \Psi_b) \mathrm{d}^4 x_1\right\} \left\{\int D_R^\mu (\overline{\Psi}_c \gamma_\mu \alpha \Psi_d) \mathrm{d}^4 x_2\right\}. \tag{5}$$

The coupling is non-local as to any accuracy it is for all intermediate boson models of the four-fermion coupling. Since, for the usual applications of this coupling, the spinor fields may be considered as changing only relatively slowly over the domain of interest, phase effects may be neglected in eq. (5) in the first approximation, and thus the only remaining effect is the Yukawa range factor corresponding to the meson in question. Thus if μ^{-1} is very much smaller than the domain of interest, or the mass μ rather large, one would find, as in the discussion of Feynman and Gell-Mann [3]), that the coupling will be practically equivalent to the local form

$$\mathscr{E}_L = C(\overline{\Psi}_a \gamma_\mu \alpha \Psi_b)(\overline{\Psi}_c \gamma_\mu \alpha \Psi_d). \tag{6}$$

If μ turns out to be of the order of the light meson masses, with a Yukawa decay length of the order of nuclear sizes, the non-locality is expected to give rise to a finite though small difference between eqs. (5) and (6), at least to the first order. In this situation the difference may be expressed in terms of a multiplying form factor F, of the order of unity, such that $\mathscr{E}_{\mathrm{NL}} = F\mathscr{E}_{\mathrm{L}}$ in effect. The form factor F is likely to be different for the different sets of four-fermions involved, by a limited percentage in this case.

To get the order of $\mathscr{E}_{NL}$, take the case μ not larger than the nucleon masses. Thus

$$\mathscr{E}_{NL} = \tfrac{1}{2}\mu^2 e^2 \int \frac{1}{4\pi r_{xx_1}} (\overline{\Psi}_a \gamma_\mu \alpha \Psi_b) \mathrm{d}^3 x_1 \int \frac{1}{4\pi r_{xx_2}} (\overline{\Psi}_c \gamma_\mu \alpha \Psi_d) \mathrm{d}^3 x_2$$

$$= \frac{\mu^2 e^2}{32\pi^2} \frac{\langle (\overline{\Psi}_a \gamma_\mu \alpha \Psi_b) \rangle \langle (\overline{\Psi}_c \gamma_\mu \alpha \Psi_d) \rangle V^2}{\langle r_{ab} \rangle \qquad \langle r_{cd} \rangle}$$

where V is an appropriate normalization volume of the order of nuclear sizes and $\langle\ \rangle$ refers to an appropriate average value over V. To derive the magnitudes of μ and e one may identify

$$\frac{\mu^2 e^2}{32\pi^2} \frac{V^2}{\langle r_{ab} \rangle \langle r_{cd} \rangle} = FC$$

with what is called in the literature [4])

$$C_V = 1.6 \times 10^{-7} \frac{1}{\mu_\pi{}^2},$$

where the π meson mass μ_π is used for normalization. There are, however, two arbitrary aspects of the otherwise natural generalization of the cohesive field that one must now countenance: firstly, will one generalize at the level of the renormalized quantities or the unrenormalized quantites and, secondly, how will one normalize the operator α? There is something to be said for generalizing with α either $(1+\gamma_5)$ or $\frac{1}{2}(1+\gamma_5)$. For definiteness the former was used in the above identification of FC. To get an idea of the magnitudes involved take μ of the order of a light meson mass, as was suggested on intuitive lines in section 2. Then V, $\langle r_{ab} \rangle$, $\langle r_{cd} \rangle$, $1/\mu$ and $/1\mu_\pi$ are all of the order of nuclear sizes, or

$$\frac{\mu^2 \mu_\pi{}^2 V^2}{\langle r_{ab} \rangle \langle r_{cd} \rangle} \approx 1.$$

Hence the fine structure constant of the cohesive boson field is

$$\alpha = \frac{e^2}{4\pi} = 8\pi \times 1.6 \times 10^{-7} = 4.0 \times 10^{-6}.$$

Since this is very much smaller than the observed electromagnetic coupling constant, all aspects of the proposed model for the four-fermion coupling can only be maintained if one supposes either a very much higher cut-off mass μ ($e^2/4\pi = 1/137$ implies [3]) $\mu \approx 80$ times the nucleon mass), or that the level at which one should generalize implies e and /or FC to be unrenormalized coupling constants. In the latter case large renormalization effects may well leave the case of $\mu <$ the nucleon mass as a possibility. No further discussion of these

points seems warranted at this stage, except to indicate one other effect of a low value of μ, say of the order of the light meson masses.

The experiments so far seem to indicate that all four-fermion couplings share a universal coupling constant, except for small deviations in the axial vector part. The fact that the strong couplings which some of the fermions partake of (in addition to the weak coupling) do not seem to make any difference in the relevant effective (renormalized) four-fermion coupling constant, was explained [3]), for the vector part at least, as probably related to microscopic conservation of the vector part of the source current J_μ above. For the vector part [3]) the elaboration of J_μ by a pion current contribution is demanded to ensure this charge conservation.

The importance of charge conservation is suggested by electrodynamics where the fact that all particles have the same charge at low energies (one then observes the total charge and not the charge distribution) appears to be intimately connected with microscopic charge conservation. It is now suggested that the axial vector part of the current J_μ may perhaps also be rigidly conserved, although no attempt will be made here to discuss what extra terms this may demand and what restrictions on the spinor fields this may imply. It is suggested that the local conservation of charge is really demanded for an intermediate vector meson model of the coupling, when for $\mu = 0$ one can insist on $\partial \Phi_\mu{}^c / \partial x_\mu = 0$ everywhere. By eq. (3) this means $\partial J_\mu / \partial x_\mu = 0$. The former equation would then be associated with the elimination of the zero spin component of the $\Phi_\mu{}^c$ field, which component has non-positive-definite energy. Now, if μ had been a very heavy meson and the ensuing couplings were hence effectively local as in (6), the conservation of the complete current on the above argument would mean a completely universal four-fermion coupling constant. That this appears not to be the case experimentally may possibly be partly due to the fact that the intermediate boson is not very heavy and that the consequent four-fermion coupling is hence really non-local as in (5). The usual experimental analysis, in terms of the local form (6), thus involves a form factor F which may be of the order of unity and may effect some discrimination between various processes. The inaccuracy of the static approximation to the energy of the charged cohesive field may effect a further discrimination.

The present discussion indicates how a cohesive field with the electrodynamic coupling constant provides a model for the four-fermion coupling. Since the latter is associated with particle instabilities, a model in terms of a cohesive field has some natural appeal. It may also be that the association of the appropriate cohesive field with the four-fermion coupling is valid even if the cohesive field is not of the simple type arising out of eq. (1), or even if the coupling constant for the charged cohesive field is not the same as that for electrodynamics.

The author would like to thank Prof. N. Bohr for the hospitality of the Theoretical Institute at Copenhagen, and Prof. L. Rosenfeld for many discussions during the course of the present research. The author is also indebted to the South African Council for Scientific and Industrial Research for a bursary and the Ernest Oppenheimer Memorial Trust for a grant in aid of the research.

References

1) H. Lehmann, Nuov. Cim. **11** (1954) 342
2) W. Heisenberg, Zeit. f. Naturf. **9a** (1954) 292;
W. Heisenberg, F. Kortel and H. Mitter, Zeit. f. Naturf. **10a** (1955) 425;
W. Heisenberg, Zeit. f. Phys. **144** (1956) 1;
W. Heisenberg, Rev. Mod. Phys. **29** (1957) 269;
W. Heisenberg, Nuclear Physics **4** (1957) 532;
H. P. Dürr, W. Heisenberg, H. Mitter, S. Schlieder and K. Yamazaki, Zeit. f. Naturf. **14a** (1959) 441
3) R. P. Feynman and M. Gell-Mann, Phys. Rev. **109** (1958) 193
4) M. Gell-Mann and A. H. Rosenfeld, Ann Rev. of Nucl. Science **7** (1957) 407

1.C:
1.D.4

Nuclear Physics 18 (1960) 161—172; © *North-Holland Publishing Co., Amsterdam*
Not to be reproduced by photoprint or microfilm without written permission from the publisher

EFFECT OF QUADRUPLE CORRELATIONS IN LIGHT NUCLEI

V. G. SOLOVIEV

Joint Institute of Nuclear Research, Dubna, USSR

Received 25 December 1959

Abstract: Quadruple correlations of nucleons having equal energies are considered on the basis of the effective Hamiltonian describing the interaction of nucleon pairs. It is shown that the formation of quadruple correlations in light nuclei is energetically favoured if the interaction among pairs is attractive. Certain laws in the binding energy of the last neutron in light nuclei are explained by taking into account pair and quadruple correlations. A criterion obtained shows at what excess of the number of neutrons over that of protons in stable nuclei, as a result of the parting of the Fermi surfaces, some outer neutrons cease to participate in quadruple correlations, which leads to the disappearance of explicit α-particle properties of nuclei.

1. Introduction

As is well known, pair correlations of nucleons in heavy nuclei are observed in both proton and neutron shells. Treatment of pair correlations by mathematical methods evolved in the theory of superconductivity [1]) resulted in an explanation of several properties of heavy nuclei. If, however, in heavy nuclei there are no proton-neutron pair correlations because of a large difference in the energies of Fermi surfaces for neutron and proton shells, in light nuclei there may be proton-neutron correlations so long as the Fermi surfaces for neutrons and protons do not part from each other. Therefore, in ref. [2]) n—p interactions were taken into account along with n—n and p—p interactions in investigating the problem of pair correlations in light nuclei. In ref. [2]) it is shown that the consideration of remaining interactions leads to the formation of a superfluid state of a light nucleus (energetically a more favourable state than that of a fully degenerate Fermi-gas in the central field), the energy of the ground state being independent of the way nucleons are paired: protons with protons, neutrons with neutrons or protons with neutrons. The consideration of pair correlations in light nuclei made it possible to understand, for example, certain regularities in binding energies. Yet a number of important properties of light nuclei cannot be explained on the basis of nucleon pair correlations alone.

In light nuclei quadruple correlations of the α-particle type between nucleons are quite pronounced, yet the α-particle properties of these nuclei disappear if the number of neutrons is in excess of that of protons in stable nuclei. A study of quadruple correlations on the basis of the α-particle model of the nuclei has made it possible to explain a number of important properties of light nuclei.

The α-particle model is nevertheless rather crude and the sphere of its application limited. It is of interest therefore to inquire into the possibility of the formation of quadruple correlations of nucleons after the pattern of pair correlations in heavy nuclei within the framework of the shell model of the nucleus, to study the properties of light nuclei having quadruple correlations of this type, and obtain a criterion for the disappearance of these correlations. These are the problems that the present paper is concerned with.

2. Effective Hamiltonian of Interaction

A study of the possibility of nucleon quadruple correlations in light nuclei will be based on the nuclear shell model with allowances for residual interactions of nucleons over the self-consistent field. The nucleon state in a nucleus will be described by a set of quantum numbers σs where $\sigma = \pm 1$ characterises the sign of the projection of the total angular momentum of the nucleon on the axis of symmetry of the nucleus.

The nucleons which are in an S-state with respect to each other in the nucleus strongly interact among themselves. It is a part of the nucleon interactions precisely of this type that leads to the formation of both pair and quadruple correlations of nucleons. The Hamiltonian of interaction therefore will be taken in the form accounting merely for the interactions of nucleons with the same quantum numbers s.

Let us assume that the quadruple correlations of nucleons arise as a result of interaction of pairs. In this case the principal contribution to the effective Hamiltonian of interaction of pairs is made by resonance interactions of nucleons with equal energies. It should be noted that our assumption on the possibility of investigating quadruple correlations by taking into account interaction of pairs is sufficiently well justified if the intrinsic binding energy of the pairs is much greater than the binding energy between them. Though this condition is not fulfilled, strictly speaking, we hold that the main properties of quadruple correlations in light nuclei may be obtained by investigating the effective Hamiltonian describing a pair interaction. The use of the effective Hamiltonian of pair interaction is unavoidable since in investigating the Hamiltonian of nucleon interaction there arise considerable difficulties.

In the case of strict isobaric invariance pairs may be constructed by various methods: either the pair is formed by a neutron and a proton in the state (σs), or it is formed by two protons (neutrons) in the states $(+s)$ and $(-s)$. Since in the following we shall consider the case when strict isobaric invariance is violated, we shall regard $b_{s\rho}$ as the operator of a pair of similar nucleons in the states $(+s)$, $(-s)$, $\rho = \pm 1$, where $\rho = +1$ corresponds to the proton pair and $\rho = -1$ to the neutron pair. The operators $b^{\dagger}_{s\rho}$, $b_{s\rho}$ are governed by te following commutation relations:

$$b^{\dagger}_{s\rho}b_{s\rho}+b_{s\rho}b^{\dagger}_{s\rho}=1, \qquad b_{s\rho}b_{s\rho}=0;$$
$$b^{\dagger}_{s\rho}b_{s'\rho'}-b_{s'\rho'}b^{\dagger}_{s\rho}=0, \quad b_{s\rho}b_{s'\rho'}-b_{s'\rho'}b_{s\rho}=0, \tag{1}$$

if $s \neq s'$ or $\rho \neq \rho'$.

The model Hamiltonian describing interactions among pairs in the case of strict isobaric invariance may be written as

$$H=\sum_{s}\{E(s)-\lambda\}\{b^{\dagger}_{s+}b_{s+}+b^{\dagger}_{s-}b_{s-}\}+\sum_{\substack{s,s'\\ s\neq s'}}J(s,s')b^{\dagger}_{s+}b^{\dagger}_{s-}b_{s'-}b_{s'+}, \tag{2}$$

where $E(s)$ is the energy of the pair in the state s, and λ is the parameter acting as a chemical potential.

Using the device suggested in ref. [3]) we introduce the auxiliary Hamiltonian

$$H'=\sum_{s}\{E(s)-\lambda\}\{b^{\dagger}_{s+}b_{s+}+b^{\dagger}_{s-}b_{s-}\}$$
$$+\sum_{\substack{s,s'\\ s\neq s'}}J(s,s')\{B^{*}(s)b_{s'-}b_{s'+}+B(s')b^{\dagger}_{s+}b^{\dagger}_{s-}-B^{*}(s)B(s')\}. \tag{3}$$

The functions $B(s)$ will be determined from the condition of minimum $\langle H'\rangle$, so that the average value $\langle H\rangle$ of the operator H in the eigenstates of the operator H' may coincide with $\langle H'\rangle$, as a result of which we obtain

$$B(s')=\langle b_{s'-}b_{s'+}\rangle. \tag{4}$$

On transforming

$$b_{s+}=\{1-2a^{\dagger}_{s-}a_{s-}\}a_{s+}, \quad b_{s-}=a_{s-}, \tag{5}$$

we note that in the states with similar s the operators $a^{\dagger}_{s\rho}$, $a_{s\rho'}$ behave as Fermi-amplitudes. The auxiliary Hamiltonian can be written in the form

$$H'=\sum_{s}\{E(s)-\lambda\}\{a^{\dagger}_{s+}a_{s+}+a^{\dagger}_{s-}a_{s-}\}$$
$$-\sum_{\substack{s,s'\\ s\neq s'}}J(s,s')\{B^{*}(s)a_{s'-}a_{s'+}+B(s')a^{\dagger}_{s+}a^{\dagger}_{s-}+B^{*}(s)B(s')\}. \tag{6}$$

3. Ground State

A study of the possibility of quadruple correlations will be conducted with the aid of the variation principle suggested by N. N. Bogolyubov [4]), using the auxiliary H' in the form of eq. (6). Let us carry out a transformation

$$a_{s+}=u_s[1-2v_s]\beta_{s+}+v_s\beta^{\dagger}_{s-}, \quad a_{s-}=u_s\beta_{s-}-v_s[1-2v_s]\beta^{\dagger}_{s+}, \tag{7}$$

where $v_s=\beta^{\dagger}_{s-}\beta_{s-}$ and $u_s^2+v_s^2=1$. The new operators of quasi-pairs $\beta^{\dagger}_{s\rho}$, $\beta_{s\rho}$ satisfy the commutation relations (1). Let us determine the new vacuum state $\beta_{s\rho}\Psi=0$ and find the average value of H' by this state

$$\langle H'\rangle=2\sum_{s}\{E(s)-\lambda\}v_s^2+\sum_{\substack{s,s'\\ s\neq s'}}J(s,s')u_sv_su_{s'}v_{s'}. \tag{8}$$

From the condition of minimum $\langle H' \rangle$ we obtain the equation

$$\{E(s)-\lambda\}u_s v_s+\tfrac{1}{2}(u_s^2-v_s^2)\sum_{s'} J(s, s')u_{s'}v_{s'} = 0, \tag{9}$$

having the same form as the equation of ref. [5]) which takes into account pair correlations. From eqs. (8) and (9) it is clear that the formation of quadruple correlations is energetically favoured under the condition that effective interaction among pairs is that of attraction. It will be noted that four nucleons which are in an S-state with respect to each other and form a quadruple are linked only through angular variables and are not connected in contrast to the α-particle model, through radial variables.

Both the asymptotic solution (9) when $J \to 0$ and the solution obtained when an integral is substituted for the sum and the J and density of states ρ in the outer shell are constant lead to the conclusion [6]) that the energy of the ground state in which all nucleons are quadrupled lies below the energy of the state in which all nucleons are paired. The first excited state connected with the disruption of a quadruple is separated from the ground state by an energy gap, viz.

$$\langle \beta_{s_0+}\beta_{s_0-}H'\beta^{\dagger}_{s_0-}\beta^{\dagger}_{s_0+}\rangle-\langle H'\rangle = 2\varepsilon(s_0), \tag{10}$$

where

$$\varepsilon(s) = \sqrt{C_s^2+\{E(s)-\lambda\}^2}, \quad C_s = \sum_{s'} J(s, s')u_s v_s.$$

It will be noted that eq. (9) may be obtained not only by the variation principle indicated above but also by the method of splitting correlations suggested by N. N. Bogolyubov [7]) on the basis of the Hamiltonian H.

4. Binding Energy of the Last Neutron in Light Nuclei

Let us consider the influence of pair and quadruple correlations of nucleons on the magnitude of the binding energy of the last neutron in light nuclei. This magnitude is no doubt more sensitive to correlations of nucleons than the average binding energy per nucleon.

The energy of the ground state in which all nucleons are quadrupled is determined by $\langle H' \rangle$, and the energy of the ground state in which there is one pair apart from quadruples has the form $\langle \beta_{s+} H' \beta^{\dagger}_{s+} \rangle$. To find the binding energy of the pair in the nucleus the following difference should be calculated:

$$\langle \beta_{s+} H' \beta^{\dagger}_{s+} \rangle_{N=2n_0\pm1} - \langle H' \rangle_{N=2n_0}.$$

In very rough approximation, considered earlier in ref. [7]), where integration is replaced by summation, and J as well as the density of states ρ are regarded as constant all over the shell, we obtain

$$\langle\beta_{s+}H'\beta^{\dagger}_{s+}\rangle_{N=2n_0+1}-\langle H'\rangle_{N=2n_0}=-\frac{\Omega-2n_0}{2\rho}-\frac{e^{\frac{2}{G}}+1}{e^{\frac{2}{G}}-1}\frac{2n_0-\Omega+1}{2\rho},$$
$$\langle\beta_{s+}H'\beta^{\dagger}_{s+}\rangle_{N=2n_0-1}-\langle H'\rangle_{N=2n_0}=-\frac{\Omega+2-2n_0}{2\rho}+\frac{e^{\frac{2}{G}}+1}{e^{\frac{2}{G}}-1}\frac{2n_0+\Omega-1}{2\rho}, \tag{11}$$

where $G=-\rho J$, Ω is the number of levels and N the number of pairs. Formulae taking into account pair correlations of nucleons have a similar form, viz.

$$\langle\alpha_{+s}H_0\alpha^{\dagger}_{+s}\rangle_{\nu=2\nu_0+1}-\langle H_0\rangle_{\nu=2\nu_0}=-\frac{\Omega+\frac{3}{2}-\nu_0}{2\rho}-\frac{e^{\frac{2}{G}}+1}{e^{\frac{2}{G}}-1}\frac{\nu_0+\frac{5}{4}-2\Omega}{4\rho},$$
$$\langle\alpha_{+s}H_0\alpha^{\dagger}_{+s}\rangle_{\nu=2\nu_0-1}-\langle H_0\rangle_{\nu=2\nu_0}=-\frac{\Omega+\frac{3}{2}-\nu_0}{2\rho}+\frac{e^{\frac{2}{G}}+1}{e^{\frac{2}{G}}-1}\frac{\nu_0-\frac{5}{4}+2\Omega}{4\rho}. \tag{12}$$

From (11) it is clear that the addition of one pair to the system where all nucleons are quadrupled changes the energy very little, while the removal of a pair from the state in which all nucleons are quadrupled, i.e. the disruption of a quadruple, requires a considerable amount of energy. Similarly, the addition of one nucleon to the system consisting of an even number of nucleons $\nu=2\nu_0$ does not lead to any essential change of energy, while the removal of one nucleon from the nucleus where there is one pair apart from quadruple correlations requires a considerable amount of energy for the disruption of the pair.

The consideration of pair and quadruple correlations illustrated in (11) and (12) makes it possible to divide all light nuclei in the region $16<A<40$ into three well-defined groups as regards the binding energy of the last neutron: 1) the last neutron does not take part either in pair or in quadruple correlations, 2) apart from the quadrupled nucleons there is one pair, which may be either (n--n) or (n—p), and 3) all neutrons are quadrupled. The binding energy of the last neutron in the nucleus classed under the first heading is determined only by its binding with the central field. The binding energy of the last neutron in the second group of nuclei is determined, roughly, by both the magnitude of the pair binding and the binding energy between the neutron and the central field. The third group comprises the α-particle type nuclei and the binding energy of the last neutron in them consists of three parts: the energy required for the disruption of the quadruple into two pairs, the binding energy of the pair and finally the binding energy between the neutron and the central field.

If we turn to the data of ref. [8]) on the binding energy of the last neutron in light nuclei, we shall see that in the nuclei referred to the first group, such as

$$_{12}Mg^{25}_{13},\quad _{12}Mg^{27}_{15},\quad _{14}Si^{29}_{15},\quad _{14}Si^{31}_{17},\quad _{16}S^{33}_{17},\quad _{16}S^{35}_{19},\quad _{18}Ar^{41}_{23},\quad _{19}K^{42}_{23},\quad _{20}Ca^{43}_{23},$$

the binding energy of the last neutron is of the order of 7 to 8 MeV. In the nuclei referred to the second group,

$$_{10}Ne^{22}_{12},\ _{11}Na^{23}_{12},\ _{12}Mg^{26}_{14},\ _{13}Al^{27}_{14},\ _{14}Si^{30}_{16},\ _{15}P^{31}_{16},\ _{16}S^{34}_{18},\ _{17}Cl^{35}_{18},\ _{18}Ar^{38}_{20},\ _{19}K^{39}_{20},$$

two outer neutrons are paired and additional energy [2]) is necessary to disrupt the pair, which is borne out by the magnitude of the binding energy of the last neutron, equal to 11 to 12 MeV. Because of the pair correlation of the outer neutron and outer proton which are in states with equal energy in the nuclei

$$_{11}Na^{22}_{11},\ _{13}Al^{26}_{13},\ _{15}P^{30}_{15},\ _{17}Cl^{34}_{17},\ _{19}K^{38}_{19},$$

the magnitude of the binding energy of the last neutron is also in the range of 11 to 12 MeV. It should be noted that if the outer proton and neutron are in different quantum states there is no correlation between them and the binding energy of the last neutron in such nuclei as

$$_{11}Na^{24}_{13},\ _{13}Al^{28}_{15},\ _{15}P^{32}_{17},\ _{17}Cl^{36}_{19},\ _{19}K^{40}_{21}$$

is in the range of 7 to 8 MeV.

In the α-particle type nuclei such as

$$_{10}Ne^{20}_{10},\ _{12}Mg^{24}_{12},\ _{14}Si^{28}_{14},\ _{16}S^{32}_{16},\ _{18}Ar^{36}_{18},\ _{20}Ca^{40}_{20},$$

all nucleons with equal quantum numbers s are quadrupled and the binding energy of the last neutron in these nuclei is in the range of 15 to 17 MeV. The difference in the binding energies of the last neutron in the nuclei included into the third and second groups roughly determines the energy necessary to disrupt a quadruple into two pairs. This makes it possible, by using eq. (11), to give a very rough estimate of the value of $-J$, which is of the order of 1 MeV. The energy gap linked with the disruption of the quadruple into pairs will be found equal to 4 to 6 MeV.

The above mentioned data confirm the presence of pair and quadruple correlations of nucleons in states with the same quantum numbers s in light nuclei. It should be noted that evidently there are no strong correlations of nucleons having different projections of the angular momentum on the axis of the symmetry of the nucleus but the same values for the other quantum numbers. This is borne out by the behaviour of nucleons in heavy nuclei in which no regularities are apparent when the number of protons (neutrons) in the outer shell is a multiple of 4.

It should be mentioned that the statistical method we have adopted averages, to a certain extent, the properties of nuclei belonging to the same group as regards the binding energy of the last neutron. However, taking into account the quantum characteristics of outer nucleons makes it possible to determine the individuality of nuclei. It is possible, therefore, to calculate the binding energy of the last neutron for each specific nucleus within the framework of the above scheme with allowances for additional factors.

5. Condition of Disappearance of Quadruple Correlations

Let us consider the behaviour of quadruple correlations in the case when the number of neutrons is in excess of that of protons. It should be noticed that the value of effective interaction among pairs $J'(s, s')$ in this case should be much less than the value $J(s, s')$ in eq. (2) pertaining to the case of strict isobaric invariance. This is due to the fact that the main contribution to the effective interaction among pairs is made by the resonance interaction of nucleons with equal energies. If the number of neutrons exceeds that of protons this resonance will fade considerably, which will lead to a considerable weakening of the interaction between pairs.

The problem of the behaviour of quadruple correlations when the number of neutrons begins to exceed that of protons will be investigated by the method of the advanced and retarded Green functions worked out by N. N. Bogolyubov and S. V. Tyablikov [9]).

Here are some general formulae which will be used in our calculations. The Green functions at zero temperature and the equations they satisfy will be written in the following form:

$$\begin{aligned} G_r(t-t') &= \langle\langle A(t)B(t')\rangle\rangle_r = -i\theta(t-t')\langle[A(t), B(t')]\rangle, \\ G_a(t-t') &= \langle\langle A(t)B(t')\rangle\rangle_a = \quad i\theta(t'-t)\langle[A(t), B(t')]\rangle, \\ i\frac{d}{dt}\langle\langle A(t)B(t')\rangle\rangle &= \delta(t-t')\langle[A(t), B(t')]\rangle + \langle\langle\{A(t)H-HA(t)\}B(t')\rangle\rangle, \end{aligned} \tag{13}$$

where $A(t)$, $B(t)$ are the operators in Heisenberg's representation. Let us go over to the Fourier transform of the Green function

$$\langle\langle A(t)B(t')\rangle\rangle = \int_{-\infty}^{\infty} \langle\langle A|B\rangle\rangle_E e^{iE(t-t')}\,dE$$

and its spectral representation (in the case of the Fermi statistics)

$$\langle\langle A|B\rangle\rangle_E = \frac{1}{2\pi}\int_{-\infty}^{\infty} I(\omega)\frac{d\omega}{E-\omega},$$

where

$$iI(E) = \langle\langle A|B\rangle\rangle_{E-i\varepsilon} - \langle\langle A|B\rangle\rangle_{E+i\varepsilon}. \tag{14}$$

The spectral representation of the correlation functions through the function $I(E)$ is expressed by

$$\langle A(t)B(t')\rangle = \int_0^{\infty} I(\omega)e^{-i\omega(t-t')}\,d\omega, \tag{15}$$

$$\langle B(t')A(t)\rangle = \int_{-\infty}^{0} I(\omega)e^{-i\omega(t-t')}\,d\omega. \tag{15'}$$

The condition of disappearance of quadruple correlations will be found by using the above formulas with the auxiliary Hamiltonian of eq. (6) written in the form

$$H' = \sum_s \{\xi_p(s)\, a^\dagger_{s+} a_{s+} + \xi_n(s) a^\dagger_{s-} a_{s-}\} - \sum_{s,s'} J(s,s')\{B^*(s) a_{s'-} a_{s'+} + B(s') a^\dagger_{s+} a^\dagger_{s-} + B^*(s) B(s')\}, \quad (16)$$

where

$$\xi_p(s) = E(s) - \lambda_p, \quad \xi_n(s) = E(s) - \lambda_n, \quad \lambda_p \neq \lambda_n.$$

For the Green functions we obtain the following equations

$$i\frac{d}{dt}\langle\langle a_{s\rho}(t)|a^\dagger_{s\rho}(t')\rangle\rangle$$

$$= \delta(t-t') + \delta_{\rho,+1}\xi_p(s)\langle\langle a_{s+}(t)|a^\dagger_{s+}(t')\rangle\rangle + \delta_{\rho,-1}\xi_n(s)\langle\langle a_{s-}(t)|a^\dagger_{s-}(t')\rangle\rangle \quad (17)$$

$$-\delta_{\rho,1}\sum_{s'\neq s} J'(s,s')B(s')\langle\langle a^\dagger_{s-}(t)|a^\dagger_{s+}(t')\rangle\rangle + \delta_{\rho,-1}\sum_{s'\neq s} J'(s,s')B(s')\langle\langle a^\dagger_{s+}(t)|a^\dagger_{s-}(t')\rangle\rangle,$$

$$i\frac{d}{dt}\langle\langle a^\dagger_{s\rho}(t)|a^\dagger_{s,-\rho}(t')\rangle\rangle$$

$$= -\delta_{\rho,1}\xi_p(s)\langle\langle a^\dagger_{s+}(t)|a^\dagger_{s-}(t')\rangle\rangle - \delta_{\rho,-1}\xi_n(s)\langle\langle a^\dagger_{s-}(t)|a^\dagger_{s+}(t')\rangle\rangle$$

$$+\delta_{\rho,1}\sum_{s'\neq s} J'(s,s')B^*(s')\langle\langle a_{s-}(t)|a^\dagger_{s-}(t')\rangle\rangle \quad (17')$$

$$-\delta_{\rho,-1}\sum_{s'\neq s} J'(s,s')B^*(s')\langle\langle a_{s+}(t)|a^\dagger_{s+}(t')\rangle\rangle.$$

Let us go over to the Fourier-transforms in time and introduce a new function

$$C_s = \sum_{s'\neq s} J'(s,s')B(s'). \quad (18)$$

Carrying out transformations and using eq. (14) we obtain

$$\langle\langle a_{s+}|a^\dagger_{s+}\rangle\rangle_{E-i\varepsilon} - \langle\langle a_{s+}|a^\dagger_{s+}\rangle\rangle_{E+i\varepsilon} = iI_+(E)$$

$$= \frac{i}{2}\left\{\left[1-\frac{\omega(s)}{\varepsilon'(s)}\right]\delta(E+\gamma+\varepsilon'(s)) + \left[1+\frac{\omega(s)}{\varepsilon'(s)}\right]\delta(E-\gamma-\varepsilon'(s))\right\}, \quad (19)$$

$$\langle\langle a_{s-}|a^\dagger_{s-}\rangle\rangle_{E-i\varepsilon} - \langle\langle a_{s-}|a^\dagger_{s-}\rangle\rangle_{E+i\varepsilon} = iI_-(E)$$

$$= \frac{i}{2}\left\{\left[1-\frac{\omega(s)}{\varepsilon'(s)}\right]\delta(E-\gamma+\varepsilon'(s)) + \left[1+\frac{\omega(s)}{\varepsilon'(s)}\right]\delta(E-\gamma-\varepsilon'(s))\right\}, \quad (19')$$

$$\langle\langle a^\dagger_{s+}|a^\dagger_{s-}\rangle\rangle_{E-i\varepsilon} - \langle\langle a^\dagger_{s+}|a^\dagger_{s-}\rangle\rangle_{E+i\varepsilon} = iI(E)$$

$$= \frac{i}{2}\frac{C_s}{\varepsilon'_{(s)}}\{\delta(E-\gamma-\varepsilon'(s)) - \delta(E-\gamma+\varepsilon'(s))\}, \quad (20)$$

where

$$\varepsilon'(s) = \sqrt{C_s^2+\omega(s)^2},\ \gamma = \tfrac{1}{2}\{\xi_n(s)-\xi_p(s)\},\ \omega(s) = \tfrac{1}{2}\{\xi_n(s)+\xi_p(s)\}.$$

We use eqs. (15) and (15′) to obtain an expression for the wave function of a quadruple as well as for the density of neutron and proton pairs, viz.

$$\langle a_{s+}^\dagger(t)|a_{s-}^\dagger(t)\rangle = \int_0^\infty dE\, e^{-iE(t-t')} I(E)$$
$$= \tfrac{1}{2}\frac{C_s}{\varepsilon'(s)}\int_0^\infty dE\, e^{-iE(t-t')}\{\delta(E-\gamma-\varepsilon'(s))-\delta(E-\gamma+\varepsilon'(s))\}, \quad (21)$$

$$\langle a_{s-}(t)|a_{s-}^\dagger(t')\rangle = \int_0^\infty dE\, e^{-iE(t-t')} I_-(E) \quad (22)$$
$$= \tfrac{1}{2}\int_0^\infty dE\, e^{-iE(t-t')}\left\{\left[1-\frac{\omega(s)}{\varepsilon'(s)}\right]\delta(E-\gamma+\varepsilon'(s))+\left[1+\frac{\omega(s)}{\varepsilon'(s)}\right]\delta(E-\gamma-\varepsilon'(s))\right\},$$

$$\langle a_{s+}(t)|a_{s+}^\dagger(t')\rangle = \int_0^\infty dE\, e^{-iE(t-t')} I_+(E) \quad (22')$$
$$= \tfrac{1}{2}\int_0^\infty dE\, e^{-iE(t-t')}\left\{\left[1-\frac{\omega(s)}{\varepsilon'(s)}\right]\delta(E+\gamma+\varepsilon'(s))+\left[1+\frac{\omega(s)}{\varepsilon'(s)}\right]\delta(E+\gamma-\varepsilon'(s))\right\}.$$

After integrating and using the formulae

$$\langle b_{s+}^\dagger b_{s-}^\dagger\rangle = -\langle a_{s+}^\dagger a_{s-}^\dagger\rangle,\quad \langle b_{s\rho}^\dagger b_{s\rho}\rangle = \langle a_{s\rho}^\dagger a_{s\rho}\rangle,\quad \langle a_{s\rho}a_{s\rho}^\dagger\rangle = 1-\langle a_{s\rho}^\dagger a_{s\rho}\rangle.$$

we obtain

$$\langle b_{s+}^\dagger b_{s-}^\dagger\rangle = \begin{cases} -\tfrac{1}{2}\dfrac{C_s}{\varepsilon'(s)} & \text{for } |\gamma| < \varepsilon'(s), \\ 0 & \text{for } |\gamma| > \varepsilon'(s); \end{cases} \quad (23)$$

$$\langle b_{s-}^\dagger b_{s-}\rangle = \begin{cases} \tfrac{1}{2}\left\{1-\dfrac{\omega(s)}{\varepsilon'(s)}\right\} & \text{for } |\gamma| < \varepsilon'(s), \\ 0 & \text{for } |\gamma| > \varepsilon'(s),\ \gamma > 0, \\ 1 & \text{for } |\gamma| > \varepsilon'(s),\ \gamma < 0; \end{cases} \quad (24)$$

$$\langle b_{s+}^\dagger b_{s+}\rangle = \begin{cases} \tfrac{1}{2}\left\{1-\dfrac{\omega(s)}{\varepsilon'(s)}\right\} & \text{for } |\gamma| < \varepsilon'(s), \\ 1 & \text{for } |\gamma| > \varepsilon'(s),\ \gamma > 0, \\ 0 & \text{for } |\gamma| > \varepsilon'(s),\ \gamma < 0; \end{cases} \quad (24')$$

We notice that in the case when the number of neutrons exceeds that of protons ($\gamma < 0$), the function C_s satisfies the following equation:

$$C_s + \tfrac{1}{2}\sum_{\substack{s' \\ s\neq s'}} J'(s,s')\frac{C_{s'}}{\sqrt{C_{s'}^2+\omega(s')^2}} = 0. \quad (25)$$

Thus, the condition of disappearance of the quadruple correlations will be obtained in the form

$$\gamma > \varepsilon'(s) \tag{26}$$

or

$$|\lambda_n - \lambda_p| > 2\varepsilon'(s), \tag{26'}$$

i.e. the disappearance of quadruple correlations begins when the difference between the energies of the neutron and proton Fermi-surfaces becomes greater than the gap connected with the disruption of quadruples into pairs in the spectrum of excited states. By using a rough estimate of the gap we can find the minimum value $|\lambda_n - \lambda_p|_{min}$ at which quadruple correlations begin to break up. For an estimate of $|\lambda_n - \lambda_p|_{min}$ we can use eq. (25) as a result of which we obtain

$$|\lambda_n - \lambda_p|_{min} \approx (-J')\Omega.$$

Both estimates yield

$$|\lambda_n - \lambda_p|_{min} \approx \eta \times 5 \text{ MeV}, \tag{27}$$

where η is the factor of weakening of interaction between pairs.

Let us see in what manner quadruple correlations break up as $|\lambda_n - \lambda_p|$ increases. Let $\lambda_n - \lambda_p = 2\varepsilon'(s_0)$; then

$$|E(s_0) - \tfrac{1}{2}(\lambda_n + \lambda_p)| = \sqrt{C_{s_0}^2 + \tfrac{1}{4}(\lambda_n - \lambda_p)^2}. \tag{28}$$

When $|\lambda_n - \lambda_p| < |\lambda_n - \lambda_p|_{min}$ all neutron pairs lying above E_F^p, the energy of the Fermi surface for a proton shell, participate in the formation of the quadruple correlations; then for $|\lambda_n - \lambda_p| > |\lambda_n - \lambda_p|_{min}$ the outer neutron pairs cease to take part in it. In the limiting case $\frac{1}{2}(\lambda_n - \lambda_p) \gg C_{s_0}$ and $E(s_0) = \lambda_p$, all the neutron pairs lying above E_F^p cease to participate in the formation, while other neutrons and protons continue to be quadrupled.

Thus, when the number of neutrons begins to exceed that of protons, quadruple correlations weaken, the outer neutrons cease to take part in the formation and thereby the explicit α-particle properties of nuclei disappear.

It should be noted that in stable nuclei there appears a tendency towards an increase in the number of neutrons as compared with that of protons in the region $30 < A < 40$, due to the beginning separation between the Fermi surface for protons and that for neutrons. However, the quadruple correlations of nucleons oppose this tendency. For $A \geqq 40$ the quantity $|\lambda_n - \lambda_p|$ apparently attains the critical value $|\lambda_n - \lambda_p|_{min}$ when the outer neutrons cease to participate in quadruple correlations, and besides, the latter weaken, which leads to the disappearance of this opposition against the increase in the number of neutrons.

Let us study the problem of the quadruple correlations of the above-mentioned type in medium and heavy nuclei. The neutrons having energies greater

than E_F^p do not participate in quadruple correlations but are paired. The protons, on the other hand, are not merely paired but also participate in the formation of quadruple correlations together with the neutrons of the same energy. The energy of the nucleus will be written in the following form:

$$\langle H' \rangle = \sum_{s<s_0} \{\xi_p(s)\langle b_{s+}^\dagger b_{s+}\rangle + \xi_n(s)\langle b_{s-}^\dagger b_{s-}\rangle\} + \sum_{s\geq s_0} \xi_n(s) + \sum_{\substack{s<s_0 \\ s'<s_0 \\ s\neq s'}} J'(s,s')\langle b_{s+}^\dagger b_{s-}^\dagger\rangle\langle b_{s'-} b_{s'+}\rangle\}. \quad (29)$$

The functions of density and wave functions of pairs are determined by eqs. (23), (24) and (24′) for $\gamma < 0$ as well as by the equation

$$C_s + \tfrac{1}{2}\sum_{\substack{s'<s_0 \\ s'\neq s}} J(s,s') \frac{C_{s'}}{\sqrt{C_{s'}^2 + \left(E(s') - \dfrac{\lambda_p+\lambda_n}{2}\right)^2}} = 0. \quad (25')$$

Whereas it is necessary to break up the pair to excite the neutron in the case of an even shell, the one-particle excitation of the proton requires not only the disruption of pair correlation but also of the quadruple correlation of two protons and two neutrons with equal energies. Hence it follows that the energy of one-particle excitation should be somewhat larger for protons than for neutrons. This conclusion agrees with the estimate of this relation derived in ref. [10]) from the mass defects as being equal to (1.5 ± 0.3) MeV.

It should be noted that the effects of quadruple correlations in compound nuclei cannot be great, firstly because of the decrease of $J'(s, s')$ as a result of the parting of the Fermi surfaces for neutrons and protons, and secondly because the main contribution to eq. (25′) is made by the terms $E(s') \approx \frac{1}{2}(\lambda_p+\lambda_n)$; eq. (29) includes C_s for which $E(s) \ll \frac{1}{2}(\lambda_p+\lambda_n)$, and therefore an essential part is played by the interactions $J'(s, s')$ with very different quantum numbers s, s', which may be less than those with neighbouring quantum numbers s, s', playing the principal role in light nuclei.

6. Conclusion

Proceeding from the presence of strong interactions of nucleons in S-state with respect to each other, we have considered the interaction of nucleon pairs which lead to the formation of the quadruple correlations if the interaction among pairs is attractive. As a result certain regularities in light nuclei understandable from the viewpoint of the α-particle nuclear model are accounted for within the framework of the shell model through taking into account quadruple correlations. The mathematical apparatus thus evolved and the general results obtained make it possible to carry out specific calculations of the influence of quadruple correlations on the properties of light nuclei.

The author is indebted to N. N. Bogolyubov for his constant interest in the present paper and valuable suggestions as well as to B. S. Dzhelepov for stimulating discussions.

References

1) N. N. Bogolyubov, V. V. Tolmachev and D. V. Shirkov, A New Method in the Theory of Superconductivity (Publishing House of the Academy of Sciences of the USSR, 1958)
2) V. B. Belyaev, B. N. Zakhariev and V. G. Soloviev, JETP **38** (1960) 952
3) N. N. Bogolyubov, D. N. Zubarev and Yu. A. Tserkovnikov, Doklady Academii Nauk SSSR **117** (1957) 788
4) N. N. Bogolyubov, Doklady Academii Nauk SSSR **119** (1958) 244
5) V. G. Soloviev, JETP **35** (1958) 823; Nuclear Physics **9** (1958/59) 655
6) V. G. Soloviev, Doklady Academii Nauk SSSR **131** (1960) 286
7) N. N. Bogolyubov, Uspekhi Fiz. Nauk **67** (1959) 549
8) D. M. Brink and A. K. Kerman, Nuclear Physics **12** (1959) 314;
I. Talmi and R. Thieberger, Phys. Rev. **103** (1956) 718
9) N. N. Bogolyubov and S. V. Tyablikov, Doklady Academii Nauk SSSR **126** (1959) 53
10) A. B. Migdal, JETP **37** (1959) 249

8.A

Nuclear Physics **18** (1960) 173—175; © *North-Holland Publishing Co., Amsterdam*

Not to be reproduced by photoprint or microfilm without written permission form the publisher

THE MEASUREMENT OF THE K_1-K_2 MASS DIFFERENCE

W. S. C. WILLIAMS

Department of Natural Philosophy, The University, Glasgow

Received 31 March 1960

Abstract: This note proposes the principle of a method of measuring the mass difference of the K_1 and K_2 neutral mesons.

The K_1-K_2 mass difference can be determined by an experiment which consists of measuring the good geometry transmission of a mono-energetic beam of K_2 mesons through a large number of thin absorbers arranged so that successive absorbers are separated by the same distance. This absorber separation can be varied so that although the total thickness of the absorbers remains the same the total distance occupied by the array of absorbers will vary. It is assumed that the source-detector separation is considerably greater than the maximum extent of the absorbers and that there are no effects on the transmission due to the more obvious aspects of the variable absorber geometry. In these circumstances the transmission will vary with the absorber separation in a manner which is directly related to the K_1-K_2 mass difference m_1-m_2 should it be in the range given by

$$10\,\lambda_1 \geqq (m_1-m_2)c^2/\hbar \geqq \lambda_1,$$

where λ_1 is the decay constant of the K_1 meson, and the other symbols have the usual meaning. In fig. 1 the transmission is plotted as a function of the absorber separation in time units of $(\lambda_1-\lambda_2)^{-1}$, where λ_2 is the decay constant of the K_2 meson. This time is the time taken to traverse the distance between successive absorbers as observed from the rest frame of the K-meson. Two curves are given in fig. 1 for mass differences corresponding to $3(\lambda_1-\lambda_2)$ and $2(\lambda_1-\lambda_2)$.

The variation in transmission comes about in the following manner. Consider a pure K_2 beam incident upon the first absorber: the difference in absorption cross-section for the K^0 and $\overline{K}^0$ fraction depletes the beam of more of its $\overline{K}^0$ than of its K^0 and the beam which emerges from the absorber is pure K_2 plus a small amount of K^0. This K^0 will undergo the usual decay-interference routine[1]) which has the feature that a certain time later there could be more $\overline{K}^0$ present in the beam than would be expected if there were no interference effects. Should the beam arrive at a second absorber at this instant, it will be in a condition to suffer more absorption than could be expected without interference. Thus the

effect of the second absorber depends upon the separation from the first and upon the mass difference. If this process is repeated many times there will be a distinct effect on the transmission, and with the absorber separation suggested by this paragraph the transmission will be a minimum. In contrast, there are times in the interference effects when the $\overline{K}^0$ content is a minimum, in which case the corresponding absorber separation will lead to a maximum in the transmission. These effects are shown in fig. 1.

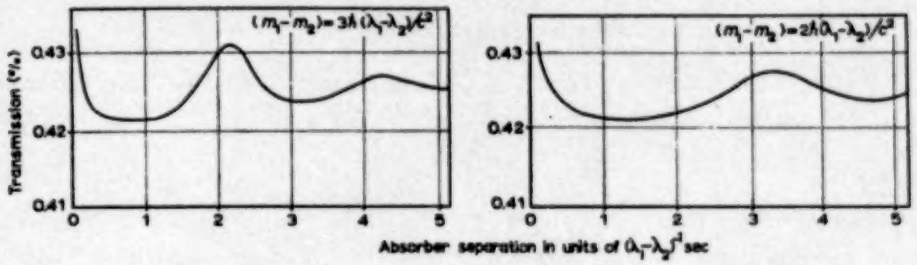

Fig. 1. Plot of transmission against absorber separation for two values of the K_1-K_2 mass difference.

The magnitude of the effect was estimated with the following assumptions. The absorbers were taken to be very thin, i.e. the time of traversal of one absorber by a K-meson was very much less than $(\lambda_1-\lambda_2)^{-1}$ sec. Thus their effect was taken to occur at one instant and to be such that the amplitude transmission was 99 % for K^0 and 97 % for $\overline{K}^0$. The result was calculated for 112 absorbers. The values of λ_1 and λ_2 used were 10^{10} sec^{-1} and 1.67×10^7 sec^{-1} respectively. The transmission was calculated by following the amplitude and phase of the beam components through the absorber array; this can be done easily using matrix algebra. The results presented have included the effect of the decay of the beam while it traverses distance not occupied by the absorbers when at less than maximum separation.

As can be seen in the figure, the transmission maxima occur at time separation corresponding to one cycle of the interference term, for example $\frac{2}{3}\pi$ for the curve for which $(m_1-m_2)c^2/\hbar = 3(\lambda_1-\lambda_2)$. As the mass difference increases the variations in transmission will become more frequent and more pronounced until such time as the period of the variation becomes comparable to the thickness of the absorbers employed.

Unfortunately, the variation in transmission is only $2\frac{1}{2}$ % and the detection of such a change in a sensible time would require an unattenuated mono-energetic K_2 beam having a detected intensity of at least 10^3 sec^{-1}. Such beams will not be available until there are some improvements in the intensity of high energy accelerators.

As described the experiment requires a mono-energetic K_2 beam. Some interesting effects could occur with a beam which is not mono-energetic if the

detector measured the energy of the transmitted K_2 mesons. In this case the effective absorber separation depends upon the energy of the K_2 meson and if all other things are equal the transmission will vary with the energy. Thus we shall expect to see interference effects superimposed upon the transmission versus energy curve at a fixed absorber separation.

There is some evidence [2]) to suggest that the mass difference corresponds to $(\lambda_1-\lambda_2)$. However, this is not conclusive and it is not inconceivable that the mass difference is very large. If it were of the order of $10^8(\lambda_1-\lambda_2)$, i.e. about 1000 eV, the interference effects would occur over distances comparable to atomic separations and the experiment could be done by using the planes of a crystalline material as the successive absorbers. Variable separation could be attained by tilting the crystal.

I am indebted to Dr. R. G. Moorhouse for assistance with the matrix algebra and to Dr. D. C. Gilles for the use of the Glasgow University Deuce Computer.

References

1) W. F. Fry and R. G. Sachs, Phys. Rev. **109** (1958) 2212
2) E. Boldt, D. O. Caldwell and Y. Pal, Phys. Rev. Lett. **1** (1958) 150

10.A

Nuclear Physics **18** (1959) 176; © *North-Holland Publishing Co., Amsterdam*

NEWS ITEM

THE AMALGAMATION OF THE INSTITUTE OF PHYSICS AND THE PHYSICAL SOCIETY

The incorporation of a new body on 17 May 1960, under the name of "The Institute of Physics and The Physical Society", marks the fulfilment of the desire expressed by the overwhelming majority of the members of the Institute and Society that the "necessary action" should be taken to implement the scheme for amalgamation prepared by a Joint Committee. The originating bodies will shortly be formally wound up and their assets handed over to the new one.

The first President of the amalgamated body is Sir John Cockcroft and the four Vice-Presidents are Dr J. Topping, Dr W. H. Taylor, Professor R. W. Ditchburn and Mr A. J. Philpot, each responsible to the Council for a defined area of the many activities to be taken over by the new organization from its predecessors. The Presidents of the predecessors (Sir George Thomson and Mr. J. A. Ratcliffe) are also members of the new Council. The other Officers are Dr. J. Taylor (Honorary Treasurer) and Dr C. G. Wynne (Honorary Secretary).

The Physical Society of London as it was then called was founded in 1874 and on the initiative of that Society's Council The Institute of Physics was founded 45 years later. The original scheme envisaged a kind of federation of societies interested in physics, to provide among other objects, rooms for meetings, a library, and a common secretariat. In fact the Institute's offices were in the Society's present rooms in South Kensington from 1927 to 1949 and the Institute provided the secretariat for The Physical Society and The Optical Society which themselves amalgamated in 1931.

At the time of its establishment no one could have foreseen the spectacular growth and influence of physics in the modern world. Broadly speaking before the war the scientific meetings and publications of the Institute were confined to applied physics while those of the Society were concerned more with pure physics. As, however, the boundary between these two aspects became less definite there has been increasing overlap in the activities of the two bodies and in their membership. It is not, therefore, surprising that during the past 20 years proposals for the amalgamation of the two bodies have been made repeatedly and from time to time detailed proposals examined, until eventually a satisfactory solution was worked out.

The qualification for the award of Fellow of The Institute of Physics, Associate of The Institute of Physics, and Graduate of The Institute of Physics will remain unchanged and members of the new body holding these diplomas will also be Fellows of The Physical Society. Besides the three Institute of Physics' grades of membership of the new body there will also be the grade to be known as "Fellow of The Physical Society". All the Fellows of the old Society will be automatically transferred to this new grade but new candidates for election to the grade will be required to possess a degree or diploma in physics recognized by the Council, or to satisfy the Council that they have a sufficient knowledge of physics.

Provision has been made for other scientists and engineers to participate in the scientific and educational work of the new body. Activities relating to the practice of the profession as such, will be strictly confined to those possessing one of the Institute's diplomas.

The Executive Officers of the new body are: *Secretary* Dr H. R. Lang, *Editor and Deputy Secretary* Dr A. C. Stickland, *Deputy Secretary* Mr N. Clarke. The registered offices and headquarters are at 47 Belgrave Square, London, S.W.1, and for the present, offices will also be retained at 1 Lowther Gardens, South Kensington, London, S.W.7.

1.C

Nuclear Physics **18** (1960) 177—195; © *North-Holland Publishing Co., Amsterdam*

Not to be reproduced by photoprint or microfilm without written permission from the publisher

ON A MODIFIED BETHE-GOLDSTONE EQUATION

AMNON KATZ

Department of Physics, The Weizmann Institute of Science, Rehovoth, Israel †

Received 6 April 1960

Abstract: A many-fermion system with Bardeen-Cooper-Schrieffer interaction is treated by a modified Bethe-Goldstone equation which takes into account a self consistent spreading of the Fermi surface. Our method employs a modified wave function which is an eigenstate of one modified Hamiltonian and from which energies are determined by another. Pairs with total momentum 0 are treated as elementary entities. All modifications are achieved by a "projection operator" which a priori takes care of the interference between pairs due to their statistics. The only case solved is the one where all interacting pairs go into the Cooper state of the modified Hamiltonian. The results are identical with those of Bardeen *et al.*

Introduction

Great progress has been made in the many-body problem since Brueckner introduced his method in 1954 [1]). The approximation consists of accounting for processes involving continued scattering of certain two particles above the Fermi sphere only. It proved successful in predicting the density and binding energy of nuclear matter. Yet it is known that this method cannot account for the peculiar ground state occurring in superconductivity theory. This case has been treated by Bardeen, Cooper and Schrieffer [2]) who applied the variation principle to a well chosen family of trial functions. Several authors [6]) have since given an equivalent treatment based on the Bogolubov canonical transformation. In the case of an infinite superconducting system the shortcoming of the Brueckner method was to be expected. In an infinite system the dependence of the energy of the superconducting state on the interaction is non-analytic. Therefore it is unobtainable by perturbation theory, on which Brueckner's method is based. But even in finite systems the Brueckner approximation fails whenever bound pairs of particles appear. An illustration to this may be found in the treatment of a degenerate shell in appendix I.

The Bethe-Goldstone equation [3]) was introduced in 1957 as an equivalent to Brueckner's method. It is a two-body Schroedinger equation which takes other particles into account only through the exclusion principle. It assigns to each pair of particles a wave funcuon based on their unperturbed single particle states and on the free states above the Fermi sea. The states occupied by other particles are totally ignored. Each pair of particles suffers an energy shift. The sum of all these shifts is considered to be the energy shift of the ground state.

† Sponsored in part by the Air Force Office of Scientific Research.

This procedure is plausible only if the wave functions of all pairs can be consistently recombined into a distribution deviating but little from the Fermi sea. In a system whose exact ground state is superconducting the ground state given by the BG equation of many pairs is a Cooper type state [4]). In such a state the pair is "bound" and its momentum distribution is spread outside the Fermi sphere. We can eliminate Cooper states by suitable boundary conditions. In this case the BG equation becomes equivalent to the Brueckner treatment. Like the latter it "skips" the superconducting ground state and describes the lowest normal state. It is our purpose in this paper to include the Cooper type solutions. We shall try to show that if this is done consistently a correct description of superconductivity can be obtained through a Bethe-Goldstone approach.

There are two hints that this can be done. First, the dependence of the Cooper energy on the strength of the interaction in an infinite system is non-analytic. It contains the same singularity as the BCS energy. Second, the ground state energy of the degenerate shell treated in appendix I is correctly given by the BG procedure, provided Cooper solutions are included.

In the general case it will be, of course, necessary to modify the BG equation. It will be necessary to generalize the Fermi distribution on which the BG equation is based. Once we have an equation which can be applied to any distribution (making use of the probability that a state is occupied or free instead of just eliminating occupied states) a consistency condition may be imposed on the distribution. We can look for the distribution which is identical with the recombination of pair wave functions derived therefrom. The sum of the energy shifts calculated from such a distribution should give the energy shift of the ground state, whether normal or superconducting. We shall carry out this idea on a special model.

1. The Model

We shall limit ourselves to the BCS reduced interaction which is of the form

$$g = \tfrac{1}{2} \sum_{kk'} g_{kk'} a_k^\dagger a_{-k}^\dagger a_{-k'} a_{k'}, \tag{1.1}$$

where the quantities a are annihilation operators of fermions, and k, k' stand for the quantum numbers defining the single fermion states. It is convenient to think of k as linear momentum although other cases may be treated as well [7]). As we see, the interaction (1.1), which conserves momentum, acts only between two particles having zero total momentum. This makes the application of the BG procedure extremely easy. It means that no particle can interact with more than one other particle. Two interacting pairs have no particle in common. With a general interaction when two independent pairs are present in the system, the latter contains six pairs. But with the BCS interaction only the original two should be considered as contributing to the energy.

It follows from the above considerations that we may limit ourselves to the subspace of states composed of pairs with zero total momentum. The ground state of the system belongs to this subspace [7]) and we wish to obtain the ground state energy.

We shall introduce labels α, β, for pairs with total momentum 0:

$$|\alpha) = |k, -k). \tag{1.2}$$

It is to be understood that different α's refer to different pairs. The pair $|-k, k)$ is denoted by the same α as (1.2). We also introduce the annihilation operator of such a pair $A_\alpha = a_{-k}a_k$, and rewrite the interaction (1.1) as

$$g = \sum_{\alpha\beta} g_{\alpha\beta} A_\alpha^\dagger A_\beta. \tag{1.3}$$

This turns our problem formally into one dealing with non-interacting entities in an external potential. The entities in question are those created by $A_\alpha^\dagger$. We shall refer to them in the following as pairs. A pair state will mean either a state of the type (1.2) or a linear combination of such states. The fact that they are pairs of fermions is reflected in their statistics. The commutation relations of the A's are discussed in appendix II. We shall only quote here the results that A's referring to different α's commute. Although a pair state of the type (1.2) can only be occupied by a single pair, a state which is a combination of many states (α) or (1.2) can accommodate many pairs.

2. Projection Operator and Consistency Condition

The elimination of occupied states is achieved in the usual BG equation by means of the projection operator P^α defined by

$$P^\alpha \sum C_\beta|\beta) = C_\alpha|\alpha) + \sum_{E_\beta > E_F} C_\beta|\beta). \tag{2.1}$$

This operator depends upon the state α to which the BG equation is applied. It eliminates all components of other states $|\beta)$ with unperturbed energy E_β below the (unperturbed) Fermi energy E_F. The effect is to modify the interaction:

$$g \to P^\alpha g P^\alpha. \tag{2.2}$$

Inserting the modified interaction (2.2) instead of g in the two-body Schroedinger equation we get the BG equation. This effectively removes the α pair from the Fermi distribution and lets it settle, subject to the interaction, in a combination of the states which are now free. The choice of states is indicated in fig. 1. It is hoped that the pair will remain most of the time in its original state α so that the wave functions of all pairs, when recombined will give rise to a distribution which is close to the step originally assumed.

This, however, is not true for model (1.1). As Cooper has shown a pair state exists with components only above the Fermi sea, but with energy E_C a finite amount below E_F. Gottfried [5]) pointed out that all pairs with unperturbed energy $E_C < E_\alpha < E_F$ would prefer a state of a similar type (with a small $|\alpha)$ component) to their corresponding "normal" states. If all these pairs are put into the Cooper state, the resulting distribution looks like fig. 2. The states between E_C and E_F remain unoccupied, as each pair considers them occupied by other pairs. This is the Gottfried paradox [5]). It shows that the Fermi distribution is not always a good approximation to the true one. If it is not, the usual BG procedure is inconsistent.

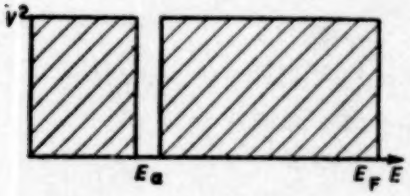

Fig. 1. Fermi distribution with the α pair removed.

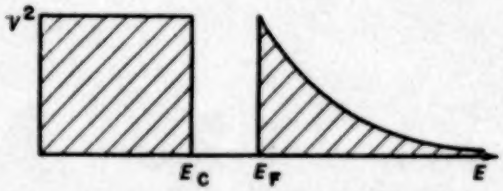

Fig. 2. The distribution resulting from the Bethe-Goldstone procedure when the Cooper state with energy E_C is taken into account.

In order to overcome this difficulty we shall generalize the procedure. Instead of starting with the Fermi distribution, we shall start from a general distribution (fig. 3) and choose it for self consistency.

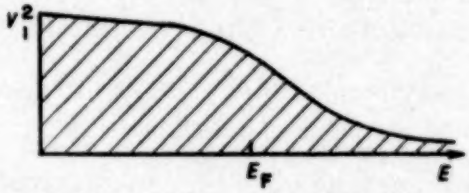

Fig. 3. A self-consistent distribution.

We shall express the spreading of the Fermi surface in the general distribution by a set of positive parameters V_α defined by

$$V_\alpha^2 = \frac{(\psi|A_\alpha^\dagger A_\alpha|\psi)}{(\psi|\psi)}, \tag{2.3}$$

where $|\psi)$ is the correct state of the whole system.

Let us also define a set of positive parameters U_α by

$$U_\alpha^2 + V_\alpha^2 = 1 \quad \text{for every } \alpha. \tag{2.4}$$

A similar set of parameters appears in the BCS [2])-Bogolubov [6]) treatment.

We must now generalize the projection operator P^α of (2.1) to apply to states only partly filled, and then formulate a consistency condition on the emerging wave function.

A simple generalization of the projection operator (2.1) is the operator Q defined by

$$Q \sum_{\alpha} C_{\alpha}|\alpha) = \sum_{\alpha} C_{\alpha} U_{\alpha}|\alpha). \tag{2.5}$$

The interaction operator g of eq. (1.3) is then replaced by

$$QgQ = \sum_{\alpha\beta} U_{\alpha} g_{\alpha\beta} U_{\beta} A_{\alpha}^{\dagger} A_{\beta}. \tag{2.6}$$

Every matrix element is weakened when the states to which it refers are partly occupied. Scattering into fully occupied states is eliminated. (A similar modification of the interaction was introduced by C. Bloch and C. De Dominici[8]) in the case of thermal spreading of the Fermi sea. There the parameters U_{α} were the temperature-dependent probabilities to find the state α free).

We neglected the change in the distribution function produced by removing a pair because we are interested in the case when many pairs go into the same state (we shall soon confine ourselves to the case when all pairs go into one and the same state). In this case the contribution of a single pair to the occupancy of the state is very small as it is already occupied by other pairs. Our projection operator Q is therefore the same for all states and there is no need for an α dependent Q^{α}.

The consistency condition can be formualted most simply as follows. Let ψ_{β}^{α} be the β component of the normalized α wave function $\sum_{\beta} \psi_{\beta}^{\alpha}|\beta)$; we then require that

$$\sum_{\alpha} |\psi_{\beta}^{\alpha}|^2 = V_{\beta}^2. \tag{2.7}$$

The arbitrary modification of the interaction and the crude consistency condition given above have been the basis for a former attempt on this problem. They were presented here because they illustrate qualitatively the modified Bethe-Goldstone philosophy. We shall see, however, that they cannot be applied directly to the case when many pairs are in the same state, they will re-emerge with their meaning somewhat changed after consideration of the peculiar features of this case.

3. Many Pairs in the Same State

We now consider the case when all pairs go into the Cooper state. In order to do this we must be familiar with the properties of a system where a pair state is filled many times over. A detailed study of this problem is given in appendix III. We shall quote here only the main results.

If the pair state in question is given by

$$\sum \psi_{\alpha}|\alpha) = \sum \psi_{\alpha} A_{\alpha}^{\dagger}|0), \tag{3.1}$$

the same state filled n times over $(\sum_\alpha \psi_\alpha A_\alpha^\dagger)^n|0)$ is well [7]) approximated (the approximation being the often used "saddle point method") by the BCS [2]) wave function

$$|\psi) = \prod_\alpha (U_\alpha + V_\alpha A_\alpha^\dagger)|0). \tag{3.2}$$

The U_α and V_α have the same meaning as in (2.3) and (2.4). They satisfy

$$\sum_\alpha V_\alpha^2 = n, \quad \frac{V_\alpha}{U_\alpha} = Z_0 \psi_\alpha, \tag{3.3}$$

where Z_0 is a parameter independent of α. The V_α's are given in terms of the ψ_α by

$$V_\alpha^2 = \frac{Z_0^2 \psi_\alpha^2}{1 + Z_0^2 \psi_\alpha^2}. \tag{3.4}$$

The dependence on n comes into (3.4) through Z_0. For Z_0 starts at 0 at $n = 0$ and goes to infinity when there are as many pairs as there are states. For small n, Z_0^2 is proportional to n which is in agreement with the consistency condition (2.7). But for large values of n as well as for large ψ_α's the dependence is far more complicated and (2.7) cannot serve as our consistency condition.

4. The Consistency Condition

The previous section has shown that when many pairs are in the same state the single pair wave function (3.1) does *not* satisfy the consistency condition (2.7):

$$\frac{n\psi_\alpha^2}{\sum_\beta \psi_\beta^2} \neq V_\alpha^2.$$

Rather, it satisfies

$$\frac{Z_0^2 \psi_\alpha^2}{1 + Z_0^2 \psi_\alpha^2} = V_\alpha^2. \tag{4.1}$$

Rather than abandon the consistency condition we shall abandon the wave function which does not satisfy it and modify it by applying the operator Q of eq. (2.5):

$$Q \sum \psi_\alpha A_\alpha^\dagger|0) = Q \sum \psi_\alpha|\alpha) = \sum \psi_\alpha U_\alpha|\alpha) = Z_0 \sum V_\alpha A_\alpha^\dagger|0). \tag{4.2}$$

The "pseudo-wave function" of a pair

$$|V) = \sum V_\alpha A_\alpha^\dagger|0) \tag{4.3}$$

satisfies

$$n \frac{V_\alpha^2}{\sum_\beta V_\beta^2} = n \frac{V_\alpha^2}{n} = V_\alpha^2. \tag{4.4}$$

This projection procedure (4.2) can be regarded intuitively as removing in advance that part of the pair wave function which would be removed by antisymmetrization with the other pairs. Therefore we leave little of components of states largely occupied and much of components referring to states which are free.

In the next section we shall devise a Hamiltonian with which to calculate energies from the pseudo-wave-function (4.3).

5. The Modified Hamiltonian

Recalling the Hamiltonian of our problem

$$H = H_0+g = \sum E_\alpha A_\alpha^\dagger A_\alpha + \sum_{\alpha\beta} g_{\alpha\beta} A_\alpha^\dagger A_\beta, \tag{5.1}$$

we shall look for a modified Hamiltonian $\mathscr{H}$ satisfying

$$(\psi|H|\psi) = n\frac{(V|\mathscr{H}|V)}{(V|V)} = (V|\mathscr{H}|V), \tag{5.2}$$

$|V)$ standing for $\sum V_\alpha A_\alpha^\dagger|0)$. The state $|\psi)$ (3.2) is normalized.

Since H_0 is diagonal we immediately see that

$$(\psi|H_0|\psi) = (V|H_0|V), \tag{5.3}$$

for

$$(\psi|H_0|\psi) = \sum E_\alpha(\psi|A_\alpha^\dagger A_\alpha|\psi) = \sum E_\alpha V_\alpha^2 = (V|H_0|V) \tag{5.4}$$

by the definition of V_α^2 (eq. (2.3)).

The same is true for the diagonal elements of the interaction g. To treat the non-diagonal elements we must find an expression for $(\psi|A_\alpha^\dagger A_\beta|\psi)$ for $\alpha \neq \beta$. Defining $|\varphi n)$ by (see appendix III, eq. (AIII.1))

$$|\varphi n) = \sum_{E_{\alpha_1}>\cdots>E_{\alpha_n}} \varphi_{\alpha_1}\cdots\varphi_{\alpha_n} A_{\alpha_1}^\dagger \cdots A_{\alpha_n}^\dagger|0), \tag{5.5}$$

where the φ_α's are given as in appendix III by

$$\varphi_\alpha = \frac{V_\alpha}{U_\alpha} = Z_0\psi_\alpha, \tag{5.6}$$

we have as in eqs. (AIII.3), (AIII.20)

$$\psi = \prod_\gamma U_\gamma \sum_n |\varphi n). \tag{5.7}$$

Using these relations we get

$$(\psi|A_\alpha^\dagger A_\beta|\psi) = \prod_\gamma U_\gamma^2 \sum_n (\varphi n|A_\alpha^\dagger A_\beta|\varphi n), \tag{5.8}$$

$$(\varphi n|A_\alpha^\dagger A_\beta|\varphi n) = \varphi_\alpha\varphi_\beta \sum_{\substack{E_{\alpha_1}>\cdots>E_{\alpha_{n-1}} \\ \alpha_i\neq\alpha,\beta}} \varphi_{\alpha_1}^2\cdots\varphi_{\alpha_{n-1}}^2, \tag{5.9}$$

$$\begin{aligned}(\psi|A_\alpha^\dagger A_\beta|\psi) &= \varphi_\alpha\varphi_\beta \prod_\gamma U_\gamma^2 \prod_{\delta\neq\alpha,\beta}(1+\varphi_\delta^2) = \varphi_\alpha\varphi_\beta U_\alpha^2U_\beta^2 \prod_{\delta\neq\alpha,\beta}(U_\delta^2+V_\delta^2) \\ &= \varphi_\alpha\varphi_\beta U_\alpha^2U_\beta^2 = V_\alpha V_\beta U_\alpha U_\beta.\end{aligned} \tag{5.10}$$

In the last sequence of equalities we have twice used the relation $\varphi = V/U$ of eq. (5.8). Summing together the different parts of

$$(\psi|H|\psi) = \sum_\alpha E_\alpha(\psi|A_\alpha^\dagger A_\alpha|\psi) + \sum_{\alpha\beta} g_{\alpha\beta}(\psi|A_\alpha^\dagger A_\beta|\psi) \tag{5.11}$$

we get

$$(\psi|H|\psi) = \sum_\alpha E_\alpha V_\alpha^2 + \sum_{\alpha\beta} V_\alpha U_\alpha g_{\alpha\beta} U_\beta V_\beta + \sum_\alpha g_{\alpha\alpha} V_\alpha^4, \tag{5.12}$$

which is, of course, identical with the expression obtained by BCS as the ground state energy. The identity of the required modified Hamiltonian becomes apparent when we rewrite (5.12) in the form

$$(\psi|H|\psi) = \sum_{\alpha\beta} V_\alpha\{(E_\alpha+g_{\alpha\alpha}V_\alpha^2)\delta_{\alpha\beta}+U_\alpha g_{\alpha\beta}U_\beta\}V_\beta. \tag{5.13}$$

The new Hamiltonian $\mathscr{H}$ is given by

$$\mathscr{H} = \sum \mathscr{H}_{\alpha\beta} A_\alpha^\dagger A_\beta, \quad \mathscr{H}_{\alpha\beta} = (E_\alpha+g_{\alpha\alpha}V_\alpha^2)\delta_{\alpha\beta}+U_\alpha g_{\alpha\beta}U_\beta. \tag{5.14}$$

Defining a "self-consistent independent-pair Hamiltonian" by

$$\mathscr{H}_0 = \sum_\alpha (E_\alpha+g_{\alpha\alpha}V_\alpha^2)A_\alpha^\dagger A_\alpha = \sum_\alpha e_\alpha A_\alpha^\dagger A_\alpha, \tag{5.15}$$

the modified Hamiltonian $\mathscr{H}$ is

$$\mathscr{H} = \mathscr{H}_0+QgQ = \sum e_\alpha A_\alpha^\dagger A_\alpha + \sum_{\alpha\beta} U_\alpha g_{\alpha\beta} U_\beta A_\alpha^\dagger A_\beta: \tag{5.16}$$

$\mathscr{H}$ is composed of an independent-pair Hamiltonian and an interaction which is the same modification of the original interaction g as suggested in eq. (2.6).

Before passing to the next section, where we shall see what should be done with the modified Hamiltonian and the modified wave function in order to solve the problem, let us remark that we shall, as most authors do, neglect the V dependence of the eigenvalues e_α. In the case of an interaction which is predominantly non-diagonal, such as the separable interaction most often treated in this connection, one may altogether neglect the difference between e_α and E_α because it stems from the diagonal elements of the interaction which are out-numbered Ω to 1 (Ω being the number of states).

6. The Variation Principle and the Eigenvalue Problem

When treating a quantal problem governed by a Hamiltonian H whose matrix elements are $H_{\alpha\beta}$, the wave function (the components of which will be denoted ψ_α) and ground state energy may be determined in either of two ways: one may either solve the Schroedinger equation

$$\sum_\beta H_{\alpha\beta}\psi_\beta = E\psi_\alpha \tag{6.1}$$

and choose E as the lowest eigenvalue and ψ as the eigenvector corresponding to it, or one may minimize the expectation of H keeping ψ normalized. In the latter case the equations are

$$\tfrac{1}{2}\frac{\partial}{\partial\psi_\alpha}\{\sum_{\beta\gamma}\psi_\beta H_{\beta\gamma}\psi_\gamma - \lambda\sum_\beta\psi_\beta{}^2\} = \sum_\gamma H_{\alpha\gamma}\psi_\gamma - \lambda\psi_\alpha = 0. \tag{6.2}$$

This equation is the same as eq. (6.1) if we identify E with the Lagrange multiplier λ.

In the above considerations we have assumed H to be given in advance and independent of the ψ which it determines. In the case of the modified Hamiltonian $\mathscr{H}$ and the pseudo-wave-function V the situation is different. The $\alpha\beta$ element of the modified interaction $QgQ = \sum U_\alpha g_{\alpha\beta}U_\beta A_\alpha{}^\dagger A_\beta$ depends on U_α and U_β, which are connected with V_α and V_β by

$$U_\alpha{}^2 + V_\alpha{}^2 = 1 \quad \text{for all } \alpha. \tag{2.4}$$

Trying to minimize $(V|\mathscr{H}|V)$, keeping V normalized (eq. (2.3)), we obtain

$$\tfrac{1}{2}\frac{\partial}{\partial V_\alpha}\{\sum_{\beta\gamma}V_\beta\mathscr{H}_{\beta\gamma}V_\gamma - \lambda\sum V^2{}_\beta\} = \sum_\gamma\left(1+V_\alpha\frac{\partial}{\partial V_\alpha}\right)\mathscr{H}_{\alpha\gamma}V_\gamma - \lambda V_\alpha = 0. \tag{6.3}$$

Thus, applying the variation method to the expectation value $(V|\mathscr{H}|V)$ of the Hamiltonian $\mathscr{H}$ corresponds to the eigenvalue problem for a further modified Hamiltonian h whose matrix elements $h_{\alpha\beta}$ are

$$\begin{aligned} h_{\alpha\beta} &= \left(1+V_\alpha\frac{\partial}{\partial V_\alpha}\right)\mathscr{H}_{\alpha\beta} = \left(1+V_\alpha\frac{\partial}{\partial V_\alpha}\right)(e_\alpha\delta_{\alpha\beta}+U_\alpha g_{\alpha\beta}U_\beta) \\ &= e_\alpha\delta_{\alpha\beta} + \frac{U_\alpha{}^2 - V_\alpha{}^2}{U_\alpha}g_{\alpha\beta}U_\beta. \end{aligned} \tag{6.4}$$

Application of the variation principle to the Hamiltonian $\mathscr{H}$ gives the correct solution of the physical problem before us, as $(V|\mathscr{H}|V) = (\psi|H|\psi)$ by eq. (5.2), and thus the variation of $(V|\mathscr{H}|V)$ coincides with the variation of $(\psi|H|\psi)$.

It is in this point that the former effort mentioned above had failed. Although the same modified Hamiltonian and consistency condition were used as those we employ here, it was not realized that $\mathscr{H}$ was the Hamiltonian for the purpo-

ses of the variation method and energy calculation only, while the wave function was an eigenfunction of a different Hamiltonian.

It is worth while to note that in an almost empty shell (see section 7), where V^2 is negligible compared to U^2, the two Hamiltonians $\mathscr{H}$ and h become asymptotically equal. In this case the operator Q becomes asymptotically equal to 1. Consequently the modified wave function approaches asymptotically the single pair wave function normalized to n. The consistency condition (2.7) also becomes applicable in this case. In this limit the methods suggested in section 2 may be applied literally. For a finite V_α^2, however, we must use the complete theory.

In the next section we shall see that the required eigenstate of h is a Cooper [4]) type state.

7. The Superconducting State as a Cooper State

The eigenvalue problem of the twice modified Hamiltonian h is equivalent, of course, to the variation problem treated by BCS [2]) and other authors [6]). A resumé of the treatment is given in appendix IV. We quote here only the main result for a special case which is most suitable for the illustration of our point. We shall treat the case of constant matrix element $g_{\alpha\beta} = -G$. We shall not deal here with the "normal" solution which always exists trivially. This solution yields the step distribution. (It is characterized by $\Delta = 0$ in the following equations). There exists also (under certain conditions) a non-trivial solution in which the distribution is

$$V_\alpha^2 = \tfrac{1}{2}\left(1 - \frac{e_\alpha - \lambda}{\sqrt{(e_\alpha-\lambda)^2+4\Delta^2}}\right), \quad \Delta \neq 0; \tag{7.1}$$

λ is the eigenvalue of the Hamiltonian h which in our case is not the energy; Δ is a parameter subject to the equation

$$G\sum \frac{1}{\sqrt{(e_\alpha-\lambda)^2+4\Delta^2}} = 1. \tag{7.2}$$

The curve of V_α^2 as a function of e_α is shown in fig. 4(a). At the point $e_\alpha = \lambda$, one has $V_\alpha^2 = \frac{1}{2}$. If we limit our considerations to a "shell" of levels between the unperturbed energies a and b and assume that no other levels exist, only part of the curve of fig. 4(a) will be used. The area under the curve must equal the number of pairs. This determines the part of the curve which falls within the shell. For an almost empty shell (fig. 4(b)) the eigenvalue λ must lie far below the shell. It is in the shell when it is half full and for an almost full shell we have $\lambda > b$. These results have been demonstrated rigorously by Belyaev [6]).

Keeping in mind the above mentioned features of our solution we now turn to the characteristics of the Cooper solution [4]). In appendix I it is shown that in a degenerate shell and with the same interaction as we have here ($g_{\alpha\beta} = -G$) the Cooper state is characterized by an eigenvalue for below the shell and a wave function spanning all unperturbed states. For a repulsive interaction the eigenvalue would have been far above the shell. The free states on the other hand deviated little from the unperturbed state and kept their unperturbed energy. The situation is not greatly changed even when the degeneracy is removed. Gottfried [5]) has shown that even then most eigenvalues of $\mathscr{H} = \mathscr{H}_0 + g$ differ little from the eigenvalues of $\mathscr{H}_0$. The remaining eigenvalue is the one corresponding to the Cooper state. It falls far below the lowest eigenvalue of $\mathscr{H}_0$ for attractive g and far above the highest eigenvalue of $\mathscr{H}_0$ when g is repul-

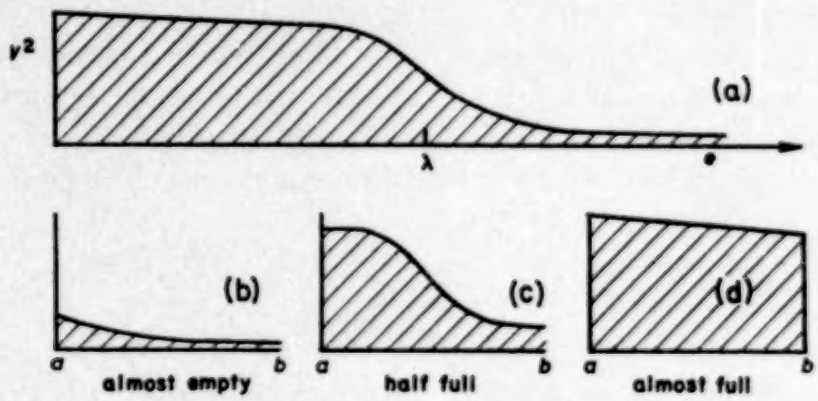

Fig. 4. The BCS distribution curve and the parts of it which fall within a shell in different cases.

sive (we still assume $g_{\alpha\beta} = \pm G$). The corresponding eigenfunction spans all eigenstates of $\mathscr{H}_0$, all components being of the same order of magnitude and differing a little according to the different values of e_α.

Our super-modified Hamiltonian h displays both regions of attractive and repulsive interaction. The original g being considered attractive, the super-modified g of eq. (6.4) is attractive wherever states are not overcrowded (wherever $V^2 < \frac{1}{2}$ to be precise); otherwise (when $V^2 > \frac{1}{2}$) it is repulsive. The eigenvalue λ lies exactly where $V^2 = \frac{1}{2}$, i.e. below the region of attraction and above the region of repulsion. In case (b) of fig. 4, i.e. when the shell is almost empty, the interaction throughout the shell is attractive, λ lies far below the shell and the components of V are all of the same order of magnitude varying a little as e varies (eq. (7.1)). Thus our solution in this case displays all the characteristics of a Cooper state. A similar statement could be made about the almost full shell (case (d) of fig. 4). As for the half full shell (case (c)), our solution still is the nearest possible thing to a Cooper state, the eigenvalue lying below the attractive region and above the repulsive region and the components of V spanning both regions and varying slowly within each of them.

Formally, the Cooper eigenvalue (as any other) must satisfy the Cooper equation [4])

$$\sum \frac{h_{\alpha\alpha}}{\lambda - e_\alpha} = 1. \tag{7.3}$$

Using

$$h_{\alpha\alpha} = \frac{U_\alpha^2 - V_\alpha^2}{U_\alpha}(-G)U_\alpha = -G\frac{e_\alpha - \lambda}{\sqrt{(e_\alpha - \lambda)^2 + 4\Delta^2}}, \tag{7.4}$$

Cooper's equation (7.3) becomes the BCS equation (7.2).

One may wonder why we get no more than two eigenstates of the Hamiltonian h. The answer is that the mutual relationship of Hamiltonian and eigenstate which we have imposed, together with the demand that V be normalized to n, while no component of it may surpass unity, have eliminated the other solutions. Other solutions should represent pair states that cannot accommodate all pairs. Treatment of a solution with different wave functions for different pairs is the natural generalization of what has been done here. Unfortunately it is mathematically far more complicated.

8. Conclusion

We have attacked the problem of a many-fermion system with a BCS [2]) reduced interaction (which acts only between pairs of particles whose total momentum is zero) using several assumptions and approximations. The main physical assumption was that all pairs go into one and the same state. We have also used the "saddle-point method" as a mathematical approximation in borrowing the BCS wave function [2]). Throughout we used the language and philosophy of the Bethe-Goldstone [3]) approach. We had to introduce the parameters U_α and V_α into the BG way of thinking in order to overcome the inconsistency in the usual procedure pointed out by Gottfried [5]). This made it in turn necessary to deal with two modified Hamiltonians. One of them serves for calculating energies with wave functions which are eigenstates of the other. The superconducting state was found to be the Cooper state of this last Hamiltonian.

I wish to thank Professor A. de-Shalit for his interest and encouragement during this work. I am indebted to him as well as to Professor I. Talmi, Dr. A. Reiner, Mr. I. Unna and others for many fruitful discussions and for constructive criticism on the form and contents of this paper. I have been guided in the presentation of material by the advice of Dr. H. J. Lipkin whom I also wish to thank.

Appendix

I. A DEGENERATE SHELL

As a special case of our model let us consider a system with 2Ω degenerate single particle states. We shall take the unperturbed energy of each particle to be zero. Denoting the single particle states by the indices $\pm 1, \pm 2, \ldots \pm\Omega$, we introduce the interaction

$$g = -G \sum_{ij} a_i^\dagger a_{-i}^\dagger a_{-j} a_j = -G \sum_{\alpha\beta} A_\alpha^\dagger A_\beta. \tag{AI.1}$$

The a's and A's are annihilation operators as in section 1. When a single pair of particles is present in the system the matrix elements of the Hamiltonian are

$$(ij|g|ji) = -G\delta(i+j). \tag{AI.2}$$

The only part of the Hamiltonian matrix which does not vanish is the one spanning the pairs α, where $|\alpha) = |i, -i)$. It is

$$H = -G \begin{pmatrix} 1\,1 \ldots 1 \\ \ldots\ldots\ldots \\ 1\,1 \ldots 1 \\ \ldots\ldots\ldots \\ 1\,1 \ldots 1 \end{pmatrix}. \tag{AI.3}$$

This matrix is of order Ω and rank one: $\Omega-1$ of its eigenvalues are 0 and the last one equals the trace $-\Omega G$. This last eigenvalue corresponds to the eigenvector $(1, 1, \ldots, 1)$. It is a bound state (negative energy), characterized by an eigenvalue far below the unperturbed energy and components which are all of the same order of magnitude (in the degenerate case exactly equal). The free states have energies close to the unperturbed energy (in the degenerate shell exactly equal to it) and components one of which is far larger than the others. In other words the free states are not much different from the unperturbed ones.

Let us now apply the BG procedure to our system when it contains $2n$ particles instead of 2. The pair problem before us now is quite similar to the one we had before. The only change is the need to ignore the states occupied by $n-1$ other pairs. As we have Ω pair states of the $|\alpha)$ type we are left with $\Omega-(n-1) = \Omega-n+1$ states for our pair problem. The lowest eigenvalue will now be $-(\Omega-n+1)G$ instead of $-\Omega G$. This is the energy shift of an $|\alpha)$ type pair. As there are n such pairs the total energy of the ground state is

$$E = -n(\Omega-n+1)G. \tag{AI.4}$$

This result is exact [7]). It is reproduced by the BCS method to within [7]) $1/\Omega$.

The Brueckner approximation is not applicable to the degenerate shell. If we start with an unperturbed Hamiltonian of the form

$$H_0 = -\tfrac{1}{2}E\sum_{i=-n}^{n} a_i^\dagger a_i, \tag{AI.5}$$

the Brueckner series is

$$\begin{aligned} E_{\mathrm{Br}} &= n\left\{-G+(-G)(\Omega-n)\frac{1}{E}(-G)+\ldots\right\} \\ &= n\left\{-G+\frac{E}{\Omega-n}\sum_{\gamma=2}^{\infty}\right\}\{-G(\Omega-n)^\gamma/E\} = n\left\{-G+\frac{G^2(\Omega-n)}{E+G(\Omega-n)}\right\}. \end{aligned} \tag{AI.6}$$

Passing to the limit $E \to 0$ we get

$$E_{\mathrm{Br}} \to n\{-G+G\} = 0, \tag{AI.7}$$

which is the energy of a "normal" state of the system.

II. PAIR STATISTICS

The pair annihilation and creation operators are defined by

$$A_\alpha = a_{-k}a_k, \quad A_\alpha^\dagger = a_k^\dagger a_{-k}^\dagger. \tag{AII.1}$$

They obey commutation relations for different α's and anticommutation relations for the same α (in the subspace under consideration):

$$\begin{aligned} &[A_\alpha, A_\beta] = [A_\alpha^\dagger, A_\beta^\dagger] = 0 \qquad (\alpha \neq \beta), \\ &A_\alpha^2 = (A_\alpha^\dagger)^2 = 0, \quad [A_\alpha, A_\alpha^\dagger]_+ = 1. \end{aligned} \tag{AII.2}$$

A pair state of the type

$$\sum \varphi_\alpha A_\alpha^\dagger|0) = \sum \varphi_\alpha|\alpha) \tag{AII.3}$$

can contain many pairs, as many as there are non-vanishing φ_α's. Putting n pairs into the same state we have the state $(\sum\varphi_\alpha A_\alpha^\dagger)^n|0)$.

While a power of $A_\alpha^\dagger$ vanishes, $A_\alpha^\dagger$'s of different α's commute. Therefore all terms in $(\sum\varphi_\alpha A_\alpha^\dagger)^n|0)$ where two α's are equal vanish and we have

$$(\sum \varphi_\alpha A_\alpha^\dagger)^n = n!\sum_{E_{\alpha_1}>E_{\alpha_2}>E_{\alpha_n}} \varphi_{\alpha_1}\varphi_{\alpha_2}\cdots\varphi_{\alpha_n}A_{\alpha_1}^\dagger\cdots A_{\alpha_n}^\dagger. \tag{AII.4}$$

As long as there are more than n φ_α's different from zero the state $(\sum\varphi_\alpha A_\alpha^\dagger)^n|0)$ does not vanish. It should, nowever, be remarked that wnen the state is very crowded — that is when n is almost equal to the number of φ_α's — the wave function loses the character of a pair state filled many times over. It becomes a state where every pair occupies a pair eigenstate of H_0 and every particle a single particle eigenstate. In the limit when n exactly equals the number of

φ_α's we have

$$(\sum_{\alpha=\alpha_1}^{\alpha_n} \varphi_\alpha A_\alpha^\dagger)^n|0) = \prod_{\alpha=\alpha_1}^{\alpha_n} \varphi_\alpha A_1^\dagger \dots A_n^\dagger|0) = \prod_{\alpha=\alpha_1}^{\alpha_n} \varphi_\alpha a_{-k_1}^\dagger a_{k_1}^\dagger a_{-k_2}^\dagger a_{k_2}^\dagger \dots a_{-k_n}^\dagger a_{k_n}^\dagger|0), \tag{AII.5}$$

which is exactly an assembly of single particles.

III. TREATMENT OF MANY PAIRS IN THE SAME STATE

The state of one pair being $\sum\varphi_\alpha A_\alpha^\dagger|0)$, we want to investigate the n pair state

$$|\varphi n) = \sum_{E_{\alpha_1}>E_{\alpha_2}>\dots>E_{\alpha_n}} \varphi_{\alpha_1}\varphi_{\alpha_2}\dots\varphi_{\alpha_n} A_{\alpha_1}^\dagger A_{\alpha_2}^\dagger \dots A_{\alpha_n}^\dagger|0). \tag{AIII.1}$$

While this function is difficult to treat it has a simple generating function

$$|\varphi(Z)) = \prod(1+Z\varphi_\alpha A_\alpha^\dagger)|0), \tag{AIII.2}$$

Z being a complex number.

A development of $|\varphi(Z))$ in powers of Z displays the n pair state $|\varphi n)$ as the coefficient of the n'th power of Z:

$$|\varphi(Z)) = \sum_n Z^n|\varphi n). \tag{AIII.3}$$

$|\varphi n)$ can be obtained from $|\varphi(Z))$ by integration over Z along a path encircling the origin:

$$|\varphi n) = \frac{1}{2\pi i}\oint |\varphi(Z))Z^{-n-1}\mathrm{d}Z. \tag{AIII.4}$$

Integrals of this type are generally evaluated in statistical mechanics by the saddle point method. This consists, save for normalization, in replacing the integral by the integrand at a point Z_0 where the logarithmic derivative of the integrand vanishes. This method is of course an approximation but it is a good one for large n. We immediately see that replacing $|\varphi n)$ by $|\varphi(Z_0))$ implies the replacement of a state of n pairs by a combination of states of different n's. However, this is what happens every time the saddle-point method is used in order to select a certain number of particles or a certain energy in statistical mechanics and in as much as we shall consider properties which are not sensitive functions of n it may serve us in the present problem as well as in any other.

The value of Z_0 is to be determined by the vanishing of the logarithmic derivative of the integrand. However, the integrand of eq. (AIII.4) cannot vanish because of its nature as a vector in a Hilbert space: it can be expressed as

$$|\varphi(Z))Z^{-n-1} = \exp\{Z\sum_\alpha \varphi_\alpha A_\alpha^\dagger - (n+1)\log Z\}|0) \tag{AIII.5}$$

and the equation

$$\left\{\sum \psi_\alpha A_\alpha^\dagger - \frac{n+1}{Z}\right\}|0) = 0 \qquad \text{(AIII.6)}$$

has no solution.

Let us, however, employ the saddle point method on another generating function

$$f(Z) = \prod_\alpha (1+Z^2|\psi_\alpha|^2) = \sum_n Z^{2n}(\psi n|\psi n). \qquad \text{(AIII.7)}$$

This $f(Z)$ is a numerical function and it determines the weights of different values of n and of different α's in $\psi(Z)$. For any positive $Z = x$ we have

$$f(x) = (\psi(x)|\psi(x)). \qquad \text{(AIII.8)}$$

The weight of the n-pair component of $\psi(Z)$ is

$$W_n = \frac{1}{2\pi i}\oint f(\sqrt{\zeta})\zeta^{-n-1}\mathrm{d}\zeta, \qquad (\zeta = Z^2). \qquad \text{(AIII.9)}$$

Evaluating this by the saddle point method we just replace W_n by $f(Z_0)$ with a value Z_0 which makes the weight of the n-component predominant in $f(Z)$. The quantity Z_0 is determined by the vanishing of the logarithmic derivative of the integrand of (AIII.9):

$$\sum_\alpha \frac{|\psi_\alpha|^2}{1+\zeta_0|\psi_\alpha|^2} - \frac{n+1}{\zeta_0} = 0, \qquad \text{(AIII.10)}$$

or

$$\sum_\alpha \frac{Z_0^2|\psi_\alpha|^2}{1+Z_0^2|\psi_\alpha|^2} = n+1. \qquad \text{(AIII.11)}$$

Let us now define

$$\varphi_\alpha = Z_0\psi_\alpha \quad (Z_0 \text{ being positive}), \qquad \text{(AIII.12)}$$

and settle on the wave function

$$|\varphi) = \prod_\alpha (1+\varphi_\alpha A_\alpha^\dagger)|0) \qquad \text{(AIII.13)}$$

as the approximation we shall use for the state of n pairs all in the state $\sum \psi_\alpha A_\alpha^\dagger|0)$. The average number of pairs in $|\psi) = |\psi(Z_0))$ is

$$\bar{n} = \left[Z^2\frac{\partial}{\partial Z^2}\log f(Z)\right]_{Z=Z_0} = \sum_\alpha \frac{Z_0^2|\psi_\alpha|^2}{1+Z_0^2|\psi_\alpha|^2} = \sum_\alpha \frac{\varphi_\alpha^2}{1+\varphi_\alpha^2} = n+1, \qquad \text{(AIII.14)}$$

the last equality being that of eq. (AIII.11). As we are dealing with an approximation which is good for large n we may neglect the difference between n and $n+1$ and be content that the value Z_0 chosen to make the weight of the n component predominant also yields n as the average number of pairs.

More insight as to the meaning of each term in the sum (AIII.14) may be gained when we evaluate V_α^2, the occupation of the α pair:

$$V_\alpha^2 = |\psi_\alpha|^2 \frac{\partial}{\partial |\psi_\alpha|^2} \log f(Z_0) = \frac{Z_0^2 |\psi_\alpha|^2}{1+Z_0^2|\psi_\alpha|^2} = \frac{|\varphi_\alpha|^2}{1+|\varphi_\alpha|^2}. \quad \text{(AIII.15)}$$

Eq. (AIII.14) can now be written as

$$\sum_\alpha V_\alpha^2 = n. \quad \text{(AIII.16)}$$

Assuming the φ_α's to be all positive (phases being absorbed by the $A_\alpha^\dagger$'s) we can sum up the relations between U_α, V_α and φ_α:

$$U_\alpha^2 = \frac{1}{1+\varphi_\alpha^2}, \quad V_\alpha^2 = \frac{\varphi_\alpha^2}{1+\varphi_\alpha^2}, \quad \varphi_\alpha = \frac{V_\alpha}{U_\alpha}. \quad \text{(AIII.17)}$$

This is in flat contradiction with the consistency condition (2.7) suggested in section 2.

Let us remark that the wave function on which we have settled

$$|\varphi) = \prod_\alpha (1+\varphi_\alpha A_\alpha^\dagger)|0) \quad \text{(AIII.18)}$$

is not normalized, for

$$(\varphi|\varphi) = f(Z_0) = \prod_\alpha (1+\varphi_\alpha^2) = \prod \left(1+\frac{V_\alpha^2}{U_\alpha^2}\right) = \prod_\alpha \frac{1}{U_\alpha^2}, \quad \text{(AIII.19)}$$

since $U_\alpha^2+V_\alpha^2 = 1$. In order to normalize it we must multiply it by $\prod U_\alpha$ and then we get

$$|\psi) = \prod_\alpha U_\alpha|\varphi) = \prod_\alpha U_\alpha(1+\varphi_\alpha A_\alpha^\dagger)|0) = \prod (U_\alpha+V_\alpha A_\alpha^\dagger)|0). \quad \text{(AIII.20)}$$

The function $|\psi)$ is nothing but the BCS trial function [2]) or the Bogoliubov ground state [6]) (or vacuum of the quasi-particles). It may be noted that the spreading in the number of pairs varies from pair to pair. It is small whenever U or V is near unity and it increases as they become equal. Quantitatively, the root mean square deviation in the occupation of a pair is given by

$$\Delta^2 = V^4U^2+(1-V^2)^2V^2 = U^2V^2, \quad \text{(AIII.21)}$$

which lies between 0 and $\frac{1}{4}$. As U and V vary with energy, V^2 starting near unity below the Fermi energy and ending near zero above it, we see that both the spreading in n and the character of the function as superposition of pairs are significant near the Fermi energy only. Far below it one may neglect U and have the state described by $\prod V_\alpha A_\alpha^\dagger|0)$ which is an assembly of independent particles and far above it one may neglect V and have the state of the system as $\prod U_\alpha|0)$ which is vacuum. Only around the Fermi energy does the special character of the function have meaning. Thus the BCS function achieves

automatically what some investigators tried to do by means of elaborate mathematical schemes — to separate the system into particles and pairs.

IV. SOLUTION OF THE EIGENVALUE PROBLEM

Inserting the Hamiltonian h of eq. (6.4) into the eigenvalue equation (6.2) we get

$$(\lambda-E_\alpha)V_\alpha = \frac{U_\alpha^2-V_\alpha^2}{U_\alpha}\sum g_{\alpha\beta}U_\beta V_\beta = \frac{U_\alpha^2-V_\alpha^2}{U_\alpha}\Delta_\alpha, \qquad \text{(AIV.1)}$$

where Δ_α is defined by

$$\Delta_\alpha = \sum g_{\alpha\beta}U_\beta V_\beta. \qquad \text{(AIV.2)}$$

(Our expressions differ from those of BCS [2]) by factors 2 in some places because we treat pairs as elementary entities while the BCS treatment is based on particles). Rewriting eq. (AIV.1) as

$$(e_\alpha-\lambda)U_\alpha V_\alpha+(U_\alpha-V_\alpha)\Delta_\alpha = 0, \qquad \text{(AIV.3)}$$

we recognize it as BCS equation (2.33). It is a quadratic equation in U and V whose solution is

$$U_\alpha^2 = \tfrac{1}{2}\left(1+\frac{e_\alpha-\lambda}{\sqrt{(e_\alpha-\lambda)^2+4\Delta_\alpha^2}}\right), \quad V_\alpha^2 = \tfrac{1}{2}\left(1-\frac{e_\alpha-\lambda}{\sqrt{(e_\alpha-\lambda)^2+4\Delta_\alpha^2}}\right). \qquad \text{(AIV.4)}$$

The parameters Δ_α and λ determining the solution are subject to the consistency of the definition of the Δ's:

$$\Delta_\alpha = \sum g_{\alpha\beta}U_\beta V_\beta = \tfrac{1}{2}\sum g_{\alpha\beta}\sqrt{1-\frac{(e_\beta-\lambda)^2}{(e-\lambda)^2+4\Delta_\beta^2}} = \sum\frac{g_{\alpha\beta}\Delta_\beta}{\sqrt{(e-\lambda)^2+4\Delta_\beta^2}}, \qquad \text{(AIV.5)}$$

and to the normalization of V (eq. (3.3)):

$$\tfrac{1}{2}\sum_\alpha\left(1-\frac{e_\alpha-\lambda}{\sqrt{(e-\lambda)^2+4\Delta_\alpha^2}}\right) = n. \qquad \text{(AIV.6)}$$

These equations are the same as those treated by Belyaev [6]). They admit a "normal" solution where n of the V_α's, those corresponding to lowest E_α's, are unity and the rest zero. (In this case $\Delta_\alpha = 0$ for all α and $E_n < \lambda < E_{n+1}$ counting E's in order of rising energy). Such a solution is a stationary state but the lowest energy belongs to a solution where Δ's differ from zero whenever such a solution exists.

In the case of a separable interaction — the one actually treated by the different authors as regards both the superconducting state and the Cooper state — the equations become simpler. Putting

$$g_{\alpha\beta} = -g_\alpha g_\beta, \qquad \text{(AIV.7)}$$

we get

$$\Delta_\alpha = -g_\alpha \sum g_\beta U_\beta V_\beta = -g_\alpha \delta, \tag{AIV.8}$$

δ being defined by

$$\delta = \sum g_\alpha U_\alpha V_\alpha. \tag{AIV.9}$$

The set of equations (AIV.5) now reduces to a single equation

$$\sum_\beta \frac{g_\beta^2}{\sqrt{(e_\beta - \lambda)^2 + 4\delta^2 g_\beta^2}} = 1 \tag{AIV.10}$$

and V_α^2 is given by

$$V_\alpha^2 = \tfrac{1}{2}\left(1 - \frac{e_\alpha - \lambda}{\sqrt{(e_\alpha - \lambda)^2 + 4\delta^2 g_\alpha^2}}\right). \tag{AIV.11}$$

For a constant matrix element $g_{\alpha\beta} = -G$ equations (AIV.10) and (AIV.11) reduce to (7.2) and (7.1) in the text. The variation of V_α^2 with e_α in this case is illustrated in fig. 4.

References

1) K. A. Brueckner, C. A. Levinson and H. Mahmoud, Phys. Rev. **95** (1954) 217;
K. A. Brueckner, Phys. Rev. **96** (1954) 508;
K. A. Brueckner and C. Levinson, Phys. Rev. **97** (1955) 1344;
K. A. Brueckner, Phys. Rev. **97** (1955) 1353
2) J. Bardeen, L. N. Cooper and J. R. Schrieffer, Phys. Rev. **108** (1957) 1175
3) H. A. Bethe and J. Goldstone, Proc. Roy. Soc. A **238** (1957) 551
4) L. N. Cooper, Phys. Rev. **104** (1956) 1189
5) K. Gottfried, unpublished
6) N. N. Bogoliubov, JETP **34**, **58**, **73** (1958);
N. N. Bogoliubov, Nuovo Cim. **7** (1958) 794;
Valatin, Nuovo Cim. **7** (1958) 843;
S. T. Belyaev, Mat. Fys. Medd. Dan. Vid. Selsk. **31**, No. 11;
S. T. Belyaev, The many-body problem (lectures given at Les Houches, 1958) (Dunod, Paris);
J. R. Schrieffer, ibid.
7) B. Mottelson, The many-body problem (Dunod, Paris 1958)
8) C. Bloch and C. De Dominicis, Nuclear Physics **10** (1959) 181, 509

1.D.1

Nuclear Physics **18** (1960) 196—223; © *North-Holland Publishing Co., Amsterdam*

Not to be reproduced by photoprint or microfilm without written permission from the publisher

SPIN-ORBIT SPLITTING AND TENSOR FORCE

AKITO ARIMA †

Physics Division, Argonne National Laboratory, Argonne, Illinois, USA ††

Received 25 April 1960

Abstract: The second-order effect of the tensor force is calculated in nuclei which have several nucleons outside closed shells. This second-order effect causes a modification of the first-order secular equation of the degenerate shell-model states $(nl)^p$, where nl is an orbit of the L-S coupling shell model and p is the number of nucleons outside closed shells. This modification is equivalent to the introduction (a) of a slight change in the one-particle energy, (b) of one-body spin-orbit interaction $\Sigma\xi\mathbf{s}_i\cdot\mathbf{l}_i$, (c) of effective nonlocal two- and three-body forces, and (d) of an energy depression that is common to all states. Here $\xi = C_0+(p-1)C_1$, where C_0 and C_1 are constant as long as the average potential of the shell model does not change. C_0 and C_1 are calculated in the (1p)-shell, and $C_0 \approx 4C_1$. The constant C_0 is about -1.0 to -1.5 MeV. In this numerical calculation, the harmonic-oscillator wave functions are adopted as individual wave functions, and either the tensor force suggested by meson theory or the phenomenological strong tensor force is assumed. It is very interesting to note that $\xi(N^{15})/\xi(He^5) \approx 3.5$.

If the three-body effect is neglected, the modified secular equation results in the intermediate-coupling shell-model Hamiltonian, provided that the two-body effective potential is replaced by the usual potential which has the same matrix elements as the effective one.

1. Introduction

The jj-coupling shell model and the optical model succeed in explaining many properties in the lower states of nuclei and the scattering of nucleons by nuclei [1, 2]). These models have averaged potentials with a strong spin-orbit interaction. Recently many attempts have been made to explain the origin of this interaction. They are divided into two groups, one of which attributes the interaction to a two-body spin-orbit interaction [3–8]) and the other to a strong tensor force [9–15]). In the second explanation, the Pauli principle plays a very important role, and one must also bear in mind that the potential suggested by meson theory involves a very strong tensor force [16]).

Almost all the papers cited above concerned nuclei which have one nucleon outside closed shells, because the experimental evidence for strong spin-orbit interaction is clearest for those nuclei. However, the jj-coupling shell model requires extension of this interaction beyond these simple nuclei [1]). It is interesting to investigate the second-order effect of the tensor force in more complicated nuclei. Let p be the number of nucleons in an orbit nl in the $L-S$ coupling shell model, and let this orbit be well separated in energy from

† On leave of absence from the Institute for Nuclear Study, University of Tokyo, Tanashi-machi, Tokyo, Japan. Permanent address after January 1961: Department of Physics, University of Tokyo, Tokyo, Japan.

†† Work performed under the auspices of the U.S. Atomic Energy Commission.

neighbouring orbits. There are many degenerate states which have the same total angular momentum J. Therefore the tensor force has non-vanishing matrix elements between these degenerate states in the first-order perturbation. Indeed, in first order, the tensor force plays an important role in explaining the long lifetime of the C^{14} decay [17–19]). The second-order effect also was estimated by Tamura [20]) and Feingold [21, 22]), the latter of whom has suggested the importance of the effective three-body spin-orbit interaction derived from the second-order closure approximation. In the customary perturbation method [23]), the secular equation of the degenerate states of $(nl)^p$ must first be solved and the eigenfunctions so obtained are used to calculate higher-order perturbations. However, in this paper the second-order effects are taken into consideration first, and these effects give the modification of the secular equation. This method was developed by Bloch and Horowitz [24]), and a rather similar method was used by Feingold [21, 22]) and by Bolsterli and Feenberg [25]). This modification is equivalent to introducing (a) a small change in the single-particle energy, (b) a one-body spin-orbit interaction, (c) non-local effective two- and three-body forces, and (d) an energy depression that is common to all states. Although only the expectation values of this spin-orbit interaction are involved, it is very interesting that there is such a $\xi \mathbf{s}\cdot\mathbf{l}$ interaction, because it seems to be difficult to derive the simple $\sum \xi \mathbf{s}_i\cdot\mathbf{l}_i$ from the tensor force. As will be shown in section 3, this ξ is written as

$$\xi = C_0 + (p-1)C_1,$$

where p is the number of nucleons outside closed shells, and C_0 and C_1 are constant if the shell-model potential does not change from nucleus to nucleus. The values of C_0 and C_1 for (1p)-nuclei are calculated numerically in section 3, where harmonic-oscillator wave functions are assumed as individual wave functions and the method developed in papers I and II (refs. [14, 15])) is used. For (1p)-nuclei

$$C_0 \approx 4C_1,$$

so that

$$\xi \approx \{1+\tfrac{1}{4}(p-1)\}C_0.$$

The constant C_0 depends on the intensity, exchange character, and radial shape of the tensor force and is also sensitive to the extent of the wave function. Two kinds of tensor force are used. They are the phenomenological tensor force of the Gaussian radial dependence, which has the Serber type of exchange character [26]), and the tensor force given by meson theory [16]). For these nuclei, C_0 is about -1.0 to -1.5 MeV; and C_1 itself is small, but $(p-1)$ becomes 10 in N^{15} and O^{15}. Therefore ξ becomes about -3.5 to -5.0 MeV. According to Kurath's results for the intermediate-coupling model, ξ seems to be about twice as large

at the end of the shell as at the beginning [27, 28]). In our case, as long as the averaged shell-model potential is constant,

$$\xi(N^{15})/\xi(He^5) \approx 3.5.$$

This figure is too large. However, it must be noticed that the average potential changes and that there are effective two-body spin-dependent forces, the dependence of which is the same as that of the two-body spin-orbit interaction. This cancels part of the one-body effect. According to Feingold [21, 22]), the sign of his effective two-body interaction is opposite to that of the phenomenological one suggested, for example, by Elliott and Lane [3]).

The nuclear binding energies are analysed by many authors on the simple assumptions that (a) the averaged well does not change in the nuclei belonging to the same unfilled shell, and (b) general two-body interactions operate between pairs of particles [29]). These simple assumptions give good agreement with the observed binding energies, especially in the $2s_{\frac{1}{2}}$ and $1d_{\frac{3}{2}}$ shells. On the same assumptions, the spectrum of Cl^{38} can be calculated by the parameters which express the integrals of the two-body interaction and can be estimated from the K^{40} spectrum [30]). The agreement with the observed spectrum is very good. Because of such evidence, it is unlikely that three-body interaction has a large effect [31]). In the (1p) shell nuclei, the above simple model does not succeed, and Feingold suggests that the three-body effect may be important for these. However, for nuclei in this region, the intermediate-coupling approximation is inevitably necessary [27, 32]) so that it is not clear what the source of the disagreement is. A three-body effect appears in our calculation, but the important question of its relative size is still unanswered. According to Lyons [33]) and Feingold [22]), the three-body potential derived by the closure approximation is too small to explain the multiplet splitting in the spectra of Li^6 and Li^7. These two-body and threebody effective potentials will be estimated in the next paper.

If this three-body effect can be neglected, and the effective two-body interaction is replaced by the usual two-body interaction which has the same matrix elements as the effective one, the usual intermediate-coupling shell-model Hamiltonian is obtained [27, 28, 32]). This Hamiltonian consists of the jj-coupling shell-model Hamiltonian and two-body forces between nucleons in the (nl)-orbit of the $L-S$ coupling shell model.

There is some doubt about the explanation of the spin-orbit interaction by the tensor force †). By the supermultiplet theory, the $B^{12} \rightarrow C^{12}$ transition is

† The author would like to express his sincere thanks to Professor E. P. Wigner for his kind correspondence and for pointing out this problem. Professor Wigner mentioned that the expectation value of the energy of tensor force is the same for the two semi-closed shells and is strongly attractive [9]). Here, a semi-closed shell contains all orbits filled with $j = l + \frac{1}{2}$ or all orbits filled with $j = l - \frac{1}{2}$. Since the expectation value is zero for the complete closed shell, the interaction between the two semi-shells must be repulsive. Hence, the tensor force in first approximation gives a self-stabilization of the semi-shells. In addition, it is shown in this paper that the strength of the spin-

forbidden and in first-order perturbation, the tensor force cannot mix the states which can decay into the ground state of C^{12}. The experimental lifetime of B^{12} is very short. However, the one-body spin-orbit interaction may explain this transition, according to Flamand and Ford [35]†; thus, at least qualitatively, the second-order effect of the tensor force offers another possible solution. The numerical calculation will be reported in the next paper.

2. Derivation of the Effective Potential

The total Hamiltonian of the nuclear system is given by

$$H = -\sum_i \frac{\hbar^2}{2m}\nabla_i^2 + \sum_{i>j} V_C(\mathbf{r}_{ij}) + \sum_{i>j} V_T(\mathbf{r}_{ij}), \tag{2.1}$$

where m is the mass of a nucleon, and V_C and V_T are the central and tensor part of the two-body potential, respectively. As the zeroth order in perturbation theory, the Hamiltonian for the $L-S$ coupling shell model is taken,

$$H_0 = -\sum\left\{\frac{\hbar^2}{2m}\nabla_i^2 + U(r_i)\right\}, \tag{2.2}$$

with

$$H_0\psi_n = E_n^{(0)}\psi_n, \tag{2.3}$$

where $U(r_i)$ is the average potential, and ψ_n is the wave function of the nth state, the energy of which is $E_n^{(0)}$. Then

$$H = H_0 + H_1 \tag{2.4}$$

and

$$H_1 = \sum_{i>j} V_C(\mathbf{r}_{ij}) + \sum_{i>j} V_T(\mathbf{r}_{ij}) - \sum_i U(r_i). \tag{2.5}$$

This brings in the problem of centre-of-mass motion which is inherent in the shell model, and the separation of the centre-of-mass coordinates is important, particularly in the light nuclei. If the harmonic-oscillator well is adopted as $U(r)$, a procedure developed by Bolsterli and Feenberg [25] avoids the complicated problem of the separation of the centre-of-mass coordinates. However, in the following, this problem is not discussed further.

In this paper, let us consider several (p) nucleons in a shell model orbit nl which is well separated in energy from neighbouring orbits. This is the case of

orbit interaction found in the second-order perturbation increases with the number of nucleons in the unfilled level. This tendency gives also a stabilization of the semi-shells. This may be responsible for the fact that the jj-coupling model is more accurate toward the end of the semi-shell than at its beginning.

† The author wishes to thank Dr. D. Kurath for calling his attention to this work and for helpful discussions of it.

the (1p)-shell nuclei. However, it would be possible to extend the same calculations as in the following to the case of many orbits, the energies of which are the same or almost the same. There are several degenerate states with the same isobaric spin T and the same total angular momentum J belonging to the configuration $(nl)^p$.

In the $L-S$ coupling scheme, the wave function of these states is

$$\psi_{0\gamma}(TJ)$$
$$= |(n_1 l_1)^{8l_1+4}(000)(n_2 l_2)^{8l_2+4}(000)\ldots(n_k l_k)^{8l_k+4}(000)(nl)^p(\alpha TSL)TJ;T_z J_z\rangle, \quad (2.6)$$

where (000) means that the resultant isobaric spin T, the spin S and the angular momentum L are all zero; $n_1 l_1$, $n_k l_k$ are principal and azimuthal quantum numbers of the closed shells; α is some quantum number; J is the total spin,

$$J = S+L$$

whose z-component is J_z; T_z is the z-component of T; and γ means all quantum numbers (αTSL).

Between these states, the perturbation Hamiltonian has non-diagonal matrix elements. Then, in the customary perturbation method, the secular equation of these degenerate states must first be solved and the eigenfunctions so obtained are used to calculate higher order perturbation [23]). However, in the following another procedure is employed. This method was developed by Bloch and Horowitz [24]) and a similar method was used by Bolsterli and Feenberg [25]) and by Feingold [21, 22]). According to Bloch and Horowitz, the perturbation energies are divided into two contributions. One of them, ΔE_c, comes from the excited states of the closed shell and this is given by the customary perturbation theory. The other energy concerns the degenerate states and is evaluated by diagonalizing the secular equation

$$\left| (\varepsilon - E_0^{(0)})\delta(\gamma,\gamma') - \langle\psi_{0\gamma}|H_1|\psi_{0\gamma'}\rangle - \sum_n \frac{\langle\psi_{0\gamma}|H_1|n\rangle\langle n|H_1|\psi_{0\gamma'}\rangle}{\varepsilon - E_n^{(0)}} \right| = 0, \quad (2.7)$$

where effects beyond third order are neglected, and all $\psi_{0\gamma}$ have the same energy $E_0^{(0)}$ in the zeroth order. In this expression, $|n\rangle$ stands for the wave functions of the higher excited states with energies $E_n^{(0)} > E_0^{(0)}$. If ε_k means the kth solution of this secular equation, the total energy of this state is given by the equation

$$E_k = \varepsilon_k + \Delta E_c.$$

Among the excited states in eq. (2.7), the states in which the closed shell is excited must be omitted, and they only contribute to ΔE_c. However, some states in which the nucleons are excited from the closed shells into the orbit nl must be included in $|n\rangle$, because the excited nucleons should be correlated with the nucleons in the (nl)-orbit so as to satisfy the Pauli principle. It has been

shown that these states have an important effect on the doublet splitting of the nuclei with a closed shell plus one nucleon [12–15]).

In the above secular equation, the last sum gives the modification of the usual first-order secular equation due to the second-order perturbation. Feingold has estimated this sum by the closure approximation, but he was concerned only with the effective two-body and three-body forces [21, 22]). Because the closure approximation does not seem to be good, this modification has to be evaluated with more precision. In this paper the perturbation effect due to the tensor force is calculated, because the central interaction does not give any spin-dependent result. Therefore, in the following the quantity

$$\mathscr{V}_{\gamma'\gamma} = \sum \frac{\langle \psi_{0\gamma'} | \sum_{i>j} V_T(\mathbf{r}_{ij}) | n \rangle \langle n | \sum_{i>j} V_T(\mathbf{r}_{ij}) | \psi_{0\gamma} \rangle}{E_0^{(0)} - E_n^{(0)}} \tag{2.8}$$

is calculated for excited configurations of various types; ε is replaced by $E_0^{(0)}$, provided that $|\varepsilon - E_0| \ll |E_0^{(0)} - E_n^{(p)}|$. This condition is somewhat questionable for the lowest excited states; however, for the present it is assumed to be satisfied.

The tensor potential is written as

$$V_T(\mathbf{r}_{ij}) = (a + b\boldsymbol{\tau}_i \cdot \boldsymbol{\tau}_j) S_{ij} V(r_{ij}),$$

where a and b are constants, $\boldsymbol{\tau}_i$ the isobaric spin operator, $V(r_{ij})$ the radial part of the potential, and $S_{ij} = 3\boldsymbol{\sigma}_i \cdot \mathbf{r}_{ij} \boldsymbol{\sigma}_j \cdot \mathbf{r}_{ij}/r_{ij}^2 - \boldsymbol{\sigma}_i \cdot \boldsymbol{\sigma}_j$, the $\boldsymbol{\sigma}$'s being Pauli spin operators. For convenience, $S_{ij} V(r_{ij})$ is rewritten as

$$S_{ij} V(r_{ij}) = (S^{(2)} \cdot L^{(2)}),$$

where

$$S_m^{(2)} = [\boldsymbol{\sigma}_i \cdot \boldsymbol{\sigma}_j]_m^{(2)}$$

and

$$L_m^{(2)} = (\tfrac{24}{5}\pi)^{\frac{1}{2}} Y_{2m}(\theta, \phi) V(r),$$

where $(r\theta\phi)$ are the relative coordinates of $\mathbf{r}_i$ and $\mathbf{r}_j$. Through the usual tensor calculus developed by Racah, the two-body matrix elements of the tensor potential become

$$\begin{aligned} &\langle l'_1 l'_2 T S' L'; JM | V_T | l_1 l_2 T S L; JM \rangle \\ &\quad = (-1)^{S'+L-J} W(S' L' S L; J2) \langle l'_1 l'_2 S' L' || S^{(2)} L^{(2)} || l_1 l_2 S L \rangle \Phi_\tau(T), \end{aligned} \tag{2.9}$$

where $l_1(l'_1)$ and $l_2(l'_2)$ are the angular momenta of two single particles and are coupled to make the state which has total isobaric spin T, total intrinsic spin $S(S')$ and total angular momentum $L(L')$; and $\Phi_\tau(T)$ is the expectation value of $a + b\boldsymbol{\tau}_1 \cdot \boldsymbol{\tau}_2$ in the state with isobaric spin T.

The excited states ψ_n, which can mix with the shell-model wave function (2.6) in the first-order perturbation, must not have more than two single-particle orbits different from the states (2.6).

I. The excited states in which the nucleons are excited from the core into empty orbits other than the nl orbit will be treated first. They are

$$\psi_{\mathrm{I_a}\,n} = |[\{(n_i l_i)^{8l_i+2}(T_1 1L_1)(n'_i l'_i, n''_i l''_i)(T_1 1L_2)\} \cdot (022)(nl)^p(\alpha TSL)](TS_3L_3)TJ; T_z J_z\rangle \quad (2.10a)$$

and

$$\psi_{\mathrm{I_b}\,n} = |[[\{(n_i l_i)^{8l_i+3}(\tfrac{1}{2}\,\tfrac{1}{2}\,l_i)(n_j l_j)^{8l_j+3}(\tfrac{1}{2}\,\tfrac{1}{2}\,l_j)\}(T_1 1L_1)(n'_i l'_i, n'_j l'_j)(T_1 1L_2)] \cdot (022)(nl)^p(\alpha TSL)](TS_3L_3)TJ; T_z J_z\rangle, \quad (2.10b)$$

which are graphically shown in figs. 1a and 1b. In these equations the resultant spin of $(n'_i l'_i, n''_i l''_i)$ and $(n'_i l'_i, n'_j l'_j)$ must be unity, because the tensor force

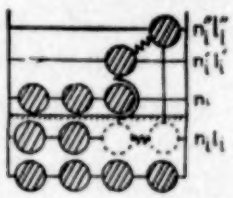

1a

Fig. 1a. Excited configuration Ia.

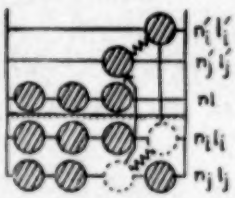

1b

Fig. 1b. Excited configuration Ib.

vanishes in the spin singlet state. These states contribute only to ΔE_c. They are easily estimated and the result is

$$\Delta E_{\mathrm{I_a}} = \sum \frac{1}{E_0^{(0)} - E_n^{(0)}} \tfrac{1}{5} \sum (2T_1+1) \cdot \langle n'_i l'_i n''_i l''_i 1L_2 || S^{(2)} L^{(2)} || n_i l_i n_i l_i 1L_1\rangle^2 \Phi_\tau^2(T_1)\delta(\gamma, \gamma'), \quad (2.11a)$$

$$\Delta E_{\mathrm{I_b}} = \sum \frac{1}{E_0^{(0)} - E_n^{(0)}} \tfrac{1}{5} \sum (2T_1+1) \cdot \langle n'_i l'_i n'_j l'_j 1L_2 || S^{(2)} L^{(2)} || n_i l_i n_j l_j 1L_1\rangle^2 \Phi_\tau^2(T_1)\delta(\gamma, \gamma'), \quad (2.11b)$$

where all two-body wave functions $|n_\alpha l_\alpha n_\beta l_\beta TSL\rangle = |n_\alpha l_\alpha n_\beta l_\beta SL\rangle\chi(T, T_z)$ should be antisymmetrized. These energies are all the same as in paper II where these configuration mixings are called the self-deformation of the closed-shell core.

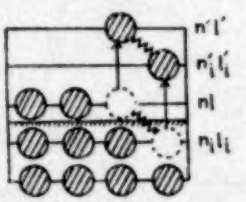

Fig. 2a. Excited configuration IIa.

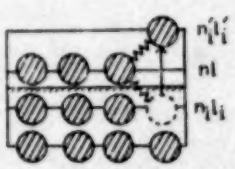

Fig. 2b. Excited configuration IIb.

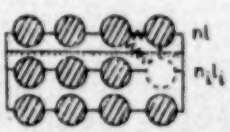

Fig. 2c. Excited configuration IIc.

IIa. A nucleon in the core can interact with a nucleon in the orbit nl, so that both of them jump into higher orbits. (see fig. 2a). These intermediate states are given by

$$\psi_{\mathrm{IIa}n} = |[\{(n_il_i)^{8l_i+3}(\tfrac{1}{2}\,\tfrac{1}{2}\,l_i)n'_il'_in'l'(T_1L_1)\} \cdot (T_2S_2L_2)(nl)^{p-1}(\beta T_3S_3L_3)](TS_4L_4)TJ;\, T_zJ_z\rangle. \quad (2.12a)$$

This kind of states contributes to $\mathscr{V}_{\gamma'\gamma}$ which thereby becomes

$$\begin{aligned}\mathscr{V}_{\mathrm{IIa}\gamma'\gamma} = {} & \frac{p}{5(8l+4)} \sum \frac{1}{E_0^{(0)} - E_n^{(0)}} \sum (2T_1+1) \\ & \cdot \langle n'_il'_in'l'\,1L_1||S^{(2)}L^{(2)}||n_il_inl1L'_1\rangle^2 \Phi_\tau^{\,2}(T_1)\delta(\gamma',\gamma) \qquad (2.13a) \\ & + \langle (nl)^p\alpha' TS'L';\, TJ;\, T_zJ_z|\sum_{i=1}^{p}\mathbf{s}_i\cdot\mathbf{l}_i|(nl)^p\alpha TSL,\, TJ;\, T_zJ_z\rangle C_{\mathrm{IIa}},\end{aligned}$$

where

$$\begin{aligned} C_{\mathrm{IIa}} = {} & -\tfrac{3}{2}\{2\cdot 3\cdot 5l(l+1)(2l+1)\}^{-\frac{1}{2}} \sum \frac{1}{E_0^{(0)} - E_n^{(0)}} \sum (-1)^{L'_1+\bar{L}'_1} \\ & \times (2T_1+1)\{(2L'_1+1)(2\bar{L}'_1+1)\}^{\frac{1}{2}} \\ & \times W(l_iL'_1l1;\, l\bar{L}'_1)W(L_1L'_121;\, 2\bar{L}'_1) \qquad (2.14a) \\ & \times \langle n'_il'_in'l'\,1L_1||S^{(2)}L^{(2)}||n_il_inl1L'_1\rangle \\ & \times \langle n'_il'_in'l'\,1L_1||S^{(2)}L^{(2)}||n_il_inl1\bar{L}'_1\rangle \Phi_\tau^{\,2}(T_1), \end{aligned}$$

provided that $n'_il'_i$ and $n'l'$ do not coincide with n_il_i and nl. The first term makes a slight change in the single-particle energy. It is very interesting to note that the second term is proportional to the matrix element of the one-body spin-orbit interaction, and therefore is diagonal in the jj-couupling representation.

IIb. In (2.12a), there is the case in which $n'l'$ can coincide with nl, i.e.,

$$\psi_{\mathrm{IIb}n} = |[(n_il_i)^{8l_i+3}(\tfrac{1}{2}\,\tfrac{1}{2}\,l_i)\{n'_il'_i(nl)^p(\beta T_1S_1L_1)\}(T_2S_2L_2)] \cdot (TS_3L_3)TJ;\, T_zJ_z\rangle, \quad (2.12b)$$

which is shown graphically in fig. 2b. For this situation $\mathscr{V}_{\mathrm{IIb}\gamma'\gamma}$ becomes

$$\begin{aligned}\mathscr{V}_{\mathrm{IIb}\gamma'\gamma} = {} & \sum \frac{1}{E_0^{(0)} - E_n^{(0)}} \left(1 - \frac{p-1}{8l+4}\right) \frac{p}{5(8l+4)} \sum (2T_4+1) \\ & \cdot \langle n'_il'_inl1L_4||S^{(2)}L^{(2)}||n_il_inl1L'_4\rangle^2 \Phi_\tau^{\,2}(T_4)\delta(\gamma,\gamma') \\ & + \langle (nl)^p\alpha' TS'L',\, TJ;\, T_zJ_z|\sum_{i=1}^{p}\mathbf{s}_i\cdot\mathbf{l}_i|(nl)^p\alpha TSL,\, TJ;\, T_zJ_z\rangle C_{\mathrm{IIb}} \qquad (2.13b) \\ & + \langle (nl)^p\alpha' TS'L',\, TJ;\, T_zJ_z|\sum_{i>j} V_{ij}^{\mathrm{IIb}}|(nl)^p\alpha TSL,\, TJ;\, T_zJ_z\rangle,\end{aligned}$$

where

$$C_{\mathrm{IIb}} = -\tfrac{3}{2}\{2\cdot 3\cdot 5l(l+1)(2l+1)\}^{-\frac{1}{2}}\left(1-\frac{p-1}{8l+4}\right)\sum\frac{1}{E_0^{(0)}-E_n^{(0)}}\sum(-1)^{L'_5+\bar{L}'_5}$$
$$\cdot(2T_5+1)\{(2L'_5+1)(2\bar{L}'_5+1)\}^{\frac{1}{2}}$$
$$\times W(l_i L'_5 l1; l\bar{L}'_5)W(L_5 L'_5 21;\ 2\bar{L}'_5)\langle n'_i l'_i nl1L_5||S^{(2)}L^{(2)}||n_i l_i nl1L'_5\rangle$$
$$\times\langle n'_i l'_i nl1L_5||S^{(2)}L^{(2)}||n_i l_i nl1\bar{L}'_5\rangle\Phi_\tau^{\,2}(T_5)$$
$$+\frac{p-1}{8l+4}\tfrac{3}{2}\{2\cdot 3\cdot 5l(l+1)(2l+1)\}^{-\frac{1}{2}}\sum\frac{1}{E_0^{(0)}-E_n^{(0)}}\sum(-1)^{L_5+\bar{L}_5} \qquad (2.14\mathrm{b})$$
$$\cdot(2T_5+1)\{(2L_5+1)(2\bar{L}_5+1)\}^{\frac{1}{2}}$$
$$\times W(l'_i L_5 l1; l\bar{L}_5)W(L'_5 L_5 21;\ 2\bar{L}_5)\langle n_i l_i nl1L'_5||S^{(2)}L^{(2)}||n'_i l'_i nl1L_5\rangle$$
$$\times\langle n_i l_i nl1L'_5||S^{(2)}L^{(2)}||n'_i l'_i nl1\bar{L}_5\rangle\Phi_\tau^{\,2}(T_5),$$

and V_{ij}^{IIb} is the effective two-body interaction which is given in the appendix. In the first term of (2.13b) the part that is proportional to p gives a slight increase in the single-particle energy, and the part proportional to $p(p-1)$ expresses the two-body effect, which depends only on the number of nucleons in the (nl) orbit. In (2.14b), C_{IIb} has also terms proportional to $(p-1)$, which come from the two-body effect again and are diagonal in the jj representation.

IIc. In (2.12a) $n'_i l'_i$ and $n'l'$ can coincide with nl (fig. 2c), i.e.,

$$\psi_{\mathrm{IIc}} = |\{(n_i l_i)^{8l_i+3}(\tfrac{1}{2}\,\tfrac{1}{2}\,l_i)(nl)^{p+1}(\beta T_1 S_1 L_1)\}(TS_2 L_2)TJ;\ T_z J_z\rangle. \qquad (2.12\mathrm{c})$$

The derivation of $\mathscr{V}_{\mathrm{IIc}\gamma'\gamma}$ for this case requires a long and tedious calculation, some details of which are given in the appendix. The result is

$$\mathscr{V}_{\mathrm{IIc}\gamma'\gamma} = \sum\frac{1}{E_0^{(0)}-E_n^{(0)}}\left\{1-\frac{2(p-1)}{8l+4}\right\}\frac{p}{5(8l+4)}\sum(2T_4+1)$$
$$\cdot\langle nlnl1L_4||S^{(2)}L^{(2)}||n_i l_i nl1L'_4\rangle^2\Phi_\tau^{\,2}(T_4)\delta(\gamma,\gamma')$$
$$+\langle(nl)^p\alpha' TS'L', TJ;T_z J_z|\sum_{i=1}^{p}\mathbf{s}_i\cdot\mathbf{l}_i|(nl)^p\alpha TSL, TJ;T_z J_z\rangle C_{\mathrm{IIc}} \qquad (2.13\mathrm{c})$$
$$+\langle(nl)^p\alpha' TS'L', TJ;T_z J_z|\sum_{i>j>k}V_{ijk}^{\mathrm{IIc}}+\sum_{i>j}V_{ij}^{\mathrm{IIc}}|(nl)^p\alpha TSL, TJ;T_z J_z\rangle,$$

where

$$C_{\mathrm{IIc}} = -\tfrac{3}{2}\{2\cdot 3\cdot 5l(l+1)(2l+1)\}^{-\frac{1}{2}}\cdot\left\{1-\frac{2(p-1)}{8l+4}\right\}\sum\frac{1}{E_0^{(0)}-E_n^{(0)}}\sum(-1)^{L'_4+\bar{L}'_4}$$
$$\cdot(2T_4+1)\{(2L'_4+1)(2\bar{L}'_4+1)\}^{\frac{1}{2}}$$
$$\times W(l_i L'_4 l1; l\bar{L}'_4)W(L_4 L'_4 21;2\bar{L}'_4)\langle nlnl1L_4||S^{(2)}L^{(2)}||n_i l_i nl1L'_4\rangle \qquad (2.14\mathrm{c})$$
$$\times\langle nlnl1L_4||S^{(2)}L^{(2)}||n_i l_i nl1\bar{L}'_4\rangle\Phi_\tau^{\,2}(T_1)$$
$$+\frac{2(p-1)}{8l+4}\tfrac{3}{2}\{2\cdot 3\cdot 5l(l+1)(2l+1)\}^{-\frac{1}{2}}\sum\frac{1}{E_0^{(0)}-E_n^{(0)}}\sum(2T_4+1)(2L'_4+1)$$
$$\times W(lL'_4 l1;lL'_4)W(L_4 L'_4 21;\ 2L'_4)\langle nlnl1L'_4||S^{(2)}L^{(2)}||n_i l_i nl1L_4\rangle^2\Phi_\tau^{\,2}(T_4).$$

The effective three-body and two-body interactions V_{ijk}^{IIc} and V_{ij}^{IIc} are given in the appendix.

The mixed configurations considered in IIa, IIb and IIc are called "the induced deformation of the closed core," because the mixings of this type are induced by the mutual interaction between the outside nucleons and the closed-shell core. Numerically speaking, $C_{\mathrm{IIa}}+C_{\mathrm{IIb}}+C_{\mathrm{IIc}}$ is small or even of opposite sign to the observed doublet splitting [36]) when $p=1$. However, Terasawa, Arima, and Takagi, Watari and Yasuno found other important excited states which give the desired contributions to the explanation of the doublet splitting by the Pauli principle [12, 14, 15]). If the Pauli principle is ignored in Ia and Ib, the nucleons can be excited from the closed shells into the outermost orbit (nl) by the mutual interaction without limitation, and these excited states only depress the total binding energy by the same amount as in the closed-shell nucleus. However, it has been shown that this exclusion effect is important for the doublet splitting.

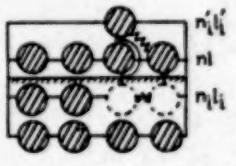

Fig. 3a. Excited configuration IIIa.

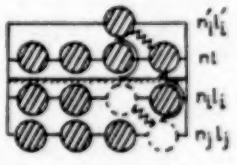

Fig. 3b. Excited configuration IIIb.

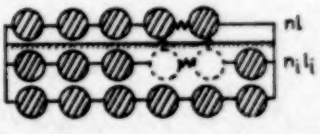

Fig. 3a′. Excited configuration IIIa′.

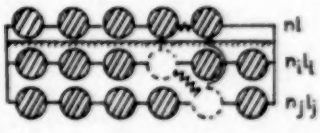

Fig. 3b′. Excited configuration IIIb′.

IIIa. When $n_i''l_i''$ coincide with nl in (2.10a), (fig. 3a), the intermediate states are given by the wave functions

$$\psi_{\mathrm{IIIa}n}=|\{(n_il_i)^{8l_i+2}(T_1 1L_1)[n'_il'_i(nl)^{p+1}(\beta T_2S_2L_2)](T_3S_3L_3)\}\cdot(TS_4L_4)TJ;T_zJ_z\rangle. \quad (2.15a)$$

Then, after a simple calculation, which will be sketched in the appendix,

$$\mathscr{V}_{\mathrm{IIIa}\gamma'\gamma}=\sum\frac{1}{E_0^{(0)}-E_n^{(0)}}\frac{1}{5}\left(1-\frac{p}{8l+4}\right)\sum(2T_1+1)\cdot\langle n'_il'_inl1L'_1||S^{(2)}L^{(2)}||n_il_in_il_i1L_1\rangle^2\Phi_\tau^2(T_1)\delta(\gamma,\gamma') \quad (2.16a)$$

$$+\langle(nl)^p(\alpha'TS'L')TJ;T_zJ_z|\sum_{i=1}^{p}\mathbf{s}_i\cdot\mathbf{l}_i|(nl)^p(\alpha TSL)TJ;T_zJ_z\rangle C_{\mathrm{IIIa}},$$

where

$$C_{\mathrm{IIIa}}=\tfrac{3}{2}\{2\cdot 3\cdot 5l(l+1)(2l+1)\}^{-\frac{1}{2}}\sum\frac{1}{E_0^{(0)}-E_n^{(0)}}\sum(-1)^{L'_1+\bar{L}'_1}\{(2L'_1+1)(2\bar{L}'_1+1)\}^{\frac{1}{2}}$$
$$\times W(l'_i L'_1 l1; l\bar{L}'_1)W(L_1 L'_1 21; 2\bar{L}'_1)\langle n_i l_i n_i l_i 1L_1||S^{(2)}L^{(2)}||n'_i l'_i nl1L'_1\rangle$$
$$\times\langle n_i l_i n_i l_i 1L_1||S^{(2)}L^{(2)}||n'_i l'_i nl1\bar{L}'_1\rangle\Phi_\tau^2(T_1). \qquad (2.17a)$$

Equations (2.16a) and (2.17a) correspond to (2.13) in paper II.

IIIb. When $n_j l_j$ coincide with nl in (2.10b), (fig. 3b), the wave functions become

$$\psi_{\mathrm{IIIb}n}=|[\{(n_i l_i)^{8l_i+3}(\tfrac{1}{2}\,\tfrac{1}{2}\,l_i)(n_j l_j)^{8l_j+3}(\tfrac{1}{2}\,\tfrac{1}{2}\,l_j)\}(T_1 1L_1)$$
$$\cdot\{n'_i l'_i(nl)^{p+1}(\beta T_2 S_2 L_2)\}(T_3 S_3 L_3)](TS_4 L_4), TJ; T_z J_z\rangle; \quad (2.15b)$$

and hence

$$\gamma_{\mathrm{IIIb}\gamma'\gamma}=\sum\frac{1}{E_0^{(0)}-E_n^{(0)}}\tfrac{1}{5}\left(1-\frac{p}{8l+4}\right)\sum(2T_1+1)$$
$$\cdot\langle n'_i l'_i nl1L'_1||S^{(2)}L^{(2)}||n_i l_i n_i l_i 1L_1\rangle^2\Phi_\tau^2(T_1)\delta(\gamma,\gamma') \qquad (2.16b)$$
$$+\langle(nl)^p(\alpha' TS'L')TJ; T_z J_z|\sum_{i=1}^{p}\mathbf{s}_i\cdot\mathbf{l}_i|(nl)^p(\alpha TSL)TJ; T_z J_z\rangle C_{\mathrm{IIIb}},$$

where

$$C_{\mathrm{IIIb}}=\tfrac{3}{2}\{2\cdot 3\cdot 5l(l+1)(2l+1)\}^{-\frac{1}{2}}\sum\frac{1}{E_0^{(0)}-E_n^{(0)}}\sum(-1)^{L'_1+\bar{L}'_1}$$
$$\cdot(2T_1+1)\{(2L'_1+1)(2\bar{L}'_1+1)\}^{\frac{1}{2}} \qquad (2.17b)$$
$$\times W(l'_i L'_1 l1; l\bar{L}'_1)W(L_1 L'_1 21; 2\bar{L}'_1)\langle n_i l_i n_j l_j 1L_1||S^{(2)}L^{(2)}||n'_i l'_i nl1L'_1\rangle$$
$$\times\langle n_i l_i n_j l_j 1L_1||S^{(2)}L^{(2)}||n'_i l'_i nl1\bar{L}'_1\rangle\Phi_\tau^2(T_1).$$

Equations (2.16b) and (2.17b) correspond to (2.15) in paper II.

IIIa′. In (2.10a) or (2.10b), both nucleons excited from the core can jump into the orbit nl, and excited states of this kind (fig. 3a′) are written as

$$\psi_{\mathrm{IIIa}'n}=|\{(n_i l_i)^{8l_i+2}(T_1 1L_1)(nl)^{p+2}(\beta T_2 S_2 L_2)\}(TS_3 L_3)TJ; T_z J_z\rangle. \quad (2.15c)$$

This contribution is

$$\gamma_{\mathrm{IIIa}'\gamma'\gamma}=\sum\frac{1}{E_0^{(0)}-E_n^{(0)}}\tfrac{1}{5}\left(1-\frac{2p}{8l+4}\right)\sum(2T_1+1)$$
$$\cdot\langle nlnl1L'_1||S^{(2)}L^{(2)}||n_i l_i n_i l_i 1L_1\rangle^2\Phi_\tau^2(T_1)\delta(\gamma,\gamma') \qquad (2.16c)$$
$$+\langle(nl)^p(\alpha' TS'L')TJ; T_z J_z|\sum_{i=1}^{p}\mathbf{s}_i\cdot\mathbf{l}_i|(nl)^p(\alpha TSL)TJ; T_z J_z\rangle C_{\mathrm{IIIa}'}$$
$$+\langle(nl)^p(\alpha' TS'L')TJ; T_z J_z|\sum_{i>j}V_{ij}^{\mathrm{IIIa}'}|(nl)^p(\alpha TSL)TJ; T_z J_z\rangle.$$

where

$$C_{\mathrm{IIIa}'} = 3\{2\cdot 3\cdot 5l(l+1)(2l+1)\}^{-\frac{1}{2}}\sum\frac{1}{E_0^{(0)}-E_n^{(0)}}\sum$$
$$\cdot(2T_1+1)(2L'_1+1)W(lL'_1l1;lL'_1) \qquad (2.17c)$$
$$\times W(L_1L'_121;2L'_1)\langle nlnl1L'_1||S^{(2)}L^{(2)}||n_il_in_il_i1L_1\rangle^2\Phi_\tau^2(T_1),$$

and $V_{ij}^{\mathrm{IIIa}'}$ will be shown in the appendix.

IIIb′. The intermediate states (fig. 3b′)

$$\psi_{\mathrm{IIIb}'n} = |[\{(n_il_i)^{8l_i+3}(\tfrac{1}{2}\,\tfrac{1}{2}\,l_i)(n_jl_j)^{8l_j+3}(\tfrac{1}{2}\,\tfrac{1}{2}\,l_j)\}$$
$$\cdot(T_11L_1)(nl)^{p+2}(\beta T_2S_2L_2)](TS_3L_3),TJ;T_zJ_z\rangle \qquad (2.15d)$$

give the result

$$\mathscr{V}_{\mathrm{IIIb}'\gamma'\gamma} = \sum\frac{1}{E_0^{(0)}-E_n^{(0)}}\frac{1}{5}\left(1-\frac{2p}{8l+4}\right)\sum(2T_1+1)$$
$$\cdot\langle nlnl1L_1||S^{(2)}L^{(2)}||n_il_in_jl_j1L_1\rangle^2\Phi_\tau^2(T_1)\delta(\gamma,\gamma') \qquad (2.16d)$$
$$+\langle(nl)^p(\alpha'TS'L')TJ;T_zJ_z|\sum_{i=1}^{p}\mathbf{s}_i\cdot\mathbf{l}_i|(nl)^p(\alpha TSL)TJ;T_zJ_z\rangle C_{\mathrm{IIIb}'}$$
$$+\langle(nl)^p(\alpha'TS'L')TJ;T_zJ_z|\sum_{i>j}V_{ij}^{\mathrm{IIIb}'}|(nl)^p(\alpha TSL)TJ;T_zJ_z\rangle,$$

where

$$C_{\mathrm{IIIb}'}=3\{2\cdot3\cdot5l(l+1)(2l+1)\}^{-\frac{1}{2}}\sum\frac{1}{E_0^{(0)}-E_n^{(0)}}\sum(2T_1+1)(2L'_1+1)W(lL'_1l1;lL'_1)$$
$$\times W(L_1L'_121;2L'_1)\langle nlnl1L'_1||S^{(2)}L^{(2)}||n_il_in_jl_j1L_1\rangle^2\Phi_\tau^2(T_1), \qquad (2.17d)$$

while $V_{ij}^{\mathrm{IIIb}'}$ will be given in the appendix.

IVa. There are new kinds of excited states which did not appear in nuclei with a closed shell plus one nucleon. They have the configurations in which one or two nucleons jump from the unfilled orbit nl into higher empty orbits. At first two nucleons are excited so that

$$\psi_{\mathrm{IVa}n} = |\{(nl)^{p-2}(\beta T_1S_1L_1)n_1l_1n_2l_2(T_21L_2)\}(TS_3L_3),TJ;T_zJ_z\rangle, \qquad (2.18a)$$

which is shown graphically in fig. 4a. In this case, $\mathscr{V}_{\mathrm{IVa}\gamma'\gamma}$ becomes

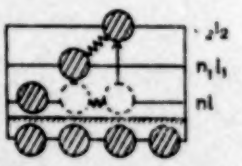

Fig. 4a. Excited configuration IVa.

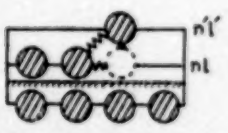

Fig. 4b. Excited configuration IVb.

$$\mathscr{V}_{\mathrm{IVa}\gamma'\gamma} = \langle(nl)^p(\alpha'TS'L')TJ;T_zJ_z|\sum_{i>j}V_{ij}^{\mathrm{IVa}}|(nl)^p(\alpha TSL)TJ;T_zJ_z\rangle, \qquad (2.19a)$$

where V_{ij}^{IVa} is again the effective two-body potential and will be given in the appendix.

IVb. Finally there is the case in which one nucleon jumps from the nl-orbit. This kind of intermediate state (fig. 4b) is expressed by the wave functions

$$\psi_{\mathrm{IVb}n} = |\{(nl)^{p-1}(\beta T_1 S_1 L_1) n' l'\}(TS_2 L_2), TJ; T_z J_z\rangle. \tag{2.18b}$$

The contribution from these states results in

$$\mathcal{V}_{\mathrm{IVb}\gamma'\gamma} = \langle (nl)^p(\alpha' TS' L')TJ; T_z J_z| \cdot \left(1-\frac{p-2}{8l+4}\right)\sum_{i>j} V_{ij}^{\mathrm{IVb}} + \sum_{i>j>k} V_{ijk}^{\mathrm{IVb}} |(nl)^p(\alpha TSL)TJ; T_z J_z\rangle, \tag{2.19b}$$

where V_{ij}^{IVb} and V_{ijk}^{IVb} represent effective two-or three-body potentials and the term $[(p-2)/(8l+4)]V_{ij}^{\mathrm{IVb}}$ is also a three-body effect. The latter may be written as a three-body force which is scalar in the space of the third particle.

The derivation of these results requires long and tedious calculations, some details of which will be shown in the appendix, where the effective two-body and three-body forces will also be given.

In the above, the central potential and averaged potential in H_1 are not considered. Their inclusion would result in an energy depression that is common to all states, a slight change in a single-particle energy, and effective interactions which are scalar in both spin and angular-momentum space. However, there is no term which can be replaced by a spin-orbit interaction, and the effective potential does not include vector and tensor parts.

3. Discussion and Conclusions

Let us evaluate $\xi = \sum_\alpha C_\alpha$ in $(1\mathrm{p})^p$ nuclei. This numerical value depends on the character of the tensor force and on the single-particle wave functions. In this section, two kinds of force are assumed as in the earlier articles I and II. One of them is the phenomenological tensor force of the Serber type,

$$V_{\mathrm{T}} = V_0\{(1-\boldsymbol{\tau}_1\cdot\boldsymbol{\tau}_2)/4\}S_{12}\exp(-r^2/r_t^2) \tag{3.1}$$

where $V_0 = -25.8$ MeV, $r_t = 2.41\times 10^{-13}$ cm and S_{12} is the tensor-force operator. This is rather stronger than the usual phenomenological one used, for example, by Feingold [10]. The other is that suggested by meson theory [16] whose potential for the triplet odd state is

$$V_{\mathrm{T}} = \begin{cases} V_{\mathrm{T}}^{(1\pi)}(\kappa r) & \text{for } \kappa r \geqq 1.0, \\ 0 & \text{for } \kappa r < 1.0, \end{cases} \tag{3.2a}$$

and for the triplet even state is

$$V_{\mathrm{T}} = \begin{cases} V_{\mathrm{T}}^{(1\pi)}(\kappa r) & \text{for } \kappa r \geqq 0.7, \\ 3V_{\mathrm{T}}^{(1\pi)}(0.7) & \text{for } \kappa r < 0.7. \end{cases} \tag{3.2b}$$

Here,

$$V_{\mathrm{T}}^{(1\pi)}(\kappa r)=\frac{g^2_{\mathrm{e}}}{4\pi}\mu c^2\frac{\tau_1\cdot\tau_2}{3}S_{12}\left(1+\frac{3}{\kappa r}+\frac{3}{\kappa^2 r^2}\right)\frac{\exp(-\kappa r)}{\kappa r}$$

where $\kappa^{-1}=\hbar/\mu c$, μ is the mass of π-meson, and $g_{\mathrm{e}}^2/4\pi$ is taken to be 0.08.

As the single-particle wave function, the harmonic-oscillator wave function is adopted. This assumption makes it possible to use the very convenient method developed in papers I and II, and also by Mayer and Lawson [37]) and by Moshinsky [38]). Wave functions of the two-particle system are transformed into those of the relative and centre-of-mass coordinate systems, and the summations over degenerate intermediate states of the same excitation energy can be carried through. The matrix elements of the states which are excluded by the Pauli principle should be subtracted.

We next divide ξ into two parts,

$$\xi=C_0+(p-1)C_1, \tag{3.3}$$

where C_0 and C_1 are given by

$$C_0=\sum_{N=1}^{\infty}\frac{3}{N\hbar\omega}\left[-\frac{1}{2^{2N}}\langle 1\mathrm{s}|V(r)|N\mathrm{d}\rangle^2\Phi_\tau^{\,2}(0)\right.$$
$$\left.+\left(1-\frac{1}{2^{2N}}\right)\frac{9}{5}\{\langle 1\mathrm{p}|V(r)|N+1\mathrm{p}\rangle^2-\langle 1\mathrm{p}|V(r)|N\mathrm{f}\rangle^2\}\Phi_\tau^{\,2}(1)\right] \tag{3.4}$$

and

$$C_1=\sum_{N=1}^{\infty}\frac{3}{4N\hbar\omega}\left[-\frac{1}{2^{2N}}\langle 1\mathrm{s}|V(r)|N\mathrm{d}\rangle^2\Phi_\tau^{\,2}(0)\right.$$
$$\left.-\frac{1}{2^{2N}}\frac{3}{5}\{(2N+2)\langle 1\mathrm{p}|V(r)|N+1\mathrm{p}\rangle^2-(2N-3)\langle 1\mathrm{p}|V(r)|N\mathrm{f}\rangle^2\}\Phi_\tau^{\,2}(1)\right]. \tag{3.5}$$

Here

$$\langle nl|V(r)|n'l'\rangle=\int_0^\infty R_{nl}(r)V(r)R_{n'l'}(r)r^2\mathrm{d}r,$$

$R_{nl}(r)$ is the radial part of the harmonic-oscillator wave function of the relative coordinate, and the quantity $\frac{3}{2}C_0$ was already calculated in paper I. Therefore, only C_1 must be calculated. Fig. 5 shows the numerical values of C_0 and C_1 as a function of the parameter $\rho(10^{-13}\ \mathrm{cm})=(\frac{1}{2}\nu)^{-\frac{1}{2}}$ which measures the extent of the harmonic-oscillator wave functions. In order to determine ρ, the Coulomb energy differences [39]) and the high-energy electron-scattering data [40]) may be used. However, in this determination, the wave function of the nucleus must be given, and then usually the shell-model wave function is assumed. By this assumption, for (1p)-nuclei, the Coulomb energy difference gives

$$2.30<\rho<2.49.$$

This estimate is questionable because of the large probability of admixing higher states into the zeroth order shell-model state. To cover this range of uncertainty, ρ runs from 1.8 to 2.5 in fig. 5.

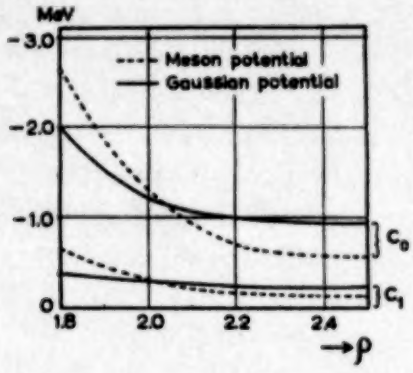

Fig. 5. The numerical values of C_0 and C_1 are shown as a function of ρ. The strength of spin-orbit interaction ξ is given by the relation $\xi = C_0 + (\rho - 1)C_1$.

As in the preceding papers I and II, C_0 is not large enough to explain the observed doublet splitting of He^5 as long as $\rho \geqq 2.3$. If ρ is smaller than this figure by 15 % to 20 %, C_0 becomes sufficiently large.

The constant C_1 itself is not large, and in these (1p)-nuclei

$$C_1 \approx \tfrac{1}{4} C_0, \tag{3.6}$$

the two quantities being exactly in the case of the Serber force. It is very interesting to note that

$$\xi(\rho = 11)/\xi(\rho = 1) \approx 3.5, \tag{3.7}$$

which means that the intensity of the one-body spin-orbit interaction becomes larger as the number of nucleons increases. There is some experimental evidence of this. The doublet splitting in He^5 is about 2.5 MeV † and that in N^{15} is about 6 MeV. According to the calculation of the intermediate-coupling shell model, the intensity of the one-body spin-orbit coupling has a tendency to increase [27, 28]. Here, it must be noticed that there are two-body and three-body effects besides the spin-orbit coupling. Some of them cancel a part of the single-body effect. Indeed, in the nuclei with a closed shell less one nucleon, the excited states IIIa and IIIb are forbidden by the Pauli principle. Therefore, in those nuclei, the effective two-body interaction $\sum_{i>j} V_{ij}^{\mathrm{IIIa}'} + \sum_{i<j} V_{ij}^{\mathrm{IIIb}'}$ must cancel the part of the one-body spin-orbit interaction $(C_{\mathrm{IIIa}'} + C_{\mathrm{IIIb}'}) \sum_i \mathbf{s}_i \cdot \mathbf{l}_i$, so that the total contribution due to IIIa′ and IIIb′ must vanish. Some of these two-body and three-body effective potentials have been estimated by Lyons [33] and Feingold [21, 22], who found that the two-body vector potential has the opposite sign

† These data are very ambiguous, because neither the $p_{\frac{1}{2}}$ nor the $p_{\frac{3}{2}}$ state is bound.

to the phenomenological one which was obtained by Elliott and Lane [3]). Terasawa [14]) has calculated the doublet splitting in N^{15}, $\Delta\Delta E(N^{15})$. The sum of the splitting energies which come from IIa, IIb and IIIa is 3.3 MeV, when $\rho = 2.34$ and the Serber potential (3.1) is assumed. In this numerical value, the two-body and three-body effects are also included. At this ρ and by this potential, $\Delta\Delta E(He^5)$ is about 1.3 MeV. Therefore, $\Delta\Delta E(N^{15})_{IIa+IIb+IIIa}/\Delta\Delta E(He^5) \approx 2.5$. The discrepancy between this value 2.5 and the value 3.5 from eq. (3.7) expresses the negative contribution of the two-body effective potentials $V_{ij}^{IIb}+V_{ij}^{IIIb}$ to the doublet splitting. He has also shown the important contributions from IVa and IVb which can be written, not as a one-body spin-orbit coupling, but as general two-body and three-body potentials. In N^{15}, they contribute 2.8 MeV to $\Delta\Delta E(N^{15})$. These effects will be estimated numerically, with inclusion of the $B^{12} \rightarrow C^{12}$ decay problem, in a subsequent paper in cooperation with Dr. T. Terasawa.

In the usual intermediate-coupling shell model, the Hamiltonian is assumed to consist of the shell-model Hamiltonian with the one-body spin-orbit coupling plus the two-body potentials interacting between nucleons in the same orbit. One term of the original Hamiltonian, eq. (2.5) is the interaction Hamiltonian which includes the two-body interaction between nucleons in all orbits. By the procedure described above, the second-order effect coming from the higher configurations is first taken into consideration, and this gives the one-body spin-orbit interaction and the effective two- and three-body forces. Therefore, if three-body effects can be neglected, the intermediate-coupling shell-model Hamiltonians are derived. Here this spin-orbit interaction increases with the number of nucleons in the unfilled level.

The author would like to express his cordial thanks to Professor T. Yamanouchi of the University of Tokyo for his kind interest and encouragement throughout the work. He also thanks Dr. D. R. Inglis and the members of the Physics Division of the Argonne National Laboratory for their hospitality and kind discussions. This paper is a continuation of earlier work with Dr. T. Terasawa, to whom the author is very grateful for many friendly and helpful discussions. His best thanks are also due to Dr. F. Throw for his kind reading of the manuscript.

Note added in proof: The numerical value of constant C_0 seems to be smaller than the observed values if the radii are fitted to the experiment. Therefore, we also calculated the doublet splitting (both the first and the second order effects) due to the L—S potentials suggested by meson theory [43]) which are in general smaller than the phenomenological L—S potentials proposed by Gammel and Thaler [44]) and Signell, Zinn and Marshak [45]).

We found that the doublet splitting due to the L—S potentials are fairly

large especially in the case of the ps—pv coupling; even in the case of ps—ps coupling, the contribution is comparable with the second order effect due to the tensor force. The details will be published elsewhere.

Appendix

The calculation of $\mathscr{V}_{\gamma'\gamma}$ is very easy in the cases of configurations Ia, Ib, IIa, IIIa and IIIb. Hence, as an illustration, let us derive eqs. (2.16a) and (2.17a) for $\mathscr{V}_{\mathrm{IIIa}\,\gamma'\gamma}$. By the usual tensor calculus, the non-diagonal matrix element between $\psi_{\mathrm{IIIa}n}$ in (2.15a) and $\psi_{0\gamma}$ in (2.6) becomes

$$
\begin{aligned}
&\langle (n_il_i)^{8l_i+4}(000)(nl)^p(\alpha TSL)TJ|\sum(S^{(2)}\cdot L^{(2)})| \\
&\quad\cdot[(n_il_i)^{8l_i+2}(T_1 1L_1)\{n'_il'_i(nl)^{p+1}(\beta T_2S_2L_2)\}(T_3S_3L_3)](TS_4L_4)TJ\rangle \\
&\quad=(-1)^{S+L_4-J}W(SLS_4L_4;J2)(\phi+1)^{\frac{1}{2}}\langle l^{p+1}\beta T_2S_2L_2\{|l,l^p(\alpha TSL)\rangle \\
&\quad\times\sum(-1)^{T_3-T-T_1}\{(2T_2+1)(2S_2+1)(2L_2+1)(2T_1+1)3(2L'_1+1) \qquad \text{(A1)}\\
&\qquad\cdot(2T_3+1)(2S_3+1)(2L_3+1)(2S_4+1)(2L_4+1)\}^{\frac{1}{2}}(2T+1)^{-\frac{1}{2}} \\
&\quad\times W(11S_4S;2S_3)W(L_1L'_1L_4L;2L_3)W(\tfrac{1}{2}\tfrac{1}{2}T_3T;T_1T_2) \\
&\qquad\cdot W(\tfrac{1}{2}\tfrac{1}{2}S_3S;1S_2)W(l'_ilL_3L;L'_1L_2) \\
&\quad\times\langle n_il_in_il_i1L_1||S^{(2)}L^{(2)}||n'_il'_inl1L'_1\rangle\Phi_\tau(T_1).
\end{aligned}
$$

Then

$$
\begin{aligned}
\mathscr{V}_{\mathrm{IIIa}\,\gamma'\gamma}=&\sum\frac{1}{E_0^{(0)}-E_n^{(0)}}\cdot\tfrac{1}{2}(\phi+1)\,[\sum\langle l^{p+1}\beta T_2S_2L_2\{|l,l^p(\alpha TSL)\}\rangle^2 \\
&\qquad\cdot(2T_2+1)(2S_2+1)(2L_2+1)(2T_1+1) \\
&\times\{(2T+1)(2S+1)(2L+1)2\cdot5(2l+1)\}^{-1} \\
&\qquad\cdot\langle n_il_in_il_i1L||S^{(2)}L^{(2)}||n'_il'_inl1L'_1\rangle^2\Phi_\tau^{\,2}(T_1)\delta(\gamma,\gamma') \\
&+\left(\frac{1}{2\sqrt{5}}\right)\sum\langle l^{p+1}\beta T_2S_2L_2\{|l,l^p(\alpha TSL)\rangle\langle l,l^p(\alpha'TS'L')|\}l^{p+1}\beta T_2S_2L_2\rangle \\
&\times(2T_2+1)(2S_2+1)(2L_2+1)3(2T_1+1) \qquad \text{(A2)}\\
&\qquad\cdot\{(2L'_1+1)(2\bar{L}'_1+1)\}^{\frac{1}{2}}(2T+1)^{-1}(-1)^{S+S'+\frac{1}{2}-S_3+L-J} \\
&\times W(\tfrac{1}{2}S'\tfrac{1}{2}S;S_21)W(S'L'SL;J1)W(L_2lL'1;L\bar{l})W(l'_il\bar{L}'_11;L'_1l) \\
&\times W(L_1L'_121;2\bar{L}'_1)\langle n_il_in_il_i1L_1||S^{(2)}L^{(2)}||n'_il'_inl1L'_1\rangle \\
&\times\langle n_il_in_il_i1L_1||S^{(2)}L^{(2)}||n'_il'_inl1\bar{L}'_1\rangle\Phi_\tau^{\,2}(T_1)].
\end{aligned}
$$

To obtain this eq. (A2), the following identities are used:

$$W(\tfrac{1}{2}\tfrac{1}{2}S_3S;\,1S_2)W(\tfrac{1}{2}\tfrac{1}{2}S_3S';\,1S_2)$$
$$=\frac{\delta(S,S')}{2\cdot 3(2S+1)}+3W(\tfrac{1}{2}1\tfrac{1}{2}1;\,\tfrac{1}{2}1)W(S1S_31;\,S'1)\;W(\tfrac{1}{2}1S_2S;\,\tfrac{1}{2}S'),$$
$$\sum(2S_3+1)W(1S_32S;\,S_41)W(1S_32S';\,S_41)W(SS_311;\,1S')=\frac{1}{2\sqrt{5}}W(S_42S1;\,S'2),$$
$$\sum(2S_4+1)W(L_4S_4L'S';\,J2)W(SS_412;\,2S')W(L_4S_4LS;\,J2)=W(JL'S1;\,S'L)W(L_4L'21;\,2L),\tag{A3}$$
$$\sum(2L_4+1)W(L_1L'_1L_4L;\,2L_3)W(L_1\bar{L}'_1L_4L';2L_3)W(L_4L'21;\,2L_1)=W(L_3L'_1L'1;\,L\bar{L}'_1)W(L_1L'_121;\,2\bar{L}'_1),$$
$$\sum(2L_3+1)W(l'_iL_3lL;\,L_2L'_1)W(L'L_31L'_1;\,\bar{L}'_1L)W(l'_iL_3lL';\,L_2\bar{L}'_1)=W(L_2lL'1;\,Ll)W(l'_il\bar{L}'_11;\,L'_1l),$$

in addition to the orthogonality relations of the W-coefficients. The relation [41] between the fractional parentages of the terms of an almost-closed shell l^{8l+4-n} and those of the terms of l^{n+1} is

$$\langle l^{p+1}\beta T_2S_2L_2\{|l^p(\alpha TSL)l\rangle$$
$$=(-1)^{-T-S-L+T_2+S_2+L_2-l+p}\{(8l+4-p)(2T+1)(2S+1)(2L+1)\}^{\frac{1}{2}}\tag{A4}$$
$$\cdot\{(p+1)(2T_2+1)(2S_2+1)(2L_2+1)\}^{-\frac{1}{2}}\langle l^{8l+3-p}(\beta T_2S_2L_2)l|\}l^{8l+4-p}\alpha TSL\rangle.$$

By this relation and the sum rule of the fractional parentages, we get

$$\mathscr{V}_{\mathrm{IIIa}\,\gamma'\gamma}=\sum\frac{1}{E_0^{(0)}-E_n^{(0)}}\frac{1}{5}\left(1-\frac{p}{8l+4}\right)\sum(2T_1+1)$$
$$\cdot\langle n_il_in_il_i1L_1||S^{(2)}L^{(2)}||n'_il'_inl1L'_1\rangle^2\Phi_\tau^{\,2}(T_1)\delta(\gamma,\gamma')$$
$$-[(8l+4-p)(-1)^{S'+L-J}W(S'L'SL;\,J1)\sum\langle l^{8l+4-p}\alpha'TS'L'\tag{A5}$$
$$\cdot\{|l^{8l+3-p}(\beta T_2S_2L_2)l\rangle$$
$$\langle l^{8l+3-p}(\beta T_2S_2L_2)l|\}l^{8l+4-p}\alpha TSL\rangle(-1)^{S_2+1-\frac{1}{2}-S}(-1)^{L_2+1-l-L}$$
$$\cdot\{(2S+1)(2L+1)(2S'+1)(2L'+1)\}^{\frac{1}{2}}$$
$$\times W(\tfrac{1}{2}S\tfrac{1}{2}S';\,S_21)W(lLlL';\,L_21)\langle\tfrac{1}{2}||\mathbf{s}||\tfrac{1}{2}\rangle\langle l||\mathbf{1}||l\rangle]C_{\mathrm{IIIa}},$$

where C_{IIIa} is given by eq. (2.17a). In this equation, the part [. . .] can be replaced by the relation [42]

$$\langle l^{8l+4-p}\alpha TS'L';\,J|\sum_i\mathbf{s}_i\cdot\mathbf{l}_i|l^{8l+4-p}\alpha TSL;\,J\rangle=[\,\ldots\,]$$
$$=-\langle l^p\alpha'TS'L';\,J|\sum\mathbf{s}_i\cdot\mathbf{l}_i|l^p\alpha TSL;\,J\rangle\tag{A6}$$

where $\langle\frac{1}{2}||\mathbf{s}||\frac{1}{2}\rangle=(\frac{3}{2})^{\frac{1}{2}}$, $\langle l||\mathbf{l}||l\rangle=\{l(l+1)(2l+1)\}^{\frac{1}{2}}$ and the conjugating relation is used. Thus (A6) becomes (2.16a).

Almost the same technique can be applied to derive $\mathscr{V}_{\mathrm{IIIa}'\gamma'\gamma}$ and $\mathscr{V}_{\mathrm{IIIb}'\gamma'\gamma}$. In this case, the relation

$$\langle l^{p+1}\alpha TSL\{|l^{p-1}(\beta T'S'L')l^2(\bar{T}\bar{S}\bar{L})\rangle$$
$$=\left[\frac{(8l+4-p)(8l+4-p+1)(2T'+1)(2S'+1)(2L'+1)}{p(p+1)(2T+1)(2S+1)(2L+1)}\right]^{\frac{1}{2}} \tag{A7}$$
$$\cdot(-1)^{T+S+L+T'+S'+L'+1}\langle l^{8l+4-(p+1)}(\alpha TSL)l^2(\bar{T}\bar{S}\bar{L})|\}l^{8l+4-(p-1)}\beta T'S'L'\rangle$$

is used instead of (A4). As a result, for example,

$$\mathscr{V}_{\mathrm{IIIa}'\gamma'\gamma}$$
$$=\langle(nl)^{8l+4-p}\alpha' TS'L';J|\sum_{\lambda}\sum_{i>j}(S_{ij}^{(\lambda)}\cdot L_{\mathrm{eff}\,ij}^{(\lambda)})(a+b\tau_i\cdot\tau_j)^2|(nl)^{8l+4-p}\alpha TSL;J\rangle \tag{A8}$$

is obtained, and in (A8)

$$\langle nlnl1L'_1||S^{(\lambda)}L_{\mathrm{eff}}^{(\lambda)}||nlnl1\bar{L}'_1\rangle$$
$$=(-1)^{\lambda}(2\lambda+1)W(1122;\lambda1)\sum\frac{1}{E_0^{(0)}-E_n^{(0)}}\sum W(2L'_1 2\bar{L}'_1;L_1\lambda)$$
$$\cdot\langle nlnl1L'_1||S^{(2)}L^{(2)}||n_il_in_il_i1L_1\rangle$$
$$\times\langle n_il_in_il_i1L_1||S^{(2)}L^{(2)}||nlnl1\bar{L}'_1\rangle,$$
$$S^{(0)}=\tfrac{1}{4}(3+\sigma_1\cdot\sigma_2),\quad S^{(1)}=(\sigma_1+\sigma_2),\quad S_m^{(2)}=[\sigma_1\cdot\sigma_2]_m^{(2)}.$$

This $(S^{(\lambda)}\cdot L_{\mathrm{eff}}^{(\lambda)})$ gives the effective two-body interactions, and hence

$$L_{\mathrm{eff}\,Q}^{(\lambda)}=4.5(2\lambda+1)^{\frac{1}{2}}W(1122;\lambda1)\langle\tfrac{1}{2}\tfrac{1}{2}1||S^{(\lambda)}||\tfrac{1}{2}\tfrac{1}{2}1\rangle^{-1}\sum\frac{1}{E_0^{(0)}-E_n^{(0)}}$$
$$\times\sum(22\,Q+\beta\,-\beta|2Q)L_{\beta+Q}^{(2)}|n_il_in_il_iL_1M_1\rangle\langle n_il_in_il_iL_1M_1|L_{-\beta}^{(2)}, \tag{A9}$$

where $\lambda=0$ corresponds to central force, $\lambda=1$ to vector force, and $\lambda=2$ to tensor force. If in the projection operator the states can run through all two-body states, this projection operator becomes unity, and then $L_{\mathrm{eff}\,Q}^{(\lambda)}$ becomes a local interaction. However, in our case, $L_{\mathrm{eff}\,Q}^{(\lambda)}$ is generally a non-local interaction. Now, let us consider a general two-body operator $T_{q_\lambda q_\mu q_\nu}^{(\lambda,\mu,\nu)}$ which is of rank λ, μ and ν in the spaces of the isobaric spin, spin and ordinary angular momentum while q_λ, q_μ, and q_ν are the third components of these vectors. Then,

$$T_{q_\lambda q_\mu q_\nu,\,ij}^{(\lambda,\mu,\nu)}=\sum_{a\cdots f}A^{(abcdef)}[f_i^{(a)}f_j^{(b)}]_{q_\lambda}^{(\lambda)}[g_i^{(c)}\cdot g_j^{(d)}]_{q_\mu}^{(\mu)}[h_i^{(e)}\cdot h_j^{(f)}]_{q_\nu}^{(\nu)}$$
$$=\sum A^{(abcdef)}[\{f^{(a)}g^{(c)}h^{(e)}\}_i\{f^{(b)}g^{(d)}h^{(f)}\}_j]_{q_\lambda q_\mu q_\nu}^{(\lambda,\mu,\nu)}, \tag{A10}$$

where $f^{(a)}$, etc. are the single-particle operators of rank a, etc. Then,

$$\sum_{i>j} T^{(\lambda,\mu,\nu)}_{q_\lambda q_\mu q_\nu,\, ij} = \frac{1}{2}\sum_{a\cdots f} A^{(abcdef)}\Big[\sum_i \{f^{(a)} g^{(c)} h^{(e)}\}_i \sum_j \{f^{(b)} g^{(d)} h^{(f)}\}_j\Big]^{(\lambda,\mu,\nu)}_{q_\lambda q_\mu q_\nu}$$
$$-\frac{1}{2}\sum_{a\cdots f}\sum_i A^{(abcdef)}[f_i^{(a)} \cdot f_i^{(b)}]^{(\lambda)}_{q_\lambda}[g_i^{(c)} \cdot g_i^{(d)}]^{(\mu)}_{q_\mu}[h_i^{(e)} \cdot h_i^{(f)}]^{(\nu)}_{q_\nu}.$$

By taking into consideration the relation [41, 42] †

$$\langle l^{8l+4-p}\alpha TSL|\sum_i \{f^{(a)}_{q_a} g^{(c)}_{q_c} h^{(e)}_{q_e}\}_i|l^{8l+4-p}\alpha' T' S' L'\rangle$$
$$= -(-1)^{a+c+e}\langle l^p \alpha TSL|\sum_i \{f^{(a)}_{q_a} g^{(c)}_{q_c} h^{(e)}_{q_e}\}_i^+|l^p\alpha' T' S' L'\rangle$$
$$+\langle l^{8l+4}000|\sum_i \{f^{(0)} g^{(0)} h^{(0)}\}_i|l^{8l+4}000\rangle\delta(\gamma,\gamma')\delta(a,0)\ldots\delta(g_e,0), \quad \text{(A11)}$$

it follows that

$$\langle l^{8l+4-p}\alpha TSL;\, T_z S_z L_z|\sum_{i>j} T^{(\lambda,\mu,\nu)}_{q_\lambda q_\mu q_\nu,\, ij}|l^{8l+4-p}\alpha' T' S' L';\, T'_z S'_z L'_z\rangle$$
$$=\tfrac{1}{2}\{(2T+1)(2S+1)(2L+1)\}^{-\frac{1}{2}}(T'\lambda T'_z q_\lambda|TT_z)(S'\mu S'_z q_\mu|SS_z)(L'\nu L'_z q_\nu|LL_z)$$
$$\times\sum A^{(abcdef)}\langle l^{8l+4-p}\alpha TSL||\sum_i\{f^{(a)}g^{(c)}h^{(e)}\}_i||l^{8l+4-p}\alpha''T''S''L''\rangle$$
$$\langle l^{8l+4-p}\alpha''T''S''L''||\sum_j\{f^{(b)}g^{(d)}h^{(f)}\}_j||l^{8l+4-p}\alpha T'S'L'\rangle$$
$$\times\{(2\lambda+1)(2\mu+1)(2\nu+1)\}^{\frac{1}{2}}W(TaT'b;\,T''\lambda)W(ScS'd;\,S''\mu)W(LeL'f;\,L''\nu)$$
$$-\tfrac{1}{2}\langle l^{8l+4-p}\alpha TSL;\, T_z S_z L_z|\sum_i T^{(\lambda,\mu,\nu)}_{q_\lambda q_\mu q_\nu,\, ii}|l^{8l+4-p}\alpha' T' S' L';\, T'_z S'_z L'_z\rangle$$

$$=\tfrac{1}{2}\langle l^p\alpha TSL;\, T_z S_z L_z|\sum_{a\cdots f}(-1)^{\Sigma a} A^{(abcdef)}\Big[\sum_i\{f^{(a)}g^{(c)}h^{(e)}\}_i^+$$
$$\cdot\sum\{f^{(b)}g^{(d)}h^{(f)}\}_j^+\Big]^{(\lambda,\mu,\nu)}_{q_\lambda q_\mu q_\nu}|l^p\alpha' T' S' L';\, T'_z S'_z L'_z\rangle$$
$$-\tfrac{1}{2}\langle l^{8l+4}000;\,000|\sum_i\{f^{(0)}g^{(0)}h^{(0)}\}_i|l^{8l+4}000;\,000\rangle\langle l^p\alpha TSL;\, T_z S_z L_z$$
$$\cdot|\sum_j(A^{(000\lambda\mu\nu)}+A^{(\lambda\mu\nu000)})(-1)^{\lambda+\mu+\nu}\{f^{(\lambda)}_{q_\lambda}g^{(\mu)}_{q_\mu}h^{(\nu)}_{q_\nu}\}_j^+|l^p\alpha' T' S' L';\, T'_z S'_z L'_z\rangle$$
$$+\tfrac{1}{2}\langle l^{8l+4}000;\,000|\sum_i\{f^{(0)}g^{(0)}h^{(0)}\}_i|l^{8l+4}000;\,000\rangle^2$$
$$\cdot A^{(000000)}\delta(\gamma,\gamma')\delta(\lambda,0)\ldots\delta(q_\nu,0)$$
$$+\tfrac{1}{2}\langle l^p\alpha TSL;\, T_z S_z L_z|\sum_i A^{(abcdef)}(-1)^{\lambda+\mu+\nu}[f_i^{(a)}\cdot f_i^{(b)}]^{(\lambda)+}_{q_\lambda}[g_i^{(c)}\cdot g_i^{(d)}]^{(\mu)+}_{q_\mu}$$
$$[h_i^{(e)}\cdot h_i^{(f)}]^{(\nu)+}_{q_\nu}|l^p\alpha' T' S' L';\, T'_z S'_z L'_z\rangle$$
$$-\tfrac{1}{2}\langle l^{8l+4}000;\,000|\sum_i[f_i^{(0)}f_i^{(0)}]^{(0)}[g_i^{(0)}g_i^{(0)}]^{(0)}[h_i^{(0)}h_i^{(0)}]^{(0)}|l^{8l+4}000;\,000\rangle$$
$$\cdot A^{(000000)}\delta(\gamma,\gamma')\delta(\lambda,0)\ldots\delta(q_\nu,0).$$

† We use the notation $\langle jm|h^{(a)+}_{q_a}|jn\rangle = \langle jm|h^{(a)\dagger}_{q_a}|jn\rangle^*$, where $\dagger$ denotes the Racah conjugation $\langle jm|h^{(a)\dagger}_{q_a}|jn\rangle = (-1)^{q_a}\langle jn|h^{(a)}_{-q_a}|jm\rangle^*$.

$$=\langle l^p\alpha TSL;\, T_z S_z L_z|\sum_{i>j}\bar{T}^{(\lambda,\mu,\nu)}_{q_\lambda q_\mu q_\nu,\,ij}|l^p\alpha' T'S'L';\, T'_z S'_z L'_z\rangle$$

$$+\tfrac{1}{2}\langle l^p\alpha TSL;\, T_z S_z L_z|\sum_{i(\lambda+\mu+\nu\neq 0)} t^{(\lambda,\mu,\nu)}_{q_\lambda q_\mu q_\nu,\,i}|l^p\alpha' T'S'L';\, T'_z S'_z L'_z\rangle$$

$$+\left\{1-\frac{2p}{8l+4}\right\}\langle l^{8l+4}000;\,000|\sum_{i>j}T^{(000)}_{ij}|l^{8l+4}000;\,000\rangle\delta(\gamma,\gamma')\delta(\lambda,0)\ldots\delta(q_\nu,0),$$

where

$$\bar{T}^{(\lambda,\mu,\nu)}_{q_\lambda q_\mu q_\nu,\,ij}=\sum(-1)^{\Sigma a}A^{(abcdef)}[f_i^{(a)+}\cdot f_j^{(b)+}]^{(\lambda)}_{q_\lambda}[g_i^{(c)+}\cdot g_j^{(d)+}]^{(\mu)}_{q_\mu}[h_i^{(e)+}\cdot h_j^{(f)+}]^{(\nu)}_{q_\nu}$$

and

$$t^{(\lambda,\mu,\nu)}_{q_\lambda q_\mu q_\nu,\,i}=\tfrac{1}{2}\sum\{(-1)^{\Sigma a}+(-1)^{\lambda+\mu+\nu}\}A^{(abcdef)}[f_i^{(a)}\cdot f_i^{(b)}]^{(\lambda)+}_{q_\lambda}[g_i^{(c)}\cdot g_i^{(d)}]^{(\mu)+}_{q_\mu}\cdot[h_i^{(e)}\cdot h_i^{(f)}]^{(\nu)+}_{q_\nu}$$

$$-\tfrac{1}{2}(A^{(000\lambda\mu\nu)}+A^{(\lambda\mu\nu000)})(-1)^{\lambda+\mu+\nu}\{f^{(\lambda)}g^{(\mu)}h^{(\nu)}\}_i+\langle l^{8l+4}000;\,000|\cdot\sum_j\{f^{(0)}g^{(0)}h^{(0)}\}_j|l^{8l+4}000;\,000\rangle.$$

The second term can be written as

$$\langle l^p\alpha TSL;\, T_z S_z L_z|\sum_i t^{(\lambda,\mu,\nu)}_{q_\lambda q_\mu q_\nu,\,i}|l^p\alpha' T'S'L';\, T'_z S'_z L'_z\rangle$$

$$=K\langle l^p\alpha TSL;\, T_z S_z L_z|\sum U^{(\lambda)}_{q_\lambda}V^{(\mu)}_{q_\mu}W^{(\nu)}_{q_\nu}|l^p\alpha' T'S'L';\, T'_z S'_z L'_z\rangle,$$

where

$$\langle\tfrac{1}{2}||U^{(\lambda)}||\tfrac{1}{2}\rangle=1,\quad \langle\tfrac{1}{2}||V^{(\mu)}||\tfrac{1}{2}\rangle=1,\quad \langle l'||W^{(\nu)}||l''\rangle=\delta(l,l')\delta(l,l'')\qquad\text{(A12)}$$

and

$$K=\langle\tfrac{1}{2}\,\tfrac{1}{2}\,l||t^{(\lambda\mu\nu)}||\tfrac{1}{2}\,\tfrac{1}{2}\,l\rangle.$$

Then,

$$\langle l^{8l+4-p}\alpha TSL|\sum_{i>j}T^{(\lambda,\mu,\nu)}_{ij}|l^{8l+4-p}\alpha' T'S'L'\rangle$$

$$=\langle l^p\alpha TSL|\sum_{i>j}\bar{T}^{(\lambda,\mu,\nu)}_{ij}|l^p\alpha' T'S'L'\rangle$$

$$+\left\{1-\frac{2p}{8l+4}\right\}\langle l^{8l+4}000|\sum_{i>j}T^{000}_{ij}|l^{8l+4}000\rangle\delta(\lambda,0)\delta(\mu,0)\delta(\nu,0)\qquad\text{(A13)}$$

$$+K\langle l^p\alpha TSL|\sum_{\substack{i\\ \lambda+\mu+\nu\neq 0}}U_i^{(\lambda)}V_i^{(\mu)}W_i^{(\nu)}|l^p\alpha' T'S'L'\rangle.$$

When this equation is used, (A8) becomes

$$\mathscr{V}_{\mathrm{IIIa}'\gamma'\gamma}=\langle(nl)^p\alpha' TS'L';\,J|\sum_{\lambda i>j}\overline{(S^{(\lambda)}_{ij}\cdot L^{(\lambda)}_{\mathrm{eff}\,ij})}(a+b\boldsymbol{\tau}_i\cdot\boldsymbol{\tau}_j)^2|(nl)^p\alpha TSL;\,J\rangle$$

$$+\sum\frac{1}{E_0^{(0)}-E_n^{(0)}}\,\frac{1}{5}\left(1-\frac{2p}{8l+4}\right)\sum(2T_1+1)\langle nlnl1L_1||S^{(2)}L^{(2)}||n_il_in_il_i1L'_1\rangle^2\,\Phi^2{}_\gamma(T_1)\delta(\gamma,\gamma')$$

$$+\langle l^p\alpha' TS'L';\,J|\sum_i\mathbf{s}_i\cdot\mathbf{l}_i|l^p\alpha TSL;\,J\rangle C_{\mathrm{IIIa}'},$$

where $C_{\mathrm{IIIa}'}$ may be derived by complicated calculation; but there is a convenient way to obtain it, because this $\mathscr{V}_{\mathrm{IIIa}'\gamma'\gamma}$ is known in the special case of $p = 1$ from paper II, and $C_{\mathrm{IIIa}'}$ is independent of p. Then $C_{\mathrm{IIIa}'}$ is obtained by comparing eq. (A14) with (2.7) in paper II. In eq. (A13), the quantities

$$V_{ij}^{\mathrm{IIIa}'} = \sum_{\lambda} \overline{(S_{ij}^{(\lambda)} \cdot L_{\mathrm{eff}\,ij}^{(\lambda)})}(a+b\boldsymbol{\tau}_i \cdot \boldsymbol{\tau}_j)^2 \tag{A14}$$

are the effective two-body non-local potentials, and may be derived by expanding (A9) into a sum as in (A10) and changing the sign of certain terms for which the sum $a+b+c+d+e+f$ is odd. However, this procedure is not practical, and a better way is to estimate (A9) directly, provided $p = 2$, and to subtract the second and third terms in (A13) which are already known.

The same argument applies in IIIb′ and $V_{ij}^{\mathrm{IIIb}'}$ can be obtained by a similar method. The result is

$$V_{ij}^{\mathrm{IIIb}'} = \sum_{\lambda} \overline{(S_{ij}^{(\lambda)} \cdot L_{\mathrm{eff}\,ij}^{(\lambda)})}(a+b\boldsymbol{\tau}_i \cdot \boldsymbol{\tau}_j)^2 \tag{A15}$$

and

$$\begin{aligned}\langle nlnl1L'_1||S^{(\lambda)}L_{\mathrm{eff}}^{(\lambda)}||nlnl1\bar{L}'_1\rangle &= (-1)^{\lambda}(2\lambda+1)W(1122;\lambda 1)\sum \frac{1}{E_0^{(0)}-E_n^{(0)}}\sum W(2L'_1 2\bar{L}'_1; L_1\lambda) \\ &\times\langle nlnl1L'_1||S^{(2)}L^{(2)}||n_il_in_jl_j1L_1\rangle\langle n_il_in_jl_j1L_1||S^{(2)}L^{(2)}||nlnl1\bar{L}'_1\rangle.\end{aligned} \tag{A16}$$

The derivations of $\mathscr{V}_{\mathrm{IIb}\gamma'\gamma}$, $\mathscr{V}_{\mathrm{IIc}\gamma'\gamma}$ and $\mathscr{V}_{\mathrm{IVb}\gamma'\gamma}$ are very complicated. In these derivations, two identities between Racah coefficients and $9j$ symbols are useful. The first is

$$\begin{aligned}&\sum_{\rho}(2\rho+1)W(a\rho hg;fl)W(d\rho el;kg)W(a\rho bc;fi)W(i\rho jd;ck) \\ &\quad= (-1)^{2b+2j+a-c+d+f-g+i+k+l}\sum_{\lambda}(2\lambda+1)U\begin{pmatrix}b & e & \lambda\\ c & d & j\\ f & g & h\end{pmatrix}U\begin{pmatrix}b & e & \lambda\\ i & k & j\\ a & l & h\end{pmatrix},\end{aligned} \tag{A17}$$

where the U-coefficients are $9j$ symbols. This equation is easily verified by the relation,

$$\begin{aligned}&\langle a[bc(f)de(g)](h)l|[ab(i)cd(j)](k)el\rangle \\ &\quad=\sum_{\rho}\langle a, fg(h)l|af(\rho)gl\rangle\langle\rho, de(g)l|\rho d(k)el\rangle\langle a, bc(f)\rho|ab(i)c\rho\rangle\langle ic(\rho)dk|i, cd(j)k\rangle \\ &\quad=\sum_{\lambda}\langle bc(f)de(g)h|be(\lambda)cd(j)h\rangle\langle a[be(\lambda)j](h)l|[ab(i)j](k)el\rangle.\end{aligned}$$

The second identity is

$$\begin{aligned}&\sum_{x,y}(2x+1)(2y+1)W(abhc;xg)U\begin{pmatrix}x & c & h\\ i & f & j\\ y & m & o\end{pmatrix}U\begin{pmatrix}a & b & x\\ d & e & i\\ k & l & y\end{pmatrix}W(klom;yn) \\ &\qquad=\sum(2z+1)W(dejf;iz)U\begin{pmatrix}b & c & g\\ e & f & z\\ l & m & n\end{pmatrix}U\begin{pmatrix}a & g & h\\ d & z & j\\ k & n & o\end{pmatrix}.\end{aligned} \tag{A18}$$

This is proved by use of the transformation coefficient

$$\langle [a, bc(g)](h)[de(i)f](j)o|ad(k)[be(l)cf(m)](n)o\rangle$$
$$= \sum_{x,y} \langle a, bc(g)h|ab(x)ch\rangle\langle xc(h)if(j)o|xi(y)cf(m)o\rangle\langle ab(x)de(i)y|ad(k)be(l)y\rangle$$
$$\langle kl(y)mo|k, lm(n)o\rangle$$
$$= \sum_{z} \langle be(l)cf(m)n|bc(g)ef(z)n\rangle\langle ad(k)gz(n)o|ag(h)dz(j)o\rangle\langle d, ef(z)j|de(i)fj\rangle.$$

In order to obtain $\mathscr{V}_{\mathrm{IIc}\gamma'\gamma}$, the same technique used to derive $\mathscr{V}_{\mathrm{IIIa}\gamma'\gamma}$ is again applied, and the eqs. (A7) and (A18) are used. After long and tedious calculation, one obtains

$$\mathscr{V}_{\mathrm{IIc}\gamma'\gamma} = p\sum \langle l^p\alpha' TS'L'\{|l, l^{p-1}(\beta T_3 S_3 L_3)\rangle\langle l, l^{p-1}(\bar{\beta}\bar{T}_3\bar{S}_3 L_3)|\}l^p\alpha TSL\rangle$$
$$\times(-1)^{S+L'-J}W(S'L'SL; Jk)(-1)^{\frac{1}{2}+\bar{T}_3-T}W(\tfrac{1}{2}T_3\tfrac{1}{2}\bar{T}_3; T\lambda)$$
$$\{(2S+1)(2S'+1)(2k+1)(2L+1)(2L'+1)(2k+1)\}^{\frac{1}{2}} \quad \text{(A19)}$$
$$\times U\begin{pmatrix}\frac{1}{2} & \frac{1}{2} & \mu\\ S_3 & \bar{S}_3 & \mu'\\ S & S' & k\end{pmatrix} U\begin{pmatrix}l & l & \nu\\ L_3 & \bar{L}_3 & \nu'\\ L & L' & k\end{pmatrix}(-1)^{1+\lambda+\mu+\nu}\langle (nl)^{8l+4-(p-1)}\beta T_3 S_3 L_3||$$
$$\sum_{i>j} T_{ij}^{(\lambda,\mu',\nu')}||(nl)^{8l+4-(p-1)}\bar{\beta}\bar{T}_3\bar{S}_3 L_3\rangle,$$

where

$$\langle nlnlT_4 1L_4||T^{(\lambda,\mu',\nu')}||nlnl\bar{T}_4 1\bar{L}_4\rangle = \sum\frac{1}{E_0^{(0)}-E_n^{(0)}}\sum(-1)^{1+\mu+\nu+k+L_4+L'_4}$$
$$\cdot(2\lambda+1)(2\nu+1)(2\nu'+1)(2\mu+1)(2\mu'+1)U\begin{pmatrix}1 & 1\mu\\ 1 & 1\mu'\\ 2 & 2k\end{pmatrix}U\begin{pmatrix}L'_4 & \bar{L}'_4\nu\\ L_4 & \bar{L}_4\nu'\\ 2 & 2\quad k\end{pmatrix}$$
$$\times\langle nlnl1L_4||S^{(2)}L^{(2)}||nln_il_i1L'_4\rangle\Phi_\tau(T_4) \quad \text{(A20)}$$
$$\cdot\langle nln_il_iT_41L'_4||U^{(\lambda)}V^{(\mu)}W^{(\nu)}||nln_il_i\bar{T}_41\bar{L}'_4\rangle$$
$$\times\langle nln_il_i1\bar{L}'_4||S^{(2)}L^{(2)}||nlnl1\bar{L}_4\rangle\Phi_\tau(\bar{T}_4).$$

Therefore, $T^{(\lambda,\mu',\nu')}$ is a two-body operator which has the rank λ, μ', and ν' in the isobaric spin, spin and angular-momentum space. By eq. (A13)

$$\mathscr{V}_{\mathrm{IIc}\gamma'\gamma} = \sum\frac{1}{E_0^{(0)}-E_n^{(0)}}\frac{p}{5(8l+4)}\left(1-\frac{2(p-1)}{8l+4}\right)\sum(2T+1)$$
$$\cdot\langle nlnl1L||S^{(2)}L^{(2)}||nln_il_i1L'\rangle^2\Phi_\tau^2(T)\delta(\gamma,\gamma') \quad \text{(A21)}$$
$$-\langle (nl)^p\alpha' TS'L'; J|\sum_i \mathbf{s}_i\cdot\mathbf{l}_i|(nl)^p\alpha TSL; J\rangle\left\{\left(1-\frac{2(p-1)}{8l+4}\right)C_{\mathrm{IIc}}^{(1)}-\frac{2(p-1)}{8l+4}C_{\mathrm{IIc}}^{(2)}\right\}$$
$$+\langle (nl)^p\alpha' TS'L'; J|\sum_{i>j}V_{ij}^{\mathrm{IIc}}+\sum_{i>j>k}V_{ijk}^{\mathrm{IIc}}|(nl)^p\alpha TSL; J\rangle,$$

where $C_{\mathrm{IIc}}^{(1)}$ is determined by comparing this equation with (2.11) in paper II. Obtaining an explicit formula for $C_{\mathrm{IIc}}^{(2)}$ is somewhat complicated, because this term vanishes when $p=1$. This term is included in the case of $\lambda=\mu=\nu=0$. Now let us consider only this case. According to (A20)

$$\mu'=\nu'=k,$$

so that this part of $\mathscr{V}_{\mathrm{IIc}\gamma'\gamma}$ in (A19) becomes

$$\begin{aligned}\Delta\mathscr{V}_{\mathrm{IIc}\gamma'\gamma}=&-\left[\frac{p}{8l+4}\right]\sum\langle l^p\alpha' TS'L'\{|l,l^{p-1}(\beta T_3S_3L_3)\rangle\langle l,l^{p-1}(\bar\beta T_3\bar S_3\bar L_3)|\}l^p\alpha TSL\rangle\\
&\times(-1)^{S+L'-J}W(S'L'SL;Jk)(-1)^{k+\frac12-S_3-S'}\{(2S+1)(2S'+1)\}^{\frac12}W(S_3\bar S_3SS';k\tfrac12)\\
&\times(-1)^{k+l-L_3-L'}\{(2L+1)(2L'+1)\}^{\frac12}W(L_3\bar L_3LL';kl)\qquad\text{(A22)}\\
&\times\langle(nl)^{8l+4-(p-1)}\beta T_3S_3L_3||\sum_{i>j}S_{ij}^{(k)}L_{\mathrm{eff}\,ij}^{(k)}(a+b\boldsymbol\tau_i\cdot\boldsymbol\tau_j)^2||(nl)^{8l+4-(p-1)}\bar\beta T_3\bar S_3\bar L_3\rangle,\end{aligned}$$

where

$$\begin{aligned}&\langle nlnl1L_4||S^{(k)}L_{\mathrm{eff}}^{(k)}||nlnl1\bar L_4\rangle\\
&\quad=(-1)^k(2k+1)W(1122;k1)\sum\frac{1}{E_0^{(0)}-E_n^{(0)}}\sum W(L_4\,2\bar L_4\,2;L'_4k)\qquad\text{(A23)}\\
&\quad\cdot\langle nlnl1L_4||S^{(2)}L^{(2)}||nln_il_i1L'_4\rangle\cdot\langle nln_il_i1L'_4||S^{(2)}L^{(2)}||nlnl1\bar L_4\rangle.\end{aligned}$$

The effective potential defined by eq. (A23) is the same as that in (A8) except for replacing $|n_il_in_il_i1L_i\rangle\langle n_il_in_il_i1L_i|$ in (A9) by $|nln_il_i1L'_4\rangle\langle nln_il_i1L'_4|$. Noting, by inspection, that as a result (A8) becomes (A14), it follows that

$$\begin{aligned}&\langle(nl)^{8l+4-(p-1)}\beta T_3S_3L_3||\sum_{i>j}S_{ij}^{(k)}L_{\mathrm{eff}\,ij}^{(k)}(a+b\boldsymbol\tau_i\cdot\boldsymbol\tau_j)^2||(nl)^{8l+4-(p-1)}\bar\beta T_3\bar S_3\bar L_3\rangle\\
&\quad=\langle(nl)^{p-1}\beta T_3S_3L_3||\sum_{i>j}\overline{S_{ij}^{(k)}L_{\mathrm{eff}\,ij}^{(k)}}(a+b\boldsymbol\tau_i\cdot\boldsymbol\tau_j)^2||(nl)^{p-1}\bar\beta T_3\bar S_3\bar L_3\rangle\\
&\quad+\{(2S_3+1)(2L_3+1)\}^{\frac12}\sum\frac{1}{E_0^{(0)}-E_n^{(0)}}\cdot\frac15\left(1-\frac{2(p-1)}{8l+4}\right)\sum(2T_1+1)\qquad\text{(A24)}\\
&\quad\cdot\langle nlnl1L_1||S^{(2)}L^{(2)}||nln_il_i1L'_1\rangle^2\Phi_\tau^{\,2}(T_1)\delta(k,0)\delta(\beta\beta')\delta(S_3,\bar S_3)\delta(L_3,\bar L_3)\\
&\quad+2C_{\mathrm{IIc}}^{(2)}\langle(nl)^{p-1}\beta T_3S_3L_3||\sum_i\mathbf{s}_i\cdot\mathbf{l}_i||(nl)^{p-1}\bar\beta T_3\bar S_3\bar L_3\rangle\delta(k,1),\end{aligned}$$

where

$$\begin{aligned}C_{\mathrm{IIc}}^{(2)}=&\tfrac{3}{2}\{2\cdot3\cdot5l(l+1)(2l+1)\}^{-\frac12}\sum\frac{1}{E_0^{(0)}-E_n^{(0)}}\sum(2T_1+1)(2L'_1+1)\\
&\cdot W(lL'_1l1;lL'_1)W(L_1L'_121;2L'_1)\qquad\text{(A25)}\\
&\times\langle nlnl1L'_1||S^{(2)}L^{(2)}||nln_il_i1L_1\rangle^2\Phi_\tau^{\,2}(T_1).\end{aligned}$$

By substituting (A24) into (A22), one obtains

$$\Delta\mathscr{V}_{\mathrm{IIc}\gamma'\gamma} = -\frac{p-2}{8l+4}\langle(nl)^p\alpha TSL;\,J|\sum_{i>j}\overline{(S_{ij}^{(k)}L_{\mathrm{eff}\,ij}^{(k)})}(a+b\boldsymbol{\tau}_i\cdot\boldsymbol{\tau}_j)^2|(nl)^p\alpha' TS'L';\,J\rangle$$

$$-\frac{p}{5(8l+4)}\left\{1-\frac{2(p-1)}{8l+4}\right\}\sum\frac{1}{E_0^{(0)}-E_n^{(0)}}\sum(2T_1+1) \qquad \text{(A26)}$$

$$\cdot\langle nlnl1L_1||S^{(2)}L^{(2)}||nln_il_i1L'_1\rangle^2\Phi_\tau^2(T_1)\delta(\gamma,\gamma')$$

$$-\frac{2(p-1)}{8l+4}C_{\mathrm{IIc}}^{(2)}\langle(nl)^p\alpha TSL;\,J|\sum_i\mathbf{s}_i\cdot\mathbf{l}_i|(nl)^p\alpha' TS'L';\,J\rangle.$$

Thus $C_{\mathrm{IIc}}^{(2)}$ is derived. In (A26), the first term is the expectation value of the effective three-body force, which is scalar in the coordinates of one of the three interacting particles. Generally,

$$V_{ijk}^{\mathrm{IIc}} = \sum_{\substack{\lambda,\mu,\nu\\ \kappa,\mu',\nu'}}(-1)^{1+\lambda+\mu+\nu}(U_i^{(\lambda)}\cdot\bar{F}_{jk}^{(\lambda)})([V_i^{(\mu)}\cdot\bar{G}_{jk}^{(\mu')}]^{(\kappa)}\cdot[W_i^{(\nu)}\cdot\bar{H}_{jk}^{(\nu')}]^{(\kappa)}), \quad \text{(A27)}$$

where

$$\bar{F}^{(\lambda)}\bar{G}^{(\mu')}\bar{H}^{(\nu')} = \bar{T}^{(\lambda,\mu',\nu')}$$
$$(\lambda+\mu+\nu\neq 0)$$

and $U^{(\lambda)}$, $V^{(\mu)}$ and $W^{(\nu)}$ are already defined in (A12). Similarly

$$V_{ij}^{\mathrm{IIc}} = \sum(-1)^{1+\lambda+\mu+\nu}(U_i^{(\lambda)}\cdot\bar{\bar{F}}_j^{(\lambda)})([V_i^{(\mu)}\cdot\bar{\bar{G}}_j^{(\mu')}]^{(\kappa)}\cdot[W_i^{(\nu)}\cdot\bar{\bar{H}}_j^{(\nu')}]^{(\kappa)}), \quad \text{(A28)}$$

where the summation takes place over λ, μ, $\nu(\lambda+\mu+\nu\neq 0)$ and κ, μ', ν' $(\lambda+\mu'+\nu'\neq 0)$. In (A28),

$$\bar{\bar{F}}_j^{(\lambda)}\bar{\bar{G}}_j^{(\mu')}\bar{\bar{H}}_j^{(\nu')}$$
$$=\tfrac{1}{2}\sum\{(-1)^{\Sigma a}+(-1)^{\lambda+\mu'+\nu'}\}A^{(abcdef)}[f_j^{(a)}\cdot f_j^{(b)}]^{(\lambda)}+[g_j^{(c)}g_j^{(d)}]^{(\mu')}+[h_j^{(e)}h_j^{(f)}]^{(\nu')}+$$
$$-\tfrac{1}{2}(-1)^{\lambda+\mu'+\nu'}(A^{(000\lambda\mu'\nu')}+A^{(\lambda\mu'\nu'000)})\{f^{(\kappa)}g^{(\mu')}h^{(\nu')}\}_j+$$
$$\langle l^{8l+4}000;\,000|\sum f_i^{(0)}g_i^{(0)}h_i^{(0)}|l^{8l+4}000;\,000\rangle.$$

Here $T^{(\lambda,\mu',\nu')}$ is expanded as in (A10). However, these two-body and three-body interactions are difficult to calculate explicitly, and again a convenient way is to estimate (A19) directly when $p=2$ and 3 and subtract known terms from these results.

A similar but easier calculation gives $\mathscr{V}_{\mathrm{IIb}\gamma'\gamma}$, and

$$V_{ij}^{\mathrm{IIb}} = \sum(U^{(\lambda)}F^{(\lambda)})([V^{(\mu)}G^{(\mu')}]^{(\kappa)}\cdot[W^{(\nu)}H^{(\nu')}]^{(\kappa)}), \qquad \text{(A29)}$$

where the sum is over $\lambda, \mu, \nu, \kappa, \mu', \nu' (\lambda+\mu+\nu \neq 0, \lambda+\mu'+\nu' \neq 0)$. In (A29)

$$\langle \tfrac{1}{2}\,\tfrac{1}{2}\,l \| F^{(\lambda)} G^{(\mu')} H^{(\nu')} \| \tfrac{1}{2}\,\tfrac{1}{2}\,l \rangle$$

$$= \sum \frac{1}{E_0^{(0)} - E_n^{(0)}} \sum (-1)^{1+\lambda+\nu+\mu'+l+l_5+L_5+L'_5+\bar{L}_5}$$

$$9 \cdot (2T_5+1)(2\bar{T}_5+1)\{(2L'_5+1)(2\bar{L}'_5+1)(2L_5+1)(2\bar{L}_5+1)\}^{\frac{1}{2}}$$

$$\times (2\lambda+1) W^2(\tfrac{1}{2}\lambda\tfrac{1}{2}T_5; \tfrac{1}{2}\bar{T}_5)(2\mu+1)(2\mu'+1) W(\tfrac{1}{2}\mu\tfrac{1}{2}1; \tfrac{1}{2}1) W(\tfrac{1}{2}1\tfrac{1}{2}1; \tfrac{1}{2}\mu') U \begin{pmatrix} 1 & 1 & \mu \\ 1 & 1 & \mu' \\ 2 & 2 & k \end{pmatrix}$$

$$\times (2\nu+1)(2\nu'+1) W(l\nu l'_i L_5; l\bar{L}_5) W(lL'_5 l\bar{L}'_5; l_i \nu') U \begin{pmatrix} L_5 & \bar{L}_5 & \nu \\ L'_5 & \bar{L}'_5 & \nu' \\ 2 & 2 & k \end{pmatrix}$$

$$\times \langle n_i l_i nl 1 L'_5 \| S^{(2)} L^{(2)} \| n'_i l'_i nl 1 L_5 \rangle \Phi_\tau(T_5)$$

$$\langle n_i l_i nl 1 \bar{L}'_5 \| S^{(2)} L^{(2)} \| n'_i l'_i nl 1 \bar{L}_5 \rangle \Phi_\tau(\bar{T}_5).$$

The derivation of $\mathscr{V}_{\mathrm{IVa}\gamma'\gamma}$ is very simple. The result is

$$V_{ij}^{\mathrm{IVa}} = \sum_\lambda (S_{ij}^{(\lambda)} \cdot L_{\mathrm{eff}\,ij}^{(\lambda)})(a + b\boldsymbol{\tau}_i \cdot \boldsymbol{\tau}_j)^2, \tag{A30}$$

where

$$\langle nlnl 1L \| S^{(\lambda)} L_{\mathrm{eff}}^{(\lambda)} \| nlnl 1\bar{L} \rangle$$

$$= (-1)^\lambda (2\lambda+1) W(1122; \lambda 1) \sum \frac{1}{E_0^{(0)} - E_n^{(0)}} \sum_{L'} W(2L2\bar{L}; L'\lambda)$$

$$\cdot \langle nlnl 1L \| S^{(2)} L^{(2)} \| n_1 l_1 n_2 l_2 1L' \rangle$$

$$\times \langle n_1 l_1 n_2 l_2 1L' \| S^{(2)} L^{(2)} \| nlnl 1\bar{L} \rangle.$$

Finally,

$$V_{ij}^{\mathrm{IVb}} = \sum_\lambda (S_{ij}^{(\lambda)} \cdot L_{\mathrm{eff}\,ij}^{(\lambda)})(a + b\boldsymbol{\tau}_i \cdot \boldsymbol{\tau}_j)^2 \tag{A31}$$

where

$$\langle nlnl 1L \| S^{(\lambda)} L_{\mathrm{eff}}^{(\lambda)} \| nlnl 1\bar{L} \rangle$$

$$= (-1)^\lambda (2\lambda+1) W(1122; 1\lambda) \sum \frac{1}{E_0^{(0)} - E_n^{(0)}} \sum W(2L2\bar{L}; L'\lambda)$$

$$\cdot \langle nlnl 1L \| S^{(2)} L^{(2)} \| nln'l' 1L' \rangle$$

$$\times \langle nln'l' 1L' \| S^{(2)} L^{(2)} \| nlnl 1\bar{L} \rangle,$$

and

$$V_{ijk}^{\mathrm{IVb}} = \sum_{\substack{\lambda,\mu,\nu \\ \kappa,\mu',\nu'}} (U_i^{(\lambda)} \cdot F_{jk}^{(\lambda)})([V_i^{(\mu)} \cdot G_{jk}^{(\mu')}]^{(\kappa)} \cdot [W_i^{(\nu)} \cdot H_{jk}^{(\nu')}]^{(\kappa)}), \tag{A32}$$

where $\lambda+\mu+\nu \neq 0$, and

$$\langle nlnlT1L||F^{(\lambda)}G^{(\mu')}H^{(\nu')}||nlnl\bar{T}1\bar{L}\rangle$$

$$= \sum \frac{1}{E_0^{(0)}-E_n^{(0)}} \sum (-1)^{\mu+\nu+\kappa+1+L_4+L'_4}(2\lambda+1)(2\mu+1)(2\mu'+1)$$

$$U\begin{pmatrix} 1 & 1 & \mu \\ 1 & 1 & \mu' \\ 2 & 2 & \kappa \end{pmatrix}(2\nu+1)(2\nu'+1)U\begin{pmatrix} L' & \bar{L}' & \nu \\ L & \bar{L} & \nu' \\ 2 & 2 & \kappa \end{pmatrix}$$

$$\times \langle nlnl1L||S^{(2)}L^{(2)}||nln'l'1L'\rangle \Phi_\tau(T)\langle nln'l'T1L'||U^{(\lambda)}V^{(\mu)}W^{(\nu)}||nln'l'\bar{T}1\bar{L}\rangle$$

$$\times \langle nln'l'1\bar{L}'||S^{(2)}L^{(2)}||nlnl1\bar{L}\rangle \Phi_\tau(\bar{T}).$$

References

1) M. G. Mayer and J. H. D. Jensen, Elementary Theory of Nuclear Shell Structure (Wiley, New York, 1955)
2) A. E. Glassgold, Progress in Nuclear Physics **7** (1959) 123
3) J. P. Elliott and A. M. Lane, Phys. Rev. **96** (1954) 1660
4) R. J. Blin-Stoyle, Phil. Mag. **46** (1955) 973
5) C. A. Pearse, Phys. Rev. **106** (1957) 545
6) B. P. Nigam and M. K. Sundaresan, Phys. Rev. **111** (1958) 284
7) J. Sawicki and R. Folk, Nuclear Physics **11** (1959) 368
8) J. Sawicki, Nuclear Physics **13** (1959) 350
9) E. P. Wigner, Symposium on New Research Techniques in Physics, Rio de Janeiro, 1952
10) A. M. Feingold, Phys. Rev. **101** (1956) 258
11) Nagata, Sasakawa, Sawada and Tamagaki, Prog. Theor. Phys. **22** (1959) 274
12) Takagi, Watari and Yasuno, Prog. Theor. Phys. **22** (1959) 154, 549
13) B. Jancovici, Prog. Theor. Phys. **22** (1959) 585
14) T. Terasawa, Prog. Theor. Phys. **22** (1959) 150; Prog. Theor. Phys. **23** (1960) 87 (this paper will be referred to as I)
15) A. Arima and T. Terasawa, Prog. Theor. Phys. **23** (1960) 115 (this paper will be referred to as II)
16) Iwadare, Otsuki, Tamagaki and Watari, Supplement of Prog. Theor. Phys. no. 3 (1956); M. Konuma, H. Miyazawa and S. Otsuki, Prog. Theor. Phys. **19** (1958) 17; S. Otsuki, Prog. Theor. Phys. **20** (1958) 171; W. Watari, Prog. Theor. Phys. **20** (1958) 181; R. Tamagaki, Prog. Theor. Phys. **20** (1958) 505; Hamada, Iwadare, Otsuki, Tamagaki and Watari, Prog. Theor. Phys. **22** (1959) 566
17) B. Jancovici and I. Talmi, Phys. Rev. **95** (1954) 289
18) J. P. Elliott, Phil. Mag. **1** (1956) 503
19) W. M. Vissher and R. A. Ferrel, Phys. Rev. **107** (1957) 781
20) T. Tamura, Phys. Rev. **105** (1957) 1808
21) A. M. Feingold, Phys. Rev. **105** (1957) 944
22) A. M. Feingold, Phys. Rev. **114** (1959) 540
23) For example L. I. Schiff, Quantum Mechanics, (McGraw-Hill, New York 1955)
24) C. Bloch and J. Horowitz, Nuclear Physics **8** (1958) 91
25) M. Bolsterli and E. Feenberg, Phys. Rev. **101** (1956) 1349
26) Kalos, Biedenharn and Blatt, Nuclear Physics **1** (1956) 233
27) D. Kurath, Phys. Rev. **101** (1956) 216
28) J. P. Elliott and A. M. Lane, Handbuch der Physik **39** (1957) 241
29) S. Goldstein and I. Talmi, Phys. Rev. **105** (1957) 995;

I. Talmi and R. Thieberger, Phys. Rev. **103** (1956) 718;
R. D. Lawson and J. L. Uretsky, Phys. Rev. **106** (1957) 1369;
I. Talmi, Phys. Rev. **107** (1957) 326;
I. Unna and I. Talmi, Phys. Rev. **112** (1958) 452;
A. Arima, Prog. Theor. Phys. **19** (1958) 421
30) S. Goldstein and I. Talmi, Phys. Rev. **102** (1956) 589;
S. Pandya, Phys. Rev. **103** (1956) 956
31) S. Pandya and J. B. French, Ann. Phys. **2** (1957) 166
32) D. R. Inglis, Rev. Mod. Phys. **25** (1953) 390
33) D. H. Lyons, Phys. Rev. **105** (1957) 936
34) I. Talmi and E. P. Wigner, Phys. Rev. **91** (1953) 443 (A)
35) G. Flamand and K. W. Ford, preprint
36) L. S. Kisslinger, Phys. Rev. **104** (1956) 1077;
B. Jancovici, Phys. Rev. **107** (1957) 631; Nuovo Cim. **7** (1958) 290
37) R. D. Lawson and M. G. Mayer, Phys. Rev. **117** (1960) 174
38) M. Moshinsky, Nuclear Physics **13** (1959) 104
39) B. C. Carlson and I. Talmi, Phys. Rev. **96** (1954) 436
40) D. G. Ravenhall, Rev. Mod. Phys. **30** (1958) 430;
R. Hofstadter, Rev. Mod. Phys. **28** (1956) 214
41) G. Racah, Phys. Rev. **62** (1942) 438; **63** (1943) 367
42) J. S. Bell, Nuclear Physics **12** (1959) 117
43) M. Sugawara and S. Okubo, Phys. Rev. **117** (1960) 605, 611
44) J. Gammel and R. Thaler, Phys. Rev. **107** (1957) 291, 1337
45) Signell, Zinn and Marshak, Phys. Rev. Lett. **1** (1958) 416

1.B:1.C

Nuclear Physics **18** (1960) 224—244; © *North-Holland Publishing Co., Amsterdam*

Not to be reproduced by photoprint or microfilm without written permission from the publisher

TREATMENT OF SPECIAL TRANSLATIONALLY INVARIANT THREE-BODY PROBLEMS BY ADAPTED COORDINATES

P. MÖBIUS

Physikalisches Institut, Technische Hochschule, Aachen

Received 16 May 1960

Abstract: An attempt is made to compute the wave functions of the considered examples as functions of adapted coordinates which are appropriately chosen combinations of the particle coordinates. The purpose of introducing the adapted coordinates is to satisfy automatically most of the conditions which exist for a many-body wave function. The fully classified and antisymmetrized wave function is written as a linear combination of products of space, spin and isobaric spin functions. The concept of one-particle functions and Slater determinants is completely eliminated. Several examples with translationally invariant interactions are treated, one containing a repulsive core.

1. Introduction

For the treatment of the time-independent nuclear many-body problem with translationally invariant interaction between A nucleons one has to look for a function $\Psi'(1 \ldots A)$ which has to obey the following equations [1]):

$$\mathscr{H}'(1 \ldots i \ldots A)\Psi'(1 \ldots i \ldots A) = E'\Psi'(1 \ldots i \ldots A), \tag{1}$$

$$\sum_{i=1}^{A} \frac{\hbar}{i} \frac{\partial \Psi'}{\partial \mathbf{r}'_i} = \mathbf{P}\Psi'(1 \ldots i \ldots A), \tag{2}$$

$$\mathscr{P}(i, k)\Psi'(1 \ldots i, k \ldots A) = -\Psi'(1 \ldots i, k \ldots A), \tag{3}$$

where $\mathscr{H}'(1 \ldots i \ldots A)$ is the Hamilton operator of the system and $\mathbf{P}$ is its total linear momentum. The number i stands for an abbreviation of the space vector $\mathbf{r}'_i$, the spin variable $\boldsymbol{\sigma}_i$ and the isobaric spin variable $\boldsymbol{\tau}_i$ of the i-th particle:

$$i = (\mathbf{r}'_i, \boldsymbol{\sigma}_i, \boldsymbol{\tau}_i).$$

Equation (3) represents the Pauli principle $\mathscr{P}(i, k)$ meaning the permutation of the particle quantities i and k. The equations (1)—(3) must always be fulfilled. But there exist other conditions for Ψ' which depend on the structure of the Hamilton operator $\mathscr{H}'$. Taking into account the charge independence of the nuclear forces Ψ' has to be also an eigenfunction of

$$\mathfrak{T}^2\Psi'(1 \ldots A) = T(T+1)\Psi'(1 \ldots A), \tag{4}$$

$$\mathfrak{T}_z\Psi'(1 \ldots A) = M_T\Psi'(1 \ldots A), \tag{5}$$

where $\mathfrak{T}$ is the operator of the isobaric spin of the system and $\mathfrak{T}_z$ is its z-component. In this paper we shall consider only those cases where the interaction depends on the particle coordinates. Then it is possible to impose on Ψ' the following additional conditions:

$$\mathfrak{S}^2\Psi'(1\ldots A) = \hbar^2 S(S+1)\Psi'(1\ldots A), \tag{6}$$

$$\mathfrak{S}_z\Psi'(1\ldots A) = \hbar M_S\Psi'(1\ldots A), \tag{7}$$

and on a function † Ψ:

$$\mathfrak{L}^2\Psi = \hbar^2 L(L+1)\Psi, \tag{8}$$

$$\mathfrak{L}_z\Psi = \hbar M_L\Psi. \tag{9}$$

Here $\mathfrak{S}$ and $\mathfrak{S}_z$ are the operators of the intrinsic spin and its z-component, while $\mathfrak{L}$ and $\mathfrak{L}_z$ are the operators of the internal orbital angular momentum and its z-component ††. If necessary a transition can be made to a representation where Ψ is classified by the quantum numbers of the total internal angular momentum $I(\mathfrak{J} = \mathfrak{J}' - \mathfrak{L}_R = \mathfrak{L} + \mathfrak{S})$, its z-component M_I and L, S instead of L, M_L, S, M_S, using the Clebsch-Gordan coefficients [2]).

The idea of this paper is to replace the single-particle quantities by such adapted combinations of the particle quantities that a solution of the equation (1) satisfies automatically the conditions (2)—(9) as far as possible. This means necessarily removing the "independent-particle aspect" from the many-body wave function. In this description it is no longer possible to make statements how the properties of the system are composed of the contributions of the single particles.

An easy way to satisfy condition (2) is to separate off the kinetic energy of the centre-of-mass motion in the Hamilton operator $\mathscr{H}'$. This can be done by a linear orthogonal coordinate transformation replacing the A particle vectors $(\mathbf{r}'_1 \ldots \mathbf{r}'_A)$ by $(A-1)$ vectors $(\mathbf{r}_1 \ldots \mathbf{r}_{A-1})$ describing the internal motion and a vector $\mathbf{r}_A$ representing the centre-of-mass. The difficulties arising from this transformation with respect to the Pauli principle are mentioned in ref. [1]). A possible transformation is

$$\mathbf{r}_i = \mathbf{r}'_i - \frac{\sqrt{A}}{\sqrt{A}-1}\mathbf{R} + \frac{1}{\sqrt{A}-1}\mathbf{r}'_A \quad (1 \leqq i \leqq A-1), \tag{10a}$$

$$\mathbf{r}_A = \sqrt{A}\mathbf{R}, \tag{10b}$$

† The primed quantities (Ψ', $\mathscr{H}'$, $\mathfrak{L}'$, $\mathfrak{J}'$, E') refer to the total system, the unprimed quantities (Ψ, $\mathscr{H}$, $\mathfrak{L}$, $\mathfrak{J}$, E) to the "internal system" from which the centre-of-mass motion is separated.

†† The internal orbital angular momentum $\mathfrak{L} = \mathfrak{L}' - \mathfrak{L}_R$ is the orbital angular momentum of the system $\mathfrak{L}'$ minus that of the centre-of-mass about a fixed point in space $\mathfrak{L}_R$.

where **R** is the centre-of-mass vector

$$\mathbf{R} = \frac{1}{A}\sum_{1}^{A} \mathbf{r}'_i.$$

Describing the centre-of-mass motion by $\varphi(\mathbf{r}_A)$, there results for Ψ' the product

$$\Psi'(1 \ldots A) = \varphi(\mathbf{r}_A)\Psi(\mathbf{r}_1 \ldots \mathbf{r}_{A-1}, \boldsymbol{\sigma}_1 \ldots \boldsymbol{\sigma}_A, \boldsymbol{\tau}_1 \ldots \boldsymbol{\tau}_A), \tag{11}$$

and the next step is to investigate how the many-body wave function $\Psi(\mathbf{r}_1 \ldots \mathbf{r}_{A-1}, \boldsymbol{\sigma}_1 \ldots \boldsymbol{\sigma}_A, \boldsymbol{\tau}_1 \ldots \boldsymbol{\tau}_A)$ depends on certain combinations of the internal coordinates $(\mathbf{r}_1 \ldots \mathbf{r}_{A-1})$, the particle spins $(\boldsymbol{\sigma}_1 \ldots \boldsymbol{\sigma}_A)$ and isobaric spins $(\boldsymbol{\tau}_1 \ldots \boldsymbol{\tau}_A)$. The equations (1)—(9) permit us to write Ψ in the form

$$\Psi(\mathbf{r}_1 \ldots \mathbf{r}_{A-1}, \boldsymbol{\sigma}_1 \ldots \boldsymbol{\sigma}_A, \boldsymbol{\tau}_1 \ldots \boldsymbol{\tau}_A) = \sum_{\nu_1 \nu_2 \nu_3} q_{\nu_1 \nu_2 \nu_3} \psi^{\nu_1}(\mathbf{r}_1 \ldots \mathbf{r}_{A-1}) \chi^{\nu_2}(\boldsymbol{\sigma}_1 \ldots \boldsymbol{\sigma}_A) \zeta^{\nu_3}(\boldsymbol{\tau}_1 \ldots \boldsymbol{\tau}_A), \tag{12}$$

where the summation goes over a restricted number of "symmetry classes" for every ν_i. In eq. (12), $\chi^{\nu}(\boldsymbol{\sigma}_1 \ldots \boldsymbol{\sigma}_A)$ and $\zeta^{\nu}(\boldsymbol{\tau}_1 \ldots \boldsymbol{\tau}_A)$ are the spin- and isobaric spin functions which fulfil the equations (6)—(7) and (4)—(5). They can be obtained for a given number of particles A and spin S or isobaric spin T as the expansion coefficients of a function $F(x, y; S, A)$ which is easy to determine [3]):

$$F(x, y; S, A) = \sum_{M_S=-S}^{+S} \chi_{SM_S} x^{S+M_S} y^{S-M_S}. \tag{13}$$

It remains to look for the space functions $\psi^{\nu}(\mathbf{r}_1 \ldots \mathbf{r}_{A-1})$. Their symmetry properties are governed by the Young tableaux [4–6]) and they are computed with the help of the adapted coordinates.

In order to become familiar with the construction of the many-body wave function by means of the adapted quantities the method will be demonstrated for the simple case of 3 particles. This is intended only as an intermediate step leading to the formulation of the method with the "many-particle variables" [1]) which give results for an arbitrary number of particles. As the standard example is taken a system of three harmonically coupled particles:

$$\mathscr{H}' = \sum_{1}^{3} -\frac{\hbar^2}{2M}\frac{\partial^2}{\partial \mathbf{r}'^2_i} + \sum_{i>k=1}^{3} \tfrac{1}{2}c(\mathbf{r}'_i - \mathbf{r}'_k)^2. \tag{14}$$

Further examples are

$$\mathscr{H}' = \sum_{1}^{3} -\frac{\hbar^2}{2M}\frac{\partial^2}{\partial \mathbf{r}'^2_i} + \sum_{i>k=1}^{3} [\tfrac{1}{2}c(\mathbf{r}'_i - \mathbf{r}'_k)^2 + k(\mathbf{r}'_i - \mathbf{r}'_k)^4], \tag{15}$$

$$\mathscr{H}' = \sum_{1}^{3} -\frac{\hbar^2}{2M}\frac{\partial^2}{\partial \mathbf{r}'^2_i} + \sum_{i>k=1}^{3} \left[\tfrac{1}{2}c(\mathbf{r}'_i - \mathbf{r}'_k)^2 + \frac{\varepsilon^2}{(\mathbf{r}'_i - \mathbf{r}'_k)^2}\right], \tag{16}$$

the last one containing a repulsive core. After the separation of the centre-of-mass motion the two internal vectors $\mathbf{r}_1, \mathbf{r}_2$ are replaced by the following adapted coordinates:

$$\rho = x_1^2+x_2^2+y_1^2+y_2^2+z_1^2+z_2^2, \quad \xi = \frac{x_1^2+x_2^2}{x_1^2+x_2^2+y_1^2+y_2^2},$$

$$\eta = \frac{x_1^2+x_2^2+y_1^2+y_2^2}{x_1^2+x_2^2+y_1^2+y_2^2+z_1^2+z_2^2} \tag{17a}$$

$$\operatorname{tg}\varphi = \frac{x_2}{x_1}, \quad \operatorname{tg}\psi = \frac{y_2}{y_1}, \quad \operatorname{tg}\vartheta = \frac{z_2}{z_1}, \tag{17b}$$

where ρ, ξ, η are invariant by a permutation of two particles, while the angles transform e.g. as follows:

$$\mathscr{P}(i,k)\varphi = \alpha(i,k)-\varphi, \quad (0 < \alpha < 2\pi). \tag{18}$$

With these adapted coordinates it is possible to make exact statements about the energy spectrum for the examples (14)—(16). The use of methods of group theory is avoided as far as possible.

2. The one-dimensional 3-Particle System

2.1. SYMMETRY PROPERTIES OF THE SPACE FUNCTIONS

For the investigation of the structure and the symmetry properties of the space functions it is sufficient to treat the one-dimensional case. The space functions can be divided in different "symmetry groups" with respect to the permutation of two particles. The groups of the totally antisymmetric and the totally symmetric space functions were already treated in ref. [1]) for the example (14). But there exist other symmetry groups in which the corresponding space functions are of "intermediate symmetry". A great help for the description of this classification is provided by the so-called "Young tableaux" [4–6]). The number of symmetry groups of a system of A particles is equal to the number of "standard frames". A standard frame is a scheme consisting of A squares put in rows and columns in such a way that the number of squares in the rows does not increase downwards and the number of squares in the column does not increase from left to right. As examples the standard frames are given for $A = 2$ and $A = 3$ in fig. 1.

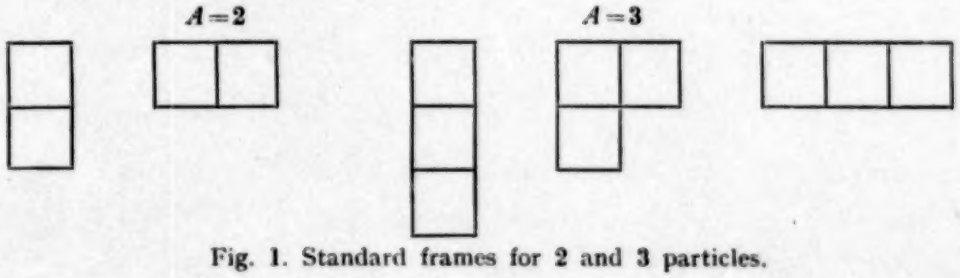

Fig. 1. Standard frames for 2 and 3 particles.

The "standard tableaux" are deduced from the standard frames by putting numbers in the squares in such a way that the numbers only increase if one goes from left to right or downwards. Their number is equal to the number of possible "symmetry classes". For the above example they are given in fig. 2.

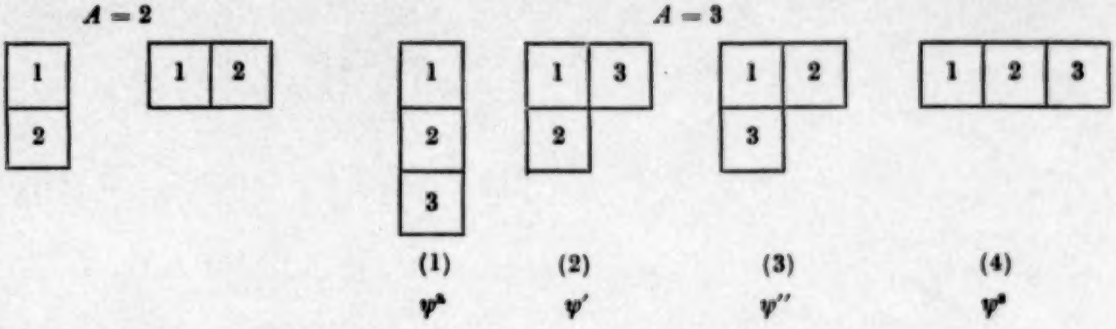

Fig. 2. Standard tableaux for 2 and 3 particles.

The number of symmetry classes is equal to, or greater than, the number of symmetry groups. For $A = 3$ there exist three symmetry groups and four symmetry classes. The functions corresponding to the standard tableaux (1)—(4) of fig. 2 will be designated by $\psi^A, \psi', \psi'', \psi^S$. All functions belonging to one standard frame form a group. We shall define the three symmetry groups in the following way:

$$\mathscr{P}(i,k)\psi^A(1,2,3) = -\psi^A(1,2,3) \quad (1 \leqq i,k \leqq 3), \tag{19}$$

$$\mathscr{P}(i,k)\psi^S(1,2,3) = +\psi^S(1,2,3) \quad (1 \leqq i,k \leqq 3), \tag{20}$$

and

$$\mathscr{P}(i,k)\psi'(1,2,3) = A(i,k)\psi'(1,2,3)+B(i,k)\psi''(1,2,3), \tag{21a}$$

$$\mathscr{P}(i,k)\psi''(1,2,3) = C(i,k)\psi'(1,2,3)+D(i,k)\psi''(1,2,3), \tag{21b}$$

with

$$A(i,k)D(i,k)-B(i,k)C(i,k) = -1. \tag{21c}$$

The two symmetry classes of the last group will be defined by

$$\mathscr{P}(1,2)\psi'(1,2,3) = -\psi'(1,2,3), \tag{22a}$$

$$\mathscr{P}(1,3)\psi''(1,2,3) = -\psi''(1,2,3). \tag{22b}$$

This is equivalent with putting $B(1,2) = 0$ and $C(1,3) = 0$. With these definitions one can interpret the standard tableaux by saying that the corresponding functions are antisymmetric with respect to the permutation of the numbers in each column.

2.2. SOLUTIONS OF THE SCHRÖDINGER EQUATIONS

After the separation of the centre-of-mass motion the Hamilton operators for the examples (14)—(16) are [1])

$$\mathscr{H} = -\frac{\hbar^2}{2M}\left(\frac{\partial^2}{\partial x_1^2}+\frac{\partial^2}{\partial x_2^2}\right)+\tfrac{3}{2}c(x_1^2+x_2^2), \tag{23}$$

$$\mathscr{H} = -\frac{\hbar^2}{2M}\left(\frac{\partial^2}{\partial x_1^2}+\frac{\partial^2}{\partial x_2^2}\right)+\tfrac{3}{2}c(x_1^2+x_2^2)+\tfrac{9}{2}k(x_1^2+x_2^2)^2, \tag{24}$$

$$\mathscr{H} = -\frac{\hbar^2}{2M}\left(\frac{\partial^2}{\partial x_1^2}+\frac{\partial^2}{\partial x_2^2}\right)+\tfrac{3}{2}c(x_1^2+x_2^2)+\left(\frac{\varepsilon}{x_1-x_2}\right)^2 + \left(\frac{\varepsilon(\sqrt{3}-1)}{(2-\sqrt{3})x_1+x_2}\right)^2+\left(\frac{\varepsilon(\sqrt{3}-1)}{x_1+(2-\sqrt{3})x_2}\right)^2. \tag{25}$$

Introducing the adapted coordinates ρ, φ given by

$$\rho = x_1^2+x_2^2, \quad \operatorname{tg}\varphi = \frac{x_2}{x_1},$$

the corresponding Schrödinger equations become

$$\left\{-\frac{\hbar^2}{2M}\left[4\rho\frac{\partial^2}{\partial\rho^2}+4\frac{\partial}{\partial\rho}+\frac{1}{\rho}\frac{\partial^2}{\partial\varphi^2}\right]+\tfrac{3}{2}c\rho\right\}\psi(\rho,\varphi) = E\psi(\rho,\varphi), \tag{26}$$

$$\left\{-\frac{\hbar^2}{2M}\left[4\rho\frac{\partial^2}{\partial\rho^2}+4\frac{\partial}{\partial\rho}+\frac{1}{\rho}\frac{\partial^2}{\partial\varphi^2}\right]+\tfrac{3}{2}c\rho+\tfrac{9}{2}k\rho^2\right\}\psi(\rho,\varphi) = E\psi(\rho,\varphi), \tag{27}$$

$$\left\{-\frac{\hbar^2}{2M}\left[4\rho\frac{\partial^2}{\partial\rho^2}+4\frac{\partial}{\partial\rho}+\frac{1}{\rho}\frac{\partial^2}{\partial\varphi^2}\right]+\tfrac{3}{2}c\rho+\frac{\varepsilon^2}{\rho}\left[\left(\frac{1}{\cos\varphi-\sin\varphi}\right)^2 + \left(\frac{\sqrt{3}-1}{(2-\sqrt{3})\cos\varphi+\sin\varphi}\right)^2+\left(\frac{\sqrt{3}-1}{\cos\varphi+(2-\sqrt{3})\sin\varphi}\right)^2\right]\right\}\psi(\rho,\varphi)=E\psi(\rho,\varphi). \tag{28}$$

All three equations can be separated exactly by the Ansatz

$$\psi(\rho,\varphi) = f(\rho)b(\varphi), \tag{29}$$

giving ordinary differential equations for $f(\rho)$ and $b(\varphi)$. The next step is to fulfil the Pauli principle. It does not act on $f(\rho)$ because ρ is invariant by a permutation of two particles. For $b(\varphi)$ we have the relations [1])

$$\mathscr{P}(1,2)b(\varphi) = b\left(\frac{3\pi}{6}-\varphi\right), \tag{30a}$$

$$\mathscr{P}(1,3)b(\varphi) = b\left(\frac{7\pi}{6}-\varphi\right), \tag{30b}$$

$$\mathscr{P}(2,3)b(\varphi) = b\left(\frac{11\pi}{6}-\varphi\right). \tag{30c}$$

which permit us in principle to construct the space functions for the different symmetry classes and to get the selection rules for the energy spectrum.

This will be demonstrated for the various examples. Let us begin with equation (26). Making the Ansatz

$$\psi_{n\lambda}(\rho, \varphi) = \rho^{\frac{1}{2}\lambda} f_{n\lambda}(\rho) b_\lambda(\varphi), \tag{31}$$

eq. (26) can be separated in the two equations

$$\rho \frac{\mathrm{d}^2 f_{n\lambda}}{\mathrm{d}\rho^2} + (1+\lambda)\frac{\mathrm{d}f_{n\lambda}}{\mathrm{d}\rho} + \frac{M}{2\hbar^2}(E_n - \tfrac{3}{2}c\rho) f_{n\lambda}(\rho) = 0, \tag{32}$$

$$\frac{\mathrm{d}^2 b_\lambda}{\mathrm{d}\varphi^2} + \lambda^2 b_\lambda(\varphi) = 0. \tag{33}$$

The solutions of eq. (32) are "Laguerre functions" [1]) with the eigenvalues

$$E_n = \hbar\omega[1+2n+\lambda], \quad (n = 0, 1, 2 \ldots), \tag{34}$$

where ω is defined by $\omega = (3c/M)^{\frac{1}{2}}$.

The selection rules for λ are obtained by looking for all solutions of (33) obeying the Pauli principle. A general solution of (33) is

$$b_\lambda(\varphi) = \sin(\lambda\varphi + \alpha_\lambda), \tag{35}$$

and all functions satisfying the condition

$$\mathscr{P}(1,2) b(\varphi) \equiv b\left(\frac{3\pi}{6} - \varphi\right) = -b(\varphi) \tag{36}$$

are

$$b'_\lambda(\varphi) = \sin\left(\lambda\varphi - \frac{\pi}{4}\lambda\right), \quad (\lambda = 1, 2, 3 \ldots), \tag{37}$$

and those satisfying

$$\mathscr{P}(1,3) b(\varphi) \equiv b\left(\frac{7\pi}{6} - \varphi\right) = -b(\varphi) \tag{38}$$

are

$$b''_\lambda(\varphi) = \sin\left(\lambda\varphi - \frac{7\pi}{12}\lambda\right), \quad (\lambda = 1, 2, 3 \ldots). \tag{39}$$

The totally antisymmetric space functions have to fulfil both conditions (36) and (38). This is the case if

$$\lambda = 3\kappa, \quad (\kappa = 1, 2, 3 \ldots). \tag{40}$$

Using the relations (19)—(22) and (36)—(40) the space functions and the corresponding energy spectra can be presented. They are

$$\psi^a = \rho^{\frac{1}{2}\kappa} f_{n\kappa}(\rho) \sin\left(3\kappa\varphi - \frac{3\pi}{4}\kappa\right), \tag{41a}$$

$$E^a = \hbar\omega[1+2n+3\kappa], \tag{41b}$$

$$(n = 0, 1, 2, \ldots; \kappa = 1, 2, 3, \ldots),$$

$$\psi^s = \rho^{\frac{1}{2}\kappa} f_{n\kappa}(\rho) \cos\left(3\kappa\varphi - \frac{3\pi}{4}\kappa\right), \tag{42a}$$

$$E^s = \hbar\omega[1+2n+3\kappa], \tag{42b}$$

$$(n, \kappa = 0, 1, 2, \ldots),$$

$$\psi' = \rho^{\frac{1}{2}\lambda} f_{n\lambda}(\rho) \sin\left(\lambda\varphi - \frac{\pi}{4}\lambda\right), \tag{43a}$$

$$E' = \hbar\omega[1+2n+\lambda], \tag{43b}$$

and

$$\psi'' = \rho^{\frac{1}{2}\lambda} f_{n\lambda}(\rho) \sin\left(\lambda\varphi - \frac{7\pi}{12}\lambda\right), \tag{43c}$$

$$E'' = \hbar\omega[1+2n+\lambda]. \tag{43d}$$

(In eqs. (43a)—(43d) we have $n = 0, 1, 2 \ldots$ and $\lambda =$ all positive integer numbers $\neq 3, 6, 9, \ldots$). The physical meaning of these spectra is given in section 3.

The example (27) can be treated in a similar way. Using (31) one obtains the two equations

$$\rho \frac{\mathrm{d}^2 f_{n\lambda}}{\mathrm{d}\rho^2} + (1+\lambda)\frac{\mathrm{d}f_{n\lambda}}{\mathrm{d}\rho} + \frac{M}{2\hbar^2}(E_n - \tfrac{3}{2}c\rho - \tfrac{9}{2}k\rho^2) f_{n\lambda}(\rho) = 0, \tag{44}$$

$$\frac{\mathrm{d}^2 b_\lambda}{\mathrm{d}\varphi^2} + \lambda^2 b_\lambda(\varphi) = 0. \tag{45}$$

Without application of perturbation theory one can only state

$$E_n = E_n(n, \lambda), \tag{46}$$

where the admissible values of n are determined by (44) and the selection rules for λ are the same as for (33).

In the case of (28) the Ansatz (31) gives the two equations

$$\rho \frac{\mathrm{d}^2 f_{n\lambda}}{\mathrm{d}\rho^2} + (1+\lambda)\frac{\mathrm{d}f_{n\lambda}}{\mathrm{d}\rho} + \frac{M}{2\hbar^2}(E_n - \tfrac{3}{2}c\rho) f_{n\lambda}(\rho) = 0, \tag{47}$$

$$\frac{\mathrm{d}^2 b_\lambda}{\mathrm{d}\varphi^2} + \left(\lambda^2 - \frac{2M\varepsilon^2}{\hbar^2} v(\varphi)\right) b_\lambda(\varphi) = 0, \tag{48}$$

with

$$v(\varphi) \equiv \left(\frac{1}{\cos\varphi-\sin\varphi}\right)^2 + \left(\frac{\sqrt{3}-1}{(2-\sqrt{3})\cos\varphi+\sin\varphi}\right)^2 + \left(\frac{\sqrt{3}-1}{\cos\varphi+(2-\sqrt{3})\sin\varphi}\right)^2. \quad (49)$$

The equation (47) is identical with (32), and therefore the energy spectrum is

$$E = \hbar\omega[1+2n+\lambda], \qquad (n = 0, 1, 2\ldots), \quad (50)$$

but the admissible values of λ are now determined by the solutions of (48) and by the requirements of the Pauli principle. A discussion of (48) will be given in a later paper.

3. Separation of the Schrödinger Equation in the 3-dimensional Case

After the separation of the centre-of-mass motion the Hamilton operators for the examples (14)—(16) are

$$\mathscr{H} = -\frac{\hbar^2}{2M}\left(\frac{\partial^2}{\partial \mathbf{r}_1^2}+\frac{\partial^2}{\partial \mathbf{r}_2^2}\right)+\tfrac{3}{2}c(\mathbf{r}_1^2+\mathbf{r}_2^2), \quad (51)$$

$$\mathscr{H} = -\frac{\hbar^2}{2M}\left(\frac{\partial^2}{\partial \mathbf{r}_1^2}+\frac{\partial^2}{\partial \mathbf{r}_2^2}\right)+\tfrac{3}{2}c(\mathbf{r}_1^2+\mathbf{r}_2^2)+\tfrac{9}{2}k(\mathbf{r}_1^2+\mathbf{r}_2^2)^2, \quad (52)$$

$$\mathscr{H} = -\frac{\hbar^2}{2M}\left(\frac{\partial^2}{\partial \mathbf{r}_1^2}+\frac{\partial^2}{\partial \mathbf{r}_2^2}\right)+\tfrac{3}{2}c(\mathbf{r}_1^2+\mathbf{r}_2^2) + \left(\frac{\varepsilon}{\mathbf{r}_1-\mathbf{r}_2}\right)^2+\left(\frac{\varepsilon(\sqrt{3}-1)}{(2-\sqrt{3})\mathbf{r}_1+\mathbf{r}_2}\right)^2+\left(\frac{\varepsilon(\sqrt{3}-1)}{\mathbf{r}_1+(2-\sqrt{3})\mathbf{r}_2}\right)^2. \quad (53)$$

As a first step the kinetic energy will be transformed in the adapted coordinates given by (17). The result is

$$\frac{\partial^2}{\partial \mathbf{r}_1^2}+\frac{\partial^2}{\partial \mathbf{r}_2^2} = 4\left(\rho\frac{\partial^2}{\partial\rho^2}+3\frac{\partial}{\partial\rho}+\frac{\eta(1-\eta)}{\rho}\frac{\partial^2}{\partial\eta^2}+\frac{(2-3\eta)}{\rho}\frac{\partial}{\partial\eta} + \frac{\xi(1-\xi)}{\rho\eta}\frac{\partial^2}{\partial\xi^2}+\frac{(1-2\xi)}{\rho\eta}\frac{\partial}{\partial\xi}\right)+\frac{1}{\rho\eta\xi}\frac{\partial^2}{\partial\varphi^2}+\frac{1}{\rho\eta(1-\xi)}\frac{\partial^2}{\partial\psi^2}+\frac{1}{\rho(1-\eta)}\frac{\partial^2}{\partial\vartheta^2}. \quad (54)$$

The potential energies in (51)—(53) are transformed in

$$V(\rho) = \tfrac{3}{2}c\rho, \quad (55)$$

$$V(\rho) = \tfrac{3}{2}c\rho+\tfrac{9}{2}k\rho^2, \quad (56)$$

$$V(\rho) = \frac{\varepsilon^2}{\rho}v(\xi, \eta, \varphi, \psi, \vartheta), \quad (57)$$

where $v(\xi, \eta, \varphi, \psi, \vartheta)$ is given by

$$\begin{aligned} v(\xi,\eta,\varphi,\psi,\vartheta) &= (1-\xi\eta\sin 2\varphi+(1-\xi)\eta\sin 2\psi+(1-\eta)\sin 2\vartheta)^{-1} \\ &+2\alpha(\xi\eta(\alpha\cos\varphi+\sin\varphi)^2+(1-\xi)\eta(\alpha\cos\psi+\sin\psi)^2+(1-\eta)(\alpha\cos\vartheta+\sin\vartheta)^2)^{-1} \\ &+2\alpha(\xi\eta(\cos\varphi+\alpha\sin\varphi)^2+(1-\xi)\eta(\cos\psi+\alpha\sin\psi)^2+(1-\eta)(\cos\vartheta+\alpha\sin\vartheta)^2)^{-1} \end{aligned} \tag{58}$$

with

$$\alpha = 2-\sqrt{3} = 0.268.$$

We shall now try to separate the corresponding Schrödinger equations. For the example (51) this can be done by standard methods. The wave function ψ is given by

$$\psi(\rho,\xi,\eta,\varphi,\psi,\vartheta) = \rho^{(n+\kappa+\frac{1}{2}(\lambda+\mu+\nu))} f_N(\rho)\xi^{\frac{1}{2}\lambda}(1-\xi)^{\frac{1}{2}\mu}g_\kappa(\xi)\eta^{(\kappa+\frac{1}{2}(\lambda+\mu))}(1-\eta)^{\frac{1}{2}\nu}p_n(\eta) \times b_\lambda(\varphi)c_\mu(\psi)e_\nu(\vartheta), \tag{59}$$

where the different functions obey the following ordinary differential equations:

$$\rho\frac{d^2f_N}{d\rho^2}+(3+2n+2\kappa+\lambda+\mu+\nu)\frac{df_N}{d\rho}+\frac{M}{2\hbar^2}(E_N-\tfrac{3}{2}c\rho)f_N(\rho)=0, \tag{60}$$

$$\xi(1-\xi)\frac{d^2g_\kappa}{d\xi^2}+(1+\lambda-(2+\lambda+\mu)\xi)\frac{dg_\kappa}{d\xi}+\kappa(\kappa+\lambda+\mu+1)g_\kappa(\xi)=0, \quad (\kappa=0,1,2\ldots), \tag{61}$$

$$\eta(1-\eta)\frac{d^2p_n}{d\eta^2}+(2+2\kappa+\lambda+\mu-(3+2\kappa+\lambda+\mu+\nu)\eta)\frac{dp_n}{d\eta} +n(n+2\kappa+\lambda+\mu+\nu+2)p_n(\eta)=0, \quad (n=0,1,2\ldots), \tag{62}$$

$$\frac{d^2b_\lambda}{d\varphi^2}+\lambda^2b_\lambda(\varphi)=0, \qquad (\lambda=0,1,2\ldots), \tag{63}$$

$$\frac{d^2c_\mu}{d\psi^2}+\mu^2c_\mu(\psi)=0, \qquad (\mu=0,1,2\ldots), \tag{64}$$

$$\frac{d^2e_\nu}{d\vartheta^2}+\nu^2e_\nu(\vartheta)=0, \qquad (\nu=0,1,2,\ldots). \tag{65}$$

The solutions of (60) are the "associated Laguerre functions" and those of (61) and (62) are the "Jacobi polynomials". From (60) one gets for the energy eigenvalues of the considered example the relation

$$E=\hbar\omega[3+2(N+n+\kappa)+\lambda+\mu+\nu], \tag{66}$$

where all six quantum numbers $N, n, \kappa, \lambda, \mu, \nu$ can be all non-negative integer numbers independently of each other.

In the case of (52) the Ansatz (59) gives the same ordinary differential equations except for (60) which becomes

$$\rho \frac{\mathrm{d}^2 f_N}{\mathrm{d}\rho^2} + (3+2n+2\kappa+\lambda+\mu+\nu) \frac{\mathrm{d}f_N}{\mathrm{d}\rho} + \frac{M}{2\hbar^2} (E_N - \tfrac{3}{2}c\rho - \tfrac{9}{2}k\rho^2) f_N(\rho) = 0. \quad (67)$$

Without application of perturbation theory one obtains only the degeneracy of the energy eigenvalues, due to the fact that E_N is only a function of two quantities

$$E_N = E_N(N, 2n+2\kappa+\lambda+\mu+\nu),$$

where the admissible values of n, κ, λ, μ, ν are the same as for the example (51).

For the treatment of the example (53) it is convenient to make for ψ the Ansatz

$$\psi(\rho, \xi, \eta, \varphi, \psi, \vartheta) = \rho^{(\sqrt{n^2+1}-1)} f_N(\rho) G(\xi, \eta, \varphi, \psi, \vartheta),$$

giving for $f_N(\rho)$ the equation

$$\rho \frac{\mathrm{d}^2 f_N}{\mathrm{d}\rho^2} + (1+2\sqrt{n^2+1}) \frac{\mathrm{d}f_N}{\mathrm{d}\rho} + \frac{M}{2\hbar^2} (E_N - \tfrac{3}{2}c\rho) f_N(\rho) = 0. \quad (68)$$

The solutions of (68) are again the "associated Laguerre functions" providing for the energy spectrum the relation

$$E = \hbar\omega[1+2N+2\sqrt{n^2+1}], \quad (N = 0, 1, 2 \ldots). \quad (69)$$

The admissible values of n must be determined by the solutions of the equation

$$\Big\{\eta(1-\eta) \frac{\partial^2}{\partial\eta^2} + (2-3\eta) \frac{\partial}{\partial\eta} + \frac{\xi(1-\xi)}{\eta} \frac{\partial^2}{\partial\xi^2} + \frac{(1-2\xi)}{\eta} \frac{\partial}{\partial\xi} + \tfrac{1}{4}\Big(\frac{1}{\eta\xi} \frac{\partial^2}{\partial\varphi^2} + \frac{1}{\eta(1-\xi)} \frac{\partial^2}{\partial\psi^2} + \frac{1}{(1-\eta)} \frac{\partial^2}{\partial\vartheta^2}\Big) - \frac{M\varepsilon^2}{2\hbar^2} v(\xi, \eta, \varphi, \psi, \vartheta) + n^2\Big\} G(\xi, \eta, \varphi, \psi, \vartheta) = 0,$$

and the requirements of the Pauli principle. A discussion of this equation will also be given in a later paper.

4. Pauli Principle

The classification of the space functions in the 3-dimensional case is completely analogous to that of the one-dimensional case. Therefore the solutions of the last section must also be assorted in the four symmetry classes characterized by the equations (19)—(22). Because the three variables ρ, ξ, η are invariant by a permutation of two particles the Pauli principle acts only on the three angles

φ, ψ, ϑ. The two important relations of the one-dimensional case (30a) and (30b) must here be modified as

$$\mathscr{P}(1,2)\psi(\rho,\xi,\eta,\varphi,\psi,\vartheta) = \psi\left(\rho,\xi,\eta,\frac{3\pi}{6}-\varphi,\frac{3\pi}{6}-\psi,\frac{3\pi}{6}-\vartheta\right), \tag{70a}$$

$$\mathscr{P}(1,3)\psi(\rho,\xi,\eta,\varphi,\psi,\vartheta) = \psi\left(\rho,\xi,\eta,\frac{7\pi}{6}-\varphi,\frac{7\pi}{6}-\psi,\frac{7\pi}{6}-\vartheta\right). \tag{70b}$$

If the space functions split in two parts, one containing only ρ, ξ, η and the other only φ, ψ, ϑ, the Pauli principle acts only on the second part. This is the case for the examples (14) and (15). Here it is sufficient to assort only the functions

$$\phi_{\lambda\mu\nu}(\varphi,\psi,\vartheta) = b_\lambda(\varphi)c_\mu(\psi)e_\nu(\vartheta).$$

For the application of the Pauli principle it is, however, convenient to develop the product $b_\lambda(\varphi)c_\mu(\psi)e_\nu(\vartheta)$ in the following four sets of functions:

$${}_1\phi_{\lambda\mu\nu} = \sin(\lambda\varphi+\mu\psi+\nu\vartheta+\alpha_\lambda+\beta_\mu+\gamma_\nu), \tag{71a}$$

$${}_2\phi_{\lambda\mu\nu} = \sin(\lambda\varphi+\mu\psi-\nu\vartheta+\alpha_\lambda+\beta_\mu-\gamma_\nu), \tag{71b}$$

$${}_3\phi_{\lambda\mu\nu} = \sin(\lambda\varphi-\mu\psi+\nu\vartheta+\alpha_\lambda-\beta_\mu+\gamma_\nu), \tag{71c}$$

$${}_4\phi_{\lambda\mu\nu} = \sin(\lambda\varphi-\mu\psi-\nu\vartheta+\alpha_\lambda-\beta_\mu-\gamma_\nu), \tag{71d}$$

where $\alpha_\lambda, \beta_\mu, \gamma_\nu$ are arbitrary phases. Because every ${}_k\phi_{\lambda\mu\nu}$ is also a solution it is now easy to assort them in the different symmetry classes. All functions ${}_k\phi'_{\lambda\mu\nu}$ fulfilling the condition

$$\mathscr{P}(1,2)\,{}_k\phi'_{\lambda\mu\nu} = -{}_k\phi'_{\lambda\mu\nu} \tag{72}$$

are, with the help of (70a),

$${}_1\phi'_{\lambda\mu\nu} = \sin\left(\lambda_1\varphi+\mu_1\psi+\nu_1\vartheta-\frac{\pi}{4}(\lambda_1+\mu_1+\nu_1)\right), \tag{73a}$$

$${}_2\phi'_{\lambda\mu\nu} = \sin\left(\lambda_2\varphi+\mu_2\psi-\nu_2\vartheta-\frac{\pi}{4}(\lambda_2+\mu_2-\nu_2)\right), \tag{73b}$$

$${}_3\phi'_{\lambda\mu\nu} = \sin\left(\lambda_3\varphi-\mu_3\psi+\nu_3\vartheta-\frac{\pi}{4}(\lambda_3-\mu_3+\nu_3)\right), \tag{73c}$$

$${}_4\phi'_{\lambda\mu\nu} = \sin\left(\lambda_4\varphi-\mu_4\psi-\nu_4\vartheta-\frac{\pi}{4}(\lambda_4-\mu_4-\nu_4)\right), \tag{73d}$$

and all functions ${}_k\phi''_{\lambda\mu\nu}$ fulfilling the condition

$$\mathscr{P}(1,3)\,{}_k\phi''_{\lambda\mu\nu} = -{}_k\phi''_{\lambda\mu\nu} \tag{74}$$

are, with the help of (70b),

$$ {}_1\phi''_{\lambda\mu\nu} = \sin\left(\lambda_1\varphi+\mu_1\psi+\nu_1\vartheta-\frac{7\pi}{12}(\lambda_1+\mu_1+\nu_1)\right), \tag{75a} $$

$$ {}_2\phi''_{\lambda\mu\nu} = \sin\left(\lambda_2\varphi+\mu_2\psi-\nu_2\vartheta-\frac{7\pi}{12}(\lambda_2+\mu_2-\nu_2)\right), \tag{75b} $$

$$ {}_3\phi''_{\lambda\mu\nu} = \sin\left(\lambda_3\varphi-\mu_3\psi+\nu_3\vartheta-\frac{7\pi}{12}(\lambda_3-\mu_3+\nu_3)\right), \tag{75c} $$

$$ {}_4\phi''_{\lambda\mu\nu} = \sin\left(\lambda_4\varphi-\mu_4\psi-\nu_4\vartheta-\frac{7\pi}{12}(\lambda_4-\mu_4-\nu_4)\right), \tag{75d} $$

where λ_k, μ_k, ν_k can be all non-negative integer numbers obeying the relation

$$ \lambda_k+\mu_k+\nu_k > 0. $$

With these relations it is possible to determine the functions belonging to the four symmetry classes represented by the standard tableaux of fig. 2. Tableau (1) characterizes the totally antisymmetric functions. They have to fulfil (72) and (74). These are all functions of (73) with

$$ \lambda_1+\mu_1+\nu_1 = 3\kappa_1+3, \quad \lambda_2+\mu_2-\nu_2 = 3\kappa_2, \quad \lambda_3-\mu_3+\nu_3 = 3\kappa_3, $$
$$ \lambda_4-\mu_4-\nu_4 = 3\kappa_4, \qquad (\kappa_i = 0, 1, 2\ldots). \tag{76} $$

To the intermediate symmetry corresponding to tableau (2) belong all functions of (73) satisfying the conditions

$$ \lambda_1+\mu_1+\nu_1 \neq 3\kappa_1, \quad \lambda_2+\mu_2-\nu_2 \neq 3\kappa_2, \quad \lambda_3-\mu_3+\nu_3 \neq 3\kappa_3, $$
$$ \lambda_4-\mu_4-\nu_4 \neq 3\kappa_4, \qquad (\kappa_i = 0, 1, 2\ldots). \tag{77} $$

Those belonging to tableau (3) are all functions of (75) satisfying also the conditions (77). For the totally symmetric functions represented by tableau (4) one obtains

$$ {}_1\phi^{s}_{\lambda\mu\nu} = \cos\left(\lambda_1\varphi+\mu_1\psi+\nu_1\vartheta-\frac{\pi}{4}(\lambda_1+\mu_1+\nu_1)\right), \tag{78a} $$

$$ {}_2\phi^{s}_{\lambda\mu\nu} = \cos\left(\lambda_2\varphi+\mu_2\psi-\nu_2\vartheta-\frac{\pi}{4}(\lambda_2+\mu_2-\nu_2)\right), \tag{78b} $$

$$ {}_3\phi^{s}_{\lambda\mu\nu} = \cos\left(\lambda_3\varphi-\mu_3\psi+\nu_3\vartheta-\frac{\pi}{4}(\lambda_3-\mu_3+\nu_3)\right), \tag{78c} $$

$$ {}_4\phi^{s}_{\lambda\mu\nu} = \cos\left(\lambda_4\varphi-\mu_4\psi-\nu_4\vartheta-\frac{\pi}{4}(\lambda_4-\mu_4-\nu_4)\right), \tag{78d} $$

where the λ_k, μ_k, ν_k have to satisfy the conditions

$$\lambda_1+\mu_1+\nu_1 = 3\kappa_1, \quad \lambda_2+\mu_2-\nu_2 = 3\kappa_2, \quad \lambda_3-\mu_3+\nu_3 = 3\kappa_3,$$
$$\lambda_4-\mu_4-\nu_4 = 3\kappa_4, \qquad (\kappa_i = 0, 1, 2 \ldots). \tag{79}$$

Comparing (79) with (76) one sees that the permitted values for λ_k, μ_k, ν_k are the same for the totally antisymmetric and totally symmetric functions ${}_k\phi_{\lambda\mu\nu}$ except for the term 0, 0, 0, which is forbidden for the former. Just this term is responsible for the fact that the spectra of the whole space functions ψ^a and ψ^s become entirely different. The selection rules for λ_k, μ_k, ν_k written in the form (76), (77), (79) have the disadvantage that some of the functions occur several times. Therefore they do not characterize the degeneracy. Because the energy (66) or (67) depends only on the expression $\lambda+\mu+\nu$ the degeneracy with respect to these three quantum numbers is obtained by looking for all independent $\phi_{\lambda\mu\nu}$ for a definite value of $\lambda+\mu+\nu$. This is done in table 1 for the four lowest values of $\lambda+\mu+\nu$.

TABLE 1

Degeneracy of the functions $\phi_{\lambda\mu\nu}$

$\lambda+\mu+\nu$	$\phi^s_{\lambda\mu\nu}$	$\phi'_{\lambda\mu\nu}, \phi''_{\lambda\mu\nu}$	$\phi^a_{\lambda\mu\nu}$
0	1		
1		3	
2	3	6	3
3	10	11	10

As an example, the totally symmetric functions $\phi^s_{\lambda\mu\nu}$ will be given for the three lowest values of $\lambda+\mu+\nu$:

$$\begin{aligned} &\lambda+\mu+\nu = 0: \quad 1, \\ &\lambda+\mu+\nu = 1: \quad \text{no function}, \\ &\lambda+\mu+\nu = 2: \quad \cos(\varphi-\vartheta), \cos(\varphi-\psi), \cos(\psi-\vartheta). \end{aligned} \tag{80}$$

5. Classification of the Space Functions

In this section we shall re-order the space functions ψ for a given energy and symmetry class in such a way that they are also eigenfunctions of the equations

$$\mathfrak{L}^2\psi = \hbar^2 L(L+1)\psi, \tag{81}$$

$$\mathfrak{L}_z\psi = \hbar M_L\psi, \tag{82}$$

where $\mathfrak{L}$ and $\mathfrak{L}_z$ are the operators of the internal orbital angular momentum ($\mathfrak{L} = \mathfrak{L}'-\mathfrak{L}_R$) and its z-component. It is advantageous to begin with the

condition (82). The operator $\mathfrak{L}_z$ has in the internal coordinates the form [1])

$$\mathfrak{L}_z = \frac{\hbar}{i} \sum_1^2 \left(x_i \frac{\partial}{\partial y_i} - y_i \frac{\partial}{\partial x_i} \right), \tag{83}$$

and the transformation of (83) in the adapted coordinates (17) yields

$$\mathfrak{L}_z = \frac{\hbar}{i} [\xi(1-\xi)]^{\frac{1}{2}} \left\{ -2 \cos(\varphi-\psi) \frac{\partial}{\partial \xi} + \sin(\varphi-\psi) \left(\frac{1}{\xi} \frac{\partial}{\partial \varphi} + \frac{1}{(1-\xi)} \frac{\partial}{\partial \psi} \right) \right\}. \tag{84}$$

Because $\mathfrak{L}_z$ does not contain the variables ρ and η it is convenient to split up the space function in two parts, one containing only the variables ρ, η and the other containing the remaining variables ξ, φ, ψ, ϑ. Calling the last one

$$Q_{\kappa\lambda\mu\nu}(\xi, \varphi, \psi, \vartheta) = \xi^{\frac{1}{2}\lambda} (1-\xi)^{\frac{1}{2}\mu} g_\kappa(\xi) \phi_{\lambda\mu\nu}(\varphi, \psi, \vartheta), \tag{85}$$

one need only to assort the $Q_{\kappa\lambda\mu\nu}$ in eigenfunctions of $\mathfrak{L}_z$. In order to do this we make the Ansatz

$$U_M = \sum_{2\kappa+\lambda+\mu+\nu=\text{const}} p_{\kappa\lambda\mu\nu} Q_{\kappa\lambda\mu\nu} \tag{86}$$

in the equation

$$\mathfrak{L}_z U_M - \hbar M_L U_M = 0, \tag{87}$$

which gives a finite homogeneous system of equations for the coefficients $p_{\kappa\lambda\mu\nu}$. Their solutions determine the functions U_M. The multiplication of U_M with the factor

$$\rho^{(n+\kappa+\frac{1}{2}(\lambda+\mu+\nu))} f_N(\rho) \eta^{(\kappa+\frac{1}{2}(\lambda+\mu))} (1-\eta)^{\frac{1}{2}\nu} p_n(\eta) \tag{88}$$

provides the whole space functions, if they fulfil at the same time the condition (81). If not, one has to repeat a similar procedure to fulfil also the equation (81) but only with functions of the same M_L.

The space functions

$$\psi^\nu_{ELM_L} \tag{89}$$

can now be classified by four quantities: the symmetry class ν and the three quantum numbers E, L, M_L for the energy, the internal orbital angular momentum and its z-component.

As examples, the totally symmetric space functions of (59) are given for the states with 0 and 2 excited quanta $\hbar\omega$. Using the number of excited quanta r instead of the energy E they are for $r = 0$:

$$\psi^s_{200} = f_0(\rho), \qquad (L = 0, M_L = 0), \tag{90a}$$

and for $r = 2$:

$$\begin{aligned}
\psi^s_{000} &= f_1(\rho), && (L = 0, M_L = 0), \\
\psi^s_{220} &= \rho f_0(\rho) p_1(\eta), && (L = 2, M_L = 0), \\
\psi^s_{22\pm1} &= \rho f_0(\rho) \sqrt{\eta(1-\eta)} [\sqrt{1-\xi} \cos(\psi-\vartheta) \mp i\sqrt{\xi} \cos(\varphi-\vartheta)], \\
& && (L = 2, M_L = \pm 1), \\
\psi^s_{22\pm2} &= \rho f_0(\rho) \eta [(1-2\xi) \mp 2i\sqrt{\xi(1-\xi)} \cos(\varphi-\psi)], && (L = 2, M_L = \pm 2).
\end{aligned} \tag{90b}$$

6. Spin and Isobaric Spin Functions

The spin and isobaric spin functions can be represented by Young tableaux having not more than two rows. Because the results are entirely analogous for both kinds of functions, we consider mainly the spin functions. If the number of squares in the upper row of the Young tableau is n_1 and that of the lower row is n_2 the spin quantum number S of the corresponding function is [4,5])

$$S = \tfrac{1}{2}(n_1 - n_2). \tag{91}$$

The number of possible multiplets with spin S for a system of A particles is equal to the number of standard tableaux having not more than two rows. The result is given in table 2.

TABLE 2

Number of multiplets with spin S as function of the number of particles ($1 \leqq A \leqq 6$)

A \ S	0	$\frac{1}{2}$	1	$\frac{3}{2}$	2	$\frac{5}{2}$	3
1		1					
2	1		1				
3		2		1			
4	2		3		1		
5		5		4		1	
6	5		9		5		1

This scheme can easily be completed for greater values of A, because the numbers in each row are the sum of the next two neighbours of the upper row, except of the first column. Here it is only the next neighbour. The $(2S+1)$ spin functions χ_{SM_S} which exist to a multiplet with spin S can be obtained as the expansion coefficients of a function F of two variables x, y [3]),

$$F(x, y; S, A) = \sum_{M_S=-S}^{+S} \chi_{SM_S} x^{S+M_S} y^{S-M_S}. \tag{92}$$

We shall now derive a rule for the construction of F. If a system of A particles has the spin S, then

$$g = \tfrac{1}{2}A - S \tag{93}$$

pairs exist in which the particles have opposite spin and

$$2S \tag{94}$$

particles have parallel spins. The corresponding standard tableau consists of g columns with two squares and $2S$ columns with only one square. Let us call the spin function of the i-th particle with spin up α_i and with spin down β_i. For

every column with two squares containing the numbers i and k we form the expression

$$\alpha_i\beta_k-\alpha_k\beta_i, \tag{95}$$

and for every column with only one square containing the number j the expression

$$\alpha_j x+\beta_j y. \tag{86}$$

The function F is now obtained by multiplying the g factors (95) with the $2S$ factors (96):

$$F(x, y; S, A) = \prod_{i,k}^{g} (\alpha_i\beta_k-\alpha_k\beta_i) \prod_{j}^{2S} (\alpha_j x+\beta_j y). \tag{97}$$

The expansion coefficients of (97) are the spin functions χ_{SM_S} without normalization factors. If a_i denotes that the i-th particle is in a proton state and b_i that it is in a neutron state, the isobaric spin functions ζ_{TM_T} are obtained from the spin functions χ_{SM_S} by replacing α_i with a_i and β_i with b_i.

In the case of three particles there exist three standard tableaux with not more than two rows. They are given in fig. 3.

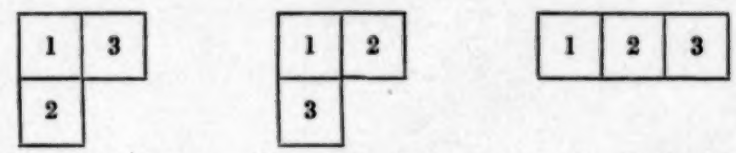

(2) $S=\frac{1}{2}$ F' (3) $S=\frac{1}{2}$ F'' (4) $S=\frac{3}{2}$ F^3

Fig. 3. Standard tableaux for the spin functions ($A = 3$).

The three corresponding functions F are

$$\begin{aligned} F' &= (\alpha_1\beta_2-\alpha_1\beta_2)(\alpha_3 x+\beta_3 y), \quad F'' = (\alpha_1\beta_3-\alpha_3\beta_1)(\alpha_2 x+\beta_2 y), \\ F^3 &= (\alpha_1 x+\beta_1 y)(\alpha_2 x+\beta_2 y)(\alpha_3 x+\beta_2 y), \end{aligned} \tag{98}$$

providing the spin functions according to (92).

7. The total Wave Function

The total wave function has to satisfy the conditions (1)—(9). It can be written as a linear combination of products of space, spin and isobaric spin functions as is done in (12). The summation over a restricted number of symmetry classes means the summation over all symmetry classes belonging to one standard frame. Because the conditions (4)—(9) are already satisfied by the single functions, the problem is next to look for such linear combinations that the total wave function fulfils the Pauli principle (3). It is convenient to assort the states by their values of S and T. A wave function with given values of S and T can only contain the corresponding spin and isobaric spin functions multi-

plied by the space functions belonging to one standard frame. The admitted combinations are then determined by applying condition (3). How to find the combinations will be demonstrated for the case of three particles.

Here exist three standard frames with the corresponding functions

$$(\psi^s), \quad (\psi', \psi''), \quad (\psi^s). \tag{99}$$

The possible combinations of spin and isobaric spin functions are

$$\text{for } T=\tfrac{3}{2}, S=\tfrac{3}{2}: \qquad q_1\chi^s\zeta^s, \tag{100a}$$

$$\text{for } T=\tfrac{3}{2}, S=\tfrac{1}{2}: \qquad (q_1\chi'+q_2\chi'')\zeta^s, \tag{100b}$$

$$\text{for } T=\tfrac{1}{2}, S=\tfrac{3}{2}: \qquad \chi^s(q_1\zeta'+q_2\zeta''), \tag{100c}$$

$$\text{for } T=\tfrac{1}{2}, S=\tfrac{1}{2}: \qquad (q_1\chi'+q_2\chi'')\zeta'+(q_3\chi'+q_4\chi''_4)\zeta'', \tag{100d}$$

where the q_i are arbitrary coefficients and χ', χ'', χ^s are the spin functions and ζ', ζ'', ζ^s are the isobaric spin functions belonging to the tableaux (2), (3), (4) of fig. 3. Every expression of (100) can be combined with the functions of one bracket of (99). A possible combination is e.g.

$$\Psi = q_1\psi^s\chi^s\zeta^s, \tag{101}$$

because the condition (3)

$$\mathscr{P}(i,k)\Psi+\Psi=0 \tag{102}$$

provides

$$q_1(-\psi^s\chi^s\zeta^s+\psi^s\chi^s\zeta^s)=0,$$

which is fulfilled for arbitrary q_1, so that (101) is permitted. This is not the case for

$$\Psi = q_1\psi^s\chi^s\zeta^s,$$

because condition (102) provides

$$q_1(\psi^s\chi^s\zeta^s+\psi^s\chi^s\zeta^s)=0,$$

which requires

$$2q_1=0.$$

Not so easy are the computations for $T=\frac{1}{2}$, $S=\frac{1}{2}$. Let us start with the Ansatz

$$\Psi = \psi^s[(q_1\chi'+q_2\chi'')\zeta'+(q_3\chi'+q_4\chi'')\zeta'']. \tag{103}$$

Using the equations (21a, b) one obtains

$$\begin{aligned}\mathscr{P}(i,k)\Psi = \psi^s[&\chi'\zeta'(q_1A^2+q_2AC+q_3AC+q_4C^2)\\ &+\chi''\zeta'(q_1AB+q_2AD+q_3AD+q_4CD)\\ &+\chi'\zeta''(q_1AB+q_2BC+q_3AD+q_4CD)+\chi''\zeta''(q_1B^2+q_2BD+q_3BC+q_4D^2)],\end{aligned}$$

and the condition (102) gives the following system of equations if one compares the coefficients by the same combinations of functions:

$$q_1(1+A^2)+q_2AC \quad +q_3AC \quad +q_4C^2 \quad = 0, \tag{104a}$$

$$q_1AB \quad +q_2(1+AD)+q_3BC \quad +q_4CD \quad = 0, \tag{104b}$$

$$q_1AB \quad +q_2BC \quad +q_3(1+AD)+q_4CD \quad = 0, \tag{104c}$$

$$q_1B^2 \quad +q_2BD \quad +q_3BD \quad +q_4(1+D^2) = 0. \tag{104d}$$

Replacing $(1+AD)$ by BC because of (21c) the equations (104b) and (104c) become identical. There remain

$$\begin{aligned} q_1(1+A^2)+(q_2+q_3)AC+q_4C^2 \quad &= 0, \\ q_1AB \quad +(q_2+q_3)BC+q_4CD \quad &= 0, \\ q_1B^2 \quad +(q_2+q_3)BD+q_4(1+D^2) &= 0, \end{aligned} \tag{105}$$

a homogeneous system of equations for the coefficients q_1, q_2+q_3, q_4 with non-vanishing determinant. This requires

$$q_1 = 0, \quad q_2+q_3 = 0, \quad q_4 = 0. \tag{106}$$

Because no further condition exists for the q_i the Ansatz (103) provides †

$$\Psi = \psi^s(\chi''\zeta'-\chi'\zeta'')q_2. \tag{107}$$

Similar calculations give the results which are presented in the table 3.

TABLE 3

Admitted combinations of space, spin and isobaric spin functions for $A = 3$

	$S = \frac{3}{2}$	$S = \frac{1}{2}$
$T = \frac{3}{2}$	$\psi^s\chi^s\zeta^s$	$(\psi'\chi''-\psi''\chi')\zeta^s$
$T = \frac{1}{2}$	$(\psi'\zeta''-\psi''\zeta')\chi^s$	$\psi^s(\chi'\zeta''-\chi''\zeta')$

TABLE 4

Sequences of states with equal values of S and T

Excitation energy in $\hbar\omega$	$T = \frac{3}{2}$, $S = \frac{3}{2}$ $\psi^a_{ELM_L}$	$T = \frac{3}{2}, S = \frac{1}{2}$; $T = \frac{1}{2}, S = \frac{3}{2}$ $\psi'_{ELM_L}, \psi''_{ELM_L}$	$T = \frac{1}{2}$, $S = \frac{1}{2}$ $\psi^s_{ELM_L}$
2	(3) $L = 1$	(6) $L = 0,2$	(6) $L = 0,2$
1		(3) $L = 1$	
0			(1) $L = 0$

† This is in disagreement with the result given by M. Verde [7]).

From table 3 one can conclude that the spectra of the space functions $\psi^{\nu}_{ELM_L}$ represent the sequences of states having the same values of S and T. In table 4 the spectrum of the example (51) is given in such a classification for the three lowest states of the system. The degeneracy of the states, which is written in the brackets (), and the values of L are presented.
So far the total wave functions have been classified by the seven quantum numbers $(E, L, M_L, S, M_S, T, M_T)$ according to (1)—(9):

$$\Psi \equiv \Psi(E, L, M_L, S, M_S, T, M_T). \tag{108}$$

A transition to a representation in which the four quantum numbers (L, M_L, S, M_S) are replaced by the quantum numbers of the total internal spin I, its z-component M_I, L and S can be made with the help of the Clebsch-Gordan coefficients [2]):

$$\Psi(E, I, M_I, L, S, T, M_T) = \sum_{M_L, M_S} C_{LS}(I, M_I, M_L, M_S)\Psi(E, L, M_L, S, M_S, T, M_T). \tag{109}$$

Eliminating M_L by the relation

$$M_L = M_I - M_S, \tag{110}$$

eq. (109) reduces to

$$\Psi(E, I, M_I, L, S, T, M_T) = \sum_{M_S=+S}^{-S} C_{LS}(I, M_I, M_I-M_S, M_S)\Psi(E, L, M_I-M_S, S, M_S, T, M_T). \tag{111}$$

As an example, the summation is worked out for the states with $S = \frac{1}{2}$, $T = \frac{1}{2}$ of table 3. For $I = L+\frac{1}{2}$, eqs. (111) and (107) yield

$$\Psi(E, L+\tfrac{1}{2}, M_I, L, S, T, M_T) = \left(\frac{L+\frac{1}{2}+M_I}{2L+1}\right)^{\frac{1}{2}} \psi^{S}_{E, L, M_I-\frac{1}{2}}(\zeta' \chi''_{\frac{1}{2},\frac{1}{2}} - \zeta'' \chi'_{\frac{1}{2},\frac{1}{2}}) \tag{112a}$$
$$+ \left(\frac{L+\frac{1}{2}-M_I}{2L+1}\right)^{\frac{1}{2}} \psi^{S}_{E, L, M_I+\frac{1}{2}}(\zeta' \chi''_{\frac{1}{2},-\frac{1}{2}} - \zeta'' \chi'_{\frac{1}{2},-\frac{1}{2}}),$$

and for $I = L-\frac{1}{2} (L > 0)$,

$$\Psi(E, L-\tfrac{1}{2}, M_I, L, S, T, M_T) = -\left(\frac{L+\frac{1}{2}-M_I}{2L+1}\right)^{\frac{1}{2}} \psi^{S}_{E, L, M_I-\frac{1}{2}}(\zeta' \chi''_{\frac{1}{2},\frac{1}{2}} - \zeta'' \chi'_{\frac{1}{2},\frac{1}{2}})$$
$$+ \left(\frac{L+\frac{1}{2}+M_I}{2L+1}\right)^{\frac{1}{2}} \psi^{S}_{E, L, M_I+\frac{1}{2}}(\zeta' \chi''_{\frac{1}{2},-\frac{1}{2}} - \zeta'' \chi'_{\frac{1}{2},-\frac{1}{2}}), \tag{112b}$$

where the quantum numbers S, M_S are added to the spin functions.

8. Concluding Remarks

The idea of this paper is to compute the wave functions for several examples by means of adapted quantities. The total wave function is written as a linear combination of products of space, spin and isobaric spin functions. Every function satisfies the corresponding conditions, contained in (1)—(9), by itself alone. A rule is derived for constructing the spin and isobaric spin functions for a given number of particles A and intrinsic spin S or isobaric spin T. The space functions are divided in different symmetry classes which are characterized by the Young tableaux. In order to compute them the particle coordinates are replaced by adapted coordinates making it easy to fulfil the conditions (1)—(9) However, no definite relation is given between the structure of the adapted coordinates and the form of the interaction. It was intended in this and the preceding paper [1]) to remove the "independent-particle aspect" as far as possible. It may be that a total elimination of the "independent-particle description" in the nuclear many-body problem will open some new aspects about the nuclear "collective coordinates".

References

1) P. Möbius, Nuclear Physics **16** (1960) 278
2) J. Blatt and V. F. Weisskopf, Theoretical Nuclear Physics (Wiley, New York, 1952)
3) B. L. van der Waerden, Die gruppentheoretische Methode in der Quantenmechanik (Springer, Berlin, 1932)
4) L. D. Landau and E. M. Lifschitz, Quantum Mechanics (Pergamon Press, London, 1958)
5) I. S. Šapiro, Fortschr. d. Phys. **7** (1959) 243 (translation from Uspechi fiz. Nauk **3** (1954) 7) (all further references are to be found in this paper)
6) M. Kretschmar, Z.f. Phys. **157** (1960) 433 and 558; **158** (1960) 284 (all further references are to be found in this paper)
7) M. Verde, in Handbuch der Physik (Springer, Berlin, 1957) Vol. 39, p. 148

1.B:2.L

Nuclear Physics **18** (1960) 245—270; © *North-Holland Publishing Co., Amsterdam*

Not to be reproduced by photoprint or microfilm without written permission form the publisher

AN IMPROVED APPROXIMATION FOR SCATTERING PROBLEMS

P. SWAN

Department of Physics, University of Melbourne

Received 16 May 1960

Abstract: A method for calculating the scattering phase-shift in atomic and nuclear collision problems is developed. In the limit of high collision energies the method reduces to a second Born approximation for the phase-shift and for low energies to the shape independent formula. The accuracy attained is an order of magnitude better than the first or second Born approximations, due to the distortion of the wave function of the scattered particle by the potential well being allowed for in a simple manner. The method applies over the whole range of energies and involves one extra integral besides the first Born approximation integral. No multiple integrals are needed as in higher Born approximations.

A detailed comparison is made between numerical results at a number of energies, for ^{3}S and ^{1}S neutron-proton scattering by four central potentials, phase-shifts being computed on the CSIRAC digital computer by numerical solution of the wave equation, by the Born approximation, and by the new method. It is found that the method gives best results for short-tailed potentials.

Many-body scattering phenomena may be treated with the same degree of simplification. Charged particle scattering is also considered and the corresponding shape independent formula derived. The latter is tested on ^{1}S proton-proton scattering.

An improved formula for binding energies, not involving any undetermined variational parameters, is obtained and tested on the deuteron.

1. Introduction

The problem of finding an improved Born approximation for the scattering phase-shift has usually been considered as one of determining a convenient Born expansion [1, 2]). However, such higher Born approximations are in general too complicated for convenient use, and in particular involve multiple integrals, the n-th correcting term to the leading term or first-order Born approximation being an n-fold integral. Application to nuclear scattering problems has also shown that there is no guarantee that the second-order Born approximation will give better results than the first-order one, implying that the convergence of the Born series may be slow.

In this paper it is shown that by dividing the scattering wave function into two parts, the one a plane wave outside a cut-off range r_a, the other a plane wave modified by a simple form factor $f_l(r)$ for $r \leqq r_a$, a greatly improved approximate formula for the elastic scattering phase-shift δ_l is obtained:

$$\tan \delta_l = B_{1l}/(1-B_{2l}), \tag{1}$$

where B_{1l} is the usual first-order Born approximation integral and B_{2l} an

integral involving the form factor $f_l(r)$ and spherical Bessel and Neumann functions. The presence of B_{2l} enables strong interference effects to occur, impossible in the first-order Born approximation

$$\delta_l = B_{1l}. \tag{2}$$

The distorting effect of the potential shape $V(r)$ on the incident wave function is explicitly allowed for in the new approximation, so that the accuracy attained is that of a high order Born approximation. Thus δ_l is obtained even at low energies to an accuracy of 1 to 2 % or better.

At high energies we have $\delta_l \to 0$ and $B_{2l} \approx 1/k^2 \to 0$, so that (1) reduces to the first Born approximation (2). On the other hand, for $k \ll 1$ and $l = 0$, (1) reduces to the form

$$k \cot \delta_0 = A + Bk^2 + Ck^4, \tag{3}$$

where numerical examples approximately identify the constants with $A = -1/a$, $B = \frac{1}{2}r_0$, $C = -Pr_0^3$, where a, r_0 and P are the zero energy scattering length, effective range and shape parameter respectively. (3) is thus an approximate form of the shape independent formula familiar in neutron-proton and proton-proton scattering [3, 4, 5]).

The above theory may be extended to charged particle scattering by replacing plane waves by the corresponding Coulomb wave functions. Application is also made to many-body scattering and to binding energies. Tensor forces are not treated in this paper.

A large number of phase-shifts (208) have been computed for ^{3}S and ^{1}S n—p scattering, using square, gaussian, exponential and Yukawa central wells, a number of values of orbital angular momentum l, and six energies ranging from 0.8 MeV to 186 MeV. The purpose is to test the approximation under a wide variety of conditions. Results are generally very much better than for the Born approximation and are usually within several percent of correct values. However, the method is best adapted to short-tailed potentials such as the square, gaussian and Woods-Saxon types. Long-talied potentials such as the exponential or Yukawa may in certain cases (k large) show no improvement. The one arbitrary quantity is the cut-off range r_α. However, results are very insensitive to any reasonable choice of r_α, except at very low energies or for singular potentials. The best results are obtained if r_α is chosen to give the experimental zero energy scattering length a, thus normalizing δ_0 correctly at zero energy. As δ_l must agree at high energies, this should give the best overall fit, besides correct values at low energies. r_α does not vary very much for different potentials.

2. Expression for the Elastic Scattering Phase-Shift

The wave equation for the scattering of neutral particles by a central potential $V(r)$ is

$$u_l''(r)+\left[k^2-\frac{l(l+1)}{r^2}-U(r)\right]u_l(r)=0, \tag{4}$$

where $U(r)=(2\mu/\hbar^2)V(r)$ and μ is the reduced mass.

We divide the potential function $U(r)$ into an 'inside' region $r\leqq r_a$ and an 'outside' region $r\geqq r_a$ such that $U(r)\approx 0$ for $r\geqq r_a$. The solution of (4) for $r>r_a$ is then approximately given by the asymptotic function

$$u_l(r\geqq r_a)=\mathscr{J}_l(kr)\cos\delta_l-\mathscr{N}_l(kr)\sin\delta_l. \tag{5}$$

Here we define $\mathscr{J}_l(kr)$ and $\mathscr{N}_l(kr)$ as the modified spherical Bessel and Neumann functions respectively, related to the corresponding spherical Bessel and Neumann functions $j_l(kr)$ and $n_l(kr)$ by

$$\mathscr{J}_l(kr)=krj_l(kr),\quad \mathscr{N}_l(kr)=krn_l(kr). \tag{6}$$

The definitions of $j_l(kr)$ and $n_l(kr)$ are those given by Schiff [6]).

We take the 'inside' solution ($r\leqq r_a$) as

$$u_l(r\leqq r_a)=\mathscr{J}_l(kr)\cos\delta_l-f_l(r)\mathscr{N}_l(kr)\sin\delta_l, \tag{7}$$

where $f_l(r)$ is a form factor. To determine $f_l(r)$, we use the boundary conditions $u_l(r_a)$, $u'_l(r_a)$ continuous and $u_l(r\to 0)\sim r^{l+1}$. Comparing (5) and (7), these require

$$f_l(r_a)=1,\quad f'_l(r_a)=0,\quad f_l(r\to 0)\approx r^{2l+1}, \tag{8}$$

where we have used the properties $\mathscr{J}_l(x\to 0)\approx x^{l+1}$, $\mathscr{N}_l(x\to 0)\approx x^{-l}$.

The integral equation for the phase [9]) is now employed:

$$\sin\delta_l=-\frac{1}{k}\int_0^\infty U(r)\mathscr{J}_l(kr)u_l(r)\mathrm{d}r. \tag{9}$$

Substitution of (5) and (7) for $u_l(r)$ in (9) gives us

$$\sin\delta_l\approx B_{1l}\cos\delta_l+B_{2l}\sin\delta_l,$$

or

$$\tan\delta_l\approx B_{1l}/(1-B_{2l}), \tag{10}$$

where

$$B_{1l}=-\frac{1}{k}\int_0^\infty U(r)\mathscr{J}_l^2(kr)\,\mathrm{d}r, \tag{11}$$

$$B_{2l}=\frac{1}{k}\int_0^\infty g_l(r)U(r)\mathscr{J}_l(kr)\mathscr{N}_l(kr)\mathrm{d}r, \tag{12}$$

$$g_l(r) = \begin{cases} f_l(r) & (r \leqq r_a), \\ 1 & (r \geqq r_a). \end{cases} \tag{13}$$

B_{1l} is the first-order Born approximation for the phase, but B_{2l} is a new term introducing a strong interference effect in δ_l.

That the forms (5) and (7) approximately satisfy the wave equation may be seen by substitution into (4). Using the fact that $\mathscr{J}_l(kr)$ and $\mathscr{N}_l(kr)$ both satisfy the wave equation for zero potential,

$$v_l''(r) + \left[k^2 - \frac{l(l+1)}{r^2}\right] v_l(r) = 0, \tag{14}$$

we get

$$U(r_a)[\mathscr{J}_l(kr)\cos\delta_l - f_l(r_a)\mathscr{N}_l(kr_a)\sin\delta_l] + 2f'_l(r_a)\mathscr{N}'_l(kr_a)\sin\delta_l + f''_l(r_a)\mathscr{N}_l(kr_a)\sin\delta_l = 0.$$

For this to hold at least approximately, we take

$$f'_l(r_a) = f''_l(r_a) = 0, \quad U(r_a) \approx 0.$$

Actually for $U(r_a)$ continuous, (4) implies $u_l''(r_a)$ continuous. Thus $f_l(r_a) = 1$ implies $f_l''(r_a) = 0$, so that the latter extra condition follows from the conditions (8). However, we shall see in practice (section 8) that the conditions (8) so constrain $f_l(r_a)$ that we may have $f_l''(r_a) \neq 0$ without affecting numerical results. Moreover results are independent to a close approximation of the choice of $f_l(r_a)$, provided it satisfies (8) and r_a is adjusted in each case.

The simplest polynomial function $f_l(r_a)$ satisfying (8) is

$$f_l(r) = \frac{1}{(m-1)}[(2l+m)(r/r_a)^{2l+1} - (2l+1)(r/r_a)^{2l+m}], \quad m \geqq 2. \tag{15}$$

Inspection of wave function solutions for an average potential (square well) suggests that $m = 3$ is a good choice:

$$f_l(r) = \tfrac{1}{2}[(2l+3)(r/r_a)^{2l+1} - (2l+1)(r/r_a)^{2l+3}]. \tag{16}$$

However, if we require $f_l''(r_a) = 0$ as well as (8), the simplest polynomial function $f_l(r)$ is

$$f_l(r) = \frac{1}{(m-1)(n-1)(n-m)}[(n-m)(2l+m)(2l+n)(r/r_a)^{2l+1} - (n-1)(2l+1)(2l+n)(r/r_a)^{2l+m} + (m-1)(2l+1)(2l+m)(r/r_a)^{2l+n}], \tag{17}$$

where $m \geqq 2$, $n \geqq 3$.

Actually $f_l(r)$ is similar in shape in each case, as seen in fig. 9, and our results turn out independent of the particular form factor used, provided r_a is suitably adjusted. This point is investigated in detail in section 8.

If we replace $U(r)$ by a spin-orbit coupling potential,

$$U(r) \to U_1(r) + \boldsymbol{\sigma} \cdot \mathbf{L} U_2(r)$$

then formulae (10)—(13) still hold, where we take for the eigenvalue

$$\boldsymbol{\sigma} \cdot \mathbf{L} = \tfrac{1}{2}\hbar^2[j(j+1) - l(l+1) - s(s+1)],$$

where the quantum numbers j, l and s relate to the total scattering system.

3. Limiting Values of the Phase-Shift Formula

For $l = 0$, we find from (11) and (12) that

$$B_{10} = -\frac{1}{k}\int_0^\infty U(r) \sin^2 kr \, dr, \tag{18}$$

$$B_{20} = -\frac{1}{2k}\int_0^\infty g_0(r) U(r) \sin 2kr \, dr. \tag{19}$$

In the limiting case of large k, $k \to \infty$, we estimate B_{10} and B_{20} by replacing $U(r)$ by the average potential (square well)

$$U(r) = \begin{cases} -U_0 & (r \leqq b), \\ 0 & (r > b). \end{cases} \tag{20}$$

This gives

$$B_{10} = \frac{U_0}{2k}\left(b - \frac{1}{2k}\sin 2kb\right), \tag{21}$$

$$B_{20} = \frac{U_0}{8k^3 b}[3j_1(2kb) - 2kb]. \tag{22}$$

In the limit as $k \to \infty$, $B_{10} \to U_0 b/2k \to 0$, $B_{20} \to -U_0/4k^2 \to 0$, giving $B_{20}/B_{10} \to -1/2kb \to 0$. Also $\delta_l \to 0$, so that (10) becomes for $l = 0$,

$$\delta_0 \to B_{10}(1 + B_{20}) \to B_{10}. \tag{23}$$

(23) thus corresponds to a second or first Born approximation for δ_0, according to whether B_{20} is retained or omitted.

For arbitrary l and $k \to \infty$, we replace $\mathcal{J}_l(kr)$ and $\mathcal{N}_l(kr)$ in (11), (12) by the asymptotic values $\sin(kr - \frac{1}{2}l\pi)$ and $-\cos(kr - \frac{1}{2}l\pi)$ respectively. This again leads to $B_{1l} \to U_0 b/2k \to 0$, $B_{2l} \to -U_0/4k^2 \to 0$, giving

$$\delta_l \to B_{1l}(1 + B_{2l}) \to B_{1l}, \tag{24}$$

equivalent to a second or first order Born approximation according to whether B_{2l} is retained or not.

The limiting case of $k \to 0$ is of interest for $l = 0$ only. We estimate (18) and

(19) by expanding sin kr and sin $2kr$ in series. Defining

$$M_n = -\int_0^\infty U(r)r^n \mathrm{d}r, \quad P_n = -\int_0^\infty g_0(r)U(r)r^n \mathrm{d}r, \tag{25}$$

we have

$$B_1 \approx kM_2 - \tfrac{1}{3}k^3M_4 + \tfrac{2}{45}k^5M_6, \tag{26}$$

$$B_2 \approx P_1 - \tfrac{2}{3}k^2P_3 + \tfrac{2}{15}k^4P_5, \tag{27}$$

which on substitution in (10) leads to the shape-independent formula (3) with small shape dependent correction term $\mathrm{O}(k^4)$:

$$k \cot \delta \approx -\frac{1}{a} + \tfrac{1}{2}r_0k^2 - Pr_0^3k^4, \tag{28}$$

where

$$-1/a = (1-P_1)/M_2, \quad r_0 = (2/3M_2)(2P_3 - M_4/a),$$

$$-Pr_0^3 = \frac{2}{45}\frac{M_6}{a} + \tfrac{1}{18}M_4\left(3r_0 + \frac{2}{a}\frac{M_4}{M_2}\right) - \tfrac{2}{15}P_5. \tag{29}$$

Numerical values of a, r_0 and P obtained from (29) are considered for n–p scattering and various well shapes in section 8.

4. Scattering Phase Shift in Many-Body Scattering Problems

Scattering by the very light nuclei, such as the deuteron, triton, ^{3}He and alpha particle, may be treated by the resonating group structure method (cf. Mather and Swan [7]). Assuming a central two-body potential interaction and neutron scattering, the wave equation reduces in radial form to the integro-differential equation

$$u_l''(r) + \left[k^2 - \frac{l(l+1)}{r^2} - U(r)\right]u_l(r) = \lambda\int_0^\infty K_l(r, r')u_l(r')\mathrm{d}r', \tag{30}$$

where $K_l(r, r')$ is a kernel term. We take (5) and (7) for the wave function $u_l(r)$ as before, but the integral equation (9) for the phase shift is modified to

$$\sin \delta_l = -\frac{1}{k}\int_0^\infty \mathscr{J}_l(kr)U(r)u_l(r)\mathrm{d}r - \frac{\lambda}{k}\int_0^\infty \mathrm{d}r\int_0^\infty \mathrm{d}r'\,\mathscr{J}_l(kr)K_l(r, r')u_l(r'). \tag{31}$$

Substitution of (5) and (7) for $u_l(r)$ in (31) gives us as before:

$$\tan \delta_l \approx \frac{B_{1l} + B_{1\lambda l}}{1 - (B_{2l} + B_{2\lambda l})}, \tag{32}$$

where B_{1l} and B_{2l} are given by (11) and (12) respectively, and

$$B_{1\lambda l} = -\frac{\lambda}{k}\int_0^\infty \mathrm{d}r \int_0^\infty \mathrm{d}r' \mathcal{J}_l(kr) K_l(r, r') \mathcal{J}_l(kr'), \tag{33}$$

$$B_{2\lambda l} = \frac{\lambda}{k}\int_0^\infty \mathrm{d}r \int_0^\infty \mathrm{d}r' \mathcal{J}_l(kr) K_l(r, r') g_l(r') \mathcal{N}_l(kr'). \tag{34}$$

Eq. (32) reduces at low energies to a shape-independent formula similar to (28).

A simple example where the analytical solution of (30) is known has been given by Buckingham and Massey [8]), who showed that s-wave neutron-deuteron scattering in the doublet spin state (mixed exchange forces) is to a good approximation described by the equation

$$u_0''(r) + k^2 u_0(r) = \lambda \int_0^\infty r r' \mathrm{e}^{-\alpha(r+r')} u_0(r') \mathrm{d}r'. \tag{35}$$

The solution is

$$u_0(r) = \sin(kr+\delta_0) - \sin\delta_0 \left[1 + \frac{1}{2k}(\alpha^2+k^2)r\right] \mathrm{e}^{-\alpha r}, \tag{36}$$

where

$$k\cot\delta_0 = -\frac{1}{2\alpha}(\alpha^2-k^2) - \frac{1}{16\alpha^5\lambda}(\alpha^2+k^2)^2[4\alpha^3(\alpha^2+k^2)^2 - (3\alpha^2+k^2)\lambda]. \tag{37}$$

We take $f_0(r)$ as (16) for $l = 0$, obtaining in our approximation

$$\begin{aligned} B_{10} = B_{20} = 0, \quad B_{1\lambda 0} &= -\frac{4k\alpha^2\lambda}{(\alpha^2+k^2)^4}, \\ B_{2\lambda 0} &= -\frac{6\alpha^2\lambda}{r_a(\alpha^2+k^2)^5}\left[(\alpha^2-3k^2) - \frac{4}{r_a^2}\frac{(\alpha^2-10\alpha^2k^2+5k^4)}{(\alpha^2+k^2)^2}\right], \end{aligned} \tag{38}$$

with

$$\tan\delta_0 = \frac{B_{1\lambda 0}}{1-B_{2\lambda 0}}. \tag{39}$$

Taking Buckingham and Massey's value $\lambda = -6.56$, $\alpha = 1.25$ and putting $k = 1$, we find $\delta_0 = 0.6934$. The corresponding first Born approximation value is $B_{1\lambda 0} = 0.7602$, giving an error of 10 %.

TABLE 1

Values of the integral B_{2l} and approximate phase δ_0 for n–d scattering

r_a (10^{-13} cm)	B_{2l}	δ_0
2	−0.05190	0.7350
3	−0.16394	0.6850
4	−0.15668	0.6881
5	−0.13783	0.6961

Also the kernel $K_0(r, r') = rr'e^{-1.25(r+r')}$ has a long tail, so that a suitable cut-off range r_a should be considerably greater than $1/1.25 = 0.8$, say $r_a > 2$. Values of $B_{2\lambda}$ and δ_0 are given in table 1 below.

We see that δ_0 is almost independent of r_a for r_a in the range 3 to 5, with $\delta_0 \approx 0.69$ agreeing well with the accurate value 0.6934. The error is $\approx 1\,\%$, about ten times smaller than the first Born approximation error.

5. Scattering of Charged Particles

We take $F_l(\alpha, \rho)$ and $G_l(\alpha, \rho)$ as the regular and irregular Coulomb wave functions respectively, where $\alpha = e^2/\hbar v = 1/2kR$, $R = \hbar^2/me^2$ and $\rho = kr$. Then we have for the 'outside' and 'inside' wave functions respectively:

$$\begin{aligned} u_l(r) &= F_l(\alpha, \rho)\cos K_l + G_l(\alpha, \rho)\sin K_l, \qquad (r \geqq r_a), \\ u_l(r) &= F_l(\alpha, \rho)\cos K_l + f_l(r)G_l(\alpha, \rho)\sin K_l, \quad (r \leqq r_a), \end{aligned} \tag{40}$$

where $f_l(r)$ is the form factor defined by conditions (18) and K_l is the phase-shift.

The integral equation for the phase is

$$\sin K_l = -\frac{1}{k}\int_0^\infty U(r)F_l(\alpha, \rho)u_l(r)\mathrm{d}r. \tag{41}$$

Substituting (40) into (41) gives

$$\tan K_l \approx B_{1l}/(1-B_{2l}), \tag{42}$$

where

$$B_{1l} = -\frac{1}{k}\int_0^\infty U(r)F_l^2(\alpha, \rho)\mathrm{d}r, \tag{43}$$

$$B_{2l} = -\frac{1}{k}\int_0^\infty g_l(r)U(r)F_l(\alpha, \rho)G_l(\alpha, \rho)\mathrm{d}r. \tag{44}$$

Although tables of $F_l(\alpha, \rho)$ and $G_l(\alpha, \rho)$ exist (see Mather and Swan [7]), they are very incomplete and require laborious double interpolation to get required values of α and ρ. However, these functions may be evaluated directly on a digital computer.

6. The Shape-Independent Formula for Charged Particles

To show that (42) reduces to the shape independent formula for charged particles (cf. Mather and Swan [7]), we use the expansions

$$F_0(\alpha,\rho)=C_0\rho\Phi_0,\quad\text{with}\quad\Phi_0=\sum_{j=1}^{\infty}A_j\rho^{j-1},\quad A_1=1,$$

$$C_0^2=2\pi\alpha/(e^{2\pi\alpha}-1),\quad A_j=(2\alpha A_{j-1}-A_{j-2})/j(j-1).$$

$$G_0(\alpha,\rho)=\Theta_0/C_0,\quad\text{with}\quad\Theta_0=\Psi_0+\rho(p\ln 2\rho+q)\Phi_0,\qquad(45)$$

$$\text{where } p=(e^{2\pi\alpha}-1)C_0^2/\pi,\quad q=p(2\gamma-1+h(\alpha)+\ln\alpha),$$

$$\Psi_0=\sum_{j=0}^{\infty}a_j\rho^j,\quad a_0=1,\quad a_1=0,\quad a_j=[2\alpha a_{j-1}-a_{j-2}-2\alpha(2j-1)A_j]/j(j-1).$$

We thus obtain

$$F_0(\alpha,\rho)=C_0\sum_{n=0}^{\infty}\frac{(-1)^n}{(2n+1)!}s_{2n+1}(r)(kr)^{2n+1},\qquad(46)$$

$$G_0(\alpha,\rho)$$

$$=\frac{1}{C_0}\sum_{n=0}^{\infty}\frac{(-1)^n}{(2n+1)!}\left[t_{2n+1}(r)(kr)^{2n}+\frac{r}{R}\left\{\ln\frac{r}{R}+2\gamma-1+h(\alpha)\right\}s_{2n+1}(r)(kr)^{2n}\right],\qquad(47)$$

where $R=\hbar^2/me^2=28{\cdot}8(15)\times10^{-13}$ cm, giving $\alpha\rho=r/2R\approx\frac{1}{20}$ for $r\approx e^2/mc^2=2{\cdot}8\times10^{-13}$ cm. Also writing $x=r/R\approx\frac{1}{10}$,

$$s_1(r)=1+\tfrac{1}{2}x+\tfrac{1}{12}x^2+\tfrac{1}{144}x^3+\tfrac{1}{2880}x^4+\tfrac{1}{86\,400}x^5+\tfrac{1}{3\,628\,800}x^6+\ldots,$$

$$s_3(r)=1+\tfrac{1}{3}x+\tfrac{1}{24}x^2+\tfrac{1}{360}x^3+\tfrac{1}{8640}x^4+\tfrac{1}{302\,400}x^5+\ldots,\qquad(48)$$

$$s_5(r)=1+\tfrac{23}{90}x+\tfrac{7}{270}x^2+\tfrac{11}{7560}x^3+\tfrac{1}{31\,104}x^4+\tfrac{13}{32\,659\,200}x^5+\ldots,$$

$$t_0(r)=1-\tfrac{3}{4}x^2-\tfrac{7}{36}x^3-\tfrac{35}{1728}x^4-\tfrac{1{\cdot}01}{864}x^5-\tfrac{7}{162\,000}x^6-\tfrac{2{\cdot}83}{2\,540\,160}x^7-\ldots,$$

$$t_2(r)=1-\tfrac{1}{9}x-\tfrac{43}{216}x^2-\tfrac{7{\cdot}7}{216}x^3-\tfrac{3{\cdot}73}{1296}x^4-\tfrac{2{\cdot}47}{18\,144}x^5-\tfrac{1{\cdot}378}{112\,896}x^6-\ldots,\qquad(49)$$

$$t_4(r)=1-\frac{0{\cdot}32}{3}x-\frac{2{\cdot}752}{25}x^2-\frac{8{\cdot}11}{567}x^3-\frac{1{\cdot}1155}{1764}x^4-\frac{x^5}{26\,733{\cdot}86103}-1{\cdot}610\,650\times10^{-6}x^6-\ldots$$

We hence find

$$F_0^2(\alpha,\rho)=C_0^2[S_1(r)(kr)^2-\tfrac{1}{3}S_3(r)(kr)^4+\tfrac{1}{180}S_5(r)(kr)^6-\ldots],$$

$$F_0(\alpha,\rho)G_0(\alpha,\rho)=\left[T_1(r)(kr)-\frac{1}{3!}T_3(r)(kr)^3+\frac{1}{5!}T_5(r)(kr)^5-\ldots\right]\qquad(50)$$

$$+\frac{1}{kR}\left[\ln\frac{r}{R}+2\gamma-1+h(\alpha)\right][S_1(r)(kr)^2-\tfrac{1}{3}S_3(r)(kr)^4+\tfrac{1}{180}S_5(r)(kr)^6-\ldots],$$

where

$$S_1(r)=s_1^2(r),\quad S_3(r)=s_1(r)s_3(r),\quad S_5(r)=5s_3^2(r)+3s_1(r)s_5(r),$$
$$T_1(r)=s_1(r)t_0(r),\quad T_3(r)=3s_1(r)t_2(r)+s_3(r)t_0(r),\qquad(51)$$
$$T_5(r)=5s_1(r)t_4(r)+10s_3(r)t_2(r)+s_5(r)t_0(r).$$

Define

$$\mathscr{M}_n = -\int_0^\infty U(r) S_{n-1}(r) r^{n-1}\,\mathrm{d}r, \qquad \mathscr{P}_{1n} = -\int_0^\infty U(r) T_n(r) r^n g_0(r)\,\mathrm{d}r,$$
$$\mathscr{P}_{2n} = -\int_0^\infty U(r) S_{n-1}(r) r^n g_0(r)\,\mathrm{d}r, \quad \mathscr{P}_{3n} = -\int_0^\infty U(r) S_{n-1}(r) r^n g_0(r) \ln\frac{r}{R}\,\mathrm{d}r. \tag{52}$$

Then the integrals (43) and (44) become

$$u = C_0^2(k\mathscr{M}_2 - \tfrac{1}{3}k^3\mathscr{M}_4 + \tfrac{1}{180}k^5\mathscr{M}_6 - \ldots),$$
$$v = (\mathscr{P}_{11} - \tfrac{1}{6}k^2\mathscr{P}_{13} + \tfrac{1}{120}k^4\mathscr{P}_{15} - \ldots) + \frac{1}{R}(2\gamma - 1 + h(\alpha))(\mathscr{P}_{22} - \tfrac{1}{3}\mathscr{P}_{24}k^2 + \tfrac{1}{180}\mathscr{P}_{26}k^4 - \ldots)$$
$$+ \frac{1}{R}(\mathscr{P}_{32} - \tfrac{1}{3}\mathscr{P}_{34}k^2 + \tfrac{1}{180}\mathscr{P}_{36}k^4 - \ldots). \tag{53}$$

On substituting (53) into (42) and defining

$$A_0 = 1 - \mathscr{P}_{11} - \frac{1}{R}\{(2\gamma - 1)\mathscr{P}_{22} + \mathscr{P}_{32}\},$$
$$A_1 = \mathscr{P}_{22},$$
$$A_2 = \mathscr{P}_{13} + \frac{2}{R}\{(2\gamma - 1)\mathscr{P}_{24} + \mathscr{P}_{34}\},$$
$$A_3 = 2\mathscr{P}_{24}, \tag{54}$$
$$A_4 = \mathscr{P}_{15} + \frac{2}{3R}\{(2\gamma - 1)\mathscr{P}_{26} + \mathscr{P}_{36}\},$$
$$A_5 = \tfrac{2}{3}\mathscr{P}_{26},$$

we find

$$C_0^2 k \cot K_0 + \frac{1}{R}h(\alpha)\frac{A_1}{\mathscr{M}_2} = -\frac{1}{a} + \tfrac{1}{2}r_0 k^2 - Pr_0^3 k^4 + \ldots, \tag{55}$$

where

$$-\frac{1}{a} = \frac{A_0}{\mathscr{M}_2},$$
$$r_0 = \frac{1}{3\mathscr{M}_2}\left[\left\{A_2 + 2\frac{\mathscr{M}_4}{\mathscr{M}_2}A_0\right\} + \left\{A_3 - 2\frac{\mathscr{M}_4}{\mathscr{M}_2}A_1\right\}\frac{1}{R}h(\alpha)\right],$$
$$-Pr_0^3 = -\frac{1}{120\mathscr{M}_2}\left[\frac{2}{3}\left\{\frac{\mathscr{M}_6}{\mathscr{M}_2} - 20\left(\frac{\mathscr{M}_4}{\mathscr{M}_2}\right)^2\right\}A_0 + \frac{20}{3}\left(\frac{\mathscr{M}_4}{\mathscr{M}_2}\right)A_2 - A_4\right. \tag{56}$$
$$\left. + \left\{\frac{2}{3}\left\{\frac{\mathscr{M}_6}{\mathscr{M}_2} - 20\left(\frac{\mathscr{M}_4}{\mathscr{M}_2}\right)^2\right\}A_1 + \frac{20}{3}\left(\frac{\mathscr{M}_4}{\mathscr{M}_2}\right)A_3 - A_5\right\}\frac{1}{R}h(\alpha)\right].$$

(55) is identical with the shape-independent formula for charged particle

scattering (cf. Mather and Swan [7])), provided $A_1/\mathcal{M}_2$ is equal to 1, at least approximately, and also that the terms in r_0 and $-Pr_0^3$ proportional to $h(\alpha)/R$ are negligible (otherwise r_0 and P would not be energy-independent constants).

To estimate $A_1/\mathcal{M}_2$, we consider the simple case of a square well, range b, and approximately take $s_1(r) = 1$ for $r < b$. Then

$$A_1 = -\int_0^\infty U(r)S_1(r)r^2 g_0(r)\mathrm{d}r \to U_0\int_0^b r^2 g_0(r)\mathrm{d}r,$$

$$\mathcal{M}_2 = -\int_0^\infty U(r)S_1(r)r^2\mathrm{d}r \to U_0\int_0^b r^2\mathrm{d}r,$$

where we take $r_\alpha = b$ and $g_0(r)$ as defined by (13) and (15). This gives $A_1/\mathcal{M}_2 = 0.8750$. In the actual case of ^{1}S proton-proton scattering below, the accurate value obtained without approximating $S_1(r)$ is 0.8775.

For other well shapes, the existence of a tail to the well for $r > r_\alpha$, in which region $g_0(r) = 1$, means that $A_1/\mathcal{M}_2$ should approximate to 1 more closely than in the square well case.

In r_0 and $-Pr_0^3$ as defined by (56), the terms proportional to $h(\alpha)/R$ should be small due to the large size of $R = 28.8(15)\times 10^{-13}$ cm. Thus the energy dependence of $h(\alpha)$ should have a negligible effect on the constants.

Equation (56) with its definition of a, r_0 and P may be tested on ^{1}S proton-proton scattering. Analysis by Swan [7]) of p−p scattering up to 18.2 MeV gives $a = (-7.75\pm 0.02)\times 10^{-13}$ cm, $r_0 = (2.78\pm 0.03)\times 10^{-13}$ cm, $P = 0.041\pm 0.007$.

Formulae supplied by Blatt [3]) and Blatt and Jackson [4]) show that the corresponding square well parameters are

$$V_0 = 11.856 \text{ MeV}, \quad b = 2.759\times 10^{-13} \text{ cm}.$$

Use of these parameters, together with $r_\alpha = b$ and $g_0(r)$ as defined by (13) and (16), in (56) leads to the values

$$a = 9.024\times 10^{-13} \text{ cm}, \quad r_0 = \{2.499 + 0.0064h(\alpha)\}\times 10^{-13} \text{ cm},$$

$$P = \{0.01385 + 0.00213h(\alpha)\}\times 10^{-13} \text{ cm}.$$

These values agree approximately with the experimental values above, and lead to phase-shifts correct to within several percent. However, better agreement could have been attained by taking r_α somewhat smaller than b and adjusting it to give the experimental value of a, thus normalizing (55) correctly for zero energy (see section 8).

As $\alpha = 1/2kR = 0.01747/k$, the experimental energy range $E = 0.1$ to 20 MeV, to which (55) is usually applied, is equivalent to $k = 0.03$ to 0.45 or to $\alpha = 0.6$ to 0.04. The corresponding range of $h(\alpha)$ is 3.0 to 0.2. Thus the $h(\alpha)$ term in r_0 is only a small fraction of 1 % of 2.499 remainder at MeV energies (where $h(\alpha) < 1$). The $h(\alpha)$ term in P, although proportionately larger, is also

very small at energies sufficiently high for the k^4 term in (55) to be important, $E \approx 15$ MeV. Here $\alpha \approx 0.2$, so that the $h(\alpha)$ term constitutes only a 3 % correction to the shape parameter term P.

Thus the $h(\alpha)$ terms in r_0 and P constitute only very small second order effects in practice and do not affect the basic shape-independent formula and its shape-dependent correction.

7. An Improved Formula for Binding Energies

We take the wave function as having the asymptotic form for large r:

$$u_l(r) \approx \exp -i(kr-\tfrac{1}{2}(l+1)\pi)-S(k)\exp i(kr-\tfrac{1}{2}(l+1)\pi), \tag{57}$$

where $S(k) = \exp 2i\delta_l$ is the scattering matrix.

A bound state is obtained if $k = -i\alpha$ and $S(k) = 0$, or

$$k = -i\alpha, \quad \cot\delta_l = -i. \tag{58}$$

Substitution of (58) into (5) and (7) for the wave function $u_l(r)$ leads to

$$u_l(r) = -i\sin\delta_l[\mathcal{J}_l(-i\alpha r)-if_l(r)\mathcal{N}_l(-i\alpha r)], \quad (r \leqq r_a) \tag{59}$$

$$u_l(r) = -i\sin\delta_l[\mathcal{J}_l(-i\alpha r)-i\mathcal{N}_l(-i\alpha r)] \quad (r \geqq r_a). \tag{60}$$

We substitute (59) and (60) into the integral equation (9) for the phase, obtaining

$$\alpha = -A_{1l}+iA_{2l}, \tag{61}$$

where

$$A_{1l} = \int_0^\infty U(r)\mathcal{J}_l^2(-i\alpha r)\mathrm{d}r, \tag{62}$$

$$A_{2l} = \int_0^\infty g_l(r)U(r)\mathcal{J}_l(-i\alpha r)\mathcal{N}_l(-i\alpha r)\mathrm{d}r, \tag{63}$$

$$\alpha^2 = (2\mu/\hbar^2)W, \tag{64}$$

where μ is the reduced mass of the system and W the modulus of the binding energy.

Eq. (61) is an improved version of the formula obtained by using (60) as the wave function everywhere, putting $f_l(r) = g_l(r) = 1$ or neglecting the well shape effect. Only the integral A_{2l} is affected.

In the special case $l = 0$, (61) reduces to

$$\alpha = -\int_0^\infty U(r)\sinh\alpha r[g_0(r)\cosh\alpha r-\sinh\alpha r]\mathrm{d}r, \tag{65}$$

the unimproved version being (putting $g_0(r) \equiv 1$)

$$\alpha = -\int_0^\infty U(r)\sinh\alpha r\,\mathrm{e}^{-\alpha r}\mathrm{d}r. \tag{66}$$

Expansion of (65) into a series in powers of α yields for small α,

$$\alpha = \frac{1}{a} + \frac{2P_3}{3M_2}\alpha^2 - \frac{M_4}{3M_2}\alpha^3 + \frac{2P_5}{15M_2}\alpha^4 - \ldots, \tag{67}$$

where a is defined by (29) and M_n and P_n by (25).

On the other hand, insertion of the conditions for a bound state (58) into the shape-independent formula (28) for scattering leads to the series for small α,

$$\alpha = \frac{1}{a} + \tfrac{1}{2}r_0\alpha^2 + Pr_0^3\alpha^4 + \ldots, \tag{68}$$

where r_0 and P are defined by (29). Eq. (68) is the usual shape-independent formula for bound states with shape-dependent correction term $Pr_0^3\alpha^4$. Eq. (67) differs not only in the coefficients of α^2 and α^4 but also in the existence of an α^3 term. Nevertheless it is easy to show that (67) and (68) are both valid series, the particular form taken depending on how the series expansion is carried out.

To see this we derive (61) again, but in the standard form (10), by substituting conditions (58) for a bound state into (10). This gives

$$\frac{1}{\alpha} = -\frac{1}{A_1}\left(1 - \frac{i}{\alpha}A_2\right), \tag{69}$$

which is equivalent to (61).

On expanding A_1 and A_2 in series involving powers of α for small α, we obtain (68). If (69) were to be inverted before expansion, yet a third series would be obtained.

Equations (65) and (66) are easily tested for a square well, range b, depth V_0, the unimproved formula (66) becoming

$$\alpha = \tfrac{1}{2}U_0\left[b - \frac{1}{2\alpha}(1 - e^{-2\alpha b})\right]. \tag{70}$$

Taking $g_0(r)$ as given by (16) for $l = 0$, eq. (65) becomes

$$\alpha = \tfrac{1}{2}U_0\left[b + \frac{1}{2\alpha}e^{-2\alpha b} + \frac{3}{8\alpha^3 b^3}\mathcal{J}_1(i2\alpha b)\right]. \tag{71}$$

For the ^{3}S ground state of the deuteron, we have the experimental parameters

$$a = 5.38 \times 10^{-13}\ \text{cm}, \quad r_0 = 1.70 \times 10^{-13}\ \text{cm}, \tag{72}$$

leading to the well parameters (cf. Blatt [3]):

$$V_0 = 36.354\ \text{MeV}, \quad U_0 = 0.87704 \times 10^{26}, \quad b = 2.0048 \times 10^{-13}\ \text{cm} \tag{73}$$

The deuteron binding energy of 2.226 MeV corresponds to $\alpha = 0.2317$. Solution

of the unimproved relation (70) for α, employing the values quoted for V_0 and b, gives $\alpha = 0.4994$. The improved relation (71) gives the value $\alpha = 0.2071$. The approximate form (68) of (71) gives, on using the approximate values

$$a = 5.745\times 10^{-13}\,\text{cm}, \quad r_0 = 1.562\times 10^{-13}\,\text{cm}$$

quoted in subsection 8.1, and putting $P = 0$, the value $\alpha = 0.2075$, in excellent agreement with (71). However, if we choose a slightly smaller cut-off range r_α, given by (78), so as to obtain the correct zero energy scattering length a, we find via (68) that $\alpha = 0.2256$, agreeing within several percent with the correct value. For wells other than square, this would be the best procedure, see section 8.

Formula (65) has the advantage over the shape-independent formula (68) of being equally valid for large α and for small α.

8. Low Energy Neutron-Proton Scattering for Various Well Shapes

In this section, computations are presented on ^{3}S and ^{1}S n—p scattering at low energies (s-waves only), using the square, gaussian, exponential and Yukawa potentials. The shape-independent formula (28) and definitions (29) of a and r_0 are employed. The effect of varying the cut-off range r_α is investigated and in one case (Yukawa potential) of varying the form factor defined by (8).

8.1. Square Well

We here assume the cut-off range r_α is not necessarily the same as the range b. Taking $f_0(r)$ as defined by (16) for $l = 0$, we get

$$-\frac{1}{a} = \frac{3}{U_0 b^3}\left[1-\tfrac{1}{2}U_0 b^2\left(1-\frac{1}{5}\frac{r_\alpha^2}{b^2}\right)\right], \tag{74}$$

$$r_0 = \frac{6}{5U_0 b}\left[1+\tfrac{1}{6}U_0 b^2\left\{2+\frac{3}{5}\frac{r_\alpha^2}{b^2}\left(1-\frac{5}{7}\frac{r_\alpha^2}{b^2}\right)\right\}\right]. \tag{75}$$

For ^{3}S n—p scattering, U_0 and b are given by (73). For ^{1}S scattering, we use the experimental values

$$a = -23.69\times 10^{-13}\,\text{cm}, \quad r_0 = 2.7\pm 0.5\times 10^{-13}\,\text{cm}, \tag{76}$$

leading to the well dimensions (cf. Blatt [3])

$$V_0 = 14.052\,\text{MeV}, \quad U_0 = 0.3390\times 10^{26}, \quad b = 2.5860\times 10^{-13}\,\text{cm}. \tag{77}$$

Fig. 1. shows r_0 and a for ^{3}S n—p scattering plotted as functions of the cut-off range r_α, represented by the left hand and right hand ordinates respectively. In particular,

$$r_\alpha = b = 2.0048\times 10^{-13}\,\text{cm gives } a = 5.745\times 10^{-13}\,\text{cm},$$

$r_0 = 1.553 \times 10^{-13}$ cm. However, from fig. 1, we see that a slightly smaller value $r_\alpha = 1.92 \times 10^{-13}$ cm gives the experimental value of a while hardly altering

$$r_\alpha = 1.92 \times 10^{-13}\,\text{cm}; \quad a = 5.38 \times 10^{-13}\,\text{cm}, \quad r_0 = 1.562 \times 10^{-13}\,\text{cm}. \quad (78)$$

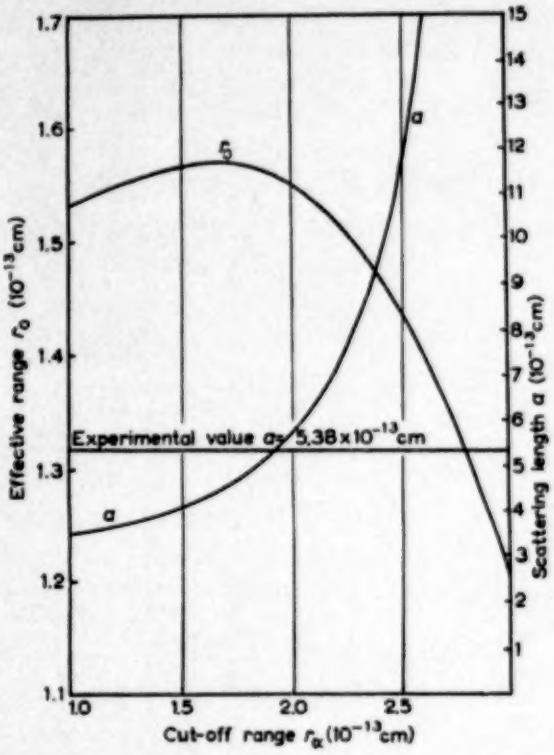

Fig. 1. Effective range r_0 and zero-energy scattering length a plotted as a function of cut-off range r_α for ^{3}S n−p scattering with a square well.

As a correct value of a normalizes the phase-shift δ_0 correctly for small k, this value of r_α should give better overall results than $r_\alpha = b$. This is found to be true in most cases given in table 2. Note that r_0 is very insensitive to r_α, particularly for $r_\alpha < b$.

TABLE 2

Calculated values of phase shift δ_0 for ^{3}S and ^{1}S n−p scattering by square wells

Spin state	k	Experimental δ_0	Theoretical δ_0 ($r_\alpha = b$)	Theoretical δ_0 ($r_\alpha \to a_{\text{exp}}$)
^{3}S	0.1	2.6283	2.6019	2.6299
	0.25	2.0590	2.0381	2.0722
	0.5	1.5176	1.5319	1.5521
^{1}S	0.1	1.0626	1.0298	1.0702
	0.25	1.1020	1.1055	1.1224
	0.5	0.9214	0.9479	0.9542

Fig. 2 present similar information on the variation of a and r_0 with r_α for ^{1}S n−p scattering. r_0 is again found insensitive to large changes in r_α, but a

changes rapidly. In particular, $r_\alpha = b = 2.586\times10^{-13}$ cm gives $r_0 = 2.492\times$ $\times10^{-13}$ cm, $a = -20.98\times10^{-13}$ cm. However, $r_\alpha = 2.51\times10^{-13}$ cm gives the experimental a:

$$r_\alpha = 2.51\times10^{-13}\,\text{cm}, \quad a = -23.69\times10^{-13}\,\text{cm}, \quad r_0 = 2.4977\times10^{-13}\,\text{cm}. \tag{79}$$

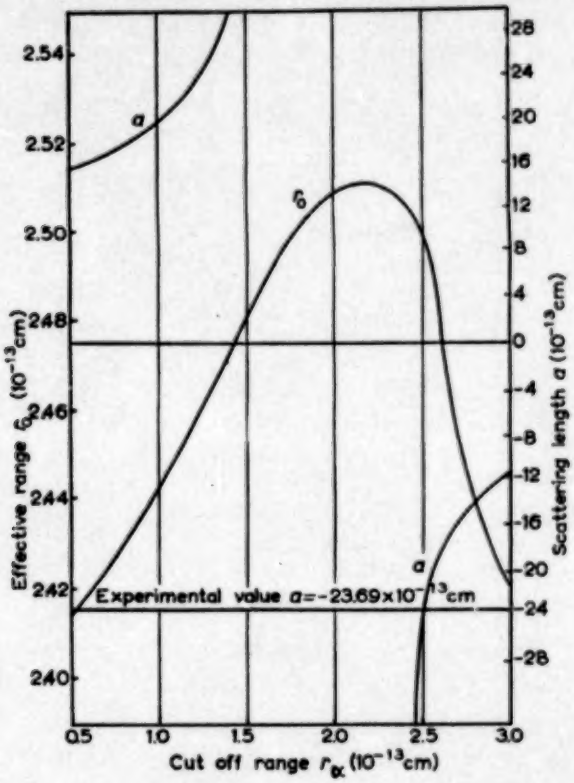

Fig. 2. Effective range r_0 and zero-energy scattering length a plotted as a function of cut-off range r_α for ^{1}S n−p scattering with a square well.

Numerical values of the phase-shift δ_0 are given in table 1, the best results coming from the cut-off range $r_\alpha = 2.51\times10^{-13}$ cm in (79).

8.2. Gaussian Well $U(r) = -U_0 e^{-r^2/b^2}$

The experimental parameters (72) and (76) lead to the n−p well dimensions

$$\text{for } ^3\text{S}: \; V_0 = 72.117\ \text{MeV}, \; U_0 = 1.7399\times10^{26}, \; b = 1.4837\times10^{-13}\,\text{cm}, \tag{80}$$

$$\text{for } ^1\text{S}: \; V_0 = 32.194\ \text{MeV}, \; U_0 = 0.77667\times10^{26}, \; b = 1.7850\times10^{-13}\,\text{cm}. \tag{81}$$

Figs. 3 and 4 show the variation of a and r_0 with r_α for ^{3}S and ^{1}S n−p scattering respectively. If we again choose r_α to give the experimental scattering length a, the best parameter sets are

$$\text{for } ^3\text{S}: \; r_\alpha = 1.87\times10^{-13}\,\text{cm}, \; a = 5.38\times10^{-13}\,\text{cm}, \; r_0 = 1.686\times10^{-13}\,\text{cm}, \tag{82}$$

$$\text{for } ^1\text{S}: \; r_\alpha = 2.395\times10^{-13}\,\text{cm}, \; a = -23.69\times10^{-13}\,\text{cm}, \; r_0 = 2.611\times10^{-13}\,\text{cm}. \tag{83}$$

Again r_0 is insensitive to r_α. Values of δ_0 found using (82) and (83) are compared in table 3 with experimental values found using (72) and (76).

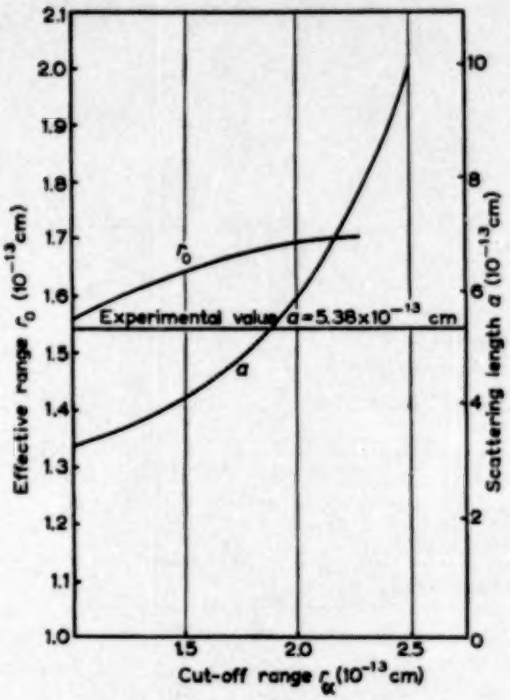

Fig. 3. Effective range r_0 and zero-energy scattering length a plotted as a function of cut-off range r_α for ^{3}S n−p scattering with a gaussian well.

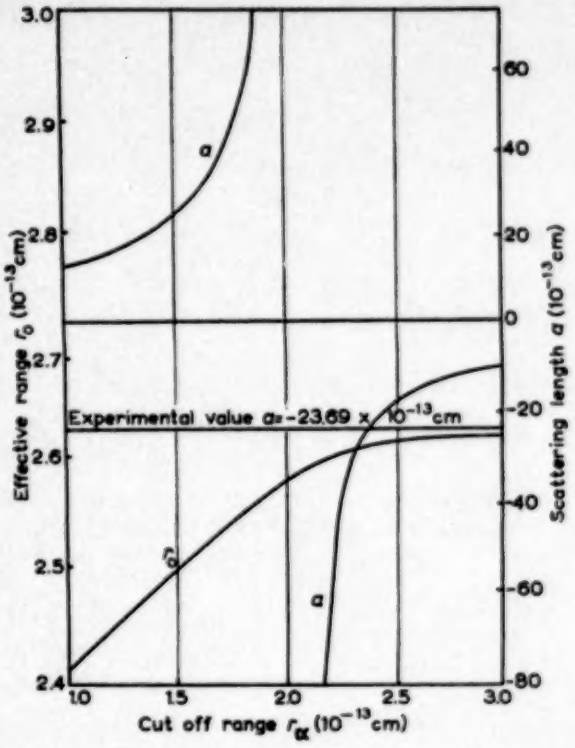

Fig. 4. Effective range r_0 and zero-energy scattering length a plotted as a function of cut-off range r_α for ^{1}S n−p scattering with a gaussian well.

TABLE 3

Calculated values of phase-shift δ_0 for ^{3}S and ^{1}S n−p scattering by various well shapes

Spin state	k	Experimental δ_0	Gaussian well δ_0	Exponential well δ_0	Yukawa well δ_0
^{3}S	0.1	2.6283	2.6284	2.6278	2.6213
	0.25	2.0590	2.0603	2.0524	2.0366
	0.5	1.5176	1.5217	1.5011	1.3774
^{1}S	0.1	1.0626	1.0659	1.0567	1.0424
	0.25	1.1020	1.1109	1.0871	1.0507
	0.5	0.9214	0.9355	0.8976	0.8426

8.3. Exponential Well $U(r) = -U_0 e^{-r/b}$

The appropriate n−p well dimensions are here

for ^{3}S: $V_0 = 216.718$ MeV, $U_0 = 5.2283\times10^{26}$, $b = 0.62798\times10^{-13}$ cm, (84)

for ^{1}S: $V_0 = 109.467$ MeV, $U_0 = 2.6409\times10^{26}$, $b = 0.71233\times10^{-13}$ cm. (85)

Figs. 5 and 6 display the dependence of a and r_0 on r_α and show the usual features such as insensitivity of r_0 to r_α, although less marked than hitherto in the ^{1}S case.

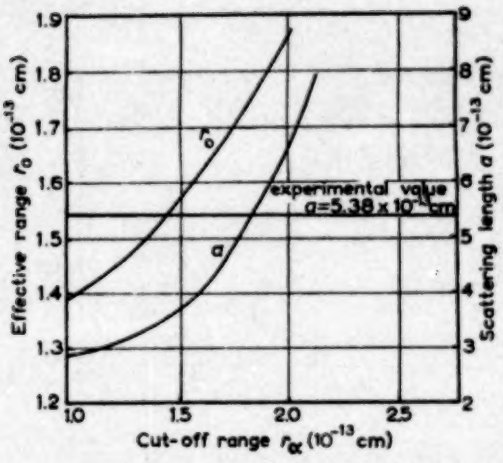

Fig. 5. Effective range r_0 and zero-energy scattering length a plotted as a function of cut-off range r_α for ^{3}S n−p scattering with an exponential well.

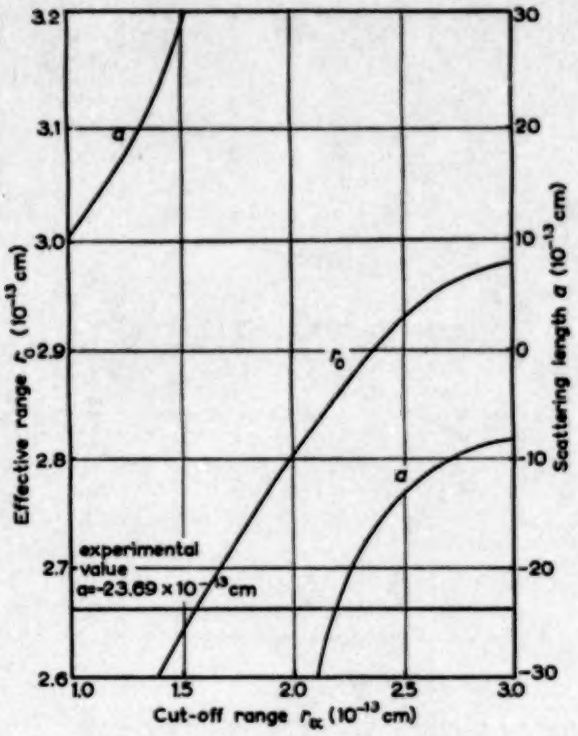

Fig. 6. Effective range r_0 and zero-energy scattering length a plotted as a function of cut-off range r_α for ^{1}S n−p scattering with an exponential well.

The parameter sets leading to the experimental values of a are

$$\text{for } ^3\text{S: } r_\alpha = 1.84\times10^{-13}\,\text{cm},\ a = 5.38\times10^{-13}\,\text{cm},\ r_0 = 1.767\times10^{-13}\,\text{cm}, \quad (86)$$

$$\text{for } ^1\text{S; } r_\alpha = 2.19\times10^{-13}\,\text{cm},\ a = -23.69\times10^{-13}\,\text{cm},\ r_0 = 2.852\times10^{-13}\,\text{cm}. \quad (87)$$

Numerical values of δ_0 obtained are compared with experimental values in table 3.

8.4. Yukawa Well $U(r) = -U_0 e^{-r/b}/(r/b)$

The n−p well dimensions employed are

$$\text{for } ^3\text{S: } V_0 = 42.237\ \text{MeV},\ U_0 = 1.0190\times10^{26},\ b = 1.5636\times10^{-13}\ \text{cm}, \quad (88)$$

$$\text{for } ^1\text{S: } V_0 = 47.701\ \text{MeV},\ U_0 = 1.1508\times10^{26},\ b = 1.1706\times10^{-13}\ \text{cm}. \quad (89)$$

As this well shape possesses both a long tail for $r > b$ and a singularity at the origin, it provides a severe test for varying the form of $f_l(r)$, as well as the cut-

off range r_α. The form factors $f_l(r)$ used were

$$f_0(r) = r/r_\alpha, \tag{90}$$

$$f_0(r) = (r/r_\alpha)[2-r/r_\alpha], \tag{91}$$

$$f_0(r) = \tfrac{1}{2}(r/r_\alpha)[3-(r/r_\alpha)^2], \tag{92}$$

$$f_0(r) = (r/r_\alpha)[3-3(r/r_\alpha)+(r/r_\alpha)^2]. \tag{93}$$

(90) satisfies the conditions $f_l(r_\alpha) = 1$ and $f_l(r \to 0) \approx r^{2l+1}$ of (8), but not $f'_l(r_\alpha) = 0$, having a discontinuous gradient of the wave function at $r = r_\alpha$.

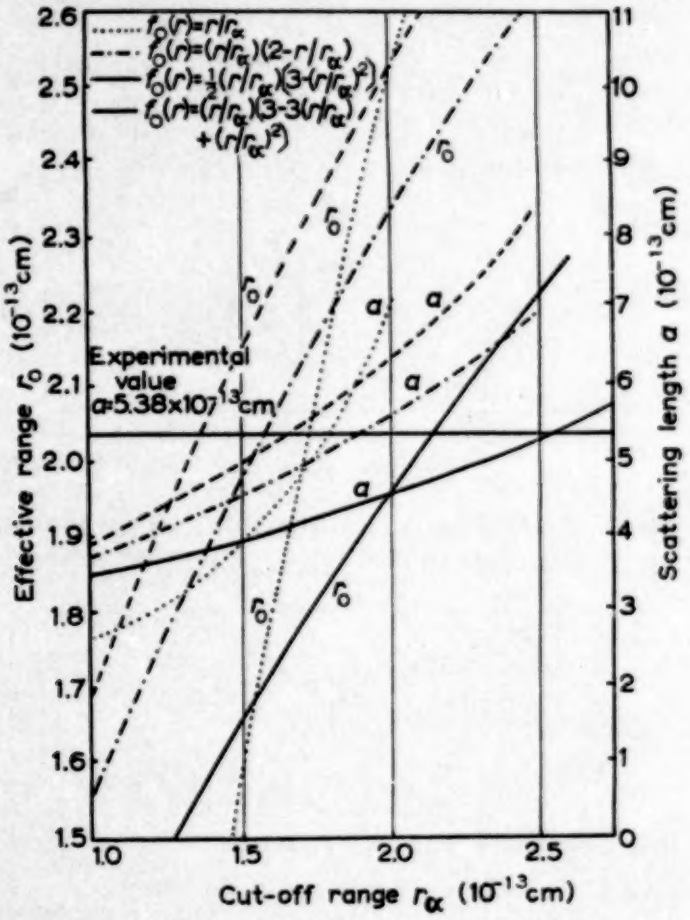

Fig. 7. Effective range r_0 and zero-energy scattering length a for a number of different form factors $f_0(r)$, plotted as a function of cut-off range r_α for ^{3}S n−p scattering with a Yukawa potential.

On the other hand, (91) and (92) satisfy all these conditions, although on analogy with the square well case (92) should be preferable. (93) satisfies all the conditions of (8) and the condition $f''_l(r_\alpha) = 0$ as well, being a particular case of (17). These functions are chosen purely because of their simple form. However, numerically they do not, apart from the too simple (90), differ appreciably, so that results obtained using them should agree fairly closely. This is in fact found to be the case.

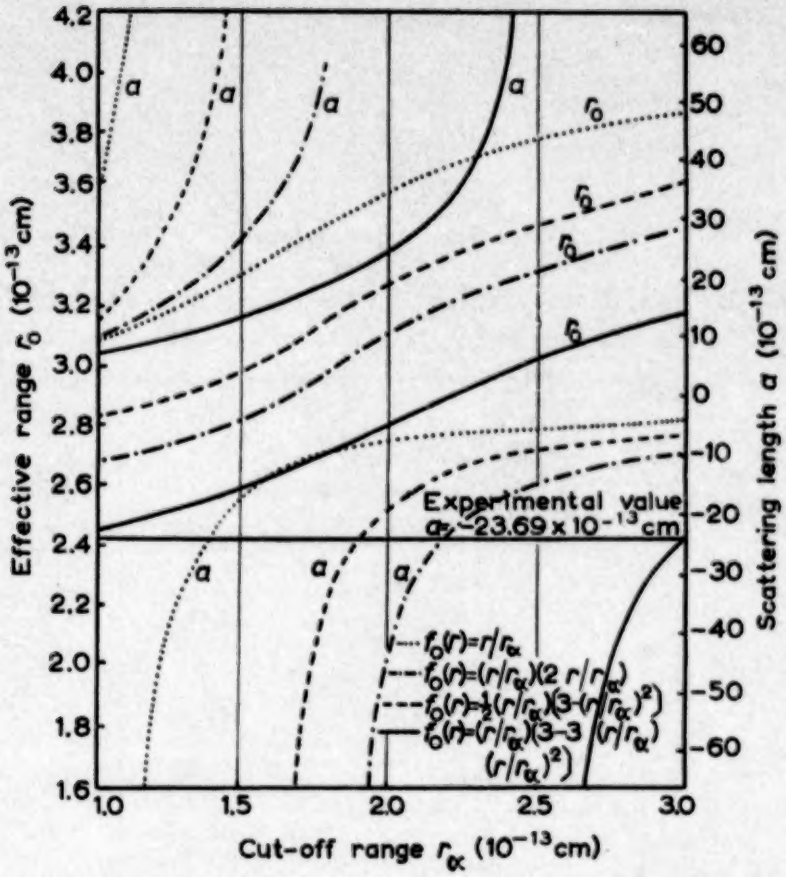
Effective range r_0 (10^{-13}cm)
Scattering length a (10^{-13}cm)
Cut-off range r_α (10^{-13}cm)
Experimental value
$a_t = -23.69 \times 10^{-13}$ cm
$f_0(r) = r/r_\alpha$
$f_0(r) = (r/r_\alpha)(2 - r/r_\alpha)$
$f_0(r) = \frac{1}{2}(r/r_\alpha)(3 - (r/r_\alpha)^2)$
$f_0(r) = (r/r_\alpha)(3 - 3(r/r_\alpha) + (r/r_\alpha)^2)$

Fig. 8. Effective range r_0 and zero-energy scattering length a for a number of different form factors $f_0(r)$, plotted as a function of cut-off range r_α for ^{1}S n−p scattering with a Yukawa potential.

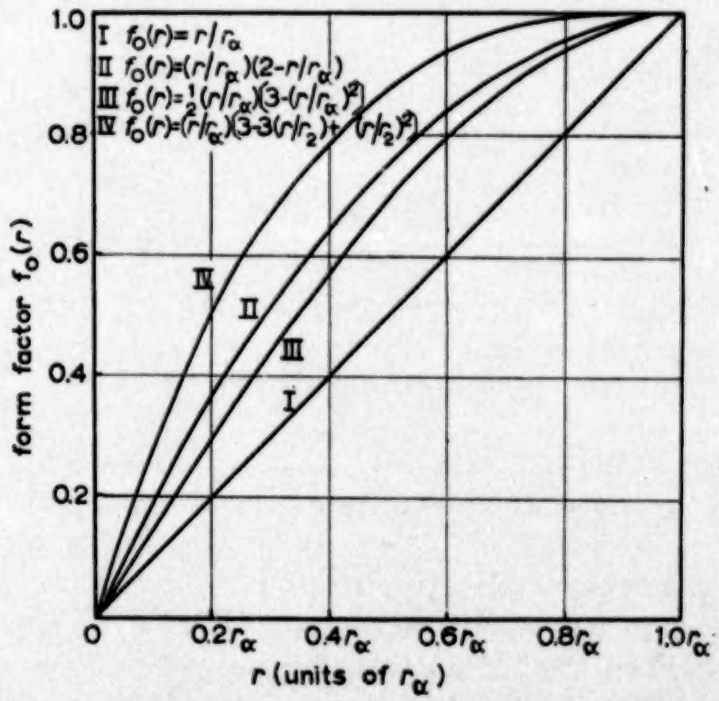
I $f_0(r) = r/r_\alpha$
II $f_0(r) = (r/r_\alpha)(2 - r/r_\alpha)$
III $f_0(r) = \frac{1}{2}(r/r_\alpha)(3 - (r/r_\alpha)^2)$
IV $f_0(r) = (r/r_\alpha)(3 - 3(r/r_2) + (r/r_2)^2)$
form factor $f_0(r)$
r (units of r_α)

Fig. 9. Form factor $f_0(r)$ plotted as a function of r_α for a number of different functions.

Fig. 9 illustrates the form factors (90)—(93) as a function of r_a for r_a equal in each case. Figs. 7 and 8 show the variations of a and r_0 with r_a for the various $f_0(r)$, for ^{1}S and ^{1}S n—p scattering respectively. We see that if we require a to be equal to its experimental value, which is done for each by taking a different r_a, then the value of r_0 obtained is the same in each case (the only appreciable difference is in the oversimplified case (90)). We list the results in table 4.

TABLE 4
Numerical results

State	Equation for $f_0(r)$	r_a (in 10^{-13} cm)	a (in 10^{-13} cm)	r_0 (in 10^{-13} cm)
^{3}S	(90)	1.528	5.38	2.178
	(91)	1.900	5.38	2.270
	(92)	1.650	5.38	2.270
	(93)	2.505	5.38	2.250
^{1}S	(90)	1.35	−23.69	3.235
	(91)	1.9075	−23.69	3.23
	(92)	2.18	−23.69	3.21
	(93)	3.029	−23.69	3.19

Thus any reasonable choice of $f_l(r)$ will give results identical within the order of the approximation, provided the cut-off range r_a is modified in each case to give, say, a fixed value of a. The extra condition $f_l''(r_a)$ satisfied by (93) does not lead to any significant change in the parameters, so for simplicity (92), and in general (16), are adopted as the form factor function.

Numerical values of δ_0 following from use of (92) as in table 4 are shown in table 3, for ^{3}S and ^{1}S n—p scattering respectively. Agreement with experimental values is good, except for $\delta_0 \approx \frac{1}{2}\pi$, due to a cancellation effect in the terms of in (28).

The Yukawa potential differs from the previous potentials considered in the much more rapid variation of r_0 with change of r_a, particularly in the ^{3}S case. This is due to the effect of the deep trough in the potential, which must make the correct r_a value much more critical. Thus for shallow potentials, results are not critical on the choice of r_a, but for singular potentials, a correct choice of r_a is much more important to get good phase-shift values. However, r_a does not differ very widely among the different potentials for each spin state.

9. Phase-Shifts δ_l for Neutron-Proton Scattering, arbitrary l

In this section, phase-shift calculations for six energies and arbitrary l values are present for the ^{3}S and ^{1}S square, gaussian, exponential and Yukawa potentials of section 8. Tables 5, 6, 7 and 8 show results for the four potential shapes

TABLE 5

Phase shifts for square well

		^{3}S n−p scattering						^{1}S n−p scattering						
	k	δ_0	δ_1	δ_2	δ_3	δ_4	δ_5	δ_0	δ_1	δ_2	δ_3	δ_4	δ_5	δ_6
Exact	0.1	2.6285	0.0009					1.0629	0.0010					
	0.25	2.0570	0.0147	0.0001				1.0947	0.0168	0.0001				
	0.5	1.4923	0.1169	0.0018				0.8710	0.1202	0.0047				
	0.75	1.1226	0.3452	0.0162	0.0005			0.6278	0.2878	0.0304	0.0019			
	1.0	0.8415	0.5543	0.0606	0.0034			0.4264	0.3805	0.0938	0.0090	0.0007		
	1.5	0.4819	0.5826	0.2602	0.0406	0.0034	0.0003	0.2502	0.2873	0.2392	0.0826	0.0150	0.0019	0.0002
Born approximation	0.1	0.2337	0.0006					0.1928	0.0009					
	0.25	0.5600	0.0097	0.0001				0.4493	0.0112	0.0001				
	0.5	0.9626	0.0698	0.0021				0.6979	0.0856	0.0043	0.0001			
	0.75	1.1200	0.1963	0.0137	0.0005			0.6858	0.2128	0.0259	0.0017	0.0001		
	1.0	1.0465	0.3594	0.0471	0.0033			0.5143	0.3268	0.0776	0.0095	0.0007		
	1.5	0.6120	0.5694	0.1993	0.0348	0.0036	0.0003	0.2548	0.3107	0.2172	0.0725	0.0139	0.0018	0.0002
Approximate method (eq. (10))	0.1	2.6320	0.0010					1.0272	0.0012					
	0.25	2.0723	0.0153	0.0001				1.0985	0.0147	0.0001				
	0.5	1.5001	0.1174	0.0025				0.9018	0.1165	0.0049	0.0001			
	0.75	1.1837	0.3318	0.0164	0.0005			0.6667	0.2771	0.0299	0.0018	0.0001		
	1.0	0.8889	0.5329	0.0601	0.0037			0.4579	0.3724	0.0907	0.0103	0.0007		
	1.5	0.5056	0.5833	0.2509	0.0404	0.0039	0.0003	0.2500	0.2985	0.2320	0.0799	0.0149	0.0019	0.0002

TABLE 6

Phase shifts for gaussian well

		^{3}S n−p scattering							^{1}S n−p scattering						
	k	δ_0	δ_1	δ_2	δ_3	δ_4	δ_5	δ_6	δ_0	δ_1	δ_2	δ_3	δ_4	δ_5	δ_6
Exact	0.1	2.6301	0.0015						1.0652	0.0013					
	0.25	2.0512	0.0228	0.0002					1.1038	0.0190	0.0003				
	0.5	1.5069	0.1349	0.0101	0.0002				0.8973	0.1190	0.0080	0.0004			
	0.75	1.1807	0.3281	0.0328	0.0024	0.0002			0.7073	0.2441	0.0388	0.0046	0.0004		
	1.0	0.9491	0.4688	0.0893	0.0132	0.0015			0.5563	0.3110	0.0915	0.0190	0.0032	0.0005	
	1.5	0.6830	0.4941	0.2290	0.0712	0.0187	0.0039	0.0007	0.3890	0.2917	0.1746	0.0751	0.0263	0.0080	0.0020
Born approximation	0.1	0.2490	0.0009						0.1926	0.0010					
	0.25	0.5881	0.0135	0.0002					0.4436	0.0147	0.0003				
	0.5	0.9682	0.0884	0.0049	0.0002				0.6746	0.0886	0.0070	0.0004			
	0.75	1.0830	0.2180	0.0267	0.0023	0.0002			0.6826	0.1937	0.0340	0.0043	0.0004		
	1.0	1.0172	0.3462	0.0737	0.0114	0.0014			0.5889	0.2701	0.0808	0.0176	0.0030	0.0004	
	1.5	0.7571	0.4660	0.2068	0.0639	0.0166	0.0036	0.0007	0.4092	0.3052	0.1737	0.0701	0.0249	0.0075	0.0019
Approximate method (eq. (10))	0.1	2.6256	0.0014						1.0728	0.0013					
	0.25	2.0556	0.0215	0.0002					1.1098	0.0191	0.0003				
	0.5	1.5529	0.1497	0.0059	0.0002				0.9114	0.1177	0.0079	0.0004			
	0.75	1.2512	0.2922	0.0301	0.0024	0.0002			0.7139	0.2426	0.0391	0.0046	0.0004		
	1.0	0.9370	0.4775	0.0948	0.0131	0.0015			0.5636	0.3047	0.0923	0.0192	0.0032	0.0004	
	1.5	0.6613	0.4916	0.2459	0.0749	0.0185	0.0039	0.0007	0.3889	0.3011	0.1820	0.0756	0.0266	0.0079	0.0020

TABLE 7

Phase shifts for Exponential well

		^{3}S n−p scattering							^{1}S n−p scattering						
	k	δ_0	δ_1	δ_2	δ_3	δ_4	δ_5	δ_6	δ_0	δ_1	δ_2	δ_3	δ_4	δ_5	δ_6
Exact	0.1	2.6310	0.0020						1.0621	0.0015					
	0.25	2.0672	0.0294	0.0006					1.1093	0.0210	0.0007				
	0.5	1.5440	0.1404	0.0162	0.0011				0.9327	0.1075	0.0120	0.0014			
	0.75	1.2900	0.2913	0.0473	0.0090	0.0014			0.7865	0.2003	0.0415	0.0092	0.0018		
	1.0	1.0890	0.3931	0.0985	0.0253	0.0062	0.0017		0.6301	0.2579	0.0798	0.0243	0.0069	0.0021	
	1.5	0.8383	0.4445	0.1901	0.0758	0.0304	0.0116	0.0050	0.5144	0.2760	0.1355	0.0610	0.0277	0.0126	0.0055
Born approximation	0.1	0.2549	0.0013						0.1871	0.0013					
	0.25	0.5892	0.0185	0.0005					0.4235	0.0168	0.0006				
	0.5	0.9286	0.1025	0.0102	0.0010				0.6332	0.0861	0.0106	0.0012			
	0.75	1.0291	0.2151	0.0410	0.0073	0.0013			0.6686	0.1668	0.0384	0.0080	0.0017		
	1.0	1.0047	0.3090	0.0891	0.0226	0.0058	0.0015		0.6390	0.2251	0.0711	0.0222	0.0066	0.0020	
	1.5	0.8539	0.4112	0.2015	0.0707	0.0284	0.0111	0.0043	0.4936	0.2735	0.1276	0.0592	0.0266	0.0116	
Approximate method (eq. (10))	0.1	2.5917	0.0019						1.0541	0.0016					
	0.25	2.0040	0.0286	0.0006					1.0883	0.0216	0.0007				
	0.5	1.4751	0.1385	0.0131	0.0011				0.9091	0.1118	0.0119	0.0013			
	0.75	1.1726	0.3198	0.0512	0.0083	0.0014			0.7526	0.2048	0.0438	0.0086	0.0018		
	1.0	0.9844	0.4039	0.1103	0.0259	0.0064	0.0016		0.6539	0.2553	0.0800	0.0243	0.0070	0.0021	
	1.5	0.7639	0.4379	0.2291	0.0806	0.0314	0.0120	0.0046	0.4342	0.2763	0.1342	0.0633	0.0282	0.0121	

TABLE 8

Phase shifts for Yukawa potential

	^{3}S n—p scattering								^{1}S n−p scattering						
	k	δ_0	δ_1	δ_2	δ_3	δ_4	δ_5	δ_6	δ_0	δ_1	δ_2	δ_3	δ_4	δ_5	δ_6
Exact	0.1	2.6203	0.0110						1.0647	0.0018					
	0.25	2.0470	0.0894	0.0080					1.1133	0.0229	0.0012				
	0.5	1.5581	0.2513	0.0589	0.0178				0.9748	0.1009	0.0189	0.0026			
	0.75	1.2946	0.3548	0.1163	0.0430	0.0247			0.8612	0.1665	0.0421	0.0132	0.0036		
	1.0	1.1151	0.3983	0.1627	0.0736	0.0349	0.0187		0.7695	0.2100	0.0705	0.0262	0.0101	0.0040	
	1.5	0.9075	0.4123	0.2141	0.1194	0.0693	0.0421	0.0255	0.6449	0.2357	0.1089	0.0541	0.0273	0.0147	0.0083
Born approximation	0.1	0.3728	0.0057						0.1798	0.0016					
	0.25	0.7615	0.0602	0.0057					0.3968	0.0195	0.0011				
	0.5	0.9853	0.1990	0.0503	0.0123				0.5813	0.0827	0.0143	0.0026			
	0.75	0.9941	0.2989	0.1196	0.0389	0.0152			0.6318	0.1445	0.0420	0.0113	0.0034		
	1.0	0.9470	0.3544	0.1818	0.0696	0.0335	0.0158		0.6294	0.1880	0.0741	0.0245	0.0096	0.0038	
	1.5	0.8326	0.4147	0.2763	0.1266	0.0700	0.0418	0.3190	0.5816	0.2383	0.1343	0.0533	0.0275	0.0138	0.0078
Approximate method (eq. (10))	0.1	2.6242	0.0104						1.0426	0.0020					
	0.25	2.0139	0.1166	0.0076					1.0624	0.0250	0.0012				
	0.5	1.4340	0.3557	0.0568	0.0131				0.8980	0.1061	0.0162	0.0028			
	0.75	1.1387	0.4402	0.1600	0.0478	0.0175			0.7718	0.1762	0.0476	0.0122	0.0036		
	1.0	0.9675	0.4464	0.2314	0.0860	0.0396	0.0181		0.6855	0.2151	0.0830	0.0266	0.0102	0.0040	
	1.5	0.7794	0.4302	0.2935	0.1457	0.0776	0.0448	0.0275	0.5790	0.2458	0.1437	0.0570	0.0296	0.0148	0.0083

as obtained from solution of the Schrödinger wave equation (4), from the first Born approximation integral B_{1l} of (11), and from the improved formula (10). The form factor $f_l(r)$ used in each case was (16). For computing convenience, the square well cut-off ranges r_a were taken equal to the range b in both ^{3}S and ^{1}S cases. However, for other well shapes, r_a was chosen as the values of section 8 for $l = 0$ giving the correct zero-energy scattering lengths a. All calculations were carried out using the CSIRAC digital computer.

Tables 5 and 6 for square and gaussian wells show good agreement between exact and approximate phases, the latter being a big improvement over the Born approximation values.

Tables 7 and 8 for exponential and Yukawa wells also show big improvements over the Born phase values, except for large k values, which are actually slightly worse than the Born values. This may be due to the long potential tails neglected for $r > r_a$ in our definition of the form factor $f_l(r)$.

The formula (10) for δ_l is of general application to potentials. However, the form factors $f_l(r)$ used in this paper, which effectively assume the asymptotic wave function for $r > r_a$, are best suited to short-tailed potentials such as the square, gaussian or Woods-Saxon potentials. Good results are also obtained for long-tailed potentials such as the exponential and Yukawa, but in some cases for $l = 0$ and for large k, the improvement over the Born phases may be negligible or the phases may even be affected adversely to a slight degree. In all these latter cases, the Born phase is already in rough agreement with the exact result. Modification of the form factor $f_l(r)$ to improve results for long-tailed potentials will be considered in another paper [10]).

References

1) R. H. Dalitz, Proc. Roy. Soc. A **206** (1951) 509
2) W. Kohn, Rev. Mod. Phys. **26** (1954) 292, 472
3) J. M. Blatt, Phys. Rev. **77** (1948) 647
4) J. M. Blatt and J. D. Jackson, Phys. Rev. **76** (1949) 18
5) H. A. Bethe, Phys. Rev. **76** (1949) 38
6) L. I. Schiff, Quantum mechanics (McGraw-Hill, New York, 1949)
7) K. B. Mather and P. Swan, Nuclear scattering (Cambridge University Press, 1958)
8) R. A. Buckingham and H. S. W. Massey, Proc. Roy. Soc. A **179** (1941-2) 123
9) N. F. Mott and H. S. W. Massey, The theory of atomic collisions (Oxford University Press, 2nd ed., 1949)
10) P. Swan, Nuclear Physics (to be published)

2.I

Nuclear Physics **18** (1960) 271—279; © *North-Holland Publishing Co., Amsterdam*

Not to be reproduced by photoprint or microfilm without written permission from the publisher

EFFECTS OF PHOTON POLARIZATION ON THE AZIMUTHAL ANGULAR DISTRIBUTION IN (γ, N) REACTIONS

A. G. de PINHO FILHO

Centro Brasileiro de Pesquisas Físicas, Rio de Janeiro, Brasil †

Received 5 April 1960

Abstract: The purpose of this note is to point out some simple features in the azimuthal angular distribution in photonuclear reactions induced by a partially plane polarized photon beam. The use of such a beam can be made of special interest as a check to the electric dipole character of the photon absorption in the giant resonance region.

1. The Angular Distributions in Photonuclear Reactions

The R-matrix formalism has been extensively discussed [1]) for the general case of a nuclear reaction $a+X \rightarrow Y+b$ in which particle a collides with nucleus X. After the collision, particle b is emitted in a direction defined by the polar angle θ and the azimuthal angle φ, the direction of reference being the axis of the beam and all quantities measured in the centre-of-mass system. The recoil nucleus Y is projected in the opposite direction. This formalism can be extended to include the case where a photon interacts with a nucleus [2]). Then the vector potential **A** plays the role of the wave function for the incident particle. If the incident photon beam travels along the z-axis and is polarized along the x-axis the multipole expansion of the vector potential $\mathbf{A}_z^x$ is given by

$$\mathbf{A}_z^x \propto \sum_{\pi} \sum_{P} \sum_{L=1}^{\infty} i^L (2L+1)^{\frac{1}{2}} (iP)^{\sigma} |\pi L P\rangle, \tag{1}$$

where π is an index giving the parity of the multipole and the connection between the $|\pi LP\rangle$ symbol and the irreducible tensor $T^P_{L,l}$ of rank L and parity $(-)^l$ used by Rose [3]) in the definition of the multipoles is easily established. The exponent $\sigma = 0$ for magnetic multipoles and $\sigma = 1$ for electric multipoles. The symbol $|LP\rangle$ shows that the photon may have angular momentum components about its direction of propagation equal to ± 1 only, since P is a polarization index that can assume these two values when the waves are left or right circularly polarized respectively. A basis of circularly polarized waves was used and the sum over P expresses the fact that a plane polarized wave can be constructed by superposing two circularly polarized waves.

† Work supported in part by Conselho Nacional de Pesquisas do Brasil.

The multipole angular momentum **L** and the spin of the bombarded nucleus $\mathbf{J}_X$ combine to give the total angular momentum of the system **J**. The spin of the emitted photoparticle is **s**, the spin of the recoil nucleus is $\mathbf{J}_Y$ and the orbital angular momentum in the final state is **l**. By vector coupling **l** with **s** we get **j** and repeating the operation we combine **j** with $\mathbf{J}_Y$ to get the same total angular momentum **J**.

From general considerations it can be easily shown that the differential cross section $d\sigma$ for the emission of a particle within the solid angle element $d\Omega$ defined by the pair of angles θ, φ in a photoreaction induced by a polarized beam on an unpolarized target (sum over final spins performed) is a linear combination of functions

$$F^{L\pi,\,L'\pi'}_{l'l'',\,jj',\,s} = (-)^{1-L+j'}\,Z(l'j'lj;\,sl'')$$
$$\times\{i^{(L-L'-l'')+(\sigma-\sigma')}[1+(-)^{L+L'-l''+(\sigma-\sigma')}](L'L,\,1-1|l''0)P^0_{l''}(\cos\theta) \qquad (2)$$
$$+\,i^{(L-L'-l'')-(\sigma+\sigma')}[e^{2i\varphi}+(-)^{L+L'-l''-(\sigma+\sigma')}e^{-2i\varphi}](L'L,\,11|l''2)P^2_{l''}(\cos\theta)\},$$

where the $P_l^m(\cos\theta)$ are the normalized Legendre's associated functions of the first kind and $(l_1l_2,\,m_1m_2|l_3m_3)$ is a Clebsh-Gordan coefficient for vector coupling. From the definition of the Z-coefficient it is clear that $F = 0$ unless $l+l'+l''$ is even, as a consequence of the conservation of parity.

For the analysis of the θ-distribution it is fundamental to consider separately the case in which only one multipole contributes to the transition. In this case l'' will be even and there will be symmetry about $\theta = \frac{1}{2}\pi$. Moreover,

TABLE 1

The φ-distribution in some simple transitions

			Parity of $l+l'$ (or parity of l'')	Parity of $L+L'-l''$	Parity of $(L+L'-l'')-(\sigma+\sigma')$
Only one multipole involved in the transition	$(\sigma=\sigma')$		even	even	even
Two multipoles involved in the transition	$\sigma=\sigma'$	E+, E+ E−, E− M+, M+ M−, M−	even	even	even
		E+, E− M+, M−	odd	even	even
	$\sigma\neq\sigma'$	E+, M+ E−, M−	even	odd	even
		E−, M+ E+, M−	odd	odd	even

a detailed knowledge of the mechanism of the reaction is not necessary to get the shape of the angular distribution, since only one term of the linear combination contributes. When radiation is unpolarized we must average over φ and the shapes of angular distribution for electric and magnetic multipoles become indistinguishable since the averaging operation removes the second term of the function F in which there is the phase factor $(i)^{-2\sigma} = (-)^{\sigma}$. When more than one multipole contribute to the transition, we lose the symmetry about $\theta = \frac{1}{2}\pi$ since odd powers of $\cos\theta$ can appear. Now the shape of the angular distribution depends on the R-reduced matrix elements and it is necessary to use some model to describe the photoreaction.

In contrast, the φ-distribution is always of a simple form, proportional to $1+\eta\cos 2\varphi$ (or proportional to $1+\mu\cos^2\varphi$) since the φ-independent term only vanishes when either $\sigma = \sigma'$ and $L+L'-l''$ is odd or $\sigma \neq \sigma'$ and $L+L'-l''$ is even, and the φ-dependence in the most simple cases is in $\cos 2\varphi$ as can be seen in table 1.

2. The Use of a Polarized Photon Beam

It is well known that the most striking feature of the low energy photonuclear reactions is the giant resonance. There is good evidence that the reaction in the giant resonance-region proceeds mostly through electric dipole absorption. The main evidence is the angular distribution of the fast photoparticles and the fact that the integrated cross section over the giant resonance nearly exhausts the sum rule for electric dipole radiation.

The emitted photoparticles may be classified in two groups. The first one includes all particles in the energy interval until about 3 MeV. Particles in this group (in most cases neutrons) are emitted by an evaporation process and present an energy distribution of the Maxwell type and a generally isotropic angular distribution. Most particles belong to this group. However, there are many particles emitted with energy greater than 4 MeV in spite of the vanishingly small probability that a compound nucleus, in which the excitation energy is about 20 MeV, evaporates particles into this energy interval. A direct process was proposed by Courant [4]) to explain this second group. In a direct interaction the nucleus has no time to "forget" the way by which radiation was absorbed and this is reflected in the angular distribution of the fast photoparticles.

When we observe the high energy tail of the photo-emitted neutrons (for the sake of simplicity we shall consider only (γ, n) reactions) the θ-angular distribution is generally expressed as $A+B\sin^2\theta$, just the angular distribution expected for electric dipole absorption.

When a polarized photon beam is used the φ-angular distribution can be studied besides the θ-distribution. If the fast neutrons are selected their angular distribution must be of the form $A+2B\sin^2\theta\cos^2\varphi$, as expected for electric

dipole transitions. The factor 2 was chosen to cancel the average value of $\cos^2\varphi$ when the beam is unpolarized.

A polarized photon beam can be obtained from some nuclear reactions or even from a betatron. It is well known that the bremsstrahlung photons produced when an electron strikes a target are polarized. The depolarization of the bremsstrahlung beam from a betatron is a consequence of the thickness of the target. Multiple scattering of electrons before bremsstrahlung occurs becomes more serious due to the fact that electrons traverse the target many times. A special arrangement can be made in such way that the accelerated electrons are allowed to traverse only once the betatron target. With this arrangement much is lost in intensity but the depolarization is greatly reduced. On the other hand, to observe any effect of polarization it is necessary to leave the axis of the photon distribution (where the intensity is the greatest) and to work in some direction with $\beta \neq 0$ (β is the angle between the direction of the electron beam and the direction of the photon, i.e., the angle of observation of the photons). The best choice depends on how much intensity may be lost and how high is the desired polarization. Miller [5]) gives curves with which it is possible to plot polarization against the photon energy with the observation angle β and the thickness of the target m as parameters, i.e. to construct the polarization function $\Pi(E_\gamma)$. Therefore it is possible to decompose the energy spectrum of the betatron $N(E_\gamma)$ into a polarized part $P(E_\gamma) \propto N(E_\gamma)\Pi(E_\gamma)$ and an unpolarized part $U(E_\gamma)$ for some prescribed pair of parameters β and m.

When a target is bombarded by this partially polarized beam each part of it acts separately and produces a number n_P and n_U of fast photoparticles respectively. The fraction of photoparticles emitted by the completely polarized part of the incident beam is $\rho = n_P/(n_P+n_U)$ and the angular distribution of the fast photoneutrons becomes

$$I(\theta, \varphi) \propto 1+[2\lambda_P\rho \cos^2\varphi+(1-\rho)\lambda_U] \sin^2\theta. \tag{3}$$

The unpolarized beam $U(E_\gamma)$ produces direct photoneutrons with an angular distribution proportional to $1+\lambda_U \sin^2\theta$. An unpolarized beam with the same energy distribution as $P(E_\gamma)$ would produce direct photoneutrons with an angular distribution proportional to $1+2\lambda_P \sin^2\theta \langle\cos^2\varphi\rangle_{Av} = 1+\lambda_P \sin^2\theta$. Since it is impossible to obtain experimentally an unpolarized beam with the same energy spectrum $P(E_\gamma)$ we cannot determine λ_P by a direct measurement. Nevertheless it is easily determined by measuring the θ-angular distribution in two different φ-planes:

$$\begin{aligned} I(\theta, \varphi = 0) &\propto 1+\lambda_0 \sin^2\theta, \\ I(\theta, \varphi = \tfrac{1}{2}\pi) &\propto 1+\lambda_{\pi/2} \sin^2\theta, \end{aligned} \tag{4}$$

where

$$\lambda_0 = 2\lambda_P\rho+(1-\rho)\lambda_U, \quad \lambda_{\pi/2} = (1-\rho)\lambda_U, \tag{5}$$

and thus

$$\lambda_U = \frac{\lambda_{\pi/2}}{1-\rho}, \qquad \lambda_P = \frac{\lambda_0 - \lambda_{\pi/2}}{2\rho}. \tag{5}$$

If the degree of polarization is not too small a considerable difference is to be expected in the parameters λ of the θ-distribution for the planes $\varphi = 0$ and $\varphi = \frac{1}{2}\pi$. Indeed, since $\lambda_0/\lambda_{\pi/2} = 1+[2\rho\lambda_P/(1-\rho)\lambda_U]$ and since in the most usual experimental circumstances $\lambda_P \approx \lambda_U$, for ρ as small as 0.20, $\lambda_0/\lambda_{\pi/2}$ will be as large as 1.5.

When electric dipole absorption takes place the fast photoparticles present a tendency to be emitted in a direction parallel to the polarization vector. An experiment can be projected to measure the ratio between the number of particles emitted in this direction and the number of particles emitted in a direction orthogonal to it. In the plane $\theta = \frac{1}{2}\pi$ the expected ratio is

$$\frac{\parallel}{\perp}(\theta = \tfrac{1}{2}\pi) = 1 + \frac{2\lambda_P\rho}{1+(1-\rho)\lambda_U} = \frac{1+\lambda_0}{1+\lambda_{\pi/2}}. \tag{6}$$

If we measure in the same experiment the three quantities $\parallel/\perp(\theta = \frac{1}{2}\pi)$, λ_0 and $\lambda_{\pi/2}$, eq. (6) is a good check to the electric dipole character of the transition. When some significant deviation is observed it is an indication that multipolarities other than electric dipole contribute to the transition, even though this is not indicated clearly by the θ-distribution alone.

3. The Calculation of ρ

Let us now consider how to calculate ρ, defined as the fraction of photoemitted neutrons due to the completely polarized part of the incident beam, as seen by some neutron counter. For a crude computation we use

$$\rho = \frac{\displaystyle\int_{(E_\alpha)_0}^{(E_\alpha)_{max}} \sigma(E_\alpha)\, e^{-\frac{R}{\Lambda(E_\alpha)}}\, T(E_\alpha)\,dE_\alpha \int_{(E_\gamma)_0}^{(E_\gamma)_{max}} dE_\gamma N(E_\gamma)\Pi(E_\gamma)\sqrt{E_\alpha - E_\gamma}\,\sigma_{\gamma n}(E_\gamma)}{\displaystyle\int_{(E_\alpha)_0}^{(E_\alpha)_{max}} \sigma(E_\alpha)\, e^{-\frac{R}{\Lambda(E_\alpha)}}\, T(E_\alpha)\,dE_\alpha \int_{(E_\gamma)_0}^{(E_\gamma)_{max}} N(E_\gamma)\sqrt{E_\alpha - E_\gamma}\,\sigma_{\gamma n}(E_\gamma)\,dE_\gamma} \tag{7}$$

where we consider a Fermi distribution of neutrons inside the nucleus; $\sigma_{\gamma n}(E_\gamma)$ is the cross section for absorption of electric dipole radiation by a neutron inside the nucleus; $\Lambda(E_\alpha)$ is the mean free path for neutrons in the nuclear matter; R is the nuclear radius (the mean distance travelled by an "excited" neutron before reaching the nuclear surface); $T(E_\alpha)$ is the transmission coefficient for a step barrier where there is a sudden modification in the mass value and $\sigma(E_\alpha)$ is the curve of sensibility of the neutron counter. The limits of inte-

gration are shown in fig. 1: E_F is the Fermi energy, equal to 58 MeV for an effective mass 0.78 times the neutron mass, S is the separation energy (about 8 MeV) and ε_0 is the energy above which the neutrons are considered directly emitted (about 4 MeV). The energy of the emitted neutrons is $\varepsilon = E_\alpha - E_F - S \approx E_\alpha - 66$ MeV.

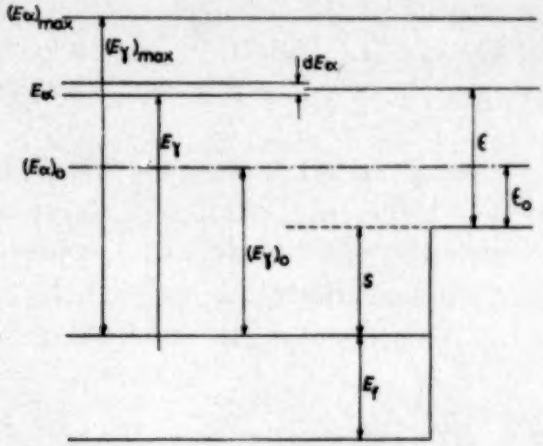

Fig. 1. Diagram indicating the limits of integration.

A crude estimate of ρ was performed with the following data:
(i) Schiff's bremsstrahlung spectrum for maximum photon energy equal to 24 MeV [6]);
(ii) Miller's curves [5]) for $\beta = 2.875\times10^{-2}$ rad and $m = (4.50\times10^{-2}ZA^{-\frac{1}{3}})t$ (mg/cm^2) = 0.6;
(iii) since the ρ value is very insensitive to the form of the cross section $\sigma_{\gamma n}(E_\gamma)$ we have used an expression of the same type as the cross section given by Courant for the direct photoprocess [4]);
(iv) $\Lambda(E_\alpha)$ is related to the imaginary part of the complex potential (averaged over distances inside the nucleus) given by Gomes [7]);
(v) the neutron counter is the reaction Si^{28}(n, p), a very usual method of detection of photoneutrons [8]).

The obtained result was $\rho = 0.13$ and the mean energies of the neutrons produced by the polarized part of the beam and by the unpolarized part were respectively $\bar{\varepsilon}_P = 7.7$ MeV and $\bar{\varepsilon}_U = 8.4$ MeV. Zatsepina *et al.* [9]) have shown conclusively that the parameter λ depends on the neutron energy (as clearly indicated by Wilkinson's theory [10])). However, the mean energies $\bar{\varepsilon}_P$ and $\bar{\varepsilon}_U$ not being too different and the peaks of the neutron spectra being very broad (half width about 4 MeV) we would expect $\lambda_P \approx \lambda_U$ (see figure 2).

A preliminary experiment was performed by Goldemberg *et al.* [11]) in the same experimental conditions as above mentioned, to measure the ratio $\|/\perp(\theta = \frac{1}{2}\pi)$. For a bismuth target with four Si detectors disposed in cross in the plane $\theta = \frac{1}{2}\pi$ the result was 0.97 ± 0.06. The θ-angular distribution was measured in a plane containing the photon beam and perpendicular to the direc-

tion of polarization at the off-centre position of the beam and the result was $\lambda_{\pi/2} \approx 1$ in accordance with previously published results. Therefore the expected ratio $\|/\perp(\theta = \frac{1}{2}\pi)$ was about 1.15 (within the approximation $\lambda_0 = \lambda_{\pi/2}$). The low value obtained for this ratio, an evidence of a possible isotropy for the φ-distribution, is not sufficiently serious to be considered as inconsistent with the theoretical estimate, specially when we consider that possible corrections tend to decrease the calculated value. The chief corrections are: (i) the effect of magnetic dipole transitions — if the θ-distributions are of the same type in the electric and magnetic dipole transitions, viz. $A+B\sin^2\theta$, the μ-parameters of

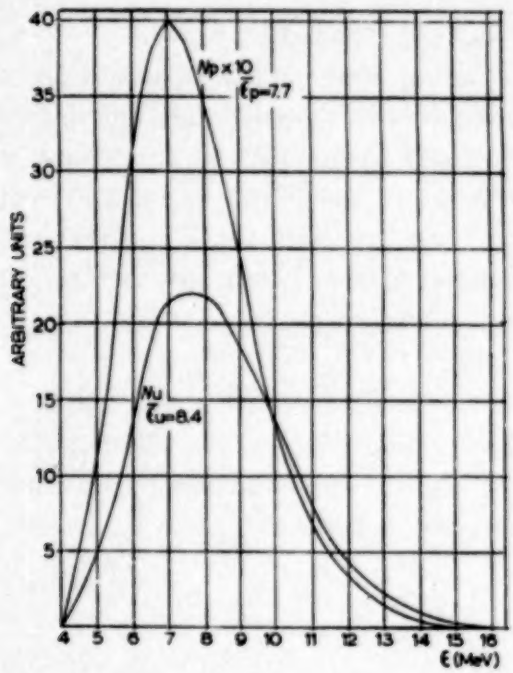

Fig. 2. The neutron spectra from a Bi target as observed by the Si detector. $\rho = 13\ \%$; $\bar{\varepsilon}_P = 7.7$ MeV; $\bar{\varepsilon}_U = 8.4$ MeV.

the φ-distribution have opposite signs and the anisotropies tend to cancel each other (electric quadrupole transitions are important only for protons owing to effective charge considerations); (ii) a neutron can be excited to a high energy level by absorbing a photon and then, after a collision, be emitted with an energy still greater than ε_0. In writing eq. (7) it was considered that all neutrons that collide before reaching the nuclear surface are removed from the high energy group of photo neutrons, and also that they are not able to produce recoil neutrons in this group. A realistic appreciation of this fact becomes very important when the photon beam is monochromatic, but it is not very important for the betatron spectrum †. A very crude estimate has indicated that for a

† We are indebted to Dr. Gomes for pointing out this fact to us.

maximum photon energy of 24 MeV the fraction of neutrons with energy greater than 4 MeV that collide before being emitted is inferior to 5 %.

It would be interesting, however, to perform a new experiment where it would be possible to measure the θ-distribution for $\varphi = 0$ and $\varphi = \frac{1}{2}\pi$ thus allowing the determination of λ_P and λ_U, as well to measure the ratio $\|/\perp$. This would be a good check for the electric dipole character of the photon absorption in the resonance region of bismuth.

4. Conclusions

As a conclusion it can be stated that:

(i) The detection of a supposed linear polarization of the photons can be checked by the examination of the azimuthal angular distribution of the products of the photoreactions; necessarily an anisotropy will be present.

(ii) Whatever may be the absorbed multipole, and even when more than one multipole contribute to the transition, the φ-distribution has the simple form $1+\mu\cos^2\varphi$ with a polarized photon beam. For electric dipole absorption and a partially polarized photon beam $\mu = 2\rho\lambda_P/[1+(1-\rho)\lambda_U] = (\lambda_0-\lambda_{\pi/2})/(\lambda_{\pi/2}+1)$ with ρ given by eq. (7).

(iii) Nevertheless the φ-distribution alone will not be sufficient to determine the character of the absorbed multipole; if we obtain in the same experiment the θ- and φ-distributions, eq. (6) being satisfied, the transition is exclusively through electric dipole, any significant deviation indicating the participation of other multipolarities in the photoreaction, for the detection of which the θ-distribution is not a sufficient information.

The author wishes to express his thanks to Professor J. Leite Lopes for his stimulating interest in this work and to Drs. J. Goldemberg and L. C. Gomes for many valuable discussions and suggestions. We are specially grateful to Dr. Goldemberg for a complete information on an unpublished work done by him, O'Connell and Dyal [11]) at the University of Illinois.

References

1) See for example J. M. Blatt and L. C. Biedenharn, Rev. Mod. Phys. **24** (1952) 258, where a complete list of references can be found
2) See for example A. Agodi, Nuovo Cim. **5** (1957) 21, where a complete list of references can be found.
3) M. E. Rose, Multipole Fields (Wiley, New York, 1955)
4) E. D. Courant, Phys. Rev. **82** (1951) 703
5) J. Miller, Rapport C.E.A. no 6555 Centre d'Études Nucléaires de Saclay
6) L. Schiff, Phys. Rev. **83** (1951) 252;
L. Katz and A. G. W. Cameron, Canad. J. Phys. **29** (1951) 518

7) L. C. Gomes, Notas de Fisica **5**, no. 8 (1959)
8) See for example F. Ferrero, L. Gonella, A. O. Hanson, R. Malvano and C. Tribuno, Nuovo Cim. **5** (1957) 242
9) G. N. Zatsepina, L. E. Lazareva and A. N. Pospelov, Soviet Physics JETP **5** (1957) 21; G. A. Price, Phys. Rev. **93** (1959) 1279
10) D. H. Wilkinson, Physica **22** (1956) 1039
11) J. Goldemberg, P. Dyal and O'Connel, unpublished paper (1958)

2.J

Nuclear Physics **18** (1960) 280—285; © *North-Holland Publishing Co., Amsterdam*

Not to be reproduced by photoprint or microfilm without written permission from the publisher

ÉTATS INDIVIDUELS AU SEUIL DE FISSION

M. DEMEUR, P. JANSSENS et J. LARDINOIS †

Université Libre de Bruxelles

Reçu le 11 mai 1960

Abstract: A dumb-bell potential has been quantized in order to find properties of individual levels in a nucleus near the fission threshold.

1. Introduction

Notre connaissance des phénomènes liés à la fission s'est accrue considérablement au cours des dernières années [1]), et différentes approches théoriques ont été proposées. Parmi celles-ci, l'étude des états collectifs du noyau fissile ayant atteint la déformation-seuil a permis de décrire des propriétés importantes [2, 3, 4])

L'étude des états intrinsèques du noyau à la déformation-seuil est restée peu développée. Il semble que seuls Hill et Wheeler [5]) et Nosov [6]) l'aient entreprise de manière détaillée; Vladimirskii [7]) a examiné certaines propriétés des nucléons plongés dans un champ de forces à symétrie axiale. Les calculs présentés ici apportent quelques réponses qualitatives au problème des états intrinsèques.

Le modèle utilisé par Hill et Wheeler est constitué par deux sphères à parois parfaitement refléchissantes, tangentes ou communiquant par un col de diamètre petit devant le rayon des sphères. Nous employons ici un champ de force dont l'équipotentielle zéro a une section méridienne ressemblant à un huit, la symétrie par rapport au plan équatorial étant assurée. Notre potentiel présente l'avantage physique de ne pas annuler identiquement la probabilité de présence d'un nucléon en dehors des deux puits attractifs représentant les fragments. L'expression analytique que nous avons choisie,

$$V = \tfrac{1}{2}kr^2 + \alpha \frac{\sin^2\theta}{r^2} - V_0 \quad (\alpha > 0), \tag{1}$$

est, par ailleurs, défavorable par le fait que toutes les équipotentielles ne simulent pas les fragments; nous l'avons cependant retenue à cause de la simplicité de sa quantification.

2. Quantification

L'équation de Schrödinger du problème

$$\left[-\frac{\hbar^2}{2m}\left(\partial^2_{rr} + \frac{2}{r}\partial_r - \frac{\mathbf{L}^2}{r^2}\right) + \tfrac{1}{2}kr^2 + \alpha\frac{\sin^2\theta}{r^2} - V_0 - E \right] \Psi = 0 \tag{2}$$

† Aspirante au Fonds National de la Recherche Scientifique

est immédiatement séparable en les variables radiale et angulaires:

$$\Psi = R(r)\Omega(\theta, \varphi).$$

Après quantification de l'équation angulaire

$$\left[\mathbf{L}^2 + \frac{2m\alpha}{\hbar^2}\sin^2\theta\right]\Omega(\theta, \varphi) = \lambda(\lambda+1)\Omega(\theta, \varphi), \quad (\lambda > 0), \tag{3}$$

il reste une équation radiale du type d'oscillateur

$$\left[\mathrm{d}_{rr}^2 + \frac{2}{r}\mathrm{d}_r - \frac{\lambda(\lambda+1)}{r^2} - \frac{km}{\hbar^2}r^2 + \frac{2m}{\hbar^2}(V_0+E)\right]R_\lambda(r) = 0$$

dans laquelle nous posons $r = ax$ avec $a^4 = \hbar^2/2m\omega$, $\omega = (k/m)^{\frac{1}{2}}$, $V_0+E = \varepsilon\hbar\omega$, et dont la solution est donnée par

$$R_{\lambda n_r} = N_{\lambda n_r} x^\lambda {}_1F_1(-n_r; \lambda+\tfrac{3}{2}; x^2)\mathrm{e}^{-\frac{1}{2}x^2}; \quad \varepsilon_{n_r,\lambda} = 2n_r+\lambda+\tfrac{3}{2}.$$

Nous en déduisons l'allure du spectre des

$$E_{n_r\lambda} = \hbar\omega(2n_r+\lambda+\tfrac{3}{2})-V_0$$

qui est donc formé par l'imbrication de spectres harmoniques construits sur les niveaux

$$E_{0\lambda} = \hbar\omega(\lambda+\tfrac{3}{2})-V_0.$$

La quantification de l'équation angulaire (3) se ramène à celle de l'équation en θ

$$\left[\mathrm{d}_\omega(1-\omega^2)\mathrm{d}_\omega - \frac{\Lambda^2}{1-\omega^2} + \lambda(\lambda+1) - \gamma(1-\omega^2)\right]\Theta(\omega) = 0, \left(\omega = \cos\theta, \gamma = \frac{2m\alpha}{\hbar^2}\right), \tag{4}$$

après séparation de la partie en φ

$$\Phi(\varphi) = (2\pi)^{-\frac{1}{2}}\exp i\Lambda\varphi, \quad (\Lambda = 0, \pm 1, \pm 2 \ldots).$$

Les solutions ne dépendent de Λ que par l'intermédiaire de Λ^2; le spectre est donc dégénéré quant au signe de Λ.

L'équation (4) est invariante pour un changement de ω en $-\omega$, étant donné la symétrie par rapport au plan équatorial; les fonctions propres se séparent en 'gerade' $\Theta^+(\omega) = \Theta^+(-\omega)$ et 'ungerade' $\Theta^-(\omega) = -\Theta^-(-\omega)$. Nous la résolvons en développant les Θ en polynômes de Legendre normés

$$\Theta_\lambda{}^\Lambda(\omega) = \sum_l a_{l,\lambda}^\Lambda P_l{}^\Lambda(\omega)$$

en restreignant $l-\Lambda$ à des valeurs paires pour les fonctions Θ^+, impaires pour les Θ^-.

Les valeurs propres λ s'obtiennent en annulant les déterminants de Hill des équations de récurrence entre les a_l. Ces calculs sont facilités par le fait que les

déterminants sont symétriques lorsque les polynômes de Legendre sont normés; ils ont été menés à bien sur un ordinateur IBM 650 en limitant les séries à $l = 25$ et pour un choix particulier des paramètres.

3. Choix des Paramètres et Résultats

Ce choix des paramètres s'effectue sur la base de deux critères:

a) L'équipotentielle zéro du potentiel (1) doit affecter la forme d'un huit avec un potentiel attractif à l'intérieur des boucles du huit, répulsif à l'extérieur.

b) Le volume contenu dans la surface $V = 0$ doit être égal à $\frac{4}{3}\pi R_0^3$ où R_0 est défini par $\frac{1}{2}k_0 R_0^2 - V'_0 = 0$.

Il faudrait en plus exiger que les potentiels non déformés $\frac{1}{2}k_0 R_0^2 - V'_0$, et déformés (1), contiennent le même nombre de nucléons; en fait, pour les paramètres que nous avons choisis cette condition est assez bien satisfaite si $V'_0 = V_0$ dans la région de 150 nucléons.

L'équation de l'équipotentielle zéro peut être ramenée à

$$\beta\rho^2 + \delta \frac{\sin^2\theta}{\beta\rho^2} = 1, \tag{5}$$

dans laquelle $\rho = r/R_0$, $\beta = k/k_0$ et $\delta = 2\alpha\beta/k_0 R_0^4$. Écrite ainsi, elle sépare un paramètre de forme δ d'un paramètre β adaptable pour satisfaire la conservation de volume.

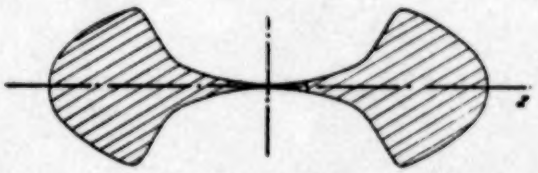

Fig. 1. Forme de l'équipotentielle zéro (5) pour $\delta = 1$, $\beta = 0.2$.

Nous avons choisi les valeurs des paramètres pour lesquelles la courbe (5) a l'allure de la fig. 1 et les critères a) et b) sont satisfaits: $\delta = 1$, $\beta = 0.2$.

Les résultats de la quantification de l'équation angulaire (4) sont reportés en appendice.

Nous présentons dans la fig. 2 l'imbrication des niveaux jusqu'à 80 particules. Il convient de remarquer que tous les niveaux possèdent une dégénérescence 'gerade-ungerade' due à la présence d'un mur de potentiel fortement répulsif dans le plan équatorial; comme ces niveaux sont en outre dégénérés en $\pm\Lambda$ et $\pm\frac{1}{2}$ (dégénérescence de spin), ils présentent la multiplicité 4 lorsque $\Lambda = 0$ et 8 lorsque $|\Lambda| \neq 0$.

La fig. 2 indique l'existence de couches après 4, 16, 40, 80 particules soit 2, 8, 20, 40 particules dans chacun des deux puits, c'est à dire d'une structure en

couche d'oscillateur à l'intérieur de ces puits. Au dessus de 80 la situation devient confuse et il n'est plus possible de mettre d'autres couches en évidence.

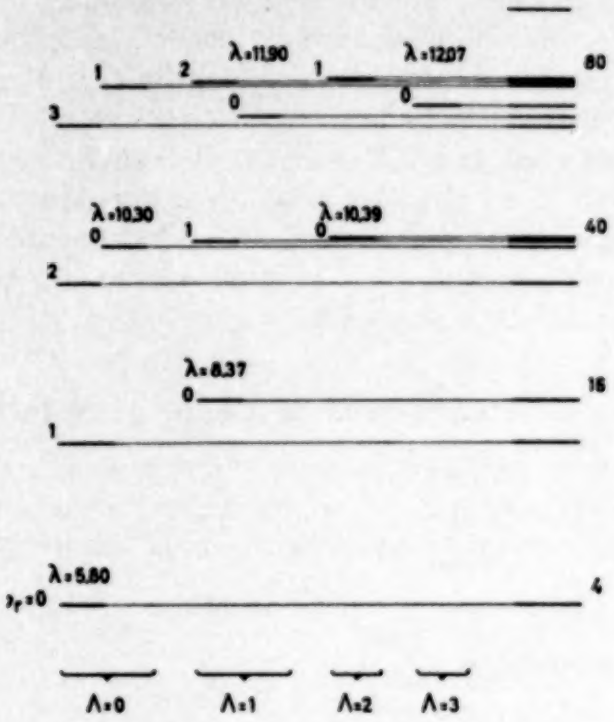

Fig. 2. Niveaux d'énergie des 80 premières particules dans le potentiel (1).

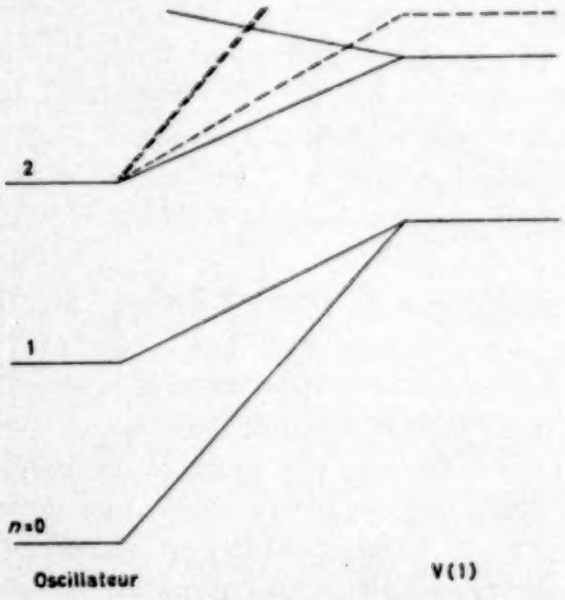

Fig. 3. Comparaison des premiers niveaux du spectre avec les niveaux de l'oscillateur de départ.

Dans la fig. 3 les premiers niveaux du spectre sont mis en correspondance avec les niveaux de l'oscillateur non perturbé de départ.

La comparaison des résultats de Hill et Wheeler [5]) avec ceux de la fig. 2 montre que les deux spectres diffèrent par l'ordre d'apparition successive des niveaux. Les deux modèles ont une propriété commune: celle de séparer les deux fragments par une barrière élevée. Chacun des spectres est donc très proche de celui que l'on obtiendrait par quantification d'un seul puits; chez Hill et Wheeler il s'agit du puits infini à symétrie sphérique, tandis que notre potentiel définit un puits très différent (d'ailleurs sans symétrie sphérique).

Les résultats sont donc sensibles à la forme détaillée du potentiel. Pour obtenir des précisions plus quantitatives il faudrait partir d'équipotentielles réalistes comme celles obtenues par Hill [8]) par exemple; le volume des calculs différerait considérablement de ceux faits ici.

4. Influence d'un Terme de Couplage Spin-Orbite

Il semble indiqué d'examiner l'influence d'un terme de couplage spin-orbite H_{so} sur l'ordre des niveaux et les propriétés de structure en couche. Ce couplage H_{so} s'écrit dans un potentiel non-central sous la forme

$$H_{so} = N\boldsymbol{\sigma} \cdot (\mathbf{v} \times \boldsymbol{\nabla} V)$$

qui se réduit dans ce cas-ci à

$$H_{so} = \frac{i\hbar N}{m}\left[\left(k - 4\alpha\frac{z^2}{r^6}\right)\mathbf{L}\cdot\boldsymbol{\sigma} + 2\alpha\frac{z}{r^4}\right](\sigma_x\partial_y - \sigma_y\partial_x).$$

La constante N est déterminée de façon à retrouver le terme de couplage spin-orbite de Nilsson [9]) pour le noyau sphérique: $N = -2/i\omega_0\kappa_{\text{Nils}}$; $\kappa_{\text{Nils}} = 0.05$. La valeur moyenne du second terme de l'opérateur H_{so} est nulle puisque les opérateurs ∂_x et ∂_y ne contiennent pas de termes diagonaux en Λ; de même l'opérateur $\mathbf{L}\cdot\boldsymbol{\sigma}$ se réduit à $L_z\sigma_z$ et le seul terme de H_{so} qui contribue à la perturbation du premier ordre est, pour le choix précédent des paramètres,

$$H_{so}^{(1)} = -0.1\left[0.2 - 152.8\frac{\omega^2}{x^4}\right]L_z\sigma_z.$$

Le couplage H_{so} n'agit donc que sur les niveaux à $\Lambda \neq 0$; il les dédouble en niveaux à spin et moment orbital parallèles $(\Lambda, \frac{1}{2})$, $(-\Lambda, -\frac{1}{2})$ et à spin et moment orbital antiparallèles $(\Lambda, -\frac{1}{2})$, $(-\Lambda, \frac{1}{2})$; et, parce que dans le bas du spectre la dégénérescence 'gerade-ungerade' n'est pas levée, aprés application de la perturbation, tous les niveaux ont la dégénérescence 4. Pour les niveaux les plus bas la contribution dominante vient du terme de déformation en $-\omega^2/x^4$, la présence du signe — indique que les niveaux sont inversés par rapport au cas sphérique; pour les niveaux plus élevés, $\langle 1/x^4\rangle$ diminue ce qui est conforme au fait que l'influence de la déformation diminue lorsque l'énergie augmente.

Pour les premiers niveaux on trouve:

$\Lambda = 1$	$\lambda = 8.37$	$n_z = 0$	$\langle H_{so} \rangle = \pm 0.10$
		$n_z = 1$	$\langle H_{so} \rangle = \pm 0.12$
$\Lambda = 2$	$\lambda = 10.39$	$n_z = 0$	$\langle H_{so} \rangle = \pm 0.14$

Après cette levée de dégénérescence les niveaux restent suffisamment proches pour que la structure en couche notée au § 3 soit conservée.

Nous remercions la société „IBM of Belgium" d'avoir mis à notre disposition les heures-machine nécessaires à la recherche des valeurs propres et des vecteurs propres des déterminants de Hill mentionnés au § 2.

Appendice

VALEURS PROPRES DE L'ÉQUATION (4)

Table des premières valeurs de λ

$\Lambda = 0$	$\Lambda = 1$	$\Lambda = 2$	$\Lambda = 3$	$\Lambda = 4$	$\Lambda = 5$
5.80					
10.30	8.37				
13.24	11.90	10.39			
15.50	14.44	13.32	12.07		
17.30	16.46	15.57	14.60	13.55	
18.74	18.09	17.37	16.60	15.77	14.88
19.69	19.38	18.80	18.22	17.57	16.87

Références

1) R. B. Leachman, Proc. 2nd Intern. Conf. Peaceful Uses Atomic Energy, Geneva 1958, Vol. 15, p. 229
2) A. Bohr, Proc. Intern. Conf. Peaceful Uses Atomic Energy, Geneva 1955, Vol. 2, p. 151
3) L. Wilets and D. M. Chase, Phys. Rev. **103** (1956) 1296
4) J. J. Griffin, Phys. Rev. **116** (1959) 107
5) D. L. Hill and J. A. Wheeler, Phys. Rev. **89** (1953) 1102
6) V. G. Nosov, cité par B. T. Geilikman dans Physics of fission, Supplement no 1 to the Soviet Journal of Atomic Energy (1957), p. 5
7) V. V. Vladimirskii, JETP **5** (1957) 673
8) D. L. Hill, Proc. 2nd Intern. Conf. peaceful Uses Atomic Energy, Geneva 1958, Vol. 15, p. 244
9) S. G. Nilsson, Mat. Fys. Medd. Dan. Vid. Selsk. **29**, No. 16 (1955)

2.G

Nuclear Physics 18 (1960) 286—295; © *North-Holland Publishing Co., Amsterdam*

Not to be reproduced by photoprint or microfilm without written permission from the publisher

ÉTUDE DE QUELQUES NIVEAUX EXCITÉS DU ^{11}B PAR LA RÉACTION ^{10}B(d, p)^{11}B

S. GORODETZKY, M. CROISSIAUX, A. GALLMANN, P. FINTZ, J. SAMUEL et G. BASSOMPIERRE

Institut de Recherches Nucléaires, Strasbourg

Reçu le 22 mars 1960

Abstract: We give some results about the angular distributions of protons, p—γ and γ—γ angular correlations for different levels which are obtained in the reaction ^{10}B(d, p)^{11}B at $E_d = 1.25$ MeV and $E_d = 4.6$ MeV. The interpretation of the results is consistent with the value $\frac{1}{2}^-$ or $\frac{3}{2}^-$ for the total angular momentum and parity of the 4.46 MeV level in ^{11}B.

1. Introduction

Les distributions angulaires des protons émis dans les réactions d—p permettent en principe, connaissant le moment angulaire et la parité du noyau cible, de déterminer la parité et les valeurs limites du moment angulaire total du niveau atteint. D'autre part, dans l'hypothèse de la théorie simplifiée de Butler, l'étude des corrélations angulaires p—γ dans un plan perpendiculaire à l'axe de recul du noyau peut également indiquer si la contribution du stripping est importante ou non. Enfin les corrélations p—γ mesurées dans le plan d—p précisent davantage les spins des niveaux en jeu. L'ensemble de ces études permet de tirer des conclusions valables sur le mécanisme de la réaction étudiée.

2. Dispositif Expérimental

Nous avons utilisé des cibles de ^{10}B isotopiquement pures (> 99 %). Pour les expériences à très basse énergie de bombardement ($E_d = 1.25$ MeV), la cible de 250 μg/cm^2 avait un support d'aluminium de 33 mg/cm^2 d'épaisseur. A cette énergie le rendement de la réaction ^{27}Al(d, p) ^{28}Al est faible vis-à-vis de celui de la réaction ^{10}B(d, p)^{11}B (fig. 1). A des énergies de deutérons plus élevées, par contre, la section efficace de la réaction ^{27}Al(d, p)^{28}Al est importante. Pour éliminer cette réaction parasite gênante nous avons, à $E_d = 4.6$ MeV, utilisé une cible de 50 μg/cm^2 de ^{10}B sur un support d'or de 19 mg/cm^2.

Le cristal de détection des protons était un scintillateur plastique (NE 102) † d'épaisseur suffisante pour absorber complètement les groupes de protons étudiés. Selon les cas, l'épaisseur était de 0.5 mm ou de 1 mm. Nous avons

† Fourni par Nuclear Enterprises Ltd., Edinburgh.

obtenu une résolution de 4.1 % pour des protons de 8.5 MeV (fig. 1). Les rayons γ étaient détectés à l'aide de cristaux de NaI(Tl) de 5.1×5.1 cm.

Les impulsions proportionnelles à l'énergie des particules venant, soit du canal proton, soit du canal γ, étaient envoyées sur un analyseur à 100 canaux R.I.D.L. Pour les distributions angulaires, nous avons utilisé une boîte en aluminium de 10 cm de diamètre, percée tous les 10 degrés d'un trou de 5 mm de diamètre. Dans ces conditions l'ouverture angulaire était de ± 3 degrés.

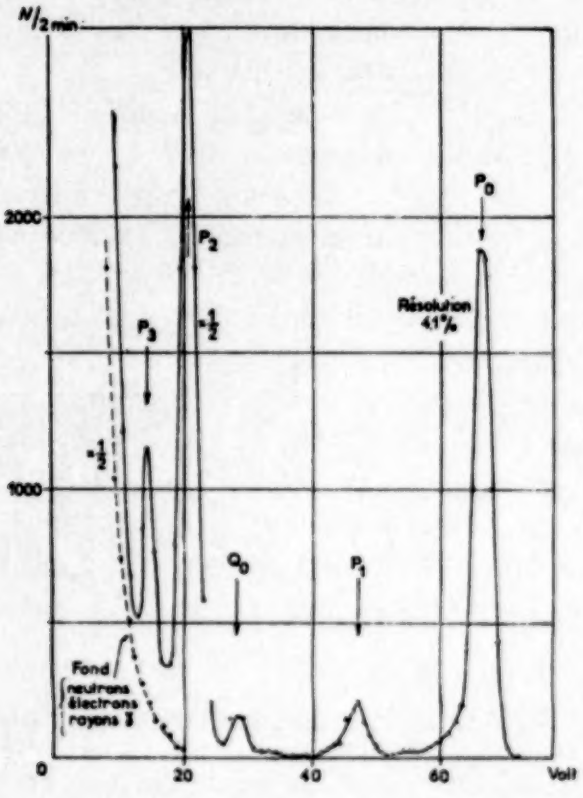

Fig. 1. Spectrographie des protons de la réaction $^{10}B(d, p)^{11}B$. Détection à 0°. Cristal de 1 mm d'épaisseur. P_0 = protons correspondant au niveau fondamental, P_1 = protons correspondant au niveau de 2.14 MeV, P_2 = protons correspondant au niveau de 4.46 MeV, P_3 = protons correspondant au niveau de 5.03 MeV et Q_0 = protons relatifs au niveau fondamental de $^{27}Al(d, p)^{28}Al$.

La boîte était sous vide et les trous fermés par une feuille de Mylar. Le centrage et la bonne marche de l'appareillage ont été vérifiés en mesurant la distribution des protons allant au niveau fondamental du ^{11}B à une énergie de bombardement de 1.06 MeV, distribution déjà faite par Redman [6]) et Burke *et al.* [1]). Le résultat trouvé était en accord avec les courbes obtenues par ces auteurs.

La mesure des corrélations angulaires $p-\gamma$ et $\gamma-\gamma$ a été faite au moyen d'un spectromètre à coïncidences du type rapide-lent, analogue à celui que nous avons utilisé dans des travaux antérieurs [2]). Le temps de résolution τ du circuit rapide était de 5×10^{-9} sec.

Pour les corrélations $p-\gamma$ nous avons utilisé un tube porte-cibles en alu-

minium de 0.2 mm d'épaisseur, le compteur proton a été fixé à $\theta_p = 20°$. L'angle sous-tendu par le scintillateur plastique était de 12°. Avec cette ouverture angulaire, l'angle de 20° englobait toujours, pour les niveaux de 4.46 MeV et 5.03 MeV, les maxima des courbes de distributions. Le taux de coïncidences fortuites était d'environ 10 % du taux de coïncidences totales. Nous avons chiffré les coïncidences parasites n—γ de la réaction ^{10}B(d, n)^{11}C, γ—γ des réactions ^{10}B(d, p)^{11}B et ^{10}B(d, n)^{11}C ainsi que celles dues au rayonnement cosmique et aux rayonnements induits par les neutrons dans la salle de mesure. L'ensemble de ces coïncidences parasites n'excédait jamais 5 %; nous en avons tenu compte dans les calculs.

Les distributions angulaires des protons relatifs aux niveaux de 6.76 et 7.30 MeV à $E_d = 1.25$ MeV n'ont pu être entreprises en spectrographie directe: en effet, au spectre des protons étudiés se superpose le spectre des particules α de la réaction ^{10}B(d, α)^{8}Be, le fond de neutrons et d'électrons de la réaction ^{10}B(d, n) et le spectre des protons de la réaction ^{12}C(d, p)^{13}C — dû au dépôt inévitable de carbone s'accumulant sur la cible. Nous les avons donc mesurées à l'aide de coïncidences p—γ [3, 4]).

Dans tout ce qui suit, nous appelerons P_0 le groupe des protons relatifs au niveau fondamental de ^{11}B, et P_1, P_2, P_3, P_4, P_5, P_6 les groupes de protons correspondant respectivement aux niveaux de 2.14, 4.46, 5.03, 6.76, 6.81 et 7.30 MeV du ^{11}B. L'intensité du groupe P_5 est faible vis-à-vis de celle du groupe P_4 à 0.8 MeV et 1.5 MeV [7, 5]). D'une façon générale quand nous parlerons du groupe P_4, il s'agira, sauf mention spéciale, de la somme des deux groupes P_4 et P_5.

3. Distributions Angulaires des Protons

Des mesures ont été faites par de nombreux auteurs [6–13]). Pour tous les niveaux, la contribution du stripping est assez faible à basse énergie de bombar-

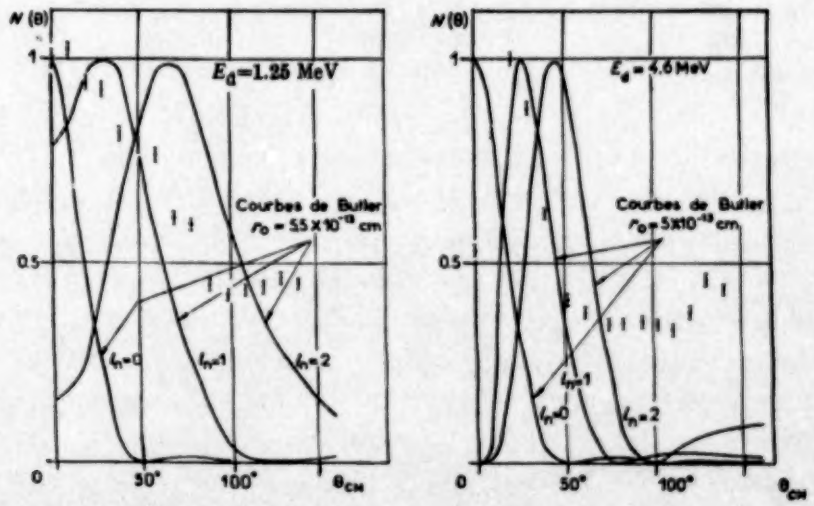

Fig. 2. Distribution angulaire des protons relatifs au niveau de 4.46 MeV.

dement; les mesures à plus haute énergie indiquent que $l_n = 1$ pour les quatre premiers niveaux. Selon Sjögren [7]) on aurait à $E_d = 0.8$ MeV, $l_n = 2$ pour le groupe P_5 et $l_n = 3$ pour le groupe P_6. Les résultats de nos mesures sont

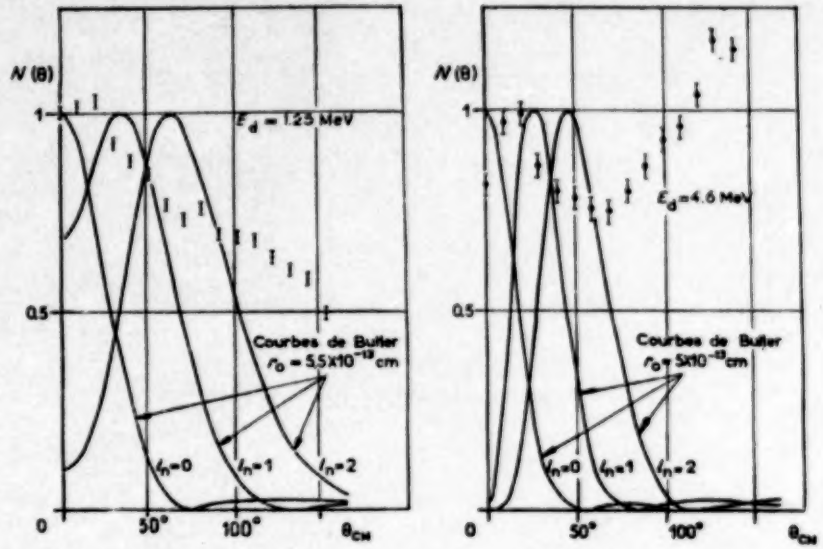

Fig. 3. Distribution angulaire des protons relatifs au niveau de 5.03 MeV.

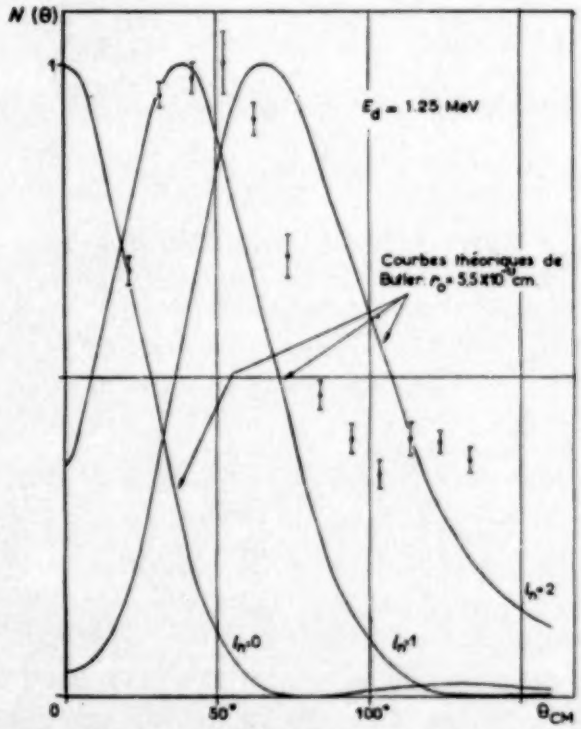

Fig. 4. Distribution angulaire des protons relatifs au niveau de 6.76 MeV (distribution expérimentale par coïncidences p−γ).

indiqués sur les figs. 2, 3, 4 et 5; ils confirment les conclusions précédentes jusqu'au groupe P_4. Pour le groupe P_6 par contre, malgré notre faible énergie de bombardement et la valeur faible du bilan Q de la réaction, le pic à 40° est assez

net pour que l'on puisse attribuer la valeur $l_n = 1$ au moment angulaire orbital du neutron capturé. La remontée aux grands angles pourrait être attribuée à une contribution du "heavy particle stripping" [14]), de même d'ailleurs que celle de la distribution du groupe P_3 à $E_d = 4.6$ MeV.

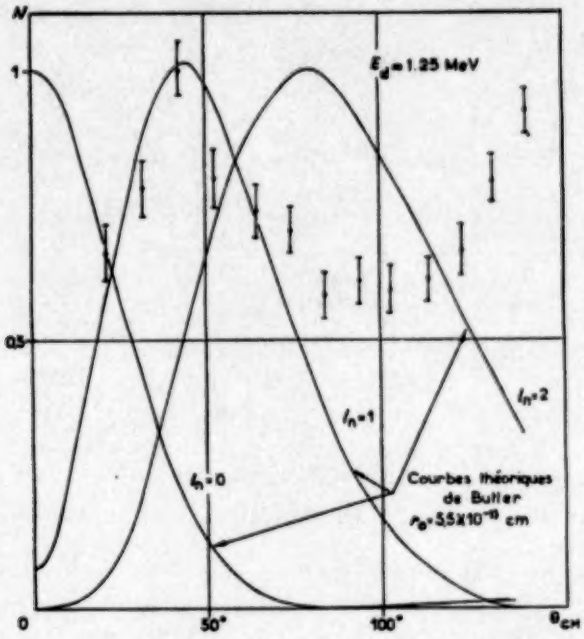

Fig. 5. Distribution angulaire des protons relatifs au niveau de 7.30 MeV (distribution expérimentale par coïncidences p$-\gamma$).

4. Corrélations Angulaires p—γ

Les corrélations angulaires dans le plan d—p mesurée par Cox et Williamson [11]) pour le niveau de 4.46 MeV à des énergies de bombardement comprises entre 2.5 et 3.9 MeV sont toutes isotropes. (A $E_d = 3.9$ MeV, le résultat est connu à 5 % près).

Nous avons mesuré les corrélations a) dans le plan d—p, b) dans un plan perpendiculaire à la direction de recul du noyau. Pour les niveaux de 6.76 MeV et 7.30 MeV, les corrélations à $E_d = 1.25$ MeV ont été trouvées isotropes à ± 7 % près. Ce résultat justifie partiellement à cette énergie la mesure des distributions des groupes P_4 et P_6 par la méthode de coïncidences [3, 4]). D'autre part, pour ces dernières, vu le grand angle solide sous-tendu par le compteur γ (mais évidemment inférieur à 2π) les corrections, s'il y a lieu, devraient être assez faibles. Pour le niveau de 4.46 MeV, les corrélations autour du noyau de recul sont isotropes à $E_d = 1.25$ MeV et 4.6 MeV. La corrélation dans le plan d—p à 1.25 MeV est isotrope. A $E_d = 4.6$ MeV, la courbe trouveé est de la forme

$$W(\theta) = 1 + (0.08 \pm 0.02) P_2(\cos\theta).$$

5. Corrélations Angulaires γ—γ

Dans la réaction ^{10}B(d, p)^{11}B les deux niveaux de 9.19 et 9.28 MeV du ^{11}B sont atteints par capture du neutron avec $l_n = 0$ [5, 17]). A l'énergie de bombardement $E_d = 1.25$ MeV, nous avons mis en évidence des coïncidences γ—γ entre deux photons d'énergie comprise entre 4.5 et 4.7 MeV. Par la suite nous avons mesuré la somme de corrélations angulaires γ—γ correspondant aux cascades

$$9.19 \text{ MeV} \rightarrow 4.46 \text{ MeV} \rightarrow 0,$$
$$9.28 \text{ MeV} \rightarrow 4.46 \text{ MeV} \rightarrow 0.$$

Le moment angulaire du niveau de 9.28 MeV est $J = \frac{5}{2}^+$ et celui de 9.19 MeV est probablement [15, 16]) $J = \frac{7}{2}^+$. La mesure des corrélations angulaires doit confirmer ou infirmer la valeur $l_n = 0$ (selon qu'elles sont toutes identiques ou non), et permettre de préciser le spin du niveau de 4.46 MeV.

Nous avons mesuré les trois corrélations suivantes dans deux plans différents:

a) $\varphi_A = 0$, $\varphi_B = 0$,
$\theta_A = 0$, $\theta_B = \theta$ (variable);
b) $\varphi_A = 0$, $\varphi_B = 0$,
$\theta_A = \frac{1}{2}\pi$, $\theta_B = \theta$ (variable);
c) $\varphi_A = 0$, $\varphi_B = \varphi$ (variable),
$\theta_A = \frac{1}{2}\pi$, $\theta_B = \frac{1}{2}\pi$.

(Les angles φ_A et θ_A déterminent la position du compteur fixe A relativement à la direction des deutérons incidents, et les angles φ_B et θ_B déterminent celle du compteur mobile B.)

Comme il était impossible d'éliminer toutes les autres cascades [3]), nous avons discriminé les impulsions des canaux latéraux de façon que l'intensité des coïncidences des cascades parasites ne dépasse pas 3 % de celle des coïncidences dues aux 2 cascades étudiées: les trois corrélations ont été trouvées isotropes à ± 3 % près.

6. Discussion

Comme les trois corrélations γ—γ ont été trouvées identiques on pourrait dire que les populations des sous-niveaux des niveaux de 9.19 et 9.28 MeV sont égales. Cela pourrait signifier que ces niveaux sont formés, soit:

a) essentiellement par stripping avec $l_n = 0$: l'hypothèse de Wilkinson [18]), selon laquelle la formation d'un niveau peut avoir lieu par stripping si l'énergie des deutérons est faible ($E_d \leqq 2$ MeV) et si le bilan de la réaction pour ce niveau est également faible ($-1 \leqq Q \leqq +1$ MeV), est alors vérifiée;

b) par formation de noyau composé: dans ce cas de nombreux niveaux rapprochés sont atteints, ce qui contrebalance ou atténue les effets dues aux différences de population des différents niveaux.

Cependant le raisonnement précédent n'est pas entièrement satisfaisant; on ne pourrait conclure comme il a été fait en (a) et (b) que si les coefficients de $P_2(\cos\theta)$ identiques dans les trois corrélations, étaient différents de zéro. En effet, le niveau de 4.46 MeV ayant un moment angulaire différent de $\frac{1}{2}$, les propriétés (spin et parité) des niveaux de 9.19 et 9.28 MeV interviennent dans le calcul des corrélations, mais ne sont généralement pas la cause directe d'une isotropie.

Dans les calculs, nous avons pris comme intensités des deux cascades celles trouvées à $E_d = 1.5$ MeV par Van Patter *et al.* [5]):

cascade $9.19 \rightarrow 4.46 \rightarrow 0$, intensité 8,

cascade $9.28 \rightarrow 4.46 \rightarrow 0$, intensité 4.

Le moment angulaire du niveau de 4.46 MeV peut alors être déduit des corrélations $\gamma-\gamma$ et p$-\gamma$.

Comme l'ont indiqué Cox et Williamson [11]), l'isotropie des corrélations p$-\gamma$ à énergie très basse peut être due à une atténuation de la corrélation obtenue à une énergie plus élevée. Une explication qualitative [19]) consiste à dire qu'à basse énergie il faut tenir compte de la distorsion des ondes planes du deuteron incident et du proton émergent. On peut donc considérer plusieurs axes de recul correspondant aux différents vecteurs $\mathbf{k}_d$ incidents à des angles très voisins. La corrélation étant rapportée à la direction de recul du noyau final dans la conception semi-classique de Butler, on a affaire à la somme incohérente d'un grand nombre de corrélations, ce qui expliquerait l'atténuation totale. Aussi nous ne considérons que le résultat à $E_d = 4.6$ MeV.

Si l'on admet que l'ordre de multipolarité du rayonnement γ de désexcitation du niveau de 4.46 MeV est unique, aucune valeur pour le moment angulaire de ce niveau ne permet d'interpréter les résultats expérimentaux. Nous sommes donc conduits à envisager le cas d'un mélange M1, E2 d'amplitude δ.

Cas $J = \frac{3}{2}^-$ *pour le niveau de* 4.46 MeV:

La corrélation $\gamma-\gamma$ conduit (fig. 6) à

$$-0.50 < \delta < -0.063,$$

ou à

$$\delta < -5.6 \text{ ou } \delta > +5.2.$$

Pour la corrélation p$-\gamma$, seul le „channel spin" $\frac{5}{2}$ est possible. Dans ce cas on est conduit à (fig. 6)

$$-0.065 < \delta < +0.065 \quad \text{ou} \quad 3.05 < \delta < 5.2.$$

On voit que la seule plage commune possible est

$$-0.065 < \delta < -0.063.$$

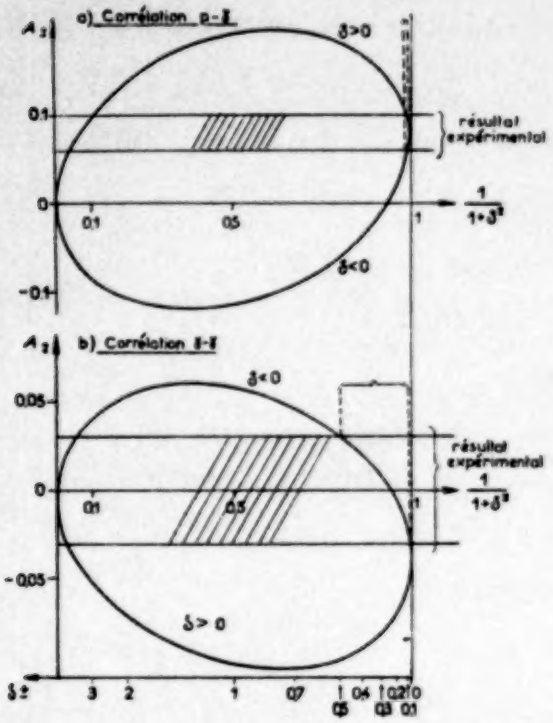

Fig. 6. Variation de A_2 en fonction du coefficient de mélange δ. Cas $J = \frac{3}{2}^-$.

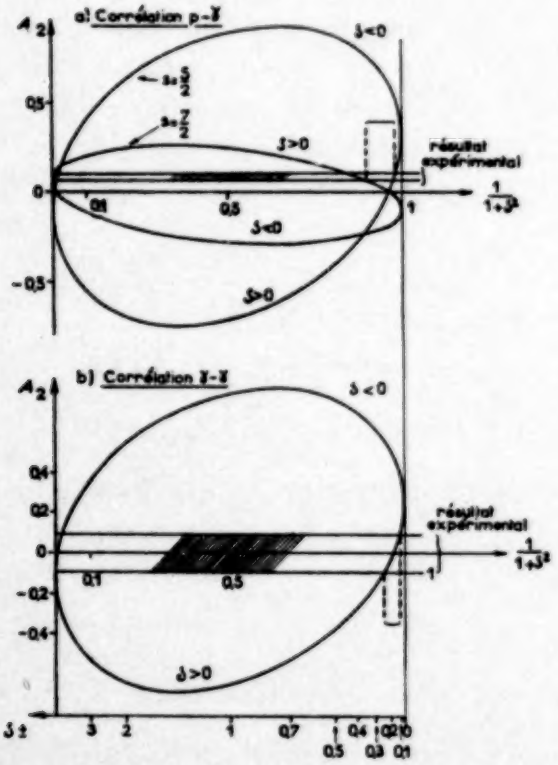

Fig. 7. Variation de A_2 en fonction du coefficient de mélange δ. Cas $J = \frac{5}{2}^-$.

Le résultat est en accord avec celui de Rasmussen *et al.* [20]) qui indiquent

$$-0.66 < \delta < 0.$$

La valeur théorique de δ calculée à partir des données de Kurath [21]) est

$$|\delta| = 0.027.$$

Cas $J = \frac{5}{2}^-$ *pour le niveau de* 4.46 MeV:

La corrélation $\gamma-\gamma$ conduit à

$$0.13 < \delta < 0.26 \quad \text{ou} \quad -29 < \delta < -6.20.$$

Pour la corrélation p$-\gamma$ les deux „channel spins" sont possibles. Dans ces conditions (fig. 7) toutes les valeurs de δ conviennent sauf les plages

$$0.155 < \delta < 0.30 \quad \text{et} \quad \delta < -7.2.$$

Les plages communes sont

$$0.13 < \delta < 0.155 \quad \text{et} \quad -7.2 < \delta < -6.20.$$

Pour ces valeurs négatives de δ, on a une contribution presque pure du quadrupole électrique. Wilkinson [22]) et Rasmussen *et al.* [20]) ont mesuré la vie moyenne de ce niveau ($\tau \approx 1.17 \times 10^{-15}$ sec). Leurs résultats sont incompatibles avec la vie moyenne estimée d'un quadrupole électrique pur pour la désexcitation de ce niveau ($\tau \approx 4 \times 10^{-13}$ sec) calculée à partir de la largeur des niveaux [21]). Les autres valeurs de δ possibles, $0.13 < \delta < 0.155$, sont en accord avec celles de Ferguson *et al.* [20]): $0 < \delta < 0.45$, et avec celle de Jones *et al.* [16]) qui trouvent que l'intensité du E2 est environ 5 % de celle du M1. Ces résultats sont à comparer à ceux que l'on peut trouver à partir des calculs de Kurath:

$$|\delta| = 0.20.$$

Cas $J = \frac{7}{2}^-$ *pour le niveau de* 4.46 MeV:

Les corrélations $\gamma-\gamma$ (avec une cascade E1$-$E2) pour ce cas sont de la forme

$$W(\theta) = 1 + 0.08 \; P_2(\cos\theta).$$

Notre résultat expérimental, (isotropie à ± 3 %) est incompatible avec une telle valeur. La valeur $J = \frac{7}{2}^-$ est donc improbable, d'autant plus que, comme dans le cas précédent, le rayon γ de désexcitation serait un quadrupole électrique pur.

7. Conclusion

Les valeurs les plus probables du spin du niveau de 4.46 MeV sont

$$J = \tfrac{5}{2}^- \quad \text{ou} \quad J = \tfrac{3}{2}^-$$

avec les mélanges indiqués ci-dessus. Les calculs pour ce niveau par le couplage intermédiaire [24]) prévoient $J = \frac{5}{2}^-$ ou $\frac{7}{2}^-$.

Nous tenons à remercier le Centre d'Études Nucléaires de Saclay qui a mis obligeamment à notre disposition l'accélérateur Van de Graaff de 5 MeV et nous sommes en particulier très reconnaissants à Monsieur E. Cotton pour l'aide qu'il nous a apportée dans la réalisation de ce travail. Les cibles de ^{10}B nous ont été fournies par les laboratoires de l'AERE à Harwell et du CEA à Saclay.

Bibliographie

1) W. H. Burke, J. R. Risser et G. C. Phillips, Phys. Rev. **93** (1954) 188
2) S. Gorodetzky, A. Gallmann, M. Croissiaux et R. Armbruster, C. R. Acad. des Sciences **241** (1955) 1743
3) M. Croissiaux, Thèse, Strasbourg (Juin, 1959)
4) S. Gorodetzky, M. Croissiaux, A. Gallmann, P. Fintz, J. Samuel et G. Bassompierre, CR. Acad. des Sciences **250** (1960) 3153
5) D. M. van Patter, W. W. Buechner et A. Sperduto, Phys. Rev. **82** (1951) 248
6) W. C. Redman, Phys. Rev. **79** (1950) 6
7) B. Sjögren, Arkiv för Fysik, **11** no. 29 (1956) 383; **12** no. 24 (1957) 537
8) P. M. Endt, C. H. Paris, H. M. Jongerius et F. P. G. Valckx, Physica **18** (1952) 423; C. H. Paris, F. P. G. Valckx et P. M. Endt, Physica **20** (1954) 573
9) W. W. Pratt, Phys. Rev. **93** (1954) 816
10) J. B. Marion et G. Weber, Phys. Rev. **103** (1956) 1408
11) S. A. Cox et R. M. Williamson, Phys. Rev. **105** (1957) 1799
12) N. T. S. Evans et W. C. Parkinson, Proc. Phys. Soc. A **67** (1954) 684
13) J. R. Holt et T. N. Marsham, Proc. Phys. Soc. A **66** (1953) 1032
14) G. E. Owen et L. Madansky, Phys. Rev. **105** (1957) 1766
15) F. Ajzenberg-Selove, T. Lauritsen, Nuclear Physics, **11** (1959) 1
16) G. A. Jones, C. M. P. Johnson et D. H. Wilkinson, Phil. Mag. **4** no. 43 (1959) 796
17) O. M. Bilaniuk et J. C. Hensel, Bull. Amer. Phys. Soc. **3** (1958) 188
18) D. H. Wilkinson, Phil. Mag. **3** (1958) 1185
19) G. R. Satchler, C. R. Cong. Int. Phys. Nucl. (Paris 1958) 112
20) V. K. Rasmussen, F. R. Metzger et C. P. Swann, Phys. Rev. **110** (1958) 154
21) D. Kurath, Phys. Rev. **106** (1957) 975
22) G. A. Jones et D. H. Wilkinson, Phil. Mag. **43** (1952) 958; D. H. Wilkinson, B. N. L. R. 1956, 2907
23) A. J. Ferguson, H. E. Gove, J. A. Kuehner, A. E. Litherland, E. Almqvist et D. A. Bromley, Phys. Rev. Letters **1** (1958) 414
24) D. R. Inglis, Rev. Mod. Phys. **25** (1953) 390; D. Kurath, Phys. Rev. **101** (1956) 216

1.B:2,F

Nuclear Physics **18** (1960) 296—302; © *North-Holland Publishing Co., Amsterdam*

Not to be reproduced by photoprint or microfilm without written permission from the publisher

INVESTIGATION OF THE INTERACTION BETWEEN THE PRODUCTS OF REACTIONS IN WHICH SEVERAL PARTICLES ARE EMITTED

V. V. KOMAROV and A. M. POPOVA

Institute of Nuclear Physics, M. V. Lomonosov Moscow State University, Moscow, USSR

Received 4 April 1960

Abstract: A method is presented for investigation of the effect of the interaction between the products of reactions which involve the emission of several particles on the energy distribution of the latter. The spectra of neutrons emitted at angles of 0° and 180° in the c.m.s. in the p+d → p+p'+n reaction are computed for a total reaction energy of ≈4 MeV, account being taken of pair interaction between nucleons in the final state. Some possible applications of the method are discussed.

The problem of the effect of the interaction of particles produced in nuclear reactions on the shape of their energy and angular distributions was first studied by Migdal [1]) in 1950 and subsequently by several other authors [2, 3]).

Later on it was shown that when several particles are emitted, due to the interaction of the reaction products peaks appear in the energy distributions whose shape and magnitude are dependent on the direction of emission of the particles [4]). Peaks of this type have been observed in the spectra of p+d → p+p'+n neutrons emitted at angles of 0° [5, 6]) (fig. 1) and 180° [6]) (fig. 2) with respect to the direction of the incident protons, the total energy of the reaction being ≈ 4 MeV. The spectrum of neutrons emitted at an angle of 0° in this reaction has been calculated in ref. [7]). Interaction between two protons in the final state was taken into account in the zero-range approximation and the Born approximation was employed to account for the interaction of the neutron with the two mutually scattered protons. From fig. 1 it can be seen that the theoretical and experimental curves agree only in the region of the peak near the upper boundary of the neutron spectrum at 0°. No agreement is obtained with the remaining part of the spectrum as there is no maximum in the computed curve in the neighbourhood of 0.6 MeV. It seems natural to assume that this peak can be explained by interaction between the neutron and proton in the final state.

In the present work, investigation of the spectrum of neutrons emitted in the p+d reaction at 0° and 180° was performed by taking into account interaction of each pair of nucleons with small relative momentum. The neutron energy distributions were computed by a method similar to that employed in refs. [4, 8]).

Interaction between nucleons with small relative momenta were taken into account exactly. The interaction parameters were derived from experimental data on nucleon-nucleon scattering. Interaction of a pair of particles with the third nucleon was treated in the Born approximation. Strictly speaking, application of the Born approximation at such low energies does not seem to be legitimate. Nevertheless, this approximation has been successfully applied in this energy region to explain the angular and energy distributions in stripping

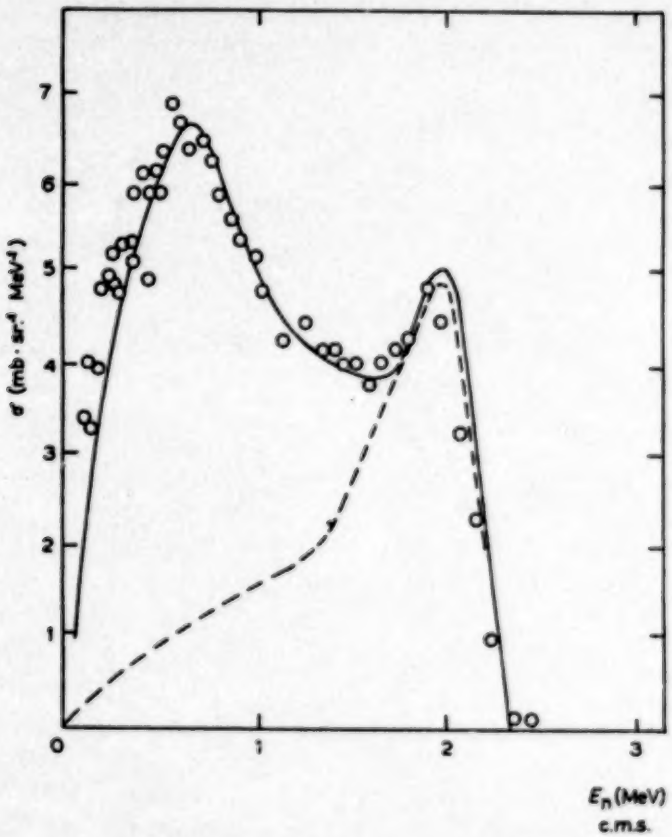

Fig. 1. Spectrum of neutrons formed in the c.m.s. at an angle of 0° in the reaction p+d → p+p'+n. Incident proton energy is 8.9 MeV. Points represent experimental data from ref. [8]). The full curve is calculated in the present paper, the dotted curve in ref. [8]).

reactions [9]) which are closely related to the process under consideration. It therefore seems natural to expect that in our case application of the Born approximation to the interaction between a pair of low relative momentum particles and a third particle should yield angular and energy distributions which closely resemble the true ones.

In order to take into account simultaneously the interaction of all particle pairs with a low relative momentum, the wave function $\psi(t)$ must obey the Schroedinger equation

$$i\hbar \frac{\partial \psi}{\partial t} = (T+V_{12}+V_{23}+V_{31}+\alpha_{12}v_{12}+\alpha_{23}v_{23}+\alpha_{31}v_{31})\psi(t), \quad (1)$$

where v_{ij} is the interaction between particles in the final state, subscripts 1 and 2 refer to the deuteron's proton and neutron and subscript 3 to the impinging proton. Coefficients α_{ij} are smooth functions of the momenta, such as

$$\alpha_{ij} = 1 \quad \text{for} \quad |\mathbf{p}_i - \mathbf{p}_j| \leqq B,$$
$$\alpha_{ij} = 0 \quad \text{for} \quad |\mathbf{p}_i - \mathbf{p}_j| \gg B.$$

Here, B is the magnitude of the relative momentum of the two particles and

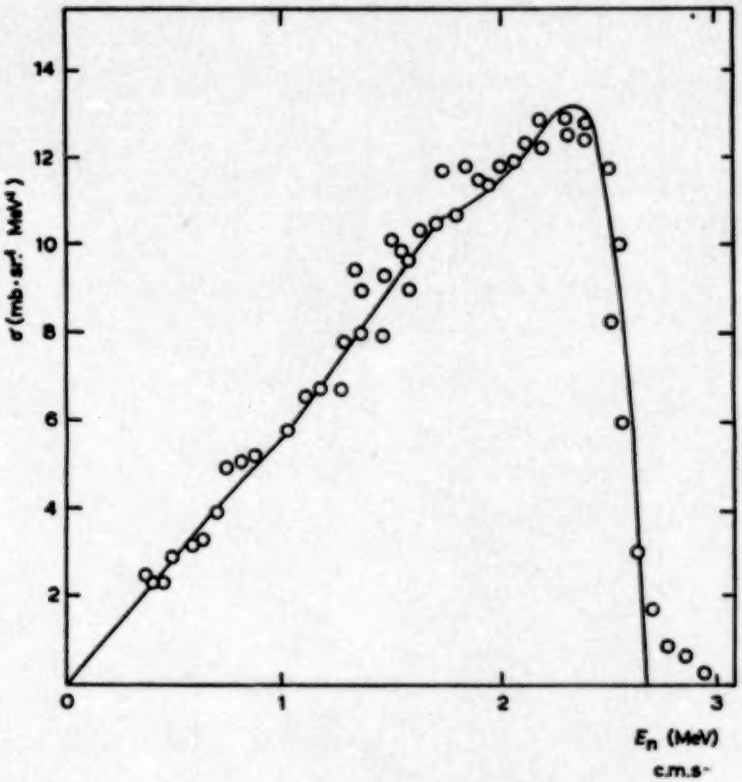

Fig. 2. Spectrum of neutrons formed in the c.m.s. at an angle of 0° in the reaction d+p → p+p'+n. Incident proton energy is 18.6 MeV. Points represent experimental data from ref. [7]). The curve is Calculated in the present paper.

corresponds to the interaction energy of two nucleons in the singlet or triplet states.

Coefficients α_{ij} can most conveniently be chosen in the form

$$\alpha_{ij} = \exp[-a^2(|\mathbf{p}_i - \mathbf{p}_j|)^2]. \tag{2}$$

Evidently if the relative momentum of two nucleons appreciably exceeds B the interaction between them can be neglected. Then the whole energy range of neutrons produced in the p+d reaction can be divided into three regions:

(a) that in which interaction between protons in the final state is important

(the relative momentum of two protons in the final state is of the order of B),

$$\alpha_{31} = 1, \qquad \alpha_{12} = \alpha_{23} = 0;$$

(b) that in which interaction between the neutron and proton in the final state is important (the relative proton-neutron momentum is of the order of B),

$$\alpha_{12} = 1, \quad \alpha_{23} = \alpha_{31} = 0 \quad \text{or} \quad \alpha_{23} = 1, \quad \alpha_{12} = \alpha_{31} = 0;$$

(c) that in which there is no pair interaction between nucleons in the final state (the relative momentum of any pair of nucleons significantly differs from B),

$$\alpha_{12} = \alpha_{23} = \alpha_{31} = 0.$$

In the Born approximation with distorted waves the transition matrix element in which account is taken of each pair of nucleons in the final state will have the form

$$H \approx \langle \psi_{123}\chi_{123} A[V_{23}+V_{31}]\psi_{12}\chi_{12}\psi_3\chi_3\rangle, \tag{3}$$

where ψ_{123} is the wave function of the final state of the system and is defined for each neutron energy region ((a), (b) or (c)) depending on the magnitude of the relative momentum between the nucleons.

In order to take into account exchange interactions between the incident nucleon and deuteron nucleons the function of the initial state of the system should be antisymmetrized. For region (a) expression (3) transforms into the integrals

$$\begin{aligned} I_{pp}^{(1)} &= \int \varphi_{2p}(\varrho)\chi_{2p}\varphi(\mathbf{r}_n)\chi_n V_{np}\psi_d\chi_d\psi(\mathbf{r}_p)\chi_p d\tau, \\ I_{pp}^{(2)} &= \int \varphi_{2p}(\varrho)\chi_{2p}\varphi(\mathbf{r}_n)\chi_n V_{pp}\psi_d\chi_d\psi(\mathbf{r}_p)\chi_p d\tau, \end{aligned} \tag{4}$$

where ψ_d is the intrinsic deuteron wave function expressed in the form of a Hulthén function; $\psi(\mathbf{r}_p)$ and $\varphi(\mathbf{r}_n)$ are wave functions of the incident proton and emitted neutron expressed in the form of plane waves; χ_d and χ_p are spin functions of the deuteron and incident proton, χ_{2p} and χ_n are spin functions of the two singlet state protons and the neutron; $\varphi_{2p}(\varrho)$ is the relative motion wave function of the two protons, chosen in such a way as to account for mutual scattering of the protons in the singlet state. If nuclear interaction between the two protons is chosen in the form of a potential well with $\rho_0 = 2.65\times 10^{-13}$ cm, the radial part of wave function $\varphi_{2p}(\varrho)$ will, for $\rho < \rho_0$, have the form $\varphi_{2p}^{(1)}(\rho) = A \sin k\rho/\rho$, where $\mathbf{k}$ is the wave vector of relative motion of the two protons inside the potential well. For $\rho > \rho_0$ Coulomb interaction between the two protons was taken into account and $\varphi_{2p}^{(2)}(\rho) = G(f\rho)+\cot\delta F(f\rho)$, where $G(f\rho)$ and $F(f\rho)$ are the Coulomb functions and $\cot\delta$ is a factor which takes into account nuclear interaction. The quantities A and $k = |\mathbf{k}|$ are defined by the

joining condition on the logarithmic derivatives and functions $\varphi_{2p}^{(1)}(\rho)$ and $\varphi_{2p}^{(2)}(\rho)$ for $\rho = \rho_0$. Variation of the ρ_0 parameter between the values $\rho_0 = 2.4\times10^{-13}$ cm and $\rho_0 = 2.8\times10^{-13}$ cm derived from proton-proton scattering experiments did not significantly affect the magnitude and shape of the differential cross section of the reaction. In formula (4), V_{np} and V_{pp} refer to the interaction between the incident proton and deuteron nucleons. The quantity V_{pn} was chosen in the form of a δ-interaction. The V_{pp} was chosen in the form of a potential well with a range of $\rho_0 = 2.65\times10^{-13}$ cm. It is not possible to choose V_{pp} in the form of a δ-interaction in the given case as $\varphi_{2p}(\varrho)$ depends on the same parameter ρ. Since in the present treatment only S waves are encountered, the choice of the form of interactions V_{pn} and V_{pp} is not important, these interactions being defined by a single parameter, the scattering length.

For region (b) expression (3) transforms into the integrals

$$I_{pn}^{(1)} = \int \varphi_{pn}(\varrho)\chi_{pn}\varphi(\mathbf{r}_p)\chi_p V_{pp}\psi_d\chi_d\psi(\mathbf{r}_p)\chi_p d\tau,$$
$$I_{pn}^{(2)} = \int \varphi_{pn}(\varrho)\chi_{pn}\varphi(\mathbf{r}_p)\chi_p V_{pn}\psi_d\chi_d\psi(\mathbf{r}_p)\chi_p d\tau, \tag{5}$$

where $\varphi_{pn}(\varrho)$ is the wave function for the relative motion of the proton and neutron and takes into account their scattering in the singlet or triplet states. When the proton-neutron interaction is chosen in the form of a potential well with $\rho_0 = 2.65\times10^{-13}$ cm, the radial part $\varphi_{pn}(\varrho)$ assumes for $\rho < \rho_0$ the form $\varphi_{pn}^{(1)}(\rho) = A' \sin k'\rho/\rho$ and for $\rho < \rho_0$ it assumes the form $\varphi_{pn}^{(2)}(\rho) = i\sqrt{\pi}[e^{-ik\rho} - e^{ik\rho}]/k\rho + 4\pi f(\theta)e^{-ik\rho}/\rho$, where $f(\theta)$ is the scattering amplitude of a proton on a neutron in the singlet or triplet state [8]). The quantities A' and k' are determined from the joining condition on the logarithmic derivatives and functions $\varphi_{pn}^{(1)}(\rho)$ and $\varphi_{pn}^{(2)}(\rho)$ for $\rho = \rho_0$. In the integrals $I_{pn}^{(1)}$ and $I_{pn}^{(2)}$, the potential V_{pp} was chosen in the form of a δ-interaction; V_{pn} was also chosen in either as a δ-interaction, if the incident proton did not enter $\varphi_{pn}(\varrho)$ or as a potential well width $\rho_0 = 2.65\times10^{-13}$ cm if the incident proton entered $\varphi_{pn}(\varrho)$.

In region (c) the integrals I_{pp} and I_{pn} become equal, since for $|\mathbf{p}_i - \mathbf{p}_j| \gg B$ distortion of the nucleon wave functions due to mutual scattering will be very small.

Account of the S state of the relative motion of the particles should be sufficient if the total energy of the p+d reaction is of the order of 4 MeV and then the total angular momentum should be either $\frac{1}{2}$ or $\frac{3}{2}$. In this case the differential cross section for disintegration of deuterons by protons should be given by the expression

$$\frac{d\sigma}{dE_n d\Omega_n} = \frac{M_n M_0}{(2\pi\hbar)^2}\frac{\rho(E_n)}{k_0}\{\tfrac{2}{3}|H_1|^2 + \tfrac{1}{3}|H_2|^2 + \tfrac{1}{3}|H_3|^2\}, \tag{6}$$

where M_0 and M_n are the reduced masses of the incident proton and the neutron

produced in the reaction, $\rho(E_n)$ is the neutron energy state density, H_1, H_2 and H_3 are transition matrix elements corresponding to total angular momentum I and spin respectively $(\frac{3}{2}, 1)$. $(\frac{1}{2}, 1)$, $(\frac{1}{2}, 0)$ of a nucleon pair possessing small relative momentum.

Since in the case under consideration the spin state of two interacting protons can only be singlet and the spin state of the interaction proton and neutron either singlet or triplet, integrals I^t_{pn} which correspond to triplet interaction between the proton and neutron enter into the matrix elements H_1 and H_2, ehereas integrals I^s_{pn} and I^s_{pn} which correspond to interaction of nucleons in the singlet state will be included in H_3.

Calculations show that $I^t_{pn} \ll I^s_{pn}$ and hence the differential cross section for the reaction should be determined by the square of matrix element H_3.

The energy spectra of neutrons emitted in the reaction $p+d \rightarrow p+p'+n$ at angles of 0° or 180° with respect to the direction of the incident protons calculated in the present paper for total reaction energies of 3.5 MeV are shown respectively in figs. 1 and 2. The calculated spectrum of neutrons emitted at 0° possesses two maxima, just as the experimental curve does. As the calculations show, the position and shape of the peaks for a neutron energy of 0.7 MeV is determined by final state interaction between the neutron and proton with small relative momentum. The peak in the neutron sepectrum near the upper boundary is due to interaction between two protons with small relative momentum. The magnitude of the cross section for the p+d reaction in the region of the maximum near $E_n \approx 0.7$ MeV is larger than the cross section in the region of the peak near the upper boundary of the neutron spectrum. This can be explained by the larger probability for stripping of a neutron from a deuteron by the impinging proton and their emission in the forward direction.

Calculations show that the spectrum of neutrons emitted at an angle of 180° with respect to the direction of the incident protons is mainly determined by interaction between protons possessing small relative momenta. This corresponds to the most probable process of stripping ot the proton by the incident proton in which the particles are emitted forward and the neutron backward.

The ratio of the areas under the experimental points is $(d\sigma/d\Omega)_{180°}/(d\sigma/d\Omega)_{0°} = 1.8 \pm 0.5$ whereas the ratio of the areas under the corresponding theoretical curves is 1.75 This fact indicates that the angular distribution of products of reactions involving the emission of several praticles can be described by employing the method of calculation discussed here.

Due to isobaric invariance it could be expected that in the spectrum of neutrons emitted at an angle of 0° with respect to the direction of the incident neutron in the c.m.s. in the $n+p \rightarrow n+n'+p$ reaction there will be two peaks if the primary energy is 10 MeV just as in the corresponding neutron spectrum for the $p+d \rightarrow p+p'+n$ reaction. The first peak at a proton energy of about 0.7 MeV should correspond to interaction between the proton and neutron,

providing their relative momentum is small, whereas the second peak near the upper boundary of the spectrum should correspond to interaction between two neutrons of low relative momentum. However, of great interest is the experimental investigation of the proton spectrum at 0° for the reaction $n+d \rightarrow n+n'+p$ since theoretical treatment by the method presented above permits one to determine the scattering length for neutrons on neutrons.

The method described in the present paper and in refs. [4, 8, 10]) can be employed to analyze the spectra of the products of reactions d+d, d+t, d+α, t+t and other similar reactions with the aim of ascertaining the role of the interaction between these reaction products and the possibility of existence of excited states of some light nuclei such as He^4, He^5, Li^5 which exhibit themselves as a resonance interaction in the final state of the products of a number of reactions involving the emission of several particles.

In conclusion the authors express their appreciation for discussion of this investigation to S. S. Vasiliev, A. S. Davydov and Yu. M. Shirokov and also to N. A. Vlasov and B. V. Rybakov for interest in our work and numerous discussions.

References

1) A. B. Migdal, JETP **28** (1955) 3
2) K. Brueckner, Phys. Rev. **82** (1951) 592
3) K. M. Watson, Phys. Rev. **88** (1952) 1163
4) V. V. Komarov and A. M. Popova, JETP **38** (1960) 253
5) M. P. Nakada, I. D. Anderson, C. C. Gardner, I. McClure and C. Wong, Phys. Rev. **110** (1958) 594
6) N. A. Vlasov, S. P. Kalinin, B. V. Rybakov and V. A. Sidorov, Reports at the International Conference on Nuclear Physics, Paris, 1958
7) W. Heckrotte and M. McGregor, Phys. Rev. **111** (1958) 593
8) V. V. Komarov and A. M. Popova, JETP **36** (1959) 1574
9) A. G. Sitenko, Uspekhi Fiz. Nauk. **67** (1958) 577
10) V. V. Komarov and A. M. Popova, JETP **38** (1960) 1559

1.B

Nuclear Physics **18** (1960) 303—399; © *North-Holland Publishing Co., Amsterdam*

Not to be reproduced by photoprint or microfilm without written permission from the publisher

ON THE CHOICE OF D-STATE WAVE FUNCTIONS IN TRITON CALCULATIONS

G. H. DERRICK †

Institute for Advanced Study, Princeton, New Jersey

Received 16 May 1960

Abstract: A set of D-state wave functions with the correct asymptotic properties is suggested for use in variation calculations of the triton energy. The matrix elements of the kinetic and potential energy operators are evaluated for these functions.

1. Introduction

In a previous paper [1]) it was shown that the triton radial wave functions [1, 2]) must have a well defined asymptotic behaviour near the two configurations at which the Euler angles are undefined, viz. (I) the three particles in a straight line (II) the three particles at the vertices of an equilateral triangle. In any variation calculation it is essential that the trial wave function has the correct asymptotic form near these positions. Otherwise the kinetic energy integrals will diverge unless the class of wave functions is restricted unnecessarily.

The conditions on the S-state and P-state functions cause no difficulty. On the other hand it is rather difficult to choose D-state radial wave functions with the correct asymptotic properties. The most straight-forward way is to replace the angular momentum and isobaric spin eigenfunctions [1, 2]) $\mathcal{I}_{8,1}$, $\mathcal{I}_{8,2}$, $\mathcal{I}_{9,1}$, $\mathcal{I}_{9,2}$, $\mathcal{I}_{10,1}$, $\mathcal{I}_{10,2}$ by six linear combinations of these; the multiplying coefficients must be functions of the interparticle distances which vanish whenever the associated $\mathcal{I}$ function becomes discontinuous ††. In this way we obtain six regular D-state eigenfunctions of the total angular momentum and isobaric spin. These functions are then combined with six *regular* radial wave functions to give an antisymmetric total D-state wave function.

In the present paper a suitable set of new D-state wave functions is suggested, and the matrix elements for these new states evaluated.

2. Notation and Definitions

For compactness we define here the functions and operators that will be needed in subsequent sections.

† Now at the Department of Mathematical Physics, University of Manitoba, Winnipeg, Canada.

†† In refs. [1, 2]) these angular momentum and isobaric spin functions were denoted by the symbol $\mathcal{Y}$ instead of $\mathcal{I}$.

r_{23}, r_{31}, r_{12} are the three interparticle distances,

$$R^2 = r_{23}^2+r_{31}^2+r_{12}^2, \quad F = 3^{-\frac{1}{2}}(r_{23}^2+r_{31}^2-2r_{12}^2), \quad G = r_{23}^2-r_{31}^2,$$

Δ = area of triangle

$$= \tfrac{1}{4}[(r_{23}+r_{31}+r_{12})(-r_{23}+r_{31}+r_{12})(r_{23}-r_{31}+r_{12})(r_{23}+r_{31}-r_{12})]^{\frac{1}{2}},$$

$$\cos\lambda = \frac{4\cdot 3^{\frac{1}{2}}\Delta}{R^2} \quad (0 \leqq \lambda \leqq \tfrac{1}{2}\pi),$$

$$\cos\theta_3 = \frac{r_{23}^2+r_{31}^2-r_{12}^2}{2r_{23}r_{31}} \text{ (}\cos\theta_1 \text{ and } \cos\theta_2 \text{ by cyclic symmetry),}$$

$$a = \frac{3^{\frac{1}{2}}}{\sin\lambda}\left(\frac{R^2\cos^2\lambda}{3r_{12}^2}-1\right), \quad b = \frac{G\cot\lambda}{r_{12}^2}, \quad a^2+b^2 = 3,$$

$$N_0 = R^4(\tfrac{1}{3}+\sin^2\lambda), \quad N_1 = \tfrac{4}{3}FR^2, \quad N_2 = \tfrac{4}{3}GR^2, \quad N_3 = \tfrac{4}{3}(G^2-F^2),$$

$$N_4 = \tfrac{8}{3}FG, \quad N_5 = R^4(\tfrac{2}{3}-\tfrac{2}{9}\sin^2\lambda),$$

$$T(f) = T(f)^\dagger \tag{1}$$

$$= -\frac{1}{r_{23}r_{31}r_{12}}\sum_{\text{cyclic}}\frac{\partial}{\partial r_{12}}\left[fr_{23}r_{31}r_{12}\left(2\frac{\partial}{\partial r_{12}}+\cos\theta_2\frac{\partial}{\partial r_{23}}+\cos\theta_1\frac{\partial}{\partial r_{31}}\right)\right]$$

(f is any function of r_{23}, r_{31}, r_{12}, and $\dagger$ denotes the hermitian conjugate),

$$\mathscr{L} = -\mathscr{L}^\dagger = 16.3^{-\frac{1}{2}}\sum_{\text{cyclic}}\frac{r_{23}^2-r_{31}^2}{r_{12}}\frac{\partial}{\partial r_{12}},$$

$$\mathscr{M}_1 = -\mathscr{M}_1{}^\dagger = 12.3^{-\frac{1}{2}}\left[(2G^2-\tfrac{1}{3}R^4\cos^2\lambda)\left(\frac{1}{r_{12}}\frac{\partial}{\partial r_{12}}-\frac{1}{2r_{23}}\frac{\partial}{\partial r_{23}}-\frac{1}{2r_{31}}\frac{\partial}{\partial r_{31}}\right)\right.$$
$$\left.+3^{\frac{1}{2}}FG\left(\frac{1}{r_{23}}\frac{\partial}{\partial r_{23}}-\frac{1}{r_{31}}\frac{\partial}{\partial r_{31}}\right)\right],$$

$$\mathscr{M}_2 = -\mathscr{M}_2{}^\dagger = -12.3^{-\frac{1}{2}}\left[2FG\left(\frac{1}{r_{12}}\frac{\partial}{\partial r_{12}}-\frac{1}{2r_{23}}\frac{\partial}{\partial r_{23}}-\frac{1}{2r_{31}}\frac{\partial}{\partial r_{31}}\right)\right.$$
$$\left.+\tfrac{1}{2}\cdot 3^{\frac{1}{2}}(2F^2-\tfrac{1}{3}R^4\cos^2\lambda)\left(\frac{1}{r_{23}}\frac{\partial}{\partial r_{23}}-\frac{1}{r_{31}}\frac{\partial}{\partial r_{31}}\right)\right]$$

$$D = \frac{R^4\cos^2\lambda}{36}\left(\frac{1}{r_{23}}\frac{\partial}{\partial r_{23}}-\frac{1}{r_{31}}\frac{\partial}{\partial r_{31}}\right), \quad D^\dagger = -D+\tfrac{2}{3}G.$$

3. The New D-State Wave Functions

Let us replace the angular momentum and isobaric spin functions $\mathcal{S}_8, \mathcal{S}_9, \mathcal{S}_{10}$ by the following set:

$$\begin{aligned}
\mathcal{S}_{11,1} &= R^2(3^{-\frac{1}{2}}\mathcal{S}_{8,1}-\sin\lambda\mathcal{S}_{9,1}), \quad \mathcal{S}_{11,2} = R^2(3^{-\frac{1}{2}}\mathcal{S}_{8,2}-\sin\lambda\mathcal{S}_{9,2}),\\
\mathcal{S}_{12} &= F(3^{-\frac{1}{2}}\mathcal{S}_{8,1}-\operatorname{cosec}\lambda\,\mathcal{S}_{9,1}-\cot\lambda\mathcal{S}_{10,1})\\
&\qquad +G(3^{-\frac{1}{2}}\mathcal{S}_{8,2}-\operatorname{cosec}\lambda\mathcal{S}_{9,2}-\cot\lambda\mathcal{S}_{10,2},\\
\mathcal{S}_{13} &= -G(3^{-\frac{1}{2}}\mathcal{S}_{8,1}-\operatorname{cosec}\lambda\mathcal{S}_{9,1}-\cot\lambda\mathcal{S}_{10,1})\\
&\qquad +F(3^{-\frac{1}{2}}\mathcal{S}_{8,2}-\operatorname{cosec}\lambda\,\mathcal{S}_{9,2}-\cot\lambda\,\mathcal{S}_{10,2}), \qquad (2)\\
\mathcal{S}_{14,1} &= F(3^{-\frac{1}{2}}\mathcal{S}_{8,1}-\operatorname{cosec}\lambda\mathcal{S}_{9,1}+\cot\lambda\mathcal{S}_{10,1})\\
&\qquad -G(3^{-\frac{1}{2}}\mathcal{S}_{8,2}-\operatorname{cosec}\lambda\mathcal{S}_{9,2}+\cot\lambda\mathcal{S}_{10,2}),\\
\mathcal{S}_{14,2} &= -G(3^{-\frac{1}{2}}\mathcal{S}_{8,1}-\operatorname{cosec}\lambda\mathcal{S}_{9,1}+\cot\lambda\mathcal{S}_{10,1})\\
&\qquad -F(3^{-\frac{1}{2}}\mathcal{S}_{8,2}-\operatorname{cosec}\lambda\mathcal{S}_{9,2}+\cot\lambda\mathcal{S}_{10,2}).
\end{aligned}$$

Under permutations of particles the two components of $\mathcal{S}_{11}$ and of $\mathcal{S}_{14}$ belong to the mixed representation, $\mathcal{S}_{12}$ is symmetric, and $\mathcal{S}_{13}$ complectely antisymmetric.

The six functions (2) are regular everywhere, and are all solutions of the equation

$$(\nabla_1^2+\nabla_2^2+\nabla_3^2)\mathcal{S} = 0.$$

This can be seen readily from the Cartesian forms of these functions. From the three second rank tensors $\mathbf{r}_{23}\mathbf{r}_{23}$, $\mathbf{r}_{31}\mathbf{r}_{31}$, $\mathbf{r}_{12}\mathbf{r}_{12}$ we can form three independent tensors of definite permutation symmetry:

$$\mathbf{S} = \mathbf{r}_{23}\mathbf{r}_{23}+\mathbf{r}_{31}\mathbf{r}_{31}+\mathbf{r}_{12}\mathbf{r}_{12},$$

$$\mathbf{M}_1 = 3^{-\frac{1}{2}}(\mathbf{r}_{23}\mathbf{r}_{23}+\mathbf{r}_{31}\mathbf{r}_{31}-2\mathbf{r}_{12}\mathbf{r}_{12}), \quad \mathbf{M}_2 = \mathbf{r}_{23}\mathbf{r}_{23}-\mathbf{r}_{31}\mathbf{r}_{31}.$$

On forming products of these three tensors with the mixed symmetry quartet functions of the spin and isobaric spin [2], $V_1 = V_1(m, \frac{1}{2}, \frac{3}{2})$ and $V_2 = V_2(m, \frac{1}{2}, \frac{3}{2})$, we obtain six linearly independent combinations:

(mixed)	$V_1\mathbf{S}, \quad V_2\mathbf{S},$
(symmetric)	$V_2\mathbf{M}_2+V_1\mathbf{M}_1,$
(antisymmetric)	$V_1\mathbf{M}_2-V_2\mathbf{M}_1,$
(mixed)	$V_2\mathbf{M}_2-V_1\mathbf{M}_1, \quad V_1\mathbf{M}_2+V_2\mathbf{M}_1.$

The functions (2) are simply the $J = \frac{1}{2}$ reduced parts of the above functions.

The total D-state wave function is obtained by forming an antisymmetric linear combination of products of the six $\mathcal{S}$ functions (2) with six functions f of the radial variables r_{23}, r_{31}, r_{12}:

$$\psi_D = -f_{11,2}\mathcal{S}_{11,1}+f_{11,1}\mathcal{S}_{11,2}+f_{12}\mathcal{S}_{12}+f_{13}\mathcal{S}_{13}-f_{14,2}\mathcal{S}_{14,1}+f_{14,1}\mathcal{S}_{14,2}.$$

Under permutations of particles the two components of f_{11} and of f_{14} belong to the mixed representation, f_{12} is antisymmetric and f_{13} symmetric. In a variation calculation we may choose for $f_{11}, f_{12}, f_{13}, f_{14}$ any functions of correct symmetry which are regular for all values of r_{23}, r_{31}, r_{12} greater than the core radius, where the functions must vanish. As a first approximation we may omit the state $f_{12}\mathscr{S}_{12}$ altogether, since an antisymmetric radial function leads to a very high kinetic energy [2]).

4. Matrix Elements with the New D-States

The conventions used in writing down the matrix elements $(\mathscr{S}_\chi, \mathscr{S}_{\chi'})$ and $(\mathscr{S}_\chi, H\mathscr{S}_{\chi'})$ are the same as in ref. [1]), except here we replace the D-state functions $\mathscr{S}_8, \mathscr{S}_9, \mathscr{S}_{10}$ by the new functions $\mathscr{S}_{11}, \mathscr{S}_{12}, \mathscr{S}_{13}, \mathscr{S}_{14}$. The sixteen functions $\mathscr{S}_\chi$ are taken in the following order: $\mathscr{S}_1, \mathscr{S}_2, \mathscr{S}_{3,1}, \mathscr{S}_{3,2}, \mathscr{S}_4, \mathscr{S}_5, \mathscr{S}_{6,1}, \mathscr{S}_{6,2}, \mathscr{S}_{7,1}, \mathscr{S}_{7,2}, \mathscr{S}_{11,1}, \mathscr{S}_{11,2}, \mathscr{S}_{12}, \mathscr{S}_{13}, \mathscr{S}_{14,1}, \mathscr{S}_{14,2}$. As in ref. [1]) a dot denotes a zero element, and elements corresponding to mixed symmetry states are grouped together into submatrices. Only the lower halves of the D-state to D-state matrices are written — the above diagonal elements are the hermitian conjugates of the elements below the diagonal.

4.1. THE D-STATE NORMALIZATION MATRIX

The new D-states are not orthogonal. The matrix elements $(\mathscr{S}_\chi, \mathscr{S}_{\chi'})$ for these states are given by (see eq. (1))

$$[N_{\chi\chi'}] = \begin{array}{c} \begin{array}{cccccc} 11 & & 12 & 13 & 14 & \end{array} \\ \left[\begin{array}{cccccc} N_0 & & & & & \\ \cdot & N_0 & & & & \\ N_1 & N_2 & N_5 & & & \\ -N_2 & N_1 & \cdot & N_5 & & \\ N_1 & -N_2 & -N_3 & -N_4 & N_5 & \\ -N_2 & -N_1 & -N_4 & N_3 & \cdot & N_5 \end{array}\right] \end{array} \begin{array}{c} 11 \\ \\ 12 \\ 13 \\ \\ 14 \end{array} \tag{3}$$

4.2. THE D-STATE KINETIC ENERGY MATRIX

The matrix elements $(\mathscr{S}_\chi, -(\nabla_1^2+\nabla_2^2+\nabla_3^2)\,\mathscr{S}_{\chi'})$ for the new D-states are given by

$$[T_{\chi\chi'}] = T(N) + \begin{array}{c} \begin{array}{cccccc} 11 & & 12 & 13 & 14 & \end{array} \\ \left[\begin{array}{cccccc} \cdot & & & & & \\ \cdot & \cdot & & & & \\ -\mathscr{M}_1 & -\mathscr{M}_2 & \cdot & & & \\ \mathscr{M}_2 & -\mathscr{M}_1 & -\mathscr{L} & \cdot & & \\ -\mathscr{M}_1 & \mathscr{M}_2 & \cdot & \cdot & \cdot & \\ \mathscr{M}_2 & \mathscr{M}_1 & \cdot & \cdot & -\mathscr{L} & \cdot \end{array}\right] \end{array} \begin{array}{c} 11 \\ \\ 12 \\ 13 \\ \\ 14 \end{array} \tag{4}$$

By $T(N)$ is meant the matrix whose $\chi-\chi'$ element is the hermitian operator $T(N_{\chi\chi'})$ (see eq. (1)), with $N_{\chi\chi'}$ given by (3). Since the differential operators $\mathscr{L}, \mathscr{M}_1, \mathscr{M}_2$ are antihermitian we must change the signs of these operators when writing the upper half of the right-hand matrix of (4).

It is not necessary to compute the full operators $T(N)$, $\mathscr{L}, \mathscr{M}_1, \mathscr{M}_2$ in a variation calculation. Symmetry yields the following equivalent forms:

$$fT(N)g \equiv 3N\left[2\frac{\partial f}{\partial r_{12}}\frac{\partial g}{\partial r_{12}} + \cos\theta_3\left(\frac{\partial f}{\partial r_{23}}\frac{\partial g}{\partial r_{31}} + \frac{\partial g}{\partial r_{23}}\frac{\partial f}{\partial r_{31}}\right)\right],$$

$$\mathscr{L} \equiv 16.3^{-\frac{1}{2}}\frac{G}{r_{12}}\frac{\partial}{\partial r_{12}}, \tag{5}$$

$$\mathscr{M}_1 \equiv 12.3^{-\frac{1}{2}}(2G^2 - \tfrac{1}{3}R^4\cos^2\lambda)\frac{1}{r_{12}}\frac{\partial}{\partial r_{12}}, \quad \mathscr{M}_2 \equiv -24.3^{-\frac{1}{2}}\frac{FG}{r_{12}}\frac{\partial}{\partial r_{12}}.$$

Here f and g are functions of r_{23}, r_{31}, r_{12}; we have omitted a divergence (which leads to a vanishing surface integral) from the first equation of (5). The expressions (5) are *not* identities, and are valid only when applied to radial wave functions of the correct symmetry, with a subsequent integration over all permissible values of r_{23}, r_{31}, r_{12} with the weight factor $r_{23}r_{31}r_{12}$.

4.3. THE POTENTIAL ENERGY MATRIX ELEMENTS

The new D-state functions $\mathscr{I}_{12}, \mathscr{I}_{13}, \mathscr{I}_{14}$ are not eigenfunctions of the Marjorana space-exchange operator P_{12}^{M}. Consequently fewer matrix elements are zero than with the old D-state functions.

The potential energy matrices ($\mathscr{I}_\chi$, $V_{12}\mathscr{I}_{\chi'}$) for the potentials (central-triplet-even), (tensor-even), and ($\mathbf{L}\cdot\mathbf{S}$-even) are each of the following form:

1	2	3	4	5	6	7	11	12	13	14	
.	.	.	.	.	.	.	.	.	.	.	11
s_0	.	.	$-s_0$	.	$-p_0$	p_0	.	$-p_0$	.	.	d_0				11
s_2	.	.	$-s_2$	.	$-p_2$	p_2	.	$-p_2$	.	.	d_2	d_4			12
s_1	.	.	$-s_1$	.	$-p_1$	p_1	.	$-p_1$	.	.	d_1	d_3	d_5		13
$-s_2$	.	.	s_2	.	p_2	$-p_2$	.	p_2	.	.	$-d_2$	$-d_4$	$-d_3^{\dagger}$	d_4	14
$-s_1$	.	.	s_1	.	p_1	$-p_1$	.	p_1	.	.	$-d_1$	$-d_3$	$-d_5$	d_3 d_5	

The matrices for the potentials (central-triplet-odd), (tensor-odd), ($\mathbf{L}\cdot\mathbf{S}$-odd), and for the Coulomb energy of He^3 between particles 1 and 2, are each of the following form

$$
\begin{array}{cccccccccccccc}
1 & 2 & & 3 & & 4 & 5 & 6 & & 7 & 11 & 12 & 13 & 14 & \\
\left[\right. & . & -s_0 & s_0 . & & p_0 & . & . & p_0 & . & p_0 & d_0 & & & \left.\right] & 11 \\
& . & . & . & . & . & . & . & . & . & . & . & & & & \\
& . & -s_1 & s_1 . & & p_1 & . & . & p_1 & . & p_1 & d_1 . & d_5 & & & 12 \\
& . & s_2 & -s_2 . & & -p_2 & . & . & -p_2 & . & -p_2 & -d_2 . & -d_3^\dagger & d_4 & & 13 \\
& . & -s_1 & s_1 . & & p_1 & . & . & p_1 & . & p_1 & d_1 . & d_5 & -d_3 & d_5 & 14 \\
& . & s_2 & -s_2 . & & -p_2 & . & . & -p_2 & . & -p_2 & -d_2 . & -d_3^\dagger & d_4 & -d_3^\dagger \; d_4 & \left.\right]
\end{array}
$$

The quantities s, p, d for the different types of potential operator are given below.

(Central-triplet-even) and (central-triplet-odd):

$$s_0 = s_1 = s_2 = p_0 = p_1 = p_2 = 0,$$

$$d_0 = N_0,\ d_1 = N_1,\ d_2 = N_2,\ d_3 = \tfrac{1}{2}N_4,\ d_4 = \tfrac{1}{2}(N_5+N_3),\ d_5 = \tfrac{1}{2}(N_5-N_3).$$

Coulomb energy of He^3 *for particles* 1 *and* 2:

As for (central-triplet-odd), except that every element is multiplied by the additional factor $2e^2/3r_{12}$.

(Tensor-even) and (tensor-odd):

$$s_0 = R^2(a\sin\lambda - 3^{-\frac{1}{2}}),$$

$$s_1 = F(a\operatorname{cosec}\lambda - 3^{-\frac{1}{2}}) + Gb\cot\lambda,\quad s_2 = G(a\operatorname{cosec}\lambda - 3^{-\frac{1}{2}}) - Fb\cot\lambda,$$

$$p_0 = R^2 b\sin\lambda,\quad p_1 = Fb\operatorname{cosec}\lambda - Ga\cot\lambda,\quad p_2 = Gb\operatorname{cosec}\lambda + Fa\cot\lambda,$$

$$d_0 = R^4[\tfrac{1}{3} + 2.3^{-\frac{1}{2}}\, a\sin\lambda - \sin^2\lambda],$$

$$d_1 = R^2[F\{3^{-\frac{1}{2}}a(\sin\lambda + \operatorname{cosec}\lambda) - \tfrac{2}{3}\} + 3^{-\frac{1}{2}}Gb\cot\lambda],$$

$$d_2 = R^2[G\{3^{-\frac{1}{2}}a(\sin\lambda + \operatorname{cosec}\lambda) - \tfrac{2}{3}\} - 3^{-\frac{1}{2}}Fb\cot\lambda],$$

$$d_3 = 3^{-\frac{1}{2}}[2FG(a\operatorname{cosec}\lambda - 3^{-\frac{1}{2}}) + (G^2 - F^2)b\cot\lambda] = 3^{-\frac{1}{2}}[Gs_1 + Fs_2],$$

$$d_4 = G^2(2.3^{-\frac{1}{2}}a\operatorname{cosec}\lambda + \tfrac{1}{3} - \operatorname{cosec}^2\lambda) - F^2\cot^2\lambda - 2.3^{-\frac{1}{2}}FGb\cot\lambda,$$

$$d_5 = F^2(2.3^{-\frac{1}{2}}a\operatorname{cosec}\lambda + \tfrac{1}{3} - \operatorname{cosec}^2\lambda) - G^2\cot^2\lambda + 2.3^{-\frac{1}{2}}FGb\cot\lambda.$$

(L · S-*even*) *and* **(L · S-*odd*)**:

$$s_0 = s_1 = s_2 = 0,$$

$$p_0 = -\hbar^2 R^2(D - \tfrac{2}{3}G)(R^2\cos\lambda)^{-1},\quad p_0^\dagger = (R^2\cos\lambda)^{-1}\hbar^2 R^2 D,$$

$$p_1 = -\hbar^2 F(D - \tfrac{2}{3}G)(R^2\cos\lambda)^{-1},\quad p_1^\dagger = (R^2\cos\lambda)^{-1}\hbar^2 FD,$$

$$p_2 = \hbar^2[-G(D - \tfrac{2}{3}G) + \tfrac{1}{6}R^4\cos^2\lambda](R^2\cos\lambda)^{-1},$$

$$p_2^\dagger = (R^2\cos\lambda)^{-1}\hbar^2[GD + \tfrac{5}{18}R^4\cos^2\lambda],$$

$$d_1 = \hbar^2\left(3\tfrac{1}{2}GD - 6Fr_{12}^2 + \frac{3\tfrac{1}{2}}{2}R^4\cos^2\lambda\right),$$

$$d_1{}^\dagger = \hbar^2\left(-3\tfrac{1}{2}GD + 2.3\tfrac{1}{2}R^2r_{12}^2 - \frac{3\tfrac{1}{2}}{2}R^4\cos^2\lambda\right),$$

$$d_2 = -\hbar^2(3\tfrac{1}{2}FD + 6Gr_{12}^2), \qquad d_2{}^\dagger = \hbar^2(3\tfrac{1}{2}FD - 2GR^2),$$

$$d_3 = \hbar^2(3\tfrac{1}{2}R^2D - 2FG), \qquad d_3{}^\dagger = \hbar^2(-3\tfrac{1}{2}R^2D + 2.3\tfrac{1}{2}Gr_{12}^2),$$

$$d_4 = -\hbar^2(2G^2 + \tfrac{1}{2}R^4\cos^2\lambda), \qquad d_5 = \hbar^2(2.3\tfrac{1}{2}Fr_{12}^2 - \tfrac{1}{2}R^4\cos^2\lambda).$$

The P-state wave functions will normally include a factor $R^2\cos\lambda$, in order to have the correct asymptotic behaviour as the three particles approach the in-line position. For this reason the factor $(R^2\cos\lambda)^{-1}$ has been written on the right of the differential operator D in the matrix elements p_0, p_1, p_2 of the $\mathbf{L}\cdot\mathbf{S}$ potential.

The author wishes to thank Professor J. R. Oppenheimer for the hospitality extended to him, and for a grant-in-aid, at the Institute for Advanced Study.

References

1) G. H. Derrick, Nuclear Physics, **16** (1960) 405
2) G. H. Derrick, and J. M. Blatt, Nuclear Physics **8** (1958) 310

7.C

Nuclear Physics **18** (1960) 310—317; © *North-Holland Publishing Co., Amsterdam*

Not to be reproduced by photoprint or microfilm without written permission from the publisher

POLARIZABILITY OF NUCLEONS

A. M. BALDIN

P. N. Lebedev Physical Institute, Academy of Sciences, Moscow, USSR

Received 18 December 1959

Abstract: Estimates of dipole polarizabilities of nucleons and the values they involve are given on the basis of data on photo-production of π-mesons and the Compton effect on nucleons. It is indicated that no upper estimate of neutron polarizability exists at present. The preliminary experimental data now available may be interpreted as indicating that a neutron has an abnormally large polarizability. The effects leading to the inapplicability of the impulse approximation for describing the reaction $\gamma+\mathrm{d} \rightarrow \mathrm{p}+\mathrm{n}+\gamma'$ are estimated. It is pointed out that the measurement of the cross section of the reaction $\gamma+\mathrm{d} \rightarrow \mathrm{d}+\gamma'$ would yield an answer for the value of neutron dipole polarizability †.

1. Introduction

As is well known from classical electrodynamics, the interactions of photons with a system of charges may be described by a fairly small number of real parameters provided the wavelength of the photon considerably exceeds the dimensions of the system and the photon's frequency is essentially less than the resonance frequencies of the system. These constants fully determine the behaviour of the system in static or slowly changing fields and are expressed through the charge, the magnetic moment and electric and magnetic polarizability tensors.

These characteristics may in particular be considered for the nucleon [1]). Of especial interest are the electric and magnetic polarizabilities of the nucleon since these are its "structural" characteristics. The aims of the present paper are: a) determination of the frequency region of photons for which the interaction of a nucleon and electromagnetic field may be described by four constants (charge, magnetic moment, electric and magnetic polarizability) with satisfactory accuracy (say, 5 %); b) discussion of possible estimates of the magnitude of the polarizability on the basis of the available experimental data and discussion of the experiments which might be worthwhile for specifying polarizability quantities.

† The main part of this paper was reported at the Padua-Venice Conference, September 1957. It was not included into the Conference Proceedings because of technical difficuities. In view of the recent interest in these estimates (see refs. [5–8])) we decided to publish them together with certain additional considerations about the Compton effect on deuterium and neutron polarizability.

2. Definition of Polarizability

In ref. [1]) it was shown that if the scattering matrix is written as

$$S = -e'_n \hat{g}_{nj} e_j (4\omega\omega')^{\frac{1}{2}}$$

(here and in the following summation over dummy indices n, $j = 1, 2, 3$ is understood; e_n and e'_j are the components of the polarization vectors of the incident and scattered photons, while ω and ω' are their frequencies), the following theorem holds in virtue of gauge invariance:

$$k'_n g_{nj} k_j = \omega'\omega \int \mathrm{d}x\mathrm{d}y \exp[-ik'x] \exp[iky] \mathrm{P}[\hat{\varrho}(x), \hat{\varrho}(y)].$$

Here $k'x$ and ky are scalar products of 4-vectors, k and k' being the 4-vectors of the photon momentum, $\hat{\varrho}(x)$ is the charge density operator, and P Dyson's time ordering operator. For purposes of orientation we may note that for Thomson scattering g_{nj} has the form:

$$\hat{g}^{\mathrm{T}}_{nj} = \delta_{nj} (2\pi)^4 i\delta(\Delta k + \Delta p) \frac{e^2}{M},$$

where the δ-function expresses the law of 4-momentum conservation.

We may now expand the mean value $\langle f|k_n g_{nj} k_j|0\rangle$ into a sum over states, where $|0\rangle$ and $|\mathrm{f}\rangle$ are the unexcited states of the nucleon:

$$\langle \mathrm{f}|k'_n \hat{g}_{nj} k_j|0\rangle = \omega'\omega \frac{(2\pi)^4}{i} \delta(\Delta k + \Delta p)$$

$$\times \sum_{\mathrm{N}} \left\{ \frac{\langle \mathrm{f}| \int \hat{\varrho}(\mathbf{x}) \exp[-i\mathbf{k}' \cdot \mathbf{x}] \mathrm{d}\mathbf{x} |\mathrm{N}\rangle \langle \mathrm{N}| \int \hat{\varrho}(\mathbf{y}) \exp[i\mathbf{k} \cdot \mathbf{y}] \mathrm{d}\mathbf{y}|0\rangle}{E_{\mathrm{N}} - E_0 - \omega} \right.$$

$$\left. + \frac{\langle \mathrm{f}| \int \hat{\varrho}(\mathbf{y}) \exp[i\mathbf{k} \cdot \mathbf{y}] \mathrm{d}\mathbf{y}|\mathrm{N}\rangle \langle \mathrm{N}| \int \hat{\varrho}(\mathbf{x}) \exp[-i\mathbf{k}' \cdot \mathbf{x}] \mathrm{d}\mathbf{x}|0\rangle}{E_{\mathrm{N}} - E_0 + \omega'} \right\}.$$

Hence it is easy to obtain the terms of zero and first orders in the expansion of the scattering amplitude with respect to the photon frequency (see ref. [1]).

The next term of the expansion $\langle \mathrm{f}|k'_n g_{nj} k_j|0\rangle$ involving excited intermediate states has the form

$$k'_n k_j \omega'\omega \frac{(2\pi)^4}{i} \delta(\Delta k + \Delta p) \sum_{\mathrm{N}} \left\{ \frac{\langle \mathrm{f}|\hat{d}_n|\mathrm{N}\rangle \langle \mathrm{N}|\hat{d}_j|0\rangle + \langle \mathrm{f}|\hat{d}_j|\mathrm{N}\rangle \langle \mathrm{N}|\hat{d}_n|0\rangle}{E_{\mathrm{N}} - E_0} \right\}$$

where the $\hat{d}_n$ are the operators of the components of the dipole moment $\int \hat{\varrho}(\mathbf{x}) \mathbf{x}_n \mathrm{d}\mathbf{x}$.

In this eq. the states $|0\rangle$ and $|\mathrm{f}\rangle$ may differ only by the quantum number m of spin orientation. The quantity $\sum\{\ldots\}$ may be written as $\langle jm'|\hat{\alpha}_{nj}|jm\rangle$, where

$\hat{\alpha}_{nj} = \hat{\alpha}_{jn}$ corresponds to the usual definition of the tensor of electric dipole polarizability of the system † (nucleon in our case). For spin $\frac{1}{2}$,

$$\langle \tfrac{1}{2} m' | \hat{\alpha}_{nj} | \tfrac{1}{2} m \rangle = \langle \tfrac{1}{2} | \alpha | \tfrac{1}{2} \rangle \delta_{m'm} \delta_{nj}.$$

Now, we have the following expression for the average value of the electric polarizability of the nucleon:

$$\bar{\alpha} = \langle \tfrac{1}{2} | \alpha | \tfrac{1}{2} \rangle = 2 \sum_{\mathrm{N}} \frac{|\langle \mathrm{N} | \hat{d}_n | 0 \rangle|^2}{E_{\mathrm{N}} - E_0}. \tag{1}$$

From eq. (1) it follows that all excited states of the system yield a positive contribution to the polarizability of the nucleon. The first state for which $\langle \mathrm{N} | \hat{d}_n | 0 \rangle \neq 0$ is a meson+ nucleon state. The square of this matrix element may be expressed through the cross section for the electric dipole photoproduction of mesons σ_{E1}. Hence a lower estimate of $\bar{\alpha}$ may be found as

$$\bar{\alpha} > \frac{1}{2\pi^2} \int \frac{\sigma_{\mathrm{E1}}}{\omega^2} \, \mathrm{d}\omega. \tag{2}$$

Apart from that, eq. (1) may yield an estimate of the mean square fluctuation of the dipole moment in the ground state. Using the completeness of the system of functions we find

$$\bar{\alpha} = \tfrac{2}{3} \frac{1}{(E_{\mathrm{N}} - E_0)} \langle 0 | \hat{d}^2 | 0 \rangle < \tfrac{2}{3} \frac{1}{\mu} \langle 0 | d^2 | 0 \rangle, \tag{3}$$

where μ is the mass of the meson; in the following we put $\mu = \hbar = c = 1$. If it turns out that the main contribution to nucleon polarizability comes from one-meson states the mean square fluctuation of the meson-nucleon distance may be estimated on the basis of eq. (3):

$$\frac{1}{e} \langle 0 | \int \hat{\varrho}(\mathbf{x}) \mathbf{x}_i \mathrm{d}\mathbf{x} \cdot \int \hat{\varrho}(\mathbf{y}) \mathbf{y}_i \mathrm{d}\mathbf{y} | 0 \rangle^{\frac{1}{2}} = \sqrt{\overline{r^2}} > \sqrt{\frac{3\bar{\alpha}}{2e^2}}, \tag{4}$$

where e is the charge. It should be mentioned that this quantity differs from $\langle 0 | \int \hat{\varrho}(\mathbf{x}) \mathbf{x}^2 \mathrm{d}\mathbf{x} | 0 \rangle$, which is measured in electron-nucleon scattering experiments.

The exact value of $\bar{\alpha}$ may in principle be obtained from the data concerning the Compton effect on nucleon in the region of low frequencies. For this purpose the cross section, obtained by adding

$$-\bar{\alpha}\omega^2 \mathbf{e}' \cdot \mathbf{e} - \bar{\beta}(\mathbf{k}' \times \mathbf{e}') \cdot (\mathbf{k} \times \mathbf{e})$$

† If we define $\hat{g}_{nj} = \hat{g}^{(\mathrm{e})}_{nj} + \hat{g}^{(\mathrm{M})}_{nj}$, where $\hat{g}^{(\mathrm{e})}_{nj}$ describes the scattering of "electrical" photons only (E → E transitions) and $\hat{g}^{(\mathrm{M})}_{nj}$ all other types of scattering (M → M, E → M; and M → E transitions) then $k'_n \hat{g}_{nj} k_j = k_n \hat{g}^{(\mathrm{e})}_{nj} k$. The amplitude $\hat{\alpha}_{nj}$ is responsible for the Rayleigh scattering part of the $\hat{g}^{(\mathrm{e})}_{nj}$.

($\bar{\alpha}$ being the electric and $\bar{\beta}$ the magnetic polarizability of the nucleon) to the amplitude of ref. [1]), should be compared with experiment.

It is not difficult to show, for example, that the cross section for scattering at an angle of 90° (in the centre of mass system) may serve as a measure of the electric dipole polarizability:

$$\left(\frac{d\sigma}{d\Omega}\right)_{90^\circ} = \left(\frac{e^2}{M}\right)^2 \left[\frac{1}{2}\left(1-2\frac{\omega}{M}\right) + \omega^2\left(\mathcal{M} - \frac{\bar{\alpha}}{\left(\frac{e^2}{M}\right)}\right)\right]. \tag{5}$$

Here $\mathcal{M}$ is the part of the cross section determined by the static magnetic moment. Even the experimental data available at present enable us to make an upper estimate of the values of the quantities (3) and (4) on the basis of eq. (5). The region of applicability of such description calls for an additional study; this is due to the fact that the experiments on Compton effect are conducted only in the region of relatively high frequencies (in the range of 50 to 100 MeV). The upper limit of frequencies ω for which this description is correct within a given guaranteed accuracy (for example $\approx 5\,\%$) may be obtained through dispersion relations for the forward amplitude [2])

$$\begin{aligned}
\mathrm{Re}\, f &= -\frac{e^2}{M} + \frac{\omega^2}{2\pi^2}\int_{\omega_0}^{\infty} \frac{\sigma(\omega')d\omega'}{\omega'^2-\omega^2} \\
&\approx -\frac{e^2}{M} + \frac{\omega^2}{2\pi^2}\left\{\int_{\omega_0}^{\infty} \frac{\sigma(\omega')d\omega'}{\omega'^2} + \omega^2\int_{\omega_0}^{\infty} \frac{\sigma(\omega')d\omega'}{\omega'^4} + \ldots\right\} \qquad (6) \\
&= -\frac{e^2}{M} + \omega^2(\alpha+\beta) + \omega^2(\alpha+\beta)\left(\frac{\omega}{\bar{\omega}}\right)^2.
\end{aligned}$$

Here $\sigma(\omega')$ is the total cross section for meson photoproduction. If it turns out that the region of large ω' contributes to the dispersion integrals the convergence of the series will be all the better. Even a rough estimate shows that the third term accounts for less than 2 % of the first one, up to photon energies in the range of 100 MeV. A number of estimates of the type of eq. (6) may be made using other disperision relations obtained on the basis of ref. [3]) and under the assumption that $\sigma(\omega')$ is determined only by low multipoles (but without using the experimental values of these). All estimates show that the contribution to the amplitude of the terms with powers of ω higher than the second does not exceed 0.03 for photon energies up to 100 MeV †. At the same time this result shows that the interaction of a nucleon and electromagnetic field can be described by four constants in a wide frequency range.

† The contribution from the difference $\alpha-\bar{\alpha} = \frac{1}{3}\frac{e}{M}\langle 0|\int \rho(\mathbf{x})\mathbf{x}^2 d\mathbf{x}|0\rangle$ between α (eq. (6)) and $\bar{\alpha}$ (eq. (1)) has the same small value.

It should be emphasized, however, that for the time being we have no test of this important proposition. The best test would be the measurement of the energy dependence of the cross section for Compton effect below the meson photoproduction threshold; i.e. it should be investigated, whether the energy dependence is of the kind

$$\frac{d\sigma}{d\Omega} = a+b\omega+c\omega^2.$$

3. Electric Polarizability of Protons

Substituting experimental values of the meson photoproduction cross-section into eqs. (2) and (6) we find

$$\bar{\alpha}_p > 0.4\times 10^{-42}\,\mathrm{cm}^3, \quad \alpha_p+\beta_p \approx 1.07\times 10^{-42}\,\mathrm{cm}^3$$

(neglecting the region of ω' higher than 1000 MeV in the dispersion integral).

Experimental data on the Compton effect [4]) show that the cross section $(d\sigma/d\Omega)_{90^\circ}$ is close to the Thomson cross section, whence the upper estimate for α_p follows:

$$\alpha_p \lesssim 1.5\times 10^{-42}\,\mathrm{cm}^3.$$

Thus for the proton we have

$$0.4\times 10^{-42} \lesssim \bar{\alpha}_p \lesssim 1.5\times 10^{-42}\,\mathrm{cm}^3. \tag{7}$$

In connection with this value it should be mentioned that an estimate of $\bar{\alpha}$ was recently made by V. S. Barashenkov and B. M. Barbashov [5]) on the basis of field theory with extended source; their result is $\bar{\alpha} = 1.8\times 10^{-42}\,\mathrm{cm}^3$. In refs. [6, 7]) estimates of $\bar{\alpha}$, obtained only on the basis of photoproduction data, are seen to coincide with our eq. (7). Recently, V. I. Goldansky *et al.* [8]) made an analysis of their new data on the Compton effect on protons at energies from 40 to 70 MeV. These authors have reduced our upper estimate to 0.9×10^{-42} cm^3.

The mean square fluctuations $\sqrt{\bar{r}^2}$ corresponding to the values of inequality (7) are 0.26×10^{-13} cm and 0.52×10^{-13} cm according to eq. (4). It is noteworthy that if we put $\overline{(E_N-E_0)} \approx 2\mu$ we obtain 0.7×10^{-13} cm on the basis of the upper estimate of α; this value is close to the "electric radius of a proton".

4. Polarizability of Neutrons

Only the lower limit for $\bar{\alpha}_n$ can be estimated on the basis of photoproduction data. These estimates differ little from those for $\bar{\alpha}_p$ according to eqs. (2) and (6). The quantity α_n should exceed α_p by something like 20 %, for the cross sections for photoproduction of neutron and proton are close to each other.

In ref. [9]) the problem was raised of a possible influence of the electric dipole

polarizability of a neutron on the scattering of neutrons on heavy nuclei at small angles. The measurements of this effect yielded an estimate $\alpha_n \approx 8\times 10^{-41}$ cm^3 which strongly contradicts eq. (7). Recently this question was again raised in ref. [6]). This paper discussed anisotropy in the scattering of slow neutrons (energy of the order of a few 100 keV) by nuclei. For a quantitative explanation of the anisotropy under study in this scattering it is necessary to assume $\alpha_n \approx 2\times 10^{-41}$ cm^3, i.e. still one order of magnitude higher than our upper limit of eq. (7).

We might confine ourselves to mentioning this contradiction, regarding the interpretation of nuclear data as ambiguous. Yet we have no strict upper estimate of α_n at present since there are no data on the Compton effect on neutrons. If, on the other hand, we turn to the Compton effect on deuterium the new data of ref. [10]) indicate an abnormally large cross section for this process, namely $\sigma_d^{\gamma\gamma'} \approx 1.6\ \sigma_H^{\gamma\gamma'}$. The authors of ref. [10]) were unable to account for this value on the basis of the impulse approximation. In general the large value of the cross section σ_d thus observed might be accounted for by an abnormally large polarizability of the neutron, which follows from the data on the scattering of neutrons on nuclei. This conclusion seems to us premature, however, for both experiment and theory of the two effects need essentially greater accuracy.

Let us consider the Compton effect on deuterium in impulse approximation; in contrast to ref. [11]) we shall consistently take into account the effects of the interaction of the nucleons. In the transition amplitude we shall consider the contribution of intermediate states corresponding to the photodisintegration of the deuteron (a correction to the impulse approximation)

$$\hat{T} = \hat{t}^p + \hat{t}^n - i\pi \sum_N |\hat{V}_e|N\rangle\langle N|\hat{V}_e|. \tag{8}$$

Here, $\hat{t}^p$ and $\hat{t}^n$ are the scattering amplitudes of free nucleons having, as is well known, the shape

$$(\boldsymbol{\sigma}\cdot\mathbf{K}+L)e^{i(\mathbf{k}'-\mathbf{k})\cdot\mathbf{r}};$$

$\hat{V}_e$ is the operator of interaction of electromagnetic field and a system of two nucleons. An accurate estimate of the third term in the amplitude is at present greatly dependent on model conceptions. Therefore, we shall merely make a rough estimate of this contribution for the simplest case. Let the interaction of the electromagnetic field with a deuteron reduce to the interaction with a proton charge and let the photodisintegration of the deuteron be of the electric dipole type. Let us also take into account that the state $|N\rangle$ describes the relative motion of two nucleons with small wavelengths. Under these assumptions we have

$$\hat{T} = \mathbf{e}\cdot\mathbf{e}'\frac{e^2}{M}\frac{2\pi}{\omega}e^{i(\mathbf{k}'-\mathbf{k})\cdot\mathbf{r}_p} - i\pi\frac{\sigma_d}{2\pi}\delta(\mathbf{r}_p-\mathbf{r}_n)\frac{\mathbf{e}'\cdot\mathbf{e}}{[\varphi_d(\mathbf{r}_p-\mathbf{r}_n)]^2}e^{\frac{1}{2}i(\mathbf{k}'-\mathbf{k})\cdot(\mathbf{r}_p+\mathbf{r}_n)}, \tag{9}$$

where σ_d is the cross section for the photodisintegration of the deuteron, φ_d is its wave function and $\mathbf{r}_p$ and $\mathbf{r}_n$ are the radii-vectors of the proton and the neutron. Calculating the cross section with $\hat{T}$ from eq. (9) and taking account of the neutron-proton interaction in the final state we find that the contribution of the interference term of the first and second parts of $\hat{T}$ are of the same order of magnitude (up to 70 %) as the cross section obtained after neglecting the second term. If no account is taken of the interaction in the final state, the interference term is equal to zero. This result shows that the interpretation of data on Compton effect on deuterium on the basis of the impulse approximation is not tenable. It should be mentioned, however, that the attempt at explaining the large value of the cross section $\sigma_d^{\gamma\gamma'}$ by the contribution of these interference terms is not successful. In integrating over the momentum ($\mathbf{p}$ of the relative motion of two nucleons the second term in eq. (9) yields a very low contribution. Yet this result does not show that the contribution of the interference terms to the cross section integrated over $\mathbf{p}$ will always be small.

In view of such uncertainty in the theory of the impulse approximation we think it rather desriable to measure the cross section of the reactions $\gamma+\mathrm{d}\to\mathrm{d}+\gamma'$ or $\gamma+\mathrm{He}^4\to\mathrm{He}^4+\gamma'$ for which no such uncertainty with respect to interference terms exists and the contribution of the second part of amplitude (9) lies beyond the accuracy of all our calculations. It should also be noted that the contribution of the Low amplitude determined by the interaction of the pair of γ-quanta with a nucleon through the virtual π^0-meson equals zero for these reactions. This fact also eliminates a number of uncertainties in the interpretation of the data.

Let us represent the cross section of the reaction $\gamma+\mathrm{d}\to\mathrm{d}+\gamma'$ in a form which does not depend on the behaviour of the wave function in the region of nuclear forces:

$$\frac{d\sigma_d^{\gamma\gamma'}}{d\Omega}=\frac{k'^3}{(2\pi)^2\left[k'+\dfrac{k'^2-(\mathbf{k}'\cdot\mathbf{k})}{2M}\right]}\cdot\left\{\frac{2}{3}|\mathbf{K}_p+\mathbf{K}_n|^2+|L_p+L_n|^2\right\}\frac{\gamma}{1-\gamma\rho_t}\left[\frac{2}{9}\operatorname{arctg}\frac{q}{2\gamma}-\rho_t\right]. \tag{10}$$

Here $\gamma=\sqrt{M\varepsilon}$ where ε is the binding energy of the deuteron and ρ_t is the triplet effective radius, $q=\sqrt{k'^2+k^2-2(\mathbf{k}'\cdot\mathbf{k})}$. Eq. (10) is very critical with respect to the polarizability of the neutron, for the first term within brackets is small ($\mathbf{K}_p$, $\mathbf{K}_n$ have opposite signs), while the signs of the amplitudes with polarizabilities in L_p and L_n are opposite to the sign of the Thomson scattering amplitude.

A large value of α_n seems improbable because of the smallness of the interval between the upper and lower estimates of eq. (7). Yet this probability should be

borne in mind, especially in connection with the data on electron-neutron scattering which have revealed an essential difference in the electromagnetic characteristics of the neutron and the proton.

References

1) F. Low, Phys. Rev. **96** (1954) 1428;
M. Gell-Mann and H. Z. Goldberger, Phys. Rev. **96** (1954) 1433;
A. Klein, Phys. Rev. **99** (1955) 998
2) M. Gell-Mann, M. L. Goldberg and W. E. Thirring, Phys. Rev. **95** (1954) 1612
3) N. N. Bogolyubov and V. D. Shirkov, DAN SSSR **113** (1957) 529
4) B. B. Govorkov, V. I. Goldansky, O. A. Karpukhin, A. V. Kutsenko and V. V. Pavlovskaya, DAN SSSR **111** (1956) 988;
G. E. Pugh, R. Gomez, D. H. Frish and G. S. Janes, Phys. Rev. **105** (1957) 982
5) V. S. Barashenkov and B. M. Barbashov (preprint of the Joint Institute for Nuclear Research, Dubna); see also L. Schiff (report at the Kiev Conference, July 1959)
6) R. M. Thaler, Phys. Rev. **114** (1959) 827
7) G. Breit and M. Z. Rustgi, Phys. Rev. **114** (1959) 830
8) V. I. Goldansky, O. A. Karpukhin, A. V. Kutsenko and V. V. Pavlovskaya (see report G. Bernardini at the Kiev Conference July, 1959)
9) Yu. A. Alexandrov and I. I. Bondarenko, JETP **31** (1956) 726;
B. S. Barashenkov, I. P. Stakhanov and Yu. A. Alexandrov, JETP **32** (1957) 154
10) L. G. Hyman, R. Ely, D. H. Frisch and M. A. Wahlig, Phys. Rev. Letters **3** (1959) 93
11) R. H. Capps, Phys. Rev. **106** (1956) 1031

8.B

Nuclear Physics **18** (1960) 318—337; © *North-Holland Publishing Co., Amsterdam*

Not to be reproduced by photoprint or microfilm without written permission from the publisher

ON THE LEPTONIC AND NON-LEPTONIC DECAY MODES OF K-MESONS

J. C. PATI † and S. ONEDA ††

University of Maryland, College Park, Maryland †††

and

B. SAKITA

University of Wisconsin, Madison, Wisconsin

Received 25 April 1960

Abstract: An attempt has been made to explain the branching ratios of the various leptonic and non-leptonic modes of K-meson decays in the framework of V—A four-fermion interaction, extended to the tetrahedron scheme. The non-leptonic modes have been investigated with the inclusion of a *new* class of diagrams for $\Lambda \to N+\pi$ decays, satisfying the strict $|\Delta I| = \frac{1}{2}$ rule, whose importance has been pointed out before [1, 2]). Final state pion-pion interactions have been neglected. It is shown that *all* the relative rates (involving ratios between different decay rates) can be explained reasonably well (at least as far as the order of magnitude is concerned), if we assume consistently that the matrix element for any process, evaluated by perturbation theory, should be damped by a factor $\approx \sqrt{3}$, whenever a pion is emitted from a closed baryon-antibaryon loop. The observed features of the approximate $|\Delta I| = \frac{1}{2}$ rule in the non-leptonic modes of K-meson decays become easy to understand by showing the marked importance of the new class of diagrams for $\Lambda \to N+\pi$ decays, which enter as virtual processes for K-meson decays. It is also possible to explain the fact that the final state in $K^+ \to \pi^+ + \pi^- + \pi^+$ decay is predominantly symmetric between the three pions.

1. Introduction

In previous papers [1, 2]) we have demonstrated a way to correlate the explanation of the approximate validity of the $|\Delta I| = \frac{1}{2}$ rule with that of the slowness of the leptonic modes compared to the non-leptonic modes of strange-particle decays. The purpose of the present paper is to consider the branching ratios of the various decay modes of K-meson along the same line. Before entering into details it would be worthwhile to summarize our standpoint.

The weak interaction phenomena involving nucleons and leptons seem to be well understood in terms of the universal V—A four-fermion-interaction [3]). The extension of this scheme to the hyperons is by no means well understood.

† This research contains part of thesis research of J.C.P. to be submitted to the University of Maryland in partial fulfilment of requirements for a Ph. D. degree in physics.

†† Now at Kanazawa University, Japan.

††† This research was supported in part by the United States Air Force through the Air Force Office of Scientific Research and Development Command, and in part by the Atomic Energy Commission (under Contract No. AT(-11-1)-30).

However, at the moment, we should prefer to choose, more or less in the spirit of the Sakata model, the simplest possibility, namely the tetrahedron scheme, which introduces the primary weak interaction amongst the leptons, the nucleons and the Λ-hyperon, and would like to pursue the possible successes of this scheme. We shall assume for the purpose of the present paper that the four-fermion interactions are *local* †. Thirdly, we shall assume that the slowness of the leptonic modes of the strange-particle decays as compared to the universal rates is not solely due to renormalization effects. The consistency of this slowness in the β-decays †† of Λ and Σ^-, as well as in $K_{\mu 2}$ (ref. [6])), $K_{\mu 3}$ (ref. [7])) and K_{e3}-decays seem to justify this assumption. Thus we prefer to adopt the point of view indicated in previous papers [1, 2]) that the strength of the weak interaction does in fact depend upon the change in strangeness. Assuming this, we therefore associate the (Λp)-vertex with a weaker coupling constant f' (referring to the dotted lines in fig. 1) than the other three vertices of the tetrahedron (referring to the solid lines in fig. 1). We further assume that the weak

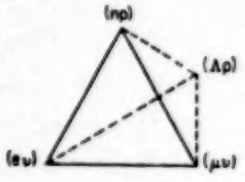

Fig. 1.

interaction current $\mathcal{J}_\alpha$ is composed only of charged positive-chiral currents. Thus, the weak interaction hamiltonian has the form

$$H_{\text{weak}} = \mathcal{J}_\alpha \mathcal{J}_\alpha^* + \text{h.c.}, \tag{1}$$

where $\mathcal{J}_\alpha$ has the unique ††† form

$$\mathcal{J}_\alpha = f\left[\bar{\nu}\gamma_\alpha(1+\gamma_5)e + \bar{\nu}\gamma_\alpha(1+\gamma_5)\mu + \bar{p}\gamma_\alpha(1+\gamma_5)n + \frac{f'}{f}\bar{p}\gamma_\alpha(1+\gamma_5)\Lambda\right]. \tag{2}$$

The coupling constant f is related to the usual Fermi coupling constant f_F (with $f_F m_p^2 \approx 10^{-5}$) by $f^2 = f_F/\sqrt{2}$. The coupling constant f' is expected to be

† The qualitative nature of the discussion of the present paper will not be altered for non-local four-fermion interaction. For the effect of non-locality on Λ-decay, see however ref. [2]) and the thesis of J. C. Pati (to be submitted to the University of Maryland).

†† Hyperon decays into leptons have been shown to be at least an order of magnitude [4]) slower than the universal rate. It does not seem possible to explain this as an accident arising from a damping due to strong interactions, since according to ref. [5]) no V-A interference term appears in the rate and the damping must take place for both V and A interactions separately. Moreover the damping must exist for both Λ and Σ-decays.

††† It may be remarked that the choice of (Λp)-current to induce strange-particle decays, which is unique in the present scheme, has the usual virtues of a $I = \frac{1}{2}$ current rule [8]) insofar as some of the predictions, like the relationships between K_{e3}^+ and K_{e3}^0 or $K_{\mu 3}^+$ and $K_{\mu 3}^0$ modes and the absence of $\Sigma^+ \to n + e^+ + \nu$ decay, etc., are consistent with present experiments [9]).

smaller than f by a factor of $\approx \sqrt{10}$ to explain the rates of the leptonic modes of strange-particle decays.

Once we adopt this scheme, we immediately face the following two problems:

(1) Can we explain the approximate validity of the $|\Delta \mathbf{I}| = \frac{1}{2}$ rule for the non-leptonic modes of strange-particle decays starting from the interaction $ff'\{(\bar{p}\Lambda)(\bar{n}p)+\text{h.c.}\}$, which contains appreciable amount of $|\Delta \mathbf{I}| = \frac{3}{2}$ transitions in addition to a $|\Delta \mathbf{I}| = \frac{1}{2}$ part?

(2) Can we correlate the faster rates of the non-leptonic modes with the slower rates of the leptonic modes of strange-particle decays without attributing the "discrepancy" to renormalization effects alone? In other words, once we adopt a weaker coupling constant for all the lines in fig. 1, linked to the (Λp)-vertex, can we still explain the observed rates of the non-leptonic modes of hyperon and K-meson decays?

In previous papers [1, 2]) we have demonstrated a way to attack both problems (1) and (2). In particular, it was pointed out that for Λ-decay a class of diagrams (fig. 3) satisfying the strict $|\Delta \mathbf{I}| = \frac{1}{2}$ rule are predominant over the usually [10]) considered diagrams (fig. 2), which contain appreciable amounts of $|\Delta \mathbf{I}| = \frac{1}{2}$ and $\frac{3}{2}$ transitions. This makes it easier to explain the approximate validity of the $|\Delta \mathbf{I}| = \frac{1}{2}$ rule. Also, since the rate given by fig. 2 (when one evaluates the contribution of the shaded loop in fig. 2 from the observed $\pi \to \mu+\nu$ rate assuming universal strength of weak interactions) is nearly half the observed rate, one can explain the observed rates of leptonic and non-leptonic modes of strange-particle decays by including the diagrams of both figs. 2 and 3 for non-leptonic processes and assuming $f'^2 \approx \frac{1}{10} f^2$. *It is the purpose of the present paper to examine how the relative rates of the various* K^+ *and* $K^0_{1,2}$ *decay-modes look like with the inclusion of the diagrams of both fig. 2 and fig. 3 as the relevant mechanism for* $\Lambda \to N+\pi$ *decays.*

In section 2, for the sake of completeness, we briefly summarize the content of the previous paper [2]), describing the mechanism of $\Lambda \to N+\pi$ decays. In section 3 we discuss the leptonic modes of K-meson decays. In section 4 we come to the discussion of non-leptonic modes, i.e. $K_{2\pi}$ and $K_{3\pi}$ modes. Both in section 3 and section 4 only the relative rates of the various modes will be discussed, so that the K-meson coupling constant will not be relevant for the discussion. Also it is expected that the relative rates, involving ratios of different decay rates may be treated reasonably by perturbation calculations. In all calculations, final state pion-pion interactions will be neglected. It will be shown that a quantitative understanding of the relative rates of *all* the observed modes of K^+ and $K^0_{1,2}$ decays can be obtained (at least in order of magnitude) if one assumes consistently that the matrix element for any process, evaluated by perturbation theory, should be damped by a factor $\approx \sqrt{3}$, whenever a pion is emitted from a closed baryon-antibaryon loop. The observed features of the approximate $|\Delta \mathbf{I}| = \frac{1}{2}$ rule in K-meson decays become easy to

understand by showing the marked importance of the diagram of fig. 3 as a virtual process in K-meson decays.

2. Mechanism of $\Lambda \to N+\pi$ Decays

Starting from the interaction given by eqs. (1) and (2) we assume that the mechanism of $\Lambda \to N+\pi$-decays is represented by figures 2 and 3 †. The matrix element of fig. 2 for the $\Lambda \to N+\pi$ decays has the form ††

$$M(\Lambda \to N+\pi) = (2\pi)^4 G \left[\bar{p}\not{\phi}_{\pi^-} + \frac{1}{\sqrt{2}}\bar{n}\not{\phi}_{\pi^0}\right](1+\gamma_5)\Lambda, \tag{3}$$

where G denotes the contribution of the shaded loop of fig. 2. On evaluating this contribution from the known rate of $\pi \to \mu+\nu$ decay and remembering

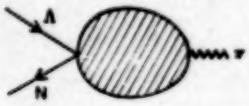

Fig. 2.

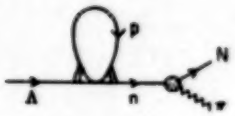

Fig. 3.

that the strangeness-violating current is associated with a weaker coupling constant than the strangeness-conserving ones, we have

$$\frac{G^2}{4\pi} m_{\pi^+}{}^2 \approx (1.83\times 10^{-15})\frac{f'^2}{f^2}. \tag{4}$$

Under the approximation adopted in ref. [2]) ‡, the matrix element of fig. 3 has the form

$$N(\Lambda \to N+\pi) = (2\pi)^4 \frac{\rho m_p g_\pi}{m_\Lambda{}^2 - m_p{}^2}[(\sqrt{2}\bar{p}-\bar{n})\not{\phi}_\pi(1+\gamma_5)\Lambda], \tag{5}$$

where g_π denotes the pion-nucleon coupling constant ($g_\pi{}^2/4\pi \approx 15$) and ρ is the dimensionless constant given by ‡‡

$$\rho = \frac{ff' m_p{}^2(B-A)}{(2\pi)^2}\frac{\lambda^2}{\lambda^2 - m_p{}^2}\frac{\lambda^2}{m_p{}^2}\left[1 - \frac{m_p{}^2}{\lambda^2 - m_p{}^2}\log_e \frac{\lambda^2}{m_p{}^2}\right], \tag{6}$$

where λ denotes the Feynmann cut-off introduced through the factor $(\lambda^2/k^2-\lambda^2)^2$ for evaluation of matrix element of fig. 3. The matrix element

† It is not easy to estimate the net effect of a class of diagrams other than fig. 3, which therefore is left as an open question. However, we adopt fig. 2 as a representative of the class of diagrams involving a $|\Delta I| = \frac{1}{2}$ part.

†† As a convention we do not write the δ-function for four-momentum-conservation in the matrix-element.

‡ In ref. [2]), the net effects of renormalization at the $(\bar{p}\Lambda)$ and $(\bar{n}p)$ vertices in fig. 3 were introduced phenomenologically by taking these vertices as $\gamma_\alpha(1+A\gamma_5)$ and $\gamma_\alpha(1+B\gamma_5)$ respectively. Hereby we neglect the other momentum-dependent corrections, whose inclusion may change the form of the matrix element. The form (5) containing $(1+\gamma_5)$ is for the case $A-B = 1-AB$.

‡‡ The form of ρ was not mentioned in ref. [2]).

given by eq. (5) can be attributed to an induced $(\bar{n}\Lambda)$-interaction of the form

$$\mathscr{H}_{n\Lambda} = \rho m_p[\bar{n}(1+\gamma_5)\Lambda + \text{h.c.}]. \tag{7}$$

As in the previous paper [2]), we choose † $B = +1.25$ and $A \approx 1$. It is then simple to check that for a choice of $\lambda \approx 1.8\, m_p$,

$$\rho \approx 9.974 \times 10^{-8} \frac{f'}{f}. \tag{8}$$

From eqs. (3)—(5), (8) we get ††

$$\left|\frac{N(\Lambda \to p+\pi^-)}{M(\Lambda \to p+\pi^-)}\right|^2 \approx 22.1. \tag{9}$$

Since fig. 2 evaluated with the usual Fermi coupling constant yields a decay rate for $\Lambda \to p+\pi^-$ decay which is nearly half the observed value, we can now explain the observed rate by including fig. 3 and taking $\lambda \approx 1.8\, m_p$ and $f'^2 \approx \frac{1}{10} f^2$. This choice of f' is also consistent with the observed rates of the leptonic modes of strange particle decays. For the purposes of K-meson decays, we choose the same value of the cut-off ($\Lambda \approx 1.8\, m_p$) as for Λ-decay, although the results are not highly sensitive to the choice of the cut-off. The choice of f' will not be relevant for our subsequent discussion, since we shall be concerned only with the ratios of various rates of K-meson decays.

Before passing on to the discussion of K-meson decays, it is worth mentioning that although the inclusion of fig. 3 makes it easier to explain the approximate $|\Delta \mathbf{I}| = \frac{1}{2}$ rule, the branching ratio of Λ-decay still deviates from the desired 2 : 1 ratio owing to the interference of the matrix elements of figs. 2 and 3 †††.

3. The Leptonic Decay Modes of K-Meson

So far two main leptonic decay modes have been observed: (1) the $K_{\mu 2}$ mode and (2) the $K_{\mu 3}$ or K_{e3} mode. In addition to discussing these two modes we shall also discuss the $K_{\mu 4}$ (see ref. [11])) and K_{e4} modes. The relevant Feynmann

† It may be mentioned that, in order to obtain a feeling of the order of magnitude of the matrix element of fig. 3, B has been chosen [2]) to be $\approx +1.25$ as in β-decay. Then A turns out to be restricted between the values $0.95 < A < 1.1$ to explain the sign and magnitude of the asymmetry parameter of $\Lambda \to p+\pi^-$ decay; so that we had chosen $A \approx 1$.

†† The importance of fig. 3. for $\Lambda \to N+\pi$-decays, revealed by the above mentioned calculation, is also expected from the point of view of a dispersion relation calculation taking the mass of Λ as a variable of the dispersion integral, in which a single neutron state is the lowest mass state contributing to the imaginary part of the matrix element.

††† This is a rather serious situation in our treatment, if we adhere to the numbers for the matrix elements of figs. 2 and 3, which we have calculated. However, since our method of evaluation of the matrix element (containing the $|\Delta \mathbf{I}| = \frac{3}{2}$ part) is rather poor, we hope that the higher order corrections may lead to a suppression of the $|\Delta \mathbf{I}| = \frac{3}{2}$ part in fig. 2 so as to give the desired branching ratio without changing our original idea. This has also been pointed out to us by Dr. H. Obayashi (private communication to B. S.).

diagrams (in lowest order perturbation theory) for these processes have been given in figs. 4, 5 and 6 respectively. The general forms of the matrix elements of $K^+_{\mu 2}$, $K^+_{\mu 3}$ and $K^+_{\mu 4}$ decays as prescribed by Lorentz invariance, are given by

Fig. 4.

Fig. 5.

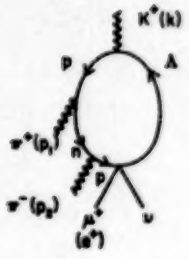

Fig. 6.

$$M(\mathrm{K}^+ \to \mu^+ + \nu) = \frac{g_\mathrm{K} f'_\mathrm{F}}{\sqrt{2}} m_\mathrm{p} I k_\alpha \bar{\nu}\gamma_\alpha(1+\gamma_5)\mu, \tag{10}$$

$$M(\mathrm{K}^+ \to \pi^0 + \mu^+ + \nu) = g_\mathrm{K} g_\pi \frac{f'_\mathrm{F}}{\sqrt{2}} [\mathcal{J}_1 k_\alpha + \mathcal{J}_2 l_\alpha]\bar{\nu}\gamma_\alpha(1+\gamma_5)\mu, \tag{11}$$

$$M(\mathrm{K}^+ \to \pi^+ + \pi^- + \mu^+ + \nu) = g_\mathrm{K}(\sqrt{2}g_\pi)^2 \frac{f'_\mathrm{F}}{\sqrt{2}} \frac{1}{m_\mathrm{p}} [K_1 p_{1\alpha} + K_2 p_{2\alpha} + K_3 l_\alpha + K_4 \varepsilon_{\alpha\beta\gamma\delta} p_{1\beta} p_{2\gamma} l_\delta / m_\mathrm{p}^2]\bar{\nu}\gamma_\alpha(1+\gamma_5)\mu, \tag{12}$$

where by convention k_α denotes the four-momentum of the incoming K-meson, $p_{i\alpha}$ the four-momentum of the ith emitted pion and l_α the sum of the four-momenta of the emitted lepton and anti-lepton. Further g_K denotes the K-meson coupling constant to $(\Lambda-\mathrm{N})$ system, and g_π the usual pion-nucleon coupling constant; $f'_\mathrm{F}/\sqrt{2}$ stands for ff'. We have kept the factors involving g_K, g_π and f'_F outside in order to compare with perturbation calculation results. The factors I, $\mathcal{J}_1$, $\mathcal{J}_2$, K_1, K_2, K_3 and K_4 are form factors denoting the contributions of the intermediate black-boxes in the above decay processes, assuming time-reversal invariance, $\mathcal{J}_1/\mathcal{J}_2$ and the ratio of any two of K_1, K_2, K_3 and K_4 are real. The form factors are dimensionless scalars and slowly varying functions of $k \cdot p_i/m_\mathrm{p}^2$ and $p_i \cdot p_j/m_\mathrm{p}^2$, where m_p denotes the mass of the nucleon †, so that it is reasonable to neglect the dependence of the form-factors on the energies of the decay pions for the range of momenta involved in the above decay processes ($\mathrm{K}^+_{\mu 3}$ and $\mathrm{K}^+_{\mu 4}$ modes). This assertion is explicitly exhibited by the results of the perturbation calculation, which will be presented in the following discussion and in the appendix.

The matrix-elements for K^+_{e2}, K^+_{e3} and K^+_{e4} decays have exactly the same forms as eqs. (10), (11) and (12) respectively, μ being replaced by e. Clearly,

† This is due to the fact that the intermediate particles in the above decays are baryons or antibaryons (with mass at least equal to nucleonic mass), so that the characteristic interaction lengths for the above decays are of the order of the baryon Compton wave lengths.

in the case of decays involving an electron (of either sign) the contribution of $\mathcal{J}_2$ and K_3-terms may be neglected owing to the smallness of the mass of the electron. The contribution of the K_4 term in $K_{\mu 4}$ and K_{e4} decays will also be neglected, since it is two orders of magnitude smaller than the other terms (in powers of m_p).

The transition probabilities for the above processes (assuming the form factors are independent of energies of the decay products) are given [12]) by

$$W(\mathrm{K}^+ \to \mu^+ + \nu) = \frac{m_\mu{}^2 m_\mathrm{K}}{2(2\pi)^9}\left(\frac{m_\mathrm{K}{}^2 - m_\mu{}^2}{m_\mathrm{K}{}^2}\right)^2 \left(g_\mathrm{K}\frac{f'_\mathrm{F}}{\sqrt{2}}\right)^2 m_\mathrm{p}{}^2 |I|^2, \tag{13}$$

$$W(\mathrm{K}^+ \to \pi^0 + \mu^+ + \nu) = \frac{m_\pi{}^5 (m_\mathrm{K}/m_\pi)}{(2\pi)^{11}}\left(g_\mathrm{K} g_\pi \frac{f'_\mathrm{F}}{\sqrt{2}}\right)^2 \cdot [0.431|\mathcal{J}_1|^2 + 0.089(\mathcal{J}_1{}^* \mathcal{J}_2 + \mathcal{J}_1 \mathcal{J}_2{}^*) + 0.0416|\mathcal{J}_2|^2], \tag{14}$$

$$W(K^+ \to \pi^0 + \mathrm{e}^+ + \nu) = \frac{m_\pi{}^5 (m_\mathrm{K}/m_\pi)}{(2\pi)^{11}}\left(g_\mathrm{K} g_\pi \frac{f'_\mathrm{F}}{\sqrt{2}}\right)^2 [0.541|\mathcal{J}_1|^2], \tag{15}$$

$$W(K^0 \to \pi^- + \mu^+ + \nu) = \frac{m_\pi{}^5 (m_\mathrm{K}/m_\pi)}{(2\pi)^{11}}\left(g_\mathrm{K} g_\pi \frac{f'_\mathrm{F}}{\sqrt{2}}\right)^2 2 \cdot [0.359|\mathcal{J}_1|^2 + 0.074(\mathcal{J}_1{}^* \mathcal{J}_2 + \mathcal{J}_2{}^* \mathcal{J}_1) + 0.034|\mathcal{J}_2|^2], \tag{16}$$

$$W(\mathrm{K}^0 \to \pi^- + \mathrm{e}^+ + \nu) = \frac{m_\pi{}^5 (m_\mathrm{K}/m_\pi)}{(2\pi)^{11}}\left(g_\mathrm{K} g_\pi \frac{f'_\mathrm{F}}{\sqrt{2}}\right)^2 2[0.456|\mathcal{J}_1|^2]. \tag{17}$$

The additional factor 2 in $\mathrm{K}^0_{\mu 3}$ and K^0_{e3} decays relative to $\mathrm{K}^+_{\mu 3}$ and K^+_{e3} decays respectively is due to the choice of our interaction $(\bar{\Lambda}\mathrm{p})\,(\bar{\nu}\mathrm{l})$, which satisfies the $I = \frac{1}{2}$ rule [8]) for the strangeness violating current. For our purposes we take the form-factors for K^0 decays to be the same as the corresponding ones for K^+ decays. This amounts to neglecting the $(\mathrm{K}^+, \mathrm{K}^0)$ and (π^+, π^0) mass differences compared to the nucleonic mass for the values of the form-factors. However, we have included these mass differences in the above expressions for the calculation of the phase space in the above decays. This is what gives rise to the slightly different expressions for K^+ and K^0 decay rates (compare with the earlier papers of ref. [12])).

From (13) and (15) we have

$$R_1 \equiv \frac{W(\mathrm{K}^+ \to \pi^0 + \mathrm{e}^+ + \nu)}{W(\mathrm{K}^+ \to \mu^+ + \nu)} \approx \frac{1}{5.2}\,\frac{|\mathcal{J}_1|^2}{|I|^2}. \tag{18}$$

The perturbation calculation (see Appendix, eqs. (51) and (52)) gives $\mathcal{J}_1 \approx 4\pi^2 i \times (-0.91)$ and $I \approx 4\pi^2 i \times (1.02)$ for cut off $\Lambda \approx 1.8\, m_\mathrm{p}$. Hence one gets

$$R_1 \approx \frac{1}{6.5}. \tag{19}$$

The observed value of $R_1 \approx \frac{1}{15}$. Thus, since the cut-off dependences for the two processes $K^+_{\mu 2}$ and K^+_{e3} are nearly the same (logarithmic), so that the ratio R_1 is rather insensitive to the choice of the cut-off, the discrepancy by a factor of ≈ 3 between the estimated and the observed ratio of the rates of K^+_{e3} and $K^+_{\mu 2}$ may be attributed to the fact that the structure of the black-boxes for the two processes differ only by the emission of an additional pion from the baryon-antibaryon loop in the former, which is absent from the latter. This suggests to assume phenomenologically that the *matrix-element for any* † *process involving emission of pions from closed baryon-antibaryon loop is effectively damped by a factor of* $\approx \sqrt{3}$. It is worthwhile to point out that a perturbation calculation of the $\pi \to \mu + \nu$-decay yields a decay rate larger than the observed value by a factor of ≈ 11 (for cut-off $\approx 1.8 m_p$), which therefore seems to indicate the plausibility of the above assumption. For the *subsequent discussion* we denote the effect of this damping of the matrix-element due to emission of a pion from a closed loop by putting $\mathscr{D} g_\pi$ instead of g_π as the *effective* coupling constant for the pion-vertex. Tentatively we assume $\mathscr{D} g_\pi \approx g_\pi/\sqrt{3}$ for all processes. It is now our task to examine how consistently we can explain *all* the relative rates of the various leptonic and non-leptonic modes of K^+ and $K^0_{1,2}$ decays with the above assumption of damping and the inclusion of fig. 3 in addition to fig. 2 for the non-leptonic decay modes. Before we enter into a discussion of non-leptonic decay modes, however, we shall give below the relative rates $K^+_{\mu 3}$ and K^+_{e4} modes compared to K^+_{e3}-decay.

From (14) and (15)

$$R_2 \equiv \frac{W(K^+ \to \pi^0 + \mu^+ + \nu)}{W(K^+ \to \pi^0 + e^+ + \nu)} \approx \frac{0.797|\mathscr{J}_1|^2 + 0.164(\mathscr{J}_1^* \mathscr{J}_2 + \mathscr{J}_1 \mathscr{J}_2^*) + 0.077|\mathscr{J}_2|^2}{|\mathscr{J}_1|^2}. \quad (20)$$

If $|\mathscr{J}_1| \approx |\mathscr{J}_2|$, then $R_2 \approx 1.20$ or 0.54 depending upon $\mathscr{J}_1 \approx +\mathscr{J}_2$ or $-\mathscr{J}_2$. By actual perturbation calculation (see appendix, eqs. (52) and (53)) $\mathscr{J}_1 \approx 4\pi^2 i \times (-0.91)$ and $\mathscr{J}_2 \approx 4\pi^2 i \times (+0.583)$ for cut-off $\Lambda \approx 1.8 m_p$, so that one obtains

$$R_2 \approx \frac{1}{1.62}. \quad (21)$$

This is in fair agreement with the experimental numbers [13]) $4.0 + 0.77$ (%) and $4.19 + 0.42$ (%) for the branching ratios of $K^+_{\mu 3}$ and K^+_{e3} decays. It is to be noted that the value of R_2 is also insensitive to the choice of the cut-off.

† The damping is, of course, expected to depend on the energy-release in a process. However, for our purposes we assume the effective damping to be nearly constant.

The amplitude for the K_{e4}^+ decay mode is convergent in perturbation calculation. The leading terms for K_1, K_2 and K_3 (obtained by perturbation calculation) are given in the appendix (see eq. (54)). Looking at these expressions, the contribution of the K_2 term (being proportional to $(m_p - m_\Lambda)$) may be neglected compared to that of the K_1 term. The decay rate of $K^+ \to \pi^+ + \pi^- + e^+ + \nu$ is then given by

$$W(K^+ \to \pi^+ + \pi^- + e^+ + \nu) \approx \frac{m_\pi{}^7}{2(2\pi)^{13}} \frac{\left[g_K(\sqrt{2}\mathscr{D}g_\pi)^2 \frac{f'_F}{\sqrt{2}}\right]^2}{m_p{}^2} \cdot 0.02|K_1|^2. \quad (22)$$

In the above expression the damping factor $\mathscr{D}$ appears owing to the assumption already mentioned. For the $K^+ \to \pi^0 + \pi^0 + e^+ + \nu$-decay, since the p_1 and p_2 terms occur in the combination $(K_1 + K_2)(p_1 + p_2)/\sqrt{2}$ in the matrix element (due to the symmetry of the two final neutral pions), the decay rate is given by

$$W(K^+ \to \pi^0 + \pi^0 + e^+ + \nu) \approx \frac{m_\pi{}^7}{2(2\pi)^{13}} \frac{\left[g_K(\mathscr{D}g_\pi)^2 \frac{f'_F}{\sqrt{2}}\right]^2}{m_p{}^2} \cdot 0.067 \left|\frac{K_1 + K_2}{\sqrt{2}}\right|^2. \quad (23)$$

From (15) and (22) we have

$$R_3 \equiv \frac{W(K^+ \to \pi^+ + \pi^- + e^+ + \nu)}{W(K^+ \to \pi^0 + e^+ + \nu)} \approx \mathscr{D}^2(2.13 \times 10^{-3}) \frac{|K_1|^2}{|\mathscr{J}_1|^2}. \quad (24)$$

In perturbation calculation (see appendix) $K_1 \approx 4\pi^2 i \times (0.56)$ and (for $\Lambda \approx 1.8 m_p$) $\mathscr{J}_1 \approx 4\pi^2 i \times (-0.91)$. Thus we get

$$R_3 \approx 2.42 \times 10^{-4}. \quad (25)$$

From (22) and (23)

$$R_4 \equiv \frac{W(K^+ \to \pi^0 + \pi^0 + e^+ + \nu)}{W(K^+ \to \pi^+ + \pi^- + e^+ + \nu)} \approx 0.42. \quad (26)$$

The predicted ratio R_3 given by (25) is smaller by an order of magnitude than the number given by Chadan and Oneda [11]). This arises from the introduction of the damping of the matrix-element due to each pion-emission and the somewhat higher choice of the cut-off adopted in the present paper. At this point it is perhaps worthwhile to point out the following:

Chadan and Oneda, adopting a value of $R_3 \approx 10^{-3}$, have recently [14]) pointed out that the hypothesis of strong final-state π–π interaction in $T = 0$, $J = 0$ state, suggested by Okubo and Marshak [15]), could lead to an enhanced value of $R_3 \approx 10^{-1}$, which would tend to disfavour the above hypothesis in view of the absence of a single K_{e4}^+ event. However, in the present scheme the enhanced value of $R_3 \approx 10^{-2}$. Hence absence of any K_{e4}^+ event in future (with accumulation of more K_{e3}^+ events) may serve to rule out the above hypothesis.

4. The Non-Leptonic Decay Modes of K-Meson

4.1. THE $K \to 2\pi$ DECAYS

There are three decays belonging to this group: (1) $K^+ \to \pi^+ + \pi^0$, (2) $K_1^0 \to \pi^+ + \pi^-$ and (3) $K_1^0 \to \pi^0 + \pi^0$. It is well known that the first process is forbidden by a strict $|\Delta I| = \frac{1}{2}$ rule, while the second and the third processes can proceed through both $|\Delta I| = \frac{1}{2}$ and $\frac{3}{2}$ channels. Therefore, the relevant diagrams (for the processes (1) and (2) only) are shown in figs. 7, 9 and 10.

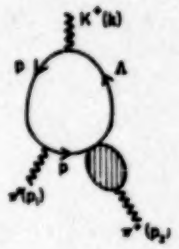

Fig. 7.

Fig. 8.

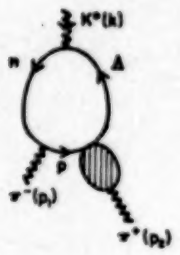

Fig. 9.

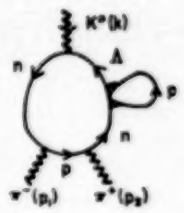

Fig. 10.

We are neglecting the contribution of diagrams of the type shown in fig. 8. With the present choice of the weak-interactions, these diagrams are known to yield a vanishing contribution without pionic corrections between successive bubbles; it is likely that their contribution even with pionic corrections between the bubbles is of the same order of magnitude as that of fig. 7, and hence may be omitted for the discussion of the present paper see ((31)). We adopt the *convention* that the matrix-elements of diagrams involving fig. 2 will be denoted by M and those involving fig. 3 by N. Remembering that in these 2π decay modes $E_{\pi_1} \approx E_{\pi_2} \approx \frac{1}{2}m_K$ (in the rest frame of the decaying K-meson), the matrix elements for the first two processes are given by

$$\begin{aligned} M(K^+ \to \pi^+ + \pi^0) &\approx 2g_K(\mathscr{D}g_\pi)G[\tfrac{1}{2}L_1 m_K{}^2 + L_2 m_\pi{}^2] \\ &\approx 2g_K \mathscr{D} g_\pi G m_\pi{}^2[6.3L_1 + L_2], \end{aligned} \tag{27}$$

$$M(K_1^0 \to \pi^+ + \pi^-) \approx \sqrt{2}g_K\sqrt{2}\mathscr{D}g_\pi G m_\pi{}^2[6.3L_1 + L_2], \tag{28}$$

$$N(K_1^0 \to \pi^+ + \pi^-) \approx \sqrt{2}g_K(\sqrt{2}\mathscr{D}g_\pi)^2 \rho m_p \mathscr{M}. \tag{29}$$

The factor 2 in $M(K^+ \to \pi^+ + \pi^0)$ is due to the possibility of interchange in the mechanisms of π^+ and π^0 emissions (see fig. 7). The factor $\sqrt{2}$ in $M(K_1^0 \to \pi^+ + \pi^-)$ is due to the definition $K_1^0 \equiv (K^0 + \bar{K}^0)/\sqrt{2}$. The factors L_1, L_2 and $\mathscr{M}$ are dimensionless scalars, denoting the contributions of the black boxes. Clearly, in the lowest order perturbation calculation, $L_1 = \mathscr{J}_1$ and $L_2 = \mathscr{J}_2$.

By eqs. (4), (8), (27) and (29)

$$\frac{|M(K^+ \to \pi^+ + \pi^0)|}{|N(K_1^0 \to \pi^+ + \pi^-)|} \approx \frac{1}{\mathscr{D} 86.73} \left| \frac{6.3 L_1 + L_2}{\mathscr{M}} \right|. \tag{30}$$

If we assume for crude estimation that $|L_1| = |L_2| = |\mathscr{M}|$, the ratio

$$\left| \frac{M(K^+ \to \pi^+ + \pi^0)}{N(K_1^0 \to \pi^+ + \pi^-)} \right| = \frac{1}{11.88 \mathscr{D}} \text{ or } \frac{1}{16.36 \mathscr{D}}$$

depending upon whether $L_1 = +L_2$ or $-L_2$. By perturbation calculation (see appendix) $L_1 \approx 4\pi^2 i \times -(0.91)$, $L_2 \approx 4\pi^2 i \times (+0.58)$ and $\mathscr{M} \approx 4\pi^2 i \times (+0.86)$ for cut-off $\Lambda \approx 1.8\, m_p$. Then one gets

$$R_5 \equiv \left| \frac{M(K^+ \to \pi^+ + \pi^0)}{N(K_1^0 \to \pi^+ + \pi^-)} \right|^2 \approx \frac{1}{211.3 \mathscr{D}^2}. \tag{31}$$

The value of R_5 is fairly insensitive to the choice of the cut-off Λ, since both fig. 7 and fig. 10 lead to logarithmically divergent amplitudes. It may be noticed from (9) and (31) that the ratio of the absolute squares of the matrix-elements of diagrams involving fig. 2 and fig. 3 respectively is diminished by a factor ≈ 10 in K-meson decays as compared to Λ-decay. *This therefore leads to a rather satisfactory explanation of the* $|\Delta \mathbf{I}| = \frac{1}{2}$ *rule in* K*-meson decays.* In fact, as shown by (31), one obtains, without damping of the pion-vertex (i.e. if we put $\mathscr{D} \approx 1$), the ratio $W(K^+ \to \pi^+ + \pi^0)/W(K_1^0 \to \pi^+ + \pi^-) \approx 1/200$. At this point it is worth remembering that since the $K^+ \to \pi^+ + \pi^0$ decay (fig. 7) proceeds through the $|\Delta \mathbf{I}| = \frac{3}{2}$ channel, the evaluation of the matrix element of fig. 7 by equating the shaded loop to that occurring in the $\pi \to \mu + \nu$ decay may be a little ambiguous. In fact, as mentioned already (see remark at the end of section 2), a suppression of the $|\Delta \mathbf{I}| = \frac{3}{2}$ part as compared to the $|\Delta \mathbf{I}| = \frac{1}{2}$ part in fig. 2 could be expected from higher order effects, in order to explain the observed 2 : 1 branching ratio of Λ decay. This suppression could therefore compensate for the damping factor $\mathscr{D}$ in the denominator of (31), and would provide a fair explanation of the observed ratio $W(K^+ \to \pi^+ + \pi^0)/W(K_1^0 \to \pi^+ + \pi^-) \approx 1/300$.

The other interesting feature of the $|\Delta \mathbf{I}| = \frac{1}{2}$ rule in $K \to 2\pi$ decays is the value of the ratio

$$R_6 \equiv \frac{W(K_1^0 \to 2\pi^0)}{W(K_1^0 \to 2\pi)}. \tag{32}$$

It is easy to check, by inspecting figs. 9 and 10, that

$$\begin{aligned} M(K_1^0 \to \pi^+ + \pi^-) &= -\sqrt{2} M(K_1^0 \to 2\pi^0), \\ N(K_1^0 \to \pi^+ + \pi^-) &= \sqrt{2} N(K_1^0 \to 2\pi^0), \end{aligned} \tag{33}$$

where M and N refer to matrix-elements of diagrams of the type of fig. 9 and fig. 10 for $K \to 2\pi$ decays, respectively. By (31), (32) and (33)

$$R_6 = \frac{|M(K_1^0 \to 2\pi^0) + N(K_1^0 \to 2\pi^0)|^2}{|M(K_1^0 \to \pi^+ + \pi^-) + N(K_1^0 \to \pi^+ + \pi^-)|^2 + |M(K_1^0 \to 2\pi^0) + N(K_1^0 \to 2\pi^0)|^2}$$
$$\approx 0.24 \quad \text{or} \quad 0.44, \tag{34}$$

where the alternative values depend upon the phase of M relative to N. In perturbation calculation the phases of $M(K_1^0 \to \pi^+ + \pi^-)$ and $N(K_1^0 \to \pi^+ + \pi^-)$ differ by 180°, which corresponds to $R_6 \approx 0.24$. This value of R_6 includes the damping factor $\mathscr{D}$ and is in good agreement with the observed [16]) value $R_6 = 0.27 \pm 0.11$. If the damping factor $\mathscr{D}$, in this case, is compensated (as mentioned before) by the suppression of the $|\Delta I| = \frac{3}{2}$ part in the matrix-element of diagrams involving fig. 2, the theoretical value for R_6 will tend more closely to 0.33, which is the value given by the strict $|\Delta I| = \frac{1}{2}$ rule.

4.2. $K \to 3\pi$ DECAYS

There are four decays belonging to this group: (1) $K^+ \to \pi^+ + \pi^- + \pi^+$, (2) $K^+ \to \pi^+ + \pi^0 + \pi^0$, (3) $K_2^0 \to \pi^+ + \pi^- + \pi^0$ and (4) $K_2^0 \to \pi^0 + \pi^0 + \pi^0$, all of which can proceed through both $|\Delta I| = \frac{1}{2}$ and $\frac{3}{2}$ channels. Two relevant † diagrams for the first process (the well-known τ^+ decay) have been shown in figs. 11 and 12. The corresponding matrix elements for these two diagrams,

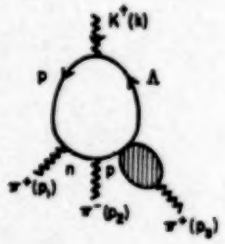

Fig. 11.

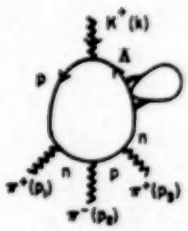

Fig. 12.

with the necessary symmetrisation between the two identical positively charged pions, are given by

$$M(K^+ \to \pi^+ + \pi^- + \pi^+) = g_K(\sqrt{2}\mathscr{D}g_\pi)^2 G \frac{1}{m_p} \frac{[2N_1 p_1 \cdot p_3 + N_2 p_2 \cdot (p_1 + p_3) + N_3(p_1^2 + p_3^2)]}{\sqrt{2}}, \tag{35}$$

$$N(K^+ \to \pi^+ + \pi^- + \pi^+) = g_K(\sqrt{2}\mathscr{D}g_\pi)^3 \rho m_p \frac{1}{m_p} \sqrt{2}\mathscr{O}, \tag{36}$$

† We postpone the discussion of the contribution of other possible diagrams in τ^+ decay for the purpose of the present paper. It is reasonable to expect that their contribution to the decay-rate will be of the same order as that of fig. 11 and since fig. 11 has a negligible contribution compared to fig. 12 (see (38)), it is justified to omit other types of diagrams for consideration of τ^+ decay rate.

where N_1, N_2, N_3 and $\mathcal{O}$ are the dimensionless scalars denoting the contribution of the black boxes in the corresponding processes. In perturbation calculation the form-factors for fig. 11 are the same as those for fig. 6, i.e. $N_1 = K_1$, $N_2 = K_2$ and $N_3 = K_3$.

By (35) and (36)

$$\left|\frac{N(\mathrm{K}^+ \to \pi^+ + \pi^- + \pi^+)}{M(\mathrm{K}^+ \to \pi^+ + \pi^- + \pi^+)}\right| \approx (25.52)\left|\frac{m_p m_\pi \mathcal{O}}{2N_1 p_1 \cdot p_3 + N_2 p_2 \cdot (p_1 + p_3) + N_3(p_1^2 + p_3^2)}\right|. \quad (37)$$

This clearly reveals that even if we assume that $N_1 = N_2 = N_3 = \mathcal{O}$ and maximise the denominator of the right hand side of (37) (by a considerable overestimation) by taking into account the nature of kinematics involved in τ^+ decay, the above ratio is still greater than 15. In perturbation calculation the N_2-term in the denominator is proportional to $(m_p - m_\Lambda)$ (See Appendix, eq. (54)), and can therefore be dropped. With the values of N_1, N_3 and $\mathcal{O}$ given in the appendix, it can be checked † that

$$\left|\frac{N(\mathrm{K}^+ \to \pi^+ + \pi^- + \pi^+)}{M(\mathrm{K}^+ \to \pi^+ + \pi^- + \pi^+)}\right| > 23. \quad (38)$$

Thus for subsequent discussion of $\mathrm{K} \to 3\pi$ decays the contribution of the type of diagrams shown in fig. 11 will be neglected.

Now it will be worthwhile to compare the rates of $\mathrm{K}^+ \to \pi^+ + \pi^- + \pi^+$ and $\mathrm{K}_1^0 \to \pi^+ + \pi^-$ decays. For $\mathrm{K}_1^0 \to \pi^+ + \pi^-$ decay rate (for reasons analogous to the situation in τ^+ decay) it is enough to consider contribution from fig. 10 only. Then the transition probabilities for $\mathrm{K}_1^0 \to \pi^+ + \pi^-$ and $\mathrm{K}^+ \to \pi^+ + \pi^- + \pi^+$ decays are given [17]) by

$$W(\mathrm{K}_1^0 \to \pi^+ + \pi^-) = \frac{\sqrt{1 - 4(m_{\pi^+}/m_\mathrm{K})^2}}{8(2\pi)^9 m_\mathrm{K}} |N(K_1^0 \to \pi^+ + \pi^-)|^2 \approx \frac{2\{g_\mathrm{K}(\sqrt{2}\mathscr{D} g_\pi)^2 \rho m_p\}^2}{8(2\pi)^9 m_{\pi^+}} 0.23 |\mathscr{M}|^2, \quad (39)$$

$$W(\mathrm{K}^+ \to \pi^+ + \pi^- + \pi^+) \approx \frac{[g_\mathrm{K}(\sqrt{2}\mathscr{D} g_\pi)^3 \rho m_p]^2 (m_\pi^2/m_\mathrm{K})}{128\pi^3 m_p^2} 0.32 |\mathcal{O}|^2. \quad (40)$$

By (39) and (40)

$$R_7 \equiv \frac{W(\mathrm{K}^+ \to \pi^+ + \pi^- + \pi^+)}{W(\mathrm{K}_1^0 \to \pi^+ + \pi^-)} \approx \frac{1}{150} \frac{|\mathcal{O}|^2}{|\mathscr{M}|^2}. \quad (41)$$

† We use the fact here that in τ^+ decay the maximum of $p_1 \cdot p_3 \approx 44\,300$ MeV^2.

By perturbation calculation (see Appendix) $\mathcal{O} \approx 4\pi^2 i \times (0.59)$ and (for $\Lambda \approx 1.8\, m_p$, $\mathcal{M} \approx 4\pi^2 i \times (0.86)$, so that

$$R_7 \approx \tfrac{1}{320}. \tag{42}$$

This may be compared with the experimental number $R_7 \approx 1/1500$. Thus, in this case there seems to be a discrepancy by a factor 5 between the observed and the estimated ratios. This, however, cannot be regarded as a serious discrepancy, particularly considering the fact that the calculated amplitude of the $K_1^0 \to \pi^+ + \pi^-$ decay is cut-off dependent while that of the $K^+ \to \pi^+ + \pi^- + \pi^+$ decay is convergent. Moreover, the above ratio does also depend upon the value of the effective damping due to emission of pion from a closed loop. This damping is expected to be dependent upon the energy release in a process, although we have assumed here that it is a constant ($\mathcal{D} \approx 1/\sqrt{3}$) for both 2π and 3π decays. It is also expected that the inclusion of final state $\pi-\pi$ interactions, neglected in the present attempt, may somewhat account for the slight discrepancy.

The matrix-element of the pure $|\Delta \mathbf{I}| = \frac{1}{2}$ diagram (fig. 12) being considerably more important (see (38)) than the other class of diagrams (fig. 11) containing both $|\Delta \mathbf{I}| = \frac{1}{2}$ and $\frac{3}{2}$ parts, it is clear that the various features † of the $|\Delta \mathbf{I}| = \frac{1}{2}$ rule (assuming a totally symmetric wave function) in $K \to 3\pi$ decays, namely

(a) $$W(K^+ \to \pi^+ + \pi^0 + \pi^0)/W(K^+ \to \pi^+ + \pi^- + \pi^+) \approx \tfrac{1}{4} \times 1.3,$$

(b) $$W(K_2^0 \to 3\pi^0)/W(K_2^0 \to \pi^+ + \pi^- + \pi^0) \approx \tfrac{3}{2},$$

(c) $$W(K_2^0 \to \pi^+ + \pi^- + \pi^0)/W(K^+ \to 3\pi) \approx \tfrac{2}{5},$$

are explained quite well in the present scheme.

So far we have not compared the rate of a leptonic mode with that of a non-leptonic mode. For this purpose we shall choose (owing to reasons, which we shall mention subsequently) a particularly suitable one, namely the rate of the K_{e3} mode compared to that of the $K_1^0 \to 2\pi$ mode.

By (15) and (39) we have

$$R_8 \equiv \frac{W(K^+ \to \pi^0 + e^+ + \nu)}{W(K_1^0 \to \pi^+ + \pi^-)} \approx (1.71 \times 10^{-4}) \frac{|\mathcal{J}_1|^2}{|\mathcal{M}|^2}. \tag{43}$$

By perturbation calculation (see Appendix), $\mathcal{J}_1 \approx 4\pi^2 i \times (-0.91)$ and $\mathcal{M} \approx 4\pi^2 i \times (0.86)$, both evaluated for cut-off $\Lambda = 1.8\, m_p$. With these values

$$R_8 \approx 1.91 \times 10^{-4}. \tag{44}$$

† The features (a) and (b) follow from any linear combination of $|\Delta \mathbf{I}| = \frac{1}{2}$ and $\frac{3}{2}$ transitions. However, (c) tests [18]) the validity of the $|\Delta \mathbf{I}| = \frac{1}{2}$ hypothesis. Out of these three features, present experiments do not bear any information on (b). However, for (a) the observed ratio [19]) 0.32 ± 0.05 agrees well with the theoretical value 0.325. The one event $K_2^0 \to \pi^+ + \pi^- + \pi^0$ observed by Crawford *et al.* [16]) is also consistent with the expected ratio (c).

Hence by (34)

$$R_9 \equiv \frac{W(K^+ \to \pi^0 + e^+ + \nu)}{W(K_1^0 \to 2\pi)} \approx 1.45 \times 10^{-4}, \tag{45}$$

and by the $I = \frac{1}{2}$ current rule †

$$R_{10} \equiv \frac{W(K^0 \to \pi^- + e^+ + \nu)}{W(K_1^0 \to 2\pi)} \approx 2.9 \times 10^{-4}, \tag{46}$$

which may be compared with the experimental †† value $R_{10} \approx 6 \times 10^{-4}$. It is pertinent to remark that, since both K_{e3}^+ and $K_1^0 \to 2\pi$ matrix elements are cut-off dependent in nearly the same manner and since in the former only the $|\Delta I| = \frac{1}{2}$ transition occurs, while in the latter the contribution of the $|\Delta I| = \frac{3}{2}$ part (coming from fig. 9) may be neglected compared to the $|\Delta I| = \frac{1}{2}$ part (coming from figs. 9 and 10), so that one does not have to worry about the ambiguity in the suppression of the $|\Delta I| = \frac{3}{2}$ part by higher order corrections, the comparison of the calculated ratio of the rates of K_{e3}^+ and $K_1^0 \to 2\pi$ decays with experiment is particularly suitable to judge the validity of our approach. The fair agreement ††† (within a factor ≈ 2) obtained with experiment in this case seems to justify our stand point.

4.3. THE ASYMMETRY IN THE ENERGY-DISTRIBUTION IN THE $K^+ \to \pi^+ + \pi^- + \pi^+$ DECAY

It is known [22, 23]) that the final state in the $K^+ \to \pi^+ + \pi^- + \pi^+$ decay is predominantly symmetric between the three pions with a small mixture of non-symmetric states. We shall briefly show that the proposed new mechanism of non-leptonic decays (inclusion of fig. 3) makes it easier to explain this fact.

By just looking at the structures of the diagrams shown in figs. 11 and 12 for the $K^+ \to \pi^+ + \pi^- + \pi^+$ decay, we may expect that fig. 12 (involving the new mechanism) would tend to favour more totally symmetric states of three pions than fig. 11 (involving the usual mechanism). This is explicitly borne out by the results of the perturbation theory calculation, in which the leading term in the matrix element of fig. 12 (see (36) and (57)) is independent of the pion energies, while the leading term in the matrix element of fig. 11 (see (35) and (57)) involves the invariant scalar products $p_1 \cdot p_3$, $p_2 \cdot p_3$ and $p_1 \cdot p_2$, which give rise to non-symmetric states. In order to have a feeling of the order of magnitude involved, we shall estimate the non-symmetric states coming from the leading term of the matrix-element of fig. 11.

† Recent observation by Crawford *et al.* [20]) on the three-body leptonic decays of K_1^0 and K_2^0 seem to be in agreement with the above rule.

†† The experimental value for R_{10} is obtained [21]) indirectly by noting the rate of K_{e3}^+ decay and applying the result of the $I = \frac{1}{2}$ current rule.

††† It may be noted that with the mechanism of $\Lambda \to N + \pi$ decays shown in fig. 2 alone, it was hard to understand the observed value of R_{10} (see Oneda [21])). The introduction of the new mechanism of Λ decay (fig. 3), however, serves to remove this difficulty.

Following Dalitz [22]) we choose as two independent variables $x \equiv \sqrt{3}(T_1-T_3)/Q$ and $y = (3T_2-Q)/Q$, where T_1 and T_3 denote the kinetic energies of the two π^+ and T_3 the kinetic energy of the π^-, while Q denotes the Q value in the τ^+ decay ($Q \approx 75.11$ MeV), so that $Q = T_1+T_2+T_3$. Denoting the invariant matrix-element for the τ^+ decay by $M(\tau^+)$, the transition rate is proportional to

$$\iint \mathrm{d}x\mathrm{d}y|M(\tau^+)|^2.$$

For fig. 11, $M(\tau^+)$ is proportional to (see (35))

$$\begin{aligned} M(\tau^+) &\propto 2N_1 p_1 \cdot p_3 + N_2 p_2 \cdot (p_1+p_3) + 2N_3 m_{\pi^+}^2 \\ &\propto 1 + Ay, \end{aligned} \tag{47}$$

where

$$A \equiv \frac{\frac{1}{3}(N_2-2N_1)m_K Q}{m_K^2 N_1 + m_\pi^2(2N_3-N_1-N_2) + m_K(m_\pi+\frac{1}{3}Q)(N_2-2N_1)} \tag{48}$$

Substituting the values of N_1, N_2 and N_3 given by perturbation theory (see Appendix) we get

$$A \approx -\frac{1}{3.77}. \tag{49}$$

Clearly the term 1 in (47) leads to a final state which is totally symmetric between the three pions, while the A term does not. A good fit to the data, obtained from the Dalitz plot [22, 23]) is given by

$$A \approx \tfrac{1}{10}. \tag{50}$$

Thus fig. 11 leads to non-symmetric states, whose intensity is about an order of magnitude larger † than that found experimentally and gives a wrong sign of A. However, as discussed in the previous subsection, the contribution of fig. 12 for the τ^+ decay is considerably larger than that of fig. 11 (see (38)), and the leading term of the matrix-element of fig. 12 being independent of the pion energies, leads to totally symmetric states.

The non-symmetric terms arise from the second order terms of the matrix element of fig. 12 and the first order terms of the matrix elements of diagrams other than fig. 12 (one of the typical ones being fig. 11). Although a reliable estimation of the above mentioned contributions to the non-symmetric term is hard to make, these together with the leading term in the matrix element of fig. 12 and some influence of the final state pion-pion interactions in an appropriate state in τ^+ decay (not the same mechanism, so as to explain the ratio $W(K^+ \to 2\pi)/W(K_1^0 \to 2\pi)$, as was suggested by Good and Holladay [24]) may

† This may be regarded as evidence against taking diagrams of the type of fig. 2 (which enters into fig. 11) as the main mechanism of the non-leptonic decays of strange-particles.

be expected to yield the experimentally observed asymmetry in τ^+ decay. (One such attempt to explain the energy-spectra of the pions in τ^+ decay on the basis of final-state interactions alone has been made by Thomas and Holladay [25]).

A compilation of our results is given in table 1.

TABLE 1

Compilation of results

	Experimental	$\mathcal{D}^2 = 1$ (No damping)	$\mathcal{D}^2 = \frac{1}{3}$	$\mathcal{D}^2 = \frac{1}{3}$ and suppression of $\lvert\Delta I\rvert = \frac{3}{2}$ part
$R_1 \equiv \frac{W(K^+ \to \pi^0+e^++\nu)}{W(K^+ \to \mu^++\nu)}$	$\frac{1}{15}$	$\frac{1}{6.5}$	$\frac{1}{19.5}$	$\frac{1}{19.5}$
$R_2 \equiv \frac{W(K^+ \to \pi^0+\mu^++\nu)}{W(K^+ \to \pi^0+e^++\nu)}$	1	$\frac{1}{1.62}$	$\frac{1}{1.62}$	$\frac{1}{1.62}$
$R_3 \equiv \frac{W(K^+ \to \pi^++\pi^-+e^++\nu)}{W(K^+ \to \pi^0+e^++\nu)}$	?	7.26×10^{-4}	2.42×10^{-4}	2.42×10^{-4}
$R_5 \equiv \frac{W(K^+ \to \pi^++\pi^0)}{W(K_1^0 \to \pi^++\pi^-)}$	$\frac{1}{300}$	$\frac{1}{210}$	$\frac{1}{70}$	$\frac{1}{250}$
$R_6 \equiv \frac{W(K_1^0 \to \pi^0+\pi^0)}{W(K_1^0 \to 2\pi)}$	0.27 ± 0.11	0.24	0.24	0.27
$R_7 \equiv \frac{W(K^+ \to \pi^++\pi^-+\pi^+)}{W(K_1^0 \to 2\pi)}$	$\frac{1}{1500}$	$\frac{1}{106}$	$\frac{1}{320}$	$\frac{1}{320}$
$R_{10} \equiv \frac{W(K^0 \to \pi^-+e^++\nu)}{W(K_1^0 \to 2\pi)}$	6×10^{-4}	0.96×10^{-4}	2.9×10^{-4}	2.9×10^{-4}

The theoretical results in the last three columns are based on perturbation theory calculations with cut-off $\Lambda = 1.8\ m_p$. $\mathcal{D}$ denotes the damping of the matrix element for each pion emission from a baryon-anti-baryon loop. In the last column we choose the suppression of $\lvert\Delta I\rvert = \frac{3}{2}$ part in the matrix-element of diagrams involving fig. 2, so as to obtain a ratio $R_5 \approx 1/250$, in spite of taking $\mathcal{D}^2 = \frac{1}{3}$.

5. Concluding Remarks

Our investigation in the present paper depends largely on perturbation calculations. However, we feel that the essential qualitative features of the present discussion involving ratios of the decay rates of the various processes are treated reasonably by such calculations. If we admit this point of view, the present investigation of K meson decays brings out the following points. The various relative rates of K^+ and $K^0_{1,2}$ decay modes seem to be explained in the scheme of Λ decay adopted here (sect. 2). It is further found that the various features of the approximate $\lvert\Delta I\rvert = \frac{1}{2}$ rule in K-meson decays can be understood in the present scheme rather successfully. These, therefore, may be

regarded as some of the attractive features of the tetrahedron scheme † of four-fermion interactions. Furthermore, from the nature of results obtained in this attempt, it may be remarked that final state pion-pion interactions in S-state, suggested †† by others, need not be very important in order to explain the observed lifetimes of K^+ and K_1^0.

The necessity of damping the matrix-element by a factor $\approx \sqrt{3}$ for emission of a pion from a closed baryon-antibaryon loop (sects. 3 and 4) to correlate the rates of processes involving different numbers of pion emissions also seems to be rather suggestive. The fact that this damping is roughly consistent with the observed rate of the $\pi \to \mu+\nu$ decay indicates the plausibility of the assumption. In addition, it is rather striking that one gets a reasonable agreement in particular for the $W(K^+ \to \pi^0+e^++\nu)/W(K_1^0 \to 2\pi)$ ratio with experiment and for the reasons mentioned at the end of sect. 4.2, this could be taken to indicate the validity of the gross features of our approach. Finally, we may conclude that the minor discrepancies (within a factor 5) for some of the ratios of decay rates, obtained in the present attempt, may be explained by the slight influence of final state $\pi-\pi$ interaction and the dependence of the damping factor $\mathscr{D}$ of the matrix-elements on the energy release in corresponding processes.

Two of us (J. C. P. and S. O.) wish to express their gratitude to Professors Snow and Sucher for discussions. One of us (S. O.) wishes to thank Professors Toll, Snow and Sucher for their hospitality during his stay at the University of Maryland.

Appendix

In this appendix, we list the results of the lowest order perturbation-theory calculations for the various form factors of the different decay modes of K-meson, which have been discussed in the text. Some of these results (for diagrams involving fig. 2 or for leptonic-modes) have been derived by others [27]). For our purposes we assume (more or less in the spirit of Sakata model) that the K-meson decays take place through virtual $(N, \bar{\Lambda})$ system. In addition, for the evaluation of the various integrals encountered in the matrix-elements, we neglect the mass difference between Λ-hyperon and nucleon in so far as their

† If the tetrahedron scheme turns out to be the true feature of weak interactions it may lend evidence in favour of the Sakata model of elementary particles, which treats only the leptons, the nucleons and the Λ-hyperon as elementary. However, there could be some experimental checks. For instance, within the framework of the Sakata model, it is impossible to have $\Delta S/\Delta Q = -1$ currents [26]). Hence occurrence of a $\Sigma^+ \to n+e^++\nu$ decay will be rather fatal to the Sakata model.

†† Okubo and Marshak [15]), starting from an interaction containing an appreciable amount of $|\Delta I| = \frac{3}{2}$ part, suggested the possibility of a strong final state $\pi-\pi$ interaction in the $T = 0$, $J = 0$ state (leading to an enhancement by a factor ≈ 100 in the rate of $K_1^0 \to 2\pi$ decay) in order to explain the ratio $W(K^+ \to 2\pi)/W(K_1^0 \to 2\pi)$. Recently Good and Holladay [24]) starting from a strict $|\Delta I| = \frac{1}{2}$ weak interaction have indicated a possible explanation of the above ratio by electromagnetic interactions and strong final state $\pi-\pi$ interaction in the $T = 2$, $J = 0$ state.

masses occur in the denominators of the matrix-elements. We maintain, however, their mass-difference in the numerator. We further adopt the convention (as an approximation) that expressions of the form $m_p{}^2x$ or $m_\Lambda{}^2x$ in the denominator will be replaced by $\bar{M}^2x$, where $\bar{M}^2 \equiv \frac{1}{2}(m_\Lambda{}^2+m_p{}^2)$. We give below only the leading terms (in powers of $m_p{}^2$) of the different form-factors. It is estimated that these approximations are not expected to lead to more than 10 % error in the various decay rates.

The following are the expressions obtained for the various form factors in the lowest order perturbation theory:

$$K^+ \to \mu^+ + \nu: \quad I \approx 4\pi^2 i \frac{\Lambda^2}{m_p{}^2}[m_p m_\Lambda I_0 - \tfrac{1}{2}m_p(m_\Lambda - m_p)I_1], \tag{51}$$

$$K^+ \to \pi^0 + \mu^+ + \nu: \quad \mathscr{J}_1 \approx -4\pi^2 i \frac{\Lambda^2}{m_p{}^2}[\tfrac{1}{2}m_p{}^2(I_1+I_2)+\tfrac{1}{2}m_p{}^3(m_\Lambda I_3+\tfrac{1}{3}m_p I_4)], \tag{52}$$

$$\mathscr{J}_2 \approx +4\pi^2 i \frac{\Lambda^2}{m_p{}^2}[m_p{}^2(I_1-\tfrac{1}{2}I_2)+\tfrac{1}{2}m_p{}^3(m_\Lambda I_3-\tfrac{1}{3}m_p I_4)], \tag{53}$$

$$K^+ \to \pi^+ + \pi^- + \mu^+ + \nu: \quad K_1 \approx 4\pi^2 i \frac{m_p+2m_\Lambda}{6m_p}, \tag{54}$$

$$K_2 \approx 4\pi^2 i \frac{m_p - m_\Lambda}{6m_p}, \quad K_3 \approx 4\pi^2 i \frac{2m_p+m_\Lambda}{6m_p},$$

$$K^+ \to \pi^+ + \pi^0: \quad L_1 = \mathscr{J}_1, \quad L_2 = \mathscr{J}_2, \tag{55}$$

$$K_1{}^0 \to \pi^+ + \pi^-: \quad \mathscr{M} \approx 4\pi^2 i \frac{\Lambda^2}{m_p{}^2}[\tfrac{1}{3}m_p{}^5 m_\Lambda I_5 + \tfrac{1}{3}m_p{}^3(m_p+m_\Lambda)I_4 + m_p{}^2 I_2], \tag{56}$$

$$K^+ \to \pi^+ + \pi^- + \pi^+: \quad N_1 = K_1, \quad N_2 = K_2, \quad N_3 = K_3, \quad \mathscr{O} \approx 4\pi^2 i(m_\Lambda/2m_p), \tag{57}$$

where

$$I_0 = \int_0^1 \frac{x}{\Lambda^2 - Bx}\,dx, \quad I_3 = \int_0^1 \frac{x^2}{(\Lambda^2 - Bx)^2}\,dx,$$

$$I_1 = \int_0^1 \frac{x^2}{\Lambda^2 - Bx}\,dx, \quad I_4 = \int_0^1 \frac{x^3}{(\Lambda^2 - Bx)^2}\,dx, \tag{58}$$

$$I_2 = \int_0^1 \frac{x^3}{\Lambda^2 - Bx}\,dx, \quad I_5 = \int_0^1 \frac{x^3}{(\Lambda^2 - Bx)^3}\,dx.$$

Here, Λ denotes the Feynman cut-off, introduced for evaluation of the above form-factors and $B \equiv \Lambda^2 - \bar{M}^2$.

References

1) B. Sakita and S. Oneda, Nuclear Physics **16** (1960) 72
2) S. Oneda, J. C. Pati and B. Sakita, Physics Department Technical Report (Maryland University) no. 160 (Phys. Rev., to be published)
3) E. C. G. Sudarshan and R. E. Marshak, Proceedings of the Padua-Venice Conference (September, 1957); Phys. Rev. **109** (1958)1860;
R. P. Feynman and M. Gellmann, Phys. Rev. **109** (1958) 193
4) D. A. Glaser, Reports on Kiev-Conference (1959). (Further references can be found here)
5) S. Weinberg, Phys. Rev. **115** (1959) 481
6) B. Sakita, Phys. Rev. **114** (1959) 1650;
C. H. Albright, Phys. Rev. **114** (1959) 1648
7) S. Oneda, Nuclear Physics **9** (1959) 476;
R. F. Sawyer, Phys. Rev. (to be published)
8) Okubo, Marshak, Sudarshan, Teutsch and Weinberg, Phys. Rev. **112** (1958) 665;
L. B. Okun, Proceedings of the Padua-Venice Conference (September, 1957)
9) Crawford, Cresti, Roger, Douglass, Good, Kalbfleisch and Stevenson, Phys. Rev. Lett. **2** (1959) 361
10) Okubo, Marshak and Sudarshan, Phys. Rev. **113** (1959) 944
11) K. Chadan and S. Oneda, Phys. Rev. Lett. **3** (1959) 292;
V. S. Mathur, Nuovo Cimento **14** (1959) 1322;
L. B. Okun and E. P. Shabalin (see report by R. E. Marshak at Kiev Conference, 1959)
12) S. Oneda, Nuclear Physics **9** (1959) 476;
A. Fujii and M. Kawaguchi, Phys. Rev. **113** (1959) 1156;
R. Gatto, Phys. Rev. **111** (1958) 1426;
R. F. Streater and J. C. Taylor, Nuclear Physics **7** (1958) 276
13) L. Okun, Ann. Rev. Nuclear Science **9** (1959) 61
14) K. Chadan and S. Oneda, Physics Department Technical Report (University of Maryland) no. 168
15) S. Okubo and R. E. Marshak, Phys. Rev. **100** (1955) 1809
16) Crawford, Cresti, Douglass, Good, Kalbfleisch, Stevenson and Ticho, Phys. Rev. Lett. **2** (1959) 266
17) S. Oneda, Nuclear Physics **9** (1959) 476;
R. H. Dalitz, Phys. Rev. **99** (1955) 915
18) R. H. Dalitz, Rev. Mod. Phys. **31** (1959) 823;
A. Pais and S. B. Treiman, Phys. Rev. **106** (1957) 1106;
Okubo, Marshak and Sudarshan, Phys. Rev. Lett. **2** (1959) 12;
M. Gellmann and A. H. Rosenfeld, Ann. Rev. Nuclear Science **1** (1957) 407
19) Birge, Perkins, Stork and Whitehead, Nuovo Cimento **4** (1956) 834;
Alexander, Johnston and O'Ceallaigh, Nuovo Cimento **6** (1957) 478
20) Crawford, Cresti, Douglass, Good, Kalbfleisch and Stevenson, Phys. Rev. Lett. **2** (1959) 361
21) S. Oneda, Nuclear Physics **9** (1959) 476
22) R. H. Dalitz, Phil. Mag. **44** (1953) 1068; Proc. Phys. Soc. A **69** (1956) 527
23) M. Gellmann and A. H. Rosenfeld, Ann. Rev. Nuclear Science **7** (1957) 407
24) M. L. Good and W. G. Holladay, Phys. Rev. Lett. **4** (1960) 138
25) B. S. Thomas and W. G. Holladay, Phys. Rev. **115** (1959) 1329
26) S. Oneda, Reports on Padua-Venice Conference (1957);
L. Okun, Ann. Rev. Nuclear Science **9** (1959) 61
27) A. Fujii and M. Kawaguchi, Phys. Rev. **113** (1959) 1156;
S. Oneda, Nuclear Physics **9** (1959) 476;
V. S. Mathur, Nuovo Cimento **14** (1959) 1322

2.E

Nuclear Physics **18** (1960) 338—345; © *North-Holland Publishing Co., Amsterdam*

Not to be reproduced by photoprint or microfilm without written permission from the publisher

A BREMSSTRAHLUNG EXPERIMENT TO MEASURE THE TIME DELAY IN NUCLEAR REACTIONS

R. M. EISBERG and D. R. YENNIE

University of Minnesota, Minneapolis 14, *Minnesota*, U.S.A.

and

D. H. WILKINSON

Clarendon Laboratory, Oxford, England

Received 29 April 1960

Abstract: It should be possible to measure the time delay in a nuclear reaction, in which both the incident and product particles are charged, by measuring the spectrum of the bremsstrahlung that is produced. The time delay enters the spectrum through a phase factor between the bremsstrahlung amplitude associated with the cessation of the current due to the incident particle and the bremsstrahlung amplitude associated with the initiation of the current due to the product particle. The classical theory of this bremsstrahlung production process is developed, and results which will be useful in estimating the feasibility of a measurement are obtained. Because of the recoil of the charged nucleus, this technique could also be used even if the incident and/or product particles are uncharged.

There are several reasons why there would be interest in a method for measuring the delay between the time at which an incident particle strikes a nucleus and the time at which a product particle is emitted. For instance, such a method would make it possible to measure the cross section for compound elastic scattering. From the point of view of the nuclear optical model, this delayed process is a reaction even though it is elastic. Therefore, in analyzing experiments with the optical model, its cross section should be subtracted from the observed cross section for elastic scattering and added to the observed cross section for reactions (addition and subtraction of cross sections is valid if the statistical assumption is satisfied). The failure to do this is probably responsible for many of the problems which have arisen in applying the optical model to the lower energy experiments [1]). A method of measuring time delay would also allow an unambiguous separation between compound nucleus reactions and direct interactions by utilizing the fact that compound nucleus reactions are delayed. We propose here a method for measuring time delay, and discuss its application to the elastic scattering problem.

Consider a charged particle entering a nucleus, and, after a time τ, a product particle being emitted elastically at some angle θ_{p_f}. In this process there will be a certain net amplitude for the emission of bremsstrahlung. One component of this net amplitude will arise from the cessation of the current associated with

the incident particle, and the other component will arise from the initiation of the current associated with the product particle. The net amplitude will depend on the charge and velocity of the particles, on the scattering angle θ_{p_t}, on the angle of emission of the bremsstrahlung θ_γ, and also on the time delay τ. The time delay comes in through the fact that it leads to a phase difference $\exp(i\omega\tau)$ between the two components. For small values of $\omega\tau$, the two components can interfere coherently (either constructively or destructively, depending on θ_{p_t} and θ_γ), producing the usual bremsstrahlung spectrum. As $\omega\tau$ increases, the interference between the two components is altered, the interference term being proportional to $\cos\omega\tau$. It is apparent then that the effect would be noticeable experimentally for bremsstrahlung energies of the order

$$E = \hbar\omega \approx \frac{\hbar}{\tau}. \tag{1}$$

In a more realistic situation, the delay time would not have a precise value, but would be distributed according to some probability law $P(\tau)$. We might assume, for a simple example, a time delay distribution of the form

$$P_1(\tau) = C\delta(\tau) + (1-C)\tau_{CE}^{-1} e^{-\tau/\tau_{CE}}, \tag{2}$$

where C is the relative amount of shape elastic scattering, $(1-C)$ is the relative amount of compound elastic scattering, τ_{CE} is the compound elastic delay time (the compound nucleus lifetime), and where we restrict ourselves to frequencies low enough so that the shape elastic scattering can be treated as instantaneous. In place of $\cos\omega\tau$, the interference term would now have the factor

$$G_1(\omega) = C + (1-C)[1+(\omega\tau_{CE})^2]^{-1}. \tag{3}$$

The bremsstrahlung spectrum would have the form sketched in fig. 1 (for fixed proton and photon directions). It is apparent that a measurement of the form of the spectrum would lead to a determination of both C and τ_{CE}.

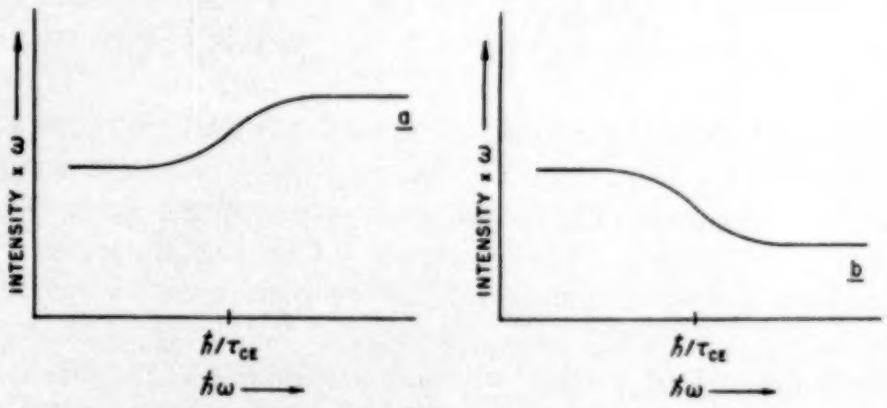

Fig. 1. Unnormalized bremsstrahlung intensity pattern for (a) case in which the interference without time delay is destructive, (b) case in which the interference without time delay is constructive.

It is also apparent that this method could be applied to any reaction in which both the incident and product particles are charged. In any of these experiments it would be, of course, necessary to operate the energy sensitive bremsstrahlung detector in coincidence with a counter which detects the emission of a product particle into the proper energy and angular range. For bremsstrahlung energies greater than several keV, a proportional counter would provide an energy sensitive detector with essentially unity efficiency and enough resolution to discriminate against the line spectrum X-rays which would be present as a background. Because these experiments involve coincidences, they would be performed most easily with a particle accelerator of high duty cycle. The elastic scattering experiment might initially use protons of about 5 MeV from a Van de Graaff. At this energy, scattering on light nuclei probably involves considerable compound elastic scattering, but scattering from heavy nuclei involves only shape elastic scattering from the Coulomb barrier. Consequently, at this energy there should be an experimentally observable change in the bremsstrahlung spectrum from light to heavy nuclei. Furthermore, for 5 MeV protons, background bremsstrahlung from delta ray electrons are of negligible intensity, at bremsstrahlung energies greater than several keV, due to the delta ray energy cut-off.

There is no way of making an accurate a priori estimate of τ_{CE} since we are dealing with excitation of the compound nucleus into its continuum states. However, an extrapolation of measured level widths from the energy region in which sharp levels can be resolved to the energy region corresponding to incident proton energies of the order of 5 or 10 MeV, using the relation $\Gamma \propto$ (kinetic energy)$^{\frac{1}{2}}$, leads to estimates ranging from $\tau_{CE} \approx 10^{-19}$ sec for light nuclei to $\tau_{CE} \approx 10^{-16}$ sec for heavy nuclei. The break in the curves of fig. 1 would thus occur at bremsstrahlung energies ranging from ≈ 6 keV for light nuclei to ≈ 6 eV for heavy nuclei. Thus for light nuclei it should be possible to make measurements which would be comprehensive enough to determine both C and τ_{CE}. For heavy nuclei it would probably only be possible to make measurements at bremsstrahlung energies $E \gg \hbar/\tau_{CE}$, but this would allow the determination of C.

We shall now give a quantitative classical treatment of this process. A quantal treatment will be given in a separate paper [2]). Since we are interested in calculating the emission of photons whose wave length is large compared to the nuclear radius, we can make certain simplifying approximations. The essence of these approximations is that the bremsstrahlung does not depend on the details of the scattering process, but only on the charge and current distributions in large regions of space (distances of order $\lambda\!\!\!^{-}_{\gamma}$). That is, as we have mentioned, it depends mainly on the properties of the trajectory of the charged particle (hereafter called proton) before entering and after leaving the scattering region.

We divide the charge-current distribution of the proton into three parts: (i) a contribution due to an idealized incident motion along a straight line at constant velocity, in which the proton arrives at the centre of the nucleus at $t' = 0$; (ii) a similar idealized motion in which the proton leaves the centre of the nucleus at $t' = \tau$; (iii) the residual contribution, which consists of the actual distribution minus the idealized ones contained in (i) and (ii). This residual contribution exists for a length of time of order τ within a spatial region of dimensions of order a, characteristic of the scattering region. (The case of the Coulomb potential in principle requires a special treatment because the scattering starts at large distances. However, a discussion by H. Suura [3]) for the case of a static Coulomb potential indicates that our arguments are valid even for long range potentials, providing the main deflection takes place in a small region). Our approximation will be to neglect this residual contribution; it will be shown to be smaller by a factor of order ka than the contribution retained. The contribution which is retained corresponds to the $d\omega/\omega$ part of the ordinary bremsstrahlung spectrum. At sufficiently small ω, this will dominate the contribution which is neglected.

The current density is accordingly written as the sum of three terms,

$$\begin{aligned}\mathbf{j}(\mathbf{x}', t') = {} & e\mathbf{V}_1\delta(\mathbf{x}'-\mathbf{V}_1t')\theta(-t') \\ & +e\mathbf{V}_t\delta(\mathbf{x}'-\mathbf{V}_tt'+\mathbf{V}_t\,\tau)\theta(t'-\tau) \\ & +\mathbf{j}'(\mathbf{x}', t'),\end{aligned} \tag{4}$$

where θ is the discontinuous function

$$\theta(\xi) = \begin{cases} 1 & (\xi > 0), \\ 0 & (\xi < 0); \end{cases}$$

$\mathbf{j}'$ is, of course, the residual contribution (iii). The radiated field (obtained by subtracting the final proper field of the proton from the total retarded field) is

$$\begin{aligned}\mathbf{A}_{\mathrm{rad}}(\mathbf{x}, t) = e\left\{\frac{\mathbf{V}_1\theta(R-ct)}{|\mathbf{x}-\mathbf{x}'|-\boldsymbol{\beta}_1\cdot(\mathbf{x}-\mathbf{x}')}\bigg|_{\mathrm{ret}} - \frac{\mathbf{V}_t\theta(R+c\tau-ct)}{|\mathbf{x}-\mathbf{x}'|-\boldsymbol{\beta}_t\cdot(\mathbf{x}-\mathbf{x}')}\bigg|_{\mathrm{ret}}\right\} \\ +\int \mathrm{d}^3x'\,\mathbf{j}'\left(\mathbf{x}', t-\frac{|\mathbf{x}-\mathbf{x}'|}{c}\right)\Big/\,|\mathbf{x}-\mathbf{x}'|,\end{aligned} \tag{5}$$

where $\boldsymbol{\beta}_1 = \mathbf{V}_1/c$, $\boldsymbol{\beta}_t = \mathbf{V}_t/c$, $R = |\mathbf{x}|$.

Next we Fourier transform with respect to the time variable. Developing the resulting expression in inverse powers of R, and keeping only the leading term, we find

$$\begin{aligned}\mathbf{A}_{\mathrm{rad}}(\mathbf{x}, \omega) &= \int_{-\infty}^{\infty}\mathbf{A}_{\mathrm{rad}}(\mathbf{x}, t)\mathrm{e}^{i\omega t}\,\mathrm{d}t \\ &\approx \frac{\mathrm{e}^{i\omega R/c}}{R}\left\{\frac{ec}{i\omega}[\boldsymbol{\lambda}_1-e^{i\omega\tau}\boldsymbol{\lambda}_t]+\int \mathrm{d}^3x'\,\mathrm{e}^{-i\mathbf{k}\cdot\mathbf{x}'}\int_{-\infty}^{\infty}\mathrm{d}t\,\mathrm{e}^{i\omega t}\mathbf{j}'(\mathbf{x}', t)\right\}.\end{aligned} \tag{6}$$

where $\mathbf{k} = \mathbf{n}\omega/c = \mathbf{n}k$, $\mathbf{n} = \mathbf{x}/|\mathbf{x}|$, $\boldsymbol{\lambda}_1 = \boldsymbol{\beta}_1/(1-\mathbf{n}\cdot\boldsymbol{\beta}_1)$ and similarly for $\boldsymbol{\lambda}_f$. To illustrate the development in inverse powers of R, the first term of eq. (6) was obtained in the following manner:

$$\int_{-\infty}^{R/c} \frac{e^{i\omega t}}{f(t)}\,dt = \frac{1}{i\omega}\frac{e^{i\omega R/c}}{f(R/c)} + \frac{1}{i\omega}\int_{-\infty}^{R/c} \frac{f'(t)e^{i\omega t}}{[f(t)]^2}\,dt.$$

Since $f \approx R$, $f' \approx V$, the second term becomes negligible as $R \to \infty$.

We can now give the expression for the bremsstrahlung associated with this vector potential. This depends on the absolute square of the component of $\mathbf{A}$ perpendicular to $\mathbf{k}$ (from the photon point of view, this includes the sum over polarization). The normalization is most easily determined by comparison with the usual bremsstrahlung formula which corresponds to $\tau = 0$. Neglecting the contribution arising from $\mathbf{j}'$, we find

$$\frac{\sigma(\hat{\mathbf{p}}_f, \hat{\mathbf{k}}, \omega)\,d\Omega_\gamma d\omega}{\sigma_{el}(\hat{\mathbf{p}}_f)} = \frac{\alpha}{(2\pi)^2}[\mathbf{n}\times\boldsymbol{\lambda}_1)^2 + (\mathbf{n}\times\boldsymbol{\lambda}_f)^2 - 2(\mathbf{n}\times\boldsymbol{\lambda}_1)\cdot(\mathbf{n}\times\boldsymbol{\lambda}_f)\cos\omega\tau]d\Omega_\gamma\,d\omega/\omega, \quad (7)$$

where $\sigma_{el}(\hat{\mathbf{p}}_f)$ is the elastic scattering cross section for the proton. The right hand side of eq. (7) is the probability that if the particle has scattered in the direction $\hat{\mathbf{p}}_f$, a photon will be emitted in the indicated angular and energy range. Averaging eq. (7) over the distribution of decay times $P(\tau)$, we find

$$\frac{\sigma(\hat{\mathbf{p}}_f, \hat{\mathbf{k}}, \omega)d\Omega_\gamma d\omega}{\sigma_{el}(\hat{\mathbf{p}}_f)} = \frac{\alpha}{(2\pi)^2}\{[\mathbf{n}\times(\boldsymbol{\lambda}_1-\boldsymbol{\lambda}_f)]^2 + 2(\mathbf{n}\times\boldsymbol{\lambda}_1)\cdot(\mathbf{n}\times\boldsymbol{\lambda}_f)[1-G(\omega)]\}d\Omega_\gamma\,d\omega/\omega, \quad (8)$$

where $G(\omega) = \int_0^\infty P(\tau)\cos\omega\tau d\tau$.

The same result is obtained in the quantal treatment [2]), where $G(\omega)$ may be expressed in terms of the scattering amplitudes f for the scattering angle θ_{p_f}, at two different energies separated by $\hbar\omega$;

$$G(\omega) = \frac{\mathrm{Re}[f^*(\theta, E_1-\hbar\omega)f(\theta, E_1)]}{|f(\theta, E_1)|^2}.$$

The quantity of theoretical interest is $G(\omega)$,and this is what is measured in the experiment. However, in a classical treatment it is convenient to relate $G(\omega)$ to the distribution of delay times $P(\tau)$ as in eq. (8). In the particular simple example $P_1(\tau)$ of eq. (2), this gives $G_1(\omega)$ of eq. (3). But in general it would probably not be possible to fit the actual experimental results by eq. (3).

The result just obtained must be modified to take into account the effect of

nuclear recoil [4]). It is simplest to consider the process in the centre of mass frame. Then, during the time interval $0 \leqq t \leqq \tau$, the current is very small; and the contribution of the nucleus to the amplitude (6) is easily obtained. The result is that $\boldsymbol{\lambda}_1$ must be redefined as follows

$$\boldsymbol{\lambda}_1 = \frac{\boldsymbol{\beta}_1}{1-\mathbf{n}\cdot\boldsymbol{\beta}_1} - \frac{ZM_P}{M_A}\boldsymbol{\beta}_1, \tag{9}$$

and similarly for $\boldsymbol{\lambda}_f$, where M_P is the proton mass and M_A is the nuclear mass (neglecting retardation for the amplitude emitted by the nucleus). This reduces the bremsstrahlung cross section approximately by the factor $(1-Z/A)^2$. It is clear that nuclear recoil will produce bremsstrahlung even if the incident or scattered particle is uncharged. If the incident particle is neutral, the first term of (9) should be dropped; similarly the definition of $\boldsymbol{\lambda}_f$ would have to be changed if the final particle is neutral. The charge Z would be that, Z_1 or Z_f, of the target or product nucleus respectively; and $M_P\boldsymbol{\beta}_1$ or $M_P\boldsymbol{\beta}_f$ the momentum of the incident or final particle, respectively. The quantity $G(\omega)$ would be expressed in terms of the trasition matrix element, instead of simply the scattering amplitude. The use of neutral incident particles might be advantageous experimentally, since it would eliminate background bremsstrahlung which might lead to accidental coincidences.

In estimating the background for a possible experiment, it is interesting to compare our result with the total cross section for production of photons with energy $\hbar\omega$ into the solid angle $d\Omega_\gamma$. Because of the factor $\sigma_{el}(\hat{p}_f)$ occurring in the cross section, most of this total cross section will come from the forward Coulomb scattering of the protons. Since the Coulomb scattering dominates, we can use the standard bremsstrahlung formula [5]) for the estimate. For simplicity, we give the expression in the non-relativistic limit:

$$\sigma_{tot}(\mathbf{k}) = \frac{Z^2\alpha^3}{\pi}\frac{1}{\omega_k{}^2} I(\theta_\gamma, E/\hbar\omega)\left(1-\frac{ZM_P}{M_A}\right)^2, \tag{10a}$$

where θ_γ is the angle of emission of the photon,

$$I(\theta_\gamma, E/\hbar\omega) = (2-\sin^2\theta_\gamma)\ln\frac{4E}{\hbar\omega} - (2-3\sin^2\theta_\gamma), \tag{10b}$$

and $E = p^2/2m$. The ratio of the expected number of coincidences to the total cross section (in the non-relativistic approximation) is given by

$$\frac{\sigma(\hat{\mathbf{p}}_f, \hat{\mathbf{k}}, \omega)\,d\Omega_{p_f}}{\sigma_{tot}(\mathbf{k})} = \frac{[\hat{\mathbf{n}}\times(\boldsymbol{\beta}_1-\boldsymbol{\beta}_f)]^2 + 2(\mathbf{n}\times\boldsymbol{\beta}_1)\cdot(\mathbf{n}\times\boldsymbol{\beta}_f)[1-G(\omega)]}{16\pi\beta^2\sin^4\frac{1}{2}\theta_{p_f} I(\theta_\gamma, E/\hbar\omega)} \times \frac{\sigma_{el}(\theta_{p_f})}{\sigma_{Ruth}(\theta_{p_f})}\,d\Omega_{p_f}, \tag{11}$$

where σ_{Ruth} is the Rutherford scattering cross section, and θ_{p_f} is the scattering angle of the proton.

We should confirm that the contribution arising from $\mathbf{j}'$ is of relative order ka, and hence negligible. The relative importance of this contribution is given by

$$\frac{k}{e\beta}\left|\int \mathrm{d}^3x e^{-i\mathbf{k}\cdot\mathbf{x}}\int_{-\infty}^{\infty}\mathrm{d}t\, e^{i\omega t}\mathbf{j}'(\mathbf{x},t).\right|. \tag{12}$$

Let us neglect possible oscillations of the nuclear system, and treat only the motion of the scattering particle. Let $\mathbf{x}(t)$ be its actual trajectory and $\mathbf{x}_1(t)$ be its idealized trajectory. Then

$$\mathbf{j}'(\mathbf{x},t) = e\left\{\frac{\mathrm{d}\mathbf{x}}{\mathrm{d}t}\delta[\mathbf{x}-\mathbf{x}(t)] - \frac{\mathrm{d}\mathbf{x}_1}{\mathrm{d}t}\delta[\mathbf{x}-\mathbf{x}_1(t)]\right\}. \tag{13}$$

Since $ka \ll 1$, we are justified in making a multipole expansion of $\exp(-i\mathbf{k}\cdot\mathbf{x})$; the first term is

$$\frac{k}{\beta}\left|\int_{-\infty}^{\infty}\left(\frac{\mathrm{d}\mathbf{x}}{\mathrm{d}t}-\frac{\mathrm{d}\mathbf{x}_1}{\mathrm{d}t}\right)e^{i\omega t}\mathrm{d}t\right| = \frac{\omega k}{\beta}\left|\int_{-\infty}^{\infty}(\mathbf{x}-\mathbf{x}_1)e^{i\omega t}\mathrm{d}t\right|. \tag{14}$$

The integrated term vanishes because $\mathbf{x} = \mathbf{x}_1$ before and after the collision. Now $|\mathbf{x}-\mathbf{x}_1| \gtrsim a$, and hence the relative contribution of $\mathbf{j}'$ is less than $ka \cdot \omega\tau/\beta$. This is probably a considerable overestimate. If the particle has many reflections from the edge of the nucleus, the time average of $(\mathbf{x}-\mathbf{x}_1)$ will be considerably smaller in magnitude than a. A random walk argument suggests that it will be of order $a/\sqrt{N}$, where N is the number of reflections in the time considered. Since $N \approx V\tau/a$, this would change the estimate to $[(ka)^3\omega\tau/\beta^3]^{\frac{1}{2}}$, providing $N \lesssim 1$. Since we are primarily interested in situations where $\omega\tau \sim 1$, $ka \ll 1$, we shall be justified in neglecting $\mathbf{j}'$. A quantal treatment [2]) shows that (8) is correct (with a certain interpretation for $G(\omega)$) within an error of order ka.

We prefer not to give detailed estimates of the feasibility of this experiment, since this depends on the details of the experimental apparatus which would be used. However, it may be of interest to indicate the order of magnitude of the effect for a special example. If we choose $\mathbf{k}$ in the direction of $(\boldsymbol{\lambda}_1-\boldsymbol{\lambda}_f)$, the probability of coincidence would be zero if there were no time delay. Because of the time delay, $G(\omega)$ differs from 1, in general, and eq. (8) reduces to

$$\left(\frac{\alpha}{\pi^2}\frac{E}{mc^2}\right)[1-G(\omega)](1-ZM_{\mathrm{p}}/M_{\mathrm{A}})^2\cos^2\tfrac{1}{2}\theta_{p_f}\mathrm{d}\Omega_\gamma\mathrm{d}\omega/\omega. \tag{15}$$

For 5 MeV protons, the coefficient $\alpha E/\pi^2mc^2$ is approximately 4×10^{-6}. This expression will vanish in the forward direction where Coulomb scattering dominates and $G(\omega) \approx 1$. If the fraction of time-delayed protons is large

($\approx \frac{1}{2}$), it should be possible to find situations in which the probability of coincidence is $\approx 0.25 \times 10^{-6} \mathrm{d}\Omega_\gamma \mathrm{d}\omega/\omega$.

For the same example (**k** parallel to $\beta_1 - \beta_f$), the ratio of the coincidence cross section to the non-coincident cross section reduces to

$$\frac{[1-G(\omega)] \cos^2 \frac{1}{2}\theta_{p_f}}{8\pi \sin^4 \frac{1}{2}\theta_{p_f}[(2-\cos^2 \frac{1}{2}\theta_{p_f}) \ln \frac{4E}{\hbar\omega} - (2-3\cos^2 \frac{1}{2}\theta_{p_f})]} \frac{\sigma_{el}(\theta_{p_f})}{\sigma_{Ruth}(\theta_{p_f})}. \tag{16}$$

For $\theta_{p_f} = 90°$, this becomes

$$\frac{[1-G(\omega)]}{\pi\left(3 \ln \frac{4E}{\hbar\omega} - 1\right)} \frac{\sigma_{el}(90°)}{\sigma_{Ruth}(90°)} \mathrm{d}\Omega_{p_f}.$$

Feasibility estimates which we have made, on the basis of equations (15) and (16), indicate tht an experiment would be difficult, but certainly possible.

It is a pleasure to acknowledge useful conservations with Drs. S. C. Frautschi, W. B. Cheston and G. E. Brown.

References

1) Proceedings of International Conference on Nuclear Optical Model (Florida State University Studies No. 32, 1959)
2) Feshbach and Yennie (to be published)
3) H. Suura, Phys. Rev. **99** (1955) 1020
4) Sommerfeld, Atombau and Spektrallinien (Vieweg, Braunschweig, 1939) Bd. II, p. 565
5) Gluckstern and Hull, Phys. Rev. **90** (1953) 1930

2.J

Nuclear Physics **18** (1960) 346—352; © *North-Holland Publishing Co., Amsterdam*

Not to be reproduced by photoprint or microfilm without written permission from the publisher

WINKELVERTEILUNGEN VON KERNSPALTUNGEN IM RESONANZBEREICH

O. HITTMAIR

Atominstitut der Österreichischen Hochschulen, Wien

Eingegangen am 19. April 1960

Abstract: An expression for the angular distribution of resonance fission is developed under the condition that the nucleus preserves its axial symmetry in the process of fission. This is achieved by reducing the representation product which describes the orientation of the nuclear symmetry axis in space with respect to the entrance channel. The result is expressed in Racah coefficients and Legendre polynomials. General predictions about the symmetry of the angular distribution and the effect of polarized incident neutrons can be made. The formula is applied to the resonance fission of Th^{232} for incident 1.60 MeV neutrons, adopting the unified model. Excellent agreement with experiment is obtained if the resonance is ascribed to rotational levels of the $\frac{1}{2}$-band of negative parity.

1. Einleitung

Winkelverteilungen von Kernspaltungen sind einerseits schwieriger zu analysieren als diejenigen normaler Kernreaktionen im Resonanzgebiet, da sich die Fülle der Ausgangskanäle der Spaltprodukte höchstens statistisch erfassen läßt. Andererseits aber liegt bei der Annahme, daß der sich spaltende Kern nach dem Sattelpunkt seine axiale Symmetrie beibehält, die Winkelverteilung schon mit der Richtung der Kernsymmetrieachse am Sattelpunkt fest. Die Winkelverteilung ist also bei dieser Annahme schon durch den Zwischenkernzustand am Sattelpunkt vollständig gegeben.

Dies legt den Gedanken nahe, das Darstellungsprodukt, das die räumliche Orientierung der Kernsymmetrieachse beschreibt [1, 2]), nach der Eingangsseite hin auszureduzieren, wo sich die Quantenzahlen der einfallenden Strahlung leichter überblicken lassen. Dies wird im folgenden durchgeführt und das Ergebnis durch Racah-Koeffizienten und Legendre-Polynome ausgedrückt. Es ergeben sich allgemeine Aussagen über die Symmetrie von Spaltungswinkelverteilungen und über Verteilungseffekte durch polarisierte Neutronen. Schließlich wird die erhaltene Formel dazu benützt, die Winkelverteilung der Spaltungsresonanz von Th^{232} für 1.60 MeV-Neutronen nach Messungen von Henkel und Brolley [3]) zu analysieren, die bereits von Wilets und Chase [4]) mit einer Verteilungsfunktion in nicht ausreduzierter Form und willkürlichen Parametern diskutiert wurde.

Spaltungswinkelverteilungen für einfallende Strahlung mittlerer Energie, die

sich im Gegensatz zu den hier betrachteten im Niveaukontinuum des Zwischenkerns vollziehen, wurden in letzter Zeit ausführlich von Halpern und Strutinskii [5]) und von Griffin [6]) behandelt.

2. Das Niveauspektrum am Sattelpunkt

Starke Anisotropien der Winkelverteilung und vor allem rasche Änderungen mit der Energie zeigen sich hauptsächlich in der Nähe der Spaltungsschwelle. Das kollektive Modell von Bohr und Mottelson erweist sich hier als nützliches Erklärungsmittel, indem es Aussagen über die verhältnismäßig wenigen Energieniveaus macht, über die sich der Spaltungsvorgang an der Schwelle vollzieht [1]). In diesem Falle ist ja ein Großteil der zugeführten Energie am Sattelpunkt, wo die Kerndeformation irreversibel wird, als potentielle Energie der Deformation vorhanden, so daß der Kern dort fast kalt ist. Aus diesem Grunde geht auch die aperiodische Bewegung über den Sattelpunkt langsam genug vor sich, daß man zwar nicht von einem stationären, aber doch von einem quasistationären Niveauspektrum sprechen kann. Die Quantenzahlen dieser Niveaus sind nach dem kollektiven Kernmodell I, K, M und Ω, wo I den Drehimpuls des sich spaltenden Kerns, K und M seine Projektion auf die Symmetrie- bzw. auf die z-Achse und Ω die Drehimpulsprojektion des etwa vorhandenen ungeraden Nukleons auf die Symmetrieachse bedeuten.

Es ist zweifelhaft, ob man auch bei höheren Energien, also schon bei Anregungen von 30 bis 40 MeV, K und Ω als gute Quantenzahlen betrachten darf. Für mittlere Energien in der Gegend von 10 MeV dient K zumindest als nützlicher Parameter für die Analysierung von Spaltungswinkelverteilungen [5,6]). Das Problem ist dort jedoch im Gegensatz zu den hier betrachteten Spaltungsresonanzen einzelner Niveaus die statistische Mittelung über ein Niveaukontinuum.

Für gerade Kerne gibt das kollektive Modell für die Rotationsbande, die sich auf dem Grundzustand aufbaut, ein Energiespektrum mit $K = \Omega = 0$,

$$E = CI(I+1), \tag{1}$$

wo die Konstante C für schwere Kerne einen Wert von ungefähr 7 keV hat. Für das Auftreten einer neuen Rotationsbande ist das Überwinden der Nukleonenpaarungsenergie von ungefähr 1 MeV nötig. Bei ungeraden Kernen hingegen liegen die inneren Zustände, auf denen sich Rotationsbanden aufbauen können, schon in Abständen von ungefähr 200 keV. Es läßt sich also abschätzen, daß an einer Spaltungsresonanz, wo das Spektrum dem des kalten Zustands ähnlich ist und die Abstände der Niveaus infolge der Deformation noch geringer sind, im allgemeinen mehrere Niveaus einer Bande und besonders im Falle ungerader Kerne mehrere Banden beteiligt sein werden.

3. Die Winkelverteilungsfunktion und die Reduktion des Darstellungsprodukts

Mit der Annahme, daß die Richtung der Spaltungsfragmente durch die Kernsymmetrieachse am Sattelpunkt bestimmt wird, liegt die Winkelverteilung schon mit den Zwischenkernquantenzahlen I, M und K am Sattelpunt fest. Für die Winkelverteilung kann man dann also schon diesen Zustand als Endzustand ansehen, da weitere Einzelheiten in der Art der Aufspaltung keinen Einfluß mehr auf sie haben. Man kann also die Reaktionsmatrix R, die durch $|R|^2$ die Wahrscheinlichkeit des betrachteten Prozesses pro Zeiteinheit angibt, als $\langle IKM|R|lsm\mu\rangle$ schreiben, wo l, s, m, μ Bahndrehimpuls und Kanalspin der einfallenden Strahlung sowie deren Projektion auf die z-Achse bedeuten. Weitere für den jeweiligen Sattelpunktzustand charakteristische, aber für die Winkelverteilung der folgenden Spaltung unwesentliche Quantenzahlen wurden weggelassen. Man erhält so für die Reaktionsamplitude

$$q_{IKM,s\mu} = -\sqrt{(2I+1)\pi} \sum_{l,m} D^I_{MK}(\varphi, \vartheta, \psi)\langle IKM|R|lsm\mu\rangle\langle lm|\Omega\rangle, \tag{2}$$

wo die Euler-Winkel φ, ϑ, ψ der Darstellung D^I der dreidimensionalen Drehgruppe sich auf die Kernsymmetrieachse beziehen und $\langle lm|\Omega\rangle$ die Strahlungskomponente (l, m) der mit Richtung Ω einfallenden Strahlung ist. Wählt man diese Richtung als z-Achse, so ergibt sich mit

$$\langle lm|0\rangle = \sqrt{\frac{2l+1}{4\pi}}\,\delta_{m0} \tag{3}$$

und

$$\sigma_{IK,s}(\vartheta) = \frac{\lambda\!\!\!^{-2}}{2s+1} \sum_{\mu=-s}^{s} |q_{IKM,s\mu}|^2 \tag{4}$$

für den differentiellen Wirkungsquerschnitt

$$\sigma_{IK,s}(\vartheta) = \frac{\lambda\!\!\!^{-2}(2I+1)}{4(2s+1)} \sum_{l,l',\mu} (sl\mu 0|IMsl)(sl'\mu 0|IMsl') \times \sqrt{(2l+1)(2l'+1)}\langle IK|R|sl\rangle\langle sl'|R^+|IK\rangle|D^I_{MK}(\varphi, \vartheta, \psi)|^2, \tag{5}$$

wo aus dem Reaktionsmatrixelement die Abhängigkeit von magnetischen Quantenzahlen durch den entsprechenden Clebsch-Gordan-Koeffizienten herausgenommen wurde; $\lambda\!\!\!^{-}$ bezieht sich auf die einfallende Strahlung.

Wenn man (5) über den vollen Raumwinkel (φ, ϑ) integriert, so erhält man das wohlbekannte Resultat für den totalen Wirkungsquerschnitt für festes I und K,

$$\sigma^{\text{tot}}_{IK,s} = \frac{\lambda\!\!\!^{-2}\pi(2I+1)}{2s+1} \sum_{l} |\langle IK|R|sl\rangle|^2. \tag{6}$$

Das Darstellungsprodukt in (5) läßt sich ausreduzieren und mit

$$(-)^{M-K} D^I_{-M\,-K} D^I_{MK} = (-)^{M-K} \sum_\nu (II-MM|\nu 0II)(II-KK|\nu 0II) P_\nu(\cos\vartheta) \quad (7)$$

und der Racah-Summierung

$$\sum_\mu (-)^\mu (sl\mu 0|IMsl)(sl'\mu 0|IMsl')(II-MM|\nu 0II) = (-)^s (2I+1)(ll'00|\nu 0ll') W(ll'II, \nu s) \quad (8)$$

ergibt sich schließlich

$$W(\vartheta)\left(\propto \sum_{I,K,s} (2s+1)\sigma_{IK,s}(\vartheta)\right) \propto \sum_{I,K,s,l,l',\nu} \langle IK|R|sl\rangle \langle IK|R|sl'\rangle^* \times (-)^{s-K}(2I+1)^2 \sqrt{(2l+1)(2l'+1)}\,(II-KK|\nu 0II)(ll'00|\nu 0ll') \times W(ll'II, \nu s) P_\nu(\cos\vartheta). \quad (9)$$

Das Ergebnis läßt sich mit einem Z'-Koeffizienten [7]) in noch kürzerer Form schreiben;

$$W(\vartheta) \propto \sum_{I,K,s,l,l'\nu} (-)^{s-K} \langle IK|R|sl\rangle \langle IK|R|sl'\rangle^* (2I+1) \times (II-KK|\nu 0II) Z'(ll'II, \nu s) P_\nu(\cos\vartheta). \quad (10)$$

4. Die Symmetrie der Winkelverteilung und der Einfluß polarisierter Teilchen mit Spin $\frac{1}{2}$

Neben der wohlbekannten Beschränkung von ν auf

$$\nu \leqq \{2l, 2I\}_{\min} \quad (11)$$

durch die allgemeinen Eigenschaften der Racah-Koeffizienten ist festzustellen, daß nur gerade ν auftreten können. Dies ist eine direkte Folge der inkohärenten Summierung über die Quantenzahlen I, die ihrerseits wieder auf die Annahme bewahrter axialer Symmetrie beim Spaltungsvorgang zurückzuführen ist. Dies bedeutet eine Symmetrie von $W(\vartheta)$ um den Winkel $\frac{1}{2}\pi$. Diese Feststellung ist trivial, solange das Experiment nicht zwischen den Spaltungsfragmenten unterscheidet, da dann natürlich für jede Vorwärts-Richtung die entsprechende Rückwärts-Richtung gleichberechtigt ist. Unterscheidet das Experiment jedoch zwischen schwerem und leichtem Spaltprodukt, so ordnet es der Spaltung eine bestimmte Richtung zwischen 0 und π zu, und eine Symmetrie inbezug auf $\frac{1}{2}\pi$ in diesen Richtungen ist eine neue Aussage.

Um die Effekte zu berechnen, die die Polarisierung einfallender Teilchen mit Spin $\frac{1}{2}$ auf die Winkelverteilung hat, ist es günstig, die Quantenzahl L für den Gesamtdrehimpuls $\mathbf{L} = \mathbf{l}+\mathbf{s}$ ($s = \frac{1}{2}$) der einfallenden Strahlung einzuführen. Das Ergebnis läßt sich dann mit dem Polarisationsvektor $\mathbf{P}$, der durch seine Richtung die Polarisationsrichtung und durch seinen Betrag das Ausmaß der

Polarisierung angibt ($1 = 100\,\%$), und dem Vektor $\mathbf{n} = \mathbf{k}_1 \times \mathbf{k}_2$ ($\mathbf{k}_1$ und $\mathbf{k}_2$ Wellenvektoren vor bzw. nach der Spaltung) nach der Umschreibung von (9) von der (s, l)- in die (L, l)-Form [7]) so schreiben, daß das Legendre-Polynom $P_\nu(\cos\vartheta)$ ersetzt wird durch

$$P_\nu = 1 + (-)^{l'+1} \frac{\mathrm{Im}\, RR'^*}{\mathrm{Re}\, RR'^*} f_\nu(LL', \tfrac{1}{2})\, \mathbf{P} \cdot \mathbf{n}\, \frac{P_\nu^1(\cos\vartheta)}{P_\nu(\cos\vartheta)}. \tag{12}$$

Die Summierung ist mit l und l' auch über alle zugehörigen L und L' zu erstrecken. RR'^* bedeutet $\langle IK|R|I_0 Ll\rangle\langle IK|R|I_0 L'l'\rangle^*$, wo I und K wieder für sämtliche Spaltungsarten stehen, die von diesem quasistationären Sattelpunktzustand aus möglich sind, und I_0 den Spin des Anfangskerns bezeichnet; f_ν ist gegeben durch

$$f_\nu(LL', \tfrac{1}{2}) = \frac{(-)^{L'+1}}{2\nu(\nu+1)} [(2L'+1) + (-)^{\nu+L+L'}(2L+1)]. \tag{13}$$

Ein Polarisationseffekt in der Verteilung ist also nur zu erwarten (bei geradem ν), wenn über L kohärent summiert wird, weil sonst f_ν verschwindet. Da aber in der Winkelverteilung (9) bzw. (10) keine Interferenzen von I auftreten, ist eine kohärente summierung über L nur gegeben, wenn I_0 von Null verschieden ist. Es läßt sich also feststellen, daß sich — axial symmetrische Spaltung vorausgesetzt — polarisierte Neutronen hinsichtlich der Spaltungswinkelverteilung nicht von unpolarisierten unterscheiden, wenn der Anfangskern Spin Null hat.

5. Die Winkelverteilung der durch 1.60 MeV Neutronen in Th^{232} angeregten Spaltung

Bei Beschießung mit Neutronen zeigt Th^{232} eine deutliche Spaltungsresonanz bei der Energie 1.60 MeV. Auch die Anisotropie der Winkelverteilung zeigt dort resonanzartiges Verhalten, so daß die Annahme nahe liegt, diese Resonanz auf das Auftreten wohldefinierter Energieniveaus am Sattelpunkt zurückzuführen. Die von Henkel und Brolley [3]) durchgeführte Messung der Winkelverteilung für diese Resonanz wurde von Wilets und Chase [4]) mittels der üblichen Symmetrieachsenverteilung des kollektiven Modells für einen axial- und reflexionssymmetrischen Kern diskutiert. Die Winkelverteilung wird auf eine $\frac{3}{2}$-Bande von Rotationsniveaus zurückgeführt, deren erste $\frac{3}{2}$, $\frac{5}{2}$ und $\frac{7}{2}$ Niveaus mit willkürlichen Gewichten und einem angepassten isotropen Anteil die gemessenen Werte gut wiedergeben. Im Gegensatz zu dieser statischen Deutungsweise der Winkelverteilung legt die den Reaktionsablauf betonende Formel (9) durch Zurückführen auf die beteiligten l-Werte des Neutronenstrahls vor allem die Frage nach deren relativen Gewichten vor. Diese werden durch die Reaktionsmatrixelemente gegeben. Nimmt man nun an, daß die Rotationsniveaus einer

Bande an sich zu der betrachteten Resonanz gleiche Beiträge leisten, also bei ungefähr konstantem Resonanznenner gleiche reduzierte Breiten aufweisen, so ist das Quadrat des Reaktionsmatrixelements jeweils dem wellenmechanischen Durchdringungskoeffizienten der betreffenden Neutron-Partialwelle proportional. Man hat also für ein gegebenes K

$$|\langle IK|R|sl\rangle|^2 \propto v_l = \frac{1}{F_l^2(R)+G_l^2(R)}, \tag{14}$$

wo F_l und G_l die reguläre bzw. irreguläre Lösung der Schrödinger-Gleichung und R den Kernradius bedeuten. Von den l-Werten kommen für eine Bande bestimmter Parität nur gerade oder ungerade in Frage.

Für die betrachtete Energie erscheint die Berücksichtigung der beiden ersten jeweils möglichen Partialwellen ausreichend. Von der $\frac{3}{2}$-Bande positiver Parität kommen also durch die l-Werte 2 und 4 die Rotationsniveaus $\frac{3}{2}^+$, $\frac{5}{2}^+$, $\frac{7}{2}^+$ und $\frac{9}{2}^+$ ins Spiel. Durch die l-Werte 1 und 3 gelangt man zu den Niveaus $\frac{3}{2}^-$, $\frac{5}{2}^-$ und $\frac{7}{2}^-$ der $\frac{3}{2}$-Bande negativer Parität. Die entsprechenden Winkelverteilungen sind nach (9) für die Niveaus positiver Parität durch

$$W(\vartheta) \propto P_0 - 0.128\, P_2 - 0.708\, P_4 - 0.096\, P_6 - 0.078\, P_8 \tag{15}$$

und für negative Parität durch

$$W(\vartheta) \propto P_0 - 0.323\, P_2 - 0.332\, P_4 - 0.345\, P_6 \tag{16}$$

gegeben. Mit einem isotropen Anteil, der durch den Meßwert bei 0° gegeben ist, ergibt dies die beiden in Figur 1 gezeigten Kurven. Man sieht, daß die Kurve für die $\frac{3}{2}$-Bande negativer Parität mit den gemessenen Werten in ausgezeichneter Übereinstimmung steht.

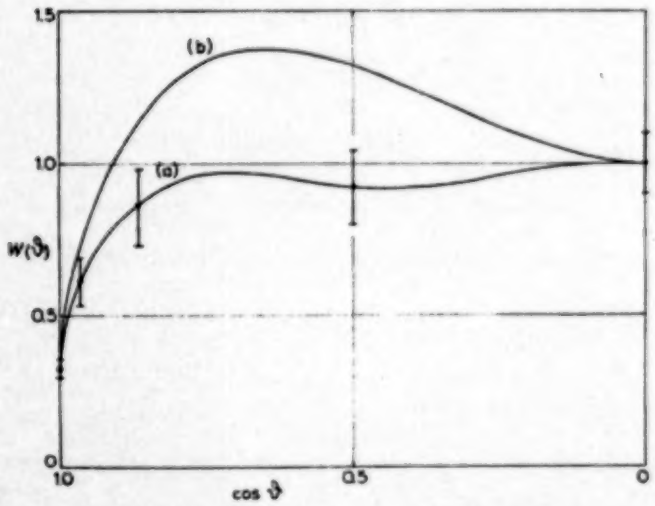

Fig. 1. Spaltungswinkelverteilungen über die Niveaus der $\frac{3}{2}$-Bande negativer Parität (Kurve (a)) und positiver Parität (Kurve (b)) mit Addition eines isotropen Teils, der den Meßwert bei 0° ergibt. Meßwerte von Henkel und Brolley [3]).

Analysiert man den Meßwert bei 0° als Beitrag einer $\frac{1}{2}$-Bande, so ergeben sich die Kurven der Figur 2. Die Kurve (b) entspricht den Meßwerten am besten. Sie umfaßt die Niveaus $\frac{1}{2}^-$, $\frac{3}{2}^-$, $\frac{5}{2}^-$ und $\frac{7}{2}^-$ der $\frac{1}{2}$-Bande. Die Niveaus dieser Bande stehen ja auch durch die Rotation-Partikel-Koppelung des kollektiven

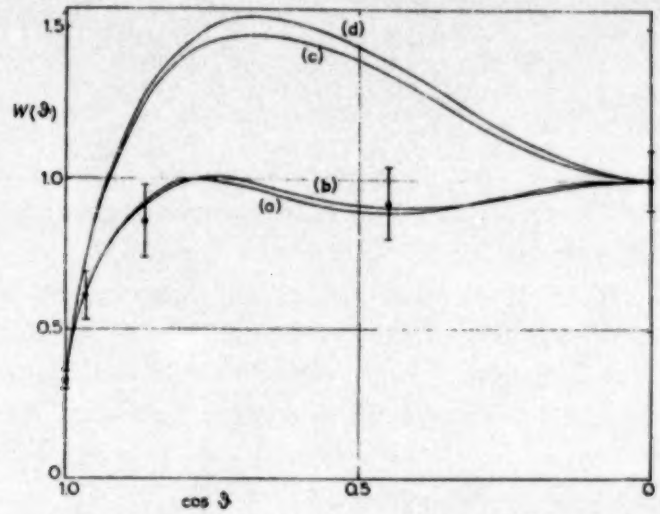

Fig. 2. Die Winkelverteilungen der $\frac{1}{2}$-Banden negativer Parität (Kurven (a) und (b)) und positiver Parität (Kurven (c) und (d)) mit Beitrag der $\frac{1}{2}$-Bande positiver Parität (Kurven (a) und (c)) und negativer Parität (Kurven (b) und (d)), der den Meßwert bei 0° ergibt.

Modells in Beziehung zu jenen der $\frac{3}{2}$-Bande negativer Parität. Die ausgezeichnete Übereinstimmung der Kurve (a), Figur 1, mit den Meßwerten könnte darauf hinweisen, daß Einflüsse vorliegen, die eine isotropere Verteilung als die betrachtete der $\frac{1}{2}$-Bande hervorrufen, doch wären für verläßliche Aussagen wohl noch mehr Meßpunkte nötig.

Literatur

1) A. Bohr, Proc. Geneva Conference **2** (1955) 151
2) V. M. Strutinskii, JETP **3** (1956) 638
3) R. L. Henkel und J. E. Brolley, Phys. Rev. **103** (1956) 1292
4) L. Wilets und D. M. Chase, Phys. Rev. **103** (1956) 1296
5) I. Halpern und V. M. Strutinskii, Proc. 2nd Geneva Conference **15** (1958) 408
6) J. J. Griffin, Phys. Rev. **116** (1959) 107
7) S. Devons und L. J. B. Goldfarb, Handbuch der Physik, Bd. **42** (Springer-Verlag, Berlin, 1957)

2.F:2.G

Nuclear Physics 18 (1960) 353—394; © *North-Holland Publishing Co., Amsterdam*

Not to be reproduced by photoprint or microfilm without written permission from the publisher

ANGULAR DISTRIBUTIONS AND POLARIZATION IN STRIPPING PROCESSES AND IN DIRECT REACTIONS

L. J. B. GOLDFARB and R. C. JOHNSON

Theoretical Physics Department, University of Manchester

Received 28 March 1960

Abstract: General expressions are found for angular distributions and polarization effects in a variety of direct reactions. These reactions include processes involving the stripping of deuterons and of heavier nuclei, in addition to inelastic-scattering phenomena which arise either from individual nucleon-nucleon encounters or from collective effects at the nuclear surface. Various selection rules are found for the existence of polarization, using the distorted-wave Born approximation and allowing for spin-dependent distortions. The influence of a neighbouring isolated resonance state of the compound nucleus is examined, and modifications are found of the general results. Expressions are given for the angular correlation of the γ-rays following de-excitation of the residual nucleus.

Introduction

During the past decade, a great deal of attention has been given to those nuclear phenomena which may be classified as direct reactions. The most well-known and useful of these are the deuteron-stripping and the related pick-up processes [1, 2, 3]). Other examples include stripping of particles heavier than deuterons and inelastic-scattering processes [1]). In the latter case, the interaction between the projectile and the nucleus is usually treated as involving either individual nucleon-nucleon encounters throughout the nuclear volume, or a collective oscillation of the nuclear surface. The factor distinguishing these phenomena is that they may be interpreted in terms of the excitation of several degrees of freedom of the nucleus, in contrast to the many parameters usually necessary for a proper description of compound-nucleus processes. The transition is represented by matrix elements measuring the degree to which the target nucleus is parent to the residual nucleus with a transfer of one or a few angular momenta to the system of incoming and outgoing radiation. In stripping and pick-up processes, these matrix elements are expressed in terms of reduced widths for transformation of the target nuclei.

Since the essential characteristic of these processes is the transfer of some angular momentum, it is of interest whether some unified approach can be given to the various processes which makes use of the mathematical techniques associated with the coupling of angular momenta. These techniques are particularly useful since besides the derivation of angular distributions, polarization effects may be handled in a systematic way.

Of particular interest to the study of direct reactions is the use of the "distorted-wave" theory [4, 5, 6]). This serves as an improvement over the use of the earlier "plane-wave" Born approximation which ignores the distortion of the incoming and outgoing waves by the target and residual nuclei, respectively. Calculations of this kind require very elaborate numerical computation which is somewhat facilitated by the use of automatic electronic computers. Tobocman recently reported [2]) the results of some numerical calculation of deuteron-stripping cross-sections and he finds in several cases a great sensitivity of the angular distributions to small variation in the optical-distorting potentials. The magnitude of the work involved in such a numerical calculation together with lack of appropriate experimental data renders very difficult any systematic search for the best parameters of the optical potentials. A similar sensitivity to the optical distorting parameters has been found by Glendenning [7]) in his calculations of neutron inelastic scattering cross-sections.

Although the optical model includes a spin-orbit interaction, this is usually ignored † in the belief that its effect is relatively small. Nevertheless, in view of the sensitivity of angular distributions to the parameters of the optical-model distortion, it would seem advisable to include information bearing the closest relation to the experimental data. In addition, the neglect of such a spin-orbit interaction leads to very restrictive selection rules concerning the polarization effects. As is well known, such effects vanish in the plane-wave approximation and therefore polarization is a direct manifestation of the optical-model distortion. One of the main purposes of this article is to find new expressions for the angular distributions and polarization. This leads to suggestions for several experimental tests to determine the presence of the spin-orbit interaction. Although the new formulae involve summation over new variables, their complexity is not felt to be great enough to warrant their neglect, particularly if powerful computing machines are already made necessary for any useful computation.

Two alternative procedures for the determination of the differential cross-sections and the polarizations produced or detected in direct reactions are given in sections 2 and 3. These procedures lead to seemingly different final expressions, which, nonetheless, are equivalent. The second set of results seems more appealing since the summation over magnetic quantum numbers is already carried out using the techniques of Racah algebra. On the other hand, for the purposes of numerical computation the formalism of section 2 is probably much more useful, particularly if many angular momenta are required in the computation.

The contribution of processes proceeding through intermediate compound-nucleus states is given in section 4. This may be of use in the neighbourhood of an isolated resonance state.

† Such is the case in the work of Tobocman [2]) for example. There are several exceptions to this, e.g. the numerical analysis of deuteron stripping by Newns and Refai [8]).

Specific applications are found in section 5 and 6. The most interesting aspect concerns processes involving a transfer of zero orbital angular momentum. In this case, measurement of the polarization effects leads to separate conclusions concerning the presence of spin-dependent distortions. In particular, it is possible to reach some conclusions concerning the spin states of the transferred radiation if it be a composite system, e.g. the two nucleons transferred in the (He^3, p) stripping process.

Most direct reactions lead to excited states of the residual nuclei. These subsequently decay with γ-ray emission. The angular correlations as found by Huby, Refai and Satchler [3]) are generalized in the last section to take into account spin-dependent distortion.

1. Notation and General Assumptions

We shall adhere to the following convention in designating angular-momentum states. Angular-momentum quantum numbers are represented by Latin letters and their components (magnetic quantum numbers), by the Greek equivalent. In the direct reactions to be considered, radiation of arbitrary spin s_1 is incident on a nucleus of spin a. There is a transfer of angular momentum j, composed of orbital angular momentum l and spin s, which leads to outgoing radiation of spin s_2 and a residual nucleus of spin c. We reserve the quantum number b to refer to the total angular momentum of intermediate states in processes involving a compound nucleus.

We shall attribute the relative orbital angular momentum to the radiation and typify the incident and outgoing orbital and total angular momentum by $l_1 j_1$ and $l_2 j_2$ together with their components. We confine ourselves to the centre-of-mass system and let initial and final linear momenta be represented by $\mathbf{k}_1$ and $\mathbf{k}_2$, respectively, where the angles are symbolically denoted by Ω_1 and Ω_2, respectively.

The matrix element of the operator $R = S-1$, where S is the Heisenberg scattering matrix, which connects initial and final states is expanded as follows:

$$\langle \mathbf{k}_2 c\gamma s_2\sigma_2|R|\mathbf{k}_1 a\alpha s_1\sigma_1\rangle = \sum_{j_1 j_2 l_1 l_2 \zeta_1 \zeta_2} \langle \Omega_2 s_2\sigma_2|j_2 l_2 \zeta_2\rangle \times \langle \Omega_1 s_1\sigma_1|j_1 l_1 \zeta_1\rangle^* \langle c\gamma (l_2 s_2) j_2 \zeta_2|R|a\alpha (l_1 s_1) j_1 \zeta_1\rangle, \quad (1.1)$$

where the expansion coefficient $\langle \Omega s\sigma|jl\zeta\rangle$ arises in the decomposition of a plane wave into a sum of spherical waves [9]).

The matrix elements in the spherical representation are evaluated by use of the first-order perturbation theory. This amounts to an evaluation of the matrix element between initial and final states of some potential operator representing the direct-interaction.

We introduce the quantity $\theta_{j(ls)}(c, a)$, which arises on integration over the internal co-ordinates of the target nucleus. This quantity, which is usually referred to in stripping processes, as a reduced-width amplitude, measures the extent to which the nucleus, with spin a is parent to the final nucleus with spin c. The phases of the nuclear eigenfunctions are chosen so that this amplitude is real. The direct-reaction involves the nuclear system only insofar as there is an energy change and there takes place a rearrangement of the nuclear configuration with the net absorption (or emission) of angular momentum with quantum numbers $j(ls)$ from (or to) the radiation system. This may or may not be accompanied by the transfer of real particles. For this interpretation to be useful, we expect only a very few quantum numbers to be associated with the angular-momentum transfer.

To be definite, we assume for the present, that the angular momentum is absorbed by the target nucleus. Integration over the remainder of the co-ordinates gives an expansion of the matrix elements as follows:

$$\langle c\gamma(l_2 s_2)j_2\zeta_2|R|a\alpha(l_1 s_1)j_1\zeta_1\rangle = \sum_{jls\zeta} [\theta_{j(ls)}(c, a)(a\alpha, j\zeta|c\gamma)] \times [\langle j_2(c)|j(ls)||j_1(a)\rangle (j_2\zeta_2, j\zeta|j_1\zeta_1)]. \quad (1.2)$$

The reduced-matrix element $\langle j_2(c)|j(ls)||j_1(a)\rangle$ corresponds to the emission of the angular momentum with quantum numbers $j(ls)$ by the initial radiation. If, for example, the distorted-wave Born approximation theory is employed, this matrix element is assumed to depend on the nuclear states through the parameters of the optical model used to describe separately the elastic scattering of the radiation by the nucleus in the incoming and outgoing channels, as well as through the angular-momentum transfer. It is expected that this dependence on nuclear properties is a weak one.

The notation for the reduced-matrix element is slightly unconventional, since double bars are used in only one side of the quantity. This is done in order to preserve the angular-momentum coupling scheme and to help distinguish absorption processes from emission processes. The reduced-matrix element is dependent on l_1, l_2 and l; however, to facilitate the reading, an abbreviated notation will be used.

Only very specialized types of interactions have been proposed, to date, to account for the various direct processes. In deuteron stripping, the operator is assumed to depend only on the neutron and proton relative co-ordinates, and even in the most elaborate calculations this is described simply by a delta-function. For inelastic scattering through volume interactions, the operator is usually chosen to be a delta function involving the coordinates of the projectile and specific nucleons in the nucleus.

An explicit discussion for each type of process is given in section 6; for the following discussion, we shall accept the validity of (1.2).

2. General Expressions for the Angular Distribution and Polarization

The general expressions for angular distribution and polarization are most directly found by use of density matrices. If $\rho^{(f)}$ and $\rho^{(i)}$ are the density matrices for the final and initial states of the system (nucleus plus radiation), these are related through the operator R, by [10])

$$\rho^{(f)} = R\rho^{(i)}R^{\dagger} \tag{2.1}$$

Choosing the representation $|\mathbf{k}_2 c\gamma s_2\sigma_2\rangle$ for $\rho^{(f)}$ and $|\mathbf{k}_1 a\alpha s_1\sigma_1\rangle$ for $\rho^{(i)}$, the matrix element of $\rho^{(f)}$ becomes

$$\langle \mathbf{k}_2 c\gamma s_2\sigma_2|\rho^{(f)}|\mathbf{k}_2 c\gamma' s_2\sigma_2'\rangle = \sum_{a\alpha'\sigma_1\sigma'} \langle \mathbf{k}_2 c\gamma s_2\sigma_2|R|\mathbf{k}_1 a\alpha s_1\sigma_1\rangle \times \langle \mathbf{k}_2 c\gamma' s_2\sigma_2'|R|\mathbf{k}_1 a\alpha' s_1\sigma_1'\rangle^* \langle \mathbf{k}_1 a\alpha s_1\sigma_1|\rho^{(i)}|\mathbf{k}_1 a\alpha' s_1\sigma_1'\rangle. \tag{2.2}$$

We now use the expressions (1.1) and (1.2) and the explicit form for $\langle \Omega s\sigma|jl\zeta\rangle$ as given in ref. [11]),

$$\langle \Omega s\sigma|jl\zeta\rangle = \frac{\hat{l}}{\sqrt{4\pi}}(l0, s\sigma|j\sigma)\mathscr{D}^{j*}_{\zeta\sigma}(\mathscr{R}). \tag{2.3}$$

In the above expressions, we denote with $\hat{x}$ the statistical factor $\sqrt{(2x+1)}$. The quantity $\mathscr{D}(\mathscr{R})$ is the rotation matrix as defined by Rose [12]), where $\mathscr{R}$ is the rotation bringing an arbitrary set of axes into a frame whose z-axis is along the propagation direction. We are thus led to the following expression for the final density matrix:

$$\begin{aligned}\langle \mathbf{k}_2 c\gamma s_2\sigma_2|\rho^{(f)}|\mathbf{k}_2 c\gamma' s_2\sigma_2'\rangle = {} & \frac{1}{(4\pi)^2}\sum \langle \mathbf{k}_1 a\alpha s_1\sigma_1|\rho^{(i)}|\mathbf{k}_1 a\alpha' s_1\sigma_1'\rangle \\ & \times \hat{l}_1\hat{l}_2\hat{l}_1'\hat{l}_2'\theta_{j(ls)}(c, a)\theta_{j'(l's')}(c, a)(a\alpha, j\zeta|c\gamma)(a\alpha', j'\zeta'|c\gamma') \\ & \times (l_1 0, s_1\sigma_1|j_1\sigma_1)(l_2 0, s_2\sigma_2|j_2\sigma_2)(l_1' 0, s_1\sigma_1'|j_1'\sigma_1')(l_2' 0, s_2\sigma_2'|j_2'\sigma_2')(j_2\zeta_2, j\zeta|j_1\zeta_1) \\ & \times (j_2'\zeta_2', j'\zeta'|j_1'\zeta_1')\langle j_2(c)|j(ls)||j_1(a)\rangle\langle j_2'(c)|j'(l's')||j_1'(a)\rangle^* \mathscr{D}^{j_2*}_{\zeta_2\sigma_2}(\mathscr{R}_2)\mathscr{D}^{j_2}_{\zeta_2'\sigma_2'}(\mathscr{R}_2) \\ & \times \mathscr{D}^{j_1}_{\zeta_1\sigma_1}(\mathscr{R}_1)D^{j_1*}_{\zeta_1'\sigma_1'}(\mathscr{R}_1),\end{aligned} \tag{2.4}$$

where the summation is over the repeated symbols for angular momenta on the right-hand side of the above expression. It is assumed that the initial and final nuclear states are sharp, i.e. their spins and parities are unique.

2.1 ANGULAR DISTRIBUTIONS

The probability of detection of the final system is given by

$$W(\Omega_1\Omega_2) = \text{trace}\,(\rho^f\varepsilon), \tag{2.5}$$

where ε is the efficiency matrix (Coester and Jauch [9])) which describes the properties of the detecting system. If we assume polarization-insensitive

detectors and unpolarized incident radiation, the following relations hold:

$$\langle \mathbf{k}_2 c\gamma s_2\sigma_2|\varepsilon|\mathbf{k}_2 c\gamma' s_2\sigma_2'\rangle = \delta_{\sigma_2\sigma_2'}\delta_{\gamma\gamma'},$$
$$\langle \mathbf{k}_1 a\alpha s_1\sigma_1|\rho^{(1)}|\mathbf{k}_1 a\alpha' s_1\sigma_1'\rangle = \frac{1}{\hat{s}_1^2}\delta_{\sigma_1\sigma_1'}\frac{1}{\hat{a}^2}\delta_{\alpha\alpha'}. \tag{2.6}$$

The probability of detection $W(\Omega_1\Omega_2)$ then simplifies to

$$W(\Omega_1\Omega_2) = \frac{1}{(4\pi)^2}\frac{\hat{c}^2}{\hat{a}^2\hat{s}_1^2}\sum_{j\zeta\sigma_1\sigma_2}\left|\sum_{ls}\frac{1}{\hat{j}}\theta_{j(ls)}(c,a)X^{j(ls)\zeta}_{\sigma_2\sigma_1}(\mathscr{R}_2\mathscr{R}_1;ca)\right|^2, \tag{2.7}$$

where

$$X^{j(ls)\zeta}_{\sigma_2\sigma_1}(\mathscr{R}_2\mathscr{R}_1;ca) = \sum_{j_1l_1\zeta_1j_2l_2\zeta_2} \hat{l}_1\hat{l}_2(l_1 0, s_1\sigma_1|j_1\sigma_1)(l_2 0, s_2\sigma_2|j_2\sigma_2)(j_2\zeta_2, j\zeta|j_1\zeta_1)$$
$$\times\langle j_2(c)|j(ls)||j_1(a)\rangle\mathscr{D}^{j_2*}_{\zeta_2\sigma_2}(\mathscr{R}_2)\mathscr{D}^{j_1}_{\zeta_1\sigma_1}(\mathscr{R}_1). \tag{2.8}$$

The operator R is defined [13]) so that the transition probability per unit time is obtained from (2.5) if one multiplies by $2\pi\rho(\mathbf{k}_2)/\hbar$, where $\rho(\mathbf{k}_2)\delta E_{\mathbf{k}_2}$ is the number of final states in the energy interval $\delta E_{\mathbf{k}_2}$, and where the wave function describing initial and final radiation states are normalized like $e^{i\mathbf{k}\cdot\mathbf{r}}$. The differential cross-section $(d\sigma/d\Omega)$ follows on division by the incident flux. One finds

$$\frac{d\sigma}{d\Omega} = \frac{m_1^* m_2^*}{64\pi^4\hbar^4}\frac{k_2}{k_1}\frac{\hat{c}^2}{\hat{a}^2\hat{s}_1^2}\sum_{j\zeta\sigma_1\sigma_2}\left|\sum_{ls}\frac{1}{\hat{j}}\theta_{j(ls)}(c,a)X^{j(ls)\zeta}_{\sigma_2\sigma_1}(\mathscr{R}_2\mathscr{R}_1;ca)\right|^2, \tag{2.9}$$

where m_1^*, m_2^* are the reduced masses of the incident and outgoing radiation in their respective centres-of-mass systems. We denote the angle between the radiations by θ such that $\cos\theta = \mathbf{k}_1\cdot\mathbf{k}_2/|\mathbf{k}_1\cdot\mathbf{k}_2|$ and also the normal to the reaction plane by $\mathbf{n} = \mathbf{k}_1\times\mathbf{k}_2/|\mathbf{k}_1\times\mathbf{k}_2|$. We then find it convenient to let the y-axis coincide with $-\mathbf{n}$ and the arbitrary z-axis with either $\mathbf{k}_1$ or $\mathbf{k}_2$. In the first case the rotations $\mathscr{R}_1$ and $\mathscr{R}_2$ are represented by the Euler angles (000) and $(0-\theta 0)$ so that

$$X^{j(ls)\zeta}_{\sigma_2\sigma_1}(\mathscr{R}_2\mathscr{R}_1;ca) \equiv A^{j(ls)\zeta}_{\sigma_2\sigma_1}(\theta;ca) = \sum_{j_1l_1j_2l_2}\hat{l}_1\hat{l}_2(l_1 0, s_1\sigma_1|j_1\sigma_1)(l_2 0, s_2\sigma_2|j_2\sigma_2)$$
$$\times(j_2\sigma_1-\zeta, j\zeta|j_1\sigma_1)\langle j_2(c)|j(ls)||j_1(a)\rangle\mathscr{D}^{j_2}_{\sigma_2\sigma_1-\zeta}(000), \tag{2.10}$$

and in the other case,

$$X^{j(ls)\zeta}_{\sigma_2\sigma_1}(\mathscr{R}_2\mathscr{R}_1;ca) \equiv B^{j(ls)\zeta}_{\sigma_2\sigma_1}(\theta;ca) = \sum_{j_1l_1j_2l_2}\hat{l}_1\hat{l}_2(l_1 0, s_1\sigma_1|j_1\sigma_1)(l_2 0, s_2\sigma_2|j_2\sigma_2)$$
$$\times(j_2\sigma_2, j\zeta|j_1\sigma_2+\zeta)\langle j_2(c)|j(ls)||j_1(a)\rangle\mathscr{D}^{j_1}_{\sigma_2+\zeta\sigma_1}(0\theta 0). \tag{2.11}$$

Either form may be used, whichever is the more convenient. The incoherent summation over j, which is characteristic of direct-reactions, is a reflection of the absence of polarization measurements of the target of residual nucleus.

2.2. POLARIZATION

In the ensuing discussion we shall concern ourselves with the polarization of radiation arising from a direct-reaction or with the angular distributions arising from incident polarized radiations. We shall ignore measurement of the polarization of the target or residual nuclei †, although the results are easily extended to this type of polarization if one interchanges the quantum numbers a and s_1 together with c and s_2.

We represent the polarization by the statistical or spin tensors $\rho_{k\kappa}(s)$ as defined in ref. [11]):

$$\rho_{k_s\kappa}(s) \equiv \langle T_{k_s\kappa}(s)\rangle \equiv \frac{\text{trace}\,[\rho T_{k_s\kappa}(s)]}{\text{trace}\,\rho}, \tag{2.12}$$

where $T_{k_s\kappa}(s)$ has matrix elements, in the spin representation

$$\langle s\sigma'|T_{k_s\kappa}(s)|s\sigma\rangle = (-)^{s-\sigma'}(s\sigma,\, s-\sigma'|k_s\kappa). \tag{2.13}$$

For $s = \frac{1}{2}$, we have

$$\rho_{00}(\tfrac{1}{2}) = \frac{1}{\sqrt{2}}, \quad \rho_{10}(\tfrac{1}{2}) = \frac{P_z}{\sqrt{2}}, \quad \rho_{1\pm1}(\tfrac{1}{2}) = \mp\tfrac{1}{2}(P_x \mp iP_y), \tag{2.14}$$

with

$$\mathbf{P} \equiv \frac{2}{\hbar}\langle \mathbf{s}\rangle. \tag{2.15}$$

For $s = 1$, we see from (2.13) that k_s takes on values 0, 1, 2. Using the convention in ref. [14]), we have

$$\rho_{00}(1) = \frac{1}{\sqrt{3}}, \quad \rho_{10}(1) = \frac{1}{\sqrt{2}}P_z, \quad \rho_{1\pm1}(1) = \mp\tfrac{1}{2}(P_x \mp iP_y), \tag{2.16}$$

$$\rho_{20}(1) = \frac{1}{\sqrt{3}}P_{33}, \quad \rho_{2\pm1}(1) = \mp\tfrac{1}{3}(P_{13} \mp iP_{23}), \quad \rho_{2\pm2}(1) = \tfrac{1}{6}(P_{11}-P_{22}) \mp \tfrac{1}{3}iP_{12},$$

where

$$\mathbf{P} \equiv \frac{1}{\hbar}\langle \mathbf{s}\rangle,$$

$$P_{ij} \equiv \frac{3}{2\hbar^2}[\langle s_i s_j + s_j s_i\rangle] - 2\delta_{ij} \quad (i, j \equiv x, y, z). \tag{2.17}$$

As a consequence of the Hermitean properties of these tensors

$$\rho_{k_s\kappa}(s) = (-)^{\kappa}\rho^{*}_{k_s-\kappa}(s). \tag{2.18}$$

† In fact, we shall consider indirectly the measurement of the polarization of the residual nucleus by means of the angular correlations of the γ-rays following de-excitation of this nucleus (see section 7).

The polarization of the outgoing radiation is readily calculated if one inserts for $\rho^{(f)}$ in (2.12) the expression (2.4). Corresponding to no polarization of either the incident radiation or the target, one finds

$$\rho_{k_{2s}\kappa}(s_2) = \frac{\sum_{jll'ss'} \frac{1}{\hat{j}^2} \theta_{j(ls)}(c,a)\theta_{j(l's')}(c,a) \sum_{\sigma_1\sigma_2\sigma_2'\zeta} (-)^{s_2-\sigma'}(s_2\sigma_2, s_2-\sigma_2'|k_{2s}\kappa) X^{j(ls)\zeta}_{\sigma_2\sigma_1}(\theta;ca) X^{j(l's')\zeta*}_{\sigma_2'\sigma_1}(\theta;ca)}{\sum_{j\zeta\sigma_1\sigma_2} \left| \sum_{ls} \frac{1}{\hat{j}} \theta_{j(ls)}(c,a) X^{j(ls)\zeta}_{\sigma_2\sigma_1}(\theta;ca) \right|^2}, \tag{2.19}$$

where $X^{j(ls)\zeta}_{\sigma_2\sigma_1}(\theta;ca)$ is given by either (2.10) or (2.11) with the z-axis along $\mathbf{k}_2$ and the y-axis along $-\mathbf{n}$.

It is possible to show, using the symmetry properties of the Clebsch-Gordan coefficients and the properties of the rotation matrices, that this latter quantity satisfies

$$X^{j(ls)-\zeta}_{-\sigma_2-\sigma_1}(\theta) = (-)^{j+l+s_1+s_2-\sigma_1-\sigma_2-\zeta} X^{j(ls)\zeta}_{\sigma_2\sigma_1}(\theta), \tag{2.20}$$

provided that parity is conserved in the process.

If we use the above relation together with (2.18) and (2.19), we find

$$\rho^*_{k_{2s}\kappa}(s_2) = (-)^{k_{2s}} \rho_{k_{2s}\kappa}(s_2). \tag{2.21}$$

This shows that the only non-vanishing polarization tensor of rank 1 (i.e. vector polarization) is pure imaginary. Using the explicit values $T_{1\kappa}(s)$ as given in ref. [14]),

$$T_{10}(s) = \frac{\sqrt{3}\, s_z}{\hbar\hat{s}\sqrt{s(s+1)}}, \quad T_{1\pm1}(s) = \frac{\mp\sqrt{3}(s_x \mp i s_y)}{\hbar\hat{s}\sqrt{2s(s+1)}}, \tag{2.22}$$

then by the definition (2.12) and the Hermitean character of the spin operators s_x, s_y and s_z, there follows the well-known result that the only non-vanishing polarization of rank 1 is along the y-direction, i.e. perpendicular to the reaction plane [15]).

For incoming polarized radiation one can write the differential cross-section using polarization-insensitive detectors in the form

$$\frac{\mathrm{d}\sigma}{\mathrm{d}\Omega} = \left(\frac{\mathrm{d}\sigma}{\mathrm{d}\Omega}\right)_0 [1 + \sum_{k_{1s}\neq 0,\,\kappa} \rho_{k_{1s}\kappa}(s_1) \varepsilon^*_{k_{1s}\kappa}(s_1)], \tag{2.23}$$

where $\rho_{k_{1s}\kappa}(s_1)$ specifies the incoming polarization and $\varepsilon_{k_{1s}\kappa}(s_1)$ is the efficiency tensor, which is defined in an analogous way to the statistical tensors [9]) but in terms of the efficiency of the detector, which in this case amounts to a measurement of the angular distribution (2.23). $(\mathrm{d}\sigma/\mathrm{d}\Omega)_0$ is the cross-section corresponding to no incoming polarization.

If the y-axis is now chosen along $+\mathbf{n}$, one readily finds, using (2.4), that the

efficiency tensor $\varepsilon^*_{k_1\kappa}(s_1)$ is given by

$$\varepsilon^*_{k_1\kappa}(s_1) = \frac{\hat{s}_1^2(-)^\kappa \sum_{jll's's'} \frac{1}{\hat{j}^2}\theta_{j(ls)}(c,a)\theta_{j(l's')}(c,a) \sum_{\sigma_1\sigma_2\sigma_1'\zeta}(-)^{s_1-\sigma_1}(s_1\sigma_1, s_1-\sigma_1'|k_1\kappa)X^{j(ls)\zeta}_{\sigma_2\sigma_1}(\theta;ca)X^{j(l's')\zeta*}_{\sigma_2\sigma_1'}(\theta;ca)}{\sum_{j\zeta\sigma_1\sigma_2}\left|\sum_{ls}\frac{1}{\hat{j}}\theta_{j(ls)}(c,a)X^{j(ls)\zeta}_{\sigma_2\sigma_1}(\theta;ca)\right|^2}, \tag{2.24}$$

where again $X^{j(ls)\zeta}_{\sigma_2\sigma_1}(\theta;ca)$ is $A^{j(ls)\zeta}_{\sigma_2\sigma_1}(\theta;ca)$ or $B^{j(ls)\zeta}_{\sigma_2\sigma_1}(\theta;ca)$, with the z-axis along $\mathbf{k}_1$ and the y-axis along $+\,\mathbf{n}$.

The efficiency tensors may be written in terms of real parameters as done † in ref. [14]). Thus, for spins $\frac{1}{2}$ and 1, we have

$$\begin{aligned}
&\varepsilon_{00}(\tfrac{1}{2}) = \sqrt{2}, && \varepsilon_{10}(\tfrac{1}{2}) = \sqrt{2}\,P^{\mathrm{d}}_z, && \varepsilon_{1\pm1}(\tfrac{1}{2}) = \mp(P^{\mathrm{d}}_x \mp iP^{\mathrm{d}}_y),\\
&\varepsilon_{00}(1) = \sqrt{3}, && \varepsilon_{10}(1) = \frac{3}{\sqrt{2}}P^{\mathrm{d}}_z, && \varepsilon_{1\pm1}(1) = \mp\tfrac{3}{2}(P^{\mathrm{d}}_x \mp iP^{\mathrm{d}}_y),\\
&\varepsilon_{20}(1) = \sqrt{\tfrac{3}{2}}\,P^{\mathrm{d}}_{33}(1), && \varepsilon_{2\pm1}(1) = \mp(P^{\mathrm{d}}_{13} \mp iP^{\mathrm{d}}_{23}), && \varepsilon_{2\pm2}(1) = \tfrac{1}{2}(P^{\mathrm{d}}_{11}-P^{\mathrm{d}}_{22}) \mp iP^{\mathrm{d}}_{12}.
\end{aligned} \tag{2.25}$$

2.3. CONSIDERATIONS BASED ON TIME-REVERSAL INVARIANCE. INVERSE PROCESSES. BOUNDARY CONDITIONS ON EIGENFUNCTIONS.

There remains the problem of the evaluation of the reduced matrix elements $\langle j(c)|j(ls)||j(a)\rangle$. The most useful procedure is to employ the distorted-wave Born approximation (Austern [1]), Gell-Mann and Goldberger [5]), Watson [16])). In this scheme, the reaction matrix, defined as the matrix element of the operator R in the representation where the radiations and nuclei are treated as well-separated and non-interacting, can be approximated as the matrix element of some operator, V_{D}, the direct-interaction operator, which acts between states that include the effects of the interactions between the radiation and nucleus. These effects give rise to compound-nucleus transitions which are accounted for in computations through the use of optical-model eigenfunctions for elastic scattering in the incident and outgoing channels. The "incoming" state is taken to be the solution corresponding asymptotically to an incident plane wave together with a distorted spherical wave, while the "outgoing" state is found to correspond to an outgoing plane-wave together with an incoming spherical wave.

Anticipating the results obtained in the specific considerations given for various types of processes as found in section 6, we note that in each case, the reduced-matrix element takes on the form

$$\langle j_2(c)|j(ls)||j_1(a)\rangle = \{\langle j_2(c)|j(ls)||j_1(a)\rangle\}\int \mathrm{d}r\, r^2 g^*_{j_2l_2}(k_2,r)U_{j(ls)}(r)f_{j_1l_1}(k_1,r), \tag{2.26}$$

† The efficiency tensors as defined in (2.25) differ from those in ref. [14]) in that the latter quantities must be multiplied by $\hat{s}^2$ in order to agree with those given here.

The quantities $f_{j_1l_1}(k_1, r)$, $g_{j_2l_2}(k_2, r)$ arise in the decomposition of distorted plane waves into spherical waves. Thus, we write

$$\langle \Omega_i s_i \sigma_i | \rangle = \sum_{j_i l_i \zeta_i} \langle \Omega_i s_i \sigma_i | j_i l_i \zeta_i \rangle \langle j_i l_i \zeta_i | \rangle, \qquad (i = 1, 2) \tag{2.27}$$

where $\langle \Omega_i s_i \sigma_i | j_i l_i \zeta_i \rangle$ is as given in (2.3) and

$$\langle j_1 l_1 \zeta_1 | \rangle = 4\pi f_{j_1 l_1}(k_1, r) \Phi^{\zeta_1}_{j_1 (l_1 s_1)}, \tag{2.28a}$$

$$\langle j_2 l_2 \zeta_2 | \rangle = 4\pi g_{j_2 l_2}(k_2, r) \Phi^{\zeta_2}_{j_2 (l_2 s_2)}, \tag{2.28b}$$

with

$$\Phi^{\zeta_i}_{j_i (l_i s_i)} = \sum_{\lambda_i \sigma_i} (l_i \lambda_i, s_i \sigma_i | j_i \zeta_i) i^{l_i} Y^{\lambda_i}_{l_i} \chi^{\sigma_i}_{s_i}. \tag{2.28c}$$

For the present, we neglect the internal structure of the radiation. The spin-angular eigenfunctions in (2.28) are chosen so that products of such eigenfunctions transform consistently with the eigenfunctions under time-reversal (Huby [17]). The function $U_{j(ls)}(r)$ is associated with one or more radial functions for bound states while the quantity $\{\langle j_2(c) | j(ls) || j_1(a) \rangle\}$ arises in the reduction of that part of the matrix element depending on the spin-angular functions. Each of the latter two quantities may be chosen to be real.

The eigenfunction $f_{j_1 l_1}(k_1, r)$ is the solution of the Schrödinger equation with the complex optical-model potential $V^{(1)}_{j_1 l_1}(r)$

$$\left\{ \frac{\mathrm{d}^2}{\mathrm{d}r^2} + k_1^2 - \frac{l_1(l_1+1)}{r^2} - \frac{2m_1^*}{\hbar^2} V^{(1)}_{j_1 l_1}(r) + V_{\mathrm{Coul}}(r) \right\} r f_{j_1 l_1}(k_1, r) = 0, \tag{2.29}$$

having an asymptotic dependence

$$f_{j_1 l_1}(k_1, r) \sim I_{l_1} - \mathrm{e}^{2i\delta_{j_1 l_1}} O_{l_1}, \tag{2.30a}$$

where I_{l_1} and $O_{l_1} (= I^*_{l_1})$ refer to incoming and outgoing waves (in the Coulomb field if the particles are charged). Alternatively,

$$f_{j_1 l_1}(k_1, r) \sim \frac{\mathrm{e}^{i(\delta_{j_1 l_1} + \sigma_{l_1})}}{k_1 r} [\cos \delta_{j_1 l_1} F_{l_1}(k_1, r) + \sin \delta_{j_1 l_1} G_{l_1}(k_1, r)], \tag{2.30b}$$

where $\delta_{j_1 l_1}$ and σ_{l_1} are the nuclear and Coulomb phase shifts, respectively, and $F_{l_1}(k_1, r)$, $G_{l_1}(k_1, r)$ are the regular and irregular Coulomb wave-functions.

The form of $g^*_{j_2 l_2}(k_2, r)$ may be found by use of the result that the reaction matrix is symmetric because of invariance under time-reversal [10]). Thus,

$$\langle c \gamma j_2 \zeta_2 | R | a \alpha j_1 \zeta_1 \rangle = \langle a \alpha j_1 \zeta_1 | R | c \gamma j_2 \zeta_2 \rangle, \tag{2.31}$$

and, therefore by use of the expansion (1.2), it follows that, except for factors depending on l, s, and j, which in any final expression, appear bilinearly having a product equal to unity, we have the following equalities

$$\langle c || j(ls) | a \rangle = \langle a | j(ls) || c \rangle; \quad \langle j_2(c) | j(ls) || j_1(a) \rangle = \langle j_1(a) || j(ls) | j_2(c) \rangle. \tag{2.32}$$

We represent $\theta_{j(ls)}(c, a)$ by $\langle c||j(ls)|a\rangle$.

Just as in (2.26), we may express the reduced matrix element $\langle j_1(a)||j(ls)|j_2(c)\rangle$ in terms of the radial eigenfunctions for the inverse process so that

$$\langle j_1(a)||j(ls)|j_2(c)\rangle = \{\langle j_1(a)||j(ls)|j_2(c)\rangle\} \int \mathrm{d}r r^2 \bar{f}^*_{j_1 l_1}(k_1, r) U_{j(ls)}(r) \bar{g}_{j_2 l_2}(k_2, r), \quad (2.33)$$

where $\bar{g}_{j_2 l_2}$ and $\bar{f}_{j_1 l_1}$ correspond to the "incoming" and "outgoing" radial solutions. The coefficients of the integrals in (2.26) and (2.33) are equal to each other and therefore it follows from (2.32) that

$$\bar{f}_{j_1 l_1}(k_1, r) = f^*_{j_1 l_1}(k_1, r); \qquad \bar{g}_{j_2 l_2}(k_2, r) = g^*_{j_2 l_2}(k_2, r). \quad (2.34)$$

Furthermore, we expect $\bar{g}_{j_2 l_2}(k_2, r)$ to be the solution of the Schrödinger equation for the inverse process

$$\left\{\frac{\mathrm{d}^2}{\mathrm{d}r^2} + k_2^2 - \frac{l_2(l_2+1)}{r^2} - \frac{2m_2^*}{\hbar^2} V^{(2)}_{j_2 l_2}(r) + V_{\mathrm{Coul}}(r)\right\} r \bar{g}_{j_2 l_2}(k_2, r) = 0, \quad (2.35)$$

where $V^{(2)}_{j_2 l_2}(r)$ is the optical-model potential for elastic scattering of radiation (2) having energy E_2 by the nucleus with spin c. The asymptotic form of $\bar{g}_{j_2 l_2}(k_2, r)$ is given by

$$\begin{aligned} \bar{g}_{j_2 l_2}(k_2, r) = g^*_{j_2 l_2}(k_2, r) &\sim I_{l_2} - \mathrm{e}^{2i\delta_{j_2 l_2}} O_{l_2} \\ &= \frac{\mathrm{e}^{i(\delta_{j_2 l_2} + \sigma_{l_2})}}{k_2 r} [\cos \delta_{j_2 l_2} F_{l_2}(k_2, r) + \sin \delta_{j_2 l_2} G_{l_2}(k_2, r)]. \quad (2.36) \end{aligned}$$

We thus see that the "outgoing" solution, $g_{j_2 l_2}(k_2, r)$, does, indeed, correspond to an outgoing plane-wave (with Coulomb distortion) together with an incoming spherical wave (with Coulomb distortion), and that this radial function is an eigenfunction [18]) of a Hamiltonian with $V^{(2)*}_{j_2 l_2}(r)$ and not $V^{(2)}_{j_2 l_2}(r)$.

The formulae in the earlier parts of this section refer to processes where the angular momentum $j(ls)$ is absorbed by the target nucleus and emitted by the incident radiation. If we repeat the calculation leading to (2.19) and (2.24) for the inverse process of emission of $j(ls)$ by the target nucleus of spin c and absorption of this radiation by the radiation of spin s_2, we are led to expressions for $\rho_{k_2 \kappa}(s_2)$ and $\varepsilon_{k_2 \kappa}(s_1)$. Making use of (2.32), we find the result previously obtained by Satchler [19]) in a slightly more general manner

$$\hat{s}_2^2 \rho^{\mathrm{I}}_{k_2 \kappa}(s_2) = \varepsilon^{\mathrm{II}*}_{k_2 \kappa}(s_2), \quad (2.37)$$

The statistical tensor refers to the polarization of radiation of spin s_2, emitted in any process I, while the efficiency tensor refers to the inverse process II, where the incoming radiation of spin s_2 is prepared in a certain polarization state. The co-ordinate axes defining these tensors are determined through use of the unit vectors $\mathbf{n} = \mathbf{k}_{\mathrm{in}} \times \mathbf{k}_{\mathrm{out}} / |\mathbf{k}_{\mathrm{in}} \times \mathbf{k}_{\mathrm{out}}|$. Thus, for the statistical tensor, the y-axis is along $-\mathbf{n}$ and the z-axis is along $\mathbf{k}_{\mathrm{out}}$, while for the efficiency tensor,

the y-axis is along $+\mathbf{n}$ (as defined for the inverse process) and the z-axis is along $\mathbf{k}_{\text{in}}$. The above relation provides the necessary directive for obtaining polarization effects for a process (say, the pick-up process) in terms of tensors associated with the inverse phenomenon (stripping). Angular distributions, not involving polarization are identical; whereas the total cross-sections are multiplied by different statistical factors and momentum factors.

The result (2.37) has immediate application to elastic scattering where the above formulation may be used provided that we put $j = l = 0$. If we consider a double process and neglect energy losses from the first to the second scattering and also deal with equal scattering angles, we get the well-known result for spin-$\frac{1}{2}$ particles that the polarization arising from the first scattering is equal to the "left-right" asymmetry $(L-R)/(L+R)$ that would arise in a scattering process if the initiating beam were fully polarized [20]). This is easily found by use of (2.23). More generally, for particles of arbitrary spin s it may be shown by use of the definition (2.12) and (2.13), that if P is the magnitude of the "vector" polarization arising from the first scattering, then the "left-right" asymmetry in another process where the initiating beam is fully polarized is equal [19]) to $3s/(s+1)P$ (i.e. where the vector polarization equals unity and there is no polarization of higher rank).

If the quantum number j does not refer to transfer of a real particle and merely describes an exchange of angular momentum between nucleus and radiation (as is the case in inelastic scattering), then it is irrelevant whether we consider this angular momentum to be absorbed or emitted by the incident radiation. We can carry out the development in the earlier parts of this section with the coupling-scheme changed so that

$$\mathbf{a} = \mathbf{c}+\mathbf{j}; \qquad \mathbf{j}_1+\mathbf{j} = \mathbf{j}_2. \tag{2.38}$$

We now obtain formulae in terms of the reduced matrix elements $\langle c|j(ls)||a\rangle$ and $\langle j_2(c)||j(ls)|j_1(a)\rangle$. This corresponds to the expansion of the matrix element (1.2) in the following way:

$$\langle c\gamma(l_2s_2)j_2\zeta_2|R|a\alpha(l_1s_1)j_1\zeta_1\rangle = \sum_{jls\zeta} \langle c|j(ls)||a\rangle (c\gamma, j\zeta|a\alpha)(j_1\zeta_1, j\zeta|j_2\zeta_2)\langle j_2(c)||j(ls)|j_1(a)\rangle, \tag{2.39}$$

which may be written as

$$\sum_{jls\zeta} \langle c|j(ls)||a\rangle \frac{\hat{a}}{\hat{c}} (-)^{a-c}(a\alpha, j\zeta|c\gamma)\frac{\hat{j}_2}{\hat{j}_1}(-)^{j_1-j_2}(j_2\zeta_2, j\zeta|j_1\zeta_1)\langle j_2(c)||j(ls)|j_1(a)\rangle. \tag{2.40}$$

Equating the above with (1.2) and ignoring factors depending on s, l and j which in any final expression appear bilinearly and equal unity, we have

$$\langle c||j(ls)|a\rangle = \frac{\hat{a}}{\hat{c}}(-)^{a-c}\langle c|j(ls)||a\rangle;$$

$$\langle j_2(c)|j(ls)||j_1(a)\rangle = \frac{\hat{j}_2}{\hat{j}_1}(-)^{j_1-j_2}\langle j_2(c)||j(ls)|j_1(a)\rangle. \quad (2.41)$$

Thus, for inelastic scattering, there exists an alternative set of expressions for the polarization and the angular distributions, corresponding to the two modes of description of the transformed radiation, i.e., according as there is absorption or emission from one system to another. These expressions are obtained from (2.10), (2.11), (2.19) and (2.24) by the replacement of the reduced matrix elements $\langle a|j(ls)||c\rangle$ and $\langle j_1(c)||j(ls)|j_2(a)\rangle$ by $\langle a||j(ls)|c\rangle$ and $\langle j_1(c)|j(ls)||j_2(a)\rangle$ as in (2.41).

3. Alternative Expressions for the Angular Distributions and Polarizations

Equivalent results to those already found may be derived by use of techniques introduced by Coester and Jauch [9]). Using the notation for quantum numbers previously defined, we can write the probability of detection of the outgoing radiation and nuclei in angles Ω_2, (with or without polarization), corresponding to initial radiation and nuclei defined by angles Ω_1, and in certain states of polarization as †

$$W(\Omega_1\Omega_2)$$
$$= \sum\langle c\gamma(l_2s_2)j_2\zeta_2C|\rho^{(f)}|c'\gamma'(l_2's_2)j_2'\zeta_2'C'\rangle\langle c'\gamma'(l_2's_2)j_2'\zeta_2'C'|\varepsilon|c\gamma(l_2s_2)j_2\zeta_2C\rangle \quad (3.1)$$

where C and C' represent quantum numbers aside from $c\gamma$, $c'\gamma'$, designating the final nuclear state.

This may be rewritten in terms of statistical and efficiency tensors as

$$W(\Omega_1\Omega_2) = \sum\rho^{(f)}_{k_c\kappa_c;\,k_2\kappa_2}[cC(l_2s_2)j_2,\, c'C'(l_2's_2)j_2']\varepsilon^*_{k_c\kappa_c}(cC,\, c'C')$$
$$\varepsilon^*_{k_2\kappa_2}[(l_2s_2)j_2,\, (l_2's_2)j_2']. \quad (3.2)$$

These tensors arise in the decomposition of densities and efficiency matrices into their spherical-tensor components. We have, for example,

$$\varepsilon_{k_c\kappa_c}(cC,\, c'C') = \sum_{\gamma\gamma'}(-)^{c'-\gamma'}(c\gamma,\, c'-\gamma'|k_c\kappa_c)\langle c\gamma C|\varepsilon|c'\gamma'C'\rangle, \quad (3.3a)$$

while the combined statistical tensor is defined as

$$\rho^{(f)}_{k_c\kappa_c;\,k_2\kappa_2}[cC(l_2s_2)j_2,\, c'C'(l_2's_2)j_2'] = \sum_{\gamma\gamma'\zeta_2\zeta_2'}(-)^{c'-\gamma'+j_2'-\zeta_2'}(c\gamma,\, c'-\gamma'|k_c\kappa_c)$$
$$(j_2\zeta_2,\, j_2'-\zeta_2'|k_2\kappa_2)\langle c\gamma(l_2s_2)j_2\zeta_2C|\rho^{(f)}|c'\gamma'(l_2's_2)j_2'\zeta_2'C'\rangle. \quad (3.3b)$$

The efficiency tensors for nucleus and radiation appear separately since, in the region of observation, the two systems are assumed to be non-interacting.

† In several of the formulae to follow, we shall omit explicit indication of the parameters over which the summation is to be made. In such instances, a convention of summation over repeated symbols is to be adopted.

If we now interpret the final nucleus as arising from the absorption of radiation with angular momentum $j(ls)$, i.e. $\mathbf{a}+\mathbf{j}=\mathbf{c}$, the statistical tensor can be expressed as follows:

$$\rho^{(f)}_{k_c\kappa_c;\,k_2\kappa_2}[cC(l_2s_2)j_2;\,c'C'(l_2's_2)j_2'] = \sum_{\substack{jj'll'AA'k\kappa \\ ss'aa'}} \rho^{(i)}_{k_a\kappa_a;\,k\kappa;\,k_2\kappa_2}[aA(ls)j(l_2s_2)j_2;\,a'A'(l's')j'(l_2's_2)j_2'] \qquad (3.4)$$

$$(k_a\kappa_a, k\kappa|k_c\kappa_c)\hat{c}^2\hat{k}\hat{k}_a \begin{Bmatrix} a & j & c \\ a' & j' & c' \\ k_a & k & k_c \end{Bmatrix} \langle cCj_2||j(ls)|aA\rangle\langle cC'j_2'||j'(l's')|a'A'\rangle^*,$$

where $\rho^{(i)}_{k_a\kappa_a;\,k\kappa k_2\kappa_2}$ is defined in a manner obvious from (3.3a) and (3.3b). The quantum numbers A, A' represent quantum numbers associated with initial states of the system aside from a, a', α and α' and they include those associated with the incident radiation.

We now decompose $\rho^{(i)}_{k_a\kappa_a;\,k\kappa k_2\kappa_2}$ to take into account the transition $\mathbf{j}_1=\mathbf{j}_2+\mathbf{j}$, so that

$$\rho^{(i)}_{k_a\kappa_a;\,k\kappa;k_2\kappa_2}\langle cCj_2||j(ls)|aA\rangle\langle cC'j_2'||j'(l's')|a'A'\rangle^* = \sum_{k_1\kappa_1 j_1 l_1 j'_1 l'_1} \rho^{(i)}_{k_a\kappa_a}(a,a')\rho^{(i)}_{k_1\kappa_1}[(l_1s_1)j_1,\,(l_1's_1)j_1'](k_2\kappa_2, k\kappa|k_1\kappa_1)\hat{j}_1\hat{j}_1'\hat{k}\hat{k}_2 \qquad (3.5)$$

$$\begin{Bmatrix} j_1 & j_2 & j \\ j_1' & j_2' & j' \\ k_1 & k_2 & k \end{Bmatrix} \langle cC||j(ls)|a\rangle\langle cC'||j'(l's')|a'\rangle^*\langle j_2(c)|j(ls)||j_1(a)\rangle\langle j_2'(c')|j'(l's')||j_1'(a')\rangle^*.$$

Again, we factorize the initial statistical tensors in accordance with the assumption of non-interacting nuclear and radiation systems.

If we assume that the target and residual nucleus are "sharp", but that no measurement is made of their states, then we find

$$W(\Omega_1\Omega_2) = \frac{\hat{c}^2}{\hat{a}^2}\sum \langle c||j(ls)|a\rangle\langle c||j(l's')a\rangle^* \frac{\hat{j}_1\hat{j}_1'}{\hat{j}^2}(-)^{j+k-j_2'-j_1}$$

$$c_{k\kappa_1}[(l_1s_1)j_1,\,(l_1's_1)j_1']c^*_{k\kappa_2}[(l_2s_2)j_2,\,(l_2's_2)j_2']W(j_1j_1'j_2j_2';\,kj)\mathscr{D}^k_{\kappa_2\kappa_1}(\mathscr{R}_2^{-1}\mathscr{R}_1) \qquad (3.6)$$
$$\langle j_2(c)|j(ls)||j_1(a)\rangle\langle j_2'(c)|j(l's')||j_1'(a)\rangle^*,$$

where $\mathscr{R}_2^{-1}\mathscr{R}_1$ is a rotation carrying the reference frame attached to the outgoing radiation to one attached to the incoming radiation, and $c_{k\kappa}$ designates the radiation parameters [21]) introduced by Racah to describe the means of preparation and detection of the radiation. For the particular case where no polarization is involved [11])

$$c_{k\kappa}[(l_1s_1)j_1,\,(l_1's_1)j_1'] = \delta_{\kappa 0}\frac{\hat{j}_1\hat{j}_1'\hat{l}_1\hat{l}_1'}{4\pi\hat{s}_1^2}(-)^{j_1+k-s_1}(l_10,\,l_1'0|k0)W(l_1l_1'j_1j_1';\,ks_1),$$
$$c^*_{k\kappa}[(l_2s_2)j_2,\,(l_2's_2)j_2'] = \delta_{\kappa 0}\frac{\hat{j}_2\hat{j}_2'\hat{l}_2\hat{l}_2'}{4\pi}(-)^{j_2+k-s_2}(l_20,\,l_2'0|k0)W(l_2l_2'j_2j_2';\,ks_2). \qquad (3.7)$$

Normalizing the wave function describing the radiations as plane waves of the form $e^{i\mathbf{k}\cdot\mathbf{r}}$ which are distorted, we finally obtain for the differential cross-section

$$\frac{d\sigma(\theta)}{d\Omega} = \frac{m_1^* m_2^*}{64\pi^4\hbar^4}\frac{k_2}{k_1}\frac{\hat{c}^2}{\hat{a}^2 \hat{s}_1^2}\sum\frac{1}{\hat{j}^2}\theta_{j(ls)}(c,a)\theta_{j(l's')}(c,a)$$

$$\hat{j}_1^2\hat{j}_1'^2\hat{j}_2\hat{j}_2'\hat{l}_1\hat{l}_1'\hat{l}_2\hat{l}_2'(-)^{k+j+j_2-j_2'-s_1-s_2}(l_1 0, l_1' 0|k0)(l_2 0, l_2' 0|k0)W(l_1 l_1' j_1 j_1'; ks_1) \quad (3.8)$$

$$W(l_2 l_2' j_2 j_2'; ks_2)W(j_1 j_1' j_2 j_2'; kj)\langle j_2(c)|j(ls)||j_1(a)\rangle\langle j_2'(c)|j(l's')||j_1'(a)\rangle^* P_k(\cos\theta).$$

It is to be noted that the above expression leads simply to the total cross-section, σ_T, which is equal to 4π times the right-hand side when $k = 0$. Thus

$$\sigma_T = \frac{m_1^* m_2^*}{16\pi^3\hbar^4}\frac{k_2}{k_1}\frac{\hat{c}^2}{\hat{a}^2\hat{s}_1^2}\sum_{jj_1j_2j_1'j_2'}\frac{\hat{j}_1^2}{\hat{j}^2}\Big|\sum_{ls}\theta_{j(ls)}(c,a)\langle j_2(c)|j(ls)||j_1(a)\rangle\Big|^2. \quad (3.9)$$

The expressions for polarization are found by inserting into (3.6) appropriate values of the radiation parameters.

If the alternative coupling scheme

$$\mathbf{a} = \mathbf{c}+\mathbf{j}, \qquad \mathbf{j}_1+\mathbf{j} = \mathbf{j}_2 \quad (3.10)$$

is used, (3.6) and (3.8) are valid, provided that we replace the matrix elements $\theta_{j(ls)}(c,a) = \langle c||j(ls)|a\rangle$ and $\langle j_2(c)|j(ls)||j_1(a)\rangle$ by

$$\frac{\hat{a}}{\hat{c}}(-)^{a-c}\langle c|j(ls)||a\rangle \quad \text{and} \quad \frac{\hat{j}_2}{\hat{j}_1}(-)^{j_1-j_2}\langle j_2(c)||j(ls)|j_1(a)\rangle,$$

respectively.

The equivalence of (3.8) with the differential cross-sections given previously, in (2.9), together with the results for polarization, are readily established by Racah algebra which may be used to prove the following equations:

$$\hat{j}_1^2\hat{j}_1'^2\hat{j}_2\hat{j}_2'(-)^{s_1-j+j_2'+l_1'+\kappa}\sum_{kk_{2l}}\hat{k}_{2l}\hat{k}_{2s}(l_2 0, l_2' 0|k_{2l}0)(k_{2l}0, k_{2s}\kappa|k\kappa)$$

$$\times\begin{Bmatrix} l_2 & l_2' & k_{2l} \\ s_2 & s_2 & k_{2s} \\ j_2 & j_2' & k \end{Bmatrix}(l_1 0, l_1' 0|k0)W(l_1 l_1' j_1 j_1'; ks_1)W(j_1 j_1' j_2 j_2'; kj)\mathscr{D}^k_{\kappa 0}(0\theta 0) \quad (3.11a)$$

$$= \sum_{\sigma_1\sigma_2\sigma_2'\zeta\zeta_2}(-)^{s_2-\sigma_2}(s_2\sigma_2, s_2-\sigma_2'|k_{2s}\kappa)(l_2 0, s_2\sigma_2|j_2\sigma_2)(l_1 0, s_1\sigma_1|j_1\sigma_1)(j_2\zeta_2, j\zeta|j_1\sigma_1)$$

$$\times(l_2' 0, s_2\sigma_2|j_2'\sigma_2)(l_1' 0, s_1\sigma_1|j_1'\sigma_1)(j_2'\zeta_2, j\zeta|j_1'\sigma_1)\mathscr{D}^{j_2}_{\sigma_2\zeta_2}(0\theta 0)\mathscr{D}^{j_2'*}_{\sigma_2'\zeta_2}(0\theta 0)$$

$$= \sum_{\sigma_1\sigma_2\sigma_2'\zeta\zeta_1\zeta_1'}(-)^{s_2-\sigma_2}(s_2\sigma_2, s_2-\sigma_2'|k_{2s}\kappa)(l_1 0, s_1\sigma_1|j_1\sigma_1)(l_2 0, s_2\sigma_2|j_2\sigma_2)(j_2\sigma_2, j\zeta|j_1\zeta_1)$$

$$\times(l_1' 0, s_1\sigma_1|j_1'\sigma_1)(l_2' 0, s_2\sigma_2|j_2'\sigma_2)(j_2'\sigma_2, j\zeta|j_1'\zeta_1')\mathscr{D}^{j_1}_{\zeta_1\sigma_1}(0\theta 0)\mathscr{D}^{j_1'*}_{\zeta_1'\sigma_1}(0\theta 0). \quad (3.11b)$$

If there is no measurement of polarization, $k_{2s} = 0$ and the above equations when inserted into (3.8) yield the corresponding result in (2.9).

3.1. COMPARISON OF THE TWO EXPRESSIONS

We note that the final expressions in this section involve no summation over magnetic quantum numbers and therefore, by reason of their compactness, these seem to be preferable to the corresponding results in the previous section. Nevertheless, the main use of such complicated expressions, as they appear in either section, is in numerical calculation, and the considerably smaller number of summation parameters in the previous section gives great advantage to the former results. Furthermore, the Clebsch-Gordan coefficients, $(l0, s\sigma|j\sigma)$, which appear in these expressions are merely combinations of phase factors and statistical factors for the case of spin-$\frac{1}{2}$ particles, whereas the corresponding simplifications in the expressions of section 3 is not nearly as great. The main drawback in the earlier result is that a separate summation over quantum numbers is required for each angle, and this is not the case in the later formulae. The presence of rotation matrices which may be of half-integral rank presents no difficulty, since these may be calculated by means of a power-series expression involving trigonometric functions of the half-angles. Considering all these factors, it would seem that if the number of parameters in the summation is large (high-energy processes), the numerical calculations are more easily done using the formulae of section 2.

It is interesting to observe that most deuteron-stripping formulae using the distorted wave formalism, have been derived using the approach of section 2, whereas almost all calculations for inelastic scattering have yielded formulae of the form of section 3.

The latter two sets of expressions do not exhaust the possibilities. It is possible to derive a new set of expressions similar to those in (2.9), provided that we replace the following factors that appear in $X^{j(ls)\zeta}_{\sigma_2\sigma_1}(\mathscr{R}_2\mathscr{R}_1)$ by the prescription

$$\hat{l}_2(l_2 0, s_2\sigma_2|j_2\sigma_2)\mathscr{D}^{j_2}_{\sigma_2\sigma_1-\zeta}(0\theta 0)\to\sqrt{4\pi}(l_2\sigma_1-\sigma_2-\zeta, s_2\sigma_2|j_2\sigma_1-\zeta)Y^{\zeta+\sigma_2-\sigma_1}_{l_2}(\theta, 0) \quad (3.12)$$

$$\hat{l}_1(l_1 0, s_1\sigma_1|j_1\sigma_1)\mathscr{D}^{j_1}_{\zeta+\sigma_2,\sigma_1}(0\theta 0)\to\sqrt{4\pi}(l_1\zeta+\sigma_2-\sigma_1, s_1\sigma_1|j_1\zeta+\sigma_2)Y^{\zeta+\sigma_2-\sigma_1}_{l_1}(\theta, 0),$$

according as one uses (2.10) or (2.11). In the first case, the z-axis is to be along $\mathbf{k}_1$ and in the second case along $\mathbf{k}_2$. There appears to be no advantage in the use of these new expressions if the calculation is to be done by means of electronic computers.

4. Contributions from Compound-Nucleus Formation

In the following discussion, we allow for the possibility of transitions from the initial to the final states which proceed through the compound-nucleus mechanism. A full discussion of these effects was first given in terms of the (n, d) and (p, d) pick-up reactions by Thomas [22]), and Breit [23]) has added some valuable comments concerning the validity of the assumptions made by Thomas. In this treatment, the compound-nucleus formation is interpreted as accounting

for most of the observed cross-section, while the direct interaction provides a perturbation. Using first-order perturbation theory one finds three contributions, two involving the separate contributions of the direct and compound-nucleus processes and, in addition, there is the interference. The latter contribution, which may vanish, if an average is made over an energy interval, large enough to include contributions from many levels, may be significant in the neighbourhood of an isolated resonance.

The two processes are assumed to originate from two distinct regions in configuration space separated by a surface, which is vaguely associated with the nuclear surface. The direct mechanism owes its origin to the direct-interaction potential V_D, which vanishes in the inner configuration. Although an interpretation of this kind seems reasonable for direct-processes with composite particles, such as He^3 or H^3, this description seems to be a very restrictive one for deuteron stripping, and is hardly valid for inelastic scattering of nucleons if this process is interpreted as occurring through direct nucleon-nucleon encounters. It is certainly not borne out by the numerical work of Tobocman concerning deuteron-stripping processes. One may consider V_D as acting internally; however, it is not clear, using the distorted-wave theory, how the contributions of the distant levels are to be dealt with, since they are accounted for both through the optical-model distortion and also in the resonance-reaction formalism. For the present discussion, we shall assume that V_D acts throughout the configuration space and leave open the proper choice of parameters typifying the nuclear distortion.

To account for the general type of process, we write the reaction matrix in the form

$$\langle c, (l_2 s_2) j_2, b, |R| a_1 (l_1 s_1) j_1, b\rangle = \langle c, (l_2 s_2) j_2, b|R_{CN}|a, (l_1 s_1) j_1, b\rangle + \langle c, (l_2 s_2) j_2, b|R_D|a, (l_1 s_1) j_1, b_1\rangle, \quad (4.1)$$

where b represents the total angular momentum of the system, i.e. $\mathbf{a}+\mathbf{j}_1 = \mathbf{b} = \mathbf{c}+\mathbf{j}_2$. Expressions for R_{CN} have been first given for one level by Wigner and Eisenbud [24]) and also by Blatt and Biedenharn [25]). By means of Green's theorem, it is possible to relate R_D with V_D (see ref. [22]))

$$\langle |R_D| \rangle = \frac{i}{\hbar} \int_\tau \psi_2^* V_D \psi_1 \mathrm{d}\tau, \quad (4.2)$$

where ψ_1 and ψ_2, representing, symbolically, the states of the incoming and outgoing radiation, are normalized to unit flux for the incoming and outgoing channels. This differs from the choice of eigenfunctions made in (2.28).

If we proceed as in the expansion of (1.2) we find, by means of (4.2)

$$\langle c, (l_2 s_2) j_2, b\beta|R_D|a, (l_1 s_1) j_1, b\beta\rangle = -\frac{4ik_1 k_2}{\hbar\sqrt{v_1 v_2}(4\pi)^2} \sum_{\alpha\gamma\zeta_1\zeta_2 j\zeta} (c\gamma, j_2\zeta_2|b\beta)(a\alpha, j_1\zeta_1|b\beta)(a\alpha, j\zeta|c\gamma)(j_2\zeta_2, j\zeta|j_1\zeta_1) \theta_{j(ls)}(c, a)\langle j_2(c)|j(ls)||j_1(a)\rangle, \quad (4.3)$$

where the reduced matrix element is defined using as eigenstates those contained in (2.28).

Noting that the left-hand side of (4.3) is independent of the magnetic quantum number β, we sum over magnetic quantum numbers and find

$$\langle c, (l_2 s_2) j_2, b\beta | R_D | a, (l_1 s_1) j_1, b\beta \rangle$$
$$= \frac{-4ik_1 k_2}{\hbar \sqrt{v_1 v_2} (4\pi)^2} \sum_{jls} \hat{c} \hat{j}_1 (-)^{b-j_2-c} W(j_1 j_2 ca; jb) \theta_{j(ls)}(c, a) \langle j_2(c) | j(ls) || j_1(a) \rangle. \quad (4.4)$$

We invert this last relation using the unitary property of the Racah coefficients, and obtain

$$\sum_{ls} \theta_{j(ls)}(c, a) \langle j_2(c) | j(ls) || j_1(a) \rangle$$
$$= i \frac{(4\pi)^2 \sqrt{v_1 v_2} \hbar}{4k_1 k_2} \frac{\hat{j}^2}{\hat{c} \hat{j}_1} \sum_b (-)^{b-j_2-c} \hat{b}^2 W(j_2 j_1 ca; jb) \langle c, (l_2 s_2) j_2, b | R_D | a, (l_1 s_1) j_1, b \rangle. \quad (4.5)$$

It is thus clear that one may obtain the differential cross-section and polarization effects and take into account compound-nucleus formation if one replaces $\sum_{ls} \theta_{j(ls)}(c, a) \langle j_2(c) | j(ls) || j_1(a) \rangle$ by

$$\sum_{ls} \theta_{j(ls)}(c, a) \langle j_2(c) | j(ls) || j_1(a) \rangle + i \frac{(4\pi)^2 \hbar \sqrt{v_1 v_2}}{4k_1 k_2} \frac{\hat{j}^2}{\hat{c} \hat{j}_1}$$
$$\times \sum_b (-)^{b-j_2-c} \hat{b}^2 W(j_2 j_1 ca; jb) \langle c, (l_2 s_2) j_2, b | R_{CN} | a, (l_1 s_1) j_1, b \rangle. \quad (4.6)$$

The differential cross-section can be written in the following form:

$$\frac{d\sigma}{d\Omega} = \left(\frac{d\sigma}{d\Omega}\right)_D + \left(\frac{d\sigma}{d\Omega}\right)_{CN} + \left(\frac{d\sigma}{d\Omega}\right)_{INT} \quad (4.7)$$

The direct-reaction contribution is given in (2.9); while the compound-nucleus contribution is given as

$$\left(\frac{d\sigma}{d\Omega}\right)_{CN} = \frac{1}{4k_1^2 \hat{a}^2 \hat{s}_1^2} \sum_{\alpha\gamma\sigma_1\sigma_2} \Big| \sum_{j_1 l_1 j_2 i_2 j i \zeta b \zeta_2} (a\alpha, j\zeta | c\gamma)(l_1 0, s_1 \sigma_1 | j_1 \sigma_1)$$
$$\times (l_2 0, s_2 \sigma_2 | j_2 \sigma_2)(j_2 \zeta_2, j\zeta | j_1 \sigma_1) \frac{\hat{l}_1 \hat{l}_2 \hat{j} \hat{b}^2}{\hat{c} \hat{j}_1} (-)^{b-j_2-c} W(j_2 j_1 ca; jb) \quad (4.8)$$
$$\times \mathscr{D}^{j_2}_{\sigma_1 \zeta_2}(000) \langle c, (l_2 s_2) j_2, b | R_{CN} | a, (l_1 s_1) j_1, b \rangle|^2.$$

This latter relation simplifies by the use of Racah algebra. Thus,

$$\sum_{j\zeta} (a\alpha, j\zeta | c\gamma)(j_2 \zeta_2, j\zeta | j_1 \sigma_1) \frac{\hat{j} \hat{b}^2}{\hat{c} \hat{j}_1} (-)^{b-j_2-c} W(j_2 j_1 ca; jb)$$
$$= \sum_\beta (a\alpha, j_1 \sigma_1 | b\beta)(c\gamma, j_2 \sigma_2 | b\beta), \quad (4.9)$$

so that

$$\left(\frac{d\sigma}{d\Omega}\right)_{CN} = \frac{1}{4k_1^2}\frac{1}{\hat{a}^2 s_1^2}\sum_{\alpha\gamma\sigma_1\sigma_2}\Big|\sum_{j_1 l_1 j_2 l_2 b\zeta_2} l_1 l_2 (l_1 0, s_1\sigma_1|j_1\sigma_1)(l_2 0, s_2\sigma_2|j_2\sigma_2)$$
$$\times (a\alpha, j_1\sigma_1|b\beta)(c\gamma, j_2\zeta_2|b\beta)\mathscr{D}^{j_2}_{\sigma_2\zeta_2}(0\theta 0)\langle c, j_2, b|R_{CN}|a, j_1, b\rangle|^2, \quad (4.10)$$

which, on further summation over magnetic quantum numbers, reduces to the formula given by [11]):

$$\left(\frac{d\sigma}{d\Omega}\right)_{CN} = \frac{1}{4k_1^2}\frac{1}{\hat{a}^2 s_1^2}\sum A_k(l_1 j_1 l_1' j_1'; abb')A_k(l_2 j_2 l_2' j_2'; cbb') \quad (4.11a)$$
$$\times\langle c, (l_2 s_2) j_2, b|R_{CN}|a, (l_1 s_1) j_1, b\rangle\langle c, (l_2' s_2) j_2', b'|R_{CN}|a, (l_1' s_1) j_1', b'\rangle^* P_k(\cos\theta),$$

where

$$A_k(l_1 j_1 l_1' j_1'; abb') \equiv (-)^{a-b'-s_1}\hat{b}\hat{b}' W(bb' j_1 j_1'; ka) Z'(l_1 j_1 l_1' j_1'; s_1 k), \quad (4.11b)$$

and $Z'(l_1 j_1 l_1' j_1'; s_1 k)$ can be found through the related coefficient

$$Z(l_1 j_1 l_1' j_1'; s_1 k) = i^{k-l_1+l_1'} Z'(l_1 j_1 l_1' j_1'; s_1 k)$$

which is extensively tabulated (see for example Sharp *et al.* [26])).

The interference term is simplified by use of (4.9) giving

$$\left(\frac{d\sigma}{d\Omega}\right)_{INT} = \frac{m_1^* m_2^*}{(4\pi\hbar)^2}\sqrt{\frac{k_2}{k_1^3}}\frac{i\hat{c}}{\hat{a}^2 s_1^2}\sum \hat{j}_1'(-)^{k+j-j_1'+s_2-s_1+c-b}$$
$$\times Z'(l_2 j_2 l_2' j_2'; s_2 k) Z'(l_1 j_1 l_1' j_1'; s_1 k) W(j_1 j_1' j_2 j_2'; kj) W(j_2 j_1 ca; jb)\theta_{j(ls)}(c, a) \quad (4.12)$$
$$\times\langle j_2'(c)||j(ls)||j_1'(a)\rangle^*\langle c, (l_2 s_2) j_2, b|R_{CN}|a, (l_1 s_1) j_1, b\rangle P_k(\cos\theta)$$
$$+\text{complex conjugate.}$$

Clearly, from the complexity of the above results, the most sensible numerical procedure would be to use eq. (2.9) together with the substitution of (4.6).

In most cases, the reaction-matrix element R_{CN} is given in the channel-spin representation. As shown by Satchler [27]) it is possible to write the relationship between the matrix elements of R_{CN} in both representations as follows:

$$\langle c, (l_2 s_2) j_2, b|R_{CN}|a, (l_1 s_1) j_1, b\rangle$$
$$= \sum_{S_1 S_2}\langle (c s_2) S_2, l_2, b|R_{CN}|(a s_1) S_1, l_1, b\rangle\langle j_1|S_1\rangle\langle j_2|S_2\rangle, \quad (4.13a)$$

where

$$\langle j_1|S_1\rangle \equiv (-)^{l_1+s_1-j_1}\hat{S}_1\hat{j}_1 W(a s_1 b l_1; S_1 j_1). \quad (4.13b)$$

5. Effects of Spin-Dependent Distortion

In the present section we shall consider the possibility of extracting information concerning the presence of spin-dependent terms in the optical-model

distorting potentials. In most considerations, this spin-dependent distortion is ignored, with the result that great restrictions are placed on the nature of the polarization arising from the direct reactions. For example, in deuteron stripping it is found [28]) that if the distortion is independent of spin, the asymmetry arising from incoming deuteron polarization is independent of second-rank polarization, and, furthermore, the effects of the first-rank polarization are correlated with the nucleon polarization arising from deuteron unpolarized beams. In addition, with this assumption concerning the distortion, no polarization effects appear at all, if the orbital angular-momentum transfer corresponds uniquely to $l = 0$.

We shall examine separately the effects of spin-dependent distortion in either the incoming and outgoing states and present the general form of the angular distribution followed by expressions for the polarization of the outgoing radiation and for the efficiency of the process in detecting polarization in the incident beam. We shall then specialize to the particular case, $l = 0$. All these results are presented in terms of reactions with radiations and nuclei of arbitrary spin. The expressions for specific direct processes are to be found in section 6.

In our present considerations, we limit ourselves to interaction operators for stripping which are not dependent on spin. This is done merely to simplify the analysis. We shall deal in the next section with situations where more than one value of s is allowed and therefore presume the presence of some type of spin-dependent operator; however, no specific calculations are made in this case. The absence of spin-dependent direct-interaction operators allows us to decouple the spin and orbital angular-momentum eigenfunctions and we find for the reduced matrix element

$$(j_2\zeta_2, j\zeta|j_1\zeta_1)\langle(l_2s_2)j_2(c)|j(ls)||(l_1s_1)j_1(a)\rangle = \sum_{\lambda\lambda_1\lambda_2\sigma\sigma_1\sigma_2} (l\lambda, s\sigma|j\zeta)(l_1\lambda_1, s_1\sigma_1|j_1\zeta_1)$$
$$\times (l_2\lambda_2, s_2\sigma_2|j_2\zeta_2)(l_2\lambda_2, l\lambda|l_1\lambda_1)(s_2\sigma_2, s\sigma|s_1\sigma_1)R_0[j_2l_2jl, j_1l_1; s_2ss_1; ca]. \quad (5.1)$$

The quantity $R_0[\ldots]$, which is independent of magnetic quantum numbers, involves the product of reduced matrix elements $\langle l_2|l||l_1\rangle$ and $\langle s_2|s||s_1\rangle$ together with a radial integral. The expression (5.1) simplifies if we make use of the 9-j symbol, in which case we find

$$\langle(l_2s_2)j_2(c)|j(ls)||(l_1s_1)j_1(a)\rangle = \hat{j}\hat{j}_2\hat{l}_1\hat{s}_1 \begin{Bmatrix} l_2 & s_2 & j_2 \\ l & s & j \\ l_1 & s_1 & j_1 \end{Bmatrix} R_0[j_2l_2jl, j_1l_1; s_2ss_1; ca]. \quad (5.2)$$

The general formulae for the cross-sections and the polarization effects are to be found in section 2. The cross-section for the inverse process, as pointed out in section 2, is obtained by multiplication by statistical and momentum factors, while simple expressions exist relating the polarization and efficiency tensors for each process. The explicit values of $R_0[\ldots]$ for specific processes will be given in section 6.

5.1. NO SPIN-DEPENDENT DISTORTION OF THE INCOMING RADIATION

In this approximation, $f_{j_1 l_1}(k_1, r)$, the incoming radial eigenfunction, and, therefore, R_0 are both independent of j_1. Inserting the expression (5.2) into (2.10), summing over j_1, and using the relation

$$\sum_{j_1} (l_1 0, s_1\sigma_1|j_1\sigma_1)(j_2\sigma_1-\zeta, j\zeta|j_1\sigma_1)\hat{j}_2\hat{j}\hat{l}_1\hat{s}_1 \begin{Bmatrix} l_2 & s_2 & j_2 \\ l & s & j \\ l_1 & s_1 & j_1 \end{Bmatrix}$$
$$= \sum_{\lambda\sigma\sigma_2'} (l_2-\lambda, l\lambda|l_1 0)(l_2-\lambda, s_2\sigma_2'|j_2\sigma_1-\zeta)(l\lambda, s\sigma|j\zeta)(s_2\sigma_2', s\sigma|s_1\sigma_1), \quad (5.3)$$

we find

$$A^{j(ls)\zeta}_{\sigma_2\sigma_1}(\theta) = \sum_{\lambda\sigma\sigma_2'} (l\lambda, s\sigma|j\zeta)(s_2\sigma_2', s\sigma|s_1\sigma_1)C^{l\lambda}_{\sigma_2\sigma_2'}(\theta), \quad (5.4a)$$

where

$$C^{l\lambda}_{\sigma_2\sigma_2'}(\theta) = \sum_{j_2 l_2 l_1} \hat{l}_1\hat{l}_2(l_2 0, s_2\sigma_2|j_2\sigma_2)(l_2-\lambda, s_2\sigma_2'|j_2\sigma_2'-\lambda)(l_2-\lambda, l\lambda|l_1 0)$$
$$\times \mathscr{D}^{j_2}_{\sigma_2\sigma_2'-\lambda}(0\theta 0)R_0(j_2 l_2 jl; l_1). \quad (5.4b)$$

The angular distributions and polarization effects are then given by insertion of (5.4a) and (5.4b) into (2.9), (2.19) and (2.24).

We now specialize to the case $l = 0$. The results are

$$\frac{d\sigma}{d\Omega} = \frac{m_1^* m_2^*}{64\pi^4\hbar^4}\frac{k_2}{k_1}\frac{\hat{c}^2}{\hat{a}^2\hat{s}^2\hat{s}_2^2}|\theta_{s0}|^2 \sum_{\sigma_2\sigma_2'} |C^{00}_{\sigma_2\sigma_2'}(\theta)|^2, \quad (5.5a)$$

$$\rho_{k_{1s}\kappa}(s_2) = \frac{\sum_{\sigma_2\sigma_2'\sigma_2''} (-)^{s_2-\sigma_2'}(s_2\sigma_2, s_2-\sigma_2'|k_{2s}\kappa)C^{00}_{\sigma_2\sigma_2''}(\theta)C^{00*}_{\sigma_2'\sigma_2''}(\theta)}{\sum_{\sigma_2\sigma_2'} |C^{00}_{\sigma_2\sigma_2'}(\theta)|^2}, \quad (5.5b)$$

$$\varepsilon^*_{k_{1s}\kappa}(s_1) \quad (5.5c)$$
$$= \frac{(-)^\kappa \hat{s}_1^2\hat{s}_2^2 W(s_2 s k_{1s} s_1; s_1 s_2)\sum_{\sigma_2\sigma_2'\sigma_2''} (-)^{s_2-\sigma_2''}(s_2\sigma_2', s_2-\sigma_2''|k_{1s}\kappa)C^{00}_{\sigma_2\sigma_2'}(\theta)C^{00*}_{\sigma_2\sigma_2''}(\theta)}{\sum_{\sigma_2\sigma_2'} |C^{00}_{\sigma_2\sigma_2'}(\theta)|^2},$$

where

$$C^{00}_{\sigma_2\sigma_2'}(\theta) = \sum_{j_2 l_2} \hat{l}_2^2(l_2 0, s_2\sigma_2|j_2\sigma_2)(l_2 0, s_2\sigma_2'|j_2\sigma_2')\mathscr{D}^{j_2}_{\sigma_2\sigma_2'}(0\theta 0)R_0(j_2 l_2 s0; l_2). \quad (5.5d)$$

The y-axis is taken along $+\mathbf{n}$ in eq. (5.5c), and along $-\mathbf{n}$ in eq. (5.5b).

By comparison of the above equations we find the polarization correlation

$$\varepsilon^*_{k\kappa}(s_1) = \hat{s}_1^2\hat{s}_2^2 W(s_2 s k s_1; s_1 s_2)\rho_{k\kappa}(s_2), \quad (5.6)$$

where we have used the relation

$$C^{00}_{\sigma_2\sigma_2'}(\theta) = (-)^{\sigma_2-\sigma_2'}C^{00}_{\sigma_2'\sigma_2}(\theta). \quad (5.7)$$

We also have the selection rule

$$0 \leqq k_{1s} \leqq 2s_2. \tag{5.8}$$

5.2. NO SPIN-DEPENDENT DISTORTION OF THE OUTGOING RADIATION

For this assumption it is best to use (2.11). One finds

$$B^{j(ls)\zeta}_{\sigma_2\sigma_1}(\theta) = \sum_{j_1 l_1 l_2 \sigma\sigma_1' \lambda} \hat{l}_1 \hat{l}_2 (l_1 0, s_1\sigma_1 | j_1\sigma_1)(l_2 0, l\lambda | l_1\lambda)(l\lambda, s\sigma | j\zeta)(l_1\lambda, s_1\sigma_1' | j_1\sigma_2+\zeta) \times (s_2\sigma_2, s\sigma | s_1\sigma_1') \mathscr{D}^{j_1}_{\zeta+\sigma_2\sigma_1}(0\theta 0) R_0(l_2 j l; j_1 l_1), \tag{5.9}$$

and for $l = 0$, the angular distribution is as in (5.5a) except for the replacement of $C^{00}_{\sigma_2\sigma_1'}(\theta)$ by $D^{00}_{\sigma_1\sigma_1'}(\theta)\hat{s}_2^2/\hat{s}_1^2$, where

$$D^{00}_{\sigma_1\sigma_1'}(\theta) = \sum_{j_1 l_1} \hat{l}_1^2 (l_1 0, s_1\sigma_1 | j_1\sigma_1)(l_1 0, s_1\sigma_1' | j_1\sigma_1') \mathscr{D}^{j_1}_{\sigma_1'\sigma_1}(0\theta 0) R_0(l_1 s 0; j_1 l_1). \tag{5.10}$$

The polarization tensors are

$$\rho_{k_{2s}\kappa}(s_2) = \frac{\hat{s}_1^2 W(s_1 s k_{2s} s_2; s_2 s_1) \sum_{\sigma_1\sigma_1'\sigma_1''} (-)^{s_1-\sigma_1''}(s_1\sigma_1', s_1-\sigma_1'' | k_{2s}\kappa) D^{00}_{\sigma_1\sigma_1'}(\theta) D^{00*}_{\sigma_1\sigma_1''}(\theta)}{\sum_{\sigma_1\sigma_1'} |D^{00}_{\sigma_1\sigma_1'}(\theta)|^2}, \tag{5.11a}$$

$$\varepsilon^*_{k_{1s}\kappa}(s_1) = \frac{(-)^\kappa \hat{s}_1^2 \sum_{\sigma_1\sigma_1'\sigma_1''} (-)^{s_1-\sigma_1'}(s_1\sigma_1, s_1-\sigma_1' | k_{1s}\kappa) D^{00}_{\sigma_1\sigma_1''}(\theta) D^{00*}_{\sigma_1'\sigma_1''}(\theta)}{\sum_{\sigma_1\sigma_1'} |D^{00}_{\sigma_1\sigma_1'}(\theta)|^2}, \tag{5.11b}$$

where the y-axis is along $+\mathbf{n}$ in eq. (5.11b) and along $-\mathbf{n}$ in eq. (5.11a). There follows the polarization correlation

$$\rho_{k\kappa}(s_2) = W(s_1 s k s_2; s_2 s_1)\varepsilon^*_{k\kappa}(s_1), \tag{5.12}$$

where we have used

$$D^{00}_{\sigma_1\sigma_1'}(\theta) = (-)^{\sigma_1-\sigma_1'} D^{00}_{\sigma_1'\sigma_1}(\theta). \tag{5.13}$$

Also we have the selection rule

$$0 \leqq k_{2s} \leqq 2s_1. \tag{5.14}$$

5.3. NO SPIN-DEPENDENT DISTORTION OF BOTH RADIATIONS

In the case of deuteron stripping, this case has been discussed by several investigators (see for example refs. [2]) and [3]).

One finds

$$\frac{\mathrm{d}\sigma}{\mathrm{d}\Omega} = \frac{m_1^* m_2^*}{64\pi^4} \frac{k_2}{k_1} \frac{\hat{c}^2}{\hat{a}^2} \sum_{jls\lambda} \left| \frac{\theta_{j(ls)} C^{l\lambda}(\theta)}{\hat{s}\hat{l}} \right|^2, \tag{5.15a}$$

$$\rho_{k_{2s}\kappa}(s_2)=\frac{\sum_{jls l's'} W(ss_1k_{2s}s_2;\, s_2s')\theta_{j(ls)}\theta^*_{j(l's')}W(l'jk_{2s}s;\, s'l)\sum_{\lambda\lambda'}(-)^{l'-\lambda'}(l\lambda, l'-\lambda'|k_{2s}\kappa)D^{l\lambda}(\theta)D^{l'\lambda}}{\sum_{jls\lambda}\left|\frac{\theta_{j(ls)}C^{l\lambda}(\theta)}{\hat{s}\hat{l}}\right|^2} \tag{5.}$$

and

$$\varepsilon^*_{k_{1s}\kappa}(s_1)$$
$$=\frac{\sum_{jls l's'}(-)^{\kappa+s-s'}\hat{s}_1^2 W(ss_2k_{1s}s_1;\, s_1s')\theta_{j(ls)}\theta^*_{j(l's')}W(l'jk_{1s}s;\, s'l)\sum_{\lambda\lambda'}(-)^{l'-\lambda'}(l\lambda, l'-\lambda'(k_{1s}\kappa)C^{l\lambda}(\theta)C^{l'\lambda'}}{\sum_{jls\lambda}\left|\frac{\theta_{j(ls)}C^{l\lambda}(\theta)}{\hat{s}\hat{l}}\right|^2} \tag{5.}$$

where

$$C^{l\lambda}(\theta)=\sqrt{4\pi}\sum_{l_1l_2}l_1Y^{\lambda}_{l_2}(\theta,0)(l_2\lambda,\, l-\lambda|l_10)R_0(l_2l,\, l_1;\, ca) \tag{5.15d}$$

and

$$D^{l\lambda}(\theta)=\sum_{\lambda'}C^{l\lambda'}(\theta)\mathscr{D}^l_{\lambda\lambda'}(0\theta0). \tag{5.15e}$$

$\varepsilon^*_{k_{1s}\kappa}(s_1)$ is referred to a set of axes with y along $+\mathbf{n}$ and z in the direction $\mathbf{k}_1$, while $\rho_{k_{2s}\kappa}(s_2)$ is referred to axes with y along $-\mathbf{n}$ and z along $\mathbf{k}_2$. The efficiency tensor, $\varepsilon^*_{k_{1s}\kappa'}(s_1)$, referred to a set of axes with the z-axis in the direction $\mathbf{k}_2$, can be found using the transformation law

$$\varepsilon^*_{k_{1s}\kappa'}(s_1)=\sum_{\kappa}\varepsilon^*_{k_{1s}\kappa}(s_1)\mathscr{D}^k_{\kappa\kappa'}(0\theta0), \tag{5.16}$$

where $\varepsilon^*_{k_{1s}\kappa}(s_1)$ is defined with respect to a set of axes with z-axis along $\mathbf{k}_1$. If we redifine $\varepsilon_{k_{1s}}\kappa(s_1)$ with respect to a z-axis along $\mathbf{k}_2$ and use (5.15e), we find

$$\varepsilon^*_{k_{1s}\kappa}(s_1)$$
$$=\frac{\sum_{jls l's'}(-)^{\kappa+s-s'}\hat{s}_1^2 W(ss_2k_{1s}s_1;s_1s')\theta_{j(ls)}\theta^*_{j(l's')}W(l'jk_{1s}s;\, s'l)\sum_{\lambda\lambda'}(-)^{l'-\lambda'}(l\lambda,l'-\lambda'(k_{1s}\kappa)D^{l\lambda}(\theta)D^{l'\lambda'*}}{\sum_{jls\lambda}\left|\frac{\theta_{j(ls)}C^{l\lambda}(\theta)}{\hat{s}\hat{l}}\right|^2} \tag{5.}$$

Continuing this approximation of no spin-dependence of the distortion we note that if we restrict ourselves to cross-sections and first-rank polarization, the summation over l is incoherent. This is not the case with the summation over s. Restricting ourselves to unique value of s, we find from (5.15b)

$$\rho_{k\kappa}(s_2)=\frac{(-)^{\kappa}}{\hat{s}_1^2}\frac{W(ss_1ks_2;\, s_2s)}{W(ss_2ks_1;\, s_1s)}\varepsilon^*_{k\kappa}(s_1). \tag{5.18}$$

There also follow the selection rules

$$0\leqq k_{1s}\leqq 2s_{\max};\quad 0\leqq k_{2s}\leqq 2s_{\max}, \tag{5.19a}$$

$$0\leqq k_{1s}\leqq 2l_{\max};\quad 0\leqq k_{2s}\leqq 2l_{\max}. \tag{5.19b}$$

From (5.19a) and (5.19b) we have the result stated at the beginning of this section, i.e. if $l = 0$, and there is no spin-dependent distortion of either radiation than $k_{1s} = k_{2s} = 0$ and therefore polarization effects are completely absent in such a reaction.

We shall discuss further applications of these selection rules when we consider specific direct processes in the following section.

6. Applications of the General Theory to Specific Direct Processes

6.1. STRIPPING REACTIONS

The considerations to follow are of immediate significance to deuteron stripping processes and to their inverse phenomena (pick-up). Since the previous analysis refers to arbitrary spins, we may, with little difficulty, interpret that which follows as applying to a process where a composite particle of spin s_1 is stripped of one portion with spin s which is absorbed by the target nucleus, leaving a residual nucleus of spin c, together with the residual element of the projectile which has spin s_2. In analogy with deuteron stripping we assume the stripping interaction to be characterized by a potential which is spin-independent and which depends only on the relative distance between the two portions of the incident radiation. To render the calculation as simple as possible, this interaction is assumed to be of a zero-range type, there being some basis for this in deuteron stripping because of the insensitivity to the range when the crude Butler theory is used. In keeping with this aim of simplicity, we disregard the internal motion of each of the portions of the incident radiation, and also disregard exchange effects.

The matrix element connecting initial and final states is written as

$$\langle c\gamma(l_2 s_2) j_2 \zeta_2 | R | a\alpha(l_1 s_1) j_1 \zeta_1 \rangle$$
$$= \int \mathrm{d}\mathbf{x}\mathrm{d}\mathbf{r}_1\mathrm{d}\mathbf{r}_2 \psi^{\dagger}_{c\gamma}(\mathbf{x}, \mathbf{r}_1)\psi^{\dagger}_{j_2\zeta_2}(\mathbf{k}_2, \mathbf{r}_2')V(|\mathbf{r}_1-\mathbf{r}_2|)\psi_{a\alpha}(\mathbf{x})\psi_{j_1\zeta_1}(\mathbf{k}_1, \mathbf{r}_1, \mathbf{r}_2), \quad (7.1)$$

where $\mathbf{r}_1$ designates the co-ordinates of the centre-of-mass of the stripped-off radiation, $\mathbf{r}_2$ those of the residual radiation, both being measured with respect to the target nucleus, while $\mathbf{r}_2' = \mathbf{r}_2 - (m_2/m_c)\mathbf{r}_1$ gives the co-ordinates of the stripped radiation with respect to the residual nucleus, m_c being its mass.

In the distorted-wave approximation, we take the eigenfunctions of space and spin, $\psi_{j_2\zeta_2}$ and $\psi_{j_1\zeta_1}$ to be those describing the elastic scattering of outgoing and incoming particles by residual and target nucleus respectively. Thus, according to the normalization used in section 2,

$$\psi_{j_2\zeta_2}(\mathbf{k}_2, \mathbf{r}_2') = 4\pi g_{j_2 l_2}(k_2, r_2')\Phi^{\zeta_2}_{j_2(l_2 s_2)}(\Omega_2), \quad (6.2a)$$

$$\psi_{j_1\zeta_1}(\mathbf{k}_1, \mathbf{r}_1, \mathbf{r}_2) = 4\pi f_{j_1 l_1}(k_1, r_1')\Phi^{\zeta_1}_{j_1(l_1 s_1)}(\Omega_1')\phi(\mathbf{r}_1-\mathbf{r}_2)$$
$$\mathbf{r}_1' = \frac{(m_1-m_2)}{m_1}\mathbf{r}_1 + \frac{m_2}{m_1}\mathbf{r}_2, \quad (6.2b)$$

where $\Phi^{\zeta}_{j(ls)}(\Omega)$ is given by eq. (2.28) and $\phi(\mathbf{r}_1-\mathbf{r}_2)$ is the internal wave function of the incident radiation. The functions $f_{j_1l_1}$ and $g_{j_2l_2}$ are as defined in section 2.3.

Carrying out the integration over $\mathbf{x}$,

$$\int \mathrm{d}\mathbf{x}\psi^{\dagger}_{c\gamma}(\mathbf{x}, \mathbf{r}_1)\psi_{a\alpha}(\mathbf{x}) = \sum_{jls\zeta} \theta_{j(ls)}(a\alpha, j\zeta|c\gamma)\psi^{\dagger}_{j(ls)\zeta}(\mathbf{r}_1), \tag{6.3}$$

where $\psi_{j(ls)\zeta}(\mathbf{r}_1)$ is the eigenfunction of the stripped radiation which is taken to be

$$\psi_{j(ls)\zeta}(\mathbf{r}) = u_{j(ls)}(r)\Phi^{\zeta}_{j(ls)}(\Omega), \tag{6.4}$$

and $\theta_{j(ls)}$ is the probability amplitude for finding this radiation bound in a state with quantum numbers $j(ls)$ to the residual nucleus (the reduced-width amplitude). The integration over the remaining co-ordinates in (6.1) gives

$$\int \mathrm{d}\mathbf{r}_1\mathrm{d}\mathbf{r}_2\psi^{\dagger}_{j_2\zeta_2}(\mathbf{k}_2, \mathbf{r}_2')\psi^{\dagger}_{j\zeta}(\mathbf{r}_1)V(|\mathbf{r}_1-\mathbf{r}_2|)\psi_{j_1\zeta_1}(\mathbf{k}_1, \mathbf{r}_1, \mathbf{r}_2) \equiv (j_2\zeta_2, j\zeta|j_1\zeta_1)\langle j_2|j||j_1\rangle, \tag{6.5}$$

where it is assumed[22]) that

$$V(|\mathbf{r}_1-\mathbf{r}_2|)\phi(\mathbf{r}_1-\mathbf{r}_2) = g\delta(\mathbf{r}_1-\mathbf{r}_2). \tag{6.6}$$

Inserting (6.6), (6.4), (6.2a) and (6.2b) into (6.5) we find after summing over magnetic quantum numbers,

$$\langle j_2|j||j_1\rangle = \hat{j}_2\hat{j}\hat{l}_1\hat{s}_1 \begin{Bmatrix} l_2 & s_2 & j_2 \\ l & s & j \\ l_1 & s_1 & j_1 \end{Bmatrix} R_0(j_2l_2jl, j_1l_1; ca), \tag{6.7}$$

where

$$R_0(j_2l_0jl, j_1l_1; ca) = (4\pi)^{\frac{1}{2}} g \frac{\hat{l}_2\hat{l}}{\hat{l}_1} (l_2 0, l0|l_1 0) i^{l_1-l_2-l} \int_0^{\infty} r^2 dr g^{*}_{j_2l_2}(k_2, r')u_{jl}(r)f_{j_1l_1}(k_1, r), \tag{6.8}$$

and $r' = (1-m_2/m_c)r$. We see that (6.7) has the form of (5.2) and therefore we can use the formulae of section 2 and the results of section 5 with $R_0(j_2l_2jl, j_1l_1; s_2ss_1; ca)$ given by (6.8).

We now present certain selection rules which arise as a consequence of the considerations in section 5. We first deal with deuteron-stripping processes.

6.1.a. Deuteron-stripping processes ($s_1 = 1$, $s_2 = s = \frac{1}{2}$).

Since $s = \frac{1}{2}$ and the summation over j is incoherent, the summation over l must also be incoherent. This is because the nuclei correspond to states of unique parity, so that the parity of l is constant. Pairs of values of l, differing by one, are therefore impossible.

To separate the effects of spin-dependent distortions, we restrict this type of distortion to the incoming or outgoing stages or to neither stage. In particular,

one easily sees, as a consequence of (5.19a), that with no spin-dependent distortion, the angular distribution is unaffected by second-rank components of deuteron-polarization [28]), and furthermore, that reactions proceeding through $l = 0$ give rise to no polarization effects. With spin-dependent distortion in both stages, there are, in general, no restrictions on the nature or degree of polarization. With $l = 0$, however, and with spin-dependent distortion operating on the outgoing nucleons, polarization effects arise; but these are limited to first-rank polarization. Second-rank deuteron polarization gives rise to asymmetries in the angular distribution for $l = 0$, only as a result of a spin-dependent deuteron interaction with the nucleus.

It is possible to relate the asymmetry arising in a process involving incoming polarized deuterons with the polarization exhibited by outgoing nucleons, where unpolarized deuterons are incident. Thus, (5.13), (5.12) and (5.6) together with the definitions (2.15), (2.16) and (2.25) give the following results:

$$l \neq 0 \quad \frac{d\sigma}{d\Omega} = \left(\frac{d\sigma}{d\Omega}\right)_0 [1+3P_{in}(1)P_{out}(\tfrac{1}{2})] \qquad \text{(no spin-dependent distortion)} \tag{6.9a}$$

$$l = 0 \quad \frac{d\sigma}{d\Omega} = \begin{cases} \left(\frac{d\sigma}{d\Omega}\right)_0 & \text{(no spin-dependent distortion)} \quad (6.9b) \\ \left(\frac{d\sigma}{d\Omega}\right)_0 [1+\frac{3}{2}P_{in}(1)P_{out}(\frac{1}{2}) + \text{sec-rank effects}] & \text{(no nucleon spin-dependent distortion)} \quad (6.9c) \\ \left(\frac{d\sigma}{d\Omega}\right)_0 [1+ P_{in}(1)P_{out}(\frac{1}{2})] & \text{(no deuteron spin-dependent distortion)} \quad (6.9d) \end{cases}$$

Here, $(d\sigma/d\Omega)_0$ is the angular distribution with unpolarized deuterons; whereas $d\sigma/d\Omega$ is the angular distribution associated with deuterons having arbitrary polarization with vector-polarization of magnitude $P_{in}(1)$ along $\mathbf{n}$. The quantity $P_{out}(\frac{1}{2})$ is the magnitude of the polarization of the outgoing nucleons which can only be along $\mathbf{n}$ for incoming unpolarized deuterons.

These results and several others are displayed in table 1. The equations (6.9a) to (6.9d) are indicated using the quantity A defined by $d\sigma/d\Omega \equiv A(d\sigma/d\Omega)_0$. They are easily applicable to the inverse pick-up process as well as to the (He^3,d) stripping process if we make use of (2.40).

A simplified demonstration of the selection rules will appear shortly in a separate publication.

6.1.b. $(He^3, p)(H^3, p)$, etc. processes ($s_1 = s_2 = \frac{1}{2}$, $s = 0,1$).

In these stripping processes, the captured nucleons may have their spins parallel or antiparallel ($s = 1$, or 0, respectively). In principle, one should expect the stripping interaction to be spin-dependent; however, to avoid the very complicated expressions that would necessarily follow, we limit our study

TABLE 1

Selection rules for stripping processes

	No spin-dependent distortion	Spin-dependent distortion	
		incoming radiation	outgoing radiation
(d, p), (d, n) processes			
magnitude of k_s $(l \neq 0)$	$k_{1s} \leqq 1$ $k_{2s} \leqq 1$		
$(l = 0)$	$k_{1s} = k_{2s} = 0$	$k_{1s} \leqq 2$, $k_{2s} \leqq 1$	$k_{1s} \leqq 1$, $k_{2s} \leqq 1$
$A \begin{cases} (l \neq 0) \\ (l = 0) \end{cases}$	$1+3P_{in}\,P_{out}$		
	1	$1+\frac{3}{2}P_{in}\,P_{out}+\cdots$	$1+P_{in}\,P_{out}$
magnitude of P_{out}	$\lvert P_{out}\rvert \leqq \begin{cases} \frac{1}{2}l/(l+1), & j = l+\frac{1}{2} \\ \frac{1}{2}, & j = l-\frac{1}{2} \end{cases}$	$\lvert P_{out}\rvert \leqq 1$	$\lvert P_{out}\rvert \leqq 1$
summation over j, l	incoherent	incoherent	incoherent
(He^3, p), (H^3, p), (H^3, n) processes			
$A \begin{cases} (s = 0) \\ (s = 1, l \neq 0) \\ (s = 1, l = 0) \end{cases}$	1	$1+P_{in}\,P_{out}$	$1+P_{in}\,P_{out}$
	$1-P_{in}\,P_{out}$		
	1	$1-3P_{in}\,P_{out}$	$1-\frac{1}{2}P_{in}\,P_{out}$
magnitude of P_{out}			
$(s = 0)$	0		
$(s = 1,\ j = l)$	$\lvert P_{out}\rvert \leqq 1/(l+1)$		
$(s = 1,\ j = l+1)$	$\lvert P_{out}\rvert \leqq l/(l+1)$		
$(s = 1,\ j = l-1)$	$\lvert P_{out}\rvert \leqq 1$		
summation over			
l $(s = 0)$	incoherent	incoherent	incoherent
l $(s = 1)$	incoherent	coherent	coherent
s	incoherent (cross-section) / coherent (polarization)	coherent	coherent
(α, p) process			
magnitude of P_{out}	$\lvert P_{out}\rvert \leqq \begin{cases} l/(l+1), & j = l+\frac{1}{2} \\ 1, & j = l-\frac{1}{2} \end{cases}$		$\lvert P_{out}\rvert \leqq 1$
summation over j, l	incoherent	incoherent	incoherent

to the consequences of the interaction proceeding through only one of the two possibilities. The various selection rules are listed in the table. One notes that in contrast to the case of deuteron stripping, both the angular distributions and the polarization effects involve coherent summation over l and s.

If we ignore spin-dependent distortions, it follows from (5.19a) and (5.19b) that no polarization effects arise if $s = 0$. Such effects arise from contributions of $s = 1$ only and from the interference between $s = 0$ and $s = 1$; thus polarization measurements provide a simple test for the presence of the latter possibil-

ity. Some interesting conclusions can also be given concerning the maximum polarization if we assume unique values of s, l and j.

We may rewrite (5.15b) in terms of the above processes as follows:

$$\rho_{11}(\tfrac{1}{2}) = -\tfrac{1}{2}\hat{s}^2\hat{l}^2 W(s\tfrac{1}{2}\,1\tfrac{1}{2};\tfrac{1}{2}s)W(lj1s;sl)\,\frac{\sqrt{6}\langle l_x - il_y\rangle}{\hbar\hat{l}\sqrt{l(l+1)}}, \qquad (6.10)$$

where $\langle (l_x - il_y)\rangle$ is the average value of the operator $l_x - il_y$ in the l-representation, having matrix elements given by

$$\langle l\lambda'|l_x - il_y|l\lambda\rangle = (-)^{l+1-\lambda'}\hbar\hat{l}\sqrt{\frac{2l(l+1)}{3}}\,(l\lambda,\, l-\lambda'|11). \qquad (6.11)$$

Now, $|\langle l_x - il_y\rangle| \leqq l\hbar$; hence, inserting the explicit values of the Racah coefficients, we find for $s = 1$, the limitations for the polarization of the outgoing radiation as shown in the table. The correlations between incoming polarization effects and outgoing polarization are found by use of the formulae in section 5.

6.1.c. (α, p), (α, He^3), (α, d), *etc. processes* ($s_1 = 0$, $s_2 = s = \frac{1}{2}$ *or* 1).

If these reactions proceed through $l \neq 0$, the outgoing particles are, in general, polarized even in the absence of spin-dependent distortion. However, if $l = 0$, such a polarization arises only as a consequence of a spin-dependent distortion. It is to be noted that the distortion gives rise to coherent summation over l for the (α, d) process.

Various specific formulae for angular distributions and polarization in several processes are to be found in the appendix.

6.2. INELASTIC NUCLEON SCATTERING

Several calculations have been performed of inelastic scattering of nucleons through direct processes, using the distorted-wave approximation and these are described by Austern [1]). Some of the calculations treat the reaction as occurring at the nuclear surface through some sort of collective oscillation, and others involve residual nucleon-nucleon interactions. The most successful [29]) of the latter kind of calculations consider interactions throughout the nuclear volume. We shall consider surface phenomena in the next sub-section. It is possible, in principle, to treat the inelastic scattering of composite systems, e.g. deuterons (the loose structure of deuterons makes the idealization of point particles somewhat dubious in this case) as occurring through volume interactions and we shall therefore present our results in a manner which is applicable in principle to the scattering or radiation of arbitrary spin.

For the purpose of simplicity, we restrict ourselves to the process considered by Lamarsh and Feshbach [30]). A nucleon with co-ordinates $\mathbf{r}$, and momentum vector $\mathbf{k}_1$, is incident on a target nucleus of spin a. This nucleus is assumed to be

composed of a core of spin j_c, with co-ordinates $\mathbf{x}$, having coupled to it, a nucleon of angular momentum $J_1(L_1\frac{1}{2})$, and co-ordinates $\mathbf{r}_1$. The interaction $V(\mathbf{r}_1, \mathbf{r})$ is assumed to act between the struck nucleon and the incident particle, leaving the core unaffected, but exciting the struck nucleon to a new state with angular momentum $J_2(L_2\frac{1}{2})$, and an outgoing nucleon with momentum $\mathbf{k}_2$.

The matrix element connecting initial and final angular momentum states is

$$\langle c\gamma(l_2\tfrac{1}{2})j_2\zeta_2|R|a\alpha(l_1\tfrac{1}{2})j_1\zeta_1\rangle = \int \mathrm{d}\mathbf{x}\mathrm{d}\mathbf{r}\mathrm{d}\mathbf{r}_1 \psi^\dagger_{c\gamma}(\mathbf{x}, \mathbf{r}_1)\psi^\dagger_{j_2\zeta_2}(\mathbf{k}_2, \mathbf{r})V(\mathbf{r}_1, \mathbf{r})\psi_{a\alpha}(\mathbf{x}, \mathbf{r}_1)\psi_{j_1\zeta_1}(\mathbf{k}_1, \mathbf{r}), \quad (6.12)$$

which becomes, using the above assumption,

$$\langle c\gamma(l_2\tfrac{1}{2})j_2\zeta_2|R|a\alpha(l_1\tfrac{1}{2})j_1\zeta_1\rangle = \sum_{\zeta_c\Lambda_1\Lambda_2} (j_c\zeta_c, J_2\Lambda_2|c\gamma)(j_c\zeta_c, J_1\Lambda_1|a\alpha) \times \int \mathrm{d}\mathbf{r}_1\mathrm{d}\mathbf{r}\psi^\dagger_{j_2\zeta_2}(\mathbf{k}_2, \mathbf{r})\psi^\dagger_{J_2\Lambda_2}(\mathbf{r}_1)V(\mathbf{r}_1, \mathbf{r})\psi_{J_1\Lambda_1}(\mathbf{r}_1)\psi_{j_1\zeta_1}(\mathbf{k}_1, \mathbf{r}), \quad (6.13)$$

where $\psi_{J_1\Lambda_1}(\mathbf{r}_1)$ and $\psi_{J_2\Lambda_2}(\mathbf{r}_1)$ are the wave functions of the struck nucleon in its initial and final states, respectively.

The interaction $V(\mathbf{r}_1, \mathbf{r})$ can be written in a general form consistent with the assumptions of section 1 as

$$V(\mathbf{r}_1, \mathbf{r}) = \sum_{jls\zeta} \chi^{\zeta\dagger}_{j(ls)}(\mathbf{r})\chi^{\zeta}_{j(ls)}(\mathbf{r}_1)\, V_{j(ls)}(r_1, r), \quad (6.14)$$

where

$$\chi^{\zeta}_{j(ls)}(\mathbf{r}) = \sum_{\lambda\sigma} T^\lambda_l(\Omega)T^\sigma_s(s)(l\lambda, s\sigma|j\zeta). \quad (6.15)$$

The quantities $T^\lambda_l(\Omega)$ and $T^\sigma_s(s)$ are spherical tensors which operate on three-dimensional and spin-space, respectively. Integrating over $\mathbf{r}_1$ in (6.16) we have

$$\langle(L_2\tfrac{1}{2})J_2||j(ls)|(L_1\tfrac{1}{2})J_1\rangle = \hat{L}_2\hat{J}_1\hat{j}\hat{\tfrac{1}{2}} \begin{Bmatrix} L_2 & L_1 & l \\ \frac{1}{2} & \frac{1}{2} & s \\ J_2 & J_1 & j \end{Bmatrix} \langle L_2||l|L_1\rangle\langle\tfrac{1}{2}||s|\tfrac{1}{2}\rangle i^{L_1-L_2}\int \mathrm{d}r_1 r_1^2 u^*_{J_2L_2}(r_1)V_{j(ls)}(r_1, r)u_{J_1L_1}(r_1), \quad (6.16)$$

where the reduced matrix elements are defined by

$$\int \mathrm{d}\Omega_1 Y^{\lambda_2*}_{L_2} T^\lambda_l Y^{\lambda_1}_{L_1} = (L_1\lambda_1, l\lambda|L_2\lambda_2)\langle L_2||l|L_1\rangle, \quad (6.17)$$

$$\chi^{\sigma_2\dagger}_{\frac{1}{2}} T^\sigma_s \chi^{\sigma_1}_{\frac{1}{2}} = (\tfrac{1}{2}\sigma_1, s\sigma|\tfrac{1}{2}\sigma_2)\langle\tfrac{1}{2}||s|\tfrac{1}{2}\rangle, \quad (6.18)$$

and $u_{J_1L_1}(r_1)$, $u_{J_2L_2}(r_1)$ are the radial wave functions of the struck nucleon in its initial and final states. These may be chosen to be real.

We note that

$$\sum_{\zeta_c\Lambda_1\Lambda_2} (j_c\zeta_c, J_2\Lambda_2|c\gamma)(j_c\zeta_c, J_1\Lambda_1|a\alpha)(J_1\Lambda_1, j\zeta|J_2\Lambda_2) = \hat{a}\hat{J}_2(-)^{j_c+j-J_2-a}W(cJ_2aJ_1; j_cj)(a\alpha, j\zeta|c\gamma). \quad (6.19)$$

Hence (6.13) becomes

$$\langle c\gamma(l_2\tfrac{1}{2})j_2\zeta_2|R|a\alpha(l_1\tfrac{1}{2})j_1\zeta_1\rangle = \sum_{jls\zeta}(a\alpha, j\zeta|c\gamma)(j_2\zeta_2, j\zeta|j_1\zeta_1)\theta_{j(ls)}(c,a)\langle j_2(c)|j(ls)||j_1(a)\rangle, \quad (6.20a)$$

where

$$\theta_{j(ls)}(c,a) = \hat{a}\hat{J}_1\hat{J}_2\hat{L}_2\hat{j}\,\hat{\tfrac{1}{2}}(-)^{j_c+j-J_2-a}W(cJ_2aJ_1; jcj)\begin{Bmatrix} L_2 & L_1 & l \\ \frac{1}{2} & \frac{1}{2} & s \\ J_2 & J_1 & j \end{Bmatrix}\langle L_2||l||L_1\rangle\langle\tfrac{1}{2}||s||\tfrac{1}{2}\rangle, \quad (6.20b)$$

and

$$(j_2\zeta_2, j\zeta|j_1\zeta_1)\langle j_2(c)|j(ls)||j_1(a)\rangle = i^{L_1-L_2}\int r_1^2\mathrm{d}r_1\,\mathrm{d}\mathbf{r}\psi^{\dagger}_{j_2\zeta_2}(\mathbf{k}_2,\mathbf{r})\chi^{\zeta\dagger}_{j(ls)}(\mathbf{r})u_{J_2L_2}(r_1)V_{j(ls)}(r_1,r)u_{J_1L_1}(r_1)\psi_{j_1\zeta_1}(\mathbf{k}_1,\mathbf{r}). \quad (6.20c)$$

We write

$$\psi_{j_2\zeta_2}(\mathbf{k}_2,\mathbf{r}) = 4\pi g_{j_2l_2}(k_2,r)\Phi^{\zeta_2}_{j_2(l_2\frac{1}{2})}(\Omega);\quad \psi_{j_1\zeta_1}(\mathbf{k}_1,\mathbf{r}) = 4\pi f_{j_1l_1}(k_1,r)\Phi^{\zeta_1}_{j_1(l_1\frac{1}{2})}(\Omega), \quad (6.21)$$

where $\Phi^{\zeta}_{j(ls)}(\Omega)$ is a spin-angular eigenfunction defined as in (2.28c). Then, proceeding as in the case of stripping reactions, we find $\langle j_2(c)|j(ls)||j_1(a)\rangle$ is of the form given in (5.2) where

$$R_0(j_2l_2jl, j_1l_1; s_2ss_1; ca) = \langle l_1||l||l_2\rangle\langle\tfrac{1}{2}||s||\tfrac{1}{2}\rangle(4\pi)^2 i^{l_1+L_1-l_2-L_2} \times\iint r_1^2r_2^2\mathrm{d}r_1\,\mathrm{d}r_2 g^*_{j_2l_2}(k_2,r)u_{J_2L_2}(r_1)V_{j(ls)}(r_1,r)u_{J_1L_1}(r_1)f_{j_1l_1}(k_1,r). \quad (6.22)$$

We may therefore use the formulae derived in sections 2, 3, 4 and 5, where $\theta_{j(ls)}(c,a)$ and R_0 are given by (6.20b) and (6.22) and where we put $s_1 = s_2 = \frac{1}{2}$.

The above assumptions are slightly more general than usually employed in calculations; $V(\mathbf{r}_1,\mathbf{r})$ is usually taken to be a δ-function interaction,

$$V(\mathbf{r}_1,\mathbf{r}) = g\delta(\mathbf{r}_1-\mathbf{r}) = g\sum_{l\lambda}\frac{\delta(r-r_1)}{r_1^2}Y^{\lambda}_l(\Omega_1)Y^{\lambda*}_l(\Omega), \quad (6.23)$$

so that $s = 0$. One then obtains

$$\theta_{j(l0)}(ca) = \frac{\hat{a}\hat{J}_1\hat{J}_2}{\sqrt{4\pi}}W(cJ_2aJ_1; j_cl)(J_1\tfrac{1}{2}, J_2-\tfrac{1}{2}|l0)(-)^{-a+j_c-\frac{1}{2}} \quad (6.24a)$$

and

$$\langle j_2(c)|j(l0)||j_1(a)\rangle = (4\pi)^{\frac{3}{2}}g(-)^{l+\frac{1}{2}-j_1}\hat{j}_2(j_1\tfrac{1}{2}, j_2-\tfrac{1}{2}|l0)i^{l_1+L_1-l_2-L_2} \times\int_0^{\infty}r^2\mathrm{d}r g^*_{j_2l_2}(k_2,r)u_{J_2L_2}(r)u_{J_1L_1}(r)f_{j_1l_1}(k_1,r), \quad (6.24b)$$

We note from (5.19a) that as long as $V(\mathbf{r}_1,\mathbf{r})$ is spin-independent ($s = 0$), polarization of the outgoing particle, or effects due to incoming polarization

will arise only as a consequence of the spin-dependence of the distorting potentials acting on the projectile. If the optical-model potential is used to describe this distortion, polarization effects arise from the spin-orbit term of the potential.

It is interesting to observe that the asymmetry arising from polarized incident nucleons is *almost* directly correlated to the polarization arising from the reaction using unpolarized incident nucleons, provided that the energy loss of the nucleons $E_1 - E_2$ is small compared to E_1. In particular, in the limit of no energy loss, the result for elastic scattering holds, i.e.

$$\left(\frac{\mathrm{d}\sigma}{\mathrm{d}\Omega}\right) = \left(\frac{\mathrm{d}\sigma}{\mathrm{d}\Omega}\right)_0 [1 + P_{\mathrm{in}}(\tfrac{1}{2}) P_{\mathrm{out}}(\tfrac{1}{2})], \tag{6.25}$$

where P_{in} is the component of incident polarization along the normal to the scattering plane and P_{out} is the polarization along the same direction that would arise if unpolarized nucleons are incident. The correlation between P_{in} and P_{out} is most easily found using the formalism of section 3, and, in particular, (3.6). If we insert into this equation the radiation parameters that are appropriate for the two experiments involved, we find that $\delta_2^2 \rho_{k_2 \kappa}(\mathrm{out})$ differs from $\varepsilon^*_{k_1 \kappa}(\mathrm{in})$ in the following way: If the statistical tensor is associated with radial integrals of the form

$$\int_0^\infty r^2 \mathrm{d}r g^*_{j_2 l_2}(k_2, r) u_{J_2 L_2}(r) u_{J_1 L_1}(r) f_{j_1 l_1}(k_1, r), \tag{6.26a}$$

then the efficiency tensor is identical to it, except that the above radial integral is replaced by

$$\int_0^\infty r^2 \mathrm{d}r f_{j_2 l_2}(k_1, r) u_{J_2 L_2}(r) u_{J_1 L_1}(r) g^*_{j_1 l_1}(k_2, r), \tag{6.26b}$$

These tensors are defined as in section 5: the statistical tensor refers to a y-axis along $-\mathbf{n}$ and the efficiency tensor to a y-axis along $+\mathbf{n}$. If (6.26a) and (6.26b) were identical, (6.25) would be valid. One also finds, using the formalism of section 2, that, if the spin-dependent distortion is confined to one state only, (6.25) is valid no matter how large the energy loss is.

The above consideration can be extended to inelastic scattering of arbitrary spin. It is then found that as long as $s = 0$, $\delta_2^2 \rho_{k_2 \kappa}(\mathrm{out})$ is *almost* equal to $\varepsilon^*_{k_1 \kappa}(\mathrm{in})$, the inequality arising from the difference of radial integrals (6.26a) and (6.26b).

The extension of these considerations to deuterons and other composite particles is not too meaningful since it is improbable that such particles would survive penetration through the nuclear surface.

Expressions for the angular distributions and polarizations for $s_1 = s_2 = \frac{1}{2}$ are to be found in the appendix.

One has avoided consideration of exchange effects by use of the δ-function

interaction in (6.23). The only contribution to the interaction in this case is when the incoming and struck nucleons are in singlet spin-states, since the antisymmetric spatial configurations give no effect. Since the singlet amplitude is twice the non-exchange amplitude, and also the probability of a singlet state configuration is $\frac{1}{4}$, there is no difference between the cross-section with exchange or without exchange (Lamarsh and Feshbach [30]).

6.3. INELASTIC SCATTERING BY SURFACE EXCITATION

A different mechanism to that discussed in section 6.2 is through the excitation of the nucleus as a whole. The optical model which previously was interpreted as providing the distortion to the incoming and outgoing radiations from plane-wave states is now considered as giving rise to deformation of the nuclear surface. The nuclei involved, which are those far away from the regions of closed shells, have their surface represented by $\rho(\theta, \phi)$, given as

$$\rho(\theta, \phi) = R(1+\sum_{j\zeta} \alpha_{j\zeta} Y_j^\zeta(\theta, \phi)), \tag{6.27}$$

where j is usually put equal to 2, corresponding to a nucleus of quadrupole shape. The earliest considerations approximate the nuclear interaction by a "square" well with the potential vanishing for $r \geqq \rho(\theta, \phi)$. On making the approximation of reasonably small deformations, the potential $V(r, \alpha_{j\zeta})$ can be put in the form

$$V(r, \alpha_{j\zeta}) = V_0(r)+V'(r), \tag{6.28}$$

where $V_0(r)$ is the optical-model potential (square well) in the absence of deformation and V' is, to first order,

$$V'(r) = RV_0(R)\delta(r-R)\sum_{j\zeta} \alpha_{j\zeta} Y_j^\zeta(\theta, \phi). \tag{6.29}$$

The potential V' is responsible for the direct inelastic scattering. If the optical model were not represented by a square well, one might postulate that the form of $V'(r)$ is as given above. The main difficulty with such a procedure is that those nuclei having prominent rotational spectra are usually those with very large values of $\alpha_{j\zeta}$. This puts the whole procedure in doubt and requires consideration of elastic and inelastic scattering in a self-consistent manner [31, 32]). Nevertheless, for the purpose of illustration we shall now derive the cross-section using an interaction given by (6.29). We shall assume the radiation is of arbitrary spin s_1.

The matrix element connecting initial and final states is

$$\langle c\gamma(l_2 s_1)j_2\zeta_2|R|a\alpha(l_1 s_1)j_1\zeta_1\rangle$$
$$=\int \mathrm{dx dr}\psi^\dagger_{j_2\zeta_2}(\mathbf{k}_2, \mathbf{r})\psi^\dagger_{c\gamma}(\mathbf{x})RV_0(R)\delta(r-R)\sum_{j\zeta}\alpha_{j\zeta}Y_j^\zeta(\theta, \phi)\psi_{a\alpha}(\mathbf{x})\psi_{j_1\zeta_1}(\mathbf{k}_1, \mathbf{r}), \tag{6.30}$$

where $\mathbf{x}$ characterizes the internal co-ordinates of the nucleus. This may be

factorized into the form

$$\sum_{j\zeta}\langle c\gamma|i^j\alpha^*_{j\zeta}|a\alpha\rangle\langle(l_2s_1)j_2\zeta_2c|V_0R\delta(r-R)Y^{\zeta*}_j i^{-j}|(l_1s_1)j_1\zeta_1a\rangle$$
$$=\sum_{j\zeta}(a\alpha,\,j\zeta|c\gamma)(j_2\zeta_2,\,j\zeta|j_1\zeta_1)\langle c||j|a\rangle\langle j_2(c)||j||j_1(a)\rangle, \quad (6.31)$$

where

$$\langle c||j|a\rangle(a\alpha,\,j\zeta|c\gamma)=\langle c\gamma|i^{+j}\alpha^*_{j\zeta}|a\alpha\rangle \quad (6.32a)$$

and

$$\langle j_2(c)||j||j_1(a)\rangle=\hat{l}_1\hat{j}_2(-)^{s_1+j-j_1-l_2}W(l_1j_1l_2j_2;\,s_1j)R_0(j_2l_2j,\,j_1l_1;\,ca) \quad (6.32b)$$

while

$$R_0(j_2l_2j,\,j_1l_1;\,ca)=(4\pi)^{\frac{1}{2}}V_0R^3(-)^{l_2}\hat{l}_2(l_10,\,l_20|l0)i^{l_1-l_2-j}g^*_{j_2l_2}(k_2R)f_{j_1l_1}(k_1R). \quad (6.32c)$$

The radial functions $g_{j_2l_2}$ and $f_{j_1l_1}$ are as given in section 2.3.

We see that (6.32b) is of the form (5.2) where $s=0$. Hence the cross-sections and polarizations are given by (2.9), (2.10) and (2.11), and in the absence of spin-dependent distortion by (5.15).

If the scattering involves nucleons, (6.32b) reduces to

$$\langle j_2(c)||j||j_1(a)\rangle$$
$$=(4\pi)^{\frac{1}{2}}V_0R^3i^{l_1-l_2-j}(-)^{j+\frac{1}{2}-j_1}\hat{j}_2(j_1\tfrac{1}{2},\,j_2-\tfrac{1}{2}|j0)\,g^*_{j_2l_2}(k_2R)f_{j_1l_1}(k_1R). \quad (6.33)$$

Inserting this into (2.9) and using (2.10) we have

$$\frac{d\sigma}{d\Omega}=\frac{(m^*V_0R^3)^2}{2\pi}\frac{k_2}{k_1}\frac{\hat{c}^2}{\hat{a}^2}\sum_j\left|\frac{\langle c||j|a\rangle}{\hat{j}}\right|^2\sum_\zeta\{|\mathscr{A}^{j\zeta}_{\frac{1}{2}\frac{1}{2}}(\theta)|^2+|\mathscr{A}^{j\zeta}_{-\frac{1}{2}\frac{1}{2}}(\theta)|^2\}, \quad (6.34a)$$

where

$$\mathscr{A}^{j\zeta}_{\sigma\frac{1}{2}}(\theta)=\sum_{j_1l_1j_2l_2}\frac{\hat{l}_1\hat{j}_2\hat{j}_1}{\sqrt{2}}(-)^{l_2}i^{l_1-l_2-j}(l_20,\,\tfrac{1}{2}\sigma|j_2\sigma)(j_2\tfrac{1}{2}-\zeta,\,j\zeta|j_1\tfrac{1}{2})$$
$$\times(j_1\tfrac{1}{2},\,j_2-\tfrac{1}{2}|j0)g^*_{j_2l_2}(k_2R)f_{j_1l_1}(k_1R)\mathscr{D}^{j_2}_{\sigma\frac{1}{2}-\zeta}(0\theta0). \quad (6.34b)$$

In the absence of spin-dependent distortion we use (5.15) and obtain

$$\frac{d\sigma}{d\Omega}=\frac{4m^{*2}}{\hbar^4}(V_0R^3)^2\frac{k_2}{k_1}\frac{\hat{c}^2}{\hat{a}^2}\sum_j|\langle c||j|a\rangle|^2\sum_\zeta|\sum_{l_1l_2}\hat{l}_2i^{l_1-l_2-j}$$
$$\times(l_2\zeta,\,j-\zeta|l_10)(l_20,\,j0|l_10)g^*_{l_2}(k_2R)f_{l_1}(k_1R)Y^\zeta_{l_2}(\theta0)|^2, \quad (6.35)$$

or the alternative formula

$$\frac{d\sigma}{d\Omega}=\frac{m^{*2}}{\pi\hbar^4}(V_0R^3)^2\frac{k_2}{k_1}\frac{\hat{c}^2}{\hat{a}^2}\sum_j\frac{|\langle c||j|a\rangle|^2}{\hat{j}^2}\sum_{l_1l_1'l_2l_2'k}(\hat{l}_1\hat{l}_1'\hat{l}_2\hat{l}_2')^2(-)^k i^{l_1+l_1'-l_2-l_2'}$$
$$\times(l_10,\,l_1'0|k0)(l_20,\,l_2'0|k0)(l_2c.\,l_10|j0)(l_2'0,\,l_1'0|j0)W(l_1l_2l_1'l_2';\,jk)$$
$$\cdot g^*_{l_2}(k_2R)f_{l_1}(k_1R)P_k(\cos\theta). \quad (6.36)$$

This is equivalent to the result of Brink [33]) and Hayakawa and Yoshida [34]).

7. The Decay of the Residual Nucleus

So far, we have restricted ourselves to measurements of the directions and polarization of the incoming or outgoing radiations. In most cases, the residual nucleus is left in an excited state, from which there is decay with the emission of further radiation. Usually the state is a low-lying one and the de-excitation is by γ-radiation to the ground state of the residual nucleus. In this section we shall derive expressions for the angular correlation between these γ-rays and the outgoing radiation of the preceding reaction.

The angular correlation is most simply found by interpreting the measurement of the direction of the γ-rays as providing information concerning the polarization state of the residual nucleus. It follows then that the efficiency matrix for the outgoing states as given in (2.6) must be amended to include quantum numbers C and C' which refer to the subsequent decay process. If the decay is by γ-rays of multipolarity L and L' to a final state where the spin is d, we have

$$\langle \mathbf{k}_2 c\gamma s_2 \sigma_2 C|\varepsilon|\mathbf{k}_2 c\gamma' s_2 \sigma_2' C'\rangle = \delta_{\sigma_2\sigma_2'} \sum_{k\kappa} \varepsilon_{k\kappa}(cC, cC')(-)^{c-\gamma'}(c\gamma, c-\gamma'|k\kappa), \quad (7.1)$$

where

$$\varepsilon_{k\kappa}(cC, cC') = \sum_{k_d\kappa_d k_L\kappa_L} \varepsilon_{k_d\kappa_d}(dd)\varepsilon_{k_L\kappa_L}(LL')\hat{c}^2\hat{k}_d\hat{k}_L \begin{Bmatrix} c & d & L \\ c & d & L' \\ k & k_d & k_L \end{Bmatrix} (k\kappa|k_d\kappa_d, k_L\kappa_L). \quad (7.2)$$

Assuming that the measurement in the decay process is limited to only the direction of the γ-radiation, the efficiency tensor for the final nuclear state vanishes unless $k_d = \kappa_d = 0$. Inserting the radiation-parameter for γ-rays in (7.2) (see ref. [11])) the above expression reduces to

$$\varepsilon_{k\kappa}(cC, cC') = \frac{\hat{c}}{4\pi}(-)^{k+L'-L}F_k(LL'dc)\mathscr{D}^k_{\kappa 0}(\mathscr{R}), \quad (7.3a)$$

where $F_k(LL'dc)$ is the tabulated function [35]) given by

$$F_k(LL'dc) = (-)^{d-c-1}\hat{c}\hat{L}\hat{L}'(L1, L'-1|k0)W(ccLL'; kd), \quad (7.3b)$$

and $\mathscr{R}$ is the rotation carrying an arbitrary z-axis into the direction of the γ-radiation.

The angular correlation is found by inserting the expression for the efficiency matrix as found from (7.1) and (7.3a), together with the density matrix for the initial states as given in (2.6) into the expression (2.4). We then find, after use of some Racah algebra,

$$W(\theta, \phi; \theta') \sim \sum \langle d|L||c\rangle\langle d|L'||c\rangle F_k(LL'dc)\theta_{j(ls)}(c, a)\theta_{j'(l's')}(c, a)\mathscr{D}^k_{\kappa 0}(\phi, \theta, 0)$$
$$\times (-)^{L'-L+j+j'+c-a}W(j'cjc; ak)\sum_{\zeta\zeta'\sigma_1\sigma_2}(-)^{-\zeta'}(j\zeta, j'-\zeta'|k\kappa)X^{j(ls)\zeta}_{\sigma_2\sigma_1}(\theta')X^{j'(l's')\zeta'*}_{\sigma_2\sigma_1}(\theta'), \quad (7.4)$$

where θ' is the angle between incoming and outgoing radiations in the direct process and (θ, ϕ) denote the direction of the γ-ray as referred to any chosen set of axes. The quantity $\langle d|L||c\rangle$ is the reduced matrix element for emission of the γ-ray and is real.

We may further simplify the above expression by interchanging primed and unprimed quantities and making use of the symmetry relation (2.20). We then find that $W(\theta, \phi; \theta')$ which must be real is of the form

$$W(\theta, \phi; \theta')$$

$$\sim \sum_{\substack{kLL'jls j'l's' \\ \kappa \geq 0}} \langle d|L||c\rangle\langle d|L'||c\rangle F_k(LL'dc)(-)^{L'-L+j-j'+c-a}\sqrt{\frac{(k-\kappa)!}{(k+\kappa)!}}\, P_k^\kappa(\cos\theta)$$

$$\times \cos\kappa\phi(2-\delta_{\kappa 0})W(j'cjc; ak)\sum_{\zeta\zeta'\sigma_1\sigma_2}(-)^{\zeta}(j\zeta, j'-\zeta'|k\kappa)\,\mathrm{Re}\,[X^{j(ls)\zeta}_{\sigma_2\sigma_1}(\theta')X^{j'(l's')\zeta'*}_{\sigma_2\sigma_1}(\theta')$$

$$\times\theta_{j(ls)}(c, a)\theta_{j'(l's')}(c, a)], \quad (7.5)$$

where $P_k^\kappa(\cos\theta)$ is as defined by Jahnke and Emde [36]).

The quantity $X^{j(ls)\zeta}_{\sigma_2\sigma_1}(\theta')$ assumes the expressions given in (2.10) or (2.11) depending on whether the z-axis is along $\mathbf{k}_1$ or $\mathbf{k}_2$. Since the nuclear states of the residual nuclei are sharp, it follows that k is even. Furthermore, it is seen from the Racah-coefficient that k does not exceed either $2j_{\max}$ or $2c$; so that if $c = \frac{1}{2}$, there is no correlation.

Equation (7.5) is the generalization of the formula of Huby *et al.* [3]), whose analysis is restricted to deuteron-stripping processes without allowance for spin-dependent distortion. If we neglect such a distortion and use (2.11) we have

$$X^{j(ls)\zeta}_{\sigma_2\sigma_1}(\theta') \equiv B^{j(ls)\zeta}_{\sigma_2\sigma_1}(\theta') = \sum_{\sigma\sigma_1'\lambda}(l\lambda, s\sigma|j\zeta)(s_2\sigma_2, s\sigma|s_1\sigma_1')\mathscr{D}^s_{\sigma_1'\sigma_1}(0, \theta' 0)D^{l\lambda}(\theta'), \quad (7.6)$$

where $D^{l\lambda}(\theta')$ is given in (5.15e). Performing the sum over magnetic quantum numbers, we obtain

$$\sum_{\zeta\zeta'\sigma_1\sigma_2}(-)^{j+\zeta}(j\zeta, j'-\zeta'|k\kappa)B^{j(ls)\zeta}_{\sigma_2\sigma_1}(\theta')B^{j'(l's')\zeta'*}_{\sigma_2\sigma_1}(\theta')$$

$$=(-)^{k+\kappa+j'+l'+s}\delta_{ss'}\hat{j}\hat{j}'\frac{\hat{s}_1^2}{\hat{s}^2}W(ljl'j'; sk)\sum_{\lambda\lambda'}(-)^{l'-\lambda'}(l\lambda, l'-\lambda'|k\kappa)D^{l\lambda}(\theta')D^{l'\lambda'*}(\theta'). \quad (7.7)$$

If we substitute (7.7) into (7.5), and consider deuteron stripping, we obtain a formula which is equivalent to that of Huby *et al.* [3]).

The complexity of the angular correlation as written in (7.5) is given by

$$k_{\max} \leqq \min\,[2L_{\max}, 2j_{\max}, 2c], \quad (7.8a)$$

whereas for no spin-dependent distortion

$$k_{\max} \leqq \min\,[2L_{\max}, 2j_{\max}, 2l_{\max}, 2c]. \quad (7.8b)$$

Thus, if $s = 0$, there is no difference in the complexity of the angular correlation in the two cases. On the other hand, if $s = 1$, a difference might arise if l were restricted to be $j-1$ and L_{max} and c were greater than j. In such an instance, it would be possible to establish contributions from $s=1$ by study of the complexity of the correlation and therefore to eliminate the ambiguities mentioned in section 6.1.b concerning (He^3, p) processes.

As pointed out by Austern [1]) the effect of distorted waves is to not seriously modify the pattern of the angular correlation. It is interesting to observe that the angular correlation, which, in fact, plays a role similar to the measurement of outgoing polarization in the primary direct-reaction, does not compare favourably with the latter measurement in isolating effects of spin-dependent distorted waves for the case $l = 0$, $s = \frac{1}{2}$. The fact is that for this situation (which applies most significantly to deuteron-stripping processes), k is even for sharp states of the residual nucleus and since j is restricted to the value $\frac{1}{2}$, it follows from (7.8a) that k must vanish.

On the other hand, if $l \neq 0$ and $c > \frac{1}{2}$, the angular correlation, which essentially gives the measurement of the polarization of the residual nucleus of spin c provides one with more independent pieces of information concerning the direct-interaction than is obtained by study of the polarization of the outgoing radiation in the direct process.

One of the main aspects of angular-correlation measurements is that, generally, a coherent summation is required over the quantities j and/or l, even though $s = 0$ or $\frac{1}{2}$. This is in contrast to the result obtained earlier that both the unpolarized and polarized angular distributions in the primary direct-reaction require an incoherent summation over l for $s = 0$ and $\frac{1}{2}$.

We end our discussion by reference to the particular expressions displayed in the appendix. These refer to the more common types of direct-reactions and include cross-sections, the tensors $\rho_{k_2\kappa}(s_2)$ describing the polarization of outgoing radiation using unpolarized incident radiation and $\varepsilon^*_{k_1\kappa}(s_1)$ which describes the efficiency of the reaction in detecting incoming polarization. The latter tensors are omitted in the cases where a simple relation exists between the efficiency and statistical tensors (see section 5). The specific parameters characterizing these tensors are displayed in (2.16) and (2.25) for the cases $s = \frac{1}{2}$ and $s = 1$, and are defined for higher spins in ref. [14]) for example.

We should finally reiterate that our analysis is far from complete because of our neglect in the case of stripping processes only of spin-dependent direct interactions which in general could contribute in a significant way to polarization. Most calculations, to date, use extremely crude models for this interaction and ignore the possibility of any spin-dependence. Yet, even in deuteron stripping, the d-state of the deuteron implies that the direct-interaction operator is non-central and spin-dependent, although this effect may be a very small one. Such effects would be more important in reactions involving heavier particles

than deuterons. Besides the neglect of the coupling of the spin of composite particles to their original configuration, we have also ignored effects of the exclusion principle, and phenomena such as heavy-particle stripping [37]).

In conclusion, we should like to acknowledge our debt to Dr. L. Castillejo, who, independently, arrived at certain results equivalent to ours, and corrected several errors that arose in our analysis.

Appendix

In this appendix we give expressions for the angular distributions and polarization tensors for some specific direct processes.

I. DIRECT INELASTIC NUCLEON SCATTERING ($s_1 = s_2 = \frac{1}{2}$)

We restrict ourselves to a spin-independent ($s = 0$) zero-range direct interaction and to the case where the target nucleus consists of a core of spin j_c and one outer nucleon with unique quantum numbers $L_1 J_1$ and $L_2 J_2$ initially and finally.

I.a. Spin-dependent distortion of the projectile

$$\frac{\mathrm{d}\sigma}{\mathrm{d}\Omega} = \frac{1}{4\pi}\left(\frac{m^* g}{\hbar^2}\right)^2 \frac{k_2}{k_1}\frac{\hat{c}^2}{\hat{a}^2}\sum_l \left[\frac{\theta_l^2}{l^2} S_l^{\mathrm{I}}(\theta)\right], \tag{A.1}$$

$$\mathbf{P}(\tfrac{1}{2}) = 2\mathbf{n}\,\frac{\sum_l \left(\frac{\theta_l}{l}\right)^2 \mathrm{Im}\sum_\zeta (-)^\zeta x_\zeta^{\mathrm{I}}(\theta) y_\zeta^{\mathrm{I}*}(\pi-\theta)}{\sum_l \left(\frac{\theta_l}{l}\right)^2 S_l^{\mathrm{I}}(\theta)}, \tag{A.2}$$

$$\mathbf{P}^{\mathrm{d}}(\tfrac{1}{2}) = 2\mathbf{n}\,\frac{\sum_l \left(\frac{\theta_l}{l}\right)^2 \mathrm{Im}\sum_\zeta x_\zeta^{\mathrm{I}}(\theta) y_{-\zeta}^{\mathrm{I}*}(\pi-\theta)}{\sum_l \left(\frac{\theta_l}{l}\right)^2 S_l^{\mathrm{I}}(\theta)}, \tag{A.3}$$

where

$$x_\zeta^{\mathrm{I}}(\theta) = \sum_{j_1 l_1 j_2 l_2} \hat{j}_1^2 \hat{j}_2 (-)^{j_2-\frac{1}{2}} (l\zeta, j_1\tfrac{1}{2}|j_2\tfrac{1}{2}+\zeta)(j_2\tfrac{1}{2}, j_1-\tfrac{1}{2}|l0) \times \mathscr{D}^{j_2}_{\frac{1}{2}+\zeta,\frac{1}{2}}(0\theta 0) R^{\mathrm{I}}(j_2 l_2 l; j_1 l_1), \tag{A.4}$$

$$y_\zeta^{\mathrm{I}}(\theta) = \sum_{j_1 l_1 j_2 l_2} \hat{j}_1^2 \hat{j}_2 (-)^{j_2-\frac{1}{2}} (l\zeta, j_1\tfrac{1}{2}|j_2\tfrac{1}{2}+\zeta)(j_2\tfrac{1}{2}, j_1-\tfrac{1}{2}|l0) \times \mathscr{D}^{j_2}_{\frac{1}{2}+\zeta,\frac{1}{2}}(0\theta 0)(-)^{l_2} R^{\mathrm{I}}(j_2 l_2 l; j_1 l_1), \tag{A.5}$$

$$S_l^{\mathrm{I}}(\theta) = \sum_\zeta \{|x_\zeta^{\mathrm{I}}(\theta)|^2 + |y_\zeta^{\mathrm{I}}(\pi-\theta)|^2\}, \tag{A.6}$$

$$R^{\mathrm{I}}(j_2 l_2 l; j_1 l_1) = i^{l_1+L_1-l_2-L_2}\int_0^\infty r^2 \mathrm{d}r g^*_{j_2 l_2}(k_2, r) u^{\mathrm{I}}_{J_2 L_2}(r) u^{\mathrm{I}}_{J_1 L_1}(r) f_{j_1 l_1}(k_1, r), \quad \text{(A.7)}$$

$$\theta_i = \frac{\hat{a}\hat{J}_1\hat{J}_2}{\sqrt{4\pi}} W(cJ_2 aJ_1; j_c l)(J_1 \tfrac{1}{2}, J_2 -\tfrac{1}{2}|l0)(-)^{a-J_c+\frac{1}{2}}, \quad \text{(A.8)}$$

and $f_{j_1 l_1}(k_1, r)$, $g_{j_2 l_2}(k_2, r)$, $u_{J_2 L_2}(r)$ and $u_{J_1 L_1}(r)$ are as defined in section 6.2.

I.b. No spin-dependent distortion of the projectile

$$\frac{\mathrm{d}\sigma}{\mathrm{d}\Omega} = \left(\frac{2m^* g}{\hbar^2}\right)^2 \frac{k_2}{k_1}\frac{\hat{c}^2}{\hat{a}^2}\sum_i \theta_i^2 \sum_{\lambda\geq 0}|z^{\mathrm{I}}_\lambda(\theta)|^2(2-\delta_{\lambda 0}), \quad \text{(A.9)}$$

$$\mathbf{P}(\tfrac{1}{2}) = \mathbf{P}^{\mathrm{d}}(\tfrac{1}{2}) = 0, \quad \text{(A.10)}$$

$$z^{\mathrm{I}}_\lambda(\theta) = \sum_{l_1 l_2} \hat{l}_2 (l_2 \lambda, l-\lambda|l_1 0)(l_2 0, l0|l_1 0) Y^\lambda_{l_2}(\theta, 0) i^{l_1+L_1-l_2-L_2} \times \int_0^\infty r^2 \mathrm{d}r g^*_{l_2}(k_2, r) u^{\mathrm{I}}_{J_2 L_2}(r) u^{\mathrm{I}}_{J_1 L_1}(r) f_{l_1}(k_1, r). \quad \text{(A.11)}$$

$u^{\mathrm{I}}_{J_2 L_2}(r)$ and $u^{\mathrm{I}}_{J_1 L_1}(r)$ are the radial wave functions of the struck nucleon in its final and initial states respectively.

II. DEUTERON STRIPPING ($s_1 = 1\ s_2 = s = \frac{1}{2}$) (d, p) (d, n)

We give formulae for the case of zero-range spin-independent neutron-proton interaction.

II.a. Spin-dependent distortion of nucleon and deuteron

$$\frac{\mathrm{d}\sigma}{\mathrm{d}\Omega} = \frac{1}{2\pi}\left(\frac{g}{\hbar^2}\right)^2 m_1^* m_2^* \frac{k_2}{k_1}\frac{\hat{c}^2}{\hat{a}^2}\sum_{ji}\theta^{\mathrm{II}2}_{ji}\hat{l}^2 S^{\mathrm{II}}_{ji}(\theta), \quad \text{(A.12)}$$

$$\mathbf{P}(\tfrac{1}{2}) = \mathbf{n}\frac{\sum_{ji}\theta^{\mathrm{II}2}_{ji}\hat{l}^2\sum_\zeta \mathrm{Im}[2(-)^{\zeta-\frac{1}{2}}x^{\mathrm{II}}_\zeta(\theta)y^{\mathrm{II}*}_\zeta(\pi-\theta)+(-)^{j+l-\zeta}z^{\mathrm{II}}_\zeta(\theta)z^{\mathrm{II}*}_\zeta(\theta)]}{\sum_{ji}\theta^{\mathrm{II}2}_{ji}\hat{l}^2 S^{\mathrm{II}}_{ji}(\theta)}, \quad \text{(A.13)}$$

$$\mathbf{P}^{\mathrm{d}}(1) = \mathbf{n}\frac{\sqrt{2}\sum_{ji}\theta^{\mathrm{II}2}_{ji}\hat{l}^2\sum_\zeta \mathrm{Im}[z^{\mathrm{II}}_\zeta(\theta)\{(-)^{l}x^{\mathrm{II}*}_\zeta(\theta)+(-)^{j-\frac{1}{2}}y^{\mathrm{II}*}_{-\zeta}(\pi-\theta)\}]}{\sum_{ji}\theta^{\mathrm{II}2}_{ji}\hat{l}^2 S^{\mathrm{II}}_{ji}(\theta)}. \quad \text{(A.14)}$$

$$P^{\mathrm{d}}_{33}(1) = \frac{\sum_{ji}\theta^{\mathrm{II}2}_{ji}\hat{l}^2\sum_\zeta\{|x^{\mathrm{II}}_\zeta(\theta)|^2+|y^{\mathrm{II}}_\zeta(\theta)|^2-2|z^{\mathrm{II}}_\zeta(\theta)|^2\}}{\sum_{ji}\theta^{\mathrm{II}2}_{ji}\hat{l}^2 S^{\mathrm{II}}_{ji}(\theta)}, \quad \text{(A.15)}$$

$$P^{\mathrm{d}}_{13}(1) = \frac{\frac{3}{\sqrt{2}}\cos\phi\sum_{ji}\theta^{\mathrm{II}2}_{ji}\hat{l}^2\sum_\zeta \mathrm{Re}\{z^{\mathrm{II}}_\zeta(\theta)[(-)^{j-\frac{1}{2}}y^{\mathrm{II}*}_{-\zeta}(\pi-\theta)+(-)^{l}x^{\mathrm{II}*}_\zeta(\theta)]\}}{\sum_{ji}\theta^{\mathrm{II}2}_{ji}\hat{l}^2 S^{\mathrm{II}}_{ji}(\theta)}, \quad \text{(A.16)}$$

$$P_{23}^{d}(1) = \tan\phi\, P_{13}^{d}(1), \tag{A.17}$$

$$P_{11}^{d}(1) - P_{22}^{d}(1) = \frac{6\cos 2\phi \sum_{jl} (-)^{j+\frac{1}{2}+l}\theta_{jl}^{\mathrm{II}2} l^2 \sum_{\zeta} \mathrm{Re}[x_{\zeta}^{\mathrm{II}}(\theta)\, y_{-\zeta}^{\mathrm{II}*}(\pi-\theta)]}{\sum_{jl} \theta_{jl}^{\mathrm{II}2} l^2 S_{jl}^{\mathrm{II}}(\theta)}, \tag{A.18}$$

$$P_{12}^{d}(1) = \tfrac{1}{2}\tan 2\phi\, [P_{11}^{d}(1) - P_{22}^{d}(1)], \tag{A.19}$$

where

$$S_{jl}^{\mathrm{II}}(\theta) = \sum_{\zeta} \{|x_{\zeta}^{\mathrm{II}}(\theta)|^2 + |y_{\zeta}^{\mathrm{II}}(\theta)|^2 + |z_{\zeta}^{\mathrm{II}}(\theta)|^2\}, \tag{A.20}$$

$$x_{\zeta}^{\mathrm{II}}(\theta) = \sum_{j_1 l_1 j_2 l_2} l_2 f_2^2 (-)^{j_2+j_1+\frac{1}{2}} \Delta(l_1 j_1)(l_2 0,\, l0|l_1 0)(j_2 1-\zeta,\, j\zeta|j_1 1) \times \begin{pmatrix} l_2 & \frac{1}{2} & j_2 \\ l & \frac{1}{2} & j \\ l_1 & 1 & j_1 \end{pmatrix} \mathscr{D}_{\frac{1}{2}1-\zeta}^{j_2}(0\theta 0) R^{\mathrm{II}}(j_2 l_2 jl;\, j_1 l_1), \tag{A.21}$$

$$y_{\zeta}^{\mathrm{II}}(\theta) = \sum_{j_1 l_1 j_2 l_2} l_2 f_2^2 (-)^{j_2+j_1+\frac{1}{2}} \Delta(l_1 j_1)(l_2 0,\, l0|l_1 0)(j_2 1-\zeta,\, j\zeta|j_1 1) \times \begin{pmatrix} l_2 & \frac{1}{2} & j_2 \\ l & \frac{1}{2} & j \\ l_1 & 1 & j_1 \end{pmatrix} \mathscr{D}_{\frac{1}{2}1-\zeta}^{j_2}(0\theta 0)(-)^{l_2} R^{\mathrm{II}}(j_2 l_2 jl;\, j_1 l_1), \tag{A.22}$$

$$z_{\zeta}^{\mathrm{II}}(\theta) = \sqrt{2} \sum_{j_1 l_1 j_2 l_2} l_1 l_2 f_2^2 (-)^{j_2+l_2-\frac{1}{2}} (l_1 0,\, 10|j_1 0)(l_2 0,\, l0|l_1 0) \times (j_2-\zeta,\, j\zeta|j_1 0) \begin{pmatrix} l_2 & \frac{1}{2} & j_2 \\ l & \frac{1}{2} & j \\ l_1 & 1 & j_1 \end{pmatrix} \mathscr{D}_{\frac{1}{2}1-\zeta}^{j_2}(0\theta 0) R^{\mathrm{II}}(j_2 l_2 jl;\, j_1 l_1), \tag{A.23}$$

$$R^{\mathrm{II}}(j_2 l_2 jl;\, j_1 l_1) = i^{l_1-l_2-l} \int_0^{\infty} r^2 \mathrm{d}r\, g_{j_2 l_2}^{*}(k_2,\, r') u_{jl}^{\mathrm{II}}(r) f_{j_1 l_1}(k_1,\, r), \qquad r' = \left(1 - \frac{m_2}{m_c}\right) r, \tag{A.24}$$

$$\Delta(l_1 j_1) = [j_1 \delta_{j_1, l_1-1} + (j_1+1)\delta_{j_1, l_1+1} + (2l_1+1)\delta_{j_1, l_1}]^{\frac{1}{2}}, \tag{A.25}$$

and ϕ is the angle between $\mathbf{n}$ and the y-axis to which the incoming polarization is referred. The z-axis is taken to be along the deuteron direction.

II.b. Spin distortion of the nucleon only.

Restricting ourselves to the case $l = 0$, we have

$$\frac{\mathrm{d}\sigma}{\mathrm{d}\Omega} = \frac{m_1^* m_2^*}{8\pi} \frac{g^2}{\hbar^4} \frac{\hat{c}^2}{\hat{a}^2} \frac{k_2}{k_1} \theta_{j0}^{\mathrm{II}2} \{|x^{\mathrm{II}}(\theta)|^2 + |y^{\mathrm{II}}(\pi-\theta)|^2\}, \tag{A.26}$$

$$\mathbf{P}(\tfrac{1}{2}) = \mathbf{n} \frac{2\,\mathrm{Im}\,\{x^{\mathrm{II}}(\theta) y^{*\mathrm{II}}(\pi-\theta)\}}{|x^{\mathrm{II}}(\theta)|^2 + |y^{\mathrm{II}}(\pi-\theta)|^2}, \tag{A.27}$$

$$x^{\mathrm{II}}(\theta) = \sum_{j_2 l_2} \hat{j}_2^2 \mathscr{D}^{j_2}_{\frac{1}{2}\frac{1}{2}}(0\theta 0) \int_0^\infty r^2 \mathrm{d}r g^*_{j_2 l_2}(k_2, r') u^{\mathrm{II}}_{j0}(r) f_{l_2}(k_1, r), \tag{A.28}$$

$$y^{\mathrm{II}}(\theta) = \sum_{j_2 l_2} \hat{j}_2^2 \mathscr{D}^{j_2}_{\frac{1}{2}\frac{1}{2}}(0\theta 0)(-)^{l_2} \int_0^\infty r^2 \mathrm{d}r g^*_{j_2 l_2}(k_2, r') u^{\mathrm{II}}_{j0}(r) f_{l_2}(k_1, r). \tag{A.29}$$

II.c. No spin distortion of the nucleon or deuteron

$$\frac{\mathrm{d}\sigma}{\mathrm{d}\Omega} = 2m_1^* m_2^* \left(\frac{g}{\hbar^2}\right)^2 \frac{k_2}{k_1} \frac{\hat{c}^2}{\hat{a}^2} \sum_{jl} \theta^{\mathrm{II}2}_{jl} \sum_{\lambda \geq 0} (2-\delta_{\lambda 0}) |z^{\mathrm{II}}_\lambda(\theta)|^2, \tag{A.30}$$

$$\mathbf{P}(\tfrac{1}{2}) = \tfrac{2}{3}\mathbf{n} \frac{\sum_{jl} (-)^{j+l+\frac{1}{2}} \left(\dfrac{\theta^{\mathrm{II}}_{jl}}{\hat{j}}\right)^2 \sum_\lambda \sqrt{(l-\lambda)(l+\lambda+1)}\ \mathrm{Im}\ \{z^{\mathrm{II}}_\lambda(\theta) z^{\mathrm{II}*}_{\lambda+1}(\theta)\}}{\sum_{jl} \theta^{\mathrm{II}2}_{jl} \sum_{\lambda \geq 0} (2-\delta_{\lambda 0}) |z^{\mathrm{II}}_\lambda(\theta)|^2}, \tag{A.31}$$

where

$$z^{\mathrm{II}}_\lambda(\theta) \tag{A.32}$$
$$= \sum_{l_1 l_2} \hat{l}_2 (l_2 - \lambda, l\lambda | l_1 0)(l_2 0, l0 | l_1 0) Y^\lambda_{l_2}(\theta, 0) i^{l_1 - l_2 - l} \int_0^\infty r^2 \mathrm{d}r g^*_{l_2}(k_2, r') u^{\mathrm{II}}_{jl}(r) f_{l_1}(k_1, r).$$

$\theta^{\mathrm{II}}_{jl}$ is the reduced-width amplitude for the stripped-off nucleon with radial eigenfunction $u^{\mathrm{II}}_{jl}(r)$ in the final nucleus.

III. (α, p) PROCESSES, etc. ($s_2 = \frac{1}{2} = s$, $s_1 = 0$)

We treat all particles as point particles and assume a spin-independent nucleon-triton interaction.

III.a. Spin-dependent nucleon distortion

$$\frac{\mathrm{d}\sigma}{\mathrm{d}\Omega} = 2m_1^* m_2^* \frac{g^2}{\hbar^4} \frac{k_2}{k_1} \frac{\hat{c}^2}{\hat{a}^2} \sum_{jl} \theta^{\mathrm{III}2}_{jl} \sum_\zeta |x^{\mathrm{III}}_\zeta(\theta)|^2, \tag{A.33}$$

$$\mathbf{P}(\tfrac{1}{2}) = 2\mathbf{n} \frac{\sum_{jl} \theta^{\mathrm{III}2}_{jl} \sum_{\zeta \geq 0} \mathrm{Im}\ \{(-)^{j+l-\zeta} x^{\mathrm{III}}_\zeta(\theta) x^{\mathrm{III}*}_{-\zeta}(\theta)\}}{\sum_{jl} \theta^{\mathrm{III}2}_{jl} \sum_\zeta |x^{\mathrm{III}}_\zeta(\theta)|^2}, \tag{A.34}$$

$$x^{\mathrm{III}}_\zeta(\theta) = \sum_{j_2 l_2 l_1} \hat{l}_1 (l_1 \tfrac{1}{2} + \zeta, j - \zeta | j_2 \tfrac{1}{2})(l_1 0, j\tfrac{1}{2} | j_2 \tfrac{1}{2}) Y^{\zeta+\frac{1}{2}}_{l_1}(\theta, 0)\, i^{l_1 - l_2 - l}$$
$$\times \int_0^\infty r^2 \mathrm{d}r g^*_{j_2 l_2}(k_2, r') u^{\mathrm{III}}_{jl}(r) f_{l_1}(k_1, r). \tag{A.35}$$

III.b. No spin-dependent distortion of the nucleon

$$\frac{\mathrm{d}\sigma}{\mathrm{d}\Omega} = 2m_1^* m_2^* \frac{g^2}{\hbar^4} \frac{k_2}{k_1} \frac{\hat{c}^2}{\hat{a}^2} \sum_{jl} \theta^{\mathrm{III}2}_{jl} \sum_{\lambda \geq 0} (2-\delta_{\lambda 0}) |z^{\mathrm{III}}_\lambda(\theta)|^2, \tag{A.36}$$

$$\mathbf{P}(\tfrac{1}{2}) = 2\mathbf{n}\,\frac{\sum_{jl}(-)^{j+l-\frac{1}{2}}\left(\frac{\theta^{\mathrm{III}}_{jl}}{\hat{j}}\right)^2 \sum_{\lambda}\sqrt{(l-\lambda)(l+\lambda+1)}\,\mathrm{Im}\{z^{\mathrm{III}}_{\lambda}(\theta)z^{\mathrm{III}*}_{\lambda+1}(\theta)\}}{\sum_{jl}\theta^{\mathrm{III}2}_{jl}\sum_{\lambda\geq 0}(2-\delta_{\lambda 0})|z^{\mathrm{III}}_{\lambda}(\theta)|^2}, \quad \text{(A.37)}$$

$$z^{\mathrm{III}}_{\lambda}(\theta) = \sum_{l_1 l_2}\hat{l}_2(l_2 0,\, l0|l_1 0)(l_2-\lambda,\, l\lambda|l_1 0)Y^{\lambda}_{l_2}(\theta,0)i^{l_1-l_2-l}\int_0^{\infty}r^2\mathrm{d}r g^{*}_{l_2}(k_2,r')u^{\mathrm{III}}_{jl}(r)f_{l_1}(k_1,r). \quad \text{(A.38)}$$

$\theta^{\mathrm{III}}_{jl}$ is the reduced-width amplitude for a triton with radial eigenfunction u^{III}_{jl} is the final nucleus.

These formulae are equally valid for $(\alpha, \mathrm{H}^3)(\alpha, \mathrm{He}^3)$ processes, provided that the radial integral and the reduced-width amplitude are modified. Thus, $\theta^{\mathrm{III}}_{jl}$ is the reduced-width amplitude for a nucleon with radial eigenfunction $u^{\mathrm{III}}_{jl}(r)$ in the final nucleus and in (A.35), $g_{j_2 l_2}(k_2, r')$ refers to the mass-3 projectile

IV. $(\mathrm{He}^3, \mathrm{p})$, $(\mathrm{H}^3, \mathrm{p})$, etc. PROCESSES $(s_1 = s_2 = \frac{1}{2})$

Restricting ourselves to $s = 0$, only, the angular distributions and polarizations are as in I, except that θ_l is identified with the reduced-width amplitude for the stripped-off nucleons with radial eigenfunctions $u^{\mathrm{IV}}_{jl}(r)$ in the final nucleus, while the quantity R^{I} is replaced by R^{IV} given by

$$R^{\mathrm{IV}}(j_2 l_2 l; j_1 l_1) = i^{l_1-l_2-l}\int_0^{\infty}r^2\mathrm{d}r g^{*}_{j_2 l_2}(k_2,r')u^{\mathrm{IV}}_{jl}(r)f_{j_1 l_1}(k_1,r). \quad \text{(A.39)}$$

References

1) N. Austern, in Fast Neutron Physics, Part II, edited by J. B. Marion and J. L. Fowler (Interscience, New York, 1960), Chapter VD
2) See for example: W. Tobocman, Phys. Rev. **115** (1959) 98;
S. T. Butler and O. H. Hittmair, Nuclear Stripping Reactions (Horvitz Publications, Sydney, 1957)
3) Huby, Refai and Satchler, Nuclear Physics **9** (1958) 94
4) B. A. Lippmann and J. Schwinger, Phys. Rev. **79** (1950) 469
5) M. Gell-Mann and M. L. Goldberger, Phys. Rev. **91** (1953) 398
6) See for example: G. E. Brown, Revs. Mod. Phys. **31** (1959) 893
7) N. K. Glendenning, Phys. Rev. **114** (1959) 1297
8) H. C. Newns and M. Y. Refai, Proc. Phys. Soc. A **71** (1958) 627
9) F. Coester and J. M. Jauch, Helv. Phys. Acta **26** (1953) 3
10) F. Coester, Phys. Rev. **89** (1953) 619
11) S. Devons, and L. J. B. Goldfarb, Handbuch der Physik **42** (Springer Verlag, Berlin, 1957) 362
12) M. E. Rose, Elementary Theory of Angular Momentum (John Wiley, New York, 1957)
13) See for example ref. [4])
14) L. J. B. Goldfarb, Nuclear Physics **7** (1958) 622
15) A. Simon and T. A. Welton, Phys. Rev. **90** (1953) 1036
16) K. M. Watson, Phys. Rev. **88** (1952) 1163
17) R. Huby, Proc. Phys. Soc. A **67** (1954) 1103
18) L. C. Biedenharn, Nuclear Physics **10** (1959) 620

19) G. R. Satchler, Nuclear Physics **8** (1958) 65
20) L. Wolfenstein and J. Ashkin, Phys. Rev. **85** (1952) 947
21) G. Racah, Phys. Rev. **84** (1951) 910
22) R. G. Thomas, Phys. Rev. **100** (1955) 25
23) G. Breit, Handbuch der Physik **41** (Springer Verlag, Berlin, 1959) 1
24) E. P. Wigner and L. Eisenbud, Phys. Rev. **72** (1947) 29
25) J. M. Blatt and L. C. Biedenharn, Revs. Mod. Phys. **24** (1952) 259
26) Sharp, Kennedy, Sears and Hoyle, Tables of Coefficients for Angular Distribution Analysis, AECL 97 (1953)
27) G. R. Satchler, Proc. Phys. Soc. A **66** (1953) 1081
28) G. R. Satchler, Nuclear Physics **3** (1958) 67
29) C. A. Levinson and M. K. Banerjee, Annals of Physics **3** (1958) 67
30) J. R. Lamarsh and H. Feshbach, Phys. Rev. **104** (1955) 1633
31) S. Yoshida, Proc. Phys. Soc. A **69** (1956) 668
32) Chase, Wilets and Edmonds, Phys. Rev. **110** (1958) 1080
33) D. M. Brink, Proc. Phys. Soc. A **68** (1955) 1037
34) S. Hayakawa and S. Yoshida, Progress Theor. Phys. **14** (1955) 1
35) M. Ferentz and N. Rosenzweig, Argonne Nat. Laboratory ANL 5234 (1953)
36) E. Jahnke and F. Emde, Tables of functions with formulae and curves (Dover Publications New York, 1945)
37) G. E. Owen and L. Madansky, Phys. Rev. **105** (1957) 1766

2.D

Nuclear Physics **18** (1960) 395—419; © *North-Holland Publishing Co., Amsterdam*

Not to be reproduced by photoprint or microfilm without written permission from the publisher

ON THE STATISTICAL PROPERTIES OF THE LEVEL-SPACINGS IN NUCLEAR SPECTRA

M. L. MEHTA †

Centre d'Études Nucléaires de Saclay, Gif-sur-Yvette (S. et O.), France

Received 5 May 1960

Abstract: The level-spacing distribution is studied under the random-matrix hypothesis. Rigorous lower and upper bounds for the distribution function of the level-spacing are given. Comparison of these with Wigner's surmise shows that it is a very good approximation. It is shown, however, that it cannot be exact even in the limiting case $n \to \infty$.

1. Introduction

In the last few years many experimental data on the statistical properties of heavy nuclei, such as distribution of neutron-widths, level-spacings, fission-widths, have been collected [1]). It is natural that such phenomena resulting from complicated many-body interactions lead to statistical theories which explain only the average properties. Thus level-densities [2]), mean angular momenta [3]) and a measure of transition rate, the strength-function [4]) are fairly well understood and widely employed.

The next natural thing for such theories to do is to find dispersions about the means or moments of the distribution to higher order, to enable one to know the distribution in more and more detail and ultimately to get the distribution function itself.

The relevance of such distributions to the theory of nuclear reactions was recognized fairly early [5]). However, the explanations to partial width distributions began to come forward [6]) some five years ago, along with the first experimental evidence of the absence of small spacings in the spacing distribution of nuclear levels (of the same spin and parity) [7]). In this paper we will be concerned only with this level-spacing distribution.

It was pointed out by Wigner [8]) and Landau and Smorodinski [9]) that under plausible assumptions on the nuclear matrix elements, this distribution should be linear for small spacings. Extrapolating this Wigner surmised a distribution for all spacings [8]).

† On leave of absence from Tata Institute of Fundamental Research, Bombay.

2. Available Theoretical Results

The random matrix hypothesis usually taken as a start is as follows. The nuclear Hamiltonian, if expressed in a system of arbitrary basic functions, is a matrix of high order with its elements distributed at random. The assumptions that every matrix element is distributed independently of the others † and that the Hamiltonian is statistically invariant under linear orthogonal transformations lead to the following conclusions [10]).

a) Every matrix element is normally distributed. All off-diagonal elements have the same mean value zero and the same variance; all the diagonal elements have the same common mean value, which can be taken as equal to zero, and equal variances. The common variance of the diagonal elements is twice that of the off-diagonal elements. This is expressed by

$$P(H_{11}, H_{12}, H_{22}, \ldots, H_{n-1,n}) = \text{const} \cdot \exp\{-\text{tr}\, H^2\}, \tag{1}$$

where the variance of the diagonal elements has been taken equal to $\frac{1}{2}$.

b) The joint probability frequency function of the eigenvalues $\theta_1, \theta_2, \ldots, \theta_n$ of H is given by

$$P(\theta_1, \theta_2, \ldots, \theta_n) = \mu_0^{-1} e^{-(\theta_1^2+\cdots+\theta_n^2)} \prod_{i<j} |(\theta_i - \theta_j)|, \tag{2}$$

with ††

$$\mu_0 = n! 2^{-\frac{1}{4}n(n-1)} \prod_{g=1}^{n} \Gamma(\tfrac{1}{2}g). \tag{2'}$$

To get the level-density, we have to calculate

$$P(\theta_1) = \int_{-\infty}^{\infty} \ldots \int_{-\infty}^{\infty} P(\theta_1, \theta_2, \ldots, \theta_n) d\theta_2 \ldots d\theta_n, \tag{3}$$

and to get the spacing distribution we have first to find

$$P(\theta_1, \theta_2) = \int' P(\theta_1, \theta_2, \ldots, \theta_n) d\theta_3 \ldots d\theta_n, \tag{4}$$

the dash on the integral sign indicating that in integrating over $\theta_3, \theta_4, \ldots$ the interval between θ_1 and θ_2 is excluded. Then we have to transform to the new variables $\theta_1 - \theta_2 = S$, $\theta_2 = \theta_2$, say, and integrate over θ_2.

The method of the preceding paragraph is difficult when n is a large number, and as one is interested in the limit of $n \to \infty$, it is prohibitive in practice. Even the integration in (3) is not simple. Certain authors [11]) have derived upper bounds for $P(\theta_1)$ in very similar problems. Wigner [12]) applied an argument of statistical mechanics to derive an integral equation for $P(\theta_1)$ in the

† However, the validity of single particle models and the existence of collective motions in nuclei indicate a strong correlation in some cases.

†† This value of μ_0, as far as we know, was first given in Hsu's paper [10]). The calculation of μ_0 given in the following section is, however, an independent proof of eq. (2').

limiting case of large n and arrived at the so called "semi-circle law"

$$P(\theta_1) = \begin{cases} \frac{2}{n\pi}\sqrt{n-\theta_1^2} & \text{for } \theta_1 < \sqrt{n}, \\ 0 & \text{for } \theta_1 > \sqrt{n}. \end{cases} \tag{5}$$

On the other hand, Porter and Rosenzweig [10]) did some Monte-Carlo machine calculations with the aim to derive $P(\theta_1)$ and spacing distributions from randomly generated matrices of orders up to $n = 20$.

We shall present here a closer study of the functions $P(\theta_1)$ and $P(\theta_1, \theta_2)$ in the centre of the distribution of eigenvalues.

We shall compute exactly the value of $P(0)$ and the first moments of $P(\theta_1)$. These values agree exactly with the "semi-circle law" in the limit $n \to \infty$.

Similarly, we shall give the exact values of the function $P(-\theta, \theta)/\theta$ and of its first derivatives at $\theta = 0$. The results obtained show that Wigner's surmise does not become rigorously exact in the limit $n \to \infty$. Lower and upper limits of the distribution function are given. They show that Wigner's surmise is at any rate a good approximation to the spacing distribution.

3. The Normalisation Constant

We give below a calculation of the normalisation constant, as the general method developed here will be frequently used later. Consider in a general way the integral

$$\rho(k, n, r, L, U) = \int_{R(L, \theta_1, \theta_2, \ldots, \theta_n, U)} e^{-(\theta_1^k + \cdots + \theta_n^k)} (\theta_1 \ldots \theta_n)^r \prod_{1 \le j < i \le n} (\theta_i - \theta_j) \prod_1^n d\theta_i, \tag{6}$$

where the region of integration R is $L \leqq \theta_1 \leqq \theta_2 \leqq \ldots \leqq \theta_n \leqq U$, k and n are positive integers and r is positive or zero. The method becomes much simpler when k is even and $L = -U$. The complication increases of course if r is non-integral and when the value of k increases.

The most important difficulty in the evaluation of (6) is that the integrand is antisymmetric. However, if the integrations over, say, θ_1, θ_3, θ_5, ..., i.e. variables with odd indices, are carried out, the remaining integrand becomes a symmetric function of the variables θ_2, θ_4, ... It will be convenient to write the integrand in the form of a determinant:

$$\rho(k, n, r, L, U) = \int_R e^{-(\theta_1^k + \cdots + \theta_n^k)} \begin{vmatrix} \theta_1^r & \ldots & \theta_n^r \\ \theta_n^{r+1} & \ldots & \theta_n^{r+1} \\ \ldots\ldots\ldots\ldots & & \\ \theta_1^{r+n-1} & \ldots & \theta_n^{r-n-1} \end{vmatrix} d\theta_1 \ldots d\theta_n. \tag{7}$$

Integration over θ_1 replaces the first column in the determinant by the column $\{F_r(\theta_2),\ F_{r+1}(\theta_2), \ldots, F_{r+n-1}(\theta_2)\}$, where the functions $F_s(\theta)$ are defined by

$$F_s(\theta) = \int_L^\theta e^{-x^2} x^s \, dx. \tag{8}$$

Now integration over θ_3 replaces the third column by the column $\{F_r(\theta_4)-F_r(\theta_2), \ldots, F_{r+n-1}(\theta_4)-F_{r+n-1}(\theta_2)\}$, but as we already have a column of $F_s(\theta_2)$ functions, we may drop the terms with a negative sign. Thus at each integration over $\theta_3, \theta_5, \ldots$ the corresponding columns are replaced by columns of single F_s functions. In the case of odd n, the last column is replaced by pure numbers $F_s(U)$. Thus we have

$$\rho(k, n, r, L, U) = \int_{R(L, \theta_2, \theta_4, \ldots, U)} e^{-(\theta_2^2+\theta_4^2+\cdots)} \cdot \begin{vmatrix} F_r(\theta_2) & \theta_2^r & F_r(\theta_4) & \theta_4^r & \ldots \\ F_{r+1}(\theta_2) & \theta_2^{r+1} & F_{r+1}(\theta_4) & \theta_4^{r+1} & \ldots \\ \ldots\ldots\ldots\ldots\ldots\ldots\ldots\ldots\ldots\ldots \\ F_{r+n-1}(\theta_2) & \theta_2^{r+n-1} & F_{r+n-1}(\theta_4) & \theta_4^{r+n-1} & \ldots \end{vmatrix} d\theta_2 d\theta_4 \ldots . \tag{9}$$

As the integrand in eq. (9) is now symmetric † in the remaining variables, we can integrate separately and independently over them on the whole interval (L, U) and divide by $[\frac{1}{2}n]!$, where $[\frac{1}{2}n]$ is the largest integer less than or equal to $\frac{1}{2}n$.

For convenience we take n even, $n = 2m$. (The case of odd n requires only slight additional care, the final results are however unchanged). The symmetry of the integrand and the independence of the variables in (9) allow us to express it as a pfaffian. It can be directly verified that

$$\rho(k, 2m, r, L, U) = \begin{vmatrix} 0 & f_r^{r+1} & f_r^{r+2} & \ldots & f_r^{r+2m-1} \\ f_{r+1}^r & 0 & f_{r+1}^{r+2} & \ldots & f_{r+1}^{r+2m-1} \\ \ldots\ldots\ldots\ldots\ldots\ldots\ldots\ldots \\ f_{r+2m-1}^r & f_{r+2m-1}^{r+1} & f_{r+2m-1}^{r+2} & \ldots & 0 \end{vmatrix}^{\frac{1}{2}}, \tag{10}$$

where the numbers f_s^t are given by

$$f_s^t = F_s^t - F_t^s, \tag{11}$$

with

$$F_s^t = \int_L^U F_s(\theta)\theta^t e^{-\theta^2} d\theta = \int_{L \le x \le \theta \le U} e^{-\theta^2 - x^2} x^s \theta^t \, dx \, d\theta. \tag{12}$$

Equation (10) is a general result. If k is even and $L = -U$, there are further

† The author wishes to express his gratitude to Mr. M. Gaudin for pointing out this symmetrization and therefore the possibility of dropping the ordering of $\theta_2, \theta_4, \ldots$.

simplifications, as we have then

$$F_s^t = (-)^{s+t} F_t^s, \tag{13}$$

giving $f_s^t = 0$ or $2F_s^t$ according as $s+t$ is even or odd. The quantity ρ is expressible in the form of a determinant (as shown in appendix I),

$$\rho(k, 2m, r, -U, U) = 2^m \begin{vmatrix} F_r^{r+1} & F_r^{r+3} & \dots & F_r^{r+2m-1} \\ F_{r+2}^{r+1} & F_{r+2}^{r+3} & \dots & F_{r+2}^{r+2m-1} \\ \dots & \dots & \dots & \dots \\ F_{r+2m-2}^{r+1} & F_{r+2m-2}^{r+3} & \dots & F_{r+2m-2}^{r+2m-1} \end{vmatrix}. \tag{14}$$

In the particular case of $k = 2$, $U = \infty = -L$, we have

$$F_i^j = 2^{-\frac{1}{2}(i+1)-\frac{1}{2}(j+1)} \Gamma\left(\frac{i+1}{2}\right) \Gamma\left(\frac{j+1}{2}\right) D_i^j, \tag{15}$$

where

$$D_i^j = \Gamma\left(\frac{i+j+2}{2}\right)^{\frac{1}{2}(j+1)} \sum_{g=1} \left\{\Gamma\left(\frac{i+1}{2} + g\right) \Gamma\left(\frac{j+3}{2} - g\right)\right\}^{-1}, \tag{16}$$

for i even and j odd. In the opposite case of i odd and j even, we can use the relation

$$D_i^j = -D_j^i, \tag{17}$$

and we do not need the value of D_i^j when both i and j are even. The numbers D_s^t have the property

$$\begin{aligned} &D_{2i}^{2j+1} = D_{2i-2}^{2j+1} + D_{2i}^{2j-1} && (i, j > 0), \\ &D_{2i}^1 = 1, && i \geqq 0. \end{aligned} \tag{18}$$

Taking $r = 0$, we have from eq. (14) and (15)

$$\int_{-\infty}^{\infty} \dots \int_{-\infty}^{\infty} e^{-(\theta_1^2 + \dots + \theta_{2m}^2)} \prod_{i<j} |(\theta_i - \theta_j)| d\theta_1 \dots d\theta_{2m}$$

$$= (2m)! \rho(2, 2m, 0, -\infty, \infty) = (2m)! 2^m \prod_{g=1}^{2m} \left\{2^{-\frac{1}{2}g} \Gamma\left(\frac{g}{2}\right)\right\} D', \tag{19}$$

where D' is the determinant

$$D' = \begin{vmatrix} D_0^1 & D_0^3 & \dots & D_0^{2m-1} \\ D_2^1 & D_2^3 & \dots & D_2^{2m-1} \\ \dots & \dots & \dots & \dots \\ D_{2m-2}^1 & D_{2m-2}^3 & \dots & D_{2m-2}^{2m-1} \end{vmatrix} = 1. \tag{20}$$

The last equality can be proved by using the relations (18) again and again to reduce D' to the triangular form having units in the principal diagonal and zeros below it.

4. The Level-Density near the Origin

As $P(\theta_1)$ is even in θ_1, it is perhaps interesting to know its maximum value $P(0)$ at $\theta_1 = 0$. The following calculation of this quantity is very similar to that of the normalization constant given in the preceding section. We have, by definition,

$$\begin{aligned}\frac{\mu_0}{(n-1)!}P(0) &= \frac{\mu_0}{(n-1)!}P(\theta_1)\Big|_{\theta_1=0} \\ &= \int_{R(0,\theta_2,\theta_3,\ldots,\theta_n,\infty)} e^{-(\theta_1^2+\ldots+\theta_n^2)} \prod_{i<j}|(\theta_i-\theta_j)|\Big|_{\theta_1=0} d\theta_2 d\theta_3 \ldots d\theta_n \\ &+ \int_{R(-\infty,\theta_1,0,\theta_3,\ldots,\theta_n,\infty)} e^{-(\theta_1^2+\ldots+\theta_n^2)} \prod_{i<j}|(\theta_i-\theta_j)|\Big|_{\theta_2=0} d\theta_1 d\theta_3 \ldots d\theta_n \\ &+ \ldots + \ldots = \mathcal{O}+\mathcal{E},\end{aligned} \tag{21}$$

where $\mathcal{O}$ includes all the integrals in which a θ with an odd index is put equal to zero, and $\mathcal{E}$ includes the other terms. If we take, for simplicity, n even, $n = 2m$, it can be seen that $\mathcal{O}$ is equal to

$$\mathcal{O} = \int_{R(-\infty,\theta_2,\theta_4,\ldots,\theta_{2m},\infty)} e^{-(\theta_1^2+\theta_3^2+\ldots+\theta_{2m}^2)} \cdot \begin{vmatrix} \varepsilon(\theta_2) & 0 & \ldots & \varepsilon(\theta_{2m}) & 0 \\ F_1(\theta_2) & \theta_2 & \ldots & F_1(\theta_{2m}) & \theta_{2m} \\ F_2(\theta_2) & \theta_2^2 & \ldots & F_2(\theta_{2m}) & \theta_{2m}^2 \\ \ldots\ldots & \ldots & \ldots & \ldots & \ldots \\ F_{2m-1}(\theta_2) & \theta_2^{2m-1} & \ldots & F_{2m-1}(\theta_{2m}) & \theta_{2m}^{2m-1} \end{vmatrix} d\theta_2 d\theta_4 \ldots d\theta_{2m}, \tag{22}$$

where $\varepsilon(\theta)$ is the Heaviside step-function

$$\varepsilon(\theta) = \begin{cases} 1 & \text{for } \theta > 0, \\ 0 & \text{for } \theta < 0. \end{cases}$$

For $\mathcal{E}$ we may integrate over $\theta_2, \theta_4, \ldots, \theta_{2m}$ in a similar way by introducing the functions

$$\phi_s(\theta) = \int_\theta^\infty e^{-x^2} x^s dx, \tag{23}$$

and by an easy transformation it may be seen that $\mathcal{O}$ and $\mathcal{E}$ are equal.

As the integrand in equation (22) is symmetric in $\theta_2, \theta_4, \ldots, \theta_{2m}$ we can integrate over these variables separately and independently over the whole range and divide by $m!$. The result can be written as a determinant (the proof, similar to that given for eq. (14), is omitted)

$$\mathcal{O} = 2^{m-1} \begin{vmatrix} \phi_1(0) & \phi_3(0) & \ldots & \phi_{2m-1}(0) \\ F_2^1 & F_2^3 & \ldots & F_2^{2m-1} \\ F_4^1 & F_4^3 & \ldots & F_4^{2m-1} \\ \ldots\ldots & \ldots & \ldots & \ldots \\ F_{2m-2}^1 & F_{2m-2}^3 & \ldots & F_{2m-2}^{2m-1} \end{vmatrix}, \tag{24}$$

where

$$\phi_i(0) = \int_{-\infty}^{\infty} e^{-x^2} \varepsilon(x) x^i \, dx = \int_0^{\infty} e^{-x^2} x^i \, dx = \tfrac{1}{2} \Gamma\left(\frac{i+1}{2}\right). \tag{25}$$

We may again factorize all common powers of 2 and gamma-functions. Collecting the results, we get, for $n = 2m$,

$$\frac{\mu_0}{(2m-1)!} P(0) = 2\mathcal{O} = 2^m \prod_{\sigma=2}^{2m} \left\{ 2^{-\frac{1}{2}\sigma} \Gamma\left(\frac{\sigma}{2}\right) \right\} V_m = \frac{\mu_0}{(2m)!} \sqrt{\frac{2}{\pi}} V_m, \tag{26}$$

where V_m is defined by

$$V_m = \begin{vmatrix} 1 & 2 & \dots & 2^{m-1} \\ D_2^1 & D_2^3 & \dots & D_2^{2m-1} \\ D_4^1 & D_4^3 & \dots & D_4^{2m-1} \\ \dots & \dots & \dots & \dots \\ D_{2m-2}^1 & D_{2m-2}^3 & \dots & D_{2m-2}^{2m-1} \end{vmatrix} = \begin{vmatrix} 1 & 1 & 2 & 2^2 & \dots & 2^{m-2} \\ D_0^1 & D_0^3 & D_0^5 & D_0^7 & \dots & D_0^{2m-1} \\ 0 & D_2^1 & D_2^3 & D_2^5 & \dots & D_2^{2m-3} \\ 0 & 0 & D_4^1 & D_4^3 & \dots & D_4^{2m-5} \\ \dots & \dots & \dots & \dots & \dots & \dots \\ 0 & 0 & 0 & 0 & \dots & D_{2m-4}^3 \end{vmatrix}. \tag{27}$$

Expanding the last determinant with respect to the last row and the last column in the Cauchy manner, we get the following recurrence relation for V_m:

$$V_m = D_{2m-4}^3 V_{m-1} - D_{2m-6}^5 V_{m-2} + \dots + (-)^{m-1} D_2^{2m-3} V_2 + (-)^m D_0^{2m-1} V_1 + (-)^{m+1} 2^{m-2}, \tag{28}$$

$$V_1 = 1. \tag{28'}$$

It is verified in appendix II that the solution of (28) is given by

$$V_m = \frac{\Gamma(m+\frac{1}{2})}{\Gamma(\frac{3}{2})\Gamma(m)}. \tag{29}$$

Finally we get for $n = 2m$.

$$P(0) = \frac{1}{2m} \sqrt{\frac{2}{\pi}} V_m = \sqrt{\frac{2}{\pi}} \frac{(2m-1)!!}{2^m m!}. \tag{30}$$

Thus, as $n \to \infty$, $P(0) \to 2/\pi\sqrt{n}$ and this is the probability that a particular level is at the origin. To get the probability that any one of the levels is at the origin, this must be multiplied by n. Thus the mean spacing at the origin D is given by

$$D^{-1} = \text{level-density} \sim \frac{2\sqrt{n}}{\pi} \quad \text{for large } n. \tag{31}$$

5. The Function $P(\theta_1, \theta_2)$

Though the result for general values of θ_1, θ_2 may be expressed in terms of certain pfaffians, we will take from the beginning $\theta_1 = -\theta_2$. It is reasonable to assume that as long as θ_1 and θ_2 are near the centre of the interval ($\theta_1, \theta_2 \lesssim 1$), $P(\theta_1, \theta_2)$ is a function of the difference $\theta_1 - \theta_2$ only. The calculation of this function is then considerably simplified when $\theta_2 = -\theta_1 = \theta$.

By definition we have

$$P(-\theta, \theta) = \frac{1}{\mu_0}(n-2)! \int e^{-2\theta^2} e^{-(\theta_1^2 + \ldots + \theta_{n-2}^2)} \begin{vmatrix} 1 & 1 & 1 & \ldots & 1 \\ -\theta & \theta & \theta_1 & \ldots & \theta_{n-2} \\ \theta^2 & \theta^2 & \theta_1^2 & \ldots & \theta_{n-2}^2 \\ -\theta^3 & \theta^3 & \theta_1^3 & \ldots & \theta_{n-2}^3 \\ \ldots & \ldots & \ldots & \ldots & \ldots \\ \ldots & \ldots & \ldots & \ldots & \ldots \end{vmatrix} d\theta_1 \ldots d\theta_{n-2}, \tag{32}$$

where the region of integration for $\theta_1, \theta_2, \ldots, \theta_{n-2}$ is $-\infty \leqq \theta_1 \leqq \theta_2 \leqq \ldots \leqq \theta_{n-2} \leqq \infty$ with no θ_i in the interval $(-\theta, \theta)$. Subtracting the first column from the second and taking the common factor 2θ out, we see that

$$P(-\theta, \theta) = \frac{1}{\mu_0}(n-2)!\, 2\theta e^{-2\theta^2} R(\theta), \tag{33}$$

where for $n = 2m$, $R(\theta)$ is

$$R(\theta) = \int e^{-(\theta_1^2 + \ldots + \theta_{2m-2}^2)} \begin{vmatrix} 1 & 0 & 1 & \ldots & 1 \\ 0 & 1 & \theta_1 & \ldots & \theta_{2m-2} \\ \theta^2 & 0 & \theta_1^2 & \ldots & \theta_{2m-2}^2 \\ 0 & \theta^2 & \theta_1^3 & \ldots & \theta_{2m-2}^3 \\ \ldots & \ldots & \ldots & \ldots & \ldots \\ 0 & \theta^{2m-2} & \theta_1^{2m-1} & \ldots & \theta_{2m-2}^{2m-1} \end{vmatrix} d\theta_1 \ldots d\theta_{2m-2} \tag{34}$$

with the same region of integration.

By integration over half the variables, we get

$$R(\theta) = \int e^{-(\theta_2^2 + \theta_4^2 + \ldots + \theta_{2m-2}^2)} \cdot \begin{vmatrix} 1 & 0 & 0 & \varepsilon(\theta_2) & 0 & \ldots & \varepsilon(\theta_{2m-2}) & 0 \\ \rho_0 & 1 & 0 & F_0(\theta_2) & 1 & \ldots & F_0(\theta_{2m-2}) & 1 \\ 0 & 0 & 1 & F_1(\theta_2) & \theta_2 & \ldots & F_1(\theta_{2m-2}) & \theta_{2m-2} \\ \rho_2 & \theta^2 & 0 & F_2(\theta_2) & \theta_2^2 & \ldots & F_2(\theta_{2m-2}) & \theta_{2m-2}^2 \\ \ldots & \ldots & \ldots & \ldots & \ldots & \ldots & \ldots & \ldots \\ 0 & 0 & \theta^{2m-2} & F_{2m-1}(\theta_2) & \theta_2^{2m-1} & \ldots & F_{2m-1}(\theta_{2m-2}) & \theta_{2m-2}^{2m-1} \end{vmatrix} d\theta_2\, d\theta_4 \ldots d\theta_{2m-2}, \tag{35}$$

where in addition to the functions F_i and ε, we have also introduced the func-

tions

$$\rho_{2i} = \rho_{2i}(\theta) = \int_{-\theta}^{\theta} e^{-x^2} x^{2i}\, dx. \tag{36}$$

The integrand in equation (35) being now symmetric, we can integrate separately and independently over all the variables from $-\infty$ to $-\theta$ and θ to ∞, dividing the result by $(m-1)!$. We introduce the functions

$$B_i^j = B_i^j(\theta) = A_i^j(\theta) - A_j^i(\theta), \tag{37}$$

with

$$A_i^j(\theta) = \left\{\int_{-\infty}^{-\theta} + \int_{\theta}^{\infty}\right\} e^{-x^2} F_i(x) x^j\, dx. \tag{38}$$

It is a great convenience to have

$$A_j^i(\theta) = 0 \quad \text{for} \quad i \quad \text{odd}, \quad j \quad \text{odd}, \tag{39}$$

which permits to express the result as a determinant. This simplification does not occur if θ_1 and θ_2 are not chosen symmetrical with respect to the centre of the interval.

It is clear that no A_i^j with i and j both even can come into the calculation as it would be multiplied by some A_i^j with i and j both odd. It is easy to verify directly, by expanding with respect to the column 1, ρ_0, ρ_2, . . ., for example, that

$$R(\theta) = -\begin{vmatrix} 0 & 0 & 1 & \theta^2 & \theta^4 & \dots & \theta^{2m-2} \\ 0 & 1 & \phi_1 & \phi_3 & \phi_5 & \dots & \phi_{2m-1} \\ 1 & \rho_0 & B_0^1 & B_0^3 & B_0^5 & \dots & B_0^{2m-1} \\ \theta^2 & \rho_2 & B_2^1 & B_2^3 & B_2^5 & \dots & B_2^{2m-1} \\ \dots & \dots & \dots & \dots & \dots & \dots & \dots \\ \theta^{2m-2} & \rho_{2m-2} & B_{2m-2}^1 & B_{2m-2}^3 & B_{2m-2}^5 & \dots & B_{2m-2}^{2m-1} \end{vmatrix}. \tag{40}$$

The following recurrence relations are easily established

$$\begin{aligned} \phi_{2j+1} - j\phi_{2j-1} &= \tfrac{1}{2}\theta^{2j} e^{-\theta^2}, \\ A_{2i}^{2j+1} - jA_{2i}^{2j-1} &= \tfrac{1}{2}\theta^{2j} e^{-\theta^2}\rho_{2i} + \tfrac{1}{2}\xi_{2(i+j)}, \\ A_{2j+1}^{2i} - jA_{2j-1}^{2i} &= -\tfrac{1}{2}\xi_{2(i+j)}. \end{aligned} \tag{41}$$

Therefore,

$$B_{2i}^{2j+1} - jB_{2i}^{2j-1} = \tfrac{1}{2}\theta^{2j} e^{-\theta^2}\rho_{2i} + \xi_{2(i+j)}, \tag{42}$$

where the functions ξ are defined by

$$\xi_{2i} = \xi_{2i}(\theta) = 2\int_{\theta}^{\infty} e^{-2y^2} y^{2i}\, dy. \tag{43}$$

Using these relations it is elementary to reduce the determinant (40) to

$$R(\theta) = -\{R_1(\theta) - R_2(\theta)\}, \tag{44}$$

where

$$R_1(\theta) = \begin{vmatrix} 0 & 1 & \theta^2 & \dots & \theta^{2m-2} \\ 1 & \xi_0 & \xi_2 & \dots & \xi_{2m-2} \\ \theta^2 & \xi_2 & \xi_4 & \dots & \xi_{2m} \\ \dots & \dots & \dots & \dots & \dots \\ \theta^{2m-2} & \xi_{2m-2} & \xi_{2m} & \dots & \xi_{4m-4} \end{vmatrix}. \tag{45}$$

and

$$R_2(\theta) = \begin{vmatrix} 0 & 0 & 1 & 2\theta^2 & \dots & (m-1)\theta^{2m-4} \\ 1 & \xi_0 & \xi_2 & \xi_4 & \dots & \xi_{2m-2} \\ \theta^2 & \xi_2 & \xi_4 & \xi_6 & \dots & \xi_{2m} \\ \dots & \dots & \dots & \dots & \dots & \dots \\ \theta^{2m-2} & \xi_{2m-2} & \xi_{2m} & \xi_{2m+2} & \dots & \xi_{4m-4} \end{vmatrix} \tag{46}$$

$$= \frac{1}{4\theta} R_1'(\theta) = \frac{1}{4\theta} \frac{\mathrm{d}}{\mathrm{d}\theta} R_1(\theta). \tag{47}$$

Equations (33), (44) and (47) allow us to write $P(-\theta, \theta)$ in the form

$$P(-\theta, \theta) = \frac{(2m-2)!}{2\mu_0} \frac{\mathrm{d}}{\mathrm{d}\theta} \{\mathrm{e}^{-2\theta^2} R_1(\theta)\}. \tag{48}$$

This is the probability that a particular level is at $-\theta$ and another particular level is at $+\theta$. Hence the probability that any one level lies at $-\theta$ and any other at $+\theta$ is

$$2m(2m-1)P(-\theta, \theta) = \frac{(2m)!}{2\mu_0} \frac{\mathrm{d}}{\mathrm{d}\theta} \{\mathrm{e}^{-2\theta^2} R_1(\theta)\}. \tag{49}$$

It is shown in appendix III that $R_1(\theta)$ as given by eq. (45) can be expressed † as an integral over $(m-1)$ variables of the square of a certain Vandermonde determinant weighted with the exponential factors, i.e. that

$$R_1(\theta) = -\frac{2^{m-1}}{(m-1)!} \int_\theta^\infty \dots \int_\theta^\infty \mathrm{d}y_1 \dots \mathrm{d}y_{m-1} \mathrm{e}^{-2(y_1^2 + \dots + y_{m-1}^2)} \cdot \prod_i (y_i^2 - \theta^2)^2 \prod_{i<j} (y_i^2 - y_j^2)^2. \tag{50}$$

Introducing new variables x_i by

$$y_i^2 = x_i^2 + \theta^2,$$

we may write

$$R_1(\theta) = -I(\theta) \mathrm{e}^{-2(m-1)\theta^2}, \tag{51}$$

† The author is thankful to Dr. C. Bloch for pointing out this possibility as well as Gram's result on determinants.

where

$$I(\theta) = \frac{2^{m-1}}{(m-1)!}\int_0^\infty \dots \int_0^\infty \mathrm{d}x_1 \dots \mathrm{d}x_{m-1} \mathrm{e}^{-2(x_1^2+\dots+x_{m-1}^2)} \cdot \prod_{i<j}(x_i^2-x_j^2)^2 \prod_i \frac{x_i^5}{\sqrt{x_i^2+\theta^2}}. \quad (52)$$

Appendix IV gives a transformation of $I(\theta)$ back to a determinantal form

$$I(\theta) = \begin{vmatrix} \eta_0 & \eta_1 & \dots \eta_{m-2} \\ \eta_1 & \eta_2 & \dots \eta_{m-1} \\ \dots & \dots & \dots \\ \eta_{m-2} & \eta_{m-1} & \dots \eta_{2m-4} \end{vmatrix}, \quad (53)$$

where

$$\eta_i = \eta_i(\theta) = 2\int_0^\infty \mathrm{e}^{-2x^2} x^{2i} \frac{x^5}{\sqrt{x^2+\theta^2}}\,\mathrm{d}x. \quad (54)$$

Equations (49) and (51) give

$$2m(2m-1)P(-\theta,\theta) = -\frac{(2m)!}{2\mu_0}\frac{\mathrm{d}}{\mathrm{d}\theta}\{\mathrm{e}^{-2m\theta^2} I(\theta)\}. \quad (55)$$

The determinantal form (53) is convenient for calculations, while the integral form (52) is convenient to find bounds for $I(\theta)$.

We may expand $I(\theta)$ in powers of θ and calculate its first terms from its form in eq. (53) by replacing the η_i by their power series. Appendix V contains this calculation. Up to terms in θ^2, we get

$$I(\theta) \approx I(0)\{1-\tfrac{2}{3}m\theta^2\}, \quad (56)$$

with

$$I(0) = \frac{\mu_0}{(2m)!}\sqrt{\frac{2}{\pi}}\frac{\Gamma(m+\frac{1}{2})}{\Gamma(\frac{3}{2})\Gamma(m)} = \frac{\mu_0}{(2m)!}\frac{1}{D}, \quad (56')$$

where D is the mean level spacing at the centre given by (31).

The function $I(\theta)$ is directly related to the *distribution function* $F(S)$ *of the level spacing* $S = 2\theta$ by

$$F(S) = \frac{2m(2m-1)}{D^{-1}}\int_0^S P(-\tfrac{1}{2}S', \tfrac{1}{2}S')\mathrm{d}S' = 1-\frac{I(\frac{1}{2}S)}{I(0)}\mathrm{e}^{-\left(\frac{\pi S}{4D}\right)^2}. \quad (57)$$

It is easy to prove (see appendix VI) that for all x_i positive

$$1-\sum_{i=1}^n \frac{\theta^2}{2x_i^2} \leqq \prod_{i=1}^n \frac{x_i}{\sqrt{x_i^2+\theta^2}} \leqq 1. \quad (58)$$

The expression (52) gives then the inequalities

$$1-\tfrac{2}{3}m\theta^2 \leqq \frac{I(\theta)}{I(0)} \leqq 1. \quad (59)$$

It follows then from (57) that we can give *rigorous upper and lower bounds* for the function $F(S)$:

$$F_0(S) \leqq F(S) \leqq F_1(S), \tag{60}$$

where

$$\begin{aligned} F_0(S) &= 1-e^{-\left(\frac{\pi S}{4D}\right)^2}, \\ F_1(S) &= 1-e^{-\left(\frac{\pi S}{4D}\right)^2}\left\{1-\tfrac{1}{3}\left(\frac{\pi S}{4D}\right)^2\right\}. \end{aligned} \tag{61}$$

If in the limit $m \to \infty$, the function $P(\theta_1, \theta_2)$ becomes invariant under translations of an amplitude equal to a large number of mean level spacings, we must have

$$\int_0^\infty S\frac{dF}{dS}dS = \int_0^\infty \{1-F(S)\}dS = D, \tag{62}$$

where D is the mean level spacing at the origin. As this relation is *exactly satisfied by the exact function* $F(S)$ (see appendix VIII), we have some reason to believe that our assumption about $P(\theta_1, \theta_2)$ is correct.

As the differences F_1-F and $F-F_0$ are everywhere positive, the differences between D and the approximate values D_0 and D_1 obtained by substituting F_0 and F_1 into (62) give a good estimation of the accuracy of the corresponding approximations to F. One obtains

$$\frac{D_0}{D}-1 = \frac{2}{\sqrt{\pi}}-1 \approx 0.13, \qquad 1-\frac{D_1}{D} = 1-\frac{5}{3\sqrt{\pi}} \approx 0.055.$$

The functions can be compared with Wigner's guess

$$F_W(S) = 1-e^{-\frac{\pi}{4}\frac{S^2}{D^2}}, \tag{63}$$

in which the parameter is adjusted from the relation (62). Figure 1 gives the plots of the functions F_W, F_0 and F_1, showing that F_W is certainly a good approximation. However, it cannot be exact, even in the limit $m \to \infty$, as will be seen (in section 7) by comparing its derivatives with the limits of the exact values.

This is perhaps the utmost information one may get about $I(\theta)$ by expanding it in powers of θ. For if we take the next higher powers

$$\frac{I(\theta)}{I(0)} = 1-\tfrac{1}{3}(2m\theta^2)+\tfrac{7}{30}(2m\theta^2)^2-\frac{512}{675\pi}(2m\theta^2)^{\frac{5}{2}}+\tfrac{101}{630}(2m\theta^2)^3+\ldots,$$

the value for the mean spacing becomes alternately larger and smaller than the true value. And the convergence of this series, if it is at all convergent, seems

to be very slow. For these reasons, to get a better result, one must search for some other method of approximation.

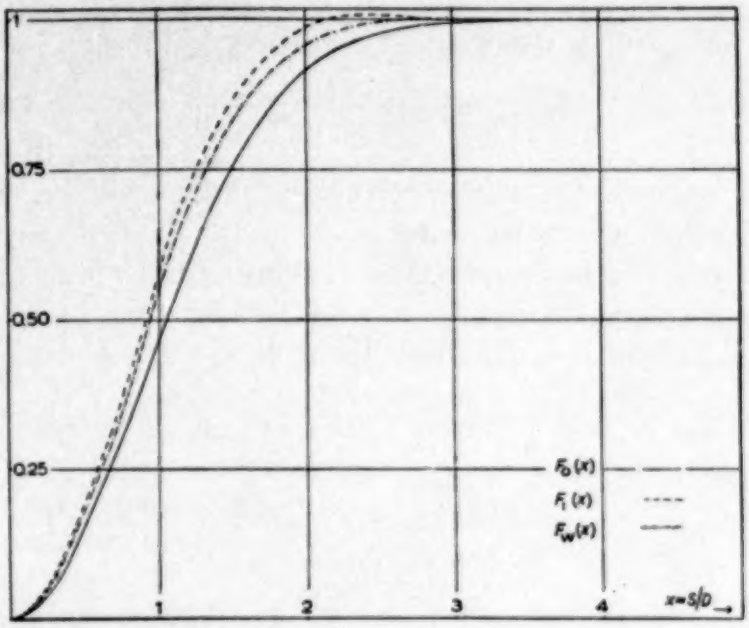

Fig. 1. The functions $F_0(x)$, $F_1(x)$ and $F_W(x)$ as given by equations (61) and (63).

6. Moments of $P(\theta_1)$

In this section, a method for calculating moments of $P(\theta_1)$ to arbitrary orders is given with some examples. The limits of these exact results for $n \to \infty$ are compared with Wigner's "semi-circle law".

6.1. ABOUT SOME GENERAL MOMENTS

It is remarkable that we may get information about certain moments without knowing the normalisation constant and without actually calculating any integral. More precisely, we can evaluate very directly quantities of the form

$$\overline{(\theta_1+\ldots+\theta_n)^{2r}(\theta_1^2+\ldots+\theta_n^2)^s}$$
$$=\int_{-\infty}^{\infty}\ldots\int_{-\infty}^{\infty}(\theta_1+\ldots+\theta_n)^{2r}(\theta_1^2+\ldots\theta_n^2)^s P(\theta_1,\ldots,\theta_n)\mathrm{d}\theta_1\ldots\mathrm{d}\theta_n, \quad (64)$$

where r and s are arbitrary positive integers or zero. For let

$$\mu_0 = n!\rho(2, n, 0, -\infty, \infty) = \int_{-\infty}^{\infty}\ldots\int_{-\infty}^{\infty} \mathrm{e}^{-(\theta_1^2+\ldots+\theta_n^2)} \prod_{i<j} |(\theta_i-\theta_j)|\mathrm{d}\theta_1\ldots\mathrm{d}\theta_n;$$

then

$$\int_{-\infty}^{\infty}\ldots\int_{-\infty}^{\infty} \mathrm{e}^{-\alpha(\theta_1^2+\ldots+\theta_n^2)-\beta(\theta_1+\ldots+\theta_n)} \prod_{i<j} |(\theta_i-\theta_j)|\mathrm{d}\theta_1\ldots\mathrm{d}\theta_n = \mu_0 \mathrm{e}^{\frac{n\beta^2}{4\alpha}} \alpha^{-\frac{n(n+1)}{4}},$$

and by differentiating this equality a sufficient number of times with respect to x and β and putting finally $\alpha = 1$, $\beta = 0$, we get the required quantity (64). Thus, in particular, we get

$$\overline{\theta_1^2} = \tfrac{1}{4}(n+1), \quad \overline{\theta_1\theta_2} = -\tfrac{1}{4}.$$

6.2. THE MOMENTS OF $P(\theta_1)$ TO ARBITRARY ORDERS

To get higher moments of $P(\theta_1)$, say $\overline{\theta_1^4}$, $\overline{\theta_1^6}$, one must resort to the method of he preceding sections. Applying it to the evaluation of $\overline{\theta_1^{2s}}$ one sees that the umber of determinants to be evaluated is the smallest of the two numbers s or $2m$. All have the same form as in eq. (14); half of them being easy to express y general formulae; while for the other half, we have not been able to give a eneral compact form. By definition we have

$$\overline{\theta_1^{2s}} = \int_{-\infty}^{\infty} \theta_1^{2s} P(\theta_1)\,d\theta_1 = \int_{-\infty}^{\infty} \cdots \int_{-\infty}^{\infty} \theta_1^{2s} P(\theta_1, \ldots, \theta_n) d\theta_1 \ldots d\theta_n$$

$$= \frac{1}{n}\int_{-\infty}^{\infty} \cdots \int_{-\infty}^{\infty} (\theta_1^{2s} + \ldots + \theta_n^{2s}) P(\theta_1, \ldots, \theta_n) d\theta_1 \ldots d\theta_n$$

$$= \frac{n!}{n\mu_0} \int_{R(-\infty, \theta_1, \ldots, \theta_n, \infty)} e^{-(\theta_1^2 + \ldots + \theta_n^2)} (\theta_1^{2s} + \ldots + \theta_n^{2s}) \prod_{n \geq i > j \geq 1} (\theta_i - \theta_j) d\theta_1 \ldots d\theta_n.$$

hen, proceeding exactly as in section 4 we get, for $n = 2m$,

$$\overline{\theta_1^{2s}} = \frac{(2m)!}{2m\mu_0} 2^m \{f_1(s) + \ldots + f_m(s)\},$$

here the determinants $f_i(s)$ may be expressed as the sum

$$f_i(s) = f_{i1}(s) + f_{i2}(s),$$

th $f_{i1}(s)$ equal to the determinant in eq. (14) for $r = 0$ except for the fact at the i^{th} row is replaced by the row $F^1_{2(i-1)+2s}, F^3_{2(i-1)+2s}, \ldots, F^{2m-1}_{2(i-1)+2s}$; d similarly $f_{i2}(s)$ is the same determinant except that the i^{th} column is re- ced by the column $\{F_0^{2i-1+2s}, F_2^{2i-1+2s}, \ldots, F_{2m-2}^{2i-1+2s}\}$.

To evaluate these, one must calculate the determinants $d_{i1}(s)$ and $d_{i2}(s)$ tained on replacing F_i^j by D_i^j in $f_{i1}(s)$ and $f_{i2}(s)$ respectively. If $s < m$, y $2s$ of them are different from zero, it is easy to set up a recurrence relation for $d_{i1}(s)$ and therefore possible to express them by closed general formulae. example, we have

$$d_{m1}(s) = \frac{\Gamma(m+s)}{\Gamma(m)\Gamma(s+1)}, \qquad s \geq 0;$$

le $d_{i2}(s)$ may be reduced to orders less than or equal to s.

his method yields for the first three non-vanishing moments of $P(\theta_1)$:

$$= \tfrac{1}{4}(n+1), \quad \overline{\theta_1^4} = \tfrac{1}{8}(n^2 + \tfrac{5}{2}n + \tfrac{5}{2}), \quad \overline{\theta_1^6} = \tfrac{1}{16}\tfrac{1}{4}(5n^3 + 22n^2 + 52n + 41). \qquad (65)$$

The limits of these for $n \to \infty$ check exactly with those given by the semi-circle law (4).

7. The Derivatives of $P(\theta_1, \theta_2)$ for $\theta_1 = 0$ and $\theta_2 = 0$

The function $P(\theta_1, \theta_2)$ is symmetric in θ_1, θ_2. As this symmetry is forced by the positive character of the integrand in the definition of $P(\theta_1, \theta_2)$, it is more convenient to consider the function

$$Q_0(\theta) = \{P(0, \theta) \times (\text{sign } \theta)\}$$

$$= \frac{(n-2)!}{\mu_0} \int e^{-(\theta_3^2 + \theta_4^2 + \ldots + \theta_n^2)} \begin{vmatrix} \theta & \theta_3 & \ldots \theta_n \\ \theta^2 & \theta_3^2 & \ldots \theta_n^2 \\ \ldots\ldots\ldots\ldots\ldots \\ \theta^{n-1} & \theta_3^{n-1} & \ldots \theta_n^{n-1} \end{vmatrix} d\theta_3 \ldots d\theta_n; \qquad (66)$$

the domain of integration over $\theta_3, \ldots, \theta_n$ being $-\infty \leqq \theta_3 \leqq \ldots \leqq \theta_n \leqq \infty$ with none of them in the interval $(0, \theta)$.

By changing the signs of the variables and by a partial inversion of the order of the columns it can be shown that $Q_0(\theta)$ is an odd function of θ:

$$Q_0(-\theta) = -Q_0(\theta). \qquad (67)$$

To study the function near $\theta = 0$, we calculate its derivatives at this point. As $Q_0(\theta)$ is odd, it follows immediately that any derivative of an even order vanishes at $\theta = 0$.

For the first two odd derivatives we find (see appendix VII) that for large $n \approx 2m$

$$Q_0'(0) = \left.\frac{dQ_0(\theta)}{d\theta}\right|_{\theta=0} = \sqrt{\frac{2}{\pi}} \frac{(2m-1)!!}{2^m m!} \frac{2}{3} \xrightarrow{m\to\infty} \frac{1}{(2m)^2} \frac{\pi^2}{6D^3}, \qquad (68)$$

$$Q_0'''(0) = \sqrt{\frac{2}{\pi}} \frac{(2m-1)!!}{2^m m!} \left(-\frac{16m}{5}\right) \xrightarrow{m\to\infty} \frac{1}{(2m)^2} \left(-\frac{\pi^4}{10D^5}\right). \qquad (69)$$

Apart from finding the mean spacing, as done in section 5, we may test the

TABLE 1

Comparison of the derivatives of several approximations

	Approximation $F_0(S)$	Approximation $F_1(S)$	Wigner's law $F_W(S)$	Approximation with correction term in θ^4	Exact
$\frac{6D^2}{\pi^2}\left(\frac{d^2F}{dS^2}\right)_{S=0}$	$\frac{3}{4} = 0.75$	1	$\frac{3}{\pi} \approx 0.955$	1	1
$-\frac{10D^4}{\pi^4}\left(\frac{d^4F}{dS^4}\right)_{S=0}$	$\frac{15}{32} \approx 0.469$	$\frac{25}{32} \approx 0.781$	$\frac{15}{2\pi^2} \approx 0.76$	1	1

approximations (61), (63) and those at the end of section 5 containing higher powers of θ by comparing their derivatives at $\theta = 0$ with the limits of the exact values given above, eq. (68) and (69). Table 1 shows this comparison.

Dr. C. Bloch, apart from suggesting the problem, guided and encouraged the work throughout. Along with Mr. M. Gaudin, he took great interest in, discussed and went through almost every detail of the calculation. It is a pleasure to express my gratitude towards them. Acknowledgements are also due to the Commissariat à l'Énergie Atomique for the hospitality extended to me at Saclay and for the award of a de Broglie fellowship.

Appendix

I. PROOF OF EQUATION (14)

We see from eq. (9) and the remarks which follow it that in the expansion of the right hand side of eq. (9), only the combinations.

$$f_i^j = F_i^j - F_j^i$$

occur. Moreover eq. (13) shows that every non-vanishing f_i^j which comes into the calculation has indices i, j one of which is odd and the other even. Thus, in $\rho(k, 2m, r, -U, U)$, which is a sum of products of m factors f_i^j, of the form

$$S\begin{pmatrix} r & r+1 & r+2 & r+3 \ldots r+2m-2 & r+2m-1 \\ a & b & c & d \ \ldots \ \ i & j \end{pmatrix} f_a^b f_c^d \cdots f_i^j,$$

$a, b, c, d, \ldots, i, j$ being the indices $r, r+1, \ldots, r+2m-1$ in some order and S the sign of the permutation indicated, we may make the convention that the lower indices are always of the same parity as r. The sum is extended to all permutations. We may always rearrange the factors in the product. Thus we may restrict the lower indices $a, c, \ldots, i$ to be in the order $r, r+2, \ldots, r+2m-2$, sum over all permutations of the upper indices and multiply the result by the number of permutations of the lower indices $m!$:

$$\rho(k, 2m, r, -U, U) = \sum S\begin{pmatrix} r+1 & r+3 \ldots r+2m-1 \\ b & d \ \ldots \ j \end{pmatrix} f_r^b f_{r+2}^d \cdots f_{r+2m-2}^j.$$

where the summation is extended to all permutations of $b, d, \ldots, j$. This is nothing but the determinant

$$\begin{vmatrix} f_r^{r+1} & f_r^{r+3} & \ldots f_r^{r+2m-1} \\ f_{r+2}^{r+1} & f_{r+2}^{r+3} & \ldots f_{r+2}^{r+2m-1} \\ \ldots\ldots\ldots\ldots\ldots\ldots\ldots \\ f_{r+2m-2}^{r+1} & f_{r+2m-2}^{r+3} & \ldots f_{r+2m-2}^{r+2m-1} \end{vmatrix}.$$

As each f is twice the corresponding F, taking the factors 2 out, we get eq. (14).

II. PROOF THAT THE EXPRESSION GIVEN BY EQUATION (29) SATISFIES THE RECURRENCE RELATION (28)

To verify this we need the following results:

$$\sum_{r=0}^{n} {}^nC_r(-)^r \frac{1}{2r+3} = \frac{2^n n!}{(2n+3)!!}, \tag{2.1}$$

$$\sum_{r=0}^{n} {}^nC_r(-)^r \frac{1}{(2r+3)(2r+5)} = \frac{2^n(n+1)!}{(2n+5)!!(1)!}, \tag{2.2}$$

$$\sum_{r=0}^{n} {}^nC_r(-)^r \frac{1}{(2r+3)(2r+5)(2r+7)} = \frac{2^n(n+2)!}{(2n+7)!!2!}, \tag{2.3}$$

etc.

To see that (2.1) is true, let

$$\sum_{0}^{n} {}^nC_r(-)^r \frac{x^{2r+3}}{2r+3} = f(x).$$

Then $f(0) = 0$, and we need $f(1)$. Differentiation of the above equation gives

$$f'(x) = \sum_{0}^{n} {}^nC_r(-)^r x^{2r+2} = x^2(1-x^2)^n.$$

Therefore,

$$f(x) = \int_0^x y^2(1-y^2)^n \, dy,$$

and

$$f(1) = \int_0^1 y^2(1-y^2)^n \, dy = \int_0^{\frac{\pi}{2}} \sin^2\theta \cos^{2n+1}\theta \, d\theta;$$

and this is equal to the right-hand side of eq. (2.1).

Once the relation (2.1) is established, we may proceed to prove successively (2.2), (2.3), etc. For example to derive (2.2), we write (2.1), replacing n by $n+1$,

$$\sum_{0}^{n+1} {}^{n+1}C_r(-)^r \frac{1}{2r+3} = \frac{2^{n+1}(n+1)!}{(2n+5)!!}.$$

Writing then ${}^{n+1}C_r = {}^nC_r + {}^nC_{r-1}$ and replacing $r-1$ by r in the second sum, we get (2.2). The same trick applied to (2.2) gives (2.3), and so on.

Next, we come to the main point of the proof. In the left hand side of the equation

$$D_0^{2m-1}V_1 - D_2^{2m-3}V_2 + \ldots + (-)^{m-2}D_{2m-4}^{3}V_{m-1} + (-)^{m-1}D_{2m-2}^{1}V_m = 2^{m-2},$$

we put

$$V_m = \frac{2m-1}{2}\,\frac{2m-3}{2} \cdots \frac{3}{2}\,\frac{1}{(m-1)!},$$

and replace $D_0^{2m-1}, D_2^{2m-3}, \ldots$ by their values,

$$D_0^{2m-1} = 1+\frac{2m-1}{2}+\frac{2m-1}{2}\frac{2m-3}{2}\frac{1}{2!}+\ldots+\frac{2m-1}{2}\frac{2m-3}{2}\ldots\frac{3}{2}\frac{1}{(m-1)!},$$

$$D_2^{2m-3} = 1+\frac{2m-1}{2}+\frac{2m-1}{2}\frac{2m-3}{2}\frac{1}{2!}+\ldots+\frac{2m-1}{2}\frac{2m-3}{2}\ldots\frac{5}{2}\frac{1}{(m-2)!},$$

etc.

Regrouping the terms in the products according to the negative powers of 2 they contain and using the relations (2.1), (2.2), ... we get

$$1+(m-2)+\frac{(m-2)(m-3)}{2!}+\ldots+1=(1+1)^{m-2},$$

and hence the verification is complete.

III. PROOF OF RELATION (50)

Equation (50) in the determinantal form reads

$$-R_1(\theta)=\frac{2^{m-1}}{(m-1)!}\int_\theta^\infty\ldots\int_\theta^\infty e^{-2(y_1^2+\ldots+y_{m-1}^2)}\begin{vmatrix}1 & 1 & \ldots 1\\ \theta^2 & y_1^2 & \ldots y_{m-1}^2\\ \theta^4 & y_1^4 & \ldots y_{m-1}^4\\ \ldots & \ldots & \ldots\\ \theta^{2m-2} & y_2^{2m-2} & \ldots y_{m-1}^{2m-2}\end{vmatrix}^2 dy_1\ldots dy_{m-1}$$

$$=\frac{2^{m-1}}{(m-1)!}\int_\theta^\infty\ldots\int_\theta^\infty e^{-2(y_1^2+\ldots+y_{m-1}^2)}$$

$$\cdot\begin{vmatrix}1+(m-1) & \theta^2+\sum_1^{m-1}y_i^2 & \ldots\theta^{2m-2}+\sum_1^{m-1}y_i^{2m-2}\\ \theta^2+\sum_1^{m-1}y_i^2 & \theta^4+\sum_1^{m-1}y_i^4 & \ldots\theta^{2m}+\sum_1^{m-1}y_i^{2m}\\ \ldots & \ldots & \ldots\\ \theta^{2m-2}+\sum_1^{m-1}y_i^{2m-2} & \theta^{2m}+\sum_1^{m-1}y_i^{2m} & \ldots\theta^{4m-4}+\sum_1^{m-1}y_i^{4m-4}\end{vmatrix} dy_1\ldots dy_{m-1}$$

$$=a_1+b_1,$$

where a_1 contains in the integrand a determinant having the same columns as in the equation just above except the first column which is replaced by $\{1, \theta^2, \theta^4, \ldots, \theta^{2m-2}\}$; and b_1 contains in the integrand the same determinant except that the first column is replaced by $\{(m-1), \sum_1^{m-1}y_i^2, \sum_1^{m-1}y_i^4, \ldots, \sum_1^{m-1}y_i^{2m-2}\}$.

In a_1 all θ can be eliminated except in the first column. As the integrand is

now symmetric in all y_i, we can replace the sums $\sum_1^{m-1} y_i^{2r}$ by $(m-1)y_1^{2r}$ in one of the columns, say the second. Then y_1 can be eliminated from the rest of the columns leaving the integrand symmetric in $y_2, y_3, \ldots, y_{m-1}$. Again in one of the columns, say the third, we can replace the sums $\sum_2^{m-1} y_i^{2r}$ by $(m-2)y_2^{2r}$ and y_2 can be eliminated from the rest of the columns. And so on, until we get

$$a_1 = 2^{m-1} \int_\theta^\infty \cdots \int_\theta^\infty e^{-2(y_1^2+\cdots+y_{m-1}^2)} \begin{vmatrix} 1 & y_1^2 & \cdots & y_{m-1}^{2m-2} \\ \theta^2 & y_1^4 & \cdots & y_{m-1}^{2m} \\ \theta^4 & y_1^6 & \cdots & y_{m-1}^{2m+2} \\ \cdots & \cdots & \cdots & \cdots \\ \theta^{2m-2} & y_1^{2m} & \cdots & y_{m-1}^{4m-4} \end{vmatrix} dy_1 \cdots dy_{m-1}$$

$$= \begin{vmatrix} 1 & \xi_2 & \cdots & \xi_{2m-2} \\ \theta^2 & \xi_4 & \cdots & \xi_{2m} \\ \theta^4 & \xi_6 & \cdots & \xi_{2m+2} \\ \cdots & \cdots & \cdots & \cdots \\ \theta^{2m-2} & \xi_{2m} & \cdots & \xi_{4m-4} \end{vmatrix}.$$

This quantity is the negative of the coefficient of 1 in the expansion, by the first row, of the determinant in eq. (45).

As to b_1, it can be written as a sum

$$b_1 = a_2 + b_2,$$

where a_2 and b_2 differ from b_1 only for the fact that the second column in the determinants of the integrands are $\{\theta^2, \theta^4, \ldots, \theta^{2m}\}$ and $\{\sum_1^{m-1} y_i^2, \sum_1^{m-1} y_i^4, \ldots, \sum_1^{m-1} y_i^{2m}\}$ for a_2 and b_2, respectively. Again a_2 can be shown to be the negative of the term in θ^2 in the expansion by the first row of the determinant in eq. (45).

One can again write b_2 as a sum

$$b_2 = a_3 + b_3,$$

and so on.

IV. PROOF OF RELATION (53)

To get equation (53), we will apply Gram's result, which may be stated as follows [13]).

Let v_i $(i = 1, 2, \ldots, n)$ be n vectors and let $v_{i\alpha} (\alpha = 1, 2, \ldots, m)$ be their components along some basis. Form the scalar products

$$b_{ij} = \sum_{\alpha=1}^{m} v_{i\alpha} v_{j\alpha} \quad (i, j = 1, 2, \ldots, n);$$

then

$$\begin{vmatrix} b_{11} & b_{12} \cdots & b_{1n} \\ b_{21} & b_{22} \cdots & b_{2n} \\ \cdots & \cdots & \cdots \\ b_{n1} & b_{n2} \cdots & b_{nn} \end{vmatrix} = \frac{1}{n!} \sum_{s_1, s_2, \ldots, s_n} \begin{vmatrix} v_{1s_1} & v_{1s_2} \cdots & v_{1s_n} \\ v_{2s_1} & v_{2s_2} \cdots & v_{2s_n} \\ \cdots & \cdots & \cdots \\ v_{ns_1} & v_{ns_2} \cdots & v_{ns_n} \end{vmatrix}^2,$$

where on the right hand side we sum over all possible ways of choosing s_1, $s_2, \ldots, s_n$ among $1, 2, \ldots, m$. The summation over m may be finite, denumerable or continuously infinite, the summation sign being replaced by an integration over a suitable measure.

For our purpose we make the correspondence

$$v_{i\alpha} \to x^{2i-2}\sqrt{2}\,\mathrm{e}^{-x^2}\frac{x^{\frac{1}{2}}}{(x^2+\theta^2)^{\frac{1}{4}}}, \quad \sum_\alpha \to \int_0^\infty \mathrm{d}x.$$

The scalar products become

$$b_{ij} = \sum_\alpha v_{i\alpha}v_{j\alpha} \to \int_0^\infty \mathrm{d}x\, 2\mathrm{e}^{-2x^2}x^{2i+2j-4}\frac{x^5}{\sqrt{x^2+\theta^2}} = \eta_{i+j-2},$$

and the theorem gives the required result.

V. CALCULATION OF THE FIRST THREE TERMS OF $I(\theta)$ IN POWERS OF θ

Expanding the integrand in eq. (54) in powers of θ and integrating, we get

$$\eta_i(\theta) = \xi_{2i+4}(0) - \tfrac{1}{2}\theta^2\xi_{2i+2}(0) + \tfrac{3}{8}\theta^4\xi_{2i}(0) + \ldots.$$

Taking terms only up to θ^4, we put this in the determinant of eq. (53). We see that writing the determinant as a sum of several ones, many of them vanish because two rows are proportional. Thus we may write

$$I(\theta) \approx I(0)\{1 - \tfrac{1}{2}\theta^2 a + \tfrac{3}{8}\theta^4(b-c)\},$$

where

$$I(0) = \begin{vmatrix} \xi_4 & \xi_6 & \ldots & \xi_{2m} \\ \xi_6 & \xi_8 & \ldots & \xi_{2m+2} \\ \ldots & \ldots & \ldots & \ldots \\ \xi_{2m} & \xi_{2m+2} & \ldots & \xi_{4m-4} \end{vmatrix}, \qquad I(0)a = \begin{vmatrix} \xi_2 & \xi_4 & \ldots & \xi_{2m-2} \\ \xi_6 & \xi_8 & \ldots & \xi_{2m+2} \\ \xi_8 & \xi_{10} & \ldots & \xi_{2m+4} \\ \ldots & \ldots & \ldots & \ldots \\ \xi_{2m} & \xi_{2m+2} & \ldots & \xi_{4m-4} \end{vmatrix},$$

$$I(0)b = \begin{vmatrix} \xi_0 & \xi_2 & \ldots & \xi_{2m-4} \\ \xi_6 & \xi_8 & \ldots & \xi_{2m+2} \\ \xi_8 & \xi_{10} & \ldots & \xi_{2m+4} \\ \ldots & \ldots & \ldots & \ldots \\ \xi_{2m} & \xi_{2m+2} & \ldots & \xi_{4m-4} \end{vmatrix}, \qquad I(0)c = \tfrac{1}{3}\begin{vmatrix} \xi_2 & \xi_4 & \ldots & \xi_{2m-2} \\ \xi_4 & \xi_6 & \ldots & \xi_{2m} \\ \xi_8 & \xi_{10} & \ldots & \xi_{2m+4} \\ \ldots & \ldots & \ldots & \ldots \\ \xi_{2m} & \xi_{2m+2} & \ldots & \xi_{4m-4} \end{vmatrix},$$

where the ξ_{2i} are the numbers

$$\xi_{2i}(0) = 2^{-(i+\frac{1}{2})}\Gamma(i+\tfrac{1}{2}).$$

Factorization and triangulation give

$$I(0) = \frac{\mu_0}{(2m)!}\sqrt{\frac{2}{\pi}}\frac{\Gamma(m+\frac{1}{2})}{\Gamma(\frac{3}{2})\Gamma(m)},$$

$$I(0)a = \frac{\mu_0}{(2m)!}\sqrt{\frac{2}{\pi}}\,2\frac{\Gamma(m+\frac{1}{2})}{\Gamma(\frac{5}{2})\Gamma(m-1)} = I(0)\;2\,\tfrac{2}{3}(m-1),$$

$$I(0)b = \frac{\mu_0}{(2m)!}\sqrt{\frac{2}{\pi}}\frac{2\sqrt{\pi}}{\Gamma(\frac{3}{2})}\frac{\Gamma(m+\frac{1}{2})\Gamma(m+1)}{\Gamma(\frac{5}{2})\Gamma(m-1)\Gamma(m)} = I(0)\;2\,\tfrac{2\cdot 2}{1\cdot 3}m(m-1),$$

$$3I(0)c = \frac{\mu_0}{(2m)!}\sqrt{\frac{2}{\pi}}\,2\frac{\Gamma(m+\frac{1}{2})}{\Gamma(\frac{7}{2})\Gamma(m-2)} = I(0)\;2\,\tfrac{2}{3}\,\tfrac{2}{5}(m-1)(m-2).$$

VI. PROOF OF THE INEQUALITIES (58)

In the following we put $u_i = \theta^2/x_i^2$, so that $u_i \geqq 0$. The second inequality in eq. (58),

$$\prod_1^n \frac{1}{\sqrt{1+u_i}} \leqq 1,$$

is immediate, as each factor in the product lies between 0 and 1.

To prove the first inequality, we proceed by induction. It is easy to see that

$$1-\tfrac{1}{2}u \leqq \frac{1}{\sqrt{1+u}}.$$

Next, suppose that

$$1-\sum_1^{n-1}\tfrac{1}{2}u_i \leqq \prod_1^{n-1}\frac{1}{\sqrt{1+u_i}}$$

is true, and let us prove that then

$$1-\sum_1^{n}\tfrac{1}{2}u_i \leqq \prod_1^{n}\frac{1}{\sqrt{1+u_i}}.$$

Let $\sum_1^n u_i \leqq 2$, for otherwise the left hand side will be negative and therefore less than the right hand side, which is positive or zero. Thus,

$$\left(1-\tfrac{1}{2}\sum_1^{n-1}u_i\right)(1-\tfrac{1}{2}u_n) \leqq \frac{1}{\sqrt{1+u_n}}\prod_1^{n-1}\frac{1}{\sqrt{1+u_i}},$$

as both quantities in the product on both sides are positive. Therefore we have

$$\prod_1^n \frac{1}{\sqrt{1+u_i}} \geqq 1-\tfrac{1}{2}\sum_1^n u_i+\tfrac{1}{4}u_n\sum_1^{n-1}u_i \geqq 1-\tfrac{1}{2}\sum_1^n u_i.$$

VII. THE DERIVATIVES OF $Q_0(\theta)$ AT $\theta = 0$

We define the series of functions

$$Q_1(\theta), Q_2(\theta), Q_3(\theta), \ldots,$$

which differ from $Q_0(\theta)$ only by the fact that the first column in the integrand of equation (66) has been replaced by its first, second, ... derivatives with respect to θ. Thus, for example,

$$Q_2(\theta) = \frac{(n-2)!}{\mu_0} \int_{\substack{(-\infty \leq \theta_3 \leq \ldots \leq \theta_n \leq \infty, \\ \text{no } \theta_i \text{ in } 0, \theta)}} e^{-\theta^2-(+\theta_3^2 \ldots +\theta_n^2)} \begin{vmatrix} 0 & \theta_3 & \ldots & \theta_n \\ 2.1 & \theta_3^2 & \ldots & \theta_n^2 \\ 3.2\theta & \theta_3^3 & \ldots & \theta_n^3 \\ \ldots & \ldots & \ldots & \ldots \\ \ldots & \ldots & \ldots & \ldots \end{vmatrix} d\theta_3 \ldots d\theta_n.$$

We also define the following series of functions:

$$Q_{10}(\theta), Q_{20}(\theta), Q_{30}(\theta), \ldots$$
$$Q_{21}(\theta), Q_{31}(\theta), Q_{41}(\theta), \ldots$$
$$Q_{210}(\theta), Q_{310}(\theta), Q_{410}(\theta), \ldots$$
$$Q_{320}(\theta), Q_{420}(\theta), \ldots.$$

The function $Q_{i0}(\theta)$ differs from $Q_i(\theta)$ only by the fact that θ_3 in the integrand is replaced by θ and that the integration over θ_3 and the appearance of θ_3 in the limits of integration are suppressed. The function $Q_{ij}(\theta)$ differs from $Q_{i0}(\theta)$ only by the fact that the second column, which is now in θ, is differentiated j times. The function $Q_{ij0}(\theta)$ differs from $Q_{ij}(\theta)$ by the fact that θ_4 in the integrand is replaced by θ and that the integration over θ_4 and its appearance in the limits of integration are suppressed, and so on.

It is easy to see that any derivative of $Q_0(\theta)$ is a linear combination of the functions defined above, with coefficients which are polynomials in θ. For example, we have

$$Q_i'(\theta) = \frac{dQ_i(\theta)}{d\theta} = Q_{i+1}(\theta) - 2\theta Q_i(\theta) - Q_{i0}(\theta) \qquad (i = 0, 1, \ldots),$$

$$Q_{i0}'(\theta) = Q_{i+1,0}(\theta) - 4\theta Q_{i0}(\theta) + Q_{i1}(\theta) \qquad (i = 1, 2, \ldots), \text{ etc.}$$

For the first three odd derivatives we have

$$Q_0'(0) = Q_1(0),$$
$$Q_0'''(0) = Q_3(0) - 6Q_1(0),$$
$$Q_0^{(5)}(0) = Q_5(0) - 20Q_3(0) + 60Q_1(0) - 5Q_{31}(0).$$

To calculate these, we note that when we put $\theta = 0$, the limits of integration over $\theta_3, \ldots, \theta_n$ become $-\infty \leqq \theta_3 \leqq \ldots \leqq \theta_n \leqq \infty$ and we can therefore

apply the procedure developed in section 3 of integrating over half of these variables which symmetrizes the integrand and finally put the result in the determinantal form. Thus

$$Q_1(0) = \frac{(n-2)!}{\mu_0} 2^{m-1} \begin{vmatrix} F_2^3 & F_2^5 & \dots & F_2^{2m-1} & F_2(\infty) \\ F_4^3 & F_4^5 & \dots & F_4^{2m-1} & F_4(\infty) \\ \dots & \dots & \dots & \dots & \dots \\ F_{2m-2}^3 & F_{2m-2}^5 & \dots & F_{2m-2}^{2m-1} & F_{2m-2}(\infty) \end{vmatrix},$$

for $n = 2m+1$; and for $n = 2m$, the last row and last column in the above disappear. It is seen that to get $-Q_3(0)/3!$ we should replace the indices 3 by 1 in the above determinant; to get $-Q_5(0)/5!$ we should replace the indices 5 by 1 and in general to get $-Q_{2r+1}(0)/(2r+1)!$ the indices $(2r+1)$ by 1. (If $r \geqq m$, $Q_{2r+1}(0) \equiv 0$).

Using the same method of factorization and maximum possible triangulation, we get

$$-\frac{Q_{2r+1}(0)}{(2r+1)!} = (-)^{r+1} \frac{2^{r+\frac{1}{2}}}{\Gamma(\frac{1}{2})r!} \frac{1}{n(n-1)} \times \begin{cases} V_m(2r+1) & \text{for } n = 2m+1, \\ \frac{1}{2}a_m(2r+1) & \text{for } n = 2m, \end{cases}$$

where

$$V_m(2r+1) = \begin{vmatrix} D_{2r+2}^3 & D_{2r+2}^5 & \dots & D_{2r+2}^{2m-1-2r} & 1 \\ D_{2r+4}^1 & D_{2r+4}^3 & \dots & D_{2r+4}^{2m-3-2r} & 1 \\ 0 & D_{2r+6}^1 & \dots & D_{2r+6}^{2m-5-2r} & 1 \\ \dots & \dots & \dots & \dots & \dots \\ 0 & 0 & \dots & D_{2m}^1 & 1 \end{vmatrix},$$

and $a_m(2r+1)$ is the same determinant, but without the last row and last column. Expanding the determinants in the Cauchy manner, we get the recurrence relations

$$V_m(2r+1) = -V_{m-1}(2r+1) + a_m(2r+1)$$

$$a_m(2r+1) = D_{2m-2}^3 a_{m-1}(2r+1) - D_{2m-4}^5 a_{m-2}(2r+1) + \dots (-)^{m-r} D_{2r+2}^{2m-1-2r} a_{r+1}(2r+1),$$

with

$$a_{r+1}(2r+1) = 1.$$

The solution of the above equations is

$$a_m(2r+1) = \left\{ \frac{\Gamma(m+\frac{3}{2})}{\Gamma(m-r)} + \frac{\Gamma(m+\frac{1}{2})}{\Gamma(m-r-1)} \right\} \frac{1}{\Gamma(r+\frac{5}{2})}.$$

The verification of this fact being straightforward and similar to that given in appendix II, though somewhat lengthy, we shall not reproduce it here.

VIII. MEAN LEVEL-SPACING USING EXACT DISTRIBUTION FUNCTION

Let us define

$$\frac{\mu(\theta)}{(2m)!} = \begin{vmatrix} \xi_0 & \xi_2 & \dots & \xi_{2m-2} \\ \xi_2 & \xi_4 & \dots & \xi_{2m} \\ \dots & \dots & \dots & \dots \\ \xi_{2m-2} & \xi_{2m} & \dots & \xi_{4m-4} \end{vmatrix},$$

where the functions ξ_{2i} were defined by eq. (43). Then it is easy to see that

$$\frac{\mathrm{d}}{\mathrm{d}\theta}\frac{\mu(\theta)}{(2m)!} = 2\mathrm{e}^{-2\theta^2}R_1(\theta) = -2\mathrm{e}^{-2m\theta^2}I(\theta),$$

$$\mu(0) = \mu_0,$$

and

$$\mu(\infty) = 0.$$

Therefore from eqs. (57) and (56'), we get

$$F(S) = 1 + \frac{D}{\mu(0)}\frac{\mathrm{d}}{\mathrm{d}S}\{\mu(\tfrac{1}{2}S)\},$$

so that

$$\bar{S} = \int_0^\infty S\frac{\mathrm{d}F}{\mathrm{d}S}\mathrm{d}S = \int_0^\infty \{1-F(S)\}\mathrm{d}S = -\frac{D}{\mu_0}\mu(\tfrac{1}{2}S)\Big|_0^\infty = D,$$

which is the mean level-spacing at the centre.

References

1) See for example:
J. A. Harvey and D. J. Hughes, Phys. Rev. **109** (1958) 471;
J. L. Rosen, Neutron resonances in U^{238}, Ph. D. Thesis (Colombia University, New-York, 1959);
C. T. Hibdon, Phys. Rev. **114** (1959) 179;
for atomic spectral data, see:
Charlotte E. Moore, Atomic energy levels, NBS Circular 467, Washington, D. C., Vol. I (June 15, 1949); Vol. II (Aug. 15, 1952); Vol. III (May 1, 1958)

2) For a discussion and earlier references see:
D. ter Haar, Elements of statistical Mechanics (Constable, London, 1954);
see further:
C. Bloch, Phys. Rev. **93** (1954) 1094;
T. D. Newton, Can. J. Phys. **34** (1956) 804

3) J. H. D. Jensen and J. M. Luttinger, Phys. Rev. **86** (1952) 907

4) For recent reviews see:
A. M. Lane and R. G. Thomas, Revs. Mod. Phys. **30** (1958) 257;
G. Breit, Handbuch der Physik **41/1** (1959);
G. Brown, Revs. Mod. Phys. **31** (1959) 893

5) E. P. Wigner, Proc. Cam. Phil. Soc. **47** (1951) 790; Ann. Math. **53** (1951) 36

6) R. G. Thomas and C. E. Porter, Phys. Rev. **104** (1956) 483;
A. Bohr, Int. Conf. on Peaceful Uses of At. En. **2** (1955) 151

7) Statistical aspects of nucleus, Brookhaven National Laboratory Report, BNL 331 (C-21), April 1955
8) E. P. Wigner, Gatlinberg Conference on Neutron Physics by time-of-flight, Oak-Ridge National Laboratory Report ORNL 2309 (1957) p. 59
9) L. Landau and Ya. Smorodinsky, Lectures on the Theory of the Atomic Nucleus (State Tech. Theo. Lit. Press, Moscow 1955); translation (Consultants Bureau, New-York 1958) p. 55
10) P. L. Hsu, Ann. Eug. **9** (1939) 250;
D. N. Nanda, Ann. Math. Stat. **19** (1948) 47;
S. N. Roy, Sankhyā (Dec., 1943);
C. E. Porter and N. Rosenzweig, Tiedeakatemian Toimituksia
11) J. V. Neumann and H. H. Goldstein, Proc. Amer. Math. Soc. **2** (1951) 188
12) E. P. Wigner, Can. Math. Cong. Proc. (1957) 174
13) Courant and Hilbert, Methoden der Mathematischen Physik (1931) Vol. I, Ch. 1, § 5

2.D

Nuclear Physics **18** (1960) 420—427; © *North-Holland Publishing Co., Amsterdam*

Not to be reproduced by photoprint or microfilm without written permission from the publisher

ON THE DENSITY OF EIGENVALUES OF A RANDOM MATRIX

M. L. MEHTA † and M. GAUDIN

Centre d'Études Nucléaires de Saclay, Gif-sur-Yvette (S. et O.) France

Received 5 May 1960

Abstract: An exact expression for the density of eigenvalues of a random-matrix is derived. When the order of the matrix becomes infinite, it can be seen very directly that it goes over to Wigner's "semi-circle law".

1. Introduction

In heavy nuclei, the interactions are so numerous and so complex that almost all the theories are statistical in nature and they try to explain only the average properties like level-density, mean square angular momenta, distribution of level-spacings, transition probability, etc. ††.

In this paper, which is essentially the continuation of the preceding one [1]), we start from the random matrix hypothesis and calculate exactly the level-density. This, in the proper limit, will be found to be the famous "semi-circle law" of Wigner [2]). The proof here is, however, mathematically rigorous.

The joint probability frequency function of the eigenvalues $\theta_1, \theta_2, \ldots, \theta_n$ of an $n \times n$ hermitian matrix, whose elements are randomly and independently distributed (these distributions being invariant under unitary transformations), is given by [3])

$$P(\theta_1, \theta_2, \ldots, \theta_n) = \mu_0^{-1} \mathrm{e}^{-\sum_{i=1}^{n} \theta_i^2} \prod_{i<j} |\theta_i - \theta_j|, \tag{1}$$

with

$$\mu_0 = n! 2^{-\frac{1}{2}n(n-1)} \prod_{g=1}^{n} \Gamma(\tfrac{1}{2}g). \tag{2}$$

To get the level-density one must integrate the expression (1) over all the variables but one, i.e.

$$P(\theta) = \int_{-\infty}^{+\infty} \ldots \int_{-\infty}^{+\infty} P(\theta, \theta_2, \theta_3, \ldots, \theta_n) \mathrm{d}\theta_2 \mathrm{d}\theta_3 \ldots \mathrm{d}\theta_n. \tag{3}$$

We shall do it explicitly for $n = 2m$. As in the preceding paper, we overcome the serious difficulty of the unfavourable symmetrical nature of the integrand in eq. (3) by integrating over half the variables, $\theta_3, \theta_5, \ldots$, say. We then drop the ordering of the variables, expressing the result in determinantal form.

† On leave of absence from Tata Institute of Fundamental Research, Bombay.

†† For a fairly extensive list of references see the preceding paper.

After some reductions this determinant will be transformed into the integral of the square of another one whose elements are Hermite polynomials. This will permit us to use the orthonormality properties of the harmonic oscillator wave functions. In this form the problem becomes that of the density of a one dimensional Fermi-gas. By taking the limit when $n \to \infty$, one gets the "semi-circle law":

$$P(\theta) = \begin{cases} \frac{2}{n\pi}\sqrt{n-\theta^2} & \text{for } \theta < \sqrt{n}, \\ 0 & \text{otherwise.} \end{cases} \tag{4}$$

2. Symmetrization and Reduction

By definition, we have

$$\begin{aligned} \frac{\mu_0}{(n-1)!} P(\theta) = & \int_{-\infty<x_1<x_2<\ldots<x_n<\infty} e^{-(x_1^2+\ldots\ x_n^2)} \begin{vmatrix} 1 & \ldots & 1 \\ x_1 & \ldots & x_n \\ \ldots & \ldots & \ldots \\ x_1^{n-1} & \ldots & x_n^{n-1} \end{vmatrix}_{x_1=\theta} dx_2 dx_3 \ldots dx_n \\ & + \int_{-\infty<x_1<x_2<\ldots<x_n<\infty} e^{-(x_1^2+\ldots+x_n^2)} \begin{vmatrix} 1 & \ldots & 1 \\ x_1 & \ldots & x_n \\ \ldots & \ldots & \ldots \\ x_1^{n-1} & \ldots & x_n^{n-1} \end{vmatrix}_{x_2=\theta} dx_1 dx_3 \ldots dx_n \\ & + \ldots + \ldots \\ & = \mathcal{O}(\theta) + \mathcal{E}(\theta), \end{aligned} \tag{5}$$

where $\mathcal{O}(\theta)$ includes the integrals in which an x with an odd index is put equal to θ, while $\mathcal{E}(\theta)$ includes the other terms. Introducing the functions

$$F_i(x) = \int_{-\infty}^{x} e^{-y^2} y^i \, dy, \tag{6}$$

and the step-function

$$\varepsilon(x) = \begin{cases} 1 & \text{if } x > \theta, \\ 0 & \text{if } x < \theta, \end{cases} \tag{7}$$

$\mathcal{O}(\theta)$ is readily seen to be

$$\mathcal{O}(\theta) = -\int_{-\infty<x_2<x_4<\ldots<\infty} e^{-(\theta^2+x_2^2+x_4^2+\ldots)} \begin{vmatrix} 0 & \varepsilon(x_2) & 0 & \varepsilon(x_4) & 0 & \ldots \\ 1 & F_0(x_2) & 1 & F_0(x_4) & 1 & \ldots \\ \theta & F_1(x_2) & x_2 & F_1(x_4) & x_4 & \ldots \\ \theta^2 & F_2(x_2) & x_2^2 & F_2(x_4) & x_4^2 & \ldots \\ \cdot & \cdot & \cdot & \cdot & \cdot & \\ \cdot & \cdot & \cdot & \cdot & \cdot & \\ \cdot & \cdot & \cdot & \cdot & \cdot & \end{vmatrix} dx_2 dx_4 \ldots . \tag{8}$$

For simplicity, we shall take n even, $n = 2m$. As for $\mathscr{E}(\theta)$ we may integrate over $x_2, x_4, \ldots$ in a similar way by introducing the functions

$$\phi_i(x) = \int_x^\infty e^{-y^2} y^i \, dy, \tag{9}$$

and by an obvious change of the variables to their negatives, it is seen that

$$\mathscr{E}(\theta) = \mathscr{O}(-\theta). \tag{10}$$

Now the integrand in eq. (8) being symmetric in $x_2, x_4, \ldots, x_{2m}$ we can integrate over these variables separately and independently over the whole range and divide the result by $m!$. It is easy to verify directly (see appendix I of the preceding article) by expanding with respect to the first column, for example, that

$$\mathscr{O}(\theta) = \mathscr{O}_{\text{even}}(\theta) + \mathscr{O}_{\text{odd}}(\theta), \tag{11}$$

with

$$\mathscr{O}_{\text{even}}(\theta) = -e^{-\theta^2} \begin{vmatrix} 0 & \phi_1(\theta) & \phi_3(\theta) & \ldots & \phi_{2m-1}(\theta) \\ 1 & f_0^1 & f_0^3 & \ldots & f_0^{2m-1} \\ \theta^2 & f_2^1 & f_2^3 & \ldots & f_2^{2m-1} \\ \ldots & \ldots & \ldots & \ldots & \ldots \\ \theta^{2m-2} & f_{2m-2}^1 & f_{2m-2}^3 & \ldots & f_{2m-2}^{2m-1} \end{vmatrix}, \tag{12}$$

and

$$\mathscr{O}_{\text{odd}}(\theta) = e^{-\theta^2} \begin{vmatrix} 0 & \theta & \theta^3 & \ldots & \theta^{2m-1} \\ \phi_0(\theta) & f_0^1 & f_0^3 & \ldots & f_0^{2m-1} \\ \phi_2(\theta) & f_2^1 & f_2^3 & \ldots & f_2^{2m-1} \\ \ldots & \ldots & \ldots & \ldots & \ldots \\ \phi_{2m-2}(\theta) & f_{2m-2}^1 & f_{2m-2}^3 & \ldots & f_{2m-2}^{2m-1} \end{vmatrix}, \tag{13}$$

where the f_i^j are the numbers

$$f_i^j = F_i^j - F_j^i, \tag{14}$$

with

$$F_i^j = \int_{-\infty}^{+\infty} e^{-x^2} F_i(x) x^j \, dx = \int_{-\infty < y < x < +\infty} e^{-(x^2+y^2)} x^j y^i \, dx \, dy. \tag{15}$$

The following recurrence relations are easily established:

$$f_i^j - \tfrac{1}{2}(j-1) f_i^{j-2} = 2^{-\frac{1}{2}(i+j)} \Gamma\left(\frac{i+j}{2}\right) \equiv \xi_{i+j-1}, \tag{16}$$

say, and

$$\phi_j(\theta) - \tfrac{1}{2}(j-1)\phi_{j-2}(\theta) = \tfrac{1}{2}\theta^{j-1} e^{-\theta^2}. \tag{17}$$

Using these recurrence relations it is elementary to reduce the determinants (12) and (13) to the forms

$$\mathcal{O}_{\text{even}} = -\tfrac{1}{2}e^{-2\theta^2}\begin{vmatrix} 0 & 1 & \theta^2 & \dots & \theta^{2m-2} \\ 1 & \xi_0 & \xi_2 & \dots & \xi_{2m-2} \\ \theta^2 & \xi_2 & \xi_4 & \dots & \xi_{2m} \\ \dots & \dots & \dots & \dots & \dots \\ \theta^{2m-2} & \xi_{2m-2} & \xi_{2m} & \dots & \xi_{4m-4} \end{vmatrix}, \tag{19}$$

and

$$\mathcal{O}_{\text{odd}} = \theta e^{-\theta^2}\begin{vmatrix} 0 & 1 & \theta^2-1 & \dots & \theta^{2m-2}-(m-1)\theta^{2m-4} \\ \phi_0(\theta) & \xi_0 & \xi_2 & \dots & \xi_{2m-2} \\ \phi_2(\theta) & \xi_2 & \xi_4 & \dots & \xi_{2m} \\ \dots & \dots & \dots & \dots & \dots \\ \phi_{2m-2}(\theta) & \xi_{2m-2} & \xi_{2m} & \dots & \xi_{4m-4} \end{vmatrix}. \tag{20}$$

Now, as

$$\phi_i(x) = (-)^i F_i(-x), \tag{21}$$

we can write the result as

$$\frac{\mu_0}{(2m-1)!}P(\theta) = T_1(\theta)+T_2(\theta)+T_3(\theta), \tag{22}$$

with

$$T_1(\theta) = 2\,\mathcal{O}_{\text{even}}(\theta), \tag{23}$$

$$T_2(\theta) = -\theta e^{-\theta^2}\begin{vmatrix} 0 & 1 & \theta^2 & \dots & \theta^{2m-2} \\ \rho_0(\theta) & \xi_0 & \xi_2 & \dots & \xi_{2m-2} \\ \rho_2(\theta) & \xi_2 & \xi_4 & \dots & \xi_{2m} \\ \dots & \dots & \dots & \dots & \dots \\ \rho_{2m-2}(\theta) & \xi_{2m-2} & \xi_{2m} & \dots & \xi_{4m-4} \end{vmatrix}, \tag{24}$$

and

$$T_3(\theta) = \theta e^{-\theta^2}\begin{vmatrix} 0 & 0 & 1 & 2\theta^2 & \dots & (m-1)\theta^{2m-4} \\ \rho_0(\theta) & \xi_0 & \xi_2 & \xi_4 & \dots & \xi_{2m-2} \\ \rho_2(\theta) & \xi_2 & \xi_4 & \xi_6 & \dots & \xi_{2m} \\ \dots & \dots & \dots & \dots & \dots & \dots \\ \rho_{2m-2}(\theta) & \xi_{2m-2} & \xi_{2m} & \xi_{2m+2} & \dots & \xi_{4m-4} \end{vmatrix}, \tag{25}$$

where the functions $\rho_{2i}(\theta)$ are defined by

$$\rho_{2i}(\theta) = \int_{-\theta}^{+\theta} e^{-x^2}x^{2i}\,dx. \tag{26}$$

We may note that

$$\frac{d}{d\theta}\left\{\frac{1}{\theta}e^{\theta^2}T_2(\theta)\right\} = -2e^{\theta^2}T_3(\theta)+2e^{\theta^2}T_1(\theta). \tag{27}$$

One can easily show that (see appendix III of the preceding paper)

$$\begin{vmatrix} 0 & a_0 & a_2 \dots\dots a_{2m} \\ b_0 & \xi_0 & \xi_2 \dots\dots \xi_{2m} \\ b_2 & \xi_2 & \xi_4 \dots\dots \xi_{2m+2} \\ \dots\dots\dots\dots\dots\dots\dots \\ b_{2m} & \xi_{2m} & \xi_{2m+2} \dots \xi_{4m} \end{vmatrix} \tag{28}$$

$$= -\frac{1}{m!}\int_{-\infty}^{+\infty} dy_1 \dots \int_{-\infty}^{+\infty} dy_m \, e^{-(y_1^2+\dots+y_m^2)} \begin{vmatrix} a_0 & 1 & \dots 1 \\ a_2 & y_1^2 & \dots y_m^2 \\ \dots\dots\dots\dots \\ a_{2m} & y_1^{2m} & \dots y_m^{2m} \end{vmatrix} \times \begin{vmatrix} b_0 & 1 & \dots 1 \\ b_2 & y_1^2 & \dots y_m^2 \\ \dots\dots\dots\dots \\ b_{2m} & y_1^{2m} & \dots y_m^{2m} \end{vmatrix}.$$

And hence we have

$$T_1(\theta) = \frac{1}{(m-1)!}\int_{-\infty}^{\infty} dy_1 \dots \int_{-\infty}^{+\infty} dy_{m-1} e^{-2(\theta^2+y_1^2+\dots+y_{m-1}^2)} \begin{vmatrix} 1 & 1 \dots\dots 1 \\ \theta^2 & y_1^2 \dots\dots y_{m-1}^2 \\ \dots\dots\dots\dots\dots \\ \theta^{2m-2} & y_1^{2m-2} \dots y_{m-1}^{2m-2} \end{vmatrix}^2, \tag{29}$$

as well as

$$\frac{1}{\theta}T_2(\theta) = \frac{1}{(m-1)!}\int_{-\infty}^{+\infty} dy_1 \dots \int_{-\infty}^{+\infty} dy_{m-1} \int_{-\theta}^{+\theta} dx \, e^{-(\theta^2+x^2)-2(y_1^2+\dots+y_{m-1}^2)} \times \begin{vmatrix} 1 & 1 \dots\dots 1 \\ \theta^2 & y_1^2 \dots\dots y_{m-1}^2 \\ \dots\dots\dots\dots\dots \\ \theta^{2m-2} & y_1^{2m-2} \dots y_{m-1}^{2m-2} \end{vmatrix} \times \begin{vmatrix} 1 & 1 \dots\dots 1 \\ x^2 & y_1^2 \dots\dots y_{m-1}^2 \\ \dots\dots\dots\dots\dots \\ x^{2m-2} & y_1^{2m-2} \dots y_{m-1}^{2m-2} \end{vmatrix}. \tag{30}$$

3. Transformation to Oscillator Wave-Functions

In the equations (29) and (30) let us put

$$z = \theta\sqrt{2}, \qquad x_i = y_i\sqrt{2}, \qquad v = x\sqrt{2}.$$

As the Hermite polynomials are linearly independent, we can express the powers of the variables as linear combinations of them. Then in each row of the determinants we can retain only those Hermite polynomials whose indices are the highest. We can also take the exponentials inside. Multiplying by the proper normalization factors according to

$$u_i(x) = (\sqrt{\pi}2^i i!)^{-\frac{1}{2}} e^{-\frac{1}{2}x^2} H_i(x),$$

we get

$$T_1(\theta) = \frac{2^{-\frac{1}{2}(m-1)}}{(m-1)!}\prod_{i=0}^{m-1}\{2^{-4i}\sqrt{\pi}(2i)!\} \times \int_{-\infty}^{+\infty} dx_1 \ldots \int_{-\infty}^{+\infty} dx_{m-1} \begin{vmatrix} u_0(z) & u_0(x_1) \ldots\ldots u_0(x_{m-1}) \\ u_2(z) & u_2(x_1) \ldots\ldots u_2(x_{m-1}) \\ \ldots\ldots\ldots\ldots\ldots\ldots\ldots\ldots \\ u_{2m-2}(z) & u_{2m-2}(x_1) \ldots u_{2m-2}(x_{m-1}) \end{vmatrix}^2, \quad (31)$$

and

$$\frac{1}{\theta}T_2(\theta) = \frac{2^{-\frac{1}{2}m-1}}{(m-1)!}\prod_{i=0}^{m-1}\{2^{-4i}\sqrt{\pi}(2i)!\}\int_{-\infty}^{+\infty} dx_1 \ldots \int_{-\infty}^{+\infty} dx_{m-1}\int_{-z}^{+z} dv$$

$$\times \begin{vmatrix} u_0(z) & u_0(x_1) \ldots\ldots u_0(x_{m-1}) \\ u_2(z) & u_2(x_1) \ldots\ldots u_2(x_{m-1}) \\ \ldots\ldots\ldots\ldots\ldots\ldots\ldots\ldots \\ u_{2m-2}(z) & u_{2m-2}(x_1) \ldots u_{2m-2}(x_{m-1}) \end{vmatrix} \times \begin{vmatrix} u_0(v) & u_0(x_1) \ldots\ldots u_0(x_{m-1}) \\ u_2(v) & u_2(x_1) \ldots\ldots u_2(x_{m-1}) \\ \ldots\ldots\ldots\ldots\ldots\ldots\ldots\ldots \\ u_{2m-2}(v) & u_{2m-2}(x_1) \ldots u_{2m-2}(x_{m-1}) \end{vmatrix}. \quad (32)$$

Multiplying the determinants and using the orthonormality properties of the oscillator wave functions $u_i(x)$

$$\int_{-\infty}^{+\infty} u_i(x)u_j(x)dx = \delta_{ij},$$

we find

$$T_1(\theta) = \sqrt{2}\,\frac{\mu_0}{(2m)!}\sum_{i=0}^{m-1} u_{2i}^2(z), \quad (33)$$

and

$$\frac{1}{\theta}T_2(\theta) = \frac{\mu_0}{(2m)!}\sum_{i=0}^{m-1} u_{2i}(z)\int_{-z}^{+z} u_{2i}(v)dv, \quad (34)$$

with $z = \theta\sqrt{2}$.

Eqs. (22), (27), (33) and (34) give

$$2mP\left(\frac{z}{\sqrt{2}}\right) = \sqrt{2}\sum_{i=0}^{m-1}\left\{u_{2i}^2(z) - u_{2i}'(z)\int_0^z u_{2i}(v)dv\right\}. \quad (35)$$

Using the recurrence relation

$$\sqrt{2}u_n' = \sqrt{n}u_{n-1} - \sqrt{n+1}u_{n+1},$$

and its integral, together with $u_{2i+1}(0) = 0$, we can transform the second term in the brackets of eq. (35) to the more suitable form

$$\sqrt{2}\sum_{i=0}^{m-1} u_{2i}'(z)\int_0^z u_{2i}(v)dv = -\sqrt{2}\sum_{i=0}^{m-2} u_{2i+1}^2(z) - \sqrt{2m-1}\,u_{2m-1}(z)\int_0^z u_{2m-2}(v)dv.$$

Therefore the final result is

$$2mP\left(\frac{z}{\sqrt{2}}\right) = \sqrt{2}\sum_{i=0}^{2m-2} u_i^2(z) + \sqrt{2m-1}\,u_{2m-1}(z)\int_0^z u_{2m-2}(x)dx. \quad (36)$$

4. The Limit $m \to \infty$

Equation (36) is exact. If the second term on the right hand side were absent, the problem would be exactly that of finding the density of a one dimensional degenerate Fermi-gas in a quadratic potential. We shall use this analogy to derive the limit in a simple way.

The equation satisfied by u_i is

$$\left(-\frac{\mathrm{d}^2}{\mathrm{d}z^2}+z^2\right)u_i = (2i+1)u_i \tag{37}$$

and therefore, classically, the Fermi-momentum for our problem is given by

$$P_F^2 = 2(2m-2)-z^2 \sim 4m-z^2, \qquad m \to \infty.$$

Also, in eq. (37) we have $\hbar = 1$, so that the density of the Fermi-gas is given by

$$\delta_F(z) = \begin{cases} \dfrac{1}{2\pi}\displaystyle\int_{-p_F}^{+p_F} \mathrm{d}p = \frac{1}{\pi}\sqrt{4m-z^2} & \text{for} \quad z^2 \leqq 4m, \\ 0 & \text{for} \quad z^2 > 4m. \end{cases}$$

Replacing the sum in (36) by this classical limit, and neglecting the second term, we get

$$2mP\left(\frac{z}{\sqrt{2}}\right) \sim \begin{cases} \sqrt{2}\dfrac{1}{\pi}\sqrt{4m-z^2} & \text{for} \quad z^2 \leqq 4m, \\ 0 & \text{for} \quad z^2 > 4m. \end{cases} \tag{38}$$

which is the same as eq. (4).

One can estimate (see appendix) that the neglected term is of the order of $1/\sqrt{m}$ when $z^2 \ll 4m$. For $z^2 \gg 4m$, the function u_{2m-1} decreases exponentially. In the neighbourhood of $z^2 = 4m$ we can say nothing, as in this neighbourhood u_{2m-1} is known to be very large.

We are thankful to Dr. C. Bloch for suggesting the problem, guidance and many helpful discussions throughout the work. One of us (M. L. M.) wishes to express his thanks to the Commissariat à l'Énergie Atomique for the kind hospitality and the award of a de Broglie fellowship.

Appendix

We divide the discussion into three parts.

1) $z \gg \sqrt{2n}$

In the differential equation (37), for $i = n$, putting

$$u_n'/u_n = -\sqrt{z^2-(2n+1)}\,v(z),$$

it is easily seen [4]) that $v(z)$ has an asymptotic expansion in powers of $\{z^2-(2n+1)\}^{-\frac{1}{2}}$ starting with the constant term unity:

$$v(z) \sim 1+\frac{a_1}{(z^2-(2n+1))^{\frac{1}{2}}}+\ldots;$$

hence

$$u_n(z) \sim A \exp\left\{-\int^z \sqrt{x^2-2n-1}\,dx+\ldots\right\},$$

where A is a const.

2) $z \ll \sqrt{2n}$

Applying the second mean value theorem to

$$u_n = -\frac{u_n''}{2n+1-z^2},$$

we get

$$\int_0^x u_n(x)dx = \frac{1}{2n+1-z^2}\{u_n'(\xi)-u_n'(z)\} \quad (\text{where } 0 \leqq \xi \leqq x)$$

$$\leqq \sqrt{2n+2}\,\{|u_{n-1}(\xi)|+|u_{n+1}(\xi)|+|u_{n-1}(z)|+|u_{n+1}(z)|\},$$

where we have used the recurrence relation

$$\sqrt{2}\,u_n' = \sqrt{n}\,u_{n-1}-\sqrt{n+1}\,u_{n+1}.$$

For estimating u_n, we may apply the WKB approximation or asymptotic methods [4]) to get

$$|u_n(z)|^2 \lesssim (2n+1-z^2)^{-\frac{1}{2}};$$

collecting all these, we have the result stated in the text.

3) $z \sim \sqrt{2n}$

As u_n^2 approaches in the mean to the classical limit

$$|u_n(z)|^2 \sim \pi^{-1}(2n+1-z^2)^{-\frac{1}{2}},$$

we know that $u_n(z)$ is large for $z \sim \sqrt{2n}$.

References

1) M. L. Mehta, Nuclear Physics **18** (1960) 395
2) E. P. Wigner, 4th Canadian Math. Cong. Proc. (1957) 174
3) P. L. Hsu, Ann. Eug. **9** (1939) 250;
D. N. Nanda, Ann. Math. Stat. **19** (1948) 47;
C. E. Porter and N. Rosenzweig, Tiedea-katemian Toimituksia
4) See for example N. G. de Bruijn, Asymptotic methods in analysis (North-Holland Publishing Company, Amsterdam, 1958) §§ 9.4, 9.5

3.B:6.A

Nuclear Physics **18** (1960) 428—445; © *North-Holland Publishing Co., Amsterdam*

Not to be reproduced by photoprint or microfilm without written permission from the publisher

DETERMINATION OF ABSOLUTE $B\rho$-VALUES OF CONVERSION LINES

C. DE VRIES

Institute of Nuclear Research, Amsterdam

Received 27 May 1960

Abstract: A recently constructed Siegbahn-Edvarson type iron-free double-focusing spectrometer has been used to determine absolute $B\rho$-values of electron lines. The abilities of the instrument with respect to high resolution (a few parts in 10^4) and high accuracy in the line positions (about $1 : 10^5$) are shown. The effects of natural line width and source thickness on the adopted line position definition are investigated. The absolute $B\rho$-values of some conversion lines occurring in the spectrum of the ThB active deposit (covering the energy range from 150 keV to 2.6 MeV) are determined with an accuracy of about one part in 10^4. Comparison with published values for these $B\rho$-values shows the linearity of the instrument to be better than $1 : 10^4$ for the energy region considered.

1. Introduction

In a recent publication[1]), henceforward to be referred to as VW, the construction and performance of an iron-free double-focusing beta ray spectrometer have been described. The instrument can be used for the accurate measurement of electron energies up to 2.6 MeV. The cooling system limits errors due to temperature effects to about one part in 10^5 in the relative $B\rho$-scale throughout this energy region. The long and short term stability of the coil current, delivered by a d.c. generator, is of the order of $1 : 10^5$. External magnetic fields are compensated; fluctuations in the most important component of these fields are automatically suppressed to less than 10^{-8} Wb/m^2. The field shape satisfies the conditions for first order focusing in the radial directions and second order focusing in the axial direction to a high degree: $\alpha = 0.500 \pm 0.003$ and $\beta = 0.39 \pm 0.02$. The maximum transmission is about 1 %; the smallest line width obtained so far has been 0.013 %.

With an ideal iron-free instrument the momentum of a focused electron line linearly proportional to the coil current. For the present instrument the coil current is determined by comparing the voltage drop across a precision resistance with a reference voltage. This reference voltage is adjustable by means of a five decade potentiometer through which a reference current is flowing. Thus the reading of this potentiometer should be linearly proportional to the magnetic field intensity and hence, with fixed geometry of source and counter, to the momentum of the focused electron lines. Therefore the $B\rho$-values of the measur-

ed lines can be calculated if the calibration constant, defined as the ratio between momentum and corresponding potentiometer reading, is known. In principle this calibration constant can be determined by measuring directly the radius of the central orbit ρ_0 and the field intensity B for one of the lines occurring in the spectrum. Both ρ_0 and B have then to be determined with an accuracy of a few parts in 10^5 because the aim of the present instrument is to measure absolute $B\rho$-values with a precision of one part in 10^4 or better. Determining ρ_0 and B with the indicated precision will be almost impossible; moreover these measurements have to be repeated for each investigation owing to the limitations to the accuracy in the positioning of the source and the counter slit. From the latter fact it follows that for high precision work the calibration constant should be obtained for each source separately. Thus, the use of conversion lines with known momentum in order to obtain the calibration constant is limited to those cases in which these lines are present in the source to be investigated. As there exist only few lines which are known with a precision comparable to the accuracy which can be reached with our instrument, the activity containing these calibration lines should be added to the activity to be considered; this procedure is troublesome and not always feasible. A very convenient method to obtain a calibration constant for each source has been proposed by Siegbahn[2]). This "self consistent" method uses two lines belonging to the same gamma-transition, e.g. a K- and a L-line. The difference in binding energy between such lines is almost always known sufficiently accurately from X-ray data. Using this difference together with the measured ratio of the potentiometer settings of both lines, the absolute $B\rho$-values of both lines can be calculated with the aid of the relativistic relation between energy and momentum. The method will be more sensitive the larger the ratio between the potentiometer settings, which means that the method is chiefly applicable for relatively low energies.

In special cases, the calibration constant may be computed from sum relations. Let γ_3 be the cross-over gamma ray of two successively emitted gamma rays γ_1 and γ_2, then e.g. their K-conversion lines satisfy the relation

$$E_1(\mathrm{K})+E_2(\mathrm{K})+B_\mathrm{K} = E_3(\mathrm{K}),$$

where B_K is the binding energy of the electrons in the K-shell. Inserting in this equation the relation between energy and momentum, the calibration constant can be computed (most easily with an interation procedure).

In the methods described above momenta of unknown lines are determined by comparing their positions with those of other lines. Thus the line position should be defined.

2. Definition of the Line Position

The calibration methods discussed in the preceding section require the comparison of line positions. The accuracy of the determination of the ratio of line

positions will be limited by the uncertainty in the exact position of the lines due to the finite line widths caused by (a) the instrumental conditions under which the lines are measured (b) the natural line width of the transitions under consideration and (c) source thickness effects.

The line shape due to (a) is independent of the momentum of the line if the positions of source and counter are fixed. In the case that the broadenings of the line due to (b) and (c) are negligible one need not be very careful in defining the line positions: the ratio of corresponding points on two different lines will always be equal to the ratio of the $B\rho$-values. In fact, there is no need even to define the line positions; the best value for the $B\rho$-ratio is obtained by matching the two lines point for point.

At high resolution this method is no longer applicable because K- and L-lines can differ considerably in line width owing to the different natural widths of the corresponding atomic levels [3]). As will be shown in section 2.3., it is then possible to compare two lines also by matching after the narrower line has been folded with a resonance curve; the width of the resonance curve should be equal to the difference in the natural line widths of both lines.

However, matching of two lines which are broadened by (energy dependent) source effects is not so simple, since the energy loss spectrum due to source thickness is not well known. In many measurements source effects cannot be avoided. Therefore it becomes important to choose a certain point on the line being representative for the true line position. Such a definition of line position is to be used also when dealing with many lines, because then matching of all the lines becomes impractical.

From the above consideration we conclude that there is need for a line position which is representative for the position of a monoenergetic line as measured with an ideal source.

Several definitions of line positions have been adopted in the literature:

a) the centre of gravity of the line;
b) the centre of the horizontal chord at half height;
c) the intersection of the diameter of horizontal chords of the upper part of the line with the top;
d) the intersection of the linearly extrapolated sides of the line;
e) the centre of the high energy rise of the line;
f) the high energy extrapolated endpoint.

The definitions a), b), e) and f) require a more careful measurement of the background of the line than the other definitions. This may be regarded as a disadvantage when dealing with many lines, because then the measurements will take so much time that possible long term drifts may spoil the precision. When determining the ratio of lines widely different in energy, the use of the definitions a), b), c) and d) will deliver erroneous results if line broadening due to source straggling occurs. The influence of source thickness will be more

pronounced for the definitions a) and b) than for c) and d). The definition f) (and probably also definition e)) has the disadvantage that this position is influenced by the broadening due to the natural line width.

The above discussion guided us to consider only the definitions c) and d). Although it is rather difficult to decide which of these definitions is the better one, we decided to adopt definition d), because definition c) depends sensitively on the result of the measurements of a few points near the top.

The intersection of the extrapolated sides of the lines is determined by most of the experimental points; the accuracy which can be reached depends on the statistical precision of the points measured. One cannot hope, however, to determine the line position with any desired accuracy by just improving the statistics, unless any systematical error can be excluded. For that reason the accuracy of the determination was mostly estimated to be 5 % of the line half width in all cases where the statistical accuracy was adequate.

When dealing with line widths in the order of 0.05 % and with the above indicated accuracy in the line position, one really should ask oneself whether the adopted definition is a good one when the lines to be compared are not equally shaped. Therefore we investigated the influence of natural line width and source thickness on the line position determination.

2.1. NATURAL LINE WIDTH

Firstly it is to be noted that the investigation given below is only necessary because the line shape for a monoenergetic line (spectrometer window curve) is in principle asymmetric as can be deduced from the image coordinates given by Shull and Dennison for the field shape used for the present instrument [4]); for a symmetric spectrometer window curve the adopted definition d) should be evidently adequate in this respect.

If the spectrometer window curve were known accurately the theoretical line shape could be constructed by folding the window curve with resonance line shapes representative for the energy distribution of the corresponding conversion electrons. Thus both the true position and the natural line width could be determined. Experimental conditions, however, may very well affect the theoretical window curve which makes this procedure not applicable. Therefore the following method † is more reliable:

Folding the L-line with resonance curves with different half-widths and comparing these results with the experimental shape of the K-line will yield the difference in natural line widths of the K- and L-line; at the same time corresponding positions can be determined by matching.

This method has been applied for the K- and L_I-line of the 238.6 keV gamma transition in ^{212}Bi shown in fig. 3. In the measurements under consideration the line half-widths were 0.038 % and 0.018 % for the K- and L_I-line

† A more extended treatment will be published by J. H. Dijkstra and C. de Vries [5]).

respectively. Fig. 1 shows the result of the folding procedure. The peaks are plotted in the $B\rho$-scale at the position of the K-line. The curve (a) is a line having the same shape and (relative) width as the L_I-line. The curves (b), (c) and (d) are obtained by folding the curve (a) with resonance curves with different

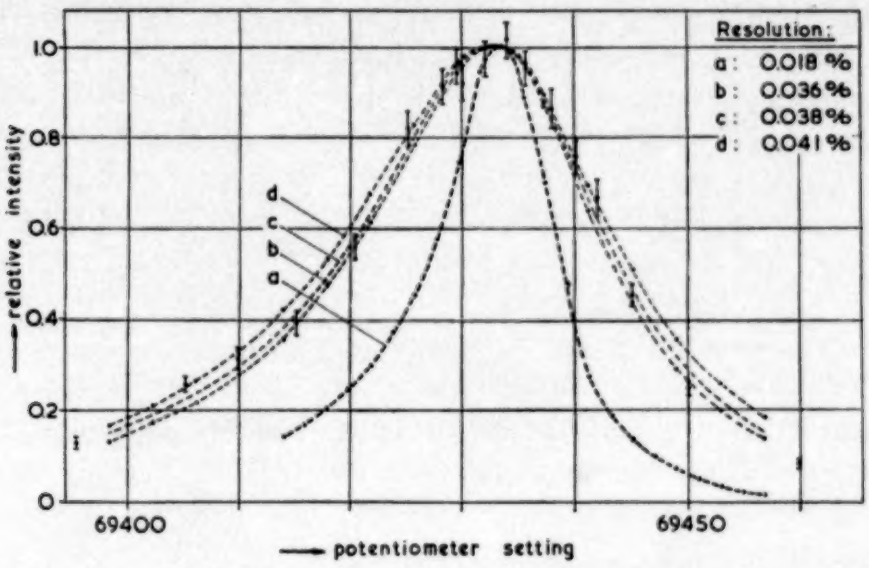

Fig. 1. Matching of the line profile as measured for the K-line (experimental points) with the line profiles (b), (c) and (d), which are obtained after folding the L_I-line (curve (a)) with resonance curves with half-widths: 47.5 eV, 52 eV and 60 eV. Curve (a) has the same shape and relative half-width as measured for the L_I-line.

half-widths: 47.5 eV, 52 eV and 60 eV. Comparison with the experimental points of the K-line indicates that the difference in natural line width between the K- and L_I-line is (52 ± 5) eV †.

† In connection with this result we want to make three remarks:

a. To be precise the difference found is somewhat too high because the natural line width of the L_I-line should have caused this line to be broader at the position of the K-line than at its actual position. Assuming the natural line half-width of this L_I-line to be 10 eV it can be calculated that the obtained result for the difference in natural line widths should be corrected to (49 ± 5) eV.

b. The difference in momentum resolution of the K-line (0.038 %) and the L_I-line (0.018 %) corresponds to 52 eV at the position of the K-line (148 keV). The obtained result therefore suggests that half-widths of lines obtained by folding resonance curves in the "window curve" equal the sum of the separate half-widths. Since it is well known that resonance curves may be mutually added linearly in this respect, the spectrometer window curve seems to behave somewhat like a resonance curve.

c. The conversion lines under consideration belong to a gamma transition in ^{83}Bi. Thus our result shows that for $Z = 83$ the difference in the natural widths of the atomic levels corresponding to the two conversion lines is (49 ± 5) eV. This is in nice agreement with the difference derived by Mladjenovic [6]) from X-ray data for ^{83}Bi. Earlier results obtained with the same K- and L_I-line have been reported by Lindström [7]), Slätis [3, 8]), Mladjenovic [6]) and Siegbahn and Edvarson [9]). If we take that the difference of true widths of the two lines is equal to the difference of the observed widths of these lines, the results of these authors indicate for the difference 80—100 eV. The discrepancy between this value and our result can only be explained assuming a better source technique at high resolution for the present investigation.

The $B\rho$-ratio of the L_I and K-line derived by this line matching procedure is

$$\text{ratio } A = 1.26328 \pm 0.00002,$$

whereas the $B\rho$-ratio obtained from the determination of the line positions separately defined as the intersection of the linearly extrapolated sides of the lines, is

$$\text{ratio } B = 1.26329 \pm 0.00003.$$

For the purpose under consideration systematic errors are not taken into account (see section 4). The result B shows that the definition adopted by us introduces only a small error relative to the more reliable ratio A. We therefore feel justified to consider this line position definition representative for the true line position to a high degree of accuracy.

2.2. SOURCE THICKNESS

The influence of source thickness on the position of the lines is investigated here because only in few cases the specific activity of the source material allows measurements with an extremely thin source; this is especially true for high precision work which as a matter of necessity has to be carried out at high resolution and thus at low luminosity.

From the review article of Marton *et al.* [10]) it is found that the energy loss spectrum due to the source material consists of several discrete lines (satellite lines) superimposed on a continuous background of inelastically scattered electrons. The characteristic energy losses connected with the appearance of the satellite lines are found to be independent of the primary energy of the electrons and the thickness of the source material. For most elements the main energy loss is about 20 eV; thus the strongest satellite peak will appear at an energy 20 eV lower than the undisturbed peak. The relative number of inelastically scattered electrons decreases with increasing primary energy and with decreasing thickness of the absorber.

Sokolowski [11]) and Nordling [12]), in their systematic study of electron binding energies with the ironfree double focusing instrument at Uppsala, discussed to what extent the position of the top of the electron line will be affected due to energy losses in the source material. These authors found that if the dominating peak is partly resolved from the undisturbed line, the top of the latter line is changed by only about 1 eV. The main satellite peak can only be resolved from the conversion line at extremely low energies (< 10 keV). As precise knowledge about the energy loss spectrum is missing for higher energies, it is impossible to compute to what extent the relative positions of the experimental lines deviate from those of the undisturbed lines. Therefore we tried to solve this problem by experiment for a special case.

A thin source and a thick one were prepared by electroplating ^{199}Au activity onto thin foils. The thickness of the thin source (0.3×10 mm) could be estimated

to be $< 50\mu g/cm^2$, while the other source (also 0.3×10 mm) was at least 25 times as thick. With these sources we measured under the same instrumental conditions the K- and L_{III}-conversion lines of the 158 keV gamma transition in ^{199}Hg. The positions of the lines were determined using the intersection of the linearly extrapolated sides of the lines (def. d) of section 2). The ratios thus obtained together with the difference between K- and L_{III}-electron binding energies, yielded absolute $B\rho$-values for the four lines. The absolute positions of these lines in the $B\rho$-scale are plotted in fig. 2.

This figure clearly shows the energy dependent influence of source thickness on the line shape. The different widths of the K- and L_{III}-lines as measured with the thin source is due to natural line width [13]). The different calculated positions of the intersection of the extrapolated sides are indicated. Even for the extremely thick source the shifts are only 1.7 and 0.9 parts in 10^4 for the K- and L_{III}-line respectively †. We also calculated the $B\rho$-values for the same line pairs using as a definition for the line position the intersection of the high energy slope with the continuum (def. f)). The values obtained in this way differ as much as one part in 10^3 for the two sources. The difference is even worse when defining the centre of the horizontal chord at half height as line position (def. b)). Thus when source thickness effects cannot be excluded definition d) is superior above definition a), b) and f).

Summarizing we may conclude from the above results and discussions that also with sources which cannot be regarded as ideal, the $B\rho$-values of lines above 75 keV can be determined with an accuracy of better than one part in 10^4.

3. Instrumental Sources of Error

In the preceding section we assumed that the uncertainty in the line position is about 5 % of the line width at half maximum, while we found that the defined line position is representative for the true line position. Now we have to consider to what extent the potentiometer readings for lines can be in error relative to each other, due to a possible non-linearity of the instrument.

Non-linearity of the instrument can be caused by

a. Remanent magnetism. The residual field intensity at the central orbit has been measured after switching off 170 A currents in both directions. The

† Using these lines for calibration in determining the energies of unknown lines of higher energies, the error in the results will be somewhere between 0 and 0.9 parts in 10^4, as can be deduced from the following reasoning: It is plausible that source straggling will shift the line positions towards lower energies and mostly so for the K-line. Thus the true energy difference between the positions of the thick lines will be larger than that for the thin lines. Inserting a too small energy difference will then cause the calculated positions of the thick lines to be still somewhat lower than their true positions. In a relative sense this "shift" is the same for the K-line and the L_{III}-line, because the ratio of the line positions is unchanged. Therefore the magnitude of this shift cannot be larger than 0.9 parts in 10^4.

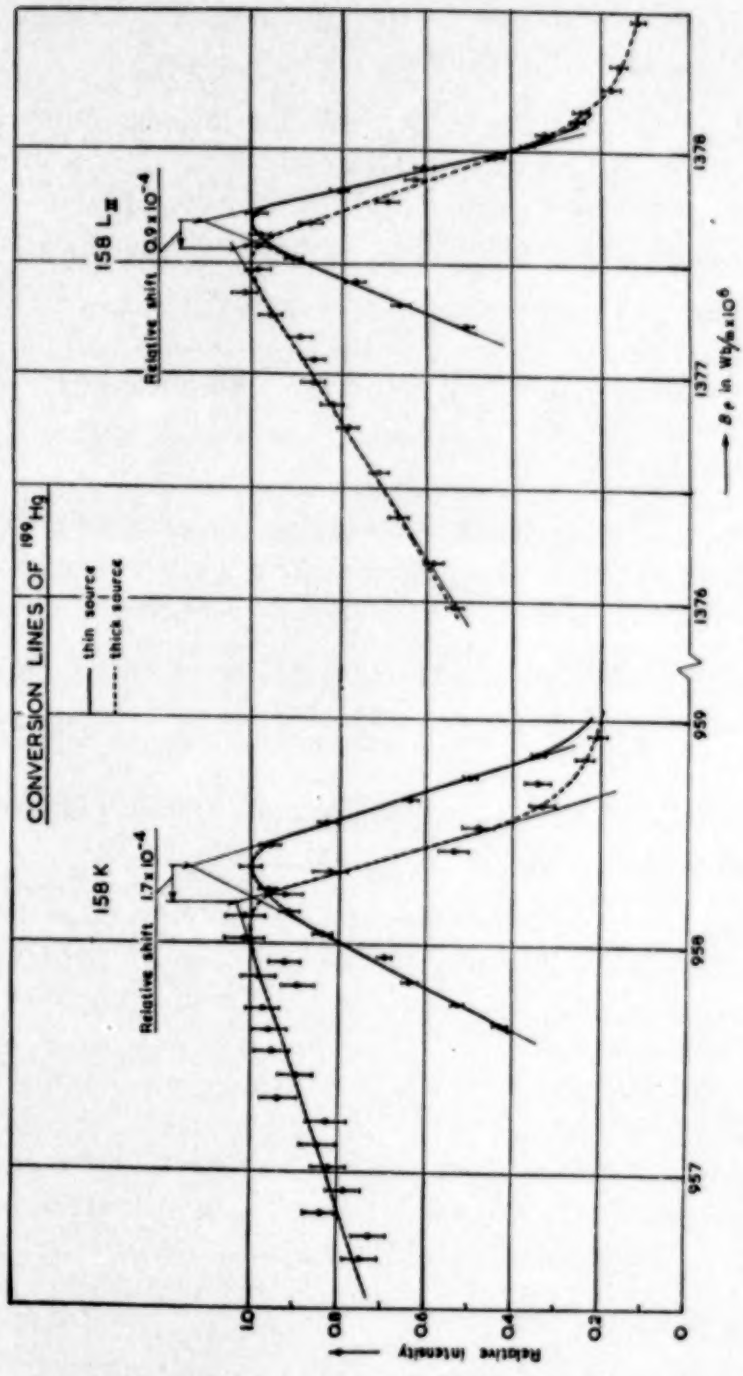

Fig. 2. K$-$L$_{III}$-line pairs as measured with a thin and a thick source. For further explanation see text.

difference between the opposite residual fields was about 10^{-7} Wb/m^2. The remanence field will therefore not cause a noticeable non-linearity of the instrument.

b. External magnetic fields. The contribution of the external field to the field generated by the coils is at most 5×10^{-8} Wb/m^2, as discussed in VW. We can neglect the effect of this error for all our measurements.

c. Variation in the geometry of the coils due to temperature fluctuations. We know from VW that an overall change in temperature of the coils causes the lines to be shifted by 4 parts in 10^5 per degree centigrade. At very high currents the line positions have to be corrected for a small systematic error.

d. Non-linearity between the potentiometer readings and the coil currents. As discussed in VW we take into account an error of 2 parts in 10^5 for each potentiometer reading, mainly in consequence of the uncertainty in the calibration of the potentiometer.

e. Long term drifts due to unknown causes. Possible long term drifts in the calibration constant can be checked by taking one or more lines as reference lines during the course of the measurements. During a typical run, stretched out over several days, no shifts have been found exceeding a few parts in 10^5.

The instrumental errors discussed above will be taken into account for the measurements described in the next sections.

4. Example of the Determination of Absolute $B\varrho$-values and Error Calculation

In this section we want to show how absolute $B\rho$-values with their errors are obtained using the method of Siegbahn described in the introduction of this chapter. As an example we take the line pair of run A of the next section (see fig. 3, tables 1 and 2).

This particular line pair has been investigated also for the effect of the natural line width (see section 2.1). Therefore the potentiometer readings as given in table 2 are obtained using fig. 1. The ratio of both line positions is $\alpha = 1.26328\pm0.00005$. The error in α can be broken down as follows:

Sources of error	Errors in parts in 10^5 for the	
	F-line	I-line
Line position (5 % of R)	1.9	1
Temperature stability of the coils $\pm0.2°$ C	1	1
Bridge circuit	2	2

Adding these errors quadratically the probable errors in the positions of the F- and I-line are found to be 3 parts and 2.5 parts in 10^5 respectively. The error in α will then be obtained by quadratic addition of the errors in the two lines separately.

Using this current ratio and the energy difference $h\nu$ between the two lines K- and L_I-line) as given from X-ray data, the absolute $B\rho$-values can be computed with the formula given by Siegbahn,

$$(B\rho)_F^2 = A + \sqrt{A^2+B},$$

where

$$A = \frac{\alpha^2+1}{(\alpha^2-1)^2}\left(\frac{1}{ce}\right)^2 (h\nu)^2, \quad B = \frac{4-s^2}{(\alpha^2-1)^2}\frac{m^2}{e^4}(h\nu)^2, \quad s = \frac{h\nu}{mc^2}.$$

The elementary constants are given by Cohen *et al.* [14]). The energy difference $h\nu$ is obtained by multiplying the frequency ν/R expressed in the Rydberg constant R_∞ as given by Cauchois and Hulubei [15]) with $RE\lambda_s$ (R and $E\lambda_s$ are given explicitly by Cohen *et al.* [14]). The frequency ν/R used for the calculation was chosen in accordance with that used by Siegbahn and Edvarson [9]) which authors took the mean value of the combinations $K\beta_3-L\beta_4$, $K\beta_1-L\beta_3$ and $K\alpha_1+L\alpha_1-L\beta_9$ as given by Cauchois and Hulubei, because the Bi $K-L_I$ transition corresponding directly to the frequency to be used is forbidden and thus very weak.

As shown for the case under consideration [9]) the following expression can be used for the determination of the relative error in the $B\rho$-values:

$$\frac{\Delta B\rho}{B\rho} = +0.65\frac{\Delta h/e}{h/e} + 0.65\frac{\Delta\nu}{\nu} - 3.3\frac{\Delta\alpha}{\alpha},$$

where the small contributions in consequence of the uncertainties in m/e and the velocity of light have been neglected. The probable relative errors in ν and h/e are 8 parts and 3.6 parts in 10^5 respectively. With these errors and the error in α given above, the relative error in $B\rho$ is obtained by quadratic addition. The computations result to

$$(B\rho)_F = (1388.28\pm0.20)\times10^{-6}\,\text{Wb/m},$$
$$(B\rho)_I = (1753.78\pm0.27)\times10^{-6}\,\text{Wb/m}.$$

It is interesting to note that, if we could neglect the error in α by increasing the resolution and the accuracy of the different parts of the instrument, the absolute errors in the above $B\rho$-values caused by the errors in the X-ray data and in the fundamental constants should be 0.08 and 0.10×10^{-6} Wb/m for the F- and I-line respectively. This means that under optimum experimental conditions there remains an error of about 6 parts in 10^5 in the determination of the momenta by this method, mainly due to uncertainties in the X-ray data.

5. Calibration Measurements

For calibration measurements several conversion lines occurring in the spectrum of the ThB active deposit have been used. These lines belong to the best known calibration lines, due to the fact that almost ideal sources can be obtained very easily. The A-, B-, F-, I-, Ia- and J-lines (notation from Ellis [16])), which cover the region from 25—235 keV, have been measured very accurately by Siegbahn and Edvarson [9]) with their iron-free double-focusing instrument. The L-line (422 keV) and the X-line (2.5 MeV) are measured by Lindström [17]) in a semicircular iron containing spectrometer. Other references are given in table 3. This whole range of calibration lines has been measured with the present instrument, partly to investigate its properties with respect to linearity and partly to check the results of the above mentioned authors. Unfortunately, it was not possible with the attainable RdTh source (about 1 millicurie) to prepare strong enough sources to measure all lines at the highest possible resolution. Therefore we performed the calibration in three steps:

a. the strongest lines (the F- and I-line) at a resolution of 0.018 %;
b. the J- and L-line at a resolution of 0.057 %;
c. the very weak X-line at a resolution of 0.12 %.

For reasons given in section 5.1 we did not investigate the low energy *A*- and *B*-lines.

5.1. EXPERIMENTAL CONDITIONS

5.1.1. *Source preparation and adjustment*

The sources are prepared on wires brought into a vessel containing RdTh. The RdTh decays through α-emission to Tn(54 sec). This noble gas diffuses throughout the vessel and decays in its turn to ThA (0.16 sec) and ThB (10 h). These atoms are left in an ionized state and can therefore be collected on the wire which is kept at a negative potential (e.g. 800 V). In this way very thin layers of the activity will be formed on the surface of the wire. However, sources prepared in this way are not quite ideal for two reasons. Firstly with thin wires it is difficult to restrict the activity to the front side only, which means that electrons emitted from the sides of the wire will loose energy when travelling through part of the wire. These electrons will contribute to the low energy side of the line. Secondly the active atoms will penetrate into the backing due to diffusion of the Tn and also due to α-recoil. This again will cause broadening of the low energy side of the lines. Extraction of the activity from an activated clean Pt wire with a drop of pure HNO_3 and evaporation to dryness onto a flat source backing [18]) seems to be the best method to avoid both source effects, but other difficulties are introduced then. Thus we used wires as a source backing material. Experimentally we only found a low energy tail for the A- and B-line with energies of 25 and 36 keV respectively. Therefore for the present we decided to refrain from determining the $B\rho$-values of these lines.

Three copper wires with a diameter of 0.07, 0.11 and 0.6 mm have been prepared. Before bringing them into the RdTh vessel, the wires were soldered to the source holder. The thinnest wire, (see VW) moreover, was stretched with a small string fitted to the source holder. Masks have been used to restrict the activity to the desired height of the source.

Evidently the use of small sources asks for a very careful alignment in the spectrometer relative to the counter slit, otherwise the line will be seriously broadened. Therefore the thinnest wire (0.07 mm) has been aligned as follows:

The source holder with the active wire was clamped to a construction fitted to the bottom of the source holder tube in such a way that an adjustment of the stretched wire relative to the axis of the supporting tube was possible. This relative position could be checked with an optical system. The relative position of the wire giving the smallest line width is determined by a trial and error procedure. This procedure has shown to be effective to obtain a resolution for the ThB I-line as low as 0.018 %.

5.1.2. *Instrumental conditions*

The dimensions of the sources and counter slits, used during the three runs, as well as the opening angles are given in table 1. These data have been chosen such that the contribution to the line width is about the same for the different components. The temperature stability of the coils during the measurements is also indicated; only for run A it was necessary to keep the fluctuations of the temperature within 0.2° C, to avoid relatively large errors due to coil temperature fluctuations (see VW). Possible imperfections in the external field compensa-

TABLE 1

Instrumental conditions

Run	Source dimensions in mm		Counter slit width in mm	Opening angles in radians		Fluctuations of the coil temperature
	height	diameter of the wire		γ_e	γ_s	
A	10	0.07	0.10	0.013	0.05	±0.2° C
B	12	0.11	0.20	0.019	0.10	±1° C
C	15	0.60	0.75	0.042	0.20	±1° C

tion system may contribute up to 5×10^{-8} Wb/m² to the spectrometer magnetic field; the systematic character of the contribution, however, causes errors in the $B\rho$-determinations in consequence of this field to be negligibly small compared to other sources of error in this work. The positions of the top of the lines have been checked several times from which we conclude that the influence of long term drifts could be neglected.

5.2. RESULTS

Fig. 3 shows the F- and I-line measured in run A. This particular line pair (K- and L_I-line of the 238 keV transition in ^{212}Bi) has been used to study the influence of the natural line width on the line position. This investigation has

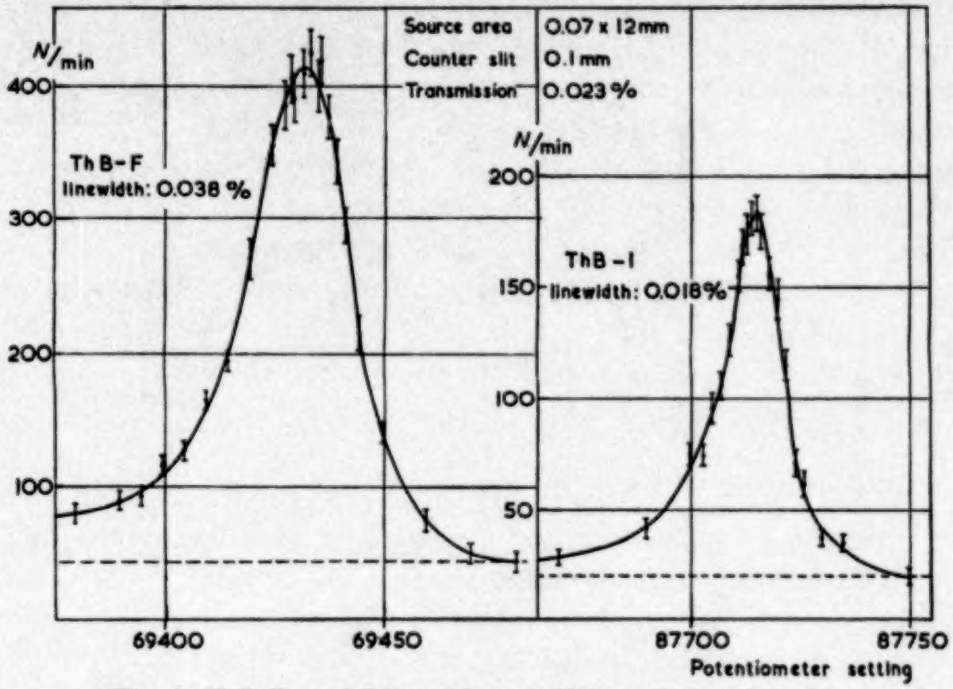

Fig. 3. ThB F- and I-line taken at high resolution (run A)

been treated in section 2.1. As can be seen from fig. 1 of that section the line shape of the F-line can readily be obtained by folding the I-line with a resonance curve (width 52 eV); this indicates at the same time that source effects do not noticeably contribute to these line shapes. The relative line positions of the two lines have also been determined from this procedure. In table 2 the potentiometer readings for these positions are given together with the readings of the lines measured in run B and run C; these latter positions have been taken to be the intersections of the high and low energy slopes of the line profiles. Table 2 gives also the line widths at which the peaks are measured.

TABLE 2

Line half-widths R and potentiometer readings P. (The null resistance of the potentiometer (0.6 units) should be added to each of the readings)

Line	run A		run B		run C	
	R in %	P	R in %	P	R in %	P
F	0.038	69434	0.08	30504	0.16	15133
I	0.018	87714.5	0.057	38535	0.13	19118
J			0.050	39793		
L			0.055	57273	0.12	28415
X					0.12	108890

In fig. 4 the X-, L-, I- and F-line are plotted on reduced scales to allow comparison of their shapes. Apart from broadening of the F-line, mainly due to natural line width, the curves indicate a constant line shape for a widely extended energy region.

From table 2 the ratio of the positions of the I- and F-line could be determined for the different runs:

run A: $I/F = 1.26328 \pm 0.000035$,

run B: $I/F = 1.26328 \pm 0.00010$,

run C: $I/F = 1.26332 \pm 0.00014$.

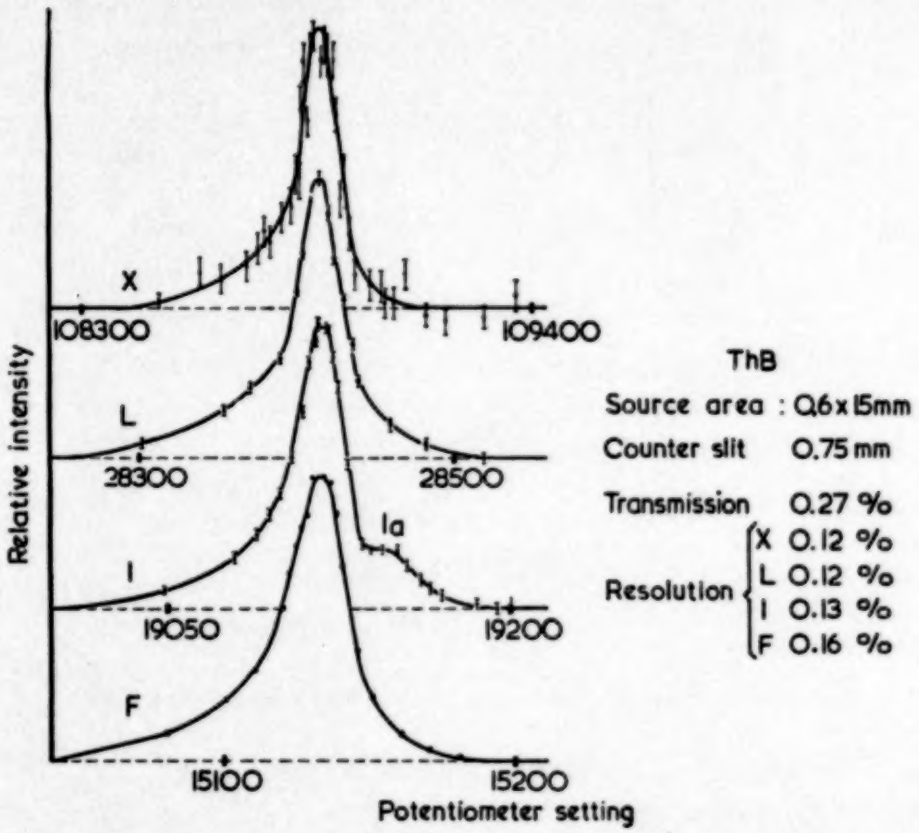

Fig. 4. Conversion lines of ThB active deposit (run C) showing the constant character of the line shape.

Siegbahn and Edvarson [9]) report that the ratio I/F becomes higher for better resolutions; they do not mention the magnitude of this effect. The above given ratios together with some results found at resolutions ranging from 0.02 % to 0.13 % for the ThB I-line are shown in fig. 5.

This figure shows that there is certainly not a pronounced trend with the resolution: all measurements are consistent with a ratio of say 1.26330. If anything, the trend is just the reverse of that reported by Siegbahn and Edvarson. Any way, in the present work the effect is certainly of minor importance.

The $B\rho$-values for the F- and the I-line (run A) are already given in the preceding section:

$$(B\rho)_F = 1388.28 \pm 0.15 \text{ Wb/m},$$
$$(B\rho)_I = 1753.78 \pm 0.20 \text{ Wb/m}.$$

The errors assigned to these $B\rho$-values are somewhat reduced relative to those given in the preceding section, because errors in the potentiometer readings due to possible sources of error in the bridge circuit are neglected for this case. Indeed we felt justified to do so, because of the consistency between the I/F ratios as found from measurements at resolutions below 0.05 %, which measurements are carried out using different measuring resistances R_m (see VW, fig. 13) and thus different ranges of the potentiometer.

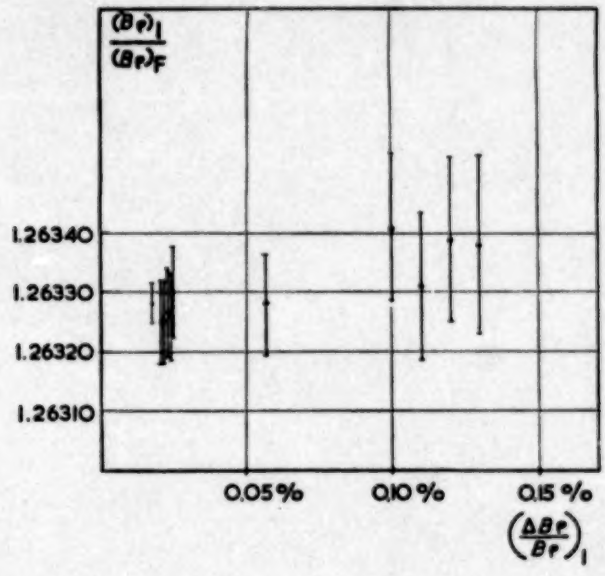

Fig. 5. I/F ratios plotted against the half-width of the I-line.

Using these two $B\rho$-values for calibration in runs B and C we found for the $B\rho$-values of the new lines measured in these runs:

$B\rho$-values in 10^{-4} Wb/m

	run B	run C
J	1811.03±0.21	
L	2606.55±0.30	2606.66±0.33
X		9989.0 ±1.5

The results of the present work are summarized in table 3 for comparison with earlier reported values.

Comparison of the tabulated values led to the conclusion that in general the agreement is rather good. Some remarks, however, should be made. All our

TABLE 3

$B\rho$-values in 10^{-6} Wb/m

Ref.	F	I	J	L	X	method	instrument
[18])					9988.4 ±2.0	absolute	semi circular spectrograph
[20])	1388.43±0.18	1753.92±0.16		2606.9 ±0.6		against W $K\alpha_1$	curved crystal
[17])	1388.56±0.15	1754.01±0.20		2607.17±0.30	9986.7±1.5	Bi $K\text{-}L_1$ and absolute	semi circular spectrograph
[21])				2607.1 ±0.6		against $2m_0c^2$	iron containing d.f. instrument
[22])	1388.56±0.21	1754.0 ±0.7		2606.9 ±1.0		against 18.5 keV electrons	ironfree lens-spectrometer
[9])	1388.44±0.10	1753.91±0.14	1811.11±0.15			Bi $K\text{-}L_1$	ironfree d.f. instrument
[23])	1388.37±0.11	1753.85±0.09				against W $K\alpha_1$	curved crystal
present work	1388.28±0.15	1753.78±0.20	1811.03±0.23	2606.60±0.30	9989.0±1.5	Bi $K\text{-}L_1$	ironfree d.f. spectrometer

$B\rho$-assignments (apart from the X-line) are lower than the other values. Although the error assignments are such that no serious discrepancies exist, we see that the effect is systematic. Indeed we systematically found the I/F ratio, the normal for all our $B\rho$-determinations, to be higher than reported by Siegbahn and Edvarson [9]). Therefore we refrained from averaging many results obtained for this ratio as done by Siegbahn and Edvarson. These authors have used the mean value of 20 determinations of this ratio obtained in essentially the same arrangement, which explains their low error assignment. Unless systematic sources of error can be excluded we think this a questionable procedure.

The $B\rho$-value of the X-line (2.5 MeV) has been obtained from the ratio of its position and those of lines as low as 150 keV and 220 keV. The agreement with the direct measurements of Brown [19]) and Lindström [17]) shows the linear behaviour of the present instrument to be satisfactory. This fact supports the hope that future determinations of conversion line energies, covering the energy region up to 2.5 MeV, will succeed with an accuracy comparable to that of the F- and I-line.

The author wishes to thank Prof. P. C. Gugelot for his continuous interest in this work and Prof. A. H. Wapstra for his invaluable advice and for many stimulating discussions. He also wishes to acknowledge the assistance during most of the measurements of Mrs. Salomons-Grobben and Mr. J. H. Dijkstra.

This work constitutes part of the research programme of the Institute for Nuclear Research, made possible by financial support from the Foundation for Fundamental Research of Matter (F. O. M.) and the Dutch Organiszation for Pure Scientific Research (Z. W. O.).

References

1) C. de Vries and A. H. Wapstra, Nuclear Instruments, to be published
2) K. Siegbahn, Ark. f. Mat. Astr. Fys. **28**B, No. 6 (1941); **30**A No. 20 (1944)
3) H. Slätis and G. Lindström, Phys. Rev. **88** (1952) 1429
4) F. Shull and D. Dennison, Phys. Rev. **71** (1947) 681; **72** (1947) 256
5) J. H. Dijkstra and C. de Vries, Nuclear Instruments, to be published
6) M. Mladjenovic, Ark. f. Fysik **8** (1954) 27
7) G. Lindström, Ark. f. Fysik **4** No. 1 (1951)
8) H. Slätis, Ark. f. Fysik **6** (1953) 415
9) K. Siegbahn and K. Edvarson, Nuclear Physics **1** (1956) 137
10) L. Marton, L. B. Leder and H. Mendlowitz, Advances in Electronics and Electron Phys. **7** (1955) 183
11) E. Sokolowski, Ark. f. Fysik **15** (1959) 1
12) C. Nordling, Ark. f. Fysik **15** (1959) 397
13) C. de Vries and J. H. Dijkstra, Nuclear Instruments, to be published
14) E. R. Cohen, J. W. M. DuMond, T. W. Layton and J. S. Rollett, Rev. Mod. Phys. **27** (1955) 363
15) Y. Cauchois and H. Hulubei, Table de constantes et données numériques (Herman, Paris, 1947)

16) C. D. Ellis, Proc. Roy. Soc. **138A** (1932) 318; **143A** (1934) 350
17) G. Lindström, Ark. f. Fysik **4** (1952) 1; Phys. Rev. **87** (1952) 678
18) J. G. Siekman, Thesis, Groningen (1959)
19) W. L. Brown, Phys. Rev. **83** (1951) 271
20) D. E. Muller, H. C. Hoyt, D. J. Klein and J. W. M. DuMond, Phys. Rev. **88** (1952) 775
21) A. Hedgran, Ark. f. Fysik **5** (1952) 1
22) D. I. Meyer and F. H. Schmidt, Phys. Rev. **94** (1954) 927
23) P. Bergvall, Ark. f. Fysik **7** (1960) 125

3.B:4.E

Nuclear Physics **18** (1960) 446—453; © *North-Holland Publishing Co., Amsterdam*

Not to be reproduced by photoprint or microfilm without written permission from the publisher

PRECISION MEASUREMENTS OF ENERGIES OF GAMMA-RAYS FOLLOWING THE DECAY OF SOME GOLD ISOTOPES

C. DE VRIES and J. H. DIJKSTRA

Institute for Nuclear Research, Amsterdam

Received 27 May 1960

Abstract: The energies of eight gamma-rays occurring in the decay of some gold isotopes have been determined from their conversion-line momenta as measured with an iron-free double-focusing spectrometer. The $B\rho$-assignments to the lines following the decay of ^{194}Au, ^{196}Au, ^{196}Au (10 h) isomer and ^{198}Au are obtained by using the conversion lines of the 158 keV transition in ^{199}Hg as calibration line. Absolute $B\rho$-values of the latter lines could be determined applying the self-consistent method of Siegbahn. Disregarding the calibration uncertainty (about one part in 10^4) the accuracy reached in the energies of the gamma-rays is about 7 parts in 10^5. Our value 411.766 ± 0.028 keV for the energy of the well known E2 transition in ^{199}Hg is in nice agreement with other values, some of which have been determined directly with a curved crystal.

1. Introduction

In the preceding paper [1]) (henceforward to be referred to as VR) one of the authors has presented calibration measurements carried out with an ironfree double focusing instrument of the Siegbahn-Edvarson type. From these measurements it can be concluded that the linear behaviour of this instrument allows an accuracy of a few parts in 10^5 in the relative momenta of conversion lines. In this work we present energy determinations of gamma-rays involved in a further study of the decay scheme of the 10 h ^{196}Au isomer as proposed by Van Lieshout *et al.* [2]): a complete description of this study will be published elsewhere.

Although the energies of some of the gamma-rays involved in this work have been reported with an accuracy comparable with that which can be obtained with the present instrument, we thought it worthwhile to determine independently the absolute $B\rho$-values of the conversion lines. The investigation is carried out in two steps: 1) the determination of the absolute $B\rho$-values of the conversion lines of the 158 keV transition in ^{199}Hg using the self consistent method of Siegbahn (see VR) and 2) the determination of the $B\rho$-values of the conversion lines relative to those of the 158 keV transition in ^{199}Hg.

The second step has been performed with a separate source, thus allowing for a better resolution (0.06 %) than was feasible with the source-material containing the other gold isotopes (0.1 %).

2. Absolute $B\varrho$-Values of the Conversion Lines of the 158 keV Transition in ^{199}Hg

Chemical separation of the gold fraction from neutron irradiated pure platinum (Harwell, one week at a flux of 10^{13}/cm^2 sec) resulted in carrier-free and isotopically pure ^{199}Au. The high specific activity of this material allowed for the preparation of a source of high quality. The preparation was performed by the electroplating technique. The $^{199}AuCl_3$, diluted in 0.1 N HCl, was plated onto a 600 μg/cm^2 silver coated, mylar film. The activity could be restricted to the desired area (0.3×10 mm) by means of a slit in the electroplate arrangement. The slit is machined such that the source position is well defined relative to the source holder frame on which the mylar foil is stuck. In its turn the source holder is brought to a well defined position in the spectrometer. As described in VR this procedure assures an accurate alignment of the narrow source relative to the counter slit, which for this investigation had the dimensions 0.3×20 mm. The opening angles γ_ρ and γ_z during the measurements given below were 0.03 and 0.12 radians, respectively. The temperature fluctuations of the coils have been kept within 0.2° C in order to keep the errors due to these fluctuations within 1 part in 10^5 [1]). The compensation of the external field perpendicular to the plane of the electron orbits has been checked with the search coil attached in the median plane and near to the central orbit of the spectrometer, both before and after the measurements. During the measurements the automatic compensation of fluctuations of this field [1]) helped to make the contribution to the errors in the positions of the conversion lines due to external fields negligible. To each current reading an error of 2 parts in 10^5 has been assigned to account for possible errors in the bridge circuit [1]).

Different runs have been made on the conversion lines of the 158 keV transition. First the whole line profiles of the K-, L- and M-lines were measured in order to determine relative conversion coefficients; these measurements are discussed elsewhere [3]). Fig. 1 shows the profiles of the L- and M-subshell conversion lines. The K- and L_{III}-line thus obtained have been used, together with those measured with a much thicker source, for the investigation of the influence of source thickness given in VR. For the special purpose under consideration the K-, L_{II}- and L_{III}-lines have been measured alternatively in four runs to check for possible long term drift influences on the line positions. To keep the measuring time short only the upper parts of the line shapes have been investigated. During these runs (measuring time about 3 hours) the positions of the lines did not change by a noticeable amount (less than 2 parts in 10^5). The line positions (intersection of the high and low sides of the lines) are representative for the true line positions to a high extent as can be deduced from (a) the investigation of the influence of source thickness as given in VR for the particular source used here and (b) the investigation of the influence of the different

natural widths of the lines given in VR for the ThB F- and I-lines. For the case under consideration a similar matching procedure of the L_{III}-line with the K-line

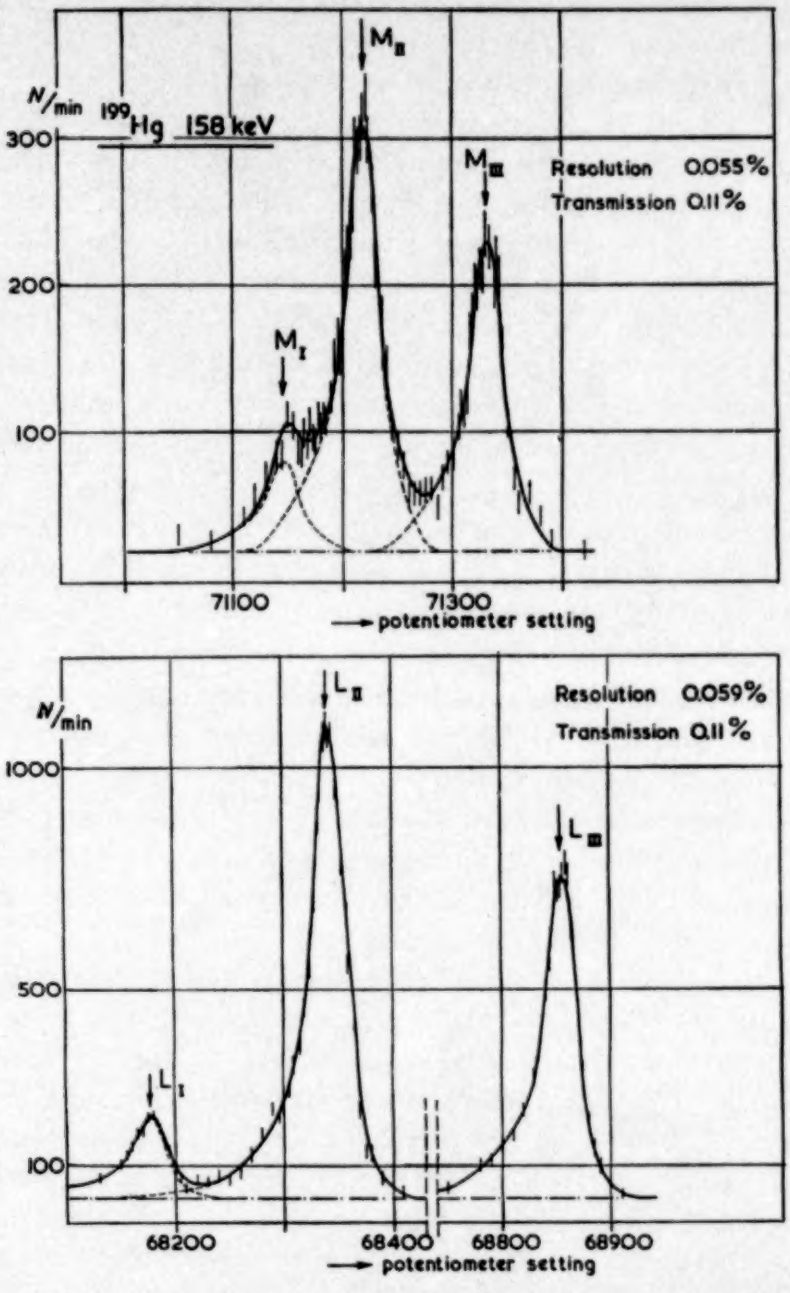

Fig. 1. Conversion spectra of the 158 keV transition in ^{199}Hg.

has been carried out †, confirming the experience obtained in VR, section 2.1 that the used line position definition yields reliable results.

In table 1 the potentiometer readings for the K-, L_{II}- and L_{III}-lines are given.

† As a result we found (50±5) eV for the difference in natural widths of the atomic levels in ^{80}Hg corresponding to the K- and L_{III}-conversion lines (see also VR, section 2.1 note).

The L_{II}/K and the L_{III}/K values found from these readings have been used to determine the absolute $B\rho$-values of these lines. The differences in binding energies are taken to be $K\alpha_1 = 70.819 \pm 0.003$ keV and $K\alpha_2 = 68.895 \pm 0.003$ keV,

TABLE 1

$B\rho$-values of conversion lines of the 158 keV transition in ^{199}Hg

Line	Resolution	Potentiometer readings [a])	$B\rho$-values in 10^{-4} Wb/m calculated from		Adopted values
			L_{II}/K	L_{III}/K	
K	0.10 %	47896	958.353±0.125	958.347±0.125	958.350±0.095
L_{II}	0.06 %	68343	1367.478±0.180		1367.474±0.137
L_{III}	0.06 %	68854		1377.693±0.180	1377.698±0.137

[a]) The null resistance of the potentiometer (0.6 units) should be added to these readings.

which values are reported by Beckman and Bergvall [4]). The results of the calculations are also given in table 1. The errors are computed in essentially the same way as indicated in VR, section 4. For the conversion from momentum to energy we adopted the $B\rho$-values given in the last column of the table. Using the value 12.285 keV for the Hg-L_{III} binding energy as measured by Sokolowski [5]), we obtain for the energy of the 158 keV gamma-ray transition

$$E_\gamma = (158.335 \pm 0.015)\text{keV}.$$

For a comparison with earlier reported values we refer to the end of the next section.

3. Energy Determinations of Gamma-Rays occurring in the Decay of ^{194}Pt, ^{196}Pt, ^{196}Au Isomer and ^{198}Hg

With the present instrument a further study of the decay scheme of the 10 h ^{196}Au isomer proposed by Van Lieshout *et al.* [2]) has been undertaken; here we will focus our attention on the energy determinations of the gamma-rays involved.

^{196}Au is obtained by bombarding Pt with (20 MeV) deuterons. Then other isotopes are also produced, e.g. ^{194}Au, ^{198}Au and ^{199}Au. As these isotopes can be obtained carrier-free, sources can be produced, which are suitable to perform precision measurements of the conversion lines. In fact the specific activity of the source (1 × 15 mm) prepared by electroplating allowed measurements of the most important conversion lines of ^{196}Au isomer, together with several of the lines belonging to the above mentioned Au isotopes, at a resolution of about 0.1 %. The transmission during this investigation was 0.25 % whereas the counter slit dimensions were 1 × 20 mm. The temperature of the coils was kept

constant at (25±1) °C. The other instrumental conditions were the same as in the preceding section.

Only the upper halves of the line profiles were determined from the conversion lines measured. Each line position was checked at least two times. During the measuring time (extending over two days) no serious long term drifts were observed.

The $B\rho$-assignments to the lines are obtained using the conversion lines of the 158 keV transition in ^{199}Hg as calibration lines (see section 2). This calibration method yielded more accurate results than should have been the case with the internal calibration method of Siegbahn. Apart from that the latter method yielded results for the $B\rho$-values which only deviate a few parts in 10^5 from those obtained with the method adopted here.

Dividing the $B\rho$-values of the calibration lines by the corresponding potentiometer readings of these lines in the present investigation gives three values for the calibration constant,

$$C_{158K} = 455381 \pm 30,$$
$$C_{158L_{II}} = 455400 \pm 30,$$
$$C_{158L_{III}} = 455377 \pm 30.$$

The average value is $C = 455386 \pm 17$.

The errors assigned here to the separate calibration constants are only those due to line position uncertainties for the determinations of which we refer to VR. The error in the $B\rho$-values themselves (1 part in 10^4) will be taken into account later on.

Applying the above given calibration constant to the potentiometer readings of the other lines yields the $B\rho$-assignments given in table 2. The uncertainties in the positions of these lines (6.7 parts in 10^5) are added quadratically to the error in the calibration constant.

Conversion of these momentum values and their errors to energies has been carried out with the aid of the tables of Gerholm [6]). Adding to these energies, also given in table 2, the corresponding binding energies yielded the different gamma-ray energies given in the table. Part of these binding energies are taken to be those measured by Sokolowski [5]) and Beckman and Bergvall [4]), whereas the remaining ones are listed by Wapstra, Nijgh and Van Lieshout [7]). The small errors in these binding energies are not taken into account.

In the last column of table 2 are given the average values for the gamma-ray energies. The errors in these values are internal errors R_i as computed by normal statistical methods, since it appears unlikely that the errors assigned to the individual results would act in the same way on the different conversion line values. In all cases the external error R_e divided by R_i, the consistency ratio, is smaller than one. The calibration uncertainties are given within brackets. The final results are given in table 3 for comparison with earlier reported values.

TABLE 2

Results of the absolute $B\rho$-determination (calibrated against the values given in table 1)

Isotope	Line	$B\rho$-value (10^{-6} Wb/m)	Energies (keV) of		Weighted average gamma-ray energy [a]) (keV)
			Conversion line	Gamma-ray	
^{196}Au isomer	148 K	901.300±0.085	67.043±0.012	147.769±0.012	
	L_I	1309.690±0.125	133.429±0.023	147.784±0.023	147.773±0.009
	L_{II}	1313.060±0.125	134.045±0.023	147.779±0.023	(±0.013)
	L_{III}	1322.896±0.125	135.849±0.023	147.768±0.023	
	175 K	1081.223±0.100	94.139±0.017	174.865±0.017	
	L_I	1453.182±0.140	160.506±0.027	174.861±0.027	174.867±0.011
	L_{II}	1456.461±0.140	161.144±0.027	174.878±0.027	(±0.018)
	L_{III}	1465.705±0.140	162.948±0.027	174.867±0.027	
^{194}Pt	294 K	1720.813±0.165	215.133±0.035	293.525±0.035	
	L_I	2012.533±0.190	279.666±0.044	293.541±0.044	293.528±0.020
	L_{II}	2015.174±0.190	280.271±0.044	293.545±0.044	(±0.037)
	L_{III}	2022.460±0.190	281.941±0.044	293.505±0.044	
	328 K	1881.154±0.180	250.037±0.039	328.429±0.039	
	L_I	2162.856±0.205	314.570±0.048	328.445±0.048	328.437±0.022
	L_{II}	2165.406±0.205	315.170±0.048	328.444±0.048	(±0.041)
	L_{III}	2172.601±0.205	316.866±0.048	328.430±0.048	
	622 K	3077.271±0.290	543.618±0.077	622.010±0.077	622.010±0.077 (±0.081)
^{196}Pt	356 L_I	2277.294±0.215	341.781±0.052	355.656±0.052	
	L_{II}	2279.753±0.215	342.372±0.052	355.646±0.052	355.651±0.030
	L_{III}	2286.903±0.215	344.088±0.052	355.652±0.052	(±0.055)
^{198}Hg	412 K	2222.375±0.210	328.658±0.050	411.762±0.050	
	L_I	2503.257±0.235	396.922±0.059	411.765±0.059	411.776±0.028
	L_{II}	2505.853±0.235	397.565±0.059	411.774±0.059	(±0.053)
	L_{III}	2513.731±0.235	399.519±0.059	411.804±0.059	

[a]) The calibration uncertainty is given between brackets.

4. Discussion

Table 3 shows that our value for the energy of the 412 keV gamma line agrees with those of Muller *et al.*, Lind and Hedgran, and the recent value of Bergvall, but that there is some disagreement with the 158 keV line as measured by Bäckström *et al.* and even more with the 328 keV line as reported by Ryde and Andersson. The $B\rho$-ratio of the 412 K-line and the 158 K-line as follows from the results given in the third column of table 3 deviates about 3 parts in 10^4 from that measured in the present work. Our calibration measurements described in VR make it rather improbable that the linearity of our instrument would be so bad as to cause the above deviation. Moreover, the present measurements

TABLE 3

Gamma-ray energies (keV)

Isotope	Line	Earlier work			Present work
		Values [a])	Ref.	Method	
^{199}Hg	158 γ	158.396±0.025	[8])	d. f. sp. (ironfree)	158.335±0.015
^{196}Au m	148 γ	149 ±2	[2])	scint. sp.	147.773±0.016
	175 γ	176 ±2	[2])	scint. sp.	174.867±0.021
^{194}Pt	294 γ	293.0 ±0.3 291.3 ±0.5	[9]) [10])	d. f. sp. lens sp.	293.528±0.042
	328 γ	329.10 ±0.08 328.1 ±0.2 326.7 ±0.5	[11]) [9]) [10])	curved crystal d. f. sp. lens sp.	328.437±0.047
	622 γ	620.1 ±1.0	[9])	d. f. sp.	622.01 ±0.11
^{196}Pt	356 γ	354.0 ±0.4	[10])	lens sp.	355.651±0.062
^{198}Hg	412 γ	411.803±0.036 411.799±0.040 411.770±0.033	[12]) [13]) [14])	curved crystal d. f. sp. curved crystal	411.776±0.060

[a]) To allow comparison these values are recalculated using the list of fundamental constants given by Cohen *et al.* [15]).

even yield an independent check on the linearity, since the sum relation between the lines in ^{194}Pt (using the values of table 2, disregarding the calibration uncertainty) is fulfilled with a precision of 45±90 eV. We are therefore inclined to believe that in the above mentioned cases our values are probably more dependable.

The authors wish to thank Prof. P. C. Gugelot for his interest during the course of the work. We are greatly indebted to Prof. A. H. Wapstra for invaluable discussions. The authors would like to thank also Mrs. N. Salomons Grobben for taking part in the measurements and Miss J. C. Kapteyn for performing the chemical separations.

This work constitutes part of the research program of the Institute for Nuclear Research, made possible by financial support from the Foundation for Fundamental Research of Matter (F. O. M.) and the Dutch Organization for Pure Scientific Research (Z. W. O.).

References

1) C. de Vries, Nuclear Physics **18** (1960) 428

2) R. van Lieshout, R. K. Girgis, R. A. Ricci, A. H. Wapstra and C. Ythier, Physica **25** (1959) 703; C. Ythier, Thesis (Paris, 1959)

3) C. de Vries, E. J. Bleeker and N. Salomons-Grobben, Nuclear Physics **18** (1960) 454
4) O. Beckman and P. Bergvall, Phys. Rev. **114** (1959) 1280
5) E. Sokolowski, Ark. f. Fysik **15** (1959) 1
6) T. R. Gerholm, in Handbuch der Physik, Band XXXIII
7) A. H. Wapstra, G. J. Nijgh and R. van Lieshout, Nuclear spectroscopy tables (North-Holland Publishing Company, Amsterdam 1959)
8) G. Bäckström, O. Bergman and J. Burde, Nuclear Physics **7** (1958) 263; **15** (1960) 566
9) M. W. Johns and S. V. Nablo, Phys. Rev. **96** (1954) 1599
10) M. T. Thieme and E. Bleuler, Phys. Rev. **101** (1956) 1031; **102** (1956) 195
11) N. Ryde and B. Andersson, Proc. Phys. Soc. **68** B (1955) 1117
12) D. E. Muller, H. C. Hoyt, D. J. Klein and J. W. M. DuMond, Phys. Rev. **88** (1952) 775
13) D. A. Lind and A. Hedgran, Ark. f. Fysik **5** (1952) 29
14) P. Bergvall, Ark. f. Fysik **17** (1960) 125

3.B

Nuclear Physics **18** (1960) 454—472; © *North-Holland Publishing Co., Amsterdam*

Not to be reproduced by photoprint or microfilm without written permission from the publisher

ABSOLUTE AND RELATIVE CONVERSION DETERMINATIONS OF PURE E2 TRANSITIONS OCCURRING IN ^{198}Hg, ^{199}Hg, ^{194}Pt AND ^{196}Pt

C. DE VRIES, E. J. BLEEKER and Mrs. N. SALOMONS-GROBBEN

Instituut voor Kernphysisch Onderzoek, Amsterdam

Received 10 June 1960

Abstract: Conversion coefficients of some pure E2 transitions following the decay of some gold isotopes have been determined using an iron-free double focusing spectrometer of the Siegbahn-Edvarson type. The α_K of the 412 keV transition in ^{198}Hg, the 328 keV transition in ^{194}Pt and the 354 keV transition in ^{196}Pt are determined using the external-internal method as recently improved by Hultberg and Stockendal. Our results indicate that the theoretical values for these conversion coefficients are 10 to 20 % too high. Some additional measurements make the explanation of the mentioned deviations by systematical errors improbable. Experimental relative conversion coefficients (K/L, $L_I/L_{II}/L_{III}$) of the 412 keV transition in ^{198}Hg indicate the deviations found for the absolute K-conversion coefficients to be present also for the L-shells. Our results for the ratios L/M of the 412 keV transition in ^{199}Hg and $M_I/M_{II}/M_{III}$ of the 158 keV transition in ^{199}Hg suggest a correction factor of 0.6 to be applied to the theoretical values of the conversion coefficients for the M-subshells, which latter values are not corrected for screening.

1. Introduction

1.1. THEORETICAL

Accurate experimental values for the internal conversion coefficients (i.c.c.) have become of interest the past few years because experimental determinations have given evidence for the i.c.c. being dependent on the properties of nuclei as well. Tralli and Goertzel [1]) and Sliv and Listengarten [2]) first realized that the finite dimensions of the nucleus can have a considerable influence on the i.c.c. Firstly, the dimensions of the nucleus will change the electron wave functions relative to those used by Rose *et al.* [3]) for the point nucleus approximation. Secondly, the movement of the nuclear particles in the field of the electrons penetrating the nucleus gives rise to new matrix elements that allow only the emission of conversion electrons and therefore may alter the conversion coefficients. Mostly the influence of these matrix elements is small compared with that of the "normal" matrix elements. Therefore, Sliv and Band [4]) took them into account in an approximate way, assuming that the nuclear currents are limited to the nuclear surface. On the other hand, Rose [5]) only considered the first, static effect in his finite size corrected tables, but together with Green [6]) he gave the data necessary to correct these tables for the influence of

the dynamic structure effect. The remarks above would indicate that the values of Sliv and Band and those of Rose should be nearly identical and indeed the differences are mostly small. Church and Weneser [7]) first pointed out that the contribution due to the dynamical effects may lead to anomalous conversion coefficients as shown especially for some slow M1 transitions. These anomalies are then caused by the increased importance of the "anomalous" matrix elements. Thus, conversion coefficient measurements may yield information about nuclear structure, as pointed out by Church and Weneser. An application of the collective model to the Church and Weneser theory given by Reiner [8]) shows that very large deviations of the Sliv conversion coefficients can occur for M1 transitions. Nilsson and Rasmussen [9]) studied the anomalies due to the intranuclear process for retarded E1 transitions both theoretically and experimentally (see also Asaro *et al.* [10])).

More or less parallel with the theoretical developments several accurate experimental values became available which in general gave support to values corrected for finite size. Wapstra and Nijgh [11]) report some measurements of conversion coefficients of some M1 transitions in the higher Z region. These measurements give values somewhat lower than the theoretical values corrected for static effects only, which suggests that dynamic effects are operative. Confirmation of the results of Wapstra and Nijgh has been obtained by Nielsen *et al.* [12]) and by McGowan and Stelson [13]).

The theoretical values of Sliv and Band and Rose for E2 transitions agree very well with each other, hence the dynamic finite size effects are expected to be small for these transitions. However, experimental results reported by McGowan and Stelson [14]) and by Wapstra *et al.* [15]) for unhindered E2 transitions indicate that possibly also the i.c.c. belonging to these transitions are dependendent on the nuclear structure. Also experimentally obtained relative L-subshell ratios for the E2 transition in the decay of ^{198}Hg are reported which disagree with theory [16]). Therefore an attempt has been made to obtain additional information for the E2 transitions.

1.2. EXPERIMENTAL

Absolute conversion coefficients are defined as N_e/N_γ: i.e. the number of (e.g. K-) conversion electrons relative to the number of gamma-rays. N_e can be determined from the measurement of the conversion line in a magnetic spectrometer. The corresponding N_γ can be obtained indirectly in different ways, e.g. (a) from the number of beta transitions feeding the initial state or depopulating the final state of the transition involved and (b) from the number of photo electrons emitted from a converter due to the gamma radiation. The first method implies a determination of the intensity of the continuous beta spectrum. Apart from the fact that the method is only applicable for very simple decay schemes, the accuracy which can be reached depends on the quality of the source

and on the instrumental response for an extended energy region. The second method can in principle also be used for the determination of the i.c.c. of a transition occurring in a complicated decay scheme because it involves only the measurement of the internal and the external conversion peak of a particular gamma ray; no information on the decay scheme is required. On the other hand, however, precise determinations require accurate knowledge of the photo-electric differential cross-sections.

Both methods have been applied for the present investigation with the use of an iron-free double focusing beta-ray spectrometer reported by de Vries and Wapstra [17]). As shown by these authors this instrument ($E_{max} = 2.6$ MeV, $\beta = \frac{3}{8}$ and $\rho_0 = 300$ mm) allows for measurements at high resolution (in the order of a few parts in 10^4) as well as for measurements at high luminosity (resolution 0.5 % at a transmission of 1 % and a source area of 140 mm^2).

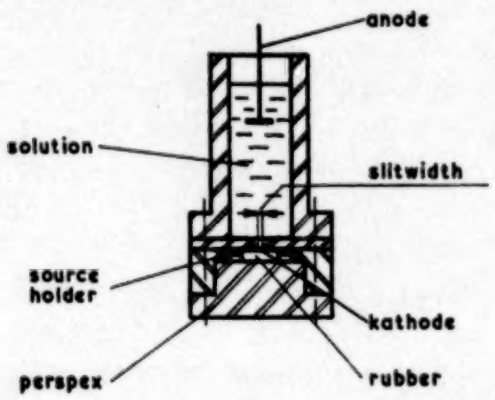

Fig. 1. Unit for preparing sources by electroplating.

Both qualities have shown to be useful for the present work. Absolute K-shell coefficients are determined for some pure E2 transitions in ^{194}Pt, ^{196}Pt and ^{198}Hg using the external-internal conversion method, the features of which are discussed in section 1.3. The measurements are described in section 2.1. For the E2 transition in the simple decay scheme of ^{198}Hg we also determined α_K from the ratio of the intensities of the internal K-conversion peak and the continuous spectrum, thus providing a check on the value obtained with the first method (see section 2.2). In section 3.1. measurements of the relative values of the i.c.c. of the latter E2 transition are presented which combined with the value of α_K yield information about the absolute conversion coefficients of the L-subshells and the M- and N-shells as well. For the 158 keV E2 transition in ^{199}Hg we determined the ratios K/L, $L_I/L_{II}/L_{III}$, L/M and $M_I/M_{II}/M_{III}$; the measurements and the results are given in section 3.2.

For all these measurements flat sources have been prepared by electroplating, using an arrangement as shown in fig. 1. The bottom plate of this perspex

equipment in which the slit is machined is interchangeable; thus the dimensions of the source area can be chosen in accordance with the requirements for a particular investigation. The source backing is pressed with a piece of rubber unto this bottom plate, assuring the acitive material to be restricted to the dimensions of the slit. The electroplating processes were performed with a solution of $AuCl_3$ in 0.1 N HCl at a current density of about 100 mA/cm^2. Further information about activities, thicknesses, backings and dimensions of the sources will be given in the different sections.

The opening angles in the spectrometer are chosen such that the line width due to spherical aberration approximately equals that due to the widths of the source and the counter slit. For the measurements described the G.M. counter was provided with defining slits varying from 0.3×20 mm to 3.2×30 mm. The counting rates are all below 15000 c/min [17]; corrections for dead time (0.38 msec) and decay are applied. Errors due to long termdrifts in the detector system are negligible as could be deduced from repeated checks at fixed points in the spectra. All the other instrumental conditions were essentially as described by de Vries and Wapstra [17]. The areas of the line profiles were determined with a planimeter. The errors assigned to the results are dependent on the statistics and on the extent to which the lines are resolved.

1.3. THE EXTERNAL-INTERNAL CONVERSION METHOD

This method has been improved considerably by Hultberg [18]. This author investigated carefully the photo-electric angular distribution for three different energies (412 keV, 662 keV and 1332 keV) using uranium as converter material. This angular distribution enters into the calculation of the conversion coefficient due to the fact that the external conversion electrons detected in the spectrometer are ejected at specified directions relative to the directions of the impinging gamma-rays. For an extensive treatment we refer to Hultberg [18]. The following formula applies to this determination:

$$\alpha_K = \frac{A_{in}}{A_{ex}} k \tau_K f_K db,$$

where A_{in} is the intensity of the internal conversion line, A_{ex} the intensity of the external conversion line, k the intensity ratio of external and internal source, τ_K the photo-electric cross section for the K-shell (barns/atom), f_K the correction factor to account for the anisotropical distribution of the external conversion electrons, d the thickness of the converter in mg/cm^2, and, finally, b the dimension factor $6.025 \times 10^4/M$ (atoms $\times$ cm^2/barns $\times$ mg), where M stands for the atomic weight of the converter atoms.

The formula given is valid if the transmission is the same for both the internal and the external conversion line measurements. In principle the same source may be used for both measurements ($k = 1$). However, we prefer to use two

sources because then counting rates differing by orders of magnitude for the two lines can be avoided. Moreover, the internal source can then be made approximately as large as the converter, which allows use of thinner sources, whereas at the same time the condition for equal transmission can be more accurately fulfilled.

The k-values for the investigations given under section 2.1 are obtained with an accuracy better than 3 % with a scintillation setup and in a special case also with a G.M. counter.

The converters used in the present investigations are made of gold rather than of uranium. The last material gives higher intensities, but high quality converters with accurately known weights could more easily be prepared from gold. Moreover, the distance in the momentum scale between the external and internal conversion lines in our investigations with Hg and Pt isotopes are then

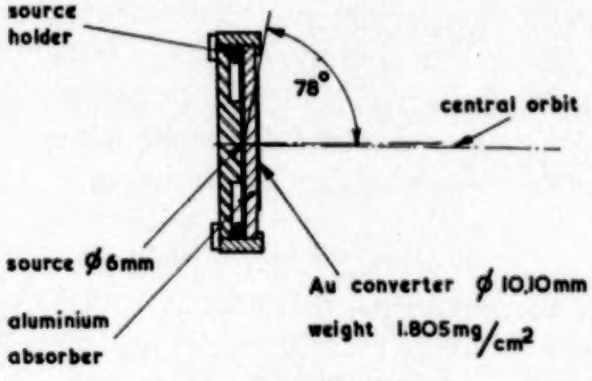

Fig. 2. External source-converter arrangement (circular geometry).

small; thus errors due to possible energy dependent effects, e.g. of the counter response, are avoided. The converters used (circular and rectangular ones) are made by stacking very thin commercially available layers of ($23\frac{1}{2}$-carat) Au foils. After weighing with a microbalance the converters were carefully glued with a diluted solution of velpon onto a (1.000 ± 0.005) mm thick aluminium support. This support serves at the same time as absorber for the internal electrons emitted by the "external" source. This source, covered by a (0.050 ± 0.005) mm thin aluminium foil, is pressed against the aluminium support as indicated in fig. 2. The arrangement shown assures an accurate position of the gamma-ray source relative to the converter. The weight of the converters could be determined with an accuracy of 1 % whereas the angles ϑ_0 under which the radius of the converter is seen from the centre of the sources are accurate within 0.5 %. The angle ϑ_0 was chosen to be 78° for the circular converter, equal to the value used by Hultberg and Stockendal [19]) for their investigation of α_K of the 662 keV transition in ^{137}Ba. (This conversion coefficient has been used in the present study to test the source-converter geometry, see appendix).

Hultberg and Stockendal have shown that for circular geometry

$$f_K = \int_0^{\Theta_0} J_K(\Theta + \Delta) \operatorname{tg} \Theta \, d\Theta \Big/ \int_0^{\pi} J_K(\Theta) \sin \Theta d\Theta.$$

The differential angular distribution functions for the photo-electric effect, $J(\Theta)$, are tabulated for uranium by Hultberg [18]) for the energies 412 keV, 662 keV and 1332 keV. Δ is the angle between the normal to the converter and the direction under which the centre of the baffle system is seen from a point on the converter; this small angle evidently varies from 0 to the maximum value for edges of the converter. In our arrangement with circular geometry Δ_{max} is 0.04 radians.

For the circular geometry we computed the f_K values of interest with the use of the tabulated $J_K(\Theta)$ functions. For the rectangular source-converter geometry the f_K value is obtained from the B.E.S.K. computer at Stockholm. The calculation program for this computer has been worked out by Hultberg in such a way that extended gamma-ray sources may be used.

It should be mentioned that the f_K-values used in this work are in principle only valid for uranium as converter material. The result of our test measurement on the 662 keV transition in ^{137}Ba given in the appendix, together with the agreement between the results obtained in the sections 2.1 and 2.2 for the α_K of the transition in ^{198}Hg supports the assumption that no large errors are introduced when applying the uranium angular distribution functions, as measured by Hultberg, to gold.

Theoretical photo-electric cross sections for the K-shell, τ_K, are to be obtained by division of the total photo-electric cross sections tabulated by G. White-Grodstein [38]) through the τ_a/τ_K values given in table 5 of this ref.

Total photo-electric cross sections for different elements are measured very precisely by Colgate [20]) for the photon energies 412 keV, 662 keV, 1332 keV and some higher energies. The corresponding τ_K values can be readily obtained from his values using the "thumb rule" $\tau_K/\tau_a = 0.80$ †. For the cases presently of interest, a comparison of the Colgate values with the tabulated τ_K's shows the latter values to be about 5 % higher. The determination of the conversion coefficient of the M4 transition in ^{137}Ba by Hultberg and Stockendal [19]) indicates Colgate's value for uranium to be more reliable. The same conclusion follows from our result given in the appendix for 662 keV on gold. Thus we felt justified to use the τ_K for 412 keV on Au as follows from Colgate's experiments. For the other energies involved in this work, 328 keV and 354 keV, no experimental values of the photo-electric cross sections are available. However, extrapolating the values determined by Colgate to these energies yields also somewhat lower values than indicated by the tables of White. Therefore we adopt for the τ_K

† This thumb rule has been verified experimentally by Hultberg [18]) for widely different energies with uranium as converter material. The investigations of this author show moreover that this thumb rule is satisfied for other elements in the high Z-region as well.

(328 keV) and τ_K (354 keV) for gold 5 % lower values than follows from ref.[38]).

2. Absolute Conversion Coefficient Measurements

2.1. INVESTIGATIONS WITH THE EXTERNAL-INTERNAL CONVERSION METHOD

2.1.1. *The* K-*shell conversion coefficient of the* 412 keV E2 *transition in* ^{198}Hg *following the decay of* ^{198}Au

The active material was obtained from Philips-Roxane N.V., it has been prepared by neutron irradiation of gold and was chemically purified. The specific activity amounted to about 10 curies per gram. The measurements have been carried out with a circular and with a rectangular source-converter geometry.

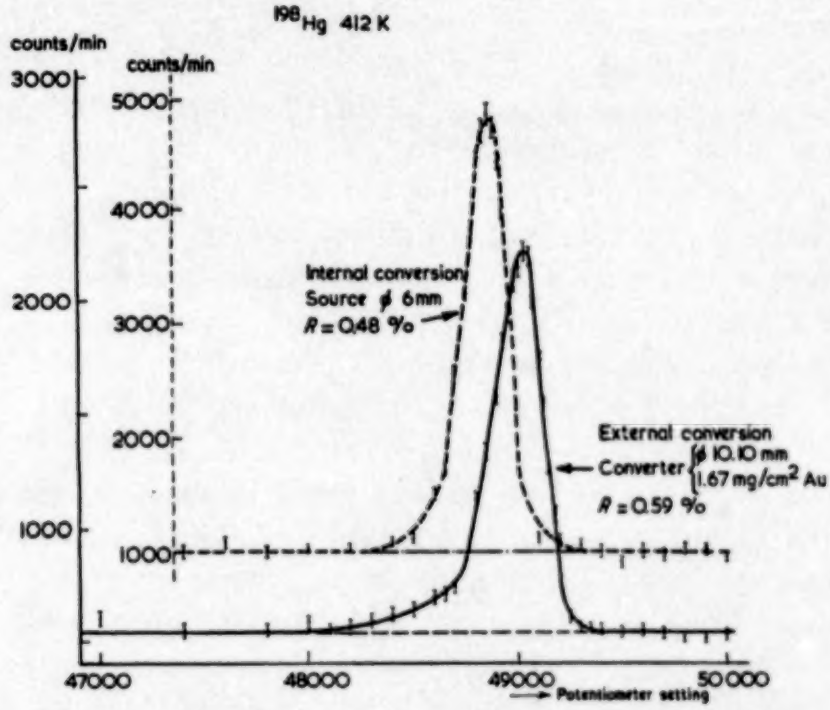

Fig. 3. K-conversion lines of the 412 keV transition (circular geometry).

For the investigations with circular geometry both the internal and the external source had a diameter of 6 mm. The internal source was backed by 0.05 mm Ag and the external source by 0.05 mm Au. The desired ratio between the source strengths could be obtained by using different electroplating times. The thickness of the internal source is estimated to be less than 10 μg/cm^2. The diameter of the converters I and II used for this geometry is (10.10 ± 0.03) mm. The measurements of the conversion lines are performed alternatively with the external source (plus converter) and the internal source in the arrangement shown in figure 2. Four pairs of lines have been measured. After the measure-

ment of each pair of lines the intensity ratio k was determined in order to check for possible errors due to damaging of the sources between the different runs. One typical line pair is shown in figure 3. The transmission of the spectrometer, kept constant throughout this investigation, was 0.7 % ($\gamma_\rho = 0.085$ rad, $\gamma_s = 0.25$ rad). The dimensions of the counter slit were 3.2×20 mm.

The radius of the external source is larger than half the radius of the converter; the f_K-value, valid for a point source, has therefore to be lowered (see Hultberg [18]). A calculation showed the required correction to be about 4 % †.

For the rectangular source-converter geometry we used a (very thin) internal source as large as 6×20 mm and an external source with an area of 4.0×14.6 mm. The dimensions of the converter were 6.95×19.97 mm. The counter slit dimensions were 3.2×30 mm. The measurements (three runs) were performed in essentially the same way as described above. The transmission was 1 %. The half-width of the external conversion peak ($R = 0.55$ %) is smaller than that obtained with the circular geometry, proving the superiority of the rectangular arrangement for the present instrument.

The data used for the computation of α_K have been summarized in table 1.

TABLE 1

Numerical data ($E_\gamma = 412$ keV)

	Source-converter geometry			Remarks
	circular		rectangular	
	converter I	converter II		
A_{in}/A_{ex}	1.747(±3 %)	1.917(±3 %)	0.676(±3 %)	mean values
d in mg/cm²	1.805(±1 %)	1.670(±1 %)	1.679(±1 %)	corrected for impurities in Au-foils
k	70.4(±3 %)		188.2(±3 %)	mean values
f_K	1.226(±3 %) [a]		1.264(±2 %) [b]	[a] corrected for extension source [b] value of B.E.S.K. (Stockholm)
τ_K in barns/atom	30.4(±2 %)		30.4(±2%)	τ_a (Colgate) × 0.80
b in $\frac{\text{atoms} \times \text{cm}^2}{\text{barns} \times \text{mg}}$	3.058×10^{-4}		3.058×10^{-4}	
$\alpha_K \times 10^4$	252(±6 %)	257(±6 %)	248(±5 %)	

† As suggested by Hultberg and Stockendal the f_K- value for circular geometry with extended source may be calculated to good accuracy using the rectangular B.E.S.K. program such that for both converter and source squares are taken with the same areas as the corresponding circles. Indeed these B.E.S.K. values showed to be in accordance within 0.5 % with our values obtained by direct calculation.

The error assignments to the results for the α_K (412 keV) which are also given in the table, have been obtained by quadratic addition of the errors in the individual data. The average results of the separate measurements is

$$\alpha_K = (252 \pm 13) \times 10^{-4}.$$

We refrained from diminishing the error in the mean value of the mutually consistent results, because the errors in the separate results are partly due to systematic errors in f_K, τ_K and d. A discussion of this result will be given below.

2.1.2. *The α_K of the* 328 keV E2 *transition in* ^{194}Pt *following the decay of* ^{194}Au.

This activity was obtained by bombarding a Pt-foil with 20 MeV deuterons in the synchro-cyclotron of this Institute. After chemical separation the carrier-free activity, containing different gold isotopes, is electroplated. The sources were prepared to be used in the circular geometry (only with converter I) and in the rectangular geometry (see subsection 2.1.1). The line profiles for one of the three runs made with the rectangular source-converter arrangement are shown in figure 4. The small peaks at the higher energy sides of these lines are K-con-

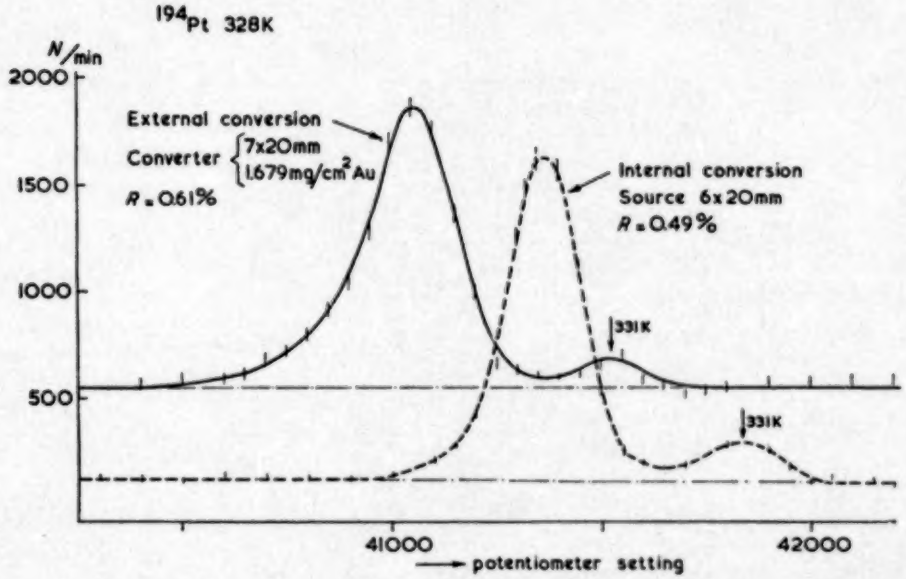

Fig. 4. K-conversion lines of the 328 keV transition (rectangular geometry).

version lines of the 331 keV ($2^+ \rightarrow 2^+$) transition in the decay of ^{196}Pt. Comparing the intensities of the 331 keV lines with the corresponding external and internal 328 keV lines yields the result that the K-conversion coefficient is 10—30 % higher than that of the pure E2 transition, in rough agreement with the reported E2/M1 mixing ratio for the 331 keV gamma ray: 5 % M1 and 95 % E2 (see Nuclear Data Sheets).

The f_K-values for the energy 328 keV are assumed to be equal to those valid

for 412 keV. Probably no large errors will be introduced by this assumption because the f_K-values for circular geometry for the energies 412 keV and 662 keV (see appendix) differ only by 1.5 %.

TABLE 2

Numerical data ($E_\gamma = 328$ keV and $E_\gamma = 354$ keV)

	Source-converter geometry			Remarks
	circular (converter I)		rectangular	
	354 keV	328 keV	328 keV	
A_{in}/A_{ex}	2.505(±5 %)	2.441(±4 %)	0.867(±4 %)	mean values
f_K	1.214(±3 %)[a])	1.201(±3 %)[a])	1.264(±2 %)	[a]) corrected for extension source
τ_K in barns/atom	44.7(±2 %)	51.9(±2 %)		τ_K (White) −5 %
k	48.9(±2 %)		139.4(±2 %)	mean values
d in mg/cm²	1.805(±1 %)		1.679(±1 %)	corrected for impurities Au foils
b in $\frac{\text{atoms} \times \text{cm}^2}{\text{barns} \times \text{mg}}$	3.058×10^{-6}			
$\alpha_K \times 10^4$	367(±7 %)	411(±6 %)	407(±5 %)	

The numerical data required for the calculation of the α_K of the 328 keV transition is given in table 2. Averaging the individual results, also presented in the table, yields

$$\alpha_K = (409 \pm 22) \times 10^{-4}.$$

Here again the error assignment to the mean value is taken equal to those in the individual results.

2.1.3. *The α_K of the* 354 keV E2 *transition in* ^{196}Pt *following the decay of* ^{196}Au

This activity was present in the same sources as used for the measurements on the 328 keV transition. Three runs have been made on this line pair with the circular geometry. The numerical data for this investigation are also given in table 2.

The results found in subsections 2.1.2 and 2.1.3 will be discussed in subsection 2.3.

2.2. THE ABSOLUTE K-CONVERSION COEFFICIENT DETERMINATION OF THE 412 keV E2 TRANSITION IN ^{198}Hg WITH THE K-PEAK TO SPECTRUM RATIO METHOD

Two sources 1 and 2 (3.0×20 mm) have been prepared using the activity obtained after neutron irradiation of gold (Philips Roxane N.V.). The specific

activity of the source material amounted to about 10 and 40 curies/gram for the sources 1 and 2, respectively. The thickness of source 1 could be estimated to be 40 $\mu g/cm^2$, whereas that of source 2 was about 15 $\mu g/cm^2$. Both sources were electroplated onto a 0.8 mg/cm^2 mylar foil which was coated with a thin layer of Ag to prevent charging of the source. The solid angle was for both investigations about 1 %, whereas the dimensions of the counter slit were 3.2×20 mm.

Although the quality of the sources was satisfactory we preferred to obtain the part of the spectrum below 300 keV from extrapolation of the measured part between 300 and 950 keV, because of the competition of the beta transitions occurring in ^{199}Au, always present in the available ^{198}Au activity, and the 290 keV beta-ray component in the continuous spectrum of ^{198}Au itself. The beta particles in the region considered are almost entirely due to the spectrum under consideration; only a very weak higher branch (the ground state transition of ^{198}Au) is present for which no corrections need to be applied. With each source two runs are taken; about 20 points per run have been used to determine the shape of the spectrum. This shape has been analyzed using the approximation for the spectral shape of first forbidden non-unique transitions as developed by Wapstra [21]). Wapstra *et al.* [15]) found that the spectrum under consideration follows rather well the shape

$$N(p)\mathrm{d}p = (W-W_0)^2 f\{1+g(W_0-W)\}^2 \mathrm{d}p,$$

with $g = 0.065 \pm 0.010$. The measured points in the runs taken with source 1 are shown in figure 5. From this plot we find $g = 0.083 \pm 0.010$. The same analysis for the experimental points as measured with source 2 yielded $g = 0.095 \pm 0.010$. Both values are thus slightly higher than that found by Wapstra *et al.*

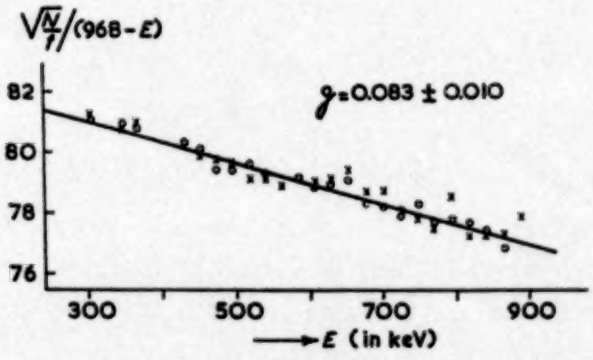

Fig. 5. "First forbidden" plot of the main beta spectrum of ^{198}Au.

For the problem of interest here this discrepancy is not serious. Extrapolation of the spectrum towards lower energies using the plot given in figure 5 yields a total intensity in the spectrum which is only a few percent higher than should have been found with a Fermi analysis with $g = 0$ (allowed shape). The analysis of the experimental values gives an end point energy of (968 ± 3) keV in agree-

TABLE 3

Absolute K-conversion coefficients ($\times 10^4$)

E2 transitions				M4 transition	
References [a])	328 keV (^{194}Pt)	354 keV (^{196}Pt)	412 keV (^{198}Hg)	References [a])	662 keV (^{137}Ba)
Rose	490	410	302	Rose	930
Sliv	490	410	298	Sliv	920
Steffen *et al.* [22])			280±70	Waggoner [26])	970±50
Huber *et al.* [23])			275±30	Heath and Bell [27])	950±50
Connors *et al.* [24])			250±50	Wapstra [28])	920±60
Wapstra *et al.* [15])			281± 5	Yoshizawa [29])	976±55
Thieme and Bleuler [25])	560±60	420±30		Hultberg and Stockendal [19])	930±60
present work	409±22	367±24	241± 9 [b]) 252±13 [c])	present work	930±50

[a]) see for a more complete list Nuclear Data Sheets.
[b]) obtained from comparison of K-conversion peak and beta spectrum.
[c]) obtained from comparison of internal and external conversion lines.

ment with the value (966±3) keV found by Wapstra *et al.* [15]). The intensity of the K-line has been determined several times during the runs.

The results of the measurements were:

$$\left.\begin{array}{l}\text{source 1: } \alpha_K = (247\pm12)\times10^{-4}\\ \text{source 2: } \alpha_K = (236\pm12)\times10^{-4}\end{array}\right\} \alpha_K = (241\pm9)\times10^{-4}.$$

The agreement with the result of subsection 2.1.1 $\alpha_K = (252\pm13)\times10^{-4}$, is satisfactory.

2.3. DISCUSSION

The results obtained in subsection 2.1 and 2.2 are summarized in table 3 for comparison with the theoretical values and earlier reported experimental ones. We also included in this table the result obtained for the K-conversion coefficient of the 662 keV M4 transition in ^{137}Ba as given in the appendix.

Table 3 shows that our results indicate lower values for the three E2 transitions than given by theory †. The agreement between our result for the M4 transition and other experimental and theoretical values indicate that the internal-external method is very probably more accurate than the difference with the theoretical values. Yet, the values reported in this work may be somewhat low. As explained before, the experimental values for the photo-electric cross sections, as measured by Colgate, are somewhat lower than the theoretical values. Accepting the theoretical values for these cross sections would bring our value for the 412 keV transition in ^{198}Hg obtained by the external-internal method in a better agreement with the earlier result of Wapstra *et al.* [15]). Our measurement of this conversion by comparison of the K-line and the continuous beta spectrum yields an even lower value. This result is, however, open to some doubt because of the possibility that the continuous spectrum may have appeared too large due to the presence of scattered electrons (e.g. against the wall of the vacuum chamber); this possibility will be investigated later.

Summarizing we may conclude that our results indicate that the conversion coefficients of the E2 transitions considered here deviate by 10—20 % from the theoretical values. These deviations cannot yet be explained as nuclear model dependent effects. Thanks especially to the recent improvements of the external-internal method by Hultberg and Stockendal, it may be expected that further experimental data on this interesting subject will become available in the near future.

3. Relative Conversion Coefficient Measurements

3.1. CONVERSION RATIOS OF THE 412 keV TRANSITION IN ^{198}Hg

The measurements of the conversion lines of the 412 keV transition following the decay of ^{198}Au have been carried out with three different sources. The

† Hultberg and Hamilton informed us that their result for the α_K of the 412 keV transition in ^{198}Hg is in excellent agreement with our values: $(244\pm8)\times10^{-4}$. (To be published.)

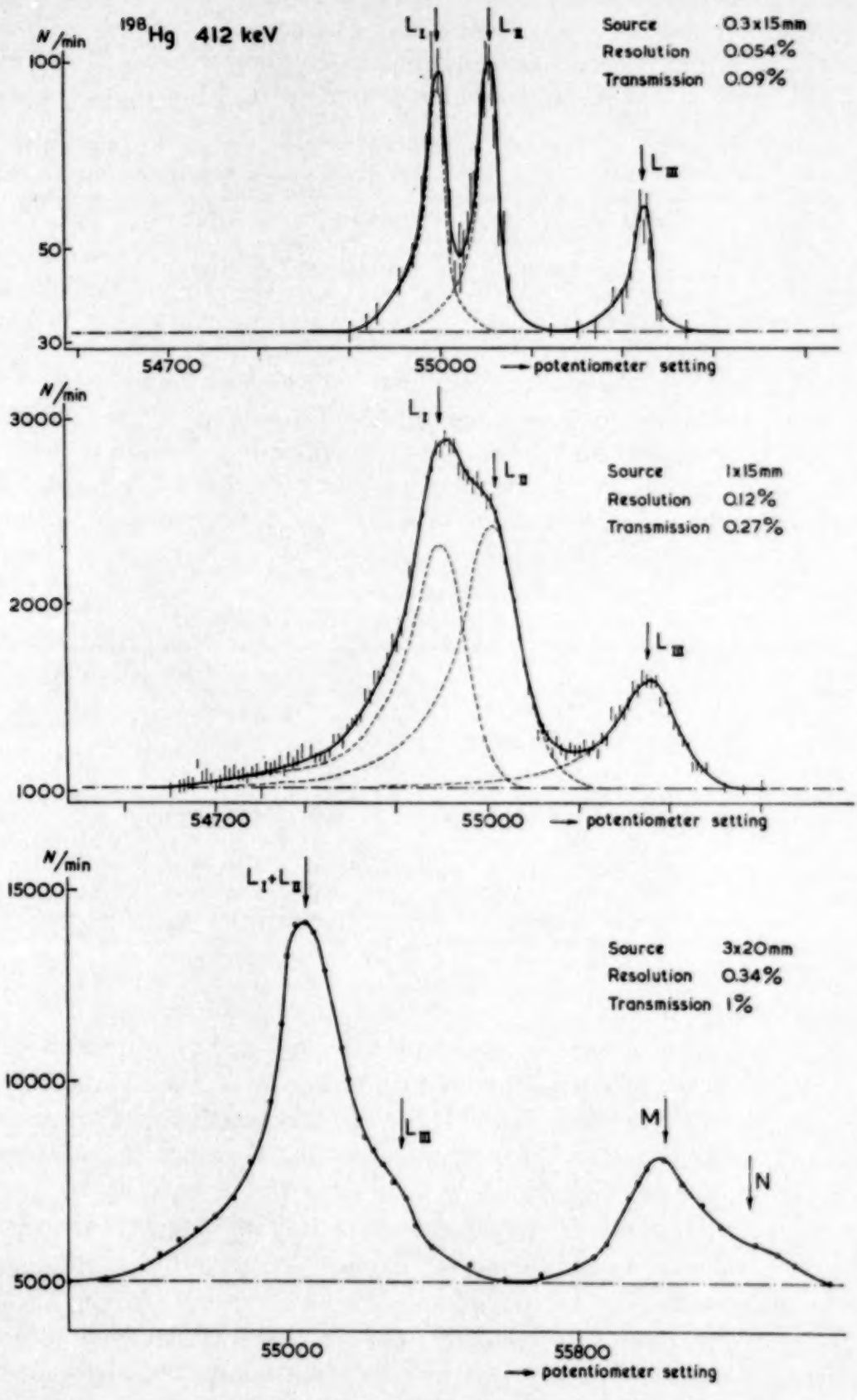

Fig. 6. Conversion spectra of the 412 keV transition in ^{198}Hg.

L_I- and L_{II}-lines could only be resolved with a source of dimensions) 0.3×15 mm which did not yield counting rates in the peaks from which the L-subshell ratios could be determined accurately (figure 6a). Another source (1×15 mm) has been used, therefore, to determine accurately $(L_I+L_{II})/L_{III}$ (figure 6b).

TABLE 4

Ratios of conversion line intensities obtained with different sources (412 keV transition in ^{199}Hg)

Source	K/ΣL	L_I/L_{II}	$(L_I+L_{II})/L_{III}$	L/ΣM	ΣL/Σ(M+N)
0.3×15 mm	2.88 ± 0.30	0.91 ± 0.07	4.65 ± 0.50		
1×15 mm	2.92 ± 0.14		4.38 ± 0.22		
3×20 mm	2.92 ± 0.14			3.94 ± 0.30	3.01 ± 0.15

The K-, L-, M- and N-lines are measured with a third source at moderate resolution (the third spectrum in fig. 6). The different resolutions and corresponding transmissions are indicated in fig. 6. The different ratios of the areas of the lines, corrected for momentum, are given in table 4. Averaging these results yields the ratios given in table 5 where they are compared with theoretical and experimental data.

TABLE 5

Relative conversion coefficients ($E_\gamma = 412$ keV (E2))

References [a])	K/ΣL	L_I/L_{III}	L_{II}/L_{III}	ΣL/ΣM	ΣL/Σ(M+N+..)
Rose	2.75	2.20	2.34	2.44 [b])	
Sliv	2.72	2.18	2.37		
Mihelich [30])			2.5		
Connors *et al.* [24])		1.9 ± 0.3	2.2 ± 0.3		
Reitmann *et al.* [16])		2.51 ± 0.24	3.12 ± 0.28	3.67 ± 0.25	
Wapstra *et al.* [15])	2.90 ± 0.13				3.13 ± 0.44
Kel'man *et al.* [31])	2.69 ± 0.02	2.22 ± 0.04	2.33 ± 0.05	3.96 ± 0.07	2.97 ± 0.10
present work	2.91 ± 0.10	2.11 ± 0.16	2.31 ± 0.17	3.94 ± 0.30	3.10 ± 0.15

[a]) See for a more complete list Nuclear Data Sheets.
[b]) Uncorrected for screening.

3.2. DISCUSSION

$K/\sum L$: Our value, in agreement with the value reported by Wapstra *et al.* [15]). is (7 ± 4) % higher than predicted by theory. The measurements reported by Kel'man *et al.* [31]) agree with theory. It is noted that together with the result of section 2 for the α_K, our $K/\sum L$ ratio indicates that the absolute L-conversion coefficient α_L deviates even slightly more from theory than α_K.

$L_I/L_{II}/L_{III}$: the results of the present work are in nice agreement with the theoretical values and with other reported results; the ratio $(L_I+L_{II})/L_{III}$ found by Reitman *et al.* [16]) is probably somewhat high.

$\sum L/\sum M$: Our value agrees with Kel'man *et al.* [31]). The main part of the discrepancy with the value predicted by theory is certainly caused by neglecting the screening effect in the M-shell calculation; the experimental results suggest

a correction factor of about 0.60. Similar large correction factors have been reported also for other transitions in the high Z-region [32–35]).

3.3. CONVERSION RATIOS OF THE 158 keV TRANSITION IN ^{199}Hg

The measurements of the conversion lines are performed with the source used also for the precision energy measurements described by de Vries and

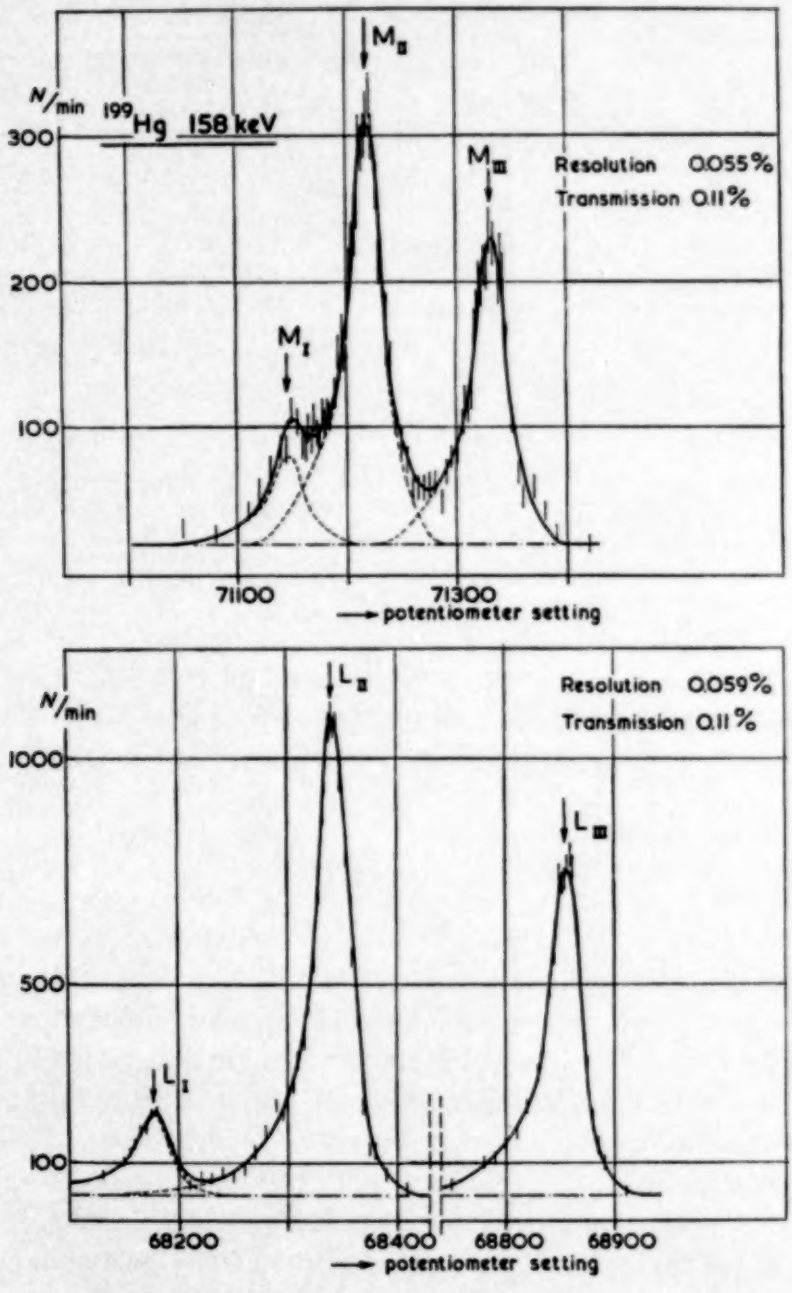

Fig. 7. Conversion spectra of the 158 keV transition in ^{199}Hg.

Dijkstra [36]). The high quality of that source (0.3×10 mm) allowed to resolve the L-subshell conversion lines (second spectrum of fig. 7) but also the M-

subshell lines (first spectrum in fig. 7). The different ratios determined from these plots are given in table 6 for comparison with the theoretical values and previous experimental values reported.

TABLE 6

Relative conversion coefficients ($E_\gamma = 158$ keV (E2))

References	$K/\Sigma L$	L_I/L_{III}	L_{II}/L_{III}
Rose	0.62	0.22	1.43
Sliv	0.62	0.21	1.45
Cressman *et al.* [33])	0.59±0.02	1.41±0.05 [a])	
Bäckström *et al.* [32])	0.54±0.06	0.23±0.03	1.37±0.14
Nall *et al.* [37])	0.62±0.02	1.72±0.05 [a])	
present work	0.59±0.04	0.25±0.02	1.50±0.10
References	$\Sigma L/\Sigma M$	M_I/M_{III}	M_{II}/M_{III}
Rose	2.22 [b])	0.24	1.47
Cressman *et al.* [33])	3.79±0.15		
Bäckström *et al.* [32])	3.85	0.166	1.33
Nall *et al.* [37])	3.72±0.15		
present work	3.75±0.20	0.28±0.05	1.40±0.10

[a]) $(L_I+L_{II})/L_{III}$.
[b]) Uncorrected for screening.

All our values are in agreement with the theoretical values if a correction factor of about 0.6 for screening is applied to all M-shell coefficients. Evidently, screening affects the M-subshell conversions to nearly the same amount, as expected by Rose [5]).

4. Appendix

The K-conversion coefficient of the 662 keV M4 transition in ^{137}Ba is one of the best measured conversion coefficients (see table 3). Most of the experimental values are in excellent agreement with the theoretical values of Rose and Sliv. Recently Hultberg and Stockendal [19]) reported an investigation of this conversion coefficient with the external-internal method using uranium as converter. In connection with the work described in this paper we reinvestigated this conversion coefficient for two reasons: (a) to test the circular source-converter geometry used for the investigations of the E2 transitions and (b) to check the assumption that the correction factor f_K computed from the angular distribution functions $J(\Theta)$ for uranium, as given by Hultberg [18]), is also valid for gold.

The angle ϑ_0 in our circular geometry (converter I) was chosen equal to that used by Hultberg and Stockendal for their investigation of the α_K of the transition under consideration. The activity used for the preparation of the

two sources was obtained from Harwell, England in 1 N nitric acid solution. The sources were backed by 0.06 mm Pt foil. The diameter of the internal source, prepared by vacuum evaporation, was 6 mm, whereas the activity of the external source (15 mR/h on 0.3 m distance) could be restricted with the droplet technique to an area with a diameter of 3.2 mm. For this investigation the same circular converter has been used as for the measurements given in section 2.1 (diameter 10.10 mm). No correction was necessary for the extension of the external source [18]). The transmission during the measurements was 1 %. The counter was provided with a 3.2×20 mm slit.

The determination of the intensity ratio of the two sources yielded $k = 235$ (± 2 %). The intensity ratio of the conversion lines ($R_{in} = 0.50$ %, $R_{ex} = 0.50$ %) has been determined as the average from three runs: $A_{in}/A_{ex} = 5.417$ (± 3 %). For the photo-electric cross section τ_K we used the value 10.2 barns/atom ± 2 % (Colgate's τ_α value $\times 0.80$). The thickness d of the converter is 1.805 mg/cm^2 ± 1 %. The f_K-value is determined in essentially the same way as described in subsection 1.3: $f_K = 1.266(\pm 3$ %). The dimension factor b is 3.058×10^{-6} (atoms $\times$ cm^2/barns $\times$ mg). From these numerical data we obtained for the K-conversion coefficient: $\alpha_K = 0.092(\pm 5$ %). A previous attempt under the same conditions but with another external source (diam. 8 mm) yielded after correction for the extension of the source: $\alpha_K = 0.095$ (± 7 %). As an average of both investigations we adopt the value:

$$\alpha_K = 0.093 \pm 0.005.$$

This result is in excellent agreement with the value $\alpha_K = 0.093 \pm 0.006$ found by Hultberg and Stockendal [19]). Hence support is given to the reliability of the circular geometry used in the present work; moreover the agreement indicates that no large errors are introduced with the assumption $f_{Au} = f_U$.

The authors wish to thank Prof. P. C. Gugelot for his interest in this work and Prof. A. H. Wapstra for many stimulating discussions. We also wish to acknowledge the fruitful discussions about the external-internal method with Dr. S. Hultberg and Dr. R. Stockendal. The authors would like to thank Drs. J. H. Dijkstra and P. F. A. Goudsmit for taking part in the measurements and Miss J. C. Kapteijn for performing the chemical separations.

This work constitutes part of the research program of the Institute for Nuclear Physics Research, made possible by financial support from the Foundation for Fundamental Research of Matter (F. O. M.) and the Netherlands' Organization for Pure Scientific Research (Z.W.O.).

References

1) N. Tralli and G. Goertzel, Phys. Rev. **83** (1951) 399
2) L. A. Sliv, JETP **21** (1951) 770;
L. A. Sliv and M. Listengarden, JETP **29** (1952) 29

3) M. E. Rose, G. Goertzel, B. Spinrad, J. Harr and P. Strong, Phys. Rev. **83** (1951) 79
4) L. A. Sliv and J. Band, Tables of internal conversion coefficients of gamma-rays (Academy of Sciences of the USSR, Moskow-Leningrad, 1956);
L. A. Sliv and J. Band, Coefficients of internal conversion of gamma radiation (Academy of Sciences of the USSR, Moskow-Leningrad, 1958)
5) M. E. Rose, Internal conversion coefficients (North-Holland Publishing Company, Amsterdam, 1958)
6) T. Green and M. E. Rose, Phys. Rev. **110** (1958) 105
7) E. Church and J. Weneser, Phys. Rev. **104** (1956) 1382
8) A. S. Reiner, Nuclear Physics **5** (1958) 544
9) S. G. Nilsson and J. O. Rasmussen, Nuclear Physics **5** (1958) 617
10) F. Asaro, F. S. Stephens, J. M. Hollander and I. Perlman, Phys. Rev. **117** (1960) 492
11) A. H. Wapstra and G. J. Nijgh, Nuclear Physics **1** (1956) 245;
G. J. Nijgh, Thesis (Amsterdam, 1955)
12) K. O. Nielsen, O. B. Nielsen and M. A. Waggoner, Nuclear Physics **2** (1956/57) 476
13) F. K. McGowan and P. H. Stelson, Phys. Rev. **103** (1956) 1133
14) F. K. McGowan and P. H. Stelson, Phys. Rev. **107** (1957) 1674
15) A. H. Wapstra, G. J. Nijgh, N. Salomons-Grobben and L. Th. M. Ornstein, Nuclear Physics **9** (1958/59) 538
16) D. Reitmann, H. Schneider and I. J. van Heerden, Phys. Rev. **110** (1958) 1093
17) C. de Vries and A. H. Wapstra, Nuclear Instruments (to be published)
18) S. Hultberg, Ark. f. Fysik **15** (1959) 307
19) S. Hultberg and R. Stockendal, Ark. f. Fysik **14** (1959) 565
20) S. A. Golgate, Phys. Rev. **87** (1952) 592
21) A. H. Wapstra, Nuclear Physics **9** (1958/59) 519
22) R. M. Steffen, O. Huber and F. Humbel, Helv. Phys. Acta **22** (1949) 167
23) O. Huber, F. Humbel, H. Schneider and A. de Shalit, Helv. Phys. Acta **25** (1952) 3
24) D. R. Connors, W. C. Miller and B. Waldman, Phys. Rev. **102** (1956) 1584
25) M. T. Thieme and E. Bleuler, Phys. Rev. **101** (1956) 1031; **102** (1956) 195
26) M. A. Waggoner, Phys. Rev. **80** (1950) 489
27) R. L. Heath and P. R. Bell, Phys. Rev. **87** (1952) 176
28) A. H. Wapstra, Ark. f. Fysik **7** (1954) 275
29) Y. Yoshizawa, Nuclear Physics **5** (1958) 122
30) J. W. Mihelich, Phys. Rev. **87** (1952) 646
31) V. M. Kel'man and R. Ya. Metskhvarishvili, Sov. Phys. JETP **9** (1959) 486
32) G. Bäckström, O. Bergman and J. Burde, Nuclear Physics **7** (1958) 263
33) P. J. Cressman and R. G. Wilkinson, Phys. Rev. **109** (1958) 872
34) I. J. van Heerden, D. Reitmann, H. Schneider, Nuovo Cim. **11** (1959) 167
35) R. Stockendal, private communication
36) C. de Vries and J. H. Dijkstra, Nuclear Physics **18** (1960) 446
37) J. C. Nall, Q. L. Baird and S. K. Haynes, to be published
38) G. White-Grodstein, Nat. Bur. of Standards Circular 583

7.C

Nuclear Physics **18** (1960) 473—491; © *North-Holland Publishing Co., Amsterdam*

Not to be reproduced by photoprint or microfilm without written permission from the publisher

ELASTIC γ-p SCATTERING AT 40 TO 70 MeV AND POLARIZABILITY OF THE PROTON

V. I. GOLDANSKY, O. A. KARPUKHIN, A. V. KUTSENKO and V. V. PAVLOVSKAYA

P. N. Lebedev Physical Institute, USSR Academy of Sciences, Moscow

Received 23 January 1960

Abstract: The elastic γ—p scattering at 40 to 70 MeV is studied and the differential cross sections are determined for angles of 45°, 75°, 90°, 120°, 135° and 150°.

The results thus obtained are compared with the Rayleigh-Powell scattering theory taking account of the anomalous magnetic moment of the proton as well as the effects of meson cloud polarization.

Study of the forward scattering cross-section calculated through dispersion relations and the angular distribution at 75° to 150° obtained from experiment warrants the conclusion that electric polarizability of the proton $\alpha_E = (9\pm2)\times10^{-43}$ cm^3 and its magnetic polarizability $\alpha_M = (2\mp2)\times10^{-43}$ cm^3. This value of proton electric polarizability corresponds to the mean quadratic fluctuation of electric dipole equal to $(3.5-5)\times10^{-14}$ cm.

1. Introduction

Elastic scattering of γ-quanta by protons essentially differs from the well-known Compton effect on electrons. This difference is attributable above all to the anomalous magnetic moment of proton. Scattering of γ-quanta by particles with spin $\frac{1}{2}$ and anomalous magnetic moment was considered in the general form by Pauli, and later the theory of this scattering was developed by Powell [1]), Gell-Mann and Goldberger [2]), Low [3]), Klein [4]) and Capps [5]).

In refs. [2–5]) additional terms linear with respect to the frequency of γ-quanta were taken into account in the amplitude of scattering alongside the Thomson term.

Correspondingly, the cross section of γ—p scattering in the laboratory system is expressed, within an accuracy of the terms of order γ^2 (where $\gamma = h\nu/Mc^2$; M is the mass of the proton) by a formula of the Powell type [1])

$$\frac{d\sigma}{d\Omega}(\theta) = \tfrac{1}{2}r_0^2\{[1-2\gamma(1-\cos\theta)+3\gamma^2(1-\cos\theta)^2](1+\cos^2\theta) + \gamma^2[(1-\cos\theta)^2+f(\theta)\}, \quad (1)$$

where $r_0 = e^2/Mc^2$, and the role of the anomalous magnetic moment is described by the term

$$f(\theta) = a_0+a_1\cos\theta+a_2\cos^2\theta. \quad (2)$$

Here, the coefficients a_0, a_1 and a_2 are the power series functions of the

anomalous part of the magnetic moment of the proton $\lambda_a = 1.7896$ and equal

$$a_0 = 2\lambda_a + \tfrac{9}{2}\lambda_a^2 + 3\lambda_a^3 + \tfrac{3}{4}\lambda_a^4 = 42.9, \tag{3}$$

$$a_1 = -4\lambda_a - 5\lambda_a^2 - 2\lambda_a^3 = -34.6, \tag{4}$$

$$a_2 = 2\lambda_a + \tfrac{1}{2}\lambda_a^2 - \lambda_a^3 - \tfrac{1}{4}\lambda_a^4 = -3.1. \tag{5}$$

Obviously, the anomalous magnetic moment leads not only to a general increase in the cross section of scattering but also to a definite change of the form of angular distribution, namely to an increase of scattering into the back hemisphere.

The effects caused by the anomaly of magnetic moment by no means exhaust the peculiarities of the scattering of γ-quanta by protons. Due to the meson cloud surrounding the proton core there arises a possibility of direct interaction between γ-quanta and this cloud, which is manifest not only in π-meson photoproduction but also in scattering. Thomson's cross section of $\gamma - \pi^+$ scattering is 45 times as great as that of γ—p scattering, and the meson effect is bound to tell on the picture of γ—p scattering not only near the threshold of photoproduction but even at essentially smaller energies.

The absorption of γ-quanta leads to the polarization of the meson cloud, the induction in the proton of electric and magnetic dipoles and subsequently their secondary radiation. Thus there arises Rayleigh scattering which is so well known in optics and the role of which in the Compton effect on the proton was noted by Capps [5]) and discussed in detail by Baldin [7]) who studied the influence of the polarizability of the proton on γ—p scattering.

The Rayleigh scattering amplitude is proportional to the square of the frequency of γ-quanta, the coefficients of proportionality for electric and magnetic dipole transitions being the constants of electric and magnetic polarizability of the proton characterizing the ability of the meson cloud to be deformed by the outer electric and magnetic fields, as well as the static distribution of electric charge and magnetic moment. We shall not discuss here the possibilities of separation of these different phenomena, but shall merely call attention to the fact that the concept of elastic polarizability used here is not altogether identical to the one commonly used for neutral particles.

Though the terms in the scattering amplitude conditioned by the polarizability of the proton are proportional to the square of frequency, they interfere only with the Thomson term and therefore lead to the terms quadratic with respect to the frequency in the formula of the cross section of scattering. Confining ourselves to such quadratic terms in the cross section of γ—p scattering we arrive at the following expression for differential angular cross sections of Rayleigh-Powell γ—p scattering in the laboratory system:

$$\frac{d\sigma}{d\Omega}(\theta) = \tfrac{1}{2} r_0^2 \{[1 - 2\gamma(1-\cos\theta) + 3\gamma^2(1-\cos\theta)^2 - 2A_E\gamma^2](1+\cos^2\theta) - 4A_M\gamma^2\cos\theta + \gamma^2[(1-\cos\theta)^2 + f(\theta)]\}, \tag{6}$$

where $f(\theta)$ has been determined above in connection with eq. (2) and the dimensionless factors A_E and A_M are the polarizabilities α_E and α_M expressed in units $(e^2/\hbar c)(\hbar/Mc)^3 = 6.8\times 10^{-44}$ cm^3.

As was shown by Petrunkin [6]), eq. (6) is obtained in the region of small frequencies as an exact corollary of dispersion relations.

Therefore eq. (6), in which two parameters: electric and magnetic polarizabilities of the proton, are to be determined, can be used in interpreting the experiments on γ—p scattering in the range of energies appreciably below the photo meson threshold (at $\gamma \ll 1$). It is clear that at low energies the difference of eq. (6) from a Powell type formula restricted to the terms γ^2 — a difference caused by the polarization of protons — has a minor effect, and therefore, despite the relative simplicity of the theoretical interpretation of the results, more exacting demands on the accuracy of the experiments have to be made than in studying the scattering of more energetic γ-quanta.

This leads us up to the aim of the present paper: ensuring as great accuracy of experiment as possible to obtain information on the polarizability of protons from the experiments on proton scattering of γ-quanta at 40 to 70 MeV.

2. Experimental Section

The experiments were conducted on the 265 MeV synchrotron of the FIAN at a maximum energy of the bremsstrahlung spectrum equal to 75 MeV, i.e., in a range of energies considerably below the threshold of π^0-meson photoproduction. Since it is possible at such energies to restrict oneself to the detection of the scattered γ-quantum (without the coincidence with the recoil proton) a sufficiently large target was used in our experiments ensuring a rate of counting from γ—p scattering of the order of 0.5 to 1 per min.

2.1. DETECTOR

As high-threshold ($\approx$ 35 MeV) detectors of γ-quanta conventional telescopes were used consisting of four scintillation counters with a lead convertor after the first one and an aluminium filter before the last (fig. 1). Every scintillation counter consisted of a glass vessel, filled with a solution of terphenyl in toluene (3 g per litre) and ФэУ —33 photomultipliers. The photomultipliers worked in a specially selected regime ($E_{\text{Photomult}} \approx$ 3—4 kV) ensuring the amplitude of output pulses of 30 to 40 V from the Co^{60} source for direct connection with the cable RK—50. Under such conditions we could do without additional amplification of input pulses from the photomultipliers.

2.2. ELECTRONICS

The block diagram of radio equipment used in experiments is shown in fig. 2. Below are some additional explanations. Two fast coincidence-circuits of

parallel-type operate on germanium D2B diodes. The first discriminator (D_1) lowering the loading of slow circuits had a compensation of the thermal drift of the threshold. As the second discriminator (D_2) the Park [8]) discriminator was used, which made it possible to use only one "triple" in the amplifier.

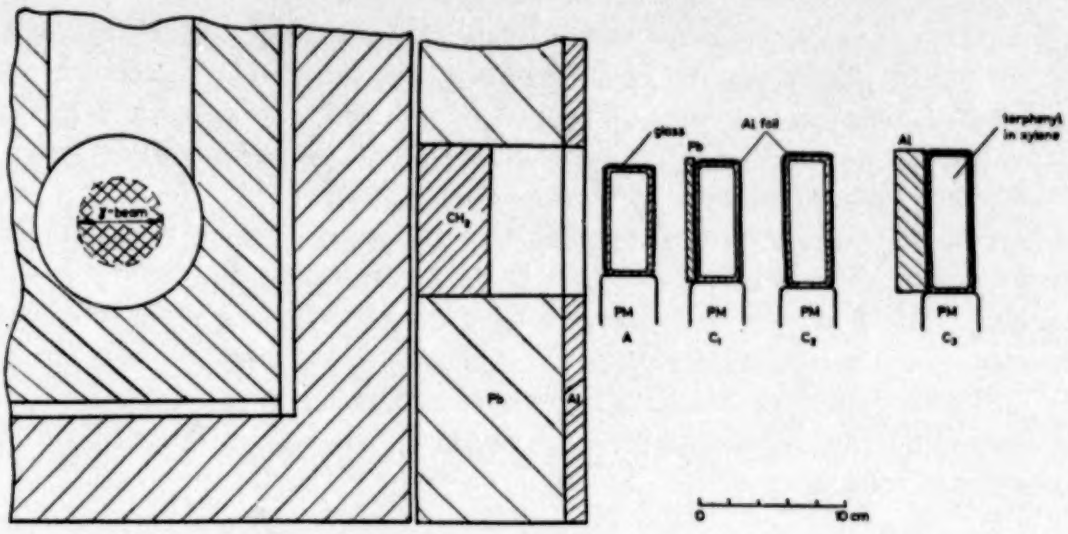

Fig. 1. Circuit of telescopes used for detecting scattered γ-quanta.

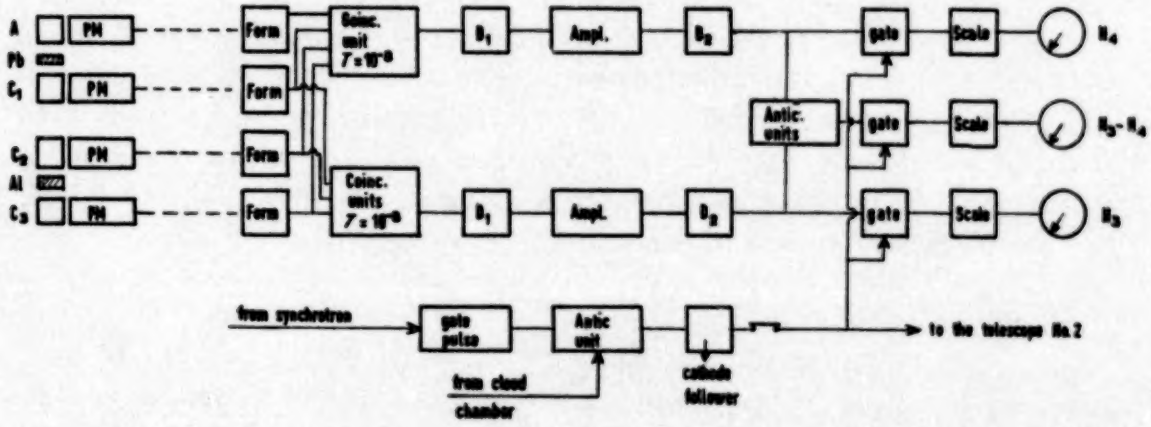

Fig. 2. Circuit of radioequipment.

The formed outputs from both coincidence-circuits were picked by the slow anti-coincidence-circuit excluding the counting of the charged particles. The possibility of simultaneous counting for all three channels made convenient the control of separate elements of the circuit.

The outputs from both coincidence-circuits and from the anti-coincidence-circuit were fed to the gate-circuits controlled by an accelerator. The counting was possible during a period only slightly greater than the duration of an intensity pulse from the synchrotron. This time-selection considerably reduces ($\approx$ to 1/50) the background caused by cosmic rays. To ensure simultaneous

work with other installations (cloud chamber, for instance) provision was made for the prohibition signal preventing the counting when the synchrotron pulses had to be changed as necessary for other installations.

2.3. PLAN OF EXPERIMENT. THE TARGET

The plan of the entire installation is represented in fig. 3. A bremsstrahlung beam from the synchrotron passed through a system of collimators and hit a liquid-hydrogen target.

The effective section of the target was a cylindrical vessel elongated by the axis of the beam (diameter 12 cm, length 30 cm) and having a capacity of some 3.5 litres. The double styrofoam walls (PS-4 with a density of some 40 mg/cm^3)

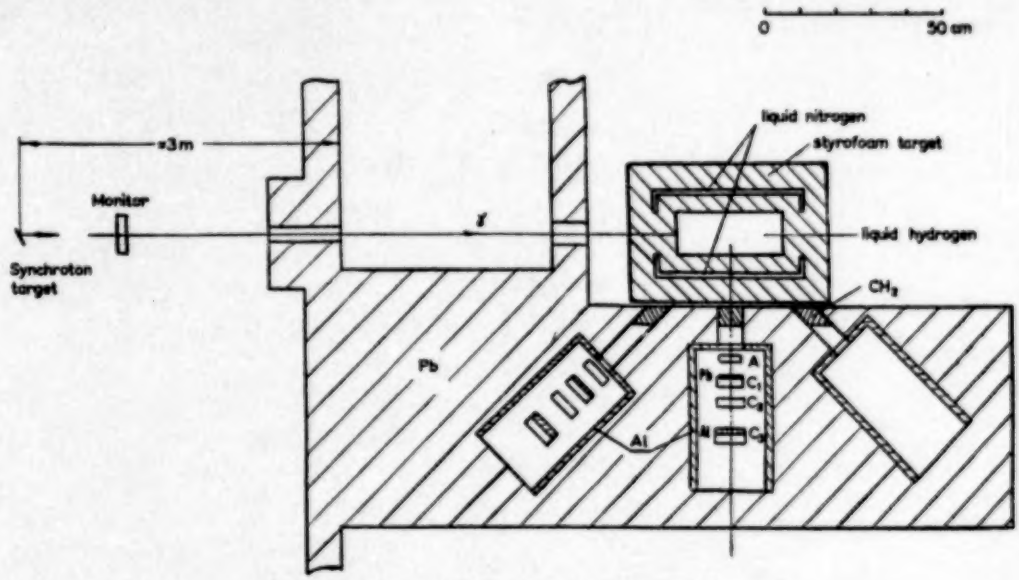

Fig. 3. Plan of experimental installation.

formed a gap of 1 cm in the non-irradiated section of the target. The gap was filled with liquid nitrogen. The total capacity of the target ($\approx$ 8.5 litres of liquid hydrogen) at an average vaporization rate of $\approx$ 0.6 litres per hour ensured $\approx$ 8 hours of constant work between refillings of the target. With an 30 cm effective length of the target its irradiated walls were "out of sight" for the detecting telescopes (except for the experiment with the angle of 150°) which considerably reduced the background from an empty target.

The scattered γ-quanta were detected simultaneously at two different angles by approximately identical telescopes with lead protection. Paraffin shields of 5 to 7 cm thick were placed at the entrance to the telescope channel, which reduced the amount of soft electrons and γ-quanta in the first counter.

2.4. MONITORS

A thin-walled ionization chamber placed in front of the first collimator served as an "intermediary" monitor. All measurements were reduced to a definite

number of counts of this chamber. The absolute value of the energy flux which had passed through the collimator at a given number of counts of the monitor was determined at regular intervals by the activation of standardized carbon detectors in the reaction $C^{12}(\gamma, n)C^{11}$, the cross section of which is known from refs. [9, 10]). To make the absolute calibration of the monitor more accurate the data on the activation of carbon were compared at intervals with the readings of a thick-wall graphite chamber with known absolute sensitivity (the so-called Lax-chamber). The values of the flux of γ-quanta obtained by the two methods coincided with an accuracy $\approx 3\ \%$.

2.5. EFFECTIVENESS OF TELESCOPES

To obtain the differential angular cross sections from the measured outputs of γ—p scattering it is necessary to know the energy dependence of the effective detection of scattered γ-quanta by the telescopes used. In the present work we employed the method we had specially worked out [11]) for determining this dependence in region from 35 to 150 MeV. The method is based on the detection of the Compton scattering of a bremsstrahlung beam on electrones at a small angle (3°). Since the spectrum of bremsstrahlung and the differential cross section of Compton scattering on electrons are known, the comparison of data at various maximum energies of bremsstrahlung yields the wanted energy

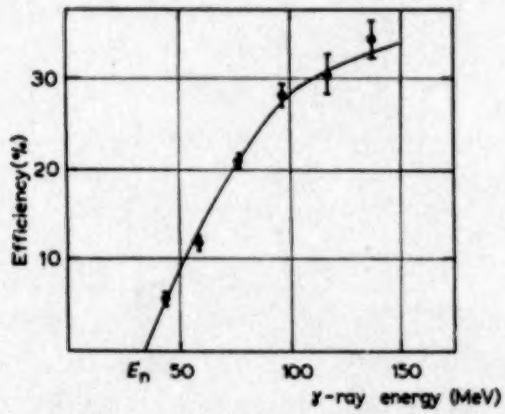

Fig. 4. Energy dependence of the effectiveness of detection of γ-quanta by the coincidence telescope.

dependence. The results of determining the energy dependence of the effectiveness of γ-quanta detection for one of the telescopes is represented in fig. 4 alongside the relevant statistical errors. The energy threshold of the telescope had been calculated by the sum of average energy losses of electrons on their leaving the convertor. The calculated figure (≈ 35 MeV) coincided with the result of the experiment.

It is essential that in the calibration experiments (as well as in the principal measurements) the entire effective surface of the telesope be irradiated at once (since in these experiments the telescope was removed at a distance of 11 m

from a carbon target of 1.5 cm thick). Besides, the absolute determination of the bremsstrahlung beam was conducted by the same method as in the principal experiments. Therefore various errors in the absolutization of the results of the principal and calibration experiments were eliminated and, in fact, direct comparison of the differential angular cross sections of Compton scattering was drawn in our experiments: the known cross sections for electrons and those to be determined for protons.

2.6. PROCEDURE OF EXPERIMENT

The maximum energy of the bremsstrahlung spectrum in the principal experiments was 75 MeV. The duration of intensity pulses (i.e., the hitting of the synchrotron target by electrons) was stretched up to ≈ 300 μs which corresponded to changes in the maximum energy of the bremsstrahlung spectrum from 62 to 75 MeV. Observation of the form of "stretching" (approximately rectangular) was visual, through a ИО-4 oscillograph synchronized with the accelerator.

The detecting telescopes were placed at angles of 45°, 75°, 90°, 120°, 135° and 150° to the direction of the bremsstrahlung beam, measurements at two angles being conducted simultaneously. Since the effectiveness of two telescopes differed somewhat, they were changed at certain intervals and the results averaged with respect to both telescopes were used for each angle.

The series of experiments with hydrogen alternated with the measurements of the background. In the experiments with the empty target the background at all angles averaged some 40 % from the rate of counting in the principal experiments.

To check the stability of the operation of the installation as a whole, control measurements of counting rate from the thick carbon target were conducted daily under working conditions as well as at a maximum energy of bremsstrahlung equal to 265 MeV.

2.7. TREATMENT OF RESULTS

The number of counts of the telescope placed at an angle of $\theta°$ correlated to a certain number of counts of the monitor chamber (say 1 000 counts) may be represented as

$$Y = \iiint a\eta(E, E_m)\mathscr{E}(E'(E))\frac{d\sigma}{d\Omega}(E, \theta)n_0 dV d\Omega dE. \quad (7)$$

Here,

$$a = \frac{E_{total}}{\int_0^{E_m}\eta(E, E_m)E dE}$$

is the beam of γ-quanta averaged by the irradiated area (per cm², for 1 000

counts); $\eta(E, E_m)$ the form of bremsstrahlung spectrum; $\varepsilon(E')$ is the effectiveness of detection of γ-quanta with the energy E' (which corresponds to the initial energy E) scattered at an angle $\theta°$; n_0 is the number of hydrogen nuclei in cm^3; dV is an element of the effective volume of the target and $d\Omega$ is the corresponding solid angle of "visibility" of the telescope (from the element dV). The integral $I_\theta = \int\int n_0 dV d\Omega$ practically does not depend on the energy of the primary γ-quanta(the account of the absorption of γ-quanta in the target will be discussed below). This integral was calculated for every angle, depending on the specific geometry of each experiment. To check the calculation the ratio $I_\theta/I_{90°}$ was compared with the data of an auxiliary experiment in which the number of counts from a "point target" of styrofoam PS-4 (a cube $2\times2\times2$ cm^3) was compared with the number of counts from the cylinder of the same material imitating the effective volume of the liquid-hydrogen target.

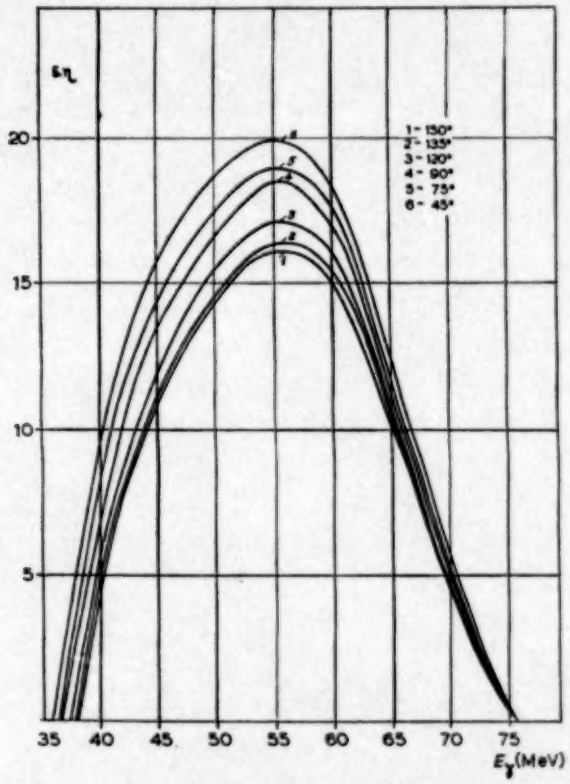

Fig. 5. The product of the effectiveness of the detection of a scattered γ-quantum by the distribution function in the primary bremsstrahlung spectrum (for different scattering angles).

Taking the cross section $\overline{d\sigma/d\Omega}$ averaged by angles and energies out of the integrand, we may isolate an integral depending on energy.

Then

$$\overline{\frac{d\sigma}{d\Omega}} = \frac{B}{aI_E I_\theta}, \tag{8}$$

TABLE 1

Experimental differential cross sections

Angle	Differential angular γp-scattering cross sections (directly from experiment) (10^{-32} cm²/sr)	Allowances for by-processes (10^{-34} cm²/sr)				Allowances for the absorption of primary and registered γ-quanta in the target $\Delta\sigma/\sigma$(%)	Differential angular γp cross sections (final quantities) (10^{-32} cm²/sr)
		Rutherford electron scattering with subsequent radiation	Production of pairs at large angles with subsequent radiation	Bremsstrahlung at large angles	Total allowances		
45°	4.66±0.28	−127	−14.1	−5.4	−146	+5.5	3.40±0.28
75°	1.21±0.08	− 10.7	− 1.4	−0.47	− 12.6	+3.5	1.12±0.08
90°	1.14±0.05	− 6.6	− 0.7	−0.3	− 7.7	+3.5	1.10±0.05
120°	1.30±0.08	− 1.4	− 0.18	−0.06	− 1.6	+4.5	1.34±0.08
135°	1.48±0.08	− 0.89	− 0.09	−0.04	− 1.0	+6.5	1.56±0.08
150°	1.82±0.07	− 0.36	− 0.04	−0.01	− 0.4	+6.5	1.93±0.07

where

$$I_E = \int_{E_{th}}^{E_{max}} \eta(E, E_{max}) \mathscr{E}(E'(E)) \mathrm{d}E.$$

The bremsstrahlung spectrum of the synchrotron for a thick target is expressed by Eyges' formula [12]) and the dependence $\mathscr{E}(E)$ was represented above in fig. 4; it is evident that the energy of the scattered quantum $E' = EMc^2/\{Mc^2 + E(1-\cos\theta)\}$ changes with the scattering angle $\theta°$ and consequently the entire integral I_E changes as well. Fig. 5 contains the products of the effectiveness of detection of the scattered γ-ray by the distribution function in the spectrum of primary bremsstrahlung for various angles of scattering depending on the energy of the incident γ-quanta. It can be seen that the curves are roughly symmetrical and have a maximum at $\approx$ 56 MeV and half width averaging about 25 MeV. The absolute value of I_E for 90° was calculated graphically. Corrections for a change in the effectiveness of detection at other angles was also calculated graphically: by the relation of the areas under the relevant curves. These corrections equalled from +5 % for 75° and put to −15.4 % for 150°. The differential cross sections of γ—p scattering for 45°, 75°, 90°, 135° and 150° thus obtained from the experiment are shown in the second column of table 1.

2.8. CORRECTIONS FOR ABSORPTION IN TARGET

For absolute determination of the average beam of γ-quanta hitting the target, carbon detectors were located in the centre of the target. Under working conditions a certain amount of bremsstrahlung is absorbed in the walls and the hydrogen of the target ($\approx$ 1.5°) and some scattered radiation is also absorbed depending on the angle: from 2.2 % for 90° up to 4.7 % for 150°. Corrections for the absorption in the paraffin shield and the walls of the telescope were eliminated due to the fact that the calibration measurements $\mathscr{E}(E)$ were also conducted with the absorbers. Corrections for the absorption of the incident, scattered and background γ-quanta in the target are represented in the seventh column of table 1 (after the allowances for the contribution of background processess).

2.9. BACKGROUND

Since we do not separate the Compton γ—p scattering by the detection of coincidences between the scattered γ-ray and the recoil proton, it is highly important to consider all possible sources of background which may contribute appreciably to the detection of γ-rays by the telescope with a threshold $\approx$ 35 MeV.

At a high threshold the possibility of detection of γ-electron Compton scattering at large angles is entirely excluded for the telescope as a whole ($\approx$ 35 MeV) as well as for each separate counter (a few MeV).

The Delbrück scattering and the radiation creation of pairs are processes

yielding γ-quanta of high energy at the angles of interest to us. The cross section of the first process [13]) on hydrogen is small ($\sigma_{tot} \approx 10^{-34}$ cm^2); and besides, the Delbrück scattering is very strongly directed forward ($\approx \theta^{-4}$) so that we can neglect it already at 45°.

There are no accurate theoretical calculations for the radiative production of pairs. According to the estimates of Feynman and Gomez cited in ref. [14]) for the laboratory angle 50° at $E_\gamma = 40$ MeV, the cross section of this process is approximately equal to that of the Compton γ—p scattering $\sigma_{\gamma p}$, while at $E_\gamma = 50$ MeV is no less than $\frac{1}{4}\sigma_{\gamma p}$. As a result of a strong energetic and angular (approximately $\approx \theta^{-4}$) dependence of the cross sections of this process, its total contribution for $E_\gamma = 56$ MeV and 75° is no more than about 3 % of γ—p-scattering. If account is also taken of the fact that only a small portion of γ-rays emitted

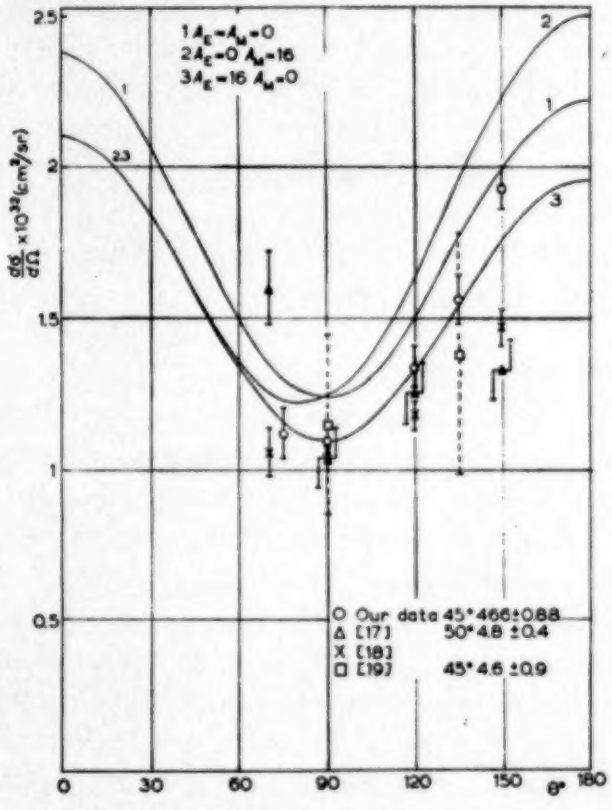

Fig. 6. Experimental data of the present paper and refs. [17–19]) on γ—p scattering at the energy of γ-quanta about 60 MeV. Between curves 2 and 3 lies the region of values of γ—p scattering cross-sections compatible with the value of the sum $A_E + A_M = 16$ (with positive A_E and A_M).

in the radiative production of pairs possess energies exceeding 35 MeV (the threshold of our telescope) it will be not difficult to conclude that the role of this process at all angles under investigation, except 45°, is negligibly small. The corresponding corrections for angles from 75° to 150° were not introduced, while the data for 45° (obviously including not only γ—p scattering) were not

used for further calculations of the polarizability of the proton because of an indefinite value of the correction to be subtracted from the cross section shown in table 1.

Other sources of background are multiple processes (occurring in the substance up to the target, in the target itself and, finally, between the target and the first counter of the telescope and leading to the penetration into the telescope of γ-rays with energies exceeding 35 MeV.

To estimate the contribution of these processes the creation of high energy electrons at small angles through Compton scattering and production of pairs in the target and in the substance before the target were calculated. Then a study was made of (a) bremsstrahlung of these electrons at large angles (according to ref. [15])) in the direction of the counters and (b) Rutherford scattering of these electrons (according to the Mott formula) in the direction of the counters with subsequent bremsstrahlung in forward direction in the substance before the telescope. Besides the production of pairs at large angles in the hydrogen of the target[16]) with the subsequent bremsstrahlung was considered. The results are shown in the third to the sixth columns of table 1. The last column of this table represents the final values of differential angular cross sections of γ—p scattering after allowances made for the background processes and the absorption in the target. Fig. 6 represents these final values alongside the data of other experimental work [17-19]) for similar energies of γ-rays ($\approx$ 60 MeV).

2.10. SYSTEMATIC ERRORS

The errors shown in table 1 in determining the cross section of γ—p scattering are merely due to the statistical errors of principal measurements. The main possible source of systematic errors: inaccuracy in determining the bremsstrahlung flux is eliminated owing to direct comparison of the Compton scattering cross sections on protons and electrons. Nevertheless there remains an error on account of two inaccuracies in determining the product of the effective volume of the target multiplied by the solid angle of the telescope's visibility in the calibration and principal (integral I_θ) experiments. This error is set down at $\pm 4\,\%$. In comparing the results of the calibration and principal experiments, additional statistical errors arise from determining the beam of γ-rays by the number of counts of the monitor in both kinds of experiments and summing the dispersions of many points at the curve of the effectiveness of the telescopes in the detection of γ-rays. Systematic errors due to possible inaccuracy in the form of the bremsstrahlung spectrum used are directed oppositely in both calibration and principal experiments and are nearly completely eliminated. The total value of possible systematic error in determining the cross section of γ—p scattering at angles from 75° to 150° is estimated as $\pm 6\,\%$.

To return to the statistical errors shown in table 1, we notice that these lie within 3.6 to $+7.2\,\%$ for five experimental points; the square root of the sum

of dispersions for all five points corresponds to 11.7 %. Thus, in using experimental points for comparison with calculated theoretical curves, the average statistical error for one point is about 2.4 % and the total error (statistic plus systematic error) about 8 %.

3. Discussion of Results

The results offered in table 1 and in fig. 6 are to be compared with eq. (6) for determining the electric and magnetic polarizabilities of the proton.

Even rejecting the obviously overestimated quantity of the cross section of $\gamma-$p scattering at 45° we have five experimental quantities for determining the two parameters of eq. (6) A_E and A_M. It will be borne in mind, however, that by no means all measurements of angular distribution are equally sensitive to the values A_E and A_M. Indeed, as is clear from eq. (6) the cross section of forward scattering (at 0°) is determined merely by the sum of A_E and A_M, and not by each of them taken separately:

$$\frac{d\sigma}{d\Omega}(0^\circ) = \tfrac{1}{2}r_0^2\{2[1-2(A_E+A_M)\gamma]^2+5.13\gamma^2\}. \tag{9}$$

On the other hand, backward scattering (at 180°) does not depend on each of the quantities A_E and A_M, but only on their difference:

$$\frac{d\sigma}{d\Omega}(180^\circ) = \tfrac{1}{2}r_0^2\{2[1-4\gamma+12\gamma^2-2(A_E-A_M)\gamma^2]+78.39\gamma^2\}. \tag{10}$$

Our experiments described the $\gamma-$p scattering mainly in the back hemisphere at laboratory angles from 75° to 150°.

Proceeding from these experimental data only A_E may be obtained with sufficient certainty, since the cross sections of $\gamma-$p scattering at angles close to 90° are little sensitive to A_M.

Relying only on the value $d\sigma/d\Omega\ (90^\circ) = (1.10\pm0.05)\times10^{-32}$ cm^2/sr we obtain $A_E = 16\pm5.8$.

Dispersion relations may be used as an additional source of information enabling us to take into account the forward $\gamma-$p scattering which was not measured in the experiment and thereby to make the value A_E more accurate as well as to estimate the magnetic polarizability A_M.

As is shown in ref. [20]) the cross sections of forward $\gamma-$p scattering ($d\sigma/d\Omega(0^\circ)$) at energies below the photomeson threshold are entirely determined by the experimental total cross section of π-meson photoproduction when acted upon by non-polarized γ-quanta. Only at higher energies is it necessary for the calculation of $d\sigma/d\Omega(0^\circ)$ to know separately the meson photo-production cross sections for γ-quanta polarized parallel and anti-parallel to the spin of the proton.

Using the relations given by Cini and Stroffolini [20]) it is easy to show that

$$\frac{d\sigma}{d\Omega}(0^\circ) = \left[\frac{e^2}{Mc^2} - \frac{\gamma^2}{4\pi^2}\frac{Mc}{\hbar}\int_0^\infty \frac{\sigma_p(\gamma')+\sigma_a(\gamma')}{\gamma'^2-\gamma^2}\,d\gamma'\right]^2$$
$$+\gamma^2\left[\frac{\lambda_a^2}{2}\frac{e^2}{Mc^2} - \frac{\gamma^2}{4\pi^2}\frac{Mc}{\hbar}\int_0^\infty \frac{\sigma_p(\gamma')-\sigma_a(\gamma')}{\gamma'(\gamma'^2-\gamma^2)}\,d\gamma'\right]^2 \qquad (11)$$
$$+\gamma^2\frac{1}{32\pi^2}\left(\frac{Mc}{\hbar}\right)^2[\sigma_p^2(\gamma)-\sigma_a^2(\gamma)],$$

where $\sigma_p(\gamma)$ and $\sigma_a(\gamma)$ are the total cross sections of meson photo-production on protons for γ-quanta with the laboratory energy γ, polarized parallel (σ_p) and anti-parallel (σ_a) to the spin of protons; the sum $\sigma_p(\gamma)+\sigma_a(\gamma) = \sigma_t(\gamma)$ is the total cross section of photo-production for a non-polarized beam of γ-quanta.

Below the threshold of meson photo-production the last term is equal to 0, and hence, with an accuracy to the terms of order γ^2,

$$\frac{d\sigma}{d\Omega}(0^\circ) = r_0^2\left\{1-\left[\frac{1}{2\pi^2}\frac{Mc}{\hbar}\frac{Mc^2}{e^2}\int_0^\infty \frac{\sigma_p(\gamma')+\sigma_a(\gamma')}{\gamma'^2-\gamma^2}\,d\gamma' - \tfrac{1}{4}\lambda_a^4\right]\gamma^2\right\}. \qquad (12)$$

Comparing (12) and (9) (bearing in mind that by the very meaning of polarizability it is determined for zero energy quanta) and changing over from A_E and A_M to α_E and α_M, we obtain

$$\alpha_E+\alpha_M = \frac{1}{2\pi^2}\frac{\hbar}{Mc}\int_0^\infty \frac{\sigma_t(\gamma)}{\gamma^2}\,d\gamma. \qquad (13)$$

Obviously, since α_E and α_M are positive, eq. (13) characterizes the upper limit of the values of each of the two polarizabilities of the proton.

Using the latest data on π-meson photo-production, given for $\pi^\pm$ in ref. [21]) and for π^0 in refs. [22, 23]) (see fig. 7), we obtain $\alpha_E+\alpha_M = 11\times10^{-43}$ cm^3, i.e., $A_E+A_M = 16$. Since eq. (13) is obtained from the most general properties of the scattering matrix there are no grounds to question it in any degree at all. Therefore if eq. (6) is accurate, i.e., the theory of Rayleigh-Powell scattering is applicable with sufficient accuracy and there is no need to take account of higher terms in the frequency of the γ-quanta, it may easily be established within what limits the cross sections of γ—p scattering should lie at any angles. Inasmuch as A_E and A_M are positive and the sum $A_E+A_M = 16$, these limits lie within the curves according to eq. (6) at $A_E = 0$, $A_M = 16$ and $A_E = 16$, $A_M = 0$.

As is clear from fig. 6, in which the region of the values $d\sigma/d\Omega(\theta)$ compatible with $A_E+A_M = 16$ lies between curves 2 and 3, all our experimental data for 75°—150° are to be found within this region, whereas the values of the cross

sections of γ—p scattering into the back hemisphere obtained in refs. [17-19]) seem somewhat underestimated.

Regarding the value $A_E+A_M = 16$ as given and calculating the value A_E offering the best agreement with our results by the method of the least squares we obtain $A_E = 13\pm3$ and $A_M = 3\pm3$, the sum of the weighted squares of errors being $D = 1.8\times10^{-66}$ cm^4/sr^2. Thus, we come to the conclusion that $\alpha_E = (9\pm2)\times10^{-43}$ cm^3 and $\alpha_M = (2\mp2)\times10^{-43}$ cm^3.

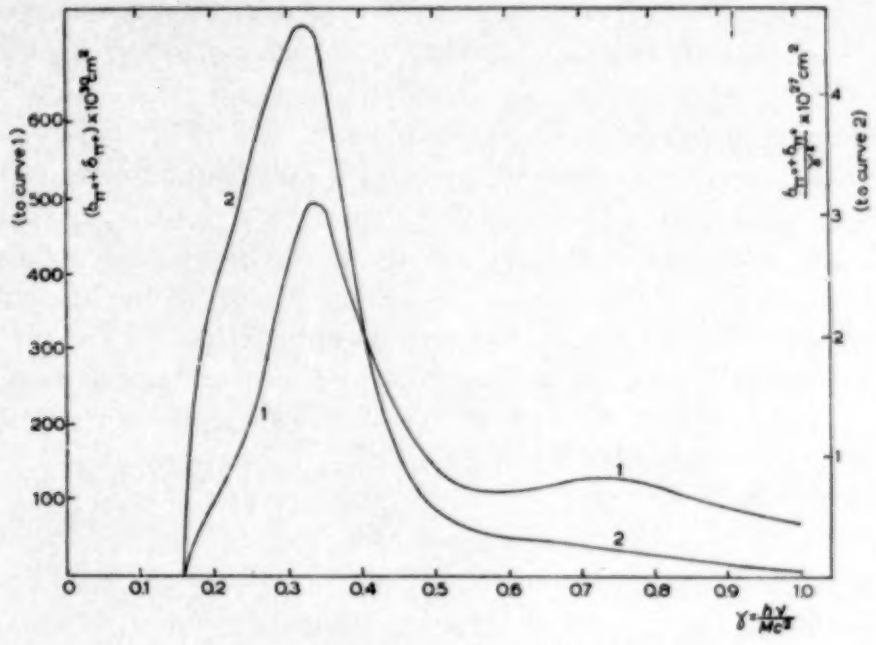

Fig. 7. Data on total photo-production cross sections of π^+ and π^0 mesons on protons used for determining the sum of electric and magnetic polarizabilities of the proton.

Thus, the magnetic polarizability of the proton is far smaller than the electric one. The determination of the former is more sensitive to the possible contribution to the cross section of γ—p scattering of the terms proportional to the high powers of the frequency of γ-quanta (over γ^2) and therefore a detailed analysis of the role of these terms is of special interest for determining A_M more accurately.

As for the electric polarizability it is clear that not only the sum A_E+A_M is in agreement with the data of our experiments, but the optimum value $A_E=13\pm3$, also coincides within errors with the data obtained above from the cross section of scattering at 90° ($A_E = 16\pm5.8$).

Direct comparison of the results of the experiment with the curve based on eq. (2) without allowances for the polarizability the proton yields a far larger sum of the weighted squares of errors than for eq. (6): $D = 10.3\times10^{-66}$ cm^4/sr^2.

The best agreement with eq. (2) is attained by increasing our experimental cross sections by 8 %, which, however, lies on the margin of possible systematic errors.

The question of the electric polarizability of nucleons has recently been widely discussed as a result of the development of theoretical concepts [24, 25]) on the role of the polarizability of neutrons in their electric scattering at small angles in the Coulomb field of heavy nuclei. The value of electric polarizability of the neutron computed by Alexandrov [26]) from an analysis of his experiment on neutron scattering $\alpha_E = (8 \pm 3.5) \times 10^{-41}$ cm^3 certainly contradicts all data on γ-rays scattering and π-meson photo-production, which was already noted in theoretical papers [7, 27–31]) and is now again confirmed by our experiments.

The latest analysis of new experiments on neutron scattering [29]) led to a reduction in the upper value of α_E namely, $0 < (\alpha_E)_n < 2.2 \times 10^{-41}$ cm^3 but yielded no more definite results. Inasmuch as $\alpha_E \approx 10^{-42}$ cm^3, neutron experiments will in general not enable us quantitatively to establish the contribution of electric polarizability. Therefore the avenue to a study of the electric and magnetic polarizabilities of the nucleon, the properties conditioned by changes in the structure of the meson cloud in the nuclei, lies in the investigation of π-meson photo-production and nucleon Compton effect.

Rough estimates of electric polarizability of a neutron on the basis of meson theories are of order of $(e^2 f^2/\hbar^2 c^2)(\hbar/\mu c)^3 = 1.6 \times 10^{-42}$ cm^3 [27, 29]) where $f^2/\hbar c = 0.08$. A result close to this estimate: $(\alpha_E)_n = (1.6 \text{ to } 1.8) \times 10^{-42}$ cm^3 was obtained [27]) by estimating the polarizability of the meson cloud in the nucleon with the help of the Chew-theory for the Gauss and exponential form-functions at the cutting parameter 5.6 $\mu c/\hbar$. Analysing the data on π-meson photo-production and γ—p scattering, Baldin [7]) obtained the quantity $(\alpha_E)_p = 4 \times 10^{-43}$ cm^3 as the lower limit of nucleon electric polarizability (under the assumption of only one-meson exchange). The upper limit $(\alpha_E)_p$ is obtained in ref. [7]) on the basis of the proximity of the cross section of γ—p scattering at 90° to Thomson's $(\frac{1}{2}r_0^2)$ and is set down at 1.4×10^{-43} cm^3.

From the data on π-meson photo-production a close estimate is obtained for the neutron in ref. [30]): $(\alpha_E)_n \lesssim 2 \times 10^{-42}$ cm^3.

It should be borne in mind that since the cross section σ^- of the process $\gamma + n \to \pi^- + p$ near the threshold exceeds the cross section σ^+ of the process $\gamma + p \to \pi^+ + n$ and the contribution of the near-threshold region to the dispersion integral (13) is considerable, the electric polarizability of the neutron should exceed the corresponding quantity for the proton by 20 to 30 % (refs. [7b, 30])). As is clear from the calculations in which eq. (13) was used, the upper limit for the electric polarizability of the proton may be lowered to $(\alpha_E)_p = 1.1 \times 10^{-42}$ cm^3.

In the final conclusion of our paper concerning the quantity $(\alpha_E)_p$ we additionally use the calculated upper value of the sum $(\alpha_E + \alpha_M)_p = 1.1 \times 10^{-42}$ cm^3; even the direct result of the experiments on the whole confirms the above-mentioned theoretical estimates of $(\alpha_E)_p$.

In conclusion we shall consider the problem of the mean quadratic fluctuation

of the displacement (allied with α_E) of the centre of electric charge distribution in the polarized proton with respect to the centre of its gravity.

According to refs. [7b, 30]) this quantity $\sqrt{\bar{r}^2}$ is connected with the electric polarizability of the proton through the common relation

$$\sqrt{\bar{r}^2} = \sqrt{\tfrac{3}{2}\alpha_E \frac{\hbar c}{e^2} \frac{\Delta E}{\hbar c}}, \qquad (14)$$

where ΔE is the difference of energies between the ground and virtual polarized states of the proton. Since the polarization is conditioned by the excitation of a meson cloud or the origin of resonance isobaric state it is worth while to accept ΔE in the range from Mc^2 to $2Mc^2$.

At $\alpha_E = 9\times10^{-43}$ cm^3 we obtain from eq. (14) for the mean quadratic fluctuation of the length of the proton electric dipole $\sqrt{\bar{r}^2} = (3.5 \text{ to } 5)\times10^{-14}$ cm.

It is certainly of interest to develop a more detailed theory of the magnetic polarizability of the proton to connect α_E and α_M with the contribution of various mechanisms of π-meson photo-production, to obtain the relevant theoretical limits for α_M and compare them with experiment as well as to compare the fluctuations of the length of electric and magnetic dipoles.

4. Conclusions

1) Elastic scattering of γ-rays with energies from 40 to 70 MeV (the average being 56 MeV) by protons has been studied. The new method of determining the effectiveness of γ-rays detection has made it possible to draw direct comparison of the cross sections of Compton scattering on protons and electrons and obtain the cross sections of γ—p scattering for 75°, 90°, 120°, 135° and 150° in the laboratory system within an average accuracy of $\pm8\%$ (with allowances for statistical as well as systematic errors).

2) The data thus obtained are compared with the theory of Rayleigh-Powell scattering of γ-rays by particles possessing anomalous magnetic moments and electric and magnetic polarizabilities. The scattering cross section at 90° corresponds to the electric polarizability $\alpha_E = (11\pm4)\times10^{-43}$ cm^3.

3) Alongside experimental data, the cross section of forward γ—p scattering (at 0°) was drawn upon for comparing with the theory. This cross section is determined by the sum of electric (α_E) and magnetic (α_M) polarizabilities of the proton:

$$\alpha_E+\alpha_M = \frac{1}{2\pi^2}\frac{\hbar}{Mc}\int_0^\infty \frac{\sigma_t(\gamma)}{\gamma^2}\,d\gamma.$$

4) On the basis of experimental data on γ—p scattering from 75° to 150° and the calculated cross section for 0°, the electric polarizability of the proton is

determined and the magnetic one estimated:

$$\alpha_E = (9 \pm 2) \times 10^{-43}\ \text{cm}^3, \quad \alpha_M = (2 \mp 2) \times 10^{-43}\ \text{cm}^3.$$

5) The electric polarizability thus found corresponds to the mean quadratic fluctuation of the length of the proton electric dipole $\sqrt{\bar{r}^2} = (3.5 \text{ to } 5) \times 10^{-14}$ cm.

The authors are greatly indebted to R. G. Vasilkov, S. P. Balatyev, Ye. V. Minarik and A. Samuillin for their assistance in conducting the experiments and G. Ivanov for his active participation in the treatment of the results obtained. We are glad to thank the entire maintenance staff of the 265 MeV synchrotron of the FIAN for ensuring many hours' experimentation for us and express our sincere acknowledgements to A. M. Baldin and V. N. Gribov for their participation in discussing the results.

Note added in proof: The general expression for the amplitude of γ—p scattering (in CMS) is of the form

$$T = R_1(ee') + R_2(ss') + iR_3(\sigma[e'e]) + iR_4(\sigma[s's]) + iR_5\{(\sigma k)(s'e) - (\sigma k')(se')\} + iR_6\{(\sigma k')(s'e) - (\sigma k)(e's)\}$$

given by Ritus [32]) and Lapidus [33]).

If we take, as in refs. [2–5]), $R_1 = 1$, $R_2 = R_5 = 0$, $R_3 = \frac{1}{2}\gamma$, $R_4 = \frac{1}{2}\gamma\lambda^2$, $R_6 = \frac{1}{2}\gamma\lambda$ (all R_i values are in $e^2/\mu c^2$ units) we obtain formula (1) for cross-sections. To obtain eq. (6) we have to take $R_1 = 1 - A_E\gamma^2$, $R_2 = A_\mu\gamma^2$.

As was shown by Aristov [34])

$$A_E = \tfrac{1}{3} r_e^2 \left(\frac{\mu c}{\hbar}\right)^2 + \tfrac{1}{4}\cos\theta + \tfrac{1}{2}\lambda_a + A^*_E,$$

where $r_e = 0.8 \times 10^{-13}$ cm is the electric radius of the proton and

$$A^*_E = \alpha^*_E \frac{e^2}{\hbar c}\left(\frac{\hbar}{\mu c}\right)^3,$$

α^*_E being the electric polarizability of the proton in conventional sense (i.e., dipole moment $\mathbf{p} = \alpha^*_E \mathbf{E}$).

References

1) J. L. Powell, Phys. Rev. **75** (1949) 32
2) M. Gell-Mann and M. Goldberger, Phys. Rev. **96** (1954) 1433
3) F. E. Low, Phys. Rev. **96** (1954) 1423
4) A. Klein, Phys. Rev. **99** (1955) 998
5) R. Capps, Phys. Rev. **106** (1957) 1031
6) V. A. Petrunkin (private communication)

7) A. M. Baldin, a) Report at the Conference on Elementary Particles at Padua-Venice (1957); b) Nuclear Physics **18** (1960)
8) E. C. Park, J. Sci. Instr. **33** (1956) 257
9) W. Barber, W. George and D. Reagan, Phys. Rev. **58** (1955) 73
10) P. S. Baranov, Thesis, P. N. Lebedev Physical Institute (1955)
11) V. I. Goldansky, O. A. Karpukhin and V. V. Pavlovskaya, Instruments and Technique of Experiment **3** (1960) **23**
12) L. Eyges, Phys. Rev. **81** (1951) 982
13) A. I. Akhiezer and V. B. Berestetsky, Quantum Electrodynamics, second edition (Fizmatizdat, 1959)
14) L. G. Hyman, MIT. Ph. D. Thesis (1959)
15) P. V. C. Hough, Phys. Rev. **74** (1948) 80
16) R. C. Miller, Phys. Rev. **95** (1954) 796
17) C. Oxley and V. L. Telegdi, Phys. Rev. **100** (1955) 435
18) C. Oxley, Phys. Rev. **110** (1958) 733
19) G. Pugh, R. Gomez, D. Frisch and G. Janes, Phys. Rev. **105** (1957) 982
20) M. Cini and R. Stroffolini, Nuclear Physics **5** (1958) 684
21) G. Bernardini, Report at the IXth Conference on High Energy Physics, Kiev (1959)
22) R. G. Vassilkov, B. B. Govorkov and V. I. Goldansky, JETP **37** (1959) 11; Nuclear Physics **12** (1959) **337**
23) K. Berkelman and J. Waggoner, Phys. Rev. **117** (1960) 1364
24) Yu. A. Alexandrov and I. Bondarenko, JETP **31** (1956) 726
25) V. S. Barashenkov, I. P. Stakhanov and Yu. A. Alexandrov, JETP **32** (1957) 1546
26) Yu. A. Alexandrov, JETP **32** (1957) 561; **33** (1957) 294
27) V. S. Barashenkov and B. M. Barbashov, Nuclear Physics **9** (1958) 426
28) D. I. Blokhintsev, V. S. Barashenkov and B. M. Barbashov, Usp. Fiz. Nauk **68** (1959) 417
29) R. M. Thaler, Phys. Rev. **114** (1959) 827
30) G. Breit and M. L. Rustgi, Phys. Rev. **114** (1959) 830
31) L. L. Foldy, Phys. Rev. Letters, **3** (1959) 105
32) V. I. Ritus, JETP **33** (1957) 1264
33) L. I. Lapidus, JETP **34** (1958) 922
34) Yu. Aristov (private communication)

2.C

Nuclear Physics **18** (1960) 492—501; © *North-Holland Publishing Co., Amsterdam*

Not to be reproduced by photoprint or microfilm without written permission from the publisher

PROTONS FROM DEUTERON BOMBARDMENT OF Be^7

R. W. KAVANAGH

Kellogg Radiation Laboratory, California Institute of Technoglogy, Pasadena, California †

Received 4 April 1960

Abstract: Protons from the reaction Be^7(d, p)Be^8 leading to Be^8 excitations up to 11 MeV have been examined with a NaI(Tl) scintillation spectrometer. No groups attributable to Be^8 are observed except those corresponding to the ground state (p_0) and first excited state (p_1), along with a continuum extending to over 11 MeV excitation. Resonances are found at bombarding energies of 0.900 ± 0.025 (p_0 and p_1) and 1.475 ± 0.010 MeV (p_1 only) with centre-of-mass widths 120 ± 40 and 71 ± 8 keV, respectively, corresponding to states in B^9 at 17.19 and 17.63 MeV. The excitation energy and width of the first excited state of Be^8 are $E_x = 2.90\pm0.06$ and $\Gamma_{cm} = 1.53\pm0.04$ MeV. The reduced width of this state and the $\alpha-\alpha$ interaction radius extracted from a single-level analysis are compared with those found in $He^4(\alpha, \alpha)$ and $B^{10}(d, \alpha)$ reactions.

1. Introduction

The bulk of the evidence regarding the energy levels of Be^8 below about 12-MeV excitation indicates the existence of just three states, all alpha-unstable: the ground state, a broad state at 2.9 MeV, and a still broader state at about 11.7 MeV [1]. The most detailed information about the parameters of these states has come from phase shift analyses of $\alpha-\alpha$ scattering, which in particular give spin-parity assignments of 0^+, 2^+ and 4^+, respectively, to these states. The alpha-scattering experiments, however, can reveal only even-even states, and other reactions must be used to test for the possible presence of states of other spin-parity character. There have, in fact, been several reports of additional states in this region, but these appear to have been negated by later work.

Some disagreement seems also to exist in the width of the first excited state, as determined from various reactions. For example, Goward and Wilkins [2] observe a width of 0.7 ± 0.15 MeV in the reaction $C^{12}(\gamma, \alpha)Be^8$, whereas Russell *et al.* [3]) deduce a width $\Gamma_{cm} = 2.0$ MeV from $\alpha-\alpha$ scattering. Other reports of intermediate values may be found in the summary of Ajzenberg-Selove and Lauritsen [1]) ††.

This report describes a study of the proton groups from the Be^7(d, p)Be^8 reaction, undertaken as a further means of clarifying the low-lying level

† Work supported in part by the joint program of the Office of Naval Research and the U. S. Atomic Energy Commission.

†† Note that the second entry for Γ in table 8.4 of ref. [1]) is a derived width, that the next-to-last should be multiplied by $\frac{1}{2}$, and that the last should read 0.7 ± 0.15.

structure of Be^8. The Q value (16.671 MeV) of this reaction is so high that even with a target in which the Be^7 is heavily outweighed by impurities, it is possible to detect protons leading to Be^8 excitation well above the first excited state. An earlier study of this reaction has been reported by Spear [4]), who found for $E_x < 5.8$ MeV only the ground state and the 2.9-MeV state, with the latter having a width of 1.6 ± 0.4 MeV. The present experiment with improved statistical accuracy extends to about 11 MeV the region in which additional states appear to be absent, and reduces by a factor of 10 the error in the observed width of the first excited state. A fairly good fit to the observed shape of this state is also obtained from the one-level dispersion formula, but with parameters which differ from those found in other reactions.

2. Experimental Procedure and Results

The target, consisting of a thin layer of Be^7O deposited on a 0.013-cm thick platinum disk, was prepared by chemical and physical separations of Be^7

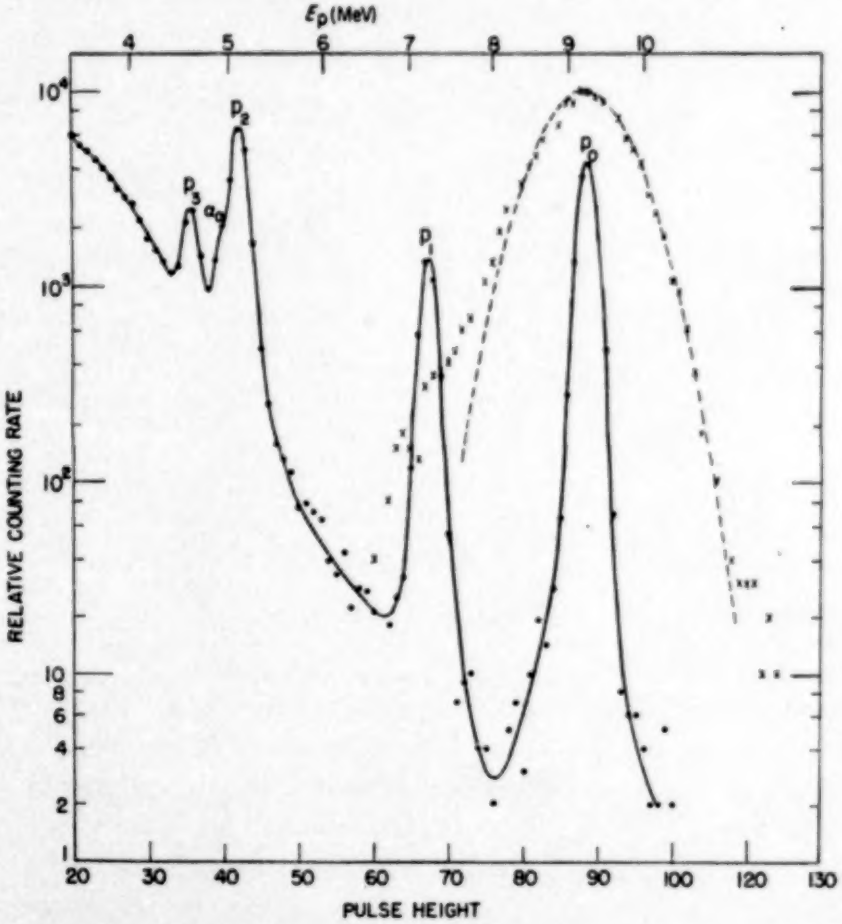

Fig. 1. The pulse-height spectrum, observed at 90°, from 1 MeV deuteron bombardment of a B^{10} target, illustrating the NaI detector response. The labels p_0, p_1, etc., refer to proton groups from $B^{10}(d, p)B^{11}$ leading to B^{11} in its ground state, first excited state, etc.; α_0 refers to the ground state group from $B^{10}(d, \alpha)Be^8$. The p_0-peak is also shown (crosses) expanded fivefold, *i.e.*, rerun with 0.2 % channel width, for comparison with a Gaussian curve (dashed) of width 3.0 %.

from lithium metal which had been bombarded with 12-MeV protons at the University of California 152-cm cyclotron. Details of target preparation have already been given [5]) in connection with a previous experiment in which the same target was used. The target was fairly uniform over a spot about 4 mm in diameter with a surface density of 10^{16} Be^7 atoms per cm^2 and a total radioactivity of 10 mc. Including impurities, the total deposit thickness was equivalent to a 1-MeV proton energy loss of less than 4 keV.

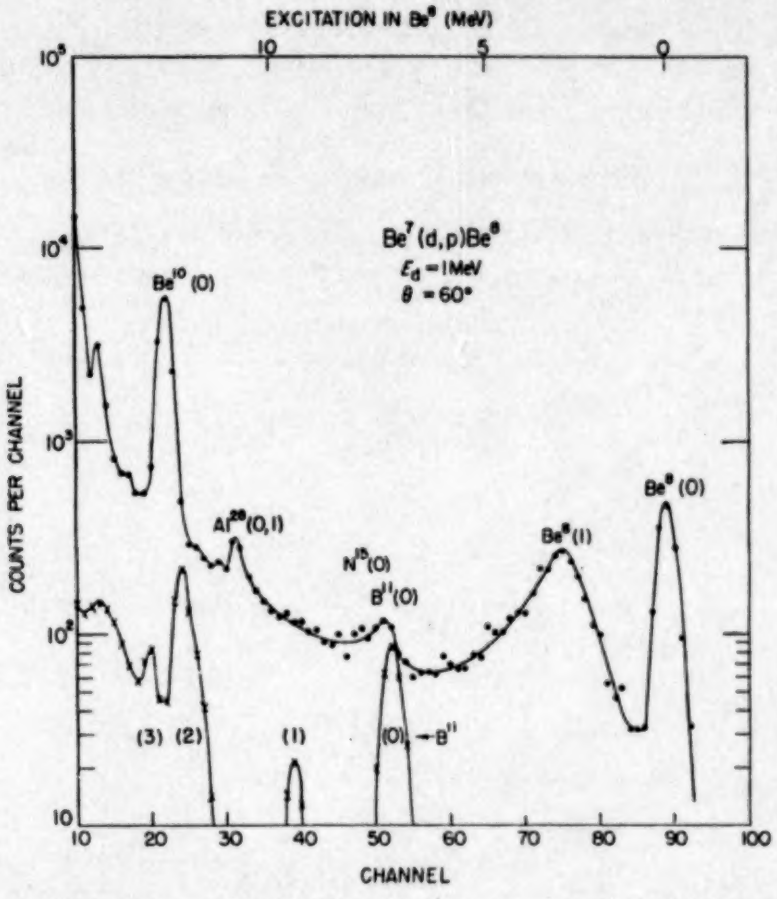

Fig. 2. The pulse-height spectrum obtained from the Be^7 target at $E_d = 1$ MeV. Peaks are labelled with the final states produced in the (d, p) reactions on Be^7 or target contaminants. The pairs $Al^{28}(0)$—$Al^{28}(1)$ and $B^{11}(0)$—$N^{15}(0)$ are unresolved. Also plotted (with arbitrary ordinate scale) are the peaks from a calibration run taken under the same conditions with a B^{10} target.

The Be^7 target was installed on the axis of a scattering chamber of 20-cm diameter which was fitted at 15° intervals with 1.11 cm diameter ports covered with 25-μm aluminium foil. For calibration purposes, a 96 % B^{10} target was also mounted on the target holder. An electrostatic accelerator provided a deuteron beam of about 1 μA, magnetically analyzed, ranging in energy from 0.7 to 1.7 MeV. To detect protons emanating from the target, a 0.16 cm wafer of NaI(Tl), covered with 13-μm aluminium foil and mounted on a Dumont 6291 photomultiplier, was moved from port to port on a 23-cm diameter circle

about the chamber axis. The response of the detector to protons from deuteron bombardment of the B^{10} target is shown in fig. 1. The exit aperture was reduced to 0.64-cm diameter for this spectrum only, giving somewhat better resolution than with the full 1.11-cm port by reducing the (non-Gaussian) broadening effects of energy variation with angle and curvature of the exit foil. That the shoulder on the p_2 peak is in fact due to $B^{10}(d, \alpha_0)Be^8$ was established by another

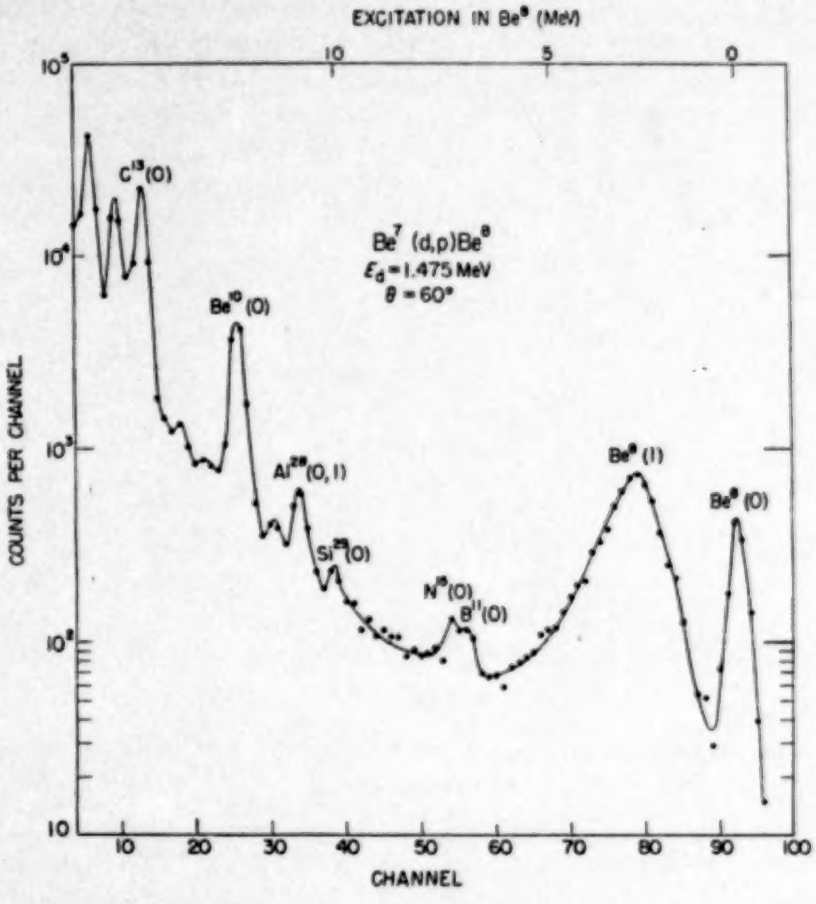

Fig. 3. Pulse-height spectrum obtained from the Be^7 target at $E_d = 1.475$ MeV.

run with an additional 13-μm Al-foil absorber, which shifted the α_0 peak below p_3.

In fig. 2 and fig. 3 are shown the spectra obtained from the Be^7 target at bombarding energies of 1 MeV and 1.475 MeV, respectively. Similar curves were obtained at 15° intervals from 60° to 150°, for deuteron energies of 1, 1.475 and 1.625 MeV, permitting unambiguous assignments to be made as indicated for the prominent proton groups. From several such curves and from B^{10}(d, p) groups, the calibration curve in fig. 4 was obtained, using the well known Q values for the various reactions.

Except for the labelled peaks in the pulse height spectra, no isolated sharp proton groups appear up to a Be^8 excitation of about 11 MeV, although they would have been seen had they been as strong as 10 % of the $Be^8(0)$ group, i.e., about half the strength of the Al^{28} peak in fig. 2. A higher limit must of course be set at regions obscured by contaminant groups, such as the vicinity of $E_x = 7.5$ MeV.

The continuum extending upwards in Be^8 excitation from 6 MeV is necessarily to be ascribed to protons from Be^7+d, since, again apart from the labelled peaks, there is no other possible source for counts in this region. (The most

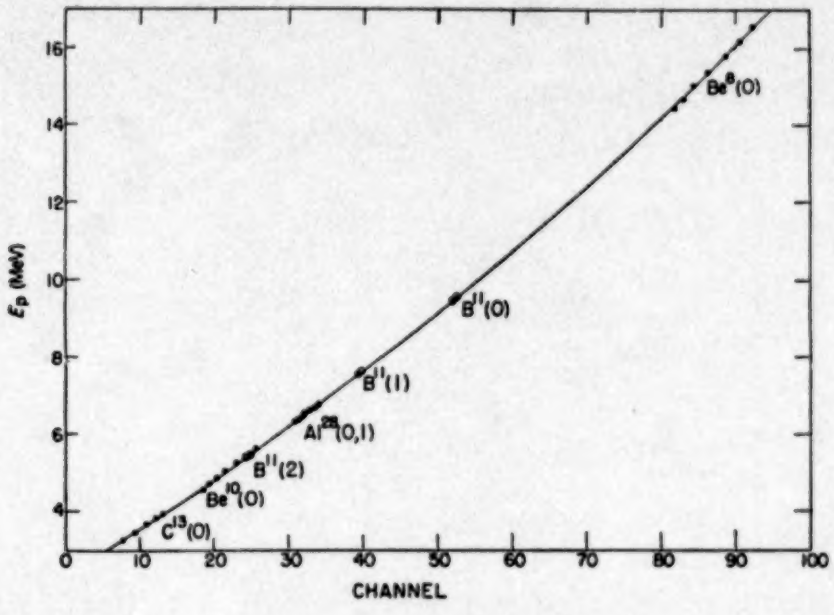

Fig. 4. Calibration curve of proton energy *versus* pulse height, from measurements at $E_d = 1.475$ MeV and at various angles with the Be^7 target (solid circles) and the B^{10} target (open circles).

energetic alpha particles, from $B^{10}(d, \alpha)Be^8$, appear at the position of the $B^{11}(2)$ peak in fig. 2.) That this continuum is distinct from the tail of the first excited state of Be^8 is manifest from the relative yields at the two bombarding energies of figs. 2 and 3: although the $Be^8(1)$ yield is up in fig. 3 by the factor 2.1, the yield in the continuum is unchanged. It is reasonable to attribute the latter to the broad G-wave state at $E_x \approx 11.7$ MeV observed in $\alpha-\alpha$ scattering by Nilson *et al.* [6]) with a width [3]) Γ_{cm} of about 6.7 MeV. Direct breakup into three alpha particles may also contribute.

From the calibration curve of fig. 4 and its counterparts at 1 and 1.625 MeV, the position of the peak of the $Be^8(1)$ state is found to be 2.90 ± 0.06 MeV (probable error) and its width at half-maximum to be $\Gamma_{cm} = 1.53 \pm 0.04$ MeV, corrected (by 6 %) for resolution but not for a possible pedestal due to extension of the continuum under the peak. (Subtracting an estimate of the latter, made by smoothly joining the low points in fig. 3, reduces the measured width

by about 7 %.) Twenty spectra were used in these determinations and the assigned probable errors are primarily an assessment of the accuracy of the calibration curves.

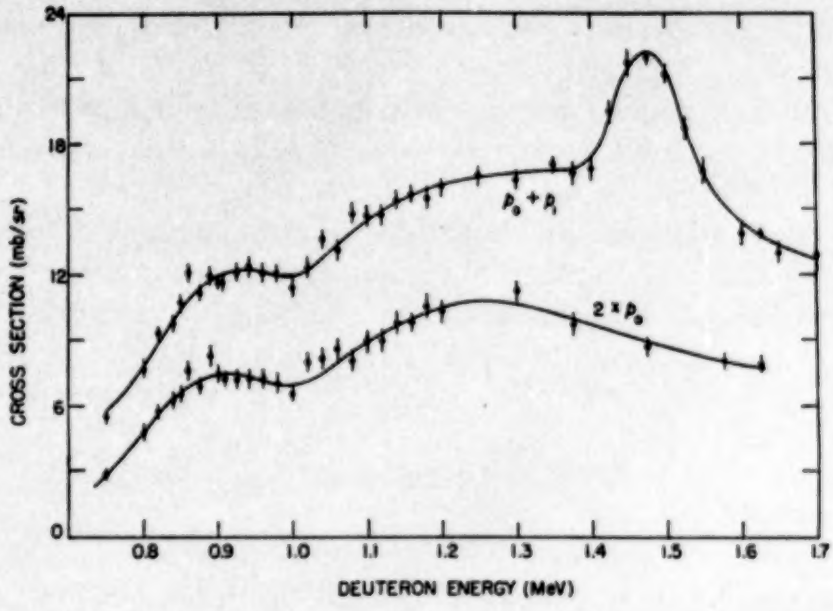

Fig. 5. Absolute cross sections (± 20 %) *versus* bombarding energy for $Be^7(d, p_0)Be^8$ and $Be^7(d, p_0+p_1)Be^8$.

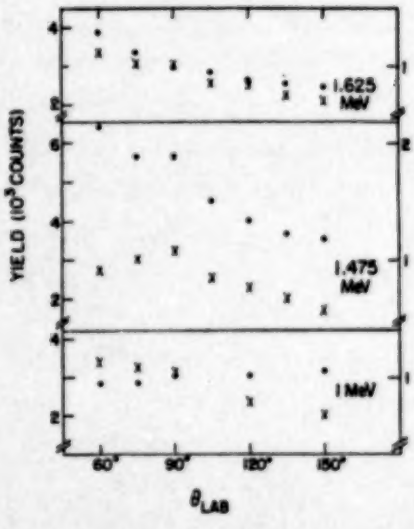

Fig. 6. Yield *versus* laboratory angle for $Be^7(d, p_0)Be^8$ (crosses, right scale) and $Be^7(d, p_1)Be^8(1)$ (circles, left scale).

The cross sections at 90° for production of Be^8 in its ground and first excited states were measured as a function of energy (see fig. 5) using two integral pulse-height discriminators biased to correspond to excitations of 1 and 6 MeV in Be^8. The target thickness was known from a previous experiment [5]). Two

resonances, superimposed on a relatively slowly varying yield, are indicated at deuteron energies of 0.900 ± 0.025 and 1.475 ± 0.010 MeV, with widths Γ_{cm} of 120 ± 40 and 71 ± 8 keV, respectively, corresponding to states in the compound nucleus B^9 at 17.19 and 17.63 MeV. The former has not hitherto been reported, while the latter has also been observed as a resonance for p_1, and not for p_0, in the $Li^6(He^3, p)Be^8$ reaction by Schiffer *et al.* [7]). It will be recalled from the comparison of figs. 2 and 3 that the distribution presumed to be due to the Be^8 4^+ state also appeared to be non-resonant at 1.475 MeV, but this was not studied in detail.

Angular distributions in the forward-angle range where useful comparison could be made with stripping theory were not obtainable due to the thick target backing. The data which were obtained by summing the counts in the $Be^8(0)$ and $Be^8(1)$ peaks of curves like fig. 2 are shown in fig. 6.

3. Discussion

In considering the significance of reported differences in the width of $Be^8(1)$, it should perhaps be emphasized that for a state with finite lifetime, different reactions of the form X(a, b)Be^{8*} should not in general exhibit the same experimental width, since each reaction rate is a function of the energy of the outgoing particle(s) b. The first inclusion of such dependence in dealing with $Be^8(1)$ appears to be that of Fowler and Lauritsen [8]), who accounted for the low-energy portion of the observed energy distribution of alpha particles from $Li^8(\beta^-)Be^8(1)$ using a product of the penetration factor for the alpha particles and a phase-space factor for the beta decay. Bonner *et al.* [9]) attempted to fit the shape of the alpha spectrum from $Li^8(\beta^-)Be^8(1)$ with the expression

$$N_\alpha dE_\alpha \propto \frac{P_{\alpha J}(Q-2E_\alpha)^5}{(E_x-2E_\alpha)^2+\frac{1}{4}\Gamma^2} dE_\alpha,$$

where $P_{\alpha J}$ is the penetration factor for outgoing alpha particles in a state of angular momentum J and $(Q-2E_\alpha)^5$ is the approximate phase-space factor for the beta decay; the width Γ was taken to be 0.8 MeV, independent of the energy E_α. The fit was not good, but only the result using $J = 4$ was shown (with a comment in proof that $J = 2$ was a better choice). Similarly, Meyer and Staub[10] achieved a fairly good fit to the alpha spectrum from $Li^7(p, \gamma)Be^8(1)$ using the form

$$N_\alpha \propto \frac{P_{\alpha 2} T_\gamma}{(E_x-2E_\alpha)^2+\frac{1}{4}\Gamma^2}, \qquad (1)$$

where the gamma ray transition probability T_γ is implicitly a function of E_α, and the best value for the constant Γ was given as 1.9 MeV.

Treacy [11]) has reported a good fit to the α_1 spectrum from $B^{10}(d, \alpha)Be^8(1)$, using the Breit-Wigner single-level formula

$$N_{\alpha_1} \propto \frac{\Gamma_\lambda \Gamma'}{(E_\lambda + \Delta_\lambda - E)^2 + \frac{1}{4}\Gamma_\lambda^2}, \tag{2}$$

where Γ' and E_λ are constants, $E = 2E_\alpha$ is the centre-of-mass energy in the $\alpha-\alpha$ scattering system, and where the level shift Δ_λ and width Γ_λ depend on J, E_α and on the assumed interaction radius a. In this case, large distortion from neglect of explicit dependence on E_{α_1} would not be expected because of the high value of E_{α_1} over the region of fit. The best fit was found with $J = 2$, $a = 4.5 \times 10^{-13}$ cm, and dimensionless reduced width $\theta^2 = \frac{2}{3}Ma^2\gamma^2/\hbar^2 = 1.9$.

In the present experiment, a fit to the observed distribution of protons from $Be^7(d, p_1)Be^8(1)$ was sought using the Breit-Wigner formula as given above, including as a small correction the phase-space factor for high-energy protons by setting $\Gamma' \propto v_p$, the velocity of the outgoing proton. The Γ_λ and Δ_λ may be expressed in terms of the amplitude A of the Coulomb wave function with $L = 2$, and the wave number k of the alpha particles from the $Be^8(1)$ breakup, as

$$\Gamma_\lambda = \frac{2\rho\gamma^2}{A^2} \quad \text{and} \quad \Delta_\lambda = -\gamma^2\left(\frac{\rho}{A}\frac{dA}{d\rho} + 1\right), \tag{3}$$

where $\rho = ka$. For comparison with parameters found from $\alpha-\alpha$ scattering, it is convenient also to write the single-level formula in terms of δ_λ, the resonant part of the alpha-scattering phase shift; we have

$$N_p \propto \frac{\frac{1}{2}v_p\Gamma_\lambda}{(E_\lambda + \Delta_\lambda - E)^2 + \frac{1}{4}\Gamma_\lambda^2} = \frac{2v_p}{\Gamma_\lambda}\sin^2\delta_\lambda. \tag{4}$$

This expression was evaluated with the aid of the tables of Bloch *et al.* [12]). The best fit was obtained in this formulation with a radius $a = 5.75 \times 10^{-13}$ cm, and with $\theta^2 = 0.64$, corresponding to a reduced width $\gamma^2 = 0.60$ MeV ($\delta_\gamma = 90°$ occurred for $E - 0.094 = E_x = 2.92$ MeV in this case). The resulting curve is shown in fig. 7, along with the experimental points from fig. 3, replotted with a small correction for detector non-linearity. No allowance has been made for a pedestal under the experimental peak; a subtraction allowing for this possibility would require a small increase in a and decrease in θ^2. Also shown in fig. 7 is a curve found using $a = 3.5 \times 10^{-13}$ cm and $\theta^2 = 1.32$, which are the values required by the phase shift analysis of $\alpha-\alpha$ scattering data given by Jones *et al.* [13]). With these values, the upper or lower side of the peak can be accounted for, but not both. On the other hand, it has been emphasized by both Jones *et al.* [13]) and Nilson *et al.* [6]) that a radius as large as 5×10^{-13} cm leads to a set of scattering phase shifts differing greatly from the empirical set, except in the region below $E_x \approx 3$ MeV. (Calculated curves illustrating this comparison for

various values of a and θ^2 may be found in both of these references.) Jones *et al.* [13]) have suggested that a conflict of this sort could be resolved through the use of a radius a which decreases with increasing energy.

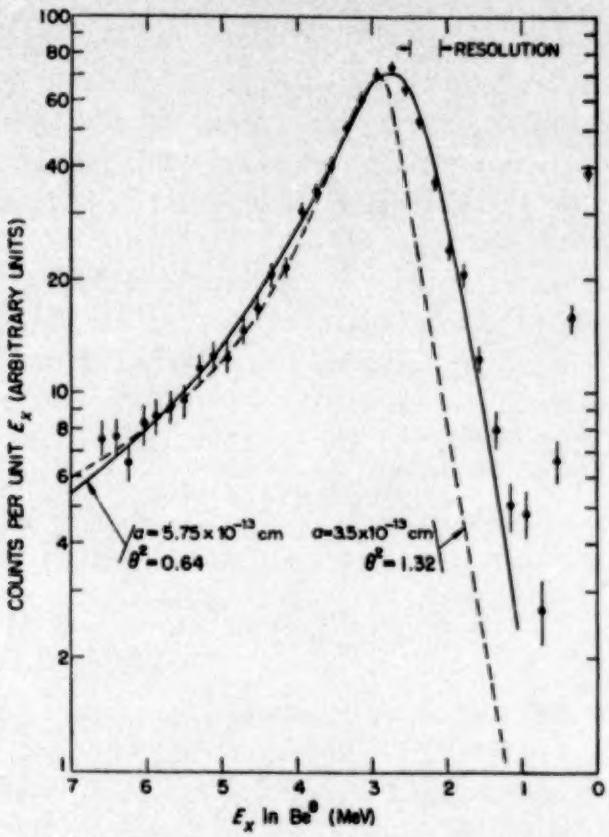

Fig. 7. The proton group to the first excited state of Be^8 from Be^7(d, p)Be^8(1). The points are the experimental data of fig. 3, and the two curves are calculated from the single-level dispersion formula for two pairs of values as indicated for the $\alpha-\alpha$ interaction radius a and the dimensionless reduced width θ^2. The curves include a correction for resolution, taken as gaussian with the indicated width; the correction in the low-E_x region shifted the steep side to the right by 0.04 MeV.

The dispersion theory parameters found in the reaction discussed above are collected for reference in table 1.

TABLE 1

Interaction radii and reduced widths found from applications of dispersion theory to Be^8(1) in three reactions

Reaction	a (in 10^{-13} cm)	θ^2	Ref.
B^{10}(d, α)	4.5	1.93	[11])
He^4(α, α)	3.5	1.32	[13])
Be^7(d, p)	5.75	0.64	This report

It is a pleasure to acknowledge the participation of Dr. Jerry B. Marion (who first suggested the feasibility of this experiment) and Professor C. A. Barnes, in early unpublished measurements of this reaction. Discussions with Professors T. Lauritsen, R. F. Christy and W. A. Fowler have also been useful and enlightening.

References

1) F. Ajzenberg-Selove and T. Lauritsen, Nuclear Physics **11** (1959) 1
2) F. K. Goward and J. J. Wilkins, Proc. Royal Soc. **228** (1955) 376
3) Russell, Phillips and Reich, Phys. Rev. **104** (1956) 135
4) R. H. Spear, Australian J. Phys. **12** (1959) 99
5) R. W. Kavanagh, Nuclear Physics **15** (1960) 411
6) Nilson, Jentschke, Briggs, Kerman and Snyder, Phys. Rev. **109** (1958) 850
7) Schiffer, Bonner, Davis and Prosser, Phys. Rev. **104** (1956) 1064
8) W. A. Fowler and C. C. Lauritsen, Phys. Rev. **51** (1937) 1103
9) T. W. Bonner and J. E. Evans, Phys. Rev. **73** (1948) 666
10) V. Meyer and H. H. Staub, Helv. Phys. Acta **31** (1958) 205
11) P. B. Treacy, Phil. Mag. **44** (1953) 325
12) Bloch, Hull, Broyles, Bouricius, Freeman and Breit, Revs. Modern Phys. **23** (1951) 147
13) Jones, Phillips and Miller, Phys. Rev. **117** (1960) 525

8.B

Nuclear Physics **18** (1960) 502—515; © *North-Holland Publishing Co., Amsterdam*

Not to be reproduced by photoprint or microfilm without written permission from the publisher

PION-PION EFFECTS IN τ-DECAY

A. N. MITRA

Department of Physics, Muslim University, Aligarh, U.P., India

Received 16 May 1960

Abstract: The effects of pion-pion interactions in resonant form in the s-states of isobaric spins 0 and 2 are studied in some details with respect to the energy and angular distributions of the unlike pion in τ-decay. The relation of the resonance picture with that of the more conventional effective range theory of pion-pion interaction is clarified. It is found that the pion-pion hypothesis is capable of explaining the observed distribution in a variety of ways, depending on the choice of the resonance parameters. In particular, an $I = 0$ interaction is by no means ruled out by experiment. However, on the basis of the present τ-decay data, and in the absence of independent information on the nature of the pion-pion interaction, it is not possible to distinguish between the various alternatives.

1. Introduction

A few years ago, we had suggested [1]) a $\pi-\pi$ interaction mechanism in the state $I = 2$ in order to understand the bias towards higher momenta of the unlike pion in τ-decay. However, the data available at that time being rather inadequate, a detailed comparison with experiment was not feasible. In the meantime the availability of more accurate data [2]) has opened up the possibility of testing the pion-pion hypothesis in greater detail. A recent calculation by Thomas and Holladay [3]) with the assumption of a zero range $\pi^+-\pi^+$ interaction gives a fairly good fit to the data. Such an approach, while it appeals immediately to intuition, does not, however, give any strong and unambiguous indication of the interaction in a charge-independent form, nor does it rule out other mechanisms for producing the observed distribution. It was mainly to clarify some of these points that the present work was undertaken.

It is now fairly well established that the τ^+-meson is pseudoscalar and that the decay particles are all emitted in mutual s-states. The evidence for this comes from the observation that the energy and angular distributions of the π^- do not vanish at zero energy and zero angle respectively. Now an s-state $\pi-\pi$ interaction can occur only in the states $I = 0,2$. There is at present a good deal of theoretical interest in these interactions, though very little is as yet known about their exact nature. Chew and Mandelstam, using the "Mandelstam representation" for the $\pi-\pi$ problem, find that both states are attractive, the $I = 0$ state being more attractive, than $I = 2$ [4]), this last fact depending entirely on isobaric spin considerations. They do not, however, find resonances in the

low energy region for these states. In this connection, it may be of some interest to note the predictions of pseudoscalar theory in the spirit of a Tamm-Dancoff type approximation which is perhaps not too misleading in the low energy region, as the famous $\frac{3}{2}-\frac{3}{2}$ resonance in $\pi-$N scattering would suggest. Such a calculation carried out some time ago [5]), indicated a resonance in the $I = 2$ state at about 25 MeV c.m. energy for each pion, while the interaction in $I = 0$ was found to be "too strong" for resonance at that energy. A more recent analysis of the $I = 0$ state [6]) seems to indicate resonance at a much higher energy ($\approx$ 250 MeV). While it is by no means suggested that these results have any quantitative significance, it would be safe to draw the following qualitative conclusion. The $I = 0$ state is a lot more attractive than $I = 2$ (in harmony with ref. [4])), and hence, if resonances occur at all, the resonance energy should be higher for $I = 0$, than for $I = 2$. As the ultimate tests of these resonances must come from indirect comparison with experiment (e.g. a high energy $\pi-\pi$ resonance is believed to be responsible for the second and third maxima in π^--p scattering in the 1 GeV region), we do not, at this stage, like to rule out the "resonance" concept (which, moreover, need not be confused with the actual occurrence of resonances). We have accordingly chosen to study the behaviour of the π^--energy distribution as a function of the resonance parameters, assuming that one or both of the interactions ($I = 0,2$) may be resonant.

In section 2, the relations between the resonance parameters and those of effective range theory are derived in an elementary manner. These relations form the necessary basis for a subsequent interpretation of our results in terms of the more familiar concepts of range and depth of the $\pi-\pi$ interaction.

In section 3, the basic formulae for the energy and angular distributions of the negative pion are derived on the assumption of both $I = 0$ and 2 resonances. The mathematical details are left over to a couple of appendices. In section 4 we discuss the numerical results as functions of the resonance parameters, individually for the $I = 0$ and 2 states, so as to make it clear under what possible conditions the experimental data can be understood.

In the following, the formalism and notation used are mostly those of A, unless otherwise specified.

2. Effective Range Interpretation of the Resonance Parameters

An s-state $\pi-\pi$ amplitude for given isobaric spin may be written as

$$W = \frac{1}{k}\,\frac{\frac{1}{2}\Gamma}{(\omega_k-\omega_r)-\frac{1}{2}i\Gamma} = \frac{1}{k}\sin\delta\, e^{i\delta}, \tag{1}$$

where δ is the corresponding phase shift given by

$$\tan\delta = \tfrac{1}{2}\Gamma/(\omega_k-\omega_r). \tag{2}$$

In the non-relativistic limit, viz. $\omega_k - \mu \approx k^2/2\mu$, etc., this expression should be compared with the standard expression of effective range theory, viz.

$$k \cot \delta = -a^{-1} + \tfrac{1}{2} r_0 k^2. \tag{3}$$

It is then immediately obvious that Γ should be proportional to k, so that we set

$$\Gamma = \gamma k, \tag{4}$$

where γ is, roughly speaking, a constant, and plays the role of a "reduced width" †.

The effective range parameters are then given by

$$a^{-1} = 2(\omega_r - \mu)/\mu, \tag{5}$$

and

$$\tfrac{1}{2} r_0 = (\gamma\mu)^{-1}. \tag{6}$$

It is clear from (1), (4), (5) and (6) that the zero range approximation is valid only when $\omega_r \gg \omega_k$, i.e. if $\omega_r \gg t_m + \mu$, t_m being the maximum kinetic energy available to any pion. In this case the distribution is governed essentially by the function (see A for notation)

$$|W|^2 \propto \frac{1}{1 + a^2 k^2} = \frac{1}{1 + \frac{1}{2} M a^2 (t_m - t)}. \tag{7}$$

This is just what was discussed by Thomas and Holladay [3]) regarding the effect of the $\pi^+ - \pi^+$ interaction. However, if $\omega_r - \mu$ is comparable to t_m, the "zero range" approximation is unjustified, and the distribution no longer has a slow monotonic behaviour as in (7). Rather, it may now exhibit a maximum over the available energy range. The sharpness of the maximum would in turn depend on the magnitude of the width parameter γ vis-a-vis the resonance parameter r. Thus it is qualitatively clear that the function

$$|W|^2 = \frac{\frac{1}{4}\gamma^2}{(\omega_k - \omega_r)^2 + \frac{1}{4}\gamma^2 k^2}, \qquad 4k^2 = 2M(t_m - t), \tag{8}$$

should pass through a fairly pronounced maximum near $t = t_m$ if the resonance energy $\omega_r - \mu$ is small and γ comparatively large. This maximum is progressively broadened and less peaked, as γ is decreased, until finally the function shows a monotonically increasing behaviour. In terms of effective range parameters, this means, according to (5) and (6), that the conditions of pronounced maximum near $t = t_m$ are 1) small r_0 and 2) large a. On the other hand, if the resonance energy is made larger, the maximum shifts to the left i.e. near $t = 0$, and

† This result which is quite familiar in resonance theory, may be generalized for a partial wave l as $\Gamma_l = \gamma_l k^{2l+1}$; c.f., the result of Gell-Mann and Watson [7]) for the width parameter of the $\frac{3}{2}-\frac{3}{2}$ resonance in π-N-scattering, viz. $\Gamma \propto k^3$.

becomes less and less pronounced as γ is decreased, until the function starts showing a monotonically decreasing trend. The actual distribution function is of course much more complicated than (8), if the $\pi-\pi$ interaction is expressed in a charge independent form. Further, as we wish to consider the effects of the interaction in both the states $I = 0,2$, their interference effects will distort the above simplified picture considerably. It should be of interest to see if, in spite of these interference effects, any qualitative conclusions about the relative roles of the interactions in these two states can be obtained from an inspection of the τ-decay data.

3. Energy and Angular Distributions

In the formalism of Dalitz [8]) and A, the transition amplitude with $\pi-\pi$ interactions in the $I = 0,2$ states and the selection rule $\Delta T = \frac{1}{2}$ is

$$\tfrac{1}{6}\sum_{\mathrm{p}}(F_0\chi_0^1+F_2\chi_2^1),$$

where

$$F_I(\mathbf{p}_1, \mathbf{p}_2, \mathbf{p}_3) = (2I+1)^{\frac{1}{2}}W_1^{(I)} = \frac{\frac{1}{2}\gamma_I(2I+1)^{\frac{1}{2}}}{(\omega_{23}-\omega_r^{(I)})-\frac{1}{2}i\Gamma_{23}^{(I)}}, \tag{9}$$

and

$$\Gamma_{ij}^{(I)} = \gamma_I k_{ij}, \qquad (i, j = 1, 2, 3). \tag{10}$$

Using (9), (10) and equations (4), (5) of A, we arrive at the following expressions (apart from a common multiplying factor) for the totally symmetric amplitude λ and the (2,1) amplitude α

$$9\lambda = 2(W_1^{(0)}+W_2^{(0)}+W_3^{(0)})+4(W_1^{(2)}+W_2^{(2)}+W_3^{(2)}); \tag{11}$$

$$9\alpha(2)^{\frac{1}{2}} = -2(2W_1^{(0)}-W_2^{(0)}-W_3^{(0)})+5(2W_1^{(2)}-W_2^{(2)}-W_3^{(2)}). \tag{12}$$

As may be seen from (11) and (12), the statistical factors due to the I-spin give some extra weight to the $I = 2$ contributions over those of $I = 0$ to these amplitudes. Thus as a hypothetical case, if the parameters of the two interactions were *identical* the distribution would be governed essentially by $I = 2$ but the anisotropy would be somewhat less pronounced, since the contributions of these states to α are of *opposite* signs. However, as is more likely, the parameters of the two interactions, particularly the resonance energy, are quite different, so that the actual interference effect is not easy to determine.

For an evaluation of the energy and angular distributions of the π^--meson, we follow closely the pattern of calculations set in A. However, some additional complications arise here, as Γ has now been assumed to be energy dependent (eq. (4)). While such a modification would not have qualitatively affected the results of A (as we were then interested only in certain integrated effects), it is

of utmost importance to our present analysis. Now the smallness of Γ had necessitated certain restrictions on the resonance parameter r and the range of the energy variable t, through the appearance of various δ-functions. The assumption of energy dependence of Γ in the present case invalidates these restrictions and consequently requires a somewhat different approach. The approximation procedures for the evaluation of the energy and angular distributions of the π^--meson are outlined in Appendices I and II respectively. The results are given below.

A) *Energy distribution*:

If t is the kinetic energy of the π^--meson, this distribution is given, apart from an overall normalizing factor, by

$$\sigma(t) = \left(1+\frac{\rho}{2}\right)\sigma_2(t)+\left(1+\frac{2}{\rho}\right)\sigma_0(t), \tag{13}$$

where

$$\rho = \gamma_0/\gamma_2, \tag{14}$$

and $\sigma_0(t)$ and $\sigma_2(t)$ are the distributions obtained on the assumption of $\pi-\pi$ interactions in the individual states $I = 0,2$. The functions σ_0 and σ_2 are listed in table 1 of Appendix I.

B) *Angular distribution*:

For this case, the angle ϕ under consideration is that between the π^--meson in the rest system of the τ^+, and the vector representing the relative momentum of the two π^+-mesons. We adopt the convention that if $\mathbf{p}_i$ and $\mathbf{p}_j$ represent the two π^+-mesons, the direction of the relative momentum vector is that of $\mathbf{p}_i-\mathbf{p}_j$ if $p_i > p_j$ and $\mathbf{p}_j-\mathbf{p}_i$ if $p_i < p_j$. Taking $\lambda = \cos\phi$, the distribution of λ is formally similar to (13), viz.

$$\Phi(\lambda) = \left(1+\frac{\rho}{2}\right)\Phi_2(\lambda)+\left(1+\frac{2}{\rho}\right)\Phi_0(\lambda), \tag{15}$$

where Φ_0 and Φ_2 express the specific contribution of $I = 0,2$ respectively, and are given by

$$\Phi_0(\lambda) = \tfrac{3}{2}f^{(0)}(t'_\lambda)-\tfrac{1}{2}f^{(0)}(0)-f^{(0)}(t_m) + \tfrac{5}{2}\left(\mathscr{I}_+^{(0)}(t'_\lambda)-\mathscr{I}_+^{(0)}(0)\right)+4\left(\mathscr{I}_-^{(0)}(t'_\lambda)-\mathscr{I}_-^{(0)}(0)\right); \tag{16}$$

and

$$\Phi_2(\lambda) = 14f^{(2)}(t_m)-\tfrac{15}{2}f^{(2)}(t'_\lambda)-\tfrac{13}{2}f^{(2)}(0) + \tfrac{15}{2}\mathscr{I}_+^{(2)}(t'_\lambda)-\tfrac{13}{2}\mathscr{I}_+^{(2)}(0)-\mathscr{I}_+^{(2)}(t_m)+\mathscr{I}_-^{(2)}(0)-\mathscr{I}_-^{(2)}(t_m). \tag{17}$$

The various symbols are defined in Appendix II.

4. Discussion

We first dispose of the angular distribution. Since this quantity is analytically more complicated and less sensitive to the $\pi-\pi$ interaction than the energy distribution, we have evaluated it only for a typical set of resonance parameters for illustration. The results for $I = 0$ and 2 are shown in fig. 1, along with the

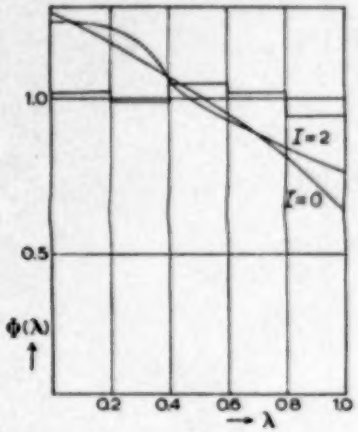

Fig. 1. The distributions of cos ϕ for the two cases of $I = 0$ and 2, taking $\theta = 1, \gamma = 0.3$ for both. The histogram represents the combined data of McKenna *et al.* and Baldo-Ceolin *et al.*

combined histogram data of Mekenna *et al.* and Baldo Ceolin *et al.* †. Both curves show a decreasing trend with $\lambda = \cos\phi$, which does not appear to be inconsistent with experiment ††. The deviation from isotropy is not large. Indeed a comparison with the corresponding curves of ref. [9]) which were obtained on the assumption of spin-parity assignments other than 0^- shows that the $\pi-\pi$ hypothesis gives a much better representation of the data than any one of them. We have, however, made no attempt to discuss the relative roles of the $I = 0$ and 2 interactions in producing the angular distribution. As this aspect is more conveniently studied with respect to the energy distribution which is analytically much simpler, we have chosen the latter alternative.

For the energy distribution, it is most convenient to plot the deviation from isotropy, which is obtained after dividing the complete distribution by the phase space factor which, in the non-relativistic limit, is proportional to $R_m = (Mt(t_m-t)/\mu)^{\frac{1}{2}}$. The corresponding experimental curve of ref. [2]) shows,

† Private communication from Drs. McKenna and O'Connell. At our request, these authors have kindly analysed the data of ref. [2]) with respect to the cos ϕ distribution and supplied them to us, along with the data of Baldo Ceolin *et al.*, as given in Dalitz [9]). We are extremely grateful to Drs. McKenna and O'Connell for this co-operation.

†† Drs. McKenna and O'Connell, however, find that their own data [2]) show an *increasing* trend near $\lambda = 1$, but these seem to be offset by Baldo-Ceolin's data. An ambiguous decision on this point will no doubt throw important light on the choice of the resonance parameters.

apart from small oscillations (which may or may not have any physical significance), a slow but monotonically increasing trend with energy. As for the theoretical distributions, we have plotted the individual quantities $\sigma_0(t)/R_m$ and $\sigma_2(t)/R_m$, appropriately normalized, in figures 2 and 3 respectively, for some

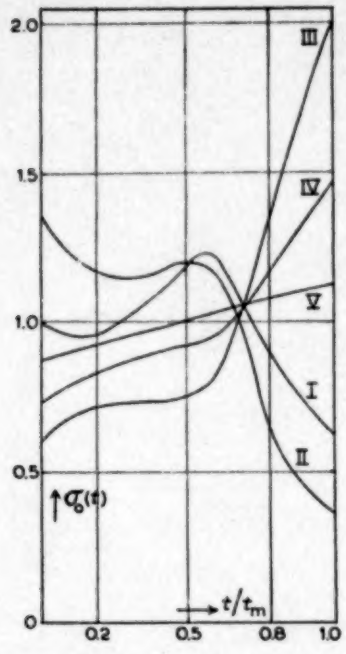

Fig. 2. The energy distribution with pure $I = 0$. Curves I–V represent respectively the cases:

$\theta=1.0$, $\gamma=0.3$; $\theta=1.0$, $\gamma=0.5$; $\theta=2.0$, $\gamma=0.3$; $\theta=2.0$, $\gamma=0.5$; $\theta=10.0$, $\gamma=0.5$.

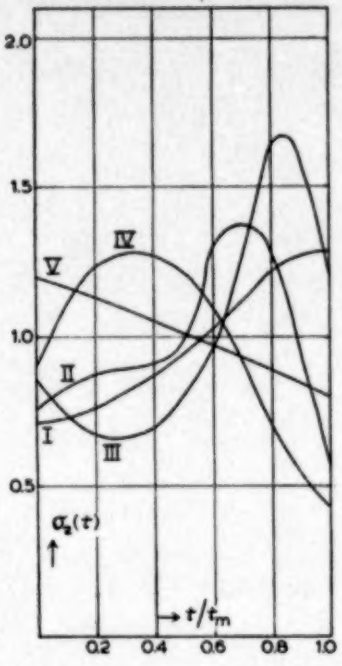

Fig. 3. The energy distribution with pure $I = 2$. Curves I–V represent respectively the cases:

$\theta=0.5$, $\gamma=0.1$; $\theta=1.0$, $\gamma=0.3$; $\theta=1.0$, $\gamma=0.5$; $\theta=2.0$, $\gamma=0.5$; $\theta=10.0$, $\gamma=0.5$

typical values of the resonance parameters in the two $\pi-\pi$ states considered. As the distributions σ_0 and σ_2 behave rather differently with the resonance parameters, we discuss separately some of their features.

From figure 2, we find that for reasonably small θ and γ, σ_0 shows a generally *decreasing* (though oscillatory) trend with energy (curve I). If γ is increased, keeping θ small and fixed, the distribution tends to be monotonic (curve II). As θ is increased, the curve starts exhibiting a monotonically *increasing* trend (curve III), the rise near $t = t_m$ being somewhat sharper for smaller γ than for a larger one (curve IV). As θ is increased to a value much beyond the available energy range for a pion, the slope while remaining positive, becomes more uniform (curve V).

As for σ_2, figure 3 shows a monotonically *increasing* trend only for very small values of θ and γ (curve I). A small increase in θ destroys the monotonicity (curve II). A disproportionate increase of γ without changing θ makes the distribution oscillatory (curve III). A further increase in σ brings in a generally

decreasing trend (curve IV). Increasing θ to a large value (beyond the energy range available to a pion) makes the decreasing trend strictly monotonic (curve V).

Before trying to analyse the implications of these curves, a word of caution regarding the roles of the two $\pi-\pi$ interactions is necessary. Prima facie it would appear that the experimentally observed small but definite high energy bias of the π^- should find explanation only with an $I = 2$ interaction which would tend to keep the two π^+-mesons together most of the time. Indeed the analysis in A (which was no doubt based on an inadequate treatment, since only certain integrated effects were considered), had appeared to confirm such a conjecture. Even the more recent analysis of Thomas and Holladay [3]) does not seem to be free from this intuitive feeling, in so far as these authors infer the existence of an $I = 2$ interaction from the agreement that a simple $\pi^+-\pi^+$ interaction gives with experiment. An examination of figures 2 and 3 shows, however, that such a point of view is misleading unless both θ and γ are small (curve I, figure 2). On the other hand, under such conditions, the "zero range" approximation of ref. [3]) is not valid (see sec. 2). Indeed, in the region of validity of the zero range approximation, the curves V (figures 2 and 3) suggest that an $I = 0$ interaction is more strongly indicated by the data than $I = 2$ (which gives the opposite slope), and this is just the opposite of the conclusion of Thomas and Holladay [3]).

There appear to be several ways of explaining the observed distribution. To understand it in terms of *pure* isobaric states, one needs either an $I = 2$ curve with small θ and γ suitably chosen, or an $I = 0$ curve with a large θ and a small γ. It is also possible to produce a gentle positive slope by taking a judicious combination of the σ_0 and σ_2 curves in accordance with eq. (13), and this can be done in a variety of ways. For example, a σ_0 curve of type III with its sharp rise near $t = t_m$, fairly well compensates for the steep fall, in this region, exhibited by a σ_2 curve of type III. The possibilities of such combinations is obviously unlimited. If we restrict them by the assumption $\omega_r^{(0)} > \omega_r^{(2)}$, as was discussed in sec. 1, the most general statement that can be made from an examination of figures 2 and 3 is that a σ_0 with a low/high γ_0 may be combined with a σ_2 having a low/high γ_2 to produce the desired effect.

To get more information about $\pi-\pi$ interaction from τ-decay data, one must look for some finer features of the latter. A close scrutiny of the end points of the energy distribution may prove particularly valuable. For example, if the experimental curve shows an initial decline near $t = 0$, and again a fall near $t = t_m$, it would strongly indicate an $I = 2$ resonance with small θ and comparatively large γ. Similar considerations hold for the angular distribution as well. Needless to say, only extremely accurate statistics can serve these ends. In the absence of such statistics at present, an analysis like the present one suggests that the phenomenon of τ-decay by itself is not a particularly good choice for

throwing any significant light on the relative roles of the $I = 0$ and 2 interactions, unless at least some information about them is forthcoming from independent experimental data.

The author is indebted to Drs. McKenna and O'Connell of the Dublin Institute of Advanced Study for supplying the data on the cos φ distribution, and to Professor P. S. Gill for his encouraging interest in this investigation.

Appendix I (Energy Distribution)

For determining the energy distribution of the π^- we have to leave the variables ω_1, ω_2 or ω_3 free from phase space integration, according as the π^- has momentum $\mathbf{p}_1$, $\mathbf{p}_2$ or $\mathbf{p}_3$ respectively, in the notation of A. With these 3 possibilities are associated the respective amplitudes A_1, A_2 or A_3 defined by eqs. (5) of A. Thus the energy distribution is given by

$$\sigma(t) = \int |A_1|^2 \frac{\mathrm{d}\tau}{\mathrm{d}\omega_1} + \int |A_2|^2 \frac{\mathrm{d}\tau}{\mathrm{d}\omega_2} + \int |A_3|^2 \frac{\mathrm{d}\tau}{\mathrm{d}\omega_3}, \tag{I.1}$$

where $\mathrm{d}\tau$ is the entire phase space element and $t = \omega_i - \mu$ is the kinetic energy of the π^- appropriate to each term. Now the A_i's can be ultimately expressed in terms of the W's via eqs. (11) and (12) of the text and eqs. (5) of A. We therefore introduce the following notations for the possible types of integrals that occur in (I.1):

$$I_{\nu i}^{(I)} = \int |W_i^{(I)}|^2 \frac{\mathrm{d}\tau}{\mathrm{d}\omega_\nu}, \tag{I.2}$$

$$J_{\nu ij}^{(I)} = \mathrm{Re} \int W_i^{(I)*} W_j^{(I)} \frac{\mathrm{d}\tau}{\mathrm{d}\omega_\nu}, \tag{I.3}$$

$$J_{\nu ij} = \mathrm{Re} \int W_i^{(0)*} W_j^{(2)} \frac{\mathrm{d}\tau}{\mathrm{d}\omega_\nu}. \tag{I.4}$$

Here the suffix ν stands for 1, 2. 3 according as the free variable is ω_1, ω_2, ω_3 respectively, i.e. according as the integrands appearing in (I.2)—(I.4) are parts of $|A_1|^2$, $|A_2|^2$, $|A_3|^2$ respectively. The superscripts (0,2) relat to the I-spin under consideration. Thus (I.2) and (I.3) are integrals for the pure states. (I.4) is a "mixed" integral for which we do not use any superscript. Note that while $J_{\nu ij}^{(I)}$ is symmetrical in i and j, $J_{\nu ij}$ is *not*.

We next express the J-integrals in terms of the I-integrals by an approximation which is best illustrated by a typical example. Consider

$$J_{123}^{(2)} = \mathrm{Re} \int \frac{\mathrm{d}R_0}{k_{12}k_{13}} \frac{\Gamma_{12}^{(2)}}{(2\omega_{12} - 2\omega_r^{(2)}) + i\Gamma_{12}^{(2)}} \frac{\Gamma_{13}^{(2)}}{(2\omega_{13} - 2\omega_r^{(2)}) - i\Gamma_{13}^{(2)}}, \tag{I.5}$$

where, for the phase space integration, the results of eqs. (A.12)—(A.15), (A.32)—(A.34) of A have been used. Substituting from (10) in (I.5) we have

$$J_{123}^{(2)} = \gamma_2^2 \int \mathrm{d}R_0 \frac{(2\omega_{12}-2\omega_r^{(2)})(2\omega_{13}-2\omega_r^{(2)})+\gamma_2^2 k_{12}k_{13}}{[(2\omega_{12}-2\omega_r^{(2)})^2+\gamma_2^2 k_{12}^2][(2\omega_{13}-2\omega_r^{(2)})^2+\gamma_2^2 k_{13}^2]} \quad \text{(I.6)}$$

The integrand is of the form

$$\frac{ab+\Gamma_1\Gamma_2}{(a^2+\Gamma_1^2)(b^2+\Gamma_2^2)},$$

for which we use an approximation analogous to eq. (A.23) of A, viz.,

$$\frac{1}{2}\left[\frac{1}{a^2+\Gamma_1^2}+\frac{1}{b^2+\Gamma_2^2}\right].$$

As was discussed in A, this approximation is rather good if γ is reasonably small, which condition is fairly well satisfied for our problem. As a result, (I.6) can be written as

$$J_{123}^{(2)} \approx \tfrac{1}{2}(I_{12}^{(2)}+I_{13}^{(2)}), \quad \text{(I.7)}$$

where, for the I-integrals, equations similar to (I.5) have been used. In a similar way all the J-integrals (including the "mixed" ones) can be transformed, and the results can be expressed as follows:

$$J_{\nu ij}^{(I)} \approx \tfrac{1}{2}[I_{\nu i}^{(I)}+I_{\nu j}^{(I)}]; \quad \text{(I.8)}$$

$$J_{\nu ij} \approx \tfrac{1}{2}\gamma_0\gamma_2[\gamma_0^{-2}I_{\nu i}^{(0)}+\gamma_2^{-2}I_{\nu j}^{(2)}]. \quad \text{(I.9)}$$

Substituting from eqs. (11) and (12) of the text and eq. (5) of A in (I.1) and using (I.8) and (I.9) to simplify the resulting expression, we obtain the energy distribution in the form of eq. (13) of the text, where (apart from a common numerical factor),

$$\sigma_0(t) \backsimeq -I_{11}^{(0)}+2(I_{12}^{(0)}+I_{13}^{(0)}+I_{21}^{(0)}+I_{31}^{(0)})+\tfrac{1}{2}(I_{22}^{(0)}+I_{33}^{(0)}+I_{23}^{(0)}+I_{32}^{(0)}), \quad \text{(I.10)}$$

$$\sigma_2(t) = 14I_{11}^{(2)}-(I_{12}^{(2)}+I_{13}^{(2)}+I_{21}^{(2)}+I_{31}^{(2)})+\tfrac{13}{2}(I_{22}^{(2)}+I_{33}^{(2)}+I_{23}^{(2)}+I_{32}^{(2)}). \quad \text{(I.11)}$$

It now remains to evaluate the I-integrals. Since they are identical in structure for both I-spins, we now drop the superscripts (0) and (2) from the various parameters and functions. Using some results of the appendix of A, we have for example,

$$I_{11} = \int^{\min(R_m,\, 3\omega_1-M)} \mathrm{d}R_0\, \xi(t), \quad \text{(I.12)}$$

where

$$\xi(t) = \gamma^2[(Q-2\omega_r)^2+\tfrac{1}{4}\gamma^2(Q^2-4\mu^2)]^{-1}, \quad \text{(I.13)}$$

and

$$Q^2-4\mu^2 = 2M(t_m-t). \quad \text{(I.14)}$$

Similar expressions hold for I_{22} and I_{33}. These quantities, which are given by different expressions for different energy ranges, are listed in table 1. As for $I_{ij}(i \neq j)$, consider

$$I_{12} = \int \mathrm{d}R_0 \gamma^2 [(2\omega_{13} - 2\omega_r)^2 + \gamma^2 k_{13}^2]^{-1},$$

where

$$2\omega_{12},\ 2\omega_{13} = 2\mu + \frac{1}{4\mu}(M\omega_1 - 3\mu^2 \pm MR_0). \tag{I.15}$$

The integration is straightforward and gives

$$\begin{aligned} I_{12} &= \eta(x_0) - \eta(x_1), \qquad t_a \leqq t \leqq t', \\ &= \eta(x_0) - \eta(x_m^-), \qquad t' \leqq t \leqq t_m. \end{aligned} \tag{I.16}$$

Here

$$\eta(x) = \frac{4\mu}{M}\left(\frac{\gamma^2}{r^2 - \frac{1}{4}\gamma^2\mu^2}\right)^{\frac{1}{2}} \tan^{-1} x, \tag{I.17}$$

$$x = \frac{1}{4\mu\gamma}(r^2 - \tfrac{1}{4}\gamma^2\mu^2)^{-\frac{1}{2}}[M\omega_1 - 3\mu^2 - 4r^2 + 2\mu^2\gamma^2 - MR_0], \tag{I.18}$$

and $x_0, x_1, x_2, x_m^+, x_m^-$ correspond respectively to the values $R_0 = 0,\ 3\omega_1 - M,\ M - 3\omega_1,\ -R_m,\ +R_m$ in (I.18). The other integrals I_{ij} can be evaluated in a similar manner, and their relevant combinations are listed in table 1. Finally, substitution of the I_{ij}'s in (I.10) and (I.11) gives the distributions $\sigma_0(t)$ and $\sigma_2(t)$ whose expressions also appear in table 1. These results complete the definition of eq. (13) of the text.

TABLE 1

The various functions needed for the energy distribution

Energy range	$0 \leqq t \leqq t_a$	$t_a \leqq t \leqq t'$	$t' \leqq t \leqq t_m$
I_{11}	0	$(3\omega - M)\xi(t)$	$R_m \xi(t)$
$I_{22} + I_{33}$	$R_m \xi(t)$	$\xi(t)\{R_m - (3\omega - M)\}$	0
$I_{12} + I_{13}$	0	$\eta(x_2) - \eta(x_1)$	$\eta(x_m^+) - \eta(x_m^-)$
$I_{21} + I_{31}$	$\eta(x_0) - \eta(x_m^-)$	$\eta(x_1) - \eta(x_m^-)$	0
$I_{22} + I_{32}$	$\eta(x_m^+) - \eta(x_0)$	$\eta(x_m^+) - \eta(x_2)$	0
$\sigma_0(t)$	$\frac{1}{2}R_m\xi(t) + \frac{1}{2}\eta(x_m^+) + \frac{3}{2}\eta(x_0) - 2\eta(x_m^-)$	$\frac{1}{2}R_m\xi(t) - \frac{3}{2}(3\omega - M)\xi(t) + \frac{3}{2}\eta(x_2) + \frac{1}{2}\eta(x_m^+) - 2\eta(x_m^-)$	$-R_m\xi(t) + 2\eta(x_m^+) - 2\eta(x_m^-)$
$\sigma_2(t)$	$\frac{15}{2}\{R_m\xi(t) + \eta(x_m^+)\} + \eta(x_m^-) - \frac{15}{2}\eta(x_0)$	$\frac{15}{2}R_m\xi(t) + \frac{15}{2}\eta(x_m^+) + \frac{15}{2}(3\omega - M)\xi(t) + \eta(x_m^-) - \frac{15}{2}\eta(x_2)$	$14R_m\xi(t) + \eta(x_m^-) - \eta(x_m^+)$

Appendix II (Angular Distribution)

For the angular distribution we integrate over the entire phase space except for the cosine of the angle between the π^- and the relative momentum of the π^+'s in their own c.m. frame. This is most conveniently done by introducing a δ-function appropriate to the amplitude A_1, A_2 or A_3 under consideration. E.g., for evaluating $\int|A_1|^2$, the appropriate δ-function is $\delta(\lambda+\hat{p}_1\cdot\hat{R})$. The phase space integral for this case is given according to eqs. (A.9)—(A.11) of A, by

$$(2\pi)^{-2}\int\delta(Q\cdot R)\delta(R^2+Q^2-4\mu^2)\delta(\hat{p}_1\cdot\hat{R}+\lambda)\mathrm{d}^4R\frac{\mathrm{d}^3p_1}{\omega_1}, \tag{II.1}$$

where

$$Q_\mu=(M-\omega_1,\,-\mathbf{p}_1).$$

The δ-functions in (II.1) give

$$\begin{aligned} Q_0R_0=\mathbf{Q}\cdot\mathbf{R}&=\lambda p_1|\mathbf{R}|,\\ |\mathbf{R}|^2&=Q^2+R_0{}^2-4\mu^2, \end{aligned} \tag{II.2}$$

so that

$$R_0{}^2(Q_0{}^2-\lambda^2p_1{}^2)=\lambda^2p_1{}^2(Q^2-4\mu^2), \tag{II.3}$$

giving in the non-relativistic limit,

$$R_0\approx\lambda\left(\frac{M}{\mu}t(t_\mathrm{m}-t)\right)^{\frac{1}{2}}=\lambda R_\mathrm{m}. \tag{II.4}$$

With the help of the δ-functions, all the variables in (II.1), except $\mathrm{d}\omega_1$, can be integrated out, giving the relativistic phase factor

$$p_1\mathrm{d}\omega_1\frac{Q_0{}^2}{Q_0{}^2-\lambda^2p_1{}^2}\cdot\left[\frac{Q^2-4\mu^2}{Q_0{}^2-\lambda^2p_1{}^2}\right]^{\frac{1}{2}}, \tag{II.5}$$

which reduces, in the non-relativistic limit, to

$$R_\mathrm{m}\mathrm{d}\omega_1=R_\mathrm{m}\mathrm{d}t. \tag{II.6}$$

It may be noted that according to (II.4) R_0 is no longer an independent variable, but a function of t, and this fact imposes the following limitations on the final t-integration: The limits of R_0 when the π^- has the momentum p_1, are $0\leqq R_0\leqq\min\,(R_\mathrm{m},\,3\omega_1-M)$; therefore, for the value $R_0=\lambda R_\mathrm{m}$ to be effective, we should have

$$3\omega-M=3\mu+3t-M\leqq\lambda R_\mathrm{m}=\lambda\left(\frac{M}{\mu}t(t_\mathrm{m}-t)\right)^{\frac{1}{2}},$$

which leads to $t'_\lambda \leqq t \leqq t_m$, where

$$\frac{t'_\lambda, t''_\lambda}{t_m} = \frac{\frac{12\mu M}{M+\mu} + \lambda^2 M \pm \frac{\lambda M}{M+\mu}\{\lambda^2(M+\mu)^2 + 8M\mu + 24\mu^2\}^{\frac{1}{2}}}{2(9\mu+\lambda^2 M)} \tag{II.7}$$

It is easy to verify the following inequalities

$$t'' \leqq t''_\lambda \leqq t_s \leqq t'_\lambda \leqq t', \tag{II.8}$$

the equality signs holding only for $\lambda = 0$ or 1.
Similarly, when the π^- has the momenta $\mathbf{p}_2$ and $\mathbf{p}_3$, the limits are respectively $t''_\lambda \leqq t \leqq t'_\lambda$ and $0 \leqq t \leqq t''_\lambda$.

Retaining the same notations for the I and J integrals (which now differ only in the phase space integration) as in Appendix I, we have

$$I_{11} = \int_{t'_\lambda}^{t_m} \frac{\gamma^2 R_m \mathrm{d}t}{(Q-2\omega_r)^2 + \frac{1}{4}\gamma^2(Q^2-4\mu^2)} \equiv f(t_m) - f(t'_\lambda). \tag{II.9}$$

Similarly,

$$I_{22} + I_{33} = f(t'_\lambda) - f(0). \tag{II.10}$$

In a similar way, the integrals $I_{ij} (i \neq j)$ may be expressed as follows

$$\begin{aligned} I_{12}, I_{13} &= \mathscr{I}_\mp(t_m) - \mathscr{I}_\mp(t'_\lambda), \\ I_{21}, I_{23} &= \mathscr{I}_\mp(t'_\lambda) - \mathscr{I}_\mp(t''_\lambda), \\ I_{31}, I_{32} &= \mathscr{I}_\mp(t''_\lambda) - \mathscr{I}_\mp(0), \end{aligned} \tag{II.11}$$

where

$$\mathscr{I}_\pm(t) = \int^t \mathrm{d}t\, R_m \gamma^2 \{x_\pm^2 + \gamma^2(\mu x_\pm + r^2)\}^{-1},$$

and

$$4\mu x_\pm = Mt + M\mu - 3\mu^2 - 4r^2 \pm M\lambda R_m. \tag{II.12}$$

The angular distribution $\Phi(\lambda)$ is given by an expression of the form (I.1), with the modifications described above for the phase space integration. Further, using the same approximation as (I.8) and (I.9), it is clear that eqs. (15) and (I.11) are valid for this case as well, except that the relations (II.9)—(II.12) must now be used for the various integrals. These considerations lead finally to eqs. (16) and (17) of the text.

References

1) A. N. Mitra, Nuclear Physics **6** (1958) 404 (referred to as A)
2) S. McKenna *et al.*, Nuovo Cimento **10** (1958) 763
3) B. Thomas and W. Holladay, Phys. Rev. **115** (1959) 1329

4) G. Chew, Proceedings of the 9th Annual International Conference on High Energy Physics, Kiev, USSR, 1959;
Chew, Mandelstam and Noyes, Phys. Rev. (to be published);
W. G. Holladay, Private communication
5) A. N. Mitra and R. P. Saxena, Phys. Rev. **108** (1957) 1083
6) Mitra, Saxena and Narayanaswamy, Nuclear Physics (to be published)
7) M. Gell Mann and K. M. Watson, Ann. Reviews of Nuc. Sci. **4** (1954)
8) R. H. Dalitz, Proc. Phys. Soc. A **69** (1956) 527
9) R. H. Dalitz, Report. Prog. Phys. **20** (1957) 195

2.A.2

Nuclear Physics **18** (1960) 516—520; © *North-Holland Publishing Co., Amsterdam*

Not to be reproduced by photoprint or microfilm without written permission from the publisher

ON THE MINIMUM NUMBER OF PARTIAL WAVES IN TWO-BODY REACTIONS

V. G. GRISHIN and V. I. OGIEVETSKI

Joint Institute for Nuclear Research, Dubna, USSR

Received 16 January 1960

Abstract: A reliable method is offered to determine the minimum number of partial waves involved in the interaction, if the total elastic cross section and differential cross section at a given angle are known.

1. Introduction

At high energies many partial waves are involved in the interaction of two particles and it is practically impossible to carry out a complete phase-shift analysis. Therefore it is important to determine what indisputable information can be obtained from the available experimental data. In particular, it is worthwhile to determine the minimum number of partial waves $L_{\min}$, necessary for describing the experimental data (when $L_{\min}$ is sufficiently large it corresponds to the minimum radius of interaction).

Rarita and Schwed [1]) have shown how to obtain $L_{\min}$ for elastic scattering, if the total cross sections of interaction are known.

In the present article inequalities are proved for the minimum number of partial waves in two-body reactions, if the total elastic and differential cross-sections at one or two angles are known. It is demonstrated that the account of the spins of the interacting particles little affects the result as compared with the zero-spin case (provided $L_{\min}$ is large). Therefore, practically, inequality (A) below can always be used.

Inequality (A) is considerably stronger than that of Rarita-Schwed [1]) when the scattering amplitude has a real part or is spin-dependent. This inequality can also be used for inelastic reactions of the type a+b → c+d.

2. Interaction of Spinless Particles

Let us first consider the case when particles have no spin. Then

$$\sigma(\theta_1) = \frac{1}{4k^2} \left| \sum_{l=0}^{\infty} (2l+1) A_l P_l(\cos\theta_1) \right|^2,$$

$$\sigma_{el} = \frac{\pi}{k^2} \sum_{l=0}^{\infty} (2l+1) |A_l|^2. \qquad (1)$$

Suppose a finite number of partial waves L can be set in these equations. Then, using the Cauchy inequality or determining the conditional minimum σ_{el} for a given $\sigma(\theta_1)$, it is possible to prove (see Appendix) that

$$\Sigma_0 \geqq \frac{4\pi\sigma(\theta_1)}{\sigma_{el}}, \tag{A}$$

where

$$\begin{aligned}\Sigma_0 &= \sum_{l=0}^{L} (2l+1)[P_l(\cos\theta_1)]^2 \\ &= \frac{(L+1)^2}{\sin^2\theta_1}\{[P_L(\cos\theta_1)]^2+[P_{L+1}(\cos\theta_1)]^2-2\cos\theta_1 P_L(\cos\theta_1)P_{L+1}(\cos\theta_1)\}\end{aligned} \tag{2}$$

The left hand side of (A) contains a monotonically increasing function L. The inequality will be fulfilled only for L greater than L_{min}. It is this number L_{min} which is the minimum number of partial waves necessary for a simultaneous description of the given σ_{el} and $\sigma(\theta_1)$.

For elastic scattering at $\theta = 0$ inequality (A) is stronger than that obtained in ref. [1]). In fact, in this case (A) can be written as

$$(L+1)^2 \geqq \frac{4\pi\sigma(0)}{\sigma_{el}} = \frac{k^2\sigma_t^2}{4\pi\sigma_{el}} + \frac{4\pi}{\sigma_{el}}[\mathrm{Re}\, f(0)]^2, \tag{A'}$$

while the Rarita-Schwed inequality [1]) is of the form

$$(L+1)^2 \geqq \frac{k^2\sigma_t^2}{4\pi\sigma_{el}} \tag{3}$$

and obviously yields smaller L_{min} than inequality (A) if the real part of the scattering amplitude is not zero.

If σ_{el}, $\sigma(\theta_1)$ and $\sigma(\theta_2)$ are assumed to be given, it is possible to obtain a stronger inequality than (A) by a similar procedure. It has a somewhat cumbersome form:

$$\rho_{11}\rho_{22}-\rho_{12}^2 \geqq \frac{1}{\sigma_{el}}\{\rho_{11}\sigma(\theta_2)-2|\rho_{12}|\sqrt{\sigma(\theta_1)\sigma(\theta_2)}+\rho_{22}\sigma(\theta_1)\}, \tag{4}$$

where

$$\begin{aligned}4\pi\rho_{ik} &= \sum_{0}^{L} (2l+1)P_l(\cos\theta_i)P_l(\cos\theta_k) \\ &= \frac{L+1}{\cos\theta_i-\cos\theta_k}[P_{L+1}(\cos\theta_i)P_L(\cos\theta_k)-P_L(\cos\theta_i)P_{L+1}(\cos\theta_k)].\end{aligned} \tag{5}$$

Sums in (5) are easily tabulated.

Other inequalities can be derived by using a greater number of experimental

points. They will certainly be even more cumbersome, but will yield a more rigorous estimate of $L_{\min}$, since any additional information can only increase $L_{\min}$.

Inequality (4) can be reversed to determine the maximum value of a differential cross section at a certain angle θ_2 if the total elastic and differential cross sections at another angle θ_1 are known:

$$\sigma(\theta_2) \leqq \frac{\sigma(\theta_1)}{\rho_{11}^2}\left\{|\rho_{12}| + \sqrt{\left(\frac{\rho_{11}\sigma_{el}}{\sigma(\theta_1)} - 1\right)(\rho_{11}\rho_{22} - \rho_{12}^2)}\right\}^2. \tag{6}$$

The upper limit on $\sigma(\theta_2)$ thus obtained depends on the number of partial waves L considered in the sums (5). If $L = L_{\min}$ the relation (6) becomes an equality. With the growth of L the right-hand side of the inequality under consideration increases. Given a reasonable number of L, definite indications on the upper limit of $\sigma(\theta_2)$ can be obtained for practical estimates.

3. Interaction of Particles with Spins

This section will deal with inequalities determining the minimum number of partial waves $L_{\min}$, if σ_{el} and $\sigma(\theta_1)$ are known for particles with spins.

a) It is proved in the Appendix that for particles with spins $\frac{1}{2}$ and 0 the inequality has the form

$$\max(\Sigma_0, \Sigma_1) \geqq \frac{4\pi\sigma(\theta_1)}{\sigma_{el}}, \tag{7}$$

where

$$\Sigma_1 = \sum_{l=1}^{L} (2l+1)\frac{(l-1)!}{(l+1)!}[P_l^{(1)}(\cos\theta_1)]^2. \tag{8}$$

b) For non-identical spin $\frac{1}{2}$ particles the following inequality can easily be derived in a similar way:

$$\max(\Sigma_0, \Sigma_1, \Sigma_2) \geqq \frac{4\pi\sigma(\theta_1)}{\sigma_{el}}, \tag{9}$$

where

$$\Sigma_2 = \sum_{l=2}^{L} (2l+1)\frac{(l-2)!}{(l+2)!}[P_l^{2}(\cos\theta_1)]^2. \tag{10}$$

c) Taking account of the identity of Dirac particles we obtain a more complicated inequality:

$$\max\{\Sigma'_0, \Sigma''_0, \Sigma'_1, \Sigma''_1, \Sigma'_2, \Sigma''_2\} \geqq \frac{4\pi\sigma(\theta_1)}{\sigma_{el}}, \tag{11}$$

where

$$\Sigma'_m = \sum_{l=m}^{L} [1+(-1)^l](2l+1)\frac{(l-m)!}{(l+m)!}[P_l^{(m)}(\cos\theta_1)]^2,$$
$$\Sigma''_m = \sum_{l=m}^{L} [1-(-1)^l](2l+1)\frac{(l-m)!}{(l+m)!}[P_l^{(m)}(\cos\theta_1)]^2. \quad (12)$$

To determine $L_{\min}$, the largest sum should be substituted into the left-hand side of inequalities (7), (9) and (11). It will be noted that at small angles Σ_0 is the largest sum, as Σ_1 and Σ_2 contain the associated Legendre polynomials. Furthermore, since at high energies $L_{\min}$ is sufficiently large, $\Sigma'_m \approx \Sigma''_m \approx \Sigma_m$. Therefore, at high energies inequality (A) can be practically used in all cases.

It should be emphasized that if a description of the experiment is limited the minimum number of partial waves obtained from the above inequalities, the terms in the corresponding scattering amplitude responsible for the spin flip are equal to zero. If they are not, the number of partial waves is larger than $L_{\min}$. If polarization is taken into account more strict conditions can be obtained for $L_{\min}$. In this case it would be possible to estimate the contribution to the cross section from the spin-dependent parts of the scattering amplitude.

4. Application to p—p Scattering at 8.5 GeV

We have come to the conclusion that inequality (A) can be used in all cases for determining the minimum number of partial waves involved in two-particle interactions at high energies. If the scattering amplitude has a real part or is spin-dependent, inequality (A) is stronger than that of Rarita-Schwed [1]).

As an example, let us consider proton-proton scattering at $E_p = 8.5$ GeV. In this case, according to the data produced by Tsyganov *et al.* [2]),

$$\sigma_{el} = (8.6\pm0.8)\,\text{mb}, \quad \sigma(2.5-5.5^\circ) = (123\pm18)\,\text{mb/sr}.$$

From inequality (A) we find

$$L_{\min} = 16\pm3. \quad (13)$$

(Fluctuations of $L_{\min}$ are due to experimental errors.) The Rarita-Schwed inequality leads to a weaker estimate

$$L_{\min} = 8\pm1, \quad (14)$$

if

$$\sigma_{tot} = (30\pm3)\text{mb}.$$

An optical model describing these experimental data [2]) yielded 16 ± 1 for the effective number of partial waves, the corresponding interaction radius R being equal to $(1.6\pm0.1)\times10^{-13}$ cm.

It follows from our results that any other model would lead to the same or to a greater interaction radius.

In conclusion it will be noted that all the results obtained fully apply not only to elastic scattering but also to inelastic two-particle reactions, e.g., $\pi^+ + p \to \Sigma^+ + K^+$, etc. In this case σ_{el} should be replaced by the total cross section of the given reaction.

The authors are indebted to L. G. Zastavenko for helpful discussions.

Appendix

As a typical example inequality (7) will be proved for a collision of particles with spins 0 and $\frac{1}{2}$.

It is convenient to write the expression for σ_{el} and $\sigma(\theta_1)$ in the form

$$\sigma(\theta_1) = \frac{1}{4k^2}\{|\sum_{l=0}^{L} x_l a_l|^2 + |\sum_{l=0}^{L} y_l b_l|^2\}, \tag{15}$$

$$\sigma_{el} = \frac{\pi}{k^2}\{\sum_{l=0}^{L} (|a_l|^2 + |b_l|^2), \tag{16}$$

where

$$x_l = \sqrt{2l+1}\, P_l(\cos\theta_1), \quad y_l = \sqrt{\frac{2l+1}{l(l+1)}}\, P_l^{(1)}(\cos\theta_1),$$

$$a_l = \frac{1}{\sqrt{2l+1}}\{(l+1)[\exp(2i\delta_{l+}) - 1] + l[\exp(2i\delta_{l-}) - 1]\}, \tag{17}$$

$$b_l = \sqrt{\frac{l(l+1)'}{2l+1}}\{\exp(2i\delta_{l+}) - \exp(2i\delta_{l-})\}.$$

Let us employ the well-known Cauchy inequality

$$|\Sigma A_i B_i|^2 \leqq (\Sigma|A_i|^2)(\Sigma|B_i|^2). \tag{18}$$

Then

$$\sigma(\theta_1) \leqq \frac{1}{4k^2}\{\Sigma x_l^2 \Sigma|a_l|^2 + \Sigma y_l^2 \Sigma|b_l|^2\} \leqq \frac{\sigma_{el}}{4\pi} \max(\Sigma x_l^2, \Sigma y_l^2)$$

$$= \frac{\sigma_{el}}{4\pi} \max(\Sigma_0, \Sigma_1). \tag{19}$$

Inequality (7) is thereby proved.

Inequalities (A), (9) and (11) can be derived in a similar manner. The method of proof described is incomparably simpler, especially for particles with spins, than the one which consists in determining the conditional extremum of σ_{el} at a given $\sigma(\theta_1)$.

References

1) W. Rarita and P. Schwed, Phys. Rev. **112** (1958) 271
2) V. I. Veksler, Report at the IX Int. High Energy Phys. Conf. Kiev, 1959

7.A:8.B

Nuclear Physics **18** (1960) 521—528; © *North-Holland Publishing Co., Amsterdam*

Not to be reproduced by photoprint or microfilm without written permission from the publisher

ANALYTICAL PROPERTIES OF THE SCATTERING AMPLITUDE FOR INELASTIC PROCESSES INVOLVING STRANGE PARTICLES

I. T. TODOROV

Laboratory of Theoretical Physics, Joint Institute for Nuclear Research, Dubna, USSR

Received 18 February 1960

Abstract: The analytical properties of the amplitudes for the processes $(N+\overline{K} \to Y+\pi)$ and $(N+\pi \to Y+K)$ are considered on the basis of the principles of covariance, causality and spectrality. Kinematic characteristics of these processes are obtained in a frame of reference which is a natural generalization of the Breit system. Dispersion relations are derived for imaginary meson masses. The Vladimirov-Logunov theorem [6]) concerning the analyticity of the anti-Hermitian part of the amplitude is extended to the case when all particles involved in the reaction possess different masses. In accordance with the results of previous investigations [3]) the region thus obtained contains no physical point.

1. Introduction

Dispersion relations for related inelastic processes involving strange particles, such as

$$N+\overline{K} \to Y+\pi, \tag{I}$$

$$N+\pi \to Y+K, \tag{II}$$

have been considered in a number of papers [1, 2, 3]).

Let p_1 and q_1 (p_2 and q_2) be the baryon and meson 4-momenta at the beginning (end) of any of these reactions. The momenta satisfy the usual relations

$$p_1^2 = M_1^2, \quad p_2^2 = M_2^2, \quad q_1^2 = m_1^2, \quad q_2^2 = m_2^2, \tag{1.1}$$

(where $pq \equiv p^0q^0 - \mathbf{pq}$),

$$p_1+q_1 = p_2+q_2. \tag{1.2}$$

It has been suggested in ref. [1]) † that the Breit system for processes of this type be defined by the equality $\mathbf{p}_1+\alpha\mathbf{p}_2 = 0$ where α assumes one of the two values for which $p_1^0 = p_2^0$. A system of this type has also been introduced in ref. [4]) in which the process $(N+\gamma \to Y+K)$ has been treated. This attempt to generalize the Breit system does not appear to be a natural approach if for no other reason that the condition $p_1^0 = p_2^0$ implies that the difference p_2-p_1 is a space-like vector which, generally speaking, (for $M_1 \neq M_2$) is not the case.

† The author is thankful to Yu. Wolf for the opportunity of learning the results of his work prior to publication.

The usual system $\mathbf{p}_1+\mathbf{p}_2 = 0$, in which the kinematic formulas are comparitively simpler, has been employed in ref. [2,3]).

Dispersion relations for processes (I) and (II) have been presented in ref. [2]), taking account of the spin and isobaric structure of the amplitudes, but no attempt has been made to prove the relations or specify their regions of applicability. Restrictions on the masses which permit one to prove the dispersion equations by available methods have been deduced in ref. [3]) (these methods are based on the principles of covariance, causality and spectrality †). It has been pointed out that for real mass values in processes (I) and (II) these conditions are not met and the problem of excluding the unobservable region in a model in which these conditions are fulfilled has been examined.

In the present work a reference system is defined which changes over to the Breit system for $M_1 = M_2$ and in which the kinematic formulas are apparently simpler and more symmetric than in the aforementioned investigations. The dispersion relations for imaginary meson masses are derived in this system and the problem of analytical continuation of the anti-Hermitian part to the real mass region is investigated. A theorem is proved which is an extension of the fundamental Vladimirov-Logunov theorem [8]) regarding the analyticity region of Fourier transforms of some invariant causal functions to the case when all four particles (two at the beginning of the reaction and two at the end) have different masses. In accordance with the results of previous investigations the analyticity region of the anti-Hermitian part of the amplitude of process (I) or (II) contains no physical point (because of the large mass of the K meson).

Underlying the deduction in the present paper is the method of N. N. Bogolubov [5]) and the integral representation of causal commutators proposed by Dyson [7]). Since similar arguments can be found in other papers (e.g., in refs. [6,8,9])) we shall confine ourselves to a presentation of the results and omit, as a rule, the intermediate calculations and proofs ††.

2. Kinematics

We introduce four-dimensional baryon velocities u_1 and u_2:

$$p_1 = M_1 u_1, \quad p_2 = M_2 u_2, \quad u_1^2 = u_2^2 = 1, \tag{2.1}$$

and define the dimensionless invariants ν and t^2 as follows:

$$\nu = \tfrac{1}{2}(u_1+u_2)\,\frac{q_1+q_2}{M_1+M_2}, \quad t^2 = -\tfrac{1}{4}(u_1-u_2)^2. \tag{2.2}$$

† The spectrality principle implies the existence of a complete system of positive energy physical states.

†† A detailed exposition of all the proofs can be found in a preprint of the author [10]).

Besides the invariants ν and t we shall also employ the total energy in the c.m.s. W and the momentum transfer Δ defined by

$$W^2 \equiv (p_1+q_1)^2 = 2M_1M_2(\nu+t^2)+M_1M_2+\frac{M_1m_2^2+M_2m_1^2}{M_1+M_2}, \qquad (2.3)$$
$$4\Delta^2 \equiv -(p_1-p_2)^2 = 4M_1M_2t^2-(M_2-M_1)^2.$$

All possible scalar products of vectors p_1, p_2, q_1, q_2 can be expressed as linear functions of the invariants ν and t^2 (or W^2 and Δ^2).

Now we introduce the reference system

$$\mathbf{u}_1+\mathbf{u}_2 = 0 \qquad (2.4)$$

(this system changes over to the Breit system for $M_1 = M_2$). In the system (2.4) the vecors p_l and q_l ($l = 1,2$) have the following form:

$$p_1 = M_1(\sqrt{1+t^2}, -t\mathbf{r}), \quad p_2 = M_2(\sqrt{1+t^2}, t\mathbf{r}),$$
$$\tfrac{1}{2}(q_1+q_2) = \left\{\frac{M_1+M_2}{2\sqrt{1+t^2}}\nu,\ \lambda(\nu)\mathbf{e}+\frac{1}{2t}\left[(M_2-M_1)\nu-\frac{m_1^2-m_2^2}{M_1+M_2}\right]\mathbf{r}\right\}, \qquad (2.5)$$
$$\tfrac{1}{2}(q_1-q_2) = \tfrac{1}{2}\{(M_2-M_1)\sqrt{1+t^2},\ (M_1+M_2)t\mathbf{r}\},$$

where $\mathbf{e}$ and $\mathbf{r}$ are three-dimensional orthogonal unit vectors ($\mathbf{e}^2 = \mathbf{r}^2 = 1$, $(\mathbf{e}\cdot\mathbf{r}) = 0$),

$$\lambda^2 = a\nu^2+2b\nu-c,$$
$$a = \frac{4M_1M_2t^2-(M_2-M_1)^2}{4t^2(1+t^2)} = \frac{\Delta^2}{t^2(1+t^2)}, \quad b = \frac{M_2-M_1}{M_2+M_1}\frac{m_1^2-m_2^2}{4t^2}, \qquad (2.6)$$
$$c = \frac{(m_1^2-m_2^2)^2}{4(M_1+M_2)^2t^2}+\frac{m_1^2+m_2^2}{2}+\Delta^2. \qquad (2.7)$$

The roots of the equation $\lambda^2(\nu) = 0$ are always real. We denote them by ν_- and $\nu_+(\nu_- < \nu_+)$. If $a > 0$ (i.e., if $\Delta^2 > 0$) the physical region for processes (I) and (II) will consist of the intervals $\nu > \nu_+$ and $\nu > -\nu_-$ respectively. If, however, $a < 0$ ($\Delta^2 < 0$) the physical region will consist of points of the finite interval $\nu_- < \nu < \nu_+$. In the following we restrict ourselves to the first case, that is, we shall assume that

$$\Delta^2 > 0, \quad \text{i.e.} \quad t^2 > \frac{(M_2-M_1)^2}{4M_1M_2}. \qquad (2.8)$$

3. Analytical Properties of the Amplitude of the Inelastic Process for Imaginary Meson Masses

In accordance with ref. [5]) the amplitude of process (I) in the physical region can be written down in the form

$$T^{\mathrm{ret}}(\tfrac{1}{2}(q_1+q_2)) = -\frac{1}{(2\pi)^3}\int \langle p_2|\frac{\delta j_1(-\frac{1}{2}x)}{\delta\varphi_2(\frac{1}{2}x)}|p_1\rangle \exp\left\{\frac{i}{2}(q_1+q_2)x\right\} \mathrm{d}_4x. \quad (3.1)$$

Currents $j_1(x)$ and $j_2(x)$ are defined by the equalities [5])

$$j_l(x) = i\frac{\delta S}{\delta\varphi_l(x)}S^+, \quad l = 1,2,$$

where $\varphi_1(x)$ and $\varphi_2(x)$ are K and π-meson field operators.

Consider a fictitious process for which (1.1) is replaced by the relations

$$q_l^2 = m_l^2+\tau = \tau_l, \quad l = 1,2. \quad (3.2)$$

Here τ is an auxiliary parameter which assumes values in the interval (for notations see (2.7))

$$\tau < -\frac{b^2}{a} - c. \quad (3.3)$$

Condition (3.3) is necessary and sufficient for the following inequality to hold (providing $\mathrm{Im}\ \nu \neq 0$):

$$|\mathrm{Im}\ \tfrac{1}{2}(q_1^0+q_2^0)| > |\mathrm{Im}\ \tfrac{1}{2}(\mathbf{q}_1+\mathbf{q}_2)|. \quad (3.4)$$

When (3.4) is valid the function T^{ret} defined by equality (3.1) is, in virtue of the Bogolubov causality condition, analytic in the upper half-plane of the complex variable ν, providing $\mathrm{Im}\ \nu > 0$, whereas the Hermite-conjugate amplitude T^{adv} is analytic in the lower half-plane ($\mathrm{Im}\ \nu < 0$). The difference between these two functions is proportional to the anti-Hermitian part of the amplitude and vanishes within a certain interval on the real axis (excluding a finite number of singularities in this interval). For example, in the case of the process $(\mathrm{N}+\overline{\mathrm{K}} \to \Lambda+\pi)$, for which $M_1 = M_{\mathrm{N}}, M_2 = M_\Lambda, m_1 = m_{\mathrm{K}}, m_2 = m_\pi$, the anti-Hermitian part vanishes in the interval $\nu_c^- < \nu < \nu_c^+$ where

$$\nu_c^- = t^2 - \frac{m_2}{M_2} + \frac{M_2^2-M_1^2+m_1^2-m_2^2}{2M_2(M_1+M_2)} + \frac{\tau}{2M_1M_2} \approx t^2+0.007+\frac{\tau}{2M_1M_2},$$

$$\nu_c^+ = -t^2 + \frac{m_2}{M_2} + \frac{M_2^2-M_1^2-m_1^2+m_2^2}{2M_1(M_1+M_2)} - \frac{\tau}{2M_1M_2} \approx -t^2+0.18-\frac{\tau}{2M_1M_2},$$

(or, for $\tau = 0$, $M_2^2+m_1^2-2M_1m_2-4\Delta^2 < W^2 < (M_2+m_2)^2$), and possesses singularities at the points

$$\nu_0^+ = -t^2 + \frac{M_\Sigma^2-M_2^2-m_2^2}{2M_1M_2} + \frac{M_2^2-M_1^2-m_1^2+m_2^2}{2M_1(M_1+M_2)}$$

$$- \frac{\tau}{2M_1M_2} \approx -t^2+0.12-\frac{\tau}{2M_1M_2},$$

$$\nu_0^- = t^2 + \frac{m_2^2}{2M_1M_2} + \frac{M_2^2 - M_1^2 + m_1^2 - m_2^2}{2M_2(M_1+M_2)} + \frac{\tau}{2M_1M_2} \approx t^2 + 0.14 + \frac{\tau}{2M_1M_2}.$$

Thus, when τ varies within the interval (3.3) the usual dispersion relations can be written for the amplitude of process (I). In order to exclude from these relations integration over negative energies the dispersion relations for process (II) should be employed (see ref. [2,3]).

4. Analytic Continuation of the Anti-Hermitian Part of the Amplitude with respect to the Auxiliary Variable τ

Since the anti-Hermitian part of the amplitude is proportional to the vacuum expectation value of the second variational derivative of the current commutator [5]) it can be represented as the sum of Fourier transforms of four translationally-invariant causality functions with the aid of the spectrality condition. Following refs. [5,6]), one can set up for each of these functions three other functions which satisfy related retarded and advanced conditions.

Thus the problem of analytic continuation of the anti-Hermitian part of the amplitude reduces to the determination of the analyticity of the Fourier transforms of the translationally invariant functions $F_{ij}(x_1, x_2, x_3, x_4)$, $(i, j = \mathrm{r}, \mathrm{a})$, which satisfy the following causality conditions †:

$$\begin{aligned}
&F_{\mathrm{rr}}(x_1, x_2, x_3, x_4) = 0 \quad \text{if} \quad x_1 \lesssim x_3 \quad \text{or} \quad x_2 \lesssim x_4,\\
&F_{\mathrm{ra}}(x_1, x_2, x_3, x_4) = 0 \quad \text{if} \quad x_1 \lesssim x_3 \quad \text{or} \quad x_2 \gtrsim x_4,\\
&F_{\mathrm{ar}}(x_1, x_2, x_3, x_4) = 0 \quad \text{if} \quad x_1 \gtrsim x_3 \quad \text{or} \quad x_2 \lesssim x_4,\\
&F_{\mathrm{aa}}(x_1, x_2, x_3, x_4) = 0 \quad \text{if} \quad x_1 \gtrsim x_3 \quad \text{or} \quad x_2 \gtrsim x_4.
\end{aligned} \tag{4.1}$$

Their Fourier transforms $\tilde{F}_{ij}(k_1, k_2, k_3, k_4)$, defined on the subspace $k_1+k_2+k_3+k_4 = 0$ by the equality

$$\begin{aligned}
&(2\pi)^4 \delta(k_1+k_2+k_3+k_4)\tilde{F}_{ij}(k_1, k_2, k_3, k_4)\\
&= \int\int\int\int F_{ij}(x_1, x_2, x_3, x_4) \exp\{i(k_1x_1+k_2x_2+k_3x_3+k_4x_4)\} \mathrm{d}_4x_1 \mathrm{d}_4x_2 \mathrm{d}_4x_3 \mathrm{d}_4x_4,
\end{aligned} \tag{4.2}$$

satisfy, in virtue of the spectrality postulate, the following conditions

$$\begin{aligned}
&\tilde{F}_{\mathrm{r}j}(k_1, k_2, k_3, k_4) = \tilde{F}_{\mathrm{a}j}(k_1, k_2, k_3, k_4), \quad \text{if} \quad k_1^2 < a_1^2 \quad \text{and} \quad k_3^2 < b_1^2;\\
&\tilde{F}_{i\mathrm{r}}(k_2, k_1, k_3, k_4) = \tilde{F}_{i\mathrm{a}}(k_1, k_2, k_3, k_4), \quad \text{if} \quad k_2^2 < a_2^2 \quad \text{and} \quad k_4^2 < b_2^2;\\
&\tilde{F}_{ij}(k_1, k_2, k_3, k_4) = 0 \qquad\qquad \text{if} \quad (k_2+k_4)^2 < c^2 \quad \text{or} \quad k_2^0+k_4^0 < 0.
\end{aligned} \tag{4.3}$$

Here the positive numbers a_l, b_l and c obey the condition

$$c > a_l - b_l \geqq 0, \quad l = 1,2.$$

† The notation $x \lesssim y$ means that $x^0 \leqq y^0$ or $(x-y)^2 < 0$.

For various terms of the expansion of the anti-Hermitian part, the parameters a_l, b_l and c assume the values (using $M_1 = M_N$, $M_2 = M_\Lambda$ or M_Σ, $m_1 = m_K$, $m_2 = m_\pi$):

$$c = M_2+m_2,\ a_1 = M_1+m_2,\ a_2 = M_2+m_2,\ b_1 = m_1+2m_2,\ b_2 = 3m_2, \quad (4.4a)$$

$$c = M_1+m_2,\ a_1 = M_1+m_2,\ a_2 = M_2+m_2,\ b_1 = 3m_2,\ b_2 = m_1+2m_2. \quad (4.4b)$$

Consideration of the anti-Hermitian part of process (II) leads to the same terms but in a different order.

The following theorem which is a generalization of the fundamental Vladimirov-Logunov theorem [8]) is found to hold.

Theorem. Let $F_{ij}(x_1, x_2, x_3, x_4)$, $(i,j = \mathrm{r}, \mathrm{a})$, be four generalized functions of four 4-vectors x_1, x_2, x_3, x_4, which are invariant under transformations from the inhomogenous orthochronous Lorentz group. These generalized functions are assumed to satisfy the retarded and advanced conditions (4.1) and their Fourier transforms $\tilde{F}_{ij}(k_1, k_2, k_3, k_4)$ satisfy conditions (4.3). Suppose, furthermore, that the positive numbers M_l^2 and real numbers $\tau_l^0 < b_l^2$ are such that†

$$\tau_l^0 \leqq \min_{W \geqq c} \left\{ W^2+M_l^2-2W\frac{a_l W+M_l^2-a_l b_l}{W+a_l-b_l} \right\}, \quad (l = 1,2). \quad (4.5)$$

Then, a function $\Phi(z_1, z_2, z_3, z_4, z_5; W)$ can be constructed which is a generalized function with respect to the real variable W and which vanishes at $W < c$ and is analytic for $W \geqq c$ with respect to the set of five complex variables $(z_1, z_2, z_3, z_4, z_5)$ in a certain domain $D(W)$ which contains all the points of the form

$$z_1 = M_1^2, \quad z_2 = M_2^2, \quad z_3 = \tau_1, \quad z_4 = \tau_2, \quad z_5 = (k_1+k_2)^2 = -4\Delta^2. \quad (4.6)$$

Here $\tau_i < \tau_i^0$ and the invariant momentum transfer $4\Delta^2$ runs over the interior of the ellipse

$$A(W, \tau_1, \tau_2)+B(W, \tau_1, \tau_2)\cos\delta+iC(W, \tau_1, \tau_2)\sin\delta, \quad (0 \leqq \delta \leqq 2\pi). \quad (4.7)$$

The functions A, B and C are defined by the formulas

$$\begin{aligned} A(W, \tau_1, \tau_2) &= \varphi_1^2(W, \tau_1)+\varphi_2^2(W, \tau_2)-\left(\frac{M_2^2-M_1^2+\tau_1-\tau_2}{2W}\right)^2, \\ \tfrac{1}{2}B(W, \tau_1, \tau_2) &= \psi_1(W, \tau_1)\psi_2(W, \tau_2) \\ &\quad +\{[\psi_1^2(W, \tau_1)-\varphi_1^2(W, \tau_1)][\psi_2^2(W, \tau_2)-\varphi_2^2(W, \tau_2)]\}^{\frac{1}{2}} \\ \tfrac{1}{2}C(W, \tau_1, \tau_2) &= \psi_1(W, \tau_1)[\psi_2^2(W, \tau_2)-\varphi_2^2(W, \tau_2)]^{\frac{1}{2}} \\ &\quad +\psi_2(W, \tau_2)[\psi_1^2(W, \tau_1)-\varphi_1^2(W, \tau_1)]^{\frac{1}{2}}. \end{aligned} \quad (4.8)$$

† It should be noted that in the particular case when $a_1 = a_2 = M+\mu$, $M_1^2 = M_2^2 = M^2$, inequality (4.5) is equivalent to equality (1.5) in ref. [8]) and, moreover, is simpler in form.

Here

$$\varphi_l^2(W,\tau_l)=\tfrac{1}{4}\left(W+\frac{M_l^2-\tau_l}{W}\right)^2-M_l^2,\quad l=1,2, \tag{4.9}$$

$$\psi_l(W,\tau_l)=\begin{cases}\left\{\varphi_l^2(W,\tau_l)+\dfrac{(a_l^2-M_l^2)(b_l^2-\tau_l)}{W^2-(a_l-b_l)^2}\right\}^{\frac{1}{2}} & \text{if}\quad \tau_l\geqq b_l\left(a_l-\dfrac{W^2}{a_l-b_l}\right),\\ \dfrac{a_l^2-M_l^2}{2W}+\dfrac{1}{2W}\{[(W+a_l)^2-\tau_l][(W-a_l)^2-\tau_l]\}^{\frac{1}{2}} & \\ \qquad\qquad\text{if}\quad \tau_l<b_l\left(a_l-\dfrac{W^2}{a_l-b_l}\right). & \end{cases} \tag{4.10}$$

It can readily be seen that in the case of inelastic scattering of K mesons on nucleons the second possibility in eq. (4.10) is realized only for $\tau_l<0$, and for the real point $\tau_l=m_l^2$, the function $\psi_l(W,\tau_l)$ is given by the upper expression in (4.10). For $\tau_l=b_l(a_l-W^2)/(a_l-b_l)$ both expressions of ψ_l in formula (4.10) are identical and equal to

$$\frac{1}{2W}\left(\frac{a_l}{a_l-b_l}W^2+a_lb_l-M_l^2\right).$$

The function $\Phi(z_1,z_2,z_3,z_4,z_5;W)$ is such that for real p_1,p_2,p_3,p_4 from subspace $p_1+p_2+p_3+p_4=0$ for which the quantities $z_1=p_1^2,\ldots,z_4=p_4^2$, $z_5=(p_1+p_2)^2$ belong to the domain $D(W)$ it can be represented as

$$\tilde{F}_{ij}(p_1,p_2,p_3,p_4)=\Phi(p_1^2,p_2^2,p_3^2,p_4^2,(p_1+p_2)^2;\sqrt{(p_2+p_4)^2}) \tag{4.11}$$

for $(p_2+p_4)^2>c^2$ and $p_2^0+p_4^0>0$.

The proof of this theorem rests on the integral representation of causal commutators [7]) and is similar to that of the basic theorem in ref. [8]) (also see ref. [10])).

The theorem formulated above in principle encompasses all processes involving two particles at the beginning and at the end of the reaction.

The region of analyticity of the anti-Hermitian part with respect to momentum transfer is not empty (for $\tau_l=\tau_l^0$) only if for $\tau_l^0=m_l^2$, $l=1,2$ inequality (4.5) is fulfilled. For example, in the case of elastic nucleon-nucleon scattering ($a_l=b_l=M+m_\pi$, $c=2m_\pi$) the right hand side of (4.5) goes through a minimum at $W=M+m_\pi$ and the inequality (4.5) with $\tau^0=M^2$ yields the well-known relation $m_\pi\geqq(\sqrt{2}-1)M$ which is not consistent with the experimental values of M and m_π.

If (4.5) be applied to the processes (I) and (II) under consideration we find that for the experimental mass values, the right hand side of (4.5) is minimum at $W=c$. The most rigorous restrictions on τ_l arise when a_l, b_l and c assume the values in (4.4b). In the case when $a_2=M_A+m_\pi$ the minimum in the right side

of (4.5) is approximately equal to $8.2\, m_\pi^2$, whereas it is required that the function be continued to the point $m_K^2 \approx 13 m_\pi^2$. Thus in this case, just as in the case when $a_2 = M_\Sigma + m_\pi$ the region of analyticity of the anti-Hermitian part derived on basis of the theorem formulated above does not contain any physical point. It may be mentioned that in the case when a_1, b_1 and c are specified by equalities (4.4a), inequality (4.5) is equivalent to the limiting condition derived by Oehme and Taylor [9]) for elastic scattering of K-mesons on nucleons (cf. also ref. [3])).

Apparently the limitations of the proof of the dispersion relations given here (as well as in the case of elastic nucleon-nucleon scattering) cannot be removed by the simple expedient of applying the causality and spectrality principles. However, the possibility exists that taking account of symmetry properties of the scattering amplitude will permit one to extend the region of analyticity with respect to the square of the meson mass τ.

In conclusion the author expresses his deep appreciation to Acad. N. N. Bogolubov for interest in this work and A. A. Logunov, V. S. Vladimirov and N. A. Chernikov for useful suggestions and discussions during the course of the investigation.

References

1) M. K. Polivanov, Doklady **118** (1958) 679;
Yu. Wolf, ZETP **37** (1959) 1379
2) Y. S. Jin, Nuovo Cimento **12** (1959) 455
3) R. F. Streater, Nuovo Cimento **13** (1959) 57
4) S. Okubo, Progr. Theor. Phys. **19** (1958) 430
5) N. N. Bogolubov, Izv. Akad. Nauk SSSR, Ser. Fiz. **19** (1955) 237;
N. N. Bogolubov, B. V. Medvedev and M. K. Polivanov, Problems of dispersion relations theory (Moscow, 1958)
6) N. N. Bogolubov and V. S. Vladimirov, Izv. Akad. Nauk SSSR, Ser. Mat. **22** (1958) 15;
A. A. Logunov, Higher School Communications, Phys. -Mat. Sciences **4** (1958) 207
7) F. J. Dyson, Phys. Rev. **110** (1958) 1460
8) V. S. Vladimirov and A. A. Logunov, Izv. Akad. Nauk SSSR, Ser. Mat. **23** (1959) 661;
D. V. Shirkov, Report at IX International Conference on High Energy Physics, Kiev, 1959
9) R. Oehme and J. G. Taylor, Phys. Rev. **113** (1959) 371
10) I. T. Todorov, Analytic properties of the amplitude for inelastic processes involving strange particles, preprint of Joint Institute for Nuclear Research (Dubna, 1960 P—464 (in Russian)).

1.E.2

Nuclear Physics **18** (1960) 529—569; © *North-Holland Publishing Co., Amsterdam*

Not to be reproduced by photoprint or microfilm without written permission from the publisher

RELATIVE NUCLIDIC MASSES

F. EVERLING †, L. A. KÖNIG, J. H. E. MATTAUCH

Max-Planck-Institut für Chemie (Otto-Hahn-Institut), Mainz

and

A. H. WAPSTRA

Instituut voor Kernphysisch Onderzoek, Amsterdam

Received 13 June 1960

Abstract: The accompanying mass table gives a complete and consistent list of nuclidic masses††, and also a few derived quantities.

In table 1 we give a complete and consistent list of nuclidic masses computed with least squares methods from all significant experimental data available to us together with the binding energies and the β^- decay energies derived from these masses. The first two columns give the number of neutrons and protons in a nucleus of the nucleide considered; columns 3 and 4 their difference and their sum (neutron excess and mass number), and column 5 the element symbol.

The columns 6 and 8 give the difference M between the nuclidic mass and the mass number (the so-called mass excess). The first quantity is measured in a scale in which the nuclidic mass of ^{12}C is exactly equal to 12 units (symbol u [1]); as accepted by the assembly of the IUPAP, Ottawa, 1960). Column 8 gives the mass excess in μu; column 6 gives the same quantity in keV for the needs of experimental physicists. The errors in these values are given in the columns 7 and 9. They are given with a two digit precision if the first digit differing from zero is less than 5. The values themselves have been abbreviated accordingly. This practice has also been followed elsewhere in this paper.

Columns 10 and 11 give the mass excesses in the old scale, in which the nuclidic mass of ^{16}O was taken equal to 16 mass units; they have been given only for the purpose of comparison with older data. The errors in these values can, for practical purposes, be taken equal to those in the columns 7 and 9. The last two groups of columns give the total binding energy and the beta decay energy with the errors in these quantities.

The masses for $A < 200$ have been derived by least squares computations from ten groups of data. In each group we distinguished between primary and

(continued on p. 568)

† Now with Nuclear Data Group, National Academy of Sciences, National Research Council, Washington 25, D.C.

†† The term (relative) nuclidic mass refers to the mass of a neutral atom of a nucleide relative to some standard atom.

TABLE 1. Nuclidic mass relative to ^{12}C and ^{16}O ind

Z	N	N−Z	A	Symbol	Mass excess ($^{12}C = 0$) (keV)		Mass excess ($^{12}C = 0$) (μu)	
0	1	1	1	n	8 071.34	± 0.41	8 665.44	± 0.43
1	0	-1	1	H	7 288.73	0.11	7 825.22	0.08
1	1	0	2	D	13 135.36	0.17	14 102.19	0.11
1	2	1	3	T	14 949.07	0.26	16 049.40	0.23
2	1	-1	3	He	14 930.94	0.26	16 029.94	0.23
2	2	0	4	He	2 425.11	0.35	2 603.61	0.37
2	3	1	5	He	11 453	20	12 296	21
3	2	-1	5	Li	11 681	37	12 541	40
2	4	2	6	He	17 604	17	18 900	18
3	3	0	6	Li	14 089.3	1.0	15 126.3	1.0
3	4	1	7	Li	14 908.0	1.1	16 005.3	1.1
4	3	-1	7	Be	15 768.7	1.1	16 929.3	1.2
3	5	2	8	Li	20 946.6	1.5	22 488.4	1.6
4	4	0	8	Be	4 944.4	0.7	5 308.3	0.8
5	3	-2	8	B	22 924.4	1.6	24 611.7	1.7
4	5	1	9	Be	11 350.3	0.9	12 185.8	0.9
5	4	-1	9	B	12 420.5	1.8	13 334.7	2.0
4	6	2	10	Be	12 607.3	2.1	13 535.3	2.3
5	5	0	10	B	12 051.9	0.7	12 938.9	0.7
6	4	-2	10	C	15 670	60	16 830	60
5	6	1	11	B	8 667.14	0.41	9 305.09	0.43
6	5	-1	11	C	10 649.5	3.1	11 433.4	3.3
5	7	2	12	B	13 368.9	1.0	14 352.9	1.0
6	6	0	12	C	0	0	0	0
7	5	-2	12	N	17 600	90	18 900	100
5	8	3	13	B	16 560	50	17 780	50
6	7	1	13	C	3 124.3	0.7	3 354.3	0.7
7	6	-1	13	N	5 345.5	1.3	5 738.9	1.4
6	8	2	14	C	3 019.67	0.38	3 241.93	0.41
7	7	0	14	N	2 863.60	0.16	3 074.38	0.17
8	6	-2	14	O	8 012	5	8 601	5
6	9	3	15	C	9 873.3	1.1	10 600.0	1.2
7	8	1	15	N	100.7	0.8	108.1	0.9
8	7	-1	15	O	2 861.3	1.8	3 071.9	1.9
7	9	2	16	N	5 672	6	6 089	6
8	8	0	16	O	-4 736.43	0.26	-5 085.06	0.28
7	10	3	17	N	7 990	200	8 580	210
8	9	1	17	O	- 807.2	0.9	- 866.6	0.9
9	8	-1	17	F	1 954.5	2.3	2 098.4	2.4

¹⁶O binding energy and β^- decay energy

	Mass excess ($^{16}O = 0$)		Binding energy (keV)		β^- decay energy (keV)	
	(keV)	(μMU)				
.43	8 367.37	8 986.11	0 ±	0	782.61 ±	0.40
.08	7 584.76	8 145.63	0	0		
.11	13 727.42	14 742.51	2 224.71	0.40		
.23	15 837.15	17 008.26	8 482.3	0.8	18.13	0.08
.23	15 819.02	16 988.78	7 717.87	0.44		
.37	3 609.22	3 876.11	28 295.0	0.9		
	12 934	13 890	27 338	20	- 227	42
	13 161	14 134	26 328	37		
	19 380	20 814	29 259	17	3 515	17
.0	15 865.4	17 038.6	31 991.0	1.5		
.1	16 980.2	18 235.8	39 243.6	1.8	- 860.7	1.1
.2	17 840.9	19 160.1	37 600.3	1.8		
.6	23 314.9	25 038.9	41 276.3	2.4	16 002.2	1.5
.8	7 312.6	7 853.4	56 495.9	1.8	-17 980.0	1.6
.7	25 292.6	27 162.9	37 733.3	2.2		
.9	14 014.6	15 050.9	58 161.3	2.1	-1 070.2	1.6
.0	15 084.7	16 200.2	56 308.5	2.7		
.3	15 567.6	16 718.8	64 975.6	3.2	555.5	2.1
.7	15 012.1	16 122.2	64 748.5	2.3	-3 620	60
	18 630	20 010	60 340	60		
.43	11 923.44	12 805.14	76 204.6	2.6	-1 982.4	3.0
.3	13 905.8	14 934.1	73 439.6	4.0		
.0	16 921.2	18 172.5	79 574.2	3.0	13 368.9	1.0
	3 552.33	3 815.01	92 160.5	2.7	-17 600	90
	21 150	22 720	73 780	90		
	20 410	21 910	84 460	50	13 430	50
.7	6 972.7	7 488.3	97 107.5	3.1	-2 221.2	1.3
.4	9 193.8	9 873.7	94 103.7	3.2		
.41	7 164.04	7 693.80	105 283.5	3.3	156.07	0.35
.17	7 007.98	7 526.19	104 656.9	3.1	-5 148	5
	12 156	13 055	98 726	6		
.2	14 313.7	15 372.2	106 501.2	3.8	9 772.6	1.4
.9	4 541.1	4 876.9	115 491.2	3.6	-2 760.6	1.5
.9	7 301.7	7 841.6	111 948.0	3.9		
	10 408	11 178	117 991	7	10 408	6
.28	0	0	127 617.0	3.5		
	13 030	13 990	123 740	200	8 800	200
.9	4 225.3	4 537.7	131 759.1	4.1	-2 761.7	2.4
.4	6 987.0	7 503.7	128 214.8	4.5		

TABLE 1 (Continued)

Z	N	N−Z	A	Symbol	Mass excess ($^{12}C = 0$) (keV)		Mass excess ($^{12}C = 0$) (μu)	
8	10	2	18	O	- 782.57	± 0.32	- 840.17	± 0.34
9	9	0	18	F	884.8	4.0	949.9	4.3
10	8	-2	18	Ne	5 100	200	5 480	210
8	11	3	19	O	3 332.1	4.0	3 577.3	4.3
9	10	1	19	F	-1 486.1	0.7	-1 595.4	0.7
10	9	-1	19	Ne	1 762	5	1 892	5
9	11	2	20	F	-13.5	3.8	-14.5	4.0
10	10	0	20	Ne	-7 041.3	0.5	-7 559.6	0.5
11	9	-2	20	Na	8 280	300	8 890	320
9	12	3	21	F	-26	25	-28	27
10	11	1	21	Ne	-5 729.1	1.6	-6 150.8	1.7
11	10	-1	21	Na	-2 207	30	-2 370	32
10	12	2	22	Ne	-8 024.9	0.6	-8 615.5	0.6
11	11	0	22	Na	-5 183.3	4.6	-5 565	5
10	13	3	23	Ne	-5 146	5	-5 525	5
11	12	1	23	Na	-9 526.2	1.5	-10 227.4	1.6
12	11	-1	23	Mg	-5 467	10	-5 869	11
10	14	4	24	Ne	-5 964	40	-6 403	43
11	13	2	24	Na	-8 413.8	2.7	-9 033.1	2.9
12	12	0	24	Mg	-13 930.1	1.8	-14 955.4	1.9
13	11	-2	24	Al	90	300	90	320
11	14	3	25	Na	-9 390	200	-10 080	210
12	13	1	25	Mg	-13 189.4	1.9	-14 160.3	2.0
13	12	-1	25	Al	-8 928	6	-9 586	7
12	14	2	26	Mg	-16 215.5	2.2	-17 409.1	2.4
13	13	0	26	Al	-12 201.5	4.7	-13 100	5
12	15	3	27	Mg	-14 581.2	3.7	-15 654.5	3.9
13	14	1	27	Al	-17 199.2	2.0	-18 465.1	2.1
14	13	-1	27	Si	-12 384	11	-13 295	12
12	16	4	28	Mg	-15 015	6	-16 120	7
13	15	2	28	Al	-16 851.5	3.6	-18 091.9	3.9
14	14	0	28	Si	-21 491.0	2.9	-23 072.9	3.1
15	13	-2	28	P	-7 690	300	-8 260	320
13	16	3	29	Al	-18 140	50	-19 470	50
14	15	1	29	Si	-21 897.4	3.4	-23 509.2	3.6
15	14	-1	29	P	-16 937	11	-18 184	11
14	16	2	30	Si	-24 440.3	4.0	-26 239.3	4.3
15	15	0	30	P	-20 193	10	-21 680	11
14	17	3	31	Si	-22 961.1	4.6	-24 651	5
15	16	1	31	P	-24 437.8	1.5	-26 236.6	1.5
16	15	-1	31	S	-19 002	17	-20 401	18
14	18	4	32	Si	-24 200	50	-25 980	50
15	17	2	32	P	-24 303.2	2.2	-26 092.1	2.4
16	16	0	32	S	-26 011.7	1.0	-27 926.2	1.1
17	15	-2	32	Cl	-13 010	300	-13 970	320

Mass excess ($^{16}O = 0$)		Binding energy (keV)	β^- decay energy (keV)
(keV)	(μMU)		
4 545.92	4 882.07	139 805.9 ± 4.3	-1 667.4 ± 4.0
6 213.3	6 672.8	137 356 6	-4 220 200
10 430	11 200	132 350 200	
8 956.6	9 618.9	143 763 6	4 818.1 4.1
4 138.5	4 444.5	147 798.1 4.4	-3 248 5
7 387	7 933	143 767 7	
5 907.1	6 343.9	154 397 6	7 027.8 3.8
-1 120.8	-1 203.6	160 642.1 4.4	-15 320 300
14 200	15 250	144 540 300	
6 191	6 649	162 480 26	5 703 25
487.5	523.6	167 401 5	-3 522 30
4 010	4 306	163 097 30	
-1 512.3	-1 624.1	177 768 5	-2 841.5 4.6
1 329.3	1 428	174 144 7	
1 662	1 785	182 961 7	4 380 5
-2 717.6	-2 918.6	186 558 5	-4 059 10
1 342	1 441	181 716 11	
1 141	1 225	191 850 41	2 450 40
-1 309.2	-1 406.0	193 517 6	5 516.3 2.7
-6 825.4	-7 330.1	198 251 6	-14 020 300
7 190	7 720	183 450 300	
-1 990	-2 140	202 560 200	3 800 200
-5 788.8	-6 216.8	205 582 6	-4 261 6
-1 528	-1 641	200 538 8	
-8 518.8	-9 148.8	216 679 6	-4 014.0 4.9
-4 504.8	-4 838	211 882 8	
-6 588.5	-7 075.7	223 116 7	2 617.9 4.0
-9 206.4	-9 887.2	224 951 6	-4 815 11
-4 391	-4 716	219 353 13	
-6 726	-7 223	231 621 9	1 837 5
-8 562.8	-9 196.0	232 675 7	4 639.5 4.2
-13 202.3	-14 178.5	236 532 7	-13 800 300
600	640	221 950 300	
-9 550	-10 260	242 030 50	3 760 50
-13 312.6	-14 297.1	245 010 7	-4 960 10
-8 353	-8 970	239 267 12	
-15 559.5	-16 710.1	255 624 8	-4 247 11
-11 313	-12 149	250 595 12	
-13 784.3	-14 804	262 216 9	1 476.7 4.6
-15 261.0	-16 389.5	262 910 7	-5 435 17
-9 826	-10 552	256 692 18	
-14 730	-15 820	271 530 50	100 50
-14 830.4	-15 927.0	270 847 8	1 708.4 2.0
-16 538.8	-17 761.8	271 773 7	-13 000 300
-3 540	-3 800	257 990 300	

TABLE 1 (Continued)

Z	N	N−Z	A	Symbol	Mass excess ($^{12}C = 0$) (keV)		(μu)	
15	18	3	33	P	-26 333.9	± 3.4	-28 272.2	± 3.7
16	17	1	33	S	-26 582.9	2.8	-28 539.5	3.0
17	16	-1	33	Cl	-21 008	12	-22 554	13
15	19	4	34	P	-24 830	200	-26 660	210
16	18	2	34	S	-29 932.4	2.9	-32 135.5	3.1
17	17	0	34	Cl	-24 512	30	-26 317	32
16	19	3	35	S	-28 842.9	2.6	-30 965.8	2.8
17	18	1	35	Cl	-29 010.2	2.6	-31 145.5	2.8
18	17	-1	35	A	-23 030	40	-24 725	43
16	20	4	36	S	-30 653	9	-32 909	9
17	19	2	36	Cl	-29 516	5	-31 688	6
18	18	0	36	A	-30 227.0	3.2	-32 451.9	3.4
16	21	5	37	S	-26 980	90	-28 960	100
17	20	3	37	Cl	-31 765.9	2.1	-34 104.1	2.2
18	19	1	37	A	-30 949.9	2.5	-33 228.0	2.7
19	18	-1	37	K	-24 830	100	-26 660	110
16	22	6	38	S	-26 800	150	-28 780	160
17	21	4	38	Cl	-29 804	8	-31 998	9
18	20	2	38	A	-34 719.9	3.2	-37 275.5	3.4
19	19	0	38	K	-28 791	11	-30 910	11
17	22	5	39	Cl	-29 803	21	-31 997	23
18	21	3	39	A	-33 233	6	-35 679	6
19	20	1	39	K	-33 798.3	2.8	-36 286.0	3.0
20	19	-1	39	Ca	-27 188	40	-29 190	43
17	23	6	40	Cl	-27 500	500	-29 600	500
18	22	4	40	A	-35 037.3	0.8	-37 616.2	0.8
19	21	2	40	K	-33 524.5	3.3	-35 992.1	3.6
20	20	0	40	Ca	-34 846.0	3.5	-37 410.8	3.7
21	19	-2	40	Sc	-20 950	400	-22 490	430
18	23	5	41	A	-33 058	11	-35 492	12
19	22	3	41	K	-35 548.3	4.3	-38 164.9	4.6
20	21	1	41	Ca	-35 135	8	-37 721	9
21	20	-1	41	Sc	-29 185	41	-31 333	44
19	23	4	42	K	-35 006	20	-37 583	22
20	22	2	42	Ca	-38 535.9	4.2	-41 372.3	4.4
21	21	0	42	Sc	-32 600	600	-35 000	600
19	24	5	43	K	-36 577	11	-39 269	12
20	23	3	43	Ca	-38 394.0	4.5	-41 220.0	4.8
21	22	1	43	Sc	-36 174	11	-38 837	12
19	25	6	44	K	-35 360	200	-37 960	210
20	24	4	44	Ca	-41 458.7	4.5	-44 510.3	4.8
21	23	2	44	Sc	-37 811	7	-40 594	7
22	22	0	44	Ti	-37 656	12	-40 427	13
20	25	5	45	Ca	-40 807.0	4.3	-43 810.6	4.6
21	24	3	45	Sc	-41 058.9	4.0	-44 081.1	4.2
22	23	1	45	Ti	-39 001	6	-41 871	6

Mass excess ($^{16}O = 0$)		Binding energy (keV)	β^- decay energy (keV)
(keV)	(μMU)		
-16 565.0	-17 789.9	280 949 ± 9	249.0 ± 2.0
-16 814.0	-18 057.3	280 415 8	-5 575 12
-11 239	-12 070	274 058 14	
-14 770	-15 860	287 520 200	5 100 200
-19 867.4	-21 336.6	291 836 8	-5 420 30
-14 447	-15 516	285 634 31	
-18 481.9	-19 848.6	298 818 9	167.34 0.19
-18 649.2	-20 028.3	298 203 8	-5 980 40
-12 669	-13 606	291 440 41	
-19 996	-21 475	308 700 13	-1 138 10
-18 859	-20 253	306 780 10	711.5 4.3
-19 570.1	-21 017.2	306 708 9	
-16 020	-17 210	313 090 90	4 790 90
-20 812.9	-22 352.0	317 101 9	-816.0 1.5
-19 996.9	-21 475.6	315 503 9	-6 120 100
-13 880	-14 900	308 600 100	
-15 560	-16 710	320 990 150	3 000 150
-18 555	-19 927	323 211 12	4 916 8
-23 470.9	-25 206.4	327 344 9	-5 929 11
-17 542	-18 839	320 632 14	
-18 258	-19 608	331 281 23	3 430 21
-21 688	-23 292	333 929 11	565 5
-22 253.3	-23 898.8	333 711 9	-6 610 40
-15 643	-16 800	326 318 41	
-15 700	-16 900	337 100 500	7 500 500
-23 196.2	-24 911.4	343 804 10	-1 512.7 3.4
-21 683.4	-23 286.9	341 509 10	1 321.5 4.5
-23 004.9	-24 706.0	342 048 10	-13 900 400
-9 100	-9 780	327 360 400	
-20 921	-22 468	349 896 15	2 490 10
-23 411.2	-25 142.4	351 604 11	-413 9
-22 998	-24 699	350 408 12	-5 950 40
-17 048	-18 309	343 675 42	
-22 573	-24 242	359 133 23	3 530 20
-26 102.8	-28 033.0	361 880 11	-5 900 600
-20 200	-21 700	355 200 600	
-23 848	-25 611	368 775 15	1 817 10
-25 664.9	-27 562.7	369 810 11	-2 220 10
-23 445	-25 179	366 807 15	
-22 330	-23 990	375 630 200	6 100 200
-28 433.6	-30 536.1	380 946 11	-3 648 5
-24 786	-26 618	376 515 12	-155 10
-24 631	-26 452	375 577 15	
-27 485.7	-29 518.2	388 365 12	252.0 1.9
-27 737.7	-29 788.8	387 835 11	-2 058.4 4.0
-25 679	-27 578	384 994 12	

TABLE 1 (Continued)

Z	N	N−Z	A	Symbol	Mass excess ($^{12}C = 0$) (keV)		Mass excess ($^{12}C = 0$) (μu)	
20	26	6	46	Ca	−43 136	± 10	−46 311	± 10
21	25	4	46	Sc	−41 754	5	−44 827	6
22	24	2	46	Ti	−44 119.2	3.5	−47 366.6	3.7
23	23	0	46	V	−36 820	400	−39 530	430
20	27	7	47	Ca	−42 370	21	−45 488	23
21	26	5	47	Sc	−44 335	8	−47 598	8
22	25	3	47	Ti	−44 935	7	−48 242	8
23	24	1	47	V	−42 023	12	−45 116	13
20	28	8	48	Ca	−44 226	14	−47 481	15
21	27	6	48	Sc	−44 494	10	−47 769	10
22	26	4	48	Ti	−48 483.6	3.4	−52 052.2	3.6
23	25	2	48	V	−44 467	6	−47 740	6
24	24	0	48	Cr	−43 070	200	−46 240	210
20	29	9	49	Ca	−41 298	15	−44 338	16
21	28	7	49	Sc	−46 490	90	−49 910	100
22	27	5	49	Ti	−48 559.1	3.3	−52 133.4	3.5
23	26	3	49	V	−47 948	6	−51 477	6
24	25	1	49	Cr	−45 388	11	−48 729	12
21	29	8	50	Sc	−45 100	500	−48 400	500
22	28	6	50	Ti	−51 425.7	4.5	−55 210.9	4.8
23	27	4	50	V	−49 213.0	3.7	−52 835.4	4.0
24	26	2	50	Cr	−50 250.6	4.2	−53 949.3	4.5
25	25	0	50	Mn	−42 600	500	−45 700	500
22	29	7	51	Ti	−49 716	20	−53 376	22
23	28	5	51	V	−52 181.3	3.9	−56 022.1	4.2
24	27	3	51	Cr	−51 428.7	4.1	−55 214.1	4.5
25	26	1	51	Mn	−48 250	50	−51 800	50
23	29	6	52	V	−51 414	7	−55 198	8
24	28	4	52	Cr	−55 407.9	3.3	−59 486.3	3.6
25	27	2	52	Mn	−50 705	9	−54 437	9
26	26	0	52	Fe	−48 322	17	−51 879	19
23	30	7	53	V	−52 750	50	−56 630	50
24	29	5	53	Cr	−55 280.0	3.4	−59 348.9	3.7
25	28	3	53	Mn	−54 683	9	−58 707	9
26	27	1	53	Fe	−50 691	40	−54 422	43
24	30	6	54	Cr	−56 930.3	4.5	−61 120.6	4.8
25	29	4	54	Mn	−55 551	6	−59 640	7
26	28	2	54	Fe	−56 239	6	−60 379	6
27	27	0	54	Co	−47 400	500	−50 900	500
24	31	7	55	Cr	−54 880	140	−58 920	150
25	30	5	55	Mn	−57 699.4	3.8	−61 946.4	4.1
26	29	3	55	Fe	−57 467.7	4.2	−61 697.6	4.6
27	28	1	55	Co	−54 008	11	−57 983	12
25	31	6	56	Mn	−56 898	5	−61 086	6
26	30	4	56	Fe	−60 607	5	−65 068	6
27	29	2	56	Co	−56 007	16	−60 130	17

Mass excess ($^{16}O = 0$) (keV)	Mass excess ($^{16}O = 0$) (μMU)	Binding energy (keV)	β^- decay energy (keV)
-29 519	-31 702	398 766 ± 15	-1 382 ± 11
-28 137	-30 217	396 601 12	2 365.2 4.4
-30 502.0	-32 757.5	398 184 11	-7 300 400
-23 200	-24 920	390 100 400	
-28 456	-30 561	406 071 24	1 965 20
-30 421	-32 671	407 253 13	600.0 2.0
-31 021	-33 315	407 070 13	-2 912 10
-28 109	-30 188	403 376 16	
-30 017	-32 236	415 998 18	268 17
-30 284	-32 524	415 483 15	3 990 9
-34 274.3	-36 808.7	418 691 11	-4 017 5
-30 257	-32 495	413 891 12	-1 400 200
-28 860	-30 990	411 710 200	
-26 793	-28 774	421 142 19	5 190 90
-31 980	-34 350	425 550 90	2 070 90
-34 053.8	-36 572.0	426 837 12	- 611 5
-33 442	-35 915	425 443 12	-2 560 10
-30 882	-33 166	422 101 16	
-30 300	-32 600	432 300 500	6 300 500
-36 624.4	-39 332.6	437 775 12	-2 213 6
-34 411.7	-36 956.3	434 780 12	1 038 6
-35 449.2	-38 070.6	435 035 12	-7 700 500
-27 700	-29 800	426 600 500	
-34 619	-37 179	444 137 24	2 465 20
-37 083.9	-39 826.2	445 820 12	- 752.6 1.5
-36 331.3	-39 017.9	444 284 12	-3 180 50
-33 150	-35 600	440 320 50	
-36 021	-38 684	453 124 14	3 994 8
-40 014.5	-42 973.5	456 335 12	-4 703 8
-35 312	-37 923	450 849 14	-2 383 15
-32 929	-35 363	447 684 20	
-37 060	-39 800	462 530 50	2 530 50
-39 590.5	-42 518.1	464 278 13	- 597 8
-38 993	-41 877	462 898 15	-3 992 41
-35 001	-37 590	458 124 42	
-40 944.8	-43 972.5	474 000 13	-1 379.0 4.7
-39 566	-42 492	471 838 14	688 8
-40 254	-43 231	471 744 13	-8 800 500
-31 500	-33 800	462 200 500	
-38 600	-41 450	480 020 140	2 820 140
-41 417.9	-44 480.7	482 058 13	- 231.7 2.2
-41 186.2	-44 231.8	481 044 13	-3 460 10
-37 726	-40 516	476 801 16	
-40 321	-43 302	489 328 14	3 709 7
-44 030	-47 286	492 254 14	-4 600 15
-39 430	-42 345	486 872 20	

TABLE 1 (Continued)

Z	N	N−Z	A	Symbol	Mass excess ($^{12}C = 0$) (keV)		(μu)	
25	32	7	57	Mn	-57 480	± 300	-61 710	± 320
26	31	5	57	Fe	-60 177	6	-64 606	6
27	30	3	57	Co	-59 607	31	-63 994	33
28	29	1	57	Ni	-56 372	34	-60 521	37
26	32	6	58	Fe	-62 153	7	-66 728	7
27	31	4	58	Co	-59 841	14	-64 246	15
28	30	2	58	Ni	-60 225	6	-64 658	6
29	29	0	58	Cu	-51 710	70	-55 510	80
26	33	7	59	Fe	-60 667	6	-65 133	7
27	32	5	59	Co	-62 230.4	4.3	-66 810.9	4.6
28	31	3	59	Ni	-61 154.6	4.8	-65 656	5
29	30	1	59	Cu	-56 356	21	-60 504	22
27	33	6	60	Co	-61 656	5	-66 194	6
28	32	4	60	Ni	-64 472	5	-69 217	6
29	31	2	60	Cu	-58 325	40	-62 618	43
27	34	7	61	Co	-62 934	40	-67 566	43
28	33	5	61	Ni	-64 224	8	-68 951	9
29	32	3	61	Cu	-61 993	10	-66 556	10
30	31	1	61	Zn	-56 190	300	-60 330	320
27	35	8	62	Co	-61 522	40	-66 051	43
28	34	6	62	Ni	-66 742	6	-71 655	7
29	33	4	62	Cu	-62 812	12	-67 436	13
30	32	2	62	Zn	-61 122	14	-65 621	16
28	35	7	63	Ni	-65 512	5	-70 334	6
29	34	5	63	Cu	-65 579	5	-70 406	6
30	33	3	63	Zn	-62 213	7	-66 792	7
28	36	8	64	Ni	-67 102	6	-72 041	6
29	35	6	64	Cu	-65 424	5	-70 239	6
30	34	4	64	Zn	-65 997	5	-70 855	5
31	33	2	64	Ga	-58 980	150	-63 320	160
28	37	9	65	Ni	-65 160	200	-69 960	210
29	36	7	65	Cu	-67 263	6	-72 214	6
30	35	5	65	Zn	-65 915	6	-70 766	6
31	34	3	65	Ga	-62 656	16	-67 267	17
28	38	10	66	Ni	-66 052	31	-70 914	33
29	37	8	66	Cu	-66 252	9	-71 129	9
30	36	6	66	Zn	-68 882	9	-73 952	10
31	35	4	66	Ga	-63 712	31	-68 401	34
29	38	9	67	Cu	-67 284	13	-72 237	14
30	37	7	67	Zn	-67 856	10	-72 851	11
31	36	5	67	Ga	-66 858	11	-71 779	12
32	35	3	67	Ge	-62 460	100	-67 060	110
30	38	8	68	Zn	-69 984	9	-75 135	9
31	37	6	68	Ga	-67 066	10	-72 003	11
32	36	4	68	Ge	-66 400	600	-71 300	600

Mass excess ($^{16}O = 0$)		Binding energy (keV)	β^- decay energy (keV)
(keV)	(μMU)		
-40 600	-43 610	497 980 ± 300	2 700 ± 300
-43 304	-46 506	499 896 14	- 570 30
-42 734	-45 894	498 543 33	-3 235 15
-39 499	-42 419	494 525 37	
-44 984	-48 310	509 943 15	-2 312 12
-42 672	-45 827	506 849 19	384 14
-43 056	-46 239	506 450 14	-8 520 70
-34 540	-37 090	497 150 70	
-43 202	-46 396	516 529 15	1 563 5
-44 764.8	-48 075.0	517 309 14	-1 075.8 2.2
-43 689.0	-46 920	515 451 14	-4 798 20
-38 891	-41 767	509 870 24	
-43 894	-47 140	524 806 15	2 816.1 2.1
-46 710	-50 164	526 839 14	-6 147 40
-40 563	-43 562	519 909 42	
-44 876	-48 194	534 155 43	1 290 40
-46 166	-49 580	534 662 16	-2 231 5
-43 935	-47 184	531 649 16	-5 800 300
-38 130	-40 950	525 070 300	
-43 169	-46 361	540 815 43	5 220 40
-48 389	-51 967	545 252 15	-3 930 10
-44 459	-47 746	540 540 18	-1 690 8
-42 769	-45 931	538 067 20	
-46 863	-50 328	552 094 15	66.76 0.47
-46 929	-50 400	551 378 15	-3 366.4 4.0
-43 563	-46 784	547 229 15	
-48 156	-51 717	561 755 16	-1 678.0 2.0
-46 478	-49 915	559 294 15	573.2 1.5
-47 051	-50 531	559 085 15	-7 020 150
-40 030	-42 990	551 280 150	
-45 920	-49 320	567 890 200	2 100 200
-48 021	-51 572	569 204 16	-1 348.3 0.8
-46 673	-50 124	567 074 16	-3 259 15
-43 414	-46 624	563 032 21	
-46 514	-49 954	576 848 35	200 30
-46 714	-50 169	576 265 18	2 630 8
-49 344	-52 993	578 112 18	-5 170 30
-44 174	-47 441	572 160 35	
-47 451	-50 959	585 369 20	572 8
-48 023	-51 574	585 158 18	- 998.4 4.0
-47 024	-50 501	583 377 19	-4 400 100
-42 620	-45 780	578 190 100	
-49 854	-53 540	595 357 18	-2 917 5
-46 936	-50 407	591 657 18	- 700 600
-46 200	-49 700	590 200 600	

TABLE 1 (Continued)

Z	N	N−Z	A	Symbol	Mass excess ($^{12}C = 0$) (keV)	(μu)
30	39	9	69	Zn	−68 318 ± 27	−73 347 ± 29
31	38	7	69	Ga	−69 223 26	−74 318 28
32	37	5	69	Ge	−66 986 28	−71 917 30
33	36	3	69	As	−63 090 300	−67 730 320
30	40	10	70	Zn	−69 534 15	−74 652 16
31	39	8	70	Ga	−68 882 16	−73 952 17
32	38	6	70	Ge	−70 532 19	−75 723 20
33	37	4	70	As	−63 990 100	−68 700 110
30	41	11	71	Zn	−67 100 210	−72 030 220
31	40	9	71	Ga	−70 005 47	−75 160 50
32	39	7	71	Ge	−69 772 47	−74 910 50
33	38	5	71	As	−67 763 47	−72 750 50
34	37	3	71	Se	−63 360 300	−68 030 330
30	42	12	72	Zn	−67 300 210	−72 260 220
31	41	10	72	Ga	−68 902 48	−73 970 50
32	40	8	72	Ge	−72 890 48	−78 260 50
33	39	6	72	As	−68 530 60	−73 570 60
31	42	11	73	Ga	−69 840 80	−74 980 80
32	41	9	73	Ge	−71 390 70	−76 640 70
33	40	7	73	As	−71 020 70	−76 240 80
34	39	5	73	Se	−68 270 70	−73 290 80
31	43	12	74	Ga	−67 790 210	−72 780 220
32	42	10	74	Ge	−73 440 50	−78 850 60
33	41	8	74	As	−70 880 50	−76 090 50
34	40	6	74	Se	−72 230 50	−77 550 60
32	43	11	75	Ge	−71 870 50	−77 160 60
33	42	9	75	As	−73 045 48	−78 420 50
34	41	7	75	Se	−72 179 48	−77 490 50
35	40	5	75	Br	−69 460 50	−74 570 60
32	44	12	76	Ge	−73 250 90	−78 640 90
33	43	10	76	As	−72 264 45	−77 583 48
34	42	8	76	Se	−75 233 45	−80 771 48
35	41	6	76	Br	−70 643 46	−75 843 49
32	45	13	77	Ge	−71 140 70	−76 380 70
33	44	11	77	As	−73 893 45	−79 332 49
34	43	9	77	Se	−74 577 44	−80 066 48
35	42	7	77	Br	−73 212 44	−78 601 48
36	41	5	77	Kr	−70 332 49	−75 510 50
32	46	14	78	Ge	−71 990 150	−77 290 160
33	45	12	78	As	−72 890 110	−78 250 120
34	44	10	78	Se	−76 986 44	−82 652 48
35	43	8	78	Br	−73 520 80	−78 930 80
36	42	6	78	Kr	−74 172.2 4.9	−79 632 5
33	46	13	79	As	−73 590 100	−79 010 110
34	45	11	79	Se	−75 893 19	−81 479 20
35	44	9	79	Br	−76 054 18	−81 652 19
36	43	7	79	Kr	−74 432 19	−79 911 20

Mass excess ($^{16}O = 0$)		Binding energy (keV)	β^- decay energy (keV)
(keV)	(μMU)		
-47 892	-51 434	601 762 ± 31	905 ± 6
-48 797	-52 406	601 885 30	-2 237 12
-46 560	-50 003	598 865 32	-3 900 300
-42 660	-45 810	594 180 300	
-48 812	-52 422	611 050 22	- 652 5
-48 160	-51 721	609 615 23	1 650 10
-49 810	-53 493	610 482 24	-6 540 100
-43 270	-46 470	603 160 100	
-46 080	-49 480	616 680 210	2 910 200
-48 988	-52 610	618 810 50	- 233 3
-48 754	-52 360	617 790 50	-2 009 7
-46 745	-50 200	615 000 50	-4 400 300
-42 350	-45 480	609 820 300	
-45 990	-49 390	624 960 210	1 600 200
-47 588	-51 110	625 770 50	3 989 10
-51 576	-55 390	628 980 50	-4 360 30
-47 220	-50 710	623 840 60	
-48 230	-51 790	634 780 80	1 552 40
-49 780	-53 460	635 550 70	- 371 30
-49 410	-53 060	634 400 80	-2 750 10
-46 660	-50 110	630 870 80	
-45 880	-49 280	640 810 210	5 600 50
-51 530	-55 340	645 670 50	-2 564 10
-48 970	-52 590	642 330 50	1 360 10
-50 330	-54 050	642 900 50	
-49 660	-53 340	652 170 50	1 178 20
-50 843	-54 600	652 570 50	- 865.4 2.0
-49 977	-53 670	650 920 50	-2 722 20
-47 260	-50 750	647 420 50	
-50 750	-54 500	661 620 90	- 980 90
-49 766	-53 446	659 857 49	2 969 10
-52 735	-56 635	662 044 48	-4 590 10
-48 145	-51 705	656 674 49	
-48 350	-51 920	667 590 70	2 750 50
-51 099	-54 878	669 560 49	684 9
-51 783	-55 612	669 459 48	-1 364 4
-50 418	-54 146	667 314 48	-2 880 20
-47 538	-51 050	663 650 50	
-48 900	-52 510	676 510 150	900 100
-49 800	-53 480	676 620 110	4 100 100
-53 896	-57 881	679 939 48	-3 470 70
-50 430	-54 160	675 690 80	650 80
-51 082.3	-54 860	675 560 19	
-50 210	-53 920	685 400 100	2 300 100
-52 507	-56 390	686 917 27	161 5
-52 668	-56 562	686 295 26	-1 621 5
-51 046	-54 821	683 892 26	

TABLE 1 (Continued)

Z	N	N−Z	A	Symbol	Mass excess ($^{12}C = 0$) (keV)		Mass excess ($^{12}C = 0$) (μu)	
33	47	14	80	As	−71 760	± 200	−77 050	± 220
34	46	12	80	Se	−77 764	16	−83 488	17
35	45	10	80	Br	−75 875	15	−81 459	16
36	44	8	80	Kr	−77 880	12	−83 612	13
37	43	6	80	Rb	−72 800	500	−78 100	500
34	47	13	81	Se	−76 510	60	−82 140	60
35	46	11	81	Br	−77 920	35	−83 656	37
36	45	9	81	Kr	−77 680	90	−83 390	100
37	44	7	81	Rb	−75 440	100	−80 990	100
34	48	14	82	Se	−77 630	70	−83 340	70
35	47	12	82	Br	−77 494	7	−83 198	8
36	46	10	82	Kr	−80 586	7	−86 517	8
37	45	8	82	Rb	−76 416	31	−82 041	33
34	49	15	83	Se	−75 530	90	−81 090	100
35	48	13	83	Br	−78 982	21	−84 795	23
36	47	11	83	Kr	−79 982	7	−85 869	8
35	49	14	84	Br	−77 730	50	−83 450	50
36	48	12	84	Kr	−82 428.6	4.9	−88 496	5
37	47	10	84	Rb	−79 776	7	−85 648	7
38	46	8	84	Sr	−80 685	11	−86 624	11
35	50	15	85	Br	−78 760	110	−84 560	120
36	49	13	85	Kr	−81 560	50	−87 570	60
37	48	11	85	Rb	−82 240	50	−88 290	60
38	47	9	85	Sr	−81 130	60	−87 100	60
36	50	14	86	Kr	−83 255	7	−89 383	8
37	49	12	86	Rb	−82 750	80	−88 840	90
38	48	10	86	Sr	−84 520	80	−90 740	80
39	47	8	86	Y	−78 510	90	−84 290	100
35	52	17	87	Br	−72 690	400	−78 040	430
36	51	15	87	Kr	−80 689	49	−86 630	50
37	50	13	87	Rb	−84 590	80	−90 820	80
38	49	11	87	Sr	−84 870	80	−91 110	80
39	48	9	87	Y	−83 180	210	−89 300	230
40	47	7	87	Zr	−79 670	220	−85 530	230
36	52	16	88	Kr	−79 920	230	−85 800	240
37	51	14	88	Rb	−82 720	100	−88 810	110
38	50	12	88	Sr	−87 920	80	−94 390	90
39	49	10	88	Y	−84 470	80	−90 690	90
37	52	15	89	Rb	−82 700	100	−88 780	110
38	51	13	89	Sr	−86 620	90	−92 990	90
39	50	11	89	Y	−88 090	90	−94 570	90
40	49	9	89	Zr	−85 240	90	−91 520	90
41	48	7	89	Nb	−81 360	130	−87 350	140
38	52	14	90	Sr	−86 330	90	−92 680	90
39	51	12	90	Y	−86 860	90	−93 260	90
40	50	10	90	Zr	−89 120	90	−95 680	90
41	49	8	90	Nb	−83 000	90	−89 110	100
42	48	6	90	Mo	−80 460	140	−86 390	150

Mass excess ($^{16}O = 0$)		Binding energy (keV)	β^- decay energy (keV)
(keV)	(μMU)		
-48 080	-51 640	691 650 ± 200	6 000 ± 200
-54 082	-58 081	696 859 25	-1 889 6
-52 193	-56 052	694 188 24	2 005 10
-54 198	-58 206	695 410 22	-5 100 500
-49 100	-52 700	689 500 500	
-52 530	-56 420	703 680 60	1 410 49
-53 942	-57 931	704 305 40	- 250 90
-53 700	-57 670	703 280 90	-2 240 30
-51 460	-55 260	700 260 100	
-53 350	-57 300	712 860 70	- 130 70
-53 220	-57 155	711 953 22	3 092 2
-56 312	-60 476	714 259 21	-4 170 30
-52 142	-55 998	709 309 37	
-50 960	-54 730	718 850 90	3 450 90
-54 412	-58 436	721 512 30	1 000 20
-55 411	-59 509	721 726 22	
-52 860	-56 770	728 330 50	4 700 50
-57 562.5	-61 819	732 244 21	-2 652 5
-54 910	-58 971	728 809 22	909 8
-55 819	-59 947	728 936 23	
-53 600	-57 570	737 440 110	2 800 100
-56 400	-60 570	739 450 60	675 7
-57 080	-61 300	739 340 60	-1 107 30
-55 970	-60 110	737 450 60	
-57 796	-62 070	749 213 23	- 510 80
-57 290	-61 520	747 920 80	1 772 5
-59 060	-63 430	748 910 80	-6 010 50
-53 050	-56 970	742 120 100	
-46 930	-50 410	747 510 400	8 000 400
-54 935	-59 000	754 720 50	3 900 90
-58 840	-63 190	757 840 80	272.3 2.4
-59 110	-63 480	757 330 80	-1 690 200
-57 420	-61 670	754 860 220	-3 510 20
-53 910	-57 900	750 570 220	
-53 870	-57 850	762 030 230	2 800 200
-56 670	-60 860	764 040 110	5 200 70
-61 870	-66 440	768 450 90	-3 447 10
-53 420	-62 740	764 220 90	
-56 350	-60 520	772 090 100	3 920 50
-60 270	-64 730	775 220 90	1 469 10
-61 740	-66 310	775 910 90	-2 842 7
-58 900	-63 250	772 290 90	-3 880 100
-55 020	-59 090	767 630 130	
-59 680	-64 100	783 010 90	535 7
-60 220	-64 670	782 760 90	2 259 10
-62 480	-67 100	784 230 90	-6 117 30
-56 360	-60 530	777 340 100	-2 540 100
-53 820	-57 800	774 020 140	

TABLE 1 (Continued)

Z	N	N−Z	A	Symbol	Mass excess ($^{12}C = 0$) (keV)	(μu)
38	53	15	91	Sr	−84 040 ± 100	−90 220 ± 100
39	52	13	91	Y	−86 710 100	−93 090 100
40	51	11	91	Zr	−88 260 100	−94 750 100
41	50	9	91	Nb	−86 660 140	−93 040 150
42	49	7	91	Mo	−82 220 140	−88 270 150
43	48	5	91	Tc	−79 680 170	−85 540 180
38	54	16	92	Sr	−83 350 120	−89 480 130
39	53	14	92	Y	−85 270 110	−91 540 120
40	52	12	92	Zr	−88 870 100	−95 410 110
41	51	10	92	Nb	−86 790 110	−93 180 120
42	50	8	92	Mo	−87 280 120	−93 710 130
43	49	6	92	Tc	−80 900 600	−86 800 700
39	54	15	93	Y	−84 590 100	−90 810 110
40	53	13	93	Zr	−87 480 100	−93 920 110
41	52	11	93	Nb	−87 540 100	−93 980 110
42	51	9	93	Mo	−87 060 110	−93 470 120
43	50	7	93	Tc	−83 900 110	−90 070 120
39	55	16	94	Y	−82 430 390	−88 490 420
40	54	14	94	Zr	−87 430 330	−93 860 360
41	53	12	94	Nb	−86 660 110	−93 040 110
42	52	10	94	Mo	−88 730 120	−95 260 130
43	51	8	94	Tc	−84 410 120	−90 620 130
40	55	15	95	Zr	−85 770 330	−92 080 360
41	54	13	95	Nb	−86 890 330	−93 280 360
42	53	11	95	Mo	−87 820 330	−94 280 360
43	52	9	95	Tc	−86 160 330	−92 500 360
44	51	7	95	Ru	−83 960 350	−90 140 370
40	56	16	96	Zr	−85 500 800	−91 800 800
41	55	14	96	Nb	−85 780 330	−92 090 360
42	54	12	96	Mo	−88 900 330	−95 450 360
43	53	10	96	Tc	−85 930 450	−92 250 480
44	52	8	96	Ru	−86 100 600	−92 400 700
40	57	17	97	Zr	−83 200 370	−89 320 400
41	56	15	97	Nb	−85 860 370	−92 180 400
42	55	13	97	Mo	−87 790 370	−94 250 400
42	56	14	98	Mo	−88 010 380	−94 490 410
43	55	12	98	Tc	−86 300 800	−92 700 800
44	54	10	98	Ru	−88 000 700	−94 500 800
45	53	8	98	Rh	−83 800 800	−90 000 800
42	57	15	99	Mo	−85 810 460	−92 130 490
43	56	13	99	Tc	−87 190 460	−93 610 490
44	55	11	99	Ru	−87 480 460	−93 920 490
45	54	9	99	Rh	−85 380 460	−91 670 490
46	53	7	99	Pd	−81 600 500	−87 600 500
42	58	16	100	Mo	−86 090 450	−92 430 490
43	59	16	102	Tc	−85 580 350	−91 880 380
44	58	14	102	Ru	−89 680 180	−96 280 200
45	57	12	102	Rh	−87 410 180	−93 850 200
46	56	10	102	Pd	−88 540 180	−95 060 190
44	59	15	103	Ru	−87 920 180	−94 390 200
45	58	13	103	Rh	−88 670 180	−95 200 200
46	57	11	103	Pd	−88 110 190	−94 590 200

Mass excess ($^{16}O = 0$)		Binding energy (keV)	β^- decay energy (keV)
(keV)	(μMU)		
-57 100	-61 320	788 790 ± 100	2 670 ± 10
-59 770	-64 190	790 680 100	1 549 4
-61 320	-65 850	791 440 100	-1 590 110
-59 720	-64 140	789 060 150	-4 443 40
-55 280	-59 370	783 840 140	-2 540 100
-52 740	-56 640	780 520 170	
-56 110	-60 260	796 170 120	1 920 40
-58 030	-62 320	797 310 110	3 600 50
-61 630	-66 190	800 120 100	-2 070 50
-59 560	-63 960	797 270 110	490 70
-60 050	-64 490	796 970 120	-6 400 600
-53 600	-57 600	789 800 600	
-57 060	-61 280	804 700 110	2 890 20
-59 950	-64 380	806 800 100	63.1 2.0
-60 010	-64 450	806 080 100	- 482 40
-59 530	-63 930	804 820 110	-3 160 30
-56 370	-60 540	800 880 120	
-54 600	-58 640	810 610 390	5 000 200
-59 600	-64 010	814 820 330	- 770 330
-58 830	-63 180	813 270 110	2 070 50
-60 900	-65 400	814 560 120	-4 320 30
-56 580	-60 760	809 460 120	
-57 640	-61 910	821 240 330	1 122 5
-58 770	-63 110	821 580 330	927.0 4.0
-59 690	-64 110	821 720 330	-1 656 20
-58 040	-62 330	819 290 330	-2 200 100
-55 840	-59 970	816 300 350	
-57 100	-61 300	829 100 800	300 800
-57 360	-61 600	828 540 330	3 130 30
-60 490	-64 960	830 880 330	-2 980 300
-57 510	-61 760	827 120 450	200 800
-57 700	-61 900	826 500 600	
-54 480	-58 510	834 810 370	2 660 30
-57 140	-61 370	836 690 370	1 932 7
-59 070	-63 440	837 840 370	
-59 000	-63 360	846 130 380	-1 700 800
-57 300	-61 600	843 700 800	1 700 200
-59 000	-63 400	844 600 700	-4 200 300
-54 800	-58 900	839 600 800	
-56 510	-60 680	852 000 460	1 380 10
-57 880	-62 170	852 600 460	293.0 2.0
-58 180	-62 480	852 110 460	-2 100 20
-56 080	-60 220	849 230 460	-3 800 200
-52 300	-56 100	844 600 500	
-56 490	-60 660	860 350 450	
-55 390	-59 480	875 210 350	4 100 300
-59 490	-63 890	878 530 180	-2 270 20
-57 220	-61 450	875 470 180	1 131 20
-58 350	-62 660	875 820 180	
-57 430	-61 680	884 830 190	750 10
-58 180	-62 480	884 800 190	- 560 30
-57 620	-61 880	883 460 190	

TABLE 1 (Continued)

Z	N	N−Z	A	Symbol	Mass excess ($^{12}C = 0$) (keV)		(μu)	
44	60	16	104	Ru	−88 000	± 370	−94 470	± 400
45	59	14	104	Rh	−87 390	180	−93 820	200
46	58	12	104	Pd	−89 830	190	−96 440	200
47	57	10	104	Ag	−85 550	190	−91 850	200
44	61	17	105	Ru	−86 350	250	−92 710	270
45	60	15	105	Rh	−88 260	250	−94 750	270
46	59	13	105	Pd	−88 820	250	−95 360	270
47	58	11	105	Ag	−86 800	500	−93 200	600
44	62	18	106	Ru	−86 600	110	−92 970	120
45	61	16	106	Rh	−86 630	110	−93 010	120
46	60	14	106	Pd	−90 160	110	−96 800	120
47	59	12	106	Ag	−87 190	110	−93 610	120
48	58	10	106	Cd	−87 600	350	−94 050	370
45	62	17	107	Rh	−86 980	120	−93 380	120
46	61	15	107	Pd	−88 480	110	−94 990	110
47	60	13	107	Ag	−88 510	110	−95 030	110
48	59	11	107	Cd	−87 070	110	−93 480	110
46	62	16	108	Pd	−89 490	110	−96 080	120
47	61	14	108	Ag	−87 650	100	−94 110	110
48	60	12	108	Cd	−89 420	110	−96 000	120
49	59	10	108	In	−84 320	150	−90 530	160
46	63	17	109	Pd	−87 650	110	−94 100	110
47	62	15	109	Ag	−88 760	110	−95 300	110
48	61	13	109	Cd	−88 610	110	−95 130	110
49	60	11	109	In	−86 590	110	−92 960	110
46	64	18	110	Pd	−88 950	300	−95 500	320
47	63	16	110	Ag	−87 510	110	−93 950	110
48	62	14	110	Cd	−90 380	110	−97 030	110
49	61	12	110	In	−86 420	110	−92 780	120
46	65	19	111	Pd	−86 030	180	−92 360	190
47	64	17	111	Ag	−88 230	180	−94 720	190
48	63	15	111	Cd	−89 280	170	−95 850	190
49	62	13	111	In	−88 040	190	−94 520	210
50	61	11	111	Sn	−85 520	190	−91 820	210
46	66	20	112	Pd	−86 160	110	−92 510	120
47	65	18	112	Ag	−86 460	110	−92 830	110
48	64	16	112	Cd	−90 500	100	−97 160	110
49	63	14	112	In	−87 890	100	−94 360	110
50	62	12	112	Sn	−88 540	110	−95 060	110
47	66	19	113	Ag	−86 850	100	−93 240	110
48	65	17	113	Cd	−88 850	90	−95 390	100
49	64	15	113	In	−89 160	90	−95 720	100
50	63	13	113	Sn	−88 470	90	−94 990	100
47	67	20	114	Ag	−85 220	410	−91 500	440
48	66	18	114	Cd	−89 820	90	−96 430	100
49	65	16	114	In	−88 400	90	−94 910	100
50	64	14	114	Sn	−90 390	100	−97 040	100
47	68	21	115	Ag	−85 010	320	−91 260	340
48	67	19	115	Cd	−87 910	100	−94 380	100
49	66	17	115	In	−89 360	100	−95 930	100
50	65	15	115	Sn	−89 860	100	−96 470	110

Mass excess ($^{16}O = 0$)		Binding energy (keV)	β^- decay energy (keV)
(keV)	(μMU)		
-57 210	-61 440	892 980 ± 370	- 610 ± 410
-56 600	-60 790	891 590 190	2 439 30
-59 040	-63 410	893 240 190	-4 280 10
-54 760	-58 810	888 180 190	
-55 270	-59 360	899 410 250	1 905 15
-57 180	-61 400	900 530 250	565 3
-57 740	-62 010	900 310 250	-2 000 600
-55 700	-59 800	897 500 500	
-55 220	-59 300	907 720 110	38 1
-55 260	-59 340	906 980 110	3 530 10
-58 790	-63 130	909 720 110	-2 970 10
-55 820	-59 940	905 970 110	410 360
-56 230	-60 380	905 600 350	
-55 300	-59 390	915 390 120	1 500 50
-56 800	-61 000	916 110 110	35 1
-56 840	-61 040	915 360 110	-1 440 10
-55 400	-59 500	913 140 110	
-57 520	-61 770	925 190 120	-1 837 49
-55 680	-59 800	922 570 110	1 770 60
-57 450	-61 700	923 560 120	-5 100 100
-52 350	-56 220	917 680 150	
-55 380	-59 480	931 430 110	1 113 5
-56 500	-60 670	931 750 110	- 158 4
-56 340	-60 510	930 820 110	-2 020 10
-54 320	-58 340	928 010 110	
-56 390	-60 560	940 800 300	-1 450 310
-54 950	-59 010	938 570 110	2 874 15
-57 820	-62 090	940 660 110	-3 960 40
-53 860	-57 840	935 920 120	
-53 170	-57 100	945 950 180	2 200 40
-55 370	-59 460	947 360 180	1 050 10
-56 420	-60 590	947 630 180	-1 240 210
-55 180	-59 260	945 610 190	-2 520 30
-52 660	-56 560	942 310 200	
-53 010	-56 930	954 150 110	300 20
-53 310	-57 250	953 670 110	4 040 30
-57 350	-61 590	956 920 110	-2 616 19
-54 730	-58 780	953 530 110	656 6
-55 390	-59 480	953 400 110	
-53 400	-57 350	962 130 110	2 000 40
-55 400	-59 490	963 340 100	310 10
-55 710	-59 830	962 870 100	- 684 4
-55 020	-59 090	961 410 100	
-51 480	-55 280	968 570 410	4 600 400
-56 080	-60 220	972 390 100	-1 420 20
-54 660	-58 700	970 180 100	1 985 4
-56 640	-60 830	971 390 100	
-50 960	-54 730	976 430 320	2 900 300
-53 860	-57 850	978 540 100	1 451 10
-55 310	-59 400	979 210 100	500 20
-55 810	-59 940	978 930 100	

TABLE 1 (Continued)

Z	N	N−Z	A	Symbol	Mass excess ($^{12}C = 0$) (keV)		Mass excess ($^{12}C = 0$) (μu)	
48	68	20	116	Cd	−88 480 ±	300	−94 990 ±	320
49	67	18	116	In	−87 890	170	−94 360	190
50	66	16	116	Sn	−91 180	180	−97 890	190
51	65	14	116	Sb	−86 480	350	−92 840	370
48	69	21	117	Cd	−86 280	350	−92 640	370
49	68	19	117	In	−88 820	170	−95 360	190
50	67	17	117	Sn	−90 290	170	−96 940	190
51	66	15	117	Sb	−88 470	180	−94 990	190
50	68	18	118	Sn	−91 470	180	−98 210	190
50	69	19	119	Sn	−89 990	180	−96 610	200
51	68	17	119	Sb	−89 410	190	−95 990	200
50	70	20	120	Sn	−91 160	130	−97 870	140
51	69	18	120	Sb	−88 430	130	−94 940	140
52	68	16	120	Te	−88 940	370	−95 490	400
53	67	14	120	I	−83 940	420	−90 120	450
50	71	21	121	Sn	−89 260	130	−95 830	140
51	70	19	121	Sb	−89 650	130	−96 250	140
50	72	22	122	Sn	−89 970	130	−96 590	140
51	71	20	122	Sb	−88 380	120	−94 880	130
52	70	18	122	Te	−90 350	120	−97 000	130
53	69	16	122	I	−86 210	130	−92 550	140
50	73	23	123	Sn	−87 860	130	−94 330	140
51	72	21	123	Sb	−89 280	130	−95 850	140
52	71	19	123	Te	−89 250	120	−95 820	130
50	74	24	124	Sn	−88 260	120	−94 760	130
51	73	22	124	Sb	−87 660	120	−94 110	130
52	72	20	124	Te	−90 580	120	−97 240	130
53	71	18	124	I	−87 390	130	−93 820	130
54	70	16	124	Xe	−87 440	150	−93 880	160
50	75	25	125	Sn	−85 930	120	−92 250	130
51	74	23	125	Sb	−88 270	120	−94 770	130
52	73	21	125	Te	−89 030	120	−95 580	130
53	72	19	125	I	−88 880	120	−95 420	130
52	74	22	126	Te	−90 125	34	−96 758	37
53	73	20	126	I	−88 010	29	−94 488	31
54	72	18	126	Xe	−89 261	29	−95 831	32
55	71	16	126	Cs	−84 460	400	−90 680	430
51	76	25	127	Sb	−86 800	50	−93 190	60
52	75	23	127	Te	−88 401	23	−94 908	25
53	74	21	127	I	−89 090	22	−95 648	23
54	73	19	127	Xe	−88 390	350	−94 900	380
55	72	17	127	Cs	−86 310	350	−92 660	380
52	76	24	128	Te	−88 760	130	−95 290	140
53	75	22	128	I	−87 725	12	−94 182	13
54	74	20	128	Xe	−89 849	9	−96 462	10
55	73	18	128	Cs	−85 850	100	−92 170	110

Mass excess ($^{16}O = 0$)		Binding energy (keV)	β^- decay energy (keV)
(keV)	(μMU)		
-54 140	-58 140	987 180 ± 300	- 580 ± 340
-53 550	-57 510	985 820 180	3 290 60
-56 840	-61 040	988 320 180	-4 700 300
-52 140	-56 000	982 840 350	
-51 650	-55 470	993 070 350	2 540 300
-54 190	-58 200	994 820 180	1 470 10
-55 660	-59 770	995 510 180	-1 820 30
-53 840	-57 820	992 910 180	
-56 540	-60 720	1 004 760 180	
-54 760	-58 810	1 011 340 190	- 579 20
-54 180	-58 190	1 009 990 190	
-55 630	-59 750	1 020 580 140	-2 723 20
-52 910	-56 820	1 017 080 140	510 390
-53 420	-57 370	1 016 800 370	-5 000 200
-48 420	-52 000	1 011 020 420	
-53 450	-57 400	1 026 760 130	383 5
-53 830	-57 810	1 026 360 130	
-53 850	-57 830	1 035 540 130	-1 590 30
-52 260	-56 130	1 033 160 130	1 971.0 4.0
-54 230	-58 240	1 034 350 130	-4 140 40
-50 090	-53 800	1 029 430 130	
-51 450	-55 250	1 041 500 130	1 420 10
-52 870	-56 780	1 042 140 130	-30 130
-52 840	-56 740	1 041 320 120	
-51 550	-55 370	1 049 970 120	- 600 170
-50 950	-54 720	1 048 590 120	2 916 3
-53 870	-57 850	1 050 720 120	-3 190 40
-50 680	-54 430	1 046 750 130	60 190
-50 740	-54 490	1 046 020 150	
-48 930	-52 540	1 055 710 120	2 340 10
-51 270	-55 060	1 057 270 120	757 6
-52 020	-55 870	1 057 240 120	- 150 30
-51 870	-55 710	1 056 320 130	
-52 825	-56 732	1 066 413 47	-2 115 20
-50 710	-54 460	1 063 516 43	1 251 5
-51 961	-55 804	1 063 984 43	-4 800 400
-47 160	-50 650	1 058 410 400	
-49 210	-52 840	1 071 950 60	1 600 50
-50 805	-54 562	1 072 766 40	689 7
-51 495	-55 303	1 072 668 39	- 700 350
-50 790	-54 550	1 071 190 350	-2 085 10
-48 710	-52 310	1 068 320 350	
-50 870	-54 630	1 081 190 130	-1 030 130
-49 834	-53 519	1 079 374 35	2 124 8
-51 958	-55 800	1 080 715 33	-4 000 100
-47 960	-51 500	1 075 940 110	

TABLE 1 (Continued)

Z	N	N−Z	A	Symbol	Mass excess ($^{12}C = 0$) (keV)	(μu)
52	77	25	129	Te	−87 019 ± 11	−93 424 ± 12
53	76	23	129	I	−88 499 10	−95 013 11
54	75	21	129	Xe	−88 688 9	−95 216 10
52	78	26	130	Te	−86 910 130	−93 300 140
53	77	24	130	I	−86 918 31	−93 315 33
54	76	22	130	Xe	−89 875 9	−96 490 9
55	75	20	130	Cs	−86 884 22	−93 279 23
56	74	18	130	Ba	−87 326 22	−93 753 24
52	79	27	131	Te	−85 156 21	−91 424 23
53	78	25	131	I	−87 436 7	−93 872 8
54	77	23	131	Xe	−88 406 7	−94 913 7
55	76	21	131	Cs	−88 051 9	−94 532 10
52	80	28	132	Te	−85 192 43	−91 463 46
53	79	26	132	I	−85 697 41	−92 005 44
54	78	24	132	Xe	−89 267 7	−95 838 8
55	77	22	132	Cs	−87 450 140	−93 890 150
56	76	20	132	Ba	−88 370 300	−94 880 320
53	80	27	133	I	−86 080 150	−92 410 160
54	79	25	133	Xe	−87 980 140	−94 450 150
55	78	23	133	Cs	−88 400 140	−94 910 150
56	77	21	133	Ba	−87 910 140	−94 390 150
54	80	26	134	Xe	−88 116 7	−94 602 8
55	79	24	134	Cs	−87 070 140	−93 480 150
56	78	22	134	Ba	−89 130 140	−95 690 150
57	77	20	134	La	−85 430 240	−91 710 260
54	81	27	135	Xe	−86 580 250	−92 960 270
55	80	25	135	Cs	−87 740 250	−94 200 270
56	79	23	135	Ba	−87 950 250	−94 430 260
53	83	30	136	I	−79 420 100	−85 260 110
54	82	28	136	Xe	−86 418 10	−92 779 10
55	81	26	136	Cs	−86 510 130	−92 870 140
56	80	24	136	Ba	−89 090 130	−95 640 140
57	79	22	136	La	−86 090 240	−92 420 250
58	78	20	136	Ce	−86 550 490	−92 900 500
55	82	27	137	Cs	−86 790 120	−93 180 130
56	81	25	137	Ba	−87 960 120	−94 440 130
55	83	28	138	Cs	−83 640 90	−89 800 100
56	82	26	138	Ba	−88 470 70	−94 990 80
57	81	24	138	La	−86 800 80	−93 190 80
58	80	22	138	Ce	−87 810 80	−94 280 80
55	84	29	139	Cs	−80 820 210	−86 770 230
56	83	27	139	Ba	−85 120 70	−91 390 80
57	82	25	139	La	−87 500 70	−93 940 80
58	81	23	139	Ce	−87 230 70	−93 650 80
59	80	21	139	Pr	−85 230 120	−91 510 130

Mass excess ($^{16}O = 0$)		Binding energy (keV)	β^- decay energy (keV)
(keV)	(μMU)		
-48 831	-52 442	1 087 526 ± 35	1 480 ± 5
-50 311	-54 031	1 088 224 34	189 5
-50 501	-54 235	1 087 625 34	
-48 420	-52 000	1 095 480 140	10 130
-48 434	-52 016	1 094 709 45	2 957 30
-51 391	-55 192	1 096 883 34	-2 991 20
-48 401	-51 980	1 093 110 39	442.0 4.0
-48 843	-52 454	1 092 769 39	
-46 376	-49 805	1 101 806 40	2 280 20
-48 656	-52 254	1 103 304 34	970 1
-49 627	-53 297	1 103 486 34	- 355 6
-49 271	-52 914	1 102 353 34	
-46 116	-49 526	1 109 910 60	505 15
-46 621	-50 068	1 109 640 50	3 570 40
-50 192	-53 903	1 112 418 34	-1 820 140
-48 370	-51 950	1 109 820 140	920 330
-49 300	-52 940	1 109 960 300	
-46 700	-50 160	1 118 090 160	1 900 70
-48 600	-52 200	1 119 200 140	428 4
-49 030	-52 660	1 118 840 140	- 490 3
-48 540	-52 130	1 117 580 140	
-48 449	-52 031	1 127 410 35	-1 040 140
-47 400	-50 910	1 125 580 140	2 055.0 2.0
-49 460	-53 120	1 126 850 140	-3 700 200
-45 760	-49 140	1 122 380 250	
-46 620	-50 070	1 133 950 250	1 160 10
-47 780	-51 310	1 134 330 250	210 5
-47 990	-51 540	1 133 750 250	
-39 160	-42 050	1 135 640 110	7 000 100
-46 159	-49 572	1 141 854 36	90 130
-46 250	-49 670	1 141 170 130	2 580 20
-48 830	-52 440	1 142 960 130	-3 000 200
-45 830	-49 220	1 139 180 240	500 500
-46 290	-49 700	1 138 850 490	
-46 230	-49 650	1 149 520 130	1 176 3
-47 410	-50 910	1 149 910 130	
-42 790	-45 960	1 154 450 100	4 830 50
-47 620	-51 140	1 158 490 80	-1 676 27
-45 950	-49 340	1 156 030 80	1 015 15
-46 960	-50 430	1 156 260 80	
-39 680	-42 610	1 159 700 220	4 300 200
-43 980	-47 230	1 163 210 80	2 381 19
-46 360	-49 780	1 164 810 80	- 270 6
-46 090	-49 490	1 163 750 80	-2 000 100
-44 090	-47 350	1 160 980 130	

TABLE 1 (Continued)

Z	N	N−Z	A	Symbol	Mass excess ($^{12}C = 0$) (keV)		Mass excess ($^{12}C = 0$) (μu)	
56	84	28	140	Ba	−83 400	± 50	−89 540	± 60
57	83	26	140	La	−84 450	50	−90 670	60
58	82	24	140	Ce	−88 223	47	−94 720	50
59	81	22	140	Pr	−84 964	46	−91 218	49
57	84	27	141	La	−83 250	50	−89 380	60
58	83	25	141	Ce	−85 681	44	−91 987	47
59	82	23	141	Pr	−86 261	43	−92 610	46
60	81	21	141	Nd	−84 461	44	−90 678	48
58	84	26	142	Ce	−84 730	70	−90 960	80
59	83	24	142	Pr	−84 025	44	−90 210	47
60	82	22	142	Nd	−86 179	44	−92 522	47
58	85	27	143	Ce	−81 805	49	−87 830	50
59	84	25	143	Pr	−83 246	48	−89 370	50
60	83	23	143	Nd	−84 180	48	−90 380	50
61	82	21	143	Pm	−83 080	160	−89 200	170
62	81	19	143	Sm	−79 580	250	−85 440	270
58	86	28	144	Ce	−80 630	50	−86 570	50
59	85	26	144	Pr	−80 942	49	−86 900	50
60	84	24	144	Nd	−83 922	48	−90 100	50
62	82	20	144	Sm	−82 290	220	−88 350	240
58	87	29	145	Ce	−78 010	170	−83 760	190
59	86	27	145	Pr	−80 010	140	−85 900	150
60	85	25	145	Nd	−81 820	140	−87 840	150
61	84	23	145	Pm	−81 680	140	−87 690	150
62	83	21	145	Sm	−81 030	140	−87 000	150
58	88	30	146	Ce	−76 130	260	−81 730	280
59	87	28	146	Pr	−77 130	240	−82 800	260
60	86	26	146	Nd	−81 330	140	−87 310	150
61	85	24	146	Pm	−80 380	120	−86 300	130
62	84	22	146	Sm	−81 130	70	−87 100	70
60	87	27	147	Nd	−78 400	50	−84 170	50
61	86	25	147	Pm	−79 302	49	−85 140	50
62	85	23	147	Sm	−79 527	49	−85 380	50
63	84	21	147	Eu	−77 700	190	−83 410	200
60	88	28	148	Nd	−77 800	150	−83 520	160
62	86	24	148	Sm	−79 580	120	−85 440	130
64	84	20	148	Gd	−76 620	240	−82 260	260
60	89	29	149	Nd	−74 670	140	−80 170	150
61	88	27	149	Pm	−76 310	120	−81 930	130
62	87	25	149	Sm	−77 370	120	−83 070	130
64	85	21	149	Gd	−75 520	210	−81 080	220
60	90	30	150	Nd	−73 850	140	−79 290	150
61	89	28	150	Pm	−73 500	420	−78 910	450
62	88	26	150	Sm	−77 300	120	−82 990	130
63	87	24	150	Eu	−74 880	150	−80 390	160
64	86	22	150	Gd	−75 950	150	−81 540	160

Mass excess ($^{16}O = 0$)		Binding energy (keV)	β^- decay energy (keV)
(keV)	(μMU)		
-41 960	-45 060	1 169 560 ± 70	1 050 ± 10
-43 010	-46 190	1 169 820 60	3 773 29
-46 780	-50 240	1 172 810 60	-3 259 19
-43 521	-46 739	1 168 770 60	
-41 510	-44 580	1 176 700 60	2 430 30
-43 941	-47 190	1 178 340 60	580 5
-44 521	-47 814	1 178 140 60	-1 800 10
-42 721	-45 880	1 175 560 60	
-42 690	-45 850	1 185 460 80	- 700 70
-41 990	-45 095	1 183 980 60	2 153 8
-44 143	-47 407	1 185 350 60	
-39 474	-42 390	1 190 610 60	1 441 10
-40 915	-43 940	1 191 270 60	933 5
-41 848	-44 940	1 191 420 60	-1 100 150
-40 750	-43 760	1 189 540 160	-3 500 200
-37 250	-40 000	1 185 260 260	
-38 000	-40 810	1 197 510 60	310 4
-38 314	-41 150	1 197 040 60	2 980 10
-41 295	-44 350	1 199 230 60	
-39 660	-42 600	1 196 040 220	
-35 090	-37 680	1 202 970 180	2 000 100
-37 090	-39 830	1 204 180 150	1 805 10
-38 890	-41 770	1 205 200 150	- 140 10
-38 750	-41 620	1 204 280 150	- 645 15
-38 110	-40 930	1 202 860 150	
-32 910	-35 340	1 209 150 270	1 000 100
-33 910	-36 410	1 209 370 250	4 200 200
-38 110	-40 930	1 212 780 150	- 950 190
-37 160	-39 910	1 211 060 130	750 100
-37 910	-40 710	1 211 020 80	
-34 890	-37 470	1 217 930 60	900 10
-35 786	-38 430	1 218 050 60	225 3
-36 011	-38 670	1 217 490 60	-1 830 190
-34 180	-36 710	1 214 880 190	
-33 990	-36 500	1 225 390 150	
-35 770	-38 420	1 225 610 120	
-32 810	-35 230	1 221 090 250	
-30 570	-32 830	1 230 340 150	1 640 90
-32 200	-34 590	1 231 200 130	1 059 49
-33 260	-35 720	1 231 470 120	
-31 410	-33 730	1 228 060 210	
-29 450	-31 630	1 237 590 150	- 350 440
-29 100	-31 250	1 236 460 420	3 800 400
-32 900	-35 330	1 239 480 120	-2 420 190
-30 480	-32 730	1 236 270 150	1 070 10
-31 550	-33 880	1 236 560 150	

TABLE 1 (Continued)

Z	N	N−Z	A	Symbol	Mass excess ($^{12}C = 0$) (keV)	(μu)
60	91	31	151	Nd	−70 590 ± 220	−75 780 ± 240
61	90	29	151	Pm	−72 990 190	−78 360 210
62	89	27	151	Sm	−74 790 170	−80 290 180
63	88	25	151	Eu	−74 860 170	−80 370 180
65	86	21	151	Tb	−71 740 210	−77 020 230
62	90	28	152	Sm	−75 130 310	−80 650 330
63	89	26	152	Eu	−73 270 310	−78 660 330
64	88	24	152	Gd	−75 080 310	−80 600 330
66	86	20	152	Dy	−70 430 260	−75 620 270
62	91	29	153	Sm	−73 040 330	−78 420 350
63	90	27	153	Eu	−73 850 330	−79 280 350
64	89	25	153	Gd	−73 640 330	−79 060 350
66	87	21	153	Dy	−69 520 210	−74 630 230
62	92	30	154	Sm	−72 960 280	−78 330 300
63	91	28	154	Eu	−72 330 260	−77 650 280
64	90	26	154	Gd	−74 300 260	−79 770 280
66	88	22	154	Dy	−70 060 150	−75 220 160
62	93	31	155	Sm	−70 630 250	−75 830 270
63	92	29	155	Eu	−72 400 240	−77 730 260
64	91	27	155	Gd	−72 640 240	−77 990 260
63	93	30	156	Eu	−69 890 250	−75 040 270
64	92	28	156	Gd	−72 430 240	−77 760 260
63	94	31	157	Eu	−69 050 270	−74 140 290
64	93	29	157	Gd	−70 750 250	−75 960 270
64	94	30	158	Gd	−70 610 250	−75 810 270
65	93	28	158	Tb	−70 400 1 000	−75 600 1 100
64	95	31	159	Gd	−69 600 1 000	−74 700 1 100
65	94	29	159	Tb	−70 500 1 000	−75 700 1 100
66	93	27	159	Dy	−70 100 1 000	−75 300 1 100
64	96	32	160	Gd	−67 720 490	−72 700 500
65	95	30	160	Tb	−68 900 900	−74 000 1 000
66	94	28	160	Dy	−70 800 900	−76 000 1 000
64	97	33	161	Gd	−66 500 900	−71 400 1 000
65	96	31	161	Tb	−68 500 900	−73 600 1 000
66	95	29	161	Dy	−69 100 900	−74 200 1 000
66	96	30	162	Dy	−69 200 900	−74 300 1 000
66	97	31	163	Dy	−67 400 900	−72 400 1 000
67	96	29	163	Ho	−65 900 800	−70 700 900
66	98	32	164	Dy	−67 000 900	−71 900 1 000
67	97	30	164	Ho	−65 600 600	−70 400 700
68	96	28	164	Er	−66 500 600	−71 400 700
66	99	33	165	Dy	−64 400 600	−69 100 700
67	98	31	165	Ho	−65 600 600	−70 400 700

Mass excess ($^{16}O = 0$)		Binding energy (keV)	β^- decay energy (keV)
(keV)	(μMU)		
-25 880	-27 800	1 242 400 ± 220	2 400 ± 100
-28 280	-30 380	1 244 020 200	1 800 100
-30 080	-32 310	1 245 040 170	76 1
-30 160	-32 390	1 244 320 170	
-27 040	-29 040	1 239 640 210	
-30 130	-32 360	1 253 440 310	-1 860 7
-28 270	-30 360	1 250 800 310	1 810 10
-30 080	-32 300	1 251 830 310	
-25 440	-27 320	1 245 620 260	
-27 750	-29 800	1 259 440 330	803 5
-28 550	-30 670	1 259 450 330	- 210 20
-28 340	-30 440	1 258 460 330	
-24 220	-26 010	1 252 780 220	
-27 370	-29 400	1 267 420 280	- 630 380
-26 740	-28 720	1 266 010 270	1 970 20
-28 710	-30 830	1 267 190 270	
-24 480	-26 290	1 261 400 160	
-24 750	-26 580	1 273 160 260	1 770 100
-26 520	-28 480	1 274 150 250	243 4
-26 760	-28 740	1 273 610 250	
-23 710	-25 460	1 279 720 250	2 540 50
-26 250	-28 190	1 281 470 250	
-22 580	-24 250	1 286 950 270	1 700 100
-24 280	-26 070	1 287 860 250	
-23 840	-25 600	1 295 790 250	- 200 1100
-23 700	-25 400	1 294 800 1 000	
-22 500	-24 200	1 302 800 1 000	944 7
-23 400	-25 200	1 303 000 1 000	- 380 20
-23 100	-24 800	1 301 800 1 000	
-20 360	-21 900	1 309 040 490	1 200 1 100
-21 600	-23 200	1 309 500 900	1 820 10
-23 400	-25 100	1 310 500 900	
-18 900	-20 300	1 315 900 900	2 000 70
-20 900	-22 400	1 317 100 900	580 20
-21 400	-23 000	1 316 900 900	
-21 200	-22 800	1 325 100 900	
-19 200	-20 600	1 331 400 900	-1 600 1 200
-17 600	-18 900	1 329 000 800	
-18 400	-19 800	1 339 000 900	-1 400 1 100
-17 000	-18 300	1 336 800 600	989 30
-18 000	-19 300	1 337 000 600	
-15 500	-16 700	1 344 500 600	1 250 20
-16 800	-18 000	1 344 900 600	

TABLE 1 (Continued)

Z	N	N−Z	A	Symbol	Mass excess ($^{12}C = 0$) (keV)		Mass excess ($^{12}C = 0$) (μu)	
66	100	34	166	Dy	−63 400	± 600	−68 100	± 600
67	99	32	166	Ho	−63 900	600	−68 600	600
68	98	30	166	Er	−65 700	600	−70 600	600
69	97	28	166	Tm	−62 600	700	−67 300	700
67	100	33	167	Ho	−63 200	600	−67 900	600
68	99	31	167	Er	−64 200	600	−68 900	600
68	100	32	168	Er	−63 900	600	−68 600	600
68	102	34	170	Er	−60 500	2 000	−64 900	2 100
71	105	34	176	Lu	−54 550	430	−58 560	460
72	104	32	176	Hf	−55 570	430	−59 660	460
70	107	37	177	Yb	−52 220	430	−56 060	460
71	106	35	177	Lu	−53 600	430	−57 550	460
72	105	33	177	Hf	−54 100	430	−58 080	460
73	104	31	177	Ta	−52 950	430	−56 840	460
72	106	34	178	Hf	−53 570	410	−57 510	440
72	107	35	179	Hf	−51 770	410	−55 580	440
72	108	36	180	Hf	−51 120	400	−54 880	430
73	107	34	180	Ta	−50 560	360	−54 280	380
74	106	32	180	W	−51 260	360	−55 030	380
72	109	37	181	Hf	−49 110	350	−52 720	380
73	108	35	181	Ta	−50 130	350	−53 820	380
74	107	33	181	W	−49 930	360	−53 610	380
73	109	36	182	Ta	−48 130	350	−51 670	380
74	108	34	182	W	−49 860	350	−53 530	380
72	111	39	183	Hf	−44 710	410	−48 000	440
73	110	37	183	Ta	−46 910	350	−50 360	380
74	109	35	183	W	−47 980	350	−51 510	380
74	110	36	184	W	−47 360	360	−50 850	390
73	112	39	185	Ta	−44 400	1 500	−47 600	1 600
74	111	37	185	W	−46 100	1 500	−49 500	1 600
75	110	35	185	Re	−46 500	1 500	−49 900	1 600
76	109	33	185	Os	−45 500	1 500	−48 900	1 600
74	112	38	186	W	−45 300	1 500	−48 600	1 600
75	111	36	186	Re	−42 770	330	−45 920	350
76	110	34	186	Os	−43 840	330	−47 060	350
74	113	39	187	W	−40 620	320	−43 610	340
75	112	37	187	Re	−41 940	320	−45 020	340
76	111	35	187	Os	−41 940	320	−45 030	340

Mass excess ($^{16}O = 0$)		Binding energy (keV)	β^- decay energy (keV)
(keV)	(μMU)		
-14 500	-15 300	1 351 600 ± 600	500 ± 5
-14 800	-15 900	1 351 300 600	1 847 5
-16 600	-17 800	1 352 400 600	-3 100 300
-13 500	-14 500	1 348 500 700	
-13 800	-14 800	1 358 700 600	1 000 100
-14 800	-15 900	1 358 900 600	
-14 200	-15 200	1 366 700 600	
-10 100	-10 900	1 379 400 2 000	
-2 450	-2 630	1 419 540 430	1 020 20
-3 470	-3 720	1 419 770 430	
180	190	1 426 060 440	1 380 50
-1 200	-1 290	1 426 660 430	497 2
-1 700	-1 830	1 426 370 430	-1 150 50
- 550	- 590	1 424 440 440	
- 880	- 940	1 433 910 410	
1 220	1 310	1 440 180 410	
2 170	2 330	1 447 600 400	- 560 350
2 730	2 930	1 446 260 360	700 20
2 030	2 180	1 446 190 360	
4 470	4 810	1 453 670 360	1 025 3
3 450	3 700	1 453 910 360	- 200 40
3 650	3 920	1 452 930 360	
5 740	6 170	1 459 980 360	1 732 10
4 010	4 310	1 460 930 360	
9 460	10 160	1 465 420 410	2 200 200
7 260	7 800	1 466 830 360	1 068 10
6 200	6 650	1 467 110 360	
7 100	7 630	1 474 570 370	
10 400	11 200	1 480 400 1 500	1 700 100
8 700	9 300	1 481 400 1 500	430 2
8 300	8 900	1 481 000 1 500	- 985 7
9 300	9 900	1 479 200 1 500	
9 800	10 500	1 488 600 1 500	-2 500 1 500
12 290	13 200	1 485 340 330	1 067 2
11 220	12 050	1 485 620 330	
14 740	15 830	1 492 050 320	1 315 10
13 420	14 410	1 492 570 320	4.1 4.0
13 420	14 410	1 491 800 320	

TABLE 1 (Continued)

Z	N	N−Z	A	Symbol	Mass excess ($^{12}C = 0$) (keV)	(μu)
75	113	38	188	Re	−39 810 ± 280	−42 740 ± 300
76	112	36	188	Os	−41 930 280	−45 020 300
77	111	34	188	Ir	−38 930 350	−41 790 370
78	110	32	188	Pt	−38 410 350	−41 230 380
79	109	30	188	Au	−33 230 360	−35 670 390
76	113	37	189	Os	−39 850 310	−42 780 330
76	114	38	190	Os	−39 660 340	−42 580 360
78	112	34	190	Pt	−38 030 380	−40 830 410
76	115	39	191	Os	−37 040 270	−39 770 290
77	114	37	191	Ir	−37 350 270	−40 100 290
76	116	40	192	Os	−36 780 320	−39 490 340
77	115	38	192	Ir	−35 370 270	−37 970 290
78	114	36	192	Pt	−36 820 270	−39 530 290
79	113	34	192	Au	−33 580 270	−36 050 290
76	117	41	193	Os	−33 950 270	−36 450 290
77	116	39	193	Ir	−35 080 270	−37 660 290
78	115	37	193	Pt	−35 030 270	−37 610 290
77	117	40	194	Ir	−32 760 220	−35 170 240
78	116	38	194	Pt	−34 990 220	−37 570 240
79	115	36	194	Au	−32 430 220	−34 810 240
78	117	39	195	Pt	−33 100 220	−35 540 240
79	116	37	195	Au	−32 830 220	−35 250 240
78	118	40	196	Pt	−32 950 220	−35 380 240
79	117	38	196	Au	−31 159 19	−33 453 21
80	116	36	196	Hg	−31 838 17	−34 181 18
78	119	41	197	Pt	−30 405 18	−32 643 20
79	118	39	197	Au	−31 155 15	−33 448 16
78	120	42	198	Pt	−30 240 280	−32 470 310
79	119	40	198	Au	−29 581 14	−31 758 15
80	118	38	198	Hg	−30 953 14	−33 231 15
78	121	43	199	Pt	−27 330 100	−29 340 110
79	120	41	199	Au	−29 112 20	−31 255 21
80	119	39	199	Hg	−29 567 19	−31 744 20
79	121	42	200	Au	−27 190 100	−29 190 110
80	120	40	200	Hg	−29 486 13	−31 656 14
81	119	38	200	Tl	−27 036 16	−29 026 17
79	122	43	201	Au	−26 150 100	−28 070 110
80	121	41	201	Hg	−27 650 17	−29 685 18
81	120	39	201	Tl	−27 240 60	−29 240 70
80	122	42	202	Hg	−27 356 21	−29 370 23
81	121	40	202	Tl	−25 960 200	−27 870 220
82	120	38	202	Pb	−25 910 200	−27 810 220

Mass excess ($^{16}O = 0$)		Binding energy (keV)	β^- decay energy (keV)
(keV)	(μMU)		
15 840	17 010	1 498 530 ± 290	2 116 ± 2
13 720	14 740	1 499 860 290	-3 000 200
16 730	17 960	1 496 080 350	- 520 50
17 250	18 520	1 494 770 350	-5 180 100
22 430	24 090	1 488 810 370	
16 100	17 290	1 505 850 320	
16 590	17 810	1 513 730 340	
18 220	19 560	1 510 540 390	
19 500	20 950	1 519 190 270	314 2
19 190	20 610	1 518 720 270	
20 060	21 540	1 526 990 320	-1 410 260
21 470	23 060	1 524 800 270	1 453 5
20 020	21 500	1 525 470 270	-3 240 50
23 260	24 980	1 521 450 270	
23 190	24 900	1 532 240 270	1 136 5
22 050	23 680	1 532 580 270	-52 30
22 100	23 740	1 531 750 270	
24 670	26 500	1 538 340 230	2 236 10
22 440	24 100	1 539 780 230	-2 566 14
25 000	26 850	1 536 440 230	
24 630	26 450	1 545 960 230	- 270 20
24 900	26 740	1 544 910 230	
25 070	26 920	1 553 880 230	-1 790 220
26 862	28 848	1 551 310 50	678 17
26 183	28 119	1 551 200 50	
27 913	29 977	1 559 420 50	750 10
27 162	29 171	1 559 380 50	
28 370	30 470	1 567 310 290	- 660 280
29 032	31 179	1 565 870 50	1 372.2 2.0
27 660	29 705	1 566 460 50	
31 580	33 910	1 572 490 110	1 780 100
29 798	32 001	1 573 480 60	455 5
29 342	31 511	1 573 150 50	
32 020	34 390	1 579 630 110	2 300 100
29 719	31 917	1 581 150 50	-2 450 10
32 169	34 548	1 577 910 50	
33 350	35 820	1 586 660 110	1 500 100
31 851	34 207	1 587 380 50	- 410 60
32 260	34 650	1 586 190 80	
32 441	34 840	1 595 160 50	-1 400 200
33 840	36 340	1 592 980 200	-50 35
33 890	36 400	1 592 140 200	

TABLE 1 (Continued)

Z	N	N−Z	A	Symbol	Mass excess ($^{12}C = 0$) (keV)		Mass excess ($^{12}C = 0$) (μu)	
80	123	43	203	Hg	−25 286 ±	37	−27 147 ±	40
81	122	41	203	Tl	−25 772	37	−27 669	40
82	121	39	203	Pb	−24 775	47	−26 600	50
83	120	37	203	Bi	−21 580	70	−23 170	70
80	124	44	204	Hg	−24 700	18	−26 518	19
81	123	42	204	Tl	−24 320	22	−26 110	24
82	122	40	204	Pb	−25 085	22	−26 931	24
83	121	38	204	Bi	−20 800	500	−22 300	500
80	125	45	205	Hg	−22 140	100	−23 770	110
81	124	43	205	Tl	−23 787	25	−25 538	27
82	123	41	205	Pb	−23 737	37	−25 484	40
83	122	39	205	Bi	−21 090	50	−22 640	50
81	125	44	206	Tl	−22 280	15	−23 920	16
82	124	42	206	Pb	−23 790	11	−25 541	12
83	123	40	206	Bi	−20 190	150	−21 680	160
84	122	38	206	Po	−18 160	200	−19 500	220
81	126	45	207	Tl	−21 008	14	−22 554	15
82	125	43	207	Pb	−22 450	11	−24 102	12
83	124	41	207	Bi	−20 050	42	−21 526	45
84	123	39	207	Po	−17 144	42	−18 406	45
85	122	37	207	At	−13 300	70	−14 280	80
81	127	46	208	Tl	−16 760	13	−17 994	14
82	126	44	208	Pb	−21 755	11	−23 356	12
83	125	42	208	Bi	−18 879	27	−20 269	29
84	124	40	208	Po	−17 451	23	−18 736	25
85	123	38	208	At	−12 600	500	−13 500	500
81	128	47	209	Tl	−13 697	42	−14 705	44
82	127	45	209	Pb	−17 610	23	−18 906	25
83	126	43	209	Bi	−18 240	25	−19 583	27
84	125	41	209	Po	−16 340	38	−17 543	41
85	124	39	209	At	−12 910	50	−13 860	50
81	129	48	210	Tl	−9 313	32	−9 998	35
82	128	46	210	Pb	−14 738	13	−15 823	14
83	127	44	210	Bi	−14 801	13	−15 890	14
84	126	42	210	Po	−15 959	11	−17 134	12
85	125	40	210	At	−12 140	150	−13 030	160
86	124	38	210	Em	−9 580	200	−10 280	220
82	129	47	211	Pb	−10 429	36	−11 197	39
83	128	45	211	Bi	−11 835	14	−12 706	15
84	127	43	211	Po	−12 436	19	−13 351	20
85	126	41	211	At	−11 647	42	−12 504	45
86	125	39	211	Em	−8 756	42	−9 400	45
82	130	48	212	Pb	−7 548	14	−8 104	16
83	129	46	212	Bi	−8 130	13	−8 729	14
84	128	44	212	Po	−10 377	11	−11 141	12
85	127	42	212	At				
86	126	40	212	Em	−8 638	24	−9 274	26
87	125	38	212	Fr	−3 600	500	−3 900	500

	Mass excess ($^{16}O = 0$)		Binding energy (keV)		β^- decay energy (keV)	
	(keV)	(μMU)				
0	34 807	37 381	1 601 160 ±	60	486 ±	3
0	34 321	36 859	1 600 860	60	-1 000	60
0	35 318	37 930	1 599 080	70	-3 190	50
0	38 510	41 360	1 595 110	80		
9	35 689	38 329	1 608 640	50	- 380	18
4	36 069	38 737	1 607 480	50	765	2
4	35 304	37 915	1 607 460	50	-4 300	500
0	39 600	42 500	1 602 400	500		
0	38 550	41 400	1 614 150	110	1 650	100
7	36 899	39 627	1 615 020	60	-50	35
0	36 949	39 681	1 614 190	60	-2 650	30
0	39 600	42 530	1 610 760	70		
6	38 702	41 563	1 621 580	50	1 510	10
2	37 192	39 942	1 622 310	50	-3 600	150
0	40 790	43 810	1 617 930	160	-2 030	250
0	42 820	45 990	1 615 120	200		
5	40 270	43 247	1 628 380	50	1 442	8
2	38 828	41 699	1 629 040	50	-2 400	40
5	41 228	44 276	1 625 860	60	-2 906	8
5	44 134	47 397	1 622 170	60	-3 850	60
0	47 980	51 530	1 617 540	80		
4	44 814	48 127	1 632 210	50	4 995	6
2	39 819	42 763	1 636 420	50	-2 876	25
9	42 695	45 852	1 632 760	60	-1 428	35
5	44 123	47 385	1 630 550	50	-4 900	500
0	49 000	52 600	1 624 900	500		
4	48 173	51 735	1 637 220	60	3 913	35
5	44 260	47 532	1 640 350	50	630	10
7	43 630	46 856	1 640 190	60	-1 900	45
1	45 530	48 896	1 637 510	60	-3 434	30
0	48 960	52 580	1 633 290	70		
5	52 853	56 761	1 640 900	60	5 425	30
4	47 428	50 935	1 645 550	60	63	1
4	47 365	50 867	1 644 830	60	1 158	6
2	46 207	49 623	1 645 200	60	-3 820	150
0	50 030	53 730	1 640 590	160	-2 560	250
0	52 590	56 480	1 637 250	200		
9	52 032	55 880	1 649 310	60	1 406	34
5	50 627	54 370	1 649 930	60	601	18
0	50 026	53 725	1 649 750	60	- 789	43
5	50 815	54 572	1 648 180	70	-2 891	9
5	53 706	57 677	1 644 500	70		
6	55 210	59 292	1 654 500	60	582	7
4	54 628	58 667	1 654 300	60	2 247	6
2	52 381	56 254	1 655 760	60		
6	54 120	58 122	1 652 460	60	-5 000	500
0	59 100	63 500	1 646 700	500		

TABLE 1 (Continued)

Z	N	N−Z	A	Symbol	Mass excess ($^{12}C = 0$) (keV)		Mass excess ($^{12}C = 0$) (μu)	
83	130	47	213	Bi	−5 282	± 29	−5 671	± 31
84	129	45	213	Po	−6 672	27	−7 163	29
85	128	43	213	At	−6 440	200	−6 910	220
82	132	50	214	Pb	− 220	60	− 240	60
83	131	48	214	Bi	−1 273	33	−1 366	35
84	130	46	214	Po	−4 479	13	−4 808	14
85	129	44	214	At	−3 420	50	−3 670	60
83	132	49	215	Bi	1 770	120	1 900	130
84	131	47	215	Po	− 495	38	− 531	41
85	130	45	215	At	−1 250	25	−1 342	26
86	129	43	215	Em	−1 240	100	−1 330	110
84	132	48	216	Po	1 786	15	1 917	16
85	131	46	216	At	2 240	33	2 405	35
86	130	44	216	Em	218	32	234	34
85	132	47	217	At	4 328	31	4 647	33
86	131	45	217	Em	3 648	41	3 917	44
87	130	43	217	Fr	4 450	280	4 780	310
84	134	50	218	Po	8 320	60	8 930	60
85	133	48	218	At	7 968	33	8 554	36
86	132	46	218	Em	5 209	16	5 592	18
87	131	44	218	Fr	7 010	70	7 520	80
85	134	49	219	At	10 580	110	11 360	120
86	133	47	219	Em	8 870	38	9 523	41
87	132	45	219	Fr	8 615	32	9 249	34
88	131	43	219	Ra	9 340	140	10 030	150
86	134	48	220	Em	10 615	15	11 396	16
87	133	46	220	Fr	11 485	44	12 330	48
88	132	44	220	Ra	10 220	38	10 972	41
87	134	47	221	Fr	13 204	32	14 176	35
88	133	45	221	Ra	12 910	50	13 860	50
89	132	43	221	Ac	14 620	300	15 690	320
86	136	50	222	Em	16 320	60	17 530	60
87	135	48	222	Fr				
88	134	46	222	Ra	14 312	19	15 365	21
89	133	44	222	Ac	16 530	90	17 750	90
87	136	49	223	Fr	18 444	38	19 802	42
88	135	47	223	Ra	17 292	37	18 565	41
89	134	45	223	Ac	17 808	37	19 119	40
90	133	43	223	Th	19 460	170	20 890	170
88	136	50	224	Ra	18 830	15	20 216	16
89	135	48	224	Ac	20 200	50	21 690	60
90	134	46	224	Th	19 913	42	21 379	46
88	137	49	225	Ra	21 906	34	23 518	37
89	136	47	225	Ac	21 556	33	23 143	35
90	135	45	225	Th	22 030	60	23 660	60

	Mass excess ($^{16}O = 0$)		Binding energy (keV)		β^- decay energy (keV)	
	(keV)	(μMU)				
1	57 772	62 044	1 659 520 ±	60	1 390 ±	10
9	56 382	60 551	1 660 130	60	- 240	200
0	56 620	60 810	1 659 110	200		
0	63 130	67 800	1 663 310	80	1 050	50
5	62 077	66 668	1 663 580	60	3 206	30
4	58 871	63 224	1 666 010	60	-1 060	50
0	59 930	64 360	1 664 170	70		
0	65 410	70 250	1 668 610	120	2 260	110
1	63 151	67 821	1 670 090	70	755	39
6	62 396	67 010	1 670 070	60	-10	100
0	62 400	67 020	1 669 270	110		
6	65 728	70 588	1 675 880	60	- 454	31
5	66 182	71 076	1 674 650	60	2 022	43
4	64 160	68 904	1 675 890	60		
3	68 566	73 636	1 680 630	60	680	33
4	67 886	72 906	1 680 530	70	- 800	280
0	68 690	73 770	1 678 940	280		
0	72 850	78 240	1 685 500	70	350	50
6	72 502	77 863	1 685 060	60	2 759	32
8	69 743	74 901	1 687 040	60	-1 800	70
0	71 540	76 830	1 684 460	90		
0	75 410	80 990	1 690 520	120	1 710	100
1	73 700	79 150	1 691 450	70	255	44
4	73 445	78 876	1 690 920	60	- 730	150
0	74 170	79 660	1 689 410	150		
6	75 741	81 342	1 697 780	60	- 870	43
8	76 611	82 276	1 696 120	70	1 260	60
1	75 346	80 917	1 696 610	70		
5	78 626	84 440	1 702 480	60	291	46
0	78 340	84 130	1 701 980	70	-1 700	300
20	80 040	85 960	1 699 500	300		
0	82 040	88 110	1 708 210	70		
1	80 030	85 948	1 708 660	60	-2 220	90
0	82 250	88 330	1 705 660	100		
2	34 458	90 703	1 713 380	70	1 152	7
1	83 306	89 466	1 713 750	70	- 516	49
0	83 822	90 020	1 712 450	70	-1 650	180
70	85 470	91 790	1 710 010	180		
6	85 140	91 436	1 720 280	60	-1 370	50
0	86 510	92 910	1 718 130	70	290	70
6	86 223	92 599	1 717 630	70		
7	88 512	95 057	1 725 280	70	350	10
5	88 162	94 681	1 724 840	70	- 480	60
0	88 640	95 190	1 723 580	80		

TABLE 1 (Continued)

Z	N	N−Z	A	Symbol	Mass excess ($^{12}C = 0$) (keV)	Mass excess ($^{12}C = 0$) (μu)
88	138	50	226	Ra	23 620 ± 60	25 360 ± 60
89	137	48	226	Ac	24 380 100	26 180 110
90	136	46	226	Th	23 184 22	24 890 23
91	135	44	226	Pa	25 890 100	27 800 110
88	139	51	227	Ra	27 217 43	29 220 47
89	138	49	227	Ac	25 907 39	27 814 41
90	137	47	227	Th	25 864 39	27 768 41
91	136	45	227	Pa	26 815 42	28 789 46
92	135	43	227	U	28 800 200	30 920 220
88	140	52	228	Ra	29 087 39	31 228 42
89	139	50	228	Ac	29 032 39	31 169 42
90	138	48	228	Th	26 778 15	28 749 16
91	137	46	228	Pa	28 830 60	30 950 60
92	136	44	228	U	29 134 44	31 278 47
90	139	49	229	Th	29 461 37	31 629 40
91	138	47	229	Pe	29 761 44	31 952 48
92	137	45	229	U	31 000 60	33 280 70
90	140	50	230	Th	30 820 60	33 080 60
91	139	48	230	Pa	32 010 22	34 366 24
92	138	46	230	U	31 600 22	33 926 24
90	141	51	231	Th	33 858 39	36 350 42
91	140	49	231	Pa	33 472 39	35 936 42
92	139	47	231	U	33 840 60	36 330 60
93	138	45	231	Np	35 640 70	38 260 70
90	142	52	232	Th	35 591 38	38 211 42
91	141	50	232	Pa	35 869 25	38 509 27
92	140	48	232	U	34 619 15	37 167 17
93	139	46	232	Np		
94	138	44	232	Pu	38 260 70	41 080 70
90	143	53	233	Th	38 588 39	41 428 42
91	142	51	233	Pa	37 358 38	40 108 40
92	141	49	233	U	36 790 38	39 498 40
93	140	47	233	Np	37 820 70	40 600 70
94	139	45	233	Pu	39 840 70	42 770 70
90	144	54	234	Th	40 590 80	43 570 80
91	143	52	234	Pa	40 400 80	43 370 80
92	142	50	234	U	38 100 60	40 900 60
93	141	48	234	Np	39 900 120	42 830 130
94	140	46	234	Pu	40 330 50	43 290 60
91	144	53	235	Pa	42 320 110	45 440 120
92	143	51	235	U	40 921 41	43 933 43
93	142	49	235	Np	41 048 42	44 069 44
94	141	47	235	Pu	42 220 70	45 330 70
92	144	52	236	U	42 598 38	45 733 40
93	143	50	236	Np	43 428 18	46 625 19
94	142	48	236	Pu	42 913 16	46 072 17

Mass excess ($^{16}O = 0$)		Binding energy (keV)		β^- decay energy (keV)	
(keV)	(μMU)				
90 520	97 210	1 731 640	± 80	- 770	± 120
91 290	98 040	1 730 090	110	1 200	100
90 086	96 748	1 730 500	60	-2 710	100
92 800	99 660	1 727 010	110		
94 415	101 397	1 736 110	70	1 310	20
93 105	99 990	1 736 630	70	43	2
93 062	99 944	1 735 900	70	- 950	50
94 013	100 965	1 734 160	70	-1 990	200
96 000	103 100	1 731 390	210		
96 581	103 723	1 742 310	70	55	3
96 526	103 664	1 741 580	70	2 254	36
94 272	101 244	1 743 050	60	-2 050	60
96 320	103 450	1 740 220	80	- 300	70
96 628	103 773	1 739 130	70		
97 251	104 443	1 748 440	70	- 300	34
97 551	104 765	1 747 360	70	-1 240	70
98 790	106 100	1 745 340	80		
98 900	106 210	1 755 160	80	-1 200	60
100 096	107 498	1 753 180	60	410	2
99 686	107 058	1 752 810	60		
102 240	109 800	1 760 190	70	386	3
101 854	109 386	1 759 790	70	-370	50
102 220	109 780	1 758 640	90	-1 800	90
104 020	111 710	1 756 060	90		
104 269	111 980	1 766 530	70	- 278	42
104 547	112 278	1 765 460	60	1 250	20
103 297	110 936	1 765 930	60		
106 940	114 840	1 760 730	90		
107 562	115 516	1 771 600	70	1 230	10
106 332	114 195	1 772 050	70	568	4
105 764	113 585	1 771 830	70	-1 030	60
106 800	114 690	1 770 020	90	-2 020	90
108 820	116 860	1 767 210	80		
109 860	117 980	1 777 670	100	192	1
109 670	117 770	1 777 080	100	2 300	50
107 370	115 310	1 778 600	80	-1 800	100
109 170	117 240	1 776 020	130	- 430	130
109 600	117 700	1 774 800	70		
111 890	120 160	1 783 230	120	1 400	100
110 487	118 658	1 783 840	70	- 127	20
110 614	118 794	1 782 930	70	-1 180	50
111 790	120 060	1 780 980	90		
112 460	120 776	1 790 240	70	- 830	38
113 290	121 667	1 788 630	60	515	7
112 775	121 115	1 788 360	60		

TABLE 1 (Continued)

Z	N	N−Z	A	Symbol	Mass excess ($^{12}C = 0$) (keV)		Mass excess ($^{12}C = 0$) (μu)	
92	145	53	237	U	45 250 ±	38	48 581 ±	41
93	144	51	237	Np	44 737	38	48 030	41
94	143	49	237	Pu	44 967	42	48 277	46
95	142	47	237	Am	46 370	80	49 780	90
92	146	54	238	U	47 280	80	50 760	80
93	145	52	238	Np	47 430	60	50 930	70
94	144	50	238	Pu	46 130	60	49 520	70
95	143	48	238	Am				
96	142	46	238	Cm	49 380	60	53 010	70
92	147	55	239	U	50 590	60	54 320	60
93	146	53	239	Np	49 309	42	52 938	45
94	145	51	239	Pu	48 585	41	52 161	44
95	144	49	239	Am	49 340	50	52 970	60
92	148	56	240	U	52 680	70	56 560	80
93	147	54	240	Np	52 320	70	56 180	80
94	146	52	240	Pu	50 274	37	53 974	40
95	145	50	240	Am				
96	144	48	240	Cm	51 698	34	55 503	37
93	148	55	241	Np	54 450	110	58 460	110
94	147	53	241	Pu	52 823	38	56 711	41
95	146	51	241	Am	52 802	38	56 689	41
96	145	49	241	Cm	53 570	70	57 510	70
94	148	54	242	Pu	54 690	80	58 710	80
95	147	52	242	Am	55 400	60	59 480	70
96	146	50	242	Cm	54 770	60	58 800	70
94	149	55	243	Pu	57 740	50	61 990	60
95	148	53	243	Am	57 174	42	61 382	46
96	147	51	243	Cm	57 169	41	61 377	44
97	146	49	243	Bk	58 600	70	62 920	80
95	149	54	244	Am	60 100	110	64 520	110
96	148	52	244	Cm	58 596	38	62 910	40
97	147	50	244	Bk				
98	146	48	244	Cf	61 413	40	65 933	43
95	150	55	245	Am	61 860	100	66 420	110
96	149	53	245	Cm	60 950	100	65 430	100
97	148	51	245	Bk	61 700	50	66 240	60
98	147	49	245	Cf	63 230	70	67 890	70
94	152	58	246	Pu	65 420	100	70 230	110
95	151	56	246	Am	65 040	90	69 830	100
96	150	54	246	Cm	62 750	80	67 370	90
97	149	52	246	Bk				
98	148	50	246	Cf	64 060	60	68 780	70
97	150	53	247	Bk	65 370	70	70 180	70
98	150	52	248	Cf	67 391	48	72 350	50
97	152	55	249	Bk	69 790	100	74 930	100
98	151	53	249	Cf	69 670	100	74 800	100
99	150	51	249	Es	70 990	70	76 220	80

	Mass excess ($^{16}O = 0$)		Binding energy (keV)		β^- decay energy (keV)	
	(keV)	(μMU)				
41	115 408	123 942	1 795 660	± 70	513	± 3
41	114 895	123 391	1 795 390	70	- 230	21
46	115 125	123 638	1 794 380	70	-1 400	80
90	116 520	125 140	1 792 190	100		
30	117 740	126 440	1 801 700	100	- 150	90
70	117 890	126 610	1 800 760	80	1 305	8
70	116 580	125 200	1 801 280	80		
70	119 830	128 690	1 796 470	80		
60	121 340	130 320	1 806 460	80	1 280	50
55	120 059	128 937	1 806 960	70	724	10
54	119 335	128 160	1 806 900	70	- 758	35
50	120 090	128 970	1 805 360	80		
80	123 730	132 880	1 812 440	90	360	20
80	123 370	132 490	1 812 010	90	2 050	60
00	121 320	130 292	1 813 280	70		
97	122 744	131 821	1 810 290	70		
00	125 800	135 100	1 817 960	120	1 630	100
01	124 165	133 347	1 818 800	70	21	1
01	124 144	133 325	1 818 040	70	- 760	50
00	124 910	134 150	1 816 500	90		
00	126 320	135 670	1 825 010	100	- 710	50
00	127 040	136 430	1 823 520	80	633	5
00	126 410	135 750	1 823 370	80		
00	129 680	139 270	1 830 030	80	570	30
06	129 108	138 656	1 829 810	70	5	12
04	129 103	138 650	1 829 040	70	-1 430	60
00	130 540	140 190	1 826 820	90		
00	132 330	142 110	1 834 960	120	1 500	100
00	130 827	140 501	1 835 680	70		
03	133 644	143 526	1 831 300	70		
00	134 390	144 330	1 841 270	110	915	16
00	133 470	143 340	1 841 400	110	- 750	80
00	134 220	144 150	1 839 870	70	-1 540	60
00	135 760	145 800	1 837 550	90		
00	138 240	148 460	1 846 570	120	375	30
00	137 870	148 060	1 846 160	110	2 290	50
00	135 580	145 600	1 847 670	100		
00	136 880	147 000	1 844 790	80		
00	138 490	148 730	1 852 340	90		
00	140 806	151 220	1 857 610	70		
00	143 500	154 120	1 864 060	110	125	2
00	143 380	153 980	1 863 400	110	-1 320	90
00	144 700	155 400	1 861 290	90		

TABLE 1 (Continued)

Z	N	N−Z	A	Symbol	Mass excess ($^{12}C = 0$) (keV)		Mass excess ($^{12}C = 0$) (μu)	
97	153	56	250	Bk	73 110	± 130	78 490	± 140
98	152	54	250	Cf	71 310	80	76 550	90
99	151	52	250	Es				
100	150	50	250	Fm	74 040	80	79 480	80
99	152	53	251	Es	74 380	80	79 850	90
100	152	52	252	Fm	76 980	50	82 650	60
99	154	55	253	Es	78 960	100	84 780	100
99	155	56	254	Es	82 070	130	88 110	140
100	154	54	254	Fm	81 040	80	87 000	90

secondary masses: the last ones have not been included in the direct least squares adjustments since they do not contribute a gain in accuracy. Table 2 gives the arrangement of the periodic table in the ten ranges and the number of

TABLE 2

Data about the separate adjustments

Range	Number of masses	Number n of primary masses	Number N of primary input data	$\sqrt{\chi^2/(N-n)}$ Computed	$\sqrt{\chi^2/(N-n)}$ Theoretical
^{1}n − ^{46}V	134	68	358	1.10	1.00±0.04
^{47}Ca − ^{70}As	95	38	103	0.98	0.09
^{71}Zn − ^{82}Se	49	27	54	1.04	0.14
^{83}Br − ^{99}Rh	77	42	76	1.29	0.13
^{99}Mo − ^{111}Sn	47	24	38	1.56	0.19
^{112}Pd − ^{119}Sb	28	14	30	0.89	0.18
^{120}Sn − ^{137}Ba	71	42	84	1.07	0.11
^{138}Cs − ^{154}Dy	69	36	62	0.85	0.14
^{154}Sm − ^{184}W	57	33	62	1.29	0.13
^{185}Ta − ^{199}Hg	43	23	50	1.15	0.13

masses and input data in each range. The last column but one gives the value for the consistency factor $\sqrt{\chi^2/(N-n)}$ following from these adjustments; it should lie with a probability of about $\frac{2}{3}$ within the range given in the last column. Customarily, the errors are multiplied with this factor if it is significantly larger than one. This has *not* been done in the present mass table (technically: we give the standard errors determined by internal consistency). In the worst case (the region ^{99}Mo—^{111}Sn) the discrepancy is known to be due to a very small group of conflicting data which give only localized extra uncertainties; and in the other

	Mass excess ($^{16}O = 0$)		Binding energy (keV)		β^- decay energy (keV)	
	(keV)	(μMU)				
40	147 110	157 990	1 868 820 ±	140	1 800 ±	100
90	145 310	156 060	1 869 830	100		
80	148 040	158 990	1 865 540	100		
90	148 680	159 680	1 874 050	110		
60	151 580	162 790	1 878 740	80		
00	153 860	165 240	1 885 610	110		
40	157 260	168 890	1 890 570	140	1 040	100
90	156 230	167 780	1 890 820	100		

cases one should not bother about corrections of only about 30 % in the errors,

A short description of the computation for $A \leqq 70$ has already been published [2]); a discussion of the range $70 < A < 200$ will follow [3]). In the region $A \geqq 200$ the number of interconnections is too low to justify a complete least squares adjustment. The computation has been done here by making a few local adjustments which gave very reasonable results. A description of this part of the adjustment will be published in the near future [4]).

References

1) T. P. Kohman, J. H. E. Mattauch and A. H. Wapstra, Naturwiss. **45** (1958) 174; J. de Chimie Physique **55** (1958) 393; Science **127** (1958) 143; Physics Today **12** (1959) 30; J. Mattauch, Zs. Naturf. **13a** (1958) 572
2) F. Everling, L. A. König, J. H. E. Mattauch and A. H. Wapstra, Nuclear Physics **15** (1960) 342
3) L. A. König, J. H. E. Mattauch and A. H. Wapstra, to be published
4) A. H. Wapstra, to be published

8.B

Nuclear Physics **18** (1960) 570—574; © *North-Holland Publishing Co., Amsterdam*

Not to be reproduced by photoprint or microfilm without written permission from the publisher

UNITARITY CONDITIONS FOR BINARY PROCESSES INVOLVING PARTICLES OF ARBITRARY SPIN

A. J. MACFARLANE

Department of Mathematics, Imperial College, London

Received 27 May 1960

Abstract: Using the helicity description of two-particle eigenstates of total angular momentum, it is found that a concise statement can be obtained of the unitarity condition, in the two-particle approximation, for processes of type A+B→C+D involving particles of arbitrary spin. As an illustration of the use of this statement a specific set of processes is discussed and some remarks are made about its application below the physical threshold.

1. Introduction

If, as in the work of Jacob and Wick [1]), one completes the specification of two-particle eigenstates of total angular momentum by specifying the helicities of the particles rather than the orbital and spin angular momentum eigenvalues, one can develop the theory of binary collisions

$$\mathrm{A}+\mathrm{B}\rightarrow\mathrm{C}+\mathrm{D} \tag{1.1}$$

in a manner offering several notable advantages. Recently Frazer and Fulco [2]) have pointed out that the partial amplitudes occurring in ref. [1]) are in certain cases particularly convenient for the discussion of analyticity properties. The present paper shows that one may use the methods of ref. [1]) to obtain a concise statement of the unitarity condition for (1.1) in the two-particle approximation.

Derivation of this statement occupies section 2, while in section 3 it is applied to a specific set of processes of type (1.1) with some remarks about the use of unitarity below the physical threshold. Amongst the results obtained is the 'phase condition', used in ref. [2]) for the partial amplitudes for the process

$$\pi+\pi\rightarrow\mathrm{N}+\bar{\mathrm{N}}. \tag{1.2}$$

2. The Unitarity Condition

S-matrix elements for processes of the type (1.1) are related to elements of the T-matrix on the energy shell by

$$\langle\mathrm{f}|S|\mathrm{i}\rangle=\delta_{\mathrm{fi}}+(2\pi)^4\mathrm{i}\delta(p_\mathrm{A}+p_\mathrm{B}-p_\mathrm{C}-p_\mathrm{D})\langle\mathrm{f}|T(P_\mu)|\mathrm{i}\rangle, \tag{2.1}$$

where P_μ is the 4-momentum of the centre of mass. All further remarks will relate to the centre of mass system: $P = 0$, $P_0 = W$.

Unitarity of S implies

$$2\langle \mathrm{f}|\mathrm{Im}\, T(W)|\mathrm{i}\rangle = (2\pi)^4 \sum_n \delta(p_\mathrm{A}+p_\mathrm{B}-p_n)\langle \mathrm{f}|T(W)|n\rangle\langle n|T^\dagger(W)|\mathrm{i}\rangle. \quad (2.2)$$

In the two-particle approximation $\sum_{n2}$ to $\sum_n$, the summation involves an integration over the momenta and a sum over the spins of the intermediate particles, E and F. The assumption that only one type of two-particle state exists has been made, the extension required on its removal being immediate.

Since all the states involved in (2.2) are two-particle states of zero total linear momentum, they can be labelled [1]) by the magnitude of the relative momentum of the particles, the polar coordinates of its direction and the helicities of the individual particles. Letting p_i and p_f be the initial and final relative momenta, p_i is in the $\theta = 0$ direction, and p_i, p_f define the $\phi = 0$ plane. The states $|p; \theta\phi, \lambda_1\lambda_2\rangle$ are related to eigenstates of the total angular momentum of the two particles by †

$$\langle p, \theta\phi, \lambda_1, \lambda_2|p, JM\lambda'_1\lambda'_2\rangle = \left[\frac{2J+1}{4\pi}\right]^{\frac{1}{2}} \delta_{\lambda_1\lambda'_1}\delta_{\lambda_2\lambda'_2} d^J_{M\lambda}(\theta)\mathrm{e}^{\mathrm{i}(M-\lambda)\phi}, \quad (2.3)$$

where $\lambda = \lambda_1 - \lambda_2$. The $d^J_{M\lambda}(\theta)$ are an orthonormal set of functions for each pair M, λ:

$$\int_{-1}^{1} \mathrm{d}\cos\theta\, d^J_{M\lambda}(\theta) d^{J'}_{M\lambda}(\theta) = \frac{2}{2J+1}\delta_{JJ'}. \quad (2.4)$$

The work of ref. [1]) now allows the resolution of Im $T(W)$ into submatrices Im $T_J(W)$ whose elements between two states are completely labelled by the particle and helicity labels of the particles involved in these states. Putting $\lambda_\mathrm{i} = \lambda_\mathrm{A} - \lambda_\mathrm{B}$, $\lambda_\mathrm{f} = \lambda_\mathrm{C} - \lambda_\mathrm{D}$, this gives

$$\begin{aligned}\langle \mathrm{f}|\mathrm{Im}\, T(W)|\mathrm{i}\rangle &= \langle \theta \quad \phi = 0, \lambda_\mathrm{C}\lambda_\mathrm{D}|\mathrm{Im}\, T(W)|\theta_0 = 0 \quad \phi_0 = 0, \lambda_\mathrm{A}\lambda_\mathrm{B}\rangle \\ &= \sum_J \frac{2J+1}{4\pi} d^J_{\lambda_\mathrm{i}\lambda_\mathrm{f}}(\theta)\langle \lambda_\mathrm{C}\lambda_\mathrm{D}|\mathrm{Im}\, T_J(W)|\lambda_\mathrm{A}\lambda_\mathrm{B}\rangle. \end{aligned} \quad (2.5)$$

Treatment of the right side of (2.2) leads (see Appendix) to

$$\begin{aligned}&\sum_{n2} \langle \mathrm{f}|T(W)|n\rangle\langle n|T^\dagger(W)|\mathrm{i}\rangle (2\pi^4)\delta(p_\mathrm{A}+p_\mathrm{B}-p_n) \\ &= \frac{p_\mathrm{i}}{16\pi^2 W}\sum_J \frac{2J+1}{4\pi} d^J_{\lambda_\mathrm{i}\lambda_\mathrm{f}}(\theta)\Big[\sum_{\lambda_\mathrm{E},\lambda_\mathrm{F}} \langle \lambda_\mathrm{C}\lambda_\mathrm{D}|T_J(W)|\lambda_\mathrm{E}\lambda_\mathrm{F}\rangle\langle \lambda_\mathrm{E}\lambda_\mathrm{F}|T_J{}^\dagger(W)|\lambda_\mathrm{A}\lambda_\mathrm{B}\rangle\Big]. \end{aligned} \quad (2.6)$$

† The notation of ref. [4]) is used for the functions $d^J_{mm'}$ and also later, for Clebsch-Gordan coefficients.

The completeness (2.4) of the $d^J_{\lambda_1\lambda_t}(\theta)$ allows one to conclude from (2.2), (2.5), (2.6) that

$$\langle\lambda_C\lambda_D|\mathrm{Im}\, T_J(W)|\lambda_A\lambda_B\rangle = \frac{p_1}{32\pi^2 W}\sum_{\lambda_E,\lambda_F}\langle\lambda_C\lambda_D|T_J(W)|\lambda_E\lambda_F\rangle\langle\lambda_E\lambda_F|T_J^\dagger(W)|\lambda_A\lambda_B\rangle, \tag{2.7}$$

which is the desired statement of the unitarity condition in the two-particle approximation.

3. Discussion

Firstly, it is to be observed that one can pass from the $|JM, \lambda_1, \lambda_2\rangle$ states to $|JMLS\rangle$ states by means of the formula [1])

$$\langle JM\lambda_1\lambda_2|JMLS\rangle = \left[\frac{2L+1}{2J+1}\right]^{\frac{1}{2}} C\langle LSJ, 0\lambda M\rangle C(s_1 s_2 S, \lambda_1 - \lambda_2 \lambda) \tag{3.1}$$

where s_1, s_2 are the individual spins. In obtaining from (2.7) the corresponding results in terms of $|JMLS\rangle$ states, one must use the results

$$\langle\lambda_1\lambda_2|T_J(W)|\lambda_3\lambda_4\rangle = \langle\lambda_3\lambda_4|T_J(W)|\lambda_1\lambda_2\rangle, \tag{3.2}$$

$$\langle\lambda_1\lambda_2|T_J(W)|\lambda_3\lambda_4\rangle = \frac{\eta_3\eta_4}{\eta_1\eta_2}(-1)^{s_1+s_2-s_3-s_4}\langle-\lambda_1-\lambda_2|T_J(W)|-\lambda_3-\lambda_4\rangle. \tag{3.3}$$

Eqs. (3.2) and (3.3) are the respective consequences of invariance under Wigner time-reversal and under the parity operation. The factor η_i is an intrinsic parity factor for the i^{th} particle: the η_i to be assigned consistently with the known relative parities of elementary particles.

Secondly, some remarks on the validity of (2.7) are needed. The unitarity condition for (1.1) is true only above the physical threshold for (1.1), but very often one seeks to use its consequence (2.7) for a range of energies below that threshold. In this case, it is necessary to justify (2.7) as an analytic continuation (in the masses of some of the particles) of the two-particle approximation to the unitarity condition.

A specific situation will now be discussed: the use of (2.7) in the energy range

$$2m_\pi < W < 4m_\pi \tag{3.4}$$

for processes involving $\pi\pi$, $\bar{\mathrm{N}}\mathrm{N}$ or $\bar{\mathrm{K}}\mathrm{K}$ initial or final states. For the energy range (3.4) one can define a real phase shift $\delta_J(W)$ for pion-pion scattering by

$$\langle\lambda_{\pi_1} = \lambda_{\pi_2} = 0|T_J(W)|\lambda_{\pi_3} = \lambda_{\pi_4} = 0\rangle = \frac{32\pi^2 W}{p_1}\sin\delta_J e^{i\delta_J}. \tag{3.5}$$

For the other processes involved, the two-particle approximation of the unitarity condition must be continued analytically in the nucleon (or K-meson) mass from a value such that (3.4) is physical up to the actual physical value of the

nucleon mass. It is to be expected that in the range (3.4) the continuation of the two-particle approximation of the unitarity condition is equal to the continuation of the exact unitarity condition, i.e. one hopes that none of the other contributions to it have anomalous thresholds. In the present example the two-particle approximation means that only 2-pion states are involved in $\sum_{n2}$.

For (1.2) Mandelstam [3] has proved that the necessary analytic continuation is admissible. Assuming the same can be done for the other cases here in view, final results will now be quoted. First one observes that parity allows only the $J, L = J \pm 1, S = 1$ states of the $\bar{\mathrm{N}}\mathrm{N}$ system to be connected to the two-pion state of angular momentum J. Hence $\mathrm{Im}\, T_J(W)$ is a 4×4 matrix, whose rows and columns will be labelled by

$$\pi\pi, \quad \bar{\mathrm{N}}\mathrm{N}(J = L+1), \quad \bar{\mathrm{N}}\mathrm{N}(J = L-1), \quad \bar{\mathrm{K}}\mathrm{K}.$$

One evaluates its elements (starting with those that involve a 2π initial or final state), using (2.7) and transfers to a J, L, S representation by means of eqs. (3.1)—(3.3). Thus, in terms of real functions, the 4×4 matrix $\mathrm{Im}\, T_J(W)$ can be written

$$\begin{bmatrix} \sin\delta_J\, e^{i\delta_J} \\ a_{J+}\, e^{i\delta_J} \\ a_{J-}\, e^{i\delta_J} \\ b_J\, e^{i\delta_J} \end{bmatrix} [\sin\delta_J e^{-i\delta_J} \quad a_{J+} e^{-i\delta_J} \quad a_{J-} e^{-i\delta_J} \quad b_J e^{-i\delta_J}], \tag{3.6}$$

apart from a factor.

Eq. (3.6) contains the phase condition of ref. [2]: that the partial amplitudes for the process (1.2), at any energy in the range (3.4), have phases equal to the corresponding pion-pion scattering phase shift at the same energy. Eq. (3.6) also contains the relation of the imaginary part of the two-pion contribution to $\mathrm{N}\bar{\mathrm{N}} \to \mathrm{N}\bar{\mathrm{N}}$ amplitudes in terms of the partial amplitudes for process (1.2). This will be relevant to partial wave dispersion relations for nucleon-nucleon scattering.

No mention of isobaric spin has been made. The remarks made above, however, apply separately to each isobaric-spin channel through which (1.1) can proceed.

I should like to express my gratitude to Dr. P. T. Matthews and to Dr. T. W. B. Kibble for advice and discussions, and to the D.S.I.R. for maintenance allowance.

Appendix

One has

$$\sum_{n2} \langle \mathrm{f}|T(W)|n\rangle\langle n|T^\dagger(W)|\mathrm{i}\rangle (2\pi)^4 \delta(p_\mathrm{A}+p_\mathrm{B}-p_n) = \frac{p_1}{16\pi^2 W} \sum_{\lambda_\mathrm{E},\lambda_\mathrm{F}} \int_{-1}^{1} \mathrm{d}\cos\theta' \int_0^{2\pi} \mathrm{d}\phi' \langle \theta\,\phi = 0\,\lambda_\mathrm{C}\lambda_\mathrm{D}|T(W)|\theta'\phi'\lambda_\mathrm{E}\lambda_\mathrm{F}\rangle \cdot \langle \theta'\phi'\lambda_\mathrm{E}\lambda_\mathrm{F}|T^\dagger(W)|00\lambda_\mathrm{A}\lambda_\mathrm{B}\rangle. \tag{A.1}$$

With $\lambda_n = \lambda_E - \lambda_F$, one obtains as in ref. [1])

$$\langle \theta' \phi' \lambda_E \lambda_F | T^\dagger(W) | 00 \lambda_A \lambda_B \rangle$$

$$= \sum_K \frac{2K+1}{4\pi} d^K_{\lambda_1 \lambda_n}(\theta') e^{i(\lambda_1 - \lambda_n)\phi'} \langle \lambda_E \lambda_F | T_K{}^\dagger(W) | \lambda_A \lambda_B \rangle, \qquad \text{(A.2)}$$

and similarly

$$\langle \theta 0 \lambda_C \lambda_D | T(W) | \theta' \phi' \lambda_E \lambda_F \rangle$$

$$= \sum_{L,N} \frac{2L+1}{4\pi} d^L_{N\lambda_1}(\theta) d^L_{N\lambda_n}(\theta') e^{i(\lambda_n - N)\phi'} \langle \lambda_C \lambda_D | T_L(W) (\lambda_E \lambda_F \rangle. \qquad \text{(A.3)}$$

One now inserts (A.2), (A.3) into (A.1) and performs the ϕ', θ' integrations in that order, finally obtaining (2.6).

References

1) M. Jacob and G. C. Wick, Annals of Physics **7** (1959) 404
2) W. R. Frazer and J. R. Fulco, UCRL 8806
3) S. Mandelstam, Phys. Rev. Letters **4** (1959) 84
4) M. E. Rose, Elementary theory of angular momentum (Wiley, New York, 1957)

2.1

Nuclear Physics **18** (1960) 575—586; © *North-Holland Publishing Co., Amsterdam*

Not to be reproduced by photoprint or microfilm without written permission from the publisher

ELECTRODISINTEGRATION OF Ta AND Au NUCLEI

W. C. BARBER and T. WIEDLING †

High-Energy Physics Laboratory, Stanford University, Stanford, California ††

Received 25 May 1960

Abstract: Yield curves were measured for the production of 5.6-d Au^{196} and 30-s Au^{195} from Au^{197}, and of 8.1-h Ta^{180}, 2.1-h Ta^{178}, and 9.3-min Ta^{178} from Ta^{181}, in foil stacks which were bombarded by electrons. The results were analyzed to compare the yields resulting from the direct effect of the electrons with those resulting from bremsstrahlung from the electrons. The comparison shows the direct effect is relatively larger than is predicted by existing theories of electrodisintegration if the transitions being excited are entirely electric dipole.

Agreement with the theory can be obtained if electric monopole and quadrupole transitions are also assumed present. The theory, however, makes use of approximations which are probably not valid for nuclei with high Z.

If there is a monopole resonance in the region of 25—40 MeV excitation, its contribution to the 2n and 3n reactions is less than 30 % of the contributions of higher multipoles to these reactions.

1. Introduction

Comparison of the cross section for the electrodisintegration of nuclei with the corresponding cross section for photodisintegration has been used to study the multipole character of the excitations resulting in disintegration. The theoretical basis of the comparison is an extension of the virtual photon concept originally proposed by Weizsäcker and Williams [1]). In its extended form the theory calculates the interaction of the nuclear electric charges and magnetic moments with the Møller potentials produced by the scattering of a relativistic electron. Contributions to this theory have been made by many people; a recent discussion of the theory, including references to earlier work, is given in the paper of Dalitz and Yennie [2]).

A number of experiments [3–6]) comparing electro- and photodisintegration of nuclei have been made with the aim of testing the multipolarity of the transitions responsible for the giant photonuclear resonance. For light and medium weight nuclei (up to Ag^{109}), the results as interpreted by the theory consistently indicate that the giant resonance is predominantly dipole, either electric or magnetic. The results lie close to the predictions for pure magnetic-dipole transitions, but they can be equally well explained by assuming a mixture of from 88 % to 95 % electric-dipole with 12 % to 5 % electric-quadrupole

† Now at Aktiebolaget Atomenergi, Stockholm Ö, Sweden.

†† Research supported by the joint program of the Office of Naval Research, the U. S. Atomic Energy Commission, and the U. S. Air Force Office of Scientific Research.

intensity. Because the theoretical explanations of the giant resonance are made in terms of electric-dipole transitions, the latter explanation is preferred.

The experiment of Brown and Wilson [3]), however, showed that the one heavy element studied, Ta^{181}, had a larger cross section for electron-induced neutron emission that is predicted by the "reasonable" mixture of electric dipole and quadrupole transitions given above. A quadrupole intensity of about 50 % would be required to give agreement with the theory. Brown and Wilson thought this unlikely, and suggested that approximations in the theory were not sufficiently valid for nuclei of high atomic number. A possible alternative explanation for the enhanced electrodisintegration is the occurrence of electric monopole transitions. Danos [7]) has shown that on the basis of certain hydrodynamical models of the giant dipole resonance, a large monopole resonance should be expected. He calculated the energy at the monopole resonance maximum to be about twice that of the dipole, which is about 14 MeV in heavy nuclei. The monopole resonance might be very broad and thus participate in disintegrations in which a single neutron is emitted.

We have studied the electrodisintegration of Ta and Au with two goals in mind: first, to see whether the enhanced electrodisintegration observed in Ta^{181} also occurs in another heavy nucleus; second, to look for the effects of a monopole resonance. With regard to the second aim, we have studied reactions in which two and three neutrons are emitted, because if the resonance is at about twice the energy of the dipole one, the emission of more than one neutron would be most likely.

The comparison of electron and photon induced reactions does not necessarily require the measurement of the entire yield curve. Some knowledge of the photon cross section as a function of energy, however, is required in making necessary corrections to the data and in interpreting the significance of the results. For this reason we have tried to measure enough points on the yield curves to derive photon cross sections sufficiently accurate for this purpose. We did not have the time or the intention to measure precise yield curves which could be analyzed to give cross-section shapes in detail.

In addition to the yield curves, we measured the relative yield of 180-d Au^{195} from Au^{197} by electrons and by bremsstrahlung at a single primary electron energy of 38 MeV.

2. Experimental Details

As an experimental method for comparing the electro-, and photodisintegration cross sections, we have used the three-foil stack first described by Brown and Wilson [3]). In this method an electron beam of well-defined energy strikes first a target foil to be activated, then a radiator whose function is the production of a known bremsstrahlung spectrum, and finally another target foil as nearly as possible identical to the first. The foil thicknesses are chosen

such that the activity N_1 in the first is primarily the result of electrodisintegration, while that of the third, N_2, is caused by electrodisintegration and photodisintegration in approximately equal amounts. If the foils were of infintesimal thickness, the ratio $N_1/(N_2-N_1)$ would give directly the relative electro- to photodisintegration yields. In practice, the foil thinness is limited by counting statistics, and a compromise must be made such that corrections for electron loss and energy degredations result in errors comparable to those from other sources. In correcting for the effects of finite foil thickness we have used the methods described by Barber [6]).

The electron beam was provided by the Stanford 45-MeV linear accelerator and its double-deflection energy-analyzing system [8]). Because the cross section for an electron to produce a reaction is of the order of α times the cross section for the photoproduction of the reaction, it is important that the number of unknown photons accompanying the electron beam be very small. This was achieved by making certain that the beam did not strike matter during its second deflection or during its subsequent transmission through a one-meter shielding wall and a two-meter flight path to the target area. The energy calibration of the system was made to an accuracy of 2 % by stuyding the elastic scattering of the emergent electrons by means of a magnetic spectrometer which was calibrated with a Cm^{244} source of 5.80-MeV α particles. The energy-analyzed electron beam passed successively through a secondary-emission monitor [9]) ("SEM"), a thin vacuum window, and the target foil stack. The Ta target foils were nominally 20.3 mg/cm^2 or 0.320×10^{-2} radiation length. The Au targets were 50 mg/cm^2 or 0.84×10^{-2} radiation length. For all experiments the radiator was 172 mg/cm^2 of Ta, or 2.71×10^{-2} radiation length. The foils of the SEM and the vacuum window made a total of 8.2×10^{-4} radiation length of aluminium in the beam directly upstream from the foil stack.

The response of the SEM as a function of the beam energy had been tested previously by comparing it with a Faraday cup [10]). It was found to yield 0.0353 ± 0.0005 secondary per primary electron independent of primary energy in the range 15—37 MeV. The data were analyzed assuming the energy-independent response continued to 42 MeV. For each bombardment the integrated secondary-emission current was recorded. For those cases where the total bombardment time was comparable with the half-life of the reaction under study, the integrated current was recorded at short periodic intervals so that corrections for the decay during bombardments, which were not necessarily uniform in time, could be made.

The activities of the foil paris were measured in two NaI scintillation counters equipped with integral pulse-height discriminators. For each bombardment, a counting program was employed to follow the decay curves of the foils so that a separation of the desired activity from the total activity could be made by the analysis of the decay curves into their components. Counting measurements

were made in alternate pairs with foils interchanged on the counters so that no systematic error in determining the relative activities of the front and back foils could result from the two counters having different efficiencies. The discriminator biases were set to emphasize the activity under study. No attempt was made to determine the relative yields of different reactions. For the study of the Au activities, the NaI crystals were 2.54 cm in diameter and 0.63 cm thick. For the Ta studies, the crystals were 3.8 cm square and 1 mm thick.

3. Results and Comparison with Theory

Yield curves of the five different radioactivities resulting from bremsstrahlung are shown in figs. 1 and 2. This activity was obtained from a corrected

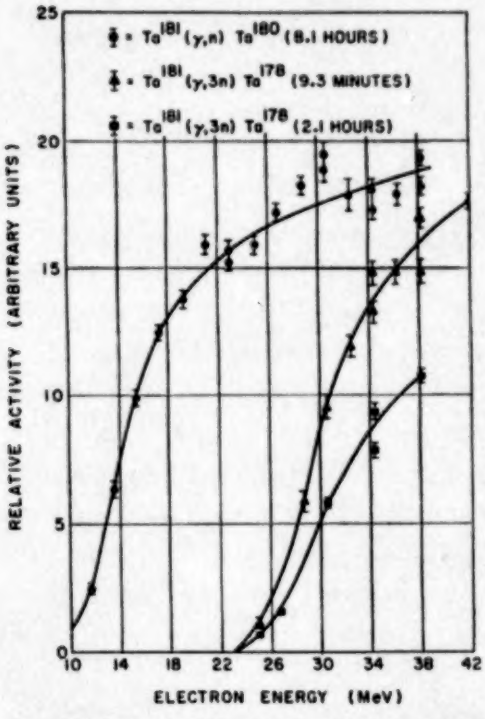
Ta181 (γ,n) Ta180 (8.1 HOURS)
Ta181 (γ,3n) Ta178 (9.3 MINUTES)
Ta181 (γ,3n) Ta178 (2.1 HOURS)
RELATIVE ACTIVITY (ARBITRARY UNITS)
ELECTRON ENERGY (MeV)

Fig. 1. Yield of Ta radioactivities resulting from the real bremsstrahlung of electrons as a function of the electron energy.

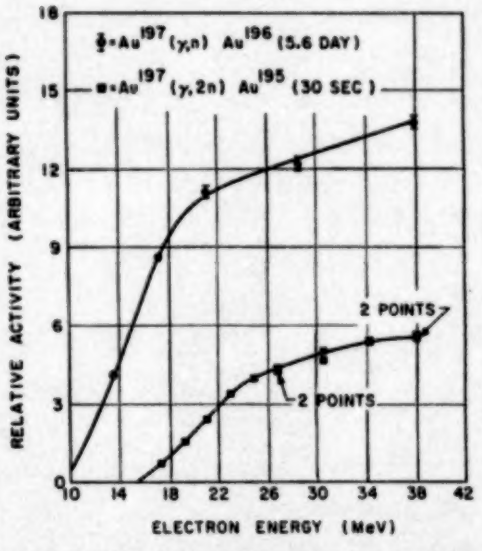

Fig. 2. Yield of Au radioactivities resulting from the real bremsstrahlung of electrons as a funtion of the electron energy.

difference in activity of the last and first target foils. The corrections were made by the method outlined in ref. [6]), and the quantities plotted in figs. 1 and 2 are the N_γ given by eq. (A-2) of ref. [6]).

The errors indicated in figs. 1 and 2 are a statistical combination of estimated errors incurred in separating the decay curves of the two target foils into constituent activities with those errors resulting from the corrections. The calculated energy losses of the electrons from ionization and radiation in traversing the foils were estimated to have errors of 10 %. Possible errors in beam

monitoring and electron energy determination, which would have only a small effect on the results, were not included.

Photon cross sections derived from the yield curves of figs. 1 and 2 by the method of Penfold and Leiss [11]) are shown in figs. 3 and 4. The histograms were

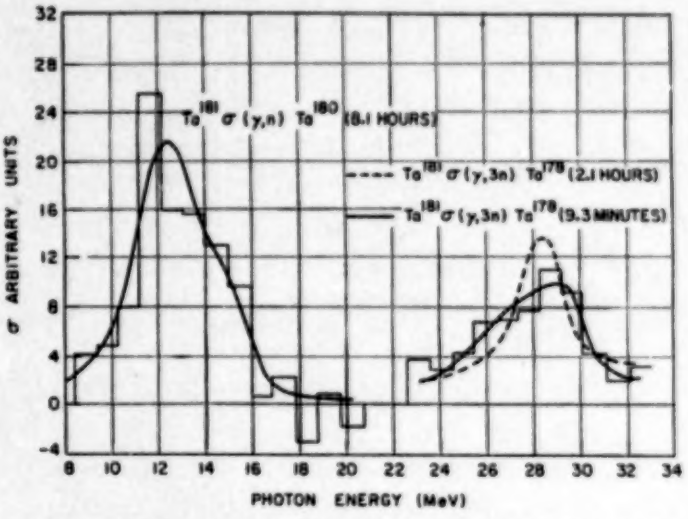

Fig. 3. Cross sections for Ta derived from the yield curves of fig. 1. The relative magnitudes of the cross section for the different reactions were drawn arbitrarily.

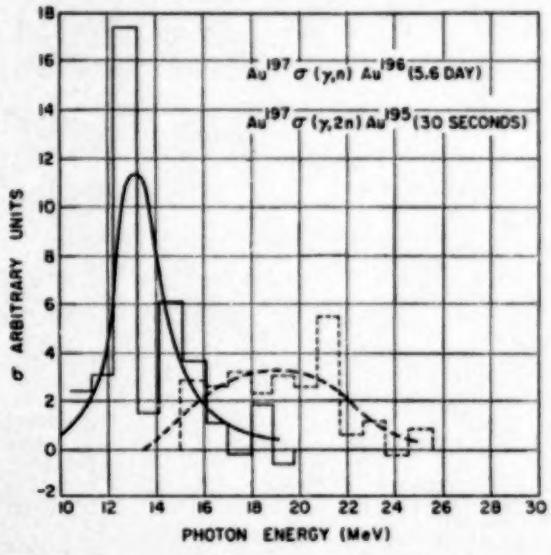

Fig. 4. Cross sections for Au derived from the yield curves of fig. 2. The relative magnitudes of the cross sections for the two reactions were drawn arbitrarily.

obtained by reading values from the smooth curves which were drawn by eye through the measured points in figs. 1 and 2. The smooth cross section curves were obtained by smoothing the running integral of the histograms, a method suggested by Penfold and Leiss [11]). The process of drawing a smooth curve through the measured yield points is so subjective that the resulting cross section curves are to be regarded as approximations. From the shape of the

yield points it is clear that the cross sections rise and then fall again. The mean energy of the cross-section curves should be correct to about 1 MeV, and in cases where other measurements are available, Ta(γ, n)[12, 13]) and Au(γ, n) [14]), we find agreement to this accuracy. The widths of the cross-section curves are probably uncertain by a factor of about 2, and therefore the difference between the cross sections shown in fig. 3 for the formation of the two isomers of Ta^{178} is probably not significant. Any conclusion about the higher moments of the curves is impossible from our data. Fortunately, the analysis of the relative electro- to photodisintegration results does not depend on detailed knowledge of the cross-section shape. This is illustrated by a comparison of the analyses of the results for the two isomers of Ta^{178}.

The experimental quantity X_e, which is plotted in figs. 5—7, is given by

$$X_e = (N_e/N_\gamma)(t/1.07), \tag{1}$$

where N_γ is the quantity plotted in figs. 1 and 2, t is the number of radiation lengths of Ta in the radiator effective in producing N_γ, N_e is the activity produced by the direct effect of electrons in the first foil, and the constant 1.07 is an empirically determined correction [15]) to take into account that the radiation length in Ta is longer than that given by the Bethe-Heitler formula. The method of obtaining N_e as well as N_γ is given in the appendix of ref. [6]). The calculation of the single value of X_e shown in fig. 7 for the 180-day isomer of Au^{195}, was made from measurement after a single long bombardment of a foil stack. The corrections were made on the assumption that the yield curve for the 180-day isomer has the same shape as the one for the 30-second isomer of Au^{195}. The value of X_e for the 5.6-day Au^{196} as obtained from that long bombardment agreed with values obtained in other bombardments.

In some previous papers [3, 6]) the results of electrodisintegration experiments have been given in terms of a quantity F which is related to X_e by the equation

$$F = \frac{4}{137}\,\frac{\ln(183Z^{-\frac{1}{3}})}{X_e}, \tag{2}$$

where Z is the atomic number of the radiator. In our case the radiator has $Z = 73$, and

$$F = 0.1105/X_e. \tag{3}$$

In calculating t and in deriving the relation between X_e and F, we have made use of the expression

$$[4\alpha Z(Z+1)r_0^2 \ln(183\,Z^{-\frac{1}{3}})]^{-1} \tag{4}$$

for the number of atoms per cm^2 in one radiation length. In expression (4), r_0 is the classical electron radius, α is the fine structure constant, and the term linear in Z comes from the assumption that each atomic electron produces the same radiation as a nucleus with $Z = 1$.

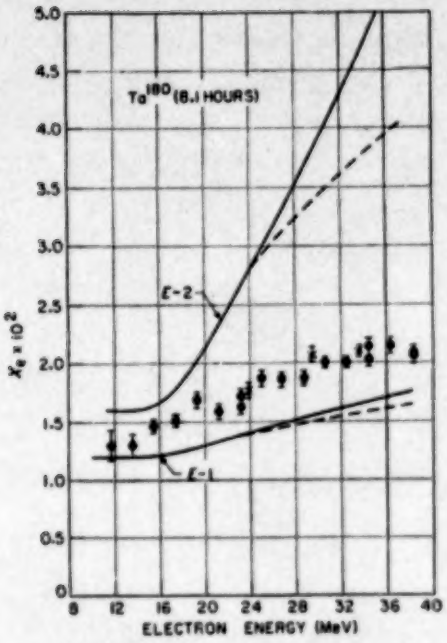

Fig. 5. Ratio of the yields of Ta^{180} from the electrodisintegration of Ta^{181} to those from the photodisintegration as a function of electron energy. The ordinate X_e is the radiation length equivalent of the electrodisintegration. The circles with standard errors indicated are the results of the experiment. The crosses are from the experiment of Brown and Wilson [3]). The theoretical ratios for a point nucleus are shown as solid curves. The dashed curves indicate an approximate correction for the nuclear size.

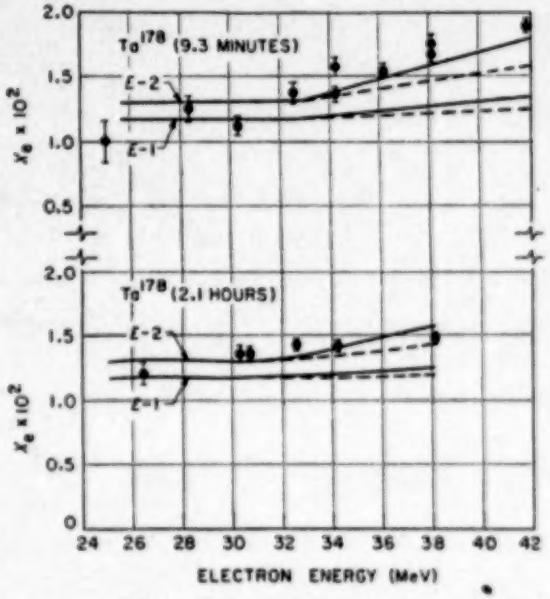

Fig. 6. The radiation length equivalent of the electrodisintegration yields of the two isomers of Ta^{178} produced from Ta^{181} as a function of electron energy. The circles with standard errors indicated are the results of the experiment. The theoretical values of X_e for a point nucleus are shown as solid curves. The dashed curves indicate an approximate correction for the nuclear size.

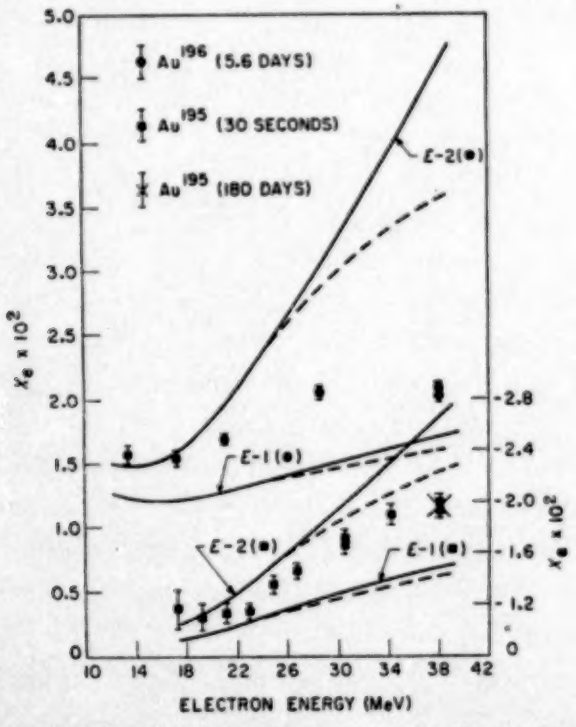

Fig. 7. The radiation length equivalent of the electrodisintegration yields of Au^{196} (ordinate scale on the left margin) and Au^{195} (ordinate scale on the right margin) produced from Au^{197} as a function of electron energy. The circles are the experimental results. Theoretical results for a point nucleus are shown as solid curves. The dashed curves indicate an approximate correction for the nuclear size.

The curves in figs. 5, 6 and 7 are the theoretically expected values of X_e for the cases that the photo-cross sections are entirely electric dipole (curves labelled E—1) or entirely electric quadrupole (curves labelled E—2). Curves for the magnetic dipole case would coincide with the corresponding electric dipole ones at the reaction threshold and would be about 15 % higher at 40 MeV. To show them would only add confusion to the figures.

The solid curves, which are valid in cases when the nuclear radius is small compared with the wave length associated with the momentum transferred to the nucleus by the electron in the excitation process, were calculated by numerical integration of the equation

$$[X_e(E_0, l)]_{\text{theor.}} = \frac{\int_0^{E_0} \sigma(k_f) N(E_0, k_f, l)(\mathrm{d}k_f/k_f)}{\eta \int_0^{E_0} \sigma(k_f)\varphi(E_0, k_f)(\mathrm{d}k_f/k_f)}. \tag{5}$$

In eq. (5), $\sigma(k_f)$ is the cross section for producing the reaction in question by photons of energy k_f; $\varphi(E_0, k_f)(\mathrm{d}k_f/k_f)$ is the bremsstrahlung cross section for electrons of energy E_0 to produce photons of energy k_f in the interval $\mathrm{d}k_f$ (we have used the Bethe-Heitler formula with intermediate screening to calculate φ); η is the number of atoms/cm^2 in one radiation length of the material producing the bremsstrahlung; and $N(E_0, k_f, l)$ can be regarded as the intensity spectrum of virtual photons of energy k_f and multipole order specified by l accompanying electrons of energy E_0.

For the case of a point nucleus,

$$N(E_0, k_f, l) = \frac{\alpha}{\pi}\left\{\left[1+\left(\frac{E_0-k_f}{E_0}\right)^2\right]\ln\frac{2E_0(E_0-k_f)}{m_0 k_f} - C(l)\right\}, \tag{6}$$

where m_0 is the rest energy of the electron; $C(l) \equiv 2(E_0-k_f)/E_0$ for electric-dipole transitions, $C(l) \equiv 0$ for magnetic-dipole transitions, and $C(l) \equiv -\frac{8}{3}(E_0-k_f)^2/k_f^2$ for electric-quadrupole transitions.

Dalitz and Yennie [2]) discuss the origin and validity of eq. (6). In particular, they consider cases when the nucleus can no longer be treated as a point. Without wave functions describing the initial and final nuclear states, it appears impossible to treat this case in a quantitative way. An approximate method for modifying the virtual photon theory for cases when the nuclear size is not negligible has been outlined by Barber [6]). We have used this method to calculate corrections to the theoretical curves for X_e; and the corrected results, where they deviate from the original point nucleus results, are indicated by dashed curves in figs. 5, 6 and 7 Although the correction terms could be wrong in magnitude by a factor of two or more, they serve to indicate the region of validity of the point theory and the general way in which electrodisintegration cross sections are reduced by the nuclear size. For the convenience of others

wishing to make calculations of this type, the equations for the corrections are given in the Appendix.

4. Discussion

For all reactions studied, the experimental values of X_e are rather consistently higher than the theoretical electric-dipole curves. The similarity of the results for two different elements and for a variety of reactions suggests that we are dealing with a rather general property of heavy nuclei and not an accident (for example, a special relation between the spin of the target nucleus and that of the residual radioactive nucleus). Since the effects of nuclear size can only reduce the expected value of X_e, they cannot be used to reconcile the disagreement.

For the reactions in which only one neutron is emitted (figs. 5 and 7), the experimental points lie nearly parallel to the dipole curve and show no evidence for the rapid rise with E_0 so characteristic of the electric-quadrupole curves. This rise, however, is reduced by the nuclear size correction, and if the correction were two or three times larger than we have estimated, it would be possible to fit the data by assuming a mixture of electric dipole and quadrupole transitions. The quadrupole intensity, however, would have to be about equal to the dipole in the case of Ta and even higher in the case of Au.

Since the (γ—n) reaction in heavy nuclei amounts to the major portion of the electric-dipole sum rule, such a large quadrupole intensity would be in disagreement with theoretical estimates [16]). Because the expected values of X_e for magnetic-dipole transitions are only slightly higher than those for electric-dipole transitions, agreement with experiment is not greatly affected by exchanging electric for magnetic dipole intensity. No problem is alleviated by this exchange because strong magnetic-dipole absorption is as difficult to explain as strong electric-quadrupole absorption. Agreement between experiment and theory can also be obtained by postulating a mixture of electric monopole and electric dipole transitions. In this case the cross section for the electron to produce monopole transitions would have to be 25 % or 30 % of that for dipole transitions.

Although there is no direct experimental evidence ruling against strong electric monopole and quadrupole transitions in the giant resonance region of heavy nuclei, their existence is unlikely from theoretical considerations. As an alternative to large amounts of exotic transitions, we should consider the possibility that the electrodisintegration theory is in error. The theory assumes plane-wave functions for the initial and final electrons and calculates the result only to the lowest order in α. These approximations will almost certainly lead to errors which increase as the atomic number of the nucleus increases. An important question is whether the errors in the case of heavy nuclei can be as

large as 20 % or 30 % and thus permit an interpretation of the experimental results in terms of electric dipole transitions alone.

For those reactions in which two or three neutrons are emitted, the E2 theoretical curves fit the experimental points better than the E1 curves. If a mixture of E1 and E2 transitions is assumed to explain the results, the required E2 intensity would be about 75 % of the total for the 2n reaction and about 100 % of the total for the 3n reactions. A mixture of about 30 % electric monopole intensity with 70 % electric dipole would also give agreement between experiment and theory.

Again, it should be noted that a 20 % or 30 % error in the theory would allow the results to be consistent with electric dipole absorption alone. An investigation of the validity of the theory will be required before any firm quantititative conclusions can be drawn from electrodisintegration experiments in heavy elements.

We should like to thank Mr. Robert Poe and Mr. William R. Dodge for aiding us in the analysis of the data and for assisting with the foil bombardments. One of us, T. Wiedling, wishes to acknowledge the support of the Swedish Atomic Energy Commission and the Alfred P. Sloan Foundation which made a stay at Stanford possible, and to thank Prof. W. K. H. Panofsky for his hospitality in making the facilities of the High-Energy Physics Laboratory available.

Appendix

APPROXIMATE CORRECTION TO THE VIRTUAL PHOTON THEORY FOR CASES WHEN THE NUCLEUS CANNOT BE TREATED AS A POINT

In calculating the virtual photon spectra, Dalitz and Yennie [2]) consider separately the contributions of the matrix elements transverse and longitudinal to the direction of the momentum transferred to the nucleus. Their result (eq. (1.5) of reference [2])) is

$$N(p, k_t) = N^t(p, k_t) + N^l(p, k_t), \tag{A-1}$$

where

$$N^t(p, k_t) = \frac{\alpha}{\pi} \int_{(p-p')^2}^{(p+p')^2} \frac{k_t^2 \mathrm{d}(k^2)}{(k_0^2 - k^2)^2} \times \left\{ \frac{[(p+p')^2 - k^2][k^2 - (p-p')^2]}{4p^2 k^2} + \frac{k^2 - k_0^2}{2p^2} \right\} \frac{\langle J_t^2(k^2) \rangle}{\langle J_t^2(k_t^2) \rangle}, \tag{A-2}$$

and

$$N^l(p, k_t) = \frac{\alpha}{\pi} \int_{(p-p')^2}^{(p+p')^2} \frac{k_t^2 \mathrm{d}(k^2)}{4k_0^2 p^2} \left[\frac{(p+p')^2}{k^2} - 1 \right] \frac{\langle J_l^2(k^2) \rangle}{\langle J_t^2(k_t^2) \rangle}. \tag{A-3}$$

The new symbols employed here are defined as follows: p and p' are the magnitudes of the electron's moment before and after scattering; k_0 and k are the energy and magnitude of the momentum transferred to the nucleus; the units are

such that $\hbar = c = 1$; k is related to the electron scattering angle θ by $k^2 = p^2+p'^2-2pp'\cos\theta$; $\langle J_t^2\rangle$ and $\langle J_l^2\rangle$ are the squares of those parts of the matrix element transverse and longitudinal to the direction of the momentum transfer. For a point nucleus the matrix element components have the values shown in table 1.

TABLE 1

Values of the ratios of the matrix elements for transitions of various multipole order when the nucleus is treated as a point

Type of transition	$\dfrac{\langle J_t^2(k^2)\rangle}{\langle J_t^2(k_f^2)\rangle}$	$\dfrac{\langle J_l^2(k^2)\rangle}{\langle J_t^2(k_f^2)\rangle}$
E1	1	1
M1	k^2/k_f^2	0
E2	k^2/k_f^2	$4k^2/3k_f^2$

Integration of eq. (A-2) and (A-3) with the values from table 1 inserted, results in the values given in table 2. In the extreme relativistic approximation that $E_0 = p$ and $E = p'$ the sum of N^t and N^l is given by eq. (6).

TABLE 2

Values of N^t and N^l for three different transitions, obtained on the assumption that kr is small compared with unity

Type of transition	N^t	N^l
E1	$\dfrac{\alpha}{\pi}\left[\dfrac{E_0^2+E^2}{p^2}\ln\dfrac{E_0E+pp'+m_0^2}{m_0(E_0-E)} - \dfrac{(E_0+E)^2}{2p^2}\ln\dfrac{p+p'}{p-p'} - \dfrac{p'}{p}\right]$	$\dfrac{\alpha}{\pi}\left[\dfrac{(E_0+E)^2}{2p^2}\ln\dfrac{p+p'}{p-p'} - \dfrac{p'}{p}\right]$
M1	$\dfrac{\alpha}{\pi}\dfrac{E_0^2+E^2}{p^2}\ln\dfrac{E_0E+pp'+m_0^2}{m_0(E_0-E)}$	0
E2	(same as M1 above)	$\dfrac{8\alpha}{3\pi}\dfrac{p'^2}{(E_0-E)^2}$

In ref. [6]) it is shown that the lowest order correction for nuclear size to the matrix element ratios of table 1 is obtained by multiplying the values in this table by the factor

$$\frac{1-\frac{1}{3}k^2\langle r^2\rangle}{1-\frac{1}{3}k_f^2\langle r^2\rangle}.$$

If eqs. (A-2) and (A-3) are integrated using the corrected ratios of the matrix elements, the results of table 3 are obtained.

The expressions in table 3 are for a definite nuclear excitation energy k_f. To obtain the theoretically expected values of X_e the values of N_r (where $N_r = N_r^t+N_r^l$) should be multiplied by the cross section and integrated over

k_f as in eq. (5). Since the correction is only an approximation, we have made it by calculating the percentage difference between N and N_r for values of k_f equal to the mean of each of the cross-section curves of figs. 3 and 4. The solid curves of figs. 5, 6 and 7 were reduced by these percentages to give the dashed curves.

TABLE 3

Values of the virtual photon intensity after correction for nuclear size.

Type of transition	$N_r^t \times (1-\frac{1}{6}k_f^2\langle r^2\rangle)$	$N_r^l \times (1-\frac{1}{6}k_f^2\langle r^2\rangle$
E1	$N^t(\mathrm{E1})-\frac{1}{6}k_f^2\langle r^2\rangle N^t(\mathrm{M1})$	$N^l(\mathrm{E1})-\frac{1}{4}k_f^2\langle r^2\rangle N^l(\mathrm{E2})$
M1	$N^t(\mathrm{M1})-\frac{\alpha}{3\pi}k_0^2\langle r^2\rangle\left\{\frac{2E_0E}{k_0^2}\left[1+\left(\frac{E}{E_0}\right)^2+\frac{E}{E_0}\right]+\left[1+\left(\frac{E}{E_0}\right)^2\right]\ln\frac{2EE_0}{m_0k_0}\right\}$	0
E2	(same as in M1 above)	$N^l(\mathrm{E2})-\frac{8\alpha}{9\pi}E_0^2\frac{\langle r^2\rangle}{k_0^2}E^2\cdot\left[1+\left(\frac{E}{E_0}\right)^2-\frac{2E}{3E_0}\right]$

The corrected values of the transverse and longitudinal parts, denoted by N_r^t and N_r^l respectively, are given in terms of the point values listed in table 2. The approximations that $E_0 = p$ and $E = p' \gg m_0$ have been used to simplify the expressions.

The values of $\langle r^2\rangle$ used in the calculations were $(5.5\times10^{-13}\,\mathrm{cm})^2$ for Ta and $(5.3\times10^{-13}\,\mathrm{cm})^2$ for Au, which are the values obtained from elastic electron scattering [17]). Since the nuclear recoil energy is small, we have assumed $k_0 = k_f$ in all calculations.

References

1) C. F. von Weizsäcker, Z. Physik **88** (1934) 612;
E. J. Williams, Mat. Fys. Medd. Dan. Vid. Selsk. **13**, No. 4 (1935)
2) R. H. Dalitz and D. R. Yennie, Phys. Rev. **105** (1957) 1598
3) K. L. Brown and R. Wilson, Phys. Rev. **93** (1954) 443
4) Scott, Hanson and Kerst, Phys. Rev. **100** (1956) 209
5) R. L. Hines, Phys. Rev. **105** (1957) 1534
6) W. C. Barber, Phys. Rev. **111** (1958) 1642
7) M. Danos, Nuclear Physics **5** (1958) 23
8) K. L. Brown, Rev. Sci. Instr. **27** (1956) 959
9) G. W. Tautfest and H. R. Fechter, Rev. Sci. Instr. **26** (1955) 229
10) W. C. Barber and V. J. Vanhuyse, Nuclear Physics **16** (1960) 381
11) A. S. Penfold and J. E. Leiss, Analysis of photo cross sections, University of Illinois Physics Research Laboratory report, May 1958 (unpublished)
12) Johns, Katz, Douglas and Haslam, Phys. Rev. **80** (1950) 1062
13) E. A. Whalin and A. O. Hanson, Phys. Rev. **89** (1953) 324
14) R. Nathans and J. Halpern, Phys. Rev. **93** (1954) 437
15) Barber, Berman, Brown and George, Phys. Rev. **99** (1955) 59
16) J. S. Levinger and H. A. Bethe, Phys. Rev. **78** (1950) 115
17) R. Hofstadter, Annual Rev. Nuc. Sci. **7** (1957) 231

1.E.2:5 *Nuclear Physics* **18** (1960) 587—595; © *North-Holland Publishing Co., Amsterdam*
Not to be reproduced by photoprint or microfilm without written permission from the publisher

ENERGIES OF ALPHA PARTICLES

AALDERT H. WAPSTRA

Instituut voor Kernphysisch Onderzoek, Amsterdam; Technical University, Delft †

Received 24 May 1960

Abstract: Energies of alpha particles emitted in ground-state transitions between nuclei with mass < 200 have been computed from experimental data obtained with magnetic spectrometers using the newest calibration results.

1. Introduction

Energies of alpha particle lines are measured most accurately by their deflection in magnetic fields. Such measurements have been made by groups in Paris [1–13]), Sydney [14, 15]), Cambridge [16, 17]), Birmingham [18]), Berkeley [19–34]) and Moscow [35, 36]); many of these results have been revised recently by Briggs [37]) and discussed by Hanna [38]). The most accurate data obtained in these measurements are ratios of $B\rho$-values; measurements of absolute $B\rho$-values are somewhat less accurate.

Measurements made before 1940 agreed rather well in most cases and were reported to give $B\rho$-values with a precision of about 0.005 %. Birmingham measurements in 1953, however, indicated that the earlier measurements were low by about 0.05 %. This discrepancy is important, among others, since natural alpha rays are used for calibration in nuclear reaction measurements, which are in their turn used to compute nuclear binding energies or mass excesses [39]). An error of 0.05 % in these $B\rho$-values therefore introduces a systematic error of 0.1 % in these data.

Recently, the energy of ^{210}Po alpha rays was remeasured by White *et al.* [40]) using the ingenious device of comparing their deflection with those of Lu ions accelerated through a well-defined potential difference. This experiment confirmed the Birmingham results. Accepting these results, it is necessary to revise earlier compilations of alpha particle energies and of nuclear reaction energies based on these energies for calibration. The first part of this work will be described in this paper for all alpha particle energies of ground state transitions in nuclei with masses above 200 measured in magnetic spectrometers.

2. The Th and Ra Series

The greatest accuracy is claimed for some measurements of ratios of velocities of alpha particles emitted by a few nucleides in the Th and Ra series to that of

† An important part of this work was done during a stay at Argonne National Laboratory, Lemont, Illinois.

the ground state alpha particles of RaC', made by Briggs [14]) and by the Cambridge group [16, 17]) in 1932 to 1934. These values were essentially computed from $B\rho$-ratios, making relativistic corrections. Since nowadays $B\rho$-values are preferred above velocities we reconverted to $B\rho$-values using second order corrections only,

$$B\rho \approx v(1+\tfrac{1}{2}v^2/c^2),$$

which is sufficient in all cases. The results are shown in table 1.

The accuracy claimed for the $B\rho$-values or velocities given by the French groups [4–9, 12]) is 0.05 to 0.1 %; ratios of $B\rho$-values computed from these results are probably somewhat more precise. They are also given in table 1, together with a few results from Birmingham [18]), Berkeley [19, 22, 34]) and Wisconsin [41]); the last results are derived from measurements with an electrostatic analyzer.

The Birmingham measurements did not include RaC'; the values given in the table were obtained by adopting a $B\rho$-value for RaC' so that in the average the $B\rho$-ratios with this value agree with the other results.

Table 1 shows that in most cases the results of the different groups agree. However, Briggs's values for Rn and RaA are somewhat higher than the averages of the other results. Recently, Walen and Bastin [13]) found that, in order to get a smooth calibration curve for their alpha ray spectrometer, they had to adopt about 8 keV higher energies for Tn and ThA as compared with Ra, Rn, RaA and RdTh than would follow from the "currently adopted" (essentially Briggs's) results; presumably better agreement could also be obtained by decreasing the Rn and RaA energies by similar amounts. Now, the first change appears rather unlikely: three experimental values for the $B\rho/B\rho$(RaC') values of both Tn and ThA in table 1 agree within one part in 5000, and the only value deviating more than this (for Tn) is even lower than the others. The only argument against the alternative change is that a Tn/^{210}Po comparison via ^{241}Am [19]) yields a result for Tn which is even slightly higher than Briggs's value. The ^{241}Am alpha energies in this early Berkeley work disagreed, however, considerably with Russian and with later Berkeley results (see below), which makes the Tn-^{210}Po comparison somewhat uncertain too. We will therefore not include Briggs's Rn and RaA value in our present calculations.

In other cases, too, Brigg's estimate of his errors may very well be somewhat optimistic. As argued elsewhere [42]) one should really have strong reasons for accepting errors smaller than about $\frac{1}{20}$ of the line halfwidths. Briggs, however, reports errors which are an order of magnitude smaller; in view of the discrepancy for Rn and RaA, these errors can hardly be accepted. As a compromise, we have rather arbitrarily assigned errors of one part in 10^4 to his $B\rho$-ratios in the Th-series. The final $B\rho$-ratios accepted here are given in the last column of table 1.

Absolute $B\rho$-values for ^{210}Po derived from various absolute measurements

TABLE 1

$B\rho$-Ratios in the Th and Ra series

		Earlier values					Adopted value
^{228}Th	RdTh	0.83985±40 [7]),	0.84013±40 [6]),			0.83999±10 [22a])	0.83999±15
^{224}Ra	ThX	0.85989±40 [7]),		0.85996 ± 3 [14]),	0.85967±50 [12])		0.85996±10
^{220}Em	Tn	0.90440±40 [7]),		0.90430 ± 3 [14]),	0.90393±50 [12]),	0.90434 [36a])	0.90430±10
^{216}Po	ThA	0.93903±50 [7]),		0.93912 ± 3 [14]),		0.93920 [36a])	0.93912±10
^{212}Bi	ThCα_1	0.89011±90 [4]),	0.88977± 3 [17]),	0.88981 ± 5 [16d]),	0.88984±20 [18])		0.88978± 5
	α_0	0.88730±40 [5]),	0.88688± 3 [17]),	0.88693 ± 5 [16d]),	0.88691±20 [18])		0.88690± 5
^{212}Po	ThC′	1.06925±50 [5]),	1.06901± 5 [17]),	1.06903 ± 3 [14]),	1.06896±25 [18])		1.06902± 5
^{230}Th	Io	0.78089±40 [9])					0.78089±40
^{226}Ra	Ra	0.78880±80 [3]),			0.78848±30 [12]),	0.78857±20 [34b])	0.78855±20
^{222}Em	Rn	0.84405±80 [3]),	0.84430±17 [17]),	(0.84503$_7$± 1$_6$ [14])),	0.84465±50 [12]),	(0.88524±25 [19c]))	0.84430±17
^{218}Po	RaA	0.88334±40 [5]),	0.88332±18 [17]),	(0.88364$_7$± 1$_1$ [14])),	0.88340±50 [12])		0.88333±17
^{214}Bi	RaC		0.84651±17 [17])				0.84651±17
^{214}Po	RaC′	1	1	1	1	1	1
^{210}Po	Po	0.83044±40 [5]),	0.83047±17 [17]),	0.83030 ±20 [41]),	0.83042±20 [18]),	0.83039±14 [36a])	0.83040±10

Values given in parentheses have not been used in determining the adopted values, for reasons given in the text of this paper. The letters added to the reference numbers refer to the following notes:

[a]) combined with the adopted value of ThX; [b]) combined with the adopted value of ^{210}Po;

[c]) comparison with ^{210}Po via α_{40} in ^{241}Am; [d]) computed from the average of α_0 and α_1 [4]), an energy difference of 39.25 keV [45]) and an intensity ratio $\alpha_0/\alpha_1 = 2.57\pm0.01$ [17]).

using these ratios are collected in table 2. The agreement between the different values is not especially good. A least squares adjustment gives an average value of 331 720±50 G. cm; the ratio of external to internal errors is $R_e/R_i = 2.3$.

TABLE 2

Magnetic rigidity of ^{210}Po alpha particles, according to different authors (in G. cm)

Briggs	331560± 45
Rosenblum *et al.*	331620±200
Sturm *et al.*	331520±170
Collins *et al.*	331760± 60
White *et al.*	331790± 30
Mass adjustment	331710± 30

As mentioned before, the ^{210}Po alpha energy enters into the problem of computing nuclear masses from experimental data since in several nuclear reaction measurements this energy has been used for calibration. A least squares adjustment of all presently known data [43]) in which this calibration energy is used as a variable gives for it an output value which is considerably more accurate than the above average of the directly determined values. The input value for the calibration energy used in this computation differed slightly from the average result of the direct measurements computed above, mainly since at that time Agapkin and Goldin's comparison [36]) of ^{210}Po and ^{220}Em was not known to us; as a consequence, the result labelled "Briggs" in table 2, which is a combination of averaged $B\rho$-ratios and Briggs's absolute RaC′ measurement, was given somewhat less weight. It is, however, easy to compute the result that would have been obtained if no input value at all had been used for this ^{210}Po alpha energy; the resulting $B\rho$-value 331711±14 G. cm is independent of the more direct determinations.

In one respect, the error in the last value should be considered with some caution. All reaction energies used in its determination have been measured using targets with thicknesses corresponding to energy losses of a few to 10 keV for the incident particles; corrections for source thickness are made but are probably not more precise than to about 10 %. This introduces a systematic error in the reaction energies used in the least squares adjustment; the result does not invalidate this adjustment but it will cause a shift of about the same relative magnitude in the resulting ^{210}Po alpha energy. We have therefore to conclude that, due to this fact, there is an error of about 1 keV in the ^{210}Po alpha energy determined in this way.

Fortunately, the value found by this adjustment happens to coincide nearly with the average of the directly determined results. We therefore propose to

use, in computing the alpha energies [44]), a value

$$B\rho(^{210}\mathrm{Po}) = 331710 \pm 30 \text{ G. cm.}$$

Moreover we propose to determine the $B\rho$-value for RaC′ (^{214}Po) from this value and the average ^{210}Po/RaC′ ratio. This procedure is not without objection, since in fact the ^{210}Po value in table 2 labelled "Briggs" has been derived from an average ^{210}Po/RaC′ $B\rho$-ratio and his reportedly more accurate RaC′ determination. However, here again Briggs estimated his error to be considerably smaller than one would expect from his linewidth which, though not given in his paper, is certainly some parts in a thousand; moreover he reported that the line shape was not perfect. We therefore preferred the outlined procedure above accepting a ^{210}Po/RaC′ ratio about 40 parts in the last decimal place higher than the five quite consistent experimental results given in table 1.

3. The Ac Series

These nuclides have been measured by several French groups [1, 3]) and in Berkeley [30]). The results expressed as ratios of $B\rho$-values to that of α_0 in RdAc are given in table 3 for all ground state transition. The results of Rosenblum

TABLE 3

$B\rho$-ratios in the Ac series

		Earlier values			Adopted value
^{227}Ac	Ac		0.90524 [3])		0.90524 ± 40
^{227}Th	RdAc	1	1	1	1
^{223}Ra	AcX		0.98581 [3]),	0.98596 [30])	0.98590 ± 20
^{219}Em	An	1.06308 [1]),	1.06223 [3]),	1.06219 [30])	1.06221 ± 20
^{215}Po	AcA	1.10588 [1]),		1.10435 [30])	1.10475 ± 60
^{211}Bi	AcC	1.04714 [1]),		1.04707 [30])	1.04710 ± 20
^{211}Po	AcC′	1.01867 [1]), 1.11268 [1])		1.01950 [30])	1.01945 ± 20

et al. have probably the same precision as his other results (0.05 %); those of Curie and Rosenblum are not better than the precision of 0.1 % claimed for the absolute $B\rho$-values, as is shown by a comparison of all subgroups as measured by them with the later results. We estimated the errors in Pilger's measurements to be about 0.02 % except for AcA for which an error of 0.075 % is claimed. Within these estimated errors, the different results agree well. The last column in table 3 gives the adopted $B\rho$-ratios.

Absolute $B\rho$-values are derived from Rosenblum and Dupouy's measure-

ment [5]) of the AcC alpha groups and from Rosenblum *et al.*'s comparison [3]) between ThC α_0 and RdAc; the $B\rho$-values for RdAc found in combination with the magnetic rigidities for the Th and Ra series given in table 4 are

TABLE 4

Magnetic rigidities and alpha particle energies in ground state transitions
References are given only for material not treated in the other tables; errors given in parentheses are our estimates

	$B\rho$ (G. cm)	E (keV)	Ref.		$B\rho$ (G. cm)	E (keV)	Ref.
^{211}Bi	370670±120	6621 ± 4		^{224}Ra	343520± 70	5686_7± 2_3	
^{212}Bi	355430± 60	6087_6± 2_0		^{226}Ra	314990± 90	4782 ± 3	
^{214}Bi	338150± 90	5410_3± 2_8		^{225}Ac	347600±150	5822(± 5)	32, 33)
^{206}Po	329020±300	5219(±10)	34)	^{227}Ac	320450±170	4949 ± 5	
^{208}Po	325590±250	5109(± 8)	34)	^{228}Th	362530±300	6333 ±10	28)
^{209}Po	318110±250	4877(± 8)	34)	^{227}Th	354000±100	6039 ± 3	
^{210}Po	331710± 30	5302_8± 1_0		^{229}Th	335540± 90	5426_4± 2_7	
^{211}Po	393110±400	7445 ±15		^{230}Th	311930±160	4690 ± 5	
^{212}Po	427030± 70	8784_1± 2_8		^{231}Pa	323730±100	5051 ± 3	
^{213}Po	416410±250	8353 ±10	32)	^{230}U	349520±150	5887 ± 5	28)
^{214}Po	399460± 60	7687_6± 2_3		^{232}U	332340± 90	5323 ± 3	26)
^{215}Po	391080±250	7369 ±10		^{233}U	316230± 50	4819_7± 1_5	35)
^{216}Po	375140± 70	6780_8± 2_4		^{234}U	314670± 70	4772_3± 2_2	35)
^{218}Po	352850± 90	6000 ± 3		^{235}U	307550±500	4559 ±15	30)
^{209}At	342290±120	5646(± 4)	33)	^{237}Np	317880±100	4870 ± 3	35)
^{210}At	338530±120	5523(± 4)	31)	^{236}Pu	346000±150	5769 ± 5	38)
^{211}At	348870± 90	5865 ± 3	31)	^{238}Pu	337670± 60	5495 ± 2	
^{217}At	382600±300	7053 ±10	32)	^{239}Pu	326930± 60	5151 ± 2	
^{218}At	372640±110	6691 ± 4	38)	^{240}Pu	327320± 60	5163 ± 2	
^{208}Em	357070±120	6144 ± 4	29)	^{241}Pu	318630±160	4893 ± 5)	34)
^{209}Em	354040± 90	6040 ± 3	29)	^{242}Pu	318790±160	4898(± 5)	34)
^{210}Em	354040± 90	6040 ± 3	29)	^{241}Am	339240± 60	5546 ± 2	
^{211}Em	348420± 90	5850 ± 3	29)	^{243}Am	333190±200	5350 ± 7	23)
^{212}Em	360630±140	6267 ± 5	29)	^{242}Cm	356080±120	6110 ± 4	
^{218}Em	384690±250	7130 ±10	28)	^{243}Cm	354560±150	6058(± 5)	21)
^{219}Em	376020±120	6813 ± 5		^{244}Cm	346940± 60	5801 ± 2	40)
^{220}Em	361230± 70	6287_8± 2_3		^{246}Cf	374450±300	6756(±10)	25)
^{222}Em	337260± 90	5481_6± 2_7		^{249}Cf	358530±300	6194(±10)	24)
^{213}Fr	364840±250	6414 ± 9	29)	^{250}Cf	353740±150	6030 ± 5	27)
^{221}Fr	362560±300	6334 ±10	32)	^{252}Cf	356320±150	6118 ± 5	27)
^{222}Ra	368920±300	6558 ±10	28)	^{253}E	371220±300	6640 ±10	33, 34)
^{223}Ra	349010±120	5870 ± 4					

354200±160, 354160±160 and 353790±250 G. cm respectively. The energies given by the Berkeley group are obtained by comparison with ^{242}Cm for which isotope an energy of 6110 keV was adopted. This value was obtained by comparison with ^{218}Po [19]); using the above result for ^{218}Po, it changes to 6116±3 keV. A $^{242-244}$Cm comparison [21]) combined with a recent measurement on ^{244}Cm [40]), interpreted here as giving a $B\rho$-ratio for ^{244}Cm and ^{210}Po yields an

energy of 6112 keV; according to a private communication of Asaro lowering the ^{242}Cm—^{244}Cm difference to 308.3 keV it would become 6107.9 keV. The agreement between these values is not especially good. It should, however, be remarked that the first value comes from the same early paper [19]) giving the questionable results about ^{210}Po—^{241}Am—^{222}Em discussed in the preceding section; it may therefore perhaps be somewhat less dependable too. We therefor propose to retain unaltered the alpha energies based on the calibration ^{242}Cm = 6110±4 keV; then, the $B\rho$-value for RdAc resulting from Pilger's measurements is 353910±100 G. cm. As an average, we will use a value $B\rho$(RdAc) = 354000±100 G. cm in computing the results given in table 4.

There remains a problem with AcC'. Curie and Rosenblum's result [1]) given in table 4 corresponds with a $B\rho$-ratio AcC'/RaC' = 0.9859; however in a somewhat later measurement on AcC, AcC' and RaC' Rosenblum [2]) confirms the given AcC'/AcC ratio but gives a direct ratio AcC'/RaC' = 0.9844. In this case alone, available range measurements may still be more dependable than these magnetic spectrometer measurements; they give [17]) 0.9839. We have adopted for the $B\rho$-ratio AcC'/RaC' = 0.9841.

4. Other Nucleides

Measurements on other nucleides have been made in Berkeley, Paris and Moscow. Some Berkeley measurements (^{243}Cm, ^{244}Cm and, partly, ^{238}Cm) are calibrated with ^{242}Cm = 6110 keV; as explained in section 3, these results have been adopted without change. Results in which nuclei of the Ra or Th series were used for calibration have been corrected using the values obtained above. ^{241}Am was used for calibration in ^{239}Am, $^{208-212}$Em, $^{210-211}$At and partly in ^{209}At; since later Berkeley measurements on ^{241}Am (private communication) gave much better agreement with the Russian value than the original ones [19]), essentially the Russian value was adopted for this calibration energy.

TABLE 5

Some nuclei as measured by different groups (energies in keV)

	Berkeley	Paris	Moscow [33])
^{231}Pa	5051(±5) [23])	5042 [10])	5053 ±3
^{238}Pu	5495 ±3 [24])		5495_4±1_5
^{239}Pu	5151 ±3 [20])	5147 [11])	5151_7±1_0
^{240}Pu	5163 ±4 [20])		5163_2±1_0
^{241}Am	5540 ±3 [19a]) 5529 ±3 [19b])		5546_5±1_5

[a]) Comparison with ^{222}Em. [b]) Comparison with ^{210}Po.

The Moscow results are calibrated with ^{210}Po = 5298.4 keV; they have been corrected using the ^{210}Po alpha energy adopted above. The Paris ^{239}Pu result was obtained in comparison with ThC = 6089 keV; the calibration for the ^{231}Pa measurement is not given. Table 5 shows the cases measured by more than one group; the averages adopted for this work are given in table 4.

An important part of this work was done at the Argonne National Laboratory; I thank Dr. T. B. Novey and Dr. J. Huizenga for their interest. This work has benefited greatly from discussions with Dr. W. B. Lewis and Mr. G. C. Hanna in Chalk River. Dr. F. Asaro in Berkeley I thank for communication of several new results.

References

1) P. Curie and S. Rosenblum, J. Phys. Radium **2** (1931) 309; C. R. (Paris) **194** (1932) 1232
2) S. Rosenblum, C. R. (Paris) **193** (1931) 848
3) P. Curie and S. Rosenblum, C. R. (Paris) **196** (1933) 1958;
S. Rosenblum, M. Perey and M. Guillot, C. R. (Paris) **202** (1936) 1274; **202** (1937) 175;
S. Rosenblum, M. Perey, M. Valadares and M. Guillot, private communication to Hollander, Seaborg and Perlman, Rev. Mod. Phys. **25** (1953) 469
4) S. Rosenblum and M. Valadares, C. R. (Paris) **194** (1932) 967
5) S. Rosenblum and G. Dupouy, C. R. (Paris) **194** (1932) 1919
6) S. Rosenblum, C. R. (Paris) **195** (1932) 317
7) S. Rosenblum and C. Chamie, C. R. (Paris) **196** (1933) 1663
8) S. Rosenblum, M. Valadares and M. Perey, C. R. (Paris) **228** (1949) 385
9) S. Rosenblum, M. Valadares and J. Vial, C. R. (Paris) **227** (1948) 1088
10) S. Rosenblum, E. Cotton and G. Bouissieres, C. R. (Paris) **229** (1949) 825
11) S. Rosenblum, M. Valadares and M. Goldschmidt, C. R. (Paris) **230** (1950) 638
12) C. Bastin Scoffier and J. Sant'ana Dionisio, C. R. (Paris) **226** (1953) 1056
13) R. J. Walen and G. Bastin, Proc. Congr. Intern. de Phys. Nucl. 1958 (Dunod, Paris, 1959)
14) G. H. Briggs, Proc. Roy. Soc. A **139** (1932) 638, **143** (1932) 604
15) G. H. Briggs, Proc. Roy. Soc. A **157** (1936) 183
16) E. Rutherford, C. E. Wynn Williams, B. V. Bowden and W. B. Lewis, Proc. Roy. Soc. A **139** (1933) 617
17) W. B. Lewis and B. V. Bowden, Proc. Roy. Soc. A **145** (1934) 235
18) E. R. Collins, C. D. McKenzie and C. A. Ramm, Proc. Roy. Soc. A **216** (1953) 219
19) F. Asaro, F. L. Reynolds and I. Perlman, Phys. Rev. **87** (1952) 277
20) F. Asaro and I. Perlman, Phys. Rev. **88** (1952) 838
21) F. Asaro, S. G. Thompson and I. Perlman, Phys. Rev. **92** (1953) 694
22) F. Asaro, F. Stephens, Jr. and I. Perlman, Phys. Rev. **92** (1953) 1495
23) F. Asaro and I. Perlman, Phys. Rev. **93** (1954) 1423
24) F. Asaro and I. Perlman, Phys. Rev. **94** (1954) 381
25) J. P. Hummel, F. S. Stephens, Jr., F. Asaro, A. Chetham-Strode, Jr., and I. Perlman, Phys. Rev. **98** (1955) 22
26) F. Asaro and I. Perlman, Phys. Rev. **99** (1955) 37
27) F. Asaro, F. Stephens, Jr., B. G. Harvey and I. Perlman, Phys. Rev. **100** (1955) 137
28) F. Asaro and I. Perlman, Phys. Rev. **104** (1956) 91
29) F. E. Momeyer, Jr., F. Asaro and E. K. Hyde, J. Inorg. Nucl. Chem. **1** (1955) 267
30) R. C. Pilger, F. S. Stephens, Jr., F. Asaro and I. Perlman, Bulletin Amer. Phys. Soc. **2** (1957) 394;
R. C. Pilger, Jr., Thesis, University of California Radiation Laboratory, Unclassified Document UCRL 3877 (1957)

31) R. W. Hoff, Thesis, University of California, Radiation Laboratory, Unclassified Document UCRL 2325 (1953)
32) F. S. Stephens, Jr., Thesis, University of California, Radiation Laboratory, Unclassified Document UCRL 2970 (1955)
33) J. P. Hummel, Thesis, University of California, Radiation Laboratory, Unclassified Document UCRL 3456 (1956)
34) Unpublished Berkeley work mentioned in the review articles by Asaro and Perlman, Rev. Mod. Phys. **26** (1954) 456; **29** (1957) 831 and by Strominger, Hollander and Seaborg, Rev. Mod. Phys. **30** (1958)
35) L. L. Goldin, G. I. Novikova, L. K. Peker and E. E. Tretyakov, Conference At. Energy (Moskow, 1955) 226; Phys. Rev. **103** (1956) 1004; Uspekhi Fiz. Nauk. **59** (1956) 459
36) I. I. Agapkin and L. L. Goldin, Izwestia Akad. Sci. USSR Ser. **21** (1957) 7
37) G. H. Briggs, Rev. Mod. Phys. **26** (1954) 1
38) G. C. Hanna, in Experimental Nuclear Physics III (Segré)
39) A. H. Wapstra, Physica **21** (1955) 367
40) F. A. White, F. M. Rourke, J. C. Sheffield, R. P. Schuman and J. K. Huizenga, Phys. Rev. **109** (1958) 437
41) W. J. Sturm and V. Johnson, Phys. Rev. **83** (1951) 542
42) A. H. Wapstra, Proc. Conf. Nucl. Masses Mainz (1957) 260
43) F. Everling, L. Konig, J. Mattauch and A. H. Wapstra, Nuclear Physics **15** (1960) 342
44) A. H. Wapstra, G. J. Nijgh and R. van Lieshout, Tables for nuclear spectroscopy (North Holland Publishing Co., Amsterdam 1959)
45) K. Siegbahn and K. Edvarson, Nuclear Physics **1** (1956) 137

1.C:
1.E.3

Nuclear Physics **18** (1960) 596—614; © *North-Holland Publishing Co., Amsterdam*
Not to be reproduced by photoprint or microfilm without written permission from the publisher

INTRINSIC QUADRUPOLE MOMENTS OF DEFORMED NUCLEI AND SUPERFLUIDITY IN NUCLEI

NORMAN K. GLENDENNING and JERZY SAWICKI †

Lawrence Radiation Laboratory, University of California, Berkeley, California ††

Received 23 May 1960

Abstract: Intrinsic quadrupole moments of deformed nuclei are calculated on a completely particle picture as a function of the atomic number Z and the parameter of spheroidal distortion of the well in which the independent particles move. The effects of the pairing force responsible for the superfluid property of the existence of an energy gap are examined by using the Green's function method of Migdal. The deformation of the single-particle potential well is treated (a) as a perturbation and (b) exactly, by using the Nilsson and Mottelson-Nilsson energy spectra and wave functions. It is necessary to include the configuration mixing with the major harmonic-oscillator shells $N' = N \pm 2$ caused by the deformation. In order to account for the observed quadrupole moments, slightly smaller values of the Nilsson deformation parameter are required than those following from the uniform-charge model. The effect of the energy gap is to smear out the shell-closure effects. As a result, the dependence of quadrupole moments on Z is similar to that predicted by the uniform-charge model.

1. Introduction

Quadrupole moments of strongly deformed nuclei have been discussed invariably in terms of the uniformly charged spheroid [1]). The connection of the intrinsic quadrupole moment with the nuclear deformation is expressed through the well-known [2]) formula $Q_0 \approx 0.8\,\delta Z R^2(1+\frac{1}{2}\delta)$. Such a model ignores the particle structure of the nucleus. Since our knowledge of nuclear deformation rests principally on the above connection, it is important to ascertain the effects of the particle structure of nuclei on their quadrupole moments.

In this work we shall adopt a particle picture of the nucleus in calculating quadrupole moments. The Z protons of the nucleus are assumed to move in a deformed spheroidal well, and the interparticle interactions are approximated by the pairing force, introduced first to account for superfluidity by Bardeen, Cooper, and Schrieffer (BCS) [3]).

Recently the BCS theory of superfluidity of systems of fermions has been applied by a number of authors to study some properties of nuclear matter and finite nuclei [4–7]). In particular, the pairing force seems to explain the well-known energy gap in even nuclei, pairing energies and the moments of inertia of deformed nuclei.

† Also from the Department of Physics, University of California, Berkeley, Calif.

†† This work was performed under the auspices of the U. S. Atomic Energy Commission.

Gorkov, using Green's function techniques, has reproduced the results of the BCS theory [8]), and Migdal extended this phenomenological model to an arbitrary system of quasiparticles with particular attention to finite nuclei [9]). Migdal's method in certain applications appears to be more straightforward and practical than Belyaev's method of canonical transformations [5]). Higher-order corrections due to perturbation interactions can be conveniently calculated by the new method.

According to Gorkov, the BCS type of pairing correlation can be derived from a weak δ-function two-body potential. Such pairing correlations, in addition to introducing an energy gap into the single-particle excitation spectrum, seem to be of crucial importance in determining the intrinsic properties of finite nuclei associated with the nuclear surface and collective motion [5]).

In this paper, we describe the effects of the particle structure of nuclei on their quadrupole moments, and, in particular, investigate the role of interparticle interactions in the form of a pairing correlation.

In section 2, the necessary equations for computing the quadrupole moments are derived. The numerical results are given in section 3. Here tables are presented from which one can deduce the nuclear deformation implied in this particle picture by an experimental measurement of the intrinsic quadrupole moment. A discussion of the methods and results follows in section 4.

2. Calculation

2.1. THE SINGLE-PARTICLE DENSITY MATRIX

The expectation value of any operator $O = \sum_{i=1}^{A} O(\mathbf{r}_i, \mathbf{p}_i)$, which is a sum of single-particle operators over the particles of the system is

$$\langle O \rangle = \mathrm{Tr}\,(\rho O) = \sum \rho_{\nu\nu'} O_{\nu'\nu}, \tag{1}$$

where ρ is the single-particle mixed density matrix for the system. It is related to the single-particle Green's function through the equation [9])

$$\rho(\mathbf{r}, \mathbf{r}') = iG(\mathbf{r}, \mathbf{r}', \tau = t - t')|_{\tau \to -0} = \frac{1}{2\pi i} \int_C G(\mathbf{r}, \mathbf{r}', \varepsilon) \mathrm{d}\varepsilon, \tag{2}$$

where $G(\mathbf{r}, \mathbf{r}', \varepsilon)$ is the time Fourier transform of $G(\mathbf{r}, \mathbf{r}', \tau)$, and the contour of integration C is the real axis plus a semicircle in the upper plane. The Green's function G is found from a set of equations describing the interactions of the Cooper pairs in a system of identical fermions interacting through a weak δ-function force. Upon introducing the eigenfunctions ϕ_ν of the single-particle Hamiltonian H_0, which in practice would be a shell-model Hamiltonian, both G and ρ can be expanded in terms of ϕ_ν, e.g.,

$$\rho(\mathbf{r}, \mathbf{r}') = \sum \rho_{\nu\nu'} \phi_\nu(\mathbf{r}) \phi_{\nu'}^*(\mathbf{r}'). \tag{3}$$

If there is no additional perturbation in the system, the zero-order density matrix is found to be

$$\rho^0_{\nu\nu'} = \tfrac{1}{2}\left(1-\frac{\varepsilon_\nu}{E_\nu}\right)\delta_{\nu\nu'}, \tag{4}$$

where

$$\varepsilon_\nu = E_\nu{}^0 - \lambda \tag{5a}$$

and

$$E_\nu = \sqrt{\varepsilon_\nu{}^2+\Delta^2}. \tag{5b}$$

Here the $E_\nu{}^0$ quantities are the single-particle eigenvalues of H_0, λ is the chemical potential, and Δ is the energy gap.

Upon inserting eq. (4) into eq. (1), the resulting expression is the same as that given by Belyaev †. The principal advantage of Migdal's method, however, lies in the fact that corrections of ρ due to the addition of a small perturbation can be computed easily. Thus, corresponding to the perturbation V, the first-order change in the density matrix is

$$\rho_{\nu\nu'} \to \rho^0_{\nu\nu'} + \rho'_{\nu\nu'}, \tag{6}$$

where

$$\rho'_{\nu\nu'} = \rho^{(1)}_{\nu\nu'} + \rho^{(2)}_{\nu\nu'}, \tag{7a}$$

$$\rho^{(1)}_{\nu\nu'} = \frac{(\varepsilon_\nu\varepsilon_{\nu'} - E_\nu E_{\nu'})V_{\nu\nu'} - \Delta^2 V^*_{\nu\nu'}}{2E_\nu E_{\nu'}(E_\nu+E_{\nu'})}, \tag{7b}$$

and

$$\rho^{(2)}_{\nu\nu'} = \frac{\varepsilon_\nu\Delta'_{\nu\nu'} + \varepsilon_{\nu'}\Delta'^*_{\nu\nu'}}{2E_\nu E_{\nu'}(E_\nu+E_{\nu'})}. \tag{7c}$$

In the above equations, Δ' is the change in the energy gap Δ, induced by the perturbation V. The expression $\mathrm{Tr}(\rho^{(1)}V)$ is the usual expression for the matrix elements of the impurities in superconductors, as given in BCS ††.

The change Δ' in Δ is related to the change F' in the function F [eq. (2) of ref. [9])] by

$$\Delta'^*(\mathbf{r}) = \gamma\int_C F'(\mathbf{r},\mathbf{r},\varepsilon)\frac{d\varepsilon}{2\pi}. \tag{8}$$

Following Migdal [9]) we assume that there is no change in γ (the strength of the correlation) resulting from the presence of V.

Now for a given γ, $\Delta'(\mathbf{r})$ has to be determined from some additional condition

† Compare, for example, with the first term of eq. (96) of ref. [5]) or the following equation for the quadrupole moment. The factor of two difference in the appearance of our expression arises from the fact that his sum is over conjugate pairs of states while ours is over each state.

†† See section IV of ref. [3]) (in particular, Tables II and III).

imposed upon it. Migdal proposes a certain condition on Δ' equivalent to a generalization of the equation relating Δ to γ [Eq. (12) of ref. [9])]. This condition leads to an integral equation for Δ'[eq. (17) of ref. [9])]. Its solution, obtained by equating all the coefficients of $\phi_\nu(\mathbf{r})\phi_{\nu'}^*(\mathbf{r})$ to zero, is physically unrealistic for our case of real V. From eq. (7) we propose instead the following equation for the matrix element of Δ'^*:

$$\Delta'^*_{\nu\nu'} = \gamma \int_C F'_{\nu\nu'}(\varepsilon) \frac{\mathrm{d}\varepsilon}{2\pi}. \tag{9}$$

Using eq. (16) of Migdal, on the right side we obtain an algebraic equation for $\Delta_{\nu\nu'}$. We have chosen Δ' to be real, for real V. The resulting solution is

$$\Delta'_{\nu\nu'} = \frac{\gamma\Delta(\varepsilon_\nu+\varepsilon_{\nu'})V_{\nu\nu'}}{2E_\nu E_{\nu'}(E_\nu+E_{\nu'})+\gamma(E_\nu E_{\nu'}+\varepsilon_\nu\varepsilon_{\nu'}-\Delta^2)}. \tag{10}$$

In the limit of vanishing pair force ($\Delta \to 0$), Tr $(\rho' V)$ goes over to the usual second-order perturbation-theory correction to the energy, induced by V.

2.2. PERTURBATION TREATMENT OF THE DEFORMATION

By introducing the nuclear deformation as a small perturbation [10])

$$V = -\tfrac{1}{3}\delta M\omega_0^2(\tfrac{16}{5}\pi)^{\frac{1}{2}}r^2Y_{20}(\theta,\phi) \tag{11}$$

on a spherical shell model †, we can use the preceding results to compute the corresponding correction induced in the density matrix by V. We shall use single-particle states labelled by the quantum numbers $(Nljm)$, where N is the oscillator quantum number, l and j are the orbital and total angular momenta, and m is the z projection of j.

The zero-order part $\rho^0_{\nu\nu'}$ of the density matix contributes nothing to the quadrupole moment in this case, because for the present choice of basic states, $E_\nu{}^0$ and hence $\rho^0_{\nu\nu'}$ are independent of the m quantum number, and we have $\sum_m\langle jm|Q_{20}|jm\rangle = 0$. The contribution of $\rho'_{\nu\nu'}$ is found from eqs. (7), (10) and (11). By using eq. (1), with

$$O(\mathbf{r}) = Q_{20} = (\tfrac{16}{5}\pi)^{\frac{1}{2}}r^2Y_{20}(\theta,\phi), \tag{12}$$

a short calculation leads to

$$\begin{aligned} Q_0 &= \sum\langle Nljm|\rho'|N'l'j'm'\rangle\langle N'l'j'm'|Q_{20}|Nljm\rangle \\ &= -\tfrac{4}{3}\delta M\omega_0^2\sum_{\nu\nu'} b_{\nu\nu'}|(r^2)_{\nu\nu'}C(j'2j;\tfrac{1}{2}0\tfrac{1}{2})|^2. \end{aligned} \tag{13}$$

In eq. (13) we define

$$\nu = \{Nlj\}, \quad \text{and} \quad b_{\nu\nu'} = b^{(1)}_{\nu\nu'}+b^{(2)}_{\nu\nu'}, \tag{14a}$$

† We use the notation of ref. [10]).

where

$$b^{(1)}_{\nu\nu'} = \frac{\varepsilon_\nu \varepsilon_{\nu'} - E_\nu E_{\nu'} - \Delta^2}{2E_\nu E_{\nu'}(E_\nu + E_{\nu'})} \tag{14b}$$

and

$$b^{(2)}_{\nu\nu'} = \frac{1}{2E_\nu E_{\nu'}(E_\nu + E_{\nu'})} \frac{-G\Delta^2(\varepsilon_\nu + \varepsilon_{\nu'})^2}{2E_\nu E_{\nu'}(E_\nu + E_{\nu'}) - G(E_\nu E_{\nu'} + \varepsilon_\nu \varepsilon_{\nu'} - \Delta^2)}. \tag{14c}$$

Here G measures the strength of the pairing correlation and is positive for attractive forces (Migdal's γ is $-G$). The value $G = 25/A$ MeV was used [11]). The term $b^{(2)}$, which corresponds to $\rho^{(2)}$ in eq. (7), was found to contribute less than 1 % to the computed quadrupole moments. Notice that in this approximation, Q_0 is proportional to the deformation.

We have calculated the intrinsic quadrupole moments of even nuclei based on eqs. (13) and (14). For the energy levels $E_\nu{}^0$, the eigenvalues of Nilsson [10]) and Mottelson and Nilsson [12]) for the spherical case were used. The matrix elements of r^2 were evaluated by using harmonic-oscillator wave functions (unperturbed by the spin-orbit term) rather than the eigenfunctions of Nilsson's Hamiltonian [10]). As a result of this approximation we can take advantage of the simple selection rules for the quantum number N. The energy gap Δ was deduced for each nucleus from experimental pairing energies when available, and otherwise interpolated. The chemical potential λ was obtained from the condition on the proton number

$$\sum_\nu \tfrac{1}{2}\left(1 - \frac{\varepsilon_\nu}{E_\nu}\right) = Z. \tag{15}$$

In principle, the sum on ν in all our equations extends over the complete set of eigenstates of H_0. In practice, the sums may be terminated at some finite point above the Fermi surface. This point will be covered in detail in the discussion of the results.

2.3. "EXACT" TREATMENT OF THE DEFORMATION

For large deformation the preceding result, which is linear in the deformation, may be inadequate. It is therefore appropriate to take account of the nonlinear dependence of Q_0 on δ by including the deformation in the Hamiltonian defining the basic states of the system to be used in eq. (1). This can be achieved for example, by using the eigenfunctions and eigenvalues for a deformed harmonic-oscillator potential with a spin-orbit term as given in the work of Nilsson [10]). The Hamiltonian for the deformed harmonic-oscillator with spin-orbit interaction is

$$H = H_0 + C\mathbf{l}\cdot\mathbf{s} + Dl^2 + V_\delta \equiv H_s + V_\delta, \tag{16}$$

where H_0 is the Hamiltonian for the isotropic harmonic oscillator, and V_δ is

the deformation term, given by

$$V_\delta = -\tfrac{1}{3}\delta M\omega_0^2 Q_{20}. \tag{17}$$

This potential connects some of the harmonic-oscillator states belonging to the shell N to those in the shells $N\pm 2$. Because of the large energy separation between shells compared to the separations between neighboring levels in a given shell, Nilsson, in calculating the eigenvalues for the deformed potential, ignored the coupling between states belonging to different oscillator quantum numbers N. The Hamiltonian that Nilsson diagonalized was therefore

$$H' = H_\delta + V_D, \tag{18}$$

where

$$V_D = V_\delta \delta_{NN'} \tag{19}$$

is diagonal in N. The eigenfunctions of eq. (18) are expanded in terms of the harmonic-oscillator eigenfunctions $|Nl\Lambda\Sigma\rangle$; for given η (the deformation parameter used by Nilsson [10])) we have

$$|N\Omega\alpha\rangle = \sum_{l\Sigma} A^{\alpha}_{l,\Omega-\Sigma}|Nl, \Omega-\Sigma, \Sigma\rangle. \tag{20}$$

Here α labels the $(N+\frac{3}{2}-\Omega)$ states corresponding to the quantum numbers N, Ω. The unnormalized coefficients $A_{l\Lambda}$ are listed in table 1 of ref. [10]) for a few values of the deformation parameter η.

Nilsson's approximation is undoubtedly valid for his purpose of calculating the eigenvalues of the deformed well. However, the term in the Hamiltonian which couples the oscillator shell N to $N\pm 2$ is just the interaction that causes the particles to follow the deformation. If some of the effects of this interaction are omitted in the eigenfunctions, the motion so described will correspond roughly to a motion in a more weakly deformed well. One may expect therefore that Nilsson's eigenfunctions will yield smaller quadrupole moments for a given deformation than one would have obtained if the eigenfunctions of H had been used. In fact, the Nilsson eigenfunctions possess the property that for a completely occupied oscillator shell, the quadrupole moment vanishes. This follows at once from the fact that the deformed Hamiltonian H' is diagonalized by finding a similarity transformation from its representation on the basic states $|Nl\Lambda\Sigma\rangle$ for fixed N, to the eigenstates $|N\Omega\alpha\rangle$. However, the states $|Nl\Lambda\Sigma\rangle$, being eigenstates of the spherically symmetric Hamiltonian H_0, possess the property

$$\sum_{l\Lambda\Sigma} \langle Nl\Lambda\Sigma|Q_{20}|Nl\Lambda\Sigma\rangle = 0. \tag{21}$$

Since the trace of any matrix is invariant under a similarity transformation, we have

$$\sum_{\Omega\alpha} \langle N\Omega\alpha|Q_{20}|N\Omega\alpha\rangle = 0, \tag{22}$$

which means that we obtain exactly no deformation polarizability of a closed-shell core in this approximation in the absence of the pairing force.

It is therefore important for the calculation of quadrupole moments to include the effect of that part of V_δ which is not included in Nilsson's eigenfunctions, namely, the part giving rise to nondiagonal (ND) elements with respect to N,

$$V_{\mathrm{ND}} = V_\delta - V_{\mathrm{D}} = V_\delta(1-\delta_{NN'}). \tag{23}$$

This can be done by treating V_{ND} as a perturbation on the Nilsson system and using eqs. (6) and (7) of subsection 2.1 to compute the correction to the density matrix. (Here V_{ND} is a perturbation because it introduces a small energy shift in the eigenvalues; it need not give a small change in the quadrupole moment, however.) We have checked the validity of the perturbation treatment of V_{ND} by examining the smallness of the expansion coefficients of the appropriate perturbed wave functions. Accordingly, using Nilsson's eigenfunctions [eq. (20)] and the perturbation V_{ND}, we find from eqs. (1), (4), (6) and (7) the quadrupole moment that corresponds to deformation η and proton number Z,

$$Q_0 = Q_{\mathrm{D}} + Q_{\mathrm{ND}} = \mathrm{Tr}(\rho^0 Q_{20}) + \mathrm{Tr}(\rho^{(1)} Q_{20}), \tag{24}$$

where

$$Q_{\mathrm{D}} = \sum_{N,\,|\Omega|,\,\alpha} \left(1 - \frac{E^0_{N\Omega\alpha}-\lambda}{[(E^0_{N\Omega\alpha}-\lambda)^2+\Delta^2]^{\frac{1}{2}}}\right) \langle N\Omega\alpha|Q_{20}|N\Omega\alpha\rangle, \tag{25}$$

$$Q_{\mathrm{ND}} = -\tfrac{4}{3}\delta M\omega_0{}^2 \sum_{N,\,|\Omega|,\,\alpha\alpha'} b^{(1)}(N\Omega\alpha;\, N+2\Omega\alpha')|\langle N\Omega\alpha|Q_{20}|N+2\Omega\alpha'\rangle|^2. \tag{26}$$

Here $b^{(1)}(\nu, \nu')$ is given by eq. (14), and the chemical potential λ is found from eq. (15). The sum extends over $\Omega > 0$ since the substates Ω, $-\Omega$ have equal contributions †.

The expression for Q_{D} has the form of a sum of single-particle quadrupole moments weighted by the occupation factor of the degenerate states $(\Omega, -\Omega)$. For levels far below the Fermi surface λ, the occupation factor approaches two. Therefore because of eq. (22), whenever all the levels belonging to the same N lie sufficiently below the Fermi surface, their contribution to Q_{D} sums to zero. This is not so in Q_{ND}. Indeed every term in eq. (26) yields a positive contribution to Q_{ND}.

The matrix elements of the quadrupole operator between Nilsson states that appear in the above expressions are

$$\langle N\Omega\alpha|Q_{20}|N'\Omega'\alpha'\rangle = 2\delta_{\Omega\Omega'} \sum_{l l' \Sigma} a^{\alpha}_{l\Omega-\Sigma} a^{\alpha'}_{l'\Omega-\Sigma} \times \langle Nl|r^2|N'l'\rangle C(l2l';\, 000)\, C(l'2l;\, \Omega-\Sigma,\, 0,\, \Omega-\Sigma), \tag{27}$$

† The factor 4 in eq. (26) comes from the reduction of the summation over N, N' $(N' = N \pm 2)$ and the reduction of the sum on Ω to positive values only.

where the a's are the normalized A's. We have calculated the intrinsic quadrupole moments of even-proton nuclei based on eqs. (24) to (27) and using Nilsson's eigenfunctions and eigenvalues, except for the $N = 5$ and 7 oscillator shells, where the Mottelson and Nilsson results were used [12]). The energy gap Δ was deduced for each nucleus from experimental pairing energies when available, and otherwise interpolated.

3. Numerical Results

3.1. PERTURBATION TREATMENT OF THE DEFORMATION

In this section we shall give and discuss the results of the calculation of nuclear quadrupole moments based on the method of subsection 2.2. According to this treatment, the quadrupole moment is proportional to the deformation. We have calculated the proportionality factor Q_0/δ. This quantity is independent of the deformation but depends on the shell structure of the nucleus. It is therefore appropriate to call it the quadrupole susceptibility for it measures the degree of susceptibility, independent of deformation, that the nucleus possesses to having a quadrupole moment.

A calculation of Q_0 alone (rather than Q_0/δ) would require an independent evaluation of the deformation δ, as might be obtained for example from an equilibrium calculation of the total energy including the pairing force. We do not have available the results of such a calculation and shall therefore content ourselves with comparing our calculation of Q_0/δ, based on a particle picture of the nucleus, with the term linear in the deformation obtained by assuming a uniform distribution of charge in a spheroidal nucleus:

$$\frac{Q_0}{\delta} = \tfrac{4}{5} Z R^2. \tag{28}$$

Figure 1 compares our results with eq. (18) for even-proton nuclei with $Z \geqq 10$. Of course treating the deformation as time-independent is valid only in the regions of strongly deformed nuclei. Our purpose in presenting results for all even-proton nuclei with $Z \geqq 10$ is merely to illustrate better the nuclear-structure dependence of the quadrupole moment and the role played by the residual internucleon forces (in the form of a pairing force).

For a vanishingly small pairing ($\Delta \to 0$) we have found that the quantity Q_0/δ as a function of Z exhibits striking shell effects, becoming small at subshell closures and rising for proton numbers that partially fill a shell.

For finite energy gaps Δ (chosen in accordance with experimental evidence when possible, as indicated in table 1), the structure dependence was considerably reduced except for the magic numbers $Z = 20$, 28, 40 and 82, as is shown in fig. 1. In the region $40 \lesssim Z \lesssim 70$, the particle model (with pairing force) and uniform model give essentially the same results. For the several strongly

deformed nuclei near Mg^{24}, however, this calculation predicts a larger quadrupole susceptibility than the uniform model, and hence suggests a smaller deformation than estimates based on the uniform model. On the other hand, near closed shells our calculation suggests that quadrupole moments should be small, not alone because the deformation is small, but because the quadrupole susceptibility of the nucleus is also small.

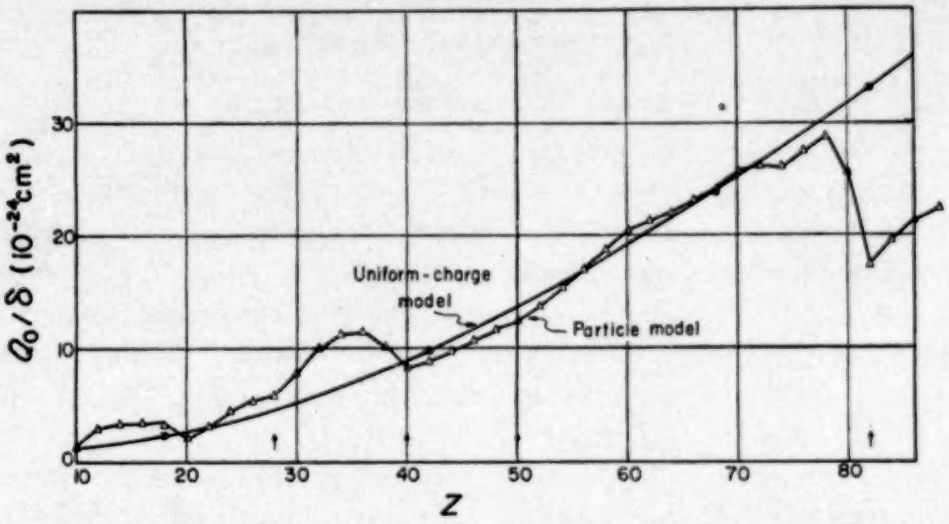

Fig. 1. Plot of Q_0/δ as a function of Z, computed on the basis of the particle picture according to the perturbation treatment of the deformation in subsection 2.2. This plot is compared with a plot of Q_0/δ corresponding to a uniformly charged spheroid (eq. (28)).

Table 1 compares the values of Q_0/δ calculated from the particle model, with the uniform model [eq. (18)], and shows the value of δ required to account for the observed quadrupole moments, when known. For strongly deformed nuclei, neighboring even and odd nuclei should have about the same quadrupole susceptibility according to the present theory, and experimental results seem to confirm this.

The sum in eq. (12) extends in principle over the complete set of eigenstates of the zero-order Hamiltonian. For the calculations presented here, the sum was terminated at the magic number $Z = 184$. To confirm that the sum had converged, we added shell-model levels from the next major shell for a few calculations in the heavy-element region, and the values of Q_0/δ changed by less than 1 %.

Quite aside from the question of convergence, it is interesting to inquire what contribution the levels above the Fermi level make to the quadrupole moment, for this is a measure of the scattering induced by the pairing force, and the quadrupole coupling to the deformation. For this purpose, table 2 shows the calculated Q_0/δ which correspond to including levels up to the magic numbers indicated and removing the contribution of all higher levels to the sum in eq. (12) for the nucleus $_{24}Cr^{52}$.

TABLE 1

Values of Q_0/δ (in 10^{-24} cm^2) of even nuclei from the perturbation treatment compared with the uniform-charge model (eq. (18))

Z	A	Proton energy gap Δ_p	Q_0/δ (Perturbation theory)	Q_0/δ (Uniform model)	Q_0 (Observed)	δ
10	20	2.45 [a])	1.40	0.85		
12	24	1.44 [b])	2.93	1.15	0.45 [e])	0.15
14	28	1.67 [b])	3.30	1.49		
60	150	1.07 [c])	20.3	19.6		
62	150	1.64 [d])	19.7	20.2	3.62 [f])	0.183
64	156	0.97 [c])	21.9	21.4	6.75 [f])	0.308
66	162	0.81 [c])	23.0	22.6	7.14 [f])	0.310
68	164	0.75 [c])	24.1	23.7	7.07 [f])	0.294
70	172	0.65 [c])	25.6	25.0	7.65 [f])	0.299
72	178	0.62 [c])	26.0	26.3	6.88 [f])	0.264
74	184	0.65 [c])	26.1	27.6	6.15 [f])	0.236
76	188	0.69 [c])	27.5	28.8		
88	226	0.83 [b])	22.2	37.7		
90	230	1.05 [d])	22.92	39.0	$\approx$8.7 [g])	$\approx$0.38
92	238	0.85 [d])	23.7	40.8	10.90 [h])	0.46

[a]) Calculated with the help of eq. (63) of ref. [9]) and the tables of mass defects of A. H. Wapstra, Physica **21** (1955) 385.

[b]) For this value, we have $\Delta_p(Z) = -\frac{1}{2}P(Z+1)$, where $P(Z+1)$ is the pairing energy given by V. A. Kravtsov, Soviet Physics J.E.T.P. **36** (1959) 871

[c]) From J. J. Griffin and M. Rich [7]). Their values of Δ were taken from: W. H. Johnson and V. B. Bhanot, Phys. Rev. **107** (1957) 1699; W. H. Johnson and A. O. Nier, Phys. Rev. **105** (1957) 1014, under the assumption $\Delta = \Delta_p = \Delta_n$ used by J. J. Griffin and M. Rich, Moments of inertia of even-even nuclei (preprint); M. Rich (Los Almos Scientific Laboratory, Los Alamos, New Mexico, USA), private communication.

[d]) From A. B. Migdal [9]), table 2

[e]) P. C. Gugelot and M. Rickey, Phys. Rev. **101** (1956) 1613; the value $Q_0(Mg^{24}) = 0.43 \times 10^{-24}$ cm^2 is given by H. E. Litherland *et al.*, Chalk River Report PD-289 (1956) (unpublished).

[f]) B. Elbek, M. C. Olesen and O. Skilbreid, Nuclear Physics, in press.

[g]) Information from R. E. Bell, S. Bjørnholm and J. Severiens, through private communication from Dr. B Elbek.

[h]) E. Skurnik, M. C. Olesen and B. Elbek, to be published; private communication from Dr. B. Elbek.

TABLE 2

Quadrupole moment of $_{24}Cr^{52}$

Z_0	50	82	126	184
Q_0/δ	2.96	4.27	4.39	4.39

The table shows the calculated quadrupole moment of Cr^{52} (in 10^{-24} cm^2) which results from omitting the contribution of all levels above the magic number Z_0.

3.2. EXACT TREATMENT OF THE DEFORMATION

In this subsection we discuss our calculation of quadrupole moments based on the method of subsection 2.3. Since we have used Nilsson's eigenfunctions and eigenvalues, our results are given for the same values of the parameter η used by Nilsson. The deformation δ is related to η through $\delta \approx \kappa\eta$, where κ measures the relative strength of the spin-orbit and oscillator phonon energy. We plot Q_0 for fixed deformation as a function of even Z for $10 \leqq Z \leqq 92$ to bring out the systematic and shell-closure effects, although, as remarked earlier, treating δ as time-independent is valid only in the strongly deformed regions of the periodic table. The numerical results based on the method of subsection 2.3 are presented graphically in figs. 2 to 5.

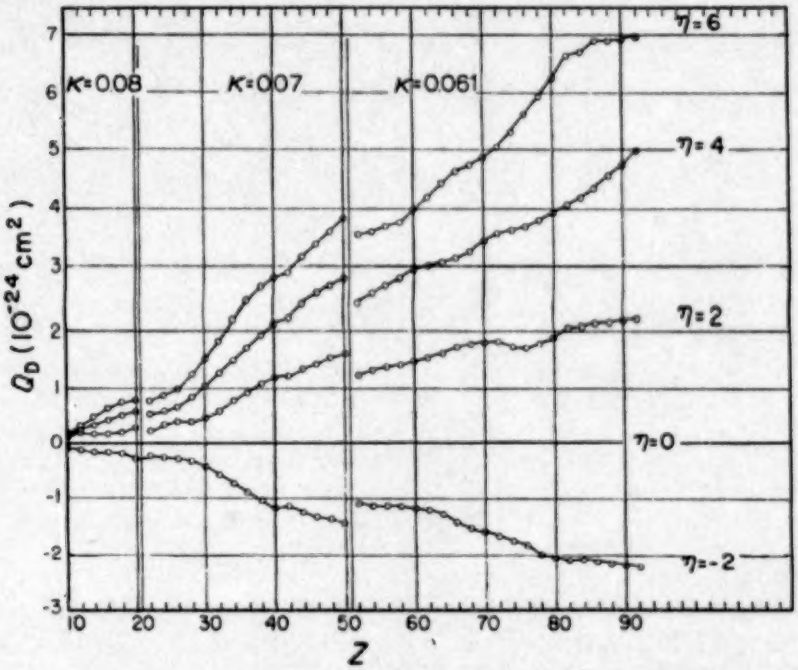

Fig. 2. The quadrupole moment Q_D computed as in subsection 2.3 using Nilsson wave functions is shown as a function of Z for five values of the deformation parameters $\eta \approx \delta/\kappa$. The moment Q_D contains no contribution from matrix elements connecting states of N to $N \pm 2$.

Figure 2 shows the intrinsic quadrupole moment as a function of Z computed by using the Nilsson wave functions, without correcting for the absence of admixtures of different oscillator states, N (see subsection 2.3). The choice of $\kappa = 0.08$ for $Z \leqq 20$, $\kappa = 0.061$ for $Z \geqq 50$ was based on Mottelson and Nilsson's work, while $\kappa = 0.07$ seems a reasonable choice in the region between. A comparison of this figure with the experimental values of Q_0 listed in table 1 shows that the Nilsson wave functions yield quadrupole moments that are too small. This is further emphasized in fig. 3, where the effect of including configuration admixture of different oscillator states N is illustrated for one deformation parameter η.

From fig. 3 we observe that the contribution to Q_0 from Q_D, the part of the density ρ, involving no admixtures of different states N, is generally equal to

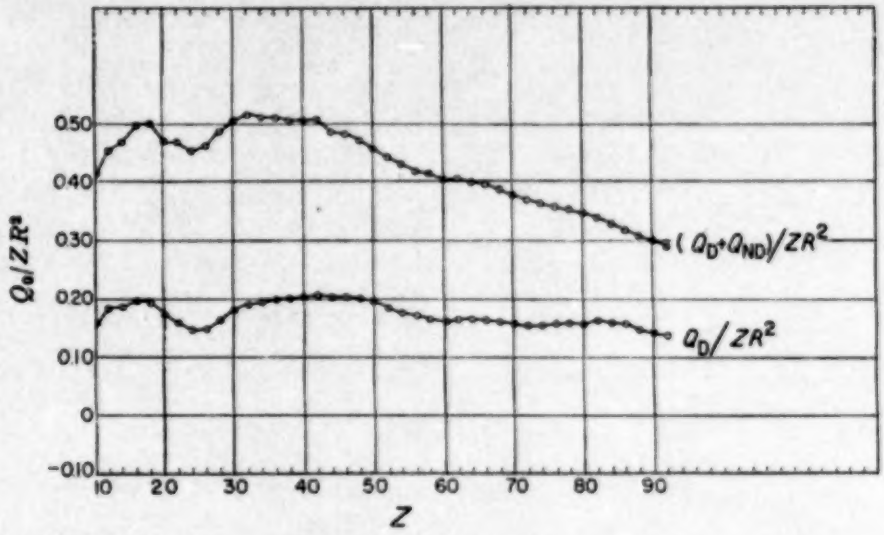

Fig. 3. The quadrupole moment computed as in subsection 2.3 is shown as a function of Z for $\delta = 0.366$. The moment Q_D contains no contribution from matrix elements connecting states of N to $N \pm 2$. The moment Q_{ND} is computed from such matrix elements only. The total intrinsic quadrupole moment is $Q_0 = Q_D + Q_{ND}$.

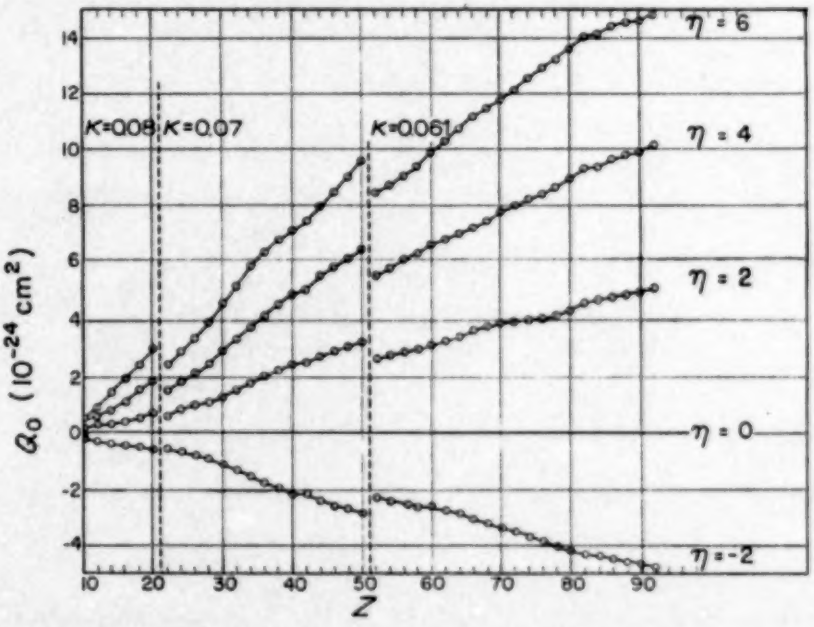

Fig. 4. The total intrinsic quadrupole moment computed in subsection 2.3 is shown for five values of the deformation $\eta \approx \delta/\kappa$.

about one half or less of the total Q_0. This result is consistent with the prediction by Moszkowski that for a pure harmonic-oscillator model, half of the quadrupole moment at equilibrium deformation is due to the diagonal in N contributions of

the protons in unfilled shells [13]). Probably the $\mathbf{l}\cdot\mathbf{s}$ and l^2 terms in H (eq. (16)) destroy the exact division into one-half in our results.

Figure 4 shows the complete calculation of the quadrupole moments including the above mentioned configuration mixing. For easiest comparison with

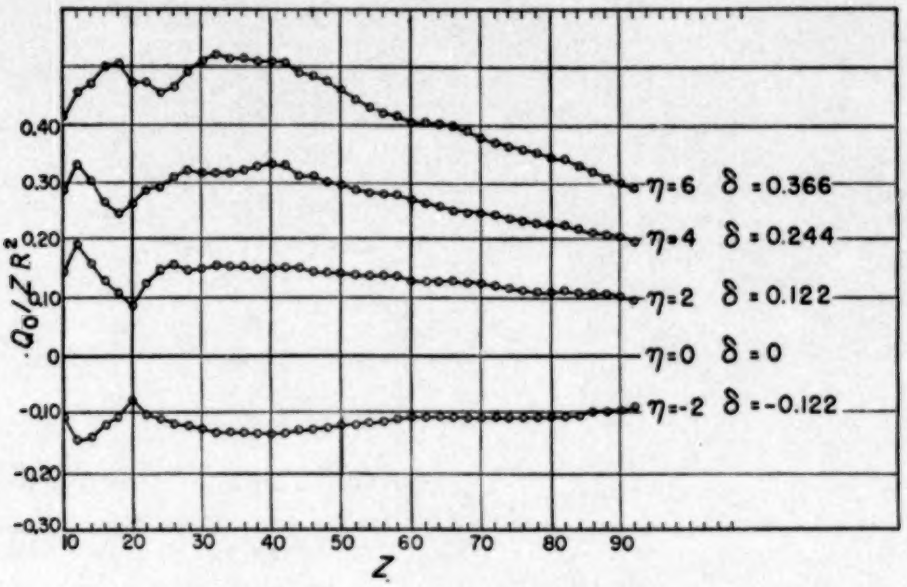

Fig. 5. The quantity Q_0/ZR^2, which for the uniform-charge model is a constant for fixed deformation (see table 3), is shown as a function of Z for five values of the deformation.

the uniform-charge model these results are given again in fig. 5, where Q_0/ZR^2 with $R = 1.2A^{\frac{1}{3}}\times 10^{-13}$ cm is shown as a function of Z. For the uniform model, this ratio is a constant for given deformations and would be represented on this graph by straight lines at the values of Q_0/ZR^2 listed in table 3.

TABLE 3

Values of Q_0/ZR^2 for the uniform-charge model

η	−2	0	2	4	6
δ	−0.122	0	0.122	0.244	0.366
Q_0/ZR^2	−0.091	0	0.103	0.219	0.346

Horizontal lines representing $Q_0/ZR^2 = {}^4/_5\delta(1+\frac{1}{2}\delta)$ for the uniformly charged spheroid are to be compared with the particle calculation of this ratio shown in fig. 3. The value of κ used is $\kappa = 0.061$

For the rare earth and heavy elements, our calculation predicts a slow depletion of the quadrupole moment with increasing Z, i.e., $\mathrm{d}(Q/ZR^2)/\mathrm{d}Z < 0$. In the light-element region, there is some trace of shell-structure effects in our results, especially around $Z = 20$, for small deformations. For the smaller

positive deformation used by Nilsson, we illustrate in fig. 6 by a dotted line, the effect of allowing the pairing interaction to vanish. It is clear that the pairing force has rather little effect on the size of the quadrupole moments, except that it does smooth out fluctuations due to the shell structure. In fact, the energy gap Δ can be changed by a factor of two without changing the calculated Q by more than several percent. The above smoothing-out effect means, in particular, that in the neighbourhood of the magic numbers (in the closed-shell regions) the pairing force decreases the quadrupole deformation required to account for the observed moment Q_{obs}, i.e., the value of δ such that the calculated $Q_0(\delta)$ is equal to Q_{obs} for a given Z. (cf. fig. 6).

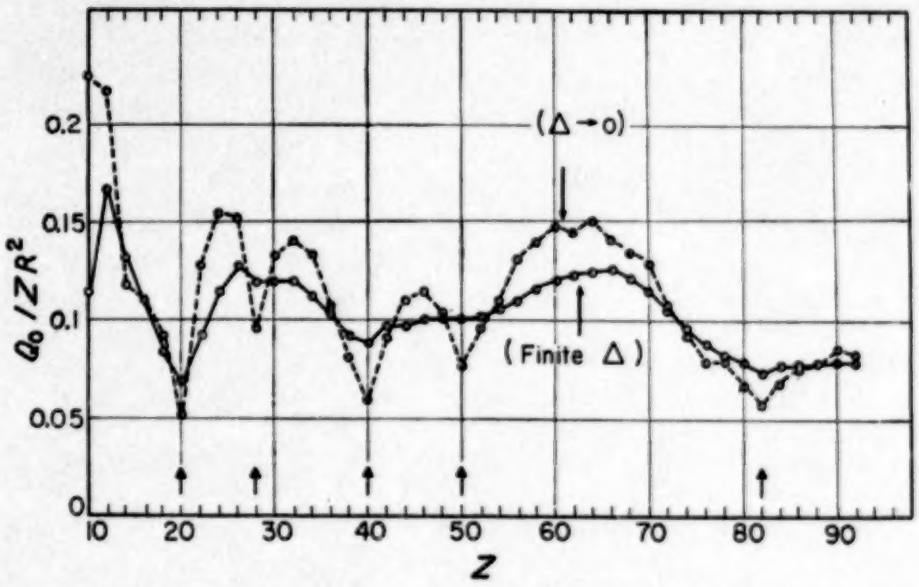

Fig. 6. The quantity Q_0/ZR^2 plotted as a function of Z for $\delta = 0.1$ ($\kappa = 0.05$) is displayed for the finite and the vanishing energy gap Δ.

It is interesting to remark here that a similar feature of the pairing force has been found by Belyaev [5]) for the equilibrium deformation (cf. fig. 1 of ref. [5])).

On the other hand, we find that in the middle of a major proton shell the quadrupole deformation is increased by the presence of an energy gap.

An examination of fig. 5 shows that for a given nucleus one can make a linear interpolation to values of the deformation between those shown. For the physical regions of our graphs (i.e., in the mass region where the nuclear deformations are permanent), we list in table 4 the calculated quadrupole moment based on the particle picture treated in this work. The nuclear deformations deduced from this table by linear interpolation to the experimental measurement of intrinsic quadrupole moments are also shown. They are smaller than the deformations obtained from the uniform-charge model, which are shown in the last column of the table.

Concerning this point, Belyaev has predicted a general reduction in the

equilibrium deformation of nuclei in the presence of the pairing force [5]). On the other hand the equilibrium deformations in the absence of the pairing force were calculated for several rare earth nuclei by Mottelson and Nilsson [12]), and are in essential agreement with the deformations deduced from the measured quadrupole moments in the uniform-charge model. This suggests therefore, that our smaller deformations deduced from experimental quadrupole moments *via* the particle model may be consistent with equilibrium deformations in the presence of the pairing force.

TABLE 4

Intrinsic quadrupole moments of strongly deformed nuclei

Z	A	Calculated Q_0			Q_{obs}	δ (this calculation)	δ (uniform model)
		$\eta = 2$	$\eta = 4$	$\eta = 6$			
12	24	0.35	0.63	0.94	0.45	0.24	0.33
62	150	3.25	6.60	10.11	3.62	0.13	0.17
62	152	3.29	6.71	10.26	5.82	0.20	0.26
64	154	3.41	6.85	10.58	5.75	0.20	0.28
64	156	3.45	6.90	10.72	6.75	0.23	0.28
64	158	3.44	6.91	10.67	7.35	0.25	0.30
64	160	3.45	6.94	10.71	7.59	0.25	0.30
66	160	3.60	7.10	11.07	6.65	0.22	0.26
66	162	3.63	7.13	11.17	7.14	0.23	0.28
66	164	3.62	7.16	11.16	7.48	0.24	0.29
68	164	3.76	7.35	11.41	7.07	0.23	0.26
68	166	3.78	7.39	11.46	7.52	0.24	0.28
68	168	3.78	7.41	11.50	7.55	0.24	0.28
68	170	3.80	7.44	11.55	7.34	0.23	0.27
70	172	3.91	7.72	11.79	7.42	0.23	0.26
72	176	3.95	7.93	12.10	7.25	0.22	0.24
72	178	3.98	7.98	12.15	6.88	0.21	0.23
72	180	3.98	7.99	12.20	6.60	0.20	0.23
74	182	3.98	8.15	12.49	6.45	0.19	0.21
74	184	3.99	8.19	12.55	6.15	0.18	0.20

Intrinsic quadrupole moments $Q_0 = Q_D + Q_{ND}$ (in 10^{-24} cm^2) for some strongly deformed nuclei calculated according to subsection 2.3 are compared with the observed moments Q_{obs}. The deformation δ deduced from this comparison is compared with the deformation implied by analyzing the experimental values of Q_0 with $Q_0 = \frac{4}{5} ZR^2\delta(1+\frac{1}{2}\delta)$ for the uniform-charge model. See table 1 details as to sources of energy gaps Δ and experimental Q_0's.

The terms in Q_{ND} connect the state N to $N+2$. By examining $b^{(1)}$ (eq. (14)), it is clear that $b^{(1)}$ is small whenever both levels N and $N+2$ lie above or below the Fermi level λ, and is appreciable only when it connects an occupied state to an unoccupied state. Since oscillator wave functions are available only up to $N = 7$, we cannot calculate the terms in Q_{ND} which connect $N = 6$ to $N = 8$. For sufficiently heavy nuclei, and at very large deformations, some of the $N = 6$ levels are occupied and would contribute significantly to Q_{ND}. (We

believe the omitted terms would increase Q_{ND} by about 20 % and therefore increase Q_0 by about 10 %). However, our results reported above indicate that for rare earth elements $\eta \approx 4$. At this deformation one can see by examining the Nilsson energy levels, that this situation does not arise until Z is about 90 or greater.

4. Discussion

We have computed intrinsic quadrupole moments of a certain model nucleus comprising Z protons moving in a permanently deformed potential well. The proton-proton interaction is approximated by a pairing force of the BCS type. Because the deformation of the potential is assumed to be time-independent, our results can have quantitative meaning for real nuclei only in the strongly deformed regions. Nevertheless, the properties of the model nucleus may have at least qualitative significance for weakly deformed nuclei near closed shells. Whether it is meaningful to consider the present form of individual particle states for nucleons far below the Fermi surface is open to some doubt. This question should be clarified by future developments of the Brueckner theory of nuclear structure. Another question is that of the validity of our particular choice of the potential model. In fact, the square-well model of Gottfried seems to predict a significantly different level spectrum than that of the Nilsson model [14]). It would be interesting to have results for such other models in order to compare the results with those obtained here.

We shall now discuss the properties of the quadrupole moments of the model nucleus, having been reminded of the possible limitations of their application to real nuclei. The particle model reproduces the general trend of quadrupole moments predicted by the uniform model for large deformations aside from a slow depletion of Q_0/ZR^2 with increasing Z, (i.e., Q_0/ZR^2 is not constant for given deformation as a function of Z in our model.)

On the other hand at a fixed small deformation, Q_0 exhibits a non-monotonic dependence on Z, reflecting the shell structure of nuclei. In the absence of the interparticle force, the effect is particularly striking, with Q_0 becoming very small at a magic number of protons. This is of course a consequence of the vanishing of the quadrupole moment for filled shells of a spherical nucleus. The effect is considerably reduced with the introduction of an interparticle force, as one might expect, because the interaction causes the particles to be boiled out of the degenerate state they occupied in its absence and to occupy with some finite probability some of the higher unfilled shells.

We find that the pairing force has negligible effect on the magnitude of quadrupole moments computed for fixed deformations at the size of deformation ($\delta \gtrsim 0.24$) appropriate to the rare-earth region. When Q_0 is plotted as a function of Z for fixed $\delta \gtrsim 0.2$, the only effect of the pairing force is to smooth

out small fluctuations from nucleus to nucleus. This, of course, does not imply that the pairing force is not important in determining equilibrium deformations.

We also find that on the basis of this particle model, the experimentally measured quadrupole moments imply consistently smaller deformations than had hitherto been expected on the basis of the uniform-charge model. This result can perhaps be understood as follows. The deformed field is created by the neutrons and protons; the electric quadrupole moment by the protons alone. The protons in the unfilled shell "take advantage" of the deformed field of the neutrons to form a more eccentric distribution within the nucleus. Such a distribution would have a larger quadrupole moment than would follow if the charge were uniformly distributed over the nuclear volume.

While we have made explicit reference to even-proton nuclei,our presentation would not predict any essential difference for strongly deformed odd-proton nuclei. In fact, within the limits of the accuracy of the method, the odd-proton nuclei can be interpolated from our graphs. The neutron number enters only in defining A, which is felt only weakly in our results through the oscillator quantum $\hbar\omega \approx 41A^{-\frac{1}{3}}$ MeV.

Finally we remark that in a model that takes account of all of the protons, the introduction of an "effective neutron charge" (see, for example, True [15]) and True and Ford [16])) is not needed, and indeed would be incorrect. The role of the neutrons has already been expressed through the deformation of the single-particle potential in which the protons move.

We are indebted to Dr. B. Elbek for a preprint of his paper on experimental measurements of quadrupole moments, and to Dr. M. Rich for a preprint and communication on energy gaps. We wish to acknowledge a stimulating discussion with Dr. S. A. Moszkowski. The numerical computations reported here were performed on an IBM 704, and the cooperation of the Computer Group is gratefully acknowledged.

Appendix

1. APPROXIMATE FORMULA FOR Q_0 IN THE PERTURBATION TREATMENT

It seems worthwhile to present a simplified approximate formula for $\mathrm{Tr}(\rho' Q_{20})$.

Following Belyaev [5]) (compare his Chapter III, § 4), and Migdal [9]), we can introduce the average level spacing $\varepsilon_\nu - \varepsilon_{\nu'} \approx d = \text{constant}$. This assumption suppresses fine effects of the shell-closure type. We can also neglect the small correction of $\rho^{(2)}$. On introducing the notation $\bar{\varepsilon}_\nu = \frac{1}{2}(\varepsilon_\nu + \varepsilon_{\nu'})$, it is easy to ascertain that $\rho^{(1)}_{\nu\nu'}$ of eq. (7) goes over into

$$\bar{\rho}'_{\nu\nu'} = -\frac{(\frac{1}{4}d^2 + 2\Delta^2)V_{\nu\nu'}}{4(\bar{\varepsilon}_\nu^{\,2} + \Delta^2)^{\frac{3}{2}}}. \tag{A.1}$$

This approximation is obviously the worse for the diagonal elements, for which we should have $d \to 0$ in order to insure the vanishing of $\rho^{(1)}$ in the limit $\Delta \to 0$. Eq. (A.1) is similar to Belyaev's eq. (144). Now we can write

$$\mathrm{Tr}(\bar{\rho}' Q_{20}) = \sum_{\nu\nu'} \bar{\rho}'_{\nu\nu'} (Q_{20})_{\nu'\nu}. \tag{A.2}$$

A similar expression can be obtained if one uses the zero-order density ρ^0 of eq. (4), but the energies ε_ν, contain the perturbation correction of first order in V of eq. (11). We can write $\varepsilon_\nu \to \varepsilon_\nu + \Delta\ \varepsilon_\nu$, or, more explicitly, $\varepsilon_{nlj} \to \varepsilon_{nlj} + \Delta\varepsilon_{njlm}$, where $\Delta\varepsilon_\nu$ depends explicitly on the magnetic number m and is proportional to $\delta(\Delta\varepsilon_\nu = V_{\nu\nu})$. In fact the first-order term in $\Delta\varepsilon_\nu$ of ρ^0 is

$$\bar{\rho}^0_{\nu\nu'} = -\frac{\Delta^2 V_{\nu\nu}}{2(\varepsilon_\nu^2 + \Delta^2)^{\frac{3}{2}}} \delta_{\nu\nu'}, \tag{A.3}$$

which corresponds to $\bar{\rho}'$ of eq. (A.2) in the limit $d \to 0$ for the diagonal matrix elements. The off-diagonal ($(njlm) \neq (n'j'l'm')$) elements are zero in this approximation.

2. REDUCED TRANSITION PROBABILITIES OF ROTATIONAL EXCITATIONS

We can also test the effect of the pairing force on the radiative transition probabilities of strongly deformed nuclei for transitions between two different members of the same rotational band ($K' = K$). The electric (e) and magnetic (m) transition operators appropriate to the 2^λ-pole radiations are

$$M_{\mathrm{e}}(\lambda\mu) = \sum_{\mathrm{p}} \tilde{e}_{\mathrm{p}} r_{\mathrm{p}}^{\lambda} Y_{\lambda\mu}(\Omega_{\mathrm{p}}) \tag{A.4}$$

and

$$M_{\mathrm{m}}(\lambda\mu) = \frac{e\hbar}{2Mc} \sum_{\mathrm{p}} \left(g_s \mathbf{s} + \frac{2}{\lambda+1} g_l \mathbf{l} \right)_{\mathrm{p}} \cdot \nabla_{\mathrm{p}} (r_{\mathrm{p}}^{\lambda} Y_{\lambda\mu}(\Omega_{\mathrm{p}})), \tag{A.5}$$

in the usual Nilsson notation [10]), where $\tilde{e}_{\mathrm{p}} = e_{\mathrm{p}} + (-)^\lambda Ze/A^\lambda$. We shall also confine ourselves to cases where either K is zero or $2K$ is greater than λ.

We shall use Nilsson's notations for the reduced probabilities of transitions from initial nuclear (spin I) states to final (spin I') states, i.e., $B(E(M)\lambda; I \to I')$, where "E" and "M" correspond to the M_{e} and M_{m} operators, respectively. Let us define the intrinsic part of that B as

$$B_{\mathrm{int}}(\mathrm{E}\lambda) = B(\mathrm{E}\lambda; I \to I')[C(I\lambda I'; K0K)]^{-2}, \tag{A.6}$$

in order to get rid of the geometrical factor. With the help of Nilsson's eqs. (35) to (37) (ref. [10])), we can write, in his notation

$$B_{\mathrm{intr}}(\mathrm{E}\lambda) = \tilde{e}_{\mathrm{p}}^2 \left(\frac{\hbar}{M\omega_0} \right)^{\lambda} \frac{2\lambda+1}{4\pi} \left[\sum_{N\Omega\alpha} \tfrac{1}{2} \left(1 - \frac{\varepsilon_{N\Omega\alpha}}{E_{N\Omega\alpha}} \right) G_{\mathrm{E}\lambda}(N\Omega\alpha) \right]^2. \tag{A.7}$$

Here the occupation factor is as in subsection 2.3 (eq. (25)) and we have

$$G_{\mathrm{E}\lambda}(N\Omega\alpha) = \sum_{ll'} \langle Nl|r^{\lambda}|Nl\rangle \left(\frac{2l+1}{2l'+1}\right)^{\frac{1}{2}} C(l\lambda l';\,000) \sum_{\Lambda} a_{l\Lambda}(\Omega) a_{l\Lambda}(\Omega) C(l\lambda l';\,\Lambda 0\Lambda). \tag{A.8}$$

Similarly, we can write

$$B_{\mathrm{intr}}(\mathrm{M}\lambda) = \left(\frac{e\hbar}{2Mc}\right)^2 \left(\frac{\hbar}{M\omega_0}\right)^{\lambda-1} \frac{1}{4} \frac{2\lambda+1}{4\pi} \left[\sum_{N\Omega\alpha} \tfrac{1}{2}\left(1 - \frac{\varepsilon_{N\Omega\alpha}}{E_{N\Omega\alpha}}\right) G_{\mathrm{M}\lambda}(N\Omega\alpha)\right]^2, \tag{A.9}$$

where $G_{M\lambda}(N\Omega\alpha)$ (with the zero projection of $\lambda-1$) is given by Nilsson's eq. (36b).

It is easy to ascertain that upon the summation over all the conjugate pairs $(\Omega, -\Omega)$ only the $B_{\mathrm{int}}(E(M)\lambda)$ with even λ are different from zero.

References

1) R. J. Blin-Stoyle, Revs. Modern Phys. **28** (1956) 75
2) B. R. Mottelson and S. G. Nilsson, Phys. Rev. **99** (1955) 1615
3) J. Bardeen, L. N. Cooper and J. R. Schrieffer, Phys. Rev. **108** (1957) 1175
4) A. Bohr, B. R. Mottelson and D. Pines, Phys. Rev. **110** (1958) 936
5) S. T. Belyaev, Mat. Fys. Medd. Dan. Vid. Selsk. **31**, No. 11 (1958)
6) V. G. Soloviev, Nuclear Physics **9** (1959) 655; Nuovo Cimento **10** (1958) 1022
7) J. J. Griffin and M. Rich, Phys. Rev. Letters **3** (1959) 342
8) L. P. Gorkov, Soviet Physics J.E.T.P. **34** (1958) 505
9) A. B. Migdal, Nuclear Physics **13** (1959) 655
10) S. G. Nilsson, Mat. Fys. Medd. Dan. Vid. Selsk. **29**, No. 16 (1955)
11) B. R. Mottelson, Lectures at the University of California (1959), unpublished
12) B. R. Mottelson and S. G. Nilsson, Mat. Fys. Skr. Dan. Vid. Selsk. **1**, No. 8 (1959)
13) S. A. Moszkowski, Phys. Rev. **103** (1956) 1328
14) K. Gottfried, Phys. Rev. **103** (1956) 1017
15) W. W. True, Phys. Rev. **101** (1956) 1342
16) W. W. True and K. W. Ford, Phys. Rev. **109** (1958) 1675

2.1

Nuclear Physics **18** (1960) 615—623; © *North-Holland Publishing Co., Amsterdam*

Not to be reproduced by photoprint or microfilm without written permission from the publisher

INTEGRATED CROSS SECTIONS FOR THE REACTIONS $A^{40}(\gamma, p)$ AND $A^{40}(\gamma, np)$

H. G. DOSCH, K. H. LINDENBERGER,

I. Physikalisches Institut der Universität Heidelberg

and

P. BRIX

Institut für Technische Kernphysik, Technische Hochschule Darmstadt

Received 25 May 1960

Abstract: The (γ, p) and (γ, np) reactions in A^{40} have been re-examined with 34 MeV bremsstrahlung by measuring the product chlorine radioactivities. Details of the sample preparation are given. Yields relative to $C^{12}(\gamma, n)$ and $Cu^{63}(\gamma, n)$ were determined by β counting. From additional measurements with a lead absorber in the beam, the following cross sections integrated to 33 MeV have been deduced: (100 ± 15) MeV · mb for (γ, p) and (25 ± 10) MeV · · mb for (γ, np). This excludes definitely the anomalously high cross section values reported in the literature. An approximate yield for the $(\gamma, 2p)$ process is also given.

1. Introduction

Contradictory data exist on the absolute cross section of the $A^{40}(\gamma, p)$ and $A^{40}(\gamma, np)$ reactions. Older values [1, 2]) for $\sigma(\gamma, p)$ were anomalously high and gave rise to some theoretical speculation. In a recent paper [3]), conservative upper limits for both cross sections were deduced which excluded such anomalous behaviour. Penfold and Garwin [4]), however, in serious disagreement with these measurements, recently published higher cross section data again. This mysterious result has been emphasized in a recent review article [5]). Since Penfold and Garwin have made use of an older absolute calibration [2]), we have repeated the earlier yield measurements [3]) as carefully as possible in order to facilitate a renormalisation of their data. We have also measured the integrated cross sections independently.

2. Experimental Procedure

2.1. IRRADIATION AND COUNTING GEOMETRY

A stainless-steell tube (42.5 cm long, 6 cm diameter) was filled with pure argon (10 atm) and irradiated with collimated bremsstrahlung of the Heidelberg 35 MeV betatron. The full aperture of the beam was 3.5°. The beam also passed through a polystyrene disc which served as an absolute monitor based

on the reaction $C^{12}(\gamma, n)$. The absorption of the bremsstrahlung in the window of the steel tube was measured separately and taken into account. A parallel plate ionization chamber served as a monitor for the relative γ-ray intensity as a function of time. The reaction products, Cl^{39} and Cl^{38}, originate in the monatomic state. Hence they have a very strong tendency to be adsorbed at surfaces from which they can be removed by chemical methods [1]).

The standard counting equipment has been described in ref. [3]). It consists of a methane-flow β-counter and a thin-bottom cuvette which enables thick liquid samples to be counted in approximately 2π geometry.

2.2. CALIBRATION OF THE 2π COUNTER FOR Cl^{39}

Carrier free samples of Cl^{39} were prepared in the following way: The walls of the steel tube were lined with plastic foil (Hostaphan, equivalent to Mylar). The tube was filled with argon and irradiated with 18 MeV bremsstrahlung, i.e. below the threshold for the $A^{40}(\gamma, d)$ reaction. After venting the tube to the atmosphere, the plastic foil was rinsed with 30 ml of destilled water. No attempt was made to remove the activity quantitatively. The solution was sucked through a glass filter. It was then evaporated almost to dryness. The last drop was transferred to a thin aluminium foil (2.1 mg/cm^2) and completely evaporated there. The samples thus obtained varied in mass between 0.1 and 0.7 mg, distributed over approximately 1 cm^2. Because the half life of Cl^{39} is 55.5 min, the evaporation time had to be kept within approximately half an hour, and therefore the activity was not deposited uniformly on the aluminium support as became obvious on autoradiography. The thickness of each sample was measured with a collimated beam of α-rays. Samples containing thick spots of more than 1 mg/cm^2 were rejected.

The radioactivity was counted in a 4π-geometry by placing the aluminium support between two of our standard 2π windowless flow-counters connected in parallel. The observed counting rate was corrected for absorption of the β-rays in the aluminium support (1.4 ± 1.2 %) and for self absorption in the sample (0.8 ± 0.8 %). A counting efficiency of (99.0 ± 1.0 %) was used. After the 4π counting, the aluminium foils carrying the samples were dissolved in diluted hydrochloric acid. The solution was transferred to the cuvette of the standard 2π counting equipment. Comparison of the counting rates in 4π- and 2π-geometry provided the desired calibration of the 2π counting equipment.

2.3. CALIBRATION OF THE 2π COUNTER FOR Cl^{38}

To prepare samples which contained both Cl^{38} and Cl^{39}, the argon was irradiated with 34 MeV bremsstrahlung. The aqueous solution obtained as described in subsection 2.2 was divided into two known fractions, one to be evaporated for the 4π counting, the other to be diluted for 2π counting. The counting rates in both counters were followed for about three hours, enabling the Cl^{39} and Cl^{38}

activities to be separated by the method of least squares (see ref. [3]) for further details and half lives used). In this way, calibration factors for Cl^{38} as well as for Cl^{39} were obtained. For Cl^{38}, the counting rate was corrected by 3.0 % to account for absorption and counting efficiency. The results and technical details have been collected in table 1.

TABLE 1

Calibration factors for 2π counting

Nucleide	Substance	ρx (mg/cm²)	ρf (mg/cm²)	ρx^* (mg/cm²)	ρx^*_{extr} (mg/cm²)
Cl^{39}	HCl(1n)	2900	5.5	80± 2	78.5±10
Cl^{38}	HCl(1n)	2900	5.5	161±14	147 ±27
C^{11}	Polystyrene	470	1.3	28± 1	

The quantity ρx^* is the calibration factor for our counting geometry which has been described in ref. [3]). The samples are β-thick, they are counted in very nearly 2π geometry. The definition of ρx^* is given by $\dot{z}/F = \rho x^* \dot{a}/m$, where $\dot{z}$ is the counting rate corrected for background and dead time, but not for foil absorption and γ sensivity, F is the area of the sample, $\dot{a}$ the disintegration rate of the sample, and m its total mass. The chemical environments of the radioactivities are listed in the second column. The mass per unit area of the sample and of the foils between sample and counting volume have been designated by ρx and ρf, respectively. The calibration factor ρx^* for Cl^{39} is a weighted mean of 79.4 mg/cm² from 5 runs as described in subsection 2.2 and 81.0 mg/cm² from two runs as mentioned in subsection 2.3. The calibration for C^{11} has been taken from ref. [6]).

The calibration factors ρx^*_{extr} in the last column are those used in the earlier paper [3]). They had been obtained by calibrating the standard counting equipment with P^{32} and assuming, in accordance with ref. [7]), that, for zero foil thickness and pure β emitters, the calibration factors are proportional to the mean ranges of the electrons averaged over the respective β spectra. The table shows that this procedure was justified within the uncertainties quoted.

2.4. SAMPLE PREPARATION FOR THE YIELD MEASUREMENT

For the yield measurement it was necessary to transfer the chlorine quantitatively from the steel tube into a solution which could be counted in our standard counting equipment. This was achieved by lining the argon tube with a thin aluminium foil which was dissolved after the end of the irradiation. The resulting solution was counted. Counting started approximately one hour after the end of the irradiation and continued for three hours. The two chlorine activities were again separated by the method of least squares. For a single run with 60 min irradiation time, typical numbers of counts were 300 000 for Cl^{39}, 100 000 for Cl^{38}, and 1 000 000 for C^{11}.

Considering the sample preparation technique described above, the following sources of error deserve attention:

1) Part of the chlorine may escape with the argon gas when the tube is vented. To test this possibility, in a separate run the argon gas was passed immediately after irradiation through two washing bottles, the first of which contained concentrated hydrochloric acid, the second soda lye. The first bottle

was found to contain 0.5 % of the total activity, the second less than 0.25 %. Normally, the tube was vented 10 min after the end of the irradiation, thus allowing some more time to collect the chlorine at the walls. A loss of activity of (0.5±0.5) % was assumed.

2) There may be some chlorine adsorbed at the walls of the steel tube rather than at the aluminium lining. To avoid errors due to this effect, the tube was rinsed with 1n HCl after each run. The counting rate of this solution provided the information necessary to correct the final yield figure. This correction amounted to between 0.5 and 1.8 %.

3) Radioactive chlorine may escape when the aluminium lining is dissolved in the hydrochloric acid. Since heat is generated on solution of aluminium in HCl, the aluminium was admitted slowly into the liquid which was cooled from the outside. The originating hydrogen gas and vapour were always passed successively through two reflux-condensors and two washing bottles containing NaOH. The content of the first washing bottle was united with the content of the dissolving vessel; the content of the second one was counted separately. It never contained more than 0.2 % of the total activity. To obtain an upper limit of the escaping activity, a special run was carried out in which the contents of the two washing bottles were counted separately. The first one contained 2.2 % of the total activity, the second 0.2 %. Assuming that the amount of activity retained in each washing bottle is proportional to the activity passing through it, a correction of (0.3±0.3) % has been applied.

This rather complicated sample preparation method has been used instead of the simple rinsing procedure described in refs. [1, 3]) in order to ascertain definitely that all radioactive chlorine was collected.

3. Relative yields

Relative yields for the photonuclear reactions were measured with the procedure described in subsection 2.4 for maximum energies E_0 of the bremsstrahlung spectrum of 30 and 34 MeV. The results are given in the first two rows of table 2. The yield is defined as

$$Y_i = \int \sigma_i(E) S(E, E_0) \mathrm{d}E,$$

where $S(E, E_0)$ represents the spectral distribution of the γ-rays and the index i the mass number of the reaction product. From the 4π-counting described in subsection 2.3, an independent and more accurate value for the ratio Y_{38}/Y_{39} was found; it is given in the third row of table 2. The quantities entered in table 2 are averages of from 2 to 5 single runs. The precision of the measure-

ments was compatible with the error resulting from activity losses as mentioned in subsection 2.4 and counting statistics. †

For comparison, table 2 contains the relative yields for $E_0 = 34$ MeV evaluated form the cross section curves of Penfold and Garwin [4]) for argon, and Barber, George and Reagan [9]) for $C^{12}(\gamma, n)$ using a Schiff forward spectrum for $S(E, E_0)$. Penfold and Garwin's experimental ratio Y_{38}/Y_{39} is 27 % larger than ours. This could be due to the fact that their counter was more sensitive to Cl^{38} with its higher energy beta rays than to Cl^{39}, whereas the authors assumed the sensitivities to be equal. The disagreement of the yields relative to $C^{12}(\gamma, n)$, however, is quite serious. The discrepancy cannot be traced to the carbon cross section, since Cook [10]), with the betatron used by Penfold and Garwin, has essentially confirmed the Stanford data [9]).

TABLE 2

Relative yields for $A^{40}(\gamma, p)$, $A^{40}(\gamma, np)$ and $C^{12}(\gamma, n)$

Method	No. of runs	E_0 (MeV)	Y_{39}/Y_{11}	Y_{38}/Y_{11}	Y_{38}/Y_{39}
2π	2	30	$2.31 \pm 0.15 (0.09)$	$0.271 \pm 0.07 (0.06)$	$0.117 \pm 0.035 (0.026)$
2π	5	34	$2.15 \pm 0.11 (0.03)$	$0.387 \pm 0.04 (0.03)$	$0.179 \pm 0.023 (0.013)$
4π	2	34			$0.175 \pm 0.004 (0.001)$
2π	4	34(f)	$2.25 \pm 0.13 (0.06)$	$0.358 \pm 0.06 (0.05)$	$0.165 \pm 0.025 (0.020)$
refs. [4, 9])		34	10.8	2.41	0.223

The definition of Y is given in the text. Errors given in parentheses are those from sample preparation and counting statistics (three times standard deviation) alone. The total errors include the uncertainties of the counter calibrations. The 34(f) in the fourth row represents a spectrum with $E_0 = 34$ MeV, filtered by 20.5 g/cm² of lead (cf. section 5). The relative yields in the last row have been calculated from the cross sections of refs. [4, 9]).

The yield of the $Cu^{63}(\gamma, n)$ reaction has been carefully measured relative to $C^{12}(\gamma, n)$ for our 34 MeV bremsstrahlung spectrum. The ratio is [6]) $Y_{62}/Y_{11} = 17.9 \pm 0.6$. With this figure, the yield ratios of table 2 can be referred to the copper, instead of the carbon, standard reaction. Our experimental ratio Y_{62}/Y_{11} coincides exactly with that evaluated from the copper cross section given by Berman and Brown [11]) and the carbon cross section of ref. [9]). Comparison of our results (table 2, row 2) with Penfold and Garwin's (table 2, row 5)

† The relative yields published earlier [3]) are confirmed by the present measurements which are completely independent and more accurate. Part of the very good agreement is, however, fortuitious because slightly improved constants have been used in the evaluation of table 2. Furthermore the new data are based on a calibration factor for C^{11} which is 9 % smaller than the one used in ref. [3]); this is because, owing to diffusion, an activity loss occurs from thin foils [8]). This effect had been neglected in the earlier calibration procedure. Actually, our (γ, p) yield is (13 ± 5) % larger than the earlier figure [3]). It seems possible that this fraction of the Cl radioactivity may have been lost with the older sample preparation technique.

indicates that their cross section curves should be multiplied by factors 0.20 for (γ, p) and 0.16 for (γ, np) to be in agreement with our measurements, these factors having the same values irrespective of whether the $C^{12}(\gamma, n)$ or the $Cu^{63}(\gamma, n)$ reaction are taken as a reference. The 30 MeV results, though less accurate, indicate the same deviation.

Penfold and Garwin did not determine absolute yields. Instead they normalized their data to the photoproton yield at 22.5 MeV measured by Spicer [2]) with photographic plates. In order to exclude the possibility that only about 20 % of all (γ, p) reactions give rise to the 55 min Cl^{39} activity, Finckh and Hegel [12]) at our laboratory have counted the photoprotons from argon directly with a CsI scintillation spectrometer. Their proton yield for the 34 MeV betatron spectrum agrees well with ours deduced from the residual activity measurement. Earlier results of Iavor [13]) (cf. table 4) were inconclusive, whereas those of Emma, Milone, Rinzivillo and Rubbino [14]), though less directly comparable, also point to the conclusion which we should like to draw, namely, that the yield given by ref. [2]) appears to be too high.

4. The Process $A^{40}(\gamma, 2p)S^{38}$

Besides Cl^{39} and Cl^{38}, the nucleide S^{38} was found as a reaction product. It originates from the process $A^{40}(\gamma, 2p)$ which so far has not been reported in the literature. The yield is so small that it could be detected only after chemical separation of the sulphur from the chlorine. This was done in the following way: The steel tube was lined with plastic foil. After the irradiation it was rinsed with a solution containing sulphur in all valence states. Then the sulphur was oxidized to S^{VI} and precipitated as $BaSO_4$. The γ-ray-spectrum from the $BaSO_4$ sample was examined with a NaI-scintillation spectrometer. A characteristic line appeared very distinctly at 1.8 MeV. It decayed with a half life of about 3 hours, in agreement with the published value [15]) of 172 min. The yield at 34 MeV relative to that of the process $A^{40}(\gamma, np)$ was estimated to be 3.5×10^{-3}. The contribution of the (γ, 2p) reaction to the yield of photoprotons at 34 MeV can, therefore, be completely neglected.

5. Integrated Cross Sections

In order to obtain the ratio of the integrated cross sections from the measured yield ratios, information on the energy dependence of the respective photonuclear reactions is necessary. As shown by Brix, Hegel, Lindenberger and Quitmann [16]), this information may be obtained by comparing the relative yields with and without a lead absorber in the bremsstrahlung beam. The results of such a measurement have been included in table 2. Only the errors given in parentheses need be considered for this comparison since the counter

efficiency cancels out when the yield ratios are formed. Using the method described in ref. [16]) and some additional data † from ref. [6]), the relative integrated cross sections shown in table 3 have been evaluated.

TABLE 3

Cross sections for $A^{40}(\gamma, p)$ and $A^{40}(\gamma, np)$, integrated to 33 MeV, as obtained by the lead absorption method

Standard	relative to standard		σ_{int} (MeV · mb)	
	(γ, p)	(γ, np)	(γ, p)	(γ, np)
$C^{12}(\gamma, n)$	1.86 ±0.23	0.46 ±0.15	94±14	23± 8
$Cu^{63}(\gamma, n)$	0.192±0.030	0.049±0.018	106±18	27±11

The values for σ_{int} have been deduced using the following cross sections integrated to 33 MeV: (50.3±4) MeV · mb for $C^{12}(\gamma, n)$ (ref. [9])) and (550±30) MeV · mb for $Cu^{63}(\gamma, n)$ (ref. [11])). They can be recalculated if newer data become available.

6. Concluding Remarks

In table 4, recent values for the integrated $A^{40}(\gamma, p)$ and $A^{40}(\gamma, np)$ cross sections have been compiled. The values read from the diagrams of Penfold and Garwin [4]) have been renormalized with the factors derived in section 3. The resulting integrated cross sections are shown in the fifth row of table 4.

TABLE 4

Summary of recent data on the integrated (γ, p) and (γ, np) cross sections of A^{40}

Authors		E_g (MeV)	σ_{int} (MeV · mb)	
			(γ, p)	(γ, np)
Iavor [13])		70	350±100	≈35
Iavor [13]), corrected		70	230± 80	≈35
Brix, Körding and Lindenberger [3])		28	<160	<35
Penfold and Garwin [4])		33	455	140
This paper	Ref. [4]) renormalized	33	91	22
	Lead absorption method	33	100± 15	25±10
Golden, Zaffarano and Martin [17])		43	179	9

E_g designates the upper limit of integration for σ_{int}. Iavor [13]) measured the yields relative to $He^4(\gamma, p)$ and assumed the yield ratio to be equal to the ratio of the integrated cross sections. This is not exactly justified for $A^{40}(\gamma, p)$ but a correction can be applied (second row) using the energy dependence of ref. [4]) for A^{40} and of ref. [18]) for He^4.

† For our 34 MeV betatron spectrum, a 20.5 g/cm² lead absorber reduces the yields of the $C^{12}(\gamma, n)$ and $Cu^{63}(\gamma, n)$ reactions by factors of 0.2569±0.0015 and 0.2974±0.0017, respectively.

They agree well with those from the lead absorption method (sixth row, averages from table 3). We should like to stress the point that the lead absorption method is completely independent of the measured shapes of the cross section curves. The renormalization, on the other hand,does not make use of the measurements with the lead absorber. The conservative upper limits given in ref. [3]) are seen to be definitely confirmed.

Golden, Zaffarano and Martin [17]) in a very recent experiment have also investigated the reactions $A^{40}(\gamma, p)$ and $A^{40}(\gamma, np)$ by measuring the Cl radioactivities, but these authors calibrated the bremsstrahlung intensity with standard ionisation chambers. Their results show the same sort of disagreement with ref. [4]) as ours.

The theoretical sum rule value for the total integrated photo-nuclear absorption cross section, up to the photomeson threshold, is about 800 MeV · mb for A^{40}. We hope to have shown conclusively that only a small fraction thereof (instead of more than one half) is exhausted by the (γ, p) process. The unexplained result of ref. [4]) that more reactions result ininitial proton emission than in initial neutron emission should, therefore, be revised. A comparison with available neutron production data [1, 4, 19]) indicates that the opposite is true as one would expect since the (γ, n) threshold is 2.2 MeV lower than the (γ, p) threshold.

Finally, a comparison can be made with the neighbouring nucleide Ca^{44}. Considering the mass numbers and particle binding energies involved, this nucleide should have a slightly larger (γ, p) cross section than A^{40}. An integrated cross section (to 31 MeV) of (125 ± 25) MeV · mb has been measured [16]) for $Ca^{44}(\gamma, p)$; again no anomalous behaviour of A^{40} is indicated.

This work was supported by the Deutsche Forschungsgemeinschaft and the Bundesministerium für Atomkernenergie und Wasserwirtschaft. The authors wish to thank Dr. H. v. Buttlar for helpful criticism of the manuscript, and Mr. D. Renner for his assistance during the experiments with the betatron.

References

1) D. McPherson, E. Pederson and L. Katz, Can. J. Phys. **32** (1954) 593
2) B. M. Spicer, Phys. Rev. **100** (1955) 791
3) P. Brix, A. Körding and K. H. Lindenberger, Z. Physik **154** (1959) 569
4) A. S. Penfold and E. L. Garwin, Phys. Rev. **114** (1959) 1139
5) D. H. Wilkinson, Annual Review of Nuclear Science **9** (1959) 1
6) P. Brix, H. Fuchs, K. H. Lindenberger and C. Salander, Z. Physik, to be published
7) J. Heintze and H. Fischbeck, Z. Physik **147** (1957) 277
8) H. Fuchs and K. H. Lindenberger, Nuclear Instruments and Methods **7** (1960) 219
9) W. C. Barber, W. D. George and D. D. Reagan, Phys. Rev. **98** (1955) 73
10) B. C. Cook, Phys. Rev. **106** (1957) 300
11) A. I. Berman and K. L. Brown, Phys. Rev. **96** (1954) 83
12) E. Finckh and U. Hegel, Z. Physik, to be published

13) I. P. Iavor, JETP **34** (1958) 983
14) V. Emma, C. Milone, R. Rinzivillo and A. Rubbino, Nuov. Cim. **14** (1959) 62
15) D. R. Nethaway and A. A. Caretto, Jr., Phys. Rev. **109** (1958) 504
16) P. Brix, U. Hegel, K. H. Lindenberger and D. Quitmann, Z. Physik **150** (1958) 461
17) S. A. Golden, D. J. Zaffarano and D. S. Martin Jr., private communication and Bull. Amer Physical Society **5** (1960) 57
18) A. N. Gorbunow and V. M. Spiridonov, JETP **6** (1958) 16
19) G. A. Ferguson, J. Halpern, R. Nathans and P. F. Yergin, Phys. Rev. **95** (1954) 776

4.E

Nuclear Physics **18** (1960) 624—627; © *North-Holland Publishing Co., Amsterdam*

Not to be reproduced by photoprint or microfilm without written permission from the publisher

A NEW ISOTOPE: CADMIUM-103

IVOR L. PREISS, PEDER J. ESTRUP † and RICHARD WOLFGANG

Sterling Chemistry Laboratory, Yale University, New Haven, Conn. ††

Received 27 May 1960

Abstract: A new activity, produced by 160 MeV O^{16} bombardments of thick molybdenum oxide targets, is assigned to Cd^{103} on the basis of chemistry and its decay to Ag^{103}. The isotope Cd^{103} has a half-life of 10 ± 1.5 min and decays by positon emission accompanied by 0.22, 0.62 and 0.85 MeV gamma-rays.

Thick natural molybdenum oxide targets were bombarded with a 160 MeV O^{16} beam in an attempt to produce the hitherto unknown isotope Cd^{103}. The expected modes of production are

$$_{42}Mo^{92-100}(_{8}O^{16}, 2p\ 3-11n)_{48}Cd^{103}.$$

Following 5 to 30 min irradiations cadmium-silver fractions were isolated from the targets by a method based on that described by Noyes and Bray [1]). Silver was removed as AgCl and the decay of the cadmium, in the form of the hydroxide, was then followed with a thin window proportional gas counter. As shown in fig. 1, the decay from 1 to 8 hours after bombardment followed a pure 60 min half-life, which may be assigned to Cd^{104} (59 min), Cd^{105} (55 min) and daughters Ag^{103} and Ag^{104}. After substraction of this component a half-life of 10 ± 1.5 min, apparently due to a new cadmium isotope, remained.

In order to confirm the elemental assignment and establish the mass number, silver was removed at regular time intervals from the chemically separated cadmium produced in other targets. Decay curves typical of these silver milkings are given in figure 2. Each of these curves could be resolved into a 27 min component corresponding [2, 3, 4]) to Ag^{104} and a 1.15 ± 0.1 h component corresponding [2, 3, 4]) to Ag^{103}. The activities were also identified by their gamma-ray spectra to energies of 1 MeV, which were found to be in accord with the published data [4, 5, 6]). (However, the previously [3]) reported 0.12 MeV Ag^{103} gamma-ray could be resolved into two components of 0.11 and 0.13 MeV.) Since the milkings were performed at regular intervals the daughter activities in the several fractions, when extrapolated to the time of milking, should decrease in activity with the half-life of the parent. As expected the Ag^{104} milkings indicated a half-life of about 57 ± 2 min for their Cd^{104} parent. The Ag^{103}

† Present address: Synchro-Cyclotron Division, CERN, Geneva, Switzerland.

†† Work supported by the U. S. Atomic Energy Commission.

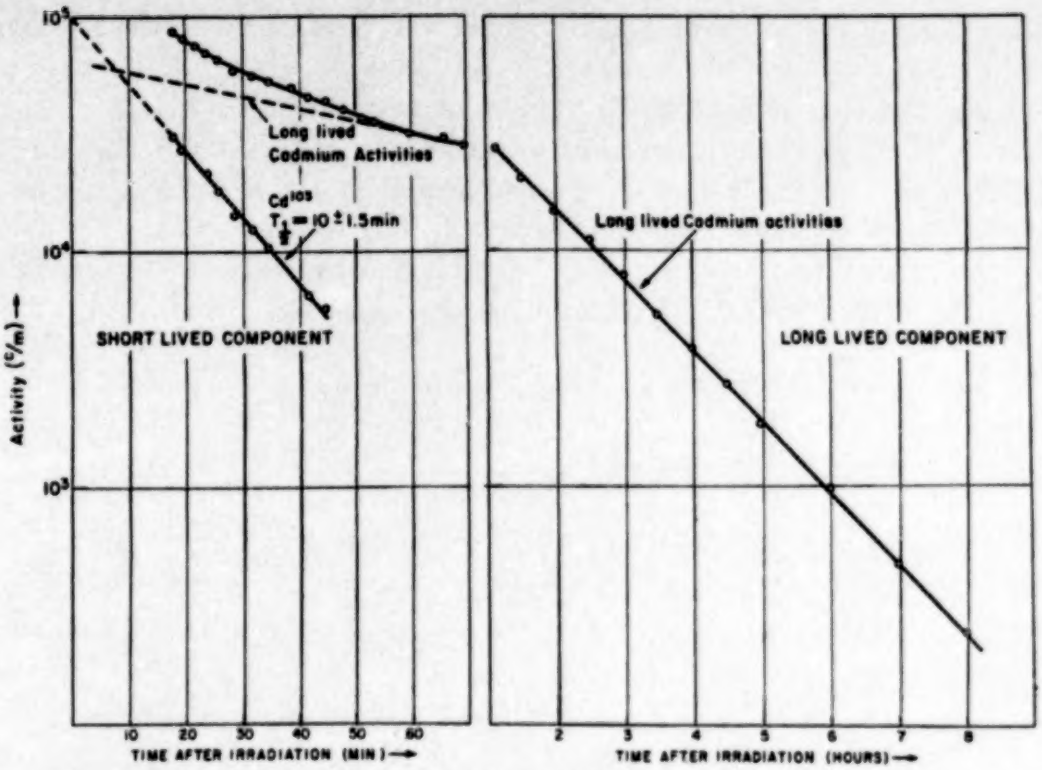

Fig. 1. Gross decay of chemically separated cadmium produced by a 5 min bombardment of Mo_2O_3 with 160 MeV O^{16}.

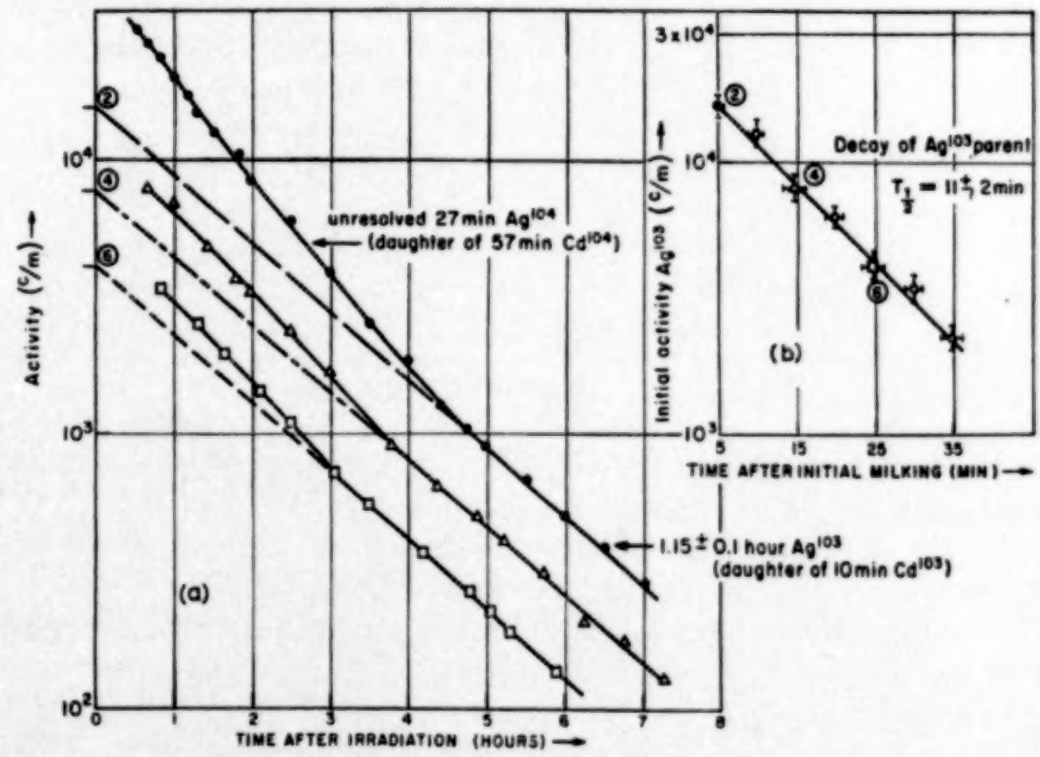

Fig. 2(a). Gross decay of silver daughters separated from the cadmium chemical fraction after a 20 min irradiation of Mo_2O_3 with 160 MeV O^{16}. (b) Initial activity of 1.15 hour Ag^{103} versus the time of separation.

milkings gave a half-life of 11 ± 2 min for Cd^{103}, in accord with the direct measurement.

To further characterize Cd^{103}, gamma-rays from the cadmium fractions resulting from short bombardments were examined using 7.6 cm$\times$7.6 cm NaI(Tl) crystal and a 400-channel pulse height analyzer. Typical spectra at various states of decay are given in fig. 3. The peaks at 0.22 ± 0.03 MeV, 0.625 ± 0.03 MeV and 0.85 ± 0.03 MeV exhibit half-lives of between 10 and 20 min, and cannot be associated with previously characterized cadmium isotopes

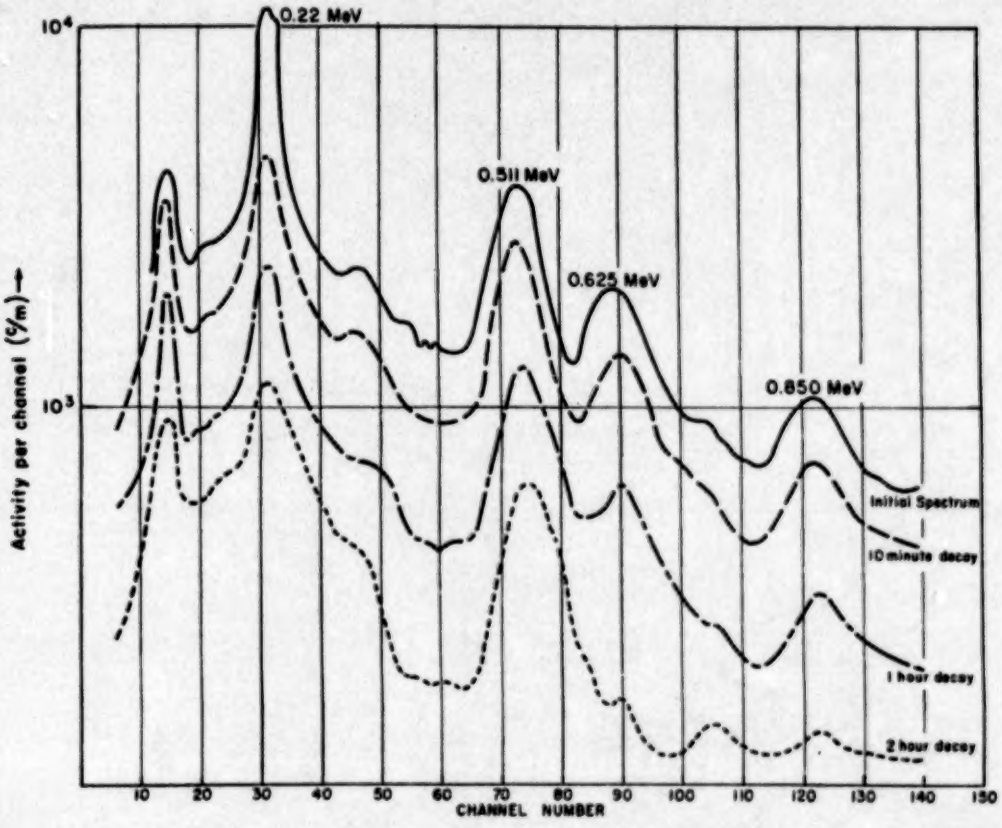

Fig. 3. Typical gamma-ray spectrum of Cd fraction after 5 min irradiation of Mo_2O_3 with 160 MeV O^{16}.

of longer half-lives. The 0.511 MeV positon annihilation peak decay could be resolved into 10—20 min and 1 h half-lives corresponding to Cd^{103} and Cd^{105}. Other peaks were observed but remain unassigned because of the background of radiation from cadmium isotopes other than Cd^{103}.

In summary, it is concluded that Cd^{103} decays, largely by positon emission, with a half-life of 10 ± 1.5 min. The associated gamma-rays observed have energies of 0.22 ± 0.03, 0.62 ± 0.03 and 0.85 ± 0.03 MeV.

The help and patience of the operating staff of the heavy ion accelerator is gratefully acknowledged.

References

1) A. A. Noyes and W. C. Bray, Qualitative analysis of the rare elements (MacMillan, London, 1927), pp 125–144
2) Strominger, Hollander and Seaborg, Rev. Mod. Phys. **30** (1958) 681
3) R. K. Girgis and R. van Lieshout, Nuclear Physics **13** (1959) 493
4) H. Nutley and J. B. Gerhart, Bul. Am. Phys. Soc. **5** (1960) 240
5) Bendel, Shore, Brown and Becker, Phys. Rev. **87** (1953) 888
6) Ames, Bernstein, Brennan, Haberstroh and Hamilton, Phys. Rev. **118** (1960) 1599

2.J

Nuclear Physics **18** (1960) 628—637; © *North-Holland Publishing Co., Amsterdam*

Not to be reproduced by photoprint or microfilm without written permission from the publisher

ABSOLUTE CROSS-SECTIONS OF $C^{12}(p, pn)C^{11}$ FROM 288 TO 383 MeV

VASTUPAL PARIKH †

Nuclear Physics Research Laboratory, Liverpool

Received 28 May 1960

Abstract: The excitation function for the reaction $C^{12}(p, pn)C^{11}$ is measured in the external proton beam of a 396 cm synchro-cyclotron. The C^{11} activity is measured by a calibrated γ-ray G. M. counter. The results are compared with those reported from other laboratories.

1. Introduction

The production of C^{11} by the bombardment of carbon by high energy protons has been studied extensively [1–8]) as this reaction provides a convenient monitor of proton flux. C^{11} decays by positon emission (0.97 MeV) and has 20.5 ± 0.3 min half-life; it is therefore quite suitable for short activation and also permits a convenient counting period. The threshold of this reaction is 18.5 ± 0.3 MeV, which helps to discriminate against low energy particle background.

In the earlier experiments, the C^{11} activity induced in carbon was measured with an end-window β-counter. This method of detection has the disadvantage that many corrections have to be applied such as those due to back-scattering, source thickness and the absorption in the window. We chose to use a gamma-ray counter as the above mentioned corrections are of little importance and hence a precise determination of efficiency is possible.

The energy of the incident protons is in the range of 288 to 383 MeV, an energy region in which there exists a lack of agreement in the measured values of the cross-section for this reaction.

2. Experimental Arrangement

2.1. EXTERNAL PROTON BEAM

A well collimated beam of protons from the 396 cm cyclotron is made available by deflecting the circulating beam by a "peeler-regenerator" system. Fig. 1 shows the path of the extracted beam of protons through various collimators before it is collected by a Faraday cup.

The "spilled-out" protons from the magnetic channel are fed into an evacuated pipe 4.5 m long and 15 cm in diameter, passing through the concrete shielding wall. In the tube the wide beam is collimated by a copper collimator 15 cm long

† Present address: Laboratoire des Hautes Énergies, B.P. No 5, Orsay (S. et O.), France.

with cross-section 1.102 cm × 3.81 cm. The beam is then deflected through 20° by the bending magnet which removes contamination in the beam due to neutrons and low energy protons produced by the premagnet collimator. The beam then travels through a 4 m long tube, at the end of which a copper collimator is placed which determines the cross-section of the beam. The beam then passes through another tube 2.5 m long at the centre of which an anti-scattering copper collimator with a hole 5.1 cm in diameter, is placed. The beam emerges from an aluminium window 0.05 mm thick, directly into air. The target was placed 60 cm beyond the end-window and the Faraday cup was fixed 1.5 m from the target. The area of the beam striking the target was 1.9 × 1.9 cm^2.

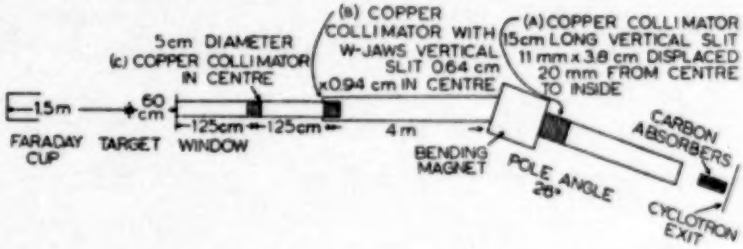
(B) COPPER COLLIMATOR WITH W-JAWS VERTICAL SLIT 0.64 cm x 0.94 cm IN CENTRE
(A) COPPER COLLIMATOR 15cm LONG VERTICAL SLIT 11 mm x 3.8 cm DISPLACED 20 mm FROM CENTRE TO INSIDE
5cm DIAMETER (C) COPPER COLLIMATOR IN CENTRE
1.5m
60 cm
1.25cm
1.25cm
4 m
FARADAY CUP
TARGET
WINDOW
BENDING MAGNET
POLE ANGLE 20°
CARBON ABSORBERS
CYCLOTRON EXIT

Fig. 1. The arrangement for exposures in the external beam of protons.

When using the maximum beam energy, with no absorber, collimator B was placed at the exit of the magnetic channel. Then the size of the beam at the target was 1 × 1 cm^2. A beam of 10^9 protons per second was available at the full energy. The energy of the protons was reduced by placing carbon absorbers at the exit of magnetic channel. At the reduced energy, the intensity was 10^7 protons per second. The energy spread of the incident beam was about ±3 MeV.

2.2. TARGETS

The targets were made of graphite 3.8 cm × 3.8 cm and 0.54 g/cm^2 thick. Only those targets were used which were uniformly thick to within a fraction of a per cent. As the targets were comparatively thick a few measurements were made on thin targets, 0.17 g/cm^2 thick, to observe the effect on C^{11} activity due to secondary nucleons produced by nuclear interaction in the target. The targets were weighed and their areas measured to an accuracy better than 0.1 %. To avoid loss or gain of activity due to recoil, polystyrene guard foils 25μm thick were placed on both sides of the target. Following the usual practice, we have not taken into consideration the 1.1 % of C^{13} present in the target in calculating the number of C^{12} atoms in the target.

2.3. BEAM MONITORING

The proton flux was collected by the Faraday cup and the charge was integrated by a circuit due to Lewis and Collinge (10).

3. The Calibration of the Gamma-ray Counter

The induced activity in carbon was measured by a gamma-ray counter. The counter was calibrated for different energies of gamma-rays emitted from Au^{198}, Co^{60} and Na^{24}. These radio-active isotopes have comparatively simple decay schemes and convenient half-lives. The calibrated sources of Au^{198} and Co^{60} were obtained from Harwell and the calibrations were checked by us by the beta-gamma coincidence method. The Na^{24} was prepared by exposing thin aluminium plates in the internal beam of synchocyclotron using the reaction $Al^{27}(p, 3pn)Na^{24}$ and the absolute strength measured in the same way.

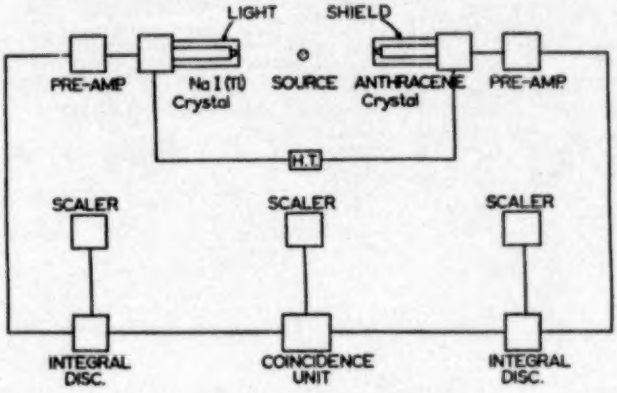

Fig. 2. Schematic diagram of the experimental arrangement used for the source calibration.

Fig. 2 shows the experimental arrangement for measuring absolute source strengths by beta-gamma coincidences.

The calibration of the sources of Co^{60} and the Au^{198} was done by using scintillation counters, and these measurements were checked by replacing scintillation counters by G.M. counters and repeating the measurements. After the precise determination of the source strength of Au^{198}, Co^{60} and Na^{24}, a gamma-ray counter supplied by Cinema, Television Ltd., was calibrated for different energies of gamma-rays emitted from these sources.

Fig. 3 shows the arrangement used for the calibration. The counter was placed in a cylindrical copper case and held by a spring against stops so that it remained in a definite position. The brass stand, which this cylindrical copper case was attached to, was divided into seven equally spaced compartments or shelves.

The sources were put into identical aluminium containers. The thickness of aluminium was sufficient to stop electrons emitted from Au^{198}, Co^{60} and Na^{24}. The voltage to the anode of the counter was from a R. F. electronically stabilized power supply. The counter was "quenched" electronically by a one-shot multivibrator circuit. The counting rate was corrected for background radiation and the "dead-time" of the counting system.

The efficiency curve as a function of gamma-ray energy, when the sources were placed on seventh shelf, is shown in fig. 4. The efficiency of the counter for the annihilation radiation, 0.51 MeV and for the gamma-ray energy of 0.48 MeV

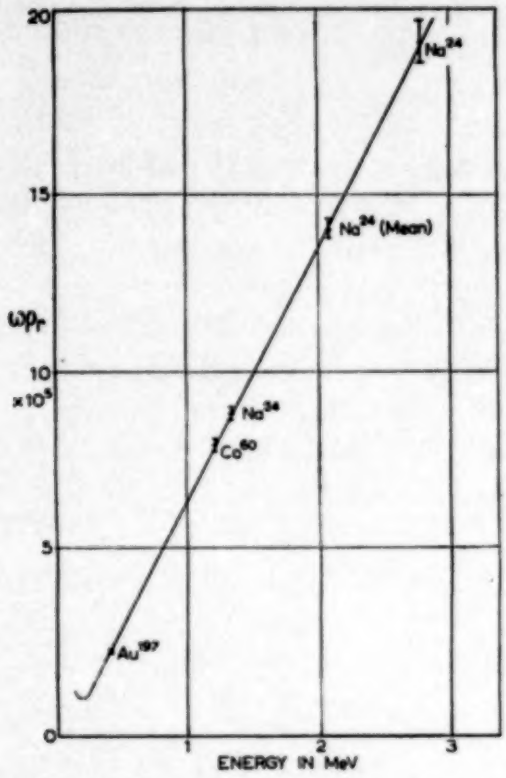

Fig. 4. Efficiency of the gamma-ray counter as a function of gamma-ray energy.

which is necessary for the evaluation of the absolute activity of positon emitting radioactive nuclei and Be^7, were determined by interpolation and were found to be

$$\omega_{E0.51} = 2.85 \times 10^{-5} \pm 2.8\ \%, \quad \omega_{E0.48} = 2.72 \times 10^{-5} \pm 2.8\ \%.$$

The errors include contributions from errors in the source strength measurements, the statistical counting error and the error involved in interpolation. The ratio $\omega_{E0.51}/\omega_{E0.48}$ is 1.048, which agrees very well with the value 1.04 reported by Dickson and Randle [11]).

The long term stability of the counter was checked from time to time with a standard Co^{60} source and the value of the efficiency was found to be constant within the counting error, throughout the experiment.

4. The Measurement of C^{11} Activity and the Corrections to be applied to the Measured Activity

The rate of decay of C^{11} activity was measured by the calibrated gamma-ray counter in an arrangement described earlier. The active source was placed on

either shelf 1 or shelf 4, depending on the strength of the source. The targets were counted for three or more half-lives and were found to follow a 20.5 min period. The disintegration rate was corrected for background radiation, dead-time of the counter and decay after the exposure. The "weighted" mean of all observations for each run was used for calculation of the cross-section.

4.1. CORRECTION DUE TO BEAM INTENSITY VARIATION DURING THE TARGET EXPOSURE

The bombardment period at full energy was 10 min, however, for the target exposure with protons of degraded energy when the flux was comparatively small, 20 min exposure were sometimes needed to obtain statistical accuracy in the counting of C^{11} activity. As the exposures were long, correction for the variation of the beam intensity was applied. At small regular intervals $\Delta t_1, \Delta t_2, \ldots, \Delta t_n (\Delta t_i = 1 \text{ min})$, the number of clicks on the integrator was noted. The interval Δt_i was small compared to the half-life of the activity. If I_n is the proton current in the interval Δt_n, after applying decay correction in this interval, we have

$$N(\Delta t_n) = I_n \sigma x \int_0^{\Delta t_n} e^{\lambda t} \mathrm{d}t = I_n \sigma x e^{\lambda \Delta t_n} \Delta t_n (1 - \tfrac{1}{2}\lambda \Delta t_n)$$

where σ is the cross-section for $C^{12}(p, pn)C^{11}$ in cm^2, x is the number of C^{12} atoms per cm^2, and where higher orders of Δt_n are neglected.

The total number of radio-active nuclei present at the end of the bombardment, after applying decay corrections in $\Delta t_1, \Delta t_2, \ldots, \Delta t_n$, is

$$\sum_{i=1}^{i=n} N(\Delta t_i) = \sigma x \{ I_1 \Delta t_1 (1 - \tfrac{1}{2}\lambda \Delta t_1) e^{\lambda(\Delta t_1 + \Delta t_2 + \ldots + \Delta t_n)} + I_2 \Delta t_2 (1 - \tfrac{1}{2}\lambda \Delta t_2) e^{\lambda(\Delta t_2 + \Delta t_3 + \ldots + \Delta t_n)} + \ldots + I_n \Delta t_n (1 - \tfrac{1}{2}\lambda \Delta t_n) e^{\lambda \Delta t_n} \}.$$

The number of radio-active nuclei decaying per second at the end of the bombardment time T is

$$\left(\frac{\mathrm{d}N}{\mathrm{d}t}\right)_T = -\lambda \{ [\sum_{i=1}^{i=n} N(\Delta t_i) e^{-\lambda T} \}.$$

The reaction cross-section can now be expressed as

$$= \frac{\left(\frac{\mathrm{d}N}{\mathrm{d}t}\right)_T}{\lambda x \{ I_1 \Delta t_1 (1 - \tfrac{1}{2}\lambda \Delta t_1) + I_2 \Delta t_2 (1 - \tfrac{1}{2}\lambda \Delta t_2) e^{-\lambda (T - \sum_1^n \Delta t_i)} + \ldots + I_n \Delta t_n (1 - \tfrac{1}{2}\lambda \Delta t_n) e^{-\lambda (T - \Delta t_n)}} \tag{1}$$

If the current is constant, the relationship (1) can be expressed as

$$\sigma = \frac{\left(\frac{\mathrm{d}N}{\mathrm{d}t}\right)_T}{Ix(1 - e^{-\lambda T})}. \tag{2}$$

In practice, the correction for the beam intensity variation was only about 1 %.

4.2. CORRECTION DUE TO THE FINITE SIZE OF THE SOURCE AND ABSORPTION OF PROTONS IN THE TARGET

During the cross-section measurements at reduced proton energy it was necessary to increase the area of the beam to obtain greater intensity. Since the efficiency of the γ-counter was determined with nearly point sources a correction for the finite size of the source had to be made.

A point Co^{60} source was counted on the horizontal plane of the shelves, parallel and perpendicular to the axis of the counter. The counting rates at various distances from the centre of the shelf were measured. It was found that when the size of the source was 1.9×1.9 cm^2, the efficiency on shelf 1 would have to be decreased 4.4 % while for the same size of the source no correction was necessary for shelf 4.

This correction was checked by measuring the absolute reaction cross-section at full energy with the beam size 1.9×1.9 cm^2 by placing the target on shelf 1 and using the value of efficiency on shelf 1 uncorrected for the size of the source. The statistical counting accuracy for C^{11} activity was less than 0.5 %. It was found that the value of cross-section obtained in this manner was 4.4 % lower than the mean value of cross-section at full energy measured on shelf 4. A correction of 4.4 % was therefore applied to the cross-section measurements for protons of degraded energy which were carried out on shelf 1.

As the targets are rather thick, a small correction for the proton absorption in the target is necessary. By taking the value of total cross section of protons of 315 MeV to be 29×10^{-26} cm^2 given by de Carvalho [12]), the correction for a 0.32 cm thick target is -0.8 % and for a 0.10 cm thick target, the correction is -0.3 %.

5. Results for the Cross-section for the $C^{12}(p, pn)C^{11}$ Reaction between 288 MeV and 383 MeV

Table 1 shows the results obtained for the cross-section at the full energy 383 MeV of the extracted beam for several independent runs. In table 2, the cross-section measurements are given at reduced proton energy.

The mean value of the cross-section at full energy for the thick target is the same as for the thin target. As there is no difference outside the counting error, it is difficult to say anything about the contribution to C^{11} activity from secondary nucleons produced in the target. We have made a crude estimate from the data of star production by protons of 400 MeV in medium heavy nuclei, by Bernardini *et al.* [13]). Assuming that the same number of neutrons are emitted as protons in a star event in a light element, the contribution to C^{11} activity from secondary nucleons is about 1 % for the thicker target. However, for the present, we have not applied this correction because of uncertain approximations involved in the calculations.

During full energy measurements collimator B in fig. 1 was not used. However, during degraded energy measurements collimator B defines the beam. As the targets were placed at 3 m from the collimator, the neutron contamination should be quite negligible as compared to the proton flux.

TABLE 1

Cross-section at 383 MeV

Target thickness (g/cm²)	Run	Date	Counts per min at end of exposure	Cross-section (mb) [a]	Mean cross-section (mb) [b]
0.54	1	24/6/55	$1.60 \times 10^3 \pm 3.1$ %	31.1 ± 3.1 %	31.6 ± 0.1 %
	2	24/10/55	$3.715 \times 10^3 \pm 0.6$ %	32.0 ± 0.6 %	
	3	24/10/55	$3.182 \times 10^3 \pm 0.7$ %	31.4 ± 0.7 %	
	4	24/10/55	$1.437 \times 10^3 \pm 1$ %	31.8 ± 1 %	
	5	24/10/55	$8.88 \times 10^2 \pm 1$ %	32.0 ± 1 %	
	6	10/12/55	$9.88 \times 10^2 \pm 2$ %	32.1 ± 2.6 %	
0.17	1	10/12/55	$2.78 \times 10^2 \pm 3.8$ %	30.1 ± 3.8 %	31.6 ± 1.6 %
	2	10/12/55	$5.56 \times 10^2 \pm 2.2$ %	31.8 ± 2.2 %	
	3	10/12/55	$3.81 \times 10^2 \pm 3.1$ %	32.6 ± 3.1 %	

[a]) Cross-section without applying correction due to absorption of protons in the target (the error shown is the "counting" error only).

[b]) Cross-section after applying correction due to absorption of proton in the target (the error shown is the "counting" error only)

TABLE 2

Cross-section from 288 to 383 MeV

Energy of protons (MeV)	Counts/min at end of exposure	Cross-section (mb) [a]
288	$1.55 \times 10^3 \pm 2.2$ %	33.7 ± 1.2
313	$3.44 \times 10^3 \pm 1.3$ %	34.8 ± 1.1
339	$3.57 \times 10^3 \pm 1.4$ %	34.9 ± 1.0
362	$4.97 \times 10^3 \pm 1.1$ %	32.4 ± 1.0
383	see table 1	31.6 ± 1.0

[a]) The error shown on the cross-section is the compounded error due to 1) 2.7 % uncertainty in efficiency calibration, 2) 1.3 % uncertainty in monitoring proton flux, 3) statistical uncertainty in counting C^{11} shown in each case.

Another possible activity present in carbon would be Be^7 from the reaction $C^{12}(p, 3p3n)Be^7$. Since it has a comparatively long half-life (54.5 d) and low production cross-section, it was not possible to detect its presence in the decay curve. The ratio of C^{11} activity to Be^7 activity obtained by exposing a carbon plate in the circulating beam was 2.4×10^5. Thus, the contribution of Be^7 activity is negligible.

6. Comparison with other Experimental Data

Fig. 5 shows the excitation function based on experimental results obtained at Berkeley, Birmingham, Chicago and Liverpool.

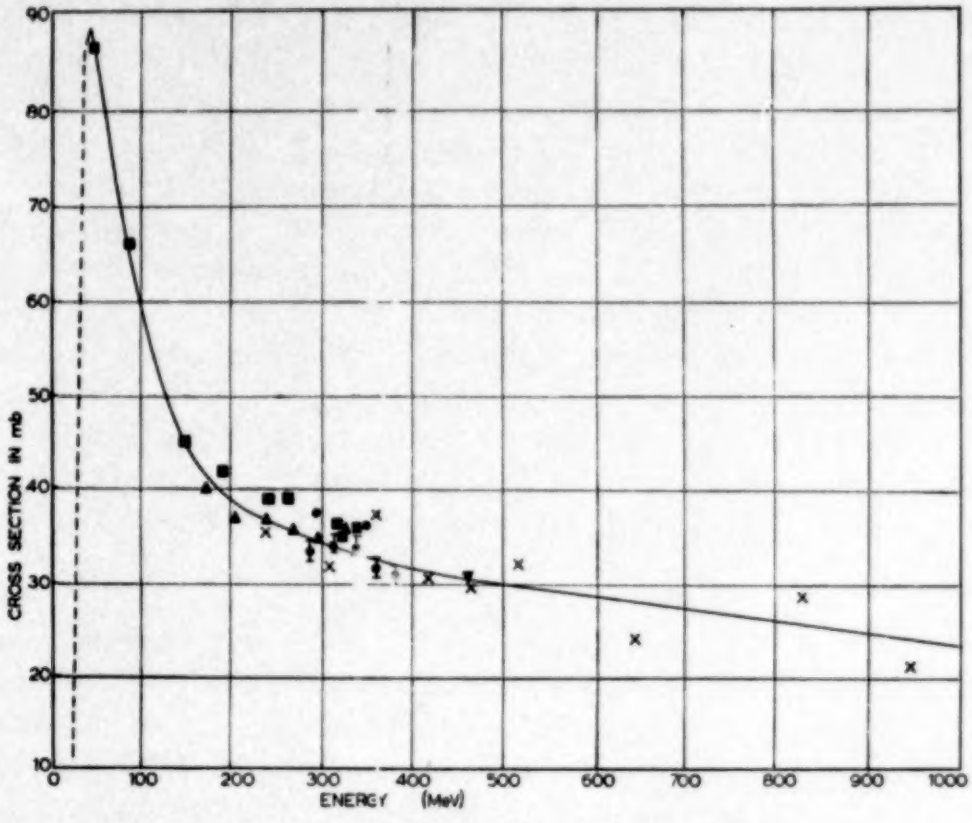

Fig. 5. Excitation function of $C^{13}(p, pn)C^{11}$.

■ Aamodt *et al.* (Corrected values)
● Good geometry } Crandall *et al.*
▲ Bad geometry }
× Burcham *et al.*
▼ Rosenfeld *et al.*
Parikh

The main differences between the earlier result obtained by Aamodt *et al.* and those obtained by others are:

1) the type of counter used for counting C^{11} activity;

2) the method of degrading the energy of incident protons. Aamodt *et al.* have assumed that the efficiency calibration of the beta-counter is the same for negatons and positons of the same energy. However, the dependence of the efficiency on the sign of the beta-particle has been demonstrated by Seliger [14]). On this basis, Rosenfeld *et al.* have estimated the error involved in the efficiency calibration of the end-window beta-counter and they reckon that the efficiency as measured by Aamodt *et al.* should be raised by 7 %. If one applies this correction, the value of the cross-section 41.2 mb $\pm$11 % at 340 MeV, obtained by Aamodt *et al.*, now becomes 38.3 mb $\pm$11 % in reasonable agreement with the value 36 mb $\pm$5 % at 350 MeV, obtained by Crandall *et al.*

The higher values of the cross-section at degraded energies obtained by Aamodt *et al.* were due to the spurious C^{11} activity generated by secondary low energy protons and neutrons produced in the absorber. This has been experimentally verified by Crandall *et al.* who have shown that the contribution of spurious C^{11} activity was 7 % for 5 to 20 cm absorber thickness of carbon. The dip in the excitation function of C^{12}(p, ph)C^{11} by Aamodt *et al.* at their highest energy disappears when corrections are made for this effect.

The points marked with a black triangle in fig. 5 are the cross-section obtained in "poor geometry" by Crandall *et al.* normalized to "good geometry" arrangement. The discrepancy between the "corrected" cross-section of Aamodt *et al.* at energy below 240 MeV and those obtained by Crandall *et al.* is not easily understood. The higher value obtained by Crandall *et al.* might possibly be due to the fact that they used copper instead of carbon for slowing down the protons.

The results of Burcham *et al.* are not easy to compare because of large experimental errors due to uncertainties involved in correcting their cross-sections for the large neutron background present around the proton synchrotron. The main uncertainties are due to

1) measurements of neutron background;

2) values of absolute cross-sections for C^{12}(n, 2n)C^{11} as a function of energy.

They have monitored the neutron flux by exposing Ilford G-5 nuclear track plates and counting stars with two or more prongs with or without primary. These measurements on stars they have compared with similar proton induced stars, and assuming the same cross-section for star production by neutron and proton they have estimated neutron contamination in the proton beam. Further, they have also assumed that the cross-section for the production of C^{11} from C^{12} by (p, pn) and (n, 2n) reactions is in the ratio 2.4 : 1; and that this ratio is independent of energy. Thus the correction in C^{11} activity due to neutron background depends on the validity of these different assumptions and can only be properly ascertained when more experimental information on these issues is available.

The target thickness which they had used in the measurements for self-absorption correction was 5 mg/cm^2 of polystyrene and the self absorption correction determined was 3 %. Rosenfeld *et al.* have used 4 mg/cm^2 of polyethylene foil and the correction they determined was less than a per cent, while Crandall *et al.*'s self-absorption curve for the same thickness of 4 mg/cm^2 of polystyrene gives 5 % self-absorption correction. A precise comparison of results obtained by different groups is thereby rendered more difficult.

Our cross-section measurement at 383 MeV agrees very well with the cross-section measurement at 461 MeV by Rosenfeld *et al.* The consistently higher value of the cross-section by Crandal *et al.* in our energy region is not easily understood.

7. Conclusion

We believe that our results obtained by employing a gamma-ray counter are at least as accurate as those from the best work with beta-counters. The only uncertainty is in the correction to be applied to C^{11} activity due to secondary nucleons generated within the target. However, this would have the effect of reducing the cross-section by less than one per cent.

The excitation function from 150 MeV upwards does not show any marked variation with energy. The π-meson production threshold in carbon is about 200 MeV and increases rapidly with increasing energy of protons. If low energy mesons were absorbed in the nucleus in which they were created, with the availability of rest mass energy of meson to the nucleus, the probability of ejecting more particles than one becomes important. As the excitation function of $C^{12}(p, pn)C^{11}$ is fairly insensitive to energy in this region, one can conclude that this process of meson absorption does not have a significant effect.

The change in the value of absolute cross-section from the earlier measurements by Aamodt *et al.*, affects those experiments whose beam monitoring was done by using this reaction. A list of experiments of which the results should be corrected has been given by Crandall *et al.*

I am thankful to the late Prof. H. W. B. Skinner for his interest and encouragement. I am indebted to Dr. J. J. Holt under whose guidance and help this experiment was carried out; his suggestions and criticisms were of great help in the writing of this paper. I am also thankful to Drs. D. Harting, A. Moore and D. Edwards for their kind assistance during the target exposures. My thanks are also due to the cyclotron crew under Mr. B. Halliday.

References

1) W. Chupp and E. McMillan, Phys. Rev. **72** (1947) 873
2) McMillian and Miller, Phys. Rev. **73** (1948) 80
3) Panofsky and Philips, Phys. Rev. **74** (1948) 1732
4) R. Aamodt, V. Peterson and R. Philips, Phys. Rev. **88** (1952) 739
5) A. M. Rosenfeld, Phys. Rev. **96** (1954) 1714
6) Crandall, Millburn, Pyle and Birnbaum, Phys. Rev. **101** (1956) 329
7) A. M. Rosenfeld, R. A. Swanson and S. D. Warshaw, Phys. Rev. **105** (1956) 413
8) W. E. Burcham, J. L. Symonds and J. Young, Proc. Phys. Soc. A **68** (1955) 1001
9) D. Harting, J. R. Holt and J. A. Moore, Proc. Phys. Soc. **71** (1958) 770
10) I. Lewis and B. Collinge, Rev. Sci. Inst. **24** (1953) 113
11) J. Dickson and I. Randle, Proc. Phys. Soc. A **64** (1951) 902
12) M. De Carvalho, Phys. Rev. **96** (1954) 399
13) Bernardini, Booth and Lindenbaum, Phys. Rev. **85** (1952) 826
14) M. M. Seliger, Phys. Rev. **88** (1952) 408

2.J

Nuclear Physics 18 (1960) 638—645; © *North-Holland Publishing Co., Amsterdam*

Not to be reproduced by photoprint or microfilm without written permission from the publisher

CROSS-SECTIONS FOR $Al^{27}(p, 3pn)Na^{24}$, $Al^{27}(p, 5p5n)F^{18}$ AND $C^{12}(p, 3p3n)Be^{7}$ RELATIVE TO $C^{12}(p, pn)C^{11}$

VASTUPAL PARIKH †

Nuclear Physics Research Laboratory, Liverpool 3

Received 28 May 1960

Abstract: The excitation functions for the reactions $Al^{27}(p, 3pn)Na^{24}$, $Al^{27}(p, 5p5n)F^{18}$ and $C^{12}(p, 3p3n)Be^{7}$, are measured relative to $C^{12}(p, pn)C^{11}$ employing internal proton beam of a 396 cm synchro-cyclotron. The results are compared with those reported from other laboratories.

1. Cross-Sections for $Al^{27}(p, 3pn)Na^{24}$ and $Al^{27}(p, 5p5n)F^{18}$

1.1. INTRODUCTION

Besides $C^{12}(p, pn)C^{11}$, another reaction which provides possibilities as a monitoring reaction is $Al^{27}(p, 3pn)Na^{24}$ and it has been studied widely [1–7]). The reaction product Na^{24} has a convenient half-life of 15.1 h and decays by electron emission (1.4 MeV) followed by two gamma-rays of 2.76 MeV and 1.38 MeV in cascade. The isotope Al^{27} is readily available in pure form.

We report here the measurements we have made by exposing in the circulating beam, an aluminium target sandwiched between two carbon plates. The measurements extend from 220 to 362 MeV, an energy region in which the result reported on this reaction by different groups are not in good agreement. We shall represent results as $\sigma_C(C^{11})/\sigma_{Al}(Na^{24})$, $\sigma_{Al}(F^{18})/\sigma_{Al}(Na^{24})$, where the subscript indicates the target from which the radio-active isotope (shown in the bracket) was produced.

The main advantage in exposing the targets in the internal beam is its high intensity compared to the intensity of the extracted beam, which is smaller by a factor of about 100. The intense activity induced in the target compensates the disadvantage of very low efficiency of the gamma-ray counter, which was used for measuring the induced activities.

1.2. EXPERIMENTAL PROCEDURE

1.2.1. *The arrangement for exposing the target.* The aluminium target sandwiched between two carbon plates was exposed to the cirulating proton beam at different radii, from 173 cm to 127 cm, by an arrangement shown in fig. 1. Semi-circular targets of 1.3 cm radius were used with the straight edge vertical.

† Present address: Laboratoire des Hautes Énergies, B.P. No 5, Orsay (S. et O.), France.

The target sandwich was filed flat along the diameter and aligned carefully so that the front edges of the three targets would equally intercept the beam. For every exposure, one of the active targets was placed on an x-ray film for a short time and the beam was found to strike fairly uniformly along the diameter of the target.

As the beam intensity was high, exposures of 5 s were quite adequate. The energy of the protons striking the targets at a given radius was calculated from the momentum and $H\rho$ relationship. The energy of the protons thus obtained was corrected for the degradation of energy due to multiple traversal of the beam through the target [8]). For a given thickness of target we calculated the effective thickness for different radii at which the target was bombarded.

The energy loss of protons after passing through this effective thickness was determined from the range-energy relation for protons. The mean energy of the protons should be accurate to ± 15 MeV, the error arising mainly from the radial oscillations of the beam.

1.2.2. *Targets.* The aluminium and carbon targets were weighed accurately to a fraction of a per cent. Two sets of targets were used: a "thick" set of 0.31 g/cm^2 carbon and 0.54 g/cm^2 aluminium, and a "thin" set of 0.08 g/cm^2 carbon and 0.05 g/cm^2 aluminium.

1.2.3. *Counting procedure.* After the irradiation, the active targets were placed in identical aluminium containers and their respective activities were measured on the fourth shelf of the calibrated counter described in an earlier communication [9]). The counting rates were corrected for the background radiation and the dead-time of the Geiger counter. The carbon targets were counted for three to four half-lives; the 'gross' decay curve due to the activities in aluminium was followed for two to three days. The short-lived activities induced in the aluminium target died out in a few hours, and the curve then became a straight line (on a logarithmic scale) following the 15.1 h half-life due to Na^{24}. Any contributions from Be^7(54.5 d) and Na^{22}(2.6 y) were negligible.

Activities in the two carbon plates on either side of the aluminium target were normalized to 1 g/cm^2 thickness of carbon. The mean of the activities in these plates was used in the calculation of $\sigma_C(C^{11})/\sigma_{Al}(Na^{24})$. The difference between them varied from 0.6 % to 8 % due to imperfect alignment. This introduced one of the main uncertainties in our measurements of $\sigma_{Al}(Na^{24})$.

1.3. RESULTS

The disadvantage of using "thick targets" comes from the production of Na^{24} by secondary neutrons generated during nuclear collisions in the target assembly. The reaction $Al^{27}(n, \alpha)Na^{24}$ has an almost geometrical cross-section for neutrons with energy of a few MeV. This contribution should be negligible for the 'thin' targets, for which the total thickness of the sandwich is 0.21 g/cm^2,

TABLE 1

$\frac{\sigma_C(C^{11})}{\sigma_{Al}(Na^{24})}$ from 202 MeV to 342 MeV

Target thickness (g/cm^2)	Energy of protons (MeV)	Al $\left(\frac{dN}{dt}\right)$ Na^{24} (counts/min at end of exposure)	C $\left(\frac{dN}{dt}\right)$ C^{11} (counts/min at end of exposure) Target A	C $\left(\frac{dN}{dt}\right)$ C^{11} (counts/min at end of exposure) Target B	Activity of targets A and B normalized to 1 g/cm^2 thickness (counts/min)	$\frac{\sigma_C(C^{11})}{\sigma_{Al}(Na^{24})}$ without correcting for spurious Na^{24} activity	4.8 % correction for Na^{24} due to secondary neutrons	$\frac{\sigma_C(C^{11})}{\sigma_{Al}(Na^{24})}$ corrected
1.16	202	$1.057\times10^4\pm0.1$ %	$4.685\times10^5\pm0.4$ %	$4.346\times10^5\pm0.4$ %	A 6.100×10^5 B 5.622×10^5	3.81	0.18	3.99 ± 0.20
	259	$1.676\times10^3\pm0.5$ %	$6.980\times10^4\pm0.4$ %	$6.825\times10^4\pm0.4$ %	A 9.706×10^4 B 8.739×10^4	3.55	0.17	3.72 ± 0.15
	294	$4.141\times10^3\pm0.4$ %	$1.580\times10^5\pm0.4$ %	$1.580\times10^5\pm0.4$ %	A 2.066×10^5 B 2.053×10^5	3.40	0.16	3.56 ± 0.14
	342	$2.276\times10^3\pm0.5$ %	$8.339\times10^4\pm0.4$ %	$8.441\times10^4\pm0.4$ %	A 1.092×10^5 B 1.086×10^5	3.31	0.16	3.47 ± 0.13
0.21	202	$5.419\times10^3\pm0.1$ %	$6.826\times10^5\pm0.4$ %	$6.610\times10^5\pm0.4$ %	A 3.447×10^6 B 3.832×10^6			3.97 ± 0.18
	342	$7.633\times10^3\pm0.4$ %	$7.726\times10^5\pm0.4$ %	$7.520\times10^5\pm0.4$ %	A 4.110×10^6 B 4.420×10^6			3.49 ± 0.25

Error shown on $\sigma_C(C^{11})/\sigma_{Al}(Na^{24})$ is the compounded error due to 1) uncertainty in the annihilation radiation efficiency (2.7 %), 2) uncertainty in the Na^{24} gamma-radiation efficiency (2.5 %), 3) statistical counting error in measuring C^{11} activity, 4) statistical counting error in measuring Na^{24} activity, 5) uncertainty in the proton flux (which is taken as half the percentage difference between C^{11} activities in two carbon targets).

as according to Crandall *et al.*, for a stack of CH and aluminium of about 0.5 g/cm², this correction is less than 1 %. Our ratio of $\sigma_C(C^{11})/\sigma_{Al}(Na^{24})$ for the "thick" targets at 202 MeV and 342 MeV was found to be 4.2 % and 5.4 % less, respectively, than that obtained for the "thin" targets, as shown in table 1. We therefore applied a mean correction of 4.8 % to the ratio $\sigma_C(C^{11})/\sigma_{Al}(Na^{24})$ obtained from the thick targets. The results obtained for different runs with "thin" and "thick" targets are presented in table 1.

In the ratio $\sigma_C(C^{11})/\sigma_{Al}(Na^{24})$ no account has been taken for losses of Na^{24} and C^{11} due to momentum transfer by incident protons. Chackett *et al.* have shown that this loss is equivalent in activity to a thickness of aluminium of 1.6 μm and 0.7 μm for F^{18} and Na^{24} respectively. The aluminium target was 0.54 g/cm² thick, so that the correction due to recoil losses should be quite negligible. The carbon targets were 0.31 g/cm² thick, so that, in the same way, the recoil losses will not be of importance.

1.4. COMPARISON WITH OTHER EXPERIMENTAL DATA

The cross-section ratio $\sigma_C(C^{11})/\sigma_{Al}(Na^{24})$ measured by us, together with measurements reported elsewhere below 1 GeV, is shown in fig. 2. The initial

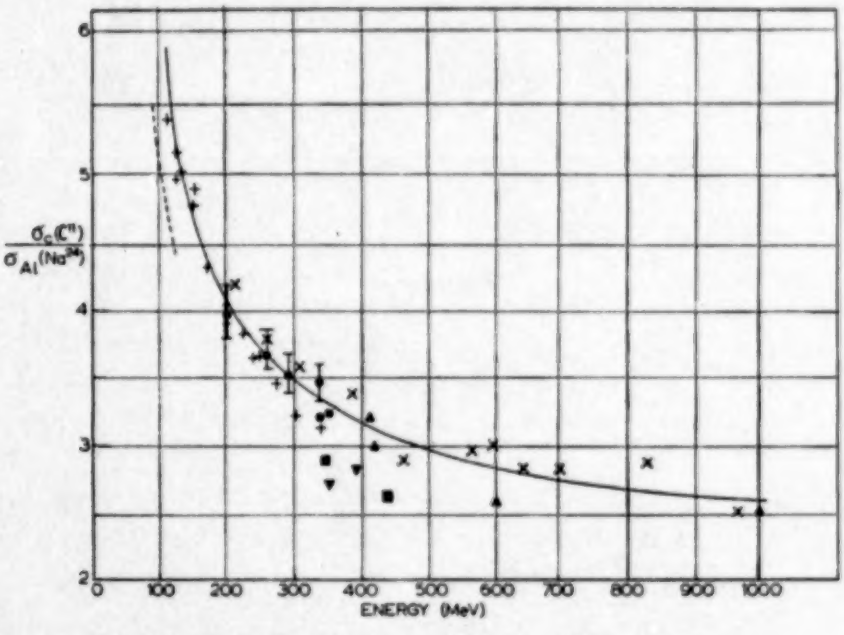

Fig. 2. The excitation function $\sigma_C(C^{11})/\sigma_{Al}(Na^{24})$.

---- Hintz and Ramsay
\+ Hicks *et al.*
× Chackett *et al.*
• Crandall *et al.*
▲ Wolfgang and Friedlander
▼ Miller
■ Turkevich
I Parikh

steep drop is based on the results of Hintz and Ramsay, which are lower in the energy range 50 to 125 MeV than the corresponding measurements by Hicks

et al. Our measurements, in the energy region corresponding to that investigated by Chackett *et al.*, are in excellent agreement with their results. However, their measurements have large errors of ± 15 %, the main uncertainty being due to the correction to be applied to the observed counting rate because of the difference between negaton and positon back-scattering. The results of Crandall *et al.* for 340 and 350 MeV protons are slightly lower than our values but are not outside the experimental error. One of the measurements by Wolfgang and Friedlander at 420 MeV agrees within experimental accuracy with our measurement at 342 MeV. The results of Hicks *et al.* indicate a steeper slope than that shown by Chackett *et al.* or by us. However, their results are not outside the experimental error of our measurements. The results obtained by Miller and also by Turkewitch are considerably lower. The discrepancy is not easy to assess as their experimental procedure is not available.

1.5. DISCUSSION

Fig. 3 shows the excitation function for the reaction $Al^{27}(p, 3pn)Na^{24}$ from 100 MeV to 1 000 MeV. The values of $\sigma_C(C^{11})$ and $\sigma_C(C^{11})/\sigma_{Al}(Na^{24})$, for a given energy have been obtained from the smooth curves drawn in fig. 5 of ref. [9]) and

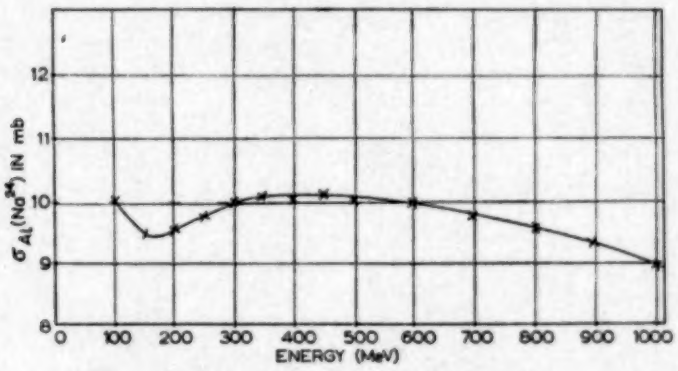

Fig. 3. The excitation function of $Al^{27}(p, 3pn)Na^{24}$.

fig. 2 of this paper. The striking feature of the curve is the slow rise in the value of cross-section from 150 to 300 MeV. The value of the cross-section remains constant from 300 MeV to 600 MeV and then slowly falls off with increasing energy of incident protons. The shape of the excitation function is quite different from that reported by Hicks *et al.*, the difference being due to the values of $\sigma_C(C^{11})$ chosen in the calculation of $\sigma_{Al}(Na^{24})$ from the value $\sigma_C(C^{11})/\sigma_{Al}(Na^{24})$. Hicks *et al.* have used the values $\sigma_C(C^{11})$ reported by Crandall *et al.*, viz. 36 mb from 200 MeV to 350 MeV, and consequently obtain a steeper rise in the cross-section $\sigma_{Al}(Na^{24})$ in this energy region.

The slight hump observed in the excitation function of $\sigma_{Al}(Na^{24})$ beyond 200 MeV is not easily understood. The meson production process is becoming important in this region. A possible explanation could be that slow mesons,

produced by the incident protons in the energy region beyond 200 MeV, are absorbed in the nucleus in which they are produced. This process would result in increasing excitation of that nucleus and consequently in increasing probability of emission of particles requisite for the production of Na^{24}. Beyond 600 MeV, however, the excitation is such that the probability for emitting many more particles than required to produce Na^{24} becomes more important. Hence the cross-section $\sigma_{Al}(Na^{24})$ begins to decrease as the energy of the incident protons increases.

1.6. RESULT FOR THE CROSS-SECTION RATIO $\sigma_{Al}(F^{18})/\sigma_{Al}(Na^{24})$

The activity due to F^{18} from the irradiated aluminium target was separated from the "gross" decay curve by a graphical method. Our measurements, together with measurements reported to date, are shown in fig. 4. All measure-

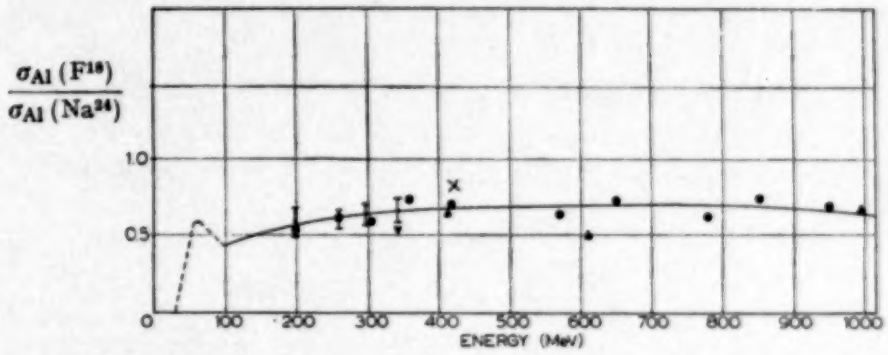

Fig. 4. The excitation function $\sigma_{Al}(F^{18})/\sigma_{Al}(Na^{24})$.

---- Hintz and Ramsay
• Chackett *et al.*
▲ Wolfgang and Friedlander
▼ Marquez and Perlman
× Marquez
I Parikh

ments shown are in excellent agreement within experimental errors. However, the accuracy of the results is such that no definite variation beyond meson production threshold could be established.

2. Cross-Section for the Reaction $C^{12}(p, 3p3n)Be^7$

2.1. INTRODUCTION

The production of Be^7 by proton bombardment of C^{12} was first reported by Dickson and Randle [10]) and the production cross-section from threshold to 155 MeV was measured by exposing carbon targets at various radii in the circulating beam of the Harwell cyclotron. The circulating beam was monitored by the $C^{12}(p, pn)C^{11}$ reaction. We have extended these measurements from 200 MeV to 352 MeV by irradiating carbon targets in the circulating beam.

2.2. THE EXPERIMENTAL PROCEDURE

The carbon targets, 0.3 cm thick, were exposed in the circulating beam at different radii; the details of the exposure and the correction to the incident proton energy due to multiple traversal of the beam through the target have been described earlier.

The targets were exposed for five minutes to the full beam and the induced C^{11} activity after a few half-lives was measured under the standard geometrical arrangement discussed in ref. [9]). The Be^7 activity was followed for 70 days after which the background became comparable to the Be^7 activity. The initial part of the decay curve showed an unidentified activity with a half-life of 12 h. possibly due to some impurity in the target. The contribution of the unidentified activity became unimportant after about two days, leaving only the Be^7 activity in the target with a half-life of 54.5 d. The activity was corrected for decay from the end of exposure of the target.

2.3. RESULTS AND DISCUSSION

Table 2 displays the measurements of $\sigma_c(C^{11})/\sigma_c(Be^7)$ for various energies of the incident protons. The main difference between our results and those reported by Dickson and Randle is that they have used 20.0 min as the half-life for

TABLE 2

$\frac{\sigma_c(C^{11})}{\sigma_c(Be^7)}$ from 202 MeV to 352 MeV

Energy of protons (MeV)	C^{11} (counts/min at the end of exposure)	Be^7 (counts/min at the end of exposure)	$\frac{\sigma_c(C^{11})}{\sigma_c(Be^7)}$
202	$9.87\times10^6\pm0.5$ %	$3.70\times10\pm0.5$ %	4.34 ± 0.12 [a])
252	$9.14\times10^6\pm0.5$ %	$3.45\times10\pm0.5$ %	4.30 ± 0.12
302	$7.77\times10^6\pm0.5$ %	$3.02\times10\pm0.5$ %	4.20 ± 0.12
342	$5.17\times10^6\pm0.5$ %	$2.12\times10\pm0.5$ %	3.97 ± 0.11
352	1) $9.39\times10^6\pm0.5$ %	$3.91\times10\pm0.5$ %	4.05 ± 0.11
	2) $9.24\times10^6\pm0.5$ %	$3.82\times10\pm0.5$ %	

[a]) The error shown on $\sigma_c(C^{11})/\sigma_c(Be^7)$ is compounded error due to the statistical uncertainty in measuring C^{11} and Be^7 activities and the uncertainty in the efficiency calibration of annihilation radiation (2.7 %); however, the relative error of each measurement is about 0.7 %.

C^{11} while we have used the more recent value 20.5 min. As the activities were measured after a few half-lives have elapsed, the difference in the two values introduces an error when the measured activities are extrapolated to the time at the end of the exposure. If one uses 20.5 min instead of 20.0 min for the half-life of C^{11} in order to compare the results, it will have the effect of reducing the cross-section ratio $\sigma_c(C^{11})/\sigma_c(Be^7)$ by 20 % according to Randle [11]). In fig. 5, we have shown the cross-sections $\sigma_c(Be^7)$ after applying this correction.

The values for the cross-section have been evaluated from the ratio $\sigma_c(C^{11})/\sigma_c(Be^7)$ at a given energy and taking corresponding values of $\sigma_c(C^{11})$ from the excitation function of $C^{12}(p, pn)C^{11}$, shown in ref. [9]).

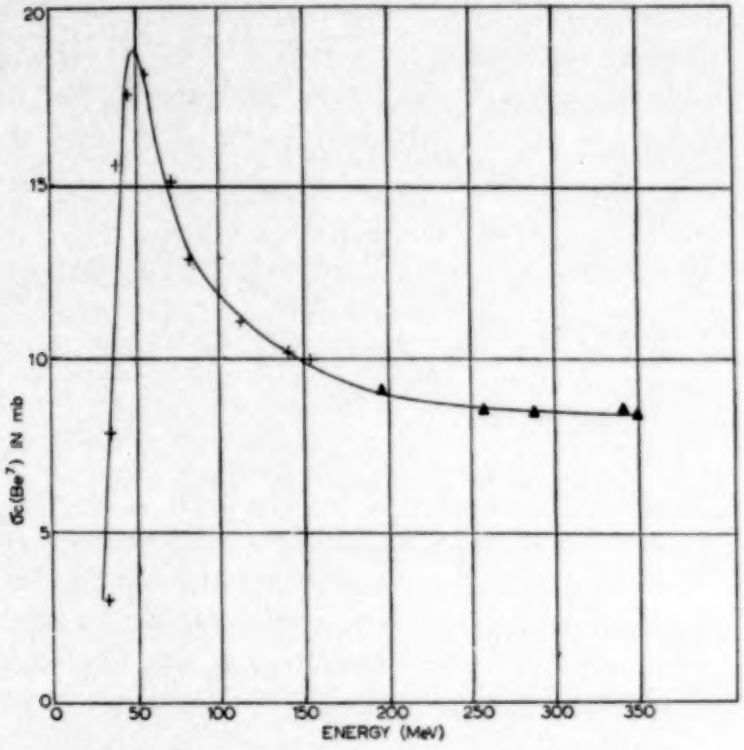

Fig. 5. The excitation function of $C^{12}(p, 3p\ 3n)Be^7$.
+ Dickson and Randle ▲ Parikh

I am thankful to the late Prof. H. W. B. Skinner for his interest and encouragement. I am indebted to Dr. J. J. Holt under whose guidance and help these experiments were carried out; his suggestions and criticisms were of great help in the writing of this paper. My thanks are also due to the cyclotron crew under Mr. B. Halliday who were most helpful during the irradiation of targets in the circulating beam.

References

1) F. Hintz and N. Ramsey, Phys. Rev. **88** (1952) 19
2) G. Chackett, K. Chackett, P. Reasbeck, J. Symonds and J. Warren, Proc. Phys. Soc. A **69** (1956) 43
3) R. Wolfgang and G. Friedlander, Phys. Rev. **96** (1954) 190
4) Crandall, Millburn, Pyle and Birnbaum, Phys. Rev. **101** (1956) 329
5) M. Hicks, P. Stevenson and W. Nervik, Phys. Rev. **102** (1956) 1390
6) L. Marquez and I. Pearlman, Phys. Rev. **81** (1951) 953
7) L. Marquez, Phys. Rev. **88** (1952) 225
8) J. Cassels, J. Dickson and J. Howlett, Proc. Phys. Soc. B **64** (1951) 590, 791
9) V. Parikh, Nuclear Physics **18** (1960) 628
10) J. Dickson and T. Randle, Nature **166** (1950) 235; Proc. Phys. Soc. A **64** (1951) 902
11) T. Randle, private communication

2.J

Nuclear Physics **18** (1960) 646—653; © *North-Holland Publishing Co., Amsterdam*

Not to be reproduced by photoprint or microfilm without written permission from the publisher

THE ACTIVITIES INDUCED IN BERYLLIUM, OXYGEN AND FLUORINE BY PROTONS OF 220 MeV TO 362 MeV

VASTUPAL PARIKH †

Nuclear Physics Research Laboratory, Liverpool 3

Received 28 May 1960

Abstract: The beryllium, oxygen and fluorine targets are bombarded in the internal proton beam of a 396 cm synchro-cyclotron. The reaction cross-sections for various spallation products are measured at different energies. The behaviour of high-energy proton induced reactions in some light elements is discussed.

1. Introduction

There is little information available on the spallation reaction products in light elements below aluminium when bombarded by high energy nucleons. High energy proton-induced stars in photographic plates give information on the disintegration of the light nuclei but since neutrons emitted in such events are not recorded, it is difficult to obtain precise information regarding the relative yields of the spallation reaction products. We have bombarded targets of beryllium, oxygen and fluorine with protons in the circulating beam of the Liverpool synchro-cyclotron and have measured the relative yields of short lived activities produced in these targets. The method of bombardment was similar to that described in a previous communication [1]). The contributions of the several radio-active products were separated from the gross decay curve by a graphical method.

We have also measured the absolute cross-section for the reaction $O^{16}(p, 3p3n)C^{11}$ using the extracted proton beam and a Faraday cup previously described [1]).

2. The Cross-sections for the Reaction $Be^9(p, p2n)Be^7$ relative to $C^{12}(p, pn)C^{11}$ at 352 MeV

The absolute cross-sections for the reaction $Be^9(p, p2n)Be^7$ have been obtained by Salter and Bird [2]) from threshold to 156 MeV, and by Batzel and Coleman [3]) from threshold to 340 MeV. There is a wide disagreement between the results reported by them. We have measured the cross-section for the above reaction at 352 MeV, in an attempt to check the reported measurements.

† Present address: Laboratoire des Hautes Énergies, B.P. No 5, Orsay (S. et O.), France.

A beryllium target 1.3 cm × 1.5 cm and 0.30 g/cm² thick was sandwiched between two similar carbon plates 0.22 g/cm² thick. The target assembly was irradiated for 3 min in the full circulating beam. After the exposure was over, the C^{11} and Be^{7} activities were measured with a calibrated gamma-ray counter in a standard geometrical arrangement. In the case of irradiated carbon targets both C^{11} and Be^{7} activities were measured. The Be^{7} activity induced in the carbon targets was followed for 70 days and the initial part of the decay curve had an unidentified activity perhaps due to impurity with a half-life of about 12 h. Its contribution became negligible after about two days and the remaining activity was due to Be^{7} with a half-life period of 54.5 d. The Be^{7} activity from

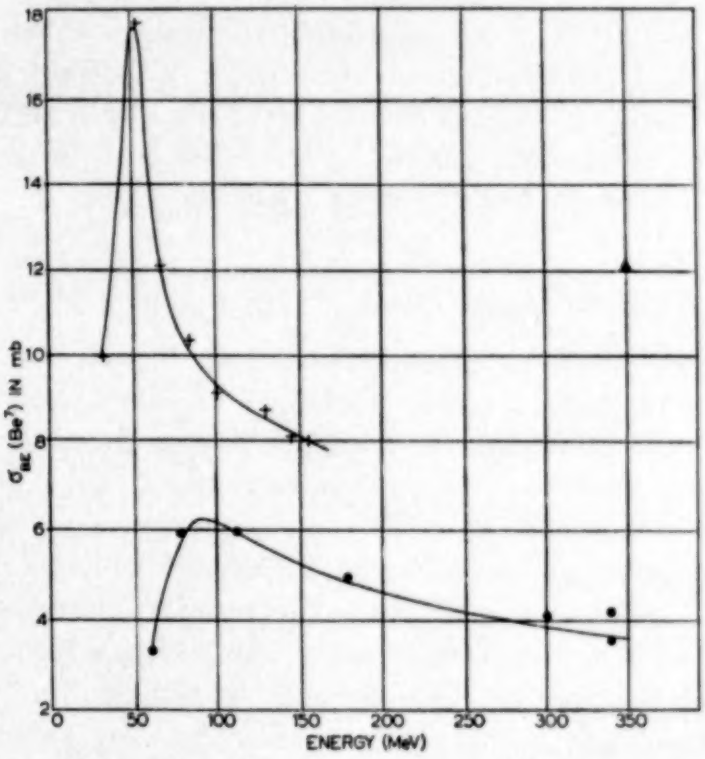

Fig. 1. The excitation function of Be^{9}(p, p 2n)Be^{7}.
+ Salter and Bird ● Batzel and Coleman ▲ Parikh

the irradiated beryllium target was followed for 120 days. The decay curve had two components. The unidentified activity, possibly due to an impurity in the target, had a half-life of about 8 d and its contribution became negligible after about 60 days, after which only the Be^{7} activity of 54.5 d half-life was left behind.

All the measurements by Salter and Bird were obtained relative to $\sigma_C(Be^7)$. They have evaluated the cross-section for $\sigma_{Be}(Be^7)$ by using their measured ratios $\sigma_{Be}(Be^7)/\sigma_C(Be^7)$ and the corresponding values of $\sigma_C(Be^7)$ measured by Dickson and Randle [4]). However, the values for the cross-section $\sigma_C(Be^7)$ were obtained by Dickson and Randle by using old measurements on $\sigma_C(C^{11})$ by

Aamodt *et al.* [5]) and the value 20.0 min as the half-life for C^{11}. We have corrected the values for $\sigma_{Be}(Be^7)$ obtained by Salter and Bird, by using the modified values of $\sigma_C(Be^7)$ obtained by Dickson and Randle as discussed in previous communications [1]). The results of Batzel and Coleman and of Salter and Bird, together with our measurements on $\sigma_{Be}(Be^7)$ at 352 MeV, are shown in fig. 1.

There is a wide discrepancy between our measurements and those by Batzel and Coleman. The main difference between our experimental procedure and theirs is that they have used a NaI crystal to detect annihilation gamma rays and a Geiger counter to detect Na^{24} activity. Also the cross section of their monitoring reaction $Al^{27}(p, 3pn)Na^{24}$ is based on old measurements by Hicks and Stevenson which are not published, so that it is difficult to say how their measurements on $\sigma_{Be}(Be^7)$ will be affected by the more recent measurements of $\sigma_{Al}(Na^{24})$ by Hicks and Stevenson [6]). Our value of $\sigma_{Be}(Be^7)$ at 352 MeV is higher than the value obtained by Salter and Bird at 156 MeV. To establish whether the cross-section really does increase between 150 MeV and 352 MeV, further measurements in this range are necessary.

3. Induced Activities in Oxygen and Fluorine

The target used for the measurement of the absolute cross-section of $O^{16}(p, 3p3n)C^{11}$ was distilled water. An aluminium container of size 3.8 cm × 3.8 cm with a small inlet at one of the corners was made and water was introduced by a syringe so that no bubbles were formed. The front and back sides of the container were made of thin aluminium sheet. After activating the target water was taken out with the syringe and was transferred to a similar aluminium container with sides sufficiently thick to stop all positons emitted by the radioactive nuclei. The weight of water and the area occupied by water inside the target container were measured permitting a determination of the number of oxygen atoms per cm^2. The volume of the measuring container was somewhat less than that of the target container so that the former could be completely filled, with a little to spare. Its volume was accurately known so that the specific activity of the water could be determined.

The target for bombarding oxygen in the circulating beam of protons was lithium hydroxide (LiOH). The possible product from lithium which can affect the measurements is Be^7 from the reaction $Li^7(p, n)Be^7$. However, as the Be^7 has a comparatively long half-life (54.5 d) the contribution due to this reaction was negligible. This was established by exposing lithium hydride (LiH) and measuring the activity due to Be^7.

Thin flakes of lithium hydroxide were prepared by adding distilled water to lithium hydride powder and drying the solution in a dessicator. The flakes of lithium hydroxide were fixed to the edge of aluminium strips which were clamped so that the beam hit the protruding edge of the flake. The initial counting

rate was about 10 000 times greater than that from a similar thickness of the lithium hydride exposed for the same time.

Fluorine was bombarded in the circulating beam in the form of lithium fluoride. The powder was sandwiched between aluminium plates, the edge projecting into the beam. To determine the absolute cross-section a special cell was constructed of carbon in which a known amount of lithium fluoride was pressed. The C^{11} activity induced in the carbon plates served to monitor the beam.

The targets were exposed in the circulating beam and the induced activities were measured with the calibrated gamma-ray counter as discussed in a previous communication. An exposure of about 5 s was quite sufficient. The "gross" decay curve was analysed graphically into its constituent components. As it was about eight minutes after the end of the exposure before the measurements of the activity could be started, it was not possible to observe the contribution of induced activities whose half-lives were less than a minute.

Table 1 gives the ratio $\sigma_0(O^{15})/\sigma_0(C^{11})$ and $\sigma_0(N^{13})/\sigma_0(C^{11})$ for proton bombarding energies of 222 MeV to 362 MeV. Table 2 gives the absolute cross-section $\sigma_0(O^{15})$. In table 3, $\sigma_F(O^{15})/\sigma_F(F^{18})$, $\sigma_F(N^{13})/\sigma_F(F^{18})$ and $\sigma_F(C^{11})/\sigma_F(F^{18})$

TABLE 1

$\frac{\sigma_0(O^{15})}{\sigma_0(C^{11})}$ and $\frac{\sigma_0(N^{13})}{\sigma_0(C^{11})}$ for proton bombarding energies 222 MeV to 362 MeV

Energy of protons (MeV)	O^{15} Activity at the end of exposure (counts/min)	N^{13} Activity at the end of exposure (counts/min)	C^{11} Activity at the end of exposure (counts/min)	$\frac{\sigma_0(O^{15})}{\sigma_0(C^{11})}$ [a]	$\frac{\sigma_0(N^{13})}{\sigma_0(C^{11})}$ [a]
222	$1.79\times10^5\pm2$ %	$1.80\times10^3\pm$ 9%	$1.30\times10^4\pm0.4$ %	1.52 ± 2 %	$0.07\pm$ 9.3 %
279	$1.09\times10^5\pm2$ %	$1.20\times10^3\pm11$%	$7.60\times10^3\pm0.5$ %	1.58 ± 2 %	0.08 ± 11.2 %
314	$8.64\times10^4\pm3$ %	$1.08\times10^3\pm20$%	$6.20\times10^3\pm0.5$ %	1.53 ± 3 %	0.09 ± 20.3 %
362	$2.02\times10^4\pm4$ %	$2.00\times10^3\pm40$%	$1.50\times10^3\pm1.2$ %	1.48 ± 4.2 %	0.07 ± 40 %

[a]) The errors shown are the compounded errors due to the statistical uncertainties in separating O^{15}, N^{13} and C^{11} activities.

TABLE 2

The absolute cross-section $O^{16}(p, 3p3n)C^{11}$ at 383 MeV

C^{11} Activity at the end of exposure	Thickness of the target	Proton current	$\sigma_0(O^{15})$ [a]
1.84×10^3 counts/min ±10 %	0.302 g/cm^2	8.28×10^9 protons/min	13.6 mb ±10.5 %

[a]) The errors shown is the compounded error due to the statistical uncertainty in measuring C^{11} activity (10 %), uncertainty in efficiency (3 %) and beam monitoring (1.3 %).

TABLE 3

$\frac{\sigma_r(O^{15})}{\sigma_r(F^{18})}$, $\frac{\sigma_r(N^{13})}{\sigma_r(F^{18})}$ and $\frac{\sigma_r(C^{11})}{\sigma_r(F^{18})}$ for proton energies from 222 MeV to 362 MeV

Energy of protons (MeV)	F^{18} Activity at the end of exposure (counts/min)	O^{15} Activity at the end of exposure (counts/min)	N^{13} Activity at the end of exposure (counts/min)	C^{11} Activity at the end of exposure (counts/min)	$\frac{\sigma_r(O^{15})}{\sigma_r(F^{18})}$ [a]	$\frac{\sigma_r(N^{13})}{\sigma_r(F^{18})}$ [a]	$\frac{\sigma_r(C^{11})}{\sigma_r(F^{18})}$ [a]
222	$3.35\times10^3\pm1$ %	$6.08\times10^4\pm1.5$ %	$1.20\times10^3\pm10$ %	$4.80\times10^7\pm2$ %	0.352 ± 1.8 %	0.032 ± 10 %	0.258 ± 2.3 %
279	$2.00\times10^3\pm1$ %	$3.01\times10^4\pm3$ %	$8.00\times10^2\pm12$ %	$3.20\times10^3\pm3$ %	0.290 ± 3.2 %	0.036 ± 12 %	0.288 ± 3.2 %
314	$2.38\times10^3\pm1$ %	$3.65\times10^4\pm1.5$ %	$1.40\times10^3\pm8$ %	$4.08\times10^3\pm3$ %	0.296 ± 1.8 %	0.053 ± 8.2 %	0.302 ± 3.2 %
362	$1.84\times10^3\pm1.8$ %	$2.80\times10^4\pm5$ %	$1.60\times10^3\pm8$ %	$3.00\times10^3\pm3$ %	0.292 ± 5.4 %	0.078 ± 8.3 %	0.293 ± 3.6 %

[a]) The errors shown are the compounded errors due to the statistical uncertainties in separating F^{18}, O^{15}, N^{13} and C^{11} activities.

TABLE 4

Absolute cross-section for $F^{19}(p, pn)F^{18}$ at 362 MeV

F^{18} Activity at the end of exposure (counts/min)	C^{11} Activity at the end of exposure (counts/min)	Thickness of Li F target (g/cm^2)	Thickness of carbon target (g/cm^2)	$\frac{\sigma_r(F^{18})}{\sigma_c(C^{11})}$	$\sigma_c(C^{11})$ (mb)	$\frac{\sigma_r(F^{18})}{(mb)}$ [a]
$2.53\times10^3\pm0.5$ %	$2.70\times10^3\pm1$ %	5.86×10^{-2}	2.96×10^{-1}	0.422 ± 1.1 %	33.2	14.2 ± 11 %

[a]) The error shown is the compounded errors due to the statistical counting error in the measurement of F^{18} and C^{11} activities, the uncertainty in the determination of the areal density of Li F target (5 %) and uncertainty in the proton current due to improper alignment of the sandwich (10 %).

for proton energies of 222 MeV to 362 MeV are shown. Finally, in table 4 the absolute cross-section $\sigma_F(F^{18})$ is given.

Results on $\sigma_O(O^{15})/\sigma_O(C^{11})$ and $\sigma_O(N^{13})/\sigma_O(C^{11})$ ratios show that they vary very slowly with the bombarding energy of protons. One conspicuous feature is the considerably lower production cross-section for N^{13} relative to O^{15} and C^{11}. A possible qualitative explanation is given in the next section.

Results on $\sigma_F(O^{15})/\sigma_F(F^{18})$ and $\sigma_F(N^{13})/\sigma_F(F^{18})$ and $\sigma_F(C^{11})/\sigma_F(F^{18})$ again show that the cross-section of the reaction which produces N^{13} is much smaller than those of the other reactions. The ratios $\sigma_F(C^{11})/\sigma_F(F^{18})$ and $\sigma_F(O^{15})/\sigma_F(F^{18})$ show little variation with energy, which probably means that the individual cross-sections are also nearly constant over this energy range. However, the ratio $\sigma_F(N^{13})/\sigma_F(F^{18})$ shows one marked increase with increasing energy, suggesting that this is a property of the reaction F^{18}(p, 3p4n)N^{13}.

4. Conclusion

Table 5 displays the cross-sections we have obtained for the different nuclear reactions in some light elements when bombarded by high-energy protons. Values quoted relate to the maximum proton energy used in each case.

TABLE 5

Absolute cross-sections of proton induced reactions in some light elements

Energy of protons (MeV)	Target	Reaction	Absolute cross-section (mb)
352	Beryllium	Be^9(p, p2n)Be^7	12.0± 4 %
383	Carbon	C^{12}(p, pn)C^{11}	31.6± 3.2 %
352		C^{12}(p, 3p3n)Be^7	8.3± 4.2 %
362	Oxygen	O^{16}(p, pn)O^{15}	20.2±10.5 %
		O^{16}(p, 2p2n)N^{13}	1.0±41 %
		O^{16}(p, 3p3n)C^{11}	13.6±12 %
362	Fluorine	F^{19}(p, pn)F^{18}	14.2±11 %
		F^{19}(p, 2p3n)O^{15}	4.2±12 %
		F^{19}(p, 3p4n)N^{13}	1.1±14 %
		F^{19}(p, 4p5n)C^{11}	4.2±12 %
342	Aluminium	Al^{27}(p, 3pn)Na^{24}	10.1± 3.8 %
		Al^{27}(p, 5p5n)F^{18}	6.8±10 %

The important fact which emerges from these results is that in each element in which the reaction (p, pn) was observed, this had a higher cross-section than any other. This has been noticed in many medium heavy nuclei too [7]). It is probable that this type of reaction for high-energy incident nucleons mainly proceeds by a "knock-on" process. According to Meadows [8]) the Goldberger model predicts highest probability for the nuclear reaction of the (p, pn) type for 100 MeV incident protons on a target nucleus of $A = 64$. As higher cross-

sections for the (p, pn) reaction are also observed in light elements, it is possible that the Goldberger model is applicable to light nuclei at least in the qualitative aspects. Also it can be seen from table 5 that the cross-section for the (p, pn) reaction decreases as the size of the nucleus increases. This is perhaps related to the fact that in a larger nucleus the colliding nucleons instead of escaping from the nucleus have a greater chance of making further collisions with the nucleons and thus giving rise to a cascade.

Another conspiciuous feature of the results shown above is the comparatively very low cross-section for the production of N^{13}, when oxygen and fluorine are bombarded with high-energy protons. A similar lower cross-section for the production of N^{13} has been observed by Marquez [9]) in the yield measurements of spallation products of aluminium. This is probably related to the weak binding energy of 2 MeV of the last proton in the N^{13} nucleus. During the later stage of the cooling of the heated nucleus, the Coulomb barrier, binding energy and the level density of the product nucleides are likely to play important roles in determining their relative yields. As N^{13} has a loose proton, the formation of N^{13} becomes less probable.

The excitations functions for the various reactions taking place in light elements as shown in previous sections, are fairly insensitive functions of the energy of the incident protons above about 200 MeV. This is consistent with Serber's suggestion that the cross-section for a given reaction would vary slowly since the probability of leaving the nucleus with a given excitation energy is determined by the mean free path, which varies slowly with the energy of the incident protons.

It has been shown by Muirhead and Rosser [10]), by the Goldberger method, that when 140 MeV protons strike a nucleus with $A = 14$, the average excitation energy transferred to the residual nucleus, following the passage of the nucleon cascade, is 23 MeV. For 360 MeV incident proton energy the average excitation energy should be higher by a few MeV. It is possible, in the case of light elements, for the excited residual nucleus to break-up completely in one act into α-particles and a few nucleons. For example, the threshold for the reaction C^{12}(p, p 3α) is only 7.3 MeV. If complete break-up into particles and nucleons were the most probable process one would expect rather small values of cross-sections for the reactions in light elements in which radio-active isotopes are produced. However, the cross-sections for such reactions shown in table 5 are appreciable fractions of the total inelastic cross-section. In the cases of fluorine and aluminium, the cross-sections for the reactions in which the radio-active isotopes are produced with emission of many nucleons have about the same values as have been measured for the production of radio-active isotopes in similar reactions with medium heavy nuclei [7]). It is perhaps quite reasonable to conclude that the excited light nucleus after the passage of nuclear cascade usually does not break-up in a single act but loses its excitation energy by

emitting particles and photons in a process similar to that which occurs in the de-excitation of highly excited medium heavy nuclei.

I am thankful to the late Professor H. W. B. Skinner for his interest and encouragement. I am indebted to Dr. J. J. Holt under whose guidance and help these experiments were carried out; his suggestions and criticisms were of great help in the writing of this paper. My thanks are also due to the cyclotron crew under Mr. B. Halliday who were most helpful during their radiation of targets in the circulating beam.

References

1) V. Parikh, Nuclear Physics **18** (1960) 628, 638
2) D. Salter and L. Bird, Phil. Mag. **44** (1953) 1305
3) R. E. Batzel and G. M. Coleman, LRL-72 (Technical information service, Oak Ridge, Tennessee)
4) V. Dikson and T. Randle, Nature **166** (1950) 235; Proc. Phys. Soc. A **64** (1951) 902
5) R. Aamodt, V. Peterson and R. Phillips, Phys. Rev. **88** (1952) 739
6) H. Hicks, P. Stevenson and W. Nervik, Phys. Rev. **102** (1956) 1390
7) A. Caretto and E. Wiig, E. Belmont and J. Miller, Phys. Rev. **103** (1956) 236; Phys. Rev. **95** (1954) 1554
8) J. Meadows, Phys. Rev. **98** (1955) 744
9) L. Marquez, Phys. Rev. **88** (1952) 225
10) H. Muirhead and W. Rosser, Phil. Mag. **46** (1955) 652

2.L

Nuclear Physics **18** (1960) 654—668; © *North-Holland Publishing Co., Amsterdam*

Not to be reproduced by photoprint or microfilm without written permission from the publisher

A METHOD FOR CALCULATING SCATTERING PHASE SHIFTS

J. N. LYNESS

Department of Applied Mathematics, University of New South Wales, Kensington, N.S.W., Australia

Received 21 May 1960

Abstract: A method, based on perturbation theory, is derived for obtaining the reflection coefficient for scattering a plane wave by a potential well of a particular type. This type is an extension of a simple potential well, whose reflection coefficient is known. This method has the advantage that exact limits can be placed on the possible error due to using the perturbation expansion. A possible application is the exact determination of the effect on the cross section of a 'tail' added to a potential well.

1. Introduction

The square well optical model, introduced by Feshbach, Porter and Weisskopf [1]), reproduced many of the experimental results for the scattering of low energy neutrons by medium and heavy nuclei. A justification of the use of a complex potential well to represent this interaction has been presented by Lane, Thomas and Wigner [2]), assuming the existence of a two-body interaction. The square well optical model is undoubtedly too simple a representation of the neutron nuclear interaction. Since the nuclear boundary is not in fact sharp, but diffuse, a more realistic shape for the radial dependence of the potential well is that of a rounded off trapezium. However, in this case the calculation of the scattering cross sections is difficult, as the radial Schrödinger equation does not in general have simple solutions in terms of known functions.

Investigations have been made of cross sections [3, 4]) using computors and it seems that at most energies it is possible to improve the experimental fit by using potentials of this type rather than a square well. In this paper, we are concerned with a method based on perturbation theory for determining the cross sections relating to low energy scattering of neutrons by medium nuclei using this sort of potential interaction.

We consider the solution of the radial Schrödinger equation which refers to the scattering of a plane wave by a potential well. The solution proposed can be applied to a well whose profile consists of two distinct sections; a central section, which is taken to be a square well of depth $V_0(1+i\zeta)$, but which can be any well which is confined to a region $r < R$ and whose reflection coefficient is known; an intermediate section $v(r)$ confined to a region $R < r < R_0$ whose depth varies from V_0 at $r = R$ to zero at $r = R_0$; the potential $v(r)$ is treated as a perturbation.

The zero order equation, discussed in section 2, is one whose solution is known. In section 3 we introduce the term $v(r)$ as a perturbation. Since we are dealing with scattering by a plane wave of known energy, no energy perturbation terms appear and carrying out the well known perturbation technique results in a series of differential equations (eq. (4)). Each of these is of the same form, expressing the r^{th} order perturbation wave function in terms of the $(r-1)^{\text{th}}$. A Green's function type of solution is written down for each of these equations.

In section 6 we consider the particular case in which $v(r)$ is constant. In this case the exact solution is known and a generating function can be set up which gives the solution of each of the differential equations. This generating function gives rise to certain recurrence relations connecting the solutions.

It turns out that these recurrence relations can also be used to establish recurrence relations connecting solutions of the perturbation wave functions in the more general case when $v(r)$ is a polynomial in r^2. These relations are exploited in section 8 to express the reflection coefficient in the latter case in terms of the reflection coefficient of the zero order well.

An additional feature on which emphasis is placed is that simple inequalities exist connecting terms of the same order of perturbation pertaining to the particular case in which $v(r)$ is constant and the general case in which $v(r)$ is not constant. However, in the former case the exact solution is known and the error involved in only using a small number of terms in the various expansions can be calculated. This leads to a knowledge of the maximum possible error in the general case in which $v(r)$ is not constant. Sections 5 and 7 are concerned primarily with this aspect of the theory.

In section 9 the formulae are specialised to the case of s-wave scattering, resulting in considerable simplification, and in section 10 possible applications are discussed.

2. The Zero Order Equation

We consider the scattering of the plane wave $\exp(ikz)$ by a potential well of the form

$$V(r) = -V_0 \qquad (r < R),$$

$$V(r) = +\frac{\hbar^2}{2m} v(r) \qquad (R < r < R_0),$$

$$V(r) = 0 \qquad (r > R_0),$$

where $v(r)$ is a polynomial in r^2 positive in the range $R < r < R_0$. The wave equation is then

$$\nabla^2\psi + \left(k^2 - \frac{2m}{\hbar^2} V(r)\right)\psi = 0.$$

On separation by the substitution

$$r\psi = \sum_{l=0}^{\infty} \psi^{(l)}(r) Y_{l,0}(\theta),$$

this gives the radial equation

$$\frac{\mathrm{d}^2}{\mathrm{d}r^2}\psi^{(l)} + \left[\begin{matrix} k^2 \\ \alpha^2 \end{matrix} - \frac{l(l+1)}{r^2}\right]\psi^{(l)} = v(r)\psi^{(l)}, \tag{1}$$

where $\begin{matrix} k^2 \\ \alpha^2 \end{matrix}$ denotes k^2 in case $r > R$ and α^2 in case $r < R$. Here $\alpha^2 = 2mV_0/\hbar^2 + k^2$ and $v(r)$ is non zero only in the region $R < r < R_0$. Under the conditions that $\psi^{(l)}(0) = 0$ and that $\psi^{(l)}(r)$ and its derivative are everywhere continuous, the solution of (1) for $r > R_0$ is

$$\psi^{(l)}(r) = \text{const}\,\{-\eta_l u_l^{(+)}(kr) + u_l^{(-)}(kr)\}, \tag{2}$$

where

$$u_l^{(\pm)}(kr) = \pm ikr\{j_l(kr) \pm i n_l(kr)\}.$$

It is the purpose of this paper to indicate a method by which η_l can be determined to any required degree of accuracy; η_0 can also be determined in the less restricted case that $v(r)$ is a polynomial in r positive in the range $R < r < R_0$. The values of η_l when known, are sufficient to determine the various scattering cross sections (Feshbach, Porter and Weisskopf [1]).

3. Treatment of $v(r)$ as a Perturbation

In the solution of equation (1) we treat the term $v(r)$ as a perturbation. Thus to zero order we have

$$\frac{\mathrm{d}^2}{\mathrm{d}r^2}\psi_0^{(l)} + \left[\begin{matrix} k^2 \\ \alpha^2 \end{matrix} - \frac{l(l+1)}{r^2}\right]\psi_0^{(l)} = 0. \tag{3}$$

This has the solution

$$\begin{aligned} \psi_0^{(l)} &= r j_l(\alpha r)/R j_l(\alpha R) && (r < R), \\ \psi_0^{(l)} &= \tfrac{1}{2}\left(j_l(kR) + i n_l(kR)\right)(\Delta_l + i s_l - f_l) && \text{(3a)} \\ &\qquad \times \left(-\eta_{l,0} u_l^{(+)}(kr) + u_l^{(-)}(kr)\right) && (r > R), \end{aligned}$$

where f_l and $\Delta_l + i s_l$ are the logarithmic derivatives of $\psi_0^{(l)}$ and $u_l^{(+)}(kr)$ respectively at $r = R$ and

$$\eta_{l,0} = \frac{f_l - \Delta_l + i s_l}{f_l - \Delta_l - i s_l} \mathrm{e}^{-2i\delta_l}. \tag{3b}$$

Here, the phase-shift δ_l is defined by the relation

$$\mathrm{e}^{-2i\delta_l} = u^{(-)}(kR)/u^{(+)}(kR).$$

The above equations and definitions are given by Blatt and Weisskopf [5]) and are reproduced here to establish the terminology.

To solve equation (1) we set up the recurrence system of differential equations

$$\frac{\mathrm{d}^2}{\mathrm{d}r^2}\psi_t(r) + \left[\begin{matrix}k^2\\ \alpha^2\end{matrix} - \frac{l(l+1)}{r^2}\right]\psi_t(r) = v(r)\psi_{t-1}(r) \quad (t = 1, 2, \ldots), \tag{4}$$

each of which satisfies the boundary condition

$$\psi_t(0) = 0. \tag{5}$$

If we then add equation (3) to equation (4) summed from $t = 1$ to ∞, we obtain

$$\frac{\mathrm{d}^2}{\mathrm{d}r^2}\sum_{t=0}^{\infty}\psi_t(r) + \left[\begin{matrix}k^2\\ \alpha^2\end{matrix} - \frac{l(l+1)}{r^2}\right]\sum_{t=0}^{\infty}\psi_t(r) = v(r)\sum_{t=0}^{\infty}\psi_t(r),$$

and as $\sum\psi_t(0) = 0$, the expression $\sum\psi_t(r)$ is the solution of eq. (1) described in eq. (2), apart from a multiplicative constant.

Equation (4) is solved by a Green's function method, described by Mott and Massey [6]). However, with only one boundary condition, ψ_t is not uniquely defined in terms of ψ_{t-1}, though the sum $\sum\psi_t$ is still a solution of equation (1), provided this sum converges. For the purposes of determining $\sum\psi_t$ it is convenient to impose arbitrarily an additional boundary condition on $\psi_t(r)$. This is sometimes done by making $\psi_t(r)$ the l-component of an outgoing wave, but this makes the formulae unnecessarily complicated. It is more convenient to make this extra boundary condition

$$\psi_t(R) = 0 \quad (t = 1, 2, \ldots), \tag{6}$$

and this can be done provided that $\psi_0(R) \neq 0$. This has the effect of normalising the solution so that

$$\psi(R) = \sum\psi_t(R) = \psi_0(R) = 1$$

and it has also the effect of making $\psi_t(r)$ small in the region where it is effective in the equation to determine ψ_{t+1}, that is where $v(r)$ is not zero.

The solution of (4) can be written

$$\frac{\psi_t}{R} = X_c(r)\int_r^b X_s(r')v(r')\psi_{t-1}(r')\mathrm{d}r' + X_s(r)\int_a^r X_c(r')v(r')\psi_{t-1}(r')\mathrm{d}r', \tag{7}$$

where $X_c(r)$ and $X_s(r)$ are any two independent solutions of equation (3) which satisfy the normalisation condition

$$X_c(r)X'_s(r) - X_s(r)X'_c(r) = \frac{1}{R},$$

and a and b are determined from the boundary conditions. We choose X_c and

X_s to be the solutions which are respectively one and zero at $r = R$ and whose derivatives are respectively zero and $1/R$ at $r = R$. This gives

$$\begin{aligned} X_c(r) &= kr\big([n(kR)+kRn'(kR)]j(kr)-[j(kR)+kRj'(kR)]n(kr)\big), \\ X_s(r) &= kr\big(-j(kr)n(kR)+n(kr)j(kR)\big), \end{aligned} \tag{8}$$

for $r > R$, which reduce to $\cos(kr-kR)$ and $(1/kR)\sin(kr-kR)$ respectively in the case $l = 0$. With this choice of X_c and X_s and with the boundary conditions (5) and (6) above, equation (7) reduces to $(t \neq 0)$

$$\psi_t(r) = 0 \qquad (0 \leqq r \leqq R), \tag{9a}$$

$$\psi_t(r) = -X_c(r)W(s, t, r)+X_s(r)W(c, t, r) \qquad (R \leqq r \leqq R_0), \tag{9b}$$

$$\psi_t(r) = -X_c(r)W(s, t, R_0)+X_s(r)W(c, t, R_0) \qquad (r \geqq R_0), \tag{9c}$$

where $W(a, t, r)$ is defined as

$$\int_R^r X_a(r')Rv(r')\psi_{t-1}(r')dr' \qquad (a = s, c).$$

If we make the arbitrary definitions

$$W(c, 0, r) = f_l, \quad W(s, 0, r) = -1,$$

expression (9) holds for $t = 0$ being in agreement with equation 3(a).

Using expression (9) and its derivative, simple manipulation yields the following expression:

$$W(a, t, r) = -R\{\psi_t(r)X'_s(r)-\psi'_t(r)X_s(r)\} \quad (a = s, c), \tag{10}$$

and by consideration of the incoming and outgoing parts of $\sum_{t=0}^{\infty}\psi_t(r)$, we have

$$\eta_l = e^{-2i\delta_l}\frac{(\Delta_l-is_l)\sum W(s,t,R_0)+\sum W(c,t,R_0)}{(\Delta_l+is_l)\sum W(s,t,R_0)+\sum W(c,t,R_0)}, \tag{11}$$

where the summations are from $t = 0$ to ∞ and δ_l, f_l, Δ_l and s_l defined in the first paragraph of this section, are to be evaluated at $r = R$.

Comparing the expression (11) for η_l with the expression (3b) for $\eta_{l,0}$ it is apparent that if we define f'_l by

$$f'_l = -\sum W(c, t, R_0)/\sum W(s, t, R_0), \tag{11a}$$

η_l is the same function of f'_l as $\eta_{l,0}$ is of f_l. Thus, if scattering results are expressed in terms of f_l, the logarithmic derivative of the wave function at $r = R$ for the unperturbed well, the results for the perturbed well can be written down by replacing f_l by f'_l. There is no need for the unperturbed well to be of the form $V(r) = \text{const.}$ for $r \leqq R$. All that is necessary is that it should be possible to calculate f_l at $r = R$. It should be borne in mind that f'_l is not the logarithmic derivative of the actual wave function anywhere. Its physical significance is

that it is the logarithmic derivative of the expression for the wave function valid when $r > R_0$, evaluated at $r = R$.

4. Change of Origin

It is convenient to change the origin and render the quantities dimensionless. This is done by setting

$$\begin{aligned} &x = kr - kR, \quad X_s(r) = \frac{1}{kR} f_0(x), \quad X_c(r) = g_0(x), \\ &v(r) = |v(R)|u(x), \quad \left(\frac{v(R)}{k}\right)^{2t} \psi_t(r) \equiv \beta^t \psi_t(r) = \phi_t(x). \end{aligned} \tag{12}$$

Then equation (7) becomes

$$\phi_t^{(l)}(x) = f_0^{(l)}(x) \int^x g_0^{(l)}(x') u(x') \phi_{t-1}^{(l)}(x') dx' - g_0^{(l)}(x) \int^x f_0^{(l)}(x') u(x') \phi_{t-1}^{(l)}(x') dx',$$

which is abbreviated to

$$\phi_t^{(l)}(x) = \mathrm{Op}^{(l)}[u(x)\phi_{t-1}^{(l)}(x)]. \tag{13}$$

The superscript l shall be dropped, except in part of section 5. Now $\phi_0(x) = (f_l/kR)f_0(x) + g_0(x)$ and we define the series

$$\begin{aligned} F_t(x) &= \mathrm{Op}\,[u(x)F_{t-1}(x)] \quad (t > 1,\ F_0(x) = f_0(x)), \\ G_t(x) &= \mathrm{Op}\,[u(x)G_{t-1}(x)] \quad (t > 1,\ G_0(x) = g_0(x)). \end{aligned} \tag{14}$$

It is then clear that

$$\phi_t(x) = \frac{f_t}{kR} F_t(x) + G_t(x),$$

and that the sum of the quantities W of equation (10) is given by

$$\begin{aligned} \sum_{t=1}^{\infty} W(\mathrm{c}, t, R_0) = &-f_t \sum_{t=1}^{\infty} \{g'_0(x_0)F_t(x_0) - g_0 F'_t(x_0)\}\beta^t \\ &-kR \sum_{t=1}^{\infty} \{g'_0(x_0)G_t(x_0) - g_0(x_0)F'_t(x_0)\}\beta^t, \end{aligned} \tag{15}$$

where $x_0 = kR_0 - kR$ and β is defined in (12). The sum $kR\sum W(\mathrm{s}, t, R_0)$ is precisely the same as (15) but with f_0 and f'_0 substituted for g_0 and g'_0.

Thus it is only necessary to evaluate the four sums in (5), and the reflection coefficients can be evaluated using (15) and (11). However, these sums are difficult to evaluate in terms of well known functions. The next section is devoted to obtaining an exact expression for $\sum\beta^t F_t(x)$ in the case that $u(x)$ is constant and showing how this can be used to obtain exact limits on the expressions $\sum\beta^t F_t(x)$, etc., in a more general case.

5. Properties of the Function Op[$A(x)$]

We now consider certain simple and useful properties of the function Op[$A(x)$] defined in (13). Direct substitution shows that if $A(x)$ and Op[$A(x)$] have power series expansions in x, viz.

$$A(x) = \sum_{r=s}^{\infty} a_r x^r \quad \text{and} \quad \text{Op}[A(x)] = \sum v_r x^r,$$

then $v_r = 0$ for $r \leqq s+1$ and $v_{s+2} = a_s/(s+1)(s+2)$. Thus it follows that if $A(x)$ and its first n derivatives at $x=0$ are zero, and if $A(x)$ is initially positive, then Op[$A(x)$] and its first $n+2$ derivatives at $x=0$ are zero and Op[$A(x)$] is initially positive. This shows that $F_n(x)$ and its first $2n$ derivatives and $G_n(x)$ and its first $2n-1$ derivatives at $x=0$ are all zero.

It also follows that if $A(x)$ is finite at $x=0$ then Op[$A(x)$] and its derivative are zero at $x=0$. Thus Op[$A(x)$] is that solution of the equation

$$\frac{\mathrm{d}^2}{\mathrm{d}x^2} F(x) + \left(1 - \frac{l(l+1)}{(x+kR)^2}\right) F(x) = A(x)$$

which satisfies the boundary conditions

$$F(0) = 0 \quad \text{and} \quad F'(0) = 0,$$

and this acts as an alternative definition of Op[$A(x)$].

Since both f_0 and g_0 satisfy the differential equation

$$\frac{\mathrm{d}^2}{\mathrm{d}x^2} f_0^{(l)}(x) + \left(1 - \frac{l(l+1)}{(x+kR)^2}\right) f_0^{(l)}(x) = 0, \tag{16}$$

and as $f_0(0) = g'_0(0) = 0$ and $f'_0(0) = g_0(0) = 1$, it can be shown that

$$g_0(x) f'_0(x) - f_0(x) g'_0(x) = 1.$$

From this it follows that both $f_0^{(l)}(x)$ and $g_0^{(l)}(x)$ are positive for all $x < x_g^{(l)}$ where $x_g^{(l)}$ is the first root of $g_0^{(l)}(x) = 0$. We can also show, by writing down the equation for Op[$A(x)$] and differentiating it, that

$$\text{Op}[A(x)] g'_0(x) - g_0(x) \frac{\mathrm{d}}{\mathrm{d}x} \text{Op}[A(x)] = -\int_0^x g_0(x') A(x') \mathrm{d}x', \tag{17}$$

so that, if $A(x) > 0$ for $0 < x < x_g^{(l)}$ and the first root of Op[$A(x)$] $= 0$ is $x = x_1$ then

$$\left| \frac{\mathrm{d}}{\mathrm{d}x} \text{Op}[A(x)] \right|_{x=x_1} g_0(x_1) = \int_0^{x_1} g_0(x') A(x') \mathrm{d}x'.$$

At the first root of a continuous quantity initially positive, the derivative must be negative or zero. Thus one of the terms $g_0(x_1)$ and $\int_0^{x_1} g_0(x') A(x') \mathrm{d}x'$ must be negative and this cannot happen unless we have $x_1 > x_g^{(l)}$. Thus we have

Result 1: If $A(x) > 0$ for $0 < x < x_g^{(l)}$ then $\mathrm{Op}[A(x)] > 0$ for $0 < x < x_g^{(l)}$.

Moreover equation (17) above holds with f_0 and f'_0 replacing g_0 and g'_0 and provides an equation for $(\mathrm{d}/\mathrm{d}x)\ \mathrm{Op}[A(x)]$. It is clear from this equation that $(\mathrm{d}/\mathrm{d}x)\ \mathrm{Op}[A(x)]$ must be positive so long as both f_0 and f'_0 are positive. If we denote the first root of $(\mathrm{d}/\mathrm{d}x) f_0^{(l)}(x) = 0$ by $x_f^{(l)}$, we have

Result 2: If $A(x) > 0$ for $0 < x < x_f^{(l)}$ then $(\mathrm{d}/\mathrm{d}x)\ \mathrm{Op}[A(x)] > 0$ for $0 < x < x_f^{(l)}$.

It remains to determine how large $x_g^{(l)}$ and $x_f^{(l)}$ are. In the case $l = 0$ both are equal to $\frac{1}{2}\pi$ as $g_0(x) = \cos x$ and $kRf_0(x) = \sin x$.

By taking the difference of equation (16) with the same equation in which $m < l$ replaces l, and using the definition of $\mathrm{Op}[A(x)]$ given in this section, we have

$$\frac{f_0^{(l)} - f_0^{(m)}}{l(l+1) - m(m+1)}\ \mathrm{Op}^{(l)}\left[\frac{f_0^{(m)}(x)}{(x+kR)^2}\right] = \mathrm{Op}^{(m)}\left[\frac{f_0^{(l)}(x)}{(x+kR)^2}\right],$$

and a similar relation is obtained by replacing f_0 by g_0 throughout. Using result 1 above, as $(x+kR)^2$ is clearly positive, $g_0^{(l)} - g_0^{(m)}$ is positive so long as either $g_0^{(l)}$ or $g_0^{(m)}$ is positive. Thus, since $l > m$, we have $x_g^{(l)} > x_g^{(m)}$ is positive. Thus, since $l > m$, we have $x_g^{(l)} > x_g^{(m)}$ and in particular $x_g^{(l)} > x_g^{(0)} = \frac{1}{2}\pi$.

Result 2 gives by the same sort of argument $x_f^{(l)} > x_f^{(m)} > x_f^{(0)} = \frac{1}{2}\pi$.

Hence we can replace Results 1 and 2 by the more easily applicable but less general

Result 3: If $A(x) > B(x) > 0$ and $0 < x < \frac{1}{2}\pi$
then $\mathrm{Op}[A(x)] > \mathrm{Op}[B(x)] > 0$
and $(\mathrm{d}/\mathrm{d}x)\ \mathrm{Op}[A(x)] > (\mathrm{d}/\mathrm{d}x)\ \mathrm{Op}\ [B(x)] > 0$.

If $A(x) \geqq C(x) \geqq B(x)$ in the region $0 \leqq x \leqq \frac{1}{2}\pi$, but there are no restrictions on the sign of any of these functions, by applying Result 3 to the functions $A(x) - C(x)$ and $C(x) - B(x)$ respectively, we have

$$\mathrm{Op}[A(x)] \geqq \mathrm{Op}[C(x)] \geqq \mathrm{Op}[B(x)], \tag{18a}$$

$$\frac{\mathrm{d}}{\mathrm{d}x}\mathrm{Op}[A(x)] \geqq \frac{\mathrm{d}}{\mathrm{d}x}\mathrm{Op}[C(x)] \geqq \frac{\mathrm{d}}{\mathrm{d}x}\mathrm{Op}[B(x)]. \tag{18b}$$

6. The Case in which $v(r)$ is Constant

Before dealing with the problem for general $u(x)$, we consider the special case in which $u(x) = +1$, $0 < x < x_0$. In this case we relabel the F_t and G_t of equation (14) by

$$f_t(x) = \mathrm{Op}[f_{t-1}(x)] \quad \text{and} \quad g_t(x) = \mathrm{Op}[g_{t-1}(x)],$$

and the differential recurrence equations for $f_t(x)$ are obtained by substituting (12) in (4) with $u(x) = 1$. This yields

$$f_t''(x) + \left(1 - \frac{l(l+1)}{(x+kR)^2}\right) f_t(x) = f_{t-1}(x),$$

and if we multiply each equation by β^t and add, we have

$$\frac{d^2}{dx^2}\sum \beta^t f_t(x) + \left(1 - \frac{l(l+1)}{(x+kR)^2}\right)\sum \beta^t f_t(x) - \beta \sum \beta^t f_t(x) = 0.$$

Applying the boundary condition at $x = 0$, the solution of this equation gives a generating function for $f_t(x)$. Similar reasoning gives generating functions for $g_t(x)$, $f'_t(x)$ and $g'_t(x)$. Putting $\gamma = (x+kR)\sqrt{1-\beta}$ and $\gamma_0 = kR\sqrt{1-\beta}$ we have

$$\sum f_t(x)\beta^t = \frac{\gamma\gamma_0}{\sqrt{1-\beta}}[j(\gamma)n(\gamma_0) - n(\gamma)j(\gamma_0)], \tag{19a}$$

$$\sum g_t(x)\beta^t = \gamma j(\gamma)\frac{d}{d\gamma_0}(\gamma_0 n(\gamma_0)) - \gamma n(\gamma)\frac{d}{d\gamma_0}(\gamma_0 j(\gamma_0)), \tag{19b}$$

$$\sum f'_t(x)\beta^t = -\left[\frac{d}{d\gamma}(\gamma j(\gamma))\right]\gamma_0 n(\gamma_0) + \left[\frac{d}{d\gamma}(\gamma n(\gamma))\right]\gamma_0 j(\gamma_0), \tag{19c}$$

and

$$\sum g'_t(x)\beta^t = -\sqrt{1-\beta}\left[-\frac{d}{d\gamma}(\gamma j(\gamma))\frac{d}{d\gamma_0}(\gamma_0 n(\gamma_0)) + \frac{d}{d\gamma}(\gamma n(\gamma))\frac{d}{d\gamma_0}(\gamma_0 j(\gamma_0))\right]. \tag{19d}$$

These generating functions give rise to the following recurrence relations:

$$4(t+2)(t+1)f_{t+2} - 2(t+1)(2t+3)f_{t+1} = -x(x+2kR)f_t + 4(t+1)kRg_{t+1}, \tag{20a}$$

$$4(t+2)(t+1)g_{t+2} - 2(t+1)(2t+1)g_{t+1} = -x(x+2kR)g_t - 4(t+1)kRf_{t+1} + 2(2t+1)kRf_t + 4l(l+1)(t+1)f_{t+1}/kR. \tag{20b}$$

These give a straightforward way of computing f_t and g_t if f_0, g_0, f_1 and g_1 are known.

Also the following relations hold for determining f'_t and g'_t in terms of f_t and g_t:

$$(x+kR)(t+1)f'_{t+1} = \tfrac{1}{2}x(x+2kR)f_t - (t+1)g_{t+1},$$
$$(x+kR)(t+1)g'_{t+1} = \tfrac{1}{2}x(x+2kR)g_t + (t+1)g_{t+1} - (t+1)\{l(l+1) - (kR)^2\}f_{t+1}/kR - 2kRf_t.$$

Equation (19) together with (15) and (11) are sufficient to determine η_t.

7. The General Case

We now consider the case in which $u(x)$ is quite general, but bounded in the region $0 \leqq x \leqq x_0$. Thus

$$+k \geqq u(x) \geqq -k. \tag{22}$$

We have to calculate the sum $\sum_t F_t(x_0)\beta^t$ and three other sums similar to it for insertion in equation (15). In the next section we shall show how the first p terms of this sum can be calculated for a certain type of $u(x)$. We shall now deal with the question of how to put limits on the error involved in leaving out the remaining terms $\sum_{t=p}^{\infty} F_t(x_0)\beta^t$. Now $u(x)$ satisfies relation (22). If we multiply this relation by $f_0(x)$ and use (18a), we have

$$kf_1(x) \geqq F_1(x) \geqq -kf_1(x).$$

Multiplication by $u(x)$ gives either of the alternatives

$$\pm kf_1(x)u(x) \geqq u(x)F_1(x) \geqq \mp ku(x)f_1(x), \tag{23}$$

the sign to be used depending on the sign of $u(x)$. Using (22) either alternative in (23) gives

$$k^2 f_1(x) \geqq u(x)F_1(x) \geqq -k^2 f_1(x),$$

and using (18a) again

$$k^2 f_2(x) \geqq F_2(x) \geqq -k^2 f_2(x).$$

Reiteration of this process gives the general result

$$k^t f_t(x) \geqq F_t(x) \geqq -k^t f_t(x), \tag{25}$$

and multiplying each term of (25) by β^t and summing for $t = p, p+1, \ldots$ we have

$$\sum f_t(x)(\beta k)^t \geqq \sum F_t(x)\beta^t \geqq -\sum f_t(x)(\beta k)^t. \tag{26}$$

The sum $\sum f_t(x)(\beta k)^t$ can be calculated from (19a).

If further restrictions are placed on $u(x)$ more restrictive inequalities than (26) result. For example if

$$u(x) \geqq 0, \tag{27a}$$

it is easy to show that $F_t(x) \geqq 0$ for all t, and so

$$\sum f_t(x)(\beta k)^t \geqq \sum F_t(x)\beta^t \geqq 0. \tag{26a}$$

If, however,

$$u(x) \leqq 0, \tag{27b}$$

which is the case in most optical model perturbations to be considered, it follows that

$$(-1)^t F_t(x) \geqq 0,$$

and the inequality (26) becomes

$$\sum_{t>\frac{1}{2}\nu} f_{2t}(x)(\beta k)^{2t} \geqq \sum_{t>\nu} F_t(x)\beta^t \geqq -\sum_{t>\frac{1}{2}\nu} f_{2t+1}(x)(\beta k)^{2t+1}. \tag{26b}$$

These summations are over integral values of t, and can be determined by elementary means from the generating function (19a).

In the case in which $u(x)$ is complex, and the real and imaginary parts of $u(x)$ are both bounded, limits of a similar nature to (26) can be obtained. For if

$$|\mathrm{Re}(u(x))| \leqq k_1 \quad \text{and} \quad |\mathrm{Im}(u(x))| \leqq k_2 \tag{27c}$$

and if we suppose that $k_1 \geqq k_2$, it can be shown by induction that

$$|\mathrm{Re}\ F_r| \leqq \tfrac{1}{2}\{(k_1+k_2)^r+(k_1-k_2)^r\}f_r$$

and (26c)

$$|\mathrm{Im}\ F_r| \leqq \tfrac{1}{2}\{(k_1+k_2)^r-(k_1-k_2)^r\}f_r.$$

Less rigorous inequalities can be obtained from these by elementary methods, viz.

$$|\mathrm{Re}\ F_r| \leqq k_1{}^r f_r \quad \text{and} \quad |\mathrm{Im}\ F_r| \leqq k_2 k_1{}^{r-1} f_r \tag{26d}$$

and these are useful when $k_1 \gg k_2$.

If $k_1 < k_2$, results analogous to (26c) and (26d) are obtained.

Results which are precisely analogous to inequalities (26) hold for the sums involving F'_t, G_t and G'_t needed in equation (15).

8. The Reflection Coefficient in the General Case

Eqs. (20) are linear relations between $x(x+2kR)f_t$, $x(x+2kR)g_t$, f_t, f_{t+1}, f_{t+2}, g_t, g_{t+1} and g_{t+2}. As such, they can be written

$$x(x+2kR)f_t = \sum_r c_{tr}^{(1,1)} f_r + \sum_r c_{tr}^{(1,2)} g_r kR, \tag{28a}$$

$$x(x+2kR)g_t = \sum_r c_{tr}^{(2,1)} f_r/kR + \sum_r c_{tr}^{(2,2)} g_r. \tag{28b}$$

TABLE 1

Non-zero values of $d_{tr}^{(\alpha\beta)} = \dfrac{2^t\, t!}{2^r\, r!}\, c_{tr}^{(\alpha\beta)}$ (see equations (28)).

Here $\mu = (kR)^2$ and $\lambda = l(l+1)-(kR)^2$

(α, β)	(1,1)	(1,2)	(2,1)	(2,2)
$r = t$	0	0	$(2t+1)\mu$	0
$r = t+1$	$2t+3$	2	2λ	$2t+1$
$r = t+2$	-1	0	0	-1

The numerical values of $c_{tr}^{(\alpha\beta)}$ can be obtained from equation (20) and are tabulated in table 1. By reiteration of these formulae, it is easily demonstrated that

$$x^n(x+2kR)^n f_t = \sum_{r_1 r_2 \cdots r_n} \sum_{\alpha_1 \alpha_2 \cdots \alpha_{n-1}} c_{tr_1}^{(1\alpha_1)} c_{r_1 r_2}^{(\alpha_1 \alpha_2)} \cdots c_{r_{n-2} r_{n-1}}^{(\alpha_{n-2} \alpha_{n-1})} \{c_{r_{n-1} r_n}^{(\alpha_{n-1} 1)} f_{r_n} + c_{r_{n-1} r_n}^{(\alpha_{n-1} 2)} kRg_{r_n}\}, \quad (29)$$

where r_3 can take any value and α_s the values 1 or 2. A similar form can be obtained for $x^n(x+2kR)^n g_t$, the only difference being that the superscripts of the first term are changed from $(1, \alpha_1)$ to $(2, \alpha_1)$. Examination of table 1 shows that, as a result of there being only seven non zero coefficients $c_{tr}^{(\alpha\beta)}$, the number of terms in (29) is severely limited. The highest contributing value of r_n is $t+2n$ and the lowest is $t+n-1$.

If $u(x)$ is restricted to being a polynomial in $x(x+2kR)$ and is written

$$u(x) = \sum_{s=0}^{n} x^s (x+2kR)^s B_s, \quad (30)$$

using equation (29) it is possible to express $u(x)f_t(x)$ as the sum of terms linear in $f_r(x)$ and $g_r(x)$ with $r = t, t+1, \ldots t+2n$. Since $\mathrm{Op}[f_r(x)] = f_{r+1}(x)$ we can then write down $\mathrm{Op}[u(x)f_t(x)]$, which is the same linear sum of $f_{r+1}(x)$ and $g_{r+1}(x)$ as $u(x)f_t(x)$ is of f_r and g_r. But as $F_1(x) = \mathrm{Op}[u(x)f_0(x)]$, $F_1(x)$ is a linear sum of f_r and g_r ($r = 1, 2 \ldots 2n+1$) and $F_2(x) = \mathrm{Op}[u(x)F_1(x)]$ gives F_2 as a linear sum of f_r and g_r with $r = 2 \ldots 4n+2$, and this can be repeated indefinitely. These relations can be written

$$\begin{aligned} F_r = &\sum_w \sum_{\lambda\mu\cdots} a_{r,r+w}^{(11)\lambda\mu\cdots} B_0^{\lambda} B_1^{\mu} \ldots (r+w)!\, 2^{r+w} f_{r+w} \\ &\times \sum_w \sum_{\lambda\mu\cdots} a_{r,r+w}^{(12)\lambda\mu\cdots} B_0^{\lambda} B_1^{\mu} \ldots (r+w)!\, 2^{r+w} kRg_{r+w}, \end{aligned} \quad (31)$$

the summations being over w with the restriction $\lambda+\mu+\ldots = r$. A similar relation holds for G_r, the first superscript in each summation being altered from 1 to 2. The values of w which provide non zero contributions to (31) are $w = 0, 1, \ldots 2rn$.

The coefficients required for the calculation of F_r, G_r ($r = 0, 1, 2, 3$) in the case where only B_0 and B_1 are non-zero are displayed in table 2.

9. The s-Wave Scattering

In determining the s-wave reflection coefficient η_0 the relations given in the preceding sections assume much simpler forms, thus making computations easier. $f_t(x)$ and $g_t(x)$ no longer depend on kR and $f_0(x)$ and $g_0(x)$ are merely $\sin x$ and $\cos x$ respectively. The generating function of equation (19) can

TABLE 2

Non-zero values of $a_{r,r+w}^{(\alpha\beta)r-p,p}$ for $r = 0, 1, 2, 3$, appearing in equation (31).

In this table $\mu = (kR)^2$ and $\lambda = l(l+1)-(kR)^2$

r	p	$r+w$	(1,1)	(1,2)	(2,1)	(2,2)
0	0	0	1	0	0	1
1	0	1	$\frac{1}{2}$	0	0	$\frac{1}{2}$
	1	2	$\frac{3}{4}$	$\frac{1}{2}$	μ	$\frac{1}{4}$
		3	$-\frac{1}{6}$	0	$\frac{1}{2}\lambda$	$-\frac{1}{6}$
2	0	2	$\frac{1}{8}$	0	0	$\frac{1}{8}$
	1	2	0	0	1	0
		3	$\frac{13}{24}$	$\frac{1}{4}$	$\frac{1}{4}\lambda$	$\frac{7}{24}$
		4	$-\frac{1}{12}$	0	0	$-\frac{1}{12}$
	2	3	$\frac{5}{6}\mu$	0	$\frac{5}{4}\mu$	$\frac{1}{3}\mu$
		4	$\frac{21}{32}+\frac{1}{8}\lambda$	$\frac{1}{2}$	$-\frac{5}{12}\mu+\frac{1}{2}\lambda$	$\frac{5}{32}+\frac{1}{8}\lambda$
		5	$-\frac{9}{40}$	$-\frac{1}{12}$	$-\frac{1}{12}\lambda$	$-\frac{17}{120}$
		6	$\frac{1}{72}$	0	0	$\frac{1}{72}$
3	0	3	$\frac{1}{48}$	0	0	$\frac{1}{48}$
	1	3	0	0	$\frac{3}{8}\mu$	0
		4	$\frac{17}{96}$	$\frac{1}{16}$	$\frac{1}{16}\lambda$	$\frac{11}{96}$
		5	$-\frac{1}{48}$	0	0	$-\frac{1}{48}$
	2	4	$\frac{13}{24}\mu$	0	$\frac{37}{24}\mu$	$\frac{7}{24}\mu$
		5	$\frac{177}{320}+\frac{1}{16}\lambda$	$\frac{1}{3}$	$-\frac{7}{24}\mu+\frac{1}{3}\lambda$	$\frac{211}{2960}+\frac{1}{16}\lambda$
		6	$-\frac{101}{720}$	$-\frac{1}{24}$	$-\frac{1}{24}\lambda$	$-\frac{71}{720}$
		7	$\frac{1}{144}$	0	0	$\frac{1}{144}$
	3	4	0	0	$\frac{7}{12}\mu^2$	0
		5	$\frac{33}{20}\mu$	$\frac{1}{6}\mu$	$\frac{45}{32}\mu+\frac{7}{24}\lambda\mu$	$\frac{29}{60}\mu$
		6	$\frac{77}{128}+\frac{2}{9}\mu+\frac{19}{96}\lambda$	$\frac{31}{64}+\frac{1}{48}\lambda$	$+\frac{179}{240}\mu+\frac{31}{64}\lambda+\frac{1}{48}\lambda^2$	$\frac{15}{128}-\frac{7}{72}\mu+\frac{17}{96}\lambda$
		7	$-\frac{573}{2240}-\frac{1}{48}\lambda$	$-\frac{2}{15}$	$-\frac{1}{18}\mu-\frac{2}{15}\lambda$	$-\frac{823}{6720}-\frac{1}{48}\lambda$
		8	$\frac{13}{480}$	$\frac{1}{144}$	$\frac{1}{144}\lambda$	$\frac{29}{144}$
		9	$-\frac{1}{1296}$	0	0	$-\frac{1}{1296}$

be written

$$\sum f_t(x)\beta^t = (1-\beta)^{-\frac{1}{2}} \sin[(1-\beta)^{\frac{1}{2}}x],$$

$$\sum g_t(x)\beta^t = \sum f'_t(x)\beta^t = \cos[(1-\beta)^{\frac{1}{2}}x],$$

$$\sum g'_t(x)\beta^t = (1-\beta)^{-\frac{1}{2}} \sin[(1-\beta)^{\frac{1}{2}}x].$$

It is interesting to note that the dependence on kR drops out when $l = 0$.

These relatively simple generating functions give rise to simple recurrence relations and equation (20) can be replaced by

$$2(t+1)f_{t+1} = (2t+1)f_t - xg_t, \quad 2(t+1)g_{t+1} = xf_t.$$

This indicates that we can calculate F_t and G_t without limiting ourselves to the case in which $u(x)$ is a polynomial in $x(x+2kR)$; if we are only interested in the $l = 0$ case, we can let $u(x)$ be any polynomial in x, or $v(r)$ be a polynomial in r.

The relations for determining the derivatives, corresponding to equation (21), become

$$f'_t = g_t, \quad g'_t = f_{t-1} - f_t.$$

In addition, simple expansions exist for f_t and g_t. Expressed as power series in x, we have

$$f_t(x) = \sum_{r=t}^{\infty} (-1)^{r+t} \frac{r!}{t!(r-t)!} \frac{x^{2r+1}}{(2r+1)!},$$

$$g_t(x) = \sum_{r=t}^{\infty} (-1)^{r+t} \frac{r!}{t!(r-t)!} \frac{x^{2r}}{2r!}.$$

They can also be expressed as a finite series in $x^r \cos x$ and $x^r \sin x$, with constant coefficients, the series for f_t or g_t consisting of $t+1$ odd or even terms respectively, the highest value of r being t. For example

$$f_3 = \tfrac{5}{16} \sin x - \tfrac{5}{16} x \cos x - \tfrac{1}{8} x^2 \sin x + \tfrac{1}{48} x^3 \cos x,$$

$$g_3 = \tfrac{1}{16} x \sin x - \tfrac{1}{16} x^2 \cos x - \tfrac{1}{48} x^3 \sin x.$$

Elementary considerations indicate that for $t \geqq 2$ the first two coefficients of f_t are of the same magnitude but opposite sign and the same is true for the second and third coefficients of g_t, the first coefficient being zero.

In the case $l = 0$, a simpler expression for the reflection coefficient results from equations (11) and (15). This is

$$\eta e^{2ikR} = -\frac{A\eta_{l,0} e^{2ikR} + B}{B^* \eta_{l,0} e^{2ikR} + A^*}, \quad (l = 0)$$

where the asterisk indicates the complex conjugate and

$$A = \sum_{t=0}^{\infty} \beta^t [(F_t(x_0) - G'_t(x_0)) - i(F'_t(x_0) + G_t(x_0))],$$

$$B = \sum_{t=0}^{\infty} \beta^t [(F_t(x_0) + G'_t(x_0)) + i(-F'_t(x_0) + G_t(x_0))].$$

10. Discussion of Possible Applications

A preliminary calculation has been made using this method to obtain the s-wave reflection coefficient corresponding to the scattering of 380 keV neutrons by medium nuclei. The interaction used was the square well optical model of Feshbach, Porter and Weisskopf [1]) with an extension. This extension made $R_0 \approx 1.4R$ and several simple functions $v(r)$ were used, both real and complex.

It was found necessary to calculate the first six terms of the summations in A and B to obtain results accurate to three decimal places. This is because $\beta \approx 100$ and $x_0 \approx 0.4$. A different incident energy has the effect of increasing x_0 and decreasing β in the same ratio and there seems to be no reason for supposing that fewer terms are necessary. Calculation of F_t becomes rapidly more extensive as t increases and without a computor the work necessary to calculate F_6 is out of proportion to the interest in exact values of the s-wave scattering coefficients.

However, it becomes a very powerful method if some application can be found which reduces β without increasing x_0. A possible example is the examination of the effect of a 'tail' on a potential well. In this case, as $\beta = v(R)/k$, the effect of a tail of depth ≈ 4 MeV and of a length of about 40 % of the radius of the well can be determined accurately.

References

1) H. Feshbach, C. E. Porter and V. F. Weisskopf, Phys. Rev. **96** (1954) 448
2) A. M. Lane, R. G. Thomas and E. P. Wigner, Phys. Rev. **98** (1955) 693
3) D. S. Saxon and R. D. Woods, Phys. Rev. **95** (1954) 577
4) G. Culler, S. Fernbach and N. Sherman, Phys. Rev. **101** (1956) 1047
5) J. M. Blatt and V. F. Weisskopf, Theoretical Nuclear Physics (Wiley, New York, 1952) Chapter VIII
6) N. F. Mott and H. S. W. Massey, The Theory of Atomic Collisions (Oxford University Press, 1949) Chapter VI

1.C

Nuclear Physics **18** (1960) 669—671; © *North-Holland Publishing Co., Amsterdam*

Not to be reproduced by photoprint or microfilm without written permission from the publisher

HOLE-HOLE INTERACTIONS AND THE PROPERTIES OF NUCLEAR MATTER

S. A. MOSZKOWSKI †

University of California, Los Angeles 24, *California*

and

A. M. SESSLER †† ‡

Ohio State University, Columbus 10, *Ohio*

Received 29 April 1960

Abstract: The contribution of hole-hole interaction to the ground state energy of nuclear matter is estimated for a mutual interaction containing a repulsive core and an exponential well outside, and is found to be only about $\frac{1}{2}$ MeV per particle.

Recently a number of authors [1, 2, 3]) have suggested modifications of the Brueckner theory of nuclear matter [4]) so as to include hole-hole interactions, as well as particle-particle interactions. Iwamoto [2]) has demonstrated that in a perturbation calculation the inclusion of hole-hole interaction makes no change in the ground-state energy to second order inclusively. The singular two-body potential between nucleons makes it difficult, however, to conclude anything about the contribution of these terms in nuclear matter. The formal similarity between the equation of Iwamoto and the equation for the energy gap in nuclear matter [5]), coupled with the fact that the energy gap is very small at normal density [6]), indicates that the effect of hole-hole interactions is probably only a very small change in the ground-state energy of nuclear matter. It is the point of this note to show that this conclusion is in fact correct, the demonstration proceeding by use of the separation method [7]) for evaluating the energy of nuclear matter.

Confining our attention to the interaction of particles with total momentum zero, we see that hole-hole interactions may be included by replacing the Bethe-Goldstone equation [8]) by [1, 2])

$$(E-T_1-T_2)\psi = (Q-P)V\psi, \tag{1}$$

where Q is an operator which projects both particles outside the Fermi sea, and

† Supported in part by the Office of Ordnance Research.

†† Supported in part by the National Science Foundation, and in part by the U. S. Atomic Energy Commission.

‡ Work done while a visitor at the Lawrence Radiation Laboratory, University of California, Berkeley, California.

P is an operator which projects both particles inside the sea. Thus $Q-P = 1$ if both particles are outside the Fermi sea, $Q-P = 0$ if one particle is outside and one inside, $Q-P = -1$ if both particles are inside the Fermi sea.

Let ϕ represent the wave function for a degenerate Fermi gas at a density appropriate to that of nuclear matter. Then the energy shift ΔE between the energy of the ideal gas and the interacting system is, in Brueckner theory [4]),

$$\Delta E = \langle \phi | t | \phi \rangle, \tag{2}$$

where, using the separation method [7]) and the modification of eq. (1) (Q replaced by $Q-P$), one obtains for t the series

$$t = (t_s+V_1)+(t_s+V_1)\frac{Q-P}{e}(t_s+V_1)-t_s\frac{1}{e_0}t_s. \tag{3}$$

The notation is the same as in ref. [7]), and the small contribution of higher-order terms has been discussed in this same paper. We may write eq. (3) as

$$t = t_0+\Delta t, \tag{4}$$

where t_0 is the usual t matrix evaluated in the absence of hole-hole interactions (cf. ref. [7])), and Δt is the correction due to hole-hole interactions,

$$\Delta t = -(t_s+V_1)\frac{P}{e}(t_s+V_1). \tag{5}$$

Thus, the solutions of the modified Bethe-Goldstone equation are quite different from the solutions of the usual Bethe-Goldstone equation. This difference, which might confuse numerical evaluation of the energy, is, however, predominantly of such a character as to cancel when the total ground-state energy is evaluated.

Indeed the second-order perturbation term for a conventional interaction $\bar{V}$ is

$$\bar{V}\frac{P}{e}\bar{V}, \tag{6}$$

which vanishes when summed over all states in the Fermi sea [2]), as a consequence of the hermiticity of $\bar{V}$. However, this cancellation does not occur in our

TABLE 1

Typical matrix elements of long and short range interactions (units f^3 MeV) for standard potential of ref. [7]). ($f = 10^{-13}$ cm)

	$k = 0.4\,f^{-1}$, $k' = 1.2\,f^{-1}$	$k = 1.2\,f^{-1}$, $k' = 0.4\,f^{-1}$
$(V_1)_{k'k}$	−357.7	−288.3
$(t_s)_{k'k}$	+ 45.2	− 53.0
$(t_s+V_1)_{k'k}$	−312.5	−341.3

case, where $\tilde{V}$ must be replaced by t_s+V_1. The long-range interaction V_1 is not quite hermitian, since the cutoff distance depends on momentum, while the short-range interaction t_s is, in fact, nearly antihermitian. The sum is also not hermitian, though more nearly so than V_1 alone. These results are illustrated in table 1.

A crude calculation of the total contribution of the second-order hole-hole term (eq. (5)) to the ground-state energy yields, in view of the cancellation commented upon above, only about $+\frac{1}{2}$ MeV per particle.

This result is dependent upon the rapid convergence of the separation method, which is certainly sufficient for the purpose of this note. The general problem of convergence has been discussed in ref. [7]), whereas the convergence rate when hole-hole interactions are included is not materially altered. It should be observed that the smallness of the correction to the ground-state energy is intimately related to the smallness of the exclusion-principle contribution in the usual theory. In fact, these two terms are comparable in magnitude, and a quantitative study of the exclusion principle contribution in nuclear matter should properly proceed from the equation including hole-hole interactions. We conclude that even in the presence of singular potentials, hole-hole interactions do not significantly affect the ground-state energy of nuclear matter, and hence leave unaltered the quantitative results of Brueckner and Gammel.

References

1) B. M. Galitzkii, JETP **34** (1958) 151 [translation **7** (1958) 104]
2) F. Iwamoto, Prog. Theoret. Phys., to be published
3) J. S. R. Chisholm and E. J. Squires, Nuclear Physics **13** (1959) 156
4) K. A. Brueckner and J. L. Gammel, Phys. Rev. **109** (1958) 1023 (references to many earlier papers may be found in this article)
5) L. N. Cooper, R. L. Mills and A. M. Sessler, Phys. Rev. **114** (1959) 1377
6) V. J. Emery and A. M. Sessler, Phys. Rev. **119** (1960) 43
7) S. A. Moszkowski and B. L. Scott, submitted to Annals of Physics
8) H. A. Bethe and J. Goldstone, Proc. Roy. Soc. A **238** (1957) 551

1.B; 1.C

Nuclear Physics **18** (1960) 672—680; © *North-Holland Publishing Co., Amsterdam*

Not to be reproduced by photoprint or microfilm without written permission from the publisher

VARIATIONAL CALCULATIONS WITH REPULSIVE CORE POTENTIALS

N. AUSTERN and P. IANO

Radiation Laboratory, University of Pittsburgh, Pittsburgh, Pa. †

Received 30 May 1960

Abstract: A variational method is described which is suitable for fairly detailed calculations with repulsive core potentials. The method employs a wave function which goes over to an exact solution of the two-body Schrödinger equation whenever two nucleons are closer together than a certain distance b. The ideas of effective range theory suggest that the results should not be sensitive to the energy parameter which characterizes the exact solution, a suggestion which is seen to be valid to great accuracy in a numerical calculation with a simple but characteristic potential. The new method is compared with straightforward variational approaches to the same problem, as well as with variational procedures based on a cutoff potential, and is found superior to them both. A practical application of the new method in calculating the Li^6 structure is also cited.

1. Introduction

Recent forms for the phenomenological interaction between two nucleons [1]) all have a repulsive core of small radius, immediately outside of which the attractive potential has a region of very great depth. Potential functions of such forms upset the accuracy of many of the theoretical approximations used in studies of nuclear structure. To some extent this difficulty can be avoided by the introduction of the reaction operator, but that method cannot treat the detailed interparticle correlations which are important in the lightest nuclei, such as H^3. Explicit variational wave functions have always been used in the past to study those correlations. It would seem worthwhile to inquire how to employ the modern potentials in such variational calculations.

Variational wave functions which are used with repulsive core potentials must be zero within the region of the core. Continuity requires that they also be zero at the surface of the core. A wave function meeting these requirements is already compelled to have at least as many variational parameters as were considered in most calculations in the past, and is difficult to employ in integrals. It is also likely to give grossly inaccurate results for the energy. The difficulty lies in the strength of the attraction just outside the core. In this region the potential and kinetic energies are orders of magnitude larger than with simpler potentials, and errors in the wave function in this region which

† Work supported by the joint program of the Office of Naval Research and the U. S. Atomic Energy Commission.

once seemed small have now very much accentuated effects on the energy. Particular attention must be given to the region of strong attraction.

It would seem desirable to establish a division in the attractive part of the potential, at some radius b, separating the region of strong attraction from the region of weaker attraction, as indicated in figure 1. Thus, let r be the separation of some one pair of particles within a nucleus. Then it seems strongly suggested that different approximation methods should be used for the system in the two regions $r < b$ and $r > b$. Such a separation is emphasized in recent work by Moszkowski [2]), who seems to have been the first to include in the "inner region" of the potential a part of the attraction. More accurate methods are used for a pair of particles if $r < b$ than if $r > b$. For $r < b$ the wave function must be very closely adapted to the exact form of $V(r)$, while for $r > b$ the wave function may be permitted to adapt itself to other features of the problem. Moszkowski exploits these ideas to obtain a rapidly converging series development. In the present article we exploit them to construct an accurate variational wave function. Thus in a many-body system the variational wave function as

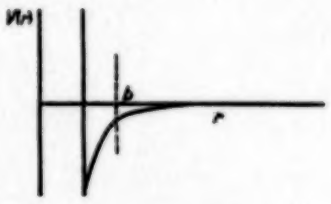

Fig. 1. A potential whose form illustrates the qualitative features of recent nucleon-nucleon interactions. The separation distance b divides the region of strong force from the region of weak force (see text).

it describes any one pair sacrifices many-body effects to two-body effects if $r < b$, but somewhat sacrifices the accuracy of the two-body correlation if $r > b$.

Methods based upon the reaction operator replace $V(r)$ in the awkward region by another operator which is better behaved. A modified potential of similar sort may be obtained very easily from Moszkowski's ideas [2]), and is described in section 2. It is based upon the observation that the inner region of $V(r)$ may be eliminated altogether if the separation radius b is chosen appropriately. This procedure has some merits of simplicity, and occasionally may be helpful. Nevertheless, if a variational calculation is performed with any sort of modified Hamiltonian there is always some doubt whether the ground state energy of the original Hamiltonian actually is the lower bound in the calculation. The method which is proposed in the present article avoids this difficulty. The original Hamiltonian is used at all times. A study of the two-body problem is used only for the purpose of introducing a suitable variational wave function for the many-body system, and not for the purpose of modifying $V(r)$ in any fashion.

In section 2 it will be shown to be feasible to employ in variational calculations a wave function which is an exact solution of the two-body problem for $r < b$. The use of such a numerically computed exact solution is kept from being burdensome by the fact that it does not matter much for what energy the exact solution is computed, an idea taken from effective range theory. This method is developed at length in section 2, and calculations which test it and compare it with other methods are given. In section 3 the results of a practical application of the method are cited.

2. Tests of Approximation Methods

In this section several variational calculations for a repulsive core potential in a two-body system are described, and the advantages of the new method are shown. Its use in many-particle systems is not discussed, this being rather deferred until section 3. The calculations with the two-body system will be of three types: (1) Straightforward application of variational wave functions adapted to the gross properties of the repulsive core potential. (2) Very simple

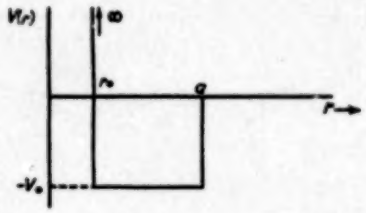

Fig. 2. Square well with repulsive core: the simple potential for which variational wave functions are tested in the present paper.

wave functions are tested with a modified potential. (3) The new method is described at length, and tested.

All the calculations are performed for a two-body system composed of spinless nucleons interacting by way of the simple repulsive core potential shown in figure 2. The parameters of the potential have values $r_0 = 0.4f$, $a = 1.971f$, $V_0 = 60.8$ MeV (nuclear parameters involving lengths are expressed in terms of the length $f = 10^{-13}$ cm). By accident these parameters do not quite give the deuteron ground state properties, with which one might wish to compare. Instead the ^{3}S-state binding energy is found to be $\varepsilon = -4.13$ MeV, and the scattering length is $2.42\,f$. The exact ground state radial wave function in this potential is

$$u(r) = \begin{cases} 0 & (r < r_0), \\ B \sin[(r-r_0)(k^2-\gamma^2)^{\frac{1}{2}}] & (r_0 < r < a), \\ e^{-\gamma r} & (a < r), \end{cases} \tag{1}$$

where

$$k^2 = MV_0/\hbar^2 = 1.462f^{-2} \quad \gamma^2 = M\varepsilon/\hbar^2 = 0.0992f^{-2}.$$

It may be noted that the simple potential of fig. 2 does not have all the awkward features of the potentials indicated by fig. 1, which are discussed in the introduction. Nevertheless calculations based upon the simple potential do adequately test the new method, even if no marked effects in the energy are obtained.

The Rayleigh-Schrödinger variational principle is employed. Thus, if $\bar{u}$ is the approximate form of u, then the corresponding approximation to the energy is

$$\bar{E} = \int_0^\infty \bar{u}\left[-\frac{\hbar^2}{M}\bar{u}'' + V(r)\bar{u}\right] dr \Big/ \int_0^\infty \bar{u}^2 dr. \tag{2}$$

This energy integral is evaluated for each of the functions to be indicated, giving $\bar{E}$ as a function of the parameters of $\bar{u}$.

2.1. STRAIGHTFORWARD METHOD

Two functional forms are tested here for the two-body system. These are

$$\bar{u}_1 = \begin{cases} 0 & (r < r_0), \\ re^{-\alpha_1 r}[1-e^{-\lambda_1(r-r_0)}] & (r > r_0), \end{cases}$$

$$\bar{u}_2 = \begin{cases} 0 & (r < r_0), \\ e^{-\alpha_2 r}[1-e^{-\lambda_2(r-r_0)}] & (r > r_0). \end{cases}$$

The function $\bar{u}_1$ is adapted from one found convenient for triton calculations, while $\bar{u}_2$ was thought to be more suitable for the deuteron. Best values for the variational parameters and the associated energies are

$$\alpha_1 = 0.79f^{-1}, \quad \lambda_1 = 3.10f^{-1}, \quad \bar{E}_1 = -3.39 \text{ MeV},$$
$$\alpha_2 = 0.28f^{-1}, \quad \lambda_2 = 0.96f^{-1}, \quad \bar{E}_2 = -2.66 \text{ MeV}.$$

Figure 3 shows a graph of the best forms of these wave functions, superimposed upon the exact wave function.

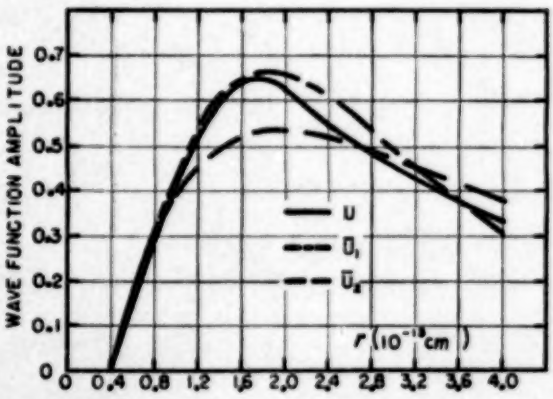

Fig. 3. The exact ground state eigenfunction u of the simple potential (solid line), and the best forms of the two variational approximations $\bar{u}_1$ (dot-dash line) and $\bar{u}_2$ (dashed line). These wave functions are normalized to unity.

Blatt and Derrick employed functions of the above forms for calculations of triton structure, using the Gammel-Thaler interaction between nucleons. Their result suggested a triton which is not bound [3]).

2.2. USE OF MODIFIED POTENTIAL

It is possible to interpret Moszkowski's ideas [2]) as suggesting a very simple modified potential $\tilde{V}$ from which the repulsive core has been eliminated. The potential $\tilde{V}$ is formed by cutting off the potential $V(r)$ at a radius b, such that $\tilde{V} = 0$ for $r < b$, and $\tilde{V} = V$ for $r > b$. Then b is adjusted to equate the logarithmic derivatives, at b, of the ground state eigenfunctions of V and $\tilde{V}$. After such adjustment the eigenfunction of $\tilde{V}$ is *the same as the eigenfunction of* V in the region $r > b$, and both eigenfunctions correspond to the same total energy. Normally b depends on the energy. For our simple potential the suitable value of b for the ground state is $b = 1.194f$, so that the modified potential has the form

$$\tilde{V}(r) = \begin{cases} 0 & r < 1.194f, \\ -V_0 & (1.194f < r < 1.971f), \\ 0 & (r > 1.971f). \end{cases} \tag{4}$$

Evidently the ground state eigenvalue of $\tilde{V}(r)$ is the same as the ground state eigenvalue of $V(r)$, and a variational calculation with $\tilde{V}(r)$ is therefore really bounded below by the exact energy. The possible convenience of conducting calculations with $\tilde{V}(r)$ lies in the fact that $\tilde{V}(r)$ is missing the awkward parts of $V(r)$. For this reason it is possible that variational wave functions of the older sort would be very successful in connection with the modified potential.

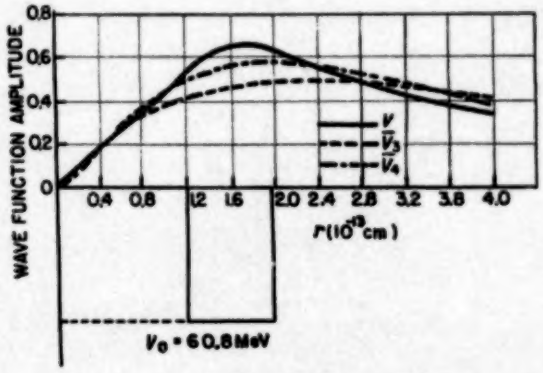

Fig. 4. The Moszkowski cutoff potential $\tilde{V}$, along with its exact eigenfunction v (solid line), and two variational approximations $\bar{v}_3$ (dashed line) and $\bar{v}_4$ (dot-dash line). (Normalized to unity).

Two forms of wave function have been tested with the modified potential. These are

$$\bar{v}_3(r) = re^{-\alpha_3 r}, \tag{5}$$

$$\bar{v}_4(r) = r(e^{-\alpha_4 r} + C_4 e^{-\beta_4 r}). \tag{6}$$

Best values of the variational parameters and the associated energies are

$$\alpha_3 = 0.4304f^{-1}, \quad \bar{E}_3 = -1.8 \text{ MeV}, \quad \alpha_4 = 0.58f^{-1},$$
$$C_4 = -0.73, \quad \beta_4 = 2.0f^{-1}, \quad \bar{E}_4 = -2.8 \text{ MeV}.$$

Figure 4 shows the potential $\bar{V}$, the best forms of the two variational functions $\bar{v}_3$ and $\bar{v}_4$, and the exact ground state eigenfunction of $\bar{V}$, $v(r)$. The wave functions used with this method are evidently simpler than those of method (1); however, the results are inferior, and the method therefore does not seem very useful.

2.3. THE EFFECTIVE RANGE METHOD

An effort is now made to obtain a wave function which may be used with the exact $V(r)$, but which gives results of much better accuracy than obtained with $\bar{u}_1$, in subsection 2.1. Once again the separation radius b is introduced. (For convenience the same numerical value as in subsection 2.2 will be employed, some discussion being given later.) In the present method the radius b is not used for any modification of the potential, but only in the specification of the variational wave function. The wave function is taken to be of simple variational form for $r > b$, but for $r < b$, the wave function is taken to be an eigenfunction $u_e(r)$ corresponding to some value e of the total energy. The explicit form considered is

$$\bar{u}_5 = \begin{cases} u_e(r) & (r < b), \\ A\,(e^{-\alpha_5 r} + C_5 e^{-\beta_5 r}) & (r > b). \end{cases} \tag{7}$$

For the present, illustrative calculations we set $e = \hbar^2\zeta^2/M$, and can write out $u_e(r)$ in detail:

$$u_e(r) = \begin{cases} 0 & (r < r_0), \\ \sin\{(r - r_0)(k^2 + \zeta^2)^{\frac{1}{2}}\} & (r_0 < r < b). \end{cases}$$

The wave function $\bar{u}_5$ depends on three variational parameters, ζ, α_5 and β_5. The constants A and C_5 are chosen to make the function and its first derivaive continuous at $r = b$. At first sight wave functions of the form of $\bar{u}_5$ would seem to be difficult ones to use in practical calculations, in which the potentials have such forms as shown in fig. 1, for in such calculations the function $u_e(r)$ for $r < b$ would have to be determined numerically for each value of ζ; i.e., for each value of e. Fortunately, the basic ideas used to develop effective range theory suggest a crucial simplification, that the exact value of e does not matter very much, provided $|e| \ll V_0$. Thus one might hope that the energy $\bar{E}_5$, computed with $\bar{u}_5$, would be insensitive to e, and that in a practical calculation e need not be varied at all. This hope will be seen to be borne out in the present example, a result which must follow even more strongly when potentials like those in fig. 1 are considered.

A complete exploration of the parameter space of ζ, α_5 and β_5 has not been performed. Instead, best values of α_5 and β_5 are determined in the case $e = 0$ (thus $\zeta = 0$), then those values of α_5 and β_5 are kept fixed and e is varied. In this manner $\bar{E}_5$ is determined as a function of e. Slightly lower values of $\bar{E}_5(e)$ could be achieved if α_5 and β_5 were varied for all $e \neq 0$, but the differences would be unimportant. The "best" values of α_5 and β_5 are

$$\alpha_5 = 0.36f^{-1}, \quad \beta_5 = 1.98f^{-1}.$$

Figure 5 shows $\bar{E}_5(e)$, and fig. 6 shows superimposed graphs of $\bar{u}_5$ for $e = 0$, and of the exact eigenfunction. It is seen that $\bar{E}_5$ is a very insensitive function of e, that $\bar{E}_5$ is very close to the exact value $\varepsilon = -4.14$ MeV, and that the variational wave function is very close to the exact wave function at *all* points.

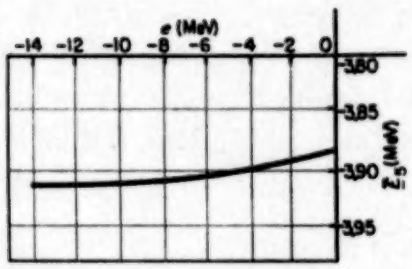

Fig. 5. The energy $\bar{E}_5$ of the effective range method shown as a function of the parameter e for fixed α_5 and β_5.

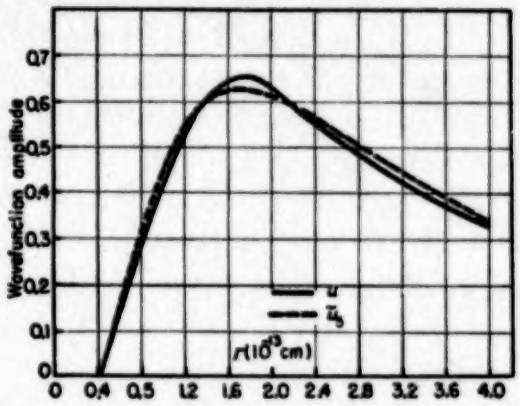

Fig. 6. The variational wave function of the effective range method, $\bar{u}_5$, is shown by the dotted line (for the case $e = 0$). The solid line is the exact eigenfunction u of the simple potential. (Normalized to unity).

A procedure for the choice of the separation radius in $\bar{u}_5$ is evidently required. The Moszkowski radius b is not unsuitable for the present study, as it includes in the inner region just enough of the attractive potential to cancel the effect of the core on the asymptotic wave function. Nevertheless in a context where we wish only to optimize certain variational results the radius b really is not uniquely indicated. The following criteria seem suitable as guides for further calculations: (1) Variational results are obviously not sensitive to the precise value of the separation. (2) We require the separation at as small a radius as possible, so that when the method is extended to use in many-body systems the inner region will not be too obtrusive. Furthermore the separation radius must be small enough so that the potential strength at that radius is great enough to swamp the uncertainty in the energy e. (3) The separation has to be at a large enough radius so that for all larger radii it is suitable to treat $V(r)$ by variational methods.

3. Conclusions

The calculations for the two-body system, in section 2, do not work out *very* badly with any of the three methods tested. This is a consequence of the flat form of the simple potential used. Enough information has been gained, however, to permit clear decisions about the three methods.

The method of subsection 2.2, which uses the cutoff potential, gives the poorest results for the energy, although these are not poor enough to disqualify it. The method does lose interest, however, because of the energy-dependent nature of the cutoff. This must interfere with its application in a many-body system, where no given two-body subsystem can be in a sharp energy eigenstate. Off-energy-shell matrix elements of the cutoff potential also are questionable. Since in the applications under discussion the method of subsection 2.2 actually was no easier to apply than the very accurate effective range method (subsection 2.3), it will not be discussed further.

The straightforward method of subsection 2.1 gives a good energy and a good wave function, for the simple potential used to test it. Nevertheless the *error* of the best energy achieved with the straightforward method was 0.74 MeV, three times the error given by the effective range method in its standard version, when $e = 0$, viz. 0.25 MeV. It is apparent that the results given by these two methods would differ markedly if a potential of the form of fig. 1 were used. For such a potential it is not surprising that the product of three functions of the "straightforward" sort gives a poor representation of the triton [3]).

The effective range method uses the exact potential, is accurate, and is not difficult to apply. Probably the most important fact shown by the calculation in subsection 2.3 is that the results are exceedingly insensitive to the parameter e, so that it appears entirely satisfactory to proceed with the one value $e = 0$. In this circumstance the variational wave function for the inner region is computed once, numerically, but has no adjustable parameters. The wave function in the outer region has two adjustable parameters but is of analytic form and easy to handle.

For many-body systems the effective range method generalizes readily. The variational wave function is taken of any suitable analytic form whenever all the particles are sufficiently separated from each other. Whenever any two particles come closer together than the separation distance, however, a single suitable, numerically computed, function $u_0(r)$, is inserted. The variational function in the outer region is adjusted so that the value and derivative of the complete wave function are continuous everywhere. At all times the wave function is subjected to the complete Hamiltonian. The numerical function in the inner region is an eigensolution of only part of the Hamiltonian, and some complications accordingly do appear because of the correlation terms in the

kinetic energy. Nevertheless the numerical function is an eigensolution of the worst part of the Hamiltonian; the correlation terms are small and are easy to carry explicitly, so that their full influence is felt. The energy computed in this way is reliably bounded below by the exact energy. Generalization for tensor forces is possible.

The effective range method has been employed in a calculation [4]) of the structure of Li^6. This nucleus is treated as a three-body system, $\alpha+n+p$. The Gammel-Thaler interaction [1]) is used between the neutron and proton. The variational wave function is taken as a product function in the three interparticle separations. Two calculations were performed for this problem: a function of the form $\bar{u}_1$ (see section 2) was employed for the neutron-proton relative motion, and a function of the form $\bar{u}_5$ was employed. Even for such a loosely bound nucleus as Li^6, in which the n—p correlation is slight, the energy computed with $\bar{u}_5$ was 3.5 MeV below that computed with $\bar{u}_1$. The value of the effective range method thus is demonstrated.

We are grateful to S. A. Moszkowski for information about the cutoff method and for some criticism of this article. We are grateful to P. H. Wackman for permission to quote his results in advance of publication.

References

1) J. Gammel and R. Thaler, Phys. Rev. **107** (1957) 291, 1337
2) S. A. Moszkowski, Bull. Amer. Phys. Soc. **4** (1959) 256, and to be published.
3) J. M. Blatt, private communication, and Proceedings of the conference of the few-nucleon problem, Univ. College, London (1959); see also G. H. Derrick and J. M. Blatt, Nuclear Physics **17** (1960) 67
4) P. H. Wackman, to be published (1960)

7.A

Nuclear Physics **18** (1960) 681—690; © *North-Holland Publishing Co., Amsterdam*

Not to be reproduced by photoprint or microfilm without written permission from the publisher

AN EQUIVALENCE THEOREM FOR PARTIALLY GAUGE-INVARIANT VECTOR MESON INTERACTIONS

ABDUS SALAM

Imperial College of Science and Technology, London

Received 21 May 1960

Abstract: Consider a massive neutral vector meson U_μ interacting with other spin zero or spin $\frac{1}{2}$ particles ϕ. If the interaction Lagrangian consists of two parts $L_1(\phi, U)+L_2(\phi)$ where $L_1(\phi, U)$ is (together with kinetic energy terms) invariant for the gauge transformations

$$\phi = \exp(iQ\Lambda)\phi', \qquad U_\mu = A_\mu - \frac{1}{\kappa}\frac{\partial \Lambda}{\partial x_\mu}$$

and L_2 is not gauge-invariant, it is shown that the conventional S-matrix T exp $i(\int L_1(\phi, U)+ +L_2(\phi))$ identically equals T exp $i\,(\int L_1(\phi, A)+L_2(\phi'))$. Since all Λ-dependent effects are now contained and displayed explicitly in $L_2(\phi')$ it is possible to give a precise discussion of the renormalization problem for vector meson theories. This is because the suspected non-renormalizability of these theories arises from $\partial\Lambda/\partial x_\mu$ terms in the conventional S-matrix.

1. Introduction

The suspicion that weak interactions may be meditated by vector mesons [1]) has led to a revival of interest in the theoretical structure of such interactions. In particular Glashow [2]) has investigated the renormalizability of vector meson theories in which a part of the Lagrangian is invariant for a certain gauge transformation leading to a "partial conservation" for the vector-meson current. His conclusion is that in special cases such theories would indeed be renormalizable. In view of the possible physical interest of these theories particularly for pseudo-vector couplings in β-decay [4]), the problem has been reinvestigated below. We prove a general equivalence theorem for vector meson interactions from which it is also possible to deduce a precise criterion for renormalizability in the conventional sense. It appears that the correct criterion is much more restrictive than that stated by Glashow and there may indeed be very few, if any, theories which satisfy this.

The equivalence theorem itself is perfectly general. In this paper we shall work it out in detail for the simple case of a neutral vector meson. In sections 2 and 3 we consider the case of a neutral pseudo-vector meson interacting with nucleons and in section 4 a vector meson interacting with mesons. In a subsequant paper the equivalence theorem will be proved for the case of a (mass-carrying) Yang-Mills [3]) triplet of vector fields.

2. Neutral Pseudovector Mesons

Consider a neutral pseudo-vector meson U_μ interacting with a fermion field ψ, the Lagrangian being

$$L = L_k + L_1 + L_2, \tag{1}$$

where

$$L_k = -(\bar{\psi}\gamma\partial\psi) - \tfrac{1}{4}\left(\frac{\partial U_\mu}{\partial x_\nu} - \frac{\partial U_\nu}{\partial x_\mu}\right)^2, \tag{2}$$

$$L_1 = -ig\bar{\psi}\gamma_\mu\gamma_5\psi U_\mu, \tag{3}$$

$$L_2 = -m\bar{\psi}\psi - \tfrac{1}{2}\kappa^2 U_\mu U_\mu. \tag{4}$$

The Lagrangian L is partially gauge invariant. Whereas the combination L_k+L_1 is form invariant when written out in terms of the fields ψ' and A_μ defined by

$$\psi = \exp\frac{i\gamma_5 g\Lambda(x)}{\kappa}\psi', \tag{5}$$

$$U_\mu = A_\mu - \frac{1}{\kappa}\frac{\partial\Lambda}{\partial x_\mu}, \tag{6}$$

this is not true of L_2. Here and in the rest of the paper we shall consider only those cases in which L_2, the non-gauge-invariant part, contains no derivative, so that the presense of L_2 does not affect the canonical commutation relations and in particular the relation

$$\delta(x_0-x'_0)[j_4(x'), \psi(x)] = -i\gamma_5 g\psi(x)\delta(x-x'), \tag{7}$$

where

$$j_\mu(x) = -\frac{\partial L}{\partial(\partial_\mu\psi)}(i\gamma_5 g)\psi = ig\bar{\psi}\gamma_\mu\gamma_5\psi. \tag{8}$$

The current $j_\mu(x)$ is partially conserved. In fact, using the equations of motion, we have

$$\frac{\partial j_\mu}{\partial x_\mu} = -\left[\frac{\partial L_2}{\partial\psi}(i\gamma_5 g)\psi + \bar{\psi}(i\gamma_5 g)\frac{\partial L_2}{\partial\psi}\right] \tag{9}$$

$$= 2mig\bar{\psi}\gamma_5\psi. \tag{10}$$

It is crucial to note that even though the meson mass term $\kappa^2 A_\mu{}^2$ in L_2 is non-gauge-invariant, it has no effect on eq. (10).

Writing

$$L_m = -m\bar{\psi}\psi, \tag{11}$$

note that †

$$\delta(x_0-x_{10})[j_4(x_1),\ j_\mu(x)] = 0, \tag{12}$$

$$\delta(x_0-x_{10})[j_4(x_1),\ L_m(x)] = \frac{\partial j}{\partial x}\,\delta^4(x-x_1). \tag{13}$$

To prove (13) notice that the right-hand side of (7) equals $\kappa(\delta\psi'(x)/\delta\Lambda(x_1))|_{\Lambda=0}$, where ψ' is given by (5). Quite generally,

$$\delta(x_0-x_{10})[j_4(x_1),\ \bar{\psi}A\psi] = \kappa\frac{\delta}{\delta\Lambda(x_1)}(\bar{\psi}'A\psi')|_{\Lambda=0} \tag{14}$$

and

$$\delta(x_0-x_{10})\delta(x_{10}-x_{20})\ldots\delta(x_{n-1,0}-x_{n0})[j_4,[\ldots[j_4,\bar{\psi}A\psi]\ldots] = \kappa^n\frac{\delta}{\delta\Lambda^n}(\bar{\psi}'A\psi')|_{\Lambda=0}. \tag{15}$$

Specializing to $A = \gamma_5\gamma_\mu$ in (14) gives (13), while setting $A = 1$, one deduces

$$L_m(\psi') = -m\bar{\psi}\exp\{-2i\gamma_5 g\Lambda/\kappa\}\psi = \sum\frac{1}{n!}\frac{1}{\kappa^n}\int\Lambda(1)\ldots\Lambda(n)\mathrm{d}1\ldots\mathrm{d}n\,\delta(x_0-x_{10})\ldots\delta(x_{n-1,0}-x_{n0}) \times[j_4(x_n)[\ldots[j_4,L_m]]\ldots]. \tag{16}$$

3. The Equivalence Theorem

The scattering matrix for the theory is given by the usual expression

$$S = \mathrm{T}\exp\left(i\int L_1\mathrm{d}^4x\right), \tag{17}$$

where $L_1 = -j_\mu U_\mu$. The fields ψ and U in this section are not Heisenberg fields but satisfy their free equations. We shall find it convenient for subsequent generalization to include the fermion mass terms (in fact all non-gauge-invariant parts of the Lagrangian except meson-mass terms) in the interaction so that

$$S = \mathrm{T}\exp i\int(-jU+L_m)\mathrm{d}^4x. \tag{18}$$

Using the free equations, note now that

$$\frac{\partial j_\mu}{\partial x_\mu} = 0. \tag{18a}$$

† Schwinger has recently [6]) emphasized that relation (12), which is a consequence of the canonical formalism, is inconsistent with the assumption that the Hamiltonian of the theory possesses only positive (energy) eigenvalues. The consideration of such questions, however, is beyond the scope of the present paper.

The S-matrix elements are written down by drawing the usual Feynman diagrams and writing a factor

$$i\langle \mathrm{T}\psi(x)\bar{\psi}(y)\rangle_0 = \frac{1}{(2\pi)^4}\frac{1}{i}\int \frac{2\pi}{\gamma k} e^{ik(x-y)} d^4k$$

for each internal fermion line and a factor

$$i\langle \mathrm{T}U_\mu(x)U_\nu(y)\rangle_0 = \left(\frac{1}{\kappa^2}\frac{\partial}{\partial x_\mu}\frac{\partial}{\partial y_\nu} - \delta_{\mu\nu}\right)\Delta^c(x-y) \tag{19}$$

for each meson line. It is well known that the possible non-renormalizability of the theory arises from terms like $\kappa^{-2}(\partial/\partial x_\mu)(\partial/\partial y_\nu)\Delta$ in (19). We now state the equivalence theorem which isolates the effect of these terms:

Theorem: The S-matrix (18) is completely equivalent to the S-matrix calculated from the expression

$$\mathrm{T}\exp\left\{i\int[-j_\mu(\psi)A_\mu + L_m(\psi')]\right\} d^4x, \tag{20}$$

where (using eq. (5) for the definition of ψ')

$$L_m(\psi') = -m\bar{\psi}\{\exp -(2i\gamma_5 \Lambda g)/\kappa\}\psi; \tag{21}$$

the matrix elements are written down with the help of conventional Feynman graphs, with the following prescriptions: (a) for all internal meson lines the factor (19) must be replaced by the factors

$$i\langle \mathrm{T}A_\mu(x)A_\nu(y)\rangle_0 = -\delta_{\mu\nu}\Delta^c(x-y), \tag{22}$$

$$i\langle \mathrm{T}\Lambda(x)\Lambda(y)\rangle_0 = \Delta^c(x-y), \tag{23}$$

$$i\langle \mathrm{T}A_\mu\Lambda\rangle_0 = 0; \tag{24}$$

(b) External mesons are created (or annihilated) by A_μ operators only.

To prove this, first consider the case when there are no external mesons in the initial or the final state. Write (18) in the form

$$S = \mathrm{T}\exp\left[\tfrac{1}{2}i\int j_\mu\left(\frac{1}{\kappa^2}\frac{\partial}{\partial x_\mu}\frac{\partial}{\partial y_\nu} - \delta_{\mu\nu}\right)j_\nu + i\int L_m\right]. \tag{25}$$

The validity of (25) is directly verified by expanding (18) and (25) in powers of the coupling constant and using the result

$$\langle \mathrm{T}U(1)\ldots U(2s)\rangle_0 = \sum_{\text{all pairs}}\langle \mathrm{T}U(1)U(2)\rangle_0\ldots\langle \mathrm{T}U(2s-1)U(2s)\rangle_0. \tag{26}$$

The number of distinct pairings on the right-hand side of (26) is $(2s-1)!!$

Since

$$\frac{(2s-1)!!}{2s!} = \frac{1}{s!\ 2^s},$$

the numerical factors in the coefficients of g^{2s} in (18) and (25) check.

Expanding (25) in the form

$$S = \mathrm{T}\left[\left(1+\frac{i}{2\kappa^2}\int \mathrm{d}1\ \mathrm{d}2\left(\frac{\partial}{\partial 1}\frac{\partial}{\partial 2}\Delta^c(1-2)\right)\right.\right.$$
$$\left.\left. j(1)j(2)+\ldots\right)\exp\int\{-\tfrac{1}{2}ij\Delta j+iL_m\}\right], \quad (27)$$

one obtains, after a partial integration,

$$S = \left(\mathrm{T}+\int\frac{i}{2\kappa^2}\Delta^c(1-2)\mathrm{d}1\ \mathrm{d}2\frac{\partial}{\partial 1}\frac{\partial}{\partial 2}\mathrm{T}j(1)j(2)+\ldots\right)\exp\int\{-\tfrac{1}{2}ij\Delta j+iL_m\}. \quad (28)$$

Using (22), (23) and (24) and relations analogous to (26) for Λ and A, one can rewrite (28) more simply as †

$$S = \left(\mathrm{T}+\frac{i^2}{2\kappa^2}\int \mathrm{d}1\,\mathrm{d}2\langle \mathrm{T}\Lambda(1)\Lambda(2)\rangle_0\frac{\partial}{\partial 1}\frac{\partial}{\partial 2}\right.$$
$$\left.\mathrm{T}j(1)j(2)+\ldots\right)\exp\int(-ijA+iL_m). \quad (29)$$

All that remains now is to differentiate a chronological product of j_μ and L_m operators.

Lemma 1.

$$\frac{\partial}{\partial x_\mu}\mathrm{T}j_\mu(x)O(y) = \mathrm{T}\frac{\partial j}{\partial x}O(y)+\frac{1}{i}\delta(x_0-y_0)[j_4(x), O(y)]. \quad (30)$$

The proof follows from the identity

$$\mathrm{T}j_\mu(x)O(y) = \tfrac{1}{2}\{j_\mu(x), O(y)\}+\tfrac{1}{2}\varepsilon(1-2)[j_\mu(x), O(y)]. \quad (31)$$

Consider two special cases:

(a) $O(y) = j_\mu(y)$. Using (12) and (18a) we have

$$\frac{\partial}{\partial x_\mu}\mathrm{T}(j_\mu(x), j_\nu(y)) = 0. \quad (32)$$

† One might have written (29) directly by starting with $S = \mathrm{T}\exp\int -ijU+iL_m = \mathrm{T}\exp\int\{-ijA+iL_m-ij(\partial\Lambda/\kappa\partial x)\}$, where use has been made of eq. (6). An expansion in powers of $\partial\Lambda/\partial x$ and a subsequent partial integration would give (29). Since Λ and A commute, $\mathrm{T}(\Lambda^n A^r) = \mathrm{T}(\Lambda^n)\mathrm{T}(A^r)$.

(b) If $O(y) = L_m(y)$ it follows from (14) that

$$\frac{\partial}{\partial x_\mu} \mathrm{T} j_\mu(x) L_m(y) = \frac{\kappa}{i} \frac{\delta}{\delta \Lambda(x)} L_m(\psi')|_{\Lambda=0}. \tag{33}$$

This result immediately generalizes to

Lemma 2.

$$\frac{\partial}{\partial x_\mu} \mathrm{T} \left\{ j_\mu(x) \exp i \int (-j_\mu A_\mu + L_m) \right\} = \frac{\kappa}{i} \frac{\delta}{\delta \Lambda(x)} \mathrm{T} \exp i \int (-j_\mu A_\mu + L_m(\psi'))|_{\Lambda=0}. \tag{34}$$

Lemma 3A.

$$\frac{\partial}{\partial 1} \frac{\partial}{\partial 2} \mathrm{T} j(1) j(2) L_m(3) = \frac{\kappa^2}{i^2} \frac{\delta^2}{\delta^2 \Lambda} L_m(\psi')|_{\Lambda=0}.$$

To prove this, note that the right-hand side equals (cf. eq. (30))

$$\frac{1}{i} \frac{\partial}{\partial 1} \mathrm{T} j(1) \delta(x_{20} - x_{30}) [j_4(2), L_m(3)] = \frac{1}{i^2} \delta(x_{10} - x_{20}) \delta(x_{20} - x_{30}) [j_4(1), [j_4(2), L_m(3)]], \tag{35}$$

which is $(\kappa^2/i^2)(\delta^2/\delta^2 \Lambda) L_m(\psi')|_{\Lambda=0}$ from (33). More generally, we have

Lemma 3B.

$$\frac{\partial}{\partial 1} \ldots \frac{\partial}{\partial n} \mathrm{T} j(1) \ldots j(n) \exp i \left(\int (-jA + L_m(\psi)) \right) = \frac{\kappa^n}{i^n} \frac{\delta^n}{\delta \Lambda^n} \mathrm{T} \exp i \left(\int -jA + L_m(\psi') \right) \Big|_{\Lambda=0}. \tag{36}$$

Substitution of (36) into (29) now trivially gives the equivalent S-matrix expression

$$S = \mathrm{T} \exp i \int \{-jA + L_m(\psi')\},$$

completing the proof of the theorem.

To include cases when mesons are present in initial or final states is a simple matter. All graphs with n external meson lines can be computed in conventional theory by considering expressions like

$$\left(A \left| \frac{\delta}{\delta \eta_a(x_1)} \ldots \frac{\delta}{\delta \eta_b(x_n)} \mathrm{T} \exp i \left(\int \{-j_\mu(U_\mu + \eta_\mu) + L_m\} \right) \right| B \right)_{\eta=0}, \tag{37}$$

where the quantities η are external source functions and states $|A)$ and $|B)$ contain no mesons. The inclusion of $ij\eta$ terms in (37) requires no change in any

of the formulae above, so that the equivalent S-matrix elements are again given by (37) with A_μ replacing U_μ and $L_m(\psi')$ replacing $L_m(\psi)$. In other words so far as external meson lines are concerned the Λ "field" does not make its appearance at all.

Note one final alteration. By considering single fermion line factors in any graph, it is clear that one may replace $L_m(\psi')$ in (20) by $L_m(\psi')-L_m(\psi)$ provided one compensates for this by changing at the same time all factors $S^c(k) = 2\pi/\gamma k$ to the conventional factors $2\pi(\gamma k+m)^{-1}$. With this change $S = \mathrm{T}\exp(-i\int jU)$ directly equals †

$$S = \mathrm{T}\exp -i\Big\{\int (jA+m\bar{\psi}[\exp(-2i\gamma_5 g\Lambda/\kappa)-1]\psi)\Big\}. \tag{38a}$$

It is clear that if the fermion interacts also with an additional field (for example π-meson field), where the non-gauge invariant part of the original Lagrangian is $L_2 = i\bar{\psi}\gamma_5\psi\pi$, in the equivalent S-matrix this term will appear as $i\bar{\psi}'\gamma_5\psi'\pi$.

4. Interaction of Vector Mesons with Scalar Particles

The proof appears complicated but its structure is essentially simple. The important step consists in observing that a string of equal time commutators of j_4 with L_m

$$[j_4, [j_4, \ldots [j_4, L_m]] \ldots]$$

on one hand equals

$$\kappa^n \frac{\delta^n}{\delta\Lambda^n} L_m(\psi')|_{\Lambda=0},$$

and on the other hand equals

$$\frac{1}{i^n}\frac{\partial}{\partial 1}\cdots\frac{\partial}{\partial n}(\mathrm{T}j(1)\ldots j(n)L_m(\psi)).$$

Also in setting up the proof (cf. eqs. (25) and (27)) it was of considerable advantage that the "gauge-invariant" part L_1 of L_m could be written in the form $-j_\mu U_\mu$ (linear in U_μ). It is always possible to do this provided one uses Schwinger's formalism [5]) and (by introducing supplementary fields) writes the Lagrangian in such a way that it contains only first order derivatives. To illustrate, in this section we demonstrate the equivalence theorem for the interaction of spin-zero particles with a neutral vector meson.

† The splitting off of $L_m(\psi)$ at this state is analogous to the converse splitting off of self-mass terms from free Lagrangians and their inclusion in interaction Lagrangians in usual renormalization theory.

Write the Lagrangian

$$L = -\chi_\mu^*(\partial_\mu+ieU_\mu)\phi-\chi_\mu(\partial_\mu-ieU_\mu)\phi^*+\mu\phi^*\phi+\mu\chi^*{}_\mu\chi_\mu+L_2+L(U), \quad (38)$$

where the quantities χ_μ are four additional dynamical variables introduced to describe spin-zero particles besides the field variable ϕ, and $L(U)$ is the free meson Lagrangian.

If L_2 (for illustrative purposes) equals $\lambda(\phi+\phi^*)$, the Lagrangian is partially gauge-invariant for the transformation

$$\phi = \exp(ie\Lambda/\kappa)\phi', \quad U_\mu = A_\mu-\frac{1}{\kappa}\frac{\partial\Lambda}{\partial x_\mu}, \quad \chi_\mu = \exp(ie\Lambda/\kappa)\chi'_\mu.$$

From Schwinger's (functional) theory [5]) of Green's functions, it can be shown that the S-matrix is given by

$$S = \mathrm{T}^* \exp\left\{i\int (L_1+L_2)\mathrm{d}^4x\right\}, \quad (39)$$

where

$$L_1 = -j_\mu U_\mu, \quad j_\mu = ie(\chi_\mu^*\phi-\chi_\mu\phi^*), \quad (40)$$

χ_μ and ϕ satisfy free field equations $\partial_\mu\phi = \mu\chi_\mu$ and $\partial_\mu\chi_\mu = \mu\phi$, and the vacuum expection value of a T*-product of 2 operators χ_μ and ϕ is given by

$$i\langle \mathrm{T}^*\phi(x)\phi^*(y)\rangle_0 = \Delta^c(x-y), \quad (41)$$

$$i\langle \mathrm{T}^*\chi_\mu(x)\phi^*(y)\rangle_0 = \frac{\partial}{\partial x_\mu}\Delta^c(x-y), \quad (42)$$

$$i\langle \mathrm{T}^*\phi(x)\chi_\mu^*(y)\rangle_0 = \frac{\partial}{\partial y_\mu}\Delta^c(x-y), \quad (43)$$

$$i\langle \mathrm{T}\chi_\mu(x)\chi_\nu^*(y)\rangle_0 = \frac{\partial}{\partial x_\mu}\frac{\partial}{\partial y_\nu}\Delta^c(x-y)-\delta_{\mu\nu}\delta(x-y). \quad (44)$$

(The T*-product of two operators differs from a T-product only for points $x_0 = y_0$).

Finally, we remark that in eqs. (39) and (40) the T*-product of more than two operators can be expressed as a Wick sum of normal products of field operators multiplied by the contractions (41) to (44). The general procedure for writing down (41) to (44) has been given by Schwinger [5]) and Glashow [2]) and will not be repeated here.

To prove the equivalence theorem we proceed now as in eqs. (25) to (29) of the last section. Since an identity analogous to (31) does not exist for T*-products, we use Wick's theorem to obtain lemmas similar to Lemmas 1 to 3 of the last section for differentiation of T*-products.

Lemma 4.

$$\frac{\partial}{\partial x_\mu} \mathrm{T}^* j_\mu(x)\phi(y) = \mathrm{T}^* \frac{\partial j}{\partial x}\phi(y) + \frac{\kappa}{i}\frac{\delta}{\delta\Lambda(x)}\phi'(y)|_{\Lambda=0}. \tag{45}$$

Proof.

From Wick's theorem

$$i\mathrm{T}^* j_\mu(x)\phi(y) = ie : \phi : \frac{\partial}{\partial x_\mu}\Delta^c(x-y) - ie : \chi_\mu : \Delta^c(x-y).$$

Thus

$$\begin{aligned}\frac{\partial}{\partial x_\mu}[i\mathrm{T}^* j_\mu(x)\phi(y)] &= i\mathrm{T}^* \frac{\partial j}{\partial x}\phi(y) + ie : \phi(x) : \left(\frac{\partial}{\partial x_\mu}\frac{\partial}{\partial x_\mu} - \kappa^2\right)\Delta^c \\ &= i\mathrm{T}^* \frac{\partial j}{\partial x}\phi(y) - ie\phi(x)\delta(x-y) \\ &= i\mathrm{T}^* \frac{\partial j}{\partial x}\phi(y) + \kappa\frac{\delta}{\delta\Lambda(x)}\phi'(y)\,|_{\Lambda=0}.\end{aligned}$$

Likewise we have

Lemma 5.

$$\frac{\partial}{\partial x_\mu} \mathrm{T}^* j_\mu(x)\chi_\nu(y) = \mathrm{T}^* \frac{\partial j}{\partial x}\chi_\nu + \frac{\kappa}{i}\frac{\delta}{\delta\Lambda}\chi'_\nu|_{\Lambda=0}, \tag{46}$$

Lemma 6.

$$\frac{\partial}{\partial x_\mu} \mathrm{T}^* j_\mu(x)A(y)B(y) - \mathrm{T}^* \frac{\partial j}{\partial x}A(y)B(y) = \frac{\kappa}{i}\frac{\delta}{\delta\Lambda(x)}\mathrm{T}^* A'(y)B'(y)|_{\Lambda=0}, \tag{47}$$

where A and B are either of the operators χ_ν or ϕ. Using Wick's theorem to write out the left-hand side and the free field equations to display $\partial j/\partial x$ explicitly, a term by term comparison of the two sides proves the result.

Using $\partial j_\mu/\partial x_\mu = 0$, it follows from Lemma 6 that

$$\frac{\partial}{\partial x_\mu} \mathrm{T}^* j_\mu(x)L_2(y) = \frac{\kappa}{i}\frac{\delta}{\delta\Lambda(x)}L_2(\phi')|_{\Lambda=0}, \tag{48}$$

and

$$\frac{\partial}{\partial x_\mu} \mathrm{T}^* j_\mu(x)j_\nu(y) = 0. \tag{49}$$

To prove (49) observe that $j_\mu(\phi', \chi') = j_\mu(\phi, \chi)$.

Lemma 7.

$$\frac{\partial}{\partial 1}\frac{\partial}{\partial 2}\mathrm{T}^* j(1)j(2)L_2(3) = \left(\frac{\kappa}{i}\right)^2\frac{\delta^2}{\delta\Lambda^2}L(\phi')|_{\Lambda=0}. \tag{50}$$

Proof:

From an extension of Lemma 6 we have

$$\frac{\partial}{\partial x_2} \mathrm{T}^* j(1) j(2) L_2(3) = \frac{\kappa}{i} \frac{\delta}{\delta \Lambda(2)} \mathrm{T}^* j(1) L_2(\phi'(3))|_{\Lambda=0}.$$

A second differentiation $\partial/\partial x_1$ proves (50).

Combining eqs. (46) to (50) we finally deduce

Lemma 8.

$$\frac{\partial}{\partial 1} \ldots \frac{\partial}{\partial n} \mathrm{T}^* j(1) \ldots j(n) \exp\left[-\int ijA + \int iL_2(\phi)\right]$$
$$= \left(\frac{\kappa}{i}\right)^n \frac{\delta^n}{\delta \Lambda^n} \mathrm{T}^* \exp\left[\int -ijA + iL_2(\phi')\right]\Big|_{\Lambda=0}. \quad (51)$$

This result is analogous to eq. (36) †. Reasoning in the same manner as in the last section, it is now trivial to complete the proof that the scattering matrix completely equivalent to (39) is indeed given by

$$\mathrm{T}^* \exp i \int \{L_1(\phi, \chi_\mu, A_\mu) + L_2(\phi')\}.$$

5. The Problem of Renormalization

Consider pseudo-vector mesons interacting with nucleons (cf sects. 2 and 3). An S-matrix of the type (38a) clearly gives rise to an infinite variety of distinct primitive divergent graphs in Dyson's sense. This is because the term $\bar{\psi}[\exp(-2i\gamma_5 g\Lambda/\kappa)]\psi$ in the exponent of (38a) means there are graphs in the theory with arbitrary numbers of Λ-lines at each vertex. It is conceivable that one may develop other techniques for removing infinities in such theories but with the techniques hitherto used a consistent removal of all infinities and their absorption in renormalization of a finite number of constants seems impossible.

The author's thanks are due to Drs. P. T. Matthews, S. Kamefuchi, G. Feldman for numerous stimulating discussions.

† Results analogous to eqs. (48) to (51) were proved in the last section for T-products (eqs. (33), (34) and (36)), using the special identity (31) which is valid only for T-products. There is no contradiction with eqs. (48) to (51) in so far as T- and T*-products are identical for the theory dealt with in section 3.

References

1) R. P. Feynman and M. Gell-Mann, Phys. Rev. **109** (1958) 193
2) J. Schwinger, Ann. Phys. **2** (1957) 407;
N. Byers and R. E. Peierls, Nuovo Cim. **10** (1958) 520;
S. L. Glashow, Nuclear Physics **10** (1959) 107;
A. Salam and J. C. Ward, Nuovo Cim. **11** (1959) 568
3) C. N. Yang and R. Mills, Phys. Rev. **96** (1954) 190;
N. Kemmer, Helv. Phys. Acta (in press)
4) R. P. Feynman, M. Gell-Mann and M. Levy, to be published
5) J. Schwinger, Phys. Rev. **91** (1953) 289
6) J. Schwinger, Phys. Rev. Letters **3** (1959) 296

8.B

Nuclear Physics **18** (1960) 691—696; © *North-Holland Publishing Co., Amsterdam*

Not to be reproduced by photoprint or microfilm without written permission from the publisher

ON SALAM'S EQUIVALENCE THEOREM IN VECTOR MESON THEORY

S. KAMEFUCHI †

Imperial College of Science and Technology, London

Received 7 June 1960

Abstract: A simple proof is given of the equivalence theorem discussed in the preceding paper by Salam [1]). Some comments are also made on renormalizability of vector meson fields.

1. Introduction

Until quite recently, vector meson theory has not attracted much attention of physicists, mainly because nature did not seem to require introduction of such particles. However, the interest has been revived recently in connection with the formulation of weak interactions, since the universal V—A interaction theory can most beatifully be formulated by assuming an intermediary vector particle.

It is well known that in most cases vector meson interactions are non-renormalizable. However, Glashow [2]) has recently claimed that they are renormalizable if "partial conservation laws" hold true. In this connection, Salam has given, in the preceding paper, a kind of equivalence theorem, which is most suitable to discuss such a renormalizability problem.

In this paper a different proof of Salam's theorem is given, which appears to be much simpler. All discussion in the following will be done in the interaction representation.

2. A Particular Example

To start with let us discuss a simple example; that is, a neutral pseudo-vector field U_μ (mass κ) in interaction with a spinor field ψ (mass m) via pseudo-vector coupling. Thus, in the interaction representation we have the following Schrödinger equation:

$$i\frac{\delta\Psi[\sigma]}{\delta\sigma(x)} = H(x)\Psi[\sigma], \tag{2.1}$$

† I. C. I. Research Fellow of The University of London. On leave of absence from Institute of Theoretical Physics, Nagoya University, Japan.

with

$$H(x) = -j_\mu U_\mu + \frac{1}{2\kappa^2}(j_\mu n_\mu)^2, \tag{2.1'}$$

where

$$j_\mu(x) = if\bar{\psi}\gamma_5\gamma_\mu\psi.$$

Further we have in that representation the ordinary commutation relations

$$\begin{aligned} \{\psi_\alpha(x),\ \bar{\psi}_\beta(x')\} &= \frac{1}{i} S_{\alpha\beta,\,m}(x-x'), \\ [U_\mu(x),\ U_\nu(x')] &= i\left(\delta_{\mu\nu} - \frac{\partial_\mu\partial_\nu}{\kappa^2}\right)\Delta_\kappa(x-x'). \end{aligned} \tag{2.2}$$

The current operator j_μ satisfies the partial conservation law

$$\partial_\mu j_\mu = -2if m\bar{\psi}\gamma_5\psi, \tag{2.3}$$

which is true also in the Heisenberg representation.

In order to discuss properties of the "longitudinal part" of the U_μ field, which leads to the more singular part $\partial_\mu\partial_\nu/\kappa^2$ in (2.2) and so eventually to non-renormalizable divergences, it is most convenient to work with the Stueckelberg formalism [3]). Thus, we may split U_μ into two parts A_μ and B as follows:

$$U_\mu(x) = A_\mu(x) + \frac{1}{\kappa}\partial_\mu B(x); \tag{2.4}$$

A_μ and B satisfy the Klein-Gordon equation $(\Box-\kappa^2)A_\mu = (\Box-\kappa^2)B = 0$, and thus have the following commutation relations:

$$\begin{aligned} [A_\mu(x),\ A_\nu(x')] &= i\delta_{\mu\nu}\Delta_\kappa(x-x'), \\ [B(x),\ \ B(x')] &= i\Delta_\kappa(x-x'). \end{aligned} \tag{2.5}$$

We have also to impose a subsidiary condition on the state vector †

$$\mathscr{R}(x)\Psi[\sigma] \equiv (\partial_\mu A_\mu(x) + \kappa B(x))\Psi[\sigma] = 0. \tag{2.6}$$

We can easily check that (2.1') satisfies the integrability condition and also that the equations (2.6) are consistent with each other and also with the Schrödinger equation (2.1). For putting

$$I(x) \equiv i\frac{\delta}{\delta\sigma(x)} - H(x),$$

we can show that $[I(x),\ I(x')] = 0$ for $x \approx x'$ and $[I(x),\ R(x')] = 0$, $[R(x),\ R(x')] = 0$ for all x and x'.

† It is to be remarked that the subsidiary condition is consistent with the equation of motion, regardless of whether the current with which the field is coupled is conserved.

It is now evident from (2.4) and (2.5) that the B-field is solely responsible for the non-renormalizable divergences. In order to separate the contribution of the B-field, we have only to carry out the following unitary transformation:

$$\Psi[\sigma] \to \Psi'[\sigma] = \exp\left[-\frac{i}{\kappa}\int_\sigma d\sigma_\mu j_\mu(x)B(x)\right]\Psi[\sigma]. \tag{2.7}$$

After a straightforward calculation we can show that in the new representation the Schrödinger equation takes the form

$$i\frac{\delta\Psi'[\sigma]}{\delta\sigma(x)} = H'(x)\Psi'[\sigma], \tag{2.8}$$

with the Hamiltonian

$$H'(x) = -j_\mu A_\mu + m\bar{\psi}(e^{-\frac{2if}{\kappa}\gamma_5 B}-1)\psi, \tag{2.8'}$$

and that the subsidiary condition is transformed into

$$\left\{\partial_\mu A_\mu(x)+\kappa B(x)+\int_\sigma \Delta_\kappa(x-x')j'_\mu d\sigma'_\mu\right\}\Psi'[\sigma] = 0. \tag{2.9}$$

The above interaction (2.8') is precisely the one obtained by Salam.

3. A More General Consideration

In this section we shall show that the result obtained in the preceding section is a consequence of a more general property of the vector meson theory. To this end let us consider the general case of interaction of the neutral vector field U_μ with an arbitrary complex field ϕ_α with spin 0, $\frac{1}{2}$, or 1. If the interaction is introduced by the gauge invariant replacement $\partial_\mu \to \partial_\mu - if U_\mu$, the most general interaction Hamiltonian in the interaction representation is of the following form:

$$H(x) = -fj_\mu(x)U_\mu - \tfrac{1}{2}f^2 j_{\mu\nu}(x, n_\lambda)U_\mu U_\nu + \frac{1}{2\kappa^2}f^2(j_\mu n_\mu)^2. \tag{3.1}$$

Here, it is to be stressed that the current operators j_μ and $j_{\mu\nu}$ are exactly identical with the corresponding quantities in the case of the electromagnetic interaction. Thus, if we omit the last term in (3.1) and replace U_μ by the electromagnetic potential, (3.1) becomes the interaction Hamiltonian in electrodynamics. The current conservation is expressed, in the interaction representation, by the following relations [4]):

$$\begin{aligned}
&\partial_\mu j_\mu = 0, \quad j_{\mu\nu}n_\nu = 0, \\
&n_\mu[j_\mu(x), j_\nu(x')] = in_\mu\partial_\rho(j_{\rho\nu}(x, n)\partial_\mu\Delta_\kappa(x-x')), \\
&n_\mu n_\nu[j_\mu(x), j_\nu(x')] = 0, \quad n_\mu[j_\mu(x), j_{\rho\nu}(x', n')] = 0.
\end{aligned} \tag{3.2}$$

Now, in the Stueckelberg formalism of this interaction there is an important theorem, which is originally due to Glauber [5]) and Umezawa [4]). It states that the unitary transformation

$$U[\sigma] = \exp\left[-\frac{if}{\kappa}\int_{\sigma} d\sigma_{\mu} j_{\mu} B\right] \tag{3.3}$$

transforms the Schrödinger equation with the Hamiltonian (3.1) into that with the new Hamiltonian

$$H'(x) = -f j_{\mu} A_{\mu} - \tfrac{1}{2} f^2 j_{\mu\nu} A_{\mu} A_{\nu}, \tag{3.4}$$

where A_{μ} and B are defined by (2.4), and also that the transformed subsidiary condition takes the same form as (2.9) above. All that is necessary in the course of proof are the general relations given by (3.2).

Now, we can generalize this theorem in the following way: Suppose that the free Hamiltonian is gauge invariant and further that in the interaction Hamiltonian there is a term which consists only of the source field variable ϕ_{α} and which may or may not violate this gauge invariance. Then our interaction Hamiltonian in this case is written in the form

$$\mathscr{H}(x) = H(x) + h(\phi_{\alpha}(x), n_{\lambda}), \tag{3.5}$$

where the gauge invariant part $H(x)$ is the same as (3.1) and the second part h, which may or may not be gauge invariant, is to be understood to be containing the normal dependent terms which are required when introducing this new interaction term. For simplicity, let us assume that h does not contain any derivative of field operators (for a field with spin 0, $\frac{1}{2}$, the normal dependent term is unnecessary in h).

Now, we notice that the transformation (3.3) is a gauge transformation and therefore, the source field variables are transformed according to †

$$\phi_{\alpha} \to \phi'_{\alpha} = U\phi_{\alpha}U^{-1} = \exp\left(-\frac{i}{\kappa} f B(x)\right)\phi_{\alpha}(x). \tag{3.6}$$

Therefore, as an immediate generalization of the Glauber-Umezawa theorem we arrive at the following theorem: The system described by the interaction Hamiltonian (3.5) is equivalent to that described by another Hamiltonian

$$\mathscr{H}'(x) = H'(x) + h(\phi'_{\alpha}(x), n_{\lambda}), \tag{3.7}$$

where $H'(x)$ is given by (3.4) and the ϕ'_{α}'s are quantities defined by (3.6). This is precisely the content of Salam's equivalence theorem. The relations (3.2) give the sufficient conditions for the validity of this theorem.

† For a spin 1 field ϕ_{α}, independent variables only are transformed in the above manner.

It can easily be seen that the example we have discussed in section 2 is also covered by our general theorem: The mass term $m\bar{\psi}\psi$ violates the invariance of the free Hamiltonian under the "gauge transformation" (2.7). Thus in order to apply our theorem we have to move this term into the interaction Hamiltonian and regard it as h. Since under the gauge transformation ψ is transformed into

$$\psi' = \exp\left(-\frac{i}{\kappa} f\gamma_5 B\right)\psi,$$

$\mathscr{H}'$ is of the form

$$\mathscr{H}'(x) = -j_\mu A_\mu + m\bar{\psi} e^{-\frac{2if}{\kappa}\gamma_5 B}\psi.$$

If we move the mass term back to the free Hamiltonian by another unitary transformation we are then led to the expression (2.8′).

4. Discussion

Finally we shall briefly discuss the renormalizability problem of the vector meson field. As is evident from our theorem, the B-field, which is the direct cause of non-renormalizability, can be completely eliminated only when h is gauge invariant. Thus, we can conclude that the theory is renormalizable only when it is gauge invariant, or, in other words, only when there is a conservation law, which is due to this invariance.

To see this more closely let us consider the example in section 2. It is at once evident that when expanded in powers of f the second term in (2.8′) leads to non-renormalizable interactions. Thus, our result is quite contrary to Glashow's statement that with partial conservation the theory is renormalizable.

The question, however, arises whether the singularity of non-renormalizable divergences can be improved when we do not expand the exponential term $\varphi \equiv \exp[-2if\gamma_5 B/\kappa]$ and treat φ as if it were a new field quantity [6]). Thus, instead of the ordinary Δ_F-function we may use something like $\Delta'_F(x-x') = \langle P(\varphi(x), \varphi(x'))\rangle_0 \propto \exp[-4f^2\Delta_F(x-x')/\kappa^2]$. However, it can immediately be seen that this function has an essential singularity near the light cone like $\exp[-f^2/\pi^2\kappa^2(x_\lambda - x'_\lambda)^2]$, which certainly gives rise to a much worse divergence than the ordinary Δ_F-function. This means that even with such a technique the theory is still non-renormalizable. Probably, Feynman's path integral method, as discussed by Arnowitt and Deser [7]), might be applicable to the above type of interaction. At the present moment, however, not much is known to what extent such a method is effective.

I would like to thank Professor A. Salam for showing me his work prior to publication.

References

1) A. Salam, Nuclear Physics **18** (1960) 681
2) S. L. Glashow, Nuclear Physics **10** (1959) 107
3) E. C. G. Stueckelberg, Helv. Phys. Acta **11** (1938) 299
4) H. Umezawa, Prog. Theor. Phys. **7** (1952) 551; Quantum field theory (North-Holland Publishing Company, Amsterdam, 1956) p. 204;
S. Kamefuchi and H. Umezawa, Prog. Theor. Phys. **8** (1952) 579
5) R. J. Glauber, Prog. Theor. Phys. **9** (1953) 295
6) R. J. Glauber, Phys. Rev. **84** (1951) 397;
S. Okubo, Prog. Theor. Phys. **11** (1954) 80
7) R. Arnowitt and S. Deser, Phys. Rev. **100** (1955) 349

1.D.4

Nuclear Physics **18** (1960) 697—712; © *North-Holland Publishing Co., Amsterdam*

Not to be reproduced by photoprint or microfilm without written permission from the publisher

GROUP THEORY OF HARMONIC OSCILLATORS
(I). The Collective Modes

V. BARGMANN and M. MOSHINSKY †

Palmer Physical Laboratory, Princeton University, Princeton, N.J.

Received 7 May 1960

Abstract: The present series of papers will deal with the classification of states of N particles moving in a harmonic oscillator common potential. In this paper we will be mainly concerned with the classification scheme that brings out a collective nature of the states. To obtain this collective behaviour, we take advantage of the invariance of the hamiltonian under both ordinary rotations and the unitary group in N dimensions.

1. Introduction and Summary

The purpose of the present series of papers is the classification of the states of N particles, when these particles move in a harmonic oscillator potential. The main advantage of using a harmonic oscillator, instead of an arbitrary common potential for the particles, stems from the fact that in the former case the hamiltonian is invariant under the rotation group and under the unitary group in N dimensions [1]), while in the latter it is only invariant under the rotation group and the permutation group of the N particles. As the permutation group of N objects is a subgroup of the unitary group in N dimensions, we can hope that the extra symmetry introduced when we take a harmonic oscillator as a common potential for the particles will greatly simplify the task of classifying the states.

In this paper we shall be mainly concerned with the classification scheme that brings out a collective nature of the states. These collective states will diagonalize the quadrupole-quadrupole interaction between particles proposed by Moszkowski [2]), an interaction that he obtained in a plausible way from the two-body potential between the particles. In the present paper, we shall obtain the rotational bands associated with the quadrupole-quadrupole interaction, while in following papers the explicit expression of the wave functions will be given, as well as the relations between the wave functions in different representations.

The present approach to the problem differs from the analysis of Elliot [3]) in emphasizing the classification with respect to the N-dimensional unitary

† Alfred P. Sloan Research Fellow on leave of absence from the Instituto de Física, Universidad de México and Instituto Nacional de la Investigación Científica, México, D.F.

group U_N, associated with the number N of particles, rather than with the unitary group U_s associated with the order s of degeneracy of the wave functions in a given shell. While the conceptions of group theory underly all the present developments, the discussion in this paper will be carried out entirely in terms of elementary algebraic procedures.

The material of the paper is arranged in the following form. In section 2 we rewrite the hamiltonian in terms of creation and annihilation operators and express the single particle wave function in terms of these operators acting on the ground state. In section 3 we deal with the problem of two particles in a harmonic oscillator potential, where the invariance with respect to the two-dimensional unitary unimodular group, (the condition of unimodularity implies no loss of generality) leads to the introduction of a new integral of motion which we call pseudo-spin. The possible values of the pseudo-spin for two-particle states of definite total energy and angular momentum are discussed. In section 4 the two-particle problem is rephrased in such a way as to permit its generalization to N particles, and in the process the pseudo-spin operator becomes the Casimir operator [4]) for the N-dimensional unitary group. In section 5 the eigenvalues of the Casimir operator are obtained with the help of the transfer operators, i.e. operators that, while commuting with the Casimir operator, transfer one unit of energy from one particle to another. In section 6 the Casimir operator is decomposed in terms of the quadrupole-quadrupole interaction, plus the square of the total angular momentum and of the hamiltonian. Finally, in section 7 the rotational bands are obtained and discussed.

2. Creation and Annihilation Operators and the One-Particle States

The hamiltonian for a system of N particles moving in a harmonic oscillator potential can be written as

$$H = \tfrac{1}{2} \sum_{s=1}^{N} \sum_{i=1}^{3} (p_{is}^2 + x_{is}^2); \tag{1}$$

here we have taken units such that $\hbar = m = \omega = 1$, when m denotes the mass of the particle, and ω the frequency of the oscillator. Indices i, j, k will be used to indicate the vector component and will run from 1 to 3, while indices such as r, s, t will indicate the particle and will run from 1 to N.

We now introduce the creation and annihilation operators by the usual definitions

$$\eta_{is} = \frac{1}{\sqrt{2}} (x_{is} - ip_{is}), \quad \xi_{is} = \eta_{is}^{\dagger} = \frac{1}{\sqrt{2}} (x_{is} + ip_{is}). \tag{2}$$

From the commutation relations between x and p, we see that

$$[\xi_{is}, \xi_{jr}] = [\eta_{is}, \eta_{jr}] = 0, \quad [\xi_{is}, \eta_{jr}] = \delta_{ij}\delta_{rs}, \tag{3}$$

so, that except for an irrelevant constant, the hamiltonian becomes

$$H = \sum_{s=1}^{N} \sum_{i=1}^{3} \eta_{is} \eta_{is}^{\dagger} = \sum_{s=1}^{N} \eta_s \cdot \xi_s \tag{4}$$

Clearly the hamiltonian (4) is invariant under the three-dimensional rotation group, and under the N-dimensional unitary transformation that affects each component of the vector η_s in the same way, i.e. under

$$\eta_{is} = \sum_{s'=1}^{N} U_{ss'} \eta'_{is'}, \tag{5}$$

where $U_{ss'}$ is a unitary matrix.

As is well known, all eigenfunctions of H may be obtained by applying products of the η_{is} to the ground state

$$|0\rangle = \pi^{-\frac{3}{4}N} \exp[-\tfrac{1}{2}(r_1^2 + r_2^2 + \ldots + r_N^2)]. \tag{6}$$

Specifically, all eigenfunctions for the energy E (where E is any non-negative integer), are linear combinations with constant coefficients of the expressions

$$\eta_{11}^{m_{11}} \eta_{21}^{m_{21}} \eta_{31}^{m_{31}} \ldots \eta_{1N}^{m_{1N}} \eta_{2N}^{m_{2N}} \eta_{3N}^{m_{3N}} |0\rangle, \tag{7a}$$

provided the sum of the exponents equals E. They may therefore be written in the form

$$P(\eta_{11}, \ldots, \eta_{3N})|0\rangle, \tag{7b}$$

where P is a homogeneous polynomial of order E. There exists therefore a one-to-one correspondence between the eigenfunctions of energy E and the homogeneous polynomials of order E, so that the polynomials may even replace the eigenfunctions.

Our treatment depends heavily on this correspondence. Thus by the action of the unitary transformation (5), the polynomial P is changed into a polynomial P' defined by

$$P'(\eta') = P(U\eta'), \tag{8}$$

in abbreviated notation.

Furthermore, in view of the commutation rules (3), for every polynomial P,

$$\xi_{is} P|0\rangle = R|0\rangle, \tag{9a}$$

where R is the polynomial $(\partial P/\partial \eta_{is})$ (as is easily verified using the fact that $\xi_{is}|0\rangle = 0$). Working with the polynomials P we may therefore set

$$\xi_{is} = \frac{\partial}{\partial \eta_{is}}. \tag{9b}$$

Consider for the moment a single particle. From (2) its hamiltonian H and

angular momentum $\mathbf{l}$ are given respectively by

$$H = \boldsymbol{\eta} \cdot \boldsymbol{\xi}, \quad \mathbf{l} = -i(\boldsymbol{\eta} \times \boldsymbol{\xi}). \tag{10}$$

Because of (9b), the eigenfunctions of energy $2n+l$ and angular momentum l with projection m, can be written as

$$|nlm\rangle = A_{nl}\eta^{2n}\mathscr{Y}_{lm}(\boldsymbol{\eta})|0\rangle, \tag{11a}$$

where A_{nl} is a normalization coeffieient, $\mathscr{Y}_{lm}$ is a normalized solid spherical harmonic [5]) in the operator $\boldsymbol{\eta}$, and $\eta^2 = \sum_{k=1}^{3}\eta_k^2$. For the coordinate $\mathbf{r}$ a solid spherical harmonic is defined

$$\mathscr{Y}_{lm}(\mathbf{r}) = r^l Y_{lm}(\theta, \varphi). \tag{11b}$$

The normalization coefficient A_{nl} can be obtained by using recurrence relations, (for example by applying η_3 to both sides of (11a) and comparing with the normalization coefficients of Laguerre polynomials) and so we get

$$A_{nl} = (-1)^n\left[\frac{4\pi}{(2n+2l+1)!!(2n)!!}\right]^{\frac{1}{2}}. \tag{11c}$$

3. The Two-Particle States

When we have one particle in a harmonic oscillator potential and specify its energy and angular momentum, the wave function for the particle is completely defined and in fact, given by (11a). For a system of two particles, this is no longer true, as wave functions with the same total energy and total angular momentum can be constructed in a variety of ways. The usual procedure for constructing the wave functions is to specify the energy and angular momentum of each particle, and to couple these angular momenta to a total angular momentum λ, i.e. the wave function is given by

$$|n_1l_1, n_2l_2, \lambda\mu\rangle = \sum_{m_1m_2}\{\langle l_1l_2m_1m_2|\lambda\mu\rangle A_{n_1l_1}\eta_1^{2n_1}\mathscr{Y}_{l_1m_1}(\boldsymbol{\eta}_1)A_{n_2l_2}\eta_2^{2n_2}\mathscr{Y}_{l_2m_2}(\boldsymbol{\eta}_2)\}|0\rangle, \tag{12}$$

where $|0\rangle$ represents now two particles in the ground state, $\langle l_1l_2m_1m_2|\lambda\mu\rangle$ is a Clebsch-Gordan coefficient, and $A_{n_1l_1}$, $A_{n_2l_2}$ are given by (11c).

Clearly the wave function (12) represents a state with total energy ρ given by

$$\rho = 2n_1+l_1+2n_2+l_2, \tag{13}$$

and total angular momentum λ that is between the limits

$$|l_1-l_2| \leqq \lambda \leqq l_1+l_2. \tag{14}$$

For a given ρ, λ, μ any set of non-negative integers n_1, l_1, n_2, l_2 that satisfy (13) and (14), will define a state. The number of states was shown by Brody [6]) to be

$$\begin{cases} \frac{1}{8}(\lambda+1)(\rho-\lambda+2)(\rho-\lambda+4), & \text{if } \rho-\lambda \text{ even}, \\ \frac{1}{8}\lambda(\rho-\lambda+1)(\rho-\lambda+3), & \text{if } \rho-\lambda \text{ odd}. \end{cases} \tag{15}$$

In general, we have quite a large degree of degeneracy if only ρ and λ are specified.

We would like to break up this degeneracy, by taking advantage of the invariance of the hamiltonian for two particles in a harmonic oscillator common potential under the two-dimensional unitary group. We could, without loss of generality, restrict ourselves to the two-dimensional unitary unimodular group, which is essentially isomorphic to the three-dimensional rotation group [7]). This immediately suggests that additional integrals of motion with the commutation rules of angular momentum can be found. To obtain these integrals of motion we first notice that we now have the creation and annihilation vector operators for two particles

$$\eta_1, \eta_2 \quad \text{and} \quad \xi_1, \xi_2, \tag{16}$$

and can construct combinations of these operators that commute with the total hamiltonian

$$H = \eta_1 \cdot \xi_1 + \eta_2 \cdot \xi_2, \tag{17}$$

and the total angular momentum

$$\boldsymbol{\lambda} = -i(\eta_1 \times \xi_1 + \eta_2 \times \xi_2). \tag{18}$$

To commute with H the combination must contain creation and annihilation operators in equal numbers, while to commute with $\boldsymbol{\lambda}$ the combination must be invariant under space rotations, i.e. must be scalar. We see then that the only bilinear combinations we can build from (16) are

$$\eta_1 \cdot \xi_1, \ \eta_1 \cdot \xi_2, \ \eta_2 \cdot \xi_1, \ \eta_2 \cdot \xi_2. \tag{19}$$

Using the commutation rules (3), we could check directly that the combinations (19) commute with H and $\boldsymbol{\lambda}$.

Of the four operators (19), one linear combination is the hamiltonian (17), and we are therefore left with three linearly independent operators which we could arrange in the form [8])

$$F_1 = \tfrac{1}{2}(\eta_1 \cdot \xi_2 + \eta_2 \cdot \xi_1), \tag{20a}$$

$$F_2 = -\tfrac{i}{2}(\eta_1 \cdot \xi_2 - \eta_2 \cdot \xi_1), \tag{20b}$$

$$F_3 = \tfrac{1}{2}(\eta_1 \cdot \xi_1 - \eta_2 \cdot \xi_2). \tag{20c}$$

From the commutation relations (3), it is immediately seen that

$$[F_1, F_2] = iF_3, \text{ etc.}, \tag{21}$$

so that the F_i's have the commutation relations of angular momentum, and fo that reason we shall denote them as the components of a pseudo-spin vector.

As the F_i's do not commute with each other, we can choose

$$\mathbf{F}^2 = F_1^2 + F_2^2 + F_3^2, \tag{22}$$

and F_3 as the additional integrals of motion. The eigenvalues of $\mathbf{F}^2$ will be denoted by $f(f+1)$ where f is, of course, an integer or half integer. The eigenvalues of F_3 will be denoted by ν, where $\nu = f, f-1, \ldots, -f$.

What are the possible values f of the pseudo-spin for a given value of ρ and λ? A simple way to find them would be to write all sets of n_1, l_1, n_2, l_2 consistent with (13) and (14), and to compute for each set the eigenvalue ν of F_3 which, from (20c), is

$$\nu = \tfrac{1}{2}[(2n_1+l_1)-(2n_2+l_2)]. \tag{23}$$

As an example, let us consider the case when $\rho = 4$, $\lambda = 0$. From (14) we have then $l_1 = l_2$, and from (13) we obtain

$$2(n_1+n_2+l_2) = 4. \tag{24}$$

TABLE 1

Eigenvalues of the F_3 component of the pseudo-spin for $\rho = 4$, $\lambda = 0$.

n_2	l_2	n_1	l_1	ν
0	0	2	0	2
0	1	1	1	1
1	0	1	0	0
0	2	0	2	0
1	1	0	1	−1
2	0	0	0	−2

We need therefore all the sets of integers n_1, n_2, l_2 whose sum is two and these are given in table 1. In the last column of the table, the corresponding values of ν are given. We clearly see that these values of ν correspond to two possibilities for the values of f,

$$f = 2 \quad \text{or} \quad f = 0. \tag{25}$$

As $\nu = f, f-1, \ldots -f$ we see from (23) and (13) that

$$0 \leqq 2f \leqq \rho. \tag{26}$$

Furthermore, f will be an integer if ρ is even, a semi-integer if ρ is odd.

For arbitrary ρ and λ the construction of tables similar to table 1 is more bothersome. Fortunately, for ρ, λ up to 12, these tables were obtained by Brody[6]) in the process of tabulating the transformation brackets for harmonic oscillator functions defined by Moshinsky [9]). A more compact procedure for correlating values of ρ, λ and f will be given in the second paper of this series.

In the example discussed in table 1, each possible value of f appears only once, and a classification in terms of pseudo-spin and its projection will therefore break down the degeneracy completely. For larger values of ρ and λ this is not, in general, the case. For example, for $\rho = 6$, $\lambda = 2$ the possible values of f are $f = 3,2,(1)^2$, i.e. the value $f = 1$ appears twice. Therefore, for the classification

of two particle states we shall need, in general, another integral of motion Ω that commutes with the hamiltonian, the angular momentum and the pseudo-spin. As this integral of motion is not relevant to the purpose of the present paper, we postpone its discussion to the second paper of this series.

The preceding discussion shows that states for two particles in a harmonic oscillator potential can be viewed in two ways. In one of them we emphasize the particles' individuality by diagonalizing the energy and angular momentum of each particle, and then coupling the angular momenta to a definite value λ. In the other, we diagonalize the total energy and angular momentum of the system plus the integrals of motion $\mathbf{F}^2$, F_3 and Ω. We shall show in the following sections that the second viewpoint emphasizes the collective character of the state.

4. The N-Particle States

When we are dealing with a state for N particles in a harmonic oscillator potential, we could start with the wave functions of the individual particles and couple their angular momenta to a definite angular momentum λ. But in this way we of course emphasize the individual particle character of the state. To find integrals of motion similar to the pseudo-spin of the previous section, we can make use of the invariance of the hamiltonian under the N-dimensional unitary group. The procedure to be followed is based on Cartan's classical method (see for example Racah [10]), but to make this procedure more accessible, we first return to the two-particle problem and rephrase it in such a way as to be able to generalize it to the N-particle case.

In the previous section we showed that it would be possible to find two-particle wave functions ψ that are simultaneously eigenfunctions of H, $\boldsymbol{\lambda}^2$, λ_3, $\mathbf{F}^2$, F_3, with eigenvalues

$$\boldsymbol{\lambda}^2\psi = \lambda(\lambda+1)\psi, \quad \lambda_3\psi = \mu\psi \tag{27a}$$

$$H\psi = \rho\psi, \quad \mathbf{F}^2\psi = f(f+1)\psi, \quad F_3\psi = \nu\psi. \tag{27b}$$

From the definition (17) and (20c) of H and F_3, we see that we can combine the first and last equations of (27b) to give

$$(\boldsymbol{\eta}_1 \cdot \boldsymbol{\xi}_1)\psi = (\tfrac{1}{2}\rho+\nu)\psi, \quad (\boldsymbol{\eta}_2 \cdot \boldsymbol{\xi}_2)\psi = (\tfrac{1}{2}\rho-\nu)\psi. \tag{28}$$

Furthermore, from the expression (22, 20) of the operator $\mathbf{F}^2$ we see that we can combine it with H^2 to give the operator

$$G\psi \equiv (2\mathbf{F}^2+\tfrac{1}{2}H^2)\psi = \sum_{r,s=1}^{2} [(\boldsymbol{\eta}_r \cdot \boldsymbol{\xi}_s)(\boldsymbol{\eta}_s \cdot \boldsymbol{\xi}_r)]\psi = [2f(f+1)+\tfrac{1}{2}\rho^2]\psi. \tag{29}$$

Clearly, instead of the ψ being defined as the eigenfunction of the operators (27b), it could be defined as the eigenfunction of $\boldsymbol{\eta}_s \cdot \boldsymbol{\xi}_s (s = 1, 2)$ and of the G of (29). This latter formulation is particularly convenient as the equations are

symmetrical in the indices of the particles. The operator G will be referred to as Casimir operator [4, 10]) for the two-dimensional unitary group †, and it obviously commutes with all $\eta_r \cdot \xi_s (r, s = 1, 2)$ as it commutes with F_i and H.

For the N-particle state, we could generalize (28, 29) by looking for a wave function ψ that besides being an eigenfunction of the total angular momentum λ as in (27a), would be an eigenfunction of the following operators

$$\eta_s \cdot \xi_s \psi = h_s \psi, \quad s = 1, 2, \ldots N, \tag{30}$$

$$G\psi = \sum_{r,s=1}^{N} [(\eta_r \cdot \xi_s)(\eta_s \cdot \xi_r)]\psi = g\psi. \tag{31}$$

Clearly this would not be a complete set of operators, as even in the two-particle case, one needs more integrals of motion. For the purpose of the present paper though, these other integrals of motion are not relevant, so we postpone their discussion to the following papers.

As ψ is an eigenfunction of the operators $\eta_s \cdot \xi_s$ we see from (9b) that it is a sum of products of homogeneous polynomials of degree h_s in $\eta_{1s}, \eta_{2s}, \eta_{3s}$ acting on the ground state for N particles. The degree of the homogeneous polynomial $P(\eta_{11}, \ldots, \eta_{3N})$ of (7b), i.e. the total energy E of the state, is given by

$$E = h_1 + h_2 + \ldots + h_N. \tag{32}$$

An important purpose in the present discussion will be to establish relations between E, g and the total angular momentum λ, in the same way as we obtained in the previous section, relations between ρ, f and λ. To establish these relations we first remark that from (3), we obtain the commutation relations

$$[\eta_r \cdot \xi_s, \eta_{r'} \cdot \xi_{s'}] = \eta_r \cdot \xi_{s'} \delta_{sr'} - \eta_{r'} \cdot \xi_s \delta_{rs'}. \tag{33}$$

If we apply $\eta_r \cdot \xi_s$ to a wave function ψ that satisfies (30), we see from (33) that

$$(\eta_t \cdot \xi_t)[(\eta_r \cdot \xi_s)\psi] = (h_t + \delta_{rt} - \delta_{st})[(\eta_r \cdot \xi_s)\psi]. \tag{34}$$

Clearly, the operator $\eta_r \cdot \xi_s (r \neq s)$ transfers one unit of energy from particle s to particle r, or equivalently, diminishes by one unit the degree of the homogeneous polynomial in $\eta_{1s}, \eta_{2s}, \eta_{3s}$ present in ψ while increasing by one unit the degree of the homogeneous polynomial in $\eta_{1r}, \eta_{2r}, \eta_{3r}$. For this reason we shall call $\eta_r \cdot \xi_s (r \neq s)$ a transfer operator. The transfer operator obviously commutes with the total hamiltonian (4). It commutes with the total angular momentum λ as it is a scalar. It also commutes with the operator G of (31), which will be referred to as the Casimir operator [4, 10]) for the N-dimensional unitary group, as can be seen directly by using (33).

† Actually the Casimir operator [4, 10]) is defined only for semi-simple groups such as, for example, the N-dimensional unitary unimodular group. For the two-dimensional unitary unimodular group, the Casimir operator is F^2. We have kept the same name for G because of its close connection with F^2.

In the next section we shall use the transfer operators to reduce the N-particle state to essentially a two-particle state.

5. The Transfer Operators and the Eigenvalues of the Casimir Operator

If we apply transfer operators $\eta_r \cdot \xi_s (r \neq s)$ to the wave function ψ that satisfies (27a, 30, 31), we obtain a new wave function with the same eigenvalues E, g, λ, μ but with different eigenvalues h_s. We would like to use the transfer operators to move as much of the energy as possible to particles of lower index, i.e. increase $h_1, h_2 \ldots$, at the expense of $h_N, h_{N-1}, \ldots$. In this way we could hope to reduce the state ψ to an essentially equivalent state with a smaller number of particles outside the ground state. We cannot apply indefinitely transfer operators to the wave function ψ. For example, if we apply $(\eta_r \cdot \xi_s)^{h_s+1}$ to ψ we get zero, as we are transferring more energy out of particle s, than this particle had originally. The transfer operations will end at the moment when, for $r < s$, we cannot transfer more energy from particle s to particle r, without the wave function vanishing. Equivalently, no more transfers can be carried out if a state ψ satisfies

$$(\eta_r \cdot \xi_s)\psi = 0, \quad \text{for all } r < s. \tag{35}$$

With the help of the transfer operators we can pass from a wave function ψ to a canonical wave function ψ_C which, besides (27a), satisfies

$$G\psi_C = g\psi_C, \quad (\eta_s \cdot \xi_s)\psi_C = h'_s\psi_C, \quad (\eta_r \cdot \xi_s)\psi_C = 0, \quad \text{for all } r < s. \tag{36}$$

With the help of the commutation relations (33), the Casimir operator G can be written as

$$\begin{aligned} G &= \sum_{r=1}^{N} (\eta_r \cdot \xi_r)^2 + \sum_{r<s} [\eta_r \cdot \xi_s, \eta_s \cdot \xi_r] + 2 \sum_{r<s} (\eta_s \cdot \xi_r)(\eta_r \cdot \xi_s) \\ &= \sum_{r=1}^{N} (\eta_r \cdot \xi_r)^2 + \sum_{r<s} (\eta_r \cdot \xi_r - \eta_s \cdot \xi_s) + 2 \sum_{r<s} (\eta_s \cdot \xi_r)(\eta_r \cdot \xi_s), \end{aligned} \tag{37}$$

so that from (36) we have

$$G\psi_C = [\sum_{r=1}^{N} h'^2_r + \sum_{r<s} (h'_r - h'_s)]\psi_C \tag{38}$$

or

$$g = \sum_{r=1}^{N} h'^2_r + (N-1)h'_1 + (N-3)h'_2 + (N-5)h'_3 + \ldots + (-N+1)h'_N. \tag{39}$$

There is therefore, a simple relation between the eigenvalues of the Casimir operator, and the h'_s for the canonical wave function ψ_C.

The next question is to determine the possible values of h'_s for ψ_C. We set

$$\psi_C = P(\eta_1, \ldots, \eta_N)|0\rangle, \tag{40}$$

and work with the polynomial P. In view of the relation (9b), we may rewrite the equations (36) in the form

$$\eta_s \cdot (\partial P/\partial \eta_s) = \sum_{i=1}^{3} \eta_{is}(\partial P/\partial \eta_{is}) = h'_s P, \tag{41}$$

$$\eta_r \cdot (\partial P/\partial \eta_s) = 0, \quad r < s. \tag{42}$$

The equation (41) implies that P is homogeneous of order h'_s in the components of η_s. Consequently, all h'_s are nonnegative integers. If $N \geqq 4$, consider first (42) for $s \geqq 4$ and $r = 1, 2, 3$. We obtain

$$\eta_1 \cdot (\partial P/\partial \eta_s) = 0, \quad \eta_2 \cdot (\partial P/\partial \eta_s) = 0, \quad \eta_3 \cdot (\partial P/\partial \eta_s) = 0, \tag{43}$$

i.e. three homogeneous equations for the partial derivatives $(\partial P/\partial \eta_{is})$, $i = 1, 2, 3$, $s \geqq 4$, with determinant

$$\Delta = (\eta_1 \times \eta_2) \cdot \eta_3. \tag{44}$$

It follows that

$$(\partial P/\partial \eta_{is}) = 0 \quad (i = 1, 2, 3;\ s \geqq 4), \tag{45}$$

since the determinant is a polynomial that does not vanish identically. Therefore, P depends only on η_1, η_2, η_3. As a consequence, $h'_s = 0$ for $s \geqq 4$, and the total energy has the value

$$E = h'_1 + h'_2 + h'_3. \tag{46}$$

For $s = 3$, we find from (41) and (42) the three equations

$$\eta_1 \cdot (\partial P/\partial \eta_3) = 0, \quad \eta_2 \cdot (\partial P/\partial \eta_3) = 0, \quad \eta_3 \cdot (\partial P/\partial \eta_3) = h'_3 P. \tag{47}$$

The same equations are satisfied by the polynomial $\Delta^{h'_3}$ as is easily verified. Introducing the rational function

$$R(\eta_1, \eta_2, \eta_3) = \Delta^{-h'_3} P(\eta_1, \eta_2, \eta_3) \tag{48}$$

we find therefore

$$\eta_r \cdot (\partial R/\partial \eta_3) = 0, \quad r = 1, 2, 3. \tag{49}$$

By (49), R is a function only of η_1 and η_2 and may be written as

$$R(\eta_1, \eta_2) = u(\eta_1, \eta_2)/v(\eta_1, \eta_2), \tag{50}$$

where u and v are two polynomials with no common factor. Hence

$$P(\eta_1, \eta_2, \eta_3) = \Delta^{h'_3} u(\eta_1, \eta_2)/v(\eta_1, \eta_2). \tag{51}$$

We use now the well known algebraic fact that the determinant is not divisible by any polynomial (except a constant), and conclude that v is a constant since

it is relatively prime to both factors of the numerator of eq. (51). Absorbing this constant in u, we obtain $R = u$ and †

$$P(\eta_1, \eta_2, \eta_3) = [(\eta_1 \times \eta_2) \cdot \eta_3]^{N_3} u(\eta_1, \eta_2). \tag{52}$$

We now define the reduced canonical wave function as

$$\psi_{RC} \equiv u(\eta_1, \eta_2)|0\rangle. \tag{53}$$

From (40) and (52), the canonical wave function ψ_C then becomes

$$\psi_C = \Delta^{N_3} \psi_{RC}. \tag{54}$$

As the determinant Δ is a scalar, it commutes with the operator of total angular momentum $\boldsymbol{\lambda}$, so that the reduced canonical wave function has the same angular momentum as the original wave function ψ, i.e. it satisfies (27a). Furthermore, from (36) and (54), we see that ψ_{RC} satisfies

$$(\eta_1 \cdot \tfrac{\xi}{S_1})\psi_{RC} = (h'_1 - h'_3)\psi_{RC}, \quad (\eta_2 \cdot \tfrac{\xi}{S_2})\psi_{RC} = (h'_2 - h'_3)\psi_{RC}, \quad (\eta_1 \cdot \tfrac{\xi}{S_2})\psi_{RC} = 0. \tag{55}$$

As $u(\eta_1, \eta_2)$ is a homogeneous polynomial in the components of η_1, η_2, we see from (53) and (55) that $h'_1 - h'_3 \geqq 0$, $h'_2 - h'_3 \geqq 0$. We shall show in a later paper that the equations (55) also imply $h'_1 - h'_2 \geqq 0$, so that $h'_1 \geqq h'_2 \geqq h'_3$.

Using (17) and (20), we could write (55) as

$$H\psi_{RC} = (h'_1 + h'_2 - 2h'_3)\psi_{RC}, \tag{56a}$$

$$F_3\psi_{RC} = \tfrac{1}{2}(h'_1 - h'_2)\psi_{RC}, \tag{56b}$$

$$(F_1 + iF_2)\psi_{RC} = 0. \tag{56c}$$

But the pseudo-spin has all the properties of angular momentum, so it is clear that the equations (56) are equivalent to (27b) if $\nu = f$. We obtain therefore the relations

$$h'_1 + h'_2 - 2h'_3 = \rho, \tag{57a}$$

$$\tfrac{1}{2}(h'_1 - h'_2) = f, \tag{57b}$$

where ρ is the energy and f the pseudo-spin of the reduced two-particle canonical state ψ_{RC}. From (46) and (57), we obtain finally

$$h'_1 = \tfrac{1}{3}E + \tfrac{1}{6}\rho + f, \tag{58a}$$

$$h'_2 = \tfrac{1}{3}E + \tfrac{1}{6}\rho - f, \tag{58b}$$

$$h'_3 = \tfrac{1}{3}E - \tfrac{1}{3}\rho. \tag{58c}$$

Because of (43), all other h'_s, $s \geqq 4$, are zero.

† A reader familiar with the representations of the unitary group will notice that we have determined the irreducible unitary representation of the unitary group, induced by the transformations (5) (see H. Weyl [11]). Our h'_s are the l_s of Weyl. Our analysis shows that only a small class of representations may occur since $h'_4 = \ldots = h'_N = 0$.

Returning to the expression (39) for the eigenvalue of the Casimir operator, we see that it is given in terms of E, ρ, f by

$$g = [\tfrac{1}{3}E^2+(N-3)E+\tfrac{1}{6}\rho(\rho+6)+2f(f+1)]. \tag{59}$$

From (46) and (57a) we have that $\rho \leqq E$, so combined with (26), we obtain

$$0 \leqq 2f \leqq \rho \leqq E, \tag{60}$$

with f being an integer if ρ is even, a semi-integer if ρ is odd. For a state of given energy, g depends only on ρ and f. The correlations between ρ, f and the angular momentum λ, are given exactly in the same way as in section 3, as the reduced canonical wave function has only two particles outside the ground state. We can therefore discuss the correlations between E, g and λ, but we first decompose the Casimir operator in terms of the quadrupole-quadrupole interaction, and the squares of the total angular momentum and hamiltonian, so as to deal directly with the eigenvalues associated with the quadrupole-quadrupole interaction.

6. The Casimir Operator and the Quadrupole-Quadrupole Interaction

Using the definitions (2) and the commutation relations (3), we see that the Casimir operator G of (31) can be written as

$$\begin{aligned} G &= \sum_{r,s=1}^{N} (\eta_r \cdot \xi_s)(\eta_s \cdot \xi_r) \\ &= \sum_{r,s=1}^{N} \{ \sum_{i,j=1}^{3} [(\eta_{ir}\xi_{jr})(\eta_{is}\xi_{js})^\dagger] + (\eta_r \cdot \xi_r) - 3(\eta_r \cdot \xi_s)\delta_{rs}\} \\ &= \sum_{r,s=1}^{N} \sum_{m,m'=-1}^{+1} [(\eta_{mr}\xi_{m'r})(\eta_{ms}\xi_{m's})^\dagger] + (N-3)\sum_{r=1}^{N} (\eta_r \cdot \xi_r), \end{aligned} \tag{61}$$

where η_{mr}, $\xi_{m'r}$, etc., stand for the spherical components of the vectors, i.e.

$$\eta_{+1r} = -\frac{1}{\sqrt{2}}(\eta_{1r}+i\eta_{2r}), \quad \eta_{0r} = \eta_{3r}, \quad \eta_{-1r} = \frac{1}{\sqrt{2}}(\eta_{1r}-i\eta_{2r}). \tag{62}$$

Introducing the Racah tensor [12]) $Q^\rho_{\tau,r}$ defined by

$$Q^\rho_{\tau,r} = \sum_{mm'} \langle 11mm'|\rho\tau\rangle \eta_{mr}\xi_{m'r}, \quad \rho = 0,1,2, \tag{63}$$

we obtain from the orthogonality property [13]) of the Clebsch-Gordan coefficients

$$\sum_{mm'=-1}^{+1} (\eta_{mr}\xi_{m'r})(\eta_{ms}\xi_{m's})^\dagger = \sum_{\rho=0}^{2} \sum_{\tau=-\rho}^{\rho} Q^\rho_{\tau,r} Q^{\rho\dagger}_{\tau,s} = \sum_{\rho,\tau} (-1)^\tau Q^\rho_{\tau,r} Q^\rho_{-\tau,s}. \tag{64}$$

Summing over the index $\tau = 1, 2, \ldots N$, we obtain the tensors

$$Q_\tau{}^\rho = \sum_{\tau=1}^{N} Q^\rho_{\tau,\tau}, \tag{65}$$

and from the explicit expressions [13]) for the Clebsch-Gordan coefficients, we have [12])

$$Q_0{}^0 = -\frac{1}{\sqrt{3}} \sum_{\tau=1}^{N} (\eta_\tau \cdot \xi_\tau) = -\frac{1}{\sqrt{3}} H, \tag{66a}$$

$$Q_\tau{}^1 = \frac{i}{\sqrt{2}} \sum_{\tau=1}^{N} (\eta_\tau \times \xi_\tau)_\tau = -\frac{1}{\sqrt{2}} (\lambda)_\tau, \tag{66b}$$

$$Q_\tau{}^2 = \sum_{\tau} \sum_{mm'} \langle 11mm' | 2\tau \rangle \eta_{m\tau} \xi_{m'\tau} \equiv Q_\tau. \tag{66c}$$

The Casimir operator (61) then becomes

$$G = \tfrac{1}{3}H^2 + (N-3)H + \tfrac{1}{2}\lambda^2 + \mathbf{Q}^2, \tag{67}$$

where

$$\mathbf{Q}^2 = \sum_{\tau} (-1)^\tau Q_\tau Q_{-\tau}. \tag{68}$$

The wave function ψ describing the N-particle state of section 4, is an eigenfunction of H, λ^2 and G, and therefore, from (67) (59), it will be an eigenfunction of $-\mathbf{Q}^2$ with the eigenvalue

$$-\mathbf{Q}^2\psi = \{-[\tfrac{1}{6}\rho(\rho+6) + 2f(f+1)] + \tfrac{1}{2}\lambda(\lambda+1)\}\psi. \tag{69}$$

For a given E, the values of ρ, f are restricted by (60). To obtain the values of the angular momentum λ compatible with given ρ and f, we make use of Brody's tables [6]). From these tables, by a procedure entirely similar to the one used in table 1 of this paper, one can obtain the values of f consistent with a given ρ and λ. Having then the compatible values of ρ, λ, f we construct table 2, in which, for given ρ, f that satisfy (60), we give all the corresponding values of λ. In the last column of table 2 we write also the value of the first term of the eigenvalue (69) of $-\mathbf{Q}^2$. The values of ρ are restricted to those available in Brody's tables, i.e. $\rho \leqq 12$.

In the previous discussion, we found that the eigenvalues of $-\mathbf{Q}^2$ can be given in terms of the energy ρ, pseudo-spin f, and angular momentum λ, of the two-particle reduced canonical wave function. If we make use of the definitions (2) and (66c), we immediately see that Q_τ is, except for irrelevant constants, just the quadrupole operator acting within a shell of Elliot [3]). We have therefore, in (69), the eigenvalues associated with the quadrupole-quadrupole interaction. In the next section, we briefly review the arguments of Moszkowski [2]) for considering this interaction as the relevant part of the potential between the nucleons. From table 2 we shall then see that this interaction gives rise to rotational bands.

TABLE 2

Rotational bands. The exponents for some values of the angular momentum λ indicate the number of times this value appears in the rotational band.

ρ	f	λ	$\frac{1}{4}\rho(\rho+6)+2f(f+1)$
0	0	0	0
1	$\frac{1}{2}$	1	$2\frac{2}{3}$
2	1	0, 2	$6\frac{2}{3}$
	0	1	$2\frac{2}{3}$
3	$\frac{3}{2}$	1, 3	12
	$\frac{1}{2}$	1, 2	6
4	2	0, 2, 4	$18\frac{2}{3}$
	1	1, 2, 3	$10\frac{2}{3}$
	0	0, 2	$6\frac{2}{3}$
5	$\frac{5}{2}$	1, 3, 5	$26\frac{2}{3}$
	$\frac{3}{2}$	1, 2, 3, 4	$16\frac{2}{3}$
	$\frac{1}{2}$	1, 2, 3	$10\frac{2}{3}$
6	3	0, 2, 4, 6	36
	2	1, 2, 3, 4, 5	24
	1	0, $(2)^2$, 3, 4	16
	0	1, 3	12
7	$\frac{7}{2}$	1, 3, 5, 7	$46\frac{2}{3}$
	$\frac{5}{2}$	1, 2, 3, 4, 5, 6	$32\frac{2}{3}$
	$\frac{3}{2}$	1, 2, $(3)^2$, 4, 5	$22\frac{2}{3}$
	$\frac{1}{2}$	1, 2, 3, 4	$16\frac{2}{3}$
8	4	0, 2, 4, 6, 8	$58\frac{2}{3}$
	3	1, 2, 3, 4, 5, 6, 7	$42\frac{2}{3}$
	2	0, $(2)^2$, 3, $(4)^2$, 5, 6	$30\frac{2}{3}$
	1	1, 2, $(3)^2$, 4, 5	$22\frac{2}{3}$
	0	0, 2, 4	$18\frac{2}{3}$
9	$\frac{9}{2}$	1, 3, 5, 7, 9	72
	$\frac{7}{2}$	1, 2, 3, 4, 5, 6, 7, 8	54
	$\frac{5}{2}$	1, 2, $(3)^2$, $(4)^2$, $(5)^2$, 6, 7	40
	$\frac{3}{2}$	1, 2, $(3)^2$, $(4)^2$, 5, 6	30
	$\frac{1}{2}$	1, 2, 3, 4, 5	24
10	5	0, 2, 4, 6, 8, 10	$86\frac{2}{3}$
	4	1, 2, 3, 4, 5, 6, 7, 8, 9	$66\frac{2}{3}$
	3	0, $(2)^2$, 3, $(4)^2$, 5, $(6)^2$, 7, 8	$50\frac{2}{3}$
	2	1, 2, $(3)^2$, $(4)^2$, $(5)^2$, 6, 7	$38\frac{2}{3}$
	1	0, 1, $(2)^2$, 3, $(4)^2$, 5, 6	$30\frac{2}{3}$
	0	1, 3, 5	$26\frac{2}{3}$
11	$\frac{11}{2}$	1, 3, 5, 7, 9, 11	$102\frac{2}{3}$
	$\frac{9}{2}$	1, 2, 3, 4, 5, 6, 7, 8, 9, 10	$80\frac{2}{3}$
	$\frac{7}{2}$	1, 2, $(3)^2$, 4, $(5)^2$, 6, $(7)^2$, 8, 9	$62\frac{2}{3}$
	$\frac{5}{2}$	1, 2, $(3)^2$, $(4)^2$, $(5)^2$, $(6)^2$, 7, 8	$48\frac{2}{3}$
	$\frac{3}{2}$	1, 2, $(3)^2$, $(4)^2$, $(5)^2$, 6, 7	$38\frac{2}{3}$
	$\frac{1}{2}$	1, 2, 3, 4, 5, 6	$32\frac{2}{3}$
12	6	0, 2, 4, 6, 8, 10, 12	120
	5	1, 2, 3, 4, 5, 6, 7, 8, 9, 10, 11	96
	4	0, $(2)^2$, 3, $(4)^2$, 5, $(6)^2$, 7, $(8)^2$, 9, 10	76
	3	1, 2, $(3)^2$, $(4)^2$, $(5)^2$, $(6)^2$, $(7)^2$, 8, 9	60
	2	0, $(2)^2$, 3, $(4)^2$, $(5)^2$, $(6)^2$, 7, 8	48
	1	1, 2, $(3)^2$, 4, $(5)^2$, 6, 7	40
	0	0, 2, 4, 6	36

7. The Rotational Bands

So far, in this paper, we have only looked into the classification of states for N spinless particles moving in a common harmonic oscillator potential. For this classification to be useful in nuclear shell theory, we would have to add the spin of the particles, take into account the Fermi statistics, introduce the spin orbit coupling in the common potential, and finally, consider the interactions between the particles. While we plan to do all this, in the present paper we shall only consider the last point, i.e. an interaction potential between the particles of the form

$$\mathscr{V} = \sum_{s<t=1}^{N} V(|\mathbf{r}_s - \mathbf{r}_t|) = \sum_{s<t=1}^{N} \sum_{k} V_k(r_s, r_t) P_k(\cos \omega_{st}), \tag{70}$$

where P_k is a Legendre polynomial, and ω_{st} is the angle between the vectors $\mathbf{r}_s$ and $\mathbf{r}_t$. If we expand V_k as a power series in r_s, r_t, we see that $\mathscr{V}$ is given as a linear combination of terms of the form

$$\sum_{\tau} r_s^{k+m} Y_{k\tau}(\theta_s, \varphi_s) r_t^{k+n} Y^*_{k\tau}(\theta_t, \varphi_t), \tag{71}$$

where $Y_{k\tau}$ are spherical harmonics, and r_s, θ_s, φ_s, etc., are the polar coordinates of the particles.

In his paper [2]), Moszkowski suggests that the interaction potential (70) would act mainly on the nuclear surface, as the exclusion principle effectively damps the interaction in the interior of the nucleus. He shows then that the terms of (71) with the lowest possible values of k, m, n, would be the most important for the interaction. If we are considering matrix elements within the shell of each particle, i.e. with h_s fixed, the parity of initial and final state is the same, and the dipole-dipole interaction term $k = 1$ vanishes. The term of lowest order, different from zero, would then be proportional to

$$\sum_{\tau} r_s^2 Y_{2\tau}(\theta_s, \varphi_s) r_t^2 Y^*_{2\tau}(\theta_t, \varphi_t), \tag{72}$$

The quadrupole term in (72) could be written as

$$r_s^2 Y_{2\tau}(\theta_s, \varphi_s) = (15/8\pi)^{\frac{1}{2}} \sum_{mm'} \langle 11\, mm' | 2\tau \rangle x_{ms} x_{m's}, \tag{73}$$

where $x_{ms} (m = +1, 0, -1)$ are the spherical components of $\mathbf{r}_s$. From (2) we see that

$$x_{ms} = \frac{1}{\sqrt{2}} (\eta_{ms} + \xi_{ms}). \tag{74}$$

If we substitute (74) in (73), and retain only the terms that act within a shell, i.e. the terms that have one creation and one annihilation operators, we see that (73) is proportional to $Q^2_{\tau,s}$, and therefore, (72) is proportional to

$\sum_\tau (-1)^\tau Q^2_{\tau,s} Q^2_{-\tau,s}$. If the potential between the particles is attractive, (72) will be multiplied by a negative constant, and under the assumption made in this paragraph, the hamiltonian, including the interaction, would be given by

$$\mathscr{H} = H - (\mathbf{Q}^2/\mathscr{I}), \tag{75}$$

where $\mathscr{I}$ is a positive constant related to the coefficient of (72).

The eigenvalues of (75) are given by (69), and therefore, for each ρ, f we have a rotational band of the form

$$\lambda(\lambda+1)/2\mathscr{I}, \tag{76}$$

with the values of λ given in table 2. The band of lowest energy would correspond to the highest value of ρ and f consistent with (60), i.e. with

$$\rho = 2f = E. \tag{77}$$

From table 2 we see that for $2f = \rho$ and ρ even, the values of λ are

$$\lambda = 0, 2, 4, 6, \ldots, \rho. \tag{78}$$

From the above discussion, we see that the classification of states in terms of the Casimir operator for the N-dimensional unitary group, brings out the collective nature of these states. In the following papers of this series, the explicit form for the eigenfunctions of the Casimir operator will be given, starting with $N = 2$, i.e. with the eigenfunctions of the pseudo-spin operator $\mathbf{F}^2$.

The authors are indebted to Prof. E. P. Wigner, Prof. C. A. Levinson and Dr. M. K. Banerjee for helpful discussions.

References

1) G. A. Baker, Jr., Phys. Rev. **103** (1956) 1119
2) S. A. Moszkowski, Phys. Rev. **110** (1958) 403
3) J. P. Elliot, Proc. Roy. Soc. **245** A (1958) 128, 562
4) H. Casimir, Proc. Kon. Acad. Amst. **34** (1931) 844
5) A. R. Edmonds, Angular momentum in quantum mechanics (Princeton University Press, Princeton, N.J., 1957) p. 69
6) T. A. Brody, Rev. Mexicana de Física **8** (1959) 139
7) E. P. Wigner, Group theory and quantum mechanics (Academic Press, New York, 1959) p. 157
8) J. M. Jauch and E. L. Hill, Phys. Rev. **57** (1940) 641
9) M. Moshinsky, Nuclear Physics **13** (1959) 104
10) G. Racah, Group theory and spectroscopy (Mimeographed notes, Institute of Advanced Study, 1951)
11) H. Weyl, Group theory and quantum mechanics (Methuen, London, 1931) p. 380
12) M. Moshinsky, Phys. Rev. **106** (1957) 117
13) M. E. Rose, Elementary theory of angular momentum (Wiley, New York, 1957) pp. 34, 225

10.A *Nuclear Physics* 18 (1960) 713—714; © *North-Holland Publishing Co., Amsterdam*

NEWS ITEMS

16th SESSION OF THE COUNCIL OF CERN

The Council of CERN held its 16th Session on June 14, 1960, in Geneva, under the presidency of Mr. F. de Rose (France). The main items of the agenda were the following.

The Director-General of CERN

The appointment of Mr. J. B. Adams (Great-Britain), as acting Director-General has been confirmed by the Council. Mr. Adams assumed the Direction of the Organization since the accidental death of Professor C. J. Bakker (Netherlands), on April 23, 1960. Discussions concerning the appointment of the future Director-General will be taken up again in the near future.

Long-Term programme

Professor E. Amaldi (Italy), Chairmant of CERN's Scientific Policy Committee, expressed the opinion that 10 years hence the state of research in high energy physics in Europe will compel CERN to use "a new tool of research". The importance of the latter will be, in 1970, comparable to that of the large 25 GeV synchrotron now operating at CERN.

The Council agreed that it was now necessary to start thinking seriously about the long-term programme of CERN. Indeed, the construction time of any large new nuclear project is very long. Furthermore, scientific and other factors are so numerous that very careful studies are necessary before a project can even be ready for consideration.

Soviet scientist at CERN

Negociations started two years ago with the Dubna research centre have come to a successful result. Mr. J. B. Adams, acting Director-General of CERN, and Professor D. I. Blokhintsev, Director of Dubna, have agreed upon the details of the coming exchange of the first three scientists between the two great centres for nuclear research in western Europe and the USSR.

Agreement with the Federal Institute of Technology (ETH), *Zurich*

CERN is building a 150 cm cloud chamber, equipped with a magnetic field. This apparatus should be completed about the end of 1960. The cost of construction and operation, staff and material included, is estimated to 3 million Swiss francs. The ETH wishes to co-operate in the construction of this machine and in the experiments undertaken by the cloud chamber group.

The agreement between CERN and the ETH stipulates that representatives of both parties will participate in the building of the apparatus. Once finished this cloud chamber will remain their joint property for two years; scientists from CERN, from ETH and from other member States will operate the chamber.

INAUGURATION AT CERN OF THE „PAULI MEMORIAL ROOM"

At the suggestion of Mrs. Pauli, the personal library of her husband, the late Professor Wolfgang Pauli, has been transferred to CERN in Geneva. On June 14, following one of the meetings of the 16th Session of CERN Council, a brief ceremony marked the inauguration of the "Pauli Memorial Room" where the volumes composing the library of the great scientist have been housed.

The library consists of some 700 books dealing with literature and philosophy in addition to theoretical physics. It also includes sets of periodicals and a unique collection of reprints.

The works in the "Pauli Memorial Room" may be consulted by those interested in the great scientist and thinker, Wolfgang Pauli.

During the inauguration ceremony, Mr. F. de Rose, President of the CERN Council, said:

"Thinking of the great work of Wolfgang Pauli, who would not feel deeply moved on entering this room and finding himself in the presence of these books which helped him to achieve so much, and in the midst of which he worked; any volume one picks up might well have been in his hands when a brilliant idea which was later to enrich universal science flashed through his mind?"

"CERN", concluded Mr. de Rose, "will treasure this gift with emotion and affection: as a symbol of confidence in CERN's mission, it is of inestimable value."

Replying to Mr. de Rose, M. Fierz, Professor of theoretical physics at the ETH at Zurich and former student of Professor Pauli, said:

"This collection shows the magnificent complexity of the means employed to make scientific discoveries. It shows that in order to understand the riddles of nature many scientists must pool their efforts. That Schopenhauer, clear, impassioned and imaginative, should have been one of Professor Pauli's favourite authors, shows what manner of man he was. Pauli was convinced that the troubles threatening the world of to-day are of spiritual as well as political origin and can only be overcome by the spirit. I hope that this permanent reminder of Professor Pauli will lead all physicists to think deeply about physics, its development and its place in our knowledge, and, last but not least, that it will cause them in spite of their modesty to meditate on their own personality."

10.D *Nuclear Physics* 18 (1960) 715—719; © *North-Holland Publishing Co., Amsterdam*

BOOK REVIEWS

R. HOBART ELLIS, Jr., *Nuclear Technology for Engineers* (McGraw-Hill, London 1959. x—284 p. 74s.)

This book gives in an easy-to-read version a rather brief review of four fundamental topics in modern nuclear technology: radio-tracer, radioactive irradiation, fission reactors, and — bringing the description up to date — fusion. It is meant as an introductory textbook, and the presentation of the material is in this respect excellent. But it is not of great help in conducting the reader into further study. There is no reference at all, which reduces the applicability of the book as a textbook. It is good only for people who want to be introduced into the nuclear field, but do not want to go any further. I find that the book may be really useful for mechanics and other technicians desirous of widening their horizon a little.

Each chapter is followed up by questions meant for discussion, and problems that will force the reader to go over the chapter once more. In chapter 3, Detection of Radiation, one observes that the older term "well-known geometry" is replaced by a newer one, "well-understood geometry", indicating the author's general intention that the reader should think instead of just accept. And this could be taken as the main impression of the book.

J. Thomas

FRANCIS H. CLAUSER (Editor), *Symposium of Plasma Dynamics* (Addison-Wesley Publishing Company, Reading, Mass. 1960. 369 p. $ 12.50).

The volume is based on an international symposium on plasma dynamics held at Woods Hole, Massachusetts, during the week June 9—13, 1958, under the sponsorship of the National Academy of Sciences and the Office of Scientific Research, Air Research and Development Command. The transcribed proceedings of the sessions served as the basis for the material compiled in the volume by a distinguished board of editors. While the subject is one of growing interest to many types of scientists, the book should be of particular value to thermonuclear physicists, missile and space engineers, astrophysicists, and electronics engineers. The book offers the broadest view yet presented of the whole field of plasma dynamics. The well-written text, the excellent editing, the beautiful drawings and remarkable photographs as well as the fascinating subject make the reading of the book a real pleasure.

H. Wilhelmsson

H. SEMAT, *Introduction à la physique atomique et nucléaire* (Gauthier-Villars, Paris 1960. xiii—599 p. 50 NF)

Cette traduction, revue par l'auteur, d'un traité élémentaire justement réputé, ne manquera de rendre les plus grands services aux étudiants en vue desquels elle a été entreprise. Il est dommage que la nature du papier employé gâche l'effet des illustrations photographiques. Au point de vue de sa production matérielle, ce volume n'a pas meilleur aspect que la plupart des livres russes destinés aux étudiants mais il coûte cinq fois plus cher.

L. R.

J. G. WILSON and S. A. WOUTHUYSEN (Editors), *Progress in elementary particle and cosmic ray physics*, vol. V (North-Holland Publishing Co., Amsterdam 1960. xii—461 p.)

This volume, which intends to survey the progress made in the last two years, offers a very judicious selection of monographs. The new developments in the question of weak interactions is described by A. Lundby; the article is divided into two parts, treating of the theoretical aspects, with some brief mention of the relevant experimental results, and of the experimental methods by which the polarization of γ-rays and electrons can be determined. J. L. Gammel and R. M. Thaler discuss the phenomenological representation of the interaction between nucleons, and J. McConnell

the theory of antinucleons on the basis of the new experimental data. Then comes an extensive account by D. H. Perkins of the peculiar "jet" cascades of cosmic radiation, produced by primaries of extremely high energy. Finally there is a survey, by R. M. Tennent, of the absorption and decay of negative μ-mesons. The production of this valuable collection is of the usual high standard. The author index would seem unnecessarily bulky: it is superfluous to repeat in it the full references already given in the lists following the individual articles.

L. R.

Who's Who in Atoms, 2nd edition (2 vol.) (Vallancey Press, London 1960. 983 p. £ 10 10s.)

Atoms have become prominent and the first edition (1959) of *Who's Who in Atoms* was out of print within two months of publication. *Who's Whos* are useful. If you want to sell something the best buyers are always those listed in a *Who's Who*. If you want to find out what that guy you met last night at an atoms meeting is really doing you might find out something from a *Who's Who*. It is always useful to know whether he is just another scientist or if he is a real big shot.

Many persons consider the most important use of a *Who's Who* to find out who is Who and who is not Who. This is the snobbish aspect of this kind of book. Maybe this point might be improved in future editions by letting the book get a more professional character. Here I would suggest three improvements: to include mailing addresses of institutions and research establishments, to include cross references by subjects so that one might find out who is working, say, in metallurgy etc., and finally to inlude cross references by countrv.

With these additions the book would be still more valuable. However, as it is, the book is quite a useful tool at any administrative or semi-administrative office dealing with atoms.

O. Kofoed-Hansen

A. Hitchcock, *Nuclear reactor stability* (Temple Press, London, 1960. ix—61 p. 12s. 6d.)

The present little book is another member of the Temple Press "Nuclear Engineering" monographs, which by now comprise an impressive collection of useful books in this important field. The series is under general edition by W. K. Mansfield.

On 60 pages a survey is given of the stability of dynamic reactor systems, illustrated by detailed considerations of temperature instability, Xenon instability and voidage instability together with a discussion of the control of instability.

In a discussion of the stability of a system as complicated as a reactor, one has to touch on many different branches of physics and engineering. Furthermore, the equations needed for a mathematical description of the system are often quite complicated and, for reactor stability calculations, necessarily highly non-linear. The present book applies the usual first approximation to this problem only, i.e. the equations are written down in terms of small deviations from a steady state; they are then linearized and analysed in terms of single modes in order that characteristic frequencies for the system may be found. If none of the characteristic frequencies show exponential increase or undamped oscillations, the system is stable. This first approximation is usually sufficient for engineering purposes, and it is treated with pedagogical insight and applied to the most important sources of instability. Consequently the present monograph can be recommended to anybody interested in this field.

O. Kofoed-Hansen

F. Halbwachs, *Théorie relativiste des fluides à spin* (Gauthier-Villars, Paris 1960. x—294 p. 60 NF)

This book may be judged from two points of view: according to the author's aims, or according to its real contents. From the former point of view it is a complete failure; worse still, it is vitiated from beginning to end by a fundamental error. Indeed, what the author intends to show, or at least suggest, is that a fermion could be faithfully pictured as a classical rotating droplet. The reason why he finds it at all possible to entertain such a preposterous idea is that he uncritically interprets mathematical quantities in physical terms, without enquiring whether such interpretations are compatible with the definitions of the physical concepts by means of appropriate

measurements. It is superfluous to point out that no classical picture contains the peculiar features of the fermion spin, e.g. the correlation between the polarizations of two fermions emitted in a single act. The superficial analogies noticed by the author (and others before him) between the spin properties and those of a classical angular momentum are sufficiently accounted for by the relation of these quantities to the rotation group.

From a sociological point of view, the author's attitude is comparable to that of the Jesuit astronomers of the XVII. Century who twisted their fertile imaginations to dodge the evidence of the Copernican system: he is blinded by the new dogmatism of the XX. century, propagated by another church, but just as fatal to the exercise of scientific thinking.

If, however, we forget about the unfortunate metaphysical background of this book, we find that it contains a well-written and extensive account of the theory of rotating fluids, in which full regard is paid to the relativity requirements; although the peculiar difficulties of this theory have long been elucidated, and excellent presentations of its main aspects (such as that in Møller's treatise) are available, the detailed treatment given here will doubtless be most helpful to anyone wishing to acquaint himself with these little-known aspects of relativistic hydrodynamics.

L. R.

M. A. MARKOW, *Hyperonen und Mesonen* (VEB Deutscher Verlag der Wissenschaften, Berlin 1960. 328 p. DM 42.80)

Professor Markow's masterly lectures of 1957 on the new discoveries of fundamental constituents of matter and the theoretical problems raised by their interpretation are now made available to those physicists who read German more easily than Russian. The translation has been revised and (to a certain extent) brought up to date by the author, who, however, has wisely retained the primitive disposition, presenting a clear picture of the gradual development of our ideas in this novel domain. An advantage of the survey of the field here given is that Russian work is more fully described in it than in most other reviews; and not the least attractive feature is the exposition of the author's own original views on the unsolved theoretical problems.

L. R.

J. G. LINHART, *Plasma physics* (North-Holland Publishing Company, Amsterdam. 1960. xi-278 p. fl. 25)

J. G. Linhart's purpose in writing this book has been to meet the heavy need for a textbook dealing with those topics of plasma physics for which the interest has been growing rapidly in recent years owing to the work that is being done to obtain controlled thermonuclear reactions. The book is specially written for postgraduate students and physicists who want to enter this part of physics. It gives a survey of the different branches of plasma physics and of some of its possible applications.

The first six chapters deal with the basic principles in plasma physics covering such topics as motion of charged particles in electric and magnetic fields, radiation from accelerated charged particles, fluid description of a plasma, equilibrium configurations, waves and instabilities in a plasma and collision and relaxation processes in a plasma. The last two chapters are concerned with applications of plasma physics. Chapter 7 deals with the fusion processes and the various approaches to the problem of obtaining controlled thermonuclear reactions. Chapter 8 treats such topics as direct conversion of heat into electricity, the use of plasma physics in rocket propulsion and its possible application to particle-accelerators.

Each chapter is followed by a list of references to works that give more detailed treatments of the subjects discussed in the chapter, and at the end of the book a detailed list of literature in plasma physics can be found.

With this book the author has written a pedagogic textbook which gives a clear and easily understandable introduction to many of the aspects of plasma physics. The major criticism of this book is that the attentive reader at some places will find weaknesses in the derivations of the formulas and that confusing misprints in the formulas are quite frequent.

Chapter 6, § 1 is a conspicuous illustration to this. In this paragraph the author uses the formulas for the angles of deflection in Coulomb-encounters without giving the assumption under which

they are valid and without giving the exact definitions of the symbols used. In the derivation of the diffusion coefficients a more detailed discussion of the approximations would be desirable, as for example that the field particles are assumed to be at rest although the temperature of the plasma appears in the formulas. In this paragraph some twenty formulas and equations are given, misprints can be found in the following four: Formula (1a) is wrong by a factor two, the equation in line 6, p. 165 is wrong owing to a simple misprint, the equation in line 12, p. 165 is wrong by a factor m and in formula (9) two misprints can be found.

However, this book should be welcomed very warmly, it satisfies a real need for a textbook in the basic principles of plasma physics. It can be recommended to any physicist who wants to get a basic knowledge in plasma physics.

V. O. Jensen

Australian Atomic Energy Symposium — 1958 — Proceedings of a Symposium on the Peaceful Uses of Atomic Energy in Australia held in Sydney from June 2 to 6, 1958. (Melbourne University Press, 1960. 788 p. £ 5.0.0.).

In the summer of 1958 the Australian Atomic Energy Commission arranged a nuclear energy symposium, which served the purpose of a local "Geneva Conference".

The minutes of this symposium, comprising some hundred papers presented at the conference and the discussions of the sessions, have now been published in book-form. The papers cover a rather wide range of subjects, reactor materials, nuclear power programs and reactors, chemical problems connected to nuclear energy, basic physics and reactor physics, application of radioisotopes, techniques in handling radioactive materials, education and fusion.

Even though more than 75 percent of the papers are written by Australians, some other countries, especially the United Kingdom and USA, have made a number of contributions.

For those interested in what is going on inside the field of nuclear energy in Australia, this book is very valuable, because it gives a good picture of the types of work that are carried out in this field in Australia. However, as a general source of information on the development and the problems of nuclear energy, these proceedings have little to offer, because the papers given only cover the different areas in an unsatisfactory way. For example the important fields of reactor technology, heat transfer and reactor physics have been given very limited attention. In view of the fact that this book is published at the same time as the proceedings of the second Geneva Conference, which gives a much more complete coverage of the different aspects of nuclear energy, it seems likely that it will raise rather limited interest.

P. L. Ølgaard

M. Rotenberg, R. Bivins, N. Metropolis, J. K. Wooten, Jr., *The 3—j and 6—j symbols* (Technology Press, M.I.T., Cambridge, Mass. 1959. viii—498 p. $ 16)

Tables extending to highest spin values 8, preceded by an excellent compendium of the properties of the symbols. It is a pity, that not *all* the analytical expressions listed in Edmonds' book are reproduced: this would have added the last touch of perfection to this useful and well-produced compilation.

L. R.

R. Herman and R. Hofstadter, *High-energy electron scattering tables* (Stanford University Press, 1960. ix—278 p. $ 8.50)

The graphs and tables collected in this book are intended as a tool for both experimental and theoretical physicists who have to analyse data on the scattering of high-energy electrons by nuclei. Special emphasis is put on scattering by protons and deuterons, and the corresponding "form factors". The theoretical background is presented, on the basis of the Born approximation, in a competent fashion; one would have liked, however, a more explicit warning about the serious insufficiencies and uncertainties of the present theoretical treatment of the charge distribution of the nucleons. In a book concerned with methods aiming at the elimination of human thinking, it is perhaps natural that no mention should be made of the theoretical work of Bodmer and Reignier, whose purpose is to reduce the recourse to numerical computation to a minimum by means of old-fashioned brain-work. The adequacy of Reignier's method, at least in the domain of lower electron energies, is well illustrated by the recent experimental paper by Bellicard and Barreau (this journal **17** (1960) 141).

L. R.

GORDON FRANCIS, *Ionization phenomena in gases* (Butterworth's Scientific Publications, London 1960. 300 p. 60s.)

The book has been written mainly for those finishing their university studies, and graduates about to begin research. Its aim is to guide the student in branches of physics which are closely connected with the fundamental processes of ionized gases.

After a short summary of atomic physics the author briefly treats the fundamental processes of gases and the similarity principle. He then devotes one chapter to alternating and high-frequency discharges, and another to ionization and excitation in the upper atmosphere. The remaining two chapters of the book describe high-current discharges and thermonuclear effects as well as plasma oscillations and waves.

In the preface the author claims to have laid stress on the physical principles, sometimes at the expense of mathematical rigour. In places this has led to oversimplification. In the introduction, for example, we find the sentence "it is the electrical forces between the electrons (of an atom) and the electrons of another atom which constitute a chemical bond", a phrase which may be misleading to the student. An application of Pauli's exclusion principle demonstrating the exchange character of molecular forces might have been justified in the introductory chapter.

Some more graphs would have helped the student to grasp the physical ideas, especially in the description of the ionosphere and in the chapter on plasma oscillations and waves. For example, the propagation constants of the waves excitable under different conditions ought to have been depicted. For further elucidation of the physical picture, an explanation of the effect of particle-drift velocity on the form of the dispersion relation as a Doppler shift (see e.g. eq. 7.66) would have been appreciated. Some unfortunate misprints are noted (e.g. the expression for the electron plasma frequency, eq. 7.69, lacks a factor 4 under the square root).

It is an open question whether astrophysical examples, such as the synchrotron radiation from the Crab nebula, the 21 cm radiation from interstellar space and some examples from solar physics, would not be well suited to widen the outlook of the student even more. Unfortunately, the astrophysical aspects are not discussed, although several questions important to the development of the thermonuclear devices originate from this field.

The student who wants to become familiar with the different fields covered in the book will, however, find in it a beatiful and stimulating presentation of the different aspects of these fascinating topics.

Hans Wilhelmsson

UNIVERSITÉ DE GRENOBLE, ÉCOLE D'ÉTÉ DE PHYSIQUE THÉORIQUE (LES HOUCHES).
The many body problem (1958) (Dunod, Paris 1959. xv—675 p. 69 NF);
La théorie des gaz neutres et ionisés (1959) (Hermanne, Paris 1960. 469 p. 68 NF)

La réputation des cours donnés à l'École d'été de physique théorique des Houches n'est plus à faire, et l'on ne peut qu'approuver la nouvelle décision des directeurs si actifs et entreprenants de cette école de rendre accessible le texte de ces cours, par les voies commerciales habituelles, aux nombreux physiciens qui en apprécient la valeur à la fois didactique et de mise au point des problèmes d'actualité. Ces éditions sont exécutées par offset de textes dactylographiés, de sorte que le résultat dépend essentiellement de la qualité de cette dactylographie. La comparaison des deux volumes couvrant respectivement les sessions 1958 et 1959 révèle une très sensible amélioration d'une année à l'autre, tant pour la netteté du texte et des formules que pour le choix d'un format plus maniable. Le prix reste malheureusement tres élevé, surtout si l'on considère que c'est aux étudiants et aux jeunes chercheurs que ce genre d'ouvrage est appelé à rendre les plus grands services.

Les deux premiers volumes se rapportent à de vastes problèmes qui ont la particularité commune d'intéresser plusieurs domaines très différents de la physique. Inutile d'insister sur la fécondité de tels rapprochements. Ainsi les développements nouveaux de la théorie de la superconductivité ont eu une notable répercussion sur celle de la structure des noyaux. De même, les questions de mécanique statistique discutées en 1959 font appel à des techniques de calcul qui peuvent venir à point dans l'étude des interactions nucléaires. De plus, les problèmes de plasmas discutés dans cette dernière session forment un domaine nouveau non sans rapports plus ou moins directs avec la physique des noyaux. Tant par le choix des professeurs que par la maîtrise avec laquelle ils ont exposé leurs sujets, ces deux volumes peuvent être recommandés comme les exposés les meilleurs et les plus complets des aspects fondamentaux de deux ensembles de problèmes d'intérêt majeur et en plein développement.

L. R.

AUTHOR INDEX

ARIMA, AKITO, Spin-orbit splitting and tensor force 196
AUSTERN, N., and P. IANO, Variational calculations with repulsive core potentials 672
BALACHANDRAN, A. P. and N. R. RANGANATHAN, A note on scattering and production amplitudes. 81
BALDIN, A. M., Polarizability of nucleons 310
BARBER, W. C. and T. WIEDLING, Electrodisintegration of Ta and Au nuclei 575
BARGMANN, V. and M. MOSHINSKY, Group theory of harmonic oscillators (I). The collective modes 697
BASSOMPIERRE, G., *see* GORODETZKY
BERNSTEIN, E. M. and J. DE BOER, Gyromagnetic factors of deformed odd-mass nuclei with $153 \leqq A \leqq 187$ 40
BLEEKER, E. J., *see* DE VRIES
BROWN, G. E., *see* GREEN
BRIX, P., *see* DOSCH
CROISSIAUX, M., *see* GORODETZKY
DE BOER, J., *see* BERNSTEIN
DEMEUR, M., P. JANSSENS et J. LARDINOIS, États individuels au seuil de fission 280
DE PINHO-FILHO, A. G., Effects of photon polarization on the azimuthal angular distribution in (γ, N) reactions 271
DERRICK, G. H., On the choice of D-state wave functions in triton calculations. 303
DE VRIES, C., Determination of absolute $B\rho$-values of conversion lines . 428
DE VRIES, C., and J. H. DIJKSTRA, Precision measurements of energies of gamma-rays following the decay of some gold isotopes 446
DE VRIES, C., E. J. BLEEKER and Mrs. N. SALOMONS-GROBBEN, Absolute and relative conversion determinations of pure E2 transitions occurring in ^{198}Hg, ^{199}Hg, ^{194}Pt and ^{196}Pt 454
DONIACH, S. and E. YAMADA, Pion-nucleon attraction at short distances. 14
DOSCH, H. G., K. H. LINDENBERGER and P. BRIX, Integrated cross sections for the reactions $A^{40}(\gamma, p)$ and $A^{40}(\gamma, np)$ 615
DIJKSTRA, J. H., *see* DE VRIES
EISBERG, R. M., D. R. YENNIE and D. H. WILKINSON, A bremsstrahlung experiment to measure the time delay in nuclear reactions 338

ESTRUP, PEDER J., *see* PREISS
EVERLING, F., L. A. KÖNIG, J. H. E. MATTAUCH and A. H. WAPSTRA, Relative nuclidic masses 529
FINTZ, P., *see* GORODETZKY
GALLMANN, A., *see* GORODETZKY
GAUDIN, M., *see* MEHTA
GLENDENNING, NORMAN, K. and JERZY SAWICKI, Intrinsic quadrupole moments of deformed nuclei and superfluidity in nuclei 596
GOLDANSKY, V. I., O. A. KARPUKHIN, A. V. KUTSENKO and V. V. PAVLOVSKAYA, Elastic γ—p scattering at 40 to 70 MeV and polarizability of the proton 473
GOLDFARB, L. J. B. and R. C. JOHNSON, Angular distributions and polarization in stripping processes and in direct reactions 353
GOODING, T. J. and H. G. PUGH, Quasi-elastic scattering of 153 MeV protons by p-state protons in C^{12}, I. Experimental 46
GOODING, T. J., *see* RILEY
GORODETZKY, S., M. CROISSIAUX, A. GALLMANN, P. FINTZ, J. SAMUEL et G. BASSOMPIERRE, Étude de quelques niveaux excités du ^{11}B par la réaction $^{11}B(d, p)^{11}B$. 286
GREEN, A. M. and G. E. BROWN, Direct interaction in the p—2p reaction 1
GRISHIN, V. G. and V. I. OGIEVETSKI, On the minimum number of partial waves in two-body reactions 516
GRISHUK, G. I., *see* VISHNEVSKY
GUPTA, V., Recoil in pion—nucleon scattering 85
GUPTA, V., Strong interactions and isobaric gauge invariance 149
HITTMAIR, O., Winkelverteilungen von Kernspaltungen im Resonanzbereich. 346
IANO, P., *see* AUSTERN
JANSSENS, P., *see* DEMEUR
JOHNSON, R. C., *see* GOLDFARB
KAMEFUCHI, S., On Salam's equivalence theorem in vector meson theory 691
KARPUKHIN, O. A., *see* GOLDANSKY
KATZ, AMNON, On a modified Bethe-Goldstone equation 177
KAVANAGH, R. W., Protons from deuteron bombardment of Be^7 . . . 492
KOMAROV, V. V. and A. M. POPOVA, Investigation of the interaction between the products of reactions in which several particles are emitted 296
KÖNIG, L. A., *see* EVERLING
KUTSENKO, A. V., *see* GOLDANSKY
LARDINOIS, J., *see* DEMEUR
LINDENBERGER, K. H., *see* DOSCH
LYNESS, J. N., A method for calculating scattering phase shifts 654

LYUBIMOV, C. A., *see* VISHNEVSKY
MACFARLANE, A. J., Unitarity conditions for binary processes involving particles of arbitrary spin 570
MATTAUCH, J. H. E., *see* EVERLING
MEHTA, M. L., On the statistical properties of the level-spacings in nuclear spectra 395
MEHTA, M. L. and M. GAUDIN, On the density of eigenvalues of a random matrix 420
MITRA, A. N., Pion-pion effects in τ-decay 502
MÖBIUS, P., Treatment of special translationally invariant three-body problems by adapted coordinates 224
MOFFAT, JOHN, W., Resonance behaviour of scattering amplitudes in dispersion relations 75
MOSHINSKY, M., *see* BARGMANN
MOSZKOWSKI, S. A. and A. M. SESSLER, Hole-hole interactions and the properties of nuclear matter 669
OGIEVETSKI, V. I., *see* GRISHIN
ONEDA, S., *see* PATI
PARIKH, VASTUPAL, Absolute cross-sections of $C^{12}(p, pn)C^{11}$ from 288 to 383 MeV 628
PARIKH, VASTUPAL, Cross-sections for $Al^{27}(p, 3pn)Na^{24}$, $Al^{27}(p, 5p5n)F^{18}$ and $C^{12}(p, 3p3n)Be^{7}$, relative to $C^{12}(p, pn)C^{11}$ 638
PARIKH, VASTUPAL, The acivitities induced in beryllium, oxygen and fluorine by protons of 220 MeV to 362 MeV 646
PATI, J. C., S. ONEDA and B. SAKITA, On the leptonic and non-leptonic decay modes of K-mesons 318
PAVLOVSKAYA, V. V., *see* GOLDANSKY
PEARLSTEIN, L. D., Y. C. TANG and K. WILDERMUTH, Low lying levels of Li^{7} and Be^{8} in the cluster model 23
PEARSON, J. M. and M. A. PRESTON, The electric quadrupole interaction in beta decay 91
PETTERSON, B. G., *see* THUN
POPOVA, A. M., *see* KOMAROV
PREISS, IVOR, L., ESTRUP, PEDER, J. and RICHARD WOLFGANG, A new isotope: cadmium-103 624
PRESTON, M. A., *see* PEARSON
PUGH, H. G., *see* GOODING
PUGH, H. G., *see* RILEY
RANGANATHAN, N. R., *see* BALACHANDRAN
RILEY, K. F., H. G. PUGH and T. J. GOODING, Quasi-elastic scattering of 153 MeV protons by p-state protons in C^{12}, II. Theoretical 65
SAKITA, B., *see* PATI

SALAM, ABDUS, An equivalence theorem for partially gauge-invariant vector meson interactions 681
SALOMONS-GROBBEN, Mrs. N., *see* DE VRIES
SAMUEL, J., *see* GORODETZKY
SATCHLER, G. R., Symmetry properties of the distorted wave theory of direct nuclear reactions 110
SAWICKI, JERZY, *see* GLENDENNING
SESSLER, A. M., *see* MOSZKOWSKI
SIEGBAHN, K., *see* THUN
SOLOVIEV, V. G., Effect of quadruple correlations in light nuclei 161
SWAN, P., An improved approximation for scattering problems 245
TADIĆ, DUBRAVKO, On the pseudoscalar interaction in $0^- \to 0^+$ beta transitions 138
TANG, Y. C., *see* PEARLSTEIN
THUN, J. E., B. G. PETTERSSON and K. SIEGBAHN, Investigation of internal bremsstrahlung cross-section with specified electron and photon energies 131
TODOROV, I. T., Analytical properties of the scattering amplitude for inelastic processes involving strange particles 521
TRETYAKOV, E. F., *see* VISHNEVSKY
VAN DER SPUY, E., A possible model for the four-fermion coupling . . . 153
VISHNEVSKY, M. E., V. A. LYUBIMOV, E. F. TRETYAKOV and G. I. GRISHUK, Investigation of polarization of internal conversion electrons emitted after β^--decay in heavy elements 122
WAPSTRA, A. H., Energies of alpha particles 587
WAPSTRA, A. H., *see* EVERLING
WIEDLING, T., *see* BARBER
WILDERMUTH, K., *see* PEARLSTEIN
WILKINSON, D. H., *see* EISBERG
WILLIAMS, W. S. C., The measurement of the K_1—K_2 mass difference . 173
WOLFGANG, RICHARD, *see* PREISS
YAMADA, E., *see* DONIACH
YENNIE, D. R., *see* EISBERG

SUBJECT INDEX

1. Nuclear Structure

1.B *Two- and three-body problems*

Treatment of special translationally invariant three-body problems by adapted coordinates, P. Möbius 224
An improved approximation for scattering problems, P. Swan 245
Investigation of the interaction between the products of reactions in which several particles are emitted, V. V. Komarov and A. M. Popova 296
On the choice of d-state wave functions in triton calculations, G. H. Derrick . 303
Variational calculations with repulsive core potentials, N. Austern and P. Iano 672

1.C *Many-particle systems*

Effect of quadruple correlations in light nuclei, V. G. Soloviev 161
On a modified Bethe-Goldstone equation, Amnon Katz 177
Treatment of special translationally invariant three-body problems by adapted coordinates, P. Möbius 224
Intrinsic quadrupole moments of deformed nuclei and superfluidity in nuclei, Norman K. Glendenning and Jerzy Sawicki 596
Hole-hole interactions and the properties of nuclear matter, S. A. Moszkowski and A. M. Sessler 669
Variational calculations with repulsive core potentials, N. Austern and P. Iano 672

1.D *Nuclear models*

1.D.1 *Shell model*

Spin-orbit splitting and tensor force, Akito Arima 196

1.D.2 *Collective model*

Gyromagnetic factors of deformed odd-mass nuclei with $153 \leqq A \leqq 187$, E. M. Bernstein and J. de Boer 40
The electric quadrupole interaction in beta decay, J. M. Pearson and M. A. Preston 91

1.D.3 *Other models*

Low lying levels of Li^7 and Be^9 in the cluster model, L. D. Pearlstein, Y. C. Tang and K. Wildermuth 23

1.D.4 *Relationship between different models*

Effect of quadruple correlations in light nuclei, V. G. Soloviev 161
Group theory of harmonic oscillators (I). The collective modes, V. Bargmann and M. Moshinsky. 697

1.E *Properties of nuclei*

1.E.1 *Energy levels*

Investigation of polarization of internal conversion electrons emitted after β^--decay in heavy elements, M. E. Vishnevsky, V. A. Lyubimov, E. F. Tretyakov and G. I. Grishuk 122

1.E.2 *Binding energies; masses*

Relative nuclidic masses, F. Eve̊ling, L. A. König, J. H. E. Mattauch and A. H. Wapstra 529
Energies of alpha particles, A. H. Wapstra 587

1.E.3 *Electric and magnetic moments*

Gyromagnetic factors of deformed odd-mass nuclei with $153 \leqq A \leqq 187$, E. M. Bernstein and J. de Boer 40
Intrinsic quadrupole moments of deformed nuclei and superfluidity in nuclei, Norman K. Glendenning and Jerzy Sawicki 596

2. Nuclear Reactions

2.A *General properties*

2.A.2 *General theory*

On the minimum number of partial waves in two-body reactions, V. G. Grishin and V. I. Ogievetski 516

2.C *Resonance reactions R-matrix theory*

Protons from deuteron bombardment of Be^7, R. W. Kavanagh 492

2.D. *Statistical model*

On the statistical properties of the level-spacings in nuclear spectra, M. L. Mehta 395
On the density of eigenvalues of a random matrix, M. L. Mehta and M. Gaudin 420

2.E *Optical model*

A bremsstrahlung experiment to measure the time delay in nuclear reactions, R. M. Eisberg, D. R. Yennie and D. H. Wilkinson 338

2.F *Direct interaction (other than stripping)*

Direct interaction in the p—2p reaction, A. M. Green and G. E. Brown 1
Quasi-elastic scattering of 153 MeV protons by p-state protons in C^{12}. I. Experimental, T. J. Gooding and H. G. Pugh 46
Quasi-elastic scattering of 153 MeV protons by p-state protons in C^{12}. II. Theoretical, K. F. Riley, H. G. Pugh and T. J. Gooding 65
Symmetry properties of the distorted wave theory of direct nuclear reactions, G. R. Satchler 110
Investigation of the interaction between the products of reactions in which several particles are emitted, V. V. Komarov and A. M. Popova 296
Angular distributions and polarization in stripping processes and in direct reactions, L. J. B. Goldfarb and R. C. Johnson 353

2.G *Stripping and pick-up*

Étude de quelques niveaux excités du ^{11}B par la réaction $^{10}B(d, p)^{11}B$, S. Gorodetzky, M. Croissiaux, A. Gallmann, P. Fintz, J. Samuel et G. Bassompierre 286
Angular distributions and polarization in stripping processes and in direct reactions, L. J. B. Goldfarb and R. C. Johnson 353

2.I *Photonuclear processes*

Effects of photon polarization on the azimuthal angular distribution in (γ, N) reactions, A. G. de Pinho Filho 271
Electrodisintegration of Ta and Au nuclei, W. C. Barber and T. Wiedling . . 575
Integrated cross sections for the reactions $A^{40}(\gamma, p)$ and $Z^{40}(\gamma, np)$, H. G. Dosch, K. H. Lindenberger and P. Brix 615

2.J *Fission and spallation*

États individuels au seuil de fission, M. Demeur, P. Janssens et J. Lardinois . 280
Winkelverteilungen von Kernspaltungen im Resonanzbereich, O. Hittmair . 346
Absolute cross-sections of $C^{12}(p, pn)C^{11}$ from 288 to 383 MeV, Vastupal Parikh 628
Cross-sections for $Al^{27}(p, 3pn)Na^{24}$, $Al^{27}(p, 5p5n)F^{18}$, and $C^{12}(p, 3p3n)Be^{7}$, relative to $C^{12}(p, pn)C^{11}$, Vastupal Parikh 638
The activities induced in beryllium, oxygen and fluorine by protons of 220 MeV to 362 MeV, Vastupal Parikh 646

2.L *Scattering processes (except two-nucleon system and meson scattering)*

An improved approximation for scattering problems, P. Swan 245
A method for calculating scattering phase shifts, J. N. Lyness 654

3. Electromagnetic Radiation

3.B *Internal conversion*

Determination of absolute $B\rho$-values of conversion lines, C. de Vries 428
Precision measurements of energies of gamma-rays following the decay of some gold isotopes, C. de Vries and J. H. Dijkstra. 446
Absolute and relative conversion determinations of pure E2 transitions occurring in ^{198}Hg, ^{199}Hg, ^{194}Pt and ^{196}Pt, C. de Vries, E. J. Bleeker and Mrs. N. Salomons-Grobben 454

3.C *Extranuclear effects*

Investigation of internal bremsstrahlung cross-section with specified electron and photon energies, J. E. Thun, B. G. Pettersson and K. Siegbahn 131

4. Beta Decay; Parity

4.A *General theory*

The electric quadrupole interaction in beta decay, J. M. Pearson and M. A. Preston 91
Investigation of polarization of internal conversion electrons emitted after β^--decay in heavy elements, M. E. Vishnevsky, V. A. Lyubimov, E. F. Tretyakov and G. I. Grishuk 122

4.B *Formulation of Fermi theory*

On the pseudoscalar interaction in $0^- \rightarrow 0^+$ beta transitions, Dubravko Tadić 138

4.E *Analysis of data*

Precision measurements of energies of gamma-rays following the decay of some gold isotopes, C. de Vries and J. H. Dijkstra 446
A new isotope: cadmium-103, Ivor L. Preiss, Peder J. Estrup and Richard Wolfgang 624

5. Alpha Decay

Energies of alpha particles, A. H. Wapstra 587

6. Methods and Instruments

6.A *Experimental*

Determination of absolute $B\rho$-values of conversion lines, C. de Vries 428

7. Quantum Field Theory

7.A *General*

Resonance behaviour of scattering amplitudes in dispersion relations, John W. Moffat 75
A note on scattering and production amplitudes, A. P. Balachandran and N. R. Ranganathan 81
Analytical properties of the scattering amplitude for inelastic processes involving strange particles, I. T. Todorov 521
An equivalence theorem for partially gauge-invariant vector meson interactions, Abdus Salam 681

7.C *π-meson field (scattering and nuclear forces)*

Pion—nucleon attraction at short distances, S. Doniach and E. Yamada . . 14
Recoil in pion-nucleon scattering, V. Gupta 85
Polarizability of nucleons, A. M. Baldin 310
Elastic γ—p scattering at 40 to 70 MeV and polarizability of the proton, V. I. Goldansky, O. A. Karpukhin, A. V. Kutsenko and V. V. Pavlovskaya . 473

8. Elementary Particles

8.A *Experimental*

The measurement of the K_1—K_2 mass difference, W. S. C. Williams 173

8.B *Theory interactions, transformation properties*

Strong interactions and isobaric gauge invariance, V. Gupta 149
On the leptonic and non-leptonic decay modes of K-mesons, J. C. Pati, S. Oneda and B. Sakita 318
Pion—pion effects in τ-decay, A. N. Mitra 502
Analytical properties of the scattering amplitude for inelastic processes involving strange particles, I. T. Todorov 521
Unitarity conditions for binary processes involving particles of arbitrary spin, A. J. MacFarlane 570
On Salam's equivalence theorem in vector meson theory, S. Kamefuchi . . . 691

8.C *Fundamental theory of matter*

A possible model for the four-fermion coupling, E. van der Spuy 153

10. News Items

10.A *News Items*

The amalgamation of the Institute of Physics and the Physical Society 176
16th Session of the council of CERN 713
Inauguration at CERN of the "Pauli Memorial Room" 713

10.D *Book Reviews*

R. Hobart Ellis, Jr., Nuclear technology for engineers (J. Thomas) 715
Francis H. Clauser (Editor), Symposium of plasma dynamics (H. Wilhelmsson) 715
H. Semat, Introduction à la physique atomique et nucléaire (L. R.) 715
J. G. Wilson and S. A. Wouthuysen (Editors) Progress in elementary particle and cosmic ray physics, vol. V (L. R.) 716
Who's who in atoms (O. Kofoed-Hansen) 716
A. Hitchcock, Nuclear reactor stability (O. Kofoed-Hansen) 716
F. Halbwachs, Théorie relativiste des fluides à spin (L. R.) 717
M. A. Markow, Hyperonen und Mesonen (L. R.). 717
J. G. Linhart, Plasma physics (V. O. Jensen) 718
Australian atomic energy symposium 1958 (P. L. Ølgaard) 718
M. Rotenberg, R. Bivins, N. Metropolis, J. K. Wooten, Jr., The 3—j and 6—j symbols (L. R.) 718
R. Herman and R. hofstadter, High-energy electron scattering tables . . . 718
Gordon Francis, Ionization phenomena in gases (Hans Wilhelmsson) . . . 719
Université De Grenoble, École D'été De Physique Théorique (Les Houches), The many body problem (1958), La théorie des gaz neutres ionisés (1959) 719